PROCEEDINGS OF THE TWENTIETH WORKSHOP ON GENERAL RELATIVITY AND GRAVITATION IN JAPAN

YUKAWA INSTITUTE FOR THEORETICAL PHYSICS, KYOTO UNIVERSITY

KYOTO, JAPAN

SEPTEMBER 21-25, 2010

Edited by

Takashi Hiramatsu, Misao Sasaki, Masaru Shibata

and Tetsuya Shiromizu

Organising Committee

Hideki Asada	(Hirosaki University)
Takeshi Chiba	(Nihon University)
Tomohiro Harada	(Rikkyo University)
Takashi Hiramatsu	(Yukawa Institute for Theoretical Physics)
Kunihito Ioka	(High Energy Accelerator Research Organization (KEK))
Hideki Ishihara	(Osaka City University)
Kenta Kiuchi	(Yukawa Institute for Theoretical Physics)
Hideo Kodama	(High Energy Accelerator Research Organization)
Yasufumi Kojima	(Hiroshima University)
Koutarou Kyutoku	(Yukawa Institute for Theoretical Physics)
Kei-ichi Maeda	(Waseda University)
Shinji Mukohyama	(Institute for the Physics and Mathematics of the Universe)
Takashi Nakamura	(Kyoto University)
Ken'ichi Nakao	(Osaka City University)
Yasusada Nambu	(Nagoya University)
Ken-ichi Oohara	(Niigata University)
Misao Sasaki	(Yukawa Institute for Theoretical Physics)
Naoki Seto	(Kyoto University)
Masaru Shibata	(Yukawa Institute for Theoretical Physics)
Tetsuya Shiromizu	(Kyoto University)
Jiro Soda	(Kyoto University)
Naoshi Sugiyama	(Nagoya University)
Takahiro Tanaka	(Yukawa Institute for Theoretical Physics)
Shoichi Yamada	(Waseda University)
Masahide Yamaguchi	(Tokyo Institute of Technology)
Jun'ichi Yokoyama	(Research Center for the Early Universe)

Programme of the Workshop

Plenary Session (Panasonic Hall, Yukawa Institute for Theoretical Physics)

Sep. 21, Tue.

9:55-10:00 Opening remark

Chair: Tetsuya Shiromizu
10:00-11:00 Gary W. Gibbons (University of Cambridge)
"What is the shape of a black hole?"
11:00-11:30 *break*
11:30-12:30 Valeri P. Frolov (University of Alberta)
"Applications of hidden symmetries to black hole physics"

12:30-14:00 *lunch*

Chair: Jiro Soda
14:00-15:00 Rong-Gen Cai (Chinese Academy of Sciences)
"Connection between thermodynamics and gravitational dynamics"
15:00-16:15 *short presentation for poster* (P1-P32)
16:15-17:15 *break + poster*
Chair: Takeshi Chiba
17:15-18:00 Nobuyoshi Ohta (Kinki University)
"Accelerating cosmologies and inflation in string theories with higher order corrections"

Sep. 22, Tue.

Chair: Shinji Mukohyama
9:30-10:30 Eric Gourgoulhon (Observatoire Paris-Meudon)
"A geometrical approach to relativistic magnetohydrodynamics"
10:30-11:00 *break*
Chair: Hideki Ishihara
11:00-11:45 Toshifumi Futamase (Tohoku University)
"A new approach of equation of motion for fast-moving self-gravitating particle"
11:45-12:30 Yasunori Fujii (Waseda University)
"An expected gravitational scalar field – Past and Future –"

12:30-14:00 *lunch*

Chair: Hideki Asada
14:00-15:00 Brandon Carter (Observatoire Paris-Meudon)
"Classical mechanics of strings and higher branes"
15:00-16:15 *short presentation for poster* (P33-P63)
16:15-17:15 *break + poster*
Chair: Ken-ichi Nakao
17:15-18:00 Yasufumi Kojima (Hirosima University)
"Radiation recoil in neutron stars"

Sep. 23, Thu.

Chair: Toshifumi Futamase

9:30-10:30 Bernard F. Schutz (Albert Einstein Institute)
"Gravitational astronomy with LIGO, VIRGO, and LCGT"
10:30-11:00 *break*
Chair: Naoki Seto
11:00-12:00 Luc Blanchet (Institut d'Astrophysique de Paris)
"Post-Newtonian methods and applications"
12:00-12:45 Masaki Ando (Kyoto University)
"Gravitational-wave observatories: LCGT and DECIGO"

12:45-16:00 *lunch* + Poster or Free discussion or Self excursion

Chair: Masaru Shibata
16:00-16:45 Kei-ichi Maeda (Waseda University)
"Dimensional reduction"
16:45-17:30 Takashi Nakamura (Kyoto University)
"Anniversary of the 20th JGRG"
17:30-18:30 walk to Holiday Inn
18:30-20:30 Banquet @ Holiday Inn, 4th floor

Sep. 24, Fri.

Chair: Yasufumi Kojima
10:00-11:00 Tsvi Piran (The Hebrew University)
"GRBs as example of extreme relativistic objects"
11:00-11:30 *break*
11:30-12:15 Kunihito Ioka (High Energy Accelerator Research Organization)
"Gravitational wave and high energy phenomena"

12:15-14:00 *lunch*

Chair: Ken-ichi Oohara
14:00-15:00 Manuela Campanelli (Rochester Institute of Technology)
"Merging binary black holes in astrophysics"
15:00-16:15 *short presentation for poster* (P64-P92)
16:15-17:15 *break + poster*
Chair: Tomohiro Harada
17:15-18:00 Takeshi Chiba (Nihon University)
"Slow-roll"

Sep. 25, Sat.

Chair: Takahiro Tanaka
9:30-10:30 David Wands (University of Portsmouth)
"Non-linear cosmological perturbations from inflation"
10:30-11:00 *break*
11:00-11:45 Shinji Tsujikawa (Tokyo University of Science)
"Inflation and dark energy -theoretical progress over 20 years"
11:45-12:30 Misao Sasaki (Yukawa Institute for Theoretical Physics)
"Summary"

Poster Presentations (Second and Third Floors, Yukawa Institute for Theoretical Physics)

Poster Place 1 (Poster Numbers P1-P46, Second Floor, Yukawa Institute for Theoretical Physics)

P01. Masaru Adachi (Hirosaki University)
"Re-analysis of the supernova data to test the effects of large-scale inhomogeneities"
P02. Takashi Torii (Osaka Institute of Technology)
"Black Holes in Effective String Theory"
P03. Fumitoshi Amemiya (Keio University)
"Quantum state of universe before big bounce"
P04. Hideyoshi Arakida (Waseda University)
"Light propagation in time-dependent gravitational field"
P05. Frederico Arroja (Yukawa Institute for Theoretical Physics)
"A note on the equivalence of a barotropic perfect fluid with a K-essence scalar field"
P06. Yu Chen (National University of Singapore)
"Black holes on gravitational instantons"
P07. Gianluca Calcagni (Max Planck Institute for Gravitational Physics)
"Fractal universe"
P08. Li-Ming Cao (Kinki University)
"Thermodyanmics of trapping horizon in FRW universe"
P09. Jinn-Ouk Gong (Instituut-Lorentz for Theoretical Physics Universiteit Leiden)
"Waterfall field in hybrid inflation and curvature perturbation"
P10. Je-An Gu (LeCosPA Center, National Taiwan University)
"f(R) Modified Gravity and its Cosmological and Solar-System Tests"
P11. Tomohiro Harada (Rikkyo University)
"Black hole candidates and the Kerr bound"
P12. Atsushi Naruko (Yukawa Institute for Theoretical Physics)
"Second order Boltzmann equation with polarization"
P13. Yuta Hiranuma (Niigata Univesity)
"Effectiveness of Empirical Mode Decomposition in Search for Gravitational Wave Signals"
P14. Kenta Hotokezaka (Kyoto University)
"Can We Confirm Neutron Stars Are Giant Hypernuclei From Gravitational Wave Observation?"
P15. Kenji Hotta (Hokkaido University)
"Creation of D9-brane–anti-D9-brane Pairs from Hagedorn Transition of Closed Strings– its application to cosmology"
P16. Tsuyoshi Houri (Osaka City University Advanced Mathematical Institute)
"Generalized hidden symmetries and the Kerr-Sen black hole"
P17. Yong-Chang Huang (Institute of Theoretical Physics, Beijing University of Technology)
"A Holographic Energy Model"
P18. Shoichi Ichinose (University of Shizuoka)
"Renormalization Group Flow and the Dark Energy Problem"
P19. Takahisa Igata (Osaka City University)
"Stable Bound Orbits around Black Rings"
P20. Koji Izumi (Hirosaki University)
"Perturbative solutions to the lens equation for multiple lens planes"
P21. Keisuke Izumi (Institute for the Physics and Mathematics of the Universe)
"Non-Gaussianity from Lifshitz Scalar"
P22. Kohei Kamada (Reserch Center for the Early Universe (RESCEU), The University of Tokyo)
"Q balls in thermal logarithmic potential"
P23. Nahomi Kan (Yamaguchi Junior College)
"Weyl invariant Dirac Born Infeld Einstein theory"
P24. Yuki Kanai (Tokyo Institute of Technology)
"Gravitational collapse in Painleve-Gullstrand coordinates"

P25. Masumi Kasai (Hirosaki University)
"Perturbative approach to a non-spherical micro-lensing effect"
P26. Tanabe Kentaro (Yukawa Institute for Theoretical Physics)
"Angular momentum at null infinity in five dimensions"
P27. Masashi Kimura (Osaka City University)
"On Non-Linear Effects of BSW Mechanism"
P28. Shunichiro Kinoshita (Yukawa Institute for Theoretical Physics)
"Non-equilibrium Condensation Process in a Holographic Superconductor"
P29. Tsutomu Kobayashi (RESCEU, The University of Tokyo)
"Inflation driven by the Galileon field"
P30. Seoktae Koh (Sogang University)
"Scalar field dynamics in nonminimally coupled hybrid inflation"
P31. Takayuki Suzuki (Yamaguchi University)
"N-body simulation on the Modified Gravity"
P32. Chih-Hung Wang (Tamkang University)
"A momentum-space representation of Feynman propagator in Riemann-Cartan spacetime"
P33. Kenta Kiuchi (Yukawa Institute for Theoretical Physics)
"Non-axisymmetric instability of toroidal magnetic field in neutron stars"
P34. Hiroshi Kozaki (Ishikawa National College of Technology)
"Dynamics of membranes with symmetry and projection formalism"
P35. Yasunari Kurita (Kanagawa Institute of Technology)
"Backreaction problem in Bose-Einstein condensates: an analogy with curved spacetime"
P36. Koutarou Kyutoku (Yukawa Institute for Theoretical Physics)
"Gravitational waves from spinning black hole-neutron star binaries"
P37. Tae-Hoon Lee (Soongsil University, Korea)
"Horava gravity coupled to the Brans-Dicke field"
P38. Satoshi Maeda (Kyoto university)
"The power spectrum of the magnetic fields generated by the second-order perturbations during the pre-recombination era"
P40. Ken Matsuno (Osaka City University)
"Multi-black strings in five-dimensional Einstein-Maxwell theory"
P41. Masato Minamitsuji (Kwansei Gakuin University)
"Dynamical solutions in the Nishino-Salam-Sezgin model and its extensions"
P42. Yosuke Misonoh (Waseda University)
"Oscillating Universe in Horava-Lifshitz gravity"
P43. Shuntaro Mizuno (University of Portsmouth)
"Trispectrum estimator in equilateral type non-Gaussian models"
P44. Yoshiyuki Morisawa (Osaka University of Economics and Law)
"Target space structure of 5-dimensionalEinstein-Maxwell-Chern-Simons theory with non-SUGRA coupling"
P45. Masaaki Morita (Nagaoka University of Technology)
"Gravitational wave background in modified-gravity dark energy models"
P46. Hayato Motohashi (Research center for the early universe, The University of Tokyo)
"Perturbation theory in f(R) gravity"

Poster Place 2 (Poster Numbers P47-P92, Third Floor, Yukawa Institute for Theoretical Physics)

P47. Kouji Nakamura (National Astronomical Observatory of Japan)
"Construction of gauge-invariant variables for linear-order perturbations on some background spacetimes"
P48. Masahiro Nakashima (The University of Tokyo, RESCEU)
"CMB Polarization in Einstein-Aether Theory"

P49. Kazunori Nakayama (High Energy Accelerator Research Organization (KEK))
"Inflation from a Supersymmetric Axion Model"
P50. Takashi Hiramatsu (Yukawa Institute for Theoretical Physics)
"Gravitational waves from Q-balls in gravity mediation"
P51. Masato Nozawa (Waseda University)
"Rotating black holes in fake supergravity"
P52. Seiju Ohashi (Kyoto University)
"No-dipole-hair theorem for higher-dimensional static black holes"
P53. Junko Ohashi (Tokyo University of Science)
"Observational constraints on assisted k-inflation"
P54. Sergey Pavluchenko (Special Astrophysical Observatory of the Russian Academy of Sciences)
"The dynamics of the flat anisotropic models in the Lovelock gravity"
P56. Margus Saal (Tartu Observatory)
"Scalar-tensor cosmologies with a potential in the general relativity limit"
P57. Norichika Sago (Yukawa Institute for Theoretical Physics)
"Gravitational self-force effect on eccentric orbits in Schwarzschild geometry"
P58. Motoyuki Saijo (Rikkyo University)
"Rapidly Rotating Dynamic Black Holes through Gravitational Collapse"
P59. Ryo Saito (The University of Tokyo, RESCEU)
"Parametric amplification of the inflaton fluctuations induced by a heavy scalar field"
P60. Nobuyuki Sakai (Yamagata University)
"Deformation of an Expanding Void in Redshift Space"
P61. Yukinori Sasagawa (Waseda University)
"AdS Black Hole Solution with nontrivial dilaton in Dilatonic Einstein Gauss-Bonnet Gravity Theory"
P62. Fabio Scardigli (LeCosPA Cosmology Center, National Taiwan University)
"Pre-inflation matter era and the CMB power spectrum"
P63. Yuichiro Sekiguchi (National Astronomical Observatory of Japan)
"Black hole and accretion disk formation in the collapsar model"
P64. Osamu Seto (Hokkai-Gakuen University)
"Curvaton with a double well potential"
P65. Masahiro Shimano (Rikkyo University)
"A note on trapped surfaces in the Oppenheimer-Snyder solution"
P66. Maresuke Shiraishi (Nagoya University)
"The CMB bispectrum from vector-mode perturbations induced by primordial magnetic fields"
P67. Kazuyuki Sugimura (Yukawa Institute for Theoretical Physics)
"The effect of multi-field interaction on false vacuum decay"
P68. Yudai Suwa (Yukawa Institute for Theoretical Physics)
"Gamma-ray bursts of the first generation of stars"
P69. Teruaki Suyama (RESCEU, The University of Tokyo, and The Universite catholic de Louvain)
"Temporal enhancement of large scale curvature perturbation in multiple curvaton decays"
P70. Ryotaku Suzuki (Kyoto University)
"Extreme charged black hole in braneworld with cosmological constant"
P71. Tomohiro Takahashi (Kyoto University)
"Linear Instability of Lovelock Black Holes"
P72. Yuichi Takamizu (RESCEU, The University of Tokyo)
"Beyond delta-N formalism for a single scalar field"
P73. Takashi Tamaki (College of Engineering, Nihon University)
"Unified picture of Q-balls and boson stars via catastrophe theory"
P74. Makoto Tanabe (Waseda University)
"Time Dependent Meta Stable Vacua in M-theory"
P75. Jun-ichirou Koga (Waseda University)
"The final fate of instability of Reissner-Nordstrom-AdS black holes"

P76. Yuko Urakawa (Waseda university)
"IR divergence and gauge-invariant initial state"
P77. Koji Uryu (University of the Ryukyus)
"Magnetized binary black holes and neutron stars in equilibrium"
P78. Ryo Wakebe (Waseda University)
"Accelerating Cosmologies in Dilatonic Einstein-Gauss-Bonnet Gravity in the String Frame"
P79. Hirotada Okawa (Yukawa Institute for Theoretical Physics)
"High-velocity BH collision in 5 dimensions"
P80. Masaaki Watanabe (Kyoto University)
"Anisotropic inflation and its imprints on the CMB"
P81. Yu-Huei Wu (National central university, Taiwan)
"Angular momentum flux from a spinning dynamical black hole"
P82. Kent Yagi (Kyoto University)
"Probing the size of extra dimension from gravitational wave astronomy"
P83. Kei Yamada (Hirosaki University)
"Euler's collinear solution to three-body problem in GR"
P84. Yuta Yamada (Osaka Institute of Technology)
"Gravitational Collapse in Five-dimensional Spacetime"
P85. Daisuke Yamauchi (Yukawa Institute for Theoretical Physics)
"Analytical model for CMB temperature angular power spectrum from cosmic (super-)strings"
P86. Kohkichi Konno (Tomakomai National College of Technology)
"Rotating black holes in Chern-Simons modified gravity"
P87. Shuichiro Yokoyama (Nagoya University)
"Iso-curvature fluctuations in modulated reheating scenario"
P88. Chul-Moon Yoo (Yukawa Institute for Theoretical Physics)
"Redshift drift in LTB universes"
P89. Hongsheng Zhang (Shanghai United Center for Astrophysics (SUCA) Shanghai Normal University)
"A new plane symmetric solution"
P91. Kazumi Kashiyama (Kyoto University)
"White Dwarf Pulsars as Possible Electron-Positron Factories"

Table of Contents

Preface

The memorial 20^{th} workshop on General Relativity and Gravitation (JGRG20) was held at Yukawa Institute for Theoretical Physics, Kyoto University, from 21st to 25th, September 2010.

The aim of the JGRG series of workshops is to overview wide and expanding topics in general relativity and its surrounding fields, including astrophysics and cosmology, and to encourage collaboration among participants of the workshop. This year was very special not just because it was the 20th anniversary of the JGRG workshops: It was the year of the 60th birthday of Professors Takashi Nakamura and Kei-Ichi Maeda, who were founding fathers of JGRG and who have been making invaluable contribution to the community of general relativity and gravitation in Japan for last forty years.

To celebrate their birthdays, we arranged a special style of scientific programme; we invited 19 world-renowned researchers and asked them to overview their research fields. We not only learned a variety of aspects of gravity, cosmology and astrophysics from their lectures, but also heard their heartfelt memories from the time when Takashi and Kei-Ichi were young. We also had 84 poster presentations by young scientists who actively discussed their works. We believe that the workshop was a great success with a plenty of stimulating discussions.

Now, JGRG has a history of 20 years! For those who are interested in the history of JGRG, we would recommend to take a look at the contribution of Takashi and/or the JGRG proceedings web-site (http://www-tap.scphys.kyoto-u.ac.jp/jgrg) maintained by Theoretical astrophysics group of Kyoto University.

We would like to deeply express our gratitude to Ms. Kiyoe Yokota, Secretary for theory groups at Department of Physics, Kyoto University. Without her effort, we could not have continued this series of JGRG meetings over twenty years. We sincerely hope that she would continue to help us for years to come.

This workshop was supported in part by JSPS Grant-in-Aid for Research (A) No. 21244033, by JSPS Grand-in-Aid for Creative Scientific Research No. 20151970, by MEXT Grant-in Aid for the Global COE program at Kyoto University, "The Next Generation of Physics, Spun from Universality and Emergence," and by the Yukawa Institute for Theoretical Physics, Kyoto University.

Kyoto, 30th of June, 2011

Takashi Hiramatsu
Misao Sasaki
Masaru Shibata
Tetsuya Shiromizu

Connections between Gravitational Dynamics and Thermodynamics

Rong-Gen Cai[1]

Key Laboratory of Frontiers in Theoretical Physics, Institute of Theoretical Physics, Chinese Academy of Sciences, P.O. Box 2735, Beijing 100190, China

Abstract

In this paper we briefly summarize three aspects of connections between gravitational dynamics and thermodynamics by focusing on three kinds of spacetime horizon: causal Rindler horizon of spacetime, black hole event horizon and apparent horizon in a Friedmann-Robertson-Walker (FRW) universe. For the causal Rindler horizon, we derive the Einstein's field equations from the Clausius relation. For black hole horizon in a static spherically symmetric spacetime, we show that at the black hole horizon, the Einstein's field equation can be cast to a form of the first law of thermodynamics. Applying to the Clauius relation to apparent horizon of a FRW universe, one is able to derive the Friedmann equations, not only in Einstein gravity, but also in Lovelock gravity. We show that there exists Hawking radiation associated with the apparent horizon in the FRW universe.

1 Introduction

According to Einstein, general relativity describes dynamics of spacetime by use of spacetime metric, while thermodynamics is another subject which describes macroscopic properties of thermal system in terms of energy, pressure, entropy and temperature etc. of the system. The first evidence for the deep connections between gravitational dynamics and thermodynamics comes from black hole thermodynamics. Black hole as a fantastic object is predicted by general relativity. Black hole thermodynamics tells us that black hole has a temperature proportional to its surface gravity and an entropy proportional to its horizon area, and the temperature, entropy and black hole mass satisfies the first law of thermodynamics. Not only the first law, other three laws of thermodynamics are also obeyed for black hole. In this sense, black hole is nothing, but an ordinary thermodynamic system. However, black hole is a special thermal system because its entropy is proportional to its horizon area, while entropy of ordinary thermal system is proportional to its volume. Another feature of black hole thermodynamics is that heat capacity of some black hole may be negative, for example, Schwarzschild black hole.

The geometric feature of black hole temperature and entropy leads one to conjecture that gravity might be an emergent phenomenon and is a coarse graining description of some underlying microscopic degrees of freedom. In fact this idea was first proposed by Sakharov in 1967 [1], before black hole thermodynamics is set up. According to Sakharov, spacetime background emerges as a mean field approximation of underlying microscopic degrees of freedom, similar to hydrodynamics or continuum elasticity theory from molecular physics.

Just in the beginning of 2010, E. Verlinde [2] proposed that gravity is not a fundamental interaction in Nature, but a kind of entropic force and gravity is caused by changes in the information associated with the positions of material bodies. With the assumption of the entropic force together with the Unruh temperature, Verlinde is able to derive the second law of Newton. Also he is able to derive Newton's law of gravitation with the assumption of the entropic force together with the holographic principle and the equipartition law of energy. This observations are also made by Padmanabhan [3]. He observed that the equipartition law of energy for the horizon degrees of freedom combing with the thermodynamic relation $S = E/2T$, also leads to Newton's law of gravity, here S and T are thermodynamic entropy and temperature associated with the horizon and E is the active gravitational mass producing the gravitational acceleration in the spacetime.

[1]Email address: cairg@itp.ac.cn

According to Verlinde, that gravity is an entropic force is more than to say that gravity has something to do with thermodynamics. In this paper, however, we will not discuss the viewpoint of gravity as entropic force more, instead we will study the connections between gravitational dynamics and thermodynamics, in particular, focus on the relation between Einstein's field equation and the first law of thermodynamics. We will investigation the relation by using of three kinds of spacetime horizons: Rindler horizon, black hole horizon and apparent horizon in a Friedmann-Robertson-Walker (FRW) universe.

The organization of this paper is as follows. In the next section, we briefly repeat the derivation process of Einstein's field equation from the first law of thermodynamics made by Jacobson by applying the latter to Rindler horizon of spacetime [4]. In Sec. 3 we focus on black hole horizon and show that the Einstein's field equations can be cast to a form of the first law of thermodynamics, not only in general relation, but also in Horava-Lifshitz gravity [5, 6]. In Sec. 4 we focus on apparent horizon of FRW universe, and investigate the relation between Friedmann equations and the first law [7–9] and show that there exists Hawking radiation associated with apparent horizon [10].

2 Rindler horizon: from the first law to Einstein's field equations

The so-called Rindler coordinate chart describes a part of flat spacetime, or say, Minkowski vacuum. This chart was introduced by Wolfgang Rindler. The Rindler coordinate sysytem or frame describes a uniformly accelerating frame of reference in Minkowski space. In special relativity, a uniformly acceleration particle undergoes a hyperbolic motion. For each such a particle a Rindler frame can be chosen in which it is at rest. For example, in the Rindler chart the Minkowski space can be written as

$$ds^2 = -x^2dt^2 + dx^2 + dy^2 + dz^2, \tag{1}$$

where $0 < x < \infty$, $-\infty < t,\ y,\ z < \infty$. The Rindler coordinate chart has a coordinate singularity at $x = 0$. The acceleration of the Rindler observers diverges there. The locus $x = 0$ in the Rindler chart corresponds to the locus $X^2 - T^2 = 0$ with $X > 0$ in the Cartesian chart of Minkwoski space, the latter consists of two null half-planes. The locus $x = 0$ is just the Rindler horizon, the Rindler observer cannot see any information outside the Rindler wedge.

According to Davies [11] and Unruh [12], for a uniformly accelerating observer with acceleration a in Minkowski space, she will detect a temperature given by $T = \frac{a}{2\pi}$, where the so-called geometric units have been taken: $c = \hbar = k_B = 1$. In the Rindler coordinate (1) , for a Rindler observer with a fixed $x = x_0$, her acceleration is $a = 1/x_0$.

Now consider a certain event P in any spacetime, by equivalent principle, one can introduce a local inertial frame around P with Riemann normal coordinates. One further transforms the local inertial frame to a local Rindler frame by accelerating along an axis with acceleration κ. Then there is a Unruh temperature associated with the local Rindler horizon as

$$T = \kappa/2\pi. \tag{2}$$

Suppose the matter in the spacetime is described by the stress-energy tensor T_{ab}. Then the heat flux across the Rindler horizon $\mathcal{H}$ is

$$\delta Q = \int_{\mathcal{H}} T_{ab}\chi^a d\Sigma^b, \tag{3}$$

where χ^a is an approximation boost Killing vector on $\mathcal{H}$. Note that the relations: $\chi^a = -\kappa\lambda k^a$ and $d\Sigma^a = k^a d\lambda dA$, where k^a is the tangent vector to the horizon generators for an fine parameter λ which vanishes at P; dA is the area element on a cross section of the horizon. Then we have

$$\delta Q = -\kappa \int_{\mathcal{H}} \lambda T_{ab}k^a k^b d\lambda dA. \tag{4}$$

Now assume that the entropy is proportional to the horizon area, so that the entropy variation associated with a piece of horizon is given by

$$dS = \eta\delta\mathcal{A}, \tag{5}$$

where η is a constant and $\delta\mathcal{A} = \int_{\mathcal{H}} \theta d\lambda dA$. Using the Raychaudhuri equation

$$\frac{d\theta}{d\lambda} = -\frac{1}{2}\theta^2 - \sigma^2 - R_{ab}k^a k^b, \tag{6}$$

and assuming the vanishing of expansion θ and shear σ at P, to the leading order of λ, one has $\theta = -\lambda R_{ab}k^a k^b$, which leads to

$$\delta\mathcal{A} = -\int_{\mathcal{H}} \lambda R_{ab}k^a k^b d\lambda dA. \tag{7}$$

By the Clausius relation $\delta Q = TdS$, one can have

$$R_{ab} + fg_{ab} = \frac{2\pi}{\eta}T_{ab}, \tag{8}$$

where f is an arbitrary function. To determine the function f, we employ the conservation law of the stress-energy tensor: $T^{ab}_{\ \ ;b} = 0$. This leads to $f = -R/2 + \Lambda$, where Λ is a constant, this is nothing, but the cosmological constant as one will see shortly. Put f back to the above equation, one arrives at

$$R_{ab} - \frac{1}{2}Rg_{ab} + \Lambda g_{ab} = \frac{2\pi}{\eta}T_{ab}. \tag{9}$$

One can see immediately from (9) that it is nothing, but the Einstein's field equation, once $G = 1/4\eta$ is identified.

Thus we simply repeated the process to derive the Einstein's field equations from the Clausius relation made by Jacobson [4]. The key idea is to demand that this relation holds for all the local Rindler causal horizons through each spacetime point, with δQ and T interpreted as the energy flux and Unruh temperature seen by an accelerated observer just inside the horizon. In this sense, the Einstein's field equation is nothing, but an equation of state of spacetime. If this viewpoint is correct, it has significant implication for quantum gravity theory: it may be no more appropriate to canonically quantize the Einstein's field equation than it would be to quantize the wave equation for sound in air.

Further remarks: 1) For $f(R)$ gravity [13] and scalar-tensor gravity [9], it turns out that a non-equilibrium thermodynamic setup has to be employed in order to produce corresponding gravitational field equations. Namely one needs an entropy production term added to the Clausius relation. 2) It is further shown that assuming the nonvanishing of the shear for Einstein gravity, the non-equilibrium setup is needed, $dS = \delta Q/T + d_i S$, where the entropy production term is proportional to the squared shear of the horizon [14]. And it leads to a universal ratio of the shear viscosity η to entropy density of the horizon: $\eta/s = 1/4\pi$. 3) For any diffeomorphism invariant theory, however, it has been shown recently that given Wald's entropy formula, by the Clausius relation, it is possible to derive the gravitational field equations [15, 16]. However, an issue exists that to have the Wald's entropy formula, one has to know first the gravity theory. In this sense, the derivation is not natural and satisfied [17].

3 Black hole horizon: equivalence between Einstein's field equations and the first law of thermodynamics

In this section we move to black hole horizon and discuss the relation between the Einstein's field equations and the first law of thermodynamics.

Let us first consider the Einstein's field equations

$$G_{ab} \equiv R_{ab} - \frac{1}{2}Rg_{ab} = 8\pi G T_{ab}, \tag{10}$$

where G_{ab} is the Einstein tensor. Consider a generic static, spherically symmetric spacetime

$$ds^2 = -f(r)dt^2 + f^{-1}(r)dr^2 + b^2(r)(d\theta^2 + \sin^2\theta d\phi^2), \tag{11}$$

where $f(r)$ and $b(r)$ are two continuous functions of r. Suppose the metric (11) describes a black hole with a nondegenerated horizon at r_+. Then the horizon has a Hawking temperature given by

$$T = \frac{1}{4\pi} f'(r_+), \tag{12}$$

where a prime denotes the derivative with respect to r. The Einstein's field equation in the metric (11) turns to be

$$G_t^t = \frac{1}{b^2}(-1 + fb'^2 + b(f'b' + 2fb'')), \quad G_r^r = \frac{1}{b^2}(-1 + bf'b' + fb'^2). \tag{13}$$

At the black hole where $f(r_+) = 0$, G_t^t and G_r^r become identical:

$$G_t^t = G_r^r = \frac{1}{b^2}(-1 + bfb')|_{r_+}. \tag{14}$$

The $r - r$ component of the Einstein field equations at the horizon can be written as

$$-1 + bf'b' = 8\pi b^2 P, \tag{15}$$

where $P = T_r^r$ is the radial pressure of matter at the horizon. Now we multiply a displacement dr_+ of the horizon on both sides of the above equation, the resulting equation can be cast as

$$Td\left(\frac{4\pi b^2}{4G}\right) - d\left(\frac{r_+}{2G}\right) = PdV, \tag{16}$$

where V is the black hole volume and $dV = 4\pi b^2 dr_+$. This equation can be clearly rewritten as

$$TdS - dE = PdV \tag{17}$$

with identifications: $S = 4\pi b^2/4G = A/4G$ and $E = r_+/2G$. Note that equation (17) is nothing, but the first law of thermodynamics. Here T is the Hawking temperature of the black hole horizon and S is the Bekenstein-Hawking entropy of the black hole. Note that here E is the Misner-Sharp energy at the horizon and is not the ADM mass of the black hole.

Thus we showed that at a black hole horizon, the Einstein's field equations can be cast to a form of the first law of thermodynamics, which implies that there exists a deep connection between gravity and thermodynamics. It is further shown that even for Horava-Lifshitz gravity, which is not a diffeomorphism invariant theory, its field equation at black hole horizon also can be cast the first law form of thermodynamics [6].

In addition, it is found that the story goes on for Lovelock gravity [18], BTZ black hole spacetime [19], stationary black holes and evolving spherically symmetric horizons [20]. However, a non-equilibrium thermodynamics setting is needed for $f(R)$ gravity [21].

4 Apparent horizon: Friedmann equation, the first law of thermodynamics and Hawking radiation

In this section we move to apparent horizon in a FRW universe.

4.1 From first law to Friedmann equation

Let us start with an $(n+1)$-dimensional FRW metric

$$ds^2 = -dt^2 + a^2(t)\left(\frac{dr^2}{1-kr^2} + r^2 d\Omega_{n-1}^2\right), \tag{18}$$

where a is the scale factor and $d\Omega_{n-1}^2$ denotes an $(n-1)$-dimensional sphere with unit radius. Without loss of generality, one can take $k = 1$, 0 or -1, corresponding to a closed, flat or open universe, respectively.

Einstein's field equations in the FRW metric (18) take the form

$$H^2+\frac{k}{a^2}=\frac{16\pi G}{n(n-1)}\rho, \tag{19}$$

$$\dot{H}-\frac{k}{a^2}=-\frac{8\pi G}{n-1}(\rho+p), \tag{20}$$

where ρ and p are energy density and pressure of the perfect fluid in the spacetime, and $H=\dot{a}/a$ is the Hubble parameter and the overdot stands for the derivative with respect to cosmic time t.

Introducing the physical radius $\tilde{r}=ar$ and the metric (18) can be rewritten as

$$ds^2=h_{ab}dx^a dx^b+\tilde{r}^2 d\Omega_{n-1}^2, \tag{21}$$

where $x^0=t$, $x^1=r$, and $h_{ab}=\mathrm{diag}(-1,a^2/(1-kr^2))$. In a FRW universe, there may exist some different horizons, for example, particle horizon, Hubble horizon, apparent horizon and event horizon etc. Here we focus on apparent horizon, which is argued to be a causal horizon of spacetime. By definition of apparent horizon, $h^{ab}\partial_a\tilde{r}\partial_b\tilde{r}=0$, we have the apparent horizon radius

$$\tilde{r}_A=\frac{1}{\sqrt{H^2+k/a^2}}. \tag{22}$$

Now we apply the first law of thermodynamics (the Clauius relation), $dE=TdS$, to the apparent horizon of the FRW universe. To do that, we assume that there exist temperature and entropy associated with the apparent horizon as

$$T=\frac{1}{2\pi\tilde{r}_A},\quad S=\frac{A}{4G}, \tag{23}$$

where $A=\tilde{r}_A^{n-1}\Omega_{n-1}$ is the apparent horizon area. Suppose the matter source in the FRW universe is a perfect fluid, its stress-energy tensor is given by $T_{ab}=(\rho+p)U_aU_b+pg_{ab}$, where U_a is the 4-velocity. Following [22], defining two physical quantities, the energy supply vector Ψ_a and work density W as

$$\Psi_a=T_a^b\partial_b\tilde{r}+W\partial_a\tilde{r},\quad W=-\frac{1}{2}T^{ab}h_{ab}, \tag{24}$$

one then can calculate the amount of energy across the apparent horizon within the time internal dt as

$$dE=A(\rho+p)H\tilde{r}_a dt. \tag{25}$$

Using the energy dE together with the temperature T and entropy S in (23), the Clausius relation leads to

$$\dot{H}-\frac{k}{a^2}=-\frac{8\pi G}{n-1}(\rho+p). \tag{26}$$

Clearly this is nothing but the second Friedmann equation (20). Further by use of the continuity equation, $\dot{\rho}+n(\rho+p)=0$, integrating (26) yields

$$H^2+\frac{k}{a^2}=\frac{16\pi G}{n(n-1)}\rho. \tag{27}$$

Here an integration constant has been put into the energy density ρ. In fact, the integration constant is just the cosmological constant. This way the cosmological constant appears as an integration constant, whose exact value should be given by initial condition. Thus the so-called cosmological constant problem does not appear here.

Thus we have derived the Friedmann equations governing the dynamics of the FRW universe by applying the first law to the apparent horizon of the spacetime with assumption (23). In fact, replacing the entropy formula in (23) by corresponding ones in Gauss-Bonnet gravity and more general Lovelcok

gravity, in the same way we are also able to derive corresponding Friedmann equations in those gravity theories [7].

The above approach can be used in more general cases [23], in fact. For example, given a relation between entropy and apparent horizon area, we are able to obtain corresponding modified Friedmann equation. Take an example, it is generally believed that quantum correction will add a logarithmic term to black hole area entropy formula as [24]

$$S = \frac{A}{4G} + \alpha \ln \frac{A}{4G}, \tag{28}$$

where α is a constant. In the same way, we obtained Friedmann equations in four dimensions

$$\begin{aligned} &\left(1 + \frac{4G\alpha}{A}\right)(\dot{H} - \frac{k}{a^2}) = -4\pi G(\rho + p), \\ &H^2 + \frac{k}{a^2} + \frac{\alpha}{2\pi}(H^2 + \frac{k}{a^2})^2 = \frac{8\pi G}{3}\rho. \end{aligned} \tag{29}$$

If the entropy is given by an arbitrary function of apparent horizon area, $S = f(x)$ where $x = A/4G$, we can have a general forms of Friedmann equations [24]

$$\begin{aligned} &(\dot{H} - \frac{k}{a^2})f'(x) = -4\pi G(\rho + p), \\ &\frac{8\pi G}{3}\rho = -\frac{\pi}{G}\int \frac{f'}{x^2}dx. \end{aligned} \tag{30}$$

4.2 Equivalence between the Friedmann equation and the first law

In this subsection we prove that the Friedmann equation at the apparent horizon can be cast to a form of the first law of thermodynamics [8].

Let us start with the FRW metric (18), by definition, $\kappa = \frac{1}{2\sqrt{-h}}\partial_a(\sqrt{-h}h^{ab}\partial_b\tilde{r})$, one has the surface gravity at apparent horizon

$$\kappa = -\frac{1}{\tilde{r}_A}(1 - \frac{\dot{\tilde{r}}_A}{2H\tilde{r}_A}). \tag{31}$$

In terms of the apparent horizon radius, the first Friedmann equation (19) can be expressed as

$$\frac{1}{\tilde{r}_A^2} = \frac{16\pi G}{n(n-1)}\rho. \tag{32}$$

Taking derivative on both sides of the above equation and using the continuity equation, one has

$$\frac{1}{\tilde{r}_A^3}d\tilde{r}_A = \frac{8\pi G}{n-1}(\rho + p)Hdt. \tag{33}$$

With identification $T = \kappa/2\pi$, and $S = A/4G$, this equation can be rewritten as

$$dE = TdS + WdV, \tag{34}$$

where $E = \rho V$, V is the volume of the region inside the apparent horizon and $W = (\rho - p)$. This is nothing, but the form of the so-called unified first law at the apparent horizon of the FRW universe. It is also shown that the form (34) also holds for the Gauss-Bonnet gravity and Lovelock gravity. Further it is found to hold in brane world scenarios [25]. With this we can obtain the entropy expression for apparent horizon in brane world scenarios. For a review, see [26].

It is interesting to note that with the first law (34), starting from some modified Friedmann equation, one is able to get entropy expression of apparent horizon in some quantum corrected gravity. Take the Friedmann equation in loop quantum cosmology as an example. In that case, the modified Friedmann equation takes the form

$$H^2 = \frac{8\pi G}{3}\rho\left(1 - \frac{\rho}{\rho_{\rm crit}}\right), \tag{35}$$

where $\rho_{\rm crit}=\sqrt{3}/(32\pi G^2\gamma^3)$, γ is the Barbero-Immirzi parameter. Clearly when $\rho=\rho_{\rm crit}$, one has a vanishing Hubble parameter. Based on this, it is argued that the big bang singularity can be avoided by bounce in loop quantum cosmology. Starting with (35), we can obtain the entropy expression associated with the apparent horizon as [24]

$$S=\frac{A}{4G}+\frac{3}{4\pi G^2\rho_{\rm crit}}\ln\frac{A}{4G}+\mathcal{O}(1/A)+C_0, \tag{36}$$

where C_0 is an undetermined constant. This way we see that a logarithmic correction term indeed appears in loop quantum gravity.

4.3 Hawking radiation of apparent horizon

In the process to derive the Friedmann equation, we have assumed that there is a Hawking temperature (23) associated with apparent horizon in a FRW universe. In this subsection, we prove this by use of the quantum tunneling approach, which is first employed by Parikh and Wilczek [27] to discuss Hawking radiation for black hole horizon.

In terms of the physical radial coordinate $\tilde{r}=ar$, the 4-dimensional FRW metric can be expressed as

$$ds^2=-\frac{1-\tilde{r}^2/\tilde{r}_A^2}{1-k\tilde{r}^2/a^2}dt^2-\frac{2H\tilde{r}}{1-k\tilde{r}^2/a^2}dtd\tilde{r}+\frac{1}{1-k\tilde{r}^2/a^2}d\tilde{r}^2+\tilde{r}^2d\Omega_2^2. \tag{37}$$

In the spherically symmetric metric (37), one can define a Kodama vector, $K^a=-\epsilon^{ab}\nabla_b\tilde{r}=\sqrt{1-k\tilde{r}^2/a^2}(\partial/\partial t)^a$. The norm of the Kodama vector is $K^2=-(1-\tilde{r}^2/\tilde{r}_A^2)$. One see that the Kodama vector is time-like, null and spacelike, inside the apparent horizon, at the apparent horizon and outside the apparent horizon, respectively. As a result, the Kodama vector can play the role as a Killing vector does in a de Sitter space in static coordinates.

Within WKB approximation, a particle with mass m in the metric (37) satisfies the Hamilton-Jacob equation:

$$g^{\mu\nu}\partial_\mu\mathbf{S}\partial_\nu\mathbf{S}+m^2=0, \tag{38}$$

where $\mathbf{S}$ is its action. In the s-wave approximation, one can define the energy and the radial wave-number of the particle as

$$\omega=-K^a\partial_a\mathbf{S}=-\sqrt{1-k\tilde{r}^2/a^2}\partial_t\mathbf{S},\quad k_{\tilde{r}}=(\partial/\partial\tilde{r})^a\partial_a\mathbf{S}=\partial_{\tilde{r}}\mathbf{S}. \tag{39}$$

And the action can be expressed as

$$\mathbf{S}=-\int\frac{\omega}{\sqrt{1-k\tilde{r}^2/a^2}}dt+\int k_{\tilde{r}}d\tilde{r}. \tag{40}$$

Then the Hamilton-Jacob equation (38) turns to be

$$-\frac{\omega^2}{1-k\tilde{r}^2/a^2}+\frac{2H\tilde{r}\omega}{\sqrt{1-k\tilde{r}^2/a^2}}k_{\tilde{r}}+(1-\frac{\tilde{r}^2}{\tilde{r}_A^2})k_{\tilde{r}}^2+m^2=0, \tag{41}$$

which has the solution as

$$k_{\tilde{r}}=\frac{-H\tilde{r}\pm\sqrt{H^2\tilde{r}^2+(1-\tilde{r}^2/\tilde{r}_A^2)[1-m^2(1-k\tilde{r}^2/a^2)/\omega^2]}}{(1-\tilde{r}^2/\tilde{r}_A^2)\sqrt{1-k\tilde{r}^2/a^2}}\omega, \tag{42}$$

where the plus/minus sign corresponds to an outgoing/incoming mode. Now we consider an incoming mode since the observer is inside the apparent horizon,like the case of particle tunneling for the cosmological event horizon in de Sitter space [28]. It is obvious that the action $\mathbf{S}$ has a pole at the apparent horizon. Through a contour integral, we obtain an imaginary part of the action

$$\begin{aligned}{\rm Im}\mathbf{S}&=-{\rm Im}\int\frac{H\tilde{r}+\sqrt{H^2\tilde{r}^2+(1-\tilde{r}^2/\tilde{r}_A^2)[1-m^2(1-k\tilde{r}^2/a^2)/\omega^2]}}{(1-\tilde{r}^2/\tilde{r}_A^2)\sqrt{1-k\tilde{r}^2/a^2}}\omega d\tilde{r}\\&=\pi\tilde{r}_A\omega.\end{aligned} \tag{43}$$

In the WKB approximation, the emission rate Γ is the square of the tunneling amplitude (here the particle tunnels from outside to inside the apparent horizon)

$$\Gamma \propto \exp(-2\mathrm{Im}\mathbf{S}). \tag{44}$$

Combining (44) with (43), one can see clearly that the emission rate can be cast in a form of thermal spectrum, $\Gamma \sim \exp(-\omega/T)$, with temperature

$$T = \frac{1}{2\pi\tilde{r}_A}. \tag{45}$$

Thus we have finished the proof that an observer inside the apparent horizon will see a thermal spectrum with temperature (45) when particles tunnel from outside the apparent horizon to inside the apparent horizon. This can be explained as Hawking radiation of apparent horizon in the same spirit in the tunneling approach proposed by Parikh and Wilczek that the Hawking radiation of black hole is expressed as a tunneling phenomenon. Furthermore, at this level of approximation, the mass of particle does not enter the emission rate. This is just the remarkable feature of thermal spectrum. In addition, let us note that the null geodesic method also leads to the same temperature [10].

5 Conclusion

A lot of evidence shows there exist deep connections between gravity and thermodynamics. In this paper we just mentioned pieces of them. The intrinsic relation between gravity and thermodynamics is required to further study. If gravity is indeed not a fundamental interaction in Nature, instead it is an induced coarse graining description of some microscopic degrees of freedom of spacetime, it is natural to see the deep connection between gravity and thermodynamics, and even further to see the relation between gravity and hydrodynamics. The latter is a very active issue under studying recently in the framework of AdS/CFT correspondence or in more general sense. Clearly to understand the nature of gravity, obviously it is worthy to deeply investigate the relation between gravity and hydrodynamics.

Acknowledgement

The author thanks the organizers of the JGRG20 for kind invitation to give the talk and for warm hospitality during the conference. It is a great honor to present on such a special occasion to celebrate the 60th birthday of Prof. Takashi Nakamura and Prof. Kei-ichi Maeda. Although I have only a chance to collaborate with Prof. Maeda with a paper "Entropy Function and Universality of Entropy-Area Relation for Small Black Holes" (R.G. Cai, C.M. Chen, K. Maeda, N. Ohta and D.W. Pang, Phys. Rev. D **77**, 064030 (2008)), I meet Prof. Maeda many times on different occasions and spend very pleasant time and enjoy various discussions including physics and others with him.

This work was partly supported by the National Natural Science Foundation of China (No. 10821504, No. 10975168 and No.11035008), and partly by the Ministry of Science and Technology of China under Grant No. 2010CB833004.

References

[1] A. D. Sakharov, Sov. Phys. Dokl. **12**, 1040 (1968) [Dokl. Akad. Nauk Ser. Fiz. **177**, 70 (1967)] [Sov. Phys. Usp. **34**, 394 (1991)] [Gen. Rel. Grav. **32**, 365 (2000)].

[2] E. P. Verlinde, arXiv:1001.0785 [hep-th].

[3] T. Padmanabhan, Mod. Phys. Lett. A **25**, 1129 (2010) [arXiv:0912.3165 [gr-qc]].

[4] T. Jacobson, Phys. Rev. Lett. **75**, 1260 (1995) [arXiv:gr-qc/9504004].

[5] T. Padmanabhan, Class. Quant. Grav. **19**, 5387 (2002) [arXiv:gr-qc/0204019].

[6] R. G. Cai and N. Ohta, Phys. Rev. D **81**, 084061 (2010) [arXiv:0910.2307 [hep-th]].

[7] R. G. Cai and S. P. Kim, JHEP **0502**, 050 (2005) [arXiv:hep-th/0501055].

[8] M. Akbar and R. G. Cai, Phys. Rev. D **75**, 084003 (2007) [arXiv:hep-th/0609128].

[9] R. G. Cai and L. M. Cao, Phys. Rev. D **75**, 064008 (2007) [arXiv:gr-qc/0611071].

[10] R. G. Cai, L. M. Cao and Y. P. Hu, Class. Quant. Grav. **26**, 155018 (2009) [arXiv:0809.1554 [hep-th]].

[11] P. C. W. Davies, J. Phys. A **8**, 609 (1975).

[12] W. G. Unruh, Phys. Rev. D **14**, 870 (1976).

[13] C. Eling, R. Guedens and T. Jacobson, Phys. Rev. Lett. **96**, 121301 (2006) [arXiv:gr-qc/0602001].

[14] C. Eling, JHEP **0811**, 048 (2008) [arXiv:0806.3165 [hep-th]].

[15] R. Brustein and M. Hadad, Phys. Rev. Lett. **103**, 101301 (2009) [Erratum-ibid. **105**, 239902 (2010)] [arXiv:0903.0823 [hep-th]].

[16] M. K. Parikh and S. Sarkar, arXiv:0903.1176 [hep-th].

[17] T. Padmanabhan, arXiv:0903.1254 [hep-th].

[18] A. Paranjape, S. Sarkar and T. Padmanabhan, Phys. Rev. D **74**, 104015 (2006) [arXiv:hep-th/0607240].

[19] M. Akbar and A. A. Siddiqui, Phys. Lett. B **656**, 217 (2007) [arXiv:1009.3749 [gr-qc]].

[20] D. Kothawala, S. Sarkar and T. Padmanabhan, Phys. Lett. B **652**, 338 (2007) [arXiv:gr-qc/0701002].

[21] M. Akbar and R. G. Cai, Phys. Lett. B **648**, 243 (2007) [arXiv:gr-qc/0612089].

[22] S. A. Hayward, S. Mukohyama and M. C. Ashworth, Phys. Lett. A **256**, 347 (1999) [arXiv:gr-qc/9810006]; S. A. Hayward, Class. Quant. Grav. **15**, 3147 (1998) [arXiv:gr-qc/9710089].

[23] M. Akbar and R. G. Cai, Phys. Lett. B **635**, 7 (2006) [arXiv:hep-th/0602156].

[24] R. G. Cai, L. M. Cao and Y. P. Hu, JHEP **0808**, 090 (2008) [arXiv:0807.1232 [hep-th]].

[25] R. G. Cai and L. M. Cao, Nucl. Phys. B **785**, 135 (2007) [arXiv:hep-th/0612144]; A. Sheykhi, B. Wang and R. G. Cai, Nucl. Phys. B **779**, 1 (2007) [arXiv:hep-th/0701198]; A. Sheykhi, B. Wang and R. G. Cai, Phys. Rev. D **76**, 023515 (2007) [arXiv:hep-th/0701261].

[26] R. G. Cai, Prog. Theor. Phys. Suppl. **172**, 100 (2008) [arXiv:0712.2142 [hep-th]].

[27] M. K. Parikh and F. Wilczek, Phys. Rev. Lett. **85**, 5042 (2000) [arXiv:hep-th/9907001].

[28] M. K. Parikh, Phys. Lett. B **546**, 189 (2002) [arXiv:hep-th/0204107]; A. J. M. Medved, Phys. Rev. D **66**, 124009 (2002) [arXiv:hep-th/0207247].

Merging binary black holes in astrophysics

Manuela Campanelli[1], Carlos O. Lousto[2], Hiroyuki Nakano[3] and Yosef Zlochower[4]

Center for Computational Relativity and Gravitation, School of Mathematical Sciences, Rochester Institute of Technology, Rochester, New York 14623, USA

Abstract

Many important advances in the understanding of black-hole physics took place after the numerical relativity breakthroughs of 2005 that allowed fully non-linear dynamical numerical simulations of the inspiral, merger and ringdown of black-hole binaries. We review recent exciting developments in the study of merging black-hole binaries and discuss future directions.

1 Introduction

According to the *no-hair theorem*, equilibrated black holes (BHs) in General Relativity are completely described by three quantities: the mass M, angular momentum J, and electric charge Q of the Kerr-Newman BH solution. However, the electric charge should be rapidly depleted by the surrounding plasma and astrophysical BHs can be completely described by their mass and spin. Although the interiors of BHs may be exotic objects where the spacetime curvature becomes singular, these regions are expected to be covered by a horizon and are thus invisible (*cosmic censorship conjecture*).

Kramer *et al.* [1] tested General Relativity to $\sim 0.05\,\%$ by calculating the inspiral rate of a double pulsar. However, there still are important open questions: Do BHs really exist in nature? Are they really represented by the Kerr solution? Are there naked singularities in the Universe? Is General Relativity the correct theory of gravity in the strong-field regime?

There is strong, but indirect, evidence that BHs exist in the Universe, with a vast range of masses from few tens to $10^9 M_\odot$. The stellar-mass BHs ($3 - 30 M_\odot$) should form from the collapse of massive stars, while intermediate-mass BHs (IMBHs, $10^2 - 10^4 M_\odot$) may assemble in globular clusters. Massive BHs (MBHs, $10^4 - 10^7 M_\odot$) and super-massive BHs (SMBHs, $10^7 - 10^9 M_\odot$) are *seen* in galactic cores by the motion of stars and/or gas surrounding them. These MBHs/SMBHs appear to be connected by the $M - \sigma$ relation [2, 3] to their host galaxies. From the electromagnetic observations, there is evidence that astrophysical BHs may be spinning relatively fast. Also note that since there is evidence that galaxies collide, it is plausible that their central BH's inspiral and collide through the stellar/gas dynamical friction, and the energy loss due to gravitational radiation below sub parsec scale (after *the final parsec problem* [4]).

We note that coalescing black-hole binaries (BHBs) are very loud gravitational-wave sources with the final merger event producing a strong burst at a luminosity of $L_{\rm GW} \sim 10^{22} L_\odot$ which makes them ideal targets for all gravitational-wave detectors (with different detectors sensitive to BHBs in different mass regimes). The gravitational waveforms from these mergers will inform us about the BH masses, (initial and final) spins, source locations, merger rates, and spacetime dynamics. These gravitational waveforms are also essential in matched filtering applications to assist gravitational-wave detection.

There are several past and ongoing ground-based gravitational-wave detector projects, including Initial LIGO (Laser Interferometer Gravitational wave Observatory, $2005 - 2010$) [5], VIRGO [6], Advanced LIGO ($10\times$ increase in sensitivity from Initial LIGO, 2016+), LCGT (Large-scale Cryogenic Gravitational wave Telescope, ~ 2017) [7], Einstein Telescope (ET, $10\times$ increase in sensitivity, 2027+) [8] and other third generation (3G) detectors. We expect that target sources for 3G detectors are not only the inspiral and merger of neutron star-neutron star binaries, neutron star-(stellar-mass) BH binaries, (stellar) BH-BH binaries, but also IMBHs at cosmological distances.

[1]Email address: manuela@astro.rit.edu
[2]Email address: lousto@astro.rit.edu
[3]Email address: nakano@astro.rit.edu
[4]Email address: yosef@astro.rit.edu

There are also plans to go to space with LISA (Laser Interferometer Space Antenna, 2025+) [9] and DECIGO (DECi-hertz Interferometer Gravitational wave Observatory, $\sim$ 2027) [10]. LISA will measure gravitational waves at low frequency ($10^{-4} - 10^{-1}$ Hz), and DECIGO will be the "bridge" between LISA and ground-based detectors with the sensitivity range (30 mHz$-$30 Hz). MBH binary mergers are one of LISA's main target, and we will learn about merger rates, the history of hierarchical galaxy mergers, and the growth of MBHs over time from its detections. Extreme mass-ratio inspirals (EMRIs) which consist of a central MBH and a stellar/intermediate-mass compact object, are also important gravitational-wave sources. From these mergers we can obtain information about the mass and spin of central objects, and as a result, they will provide a census of MBHs in galaxies and the MBHs growth mechanisms (i.e. do these massive objects arise from the merger of comparable mass smaller objects or by accretion onto a large central object).

Merging MBH/IMBH binaries will not only be observed through gravitational-waves, but also likely to be accompanied by electromagnetic counterparts. From correlations between the electromagnetic and gravitational-wave spectra, we will obtain important astrophysical information. This includes an improvement in the sky localization of the source and identification of the host galaxy morphology, tests of galaxy merger scenarios, and detection rates for gravitational-wave sources. Importantly, these observation will provide a novel measurements of the luminosity distance (from the gravitational waveform) to redshift relation out to cosmological distances (*cosmological standard sirens*), as well as provide tests of the fundamental principles of General Relativity (e.g. graviton's speed). They will also improve our understanding of BH accretion physics and magneto-hydrodynamics, circumbinary disks, as well as gravitational kicks. Consequently, these studies are very important to our understanding of the dynamics of our Universe (see Astro2010 Decadal Survey White papers [11, 12]).

2 Simulation of Black-Hole Binaries

In Numerical Relativity, we solve numerically General Relativity's field equations for a dynamical spacetime. The goals are to understand gravity at its strongest manifestation, to inform gravitational-wave detection, and to determine characteristics of compact objects. To simulate black-hole binaries in Numerical Relativity, we need tackle many challenges, 1) several scales required for the physics that arise from the mass of the smallest black hole, black hole's spins, and the wavelength of the emitted gravitational waves in the wave zone, 2) long waveforms matching the early post-Newtonian inspiral phase, 3) large parameter space of black-hole binaries, mass ratio, individual spins, eccentricity, etc.

The first simulation in Numerical Relativity was done by Hahn and Lindquist [13] in 1964 for a head-on collision of two equal-mass black holes in two dimensional (2D) space. In 1990s, there was a big effort by the Binary Black Hole Grand Challenge Alliance (e.g. [14]) to solve the BBH problem. We then saw various development in the evolution system (NOK-BSSN [15–17]), initial data ("puncture" initial data [18]), and gauge conditions ("fixed puncture" evolutions [19]) in black-hole binary simulations. In the Lazarus project (see [20]), the final moments of the merger of black-hole binaries in the three dimensional (3D) simulations has been modeled through the identification of perturbations at late times. In 2004, [21] presented a simulation of black-hole binaries for about one orbital period.

After 40+ years of hard work, the black-hole binary problem in full General Relativity has been solved with the breakthroughs of 2005 by the "generalized harmonic" [22] and the "moving punctures" [23, 24] methods. In these works, the first successful fully non-linear dynamical numerical simulations were done for the inspiral, merger, and ringdown of orbiting black-hole binary systems. In particular, the moving punctures approach, developed independently by the Numerical Relativity groups at UTB (Now RIT) and NASA/GSFC, has become the most widely used method in the field and was successfully applied to evolve generic black-hole binaries. In this approach, a singular term in the spacetime metric is numerically regularized and the black holes move across the computational domain. The generalized harmonic approach has also been successfully applied to accurately evolve generic BHBs for tens of orbits with the use of pseudospectral codes [25, 26].

There have been since 2005 many important advances in the understanding of black-hole physics: studies of the orbital dynamics of spinning black-hole binaries [27–33], calculations of recoil velocities from the merger of unequal mass black-hole binaries [34–36], and the surprising discovery that very large recoils can be acquired by the remnant of the merger of two spinning black holes [30, 37–52], empirical

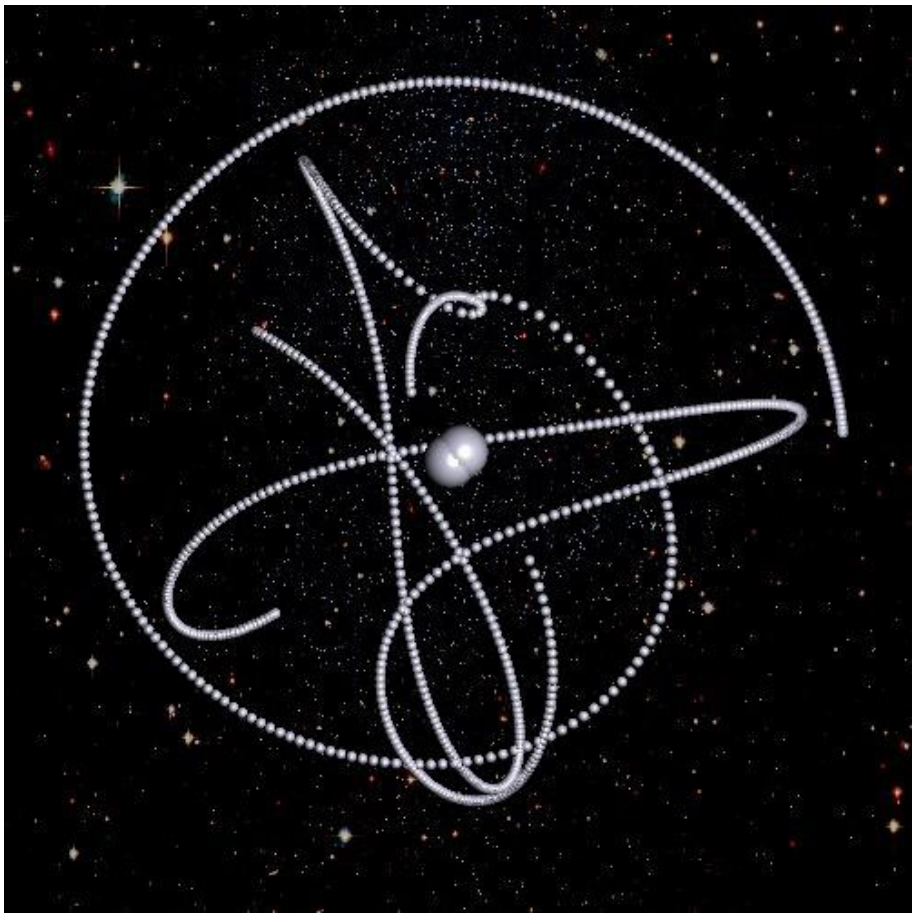

Figure 1: **[Simulation: Manuela Campanelli, Carlos Lousto, Yosef Zlochower, Visualization: Hans-Peter Bischof]** Inspiral and merger of three black holes. The small dots show their trajectories. This movie is downloadable from http://ccrg.rit.edu/movies.

models relating the final mass and spin of the remnant with the spins of the individual black holes [53–60], and comparisons of waveforms and orbital dynamics of black-hole binary inspirals with post-Newtonian predictions [61–68].

3 *LazEv* code results

We can accurately and stably evolve black-hole binaries (and multiplets, e.g. [69–71] and Figure 1) for a vast range of mass-ratios and spins, and compute the gravitational-wave radiation, black-hole remnant and spacetime dynamics. In the following, we summarize some work using the *LazEv* [72] implementation of the moving puncture approach.

3.1 Merger of Spinning Black Holes: Hang-Up Orbits

To understand the dynamics of highly spinning black-hole binaries, we accurately simulated the inspiral orbit of black-hole binaries with two equal mass m and individual spins with equal amplitude $S/m^2 = 0.757$ parallel to the orbital angular momentum in [27]. The simulations start from the orbital frequency $\Omega = 0.05/M_{\rm ADM}$ where $M_{\rm ADM}$ denotes the ADM mass of the system.

We found that the *orbital hang up* effect (spin-orbit coupling) delays the onset of the plunge phase (compared to the non-spinning case) when the spins are aligned with the orbital angular momentum, while in the anti-aligned case the plunge phase is hastened. This effect can be considered as the leading

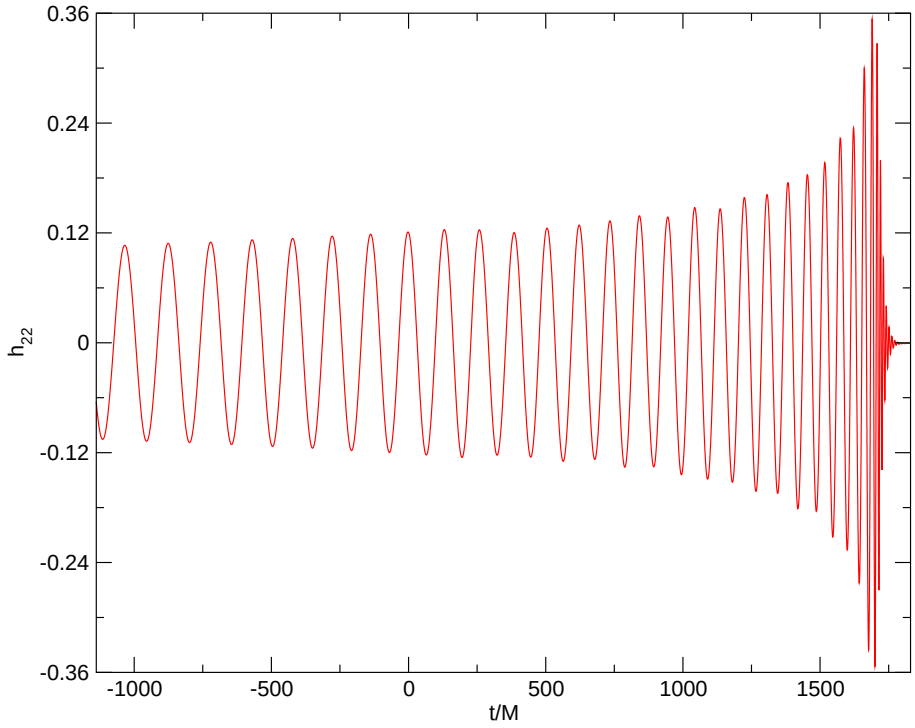

Figure 2: The real part of the $\ell = 2$, $m = 2$ mode of the hybrid gravitational waveform for a precessing black-hole binary [75]. This is created by matching the NR waveform to the waveform derived from the 3.5 post-Newtonian order equations of motion, and the matching starts around $t = 226M_{\rm ADM}$.

order spin-orbit coupling (the 1.5 post-Newtonian order interaction) in the post-Newtonian equations of motion. The total radiated energy $E_{\rm rad}/M_{\rm ADM}$ is $(6.7 \pm 0.2)\,\%$ for the aligned case, while for the anti-aligned case it is only $(2.2 \pm 0.1)\,\%$ (compared to the non-spinning case $(3.5 \pm 0.1)\,\%$). And in all cases the black holes merged to form a single final Kerr black hole with sub-maximal spin (the non-dimensional spin $\chi < 1$), i.e., the *cosmic censorship conjecture* holds in our all cases.

3.2 Merger of Generic, Precessing Black-Holes

In [73], we compared Numerical Relativity and post-Newtonian waveforms of a generic black-hole binary, i.e., a binary with unequal masses, with mass ratio $q = m_1/m_2 = 0.8$ and unequal, non-aligned, precessing spins of magnitude, $S_1/m_1^2 = 0.4$ and $S_2/m_2^2 = 0.6$. The numerical simulation starts with an initial separation of $r \sim 11M_{\rm ADM}$, and has 9 orbits prior to the merger. To obtain the initial data (the positions, momenta, and spins of each black hole), we considered purely post-Newtonian evolutions of a nearly quasi-circular binary with initial orbital separation $r \sim 50M_{\rm ADM}$ by the procedure in [74], extended to spinning particles.

Comparison of numerical simulations with post-Newtonian ones have several benefits aside from the theoretical verification of the post-Newtonian calculations. From a practical point of view, one can directly propose a phenomenological description and thus make predictions in regions of the parameter space still not explored by numerical simulations. From the theoretical point of view, an important application is to have a calibration of the post-Newtonian error (and fitting parameters in the Effective-One-Body approach) in the last stages of the binary merger. Also, combining the post-Newtonian waveform from large separations and smoothly attaching this waveform to the corresponding Numerical Relativity waveform produced by the binary during the late-inspiral, we can provide a hybrid waveform [75]. The waveform in Figure 2 is available for download from http://ccrg.rit.edu/downloads/waveforms[5].

[5] We would like to introduce an interesting website: http://www.black-holes.org/. Some numerically-generated gravitational waveforms are also publicly available from this website.

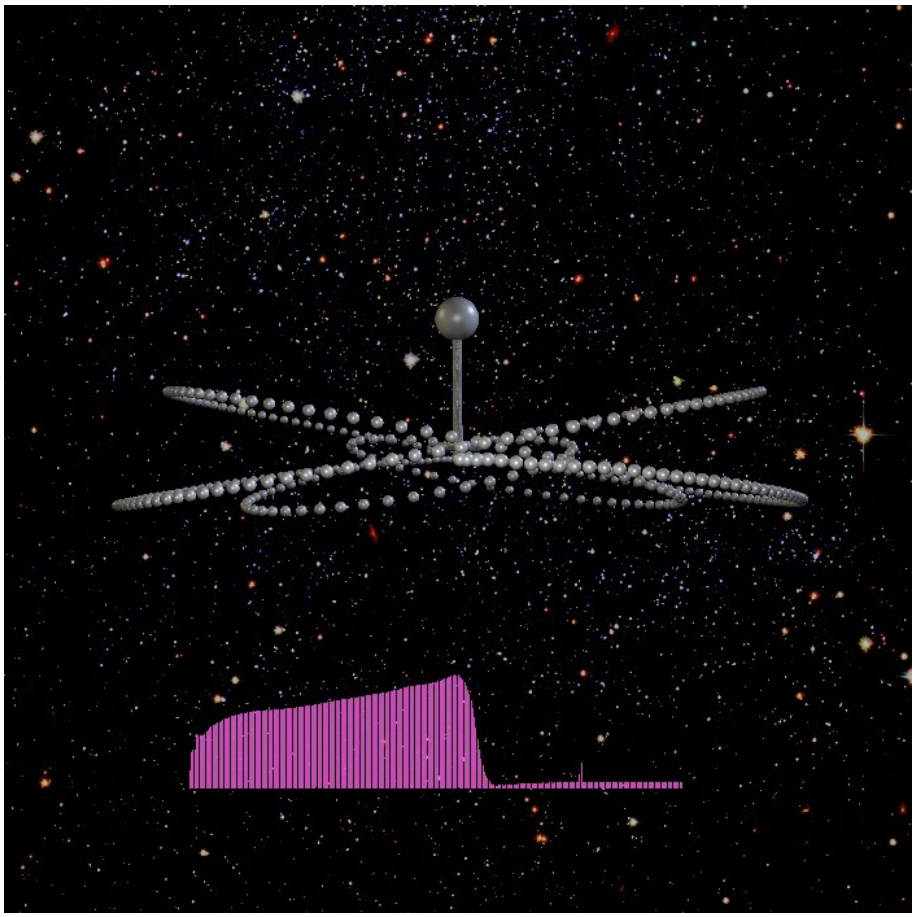

Figure 3: **[Simulation: Manuela Campanelli, Carlos Lousto, Yosef Zlochower, Visualization: Hans-Peter Bischof]** Remnant gravitational recoil of the merger of a black-hole binary. We see the bobbling and merger of two black hole and the resulting merger superkick. The bar at the bottom indicates the speed of the black holes. This movie is downloadable from http://ccrg.rit.edu/movies.

3.3 Gravitational Recoiling Black-Holes

We have modeled the remnant gravitational kick of the merger of black-hole binaries with very large recoil velocities due to gravitational radiation since the discovery [38, 39] (see Figure 3) in the numerical simulations of generic spinning binaries. The spins of the black holes play a crucial role in producing recoils of up to 4000 km/s which allow remnant black holes to escape from major galaxies. The large gravitational recoils found had a significant impact on astrophysics since, the gravitational kicks affect the SMBH retention rates in galaxies, the IMBH retention rates in globular clusters, galactic core dynamics and accretion disk dynamics. Direct observation of them can lead to the first confirmation of a prediction of General Relativity in the highly-dynamical, strong-field regime.

Based on the notion [40, 76] that the leading description of the recoil can be modeled by the post-Newtonian dependence [77, 78], empirical formulae for the final remnant black-hole recoil velocity (also mass and spin) from merging black-hole binaries were obtained in [60] (and references therein). In [79], considering cubic and possible fifth-order corrections [54], we obtained enhanced recoil formulae for the "maximum kick" configurations, and have predicted that the maximum recoil will be 3680 ± 130 km/s. In [80] we confirmed that the recoil formula is accurate to within a few km/s in the comparable mass-ratio regime for the out-of-plane recoil by using a new set of 20 numerical simulations.

In [81], we studied the statistical distributions of the spins of generic black-hole binaries during the 'dry' inspiral (i.e. gravitational radiation driven) and merger, as well as the distributions of the remnant mass, spin, and recoil velocity. In the statistical results, we found a small bias towards counter-alignment

of the vectors $\vec{\Delta}$ and $\vec{S}$ with respect to the orbital angular momentum $\vec{L}$ just prior to merger, where $\vec{S} = \vec{S}_1 + \vec{S}_2$, $\vec{\Delta} = (m_1 + m_2)(\vec{S}_2/m_2 - \vec{S}_1/m_1)$. This effect essentially takes place at close separations and can be studied analytically at low post-Newtonian orders. The anti-alignment effect is associated with the late-time precession of the orbital plane due to gravitational radiation reaction. This effect for dry mergers seems to oppose the alignment mechanism observed in 'wet' mergers [82, 83]. After the initial inspiral regime, we studied the merger of black-hole binaries using full numerical simulations. We found that the merged black holes have a considerable probability (23 %) to reach recoil velocities above 1000 km/s and the distribution is highly peaked along the orbital angular momentum (see Table 1).

Table 1: The probability to obtain large recoil velocities, and large recoil velocities along the line of sight assuming a uniform distribution of mass ratios [81]. Large recoil magnitudes are highly probable, but less observable.

v [km/s] $\geq$	500	1000	2000	2500
Recoil	50.2 %	23.2 %	2.2 %	0.24 %
Observer	22.6 %	6.4 %	0.22 %	0.01 %

3.4 Simulations of Small Mass-Ratio Black-Hole Binaries

According to [84], small mass-ratios black-hole binaries in the range $0.01 < q = m_1/m_2 < 0.1$ are most likely to occur. Current Numerical Relativity simulations have focused on the comparable mass-ratio regime, and black-hole binaries in the very small mass-ratio regime can, in principle, be modeled accurately with the black hole perturbation approach. The small mass-ratio regime is hard to model with Numerical Relativity simulations.

In [85] we introduced a new technique that makes use of the trajectories obtained in the Numerical Relativity simulations and efficient perturbative evolutions to compute waveforms at large radii for the leading and non-leading modes in the black hole perturbation approach, i.e., the Regge-Wheeler-Zerilli (RWZ) formalism [86, 87]. As a proof-of-concept, we computed waveforms for a relatively close binary with mass ratio $q = 1/10$.

In the next paper [88], we reached smaller mass ratios, to the $q = 1/15$ case, and extended the RWZ formalism for the Schwarzschild perturbations by including, perturbatively, a term linear in the spin of the larger black hole (SRWZ formulation). For intermediate mass-ratio black-hole binaries with the mass ratio $q = 1/10$ and $1/15$, we have found good agreement in the Numerical Relativity and SRWZ waveforms which include the late inspiral, plunge, merger and ringdown phases (see Figure 4).

Recently, the merger of a mass ratio 100 : 1 black-hole binary has been simulated in [89] using an optimal choice of the mesh refinement structure around the smaller black hole. Using the techniques presented in this paper, we can simulate even smaller mass-ratios q and initially spinning black holes. It is also important to choose quasi-circular orbital parameters (see [90]) and to evolve initial data with lower spurious radiation content to obtain realistic true inspiral wave information [91, 92].

4 Community-Wide Collaborations

The *NINJA* (Numerical INJection Analysis, https://www.ninja-project.org/doku.php?id=ninja:home) is a collaborative effort between members of the numerical relativity and gravitational-wave data analysis communities. In *NINJA-1* [93, 94] with ten numerical relativity groups providing gravitational waveforms and data analysis contributions from nine different groups, short Numerical Relativity waveforms from the merger of black-hole binaries without any hybrids, i.e., attaching post-Newtonian inspiral waveforms, have been used for the injections. The data set did not include the type of non-Gaussian transients seen in real gravitational-wave detector data. In *NINJA-2* with more groups, we are now attempting to use various (including different mass-ratios and spins) hybrid waveforms for LIGO and VIRGO data analysis.

To develop accurate analytical gravitational-wave template banks of black-hole binaries for the data analysis, a larger region of the parameter space including spin precessing systems, has been simulated

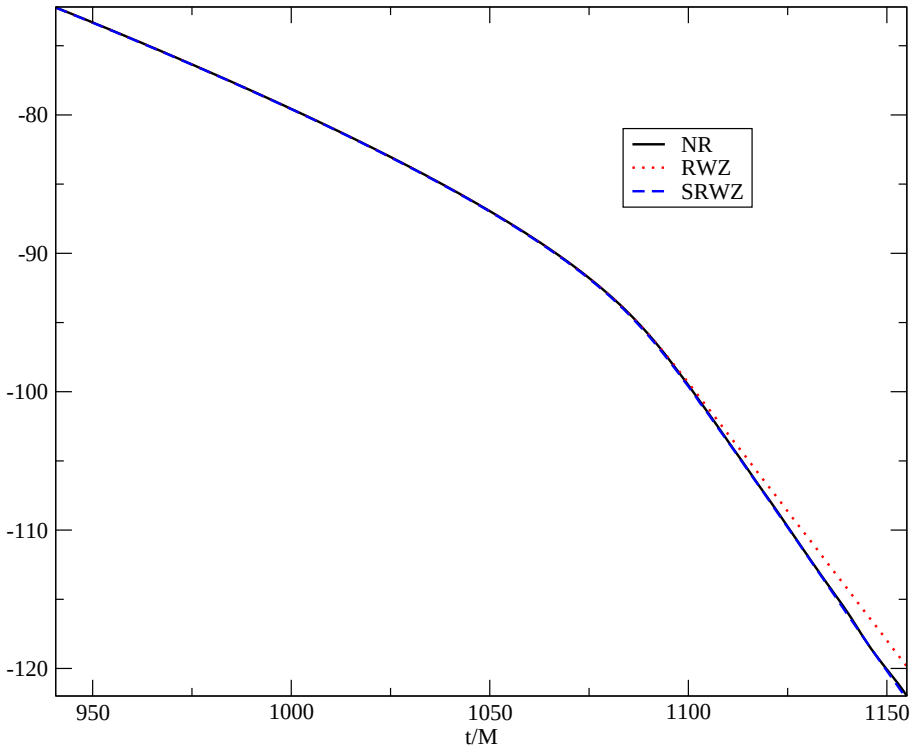

Figure 4: The phase evolution of the ($\ell = 2$, $m = 2$) wave for the $q = 1/10$ case [88]. The (black) solid, (red) dotted, and (blue) dashed curves show the Numerical Relativity, RWZ (spin-off), and SRWZ (spin-on) calculations, respectively. Note that although the initial part of the three curves show almost the same evolution, we can see differences after the merger.

on the TeraGrid machine Kraken, and the precise full numerical gravitational waveforms have been computed in the *NRAR* collaboration (Numerical-Relativity and Analytical-Relativity, https://www.ninja-project.org/doku.php?id=nrar:home).

The *Einstein Toolkit* (http://einsteintoolkit.org/) is a state of the art, open, community developed software infrastructure for relativistic astrophysics. The targets are black holes, neutron stars, core-collapse supernovae, etc. This type of a collaborative work will be needed in the future directions discussed next.

5 Future Directions

As mentioned in the Introduction, coincident detections of gravitational-wave and electromagnetic signatures from merging black-hole binaries give us varied astrophysical information. Observable consequences of large gravitational recoils include effects of a SMBH passing through an accretion disk. The disk around the kicked black hole will have broader spectrum and be shifted with respect to the host disk. The sudden loss of mass of the central black hole will perturb the disk, MBHs will be displaced or wandering from the core of the host structure, and the kicks lead the reorientation of jets, e.g. X-shaped radio-morphologies.

Studies of electromagnetic counterparts of merging black-hole binaries should include the gaseous environment. The scale problem, from 10^5 pc to 10^{-5} pcs, represents a huge computational challenge. One should split the problem into stages, the capture, pre-merger, merger and post-merger (e.g. kicked) stages. Simulations of the merger require full General Relativity-magneto-hydrodynamics (GR-MHD) and radiation physics modeling.

Regarding the gaseous environment close to the merging black-hole binaries, (at scales < 0.01 pc) there are some initial explorations about the electromagnetic fields [95] and radiatively inefficient hot gas clouds [96] around them. One may also consider alternative models, e.g. thin circumbinary disk. The

most important point is to create reliable GR-MHD codes which properly account for accretion rates, electromagnetic fields, radiation transport, and the required numerical resolution. To complete the above studies we will need large collaborative efforts.

6 Conclusions

Exciting new astrophysical phenomena have been found thanks to Numerical Relativity's black-hole binary simulations. We can accurately and stably evolve almost arbitrary black-hole binaries. The gravitational waveforms are accurately produced for use in gravitational wave data analysis for ground and space-based detectors. The results can be compared with the post-Newtonian (including Effective-One-Body) and black hole perturbation theories, and be used to calibrate them. The remnant mass-loss reaches up to 10% of the total mass of the system, and depending on the spins magnitude and orientation we can observe the gravitational superkicks.

On the other hand, we still have some open challenges for the numerical simulations of black-hole binaries, 1) extreme black-hole binaries, nearly maximal spins and extreme mass-ratios are still very hard to accurately simulate, 2) long, accurate simulations and multiple physical scales require more efficient evolution codes, and 3) better initial data are needed especially for highly spinning black-hole binaries and for the inclusion of matter.

The possibility of observing electromagnetic counterparts from binary black-hole mergers is a very exciting topic. This study requires 1) careful pre-merger modeling efforts, 2) a comprehensive approach and reliable GR-MHD codes, and 3) open source codes for general relativistic astrophysics, such as (http://einsteintoolkit.org/).

Astrophysicists can now test General Relativity in the highly-nonlinear regime. The simulations of black-hole binaries can soon be used to look for gravitational waves reaching earth opening thus up a brand new window onto the Universe.

Acknowledgments

We gratefully acknowledge the NSF for financial support from Grants No. PHY-0722315, No. PHY-0653303, No. PHY-0714388, No. PHY-0722703, No. DMS-0820923, No. PHY-0929114, No. PHY-0969855, No. PHY-0903782, No. CDI-1028087; and NASA for financial support from NASA Grants No. 07-ATFP07-0158 and No. HST-AR-11763.

Finally, it is our pleasure to celebrate Takashi Nakamura and Kei-ichi Maeda's sixtieth birthday.

References

[1] M. Kramer et al. (2005), astro-ph/0503386.

[2] L. Ferrarese and D. Merritt, Astrophys. J. **539**, L9 (2000), astro-ph/0006053.

[3] K. Gebhardt et al., Astrophys. J. **539**, L13 (2000), astro-ph/0006289.

[4] M. Milosavljevic and D. Merritt, AIP Conf. Proc. **686**, 201 (2003), astro-ph/0212270.

[5] B. Abbott et al. (LIGO Scientific), Rept. Prog. Phys. **72**, 076901 (2009), 0711.3041.

[6] F. Acernese et al., Class. Quantum Grav. **25**, 114045 (2008).

[7] K. Kuroda et al. (LCGT Collaboration), Class. Quantum Grav. **27**, 084004 (2010).

[8] M. Punturo et al., Class. Quantum Grav. **27**, 194002 (2010).

[9] K. Danzmann et al., Max-Planck-Inistitut für Quantenoptik, Report MPQ **233** (1998).

[10] M. Ando et al., Class. Quantum Grav. **27**, 084010 (2010).

[11] E. S. Phinney (2009), 0903.0098.

[12] J. S. Bloom et al. (2009), 0902.1527.

[13] S. G. Hahn and R. W. Lindquist, Ann. Phys. **29**, 304 (1964).

[14] G. B. Cook et al., Phys. Rev. Lett **80**, 2512 (1998).

[15] T. Nakamura, K. Oohara, and Y. Kojima, Prog. Theor. Phys. Suppl. **90**, 1 (1987).

[16] M. Shibata and T. Nakamura, Phys. Rev. D **52**, 5428 (1995).

[17] T. W. Baumgarte and S. L. Shapiro, Phys. Rev. D **59**, 024007 (1999), gr-qc/9810065.

[18] S. Brandt and B. Brügmann, Phys. Rev. Lett. **78**, 3606 (1997), gr-qc/9703066.

[19] M. Alcubierre, W. Benger, B. Brügmann, G. Lanfermann, L. Nerger, E. Seidel, and R. Takahashi, Phys. Rev. Lett. **87**, 271103 (2001), gr-qc/0012079.

[20] M. Campanelli, Class. Quantum Grav. **22**, S387 (2005), astro-ph/0411744.

[21] B. Brügmann, W. Tichy, and N. Jansen, Phys. Rev. Lett. **92**, 211101 (2004), gr-qc/0312112.

[22] F. Pretorius, Phys. Rev. Lett. **95**, 121101 (2005), gr-qc/0507014.

[23] M. Campanelli, C. O. Lousto, P. Marronetti, and Y. Zlochower, Phys. Rev. Lett. **96**, 111101 (2006), gr-qc/0511048.

[24] J. G. Baker, J. Centrella, D.-I. Choi, M. Koppitz, and J. van Meter, Phys. Rev. Lett. **96**, 111102 (2006), gr-qc/0511103.

[25] M. A. Scheel et al., Phys. Rev. **D79**, 024003 (2009), 0810.1767.

[26] B. Szilagyi, L. Lindblom, and M. A. Scheel, Phys. Rev. **D80**, 124010 (2009), 0909.3557.

[27] M. Campanelli, C. O. Lousto, and Y. Zlochower, Phys. Rev. D **74**, 041501(R) (2006), gr-qc/0604012.

[28] M. Campanelli, C. O. Lousto, and Y. Zlochower, Phys. Rev. D **74**, 084023 (2006), astro-ph/0608275.

[29] M. Campanelli, C. O. Lousto, Y. Zlochower, B. Krishnan, and D. Merritt, Phys. Rev. **D75**, 064030 (2007), gr-qc/0612076.

[30] F. Herrmann, I. Hinder, D. M. Shoemaker, P. Laguna, and R. A. Matzner, Phys. Rev. **D76**, 084032 (2007), 0706.2541.

[31] P. Marronetti et al., Class. Quantum Grav. **24**, S43 (2007), gr-qc/0701123.

[32] P. Marronetti, W. Tichy, B. Brugmann, J. Gonzalez, and U. Sperhake, Phys. Rev. **D77**, 064010 (2008), 0709.2160.

[33] E. Berti et al., Phys. Rev. **D76**, 064034 (2007), gr-qc/0703053.

[34] F. Herrmann, D. Shoemaker, and P. Laguna, AIP Conf. **873**, 89 (2006), gr-qc/0601026.

[35] J. G. Baker et al., Astrophys. J. **653**, L93 (2006), astro-ph/0603204.

[36] J. A. González, U. Sperhake, B. Brugmann, M. Hannam, and S. Husa, Phys. Rev. Lett. **98**, 091101 (2007), gr-qc/0610154.

[37] F. Herrmann, I. Hinder, D. Shoemaker, P. Laguna, and R. A. Matzner, Astrophys. J. **661**, 430 (2007), gr-qc/0701143.

[38] M. Campanelli, C. O. Lousto, Y. Zlochower, and D. Merritt, Astrophys. J. **659**, L5 (2007), gr-qc/0701164.

[39] M. Campanelli, C. O. Lousto, Y. Zlochower, and D. Merritt, Phys. Rev. Lett. **98**, 231102 (2007), gr-qc/0702133.

[40] C. O. Lousto and Y. Zlochower, Phys. Rev. D **79**, 064018 (2009), 0805.0159.

[41] D. Pollney et al., Phys. Rev. **D76**, 124002 (2007), 0707.2559.

[42] J. A. González, M. D. Hannam, U. Sperhake, B. Brugmann, and S. Husa, Phys. Rev. Lett. **98**, 231101 (2007), gr-qc/0702052.

[43] B. Brugmann, J. A. Gonzalez, M. Hannam, S. Husa, and U. Sperhake, Phys. Rev. **D77**, 124047 (2008), 0707.0135.

[44] D.-I. Choi et al., Phys. Rev. **D76**, 104026 (2007), gr-qc/0702016.

[45] J. G. Baker et al., Astrophys. J. **668**, 1140 (2007), astro-ph/0702390.

[46] J. D. Schnittman et al., Phys. Rev. **D77**, 044031 (2008), 0707.0301.

[47] J. G. Baker et al., Astrophys. J. **682**, L29 (2008), 0802.0416.

[48] J. Healy et al., Phys. Rev. Lett. **102**, 041101 (2009), 0807.3292.

[49] F. Herrmann, I. Hinder, D. Shoemaker, and P. Laguna, Class. Quantum Grav. **24**, S33 (2007).

[50] W. Tichy and P. Marronetti, Phys. Rev. **D76**, 061502 (2007), gr-qc/0703075.

[51] M. Koppitz et al., Phys. Rev. Lett. **99**, 041102 (2007), gr-qc/0701163.

[52] S. H. Miller and R. A. Matzner, Gen. Rel. Grav. **41**, 525 (2009), 0807.3028.

[53] L. Boyle, M. Kesden, and S. Nissanke, Phys. Rev. Lett. **100**, 151101 (2008), 0709.0299.

[54] L. Boyle and M. Kesden, Phys. Rev. **D78**, 024017 (2008), 0712.2819.

[55] A. Buonanno, L. E. Kidder, and L. Lehner, Phys. Rev. **D77**, 026004 (2008), 0709.3839.

[56] W. Tichy and P. Marronetti, Phys. Rev. **D78**, 081501 (2008), 0807.2985.

[57] M. Kesden, Phys. Rev. **D78**, 084030 (2008), 0807.3043.

[58] E. Barausse and L. Rezzolla, Astrophys. J. Lett. **704**, L40 (2009), 0904.2577.

[59] L. Rezzolla, Class. Quantum Grav. **26**, 094023 (2009), 0812.2325.

[60] C. O. Lousto, M. Campanelli, Y. Zlochower, and H. Nakano, Class. Quantum Grav. **27**, 114006 (2010), 0904.3541.

[61] A. Buonanno, G. B. Cook, and F. Pretorius, Phys. Rev. **D75**, 124018 (2007), gr-qc/0610122.

[62] J. G. Baker, J. R. van Meter, S. T. McWilliams, J. Centrella, and B. J. Kelly, Phys. Rev. Lett. **99**, 181101 (2007), gr-qc/0612024.

[63] Y. Pan et al., Phys. Rev. **D77**, 024014 (2008), 0704.1964.

[64] A. Buonanno et al., Phys. Rev. **D76**, 104049 (2007), 0706.3732.

[65] M. Hannam, S. Husa, U. Sperhake, B. Brugmann, and J. A. Gonzalez, Phys. Rev. **D77**, 044020 (2008), 0706.1305.

[66] M. Hannam, S. Husa, B. Bruegmann, and A. Gopakumar, Phys. Rev. **D78**, 104007 (2008), 0712.3787.

[67] A. Gopakumar, M. Hannam, S. Husa, and B. Bruegmann, Phys. Rev. **D78**, 064026 (2008), 0712.3737.

[68] I. Hinder, F. Herrmann, P. Laguna, and D. Shoemaker, Phys. Rev. **D82**, 024033 (2010), 0806.1037.

[69] C. O. Lousto and Y. Zlochower, Phys. Rev. **D77**, 024034 (2008), 0711.1165.

[70] G. Jaramillo and C. O. Lousto (2010), 1008.2001.

[71] M. Ponce, C. Lousto, and Y. Zlochower (2010), 1008.2761.

[72] Y. Zlochower, J. G. Baker, M. Campanelli, and C. O. Lousto, Phys. Rev. D **72**, 024021 (2005), gr-qc/0505055.

[73] M. Campanelli, C. O. Lousto, H. Nakano, and Y. Zlochower, Phys. Rev. D **79**, 084010 (2009), 0808.0713.

[74] S. Husa, M. Hannam, J. A. Gonzalez, U. Sperhake, and B. Brugmann, Phys. Rev. **D77**, 044037 (2008), 0706.0904.

[75] M. Campanelli et al., Class. Quantum Grav. **27**, 084034 (2010), 1001.3834.

[76] C. O. Lousto and Y. Zlochower, Phys. Rev. **D77**, 044028 (2008), 0708.4048.

[77] L. E. Kidder, Phys. Rev. D **52**, 821 (1995), gr-qc/9506022.

[78] E. Racine, A. Buonanno, and L. E. Kidder, Phys. Rev. **D80**, 044010 (2009), 0812.4413.

[79] C. O. Lousto and Y. Zlochower, Phys. Rev. **D83**, 024003 (2011), 1011.0593.

[80] Y. Zlochower, M. Campanelli, and C. O. Lousto (2010), 1011.2210.

[81] C. O. Lousto, H. Nakano, Y. Zlochower, and M. Campanelli, Phys. Rev. **D81**, 084023 (2010), 0910.3197.

[82] T. Bogdanovic, C. S. Reynolds, and M. C. Miller, Astrophys. J. **661**, L147 (2007), astro-ph/0703054.

[83] A. Perego, M. Dotti, M. Colpi, and M. Volonteri, Mon. Not. R. Astron. Soc. **399**, 2249 (2009), 0907.3742.

[84] M. Volonteri and P. Madau, Astrophys. J. **687**, L57 (2008), 0809.4007.

[85] C. O. Lousto, H. Nakano, Y. Zlochower, and M. Campanelli, Phys. Rev. Lett. **104**, 211101 (2010), 1001.2316.

[86] T. Regge and J. A. Wheeler, Phys. Rev. **108**, 1063 (1957).

[87] F. J. Zerilli, Phys. Rev. D **2**, 2141 (1970).

[88] C. O. Lousto, H. Nakano, Y. Zlochower, and M. Campanelli, Phys. Rev. **D82**, 104057 (2010), 1008.4360.

[89] C. O. Lousto and Y. Zlochower Phys. Rev. Lett. **106**, 041101 (2011), 1009.0292.

[90] H. P. Pfeiffer et al., Class. Quantum Grav. **24**, S59 (2007), gr-qc/0702106.

[91] B. J. Kelly, W. Tichy, Y. Zlochower, M. Campanelli, and B. F. Whiting, Class. Quantum Grav. **27**, 114005 (2010), 0912.5311.

[92] B. C. Mundim, B. J. Kelly, Y. Zlochower, H. Nakano, and M. Campanelli (2010), 1012.0886.

[93] B. Aylott et al., Class. Quantum Grav. **26**, 165008 (2009), 0901.4399.

[94] B. Aylott et al., Class. Quantum Grav. **26**, 114008 (2009), 0905.4227.

[95] C. Palenzuela, L. Lehner, and S. L. Liebling, Science **329**, 927 (2010), 1005.1067.

[96] T. Bode, R. Haas, T. Bogdanovic, P. Laguna, and D. Shoemaker, Astrophys. J. **715**, 1117 (2010), 0912.0087.

Classical dynamics of strings and branes, with application to vortons

Brandon Carter

LUTH (CNRS), Observatoire Paris - Meudon

Abstract

These notes offer an introductory overview of the essentials of classical brane dynamics in a space-time background of arbitrary dimension, using a systematic geometric treatment emphasising the role of the second fundamental tensor and its trace, the curvature vector K^μ . This approach is applied to the problem of stability of vorton equilibrium states of cosmic string loops in an ordinary 4-dimensional background.

1 Worldsheet Curvature Analysis

1.1 The first fundamental tensor

Earlier treatments of the classical dynamics of strings and higher p-branes were inclined to rely too much on gauge dependent auxiliary structures such as internal coordinates σ^i on the d=p+1 dimensional worldsheet, which can be useful for various computational purposes but tend to obscure what is essential. The present notes offer an introductory overview of a more geometrically elegant approach [1] that is particularly useful for work in a background spacetime whose dimension n is 5 or more [2–4], but that I originally developed for the purpose of studying cosmic string loops and particularly the question of the stability of their vorton equilibrium states [5] in a background of dimension n=4. Following the strategy originally advocated by Stachel[6], the guiding principle of this approach [1] is to work as far as possible with a single kind of tensor index, which must of course be the one that is most fundamental, namely that of the n-dimensional coordinates, x^μ , on the background spacetime with metric $g_{\mu\nu}$.

The idea is to avoid unnecessary use of the internal coordinate indices, which are lowered and raised by contraction with the induced metric $\eta_{ij} = g_{\mu\nu}x^\mu{}_{,i}x^\nu{}_{,j}$ (using the notation $x^\mu{}_{,i} = \partial x^\mu/\partial\sigma^i$) on the worldsheet, and with its contravariant inverse η^{ij} . This is achieved by working instead with the (first) fundamental tensor as given by projection back onto the background according to the prescription

$$\eta^{\mu\nu} = \eta^{ij}x^\mu{}_{,i}x^\nu{}_{,j}\,, \tag{1}$$

(in the manner that is applicable to the contravariant version of any worldsheet tensor) so that $\eta^\mu{}_\nu$ will be the tangential projector. The complementary orthogonal projector is $\perp^\mu{}_\nu = g^\mu{}_\nu - \eta^\mu{}_\nu$. As well as having the properties $\eta^\mu{}_\rho\eta^\rho{}_\nu = \eta^\mu{}_\nu$, and $\perp^\mu{}_\rho\perp^\rho{}_\nu = \perp^\mu{}_\nu$ these projection tensors will evidently be related by $\eta^\mu{}_\rho\perp^\rho{}_\nu = 0 = \perp^\mu{}_\rho\eta^\rho{}_\nu$.

1.2 The second fundamental tensor

In so far as we are concerned with tensor fields such as the frame vectors whose support is confined to the d-dimensional world sheet, the effect of Riemannian covariant differentation ∇_μ along an arbitrary directions on the background spacetime will not be well defined, only the corresponding tangentially projected differentiation operation

$$\overline{\nabla}_\mu \stackrel{\text{def}}{=} \eta^\nu{}_\mu\nabla_\nu\,, \tag{2}$$

being meaningful for them, as for instance in the case of a scalar field φ for which the tangentially projected gradient is given in terms of internal coordinate differentiation simply by $\overline{\nabla}^\mu\varphi = \eta^{ij}x^\mu{}_{,i}\,\varphi_{,j}$. The action of this operator on the first fundamental tensor $\eta^{\mu\nu}$ itself gives the entity

$$K_{\mu\nu}{}^{\rho} \stackrel{\text{def}}{=} \eta^{\sigma}{}_{\nu}\overline{\nabla}_\mu\eta^{\rho}{}_{\sigma} \tag{3}$$

that we refer to [1] as the *second fundamental tensor*.

As this second fundamental tensor, $K_{\mu\nu}{}^{\rho}$ will play an important role in the work that follows, it is worth lingering [1] over its essential properties. The expression (3) could of course be meaningfully applied not only to the fundamental projection tensor of a d-surface, but also to any (smooth) field of rank-d projection operators $\eta^{\mu}{}_{\nu}$ as specified by a field of arbitrarily orientated d-surface elements. What distinguishes the integrable case – in which the elements mesh together to form a well defined d-surface through the point under consideration – is the *Weingarten identity*, whereby that the tensor defined by (3) will have the symmetry property

$$K_{[\mu\nu]}{}^{\rho} = 0\,, \tag{4}$$

an integrability condition that is derivable [1] as a version of the well known Frobenius theorem.

As well as being symmetric, the tensor $K_{\mu\nu}{}^{\rho}$ is obviously tangential on the first two indices and also orthogonal on the last: $\perp^{\sigma}_{\mu}K_{\sigma\nu}{}^{\rho} = K_{\mu\nu}{}^{\sigma}\eta_{\sigma}{}^{\rho} = 0$. It fully determines the tangential derivatives of the first fundamental tensor $\eta^{\mu}{}_{\nu}$ by the formula

$$\overline{\nabla}_\mu\eta_{\nu\rho} = 2K_{\mu(\nu\rho)}\,, \tag{5}$$

(using round brackets to denote symmetrisation) and it is characterisable by the condition that the orthogonal projection of the acceleration $\dot{\boldsymbol{u}}^\mu = \boldsymbol{u}^\nu\nabla_\nu\boldsymbol{u}^\mu$ of any tangential unit vector field $\boldsymbol{u}^\mu$ (with $\boldsymbol{u}^\mu\boldsymbol{u}_\mu = -1$) will be given by $\boldsymbol{u}^\mu\boldsymbol{u}^\nu K_{\mu\nu}{}^{\rho} = \perp^{\rho}_{\mu}\dot{\boldsymbol{u}}^\mu$.

1.3 Extrinsic curvature vector and Conformation tensor

It is very practical for a great many purposes to introduce the *extrinsic curvature vector* K^μ , defined [1] as the trace of the second fundamental tensor,

$$K^\mu \stackrel{\text{def}}{=} K^{\nu}{}_{\nu}{}^{\mu} = \overline{\nabla}_\nu\eta^{\mu\nu}\,, \tag{6}$$

which is automatically orthogonal to the worldsheet, $\eta^{\mu}{}_{\nu}K^\nu = 0$. It is useful for many specific purposes to work this out in terms of the intrinsic metric η_{ij} and its determinant $|\eta|$. For the tangentially projected gradient of a scalar field φ on the worldsheet, it suffices to use the simple expression $\overline{\nabla}^\mu\varphi = \eta^{ij}x^\mu{}_{,i}\varphi_{,j}$. However for a tensorial field (unless one is using Minkowski coordinates in a flat spacetime) the gradient will also have contributions involving the background Riemann Christoffel connection $\Gamma_{\mu}{}^{\nu}{}_{\rho} = g^{\nu\sigma}\left(g_{\sigma(\mu,\rho)} - \frac{1}{2}g_{\mu\rho,\sigma}\right)$. The curvature vector is thus obtained in explicit detail as

$$K^\nu = \frac{1}{\sqrt{\|\eta\|}}\left(\sqrt{\|\eta\|}\eta^{ij}x^\nu{}_{,i}\right)_{,j} + \eta^{ij}x^\mu{}_{,i}x^\rho{}_{,j}\Gamma_{\mu}{}^{\nu}{}_{\rho}\,. \tag{7}$$

This expression is useful for specific computational purposes, but much of the literature on cosmic string dynamics has been made unnecessarily heavy by a tradition of working all the time with long strings of non tensorial terms such as those on the right of (7) rather than exploiting more succinct tensorial expressions, such as $K^\nu = \overline{\nabla}_\mu\eta^{\mu\nu}$.

As an alternative to the universally applicable tensorial approach advocated here, there is of course another more commonly used method of achieving succinctness in particular circumstances, which is to sacrifice gauge covariance by using specialised kinds of coordinate system. In particular, for the case of a string, i.e. for a 2-dimensional worldsheet, it is standard practise to use conformal coordinates σ^0 and σ^1 so

that the corresponding tangent vectors $\dot{x}^\mu = x^\mu_{,0}$ and $x'^\mu = x^\mu_{,1}$ satisfy the restrictions $\dot{x}^\mu x'_\mu = 0$, $\dot{x}^\mu \dot{x}_\mu + x'^\mu x'_\mu = 0$, which implies $\sqrt{\|\eta\|} = x'^\mu x'_\mu = -\dot{x}^\mu \dot{x}_\mu$, so that (7) simply gives $\sqrt{\|\eta\|}\, K^\nu = x''^\nu - \ddot{x}^\nu + (x'^\mu x'^\rho - \dot{x}^\mu \dot{x}^\rho)\Gamma_{\mu\ \rho}^{\ \nu}$.

The physical specification of the extrinsic curvature vector (6) for a timelike d-surface in a dynamic theory provides what can be taken as the equations of extrinsic motion of the d-surface [1], the simplest possibility being the "harmonic" condition $K^\mu = 0$ that is obtained (as shown below) from a surface measure variational principle such as that of the Dirac membrane model [7], or of the Goto-Nambu string model [8] whose dynamic equations in a flat background are therefore expressible with respect to a standard conformal gauge in the familiar form $x''^\mu - \ddot{x}^\mu = 0$,

There is a certain analogy between the Einstein vacuum equations, which impose the vanishing of the trace $\mathcal{R}_{\mu\nu}$ of the background spacetime curvature $\mathcal{R}_{\lambda\mu}{}^\rho{}_\nu$, and the Dirac-Gotu-Nambu equations, which impose the vanishing of the trace K^ν of the second fundamental tensor $K_{\lambda\mu}{}^\nu$, Moreover, just as it is useful to separate out the Weyl tensor [9], i.e. the trace free part of the Ricci background curvature which is the only part that remains when the Einstein vacuum equations are satisfied, so also analogously, it is useful to separate out the the trace free part of the second fundamental tensor, namely the extrinsic conformation tensor [1], which is the only part that remains when equations of motion of the Dirac - Goto - Nambu type are satisfied.

Explicitly, the trace free *extrinsic conformation* tensor $C_{\mu\nu}{}^\rho$ of a d-dimensional imbedding is defined [1] in terms of its first and second fundamental tensors as

$$C_{\mu\nu}{}^\rho \stackrel{\text{def}}{=} K_{\mu\nu}{}^\rho - \frac{1}{\mathrm{d}}\eta_{\mu\nu}K^\rho\ , \qquad C^\nu{}_\nu{}^\mu = 0\ . \tag{8}$$

Like the Weyl tensor $\mathcal{W}_{\lambda\mu}{}^\rho{}_\nu$ of the background metric (whose definition is given implicitly by (13) below) this conformation tensor has the noteworthy property of being invariant with respect to conformal modifications of the background metric: $g_{\mu\nu} \mapsto \mathrm{e}^{2\alpha} g_{\mu\nu}$ $\Rightarrow$

$$K_{\mu\nu}{}^\rho \mapsto K_{\mu\nu}{}^\rho + \eta_{\mu\nu}\perp^{\rho\sigma}\nabla_\sigma\alpha\,, \qquad C_{\mu\nu}{}^\rho \mapsto C_{\mu\nu}{}^\rho\,. \tag{9}$$

This is useful [10] for work like that of Vilenkin [11] in a Robertson-Walker cosmological background, which can be obtained from a flat spacetime by a conformal transformation for which e^α is a time dependent Hubble expansion factor.

1.4 Codazzi, Gauss, and Schouten identities

As the higher order analogue of (3) we can go on to introduce the *third* fundamental tensor[1] as

$$\Xi_{\lambda\mu\nu}{}^\rho \stackrel{\text{def}}{=} \eta^{\ \sigma}_{\mu}\eta^{\ \tau}_{\nu}\perp^\rho_\alpha \overline{\nabla}_\lambda K_{\sigma\tau}{}^\alpha\,, \tag{10}$$

which by construction is obviously symmetric between the second and third indices and tangential on all the first three indices. In a spacetime background that is flat (or of constant curvature as is the case for the DeSitter universe model) this third fundamental tensor is fully symmetric over all the first three indices by what is interpretable as the *generalised Codazzi identity*.

In a background with arbitrary Riemann curvature $\mathcal{R}_{\lambda\mu}{}^\rho{}_\sigma$ the *generalised Codazzi identity* is expressible [1] as

$$\Xi_{\lambda\mu\nu}{}^\rho = \Xi_{(\lambda\mu\nu)}{}^\rho + \tfrac{2}{3}\eta^{\ \sigma}_{\lambda}\eta^{\ \tau}_{(\mu}\eta^{\ \alpha}_{\nu)}\mathcal{R}_{\sigma\tau}{}^\beta{}_\alpha\perp^\rho_\beta \tag{11}$$

A script symbol $\mathcal{R}$ is used here in order to distinguish the (n- dimensional) background Riemann curvature tensor from the intrinsic curvature tensor of the (d- dimensional) worldsheet to which the ordinary symbol R has already allocated. For many of the applications that will follow it will be sufficient just to treat the background spacetime as flat, i.e. to take $\mathcal{R}_{\sigma\tau}{}^\beta{}_\alpha = 0$.

For $n > 2$, the background curvature tensor will be decomposible (if present) in terms of the background Ricci tensor and its scalar trace,

$$\mathcal{R}_{\mu\nu} = \mathcal{R}_{\rho\mu}{}^{\rho}{}_{\nu} \,, \qquad \mathcal{R} = \mathcal{R}^{\nu}{}_{\nu} \,, \tag{12}$$

and of its trace free conformally invariant Weyl part $\mathcal{W}_{\mu\nu}{}^{\rho}{}_{\sigma}$ – which can be non zero only for $n \geq 4$ – in the well known [9] form

$$\mathcal{R}_{\mu\nu}{}^{\rho\sigma} = \mathcal{W}_{\mu\nu}{}^{\rho\sigma} + \tfrac{4}{n-2} g^{[\rho}{}_{[\mu} \mathcal{R}^{\sigma]}{}_{\nu]} - \tfrac{2}{(n-1)(n-2)} \mathcal{R} g^{[\rho}{}_{[\mu} g^{\sigma]}{}_{\nu]} \,. \tag{13}$$

In terms of the tangential projection of this background curvature, the corresponding *internal* curvature tensor takes the form

$$R_{\mu\nu}{}^{\rho}{}_{\sigma} = 2K^{\rho}{}_{[\mu}{}^{\tau} K_{\nu]\sigma\tau} + \eta^{\kappa}{}_{\mu} \eta^{\lambda}{}_{\nu} \mathcal{R}_{\kappa\lambda}{}^{\alpha}{}_{\tau} \eta^{\rho}{}_{\alpha} \eta^{\tau}{}_{\sigma} \,, \tag{14}$$

which is the translation into the present scheme of what is well known in other schemes as the *generalised Gauss identity*.

The less well known analogue (attributable [9] to Schouten) for the (trace free conformally invariant) *outer* curvature is expressible [1] in terms of the relevant projection of the background Weyl tensor as

$$\Omega_{\mu\nu}{}^{\rho}{}_{\sigma} = 2\, C_{[\mu}{}^{\tau\rho}\, C_{\nu]\tau\sigma} + \eta^{\kappa}{}_{\mu} \eta^{\lambda}{}_{\nu} \mathcal{W}_{\kappa\lambda}{}^{\alpha}{}_{\tau} \perp^{\rho}_{\alpha} \perp^{\tau}_{\sigma} \,. \tag{15}$$

In a background that is flat or conformally flat (for which it is necessary, and for $n \geq 4$ sufficient, that the Weyl tensor should vanish) the vanishing of the extrinsic conformation tensor $C_{\mu\nu}{}^{\rho}$ will therefore be sufficient (independently of the behaviour of the extrinsic curvature vector K^{μ}) for vanishing of the outer curvature tensor $\Omega_{\mu\nu}{}^{\rho}{}_{\sigma}$, which is the condition for it to be possible to construct fields of vectors λ^{μ} orthogonal to the surface and such as to satisfy the generalised Fermi-Walker propagation condition to the effect that $\perp^{\rho}_{\mu} \overline{\nabla}_{\nu} \lambda_{\rho}$ should vanish.

2 Laws of motion for a regular brane complex

2.1 Definition of brane complex

The term p-brane has come [12, 13] to mean a dynamic system localised on a timelike support surface of dimension $d{=}p{+}1$, in a spacetime background of dimension $n{>}\ p$. Thus a zero - brane means a "point particle", and a 1-brane means a "string", while a 2-brane means what is commonly called a "membrane". At the upper extreme an $(\ n\text{-}1)$-brane is what is commonly referred to as a "medium" (as exemplified by a simple fluid). The codimension-1 (hypersurface supported) case of an $(\ n\text{-}2)$-brane (as exemplified by a cosmological domain wall) is what may be referred to as a "hypermembrane", while the codimension-2 case of an $(\ n\text{-}3)$-brane is what may analogously be referred to as a "hyperstring".

A set of branes forms a "brane complex" if the support surface of each (d-1)-brane member is a smoothly imbedded d-dimensional timelike submanifold of which the boundary, if any, is a disjoint union of support surfaces of lower dimensional members of the set. For the complex to qualify as regular [1] it is required that a p-brane member can act directly only on an (p-1)-brane member on its boundary or on a $(p+1)$-brane member on whose boundary it is itself located, though it may be passively influenced by higher dimensional background fields.

Direct mutual interaction between branes with dimension differing by 2 or more would usually lead to divergences, symptomising the breakdown of a strict – meaning thin limit – brane description. To cure that properly, a more elaborate treatment – allowing for finite thickness – would be needed, but it may suffice to use a thin limit approximation [15] whereby the divergence is absorbed [16, 17] in a renormalisation.

In the case of a brane complex, the total action $\mathcal{I}$ will be given as a sum of contributions from the various $(d\text{-}1)$-branes of the complex, of which each has its own Lagrangian d-surface density scalar ${}^{(d)}\overline{L}$ say. Each supporting d-surface will be specified by a mapping $\sigma \mapsto x\{\sigma\}$ giving the local background coordinates x^{μ}

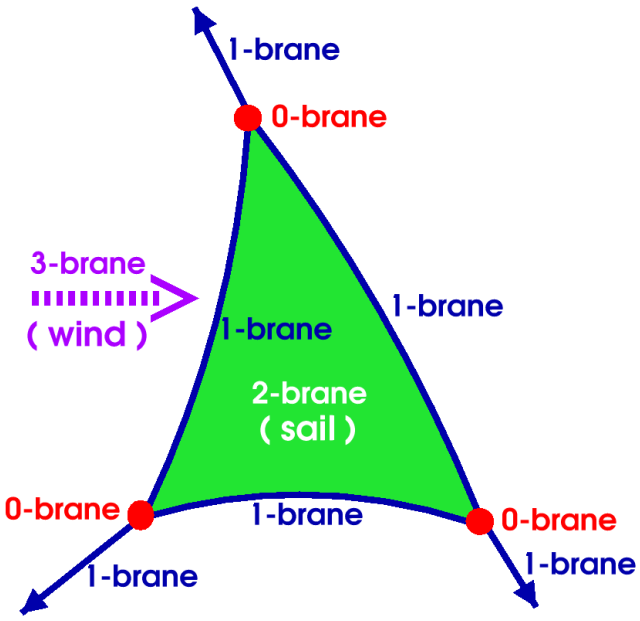

Figure 1: Nautical archetype of a regular brane complex in which a 3-brane (the wind) acts (by pressure discontinuity) on a 2-brane (the sail) hemmed by three 1-branes (bolt ropes) terminating on 0-branes (shackles) that are held in place by three more (free) 1-branes (external stay/sheet ropes).

($\mu = 0, \ldots, \text{n-1}$) as functions of local internal coordinates σ^i ($i = 0, \ldots, \text{d-1}$). The corresponding d-dimensional surface metric tensor ${}^{(\text{d})}\eta_{ij}$ induced as the pull back of the n-dimensional background spacetime metric $g_{\mu\nu}$, determines the surface measure, ${}^{(\text{d})}\bar{\mathcal{S}}$, in terms of which the total action will be expressible as

$$\mathcal{I} = \sum_{\text{d}} \int {}^{(\text{d})}\bar{\mathcal{S}}\, {}^{(\text{d})}\bar{L}\,, \qquad {}^{(\text{d})}\bar{\mathcal{S}} = \sqrt{\|{}^{(\text{d})}\eta\|}\, \text{d}^{\text{d}}\sigma\,. \tag{16}$$

2.2 Conserved current and the stress-energy tensor

As well as on its own internal (d-1)-brane surface fields and their derivatives, and those of any attached d-brane, each contribution ${}^{(\text{d})}\bar{L}$ will also depend (passively) on the spacetime metric $g_{\mu\nu}$ and perhaps other background fields, of which the most common example is a Maxwellian gauge potential A_ν, for which the corresponding field $F_{\mu\nu} = 2\nabla_{[\mu}A_{\nu]}$, is invariant under gauge changes $A_\nu \mapsto A_\nu + \nabla_\nu\alpha$, and is automatically closed, $\nabla_{[\rho}F_{\mu\nu]} = 0$, Subject to the internal dynamic equations of motion given by the variational principle stipulating preservation of the action by variations of the independent field variables, the effect of arbitrary infinitesimal "Lagrangian" variations $\underset{\text{L}}{\delta}A_\nu$, $\underset{\text{L}}{\delta}g_{\mu\nu}$, of the background fields will be to induce a corresponding variation

$$\delta\mathcal{I} = \sum_{\text{d}} \int {}^{(\text{d})}\bar{\mathcal{S}}\left({}^{(\text{d})}\bar{j}^{\mu}\underset{\text{L}}{\delta}A_\mu + \tfrac{1}{2}\,{}^{(\text{d})}\bar{T}^{\mu\nu}\underset{\text{L}}{\delta}g_{\mu\nu}\right), \tag{17}$$

from which, for each (d−1)-brane, one can read out the electromagnetic surface current vector ${}^{(\text{d})}\bar{j}^{\mu}$, and also (since $\underset{\text{L}}{\delta}\left({}^{(\text{d})}\bar{\mathcal{S}}\right) = \frac{1}{2}\,{}^{(\text{d})}\eta^{\mu\nu}\left(\underset{\text{L}}{\delta}g_{\mu\nu}\right){}^{(\text{d})}\bar{\mathcal{S}}$,) the *surface stress momentum energy* tensor

$${}^{(\text{d})}\bar{T}^{\mu\nu} = {}^{(\text{d})}\bar{T}^{\nu\mu} = 2\frac{\partial\,{}^{(\text{d})}\bar{L}}{\partial g_{\mu\nu}} + {}^{(\text{d})}\bar{L}\,{}^{(\text{d})}\eta^{\mu\nu}\,. \tag{18}$$

For any d-dimensional support surface ${}^{(\mathrm{d})}\overline{\mathcal{S}}$, Green's theorem gives

$$\int {}^{(\mathrm{d})}\mathrm{d}\overline{\mathcal{S}}\, {}^{(\mathrm{d})}\overline{\nabla}_\nu\, {}^{(\mathrm{d})}\overline{j}^\nu = \oint {}^{(\mathrm{d}-1)}\mathrm{d}\overline{\mathcal{S}}\, {}^{(\mathrm{d})}\lambda_\nu\, {}^{(\mathrm{d})}\overline{j}^\nu \,, \tag{19}$$

taking the integral on the right over the boundary $(\mathrm{d}\text{-}1)$-surface of $\partial\, {}^{(\mathrm{d})}\overline{\mathcal{S}}$ of ${}^{(\mathrm{d})}\overline{\mathcal{S}}$, where ${}^{(\mathrm{d})}\lambda_\nu$ is the (uniquely defined) outward directed unit tangent vector on the d-surface at its $(\mathrm{d}\text{-}1)$-dimensional boundary.

The Maxwell gauge invariance condition (independence of α) is thus seen to be equivalent to the electric current conservation condition

$${}^{(\mathrm{p})}\overline{\nabla}_\mu\, {}^{(\mathrm{p})}\overline{j}^\mu = \sum_{\mathrm{d}=\mathrm{p}+1} {}^{(\mathrm{d})}\lambda_\mu\, {}^{(\mathrm{d})}\overline{j}^\mu \,, \tag{20}$$

which means that the source of charge injection into any particular $(\mathrm{p}\text{-}1)$-brane is the sum of the currents flowing in from the p-branes to which it is attached.

2.3 Force and the stress balance equation

The condition of being "Lagrangian" means that $\underset{\mathrm{L}}{\delta}$ is comoving as needed to be meaningful for fields with support confined to a particular brane. However for background fields one can also define an "Eulerian" variation, $\underset{\mathrm{E}}{\delta}$, with respect to some appropriately fixed reference system, in which the infinitesimal displacement of the brane complex is specified by a vector field ξ^μ. The difference will be given by $\underset{\mathrm{L}}{\delta} - \underset{\mathrm{E}}{\delta} = \vec{\xi}\pounds$, where the $\vec{\xi}\pounds$ is the Lie differentiation operator, which will be given for the relevant background fields by the familiar formulae $\vec{\xi}\pounds A_\mu = \xi^\rho \nabla_\rho A_\mu + A_\rho \nabla_\mu \xi^\rho$, and $\vec{\xi}\pounds g_{\mu\nu} = 2\nabla_{(\mu}\xi_{\nu)}$.

In a fixed Eulerian background, the background fields will have Lagrangian variations given just by their Lie derivatives with respect to the displacement ξ^μ. Subject to the internal field equations, the action variation $\delta\mathcal{I}$ due to the displacement of the branes will therefor just be $\sum_{\mathrm{d}} \int {}^{(\mathrm{d})}\mathrm{d}\overline{\mathcal{S}} \left({}^{(\mathrm{d})}\overline{j}^\nu\ \vec{\xi}\pounds A_\nu + \tfrac{1}{2}\, {}^{(\mathrm{d})}\overline{T}^{\mu\nu}\ \vec{\xi}\pounds g_{\mu\nu} \right)$. The postulate that this vanishes for any ξ^μ entails the further d-surface tangentiality restriction ${}^{(\mathrm{d})}\overline{\perp}^\mu{}_\nu\, {}^{(\mathrm{d})}\overline{T}^{\nu\rho} = 0$ and (by the Green theorem) the dynamic equations

$${}^{(\mathrm{p})}\overline{\nabla}_\mu\, {}^{(\mathrm{p})}\overline{T}^\mu{}_\rho = {}^{(\mathrm{p})}f_\rho \,, \tag{21}$$

in which total force density,

$${}^{(\mathrm{p})}f_\rho = {}^{(\mathrm{p})}\overline{f}_\rho + {}^{(\mathrm{p})}\check{f}_\rho \,, \tag{22}$$

includes the Faraday-Lorenz contribution ${}^{(\mathrm{p})}\overline{f}_\rho = F_{\rho\mu}\, {}^{(\mathrm{p})}\overline{j}^\mu$, from the background, while on each $(\mathrm{p}\text{-}1)$-brane, the contact force exerted by attached p-branes is

$${}^{(\mathrm{p})}\check{f}_\rho = \sum_{\mathrm{d}=\mathrm{p}+1} {}^{(\mathrm{d})}\lambda_\mu\, {}^{(\mathrm{d})}\overline{T}^\mu{}_\rho \,, \tag{23}$$

in which it is to be recalled that, on the $(\mathrm{p}\text{+}1)$-dimensional support surface of each attached p-brane, ${}^{(\mathrm{d})}\lambda_\mu$ is the unit vector that is directed normally towards the bounding $(\mathrm{p}\text{-}1)$-brane.

The tangential force balance equations will hold as identities when the internal field equations are satisfied (because a surface tangential displacement has no effect). The non-redundent information governing the extrinsic motion of a $(\mathrm{d}-1)$-brane will be given just by the orthogonal part. Integrating by parts, as the surface gradient of the rank-$(\mathrm{n}-\mathrm{d})$ orthogonal projector ${}^{(\mathrm{p})}\overline{\perp}^\mu{}_\nu$ will be given in terms of the second fundamental tensor ${}^{(\mathrm{p})}K_{\mu\nu}{}^\rho$ of the d-surface by

$${}^{(\mathrm{p})}\overline{\nabla}_\mu\, {}^{(\mathrm{p})}\overline{\perp}^\nu{}_\rho = -\, {}^{(\mathrm{p})}K_{\mu\nu}{}^\rho - {}^{(\mathrm{p})}K_\mu{}^\rho{}_\nu \,, \tag{24}$$

the extrinsic equations of motion are finally obtained in the form

$$ {}^{(\mathrm{p})}\overline{T}^{\mu\nu}\,{}^{(\mathrm{p})}K_{\mu\nu}{}^{\rho} = {}^{(\mathrm{p})}\underline{L}^{\rho}_{\mu}\,{}^{(\mathrm{p})}f^{\mu}\,. \tag{25}$$

It is to be remarked that this is valid not just for a conservative force such as the electromagnetic example considered above, but also for dissipative forces such as frictional drag[10] by a relatively moving background medium.

The most familiar application is to the case $p = 1$ of a point particle of mass m with unit velocity vector $\dot{x}^{\mu}$ and orthogonally directed acceleration vector $\ddot{x}^{\mu}$, for which one has $\eta^{\mu\nu} = -\dot{x}^{\mu}\dot{x}^{\nu}$, $\overline{T}^{\mu\nu} = m\,\dot{x}^{\mu}\dot{x}^{\nu}$, $K^{\mu\nu\rho} = \dot{x}^{\mu}\dot{x}^{\nu}\ddot{x}^{\rho}$, so that $K^{\rho} = -\ddot{x}^{\rho}$ and $\overline{T}^{\mu\nu}K_{\mu\nu}{}^{\rho} = m\,\ddot{x}^{\rho}$.

3 Canonical Liouville and symplectic currents

3.1 Canonical formalism for Branes

For the study of small perturbations, and particularly for the systematic derivation of conservation laws associated with symmetries, it is useful to employ a treatment of the canonical kind that was originally developped in the context of field theory (as a step towards quantisation) by Witten, Zuckerman, and others [18–24]. This section describes the generalisation of this procedure to brane mechanics in the manner initiated by Cartas-Fuentevilla [25, 26] and developed in collaboration with Dani Steer [27]. After a general presentation, including a review of the relationships between the various (Lagrangian, Eulerian and other) relevant kinds of variation, the procedure is illustrated by application to a particular category that includes the case of branes of purely elastic type.

Consider a generic conservative p-brane model whose mechanical evolution is governed by an action integral of the form

$$ \mathcal{I} = \int \mathcal{L}\,\mathrm{d}^{\mathrm{p}+1}\sigma\,, \tag{26}$$

over a supporting worldsheet with internal co-ordinates σ^{i} $(i = 0, 1, \ldots \mathrm{p})$, and induced metric $\eta_{ij} = g_{\mu\nu}x^{\mu}_{,i}x^{\nu}_{,j}$ in a background with coordinates x^{μ}, $(\mu = 0, 1, \ldots \mathrm{n}-1)$, $(\mathrm{n} \geq \mathrm{p}+1)$ and (flat or curved) space-time metric $g_{\mu\nu}$. The relevant Lagrangian scalar density $\mathcal{L} = \|\eta\|^{1/2}\overline{L}$, is given as a function of a set of field components q^{A} – including background coords – and of their surface deriatives, $q^{\mathrm{A}}_{,i} = \partial_i q^{\mathrm{A}} = \partial q^{\mathrm{A}}/\partial\sigma^{i}$. The relevant field variables q^{A} can be of internal or external kind, the most obvious example of the latter kind being the background coordinates x^{μ} themselves.

The generic action variation,

$$ \delta\mathcal{L} = \mathcal{L}_{\mathrm{A}}\delta q^{\mathrm{A}} + p^{i}_{\mathrm{A}}\delta q^{\mathrm{A}}_{,i}\,, \tag{27}$$

specifies partial derivative components $\mathcal{L}_{\mathrm{A}}$ and and corresponding generalised momentum components p^{i}_{A}. The variation principle characterises dynamically admissible "on shell" configurations by the vanishing of the Eulerian derivative

$$ \frac{\delta\mathcal{L}}{\delta q^{\mathrm{A}}} = \mathcal{L}_{\mathrm{A}} - p^{i}_{\mathrm{A}\,,i}\,. \tag{28}$$

In terms of this Eulerian derivative, the generic Lagrangian variation will have the form

$$ \delta\mathcal{L} = \frac{\delta\mathcal{L}}{\delta q^{\mathrm{A}}}\delta q^{\mathrm{A}} + \left(p^{i}_{\mathrm{A}}\delta q^{\mathrm{A}}\right)_{,i}\,. \tag{29}$$

There will be a corresponding pseudo-Hamiltonian scalar density

$$ \mathcal{H} = p^{i}_{\mathrm{A}}q^{\mathrm{A}}_{,i} - \mathcal{L}\,, \tag{30}$$

for which

$$ \delta\mathcal{H} = q^{\mathrm{A}}_{,i}\delta p^{i}_{\mathrm{A}} - \mathcal{L}_{\mathrm{A}}\delta q^{\mathrm{A}}\,. \tag{31}$$

(The covariance of such a pseudo-Hamiltonian distingushes it from the ordinary kind of Hamiltonian, which depends on the introduction of some preferred time foliation.)

For an on-shell configuration, i.e. when the dynamical equations

$$\frac{\delta \mathcal{L}}{\delta q^{\mathrm{A}}} = 0 \,, \tag{32}$$

are satisfied, the Lagrangian variation will reduce to a pure surface divergence,

$$\delta \mathcal{L} = \left(p_{\mathrm{A}}^{\ i} \delta q^{\mathrm{A}} \right)_{,i} \,, \tag{33}$$

and the correponding on-shell pseudo-Hamiltonian variation will take the form

$$\delta \mathcal{H} = q^{\mathrm{A}}_{\ ,i} \delta p_{\mathrm{A}}^{\ i} - p_{\mathrm{A}}^{\ i}{}_{,i} \delta q^{\mathrm{A}} \,. \tag{34}$$

3.2 Symplectic structure

The generic first order variation of the Lagrangian will be given by

$$\delta \mathcal{L} = \frac{\delta \mathcal{L}}{\delta q^{\mathrm{A}}} \delta q^{\mathrm{A}} + \vartheta^{i}{}_{,i} \,. \tag{35}$$

in terms of the generalised Liouville 1-form (on the configuration space cotangent bundle) defined by

$$\vartheta^{i} = p_{\mathrm{A}}^{\ i} \delta q^{\mathrm{A}} \,. \tag{36}$$

Now consider a pair of successive independent variations $\acute{\delta}$, $\grave{\delta}$, which will give a second order variation of the form

$$\grave{\delta} \acute{\delta} \mathcal{L} = \grave{\delta} \Big(\frac{\delta \mathcal{L}}{\delta q^{\mathrm{A}}} \Big) \acute{\delta} q^{\mathrm{A}} + \frac{\delta \mathcal{L}}{\delta q^{\mathrm{A}}} \grave{\delta} \acute{\delta} q^{\mathrm{A}} + \big(\grave{\delta} p_{\mathrm{A}}^{\ i} \acute{\delta} q^{\mathrm{A}} + p_{\mathrm{A}}^{\ i} \grave{\delta} \acute{\delta} q^{\mathrm{A}} \big)_{,i} \,. \tag{37}$$

Thus using the commutation relation $\grave{\delta} \acute{\delta} = \acute{\delta} \grave{\delta}$ one gets

$$\grave{\delta} \Big(\frac{\delta \mathcal{L}}{\delta q^{\mathrm{A}}} \Big) \acute{\delta} q^{\mathrm{A}} - \acute{\delta} \Big(\frac{\delta \mathcal{L}}{\delta q^{\mathrm{A}}} \Big) \grave{\delta} q^{\mathrm{A}} = \hat{\varpi}^{i}{}_{,i} \,, \tag{38}$$

where the symplectic 2-form (on the configuration space cotangent bundle) is defined by

$$\hat{\varpi}^{i} = \acute{\delta} p_{\mathrm{A}}^{\ i} \grave{\delta} q^{\mathrm{A}} - \grave{\delta} p_{\mathrm{A}}^{\ i} \acute{\delta} q^{\mathrm{A}} \,. \tag{39}$$

For an on-shell perturbation we thus obtain

$$\frac{\delta \mathcal{L}}{\delta q^{\mathrm{A}}} = 0 \qquad \Rightarrow \qquad \delta \mathcal{L} = \vartheta^{i}{}_{,i} \,, \tag{40}$$

while for a pair of on-shell perturbations we obtain

$$\acute{\delta} \Big(\frac{\delta \mathcal{L}}{\delta q^{\mathrm{A}}} \Big) = \grave{\delta} \Big(\frac{\delta \mathcal{L}}{\delta q^{\mathrm{A}}} \Big) = 0 \qquad \Rightarrow \qquad \hat{\varpi}^{i}{}_{,i} = 0 \,. \tag{41}$$

The foregoing surface current conservation law is expressible in shorthand as

$$\varpi^i{}_{,i} = 0\,, \tag{42}$$

in which the closed (since manifestly exact) symplectic 2-form (39) is specified in concise wedge product notation as

$$\varpi^i = \delta \wedge \vartheta^i = \delta p^i_{\rm A} \wedge \delta q^{\rm A}\,. \tag{43}$$

Some authors prefer to use an even more concise notation system in which it is not just the relevant distinguishing (in our case acute and grave accent) indices that are omitted but even the wedge symbol $\wedge$ that indicates the antisymmetrised product relation. However such an extreme level of abbreviation is dangerous [25] in contexts in which symmetric products are also involved.

3.3 Translation into strictly tensorial form

To avoid the gauge dependence involved in the use of auxiliary structures such as local frames and internal surface coordinates, by working [28] just with quantities that are strictly tensorial with respect to the background space, one needs to replace the surface current densities whose components ϑ^i and ϖ^i depend on the choice of the internal coordinates σ^i, by vectorial quantities with strictly tensorial background coordinate components given by

$$\Theta^\nu = \|\eta\|^{-1/2} x^\nu_{,i} \vartheta^i\,, \qquad \Omega^\nu = \|\eta\|^{-1/2} x^\nu_{,i} \varpi^i\,. \tag{44}$$

and with strictly scalar divergences given by

$$\overline{\nabla}_\nu \Theta^\nu = \|\eta\|^{-1/2} \vartheta^i{}_{,i}\,, \qquad \overline{\nabla}_\nu \Omega^\nu = \|\eta\|^{-1/2} \varpi^i{}_{,i}\,. \tag{45}$$

In terms of the surface projected covariant differentiation operator defined in terms of the fundamental tensor $\eta^{\mu\nu} = \eta^{ij} x^\mu_{,i} x^\nu_{,j}$ by $\overline{\nabla}_\nu = \eta^\mu{}_\nu \nabla_\mu$, one thus obtains a Liouville current conservation law of the form

$$\overline{\nabla}_\nu \Theta^\nu = 0 \tag{46}$$

for any symmetry generating perturbation, i.e. for any infinitesimal variation $\delta q^{\rm A}$ such that $\delta \mathcal{L} = 0$. Similarly a symplectic current conservation law of the form

$$\overline{\nabla}_\nu \Omega^\nu = 0 \tag{47}$$

will hold for any pair of perturbations that are on-shell, i.e. such that $\delta(\delta\mathcal{L}/\delta q^{\rm A}) = 0$.

3.4 Application to hyperelastic case

In typical applications, the relevant set of configuration components $q^{\rm A}$ will include a set of brane field components φ^α as well as the background coords x^μ, so that in terms of displacement vector $\xi^\mu = \delta x^\mu$ the Liouville current will take the form

$$\Theta^\nu = \|\eta\|^{-1/2} x^\nu_{,i} \big(p_\alpha{}^i\, \delta\varphi^\alpha + p_\mu{}^i\, \xi^\mu \big) = \pi_\alpha{}^\nu\, \delta\varphi^\alpha + \pi_\mu{}^\nu\, \xi^\mu\,, \tag{48}$$

in which the latter version replaces the original momentum components by the corresponding background tensorial momentum variables, which are given by $\pi_\alpha{}^\nu = \|\eta\|^{-1/2}\, x^\nu_{,i}\, p_\alpha{}^i$ and $\pi_\mu{}^\nu = \|\eta\|^{-1/2}\, x^\nu_{,i}\, p_\mu{}^i$.

The hyperelastic category [29] (generalising the case of an ordinary elastic solid which includes the special case of an ordinary barotropic perfect fluid) consists of brane models in which – with respect to a suitably comoving internal reference system σ^i – there are no independent surface fields at all – meaning that the φ^α

and the $p_\alpha{}^i$ are absent – and in which the only relevant background field is the metric $g_{\mu\nu}$ that is specified as a function of the external coordinates x^μ . In any such case, the generic variation of the Lagrangian is determined just by the surface stress momentum energy density tensor $\overline{T}^{\mu\nu}$ according to the standard prescription

$$\delta\mathcal{L} = \frac{1}{2}\|\eta\|^{1/2}\,\overline{T}^{\mu\nu}\,\underset{\text{L}}{\delta} g_{\mu\nu}\,, \tag{49}$$

whereby $\overline{T}^{\mu\nu}$ is specified in terms of partial derivation of the action density with respect to the metric.

In a fixed background (i.e. in the absence of any Eulerian variation of the metric) the Lagrangian variation of the metric will be given by $\underset{\text{L}}{\delta} g_{\mu\nu} = \vec{\xi}\pounds g_{\mu\nu} = 2\nabla_{(\mu}\xi_{\nu)}$. Comparing this to canonical prescription $\delta\mathcal{L} = \mathcal{L}_\mu\xi^\mu + p_\mu{}^i\xi^\mu_{,i}$ with $\xi^\mu = \delta x^\mu$ shows that the relevant partial derivatives will be given by the (non-tensorial) formulae $\mathcal{L}_\mu = \|\eta\|^{1/2}\,\Gamma_\mu{}^\nu{}_\rho\overline{T}_\nu{}^\rho$, $p_\mu{}^i = \|\eta\|^{1/2}\,\overline{T}_{\mu\nu}\eta^{ij}x^\nu{}_{,j}$. It can thus be seen that in the hyperelastic case, the canonical momentum tensor $\pi_\mu{}^\nu$ and the Liouville current Θ^ν will be given just in terms of surface stress tensor $\overline{T}^{\mu\nu}$ by the very simple formulae

$$\pi_\mu{}^\nu = \overline{T}_\mu{}^\nu\,, \qquad \Theta^\nu = \overline{T}_\mu{}^\nu\xi^\mu\,. \tag{50}$$

In order to proceed, we must consider the second order metric variation, whereby (following Friedman and Schutz [30]) the hyper Cauchy tensor (generalised elasticity tensor) $\overline{\mathfrak{C}}^{\mu\nu\rho\sigma} = \overline{\mathfrak{C}}^{\rho\sigma\mu\nu}$ is specified [31] in terms of Lagrangian variations by a partial derivative relation of the form

$$\underset{\text{L}}{\delta}\big(\|\eta\|^{1/2}\,\overline{T}^{\mu\nu}\big) = \|\eta\|^{1/2}\overline{\mathfrak{C}}^{\mu\nu\rho\sigma}\underset{\text{L}}{\delta} g_{\rho\sigma}\,. \tag{51}$$

The symplectic current is thereby obtained in the form

$$\Omega^\nu = \mathfrak{O}_\mu{}^\nu \wedge \xi^\mu\,, \tag{52}$$

where

$$\mathfrak{O}_\mu{}^\nu = 2\overline{\mathfrak{C}}_\mu{}^\nu{}_\rho{}^\sigma\overline{\nabla}_\sigma\xi^\rho + \overline{T}^{\nu\rho}\overline{\nabla}_\rho\xi_\mu\,. \tag{53}$$

4 Brane perturbation by gravitational radiation

4.1 Generic case

A background metric perturbation $\delta g_{\mu\nu} = h_{\mu\nu}$ will provide an extra Lagrangian and stress contributions $\delta\overline{L} = \frac{1}{2}\overline{T}^{\rho\sigma}h_{\rho\sigma}$, and $\delta\overline{T}^{\mu\nu} = \overline{\mathfrak{C}}^{\mu\nu\rho\sigma}h_{\rho\sigma}$, whence a corresponding force increment $\delta\overline{f}^\mu = \frac{1}{2}\overline{T}^{\nu\sigma}\nabla^\mu h_{\nu\sigma} - \overline{\nabla}_\nu\big(\overline{T}^{\nu\sigma}h_\sigma{}^\mu\big)$. The effect of this is expressible as the inclusion of an extra term $\overline{f}_{\text{G}}{}^\mu$ on the right of the original force balance equation, as expressed in terms of the unperturbed values of the metric $g_{\mu\nu}$, stress tensor $\overline{T}^{\mu\nu}$, and force density f^μ , so as to obtain a perturbed force balance of the form

$$\overline{\nabla}_\nu T^{\nu\mu} = f^\mu + \overline{f}_{\text{G}}{}^\mu\,, \tag{54}$$

in which the effective gravitational perturbation contribution is given by

$$\overline{f}_{\text{G}}{}^\mu = \tfrac{1}{2}\overline{T}^{\nu\sigma}\nabla^\mu h_{\nu\sigma} - \overline{\nabla}_\nu\big(\overline{T}^{\nu\sigma}h_\sigma{}^\mu + \overline{\mathfrak{C}}^{\mu\nu\rho\sigma}h_{\rho\sigma}\big)\,, \tag{55}$$

a formula that was not so well known until relatively recently [31].

4.2 The case of a simple Dirac-Nambu-Goto type brane

The simplest dimensionally unrestricted application, is to a p-brane of the Dirac-Nambu-Goto type, for which the relevant master function is simply constant, so given in terms of a corresponding Kibble mass M_{K} by $\overline{L} = -\mathrm{M}_{\mathrm{K}}^{\mathrm{p}+1}$. (In the context of superstring theory M_{K} is typically of the order of magnitude of the Planck mass M_{P}, whereas in the context of cosmic string theory the Kibble mass is expected to comparable with the relevant Higgs mass, M_{X} .) In this special case, the surface stress momentum energy tensor is of course simply proportional to the fundamental tensor:

$$\overline{T}^{\mu\nu} = -\mathcal{T}\,\eta^{\mu\nu}\,, \qquad \mathcal{T} = \mathrm{M}_{\mathrm{K}}^{\mathrm{p}+1} \tag{56}$$

so its trace will be given by $\overline{T} = -\,(\mathrm{p}+1)\,\mathcal{T}$, where $\mathcal{T}$ is interpretable as the surface tension. The corresponding the hyper-Cauchy tensor is found[31] to be

$$\overline{\mathfrak{C}}^{\mu\nu\rho\sigma} = \mathcal{T}\left(\eta^{\mu(\rho}\eta^{\sigma)\nu} - \tfrac{1}{2}\eta^{\mu\nu}\eta^{\rho\sigma}\right). \tag{57}$$

The dynamical equation of motion (54) will therefor reduce to the form

$$\mathcal{T}\,K^{\rho} = -f^{\rho}\,, \tag{58}$$

in which (as well as the possibility of drag) the right hand side will include an effective gravitational contribution expressible[31] in the form ${f_{\mathrm{G}}}^{\mu} = {f_{\mathrm{I}}}^{\mu} + {f_{\mathrm{II}}}^{\mu}$, with

$${f_{\mathrm{I}}}^{\mu} = \mathcal{T}\,\perp^{\mu\nu}\eta^{\rho\sigma}\left(\nabla_{\rho}h_{\nu\sigma} - \tfrac{1}{2}\nabla_{\nu}h_{\rho\sigma}\right), \tag{59}$$

$${f_{\mathrm{II}}}^{\mu} = \mathcal{T}\left(\perp^{\mu\nu}K^{\rho} + \tfrac{1}{2}\eta^{\rho\nu}K^{\mu} - K^{\nu\rho\mu}\right)h_{\nu\rho}\,. \tag{60}$$

It was observed by Battye[32, 33] that the early work on gravitational perturbations of strings cited by Vilenkin and Shellard in their 1994 treatise [34] was seriously flawed by the use for estimating ${f_{\mathrm{G}}}^{\mu}$ of a formula (7.7.3) without the orthogonal projection operator $\perp^{\mu\nu}$ in the expression (59) for ${f_{\mathrm{I}}}^{\mu}$, and entirely lacking the contribution ${f_{\mathrm{II}}}^{\mu}$ which might be relatively negligible for high frequency radiation[32] of external origin, but not in the case of self-interaction for which the two contributions will be comparable. The self interaction contributions from (59) and (60) will be separately divergent, but in the "hyperstring" case these divergences will actually cancel each other. Thus (contrary to what was claimed in (7.7.7) [34]) the total self-interaction will remain finite[16, 17, 33] whenever the codimension is 2, as for an ordinary string in 4 dimensions (or for a "brane-world" in 6 dimensions).

4.3 Regularisation of self-interaction

To treat such self-interaction one must face the problem that the regularity condition (see Figure 1) is violated whenever a brane of dimension $\mathrm{d} = \mathrm{p}+1$ acts on a background of dimension $\mathrm{n} \geq \mathrm{d}+2$, . To cure this, a physically realistic regularisation involves replacing the infinitely thin worldsheet by a support of finite thickness. The divergent self-interaction fields such as A_{μ} and $h_{\mu\nu}$ are then replaced by regularised averages $\widehat{A}_{\mu}$ and $\widehat{h}_{\mu\nu}$ with dominant contribution proportional to the relevant source [16, 17]. This means $\widehat{A}_{\mu} \propto \overline{j}^{\mu}$ and $\widehat{h}_{\mu\nu} \propto (\mathrm{n}-2)\overline{T}_{\mu\nu} - \overline{T}_{\sigma}{}^{\sigma}g_{\mu\nu}$, which for a Nambu-Goto hyperstring, $\mathrm{p} = \mathrm{n}-3$, gives $\widehat{h}^{\mu\nu} \propto (\mathrm{p}+1)\mathcal{T}\perp^{\mu\nu}$, with a proportionality coefficient that diverges as the thickness tends to zero. On such world sheet confined fields, the ordinary gradient operator ∇_{ν} must be replaced by the corresponding regularised operator $\widehat{\nabla}_{\nu}$, so that for example the field $F_{\mu\nu} = 2\nabla_{[\mu}A_{\nu]}$ will have the regularised average $\widehat{F}_{\mu\nu} = 2\widehat{\nabla}_{[\mu}\widehat{A}_{\nu]}$, as needed for the electromagnetic self-interaction force density $\widehat{f}_{\rho} = \widehat{F}_{\rho\mu}\overline{j}^{\mu}$. The required result, giving zero gravitational contribution, ${\widehat{f}_{\mathrm{G}}}^{\mu} = 0$, for Nambu-Goto hyperstrings (including [33] the ordinary string case p=1 with n=4) has been shown [15] to be provided generally by the conveniently simple and easily memorable formula $\widehat{\nabla}_{\nu} = \overline{\nabla}_{\nu} + \frac{1}{2}K_{\nu}$.

5 Vorton equilibrium states of elastic string loops

5.1 The category of simple elastic string models

For any string model the fundamental tensor of the 2 dimensional worldsheet will be expressible in terms of any orthonormal diad of space like and timelike vectors $\boldsymbol{u}^\nu$, $\widetilde{\boldsymbol{u}}^\nu$ as $\eta^\mu{}_\nu = -\boldsymbol{u}^\mu\,\boldsymbol{u}^\nu + \widetilde{\boldsymbol{u}}^\mu\,\widetilde{\boldsymbol{u}}^\nu$. There will generically be a prefered diad with respect to which the symmetric surface stress energy tensor will be expressible as

$$\overline{T}^{\mu\nu} = \mathcal{U}\,\boldsymbol{u}^\mu\,\boldsymbol{u}^\nu - \mathcal{T}\,\widetilde{\boldsymbol{u}}^\mu\,\widetilde{\boldsymbol{u}}^\nu \tag{61}$$

where $\mathcal{T}$ is the string tension, and $\mathcal{U}$ is the surface energy density, which, in the elastic case, is determined as a function of $\mathcal{T}$ by an equation of state.

In addition to the extrinsic (transversely polarised)"wiggle" perturbations which, as in any string model, travel with a characteristic velocity $v = \sqrt{\mathcal{T}/\mathcal{U}}$ such a model has perturbation modes of only one other kind: these are sound type (longitudinal compression) "woggle" modes, which propagate relative to the locally preferred frame with speed given by the formula $v_{\rm L} = \sqrt{-{\rm d}\mathcal{T}/{\rm d}\mathcal{U}}$. A particularly important special case is that of models of the integrable transonic type [35] for which the "wiggle" and "woggle" speeds coincide, which occurs when the equation of state is specified simply by the specification of a fixed value for the product $\mathcal{U}\mathcal{T}$. The kind of model appropriate for representing such familiar technical applications as bow strings, or the strings of musical instruments, will generally be of subsonic type, meaning that the wiggle speed v is less than the sonic speed $v_{\rm L}$, while on the other hand it has been shown by Peter [36] that models of supersonic type will commonly be needed for the representation of cosmic strings of the conducting vacuum vortex type envisaged by Witten [37].

A model of any such elastic type is specifiable in variational form by a string Lagrangian L depending only on the magnitude of the gradient of some stream function φ (which in the Witten case represents the phase of a complex scalar field). This means that the string model is characterised by a single variable equation of state giving L as a function of the scalar $w = \eta^{ij}\varphi_{,i}\varphi_{,j}$. It is useful [14, 38] to introduce the corresponding adjoint formulation in terms of the quantity $\Lambda = L + w\kappa$, with $\kappa = -2\,{\rm d}L/{\rm d}w$. When $w < 0$, one finds that the tension and energy density will be given by $\mathcal{T} = -L$, $\mathcal{U} = -\Lambda$, while when $w > 0$ they will be given by $\mathcal{T} = -\Lambda$, $\mathcal{U} = -L$. In all cases the phase gradient is proportional to a surface current, $\overline{c}^\mu = x^\mu_{,i}\overline{c}^i$, $\overline{c}^i = \kappa\eta^{ij}\varphi_{,j} = -\partial L/\partial\varphi_{,i}$, that has the property of being conserved, $(\sqrt{-\eta}\,\overline{c}^i)_{,i} = 0$, whenever there is no external force, so that the equation of motion of the worldsheet reduces to the simple form $\overline{T}^{\mu\nu}K_{\mu\nu}{}^\rho = 0$, with $\overline{T}^{\mu\nu} = 2\kappa^{-1}\overline{c}^\mu\overline{c}^\nu + L\eta^{\mu\nu}$.

When he originally introduced the concept of conducting cosmic strings [37] Witten suggested that a simple linear action formula, $L = -m^2(1+\delta_*^2\,w)$, involving just a single extra parameter (namely a lengthscale δ_*) might be used as a good approximation, least in the weak current limit for which w is sufficiently small. However it subsequently became clear that such a linear formula is inadequate even in the weak current limit, since it implies that wiggle propagation would always be subsonic $v^2 < v_{\rm L}^2$, whereas detailed examination of the relevant kind of vacuum vortex by Peter [36] revealed that the wiggle propagation in such a case would typically be supersonic $v^2 > v_{\rm L}^2$ As a more satisfactory replacement for Witten's direct linearity ansatz, it has been found [39, 40] that at the cost of introducing one more mass scale $m_\star$, a reasonably good representation is obtainable by using an ansatz of logarithmic form $L = -m^2 - \frac{1}{2}m_\star^2\ln\{1+\delta_\star^2\,w\}$.

5.2 Stationary string states in flat background

We shall conclude this overview by considering what can be said about stationary equilibrium states, as characterised, in a flat background a world sheet that is tangent to a timelike unit static Killing vector satisfying $\nabla_\mu k^\nu = 0$. In such a worldsheet there will also be an orthogonal (and therefor spacelike) unit tangent vector e^μ satisfying the invariance condition $k^\nu\nabla_\nu e^\mu = 0$. For such a worldsheet, the first fundamental tensor will be given by $\eta^{\mu\nu} = -k^\mu k^\nu + e^\mu e^\nu$, while in terms of the curvature vector, $K^\mu = e^\nu\nabla_\nu e^\mu$, the second fundamental tensor will be given by $K_{\mu\nu}{}^\rho = e_\mu e_\nu K^\rho$.

Within the worldsheet, the preferred timelike eigenvector of the stress energy tensor, as characterised by

the relation $\overline{T}^{\mu}_{\nu}u^{\nu} = -\mathcal{U}u^{\nu}$, will be expressible in the form

$$u^{\mu} = (1-v^2)^{-1/2}(k^{\mu}+v\,e^{\mu}) \tag{62}$$

which defines the relative flow velocity v. Under these conditions, the free dynamical equation (5.1) can be seen to reduce to the simple form $(\mathcal{U} - v^2\mathcal{T})K^{\rho} = 0$.

For an infinitely long string this equation can of course be solved in a trivial manner by choosing a configuration that is straight, which means $K^{\rho} = 0$, in which case the value of v is unrestricted. However for a finite closed loop the curvature cannot vanish everywhere, and where K^{ρ} is non-zero the only way of satisfying the extrinsic equilibrium condition(5.2) is for the relative flow velocity to bethe same as the relevant wiggle propagation speed: $v = \sqrt{\mathcal{T}/\mathcal{U}}$, while to satisfy the intrinsic (current conservation) equilibrium condition it is trivially sufficient (and generically necesssary) for the value of this speed to be uniform. Provided this centrifugal equilibrium condition is satisfied, there is no retriction on the curvature, which need not be uniform: thus the equilibrium configuration of the string loop need not be circular, but may have an arbitrary shape.

After thus obtaining the generic condition for string loop equilibrium, the next problem is to find which of such vorton equilibrium states are stable. This question has so far been dealt with [5, 41] only in the simple case of equilibrium configurations that are circular.

5.3 Stability criterion for circular vorton states

It is easy to see that the stability of a uniform circular equilibrium state of an elastic string loop in a flat background will depend just on the extrinsic (wiggle type) and longitudinal (sound type) perturbation speeds, v and $v_{\rm L}$. Moreover it is fairly easy to show [5] that such a state will always be stable in the subsonic case, $v^2 \leq v_{\rm L}^2$, which is what is most likely to be relevant in a terrestrial engineering context.Even in the supersonic case, it has been shown [5] that monopole $n = 0$ and dipole $n = 1$ perturbation modes are always stable. However instability may occur for higher modes, $n \geq 2$ for which, in a state with radius a, the eigenfrequency ω is given by the solution of an equation of the cubic form $x^3 + b_2x^2 + b_1x + b_0 = 0$, for the quantity $x = a\,\omega/v_{+}\,n$, where $v_{+} = 2v/(1+v^2)$, is the relative velocity of orthogonaly polarised forward propagating wiggles, and the coefficients of the cubic are given by $b_2 = \Gamma - 2 - \xi$, $b_1 = -2\Gamma + (1+\xi)(1-n^{-2})$, $b_0 = \Gamma(1-n^{-2})$, using the notation $\xi = \Gamma(1-v_{+}^2)$, $\Gamma = v_{+}^{-2}(v_{\rm L}^2 - v^2)/(1-v_{\rm L}^2\,v^2)$.

The stability criterion, for all the roots to be real, is the positivity of a discriminant $\Delta = b_2^2b_1^2 + 18b_2b_1b_0 - 4b_1^3 - 4b_2^3b_0 - 27b_0^2$. Figure 2 shows the zones of negativity (instability) for the lowest relevant mode numbers, $n = 2, 3, \ldots$ by Martin [41]. In the ultrarelativistic limit $v \longrightarrow 1$, $v_{\rm L} \longrightarrow 1$ that is relevant for weak currents in conducting cosmic strings, one gets $\xi \longrightarrow 0$ and

$$\Delta \longrightarrow 4n^{-2}(\Gamma+1+n^{-1})^2(\Gamma+1-n^{-1})^2, \tag{63}$$

which is strictly positive (implying stability) almost always, the unstable exceptions being on the lines converging in the plot to the limit point $v^2 = 1$, $v_{\rm L}^2 = 1$ with gradient given in terms of the corresponding node number by $1/(2n-1)$.

The upshot is that although some circular vorton states are unstable, there are plenty more – the ones that would presumably be selected under natural conditions – that are stable, at least with respect to macroscopic string perturbations. It is however to be remarked that – since it deals only with the thin string limit – the kind of analysis described here can not resolve the (sensitively model dependent) issue of stability with respect to quantum effects or other processes involving the microscopic internal structure of the vacuum vortex or whatever else may constitute the string.

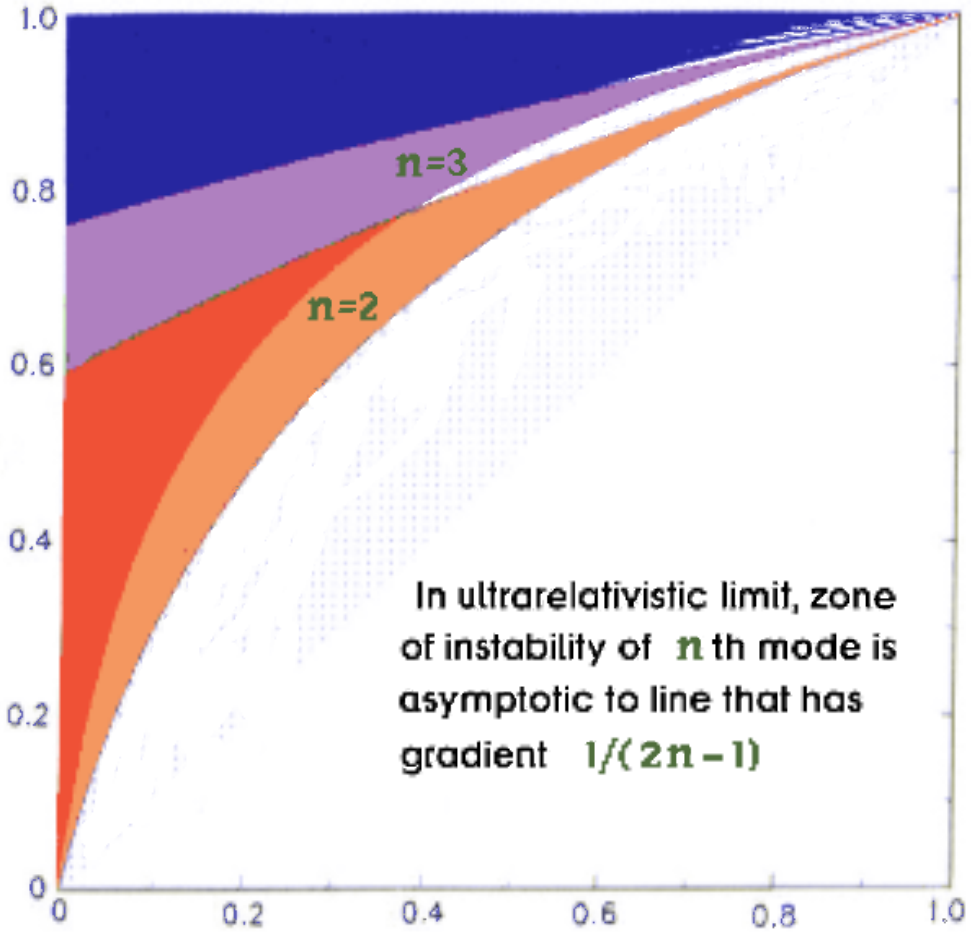

Figure 2: Zones of instability of circular vorton states, as obtained by X. Martin on plot of squared rotation (and wiggle) speed, v^2, against squared "sonic" speed $v_{\rm L}^2$.

References

[1] B. Carter,"Essentials of classical brane dynamics", (in Proc. Peyresq workshop, June 2000, ed. E. Verdaguer) *Int. J. Theo. Phys.* **40** (2001) 2099-2129. [gr-qc/0012036]

[2] V. Niarchos, "Phases of Higher Dimensional Black Holes", *Mod. Phys. Lett.* **A23** (2008) 2625-2643. [arXiv: 0808.2776]

[3] L.M. Cao, "Deformation of Codimension-2 Surface and Horizon Thermodynamics", [arXiv: 1009.4540]

[4] R. Emparan, T. Harmark, V. Niarchos, N.A. Obers, "Essentials of Blackfold Dynamics" *J.H.E.P.* **1003** (2010) 063. [arXiv: 0910.1601]

[5] B. Carter, X. Martin, "Dynamic Instability criterion for Circular String Loops", *Ann. Phys.* **227** (1993) 151-171. [hep-th/0306111]

[6] J. Stachel, "Thickenning the string: the perfect string dust", Phys. Rev. **D21** (1980) 2171-81.

[7] P.A.M. Dirac, "An extensible model of the electron", *Proc. Roy. Soc. Lond.* **A268** (1962) 57-67.

[8] T.W.B. Kibble, "Topology of cosmic domains and strings", *J. Phys.* **A9** ((1976) 1387-98.

[9] J.A. Schouten, *Ricci Calculus* (Springer, Heidelberg, 1954).

[10] B. Carter, M. Sakellariadou, X. Martin, "Cosmological expansion and thermodynamic mechanisms in cosmic string dynamics", *Phys. Rev.* **D50** (1994) 682-99.

[11] A. Vilenkin, "Cosmic string dynamics with friction", *Phys. Rev.* **D43** (1991) 1060-62.

[12] A. Achúcarro, J. Evans, P.K. Townsend, D.L. Wiltshire, "Super p-branes", *Phys. Lett.* **198 B** (1987) 441-446.

[13] I. Bars, C.N. Pope, "Anomalies in super p-branes", *Class. Quantum Grav.,* **5** (1988) 1157-1168.

[14] B. Carter, "Dynamics of cosmic strings and other brane models", in *Formation and Interactions of Topological Defects* (NATO ASI **B349**), ed. R. Brandenberger, A.-C. Davis, (Plenum, New York, 1995) 303-348. [arXiv: [hep-th/9611054]

[15] B. Carter, R.A. Battye, J.-P. Uzan, "Gradient formula for linearly self-interacting branes", *Commun. Math. Phys.* **235** (2003) 289-311 . [hep-th/0204042]

[16] R.A. Battye, B. Carter, A. Mennim, "Regularization of the linearized gravitational self-force for branes", *Phys. Rev. Lett.* **92** (2004) 201305. [hep-th/0312198]

[17] R.A. Battye, B. Carter, A. Mennim. "Linearized self-forces for branes", *Phys. Rev.* **D71** (2005) 104026. [hep-th/0412053]

[18] E. Witten, "Interacting field theory of open superstrings", *Nucl. Phys.* **B276** (1986) 291-324.

[19] C. Crncovic, E. Witten, "Covariant description of canonical formalism in geometric theories" in *300 years of Gravitation*, ed. S.W. Hawking, W. Israel (Cambridge U.P., 1987) 676-684.

[20] G.J Zuckerman, in *Mathematical elements of string theory*, ed. S.T. Yau (World scientific, Singapore, 1987).

[21] K-S. Soh, "Covariant symplectic structure of two-dimensional dilaton gravity" *Phys. Rev.* **D49** (1994) 1906-1911.

[22] R. Cartas-Fuentevilla, "Symplectic current for the field perturbatios in dilaton axion gravity coupled with Abelian fields" *Phys. Rev.***D57** (1998) 3443-3448.

[23] Y. Nutku, "Covariant symplectic structure of the complex Monge-Ampere equation" *Phys. Lett.***A268**(2000) 293. [hep-th/0004164]

[24] C. Rovelli, "Covariant Hamiltonian formalism for field theory: symplectic structure and Hamilton-Jacobi structure on the space G", *Lecture Notes in Physics* **633** (Springer, 2003) 36-62 [gr-qc/0207043]

[25] R. Cartas-Fuentevilla, "Identically closed two-form for covariant phase space quantisation of Dirac - Nambu - Goto p-branes in a curved space-time", *Phys. Lett.* **B536** (2002) 283 - 288. [hep-th/0204133]

[26] R. Cartas-Fuentevilla "Global symplectic potentials in the Witten covariant phase space for bosonc extendons" *Phys.Lett.* **B536** (2002) 289-293. [hep-th/0204135]

[27] B. Carter, D. Steer, "Symplectic structure for elastic and chiral conducting cosmic string models",*Phys. Rev.* **D 69** (2004) 125002. [hep-th/0302084]

[28] B. Carter, "Perturbation dynamics for membranes and strings governed by the Dirac - Goto - Nambu action in curved space", *Phys. Rev.* **D48** (1993) 4835-4838.

[29] B. Carter, "Poly-essential and general Hyperelastic World (brane) models", *Int. J. Theor. Phys.* **46** (2007) 2299-2312. [hep-th/0604157]

[30] J. Friedman, B.A. Schutz, "On the stability of relativistic systems" *Astrop. J.* **200** (1975) 204-220.

[31] R. A. Battye, B. Carter, "Gravitational perturbations of relativistic membranes and strings", *Phys. Letters* **B357** (1995) 29-35 [hep-th/9507059]

[32] R.A. Battye "Gravitational radiation and backreaction for cosmic strings", *DAMTP preprint* **R95/18** (1995).

[33] B. Carter, R.A. Battye, "Non-divergence of gravitational self interactions for Nambu-Goto strings", *Phys. Letter* **B 430** 49-53 [hep-th/9803012]

[34] A. Vilenkin, E.P.S. Shellard, *Cosmic strings and other topological defects* (Cambridge University Press, 1994) 215-216.

[35] B. Carter, "Transonic elastic model for wiggly Goto-Nambu string", *Phys. Rev. Letters* **B74** (1995) 3098-3101 [hep-th/9411231]

[36] P. Peter, "Superconducting cosmic string: Equation of state for spacelike and timelike current in the neutral limit" *Phys. Rev.* **D45** (1992) 1091-1102.

[37] E. Witten, "Superconducting cosmic strings", *Nucl. Phys.* **B249** (1995) 557-592.

[38] "Avoidance of collapse by circular current-carrying cosmic string loops", B. Carter, P. Peter & A. Gangui, *Phys. Rev.* **D55** (1997) 4647-4662. [hep-ph/9609401].

[39] B. Carter, P. Peter, "Supersonic string model for Witten vortices" *Phys. Rev* **D52** (1995) R1744-1748.

[40] B. Hartmann, B. Carter, "Logarithmic equation of state for superconducting cosmic strings", *Phys. Rev.* **D77** (2008) 103516 [arXiv:0803.0266]

[41] X. Martin, "Zones of dynamical instability for rotating string loops", *Phys. Rev.* **D50** (1994) 7479-7492.

Slow-roll Dark Energy

Takeshi Chiba,

Department of Physics, College of Humanities and Sciences,
Nihon University, Tokyo 156-8550, Japan

Abstract

We derive slow-roll conditions for thawing quintessence. We solve the equation of motion of ϕ for a Taylor expanded potential (up to the quadratic order) in the limit where the equation of state w is close to -1 to derive the equation of state as a function of the scale factor. We find that the evolution of ϕ and hence w are described by only two parameters, w_0 (the present-day value of w), and the K, which parametrizes the curvature of the potential, and $w(a)$ is model-independent. We derive observational constraints on these two parameters. We also derive the slow-roll conditions for a non-minimally coupled scalar field (extended quintessence) during the radiation/matter dominated era extending our previous results for thawing quintessence. We find that the ratio $\ddot{\phi}/3H\dot{\phi}$ becomes constant but negative, in sharp contrast to the ratio for the minimally coupled scalar field. We also find that $w(a)$ asymptotically approaches that of the minimally coupled thawing quintessence.

1 Introduction

It is my great pleasure to give my talk at this special occasion celebrating Prof. Maeda and Prof. Nakamura's 60th birthday. I have several joint papers with both of them about black holes and cosmic no hair conjecture, which I am very proud of. The topic I discuss is dark energy, about which I wrote several papers (including X-matter paper [1]) with Takashi Nakamura more than ten years ago when I was a postdoc at Yukawa Institute. More specifically, I consider slow-roll dark energy. Firstly I explain the motivation of my study and then I derive the slow-roll conditions of a certain type of scalar field dark energy models (called thawing model) and derive the equation of state of such a dark energy model. I also fit the equation of state to observational data and put constraints on the parameters involved in the equation of state. Next, I extend the dark energy model to include non-minimal coupling with gravity. I derive the slow-roll conditions of such a non-minimally coupled quintessence and find such a dark energy behaves very differently from a minimally coupled quintessence. I also find however that the equation of state approaches to that of minimally coupled quintessence. Finally I summarize my talk.

2 Slow-roll Dark Energy

There is strong evidence that the Universe is dominated by dark energy, and the current cosmological observations seem to be consistent with ΛCDM. The equations of state of dark energy, w, is close to -1 within 10% or less. However, how much is a dark energy model close to the cosmological constant? In order to quantify such "distance from the cosmological constant" in the dark energy theory space, we need to introduce a parametrization of the equation of state, $w(a)$, which parametrizes the deviation from the cosmological constant, $w = -1$. Moreover, since w is close to -1 This implies that even if a scalar field (dubbed "quintessence" [2]) plays the role of dark energy, it should roll down its potential slowly because its kinetic energy density should be much smaller than its potential. In this situation, as in the case of inflation, it is useful to derive the slow-roll conditions for quintessence because the dynamics of the scalar field can be discussed only by simple conditions without having to solve its equation of motion directly. Quintessence models are classified according to their motion [3]: In "thawing" models the scalar fields hardly move in the past and begin to roll down the potential recently, while in "freezing" models the scalar fields move in the opposite ways and gradually slow down the motion. We will mostly consider the slow-roll conditions for thawing models since the observational data already favor them and there

are several particle physics models for them. Note however that our consideration will not be limited to quintessence but will be applied to the case when the scalar fields which are subdominant components in the universe move slowly. Axions, curvatons, and moduli before the oscillation can be such fields.

2.1 Slow-roll Conditions

We first derive the slow-roll conditions for thawing quintessence models [4]. Working in units of $8\pi G = 1$, the basic equations in a flat universe are

$$\ddot{\phi} + 3H\dot{\phi} + V' = 0, \tag{1}$$

$$H^2 = \left(\frac{\dot{a}}{a}\right)^2 = \frac{1}{3}(\rho_B + \rho_\phi), \tag{2}$$

$$\dot{H} = -\frac{1}{2}\left((\rho_B + p_B) + (\rho_\phi + p_\phi)\right) = -\frac{1}{2}\left((1+w_B)\rho_B + \dot{\phi}^2\right), \tag{3}$$

where $V' = dV/d\phi$, $H = \dot{a}/a$ is the Hubble parameter with a being the scale factor, $\rho_B(p_B)$ is the energy density (pressure) of matter/radiation, $\rho_\phi = \dot{\phi}^2/2 + V(\phi)(p_\phi = \dot{\phi}^2/2 - V(\phi))$ is the scalar field energy density (pressure), and w_B is the equation of state of matter/radiation.

By slow-roll quintessence we mean a model of quintessence whose kinetic energy density is much smaller than its potential,

$$\frac{1}{2}\dot{\phi}^2 \ll V. \tag{4}$$

Unlike the case of inflation, we do not require that $\ddot{\phi}$ is smaller than the friction term $3H\dot{\phi}$ in Eq. (1) since H is not determined by the potential alone, but by the matter/radiation along with the scalar field energy density.

With fixed w_0, slowly rolling thawing models correspond to the equation of state $w = p_\phi/\rho_\phi$ very close to -1, so that the Hubble friction is not effective and hence $\ddot{\phi}$ is not necessarily small compared with $3H\dot{\phi}$ in Eq. (1). Slowly rolling freezing models correspond to models whose w is not so close to -1 compared with thawing models so that the Hubble friction is effective and $\ddot{\phi}$ is smaller than $3H\dot{\phi}$ in Eq. (1).

We derive the slow-roll conditions for thawing quintessence during the matter/radiation dominated epoch. We first introduce the following function :

$$\beta = \frac{\ddot{\phi}}{3H\dot{\phi}}. \tag{5}$$

As stated above, for thawing models, β is a quantity of $\mathcal{O}(1)$. We assume β is an approximately constant in the sense $|\dot{\beta}| \ll H|\beta|$, and the consistency of the assumption will be checked later. In terms of β, using Eq. (1), $\dot{\phi}$ is written as

$$\dot{\phi} = -\frac{V'}{3(1+\beta)H}, \tag{6}$$

and the slow-roll condition Eq. (4) becomes

$$\epsilon := \frac{V'^2}{6H^2V} \ll 1, \tag{7}$$

where we have omitted $1+\beta$ since it is an $\mathcal{O}(1)$ quantity and introduced the factor of $1/6$ so that ϵ coincides with the inflationary slow-roll parameter, $\epsilon = \frac{1}{2}(V'/V)^2$, if the scalar field dominates the expansion: $H^2 \simeq V/3$. Eq. (7) is a quintessence counterpart of the inflationary slow-roll condition $(V'/V)^2 \ll 1$.

Similar to the case of inflation, the consistency of Eq. (5) and Eq. (1) should give the second slow-roll condition. In fact, from the time derivative of Eq. (6)

$$\ddot{\phi} = \frac{V''V'}{9(1+\beta)^2H^2} - \frac{1+w_B}{2(1+\beta)}V' + \frac{\dot{\beta}V'}{3(1+\beta)^2H}, \tag{8}$$

where we have used $\dot{H}/H^2 \simeq -3(1+w_B)/2$ from Eq. (2) and Eq. (3). On the other hand, from Eq. (5) and Eq. (6), $\ddot{\phi} = 3\beta H\dot{\phi} = -\beta V'/(1+\beta)$, and so we obtain

$$\beta = -\frac{V''}{9(1+\beta)H^2} + \frac{(1+w_B)}{2} - \frac{\dot{\beta}}{3(1+\beta)H} \simeq -\frac{V''}{9(1+\beta)H^2} + \frac{(1+w_B)}{2}, \tag{9}$$

where we have used $\dot{\beta} \ll H\beta$. While the left-hand-side of Eq. (9) is an almost time-independent quantity by assumption, the first term in the right-hand-side is a time-dependent quantity in general. Therefore the equality holds if the first term is negligible:

$$\eta := \frac{V''}{3H^2}; \qquad |\eta| \ll 1, \tag{10}$$

so that β becomes

$$\beta = \frac{1+w_B}{2}, \tag{11}$$

or the left-hand-side is negligible:

$$|\beta| \ll 1, \tag{12}$$

so that

$$\eta = \frac{3}{2}(1+w_B). \tag{13}$$

The former condition corresponds to the slow-roll thawing models, while the latter corresponds to the slow-roll freezing models. β given by Eq. (11) is an approximately constant, which is consistent with our assumption. Here the factor $1/3$ is introduced in Eq. (10) so that η coincides with the inflationary slow-roll parameter, $\eta = V''/V$, if $H^2 \simeq V/3$. Eq. (10) is a quintessence counterpart of the inflationary slow-roll condition $|V''|/V \ll 1$.

Eq. (7) and Eq. (10) constitute the slow-roll conditions for thawing quintessence during the matter/radiation epoch. Moreover once the universe becomes dominated by the scalar field, the two conditions reduce to the usual inflationary slow-roll conditions from $H^2 \simeq V/3$. Therefore, these conditions (Eq. (7) and Eq. (10)) are the slow-roll conditions for thawing quintessence at all times, both during the matter/radiation era and during the scalar field dominated era. Note that since $H^2 \gtrsim V/3$, the inflationary slow-roll conditions are sufficient conditions for slow-roll thawing quintessence during the matter/radiation era, not necessary conditions. In Fig. 1, the evolution of β is shown for a thawing quintessence model ($V = M^4(1-\cos\phi)$). The evolution of β agrees nicely with Eq. (11).

2.2 Equation of State

Next we derive general solutions of ϕ in the limit of $|1+w| \ll 1$ and derive w as a function of a. To do so, we first note that the Hubble friction term in Eq. (1) can be eliminated by the following change of variable

$$u = (\phi - \phi_i)a^{3/2}, \tag{14}$$

where ϕ_i is an arbitrary constant, which is introduced for later use, and then Eq. (1) becomes

$$\ddot{u} + \frac{3}{4}(p_B + p_\phi)u + a^{3/2}V' = 0. \tag{15}$$

We assume a universe consisting of matter and quintessence with $w \simeq -1$. Then the pressure is well approximated by a constant: $p_B + p_\phi \simeq p_\phi \simeq -\rho_{\phi 0}$, where $\rho_{\phi 0}$ is the nearly constant density contributed by the quintessence in the limit $w \simeq -1$. Eq. (15) then becomes

$$\ddot{u} - \frac{3}{4}\rho_{\phi 0}u + a^{3/2}V' = 0. \tag{16}$$

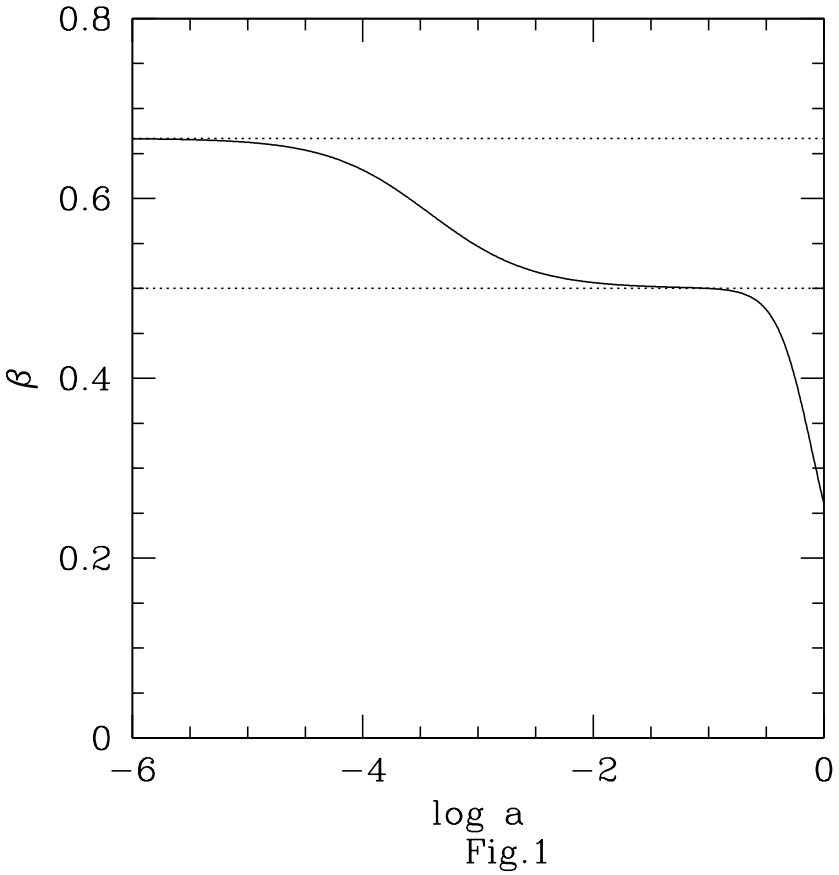

Figure 1: β as a function of a for thawing quintessence model with the axion-like potential $V = M^4(1-\cos\phi)$. The dotted lines are $\beta = 2/3, 1/2$, respectively.

Since we consider a slow-roll scalar field, the potential may be generally expanded around some value ϕ_i, which we identify with the initial value, in the form (up to the quadratic order)

$$V(\phi) = V(\phi_i) + V'(\phi_i)(\phi - \phi_i) + \frac{1}{2}V''(\phi_i)(\phi - \phi_i)^2. \tag{17}$$

Substituting the expansion Eq. (17) into Eq. (16) and taking $\rho_{\phi 0} = V(\phi_i)$ gives

$$\ddot{u} + \left(V''(\phi_i) - \frac{3}{4}V(\phi_i)\right) u = -V'(\phi_i)a^{3/2}. \tag{18}$$

Being consistent with $|w+1| \ll 1$, we assume $a(t)$ is well approximated by its value in the ΛCDM model which is given by

$$a(t) = \left(\frac{1-\Omega_{\phi 0}}{\Omega_{\phi 0}}\right)^{1/3} \sinh^{2/3}(t/t_\Lambda), \tag{19}$$

where $\Omega_{\phi 0}$ is the present-day value of density parameter of quintessence, $a = 1$ at present, and t_Λ is defined as $t_\Lambda = 2/\sqrt{3\rho_{\phi 0}} = 2/\sqrt{3V(\phi_i)}$. Since Eq. (18) is a second order linear ordinary differential equation, it can be solved analytically. The solution, which is valid if the initial time is much earlier than the present time, is [4]

$$\phi(t) = \phi_i + \frac{V'(\phi_i)}{V''(\phi_i)}\left(\frac{\sinh(kt)}{kt_\Lambda \sinh(t/t_\Lambda)} - 1\right), \tag{20}$$

where $k = \sqrt{(3/4)V(\phi_i) - V''(\phi_i)}$. Then the equation of state becomes [4]

$$1 + w(a) = (1+w_0)a^{3(K-1)}\left(\frac{(K-F(a))(F(a)+1)^K + (K+F(a))(F(a)-1)^K}{(K-\Omega_{\phi 0}^{-1/2})(\Omega_{\phi 0}^{-1/2}+1)^K + (K+\Omega_{\phi 0}^{-1/2})(\Omega_{\phi 0}^{-1/2}-1)^K}\right)^2, \tag{21}$$

where

$$K = kt_\Lambda = \sqrt{1 - \frac{4}{3}\frac{V''(\phi_i)}{V(\phi_i)}}, \tag{22}$$

$$F(a) = \sqrt{1 + (\Omega_{\phi 0}^{-1} - 1)a^{-3}}. \tag{23}$$

We also studied the slow-roll conditions for k-essence [5] and find that the equation of state obeys the same functional form as Eq. (23) since the k-essence Lagrangian can be Taylor-expanded for small kinetic energy, $X = \dot{\phi}^2/2$, if it is analytical

$$p(X,\phi) = p(0,\phi) + (\partial p/\partial X)X + \ldots, \tag{24}$$

and it reduces to that of canonical scalar field by field redefinition [6].

2.3 Observational Constraints

The results of this paper indicate that Eq. (21) applies both to quintessence models and to a subset of k-essence models with $w \simeq -1$. Hence Eq. (21) is a useful and physically well-motivated parametrization for $w(a)$ that can be compared with the observations. So, in this section, we present the observational constraints on the equation of state parameters w_0 and on K [6].

First, we note that the cosmological constant corresponds to a *line* in the (w_0, K) plane: $w_0 = -1$ *irrespective of* K. This can be understood for a canonical scalar field by noting that $w_0 = -1$ corresponds to the case where the scalar field sits at the minimum ($K < 1$) or the maximum ($K > 1$) of the potential.

As observational data we consider the recent compilation of 397 Type Ia supernovae (SNIa), called the Constitution set with the light curve fitter SALT, by Hicken et al. [7] and the measurements of BAO from the recent SDSS data [8].

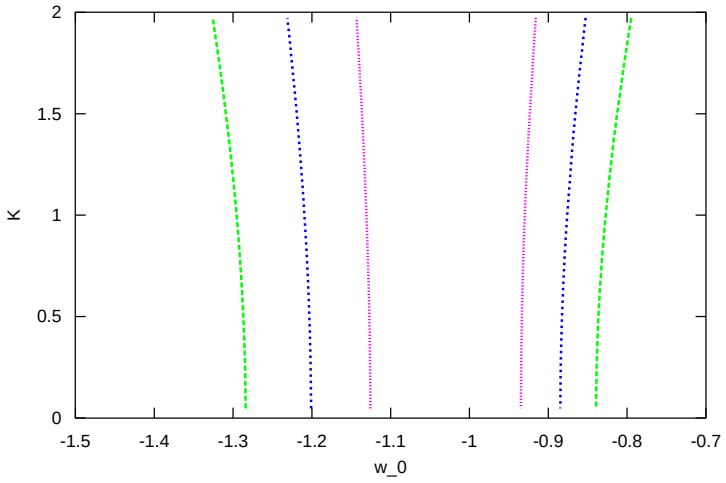

Figure 2: Contours at 68.3% (red, inner), 95.4% (blue, middle), 99.7% (green, outer) confidence level on w_0 and K. The Constitution SN set was combined with BAO constraint.

BAO measurements from the SDSS data provide a constraint on the distance parameter A defined by

$$A(z) = (\Omega_m H_0^2)^{1/2} \left(\frac{1}{H(z)z^2}\right)^{1/3} \left(\int_0^z \frac{dz'}{H(z')}\right)^{2/3} \tag{25}$$

to be $A(z = 0.35) = 0.493 \pm 0.017$ [8].

The joint constraints from SNIa and BAO are shown in Fig. 2. We marginalize over Ω_m to derive the constraints. The allowed range of w_0 is narrow: $-1.14 \lesssim w_0 \lesssim -0.92(1\sigma)$. We find that the cosmological constant $w_0 = -1$ is fully consistent with the current data. Note that K, which parametrizes the curvature of $V(\phi_i)$, is not well-constrained by current SNIa and BAO data.

3 Slow-roll Extended Quintessence

In this section, we further study the slow-roll conditions for a scalar field *non-minimally coupled* to gravity (called extended quintessence) and examine to what extent the results for minimally coupled quintessence are universal [9].

We consider the cosmological dynamics described by the action

$$S = \int d^4x\sqrt{-g}\left[\frac{1}{2\kappa^2}R - F(\phi)R - \frac{1}{2}(\nabla\phi)^2 - V(\phi)\right] + S_m. \tag{26}$$

Here $\kappa^2 \equiv 8\pi G_{bare}$ is the bare gravitational constant, $F(\phi)$ is the non-minimal coupling and S_m denotes the action of matter (radiation and nonrelativistic particle).

The equations of motion in a flat FRW universe model are

$$\ddot{\phi}+ \quad 3H\dot{\phi} \quad +V'(\phi)+6F'(\phi)\left(\dot{H}+2H^2\right)=0, \tag{27}$$

$$3H^2 \quad = \quad \kappa^2\left(\rho_B+\frac{1}{2}\dot{\phi}^2+U\right) =: \kappa^2(\rho_B+\rho_\phi) =: \kappa^2\rho_{\rm tot}, \tag{28}$$

$$2\dot{H} \quad = \quad -\kappa^2\left(\rho_B+p_B+\rho_\phi+\dot{\phi}^2/2-V-2\ddot{F}-4H\dot{F}-2F(2\dot{H}+3H^2)\right) \tag{29}$$

$$=: \quad -\kappa^2\left((1+w_B)\rho_B+\rho_\phi+p_\phi\right),$$

$$U \quad := \quad V+6H\left(\dot{F}+HF\right), \tag{30}$$

where $' = d/d\phi$, ρ_B and p_B denote the background (radiation and matter) energy density and pressure, respectively, and $w_B = p_B/\rho_B$ is the equation of state of radiation and matter.

3.1 Slow-roll Conditions

We derive the slow-roll conditions for extended (thawing) quintessence during the matter/radiation dominated epoch [9]. Eq. (27) then becomes

$$\ddot{\phi}+3H\dot{\phi}+V'_{\rm eff}=0, \tag{31}$$

$$V'_{\rm eff} \equiv V'+3F'H^2(1-3w_B). \tag{32}$$

By "slow-roll", we mean that the movement of ϕ during one Hubble time is much smaller than ϕ. On the other hand, the condition that the kinetic energy density of the scalar field is much smaller than the potential U (Eq. (30)) in the energy density of the scalar field ρ_ϕ (Eq. (28))

$$\frac{1}{2}\dot{\phi}^2 \ll U, \tag{33}$$

implies that

$$\dot{\phi}^2H^{-2} \ll \kappa^{-2} \lesssim \phi^2, \tag{34}$$

from $U \ll \rho_{\rm tot} \simeq \kappa^{-2}H^2$ if $\kappa\phi \gtrsim 1$. Hence we regard Eq. (33) as the slow-roll condition.

We derive the consistent set of the slow-roll conditions. We again consider the ratio,

$$\beta = \frac{\ddot{\phi}}{3H\dot{\phi}}. \tag{35}$$

For slow-roll (thawing) models, we first assume that β is an $\mathcal{O}(1)$ approximately constant quantity not equal to -1 in the sense $|\dot{\beta}| \ll H|\beta|$, and the consistency of the assumption will be checked later. In terms of β, using Eq. (31), $\dot{\phi}$ is rewritten as

$$\dot{\phi} = -\frac{V'_{\rm eff}}{3(1+\beta)H}, \tag{36}$$

and the condition Eq. (33) gives the first one of the slow-roll conditions

$$\epsilon := \frac{V'^2_{\rm eff}}{6H^2U} \ll 1, \tag{37}$$

where we have omitted $1+\beta$ since it is an $\mathcal{O}(1)$ quantity and introduced the factor of $1/6$ in ϵ so that ϵ coincides with the inflationary slow-roll parameter, $\epsilon = \frac{1}{2}\left(\frac{V'}{\kappa V}\right)^2$, if the scalar field dominates the expansion: $H^2 \simeq \kappa^2V/3$ and $U \simeq V_{\rm eff} \simeq V$.

Similar to the case of inflation, the consistency of Eq. (35) and Eq. (31) should give the second slow-roll condition. In fact, from the time derivative of Eq. (36)

$$\ddot{\phi} \quad = \quad -\frac{\dot{H}}{H}\dot{\phi}-\frac{V''}{3(1+\beta)H}\dot{\phi}-\frac{F''H(1-3w_B)}{1+\beta}\dot{\phi}+\frac{3F'H^2(1-3w_B)}{1+\beta}-\frac{\dot{\beta}}{1+\beta}\dot{\phi}, \tag{38}$$

where we have used $(H^2(1-3w_B))^{\cdot} \simeq -3H^3(1-3w_B)$. On the other hand, from Eq. (35) and Eq. (36), $\ddot{\phi} = 3\beta H\dot{\phi} = -\beta V'_{\rm eff}/(1+\beta)$, and so we obtain

$$\begin{aligned}\beta = \frac{\ddot{\phi}}{3H\dot{\phi}} &\simeq -\frac{\dot{H}}{3H^2} - \frac{V''}{9(1+\beta)H^2} - \frac{F''(1-3w_B)}{3(1+\beta)} - \frac{V'_{\rm eff}-V'}{V'_{\rm eff}}, \\ &= \frac{w_B-1}{2} - \frac{V''}{9(1+\beta)H^2} - \frac{F''(1-3w_B)}{3(1+\beta)} + \frac{V'}{V'_{\rm eff}},\end{aligned} \tag{39}$$

where we have used $3F'H^2(1-3w_B) = V'_{\rm eff} - V'$ and $|\dot{\beta}| \ll H|\beta|$. While the left-hand-side of Eq. (39) is assumed to be an almost time-independent quantity, the terms other than the first in the right-hand-side are time-dependent quantities in general. Therefore the assumption is consistent if they are negligible:[1]

$$\eta := \frac{V''}{3H^2}; \qquad |\eta| \ll 1 \qquad \text{and} \qquad |F''(1-3w_B)| \ll 1 \qquad \text{and} \qquad \left|\frac{V'}{V'_{\rm eff}}\right| \ll 1, \tag{40}$$

so that β becomes

$$\beta = \frac{w_B-1}{2}. \tag{41}$$

β given by Eq. (41) is consistently an $\mathcal{O}(1)$ constant not equal to -1. Here the factor $1/3$ is introduced in η so that η coincides with the inflationary slow-roll parameter, $\eta = V''/\kappa^2 V$, if $H^2 \simeq \kappa^2 V/3$. The conditions in Eq. (40) are quintessence counterparts of the inflationary slow-roll condition $|V''|/\kappa^2 V \ll 1$.

Eq. (37) and Eq. (40) constitute the slow-roll conditions for extended quintessence during matter/radiation epoch. β (Eq. (41)) is negative and is quite different from that for a minimally coupled scalar field (Eq. (11)) which is positive. Therefore, this can be a discriminating probe of the non-minimal coupling of the scalar field. Although it may be difficult to determine the thawing dynamics from distance measurements, the ratio β may be determined by measuring the time variation of the fine structure constant α if ϕ induces such a variation and α depends linearly on ϕ.

In Fig. 3, the evolution of β is shown for a massive scalar field ($V = \frac{1}{2}m^2\phi^2$) with a non-minimal coupling $F = \frac{1}{2}\xi\phi^2$ with $\xi = 10^{-2}$. The evolution of β agrees nicely with Eq. (41).

3.2 The Equation of State

Next we derive analytically the equation of state [9]. We consider the case that the non-minimal coupling is given by $F(\phi) = \frac{1}{2}\xi\phi^2$. In terms of u defined in Eq. (14), the equation of motion Eq. (27) becomes

$$\ddot{u} + \left[-\frac{3}{2}\left(\dot{H} + \frac{3}{2}H^2\right) + 6\xi\left(\dot{H} + 2H^2\right)\right]u + \left[V' + 6\xi\phi_i\left(\dot{H} + 2H^2\right)\right]a^{\frac{3}{2}} = 0. \tag{42}$$

Since we are interested in the slow-roll motion of the quintessence field ϕ, we may expand the potential $V(\phi)$ around the initial value ϕ_i up to the quadratic order as in Eq. (17). Moreover we assume that the scale factor $a(t)$ is well approximated by that in the ΛCDM model Eq. (19). Then the approximate solution, which is valid as far as $t \gg t_\Lambda$ and $t \gg t_i$, is given by [9]

$$\phi(t) = \phi_i + \frac{V'(\phi_i) + 4\xi\kappa^2\phi_i V(\phi_i)}{V''(\phi_i)}\left[\frac{\sinh(kt)\cosh\left(\frac{t_i}{t_\Lambda}\right)}{kt_\Lambda\sinh\left(\frac{t}{t_\Lambda}\right)} - 1\right], \tag{43}$$

with $k \equiv \sqrt{\left(\frac{3}{4} - 4\xi\right)\kappa^2 V(\phi_i) - V''(\phi_i)}$. The equation of state w is then given by [9]

$$1 + w = (1+w_0)a^{3(K-1)}\left[\frac{(K-F(a))(F(a)+1)^K + (K+F(a))(F(a)-1)^K}{(K-\Omega_{\phi 0}^{-1/2})(\Omega_{\phi 0}^{-1/2}+1)^K + (K+\Omega_{\phi 0}^{-1/2})(\Omega_{\phi 0}^{-1/2}-1)^K}\right]^2, \tag{44}$$

[1] The exception is the case of $F'' = $ const. In this case F'' needs not to be small. For example, if $F = \frac{1}{2}\xi\phi^2$, then β satisfies $\beta = -\frac{1}{3}$ during the radiation era and $\beta = -\frac{1}{2} - \frac{\xi}{3(1+\beta)}$ so that $\beta = \frac{-9+\sqrt{9-48\xi}}{12}$ during the matter era.

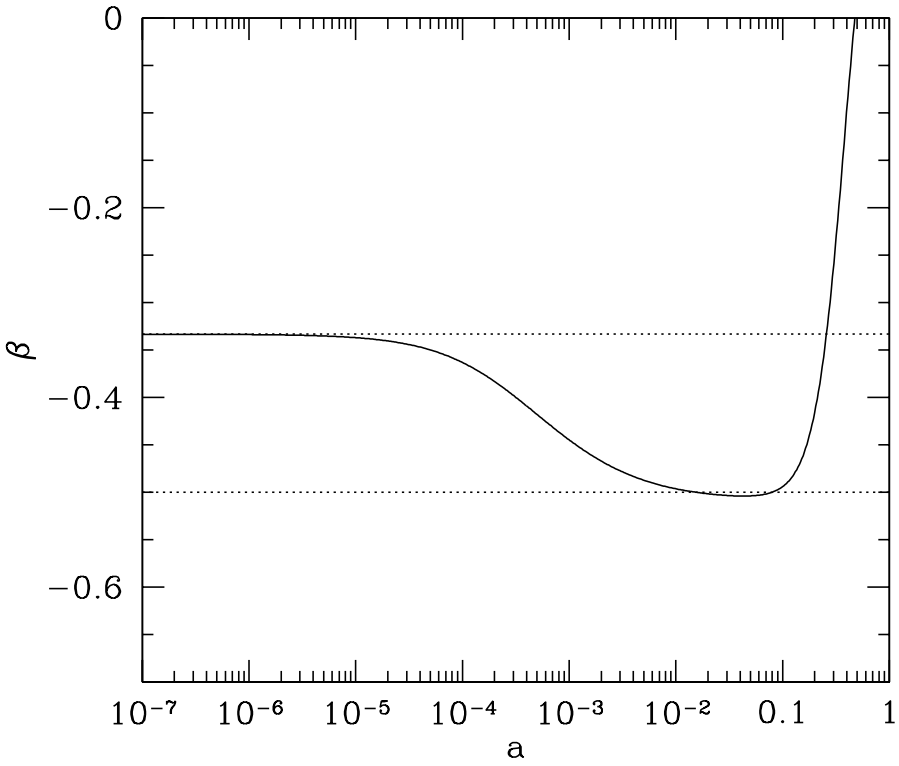

Figure 3: β as a function of a for a massive scalar field model with $F = \frac{1}{2}\xi\phi^2$ with $\xi = 10^{-2}$. The dotted lines are $\beta = -\frac{1}{3}, -\frac{1}{2}$, respectively.

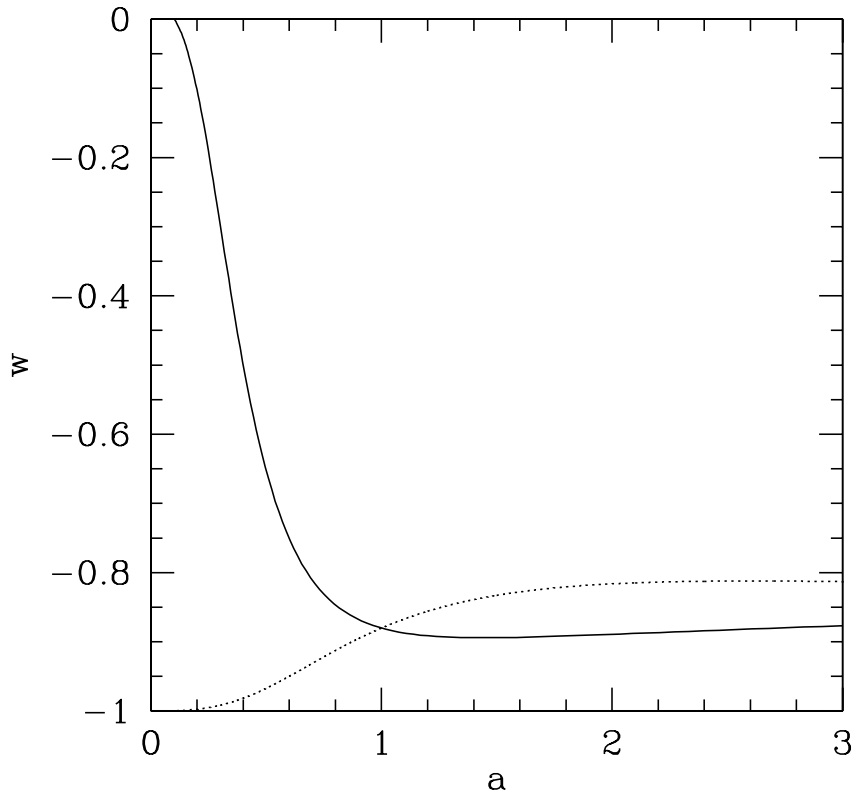

Figure 4: w_ϕ as a function of a. The solid line is the numerical solution, while the dotted line is the asymptotic solution Eq. (44).

where $K = kt_\Lambda = \sqrt{1 - \frac{16\xi}{3} - \frac{4}{3}\frac{V''(\phi_i)}{\kappa^2 V(\phi_i)}}$. We have normalized the expression to $w_{\phi 0}$ in Eq. (44). This expression completely coincides with that in the minimal coupling Eq. (21). It is noted, however, that this expression applies only for $t \gtrsim t_\Lambda$ and that the definition of K is different but, when ξ approaches 0, reduces to that of the minimally coupled scalar field.

In Fig. 4, w_ϕ is shown as a function of a. We find that apart from the slight offset w_ϕ approaches the asymptotic solution given by Eq. (44). This, together with [6], makes the functional form of $w_\phi(a)$, Eq. (21), even more useful.

4 Summary: What is the Kepler's law of Dark Energy?

We have derived slow-roll conditions for thawing quintessence models, Eq. (7) and Eq. (10). We have also solved the equation of motion of the slow-roll thawing quintessence and obtained the equation of state as a function of the scale factor $w(a)$, Eq. (21), which involves only two parameters. We have found that this $w(a)$ is in general not fit by a linear evolution in a which is frequently used in the literature. We have also found that this $w(a)$ applies to quintessence models and to k-essence models with $w \approx -1$ and also to extended quintessence models. Applying this parametrization to SNIa data and BAO, we find that the present-day value of w is constrained to lie near -1, while the curvature parameter K is poorly constrained by the observations. Further, we see that the cosmological constant limit of these models is consistent with the current data. As an extension, we have also derived the slow-roll conditions for non-minimally coupled scalar field during the radiation/matter dominated epoch. We have also derived

the slow-roll equation of motion of the scalar field and found that the ratio $\ddot{\phi}/3H\dot{\phi}$ becomes constant but negative, in sharp contrast to the result for the minimally coupled scalar field. This ratio can be a discriminating probe of the non-minimal coupling of the scalar field.

Finally, I would like to ask a provocative question. When I teach classical mechanics to freshman, I am always impressed by the role which the Kepler's laws of the planetary motion played in formulating the Newtonian mechanics. As we know, every law is essential in establishing the universal attractive force of gravity: the second law shows that the force depends only on the distance between the planet and the Sun (central force); from the first law, the force is found to be proportional to inverse square of the distance; the third law establishes the force depends only on the mass of each body with the universal constant: the Newton's constant. Being impressed by the success of Kepler's law as a phenomenological law, I cannot help asking "What is the Kepler's law of dark energy (or the Universe)?".

Truly finally, I would like to say "Happy birth day to Prof. Maeda and Prof. Nakamura!"

References

[1] T. Chiba, N. Sugiyama and T. Nakamura, Mon. Not. Roy. Astron. Soc. **289**, L5 (1997) [arXiv:astro-ph/9704199]; T. Chiba, N. Sugiyama and T. Nakamura, Mon. Not. Roy. Astron. Soc. **301**, 72 (1998) [arXiv:astro-ph/9806332].

[2] R. R. Caldwell, R. Dave and P. J. Steinhardt, Phys. Rev. Lett. **80**, 1582 (1998).

[3] R. R. Caldwell and E. V. Linder, Phys. Rev. Lett. **95**, 141301 (2005) [arXiv:astro-ph/0505494].

[4] T. Chiba, Phys. Rev. D **79**, 083517 (2009) [Erratum-ibid. D **80**, 109902 (2009)] [arXiv:0902.4037 [astro-ph.CO]].

[5] T. Chiba, T. Okabe and M. Yamaguchi, Phys. Rev. D **62**, 023511 (2000) [arXiv:astro-ph/9912463]; C. Armendariz-Picon, V. F. Mukhanov and P. J. Steinhardt, Phys. Rev. Lett. **85**, 4438 (2000) [arXiv:astro-ph/0004134].

[6] T. Chiba, S. Dutta and R. J. Scherrer, Phys. Rev. D **80**, 043517 (2009) [arXiv:0906.0628 [astro-ph.CO]].

[7] M. Hicken *et al.*, Astrophys. J. **700**, 1097 (2009) [arXiv:0901.4804 [astro-ph.CO]].

[8] B. A. Reid *et al.*, arXiv:0907.1659 [astro-ph.CO]; W. J. Percival *et al.*, arXiv:0907.1660 [astro-ph.CO].

[9] T. Chiba, M. Siino and M. Yamaguchi, Phys. Rev. D **81**, 083530 (2010) [arXiv:1002.2986 [astro-ph.CO]].

Applications of hidden symmetries to black hole physics

Valeri Frolov[1]

Institute of Theoretical Physics, Department of Physics University of Alberta, Edmonton, Alberta, T6G 2G7, CANADA

Abstract

This work is a brief review of applications of hidden symmetries to black hole physics. In physics and mathematics the symmetry allows one to simplify a problem, and often to make it solvable. According to the Noether theorem symmetries are responsible for conservation laws. Besides evident (explicit) spacetime symmetries, responsible for conservation of energy, momentum, and angular momentum of a system, there also exist what is called hidden symmetries, which are connected with higher order in momentum integrals of motion. A remarkable fact is that black holes in four and higher dimensions always possess a set ('tower') of explicit and hidden symmetries which make the equations of motion of particles and light completely integrable. The paper gives a general review of the recently obtained results.

1 Introduction

In this paper we discuss higher dimensional rotating black holes and their properties. We consider black holes with the spherical topology of the horizon in a spacetime which is either asymptotically flat (vacuum) or (Anti)deSitter (with cosmological constant). We demonstrate that such solutions of the Einstein equations always possess a "tower" of symmetries, which make the equations of geodesic motion completely integrable. This 'tower' is generated by a single object, which we call a *principal conformal Killing-Yano tensor*. This object is responcible for a set of Killing vectors reflecting a spacetime symmerty. It also generates a set of Killing tensors, connected with hidden symmetries of the spacetime. The corresponding conserved quantities, which are first and second order in the momentum, form a complete set of integrals of motion which make the geodesic equation completely integrable. The purpose of the paper is to describe a general scheme of this construction, and to discuss its application to concrete problems connected with particle motion and field propagation in the higher dimensional black holes. We also describe a class of metrics which admit the principal conformal Killing-Yano tensor and its generalizations.

2 Complete integrability

2.1 Phase space

Let us first remind three related notions which play an important role in study of dynamical systems: (i) complete integrability, (ii) separation of variables, and (iii) hidden symmetries (for more details see [1, 2]).

A *phase space* is a set of three items $\{M^{2m}, \Omega, H\}$. M^{2m} is a $2m-$dimensional differential manifold. A symplectic form Ω is a closed, $d\Omega = 0$, non-degenerate 2-form. The non-degeneracy means that the corresponding matrix of its coefficient has the rank $2m$. Locally $\Omega = 0$ can be presented in the form

$$\Omega = d\alpha\,, \tag{1}$$

where α is a 1-form. H is a scalar function on M^{2m} called a *Hamiltonian*. We denote coordinates on M^{2m} by z^A $(A = 1, \dots, 2m)$. A set of coordinates which covers all the manifold is called an *atlas*.

[1]Email address: vfrolov@ualberta.ca

Since the symplectic form is non-degenerate, the tensor Ω_{AB} has an inverse one Ω^{AB}, defined by the relation $\Omega^{AB}\Omega_{BC} = \delta^A_C$. The tensors Ω_{AB} and Ω^{AB} can be used to relate tensors with upper and lower position of indices. For example,

$$\eta^A = \Omega^{AB} H_{,B} \tag{2}$$

is a vector generating the Hamiltonian flow. The equation of motion of a particle in the phase space is

$$\dot{z}^A = \eta^A \,. \tag{3}$$

Poisson bracket for two functions on the phase space A and B is defined as

$$\{A, B\} = \Omega^{AB} A_{,A} B_{,B} \,. \tag{4}$$

One says that these function are in *involution* if their Poisson bracket vanishes. The Poisson brackets for any three functions A, B, and C on the symplectic manifold obey the *Jacobi identity*

$$\{\{A, B\}, C\} + \{\{B, C\}, A\} + \{\{C, A\}, B\} = 0 \,. \tag{5}$$

If $F(z)$ is a function on the phase space, the equation of motion Eq.(3) determines its evolution $F_t = F(z(t))$

$$\dot{F}_t = \{H, F_t\} \,. \tag{6}$$

A function F for which $\{H, F\} = 0$ is an integral of motion of the Hamiltonian system. The Hamiltonian itself is a trivial integral of motion.

According to *Darboux theorem*, in the vicinity of any point of the phase space it is always possible to choose *canonical coordinates* $z^A = (q_1, q_2, \ldots, q_m, p_1, p_2, \ldots, p_m)$ in which the symplectic form is

$$\Omega = \sum_{i=1}^{m} dp_i \wedge dq_i \,. \tag{7}$$

In such canonical coordinates many relations are simplified and take a well known form. A set of canonical coordines which covers the phase space is called a *canonical atlas*.

2.2 Integrability

Integrability of equations of a dynamical system generically means that these equations can be solved by quadratures. Integrability is linked to 'existence of constants of motion'. For the integrability it is important to know: (i) How many constants of motion exist? (ii) How precisely are they related? and (iii) How the phase space is foliated by their level sets?

A system of differential equations is said to be integrable by quadratures if its solution can be found after a finite number of steps involving algebraic operations and integration. The following theorem (Bour, 1855; Liouville, 1855) establishes conditions required for the complete integrability of a Hamiltoniam system:

If a Hamiltonian system with m degrees of freedom has m integrals of motion $F_1 = H, F_2, \ldots, F_m$ in involution which are functionally independent on the intersection sets of the m functions, $F_i = f_i$, the solutions of the corresponding Hamiltonian equations can be found by quadratures.

The main idea behind Liouville's theorem is that the first integrals of motion F_i can be used as m coordinates. The involution condition implies that the m vector fields generated by gradients of F_i commute with each other and provide a choice of canonical coordinates. In these coordinates, the Hamiltonian is effectively reduced to a sum of m decoupled Hamiltonians that can be integrated.

We denote by M_f an intersection of the level sets $F_i = f_i$ for m integrals of motion (see Figure 1). Since the integrals of motion are independent, the tangent to M_f vectors $X^A_i = \Omega^{AB} F_{i,B}$ are linearly independent and M_f is a $m-$dimensional submanifold of the phase space. The condition that the integrals of motion are in involution implies

$$[X_i, X_j] = 0 \,. \tag{8}$$

One also has

$$\Omega_{AB} X^A_i X^B_j = \{F_i, F_j\} = 0 \,. \tag{9}$$

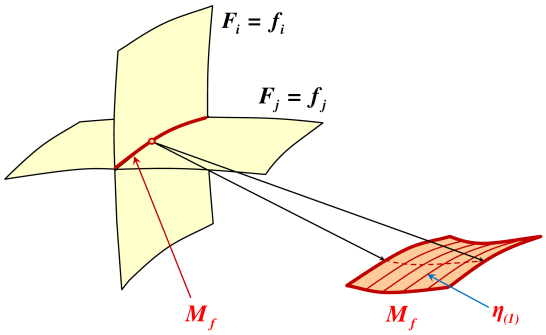

Figure 1: Illustration to the proof of Liouville theorem.

Let us use the equations $F_i(p,q) = f_i$ to get $p_i = p_i(f,q)$. Denote

$$S(F,q) = \int_{q^0}^{q} \sum_{i=1}^{m} p_i(f,q) dq_i \,. \tag{10}$$

The integral is taken over a path on M_f connecting two its points q^0 and q. The relation Eq.(9) implies that $S(F,q)$ does not depend on the choice of the path. Denote

$$\Psi_i = \frac{\partial S}{\partial F_i} \,, \tag{11}$$

then

$$dS = \sum_{i=1}^{m} \left(\Psi_i dF_i + p_i dq_i \right) \,. \tag{12}$$

Since the symplectic form Ω is closed, one has $d^2 S = 0$ and hence

$$\Omega = \sum_{i=1}^{m} dp_i \wedge dq_i = \sum_{i=1}^{m} d\Psi_i \wedge dF_i \,. \tag{13}$$

This result means that there exists a canonical transformation (p_i, q_i) to (F_i, Ψ_i). To obtain 'new' canonical coordinates two operations are required: (1) finding of $p_i = p_i(f,q)$, and (2) calculation of some integrals. In the new variables the Hamiltonian equations take the form

$$\dot{F}_i = \{H, F_i\} = 0 \,, \tag{14}$$

$$\dot{\Psi}_i = \{H, \Psi_i\} = \frac{\partial H}{\partial F_i} = \delta_i^1 \,. \tag{15}$$

The solution of this system is trivial

$$F_i = \text{const} \,, \qquad \Psi_i = a_i + \delta_i^1 t \,. \tag{16}$$

Complete integrability and chaotic motion are at the two ends of 'properties' of a dynamical system. The integrability is exceptional, while the chaoticity is generic. In all cases, integrability seems to be deeply related to some symmetry, which might be partially hidden. The existence of integrals of motion reflects the symmetry.

Important known examples of completely integrable mechanical systems include:

1. Motion in Euclidean space under a central potential;
2. Motion in the two Newtonian fixed centers;
3. Geodesics on an ellipsoid;
4. Motion of a rigid body about a fixed point;
5. Neumann model[2].

3 Separation of variables and integrability

Complete integrability of the Hamiltonian systems is closely related with the separation of variables in the Hamilton-Jacobi equation. For a Hamiltonian $H(P,Q)$, $P = p_1,\dots,p_m$ and $Q = q_1,\dots,q_m$, the *Hamilton-Jacobi equation* is

$$H(\partial_Q S, Q) = 0\,, \qquad \partial_Q S = (\partial_{q_1} S,\dots,\partial_{q_m} S)\,. \tag{18}$$

If a variable q_1 and a derivative $\partial_{q_1} S$ enter this equation in a form of single expression $\Phi_1(\partial_{q_1} S, q_1)$, than one says that the variable q_1 is separated. In such a case one may try to search a solution in the form

$$S = S_1(q_1) + S'(q_2,\dots,q_m)\,. \tag{19}$$

Putting

$$\Phi_1(\partial_{q_1} S, q_1) = C_1\,, \tag{20}$$

one obtains an equation with a less number of variables

$$H_1(\partial_{q_2} S',\dots,\partial_{q_m} S', q_2,\dots,q_m; C_1) = 0\,. \tag{21}$$

Let $S'(q_2,\dots,q_m;C_1)$ be a solution of this equation depending on a parameter C_1, then Eq.(19) is a solution of Eq.(18) when S_1 obeys an ordinary differential equation Eq.(20), which is easily solvable by quadratures. If a variable q_2 can be separated in a new equation Eq.(21) one can repeat this procedure again. One says that the Hamilton-Jacobi equation Eq.(18) allows a *complete separation of variables* if after m steps we obtain a solution of the initial equation Eq.(18) which contains m constants C_i

$$S = S_1(q_1, C_1) + S_2(q_2; C_1, C_2) + \ldots + S_m(q_m; C_1,\dots,C_m)\,. \tag{22}$$

In this case one obtains a complete solution of the Hamilton-Jacobi equation which depends on m parameters and the corresponding Hamilton equations are integrable by quadratures (*Jacobi theorem*).

The constants $C_1,\dots,C_m$ for a completely separable Hamilton-Jacobi equation can be considered as functions on the phase space where they are integrals of motion. In a case, when these integrals on motion are independent and in involution, the system is completely integrable in the sense of Liouville.

4 Particle motion in General Relativity

4.1 Equation of motion in the Hamiltonian form

Consider a particle motion of mass μ in the gravitational field. Its equation of motion is

$$\frac{D^2 x^\mu}{d\tau^2} = 0\,. \tag{23}$$

[2]The Lagrangian of the Neumann model is

$$L = \frac{1}{2}\sum_{k=1}^{N}\left[\dot{x}_k^2 - a_k x_k^2 + \Lambda(x_k^2 - 1)\right]\,. \tag{17}$$

Here, $D/d\tau$ is the covariant derivative with respect to the proper time τ. Introduce the affine parameter $\lambda = \tau/\mu$ and denote a derivative with respect to it by a dot. The Lagrangian for Eq.(23) is

$$L = \frac{1}{2} g_{\mu\nu} \dot{x}^\mu \dot{x}^\nu \,. \tag{24}$$

The momentum p_μ is defined as follows

$$p_\mu = \frac{\partial L}{\partial \dot{x}^\mu} = g_{\mu\nu} \dot{x}^\nu \,. \tag{25}$$

Denote by D the dimensionality of the spacetime. Coordinates (p_μ, x^μ) are canonical on the phase space M^{2D}. In these coordinates the symplectic form is

$$\Omega = \sum_{\mu=1}^{D} dp_\mu \wedge dx^\mu \,. \tag{26}$$

The Hamiltonian of the particle is

$$H = \frac{1}{2} g^{\mu\nu} p_\mu p_\nu \,. \tag{27}$$

It gives trivial integral of motion

$$H = -\frac{1}{2}\mu^2 \,. \tag{28}$$

For null rays one must put $\mu = 0$. The Hamiltonian equations of motion

$$\dot{x}^\mu = \{H, x^\mu\} = g^{\mu\nu} p_\nu \,, \tag{29}$$

$$\dot{p}_\mu = \{H, p_\mu\} = -\frac{1}{2} g^{\nu\lambda}{}_{,\mu} p_\nu \,, \tag{30}$$

are equivalent to the geodesic equation Eq.(23), which can be written in the form

$$p^\nu p_{\mu;\nu} = 0 \,. \tag{31}$$

4.2 Integrals of motion and Killing tensors

Consider a special monomial in the momentum on the phase space of the relativistic particle of the form

$$\mathcal{K} = K^{\mu_1 \dots \mu_s} p_{\mu_1} \dots p_{\mu_s} \,. \tag{32}$$

A condition that this is an integral of motion implies

$$K^{(\mu_1 \dots \mu_s ; \nu)} = 0 \,. \tag{33}$$

The symmetric tensor of the rank s, $K_{\mu_1 \dots \mu_s}$, which obeys the equation Eq.(33), is called a *Killing tensor*. The metric $g_{\mu\nu}$ is a trivial example of the Killing tensor of rank 2.

Suppose we have two integrals of motion, $\mathcal{K}_{(s)}$ and $\mathcal{K}_{(t)}$, connected with the Killing tensors $K^{\mu_1 \dots \mu_s}_{(s)}$ and $K^{\nu_1 \dots \nu_t}_{(t)}$, respectively. Using the *Jacobi identity* Eq.(5) it is easy to check that $\{\mathcal{K}_{(s)}, \mathcal{K}_{(t)}\}$ also commutes with the Hamiltonian H and hence is an integral of motion. This commutator is a monomial of the power $s + t - 1$ in the momentum. The corresponding Killing tensor of the rank $s + t - 1$ is

$$[K_{(s)}, K_{(t)}] = K_{(s+t-1)} \,, \tag{34}$$

$$K^{\mu_1 \dots \mu_{s-1} \lambda \nu_1 \dots \nu_{t-1}}_{(s+t-1)} = s\, K^{\epsilon(\mu_1 \dots \mu_{s-1}}_{(s)} \partial_\epsilon K^{\lambda \nu_1 \dots \nu_{t-1})}_{(t)} - t\, K^{\epsilon(\nu_1 \dots \nu_{t-1}}_{(t)} \partial_\epsilon K^{\lambda \nu_1 \dots \mu_{s-1})}_{(s)} \tag{35}$$

The introduced operation for the Killing tensors is known as the *Schouten-Nijenhuis brackets*. Killing tensors form a Lie subalgebra of a Lie algebra of all totally symmetric contravariant tensor fields on the manifold with respect to these operations. The Killing tensors for which the Schouten-Nijenhuis bracket vanishes are said to be in involution.

In a simplest case when a monomial is of the first order in the momentum, the Killing tensor coincides with the Killing vector, and the *Schouten-Nijenhuis bracket* reduces to a usual commutator of two vector fields.

If there exist D non-degenerate functionally independent Killing tensors[3] in involution then the

[3] Some of them can be Killing vectors.

geodesic equations in $D-$dimensional spacetime are completely integrable.

Geodesic motion in the gravitational field of the most general solution describing a rotating black hole in 4 and higher dimensional spacetimes, which are asymptotically either flat or (A)dS, is a new class of physically interesting completely integrable systems.

5 Killing-Yano tensors

5.1 Definitions

Killing tensors are natural symmetric generalizations of a Killing vector. Let us discuss another important generalization, known as a Killing-Yano tensor. We define first a *conformal Killing-Yano tensor* of rank p. It is an antisymmetric tensor $k_{\mu_1\dots\mu_p}$ which obeys the following equation

$$\nabla_{(\mu_1}k_{\mu_2)\mu_3\dots\mu_{p+1}} = g_{\mu_1\mu_2}\tilde{k}_{\mu_3\dots\mu_{p+1}} - (p-1)g_{[\mu_3(\mu_1}\tilde{k}_{\mu_2)\mu_4\dots\mu_{p+1}]}\,. \tag{36}$$

By tracing both sides of this equation one obtains

$$\tilde{k}_{\mu_2\mu_3\dots\mu_p} = \frac{1}{D-p+1}\nabla^{\mu_1}k_{\mu_1\mu_2\dots\mu_p}\,. \tag{37}$$

In the case when $\tilde{k}_{\mu_2\dots\mu_p} = 0$ one has a *Killing–Yano* (KY) tensor. For the KY tensor $\mathbf{k}$ the quantity

$$L_{\mu_1\mu_2\dots\mu_{p-1}} = k_{\mu_1\mu_2\dots\mu_p}p^{\mu_p}\,, \tag{38}$$

is parallel-propagated along the geodesic.

The 'square' $\mathbf{K}$ of KY tensor $\mathbf{k}$, defined by the relation

$$K_{\mu\nu} = (\mathbf{k}\circ\mathbf{k})_{\mu\nu} \equiv (p-1)!\,k_{\mu\mu_2\dots\mu_p}k_{\nu}{}^{\mu_2\dots\mu_p}\,, \tag{39}$$

is a Killing tensor. Notice that not an arbitrary Killing tensor can be written in the form .

5.2 Properties of conformal Killing-Yano tensors

The (conformal) Killing-Yano tensors have the following properties:

1. Hodge dual of a conformal Killing-Yano tensor is a conformal Killing-Yano tensor;
2. Hodge dual of a closed conformal Killing-Yano tensor is a Killing-Yano tensor;
3. Hodge dual of a Killing-Yano tensor is a closed conformal Killing-Yano tensor;
4. Exterior product of two closed conformal Killing-Yano tensor is a closed conformal Killing-Yano tensor.

Figure 2 schematically illustrates these properties. The last of these statements was proved in [3, 4].

5.3 Principal conformal Killing-Yano tensor

Consider an antisymmetric tensor of rank 2 $h_{\mu\nu}$ which obeys the following equation

$$\nabla_\gamma h_{\mu\nu} = g_{\gamma\mu}\xi_\nu - g_{\gamma\nu}\xi_\mu\,. \tag{40}$$

This is a conformal Killing-Yano tensor. Equation (40) implies the following relations

$$\nabla_{[\gamma}h_{\mu\nu]} = 0\,, \qquad \xi_\mu = \frac{1}{D}\nabla^\nu h_{\nu\mu}\,. \tag{41}$$

The first of these relations means that $\mathbf{h}$ is closed. Here $D = 2n+\varepsilon$ is the spacetime dimension. For even number of dimensions $\varepsilon = 0$, while for the odd number $\varepsilon = 1$. The tensor $\mathbf{h}$ is non-degenerate if its matrix rank is $2n$. A *principal conformal Killing-Yano tensor* is a non-degenerate closed conformal Killing-Yano tensor of rank 2. The existence of the principal conformal Killing-Yano tensor for the most general known solution [5] for higher dimensional rotating black holes with spherical topology of the horizon was proved in [6, 7].

It is possible to show that the vector ξ^μ defined by the second equation in (41) is a Killing vector. We call it a *primary Killing vector* [8].

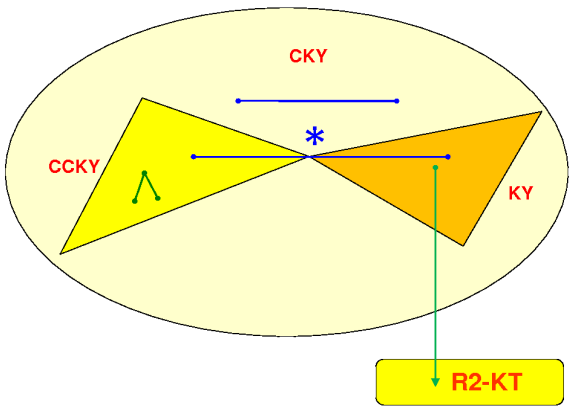

Figure 2: Schematical illustration of the properties of closed conformal Killing-Yano tensors (CCKY), Killing-Yano tensors (KY), and Killing tensors of rank 2 (R2-KT).

6 Killing-Yano 'tower'

In a spacetime with a principal conformal Killing-Yano tensor it is possible to construct a set of Killing vectors and tensors, which we call a *Killing-Yano 'tower'*. The idea of this constuction is following. For a given principal conformal Killing-Yano tensor $\mathbf{h}$ one can define the a set of $n-1$ objects

$$\mathbf{h}^{\wedge j} = \underbrace{\mathbf{h} \wedge \mathbf{h} \wedge \ldots \wedge \mathbf{h}}_{j \text{ times}}, \qquad j = 1, \ldots, n-1\,. \tag{42}$$

Each of these objects is a closed conformal Killing-Yano tensor, so that their Hodge dual are Killing-Yano tensors

$$\mathbf{k}_{(j)} = *\mathbf{h}^{\wedge j}\,. \tag{43}$$

By taking 'squares' of these tensors one obtains $n-1$ Killing tensors of the second rank

$$\mathbf{K}_{(j)} = \mathbf{k}_{(j)} \circ \mathbf{k}_{(j)}\,. \tag{44}$$

If ξ^ν is a primary Killing vector then it is possible to show that

$$\xi^\mu_{(j)} = K^\mu_{(j)\nu}\xi^\nu \tag{45}$$

are again Killing vectors. Thus one obtains n Killing vectors. In the odd dimensional spacetime there exists an additional Killing vector $\eta = *\mathbf{h}^{\wedge n}$. A set of constructed $n+\varepsilon$ Killing vectors, $n-1$ Killing tensors, and one trivial Killing tensor ($\mathbf{g}$) gives D conserved quantities for the geodesic motion. It is possible to show that the corresponding integrals of motion are independent and in involution. Thus geodesic motion equations are completely integrable in a spacetime with a principal conformal Killing-Yano tensor [9–11].

7 Canonical form of metric

7.1 Canonical coordinates

In a spacetime with a principal conformal Killing-Yano tensor $\mathbf{h}$ there exists a special convenient choice of coordinates. Consider the following eigen-value problem

$$h^\mu{}_\nu m^\nu_{\pm a} = \mp i x_a m^\mu_{\pm a}\,. \tag{46}$$

Complex eigen-vectors $m^{\mu}_{\pm a}$ can be written as

$$m^{\mu}_{\pm a} = e^{\mu}_{a} \pm i e^{\mu}_{\hat{a}}\,, \tag{47}$$

where $\mathbf{e}_a$ and $\mathbf{e}_{\hat{a}}$ are mutually orthogonal normalised real vectors. A non-degerate $\mathbf{h}$ has n different eigen-values x_a $(a = 1, \dots, n)$, and the corresponding eigen-space for each of these eigen-values is two dimensional (see [12]). One can use x_a as n coordinates on the spacetime manifold. We call them *Darboux coordinates*. For each of the Killing vectors ξ from the Killing-Yano 'tower' one can introduce a Killing parameter so that the integral line of this vector field is a solution of the equation

$$\frac{dx^{\mu}}{d\psi} = \xi^{\mu}\,. \tag{48}$$

This gives us $n + \varepsilon$ Killing coordinates ψ_j $(j = 0, \dots, n - \varepsilon)$. Total number of Darboux and Killing coordinates is D, which is sufficient for using as coordinate system in the D dimensional spacetime manifold. We call these coordinates *canonical*.

7.2 Off-shell canonical metric

The metric of the spacetime which possesses a principal conformal Killing-Yano tensor in the canonical coordinates is of the form [13–15]

$$ds^2 = \sum_{a=1}^{n} \left[\frac{U_a}{X_a} (dx_a)^2 + \frac{X_a}{U_a} \left(\sum_{j=0}^{n-1} A^{(j)}_a d\psi_j \right)^2 \right] - \frac{\varepsilon c}{A^{(n)}} \left(\sum_{j=0}^{n} A^{(j)} d\psi_j \right)^2 . \tag{49}$$

Here

$$U_a = \prod_{b \neq a} (x_b^2 - x_a^2)\,, \qquad X_a = X_a(x_a)\,, \tag{50}$$

$$\prod_{a=1}^{n} (1 + \lambda x_a^2) = \sum_{j=0}^{n} \lambda^j A^{(j)}\,, \qquad (1 + \lambda x_b^2) \prod_{a=1}^{n} (1 + \lambda x_a^2) = \sum_{k=0}^{n-1} \lambda^k A^{(k)}_b\,. \tag{51}$$

A potential $\mathbf{b}$, which generates the principal conformal Killing-Yano tensor $\mathbf{h}$,

$$\mathbf{h} = d\mathbf{b}\,, \tag{52}$$

in the canonical coordinates is

$$\mathbf{b} = \frac{1}{2} \sum_{k=0}^{n-1} A^{(k+1)} d\psi_k\,. \tag{53}$$

The metric (49) is of the algebraical type D. As we indicated above, geodesic equations in this metric are completely integrable. Besides this, it also has the following nice properties. In the metric (49):

1. Hamilton-Jacobi and Klein-Gordon equations allow complete separation of variables [16];
2. Massive Dirac equation is separable [17];
3. Stationary string equations are completely integrable [18];
4. Tensorial gravitational perturbation equations are separable [19];
5. Equations of the parallel transport along timelike and null geodesics can be integrated [20, 21];

7.3 On-shell metric

The metric (49) is valid for any geometry with a principal conformal Killing-Yano tensor. We call this metric *off-shell*, since it does not obey the Einstein equations. Let us consider now on-shell geometry, that is assume that the metric obeys the equations

$$R_{\mu\nu} = (D-1)\Lambda g_{\mu\nu}\,. \tag{54}$$

Λ is the cosmological constant. The Einstein equations restrict arbitrary functions $X_a(x_a)$, which enter (49), so that they take the form of polynomials [5, 23]

$$X_a = b_a x_a + \sum_{k=0}^{n} c_k x_a^{2k}\,. \tag{55}$$

As a result, the solution depends on $D-\varepsilon$ arbitrary parameters. This solution coincides with the most general solution for higher dimensional black holes in either asymptotically flat ($\Lambda = 0$), or asymptotically (A)dS spacetime, obtained in [5]. Arbiraty constants, which enter this solutions are: the cosmological constant Λ, the mass M, rotation parameters, and 'NUT' parameters. In the 4D case this is a Kerr-NUT-(A)dS metric.

7.4 Charged particle motion in weakly charged black holes

Another example of a completely integrable system is the case of a charged particle motion in a spacetime of a weakly charged higher dimensional black hole [22]. Its equation of motion is

$$\mu\,\frac{D^2x^\mu}{d\tau^2} = qF^\mu{}_\nu\frac{Dx^\nu}{d\tau}\,. \tag{56}$$

Here μ is mass and q is charge of the particle, $D/d\tau$ is the covariant derivative with respect to the proper time τ. It is useful to introduce the affine parameter $\lambda = \tau/\mu$. Denoting by the dot $\dot{}$ a covariant derivative with respect to parameter λ, the equation of motion can be rewritten as

$$\ddot{x}^\mu = qF^\mu{}_\nu\,\dot{x}^\nu\,. \tag{57}$$

If $K_{\mu\nu}$ is the Killing tensor, and the field obeys the condition

$$K_{(\mu}{}^\lambda F_{\lambda)} = 0\,, \tag{58}$$

then the following quantity is conserved

$$\dot{x}^\mu K_{\mu\nu}\,\dot{x}^\nu\,. \tag{59}$$

The equation of motion (57) follows from the Lagrangian

$$L = \frac{1}{2}g_{\mu\nu}\dot{x}^\mu\dot{x}^\nu + qA_\mu\dot{x}^\mu\,. \tag{60}$$

To write a Hamiltonian one defines the momentum

$$p_\mu = \frac{\partial L}{\partial\dot{x}^\mu} = g_{\mu\nu}\dot{x}^\nu + qA_\mu\,, \tag{61}$$

and the corresponding Hamiltonian reads

$$H = \frac{1}{2}g^{\mu\nu}(p_\mu - qA_\mu)(p_\nu - qA_\nu)\,. \tag{62}$$

Since it does not depend on λ, the Hamiltonian is the integral of motion. For our choice of the affine parameter λ one finds that its value is given by

$$H = -\frac{1}{2}\mu^2\,. \tag{63}$$

The conservation law (63) with Hamiltonian (62) implies the following Hamilton–Jacobi equation for the classical action $\mathcal{S} = -\frac{1}{2}\lambda\mu^2 + S(x^\mu)$:

$$-\mu^2 = g^{\mu\nu}\big(\partial_\mu S - qA_\mu\big)\big(\partial_\nu S - qA_\nu\big)\,. \tag{64}$$

From the same Hamiltonian one obtains the equation for a charged massive field φ by substituting $p_\mu \to -i\nabla_\mu$. The corresponding Klein-Gordon equation is

$$\big[[\nabla_\mu - iqA_\mu]\, g^{\mu\nu}\,[\nabla_\nu - iqA_\nu] - \mu^2\big]\varphi = 0\,. \tag{65}$$

Consider now a Ricci-flat spacetime, $R_{\mu\nu} = 0$, which possesses a Killing vector ξ^μ. Then, in the Lorentz gauge $\nabla_\nu A^\nu = 0$, the Maxwell equations $\nabla_\nu F^{\mu\nu} = 0$ reads $\nabla_\nu\nabla^\nu A_\mu = 0$. The Killing vector ξ^μ obeys the same equation $\nabla_\nu\nabla^\nu\xi_\mu = 0$. This means that the Killing vector field can be used as a potential of a special test electromagnetic field

$$A_\mu = Q\,\xi_\mu\,. \tag{66}$$

Here, Q is a normalization constant parameterizing the strength of the field.

Let us assume that the background spacetime allows the separability of uncharged Hamilton–Jacobi and Klein–Gordon equations. It is natural to ask, what happens with these equations when one consider the system with the test Killing electromagnetic field (66). If the separation takes place with respect to the Killing coordinate corresponding to the Killing vector ξ^μ,

$$\xi^\mu\partial_\mu S = \Psi\,, \quad \xi^\mu\partial_\mu\varphi = \Psi\,\varphi\,, \tag{67}$$

with Ψ being the separation constant, the charged Hamilton–Jacobi (64) and Klein–Gordon equations (65) take the form

$$g^{\mu\nu}\,\partial_m uS\,\partial_n uS + M^2 = 0\,, \tag{68}$$

$$\big[g^{\mu\nu}\,\nabla_\mu\nabla_\nu - M^2\big]\varphi = 0\,. \tag{69}$$

Here, the function M^2 is given by ($e = qQ$)

$$M^2 = \mu^2 - 2e\Psi + e^2\xi^2\,. \tag{70}$$

The remarkable property of a spacetime which admits a principal conformal Killing-Yano tensor is that these equations are completely separable for the case when ξ^μ is the primary Killing vector of the system.

To illustrate this property for the Hamilton-Jacobi equation, we use the following ansatz for the action function S

$$S = \sum_{a=1}^{n} S_a(x_a) + \sum_{k=0}^{n-1}\Psi_k\psi_k\,, \tag{71}$$

where the functions $S_a(x_a)$ are functions of just one variable x_a. Substituting it into Eq.(64) for the metric Eq.(49) one obtains the following equations

$$\begin{aligned} (S_a')^2 &= \frac{Ba}{X_a} - \left(\frac{C_a}{X_a} - e\right)^2\,, \\ C_a &= \sum_{k=0}^{n-1}\Psi_k(-x_a^2)^{n-1-k}\,, \quad B_a = \sum_{k=0}^{n-1}\Xi_k(-x_a^2)^{n-1-k}\,. \end{aligned} \tag{72}$$

Here Ξ_k are separation constants.

Similarly, substituting the separability ansatz

$$\varphi = \prod_{a=1}^{n} R_a(x_a)\prod_{k=0}^{n-1}\exp\big(i\Psi_k\psi_k\big)\,, \tag{73}$$

in the Klein-Gordon equation Eq.(69) we find that the separation of variables really takes place and for the modes $R_a(x_a)$ one obtains the following second order ordinary differential equations

$$\big(X_aR_a'\big)' + \Big(B_a - \frac{1}{X_a}\big(C_a - eX_a\big)^2\Big)R_a = 0\,. \tag{74}$$

For more details see paper [22].

7.5 Further developments

Let us mention two recent developments of the above described results.

(1) In our discussion we assumed that the closed conformal Killing-Yano tensor is non-degenerate. In particular, this implies that there exists a set of n different eigen-values of $\mathbf{h}$, which we used as Darboux coordinates. In a degenerate case, there may exist several eigen-values which are constants, and some of these constants can vanish. The general form of the canonical metric for such degenerate cases was constucted in [12].

(2) We discussed vacuum (with cosmological constant) solutions of the higher dimensional Einstein equations. An interesting generalization to a non-vacuum case was obtained recently in [24]. The authors consider a *five dimensional* minimally coupled gauged supergravity, which includes gravity and the Maxwell field with a Chern-Simons term. The corresponding Largrangian density is

$$L = *(R + \Lambda) - \frac{1}{2} F \wedge *F + \frac{1}{3\sqrt{3}} F \wedge F \wedge A \,. \tag{75}$$

The corresponding Einstein-Maxwell equations are

$$R_{\mu\nu} + \frac{1}{3}\Lambda = \frac{1}{2}(F_{\mu\lambda}F_{\nu}{}^{\lambda} - \frac{1}{6} g_{\mu\nu} F^2) \,, \tag{76}$$

$$dF = 0 \,, \qquad d * F - \frac{1}{\sqrt{3}} F \wedge F = 0 \,. \tag{77}$$

The main result of this work is the following. One can modify the covariant derivative by including a non-vanishing torsion $T = \frac{1}{\sqrt{3}} * F$, and generalize the equation (40), by subsituting the modified derivative insted of the covariant one. The authors demonstrated that the generalized principal conformal Killing-Yano tensor generates a 'tower' of integrals of motion which provides complete integrability of a charged particle motion in these spaces. An interesting example of a charged rotating black hole solution in this theory was obtained in [25]. It is interesting, that the corresponding metric is of a general algebraical type.

7.6 Acknowledgments

The author is grateful to the Natural Sciences and Engineering Research Council of Canada and the Killam Trust for their support.

References

[1] Arnold V I 1989 *Mathematical Methods of Classical Mechanics* Springer

[2] Babelon O, Bernard D, and Talon M 2003 Introduction to Classical Integrable Systems Cambridge Univ. Press.

[3] Krtouš P, Kubizňák D, Page D N, and Frolov V P 2007 *J. High Energy Phys.* **02** 004

[4] Frolov V P 2008 *Prog.Theor.Phys.Suppl.* **172** 210

[5] Chen W, Lü H, and Pope C N 2006 *Class. Quant. Grav.* **23** 5323

[6] Frolov V P and Kubizňák D 2007 *Phys.Rev.Lett* **98** 011101

[7] Kubizňák D and Frolov V P 2007 *Class. Quant. Grav.* **24** F1

[8] Frolov V P and Kubizňák D 2008 *Class.Quant.Grav.* **25** 154005

[9] Page D N, Kubizňák D, Vasudevan M, and Krtouš P 2007 *Phys. Rev. Lett.* **98** 061102

[10] Krtouš P, Kubizňák D, Page D N, and Vasudevan M 2007 *Phys. Rev.* D **76** 084034

[11] Houri T, Oota T and Yasui Y 2008 *J. Phys.* A **41** 025204

[12] Houri T, Takeshi Oota T and Yasui Y 2008 *Phys.Lett.* B **666** 391

[13] Houri T, Oota T and Yasui Y 2007 *Phys. Lett.* B **656** 214

[14] Houri T, Oota T and Yasui Y, 2009 *Class.Quant.Grav.* **26** 045015

[15] Krtous P, Frolov V P, and Kubiznak D 2008 *Phys.Rev.* D **78** 064022

[16] Frolov V P, Krtouš P, and Kubizňák D 2007 *J. High Energy Phys.* **02**) 005

[17] Oota T and Yasui Y 2008 *Phys.Lett.* B **659** 688

[18] Kubiznak D and Frolov V P 2008 *JHEP* **0802** 007

[19] Oota T and Yasui Y 2008 *Int.J.Mod.Phys.* A **25** 3055

[20] Connell P, Frolov V P and Kubiznak D 2008 *Phys.Rev.* D **78** 024042

[21] Kubiznak D, Frolov V P, Krtouš P, and Connell P 2009 *Phys.Rev.* D **79** 024018

[22] Frolov V and Krtouš P, 2011 *Phys.Rev.* D **83** 024016.

[23] Hamamoto N, Houri T, Oota T, and Yasui Y 2007 *J. Phys.* A **40**, F177

[24] Kubiznak D, Kunduri H K and Yasui Y 2009 *Phys.Lett.* B **678** 240

[25] Chong Z W, Cvetic M, Lu H and Pope C N 2005 *Phys. Rev. Lett.* **95** 161301

An expected gravitational scalar field – Past and Future –

Yasunori Fujii[1]

Advanced Research Institute for Science and Engineering, Waseda University, Tokyo 169-8555

Abstract

The paper consists of two parts. In the first half – Past, Chapters 1-3, we begin with recalling a historical development of the gravitational scalar field, hypothesized as a Nambu-Goldstone boson associated with scale invariance in particle physics. We then re-emphasize how we can understand the accelerating universe, related inseparably to today's version of the cosmological constant problem, in terms of the gravitational scalar field, particularly in the context of the scalar-tensor theory originally due to P. Jordan. In the second half – Future, Chapters 4-6, we propose an experimental search for the scalar field as a constituent of Dark Energy, by means of a precision measurement on photon-photon scattering taking place inside a high-intensity laser beam. This part is based on the collaboration with Kensuke Homma. Some of the footnotes are for additional comments not delivered on the occasion of the talk.

1 Historical introduction

I have been attracted to the idea of the gravitational scalar field since the early 1970's when I was interested in scale invariance in particle physics, broken spontaneously in terms of Nambu-Goldstone boson, a massless scalar field called *dilaton* [1]. I was also convinced that the scalar field, unlike the genuine gauge fields like photon or graviton, has no immunity against acquiring nonzero self-energy. Consider, for example, the scalar field diagram in which we have quarks and leptons coupled gravitationally in the closed loop. We then derived m_σ, the mass of the scalar field [2],[3],

$$m_\sigma^2 \sim \frac{m_{\rm q}^2 M_{\rm ssb}^2}{M_{\rm P}^2} \sim \left(10^{-9}{\rm eV}\right)^2, \tag{1}$$

where $m_{\rm q}, M_{\rm ssb}, M_{\rm P}$ are for the light-quark mass $\sim$ MeV, the supersymmetric breaking mass scale $\sim$ TeV and the Planck mass $\sim 10^{18}$GeV, respectively, allowing us for the latitude of a few orders of magnitude in both directions. More surprising was its inverse, or the force-range $\lambda = m_\sigma^{-1}$, estimated to be $\sim$ 100m, a macroscopic distance which had never been explored before. I then proposed "non-Newtonian gravity," with the static potential;[2]

$$V_{ij}(r) = -\frac{Gm_i m_j}{r}\left(1 + \alpha_{5(ij)} e^{-r/\lambda}\right). \tag{2}$$

If the coefficient $\alpha_{5(ij)}$ turns out to be independent of any specific natures of the objects i, j, then the concept of Weak Equivalence Principle (WEP) must have been respected. After years of extensive studies in precision measurements not only in physics but also in such versatile areas including geology and space sciences, however, no solid evidence has been reported for the presence of a new type of force. The data accumulated in the past has then been recorded only in the diagrams like Fig. 1, originally invented by G.W. Gibbons and B.F. Whiting,[4] who provided with a convenient way to express the observational upper bounds on the deviations from the inverse-square law and on WEP violation.

I was, on the other hand, a theorist who was frequently asked the question, on whether everything is consistent with Einstein's idea on General Covariance. Some of the people including J. O'Hanlon, and R. Acharia and P. A. Hogan [7] helped me by providing me with an affirmative view based on the scalar-tensor theory (SST) [8]. Since then I have been attracted to SST. The following discussions, particularly throughout the first three sections, will be largely based on Ref. [3].

[1]Email address: fujii@e07.itscom.net

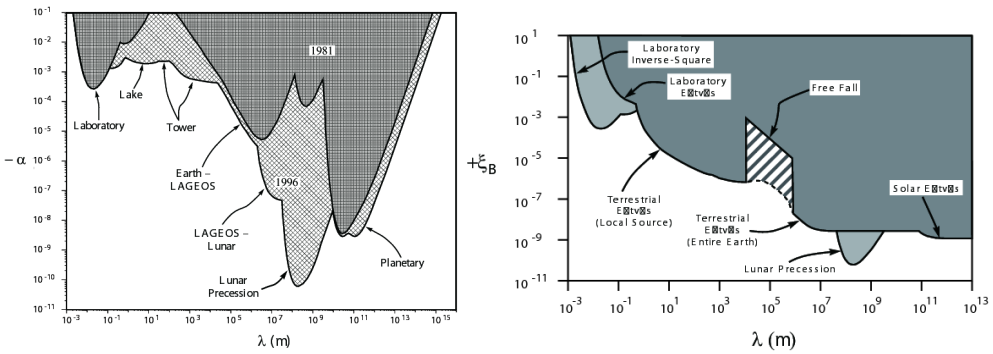

Figure 1: The left and right diagrams obtained from the composition-independent (for any departure from the inverse-square law) and -dependent (for WEP violation) experiments, respectively, plot the observed upper bounds on the coefficients equivalently to α_5 in (2), against the assumed force-range λ. They are taken from Figs. 2.13 and 4.16-17 of Ref. [5]. For more recent results, particularly on the mm range, see Ref. [6] and papers cite therein.

In 1955 P. Jordan came up with the Lagrangian [8][2]

$$\mathcal{L} = \sqrt{-g}\left(\frac{1}{2}\xi\phi^2 R - \epsilon\frac{1}{2}g^{\mu\nu}\partial_\mu\phi\partial_\nu\phi + L_{\rm matter}\right), \tag{3}$$

which features a *nonminimal coupling term*, $(\xi\phi^2/2)R$, in place of the standard Einstein-Hilbert term, where we use the *Reduced Planckian Units* (P Units) defined by $c = \hbar = M_{\rm P}(= (8\pi G)^{-1/2}) = 1$. Notice that the present age of the universe is $t_0 = 1.37 \times 10^{10}{\rm y} \approx 10^{60.2}$ in units of the Planck time.

Obviously one of Jordan's motivations was to offer a generally covariant theory which accommodates the spacetime-dependent effective gravitational constant defined by $(8\pi G_{\rm eff}(x))^{-1} = \xi\phi^2(x)$ in accordance with Dirac's suggestion [9].

We also make use of the conformal transformation/frame defined by $g_{\mu\nu} \to g_{*\mu\nu} = \Omega^2(x)g_{\mu\nu}$, representing locally rescaling the metric tensor. By this transformation, the same Lagrangian in (3) can be re-expressed in terms of the new metric $g_{*\mu\nu}$. By a special choice $\Omega^2 = \xi\phi^2$, the re-expressed Lagrangian is found to be

$$\mathcal{L} = \sqrt{-g_*}\left(\frac{1}{2}R_* - {\rm Sgn}(\zeta^2)\frac{1}{2}g_*^{\mu\nu}\partial_\mu\sigma\partial_\nu\sigma + L_{*\rm matter}\right), \tag{4}$$

which features $8\pi G_* = 1$, hence back to the Einstein-Hilbert term, where $\zeta^2 = (6 + \epsilon\xi^{-1})^{-1}$. For this reason we are now in what is called the Einstein frame (Efr), whereas (3) is the Lagrangian in the Jordan frame (Jfr). We may say that Dirac was right when he was in Jfr, but obviously not if he lived in Efr. The question is then which frame is *physical*.

Note that the canonical scalar field in Efr is σ, which is not the same as ϕ in Jfr, but is related to it by $\phi = \xi^{-1/2}e^{\zeta\sigma}$.

Also the scale factor a and the cosmic time t in cosmology are also subject to the changes; $a_* = \Omega a$ and $dt_* = \Omega dt$ [10]. In this context the way of the cosmological expansion may differ from frame to frame.

Then came the year 1998, when the *accelerating universe* was finally approved by the observation [11]. This also left us with *today's version of the cosmological constant problem*, featuring the two questions; fine-tuning and the coincidence problems, the first of which will be discussed briefly. According to the observed result $\Omega_\Lambda = \Lambda/\rho_{\rm cr} \approx 0.7$ [11], we find the size of the cosmological constant; $\Lambda_{\rm obs} \approx 10^{-120}$ in the P Units, to be compared with the theoretical estimate $\Lambda_{\rm th} \sim 1$ in the same units, from almost any of the unification-oriented theories, implying a huge discrepancy of nearly 120 orders of magnitude. In order to better understand the cosmological constant problem, perhaps the most promising is to assume the presence of a scalar field. In a sense the scalar field started then to live an entirely new life. Also many kinds of theories started to be discussed on the scalar field. But perhaps the simplest theoretical

[2] $\epsilon = \pm 1$ and ξ are related to the widely used symbols by $4\omega = \epsilon\xi^{-1}$, with $\epsilon = {\rm Sgn}(\omega)$.

idea due to Jordan appears to come to a unique finding on the most integral aspect of the cosmological constant problem, as we are going to show from now on.

For this purpose we start with the Lagrangian in Jfr but with an added constant Λ, which is "large," meant to be of the order one in the P Units;[3]

$$\mathcal{L} = \sqrt{-g}\left(\frac{1}{2}\xi\phi^2 R - \epsilon\frac{1}{2}g^{\mu\nu}\partial_\mu\phi\partial_\nu\phi - \Lambda + L_{\rm matter},\right). \tag{5}$$

We may compare this with the effective Lagrangian for the closed strings in higher-dimensional spacetime [12];

$$\mathcal{L}_{\rm string} = \sqrt{-\bar{g}}e^{-2\Phi}\left(\frac{1}{2}\bar{R} + 2g^{\bar{\mu}\bar{\nu}}\partial_{\bar{\mu}}\Phi\partial_{\bar{\nu}}\Phi - \frac{1}{12}H_{\bar{\mu}\bar{\nu}\bar{\lambda}}H^{\bar{\mu}\bar{\nu}\bar{\lambda}}\right). \tag{6}$$

Notice the presence of a scalar field Φ sharing basically the same nonminimal coupling term as in (5) [4]. For this reason, Jfr is sometimes called the string frame.[5]

We move to Efr;

$$\mathcal{L} = \sqrt{-g_*}\left(\frac{1}{2}R_* - {\rm Sgn}(\zeta^2)\frac{1}{2}g_*^{\mu\nu}\partial_\mu\sigma\partial_\nu\sigma - \Lambda e^{-4\zeta\sigma} + L_{*\rm matter}\right). \tag{7}$$

To be noticed is that the "constant" term Λ in (5) has been converted to a potential $V(\sigma) = \Lambda e^{-4\zeta\sigma}$.

On these bases we now discuss simple cosmology.

2 Lambda cosmology and choosing a physical frame

By assuming the spatially flat FRW metric, also radiation-dominated universe for simplicity, we derive the cosmological equations, discussing the solutions. Fortunately we find asymptotic and attractor solutions, which are rather simple [13]. We examine their behaviors somewhat in detail, on both of Jfr and Efr separately.

First in Jfr, we find an extremely simple solution:

$$a = {\rm const}, \quad \phi = 2\zeta\sqrt{\Lambda\xi^{-1}}\,t, \quad \rho = -3\Lambda\zeta^2\left(2 + \epsilon\xi^{-1}\right). \tag{8}$$

The first equation represents simply, and almost trivially, a *static* universe. For this reason the Jfr cannot be accepted as a physical frame. Note that these solutions do not allow a smooth limit as $\Lambda \to 0$.

We add an important comment on what is known as the Brans-Dicke (BD) *model* [14], in which BD required a constraint that ϕ should be decoupled from $L_{\rm matter}$, leaving ϕ to be coupled only through the nonminimal coupling term, to save WEP. The same requirement entails another condition that m, mass of any of the matter fields, is constant;

$$m = {\rm const}. \tag{9}$$

With this constant particle mass, we may prepare a microscopic clock or meter-stick. As an example, the electron mass inverse, $m_{\rm e}^{-1}$ provides with the unit, or standard, of the atomic clock. We then find that we have no way to detect any possible time change of the unit itself, as long as we stick to the use of the same atomic clock, in other words, unless we use other kind of clocks. This simple finding might be elevated to a principle; *Own Unit Insensitivity Principle* (OUIP) [10], according to which any unit is a constant in the current frame which we live in.

[3] The constant term Λ might be slightly extended by multiplied by a monomial of the scalar field; ϕ^q. The corresponding Lagrangian is, however, transformed to an Efr form of the Lagrangian, then again back to the Jfr form now with Λ without the ϕ-dependence. More precisely, we start with a theory with the modified term $\phi^q\Lambda'$, also with ξ' and ϵ'. We introduce $\zeta' = (6 + 4\omega')^{-1/2}$ where $\omega' = \epsilon'\xi'^{-1}/4$. The new form of the Jfr Lagrangian with the unmodified Λ term is reached simply by the substitutions; $\Lambda = \Lambda'\xi'^{-q/2}$ and $\zeta = (6 + 4\omega)^{-1/2} = \zeta'(1 - q/4)$ where $\omega = \epsilon\xi^{-1}/4$.

[4] A more precise identification follows for $\phi = 2e^{-\Phi}$ with $\xi = 1/4$ and $\epsilon = -1$. The last condition never implies a ghost of negative energy. The *diagonalized* field σ has a positive energy as shown in the second term on RHS of (4).

[5] It even seems as if Jordan invented his theory having expected it to be applied to string theory decades later.

Now let us move to Efr. The solutions are;

$$a_* = t_*^{1/2} \sim t, \tag{10}$$
$$\sigma = \bar{\sigma} + (1/2)\zeta^{-1} \ln t_*, \tag{11}$$
$$3H_*^2 = \rho_\sigma + \rho_*, \tag{12}$$
$$\rho_\sigma = \frac{1}{2}\dot{\sigma}^2 + V(\sigma) = \Lambda_{\rm eff} = \frac{3}{16}\zeta^{-2} t_*^{-2}, \tag{13}$$
$$\rho_* = \frac{3}{4}\left(1 - \frac{1}{4}\zeta^{-2}\right) t_*^{-2}, \tag{14}$$
$$m_* = t_*^{-1/2}. \tag{15}$$

The universe now expands, as shown in (10), where a_* and t_* are the scale factor and the cosmic time, respectively, in Efr. It also does in accordance with the assumed radiation dominance. It even sounds like a good news, because it appears to allow us to accept Efr as a physical frame. We must be careful, however, before reaching a conclusion; we look into other portion of the solution.

Equation (11) tells us how the scalar field evolves with the cosmic time. Eq. (12) is Einstein's equation in the conventional sense, but with RHS consisting of two terms. The first term ρ_σ defined by (13) can be interpreted as an effective cosmological constant, $\Lambda_{\rm eff}$, or called Dark Energy. It falls off like t_*^{-2}, as shown by the last term. This is one of the most useful results in the current analysis. On the other hand, ρ_* is for the ordinary matter density in radiation-dominance, again falling off like t_*^{-2}, according to (14).

Then we have come to the solution for m_*, the particle mass in Efr. It should behave like $\sim t_*^{-1/2}$. I am going to tell how I come up with this solution, in the first place. Perhaps the simplest way is to make use of the relation

$$am = a_* m_*. \tag{16}$$

On LHS, a is the scale factor in Jfr, which was shown to be a constant according to the first of (8). We also found $m = $ const as in (9) in accordance with BD model. As we also find, the product am happens to be invariant under conformal transformation. Combining these with the solution (10) we have no way to avoid (15), hence in conflict with OUIP. From this point of view, (15) is in fact a bad news. We fail to accept Efr as a physical frame.

Naturally we may wonder if Efr can be still saved by revising part of the theory in such a way that we come up with the conclusion $m_* = $ const acceptable for the physical frame. We are going to show very briefly how we can do this.

For the sake of illustration, let us assume that the matter fields can be represented by a single, free and massive fermion field, ψ, so that the matter Lagrangian in Jfr is given by

$$L_{\rm matter} = -\overline{\psi}\,(\partial\!\!\!/ + m)\,\psi. \tag{17}$$

The second term on RHS is a constant mass term, a consequence of appreciating the BD model, as we explained before. We attempt, however, to replace this term by the Yukawa interaction term;

$$L_{\rm matter} = -\overline{\psi}\,(\partial\!\!\!/ + f\phi)\,\psi, \tag{18}$$

where f is a dimensionless coupling constant. This is obviously against BD's premise, hence at the risk of WEP violation. This by no means keeps us, on the other hand, from applying a conformal transformation to move to Efr in which we find the matter Lagrangian;

$$L_{*\rm matter} = -\overline{\psi}_*\,(\partial\!\!\!/_* + m_*)\,\psi_*, \tag{19}$$

where we introduced ψ_* defined by $\psi_* = \Omega^{-3/2}\psi$ together with the same for $\overline{\psi}$. By this transformation we then determine m_* to be given by

$$m_* = \xi^{-1/2} f, \tag{20}$$

which is a constant, in consistency with our goal stated above. This is the way we successfully save Efr as a physical frame, though with certain problems, as will be discussed again briefly.

At this moment, however, we notice that the matter Lagrangian (19) contains no scalar field σ. Thanks to this decoupling, we may find no way to detect WEP violation as long as we use the matter field, represented by ψ_* in the above simplified illustration, to measure the effects. This is true, somewhat curiously, in spite of BD's general argument in Jfr ruling out WEP. In fact the absence of the scalar field in the matter Lagrangian in Efr provides us with an alternative way to save WEP, like the Jfr counterpart stated in BD's premise.

As it turns out, however, the decoupling and undetectability just mentioned in Efr are true only *classically*. In fact *quantum* effects come in easily arising from the relativistic quantum field theory to be developed in tangential Minkowski spacetime. Consequently, WEP violation re-emerges again in the realistic environments. Quantitative estimates are derived through what is known as quantum-anomaly calculations, which reveal, at the same time, that the effects are rather weak.[6]

3 Decaying cosmological constant and Dark Energy

We have come to summarizing what we have achieved. Our Jfr is a theoretical frame, sometimes called string frame, in which we have a theoretical cosmological constant $\Lambda_{\rm th} \sim 1$, while our Efr is nearly identified with the physical, or the observational frame, to a good approximation, only up to quantum effects estimated rather weak. We have the effective cosmological "constant" given essentially by ρ_* falling off like t_*^{-2} according to (13).

More precisely, the identification for the physical frame needs more scrutiny. Due to the quantum effects, in fact, the truly physical frame is somewhat different from the pure Efr. But before going into details, we test how good the Efr relation at the present epoch, now put into the form;

$$\Lambda_{\rm eff0} \sim t_{*0}^{-2}, \tag{21}$$

where the suffix 0 is for the present epoch. LHS was shown, in the paragraph preceding (5), to be 10^{-120} in P Units based on the observation, while $t_{*0} \sim 10^{60}$ in the same units, as was also noted following (3). By substituting this into RHS of (21), we come across a fully impressive agreement with LHS, to be hardly dismissed as a mere coincidence. We call this *Scenario of a decaying cosmological constant*, which will turn out later to be applied to a considerable portion of the entire history of the universe.

According to this *Scenario*, today's value of the observed value $\Lambda_{\rm eff}$ is this small simply because we are *old cosmologically*, but *not* because we fine-tuned any of the theoretical parameters. It sounds as if we are rediscovering Dirac in 1937, now applied to Λ but not to G.

We may also repeat what we stated before: The simplest approach due to Jordan has now reached the above *Scenario* by leaving the BD model, at the risk of WEP violation hopefully barely below the observational upper bounds. We have also come through non-trivial arguments on how the physical frame is selected. We also add that there seems to be no other theoretical ideas, simple still natural, to account for the simple yet highly remarkable observational achievement (21), the central message of today's version of the cosmological constant problem.[7]

Before closing my first half of today's presentation, I am going to discuss briefly two related subjects.

Scaling *vs* tracking behaviors?

This is related to (13) and (14), on ρ_σ and ρ_* for $\Lambda_{\rm eff}$, or Dark Energy and the ordinary matter densities, respectively, but sharing the same manner of falling off $\sim t_*^{-2}$ in Efr, called the scaling behavior.

[6] The WEP violating terms in the Jfr matter Lagrangian turn out to come with dimensionless coupling constants, as shown generically in the the Yukawa interaction term in (18). The simplicity of BD's premise, decoupled ϕ field in Jfr, is now replaced, miraculously, by scale invariance of equal simplicity, except for the Λ-dependent potential as in (7). This will eventually result literally in the spontaneously broken scale invariance with σ as a Nambu-Goldstone boson in a strict sense, somewhat like a rebirth of the idea as mentioned at the beginning of Section 1. Also the quantum-anomaly-type regularization of the loop integrals parametrized by D-dimensional spacetime off 4 dimensions is closely connected with a technical way to implement a breaking of scale invariance, or dilatation symmetry, in the Lagrangian in $D \neq 4$. Through this line of arguments we find a fascinated interplay between scale invariance and WEP. For more details, see Ref. [3]

[7] This result itself had been foreseen much earlier by Y. F. in 1982 [15], also by O. Bertolami in 1986 [16], though the way of deriving the result is in a much better shape at present than it used to be.

This is, however, not the way we expect an extra acceleration of the universe. Observed result appears to require a nearly constant ρ_σ, called the tracking behavior, which obviously demands us a remedy. Skipping all the details, we simply show the diagrams in Fig. 2. In the bottom panel, we plotted two densities ρ_σ (also similar to ρ_s) and ρ_* as functions of t_* in the log-log scale. The two densities behave $\sim t_*^{-2}$ as overall behaviors, thus inheriting the Scenario of the decaying cosmological constant, applied, rather unintentionally, to a long time-scale starting right after the primordial inflation. Looking into more closely reveals, however, we notice certain non-smooth behaviors, particularly occasional plateau behavior of $\Lambda_{\rm eff}$, with a concomitant sharp rise of the scale factor, causing a mini-inflation, as shown in the top panel. An interlacing behaviors between two densities are also noted.

These are the behaviors designed rather phenomenologically supposed to come from quantum effects hence departing from the pure Efr solutions. Underneath such local behaviors to fit the observations,[8] we still find an unmistakable sign of the persistent and dominant overall trend based on the simple scalar-tensor theory.

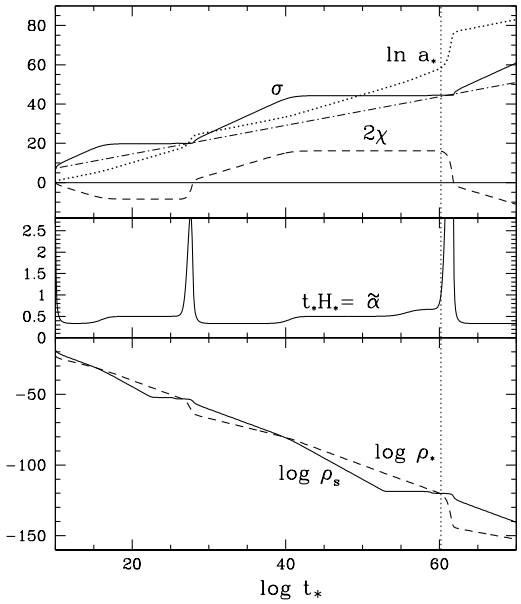

Figure 2: In the bottom panel, we plot ρ_*, denoted here by ρ_s for $\Lambda_{\rm eff}$ and ρ_* for the ordinary matter density as functions of the cosmic time in the log-log scale, so that the present epoch is around 60. In addition to the overall behaviors $\rho_s \sim \rho_* \sim t_*^{-2}$, to be understood in terms of the simplest version of the scalar-tensor theory, we note certain non-smooth and local behaviors. In particular, plateau behaviors of ρ_s triggers the mini-inflation of the scale factor a_* as shown in the top panel. Taken from Fig. 5.8 of Ref. [3].

Locally massive *vs* globally massless behaviors?

By a locally massive behavior we simply mean a nonzero mass of the scalar field σ somewhere around $\sim 10^{-9}$eV, basically given by (1). By a globally massless behavior, on the other hand, we mean the Efr solution given by (11), which can be traced back to the exponential potential $V(\sigma) = \Lambda e^{-4\zeta\sigma}$ as shown in (7). This potential is so smooth that we have no local minimum as an indication of a nonzero mass, hence described roughly as a massless behavior. These two behaviors may appear contradictory with each other, but might be two different ways in which the same thing σ shows itself in two utterly different surroundings.

[8] For more details, see our Ref. [3], together with Refs [17].

Equation (11) even appears to display a purely classical evolution of the *entire* universe, whereas the nonzero mass is a quantum effect of the field exchanged between two *local* objects. We are now going to discuss another local phenomena in which σ mediates a force between two photons inside a laser beam, now in the second half of my talk.

4 Attempted experimental search for the scalar field

We want naturally to probe experimentally the gravitational scalar field supposed to be as light as $m_\sigma \sim 10^{-9}$eV, as a bench mark, though the latitude of a few orders of magnitude is to be understood. An obvious issue is how we can overcome the σ-matter coupling as weak as the gravitational coupling, or $M_{\rm P}^{-1}$, by some non-gravitational means. In the past searches for non-Newtonian gravity or the fifth force, huge and heavy objects were often used, sometimes even appealing to natural environments, like water reservoirs, bore holes, cliffs, and so on, still ending up only with unavoidable and uncontrollable uncertainties [5],[18]. This time, in contrast, we are going to propose laboratory experiments by means of precision measurements on photon-photon scattering taking place in high-intensity laser beams. The content of the following part of the present paper is based largely on our joint work with Kensuke Homma [19].

We start with assuming the scalar-field-dominated processes, as shown diagrammatically in Fig. 3.

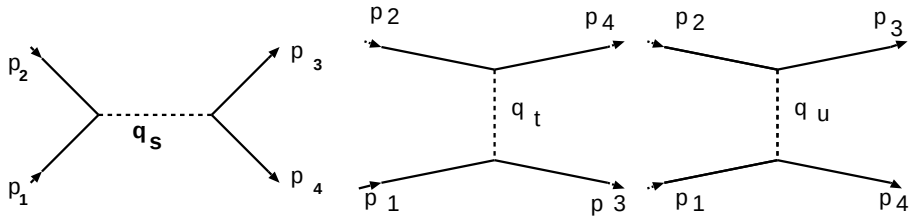

Figure 3: σ-dominated diagrams for the photon-photon scattering. Solid lines are for the photons with the attached momenta p's while the dashed lines for σ, in the s-, t-, and u-channels, respectively.

We avoid loop diagrams as often used in the QED box diagrams [20]. We are particularly interested in the s-channel process in which the scalar field occurs as a real resonance hence making an overwhelming contributions.

Unlike conventional CM or Lab frames, we prefer the frame in which we have the quasi-parallel incident beams, as shown Fig. 4.

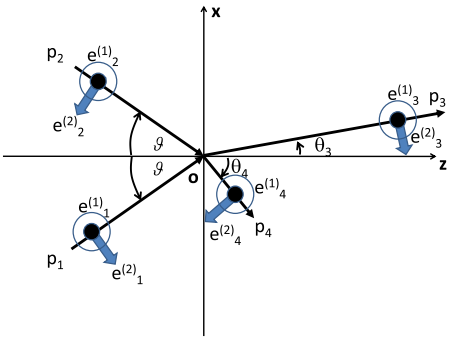

Figure 4: The two photons with the momenta p_1 and p_2 are incident nearly parallel to each other, making a small angle 2ϑ. At the middle we set up the z axis. The outgoing photons p_3 and p_4 are also shown. The polarization vectors are shown, but with the related details skipped in the present text.

The incident photon momenta are parametrized as

$$\begin{aligned} p_1 &= (\omega \sin\vartheta, 0, \omega\cos\vartheta; \omega)\,, \\ p_2 &= (-\omega \sin\vartheta, 0, \omega\cos\vartheta; \omega)\,, \end{aligned} \tag{22}$$

where ω is the common frequency, while the outgoing photon momenta are

$$\begin{aligned} p_3 &= (\omega_3 \sin\theta_3, 0, \omega_3\cos\theta_3; \omega_3)\,, \\ p_4 &= (-\omega_4 \sin\theta_4, 0, \omega_4\cos\theta; \omega_4)\,, \end{aligned} \tag{23}$$

where the axial symmetry around the z axis is assumed for the s-channel reaction. Details on the polarizations will be omitted in what follows.

We choose ϑ as small as $\sim 10^{-9}$ so that we have the relation

$$\vartheta \approx \frac{m_\sigma}{\omega_1}, \tag{24}$$

in which we use the symbol $\omega_1 \equiv 1\text{eV}$ which provides us with a typical energy scale of the processes to be discussed. In (23), we choose $0 < \theta_3 < \vartheta < \theta_4 < \pi$ so that $0 < \omega_4 < \omega_3 < 2\omega$.

Notice also that the frame we mentioned can be obtained from the CM frame in which the two photons collide each other head-on along the x axis, and Lorentz boosted in the z direction with the velocity $\beta_z = \cos\vartheta$.

We compute the differential cross section with respect to p_3;

$$\frac{d\sigma}{d\Omega_3} = \left(\frac{1}{8\pi\omega}\right)^2 \sin^{-4}\vartheta \left(\frac{\omega_3}{2\omega}\right)^2 |\mathcal{M}|^2, \tag{25}$$

where $\mathcal{M}$ is an invariant scattering amplitude, which may depend on ω_3, for example. In the context of the σ-dominance, however, we find no such dependence in $\mathcal{M}$. In this sense, possible ω_3-dependence comes only through the kinematical factor $(\omega_3/2\omega)^2$.

Out of $\sin^{-4}\vartheta$, two come from the phase-volume integral, whereas the remaining is due to the flux of the two-photon beam [21];

$$1/\sqrt{(p_1 p_2)^2} \approx 1/\left(2\omega^2 \sin^2\vartheta\right). \tag{26}$$

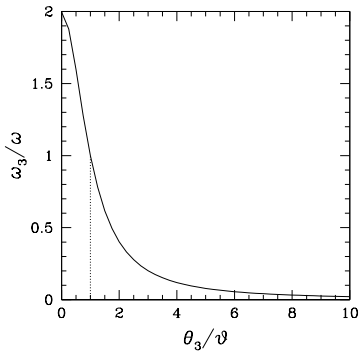

Figure 5: ω_3/ω plotted against θ_3/ϑ. Note that the forward peak is extremely narrow with the angular width $\sim \vartheta \sim 10^{-9}$.

We also find

$$\omega_3 = \frac{\omega \sin^2\vartheta}{1 - \cos\vartheta\cos\theta_3}, \tag{27}$$

implying that ω_3 shows a sharp forward peak toward $\theta_3 \to 0$, confined to the angle ϑ, which is much smaller than any of the practical angular resolution, as shown by Fig. 5. The peak reaches a top with $\omega_3 = 2\omega$, carrying the entire incident energy, providing an observational signature unique to the frame with quasi-parallel incident beams.

It is important to notice, however, that the peak is too narrow to be measured directly. On the other hand, ω_3/ω can be measured accurately, hence allowing to set up a threshold $\bar{\omega}_3$, accepting the events only for $\omega_3 > \bar{\omega}_3$. Choosing $\bar{\omega}_3 > \omega$ turns out to be highly convenient to remove the large amount of the unwanted background photons coming non-interacting flowing out also to the forward direction.

According to Fig. 5, also from (27), we then define the angular boundary $\theta_3 \le \bar{\theta}_3 = \vartheta\sqrt{\delta/2}$, where δ is defined by $\bar{\omega}_3/\omega = 2 - \delta$. This $\bar{\theta}_3$ is of the same order of magnitude as ϑ which is extremely small. Nearly automatically, we are then considering the *partially integrated* cross section defined by

$$\overline{\sigma} \equiv 2\pi \int_0^{\bar{\theta}_3} \left(\frac{d\sigma}{d\Omega_3}\right) \sin\theta_3 d\theta_3 \sim \left(\frac{d\sigma}{d\Omega_3}\right)_0 2\pi \int_0^{\bar{\theta}_3} \left(\frac{\omega_3}{2\omega}\right)^2 \sin\theta_3 d\theta_3 \approx \left(\frac{d\sigma}{d\Omega_3}\right)_0 \pi\vartheta^2 \frac{\delta}{2}, \tag{28}$$

where the subscript 0 implies the value estimated at the forward direction, also to the linear approximation with respect to δ. The dependence on ϑ^2 found on the far RHS can be understood because the integrand is approximately proportional to θ_3. We thus find that we can make use only of a tiny portion of solid angle which is reasonably sized to detect the desired events, though the ultimate reason can be traced back to the narrow forward peak of ω_3. The consequence will be discussed later again in connection with the whole analysis of enhancing the signals.

In Fig. 6 we show a simplified experimental setup. The incident laser beams will meet at a point to make an angle 2ϑ. The nearly frequency-doubled photon will give a signal in the detector placed along the z axis. This setup, though easy to understand the principle, is too naive particularly for $\vartheta \ll 1$. A more practical setup will be presented later.

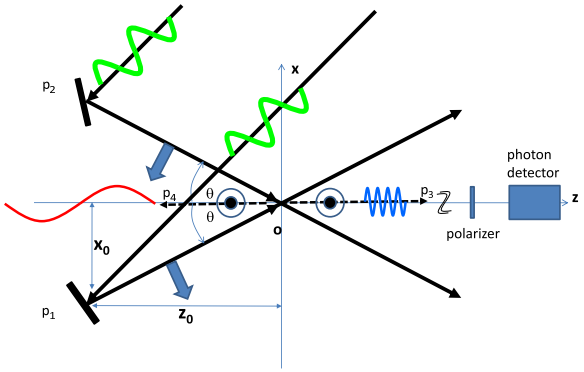

Figure 6: A simplified experimental setup. Two laser beams will collide each other to produce the photon p_3 to be detected at the detector. More practical setup will be shown later.

5 Resonance amplitude

In Fig. 3 we assumed a vertex for the photon-photon-σ coupling, which can be derived from the scalar-tensor theory, described by the interaction Lagrangian;

$$-L_{\mathrm{mx}\sigma} = \frac{1}{4} B M_{\mathrm{P}}^{-1} F_{\mu\nu} F^{\mu\nu} \sigma, \tag{29}$$

where we start to re-install M_{P} explicitly to demonstrate the gravitational nature. In addition, the factor $B = (2/9)(\alpha/\pi)\mathcal{Z}\zeta$ includes the fine-structure constant together with certain parameters.[9] In

[9] $\mathcal{Z}$ represents an effective number of such fundamental fields, like quarks and leptons. For more details see Ref. [3], in which the factor (1/12) in (6.181) has been multiplied by 8/3 to give (2/9) when the complex scalar matter fields in the loop

fact the coupling (29) is a consequence of a quantum effect derived through the quantum-anomaly-type calculation, hence WEP violating, as was discussed toward the end of Section 2.

We immediately compute the decay rate of σ into two photons;

$$\Gamma_\sigma = (16\pi)^{-1} \left(BM_{\rm P}^{-1}\right)^2 m_\sigma^3, \tag{30}$$

giving the decay lifetime $\Gamma_\sigma^{-1} \sim 3 \times 10^{54} t_0$, where t_0 is the age of the universe.

We also compute the Feynman amplitude for the first diagram of Fig. 3 in the s-channel process;[10]

$$\mathcal{M}_{1111s} = -\left(BM_{\rm P}^{-1}\right)^2 \frac{\mathcal{N}}{(p_1+p_2)^2 + m_\sigma^2} = -\left(BM_{\rm P}^{-1}\right)^2 \frac{\omega^4(\cos 2\vartheta - 1)^2}{2\omega^2(\cos 2\vartheta - 1) + m_\sigma^2}, \tag{31}$$

where the denominator in the first equation is the propagator of σ, while $\mathcal{N}$ is a well-defined but complicated combination of the momenta and the polarization vectors. Re-expressing them in terms of ω and ϑ according to (22), we arrive at the second equation. We also replace m_σ by $m_\sigma - i\Gamma_\sigma/2$ for a nonzero width of σ as a resonance.

We want to make the resonance nature more explicit. For this purpose we introduce a variable ξ defined by

$$\xi = \omega^2 - \omega_r^2, \tag{32}$$

where

$$\omega_r^2 = \frac{m_\sigma^2/2}{1 - \cos 2\vartheta}, \tag{33}$$

corresponding to m_σ^2. Also corresponding to Γ_σ we define

$$a = \frac{m_\sigma \Gamma_\sigma/2}{1 - \cos 2\vartheta}. \tag{34}$$

The resonance condition, $(p_1+p_2)^2 + m_\sigma^2 = 0$, is now translated into $\xi = 0$. In this neighborhood, we approximate (31) by

$$\mathcal{M}_r(\xi) \approx -4\pi \frac{a}{\xi + ia}, \quad \text{hence} \quad |\mathcal{M}_r(\xi)|^2 \approx (4\pi)^2 \frac{a^2}{\xi^2 + a^2}, \tag{35}$$

precisely the Breit-Wigner one-level formula. Remarkably enough we reconfirm what has been well-known;

$$\mathcal{M}_r(\xi) = 4i\pi, \quad \text{or} \quad |\mathcal{M}_r(\xi)|^2 = (4\pi)^2, \tag{36}$$

where RHS's are finite constants *independent of strength* of the coupling. This implies that our amplitude right at the resonance is by no means small even if we started from (31) which is multiplied by $M_{\rm P}^{-2} \sim G$.

It is true that this result is verified only in the extremely limited range of $|\xi| \lesssim a$ for the second of (35), where $a \sim M_{\rm P}^{-2} \sim 10^{-77}\omega_1^2$ according to the estimate of (30) and (34), with $\omega_1 \equiv 1\text{eV}$ introduced after (24) as a typical energy scale of the system. We also keep it in mind that the presence of $M_{\rm P}^{-2}$ in (31) constrains the size of $|\mathcal{M}|^2$ as small as $\sim M_{\rm P}^{-4}$ as a whole including non-resonance contributions. We will nevertheless exploit the *huge gain* of $\mathcal{O}(M_{\rm P}^4)$ when $|\mathcal{M}_r|^2$ at $\xi = 0$ is compared with the overall size in our efforts to enhance the gravitationally weak signals.[11]

in the toy model are replaced with the more realistic Dirac fields. The same type of the interaction had been introduced from a rather phenomenological point of view [22] and in other references. It was shown, on the other hand, that this type of the coupling is left unconstrained by the solar-system experiment, as long as the force-range of σ is shorter than the solar radius, whatever the origin [23].

[10] The numerals in the suffix on LHS are for the photon polarizations, not to be discussed in the text.

[11] This is precisely a consequence of exploiting the scattering amplitude in a full context. This makes a difference from the LSW approach in the axion search [24], in which the "wall" was inserted to remove the residual photons after producing a long-lived resonance, hence failing to enhance the weak signals to the maximum. Also the enhancement due to the resonance contributes to outnumber the result of the QED box-diagram [20] by as much as 50 orders of magnitude particularly in the forward direction. Notice also this type of enhancement makes it possible to ignore the contributions from the t- and u-channels.

The first issue arising from the small width $a \ll \omega_1^2$, allowing practically no direct measurement of the resonance peak in any energy scale of ω_1, can be dealt with by an *averaging* process;

$$\overline{|\mathcal{M}_r|^2} \equiv \frac{1}{2\tilde{a}} \int_{-\tilde{a}}^{\tilde{a}} |\mathcal{M}_r(\xi)|^2 d\xi = (4\pi)^2 \eta^{-1} \frac{\pi}{2} \hat{\eta}, \tag{37}$$

where we have introduced $\tilde{a}$ as large as ω_1^2, with $\eta \equiv \tilde{a}/a \gg 1$. The occurrence of η^{-1} on RHS will be justified as long as we substitute the integrand $|\mathcal{M}_r(\xi)|^2$ exactly from the second of (35), where $\hat{\eta} \to 1$ in the limit $\eta \to \infty$. But we may interpret this intuitively as a probability of hitting a small target width a aiming from a wider platform as large as $\tilde{a}$. Notice also that $\eta^{-1} \sim 10^{-77}$ is somewhat close to $(m_\sigma/M_{\rm P})^2 \sim 10^{-72}$.

We now sketch briefly what we have done and what we are going to do for the likely enhancement of the weak signals. First our comparison of $|\mathcal{M}_r(0)|^2 \sim M_{\rm P}^0$ with $|\mathcal{M}|^2 \sim M_{\rm P}^{-4}$ as a whole might be represented by a gigantic leap shown near the left end of Fig. 7. This will be followed by a setback by $\eta^{-1} \sim 10^{-72}$ corresponding to the averaging process given by (37). Remarkably, we are still at the middle, still up by more than 70 orders of magnitude from the bottom.

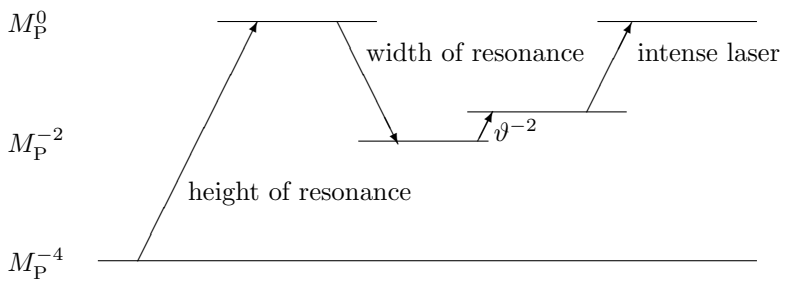

Figure 7: Schematic representation of enhancing the gravitationally weak signals $\sim M_{\rm P}^{-4}$ finally to those at the level of $\sim M_{\rm P}^0$.

We further attempt to go up by substituting the value $\vartheta \sim 10^{-9}$ into (25) to obtain $\vartheta^{-4} \sim 10^{36}$.[12] But this is the time when we should revisit the discussion around (28). With the averaged resonance contribution (37), the partially integrated cross section (28) goes like this;

$$\overline{\sigma} = 2\pi \int_0^{\bar{\theta}_3} \left(\frac{1}{8\pi\omega}\right)^2 \vartheta^{-4} \left(\frac{\omega_3}{2\omega}\right)^2 \sin\theta_3 d\theta_3 (4\pi)^2 \eta^{-1} \frac{\pi}{2} = \frac{\pi^2}{16\omega^2} \vartheta^{-2} \eta^{-1} \delta. \tag{38}$$

Due to the factor ϑ^2 in (28), we have now $\vartheta^{-2} \sim 10^{18}$ rather than ϑ^{-4} expected previously in (25). This reduced gain is probably one of the prices we have to pay for reaching realistic goals.

We are then somewhat above the "middle" as also shown in Fig. 7. We are still short of achieving the goal of $\mathcal{O}(M_{\rm P}^0)$ by something like 54 orders of magnitude. We aim to fill this up finally by appealing to the intensity of the laser beam.

It might be appropriate now to show a more realistic experimental setup in Fig. 8 in which we adopt one-beam focusing inside the beam itself in place of the two-beam focusing illustrated in Fig. 6.

A pulse of laser with a frequency held fixed to ω_1 comes from the left of the lens system, which focus the beam toward the interaction volume denoted by D. Pairs of photons will collide each other, as before, then producing the outgoing photon p_3 with the frequency nearly 2ω, finally reaching the detector. We

[12] This can be done without potential danger of suffering from an infinity in $\overline{\sigma}$ in the limit $\vartheta \to 0$, because the far RHS of (31) is shown to behave like $\sim \vartheta^4$ for $\vartheta^2 \ll (1/4)(m_\sigma^2/\omega^2)$.

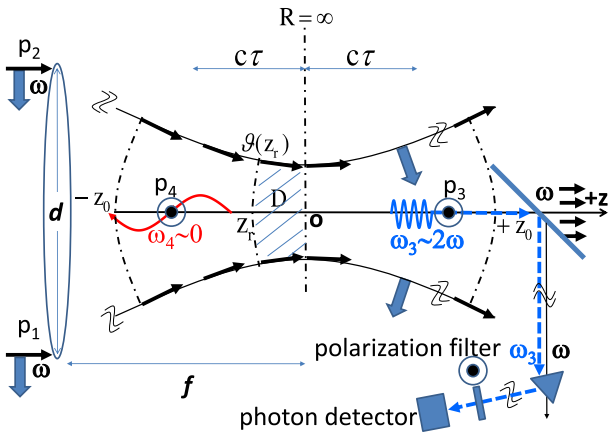

Figure 8: A one-beam focusing setup in which the beam is focused by means of a lens system, to the interaction volume D. Also the frequency of the incident laser pulse is fixed, while the incident angle varies around the value $\sim 10^{-9}$.

find that the angle ϑ somewhat distributed around the value $\sim 10^{-9}$. Combining (32) and (33) with $\omega = \omega_1$ we find

$$\xi \approx \omega_1^2 - \frac{m_\sigma^2}{4\vartheta^2}. \tag{39}$$

The averaging process (37) might then be re-expressed as an integral with respect to ϑ. Corresponding to $\xi = 0$, we have the resonance condition for the angle;

$$\vartheta_r = \frac{m_\sigma}{2\omega_1}, \tag{40}$$

which is naturally $\sim 10^{-9}$ according to (24).

6 Required laser intensity

Given the partially integrated averaged cross section $\Delta\sigma$ (28) we obtain the yield by[13]

$$\mathcal{Y} = \mathcal{L}\Delta\sigma \tag{41}$$

with the luminosity $\mathcal{L}$ given by

$$\mathcal{L} \approx \frac{\bar{N}^2/2}{\pi\lambda^2}, \tag{42}$$

where the numerator is for the combinatorics to pick up a pair of two photons out of the averaged photon number $\bar{N}$ in a pulse of the laser, while λ is its wavelength.

Using the numerical values for $\omega = \omega_1$ and $\delta \approx 0.1$, also integrating over the time interval of a pulse, we find

$$\mathcal{Y} \approx 10^{-63}\bar{N}^2. \tag{43}$$

With $\mathcal{Y} \sim 1$, expecting to find *an event per pulse* focusing, we then obtain the required photon number, $\bar{N}_1 \sim 10^{32}$ which is disappointingly larger than 10^{22}, corresponding to what appears to be rather close to the strongest pulse available at present or near future [25]. Sticking to using this so-called 1kJ beam as a convenient reference would imply $\mathcal{Y} \sim 10^{-18}$ per pulse, hence it takes $\sim 10^{10}$y even operated with repetition period of 10 Hz.

We still point out that there are certain aspects which have been left unscrutinized but possibly break through the impasse we face currently. In the first diagram of Fig. 3 we consider the left vertex in which

[13]The discussion in this section represents a technical status at the time of delivering the talk. Further scrutinies from wider perspectives, hence even possible revisions, will be made in our future publications.

two photons annihilate, unrealistically into the *vacuum*, also creating σ. In reality, they annihilate into the interaction volume shown in Fig. 8, thus into the *sea of photons* having been prepared in the initial state of the laser. We may even focus upon each photon, the one with the momentum p_1, for example. There must be other photons which are in the quantum state sharing the same quantum numbers as p_1. Suppose there are n of them. What is relevant here is the transition amplitude

$$< n|a|n+1 >= \sqrt{n+1}, \tag{44}$$

derived in accordance with the commutation relations on the annihilation operator a and the creation operator $a^\dagger$, respectively. This is what has been long known in connection with the *induced* absorption of light by atoms. Leaving this traditional association with atomic transitions, we may consider creation and annihilation of photons of their own merit, though some kind of association is always required, this time with the scalar-field coupling.

With the choice $n = 0$, (44) reduces to

$$< 0|a|1 >= 1, \tag{45}$$

representing a *spontaneous* annihilation, which is precisely computed by means of the Feynman rules.

We then may attempt an extension of the conventional estimate due to the Feynman diagrams, by the rule summarized symbolically;

$$\left.\begin{array}{l}\text{Feynman amplitude}\\ \mathcal{Y}_{\rm conv}\end{array}\right\} \text{ to be corrected by } \times \left\{\begin{array}{l}\sqrt{n+1},\\ n+1.\end{array}\right. \tag{46}$$

So far the discussions have been restricted obviously to discrete states. Transitions to the realistic continuous states can be achieved basically by replacing n by a distribution function $n(\vartheta)$;

$$n+1 \sim n \to n(\vartheta)\bar{N}, \tag{47}$$

with the normalization condition

$$\int n(\vartheta)d\vartheta = 1, \tag{48}$$

extending the obvious condition $\sum n = \bar{N}$. We also assumed that the distribution function depends on the slope of the photon momenta with its frequency fixed to ω_1, apart from the polarization states.

We may repeat nearly the same about another photon p_2, with an approximate assumption that the same function $n(\vartheta)$ can be used. On the other hand, the same type of process may not be applied to the outgoing photons p_3 and p_4, because these momenta are most likely close to 2ω and 0, respectively, according to (27) and Fig. 5, then entirely off the range included in the initial degenerated state, which also includes little of the scalar field σ. For these reasons the modification (46) should apply only to the two incident photons in the present circumstances.

We also recall that the momenta p_1 and p_2 are such that they are connected to the σ line as shown in the first diagram of Fig. 3. This implies that the averaging integral in (37) is now multiplied by $n^2(\vartheta(\xi))\bar{N}^2$ inside the integration. In view of the fact that $|\mathcal{M}_r(\xi)|$ is peaked sharply at $\xi = \xi_r = 0$, corresponding to $\vartheta = \vartheta_r \equiv (1/2)(m_\sigma/\omega_1)$ defined by (40), we find that the function $n(\vartheta)$ can be taken outside the integral to be $n(\vartheta_r)$. In this way we have

$$\mathcal{Y}_{\rm conv} \to \mathcal{Y} = \mathcal{Y}_{\rm conv} \times n^2(\vartheta_r)\bar{N}^2 \approx 10^{-63} n^2(\vartheta_r)\bar{N}^4, \tag{49}$$

where we have substituted (43) in obtaining the far RHS. This indicates an obvious enhancement by including the induced effects, though depending on the value of $n(\vartheta_r)$.

For a one-beam focusing, we expect a Gaussian behavior of $n(\vartheta)$, hence suggesting a rather flat function near ϑ_r. A preliminary analysis shows $n(\vartheta_r) \sim 10^5$, hence $\bar{N}_1 \sim 10^{13}$, considerably smaller than 1kJ beam. Obviously, however, more scrutinized studies will be needed to reach reliable final results on $\bar{N}_1$.

References

[1] C. B. Chiu, Y. Fujii and W. W. Wada, Lett. Nuovo Cimento **1** (1971), 110.

[2] Y. Fujii, Nature Phys. Sci. **234** (1971), 5.

[3] Y. Fujii and K. Maeda, *The Scalar-Tensor Theory of Gravitation*, Cambridge University Press (2003).

[4] G. W. Gibbons and B. F. Whiting, Nature **291** (1981), 636.

[5] E. Fishcbach and C. Talmadge, *The Search for Non-Newtonian Gravity*, AIP/Springer, (1998).

[6] S. Schlamminger et al, Phys. Rev. Lett. **100** (2008), 041101.

[7] J. O'Hanlon, Phys. Rev. Lett. **29** (1972), 137. R. Acharia and P. A. Hogan, Lett. Nuovo Cim., **6** (1973), 668.

[8] P. Jordan, *Schwerkraft und Weltall*, Friedrich Vieweg und Sohn, 1955.

[9] P.A.M. Dirac, Nature **139** (1937),323; Proc.Roy.Soc.**A165** (1938),199.

[10] Y. Fujii, Prog. Theor. Phys. **118** (2007), 983.

[11] A. G. Riess et al., Astron. J. **116** (1998), 1009. S. Perlmutter et al., Nature **391** (1998), 51; Astrophys. J. **517** (1999), 565.

[12] M. B. Green, J. H. Schwarz and E. Witten, *Superstring Theory* (Cambridge University Press, 1987).

[13] K. Maeda and Y. Fujii, Phys. Rev. **D79** (2009), 084026.

[14] C. Brans and R. H Dicke, Phys. Rev. **124** (1961), 925.

[15] Y. Fujii, Phys. Rev. **D26** (1982), 2580.

[16] O. Bertolami, Nuovo Cimento **B93** (1986), 36.

[17] Y. Fujii, Phys. Lett. **B616** (1950), 141. Y. Fujii and S. Mizuno, Int. J. Mod. Phys. **D14** (1905), 677. Y. Fujii, Phys. Lett. **B660** (2008); 87, **B671** (2009), 207; arXiv:0908.4324; Proc. IAU 2009 JD9, 03-14 Aug. 2009, Mem. S.A.It. Vol. 75, 282, arXiv:0910.5090.

[18] A. Franklin, *The Rise and Fall of the Fifth Force*, (AIP, 1993).

[19] Y. Fujii and K. Homma, arXiv:1006.1762, though a preliminary version.

[20] W. Dittrich and H. Gies, *Probing the Quantum Vacuum* (Springer 2007).

[21] J. M. Jauch and F. Rhorlich, *The Theory of Photons and Electrons*, (Addison-Wesley, 1954). See also (3.78) in W. Greiner and J. Reinhardt, *Quantum Electrodynamics*, (Springer 1994).

[22] J. D. Bekestein, Phys. Rev. **D25** (1982), 1527.

[23] Y. Fujii and M. Sasaki, Phys. Rev. **D75** (2007), 064028.

[24] See, for example, G. Mueller, P. Skivie, D. B. Tanner and Karl van Bibber, arXiv: 0907.5387. A. Lindner, arXiv:0910.1686.

[25] See, for example, http://www.extreme-light-infrastructure.eu/

Radiation Recoil Velocity of a Neutron Star

Yasufumi Kojima [1]

Department of Physics, Hiroshima University, Higashi-Hiroshima 739-8526

Abstract

Kick velocity of a compact star is discussed. In particular, the recoil is calculated as a back reaction to the magnetic dipole and quadrupole radiations from a pulsar/magnetar born with rapid rotation. The process is slow one operating on a spin-down timescale. Resultant velocity depends on not the magnitude, but rather the ratio of the two moments and their geometrical configuration. The model does not necessarily lead to high spatial velocity for a magnetar with a strong magnetic field, which is consistent with the recent observational upper bound. The maximum velocity predicted with this model is slightly smaller than that of observed fast-moving pulsars.

Preface

It is a great pleasure to talk at this JGRG20 meeting for the 60th birthday of Takashi Nakamura Sensei and Kei-ichi Maeda Sensei. This meeting started two decades ago under their enthusiastic leadership, and has been developed successfully. Young generation including me has grown up through the meeting. I would like to express special thanks on this occasion.

1 Introduction

Formation of black holes and neutron stars is most violent energetic event in astronomy. However, the event rate is rare, so that the direct observation is very difficult. The obstacle can be overcome by observing into deep universe with advanced technology. Another approach to infer the past powerful happening may be possible by looking for some evidence. Velocity of the proper motion belongs to the category. High velocity of compact stars suggests the violent event at birth.

This kind of idea has been discussed since the beginning of relativistic astrophysics in the 1970's. For example, some black holes may have large velocity (>300km s^{-1}), and migrate from the Galaxy. One of the important mechanisms for high velocity is gravitational radiation. Beckenstein(1973) [1] formulated the linear momentum radiation for collapsing two-body problem in post-Newtonian approximation. Note that net linear momentum is radiated by the interference between different multipoles. (See Appendix for a simple demonstration.) Quadrupole and the next order octopole radiation generate it in the lowest order. The energy is a sum of each multipole radiation $\Delta E = \Delta E_2 + \Delta E_3 + \cdots$, whereas the linear momentum is $\Delta Pc \approx (\Delta E_2 \Delta E_3)^{1/2} \approx \varepsilon \Delta E$, where ΔE_l is the radiation by quadrupole ($l = 2$) and octopole ($l = 3$), and ε is the efficiency. Thus, a compact star with mass M gets the magnitude of velocity $v/c \approx \varepsilon(\Delta E/Mc^2)$ as a back reaction of linear momentum emission. Higher velocity is achieved in more relativistic system. The treatment is weak field approximation, so that it may be questionable to apply it to the events in strong gravity regime. The linear momentum radiation is also calculated for various cases by using linear perturbation of black hole space-time. See Ref.[2] for the summary of Kyoto group in the 1980's. The treatment is applicable to the events in strong gravity, but extremely small mass ratio of the binary is assumed. Radiation reaction is also ignored. Recently, full relativistic simulations of collision of two back holes have been performed, e.g., [3, 4]. See also Campanelli in this volume.

Interesting thing is that high velocity components in QSOs have been observed;for example ∼2500km s^{-1} in SDSSJ092712.65+294344.0[5] and ∼2100km s^{-1} in E1821+643[6]. These sources are candidates of gravitational radiation recoil. Gravitational radiation is very important mechanism to produce such high velocities especially in the merger of super-massive black hole binary. For the formation of stellar black

[1]Email address: kojima@theo.phys.sci.hiroshima-u.ac.jp

holes, there are many competing mechanisms. Supernova explosion is one of complicated physics. In addition to the gravitational radiation, anisotropic emission of neutrinos, (magneto-)hydrodynamical waves and electromagnetic waves may cause the kick velocity.

Possible origins of kick velocity of a neutron star are discussed in this paper. The understanding may become a useful hint for the black hole system. Observation of pulsar proper motion and some proposed scenarios are briefly reviewed in Section 2. In Section 3, a rocket mechanism is discussed in detail by electromagnetic radiation from rotating dipole and quadrupole moments in vacuum, which is recently considered[7]. Section 4 presents our conclusions.

2 Pulsar proper motion

Pulsar velocities are determined from measurements of their proper motion and distance. The position of pulsars is recorded by the periodic pulse, so that the proper motion of pulsars is easily determined than that of black holes. Manchester et al.(1974)[8] for the first time achieved it for PRS1133+16, using timing observation over a four-year period. Observational progress over three decades has provided some interesting results. Firstly, number of pulsars has been increased up to ∼1000. The statistical property becomes better. Hobbs et al.(2005)[9] analyzed a catalog of 233 pulsars, and found that the mean three-dimensional velocity is 400 km s^{-1}, which is converted from observed two-dimensional velocity $v_\perp$ on the sky. Second interesting discovery is fast moving pulsars. Very high velocities have been reported; B1508+55 ($v_\perp \sim 1000$ km s^{-1} [10]) and PSR2224+45 ($v_\perp > 800$ km s^{-1} [11]). Third one is existence of a magnetar, a class of neutron stars with super strong magnetic field strength $B_s \sim 10^{14-15}$G. The velocity is very interesting. At moment, the upper limit of the transverse velocity $v_\perp$ has been reported, although there is uncertainty in the value. For example, $v_\perp \sim 210$ km s^{-1} for AXP XTEJ1810-197[12], $v_\perp < 1300$ km s^{-1} for SGR 1900+14 [13, 14] and $v_\perp < 930$ km s^{-1} for AXP 1E2259+586[13]. On the other hand, the magnetic fields for the fast moving pulsars are quite ordinary, B_s ∼2-3 $\times 10^{12}$G. Thus, there is no clear correlation between the field strength and the velocity in the present sample.

A number of pulsar kick mechanisms have been proposed. See e.g, Ref.[15] for a review. They are classified by working epoch, pre-natal, natal and post-natal mechanisms. The pre-natal mechanisms is a binary breakup at the supernova explosion. Resultant escape velocity is not large, ∼ a few hundreds km s^{-1}. Next is the natal mechanisms. Several kick mechanisms operative at the core bounce of the supernova explosion have been proposed to date: anisotropic emissions of neutrinos (e.g., [16, 17]), hydrodynamical waves (e.g., [18, 19]), and MHD effects (e.g., [20]). Large-scale simulations are required to check any of these mechanisms, and are still in progress. Among these scenarios, a strong magnetic field may play a key role, since it naturally causes one preferable direction. However, very strong field strength $> 10^{15-16}$G seems to be needed. The origin of the strong fields is also a problem, fossil or dynamo action. Kick mechanisms at birth end on a dynamical timescale of the order of milliseconds or the cooling timescale of ∼ 10 s. If the strong magnetic fields are generated on a longer timescale, some natal kick mechanisms involved the magnetic-field-driven anisotropy do not work effectively. Recoil driven by electromagnetic radiation, which is operative on a longer spindown timescale of $\sim 10^3 (B/10^{15}\mathrm{G})^{-2} (P_i/1\mathrm{ms})^2$ s, has been proposed as a post-natal kick mechanism[21] (see also [15] for the corrected expression). The model is revisited as one of possible mechanisms in the next section. This does not mean that other scenarios are inadequate.

3 Kick driven by radiation

3.1 Generation of magnetic fields

The surface magnetic field strength B_s of a pulsar is conventionally estimated by matching the rotational energy loss rate with the magnetic dipole radiation rate, that is, $B_s \approx (3c^3 I P \dot{P})^{1/2}/(2\sqrt{2}\pi R_s^3)$, where I is the inertial moment, R_s is the stellar radius, P is the spin period, and $\dot{P}$ is the time derivative of the spin period. The precision of this approximation is only at the order of magnitude level because actual energy loss is not well described by magnetic dipole radiation in a vacuum. A more realistic model with current flows and radiation losses is required, but has not yet been established. A simple estimate

provides $B_s \approx 10^{12}$G for typical radio and X-ray pulsars, and $B_s \approx 10^{13}$-10^{15}G for magnetars, although the level of the approximation must be noted. Dynamo action in a rapidly rotating proto-neutron star with $P \approx 1$ ms is proposed as a mechanism for this amplification by 2-3 orders of magnitude (see e.g., [22, 23]).

Recent numerical simulations of dynamo action can be used to study the large-scale fields in fully convective rotating stars. For example, non-axisymmetric fields are generated in the case of uniform rotation [24], while mostly axisymmetric fields with a mixture of the first few multipoles are formed in the case of a differentially rotating star[25]. The results may not directly apply to pulsars or magnetars, but suggest that the magnetic field configuration of neutron stars may not be an ordered dipole. If there are higher-order multipoles, these will also contribute to the radiation loss. The upper bounds on their surface magnetic fields are rather loose. See Ref.[26] for a discussion of the magnetic fields of millisecond pulsars. The magnetic field strength B_{lm} relevant to the multipole moment of order (l, m) is limited to $B_{lm} \leq B_s/(mR_s\Omega/c)^{l-1}$, where $\Omega = 2\pi/P$ is angular velocity, and the radiation of each multipole $L_{lm} \sim c(mR_s\Omega/c)^{2l+2}\ (B_{lm}R_s)^2$ is assumed to be smaller than that of a dipole. Thus, a model with complex magnetic configuration at surface $B_{lm} \geq B_s$ $(l > 1)$ is allowed because of the small factor $R_s\Omega/c \ll 1$ for observed stars.

In the original work of the rocket mechanism[21], an oblique dipole moment displaced by a distance s from the stellar center rotates. This causes the radiation of higher order multipoles, whose superposition is generally asymmetric in the spin direction, leading to the kick velocity. In the off-center model, the quadrupole field B_2 of order $B_2 \sim (s/R_s) \times B_1 \sim B_1$ is involved. It is interesting to study the case where $B_2 \gg B_1$, because the constraint of the higher order component by the radiation is very weak, for example, $B_2 \sim (c/(R_s\Omega)) \times B_1 \gg B_1$. In this paper, the kick velocity induced by electromagnetic radiation is examined: A star rotates with both dipole and quadrupole magnetic fields, in which a larger quadrupole field $B_2 \gg B_1$ at the surface is allowed. The maximum kick velocity as a recoil of momentum radiation is evaluated. Evolution of the spin and spatial velocity is calculated.

3.2 Electromagnetic fields

Maxwell equations are solved for the fields outside a rotating object with angular frequency Ω in vacuum; the object has a magnetic dipole and quadrupole moments. The dipole moment is denoted by μ, and the direction is inclined from the spin axis by χ_1. Quadrupole moment is denoted by Q and the inclination angle of the symmetric axis is χ_2 from the spin axis. The electromagnetic fields outside the rotating magnetized object are described by the magnetic mupltipoles of order $l = 1, 2, |m| \leq l$, for which $E_r = \mathbf{E} \cdot \mathbf{r} = 0$ [27]. The explicit forms are written in Ref.[7]. Their characteristics are described below.

The electromagnetic fields for a rotating magnetic dipole are discussed at first. Near the stellar surface $R_s \leq r \ll c/\Omega$, the magnetic field reduces to

$$\mathbf{B} \to \mathbf{B}_{\rm near} = \frac{2\mu e^{i\lambda}}{r^3}\cos(\theta - \chi_1)\mathbf{e}_r + \frac{\mu e^{i\lambda}}{r^3}\sin(\theta - \chi_1)\mathbf{e}_\theta, \tag{1}$$

where $\lambda = \phi - \Omega(t - r/c)$. It is clear that the field near the surface represents a magnetic dipole inclined by the angle χ_1, which rotates in the azimuthal direction with $\phi = \Omega t$. The electromagnetic fields in the radiative region $(r \gg c/\Omega)$ are given by

$$\mathbf{B} \to \mathbf{B}_{\rm rad} = \frac{\mu\Omega^2}{c^2 r}P_1^1(\chi_1)P'^1_1(\theta)e^{i\lambda}\mathbf{e}_\theta + \frac{i\mu\Omega^2}{c^2 r}P_1^1(\chi_1)e^{i\lambda}\mathbf{e}_\phi, \tag{2}$$

$$\mathbf{E} \to \mathbf{E}_{\rm rad} = \frac{i\mu\Omega^2}{c^2 r}P_1^1(\chi_1)e^{i\lambda}\mathbf{e}_\theta - \frac{\mu\Omega^2}{c^2 r}P_1^1(\chi_1)P'^1_1(\theta)e^{i\lambda}\mathbf{e}_\phi, \tag{3}$$

where $P_l^m(x)$ is the associated Legendre function and the prime denotes the derivative with respect to x.

The electromagnetic fields for a rotating magnetic quadrupole are similarly discussed.The near-field is

$$\mathbf{B} \to \mathbf{B}_{\rm near} = \frac{3Qe^{i\lambda_2}}{2r^4}P_2^0(\theta - \chi_2)\mathbf{e}_r - \frac{Qe^{i\lambda_2}}{2r^4}P'^0_2(\theta - \chi_2)\mathbf{e}_\theta, \tag{4}$$

where the phase λ_2 is shifted by $\lambda_2 = \lambda + \delta$, because the meridian plane in which the symmetric axis of the quadrupole is located may differ by the azimuthal angle δ from that of the dipole. Equation (4)

represents the magnetic field of a rotating quadrupole, whose inclination angle is χ_2. Radiative fields in $r \gg c/\Omega$ become

$$\begin{aligned}\mathbf{B} \to \mathbf{B}_{\rm rad} &= -\frac{iQ\Omega^3}{36c^3 r}\left[P_2^1(\chi_2)P'^1_2(\theta)e^{i\lambda_2} + 2P_2^2(\chi_2)P'^2_2(\theta)e^{2i\lambda_2}\right]\mathbf{e}_\theta \\ &+ \frac{Q\Omega^3}{12c^3 r}\left[P_2^1(\chi_2)\cos\theta e^{i\lambda_2} + 4P_2^2(\chi_2)\sin\theta e^{2i\lambda_2}\right]\mathbf{e}_\phi, \end{aligned} \tag{5}$$

$$\begin{aligned}\mathbf{E} \to \mathbf{E}_{\rm rad} &= \frac{Q\Omega^3}{12c^3 r}\left[P_2^1(\chi_2)\cos\theta e^{i\lambda_2} + 4P_2^2(\chi_2)\sin\theta e^{2i\lambda_2}\right]\mathbf{e}_\theta \\ &+ \frac{iQ\Omega^3}{36c^3 r}\left[P_2^1(\chi_2)P'^1_2(\theta)e^{i\lambda_2} + 2P_2^2(\chi_2)P'^2_2(\theta)e^{2i\lambda_2}\right]\mathbf{e}_\phi. \end{aligned} \tag{6}$$

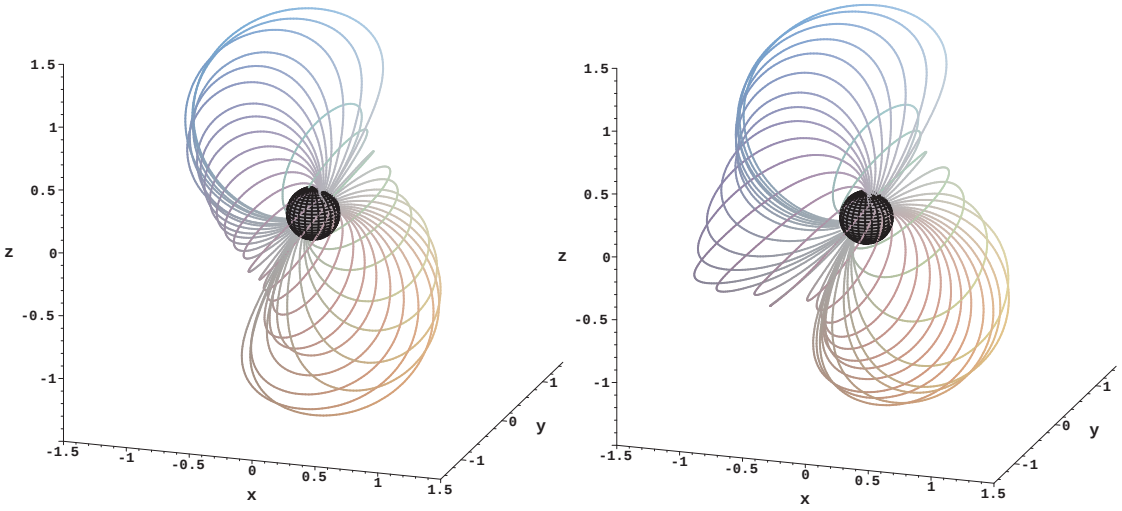

Figure 1: Closed magnetic field lines in the cases of pure dipole (left) and dipole plus quadrupole (right). The magnetic axis is inclined by angle $\chi_1 = \chi_2 = \pi/4$ from the spin axis z, and the azimuthal angle between moments is $\delta = \pi/2$. A sphere of radius $0.2c/\Omega$ at the origin is also shown. Distance is scaled by c/Ω.

The combination of dipole and quadrupole fields is compared with the case of a pure dipole. A snapshot of almost-closed magnetic field lines near the light cylinder is shown in Figure 1. Both inclination angles are the same $\chi_1 = \chi_2 = \pi/4$, but the meridian planes are perpendicular, that is, $\delta = \pi/2$. Field strength is set as $Q = 0.2\mu c/\Omega$. It is clear that the quadrupole field is added to the dipole one. The quadrupole field increases more rapidly with the decrease of the radius r, and dominates for $r < r_q \approx 0.2c/\Omega$ for the model parameter, since $B_1 \sim \mu/r^3$ and $B_2 \sim Q/r^4$.

Contour of outgoing flux is shown in Figure 2. This pattern by almost $m = 1$ mode rotates with the angular frequency Ω. There is a symmetry between upward and downward fluxes, in the case that two directions of dipole and quadrupole are parallel, $\delta = 0$. On the other hand, there is a small asymmetry in the case that two axes are perpendicular, $\delta = \pi/2$. This asymmetry causes net linear momentum and hence the recoil velocity.

3.3 Radiation

The radiation energy per unit time is obtained by integrating the time-averaged Poynting flux over the solid angle at the wave zone $r \gg c/\Omega$. The luminosity for a combination of electromagnetic fields described by eqs.(2),(3) and eqs.(5),(6) is given by

$$L = \int \frac{c}{4\pi}\overline{(\mathbf{E}_{\rm rad} \times \mathbf{B}_{\rm rad})} \cdot \mathbf{e}_r r^2 \sin\theta d\theta d\phi = \frac{2\mu^2\Omega^4}{3c^3}\sin^2\chi_1 + \frac{Q^2\Omega^6}{160c^5}\sin^2 2\chi_2 + \frac{2Q^2\Omega^6}{5c^5}\sin^4\chi_2. \tag{7}$$

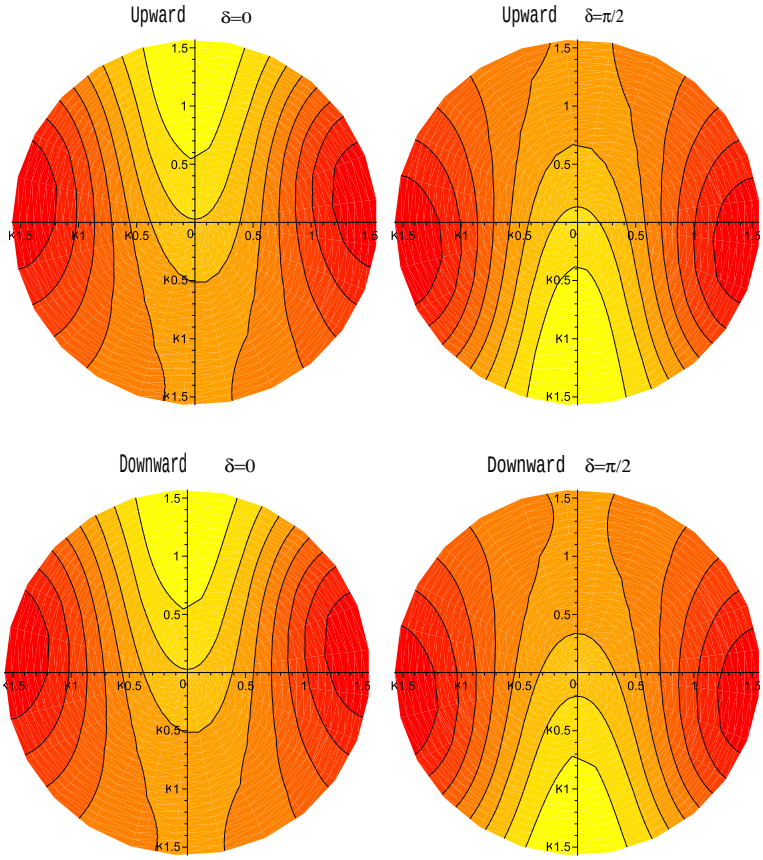

Figure 2: Contour of Poynting flux going in $+z$ direction(upper panel) and going in $-z$ direction(lower panel). Left ones are for the parallel case of dipole and quadrupole axes $\delta = 0$, whereas right ones for orthogonal case $\delta = \pi/2$.

The luminosity is the sum of the contributions from multipole radiation. Our model consists of three components, the magnetic dipole radiation $M_{1,1}$ specified by spherical harmonics index $(l, m) = (1, 1)$, and the quadrupole radiation $M_{2,1}$ and $M_{2,2}$. They correspond to the first, second and third terms in eq.(7). The third term is larger than the second term roughly by a factor $m^6 = 2^6$, which comes from the frequency of time variation.

The linear momentum radiated per unit time in the direction z is similarly calculated as

$$F = \int \frac{1}{4\pi} \overline{(\mathbf{E}_{\rm rad} \times \mathbf{B}_{\rm rad})} \cdot \mathbf{e}_z r^2 \sin\theta d\theta d\phi = \frac{\mu Q \Omega^5}{20c^5} \sin\chi_1 \sin 2\chi_2 \sin\delta. \tag{8}$$

The net flux arises from the interference of two multipoles, namely, the magnetic dipole $M_{1,1}$ and the quadrupole $M_{2,1}$. The angle χ_l governs the radiation strength of each multiple l, while the angle δ governs the interference. The most efficient configuration is realized when the two magnetic multipole moments are orthogonal, $\delta = \pi/2$. On the other hand, when both of the multipole moments lie in the same meridian plane (i.e., $\delta = 0$), the net linear momentum vanishes. This property can be understood from the fact that radiative electromagnetic fields in vacuum are expressed by the spherical Hankel function h_l and the asymptotic form for $\xi = \Omega r/c \gg 1$ is $h_l \sim \exp[i(\xi - l\pi/2)]/r$ for the multipole l. There is a phase shift $\pi/2$ between dipole and quadrupole fields, and this shift is important in the wave interference.

Table 1: Comparison of models.

Model	Multipole	α	β	γ	$\gamma/(\alpha\beta)^{1/2}$
Off-center dipole	$M_{1,1}, M_{2,1}, E_{1,1}$	0.33	0.83×10^{-2}	0.47	9.0
Dipole-quadrupole	$M_{1,1}, M_{2,1}, M_{2,2}$	0.33	0.10	0.18	0.97

3.4 Comparison

Our dipole-quadrupole model is compared with the off-center dipole one [15, 21]. The rates of energy and linear momentum are written in term of the magnetic dipole moment (μ_R, μ_ϕ, μ_z) in cylindrical coordinate and distance s from the spin axis as follows:

$$L = \frac{2\Omega^4}{3c^3}\left(\mu_R^2 + \mu_\phi^2\right) + \frac{4\Omega^6}{15c^5}s^2\mu_z^2. \tag{9}$$

The first term is the magnetic dipole radiation $M_{1,1}$. Correspondence to our expression is clear by replacing $\mu_R^2 + \mu_\phi^2 = \mu^2 \sin^2\chi_1$. The second term is derived from the sum of electric dipole radiation $E_{1,1}$ and magnetic quadrupole radiation $M_{2,1}$. Their contributions are $\Omega^6 s^2\mu_z^2/(6c^5)$ by $E_{1,1}$ and $\Omega^6 s^2\mu_z^2/(10c^5)$ by $M_{2,1}$, respectively. The parameter in the off-center dipole model corresponds to $Q\sin 2\chi_2 = 4s\mu_z$ except for a complex phase factor. There is a constraint on the quadrupole moment Q as $Q\sin 2\chi_2 \le 4\mu R_s \cos\chi_1$, since $s \le R_s$. In our model, it is possible to consider the case of $Q \gg \mu R_s$ in magnitude.

The linear momentum in the off-center dipole model is evaluated as[15]

$$F = \frac{8\Omega^5 s\mu_\phi\mu_z}{15c^5}. \tag{10}$$

Net linear momentum flux arises from two types of interference. One is between magnetic dipole radiation $M_{1,1}$ and electric dipole radiation $E_{1,1}$. The other is between magnetic dipole radiation $M_{1,1}$ and magnetic quadrupole radiation $M_{2,1}$. These contributions are expressed by $\Omega^5 s\mu_\phi\mu_z/(3c^5)$ and $\Omega^5 s\mu_\phi\mu_z/(5c^5)$, respectively. The latter reduces to eq.(8) if $s\mu_z = Q\sin 2\chi_2/4$ and $\mu_\phi = \mu\sin\chi_1\sin\delta$.

Although there is a slight difference in the radiative components between the off-center dipole and dipole-quadrupole models, both formulae for eqs. (7),(8) and eqs. (9),(10) are parameterized as

$$L = \alpha\frac{\mu^2\Omega^4}{c^3} + \beta\frac{Q^2\Omega^6}{c^5}, \tag{11}$$

$$F = \frac{\gamma}{10}\frac{\mu Q\Omega^5}{c^5}, \tag{12}$$

where α, β and γ are dimensionless numbers that depend on only the geometrical configuration. The typical values are listed in Table 1 for the simple assumption that $\sin\chi_l, \sin\delta \to 1/\sqrt{2}$, that is, the directional average of $\langle\sin^2\chi_l\rangle = \langle\sin^2\delta\rangle = 1/2$. It is clear that the coefficient β in our model is considerably larger than that in the off-center model. This comes from the radiation of $m = 2$.

3.5 Evolution

The angular velocity $\Omega(t)$ is determined by equating the loss rate of rotational energy with the luminosity L in eq.(11), and the velocity $V(t)$ is determined from the momentum emission F in eq.(12). In terms of the mass M and inertial moment I, we have

$$I\Omega\dot{\Omega} = -\alpha\frac{\mu^2\Omega^4}{c^3} - \beta\frac{Q^2\Omega^6}{c^5}, \tag{13}$$

$$M\dot{V} = -\frac{\gamma}{10}\frac{\mu Q\Omega^5}{c^5}. \tag{14}$$

By using the approximation $I = 2MR_s^2/5$, where R_s is the stellar radius, the magnitude of the velocity gained from the initial angular velocity Ω_i is given by

$$\Delta V = \frac{\gamma Q R_s^2}{25\mu}\int_{\Omega_0}^{\Omega_i}\frac{\Omega^2}{\alpha c^2+\beta(Q/\mu)^2\Omega^2}d\Omega \le \Delta V_* \equiv \frac{\gamma}{25c(\alpha\beta)^{1/2}}\left(\Omega_i R_s\right)^2 X^{-2}\left[X-\tan^{-1}X\right], \tag{15}$$

where $X \equiv (\beta/\alpha)^{1/2}Q\Omega_i/\mu$ and the present angular velocity $\Omega_0 = 0$ is used in the last inequality. The function ΔV_* is determined by the ratio $Q/(\mu R_s)$ of the two multipole moments for the fixed geometrical configuration and the initial angular velocity Ω_i. Two limiting cases of ΔV_* are approximated as

$$\frac{\Delta V_*}{c} \approx \begin{cases} \frac{\gamma}{75\alpha}\left(\frac{Q}{\mu R_s}\right)\left(\frac{\Omega_i R_s}{c}\right)^3 & \text{for } 0 < X \ll 1 \\ \frac{\gamma}{25\beta}\left(\frac{Q}{\mu R_s}\right)^{-1}\left(\frac{\Omega_i R_s}{c}\right) & \text{for } X \gg 1. \end{cases} \tag{16}$$

The value ΔV_* increases as the ratio $Q/(\mu R_s)$ increases, while $Q/(\mu R_s) \ll 1$, but begins to decrease for $Q/(\mu R_s) \to \infty$. Thus, it has a maximum with respect to the magnetic moment ratio:

$$\frac{\Delta V_*}{c} \approx 9.2\times10^{-3}\frac{\gamma}{(\alpha\beta)^{1/2}}\left(\frac{\Omega_i R_s}{c}\right)^2 \quad \text{at } \frac{Q}{\mu R_s} \approx 1.5\left(\frac{\alpha}{\beta}\right)^{1/2}\left(\frac{\Omega_i R_s}{c}\right)^{-1}. \tag{17}$$

The magnetic moment ratio at the maximum means that the quadrupole field $B_2 \sim Q/R_s^4$ is stronger than the dipole field $B_1 \sim \mu/R_s^3$ at the surface. The energy loss rate L_l of each multipole is approximately the same at the beginning, $L_2 = \beta Q^2\Omega_i^6/c^5 \approx 2.3\times\alpha\mu^2\Omega_i^4/c^3 = 2.3L_1$, but the contribution of L_2 and becomes smaller as Ω is decreased. The velocity using the canonical values is evaluated as

$$\Delta V_* \approx 120\left(\frac{P_i}{1\text{ms}}\right)^{-2}\times\frac{\gamma}{(\alpha\beta)^{1/2}}\ \text{km s}^{-1} \tag{18}$$

For the off-center dipole model, $V_* \sim 10^3(P_i/1\text{ms})^{-2}$ km s^{-1} is allowed for an initially rapid rotator, the initial period $P_i = 1$ ms, using typical values given in Table 1. On the other hand, the typical value is small, $V_* \sim 10^2(P_i/1\text{ms})^{-2}$ km s^{-1}, for the dipole-quadrupole model. The difference comes from the presence of radiation of $m = 2$, which causes efficient energy loss, as discussed in the previous section. Nevertheless, extremely high velocity is possible for a specific configuration even in the present model. Small β corresponds to high velocity. For small χ_2 in eq.(7), we have $\beta = \sin^2 2\chi_2/160$. Because $\alpha = 2\sin^2\chi_1/3$, $\gamma = \sin\chi_1\sin 2\chi_2/2$ for $\sin\delta = 1$; the combination of parameters reduces to $\gamma/(\alpha\beta)^{1/2} = 7.7$. The resultant kick velocity increases up to $\sim 930(P_i/1\text{ms})^{-2}$ km s^{-1}. This optimal case corresponds to the magnetic configuration with an inclined dipole and a nearly axially symmetric quadrupole. The ratio of the moments is $Q/(\mu R_s) \sim 74(\sin\chi_1/\sin\chi_2)(P_i/1\text{ms})$.

Time evolution of spin and velocity is calculated for the optimized relation (17). Once the quadrupole field strength is fixed, the evolution of $\Omega(t)$ in eq.(13) is scaled by characteristic time t_* of the dipole radiation loss for the initial angular velocity $\Omega_i = 2\pi/P_i$:

$$t_* = \frac{Ic^3}{\alpha\mu^2\Omega_i^2} \approx 0.8\left(\frac{\alpha}{0.33}\right)^{-1}\left(\frac{P_i}{1\text{ms}}\right)^2\left(\frac{\mu}{10^{31}\text{Gcm}^3}\right)^{-2}\ \text{yr}, \tag{19}$$

where magnetic dipole field at the surface is chosen as $B_1 \sim 10^{13}$ G. Figure 3 shows the evolution of $\Omega(t)/\Omega_i$ as a function of $\tau = t/t_*$. The ratio of quadrupole to the total energy loss rate, $L_2/(L_1+L_2)$ is also plotted. The ratio at $t = 0$ is approximately 0.7 because of $L_2 \approx 2.3L_1$, but monotonically decreases. At $t = t_*$, the angular velocity becomes $\Omega \sim 0.5\Omega_i$ and the contribution of quadrupole radiation also decreases as $L_2 \sim 0.5L_1$. The velocity $V(t)$ normalized by the terminal one (eq.(18)) is also shown in Figure 3. The magnitude attains to almost terminal value, $V \sim 0.8\Delta V_*$ before $t = t_*$.

3.6 Implication

Magnetic field strength itself is critical in most kick mechanisms. For example, $B_s > 10^{15}$ G at the surface is required in asymmetric neutrino emission (e.g., [16]), as well as in asymmetric magnetized core collapse

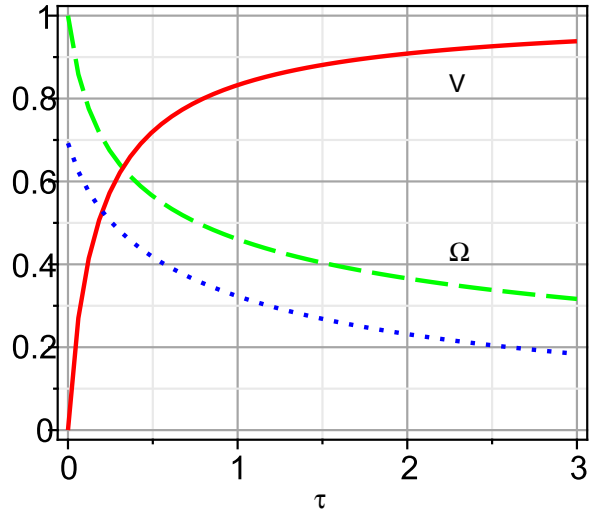

Figure 3: Time evolution of velocity, spin and energy loss rates as a function of dimensionless time $\tau = t/t_*$. Solid red line represents the linear velocity normalized by the terminal one ΔV_*, and dashed green line the angular velocity normalized by initial one Ω_i. Dotted blue line is the radiation loss ratio $L_2/(L_1 + L_2)$.

(e.g., [20]). The resultant velocity increases with the field strength because the asymmetry arises from the magnetic field. Magnetars are therefore expected to have high velocity if one of these mechanisms is operative. Recent observations do not support the high velocity, as discussed in Section 2. There is no clear evidence in the present observation about correlation between the field strength and the kick velocity.

The electromagnetic rocket mechanism considered in [21] and in this paper does not depend on field strength if the spin evolution is determined from the radiation loss. In our model, the ratio of dipole and quadrupole moments is important. The condition for high velocity is that the quadrupole field is large enough in magnitude for the radiation loss to be of the same order as the dipole field. The velocity also depends on the geometrical configuration of the multipole moments, that is, each inclination angle from the spin axis and the angle between the axes of symmetry of the moment. Assuming that the directions of moments are random, and that they are equally likely to be oriented in any direction, it is found that the mean velocity with respect to the configuration is not so large, $\sim 120(P_i/1\mathrm{ms})^{-2}$ km s^{-1}, for the optimized dipole-quadrupole ratio. The maximum velocity is realized for a specific configuration in which the inclination angle of the quadrupole moment is small, and the meridian plane in which the quadrupole moment lies is perpendicular to the plane of the dipole. The velocity increases up to $\sim 930(P_i/1\mathrm{ms})^{-2}$ km s^{-1}. This value is slightly smaller than the maximum observed velocity of a pulsar.

The configuration is unknown, and is closely related to the origin of the magnetic field, dynamo or fossil. Nevertheless, interesting results are reported within the mean-field dynamo theory[23]: (1)Strong large-scale and weak small-scale fields are generated only in a star with a very short initial period, that is, the Rossy number is small: (2)Maximum strength decreases and small-scale fields become dominant with the decrease of the initial period. Thus, magnetars may have an ordered dipole with a strong field, while some pulsars may have rather irregular fields with higher multipoles. Through the superposition of higher multipoles, pulsars in general come to have a larger radiation recoil velocity than magnetars.

Finally, if the kick velocity of pulsars and magnetars is governed by the same mechanism, it either should not simply depend on magnetic field, or should depend on only the configuration. The latter possibility was explored here. Present argument is recognized as the order of magnitude level due to the rotating model in vacuum. Further improvement of the magnetosphere will be of importance to explore the idea.

4 Conclusions

Some proto-neutron stars are conjectured to be born in hypothetical extreme state of rapid rotation $P \approx 1$ ms with an ultra strong magnetic field $B_s \approx 10^{15}$G. Such rapidly rotating magnetars are also considered as one of models for gamma-ray bursts. Is there any remaining evidence of this stage within our Galaxy? The proper motion can possibly be used as a probe. Observationally, there is no correlation between the field strength and the kick velocity. The velocity should depend on magnetic field in a complicated manner. The kick velocity is an indirect evidence of past violent energetic event, so that a number of speculations are allowed. Direct observations by gravitational waves by LIGO/VIRGO/LCGT and by many electromagnetic bands would be of importance as a witness.

Acknowledgements

This work was supported in part by the Grant-in-Aid for Scientific Research (No.21540271) from the Japanese Ministry of Education, Culture, Sports, Science and Technology.

Appendix

This appendix demonstrates how net linear momentum originates from the interference between multipole radiations. For example, the field is assumed to be described by a sum of modes with spherical harmonics Y_{lm}

$$h = \sum_{lm} A_{lm}(t,r) Y_{lm}(\theta,\phi).$$

Time averaged energy radiation rate carried away by waves is given by

$$\frac{dE}{dt} \propto \int d\Omega \sum_{l'm'lm} (A_{l'm'} Y_{l'm'})^* A_{lm} Y_{lm} = \sum_{lm} |A_{lm}|^2,$$

where orthogonal property of Y_{lm} is used. The total power radiated is just an incoherent sum of contributions from different multipoles. The linear momentum radiation is calculated with directional cosine. For example, z-component is given by

$$\frac{dP_z}{dt} \propto \int d\Omega \sum_{l'm'lm} (A_{l'm'} Y_{l'm'})^* \cos\theta (A_{lm} Y_{lm}) = \sum_{lm} c^{\pm}_{lm} A^*_{l\pm 1 m} A_{lm},$$

where $c^{\pm}_{lm}$ is a coefficient, and there is a coupling between l and $l \pm 1$ due to the combination rule. In this example, the field h is decomposed by scalar spherical harmonics($s = 0$). The harmonics are replaced by vector harmonics for the electromagnetic wave ($s = 1$), and by tensor harmonics for the gravitational wave ($s = 2$).

References

[1] Bekenstain, J. D. 1973, ApJ, 183, 657

[2] Nakmura, T. Oohara, K. & Kojima, Y. 1987, Prog. Theor. Phys. Suppl. 90, 1

[3] Baker, J. G. et al. 2006 ApJ, 659, L93

[4] Campanelli, M., Lousto, C. O., Zlohcower, Y., & Merritt, D. 2007, Phys. Rev. Lett. 98, 231102

[5] Komossa, S.,Zhou, H. & Lu, H. 2008 ApJ, 678, L81

[6] Robinson, A., Young, S., Axon, D. J. Kharb, P. & Smith, J. E. 2010 ApJ, 717, L122

[7] Kojima, Y. & Kato E. Y. arXiv:1012.1376, 2011, ApJ, 727 in press

[8] Manchester, R. N., Taylor, J. H. & Van, Y. Y. 1974 ApJ, 189, L119

[9] Hobbs, G., Lorimer, D. R., Lyne, A. G., & Kramer, M. 2005 Mon. Not. R. Astron. Soc., 360, 974

[10] Chatterjee, S., Vlemmings, W. H. T., Brisken, W. F., Lazio, T. J. W., Cordes, J. M., Goss, W. M., Thorsett, S. E., Fomalont, E. B., Lyne, A. G., & Kramer, M. 2005, ApJ, 630, L61

[11] Cordes, J. M., Romani, R. W., & Lundgren, S. C. 1993, Nature, 362, 133

[12] Helfand, D. J., Chatterjee, S., Brisken, W. F., Camilo, F., Reynolds, J., van Kerkwijk, M. H., Halpern, J. P., & Ransom, S. M. 2007, ApJ, 662, 1198

[13] Kaplan, D. L., Chatterjee, S., Hales, C. A., Gaensler, B. M., & Slane, P. O. 2009, AJ, 137, 354

[14] De Luca, A., Caraveo, P. A., Esposito, P., & Hurley, K. 2009, ApJ, 698, 250

[15] Lai, D., Chernoff, D. F., & Cordes, J. M. 2001, ApJ, 549, 1111

[16] Arras, P., & Lai, D. 1999, ApJ, 519, 745

[17] Fryer, C. L., & Kusenko, A. 2006, ApJS, 163, 335

[18] Scheck, L., Kifonidis, K., Janka, H.-Th., & Müller, E. 2006, A&A, 457, 963

[19] Nordhaus, J., Brandt, T. D., Burrows, A., Livne, E.& Ott, C. D. 2010, arXiv:1010.0674

[20] Sawai, H., Kotake, K., & Yamada, S. 2008, ApJ, 672, 465

[21] Harrison, E. R., & Tademaru, E. 1975, ApJ, 201, 447

[22] Thompson, C., & Duncan, R. C. 1993, ApJ, 408, 194

[23] Bonanno, A., Urpin, V., & Belvedere, G. 2006, A&A, 451, 1049

[24] Chabrier, G., & Küker, M. 2006, A&A, 446, 1027

[25] Dobler, W., Stix, M., & Brandenburg, A. 2006, ApJ, 638, 336

[26] Krolik, J. H. 1991, ApJ, 373, L69

[27] Jackson, J. D. 1975, *Classical Electrodynamics* 2nd ed., (Wiley, New York)

Anniversary of the 20th Japan General Relativity and Gravitation (JGRG)

Takashi Nakamura[1]

Department of Physics , Kyoto University, Kyoto 606-8502

1 How did Numerical Relativity in Kyoto start?

I was born in 1950. I was admitted to faculty of science, Kyoto university in April 1969. In Japan, the academic year of university starts in April and ends in March usually. However 1969 was an unusual year. In university of Tokyo, some radical students occupied the main buildings for an year or so. Finally the police entered the university to get rid of these students. In these confusions, the entrance examination to university of Tokyo had to be cancelled in 1969. In Kyoto university also, some radical students occupied many buildings so that there were no lectures for an year or so. I had only one minute entrance ceremony because the radical students were against the ceremony and lectures.

In faculty of science of our university, one can choose what one studies in university after one is admitted. My first plan was to study biophysics. However my high school teacher said to me that at first I had better study various fields of science in university so that I studied also astrophysics and found it very, very interesting. In 1970, professor C. Hayashi in our faculty got Eddington medal of Royal Astronomical Society for the discovery of "Hayashi Phase". I noticed this fact through the scientific journal for non-experts. Then I attended Hayashi's seminar in the fourth grade and was admitted to Hayashi group as an graduate student after the entrance examination.

Brief History of Chushiro Hayashi is as follows:

1920	born.
1957-1984	professor in department of physics as a leader of nuclear astrophysics group.
1977-1979	dean of faculty of science.
1970	awarded Eddington Medal.
1971	awarded Japan academy prize and imperial prize.
1987	life member of Japan academy.
2010 Feb. 28	passed away.

Main subjects were stellar evolution such as Hayashi phase, origin of solar system called Kyoto model and cosmology such as n-p ratio.

In my undergraduate student age, I had an unusual experience. I took a course of lectures on Lebesgue integral by professor Mizohata. In the end of his last lecture he said, "I will retire this March so that this is the final lecture. Now I would like to say something to you. Suppose that there is a problem in mathematics that you can not solve. In this situation there are two attitudes to the problem. The first one is; You are bad. You should study harder to solve the problem. However there is another attitude; The problem is bad. You had better arrange the problem which you can solve. Please remember this second attitude." I had never considered the second attitude. I had never considered a possibility that the problem is bad. The problem should not be bad but it is the thing that should be solved. After Mizohata's short talk, I thought that this second attitude should be the research. Then I could understand what professor Mizohata wanted to say although I could not understand Lebesgue integral itself almost everywhere.

When I was in master course, over doctor problem became severe. Here the over doctor problem (=Japanese English?) means that many graduate students can not find permanent positions even after they received Ph.D. At that time, the job meant the permanent position in Japan. I wondered what would happen when I would receive Ph.D five years later. Then Professor Humitaka Sato in Yukawa Institute for Theoretical Physics said to me that the problem would be resolved when I would receive

[1]Email address: takashi@tap.scphys.kyoto-u.ac.jp

Ph.D. In my graduate student age, I first wrote papers on density wave theory of spiral arms with S. Ikeuchi and F. Takahara and the restoration of broken symmetry in astrophysical situation with K. Sato. However around the age of 26 or so, the over doctor problem became more severe since even K. Sato and K. Nomoto could not find permanent positions. I was deeply disappointed since K. Sato and K. Nomoto were already famous in the world. One day in such disappointed days, professor Hayashi came into the graduate student room and said to me, "What will happen when two rocks collide is a very important problem in relation to the formation theory of planets. Can you study this problem with us?" I answered, "Thank you and I will consider the problem for a while." However I could neither find reference papers for this problem nor imagine what to do. Later I went to his office and said, "I decline to study what will happen when two rocks collide since I could not find any reference papers." Then professor Hayashi said, "A problem with no or little reference papers is a good problem. If there are many reference papers on the problem, that means that your contribution to the field will be very small ." This was completely unexpected statement for me. Usually graduate students like to study the problem with many references. What professor Hayashi said is , however, in reality correct. He himself did study the problems with no or little references such as the stellar evolution in 1960s and the origin of solar system in 1980s. To overcome over doctor problem, I thought that I should do something big. For this purpose I combined the statements of professors Mizohata and Hayashi as ; Find the solvable problem for the important theme with no or little reference papers.

I consulted Maeda what we should start. Three possible problems were considered. 1) jet formation from accretion disk, 2) high energy cosmic rays and 3) numerical simulations of collapse of rotating stars to black holes. Two graduate students Miyama and Sasaki joined our group. Finally we decided to study non-spherical collapse of the star leading to the formation of black holes, called numerical relativity later. We started seminars with no time limit in 1977. In reality we started from zero. We heard from many seniors that our challenge is hopeless and the result should be the failure. However after two years or so, finally we submitted four papers in 1979 and accepted for publication:

- General Relativistic Collapse of an Axially Symmetric Star by Takashi Nakamura, Kei-ichi Maeda, Shoken Miyama and Misao Sasaki, Prog.Theor. Physics **63** (1980) 1229
- A New Formalism of the Einstein Equations for Relativistic Rotating Systems by Kei-ichi Maeda, Misao Sasaki, Takashi Nakamura and Shoken Miyama , Prog.Theor. Physics **63** (1980) 719
- An Analytic Solution of Initial Data for Slowly Rotating Dust Sphere under Maximal Slicing Condition by Kei-ichi Maeda, Shoken Miyama, Misao Sasaki and Takashi Nakamura , Prog.Theor. Physics **63** (1980) 1048
- A Method of Determining Apparent Horizons in (2+1)+1-formalism of the Einstein Equations by M. Sasaki, K.Maeda, S. Miyama and T. Nakamura, Prog. Theor. Phys. **63** (1980) 1051

We also presented early results of non-spherical collapse of dust and gravitational waves at 2nd Marcel Grossman Meeting at Trieste Italy in 1979, where I met Tsvi Piran first.

In 1981 Miyama published axially symmetric time evolution of pure gravitational waves (S. Miyama, Prog. Theor. Phys. **65** (1981)). While I wrote a paper on general relativistic collapse of axially symmetric stars leading to the formation of rotating black holes (T. Nakamura, Prog. Theor. Phys. **65** (1981) 1876) which is the first numerical example of the formation of rotating black hole. In 1987, I wrote 218 pages review paper on "General Relativistic Collapse to Black Holes and Gravitational Waves from Black Holes" (Prog.Theor.Phys. suppl**90**) with Oohara and Kojima. One of the conclusions of this review paper was that non-axially symmetric systems , i.e. ,3D numerical relativity was strongly needed. From page 88 to 101 of this paper, I presented the time evolution of 3D pure gravitational waves as an example of 3D numerical relativity where the basic idea called BSSN formalism at present was shown.

2 When and How the study of laser Interferometer gravitational waves detector in Japan started ?

In 1988 March 23, I received a letter from president of Nagoya university, Sachio Hayakawa. He met Hayashi on his way to Tokyo and back to Nagoya and knew that I was interested in gravitational waves.

His friend Mizushima in Colorado, asked Hayakawa to organize the research group on the laser interferometer gravitational wave detectors in space using two artificial satellites. He already discussed this with laser physicist professor Takuma in Univ. Electro-Communication, M. Fujimoto in NAO (National Astronomical Observatory) and ATR (Advanced Telecommunication Research) company. Hayakawa answered to Mizushima that he wanted to organize the research group on the laser interferometer in Japan after the discussion with Takuma. He was impressed by the talk of Kip Thorne when he invited Kip to talk on LIGO at Nagoya University in 1986 after Yamada conference in Kyoto. In the letter, Hayakawa asked me to join the group. I answered, "Yes". In 1988 June, we first had a small meeting at ATR in Osaka. We felt that we had a bigger meeting with more experts to discuss how we should start the research on laser interferometer gravitational wave detectors in Japan.

Brief History of Sachio Hayakawa is as follows:

1923	born
1954-1959	Professor in YITP
1959-1987	Professor in Nagoya University
1987-1992	President of Nagoya University
1991	awarded Japan Academy Prize
1992 Mar. 5	passed away

Main subjects were Elementary Particle Physics, Cosmic Ray Physics and Gamma Ray and X-Ray Astronomy.

We had Molecule Type workshop[2] in YITP entitled "Dynamical Space Time and Gravitational Waves". We had the workshop in 1988 September. Participants were Hayakawa, Kawashima(ISAS), Takuma (Univ, Electro-Communication), Tsubono(Univ.Tokyo), Fujimoto(NAO), Morimoto(KEK), Nakamura, Madea, Sasaki, Miyama, Kojima, Oohara, Futamase, and Nagasawa. Professor Hirakawa in Univ. Tokyo had been trying to observe the continuous gravitational waves from Crab pulsar using cooled resonant type antenna. Unfortunately he passed away in 1986. Tsubono succeeded to Hirakawa's group in Univ. Tokyo. Morimoto continued the experiment by Hirakawa in KEK. Kawashima made 10m delay line laser interferometer in ISAS[3]. The main purpose of this workshop was to discuss and decide what we should do next several years.

Resolutions were: 1) Apply to the grant-in-aid of Type B with 3M Yen(about 30,000 Euro now) to prepare for the bigger grant-in-aid. 2) Simultaneously apply to the grant-in-aid on Priority Area of ministry of education with 600M YEN(about 6M Euro now). 3) P.I : prof. Hayakawa. Next year(1989) we were informed that the Type B grant was approved but the priority area was not. In 1989 June, prof. Hayakawa proposed to write a conceptual design of the interferometer. The design started in June mainly by Mio and Ohashi and ended in February 1990. However the ministry of education was anxious about the research by the president of the university. In short, the president of the university should not be the leader of the big grant-in-aid such as priority area. Hayakawa then asked me to be P.I. I obeyed his order. We again applied to the grant-in-aid on Priority Area "gravitational wave astronomy" in 1990 with 600M YEN(about 6M Euro now). The cover title of application form for the grant-in-aid on the priority area was "Gravitational Wave Astronomy" for 1991-1994. This was approved. That is, we started the priority area (1991-1994) with 600M Yen(about 6M Euro now). At that time, we do not know which is better, Fabry Perot or Delay Line? The best interferometer then was MPI 30m in which Delay Line was adopted. We decided to develop both as

- organization of the priority area
- Sub Project A1) Construction of FP type 20m interferometer (Leader Fujimoto in NAO)
- Sub Project A2) Construction of 100m Delay Line interferometer (Leader Kawashima in ISAS)
- Sub project B) Development of high power and stable laser such as Nd:YAG laser 200mW with $\delta\nu/\nu \sim 10^{-19}/\sqrt{\text{Hz}}$. (Leader K. Ueda in Univ, electro-communications)

[2]Molecule type means that the number of participants is 10 or so
[3]Institute for Space and Aeronautics Science

- Sub project C) Development of various elements such as seismic isolation and control of mirror. (Leader K. Tsubono in Univ. Tokyo)
- Sub project D) Research on sources of gravitational waves and numerical simulations. (Leader T. Nakamura in YITP)

Unfortunately Prof. Hayakawa passed away in 1992 March 5. What he did was extremely important. Without his activity, present gravitational wave research group in Japan could not exist. Especially important is that he proposed to exchange MOU (Memorandum Of Understanding) among NAO, KEK and ICRR. This MOU has been continuing even now. Its content is: "The presidents(directors) of NAO, KEK and ICRR (three big institutes in Japan) agree to work and cooperate together to construct the ground based 3km size gravitational wave detector in Japan." He also encouraged to write the conceptual design. This was also very ,very important.

I did not expect that I became P.I. of the experimental project. Moreover the ministry of education requested me to achieve something very new in the world. I knew nothing about the laser interferometer so that I began to read the document of the conceptual design. I found that the thermal noise was important so that I proposed to cool down the mirror to 4K. Then I received many objections; "How do you cool the mirror in the vacuum? Do you shed the cool gas to the mirror and absorb it from somewhere to keep the level of vacuum? That is extremely difficult.", "How about keeping all the vacuum tube 4K and cooling the mirror by its emission of radiation?", "It would be OK for end mirrors disregarding the cost. However near mirrors should absorb the laser light more or less so that the temperature of the near mirror would be at most 200K or so. 200K mirror does not help to increase the sensitivity.", "We have been studying the resonant detectors to catch the continuous gravitational wave from Crab pulsar. We knew various problems in cooling the detector. We started the study of laser interferometer since we heard that the cooling is not needed. Are you saying that we should cool again?" The discussions ended at that time. However ten years later in 2000, Kuroda in ICRR succeeded in cooling the mirror to 20K by the conduction of the wire which sustains the mirror. This opened the way to LCGT.

3 The birth of JGRG (Japan General Relativity and Gravitation)

To support the experimental effort for the detection of gravitational waves, Maeda and I considered to make the theoretical community related to general relativity and gravitation. Contents are

1) Once a year we will have $\sim$ five days conference on general relativity and gravitation.
2) We will publish the proceedings in English.
3) Priority Area "Gravitational Wave Astronomy" will support the cost of the proceedings and a part of the travel and living expenses for invited speakers.
4) The place of conference will be changed every year to promote general relativity and gravitation.
5) The contents of the conference should be as wide as possible. Any talks related to general relativity and gravitation are OK.
6) We also expected that some young people in JGRG move to data analysis and experiments.

In Appendix A, I show the list of JGRG from the first one to the 20th (this conference).

The Priority Area itself ended with great success. The judge of the priority area , Takuma (laser physicist) and I agreed as "Any apparatus considered by scientists will be constructed sooner or later, unless it conflicts with major laws of physics such as energy conservation, uncertainty principle and the principle of increase of entropy." New program followed the priority area.

New program on "gravitational wave astronomy" (a Grant in-Aid for Creative Basic Research from the Ministry of Education 09NP0801) was a top-down program. One could not apply to this program. Principal Investigator was Y. Kozai who was a former director of NAO (National Astronomical Observatory). The total cost was 1560M Yen (about 15.6M Euro now). The TAMA 300 was constructed by

this program and I was a leader of theory group. However I was against this project since 300m is not long enough to detect gravitational waves. I said, "Although this is a top down project, please reject the project. We had better ask and wait for the funding of 3km size interferometer." Answer was: "It is too risky to extend the arm length two orders of magnitude (from 20m to 3km). Even by TAMA 300, if we are lucky enough we may detect the gravitational wave first in the world. Then we can ask for 3km size antenna", "If we reject the project, how can we get the fund for experiments?" My answer to this question was "·····."

Then let us consider the source of gravitational waves that TAMA300 might detect[4]

1) At this time, using gravitational microlensing, dark matter in our galaxy might consist of MACHO (MAssive Compact Halo Object) of mass about 0.5 solar mass.

2) If MACHO is a black hole, it should have been formed in the early universe when the temperature T was ∼1GeV.

3) MACHO black holes were formed randomly in space so that binary black hole was formed due to the tidal force of the third near-by black hole.

4) Coalescence rate would be about once per 20 years by TAMA300. That is, the probability of detection is 5% per year or so, which is the same as the consumer tax rate in Japan. That is neither large nor small.

2001 was thirteen years after we started from zero. We succeeded in 1038 hours operation of TAMA300 with 87% duty cycle in 2001[5]. We theoretical group members also took part in 8-hours shift each. In 2003, 1157 hours operation was done and achieved the sensitivity that the coalescing binary neutron stars event in our galaxy can be detected.

New program ended with a great success in 2001 and next program called "New development in the research of gravitational wave" (Grant-in- Aid for Scientific Research on Priority Area of Ministry of Education) followed. "New development in the research of gravitational wave" was as follows:

- This was approved for 2002-2005.
- Principal Investigator: Kimio Tsubono (Univ. Tokyo)
- The total cost: 1430M Yen (about 14.3M Euro now)
- Main purposes of the program were:
  1) Observations using TAMA300.
  2) Basic technical research on LCGT(Large Cryogenic Gravitational wave Telescope with 3km arm length) using 100m proto type CLIO.
  3) Theory and data analysis [6]

Project DECIGO (DECi hertz Interferometer Gravitational wave Observatory) was born in this priority area. Motivation to DECIGO comes from extra solar planets. Many extra solar planets are found using many absorption lines (∼5000) of nearby G type stars since small orbital motion up to 10m/s can be measured. Loeb[7] proposed to apply this techniques to many QSO absorption lines so that two observations between several years or so yield direct measurement of cosmic acceleration and thus dark energy. Our point is to use gravitational waves from coalescing binary neutron stars at z∼1 instead of QSO absorption lines. Then a year to ten years before coalescence, the frequency of gravitational wave should be 0.1 Hz band where little proposal for detectors existed [8]. Punch Point of Ultimate DECIGO with $10^{-26}/\sqrt{\mathrm{Hz}}$ at 0.1Hz is as follows:

[4] Gravitational Waves from Coalescing Black Hole Macho Binaries, T. Nakamura, M. Sasaki, T. Tanaka and K. S Thorne, Astrophys. J.**487**(1997) L139-L142

[5] Stable Operation of a 300-m Laser Interferometer with Sufficient Sensitivity to Detect Gravitational-Wave Events within our Galaxy, Masaki Ando, et al, the TAMA collaboration Physical Review Letters **86** 3950 (2001)

[6] Nakamura and Sasaki were leaders of thory and data analysis groups, respectively and they supported JGRG.

[7] A.Loeb, Astrophys. J. Letters **499** L111 (1998)

[8] Direct Measurement of the Acceleration of the Universe using 0.1Hz Band Laser Interferometer Gravitational Wave Antenna in Space, Naoki Seto, Seiji Kawamura, Takashi Nakamura, Physical Review Letters **87** 221103 (2001))

- ∼100,000 mass of neutron stars and black hole per year will give us mass functions of NS and BH.
- Direct measurement of acceleration of the universe which is independent measurement of the curvature of the universe so that the independent information of EOS of the universe is available.
- Background gravitational waves predicted by inflation model up to $\Omega_{GW} \sim 10^{-20}$ can be detected. This is a completely independent information from WMAP and PLANCK because the frequency of gravitational wave is completely different.
- If the fundamental scale is TeV, then the redshifted gravitational wave at T=TeV is just 0.1Hz band. We may see something.

For practical DECIGO with $10^{-23}/\sqrt{\text{Hz}}$ at 0.1Hz, the angular resolution of ∼1 arcminute can be achieved a week before the coalescing binary neutron stars event at ∼ 300Mpc[9]. Then we can point all the detectors to coalescing binary neutron star (black hole) event. Since the direction as well as the time (within ∼0.1 sec accuracy) of the event are known beforehand, all band electromagnetic detectors from radio to ultrahigh energy gamma rays can be pointed to the source with possible neutrino detectors. Even the high frequency gravitational wave detectors can be tuned to catch ISCO, QNM and so on.

4 The dark age of Japanese Gravitational wave group

In 2005, we applied to Grant-in- Aid for Scientific Research on Priority Area of Ministry of Education called, "Frontiers of all wave length gravitational waves astronomy" with 2100M Yen (about 21M Euro now) for 2006-2011. Contents of the project are as follows:

- P.I.: T. Nakamura
- Sub Project A01) Pulsar Timing Array (Leader T. Daishido)
- Sub Project A02) DECIGO (Leader S. Kawamura)
- Sub Project A03) CLIO(100m proto-type of LCGT) (Leader M. Oohashi)
- Sub Project A04) High Frequency GW (Leader K. Arai)
- Sub Project A05) Theory and Data Analysis (Leader T. Tanaka and N.Kanda)

The meaning of all wavelength Gravitational wave astronomy can be explained as

- Gravitational Wave Astronomy $\Longleftrightarrow$ Electro Magnetic Wave Astronomy
- GHz GW? $\Longleftrightarrow$ gamma ray Astronomy
- MHz GW? $\Longleftrightarrow$ X-ray Astronomy
- 10kHz GW $\Longleftrightarrow$ UV Astronomy
- Ground Detectors ∼100Hz$\Longleftrightarrow$ Optical Astronomy
- Deci Hertz GW $\Longleftrightarrow$ Infrared Astronomy
- LISA (mHz Band) $\Longleftrightarrow$ Radio Astronomy
- Pulsar Timing Array (10nHz Band) $\Longleftrightarrow$ Low Frequency Radio Astronomy

In 2006, we were informed that the project was not approved. The comment of the judges was "We understand the scientific purposes of all wave length gravitational wave astronomy but it is too early to start it simultaneously in the time when no gravitational wave is detected." However in electromagnetic waves all wave length astronomy started almost simultaneously in Japan. We proposed similar priority areas in 2007,2008 and 2009 changing P.I.. However they were not approved. ICRR also requested the construction of LCGT to Ministry of Education in these years but LCGT was not approved in spite of recommendation by GWIC and Science Council of Japan.

[9]Deci hertz Laser Interferometer can determine the position of the Coalescing Binary Neutron Stars within an arc minute a week before the final merging event to Black Hole, Ryuichi Takahashi and Takashi Nakamura, Astrophys. J. Letters **596** L231-L234(2003)

5 Dark age ended in 2010 July 20 !!

Very recently a part of LCGT plan which amount to 9800M Yen = about 98M Euro was approved. We are now preparing application form to the Grant-in- Aid for Scientific Research on Priority Area of Ministry of Education called, "Frontier of physics and astronomy opened by the detection of gravitational waves" for 2011-2015. This Priority Area will support the construction and operation of LCGT in every sense including the basic research for upgrade the present LCGT design.

In conclusion,

- JGRG was born 20 years ago in relation to start of the research on detection of gravitational waves in Japan.
- This year a part of LCGT was approved. JGRG will support LCGT in every sense.
- We will apply to grant-in-aid on priority area to support LCGT and JGRG. We hope that this will be approved.
- Next project after LCGT will be DECIGO in 2020's.
- In Japan, one has the right to vote after 20 years old. In this sense, JGRG becomes an adult this year.

A List of JGRG(Japan General Relativity and Gravitation)

1st: 1991.12.4-6 ,Tokyo Metropolitan Univ. , 44 talks,120 participants , 399 page English proceedings, supported by Priority Areas "Gravitational Wave Astronomy"

2nd: 1993. 1.18-20, Waseda Univ. , 57 talks, 142 participants, 476 page English proceedings, supported by Priority Areas "Gravitational Wave Astronomy"

3rd: 1994. 1. 17-20, Univ. Tokyo, 64 talks, 155 participants, 516 page English proceedings, supported by Priority Areas "Gravitational Wave Astronomy"

4th: 1994. 11.28-12.1, Kyoto Univ. YITP , 56 talks, 105 participants, 475 page English proceedings, supported by Priority Areas "Gravitational Wave Astronomy"

5th: 1996. 1.22-25, Nagoya Univ., 57 talks, 110 participants, 463 page English proceedings, supported by New Program "Gravitational Wave Astronomy" (TAMA project was started as a part of this program.)

6th: 1996. 12.2-5, Tokyo Inst. Tech., 60 talks, 120 participants, 481 page English proceedings, supported by New Program "Gravitational Wave Astronomy"

7th: 1997. 10.27-30, Kyoto Univ. YITP, 52 talks, 93 participants, 364 page English proceedings, supported by New Program "Gravitational Wave Astronomy"

8th: 1998. 10.19-22, Niigata Univ., 59 talks, 110 participants, 392 page English proceedings, supported by New Program "Gravitational Wave Astronomy"

9th: 1999. 10.27-30, Hiroshima Univ., 74 talks, 120 participants, 502 page English proceedings, supported by New Program "Gravitational Wave Astronomy"

10th: 2000. 9.11-14, Osaka Univ., 60 talks, 120 participants, 431page English proceedings, supported by New Program "Gravitational Wave Astronomy"

From JGRG10 Talks should be in English .

11th: 2002. 1.9-12, Waseda Univ., 79 talks, 150 participants, 445 page English proceedings, supported by New Program "Gravitational Wave Astronomy"

12th: 2002. 11.25-28, Univ. Tokyo Komba, 67 talks, 150 participants, 469 page English proceedings, supported by "New Development of GW Research "

13th: 2003. 12.1-4, Osaka City Univ., 55 talks, about 150 participants, 307 page English proceedings, supported by "New Development of GW Research "

14th: 2004. 11.29-12.3, Kyoto Univ. YITP, 49 talks, about 150 participants, 465 page English proceedings, supported by "New Development of GW Research "

15th: 2005. 11.28-12.2, Tokyo Inst. Tech., 47 talks, about 150 participants, 347 page English proceedings, supported by "New Development of GW Research "

16th: 2006. 11.27-12.1, Niigata Univ. 57 talks, 150 participants, 282page English proceedings, supported by funds from MEXT.

17th: 2007. 12.3-7, Nagoya Univ. , 62 talks, 170 participants, 396 page English proceedings, supported by JSPS Scientific Research(B) and MEXT Creative Scientific Research

18th: 2008. 11.17-21, Hiroshima Univ. , 69 talks, about 150 participants, 318 page English proceedings, supported by JSPS Scientific Research(B) and MEXT Creative Scientific Research

19th: 2009. 11.20-12.4, Rikkyo Univ. , 70 talks, 185 participants, 427 page English proceedings, supported by Rikkyo Univ. and MEXT Creative Scientific Research

20th: this conference 2010. 9.21-9.24

Proceedings are available (http://www-tap.scphys.kyoto-u.ac.jp/jgrg/pastjgrg.html).

Accelerating cosmologies and inflation in string theories with higher order corrections

Nobuyoshi Ohta[1]

Department of Physics, Kinki University, Higashi-Osaka, Osaka 677-8502

Abstract

We discuss how to obtain inflationary and accelerating cosmological solutions in the context of string theories and M-theory. First, we review the no-go theorem which forbids such solutions in the low-energy effective string theories, i.e. supergravities. Then we show that this can be avoided if we consider time-dependent internal space. This is given by the S-brane solutions in string and M theories. Unfortunately these solutions do not give enough e-folding. We then argue that higher order corrections in string and M theories can give inflationary solutions with big enough e-folding.

1 Introduction

First of all, I would like to thank the organizers for inviting me to this special occasion of 20th anniversary of JGRG, and also the occasion of the 60th birthdays of Prof. Maeda and Prof. Nakamura. Congratulation on the 60th birthday, both Prof. Maeda and Prof. Nakamura.

It is my great pleasure and honour to be acquainted with both of you, and in particular to collaborate with Prof. Maeda on various interesting subjects. As other people, I wish both of you a good health and future prosperity.

My real encounter with Prof. Maeda was at the occasion when I was invited as a speaker in a workshop on brane world (2002 Jan.) which was organized by those people. In retrospect, it was this occasion that I started looking at time-dependent solutions in the context of string and supergravity theories; I remember that in some evening I had an early dinner and then was deriving such solutions now known as S-brane solutions. Such time-dependent solutions later became a subject to study together.

It was then one or two years later at one of this series of JGRG at Osaka City University (2003 Dec.) that we really discussed seriously collaboration on cosmological solutions in superstring/M-theory.

So I think that it is appropriate to talk about this subject in this occasion. This is also good because all the former speakers talked about other aspects of his work on black holes.

2 Models of inflation and no-go theorem

Superstring is the most promising candidate for the unified theory of all interactions of elementary particles including gravity. It is an urgent problem to give any check of superstring and/or predictions. To achieve this task, we should look for circumstances where quantum effects of gravity are most significant such as black holes and the early universe both of which involve singularity. It is extremely important to study if superstrings can give predictions consistent with observation and also resolve the problem of singularity. Here we focus on the problems associated with the early universe.

First let us briefly recall why inflation is necessary. There are two major cosmological questions.

- Horizon problem: It is found that the universe is homogeneous in the large scale beyond the distance causally connected. Why and how is such homogeneity realized?

- Flatness problem: It is also found that the present universe is very flat, but it is quite unnatural to have it at the very present. Why is this so?

[1]Email address: ohtan@phys.kindai.ac.jp

Inflation, the rapid expansion of the universe at the early stage, can resolve both these problems because of the rapid expansion of the initial causally connected region. As an important byproduct from the observational viewpoint, it turns out that this rapid expansion at the early stage produces scale invariant density perturbation which agrees with recent observations. If the grand unified theory of elemantary particles is correct, there will be lots of monopoles produced at the early universe, and inflation will also be needed to dilute these.

More surprising is that it has been discovered that the expansion of the present universe is accelerating! Naively we expect that the expansion is decelerating because the gravity is attractive force. The acceleration means that there is some source causing this acceleration, typically a tiny cosmological constant. This is called late-time acceleration.

Thus the correct theory of gravity must explain not only the inflation at early epoch but also the present accelerating expansion. It is this question about superstring that we address.

The first model of inflation was proposed by Guth and Sato in 1981 [1, 2]. Motivated by grand unified theories which involve change of vacuum energy due to phase transition, they considered effective cosmological constant, which produces exponential expansion of the scale factor of our FLRW universe when it is positive.

Actually another model of inflationary expansion had been proposed before by Starobinsky. This is caused by higher order corrections such as R^2 [3].

Without introducing artificial potential, we would like to have this behavior as a prediction of the fundamental theory, the superstring. However there is a no-go theorem [4–6] that forbids this. Let us briefly see how this result is obtained.

The Einstein equations give

$$\frac{\ddot{a}}{a} = -\frac{4\pi G}{3}(\rho + 3P), \quad \left(\frac{\dot{a}}{a}\right)^2 + \frac{k}{a^2} = \frac{8\pi G}{3}\rho, \tag{1}$$

where a is the scale factor in the FLRW universe, G the gravitational constant, k the signature of the curvature of our space, ρ the energy density and P pressure, respectively. To have inflation, we must have $\ddot{a} > 0$ i.e. $\rho + 3P < 0$ ($w \equiv \frac{P}{\rho} < -\frac{1}{3}$). This means that the gravity works as repulsive force! A famous example of this anti-gravity is the cosmological constant with

$$\rho = \Lambda, \quad P = -\Lambda, \tag{2}$$

The following theorem has been shown [4–6]:

Theorem: If $D(> 2)$-dimensional supergravity is compactified on smooth manifold without boundary and the following is true,

1. gravitational interactions do not contain higher derivative terms than ordinary Einstein theory,
2. all massless fields have positive kinetic term (not ghost),
3. d-dimensional Newton constant is finite,

then we cannot obtain accelerating expansion. •

Now the challenge is how to avoid this no-go theorem. The following possibilities immediately come to our mind.

- Consider additional degrees of freedom such as D-branes. This has been considered by Dvali-Tye [7], KKLT [8] and [9].
- We can consider time-dependent internal space, which leads to the S-brane [11] and will be briefly discussed in the following.
- We can also consider higher order corrections existing in superstring/M-theory (like Starobinsky). This is closely related to our work [12] with Prof. Maeda.
- Introduce scalar fields with negative kinetic terms, which is called phantom cosmology. We will not consider such a pathological theory.
- Consider non-compact space and/or space with boundary, which is the approach called brane world.

In what follows, we discuss the second and third possibility.

3 S-brane

A Vacuum solution which exhibits accelerating expansion was found in higher-dimensional Einstein gravity if we consider hyperbolic space for the internal space [13]. It was then immediately identified as a special case (0 flux) of S-brane [10, 11], i.e. SM2-brane (S2-brane in M-theory with 3-dimensional space) which is given as

$$\begin{aligned} ds_d^2 &= [\cosh 3c(t-t_2)]^{2/(n-1)}\Big[-e^{2ng(t)-6c'/(n-1)}dt^2 \\ &\quad +e^{2g(t)-6c'/(n-1)}d\Sigma_{n,\sigma}^2 + [\cosh 3c(t-t_2)]^{-2(n+2)/3(n-1)}e^{2c'}d\boldsymbol{x}^2\Big], \end{aligned} \tag{3}$$

where c, c' are constant, $\boldsymbol{x}$ represent three-dimensional space, $d = 4+n$ and $d\Sigma_{n,\sigma}^2$ is n-dimensional sphere ($\sigma = +1$), flat ($\sigma = 0$) or hyperbolic ($\sigma = -1$) spaces. Here

$$g(t) = \begin{cases} \frac{1}{n-1}\ln\frac{\beta}{\cosh[(n-1)\beta(t-t_1)]} & : \sigma = +1, \\ \pm\beta(t-t_1) & : \sigma = 0, \\ \frac{1}{n-1}\ln\frac{\beta}{\sinh[(n-1)\beta|t-t_1|]} & : \sigma = -1, \end{cases} \tag{4}$$

with a constant β.

When compactified, the 4-dimensional Einstein frame is defined as

$$ds^2 = \delta^{-n}(t)ds_E^2 + \delta^2(t)d\Sigma_{n,\sigma}^2, \quad ds_E^2 = -a^6(t)dt^2 + a^2(t)d\boldsymbol{x}^2, \tag{5}$$

where we have defined

$$\begin{aligned} \delta(t) &= [\cosh 3c(t-t_2)]^{1/(n-1)}e^{g(t)-3c'/(n-1)}, \\ a(t) &= [\cosh 3c(t-t_2)]^{(n+2)/6(n-1)}e^{ng(t)/2-(n+2)c'/2(n-1)}. \end{aligned} \tag{6}$$

The cosmic time is then defined by

$$d\tau = a^3(t)dt, \tag{7}$$

If $\frac{da}{d\tau} > 0$, then 4-dimensional universe expands. The condition for $n = 7$ is given by

$$n(t) \equiv \frac{3}{4}\tanh[3c(t-t_2)] - \frac{\sqrt{21}}{4}\coth(3\sqrt{3/7}ct) > 0, \tag{8}$$

The behavior of this quantity is depicted by the solid line in Fig. 1 (a) as a function of the original time t. For $\frac{d^2a}{d\tau^2} > 0$, the universe exhibits accelerating expansion:

$$\frac{9}{8}\left(\frac{1}{\cosh^2[3c(t-t_2)]} + \frac{1}{\sinh^2(3\sqrt{3/7}ct)}\right) - n^2(t) > 0. \tag{9}$$

The behavior of the lhs is also shown by the dotted line in Fig. 1 (a), and the scale factor in Fig. 1 (b).

Unfortunately examining the behavior of the scale factor, alas, we find that the obtained e-folding during accelerating expansion is very small only around $2-3$!!

The basic mechanism that causes this accelerating expansion can be understood from the effective four-dimensional viewpoint as follows [14]. Consider the product of d-dimensional universe and n-dimensional space whose metric is given by

$$ds^2 = \mathrm{e}^{-2\sum_i m_i\phi_i/(d-1)}ds_{d+1}^2 + \sum_i \mathrm{e}^{2\phi_i(x)}d\Sigma_{m_i,\epsilon_i}^2, \tag{10}$$

where $\sum_i m_i = n$ and ϵ_i is the signatures of the curvatures of internal m_i-dimensional spaces. The size of each internal space is determined by ϕ_i. We find that the d-dimensional effective potential is given by [15]

$$V = \sum_i(-\epsilon_i)\frac{m_i(m_i-1)}{2}\mathrm{e}^{-\frac{2}{d-1}\left((m_i+d-1)\phi_i+\sum_{j(\neq i)}m_j\phi_j\right)} - \epsilon_0\frac{(d-1)^2}{2a^2}. \tag{11}$$

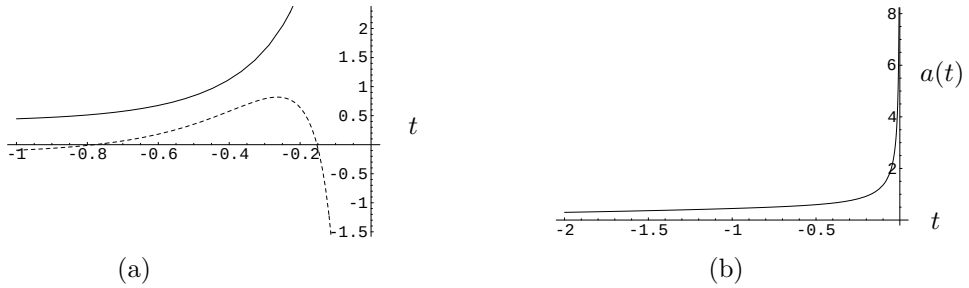

(a) (b)

Figure 1: (a) $\frac{da}{d\tau}$ (solid line) and $\frac{d^2}{d\tau^2}$ (dotted line) for $\sigma = -1, n = 7$. (b) scale factor $a(t)$.

For simplicity, we consider $\phi_1 = \phi_2 = \cdots \equiv \phi$. There is additional contribution when we have four-form flux. Then the effective potential for the 4-dimensional case takes the form shown in Fig. 2. The potential is always bounded below for the case with flux, but there is no lower bound on the potential in the case without flux for spheirical space ($\epsilon = +1$). The case of $\epsilon = -1$ is similar to that with flux, and there is no potential for $\epsilon = 0$.

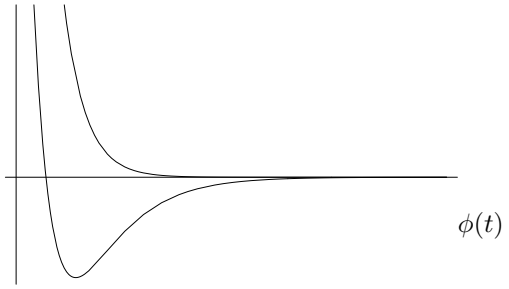

Figure 2: Scalar potential. The upper one is for hyperbolic internal space with and without flux, and the lower one is for spherical case with flux. The potential for spherical space without flux goes to minus infinity for $\phi \to -\infty$.

From this figure, we can understand how the above temporary accelerating expansion takes place [14]. Suppose that the scalar field ϕ comes in from the right, then it climbs up the slope but turns around after some time. While the scalar field is up on the slope, the potential gives an effective positive cosmological constant and the inflation occurs, but this ceases after some time. It is also obvious that the size of internal space will become large eventually.

In this picture, it is clear that the accelerating expansion is possible only for hyperbolic internal space if we consider solutions of higher-dimensional Einstein equation without flux [13], but this is always possible for S-branes with flux even for $\epsilon_i > 0$ [11]. This is a striking contrast and excellent feature of the S-brane solutions. So far so good. The only unfortunate result is that the obtained e-folding is very small. These solutions are very interesting because they clearly show that it is possible to evade the no-go theorem by considering time-dependent solutions.

If we use hyperbolic space for our space, it has been found that there is accelerating ever-expanding solution in the higher-dimensional Einstein theory [15]. This solution is found for $m \geq 6$, and the behavior of the scale factor, when it is reduced to four-dimensional FLRW universe, is given by

$$a(\tau) = \tau + A\tau^{-\sqrt{(m-6)/(m+2)}}. \tag{12}$$

For $m = 6$, it may appear that this solution does not give accelerating expansion. However a closer look reveals that the solution involves logarithmic term and gives such expansion [16]. It is very interesting that the minimal dimension $m = 6$ precisely coincides with the critical dimension of the string theory, and M-theory is also allowed! The solution may be useful to describe the present accelerating expansion.

4 Higher order corrections in M-theory

From the analysis of the previous section, it is rather clear that the S-brane solutions cannot be used for inflation at early universe because

1. it does not give large enough inflation,
2. it leads to big internal space.

However, it is known that there are always higher-order quantum corrections in string theory. Considering Starobinsky's approach mentioned in Sec. 2, this gives us the hope to have the inflation within the context of string and/or M theory. These higher-order terms must be important in the early universe. In M-theory, they are given as

$$S = S_{\rm EH} + S_4, \tag{13}$$

$$S_{\rm EH} = \frac{1}{2\kappa_{11}^2}\int d^{11}x\sqrt{-g}R, \qquad S_4 = \frac{1}{2\kappa_{11}^2}\int d^{11}x\sqrt{-g}\left[\alpha_4\tilde{E}_8 + \gamma L_W + \delta R^4\right]. \tag{14}$$

where

$$\tilde{E}_8 = -\frac{1}{2^4\times 3!}\epsilon^{\alpha\beta\gamma\mu_1\nu_1\ldots\mu_4\nu_4}\epsilon_{\alpha\beta\gamma\rho_1\sigma_1\ldots\rho_4\sigma_4}R^{\rho_1\sigma_1}{}_{\mu_1\nu_1}\cdots R^{\rho_4\sigma_4}{}_{\mu_4\nu_4}, \tag{15}$$

$$L_W = C^{\lambda\mu\nu\kappa}C_{\alpha\mu\nu\beta}C_\lambda{}^{\rho\sigma\alpha}C^\beta{}_{\rho\sigma\kappa} + \frac{1}{2}C^{\lambda\kappa\mu\nu}C_{\alpha\beta\mu\nu}C_\lambda{}^{\rho\sigma\alpha}C^\beta{}_{\rho\sigma\kappa}. \tag{16}$$

Here $C_{\lambda\mu\nu\kappa}$ is the Weyl tensor, $\alpha_4 = \frac{\kappa_{11}^2\ T_2}{3^2\times 2^9\times(2\pi)^4}$, $\gamma = \frac{\kappa_{11}^2\ T_2}{3\times 2^4\times(2\pi)^4}$, and $T_2 = (2\pi^2/\kappa_{11}^2)^{1/3}$ is the membrane tension. Considering the relation

$$L_W(R) \sim L_W(C) + \frac{60}{(D-1)^2(D-3)^3}R^4, \tag{17}$$

it is natural to consider $\delta \sim 10^{-3}\gamma$ because the coefficient in the second term in (17) is 10^{-3} for $D = 10$ or 11. Otherwise we also find that R^4 is dominant and the system does not give any interesting solution.

Take the general metric [6, 12]

$$ds_D^2 = -e^{2u_0(t)}dt^2 + e^{2u_1(t)}ds_p^2 + e^{2u_2(t)}ds_q^2, \quad D = 1+p+q, \tag{18}$$

where σ_p and σ_q are the signs of the $p = 3$- and $q = 7$-dimensional spaces, respectively.

Since there are too many possible solutions, we restrict the possible solutions to those given by

$$u_0 = \epsilon t, \quad u_1 = \mu t + \ln a_0, \quad u_2 = \nu t + \ln b_0. \quad (\epsilon = 0, 1) \tag{19}$$

It is clear that $\epsilon = 0$ gives generalized de Sitter solution ("generalized" in the sense that it contains time-dependent internal space) and $\epsilon = 1$ gives power expanding solution in terms of the cosmic time.

By varying the above action, we find three basic (Einstein) equations:

$$F \equiv \sum_{n=1}^{4} F_n + F_W + F_{R^4} = 0\ , \tag{20}$$

$$F^{(p)} \equiv \sum_{n=1}^{4} f_n^{(p)} + X\sum_{n=1}^{4} g_n^{(p)} + Y\sum_{n=1}^{4} h_n^{(p)} + F_W^{(p)} + F_{R^4}^{(p)} = 0\ , \tag{21}$$

$$F^{(q)} \equiv \sum_{n=1}^{4} f_n^{(q)} + Y\sum_{n=1}^{4} g_n^{(q)} + X\sum_{n=1}^{4} h_n^{(q)} + F_W^{(q)} + F_{R^4}^{(q)} = 0\ , \tag{22}$$

where we have defined $X = \ddot{u}_1 - \dot{u}_0\dot{u}_1 + \dot{u}_1^2$, $Y = \ddot{u}_2 - \dot{u}_0\dot{u}_2 + \dot{u}_2^2$, and other functions involving time derivatives of the metric functions. Due to the generalized Bianchi identity, only two out of these three equations are independent.

Solutions are summarized below [12]:

4.1 $\delta = \sigma_3 = \sigma_7 = 0$

Here we obtain generalized de Sitter solutions.

$$\mathrm{ME1}_{\pm}(\tilde{\mu}, \tilde{\nu}) \quad = \quad (\pm 0.10465, \mp 0.93666). \tag{23}$$

In this case, the scale factor $a(\tau)$ exhibits "super-inflation" in the Einstein frame.

We do not find exact solution in power-law solutions but asymptotic solutions are found.

4.2 $\delta = \sigma_3 = 0, \sigma_7 \neq 0$ **or** $\delta = \sigma_7 = 0, \sigma_3 \neq 0$

In this case, there is no generalized de Sitter solution. We find exact solution in power-law solution

$$\mathrm{ME12}(\mu, \nu, \sigma_7) = (0, 1, -1). \tag{24}$$

4.3 $\delta \neq 0$

Here we find more solutions for $\delta < 0$. See Figs. 3 and 4 and Table 1.

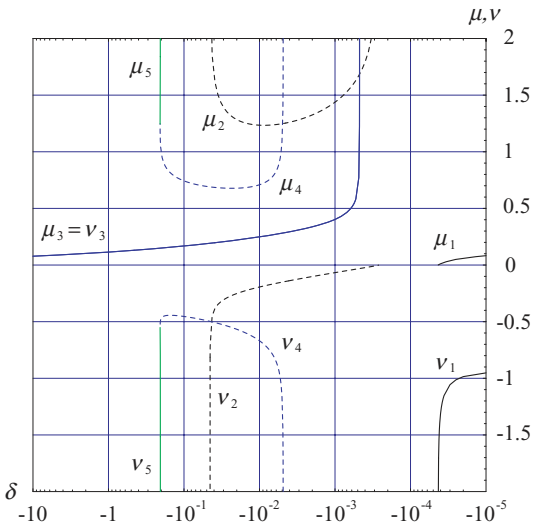

Figure 3: Five de Sitter solutions for $\sigma_p = \sigma_q = 0, \delta < 0$.

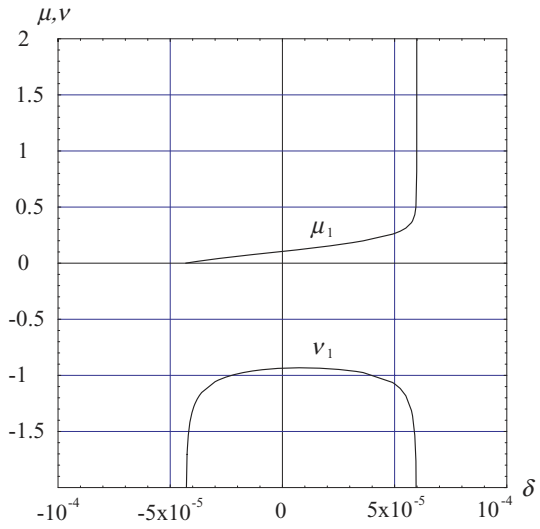

Figure 4: de Sitter solutions for $\delta \sim 0, \sigma_p = \sigma_q = 0$.

The conditions for good inflation are

1. $\mu > \nu, \mu \geq 0$
2. 60 e-folding
3. almost stable but the existence of small instability is desirable in order to have inflation ending after some time.

Closer study shows that enough inflation cannot be obtained only with the exact solution. It turns out that some exact solutions have unstable modes, so we should study the evolution after the exact solution decays in the direction of unstable mode. In particular, the solution $\mathrm{ME6}_+$ in Table 1 looks promising. We therefore performed numerical study and found a solution which comes close to $\mathrm{ME6}_+$ and then goes away. We thus find that there is a case in which we can obtain large e-folding as shown in Figs. 5 and 6.

The feature of general solutions is that the size of the internal space is larger than the Planck scale. For example, if we obtain 60 e-folding for MN1 (see the numerical solution in Fig. 6), we will have

$$R_0 \sim 4000 m_{11}^{-1}, \tag{25}$$

Table 1: Solutions MEi_+ ($i = 1, \cdots, 5$) for various δ. (ms,nu) means that there are m stable and n unstable modes. The solution is stable if 10-dimensional volume expansion rate $3\mu + 7\nu$ is positive.

Solution	Property	Range	Stability	$3\mu_i + 7\nu_i$
ME1$_+$	$\nu_1 < 0 < \mu_1$	$-0.000\,043\,11 < \delta < 0$	(0s,5u)	$-$
		$\delta = 0$	(1s,2u)	$-$
		$0 < \delta < 0.000\,059\,88$	(1s,4u)	$-$
ME2$_+$	$\nu_2 < 0 < \mu_2$	$-0.045\,20 < \delta < -0.002\,649$	(4s,1u)	$+$
ME3$_+$	$0 < \mu_3 = \nu_3$	$\delta < -0.000\,4732$	(3s,0u)	$+$
ME4$_+$	$\nu_4 < 0 < \mu_4$	$-0.2073 < \delta < -0.004\,852$	(1s,4u)	$-$
ME5$_+$	$\nu_5 < 0 < \mu_5$	$-0.2073 < \delta < -0.2056$	(2s,3u)	$-$
ME6$_+$	$\nu_6 = 0,\ 0 < \mu_6, \tilde{\sigma}_{q(6)}$	$\delta < -0.000\,5589$	(5s,1u)	$+$
ME7$_+$	$\nu_7 = 0,\ \tilde{\sigma}_{q(7)} < 0 < \mu_6$	$0.002\,999 < \delta$	(4s,2u)	$+$
ME8$_+$	$\mu_8 = 0,\ 0 < \tilde{\sigma}_{p(8)}, \nu_8$	$-0.003\,163 < \delta < -0.000\,5650$	(4s,2u)	$+$
ME9$_+$	$\mu_9 = 0,\ 0 < \tilde{\sigma}_{p(9)}, \nu_9$	$\delta < -0.000\,5657$	(5s,1u)	$+$
ME10$_+$	$\mu_{10} = 0,\ \tilde{\sigma}_{p(10)} < 0 < \nu_{10}$	$\delta < -0.000\,043\,49$	(5s,1u)	$+$
ME11$_+$	$\mu_{11} = 0,\ \tilde{\sigma}_{p(11)} < 0 < \nu_{11}$	$-0.085\,22 < \delta < -0.003\,164$	(4s,2u)	$+$

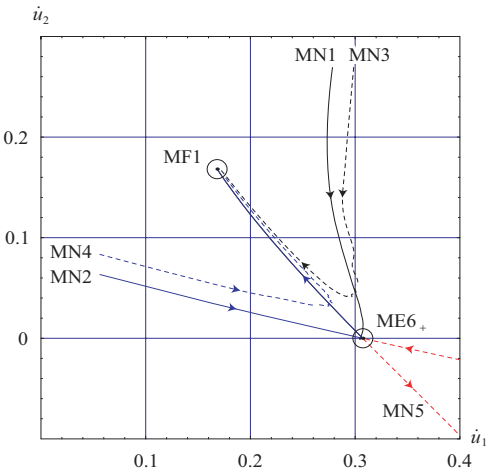

Figure 5: numerical results near ME6$_+$ on the $\dot{u}_1$-$\dot{u}_2$ plane for $\delta = -0.1$. Shown are ME6$_+$ and MF1

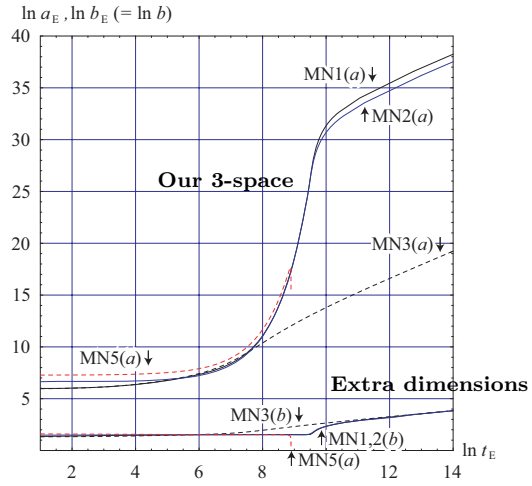

Figure 6: Sizes of the space for $\delta = -0.1$. MNi(a) represents ln a_E of MNi solutionsB

where R_0 is the radius of the internal six-dimensional space. This is rather big and gives large extra dimensions. From the relation

$$m_4^2 = R_0^7 m_{11}^9, \tag{26}$$

we get

$$m_{11} \sim 2 \times 10^{-13} m_4 \sim 600 \text{ TeV}, \tag{27}$$

which is quite low energy. If true, we may attain the energy scale of quantum gravity near future. But of course the present estimate strongly depends on the initial condition and there is no surprize if we do not see such effects in low energy.

5 Gauss-Bonnet theory with dilaton

5.1 Solution space

We have also studied similar solutions in Gauss-Bonnet theory with dilaton (effective heterotic string) [17]

$$S = \frac{1}{2\kappa_D^2}\int d^D x\sqrt{-\tilde{g}}\, e^{-2\tilde{\phi}}\left[\tilde{R} + 4(\partial_\mu\tilde{\phi})^2 + \alpha_2\tilde{R}^2_{\rm GB}\right], \tag{28}$$

The field equations gives autonomous system. We looked for fixed points in the time evolution, and found that general solutions are those starting from one fixed point to another fixed point. We find seven fixed

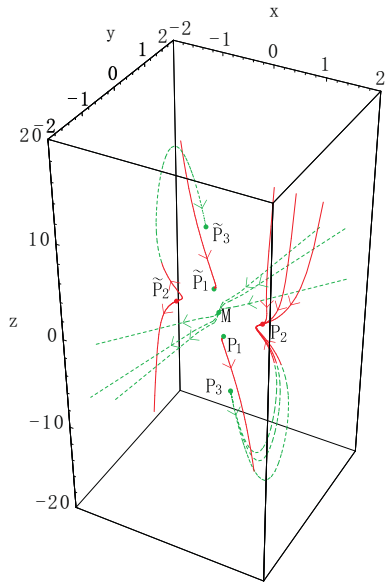

Figure 7: The Solution space with dilaton. Solid (red) line for $d^2a/d\tau^2 > 0$, and dotted (green) line for $d^2a/d\tau^2 < 0$.

points:

$$\begin{aligned}(x,y,z) \;=\; & \mathrm{M}(0,0,0),\quad \mathrm{P}_1(\mp 0.292373, \pm 0.36066, \pm 0.954846),\\ & \mathrm{P}_2(\pm 0.91822, \mp 0.080285, \pm 0.585906), \qquad (29)\\ & \mathrm{P}_3(\pm 0.161307, \pm 0.161307, \mp 9.30437), \qquad (30)\end{aligned}$$

Only P_2 gives accelerated expansion. But actually P_2 gives

$$a(\tau) = e^{u_1+3u_2} = e^{0.677T} \sim |\tau|^{-1.75} \quad (\tau : \text{cosmic time}) \tag{31}$$

We have also examined how large region of the initial conditions can give solutions approaching these fixed points. The result is that there are certain regions which approach the solutions, as shown in Fig. 7. Thus the problem with the initial conditions are not so severe.

This approach is being reconsidered with Prof. Maeda and Wakebe [18] in the string frame, but the result does not seem to be so much different. If the field redefinition ambiguity is taken into account, the result turns out to change very much and we find that de Sitter solutions are possible.

5.2 Density perturbation

Given some inflationary solutions, it is important to study if inflation by higher order corrections can produce scale invariant density perturbation [19]. Here we consider a toy model with GB and dilaton

higher derivative kinetic terms:

$$\mathcal{L}_c = -\frac{1}{2}\alpha'\xi(\phi)\left[c_1 R^2_{\rm GB} + c_2(\nabla\phi)^4\right] \ , \quad \xi(\phi) = \lambda e^{\mu\phi} \ (\mu = \pm 1 \text{ at tree level.}) \tag{32}$$

Typically $\lambda = -\frac{1}{4}, c_1 = 1, c_2 = -1$. Our approach is to consider no terms other than those from superstrings. We find several relevant solutions given in Table 2.

Parameters	$n_{\mathcal{R}}$	n_T	r
$\lambda = -1/4, c_1 = 1, c_2 = -1, \mu = 1$	3.28	2.28	–
$\lambda = -1/4, c_1 = 1, c_2 = -1, \mu = 10^{-2}$	1.0027	2.7×10^{-3}	–
$\lambda = -1/4, c_1 = 1, c_2 = 0, \mu = 10^{-2}$	1.011	0.011	–
$\lambda = 1/4, c_1 = 1, c_2 = -1, \mu = 1$	0.174	-0.826	46.4
$\lambda = 1/4, c_1 = 1, c_2 = -1, \mu = 10^{-2}$	0.9650	-0.0350	7.1×10^{-3}
$\lambda = 1/4, c_1 = 1, c_2 = -1, \mu = 10$	-12.4	-13.4	–
$\lambda = 1/4, c_1 = 1, c_2 = -1, \mu = 10$	-17.4	-18.4	–
$\lambda = 1/4, c_1 = 1, c_2 = -1, \mu = 10$	9.7×10^{-3}	-0.99	5.73
$\lambda = 1/4, c_1 = 1, c_2 = 0, \mu = 1$	0.37	-0.63	1.15×10^3
$\lambda = 1/4, c_1 = 1, c_2 = 0, \mu = 10^{-2}$	0.99	-0.01	–
$\lambda = 1/4, c_1 = 1, c_2 = 0, \mu = 10$	9.8×10^{-3}	-0.99	5.73

Table 2: de Sitter solutions for various λ, c_1, c_2, μ and $\omega_0 = -1$, spectral index $n_{\mathcal{R}}$ of scalar perturbation, and n_T for tensor mode tensor-to-scalar ratio r.

The result is that if GB is dominant, there is no good solution. We find that if higher kinetic term is dominant, there are good solutions.

6 Conclusion

Here we thus find that no-go theorem can be overcome. We find that various models are possible, but fine tuning may be necessary. In most models, quantum corrections seems to be important. An example is [8].

We have discussed S-brane solutions that

- gives accelerating expansion,
- but unfortunately only gives small e-folding.

We have also found that higher order corrections are important in the early universe, and they can give generalized de Sitter solutions. The obtained desirable features are

- it gives enough e-folding,
- it also gives relatively large internal space which could be tested experimentally,
- the size of the internal space can be stabilized,
- it can produce density perturbation.

There are still several problems that should be studied further:

- There is a question of frame-dependence: Einstein or string (Jordan) frames. The question is whether the difference of the frames produces any qualitative difference in the result [18].
- It seems that fine tuning of the initial conditions is necessary. Whether this is a general result or not should be studied.

- It is also interesting to study density perturbation [19]. It is interesting and important to extend this GB case to M-theory and check if the realization of graceful exit is possible.

It is also known that KKLT [8] need complicated and ad hoc settings. It is important to examine whether nature likes that or not. In this connection, we probably have to take string landscape and anthropic principle into account.

Another important question is how to derive 4 dimensions. We have seen that it is possible to obtain 4 dimensions as a solution, but it is not clear if it is natural or why other dimensions are excluded. This is a serious question because it is possible to show that there are solutions which allow other dimensions. The fact that there is 4-form in M-theory may be important in the realization of four dimensions. But to study this problem, we may need higher order corrections in 4-form, which is not known at the moment.

Acknowledgement

Again it is a great pleasure to thank Prof. Maeda for collaboration, and the organizers for invitation to this conference. This work was supported in part by the Grant-in-Aid for Scientific Research Fund of the JSPS (C) No. 20540283, No. 21· 09225 and (A) No. 22244030.

References

[1] A. H. Guth, Phys. Rev. D **23** (1981) 347.

[2] K. Sato, Mon. Not. Roy. Astron. Soc. **195** (1981) 467.

[3] A. A. Starobinsky, Phys. Lett. B **91** (1980) 99.

[4] G. W. Gibbons, Proceedings of the GIFT Seminar 1984, edited by F. Del Aguila, J. A. de Azcarraga and L. E. Ibanez, pp. 123-146 (World Scientific, 1984).

[5] J. M. Maldacena and C. Nunez, Int. J. Mod. Phys. A **16** (2001) 822 [arXiv:hep-th/0007018].

[6] N. Ohta, Int. J. Mod. Phys. A **20** (2005) 1 [arXiv:hep-th/0411230].

[7] G. R. Dvali and S. H. H. Tye, Phys. Lett. B **450** (1999) 72 [arXiv:hep-ph/9812483].

[8] S. Kachru, R. Kallosh, A. D. Linde and S. P. Trivedi, Phys. Rev. D **68** (2003) 046005 [arXiv:hep-th/0301240].

[9] S. Kachru, R. Kallosh, A. D. Linde, J. M. Maldacena, L. P. McAllister and S. P. Trivedi, JCAP **0310** (2003) 013 [arXiv:hep-th/0308055].

[10] M. Gutperle and A. Strominger, JHEP **0204** (2002) 018 [arXiv:hep-th/0202210];
C. M. Chen, D. V. Gal'tsov and M. Gutperle, Phys. Rev. D **66** (2002) 024043 [arXiv:hep-th/0204071];
N. Ohta, Phys. Lett. B **558** (2003) 213 [arXiv:hep-th/0301095].

[11] N. Ohta, Phys. Rev. Lett. 91 (2003) 061303 [arXiv:hep-th/0303238]; Prog. Theor. Phys. **110** (2003) 269 [arXiv:hep-th/0304172].

[12] K. Maeda and N. Ohta, Phys. Lett. B **597** (2004) 400 [arXiv:hep-th/0405205]; Phys. Rev. D **71** (2005) 063520 [arXiv:hep-th/0411093];
K. Akune, K. Maeda and N. Ohta, Phys. Rev. D **73** (2006) 103506 [arXiv:hep-th/0602242].

[13] P. Townsend and M. Wohlfarth, Phys. Rev. Lett. 91 (2003) 061302 [arXiv:hep-th/0303097].

[14] R. Emparan and J. Garriga, JHEP **0305** (2003) 028 [arXiv:hep-th/0304124].

[15] C. M. Chen, P. M. Ho, I. P. Neupane, N. Ohta and J. E. Wang, JHEP **0310** (2003) 058 [arXiv:hep-th/0306291].

[16] C. M. Chen, P. M. Ho, I. P. Neupane, N. Ohta and J. E. Wang, JHEP **0611** (2006) 044 [arXiv:hep-th/0609043].

[17] K. Bamba, Z. K. Guo and N. Ohta, Prog. Theor. Phys. **118** (2007) 879 [arXiv:0707.4334 [hep-th]].

[18] K. Maeda, N. Ohta and R. Wakebe, in preparation.

[19] Z. K. Guo, N. Ohta and S. Tsujikawa, Phys. Rev. D **75** (2007) 023520 [arXiv:hep-th/0610336].

Inflation and dark energy–theory and observational signatures

Shinji Tsujikawa[1]

Department of Physics, Faculty of Science, Tokyo University of Science, 1-3, Kagurazaka, Shinjuku-ku, Tokyo 162-8601, Japan

Abstract

The theories of inflation and dark energy are reviewed paying particular attention to their observational signatures. We discuss the classification of inflationary models, primordial density perturbations including non-Gaussianities, and modified gravity models of inflation. We also review theoretical attempts for finding out the origin of dark energy–such as the cosmological constant, modified matter models, and modified gravity models.

1 Introduction

The inflationary paradigm has been the backbone of high-energy cosmology over the past 30 years. Inflation was first introduced [1, 2] as a way of addressing a number of cosmological problems such as horizon and flatness problems. The striking feature of the inflationary cosmology is that it predicts nearly scale-invariant, gaussian, adiabatic density perturbations in its simplest form [3]. This prediction shows an excellent agreement with all existing and accumulated data within observational errors. In particular the temperature anisotropies of Cosmic Microwave Background (CMB) measured by the Wilkinson Microwave Anisotropy Probe (WMAP) [4, 5] have provided the high-precision dataset from which inflationary models can be seriously constrained.

The first model of inflation proposed by Starobinsky [1] is based on a conformal anomaly in quantum gravity. The model in which the Lagrangian density is given by $f(R) = R + \alpha R^2$, where R is a Ricci scalar, can lead to the sufficient cosmic acceleration with a successful reheating [6]. Moreover this model is still allowed from the recent observations of the CMB temperature anisotropies [7]. The idea of "old inflation" [2], which is based on the theory of supercooling during the cosmological phase transition, turned out to be unviable, because the Universe becomes inhomogeneous by the bubble collision after inflation. The revised version dubbed "new inflation" [8, 9], where the second-order transition to true vacuum is responsible for cosmic acceleration, is plagued by a fine-tuning problem for spending enough time in false vacuum. However these pioneering works opened up a new paradigm for the construction of workable inflation models based on particle physics such as superstring theory and supergravity (see e.g., Refs. [10, 11]).

Most of the inflation models, including the Linde's chaotic inflation [12], have been constructed by using a slow-rolling scalar field with a sufficiently flat potential. One can discriminate between a host of slow-roll inflation models by comparing the theoretical prediction of the spectral index of scalar metric perturbations as well as the ratio between scalar and tensor perturbations with the temperature anisotropies in CMB (see e.g., [13–15]). There are other classes of models called k-inflation [16] in which the field kinetic energy plays an important role to drive cosmic acceleration. Since in k-inflation the scalar propagation speed is different from the speed of light [17], this can give rise to large non-Gaussianities of primordial perturbations [18, 19]. The models based on the modification of gravity (including the Starobinsky's model [1]) can lead to some peculiar theoretical predictions for inflationary observables. We shall discuss how a host of models can be distinguished from observations.

The observations of supernovae type Ia [20, 21] have shown that the Universe entered the phase of cosmic acceleration after the matter-dominated epoch. The discovery of this late-time accelerated expansion has opened up a new research field called dark energy (DE), see e.g., [22]. If we try to explain the origin of DE based on particle physics, we encounter a problem associated with a very small energy scale. For example, the vacuum energy appearing in particle physics is usually significantly larger than

[1]Email address: shinji@rs.kagu.tus.ac.jp

the observed energy density of dark energy ($\rho_{\rm DE}^{(0)} \simeq 10^{-47}$ GeV^4) [23]. In this case we need to find out a mechanism to obtain a tiny value of the cosmological constant Λ consistent with observations.

The first step toward understanding the nature of DE is to clarify whether it is a simple cosmological constant or it originates from other sources that dynamically change in time. The dynamical DE models can be distinguished from the cosmological constant by considering the evolution of the equation of state of DE ($= w_{\rm DE}$). The scalar field models of DE such as quintessence [24, 25] and k-essence [26, 27] predict a wide variety of variations of $w_{\rm DE}$, but still the current observational data are not sufficient to provide some evidence for the preference of such models over the ΛCDM model. Moreover we require that the field potentials are sufficiently flat, such that the field evolves slowly enough to drive the cosmic acceleration today. This demands that the field is extremely light ($m_\phi \simeq 10^{-33}\,$eV) relative to typical mass scales appearing in particle physics. However it is not entirely hopeless to construct viable scalar-field dark energy models in the framework of particle physics.

There exists another class of dynamical DE models that modify Einstein gravity. The models that belong to this class are $f(R)$ gravity [28, 29] (f is a function of the Ricci scalar R), scalar-tensor theories [30], Dvali, Gabadadze and Porrati (DGP) braneworld model [31], Galileon gravity [32], and so on. The attractive feature of these models is that the cosmic acceleration can be realized without recourse to a dark energy component. If we modify gravity from General Relativity, however, there are in general stringent constraints coming from local gravity tests as well as a number of observational constraints. Hence the restriction on modified gravity models is quite tight compared to modified matter models such as quintessence and k-essence.

We shall review the above mentioned dark energy models and also discuss the current status of observational and experimental constraints on those models.

2 Inflation

2.1 Dynamics and models of inflation

Most of inflationary models are based on a minimally coupled scalar field ϕ ("inflaton") with a potential $V(\phi)$. In the flat Friedmann-Lemaître-Robertson-Walker (FLRW) background with a scale factor $a(t)$, the energy density and the pressure of the inflaton are given, respectively, by

$$\rho_\phi = \dot\phi^2/2 + V(\phi)\,, \qquad P_\phi = \dot\phi^2/2 - V(\phi)\,, \tag{1}$$

where a dot represents a derivative with respect to cosmic time t. From the Friedmann equation $3H^2 = 8\pi G\rho_\phi$ ($H \equiv \dot a/a$ is the Hubble parameter and G is gravitational constant) and the continuity equation $\dot\rho_\phi + 3H(\rho_\phi + P_\phi) = 0$, it follows that

$$H^2 = \frac{8\pi}{3m_{\rm pl}^2}\left[\frac{1}{2}\dot\phi^2 + V(\phi)\right], \qquad \ddot\phi + 3H\dot\phi + V_{,\phi}(\phi) = 0\,, \tag{2}$$

where $m_{\rm pl} = G^{-1/2}$ is the Planck mass, and $V_{,\phi} \equiv {\rm d}V/{\rm d}\phi$. Combination of these equations gives $\ddot a/a = 8\pi(V - \dot\phi^2)/(3m_{\rm pl}^2)$, which means that cosmic acceleration ($\ddot a > 0$) occurs for $\dot\phi^2 < V$. Inflation can be realized by a sufficiently flat potential along which the field evolves slowly. Under the slow-roll conditions $\dot\phi^2 \ll V(\phi)$ and $|\ddot\phi| \ll |3H\dot\phi|$, we have $H^2 \simeq 8\pi V(\phi)/(3m_{\rm pl}^2)$ and $3H\dot\phi \simeq -V_{,\phi}(\phi)$ from (2).

We define the so-called slow-roll parameters [13]

$$\epsilon_V = \frac{m_{\rm pl}^2}{16\pi}\left(\frac{V_{,\phi}}{V}\right)^2, \qquad \eta_V = \frac{m_{\rm pl}^2 V_{,\phi\phi}}{8\pi V}\,, \qquad \xi_V^2 = \frac{m_{\rm pl}^4 V_{,\phi}V_{,\phi\phi\phi}}{64\pi^2 V^2}\,. \tag{3}$$

The sufficient amount of inflation is realized provided that $\{\epsilon_V, |\eta_V|, |\xi_V^2|\} \ll 1$. At leading order in the slow-roll expansion the parameters (3) reduce to $\epsilon_V \simeq \epsilon \equiv -\dot H/H^2$, $\eta_V \simeq 2\epsilon - \dot\epsilon/(2H\epsilon)$, and $\xi_V^2 \simeq [2\epsilon - \dot\eta/(H\eta)]\eta$ [33]. The cosmic acceleration ends when ϵ_V and η_V grow to of order unity. A useful quantity to describe the amount of inflation is the number of e-foldings, defined by

$$N \equiv \ln\frac{a_f}{a} = \int_t^{t_f} H\,dt \simeq \frac{8\pi}{m_{\rm pl}^2}\int_{\phi_f}^{\phi}\frac{V}{V_{,\tilde\phi}}\,d\tilde\phi = \frac{2\sqrt{\pi}}{m_{\rm pl}}\int_{\phi_f}^{\phi}\frac{d\tilde\phi}{\sqrt{\epsilon_V}}\,, \tag{4}$$

where the subscript f denotes the evaluation of the quantity at the end inflation. In order to solve the horizon and flatness problems we require that N is larger than 60 [14].

The inflationary models based on a scalar field can be roughly classified in the following way [34]. The first class (type I) consists of the "large field" models, in which the field evolves over a super-Planckian range during inflation, $\Delta\phi > m_{\rm pl}$. Chaotic inflation [12] is one of the representative models of this class. The second class (type II) consists of the "small field" models, in which the field moves over a small (sub-Planckian) distance: $\Delta\phi < m_{\rm pl}$. New inflation [8, 9] and natural inflation [35] are the examples of this type (although in these models there are some cases in which the field evolves over a super-Planckian range). In the first class one usually has $V_{,\phi\phi} > 0$, whereas $V_{,\phi\phi}$ can change the sign in the second class. The third class (type III) consists of the hybrid inflation models [36, 37], in which inflation typically ends by a phase transition triggered by the presence of a second scalar field. The fourth class (type IV) consists of the double inflation models in which there exist two dynamical scalar fields leading to the two stages of inflation. A simple example is two light massive scalar fields [38] (see also Refs. [39]).

We note that several models of inflation cannot be classified in the above four classes. For example, there are some models in which the potential does not have a minimum–such as inflation with an exponential potential [40], quintessential inflation [41], and tachyon inflation [42]. Typically these scenarios suffer from a reheating problem unless some modifications to the potential are taken into account. There exist other models of inflation in which an accelerated expansion is realized without using the potential of the inflaton. For example, k-inflation [16] and ghost inflation [43] belong to this class. In this case inflation occurs in the presence of non-linear kinetic terms of the scalar field. Inflation can also be realized by higher-order curvature terms [1, 44].

2.2 Linear density perturbations and observational constraints

It is possible to distinguish between a host of inflationary models from primordial density perturbations generated during inflation. Consider the general theories [16] described by the action

$$S = \int d^4x \sqrt{-g} \left[\frac{M_{\rm pl}^2}{2} R + P(\phi, X) \right] , \tag{5}$$

where $M_{\rm pl} = (8\pi G)^{-1/2}$ is the reduced Planck mass, R is a Ricci scalar, and $P(\phi, X)$ is the Lagrangian dependent on the field ϕ and the kinetic energy $X = -(1/2)g^{\mu\nu}\partial_\mu\phi\partial_\nu\phi$. In addition to the standard canonocal field with a potential, the action (5) includes a wide variety of theories such as low energy effective string theory with derivative terms [45], ghost condensate model [46], tachyon field [47], and DBI theories [48]. In the following we shall use the unit $M_{\rm pl}^2 = 1$, but we sometimes restore $M_{\rm pl}$ when the dimension matters.

The line-element describing scalar perturbations Ψ, B, Φ, E and tensor perturbations h_{ij} about the flat FLRW background is given by [50]

$$ds^2 = -(1+2\Psi)dt^2 + 2a(t)B_{,i}dx^i dt + a^2(t)\left[(1+2\Phi)\delta_{ij} + 2E_{,ij} + h_{ij}\right] dx^i dx^j , \tag{6}$$

One can derive the action for the scalar functions Ψ, B, Φ, E together with the inflaton fluctuation $\delta\phi$. Integrating the action (5) by parts and using the background equations of motion, the second-order action for these perturbations can be written in terms of the gauge-invariant comoving curvature perturbation [51]

$$\mathcal{R} = \Phi - H\delta\phi/\dot{\phi} . \tag{7}$$

Choosing the comoving gauge $\delta\phi = 0$, for example, the second-order action for the curvature perturbation takes the following form [17]

$$S_2 = \int dt\, d^3x\, a^3 \frac{\epsilon}{c_s^2} \left[\dot{\mathcal{R}}^2 - \frac{c_s^2}{a^2} \partial^i\mathcal{R}\partial_i\mathcal{R} \right] , \tag{8}$$

where $\epsilon = -\dot{H}/H^2$, and c_s^2 is the scalar propagation speed squared, given by [17]

$$c_s^2 = \frac{P_{,X}}{P_{,X} + 2XP_{,XX}} . \tag{9}$$

We write $\mathcal{R}$ in Fourier space with the comoving wave number $\mathbf{k}$, as

$$\mathcal{R}(\tau,\mathbf{x}) = \frac{1}{(2\pi)^3}\int d^3\mathbf{k}\,\mathcal{R}(\tau,\mathbf{k})e^{i\mathbf{k}\cdot\mathbf{x}}\,, \qquad \mathcal{R}(\tau,\mathbf{k}) = u(\tau,\mathbf{k})a(\mathbf{k}) + u^*(\tau,-\mathbf{k})a^\dagger(-\mathbf{k})\,, \tag{10}$$

where $a(\mathbf{k})$ and $a^\dagger(\mathbf{k})$ are the annihilation and creation operators, respectively, satisfying the commutation relations $\left[a(\mathbf{k}_1), a^\dagger(\mathbf{k}_2)\right] = (2\pi)^3\delta^{(3)}(\mathbf{k}_1-\mathbf{k}_2)$, $[a(\mathbf{k}_1), a(\mathbf{k}_2)] = \left[a^\dagger(\mathbf{k}_1), a^\dagger(\mathbf{k}_2)\right] = 0$. Note that $\tau = \int a^{-1}dt$ is a conformal time, which can be expressed as $\tau = -1/(aH)$ in the de Sitter background.

The equation for the Fourier mode u follows from the action (8). Introducing new variables $v = zu$ and $z = (a\sqrt{2\epsilon}/c_s)u$, it follows that

$$v'' + \left(c_s^2k^2 - z''/z\right)v = 0\,, \tag{11}$$

where a prime represents a derivative with respect to τ. In the quasi de Sitter background with a slow variation of c_s^2 we can approximate $z''/z \simeq 2/\tau^2$. The solution to Eq. (11), which recovers the Bunch-Davis vacuum state $v = e^{-ic_sk\tau}/\sqrt{2c_sk}$ in the asymptotic past, $(k\tau \to -\infty)$ is given by

$$u = i\frac{e^{-ic_sk\tau}}{2k^{3/2}\sqrt{\epsilon c_s}}H(1+ic_sk\tau)\,. \tag{12}$$

After the perturbations leave the Hubble radius ($c_sk \ll aH$), the asymptotic solution for $k\tau \to 0$ is described by $u \simeq H/[2k^{3/2}\sqrt{\epsilon c_s}]$. The power spectrum $\mathcal{P}_\mathcal{R}$ of the curvature perturbation is defined by $\langle\mathcal{R}(\mathbf{k}_1)\mathcal{R}(\mathbf{k}_2)\rangle = (2\pi^2/k_1^3)\mathcal{P}_\mathcal{R}(k_1)\cdot(2\pi)^3\delta^{(3)}(\mathbf{k}_1+\mathbf{k}_2)$. We then obtain [17]

$$\mathcal{P}_\mathcal{R} = \frac{1}{8\pi^2M_{\rm pl}^2}\frac{H^2}{c_s\epsilon}\,, \tag{13}$$

which is evaluated at $c_sk = aH$. The spectral index is

$$n_\mathcal{R} - 1 \equiv \left.\frac{d\ln\mathcal{P}_\mathcal{R}}{d\ln k}\right|_{c_sk=aH} = -2\epsilon - \eta - s\,, \tag{14}$$

where

$$\epsilon = -\dot{H}/H^2\,, \qquad \eta = \dot{\epsilon}/(H\epsilon)\,, \qquad s = \dot{c}_s/(Hc_s)\,. \tag{15}$$

The tensor perturbation h_{ij} satisfies the same equation as that for a massless scalar field. The spectrum of tensor perturbations and its spectral index are given by

$$\mathcal{P}_T = \frac{2H^2}{\pi^2M_{\rm pl}^2}\,, \qquad n_T \equiv \left.\frac{d\ln\mathcal{P}_T}{d\ln k}\right|_{c_sk=aH} = -2\epsilon\,. \tag{16}$$

The tensor-to-scalar ratio is

$$r \equiv \frac{\mathcal{P}_T}{\mathcal{P}_\mathcal{R}} = 16c_s\epsilon = -8c_sn_T\,. \tag{17}$$

In inflation models with a standard kinetic term (i.e. $P = X - V(\phi)$) the propagation speed is $c_s = 1$. In this case it follows that

$$n_\mathcal{R} - 1 = -6\epsilon_V + 2\eta_V\,, \qquad n_T = -2\epsilon_V\,, \qquad r = 16\epsilon_V\,, \tag{18}$$

where we used the slow-roll parameters defined in Eq. (3). The runnings of the spectral indices are given by

$$\alpha_\mathcal{R} \equiv \left.\frac{dn_\mathcal{R}}{d\ln k}\right|_{k=aH} = 16\epsilon_V\eta_V - 24\epsilon_V^2 - 2\xi_V^2\,, \qquad \alpha_T \equiv \left.\frac{dn_T}{d\ln k}\right|_{k=aH} = -4\epsilon_V(2\epsilon_V - \eta_V)\,. \tag{19}$$

We can evaluate the above observables for given inflaton potentials. Let us consider chaotic inflation [12] with the potential $V(\phi) = V_0\phi^n$. In this case the number of e-foldings is given by $N = 4\pi/(nm_{\rm pl})(\phi^2-\phi_f^2)$,

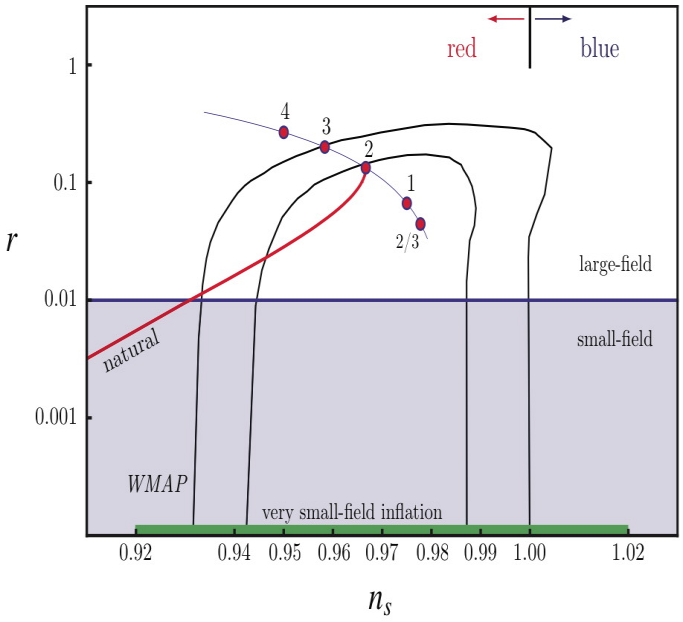

Figure 1: Observational constraints (1σ and 2σ contours) on single-field inflation models in the $(n_{\mathcal{R}}, r)$ plane ($n_{\mathcal{R}}$ is denoted as n_s in the figure). We also show the theoretical prediction of chaotic inflation with $V(\phi) = V_0\phi^n$ (the power $n = 4, 3, 2, 1, 2/3$) and natural inflation with $V(\phi) = V_0[1-\cos(\phi/\mu)]$. The border between large-field and small-field models is characterized by $r = 0.01$. From Ref. [53].

where $\phi_f = nm_{\rm pl}/4\sqrt{\pi}$ is value of inflaton at the end of inflation (at which $\epsilon_V = 1$). The scalar spectral index $n_{\mathcal{R}}$ and the tensor-to-scalar ratio r are given by

$$n_{\mathcal{R}} = 1 - \frac{2(n+2)}{4N+1}\,, \qquad r = \frac{16n}{4N+1}\,. \tag{20}$$

The number of e-foldings relevant to the CMB anisotropies corresponds to $N_{\rm CMB} = 50$-60. Figure 1 shows theoretical predictions for the models $n = 4, 3, 2, 1, 2/3$ ($N_{\rm CMB} = 60$), with the bounds constrained by the WMAP 5-year data [52]. The models with $n \leq 3$ are within the 2σ contour, but the self-coupling model ($n = 4$) is not allowed observationally. Hybrid inflation [36] gives rise to the scalar spectral index $n_{\mathcal{R}}$ larger than 1 with a suppressed tensor-to-scalar ratio ($r \ll 1$), which is also in tension with observations.

From Eqs. (4) and (17) we find that r is related to the variation of the field ϕ, as $r = (8/M_{\rm pl}^2)(d\phi/dN)^2$. The total variation of the field between the time when the perturbations exited the Hubble radius (at $N = N_{\rm CMB}$) and the end of inflation (at $N = N_f$) is then given by $\Delta\phi/M_{\rm pl} = \int_{N_f}^{N_{\rm CMB}} dN\sqrt{r/8}$. Provided that the variation of r is not much, we obtain the Lyth's bound [54]

$$\Delta\phi/M_{\rm pl} = \mathcal{O}(1) \times (r/0.01)^{1/2}\,. \tag{21}$$

For large-field inflation with $\Delta\phi > M_{\rm pl}$ we have $r > 0.01$ (as in chaotic inflation). The small-field models ($\Delta\phi < M_{\rm pl}$) gives rise to a suppressed tensor-to-scalar ratio: $r < 0.01$. The natural inflation model with the potential $V(\phi) = V_0[1-\cos(\phi/\mu)]$ belongs to either large-field or small-field, depending on the initial conditions of ϕ. The models motivated by string theory, such as D-brane inflation [55], racetrack inflation [56], and Kähler inflation [57] usually predict a very small tensor-to-scalar ratio ($r < 10^{-3}$). It may be difficult to see the signatures of those models even with the Planck satellite.

In k-inflation the propagation speed c_s is different from 1, so we need to use the results (14) and (17) to confront the models with observations. In such models the non-Gaussianity of curvature perturbations can be large, as we will see in what follows.

2.3 Non-Gaussian perturbations

The standard inflation with a canonical kinetic term predicts a nearly Gaussian distribution of primordial perturbations [58, 59], but in k-inflation it is possible to give rise to large non-Gaussianities. The first non-trivial statistics describing the non-Gaussianities of the curvature perturbation $\mathcal{R}$ is the bispectrum defined by

$$\langle \mathcal{R}(\mathbf{k}_1)\mathcal{R}(\mathbf{k}_2)\mathcal{R}(\mathbf{k}_3)\rangle = (2\pi)^3\delta^{(3)}(\mathbf{k}_1+\mathbf{k}_2+\mathbf{k}_3)(\mathcal{P}_\mathcal{R})^2 B(k_1,k_2,k_3)\,, \tag{22}$$

where B depends on inflation models.

Let us consider k-inflation models described by the action (5). The vacuum expectation value of the three-point correlation function of $\mathcal{R}$ can be obtained by using the interaction picture in quantum field theory, as [60]

$$\langle \mathcal{R}(t,\mathbf{k}_1)\mathcal{R}(t,\mathbf{k}_2)\mathcal{R}(t,\mathbf{k}_3)\rangle = -i\int_{t_0}^{t} d\tilde{t}\langle 0|[\mathcal{R}(t,\mathbf{k}_1)\mathcal{R}(t,\mathbf{k}_2)\mathcal{R}(t,\mathbf{k}_3), H_I(\tilde{t})]|0\rangle\,, \tag{23}$$

where t_0 is the initial time during inflation (at which the perturbations are deep inside the Hubble radius) and t is some time after the Hubble radius crossing. The interaction Hamiltonian H_I can be derived by expanding the action (5) at the third-order in perturbations, as $H_I = -L_3$, where L_3 is the third-order Lagrangian (i.e. $S_3 = \int dt\, L_3$).

In order to evaluate the third-order Lagrangian $\mathcal{L}_3$ it is convenient to use the ADM metric $ds^2 = -N^2dt^2 + h_{ij}(dx^i + N^i dt)(dx^j + N^j dt)$ with $h_{ij} = a^2 e^{2\mathcal{R}}\delta_{ij}$. In this case we only need to consider the perturbations of N and N^i at first-order in $\mathcal{R}$, with the comoving gauge $\delta\phi = 0$ [59]. Using the first-order solution (12) and commutation relations for the creation and annihilation operators, we obtain the three-point correlation long after the Hubble radius crossing [19]:

$$\langle \mathcal{R}(\mathbf{k}_1)\mathcal{R}(\mathbf{k}_2)\mathcal{R}(\mathbf{k}_3)\rangle = (2\pi)^7\delta^{(3)}(\mathbf{k}_1+\mathbf{k}_2+\mathbf{k}_3)(\mathcal{P}_\mathcal{R})^2\mathcal{A}/(k_1^3k_2^3k_3^3)\,, \tag{24}$$

with

$$\begin{aligned}
\mathcal{A} &= \left(\frac{1}{c_s^2}-1-\frac{2\lambda}{\Sigma}\right)\frac{3k_1^2k_2^2k_3^2}{2K^3} + \left(\frac{1}{c_s^2}-1\right)\left(-\frac{1}{K}\sum_{i>j}k_i^2k_j^2 + \frac{1}{2K^2}\sum_{i\neq j}k_i^2k_j^3 + \frac{1}{8}\sum_i k_i^3\right) \\
&+ \frac{\epsilon}{c_s^2}\left(-\frac{1}{8}\sum_i k_i^3 + \frac{1}{8}\sum_{i\neq j}k_ik_j^2 + \frac{1}{K}\sum_{i>j}k_i^2k_j^2\right) + \frac{\eta}{c_s^2}\left(\frac{1}{8}\sum_i k_i^3\right) \\
&+ \frac{s}{c_s^2}\left(-\frac{1}{4}\sum_i k_i^3 - \frac{1}{K}\sum_{i>j}k_i^2k_j^2 + \frac{1}{2K^2}\sum_{i\neq j}k_i^2k_j^3\right)\,,
\end{aligned} \tag{25}$$

where $K = k_1+k_2+k_3$, $\Sigma = XP_{,X}+2X^2P_{,XX}$, and $\lambda = X^2P_{,XX}+2X^3P_{,XXX}/3$. We take a factorizable shape function B in the form $B = (2\pi)^4(9f_{nl}/10)[-1/(k_1^3k_2^3) - 1/(k_1^3k_3^3) - 1/(k_2^3k_3^3) - 2/(k_1^2k_2^2k_3^2) + 1/(k_1k_2^2k_3^3) + (5\ \text{perm.})]$, where the permutations act on the last term in parenthesis. For the equilateral triangles where $k_1 = k_2 = k_3$ it follows that [18, 19]

$$f_{nl}^{\rm equil} = -\frac{85}{324}\left(\frac{1}{c_s^2}-1+\frac{8}{17}\frac{\lambda}{\Sigma}\right) + \frac{55}{36}\frac{\epsilon}{c_s^2} + \frac{5}{12}\frac{\eta}{c_s^2} - \frac{85}{54}\frac{s}{c_s^2}\,. \tag{26}$$

In standard inflation with a canonical kinetic term one has $c_s^2 = 1$, $\lambda = 0$, and $s = 0$, so that $f_{nl}^{\rm equil}$ is of the order of the slow-roll parameters ϵ and η. In k-inflation models such as DBI inflation [48] one has $|f_{nl}^{\rm equil}| \gg 1$ for $c_s^2 \ll 1$, which can be testable in future observations. Non-Gaussianities in multi-field inflation has been also studied by a number of authors [61]. For the k-inflation models described by the action $P = Xg(Y)$, where g is an arbitrary function in terms of $Y = Xe^{\mu\phi/M_{\rm Pl}}$ (μ is a constant), assisted inflation [62] occurs in the presence of multiple scalar fields [63]. It is of interest to see whether such assisted k-inflation models can give rise to large non-Gaussianities.

2.4 Modified gravitational models of inflation

There are a number of inflation models based on the modification of gravity–such as $f(R)$ gravity and scalar-tensor theories. Let us consider the action in $f(R)$ gravity

$$S = \frac{M_{\rm pl}^2}{2}\int d^4x\sqrt{-g}\, f(R)\,, \tag{27}$$

where f is an arbitrary function in terms of the Ricci scalar R. In the Starobinsky's model described by the Lagrangian $f(R) = R + R^2/(6M^2)$ [1] the slow-roll parameter $\epsilon = -\dot{H}/H^2$ is approximately given by $\epsilon \simeq M^2/(6H^2)$, so that inflation occurs for $H \gtrsim M \simeq 10^{13}\,{\rm GeV}$. The mass scale M is determined by the WMAP normalization of the CMB temperature anisotropies [7]. The dynamical analysis of this model was carried out in Refs. [65].

The spectra of scalar and tensor perturbations can be evaluated directly for the Jordan frame action (27). Another way is to transform the action (27) to that in the Einstein frame under the conformal transformation $\tilde{g}_{\mu\nu} = Fg_{\mu\nu}$, where $F \equiv \partial f/\partial R$. The action in the Einstein frame is given by [66]

$$S_E = \int d^4x\sqrt{-\tilde{g}}\left[\frac{M_{\rm pl}^2}{2}\tilde{R} - \frac{1}{2}\tilde{g}^{\mu\nu}\partial_\mu\phi\partial_\nu\phi - V(\phi)\right]\,, \tag{28}$$

where $\phi = \sqrt{3/2}M_{\rm pl}\ln F$ and $V(\phi) = (FR - f)M_{\rm pl}^2/(2F^2)$. Under the conformal transformation the perturbed metric (6) is transformed as

$$d\tilde{s}^2 = Fds^2 = -(1+2\tilde{\Psi})d\tilde{t}^2 + 2\tilde{a}(\tilde{t})\tilde{B}_{,i}d\tilde{x}^i d\tilde{t} + \tilde{a}^2(\tilde{t})\left[(1+2\tilde{\Phi})\delta_{ij} + 2\tilde{E}_{,ij} + \tilde{h}_{ij}\right]d\tilde{x}^i d\tilde{x}^j\,, \tag{29}$$

where $d\tilde{t} = \sqrt{F}dt$ and $\tilde{a} = \sqrt{F}a$. We decompose the conformal factor $F(t,\mathbf{x})$ into the background and perturbed parts: $F(t,\mathbf{x}) = \bar{F}(t)\left[1 + \delta F(t,\mathbf{x})/\bar{F}(t)\right]$. In what follows we omit a bar from F. The transformation of scalar metric perturbations is given by

$$\tilde{\Psi} = \Psi + \delta F/(2F)\,, \qquad \tilde{B} = B\,, \qquad \tilde{\Phi} = \Phi + \delta F/(2F)\,, \qquad \tilde{E} = E\,, \tag{30}$$

whereas $\tilde{h}_{ij} = h_{ij}$ for tensor perturbations. Under the above transformation one can easily show that the curvature perturbation $\mathcal{R} = \Phi - H\delta F/\dot{F}$ is invariant, i.e. $\tilde{\mathcal{R}} = \mathcal{R}$. Since the tensor perturbation is also invariant, the tensor-to-scalar ratio $\tilde{r}$ in the Einstein frame is identical to that in the Jordan frame.

For example, let us consider the model $f(R) = R + R^2/(6M^2)$. For this model the potential $V(\phi)$ in the Einstein frame is given by

$$V(\phi) = \frac{3}{4}M^2M_{\rm pl}^2\left(1 - e^{-\sqrt{2/3}\phi/M_{\rm pl}}\right)\,, \qquad \phi = \sqrt{3/2}\,M_{\rm pl}\ln[1 + R/(3M^2)]\,. \tag{31}$$

In the regime $\phi \gg M_{\rm pl}$ this potential is nearly constant ($V(\phi) \simeq 3M^2M_{\rm pl}^2/4$), which leads to slow-roll inflation. Meanwhile, in the regime $\phi \ll M_{\rm pl}$, one has $V(\phi) \simeq (1/2)M^2\phi^2$, so that the field oscillates around $\phi = 0$ with a Hubble damping. During inflation the slow-roll parameters defined in Eq. (15) are approximately given by $\epsilon \simeq 3/(4N^2)$ and $\eta \simeq 3/(4N^2) - 1/N$, where $N \simeq (3/4)e^{\sqrt{2/3}\phi/M_{\rm pl}}$ is the number of e-foldings from the end of inflation to the epoch of the first horizon crossing during inflation. From Eq. (18) the spectral index of curvature perturbations and the tensor-to-scalar ratio are given, respectively, by

$$n_{\mathcal{R}} - 1 \simeq -2/N\,, \qquad r \simeq 12/N^2\,, \tag{32}$$

where we have ignored the term of the order of $1/N^2$ in the expression of $n_{\mathcal{R}}$. For the typical value $N = 55$ relevant to the CMB anisotropies we have $n_{\mathcal{R}} \simeq 0.964$ and $r \simeq 4.0 \times 10^{-3}$. These values are allowed by the WMAP5 year constraints: $n_{\mathcal{R}} = 0.960 \pm 0.013$ and $r < 0.22$ (for the negligible running) [52]. The tensor-to-scalar ratio is suppressed compared to chaotic inflation with the potential $V(\phi) = V_0\phi^n$ ($n = 2, 4$), because the potential (31) is almost flat in the regime $\phi \gtrsim M_{\rm pl}$.

For the model $f(R) = R + R^2/(6M^2)$, reheating proceeds gravitationally through the oscillation of R in the regime $H \lesssim M$ [6]. If a field χ is non-minimally coupled to R through the coupling $\xi R\chi^2/2$,

non-perturbative particle creation called preheating can occur through parametric resonance [67]. In Ref. [68] it was shown that preheating occurs for $|\xi|$ larger than 1.

The equivalence of the curvature perturbation between the Jordan and Einstein frames also holds for scalar-tensor theory with the Lagrangian $\mathcal{L} = F(\phi)R/(2\kappa^2) - (1/2)\omega(\phi)g^{\mu\nu}\partial_\mu\phi\partial_\nu\phi - U(\phi)$ [69]. For a non-minimally coupled scalar field with $F(\phi) = 1-\xi\kappa^2\phi^2$ [70, 71] the spectral indices of scalar and tensor perturbations have been derived by using such equivalence [72]. In particular the self-coupling potential $U(\phi) = \lambda\phi^4/4$ with a largely negative non-minimal coupling ($|\xi| \gg 1$) gives rise to the similar potential to Eq. (31) in the Einstein frame. In this case $n_{\mathcal{R}}$ and r are the same as those given in Eq. (32) [72], so the model can be allowed observationally. Preheating in this model was studied in detail in Ref. [73]. We note that the self-coupling potential with a non-minimal coupling was recently revived as a "Higgs inflation" as a way of realizing inflation with a Higgs field [74].

3 Dark energy

In this section we discuss a number of approaches that have been adopted to try and explain the origin of dark energy. The difference between inflation and dark energy is their associated energy scales–the former is about 10^{13} GeV and the latter is about 10^{-42} GeV. From the view point of particle physics dark energy is more difficult to identify its origin, but still it is not entirely hopeless to do so. In inflationary cosmology the energy density of a scalar degree of freedom should vary in time to end inflation, but dark energy can be either the cosmological constant (constant energy density) or some other dynamical source.

3.1 Cosmological constant

The cosmological constant Λ is the simplest candidate of dark energy and it is favored by a number of observations [5, 20, 21, 75]. However it suffers from a serious problem of energy scale if it originates from a vacuum energy appearing in particle physics. The zero-point energy of some field of mass m with momentum k and frequency ω is given by $E = \omega/2 = \sqrt{k^2+m^2}/2$ (in the units of $\hbar = c = 1$). Summing over the zero-point energies of this field up to a cut-off scale $k_{\rm max}$ ($\gg m$), we obtain the vacuum energy density

$$\rho_{\rm vac} = \int_0^{k_{\rm max}} \frac{4\pi k^2 dk}{(2\pi)^3}\frac{1}{2}\sqrt{k^2+m^2} \approx \frac{k_{\rm max}^4}{16\pi^2}\,, \tag{33}$$

where we have used the fact that the integral is dominated by the mode with k larger than m. Taking the cut-off scale $k_{\rm max}$ to be the Planck scale $m_{\rm pl}$, the vacuum energy density can be estimated as $\rho_{\rm vac} \simeq 10^{74}$ GeV^4. This is about 10^{121} times larger than the observed value $\rho_{\rm DE}^{(0)} \simeq 10^{-47}$ GeV^4.

Before the observational discovery of dark energy in 1998 [20, 21], most people believed that the cosmological constant was exactly zero and tried to explain why it is so. The vanishing of a constant may imply the existence of some symmetry. In supersymmetric theories the bosonic degree of freedom has its Fermi counter part that contributes to the zero point energy with an opposite sign. If supersymmetry is unbroken, an equal number of bosonic and fermionic degrees of freedom is present such that the total vacuum energy vanishes. However it is known that supersymmetry is broken at sufficient high energies (for the typical scale $M_{\rm SUSY} = 10^3$ GeV). Hence the vacuum energy is generally non-zero in the world of broken supersymmetry.

Even if supersymmetry is broken there is a hope to obtain a vanishing Λ or a tiny amount of Λ. In supergravity theory an (effective) cosmological constant is given by an expectation value of the potential V for chiral scalar fields φ^i:

$$V(\varphi,\varphi^*) = e^{\kappa^2 K}\left[D_iW(K^{ij^*})(D_jW)^* - 3\kappa^2|W|^2\right]\,, \tag{34}$$

where $\kappa^2 = 8\pi G = 1/M_{\rm pl}^2$, K and W are the so-called Kähler potential and the superpotential, respectively (which are functions of φ^i and φ^{i*}). The quantity K^{ij^*} is the inverse of the derivative $K_{ij^*} \equiv \partial^2 K/\partial\varphi^i\partial\varphi^{j^*}$, whereas the derivative D_iW is defined by $D_iW \equiv \partial W/\partial\varphi^i + \kappa^2 W(\partial K/\partial\varphi^i)$.

The breaking of the supersymmetry corresponds to the condition $D_iW \neq 0$. In this case it is possible to find scalar field values giving the vanishing potential ($V = 0$), but this is not in general an equilibrium

point of the potential V. Nevertheless there is a class of Kähler potentials and superpotentials giving a stationary scalar-field configuration at $V = 0$. Consider, for example, the gluino condensation in $E_8 \times E_8$ superstring theory [76]. The reduction of the 10-dimensional action to 4-dimensions gives rise to a so-called modulus field T. This field characterizes the scale of the compactified 6-dimensional manifold. There exists another complex scalar field S of 4-dimensional dilaton/axion fields. The fields T and S are governed by the Kähler potential

$$K(T, S) = -(3/\kappa^2) \ln (T + T^*) - (1/\kappa^2) \ln (S + S^*) , \tag{35}$$

where $(T + T^*)$ and $(S + S^*)$ are positive definite. The field S couples to the gauge fields, while T does not. An effective superpotential for S can be obtained by integrating out the gauge fields under the use of the R-invariance [77]:

$$W(S) = M_{\rm pl}^3 \left[c_1 + c_2 \exp(-3S/2b) \right] , \tag{36}$$

where c_1, c_2, and b are constants.

Substituting Eqs. (35) and (36) into Eqs. (34), we obtain the field potential

$$V = \frac{M_{\rm pl}^4}{(T + T^*)^3 (S + S^*)} \left| c_1 + c_2 \exp(-3S/2b) \left\{ 1 + \frac{3}{2b} (S + S^*) \right\} \right|^2 . \tag{37}$$

This potential is positive because of the cancellation of the last term in Eq. (34). The stationary field configuration with $V = 0$ is realized under the condition $D_S W = \partial W/\partial S - W/(S + S^*) = 0$. Note that the derivative, $D_T W = \kappa^2 W \partial K/\partial T = -3W/(T + T^*)$, does not necessarily vanish. When $D_T W \neq 0$ the supersymmetry is broken with a vanishing potential energy. Hence it is possible to obtain a stationary field configuration with $V = 0$ even if supersymmetry is broken.

The discussion above is based on the lowest-order perturbation theory. This picture is not necessarily valid to all finite orders of perturbation theory because the non-supersymmetric field configuration is not protected by any symmetry. Moreover some non-perturbative effect can provide a large contribution to the effective cosmological constant. The so-called flux compactification in type IIB string theory allows us to realize a metastable de Sitter (dS) vacuum by taking into account a non-perturbative correction to the superpotential (coming from brane instantons) as well as a number of anti D3-branes in a warped geometry [78]. Hence it is not hopeless to obtain a small value of Λ or a vanishing Λ even in the presence of some non-perturbative corrections.

Kachru, Kallosh, Linde and Trivedi (KKLT) [78] constructed dS solutions in the type II string theory compactified on a Calabi-Yau manifold in the presence of flux. The construction of the dS vacua in the KKLT scenario consists of two steps. The first step is to freeze all moduli fields in the flux compactification at a supersymmetric anti de Sitter (AdS) vacuum. Then a small number of the anti D3-brane is added in a warped geometry with a throat, so that the AdS minimum is uplifted to yield a dS vacuum with broken supersymmetry. If we want to use the KKLT dS minimum derived above for the present cosmic acceleration, we require that the potential energy $V_{\rm dS}$ at the minimum is of the order of $V_{\rm dS} \simeq 10^{-47}\,{\rm GeV}^4$. Depending on the number of fluxes there are a vast of dS vacua, which opened up a notion called string landscape [79]. The question why the vacuum we live in has a very small energy density among many possible vacua has been sometimes answered with anthropic arguments. Some people have studied landscape statistics by considering the relative abundance of long-lived low-energy vacua [80]. These statistical approaches are still under study, but it will be interesting to pursue the possibility to obtain high probabilities for the appearance of low-energy vacua.

In the following we shall consider alternative models of dark energy to the cosmological constant, under the assumption that the cosmological constant problem is solved in such a way that it vanishes completely.

3.2 Modified matter models

In this section we discuss "modified matter models" in which the energy-momentum tensor $T_{\mu\nu}$ on the r.h.s. of the Einstein equations contains an exotic matter source with a negative pressure. The models that belong to this class are quintessence [24, 25], k-essence [26, 27], and perfect fluid models. In what follows we shall discuss quintessence and k-essence. Note that there is a perfect fluid model described by

the equation of state $P = -A/\rho$ ($A > 0$) (Chaplygin gas) [81], but this model was already excluded by the observations of large-scale structure [82].

3.2.1 Quintessence

Many scalar fields are present in particles physics–including string theory and supergravity. We use "quintessence" [25] to denote a canonical scalar field ϕ with a potential $V(\phi)$. The action of quintessence is described by [24]

$$S = \int d^4x\sqrt{-g}\left[\frac{M_{\rm pl}^2}{2}R - \frac{1}{2}g^{\mu\nu}\partial_\mu\phi\partial_\nu\phi - V(\phi)\right] + S_M\,, \tag{38}$$

where $M_{\rm pl}$ is the reduced Planck mass, and R is the Ricci scalar. As a matter action S_M we consider a perfect fluid with the energy density ρ_M, the pressure P_M, and the equation of state $w_M = P_M/\rho_M$.

In a flat FLRW background the perfect fluid satisfies the continuity equation $\dot{\rho}_M + 3H(\rho_M + P_M) = 0$ and the field ϕ obeys the second of Eq. (2). The field equation of state is given by

$$w_\phi \equiv \frac{P_\phi}{\rho_\phi} = \frac{\dot{\phi}^2 - 2V(\phi)}{\dot{\phi}^2 + 2V(\phi)}\,, \tag{39}$$

where ρ_ϕ and P_ϕ are given in Eq. (1). We also have the following Friedmann equation

$$H^2 = \frac{1}{3M_{\rm pl}^2}\left[\frac{1}{2}\dot{\phi}^2 + V(\phi) + \rho_M\right]\,. \tag{40}$$

During radiation and matter dominated epochs, the energy density ρ_M of the fluid dominates over that of quintessence, i.e. $\rho_M \gg \rho_\phi$. We require that ρ_ϕ tracks ρ_M so that the dark energy density dominates at late times. Whether this tracking behavior occurs or not depends on the form of the potential $V(\phi)$. If the potential is steep so that the condition $\dot{\phi}^2/2 \gg V(\phi)$ is always satisfied, we have $w_\phi \simeq 1$ from Eq. (39). In this case the energy density of the field evolves as $\rho_\phi \propto a^{-6}$, which decreases much faster than the background fluid density.

We require the condition $w_\phi < -1/3$ to realize the late-time cosmic acceleration, which translates into the condition $\dot{\phi}^2 < V(\phi)$. Hence the scalar potential needs to be shallow enough for the field to evolve slowly along the potential. This situation is similar to that in inflationary cosmology and it is convenient to introduce the following slow-roll parameters given in Eq. (3). If the conditions $\epsilon_V \ll 1$ and $|\eta_V| \ll 1$ are satisfied, the evolution of the field is sufficiently slow so that $|\ddot{\phi}| \ll |3H\dot{\phi}|$ and $\dot{\phi}^2 \ll V(\phi)$.

The deviation of w_ϕ from -1 is given by

$$1 + w_\phi = \frac{V_{,\phi}^2}{9H^2(\mu+1)^2\rho_\phi}\,, \tag{41}$$

where $\mu \equiv \ddot{\phi}/(3H\dot{\phi})$. This shows that w_ϕ is always larger than -1 for the positive potential. In the slow-roll limit, $|\xi_s| \ll 1$ and $\dot{\phi}^2/2 \ll V(\phi)$, we obtain $1 + w_\phi \simeq 2\epsilon_V/3$ by neglecting the matter fluid in Eq. (40), i.e. $3H^2 \simeq V(\phi)/M_{\rm pl}^2$. The deviation of w_ϕ from -1 is characterized by the slow-roll parameter ϵ_V.

So far many quintessence potentials have been proposed. Crudely speaking they have been classified into (i) "freezing models" and (ii) "thawing" models [83]. In the class (i) the field was rolling along the potential in the past, but the movement gradually slows down after the system enters the phase of cosmic acceleration. In this case the field equation of state w_ϕ decreases toward -1. In the class (ii) the field (with mass m_ϕ) has been frozen by Hubble friction (i.e. the term $H\dot{\phi}$) until recently and then it begins to evolve once H drops below m_ϕ. In this case the equation of state of dark energy is $w_\phi \simeq -1$ at early times, which is followed by the growth of w_ϕ. The representative potentials that belong to these two classes are

- Freezing models:
  (A) $V(\phi) = M^{4+n}\phi^{-n}$ $(n > 0)$, (B) $V(\phi) = M^{4+n}\phi^{-n}\exp(\alpha\phi^2/m_{\rm pl}^2)$.

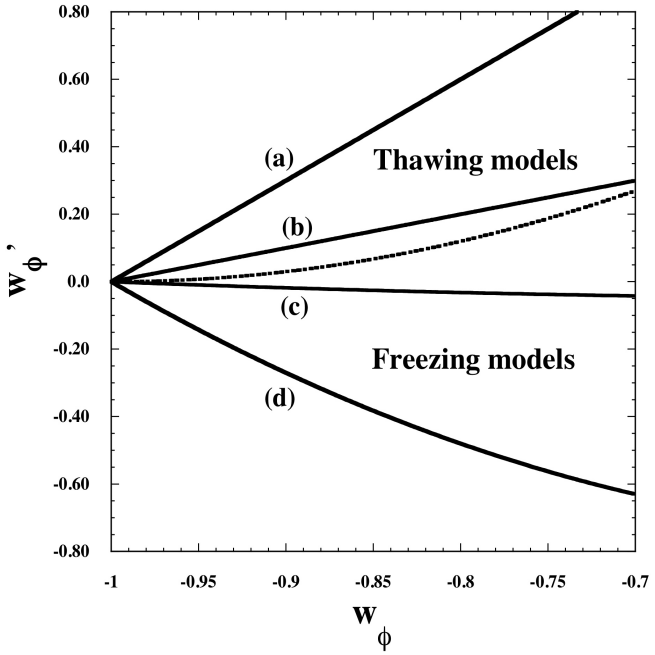

Figure 2: The allowed region in the (w_ϕ, w'_ϕ) plane for thawing and freezing models of quintessence (here primes denote the derivative with respect to $N = \ln a$). The thawing models correspond to the region between two curves: (a) $w'_\phi = 3(1 + w_\phi)$ and (b) $w'_\phi = 1 + w_\phi$, whereas the freezing models are characterized by the region between two curves: (c) $w'_\phi = 0.2w_\phi(1 + w_\phi)$ and (d) $w'_\phi = 3w_\phi(1 + w_\phi)$. The dotted line shows the border between the acceleration and deceleration of the field ($\ddot{\phi} = 0$), which corresponds to $w'_\phi = 3(1 + w_\phi)^2$.

- Thawing models:

  (C) $V(\phi) = V_0 + M^{4-n}\phi^n \quad (n > 0), \qquad$ (D) $V(\phi) = M^4 \cos^2(\phi/f).$

The potential (A) does not possess a minimum and hence the field rolls down the potential toward infinity [24, 25]. This appears, for example, in the fermion condensate model as a dynamical supersymmetry breaking [84]. The potential (B) has a minimum at which the field is eventually trapped (corresponding to $w_\phi = -1$). This potential can be constructed in the framework of supergravity [85].

The potential (C) is similar to the one of chaotic inflation ($n = 2, 4$) used in the early Universe (with $V_0 = 0$). while the mass scale M is very different. Note that the model with $n = 1$ was originally proposed by Linde [86] to replace the cosmological constant by a slowly varying field and then it was revised [87] in connection with the possibility to allow for negative values of $V(\phi)$. The Universe will collapse in the future if the system enters the region with $V(\phi) < 0$. The potential (D) appears as that of the Pseudo-Nambu-Goldstone Boson (PNGB). This was introduced by Frieman *et al.* [88] in response to the first tentative suggestions that the universe may be dominated by the cosmological constant. The small mass of the PNGB model required for the late-time cosmic acceleration is protected against radiative corrections, so this model is favored theoretically. In this model the field is nearly frozen at the potential maximum during the period in which the field mass m_ϕ is smaller than H, but it begins to roll down around the present ($m_\phi \simeq H_0$).

The freezing models and the thawing models are characterized by the conditions $w'_\phi \equiv \mathrm{d}w_\phi/\mathrm{d}\ln(a) < 0$ and $w'_\phi > 0$, respectively. More precisely the allowed regions for the freezing and thawing models are given by $3w_\phi(1+w_\phi) < w'_\phi \lesssim 0.2w_\phi(1+w_\phi)$ and $1+w_\phi \lesssim w'_\phi \lesssim 3(1+w_\phi)$, respectively [83]. In Fig. 2 we illustrate these borders in the (w_ϕ, w'_ϕ) plane. While the observational data up to now are not sufficient to distinguish freezing and thawing models by the variation of w_ϕ, we may be able to do so with the next decade high-precision observations.

In supernovae Ia observations the Hubble parameter $H(z)$ is estimated by measuring a luminosity distance d_L. From the observational data it is possible to reconstruct quintessence potentials [89]. The reconstruction process is however subject to two general problems. The first is that finding a model containing a trajectory with a given expansion rate does not guarantee that the trajectory is stable. The second is that the actual observational data such as d_L are known at discrete values of redshifts, so we require some smoothing process for the reconstruction. In spite of these potential problems it will be of interest how the future high-precision observations can restrict the forms of quintessence potentials.

3.2.2 k-essence

Let us consider dark energy models in which the late-time cosmic acceleration is driven by a kinetic energy of a scalar field. The action for such models is described by (5) in the presence of matter fluids:

$$S = \int d^4x\sqrt{-g}\left[\frac{M_{\rm pl}^2}{2}R + P(\phi, X)\right] + S_M\,. \tag{42}$$

The application of these theories to dark energy was first carried out by Chiba *et al.* [26]. Later this was extended to more general cases and the models based on the action (42) were named "k-essence" [27].

The energy density ρ_ϕ and the pressure P_ϕ of the field are given by $\rho_\phi = 2XP_{,X} - P$ and $P_\phi = P$, respectively. The equation of state of k-essence is

$$w_\phi = \frac{P_\phi}{\rho_\phi} = \frac{P}{2XP_{,X} - P}\,. \tag{43}$$

As long as the condition $|2XP_{,X}| \ll |P|$ is satisfied, w_ϕ can be close to -1. For example, in the ghost condensate model [46] given by $P = -X + X^2/M^4$, we have

$$w_\phi = \frac{1 - X/M^4}{1 - 3X/M^4}\,, \tag{44}$$

which gives $-1 < w_\phi < -1/3$ for $1/2 < X/M^4 < 2/3$. In particular a de Sitter solution ($w_\phi = -1$) is realized at $X/M^4 = 1/2$. Since the field energy density is $\rho_\phi = M^4/4$ at the de Sitter point, it is possible to explain the present cosmic acceleration for $M \sim 10^{-3}$ eV. There is also a modified version of the above model, $P = -X + e^{\lambda\phi/M_{\rm pl}}X^2/M^4$, which is called dilatonic ghost condensate model [49]. The correction of the type $e^{\lambda\phi/M_{\rm pl}}X^2/M^4$ can arise as a dilatonic higher-order correction to the tree-level string action.

In k-essence it can happen that the linear kinetic energy in X has a negative sign. Such a field, called a phantom or ghost scalar field [90], suffers from a quantum instability problem unless higher-order terms in X or ϕ are taken into account in the Lagrangian density. In the (dilatonic) ghost condensate scenario it is possible to avoid this quantum instability by the presence of the term X^2. The quantum stability conditions for k-essence which come from the positive definiteness of the Hamiltonian are given by [49]

$$P_{,X} + 2XP_{,XX} \geq 0\,, \qquad P_{,X} \geq 0\,, \tag{45}$$

$$P_{,\phi\phi} \leq 0\,. \tag{46}$$

The instability prevented by the condition (46) is of the tachyonic type and generally much less dramatic than the conditions (45). The scalar propagation speed c_s is defined in Eq. (9), which is positive under the conditions (45).

In the dilatonic ghost condensate model ($P = -X + e^{\lambda\phi/M_{\rm pl}}X^2/M^4$), for example, the conditions (45) are ensured for $e^{\lambda\phi/M_{\rm pl}}X/M^4 \geq 1/2$ with the sound speed smaller than 1 (speed of light). Some k-essence models have been proposed to solve the coincidence problem of dark energy by the existence of tracker solutions [27]. In such cases, however, it was shown that the sound speed becomes superluminal ($c_s > 1$) before reaching the accelerated attractor [91].

3.3 Modified gravity models

There is another class of dark energy models in which gravity is modified from General Relativity (GR). We discuss a number of cosmological and gravitational aspects of $f(R)$ gravity and DGP braneworld.

3.3.1 $f(R)$ gravity

Let us consider the action (27) in $f(R)$ gravity in the presence of matter fluids:

$$S = \frac{M_{\rm pl}^2}{2}\int {\rm d}^4x\sqrt{-g}\, f(R) + S_M\,, \tag{47}$$

where f is a function of the Ricci scalar R, and S_M is a matter action for perfect fluids. The field equation can be derived by varying the action (47) with respect to $g_{\mu\nu}$:

$$F(R)R_{\mu\nu}(g) - \frac{1}{2}f(R)g_{\mu\nu} - \nabla_\mu\nabla_\nu F(R) + g_{\mu\nu}\Box F(R) = T_{\mu\nu}/M_{\rm pl}^2\,, \tag{48}$$

where $F(R) \equiv \partial f/\partial R$, and $T_{\mu\nu}$ is an energy-momentum tensor of matter[2]. The trace of Eq. (48) is given by

$$3\,\Box F(R) + F(R)R - 2f(R) = T/M_{\rm pl}^2\,, \tag{49}$$

where $T = g^{\mu\nu}T_{\mu\nu} = -\rho_M + 3P_M$. Here ρ_M and P_M are the energy density and the pressure of matter, respectively.

The de Sitter fixed point corresponds to a vacuum solution at which the Ricci scalar is constant. Since $\Box F(R) = 0$ at this point, we obtain

$$F(R)R - 2f(R) = 0\,. \tag{50}$$

The model $f(R) = \alpha R^2$ satisfies this condition and hence it gives rise to an exact de Sitter solution. It is possible to construct viable dark energy models based on $f(R)$ theories having the late-time de Sitter solution satisfying the condition (50).

The possibility of the late-time cosmic acceleration in $f(R)$ gravity was first suggested by Capozziello [28] in 2002. An $f(R)$ model of the form $f(R) = R - \mu^{2(n+1)}/R^n$ $(n > 0)$ was proposed to be responsible for dark energy [29], but this model suffers from a number of problems such as the matter instability [92], absence of the matter era [93], and inability to satisfy local gravity constraints [94]. There are a number of conditions under which $f(R)$ dark energy models are viable. Below we summarize those conditions.

- (i) $f_{,R} > 0$ for $R \geq R_0$, where R_0 is the Ricci scalar today. This is required to avoid the appearance of a ghost.
- (ii) $f_{,RR} > 0$ for $R \geq R_0$. This is required to avoid the negative mass squared of a scalar-field degree of freedom (tachyon) [95].
- (iii) $f(R) \to R - 2\Lambda$ for $R \geq R_0$. This is required to for the presence of the matter era [93] and for consistency with local gravity constraints [96, 97].
- (iv) $0 < \frac{Rf_{,RR}}{f_{,R}}(r=-2) < 1$ at $r = -\frac{Rf_{,R}}{f} = -2$ [98, 99]. This is required to for the stability and the presence of a late-time de Sitter solution. Note that there is another fixed point that can be responsible for the acceleration [99] (with an effective equation of state $w_{\rm eff} > -1$).

The examples of viable models that satisfy all these requirements are [96, 97, 100]

$$\text{(A)}\ f(R) = R - \mu R_c\frac{(R/R_c)^{2n}}{(R/R_c)^{2n}+1} \qquad \text{with}\ \ n, \mu, R_c > 0\,, \tag{51}$$

$$\text{(B)}\ f(R) = R - \mu R_c\left[1 - \left(1 + R^2/R_c^2\right)^{-n}\right] \qquad \text{with}\ \ n, \mu, R_c > 0\,, \tag{52}$$

$$\text{(C)}\ f(R) = R - \mu R_c \tanh\left(R/R_c\right) \qquad \text{with}\ \ \mu, R_c > 0\,, \tag{53}$$

where μ, R_c, and n are constants. R_c is roughly of the order of the present cosmological Ricci scalar R_0. A similar model to (C) was also proposed by Appleby and Battye [101]. If $R \gg R_c$ the models are close to the ΛCDM model ($f(R) \simeq R - \mu R_c$), so that GR is recovered in the region of high density. Meanwhile

[2]There is another way for the variation of the action (47) called the Palatini formalism.

the deviation from GR becomes important when R decreases to the order of R_c. The equation of state $w_{\rm DE}$ of dark energy to confront with supernovae Ia observations can be smaller than -1 for viable $f(R)$ models without the appearance of ghosts [96, 100, 102]. We note, however, that the effective equation of state $w_{\rm eff} = -1 - 2\dot{H}/(3H^2)$ remains to be larger than -1 as long as the conditions (i)-(iv) listed above are satisfied (apart from small oscillations around the de Sitter attractor if it is a stable spiral). Since the deviation of $w_{\rm DE}$ from that in the ΛCDM model ($w_{\rm DE} = -1$) is not so significant [96, 103], the viable models such as (51)-(53) can be consistent with the supernovae Ia data fairly easily.

The modification of gravity manifests itself in the effective gravitational coupling that appears in the equation of cosmological perturbations. The matter density perturbation δ_m satisfies the following equation under a quasi-static approximation on sub-horizon scales [104]

$$\ddot{\delta}_m + 2H\dot{\delta}_m - 4\pi G_{\rm eff}\rho_m\delta_m = 0\,, \tag{54}$$

where ρ_m is the energy density of non-relativistic matter, and

$$G_{\rm eff} = \frac{G}{f_{,R}}\frac{1+4m\,k^2/(a^2R)}{1+3m\,k^2/(a^2R)}\,. \tag{55}$$

Here $m \equiv Rf_{,RR}/f_{,R}$ is the deviation parameter from the ΛCDM model [99]. In the regime where the deviation from the ΛCDM model is small such that $m\,k^2/(a^2R) \ll 1$, the effective gravitational coupling $G_{\rm eff}$ is very close to the gravitational constant G. Then the matter perturbation evolves as $\delta_m \propto t^{2/3}$ during the matter dominance. Meanwhile in the regime $m\,k^2/(a^2R) \gg 1$ one has $G_{\rm eff} = 4G/(3f_{,R})$, so that the evolution of δ_m during the matter era is given by $\delta_m \propto t^{(\sqrt{33}-1)/6}$.

This unusual evolution of δ_m leaves a number of interesting signatures such as the modification to the matter power spectrum and the effect on weak lensing. For the models (A) and (B), for example, the difference between the spectral indices between the matter power spectrum and the CMB spectrum can be estimates as [97]

$$\Delta n_s = \frac{\sqrt{33}-5}{6n+4}\,. \tag{56}$$

Observationally we do not find any strong signature for the difference of slopes of the two spectra. If we take the mild bound $\Delta n_s < 0.05$, we obtain the constraint $n > 2$. Local gravity constraints on solar system scales can be satisfied for $n > 0.9$ [105] through the chameleon mechanism [106]. Hence, as long as $n > 2$, the models (A) and (B) can be consistent with both cosmological and local gravity constraints. The model (53) can easily satisfy local gravity constraints because of the rapid approach to the ΛCDM model in the regime $R \gg R_c$.

In the strong gravitational background (such as neutron stars), Kobayashi and Maeda [107, 108] pointed out that for the $f(R)$ models such as (51) and (52) it is difficult to obtain thin-shell solutions inside a spherically symmetric body with constant density. For chameleon models with general couplings Q, a thin-shell field profile was analytically derived in Ref. [109] by employing a linear expansion in terms of the gravitational potential Φ_c at the surface of a compact object with constant density. Using the boundary condition set by analytic solutions, Ref. [109] also numerically confirmed the existence of thin-shell solutions for $\Phi_c \lesssim 0.3$ in the case of inverse power-law potentials $V(\phi) = M^{4+n}\phi^{-n}$. Ref. [110] also showed that static relativistic stars with constant density exists for the model (52). The effect of the relativistic pressure is important around the center of the body, so that the field tends to roll down the potential quickly unless the boundary condition is carefully chosen. Realistic stars have densities $\rho_A(r)$ that globally decrease as a function of r. Numerical simulations of Refs. [111] demonstrate that thin-shell solutions are present for the $f(R)$ model (52) by considering a polytropic equation of state even in the strong gravitational background.

3.3.2 DGP model

There is another class of modified gravity models of dark energy based on braneworlds. In braneworlds standard model particles are confined on a 3-dimensional (3D) brane embedded in 5-dimensional bulk spacetime with large extra dimensions. Dvali, Gabadadze, and Porrati (DGP) [31] proposed a braneworld model in which the 3-brane is embedded in a Minkowski bulk spacetime with infinitely large extra

dimensions. Newton's law can be recovered by adding a 4D Einstein-Hilbert action sourced by the brane curvature to the 5D action. The presence of such a 4D term may be induced by quantum corrections coming from the bulk gravity and its coupling with matter on the brane. In the DGP model the standard 4D gravity is recovered for small distances, whereas the effect from the 5D gravity manifests itself for large distances. Interestingly it is possible to realize the late-time cosmic acceleration without introducing a dark energy component [112].

The action for the DGP model is given by

$$S = \frac{1}{2\kappa_{(5)}^2}\int d^5X\sqrt{-\tilde{g}}\,\tilde{R} + \frac{1}{2\kappa_{(4)}^2}\int d^4X\sqrt{-g}R - \int d^5X\sqrt{-\tilde{g}}\,\mathcal{L}_M\,, \tag{57}$$

where $\tilde{g}_{AB}$ is the metric in the 5D bulk and $g_{\mu\nu} = \partial_\mu X^A \partial_\nu X^B \tilde{g}_{AB}$ is the induced metric on the brane with $X^A(x^c)$ being the coordinates of an event on the brane labelled by x^c. The 5D and 4D gravitational constants, $\kappa_{(5)}^2$ and $\kappa_{(4)}^2$, are related with the 5D and 4D Planck masses, $M_{(5)}$ and $M_{(4)}$, via $\kappa_{(5)}^2 = 1/M_{(5)}^3$ and $\kappa_{(4)}^2 = 1/M_{(4)}^2$.

The first and second terms in Eq. (57) correspond to Einstein-Hilbert actions in the 5D bulk and on the brane, respectively. The matter action consists of a brane-localized matter whose action is given by $\int d^4x\sqrt{-g}\,(\sigma + \mathcal{L}_M^{\rm brane})$, where σ is the 3-brane tension and $\mathcal{L}_M^{\rm brane}$ is the Lagrangian density on the brane. Since the tension is not related to the Ricci scalar R, it can be adjusted to be zero.

The Friedmann equation on the flat FLRW brane is given by [112]

$$H^2 - \frac{\epsilon}{r_c}H = \frac{\kappa_{(4)}^2}{3}\rho_M\,, \tag{58}$$

where $\epsilon = \pm 1$, $r_c \equiv \kappa_{(5)}^2/(2\kappa_{(4)}^2)$ is a crossover scale, and ρ_M is the matter energy density on the brane satisfying the continuity equation

$$\dot{\rho}_M + 3H(\rho_M + P_M) = 0\,. \tag{59}$$

If the crossover scale r_c is much larger than the Hubble radius H^{-1}, the first term in Eq. (58) dominates over the second one. In this case the standard Friedmann equation, $H^2 = \kappa_{(4)}^2\rho_M/3$, is recovered. Meanwhile, in the regime $r_c < H^{-1}$, the presence of the second term in Eq. (58) leads to a modification to the standard Friedmann equation. In the Universe dominated by non-relativistic matter ($\rho_M \propto a^{-3}$), the Universe approaches a dS solution for $\epsilon = +1$:

$$H \to H_{\rm dS} = 1/r_c\,. \tag{60}$$

Hence it is possible to realize the present cosmic acceleration provided that r_c is of the order of the present Hubble radius H_0^{-1}.

Although the DGP braneworld is an attractive model allowing a self acceleration, the joint constraints from data of supernovae Ia, baryon acoustic oscillations, and the CMB shift parameter shows that this model is under strong observational pressure [113]. Moreover, this model contains a ghost mode [114] with the effective Brans-Dicke parameter $\omega_{\rm BD}$ smaller than $-3/2$. Hence the original DGP model is effectively ruled out from observational constraints as well as from the ghost problem. It is however possible to construct a generalized DGP model free from the ghost problem by embedding our visible 3-brane with a 4-brane in a flat 6D bulk [115].

In the DGP model a brane-bending mode ϕ (i.e. longitudinal graviton) gives rise to a field self-interaction of the form $\Box\phi(\partial^\mu\phi\partial_\mu\phi)$ through a mixing with the transverse graviton [116]. This can lead to the decoupling of the field ϕ from gravitational dynamics in the local region by the so-called Vainshtein mechanism [117]. It is possible to generalize the field self-interaction $\Box\phi(\partial^\mu\phi\partial_\mu\phi)$ to more general forms in the 4D gravity, such that the Lagrangian is invariant under the the Galilean shift $\partial_\mu\phi \to \partial_\mu\phi + b_\mu$ [32]. In such "Galileon gravity" the late-time cosmic acceleration can be realized without the appearance of ghosts [118].

4 Conclusions

We have discussed theoretical attempts for finding the origin of inflation and dark energy, paying particular attention to their observational signatures. The WMAP observations already ruled out some models

of inflation (such as $V(\phi) = \lambda\phi^4/4$). The future observations such as the Planck will be able to constrain inflationary models further. In particular the detection of gravitational waves and non-Gaussianities will allow us to discriminate between a host of inflation models.

The important step for approaching the origin of dark energy is to clarify whether it is a cosmological constant or it originates from some dynamical source. In doing so, it is important to find some observational signatures for the deviation of the dark energy equation of state from -1. Modified gravity models of dark energy can be distinguished from other models at the level of perturbations because of the modification of the effective gravitational coupling. The upcoming high-precision observations of large-scale structure, weak lensing, and cosmic microwave background may allow us to discriminate those models from the ΛCDM.

Acknowledgements

S. T. would like to give warm regards to Profs. Kei-chi Maeda and Takashi Nakamura for the celebration of their 60-th birthdays. S. T. also thanks organizers of the JGRG20 workshop for inviting him to have a talk.

References

[1] A. A. Starobinsky, Phys. Lett. B **91** (1980) 99.

[2] D. Kazanas, Astrophys. J. **241** L59 (1980); K. Sato, Mon. Not. R. Astron. Soc. **195**, 467 (1981); Phys. Lett. **99B**, 66 (1981); A. H. Guth, Phys. Rev. D **23**, 347 (1981).

[3] V. F. Mukhanov and G. V. Chibisov, JETP Lett. **33**, 532 (1981); A. H. Guth and S. Y. Pi, Phys. Rev. Lett. **49** (1982) 1110; S. W. Hawking, Phys. Lett. B **115**, 295 (1982); A. A. Starobinsky, Phys. Lett. B **117** (1982) 175; J. M. Bardeen, P. J. Steinhardt and M. S. Turner, Phys. Rev. D **28**, 679 (1983).

[4] D. N. Spergel *et al.* [WMAP Collaboration], Astrophys. J. Suppl. **148**, 175 (2003).

[5] E. Komatsu *et al.*, arXiv:1001.4538 [astro-ph.CO].

[6] A. A. Starobinsky, in: Proc. of the 2nd Seminar, "Quantum Gravity" (Moscow, 13-15 Oct. 1981), INR Press, Moscow, 1982, pp. 58-72; reprinted in: Quantum Gravity, eds. M. A. Markov and P. C. West, Plenum Publ. Co., N. Y., 1984, pp. 103-128; A. Vilenkin, Phys. Rev. D **32**, 2511 (1985); M. B. Mijic, M. S. Morris and W. M. Suen, Phys. Rev. D **34**, 2934 (1986).

[7] J. c. Hwang and H. Noh, Phys. Lett. B **506**, 13 (2001).

[8] A. D. Linde, Phys. Lett. B **108**, 389 (1982).

[9] A. Albrecht and P. Steinhardt, Phys. Rev. Lett. **48**, 1220 (1982).

[10] D. H. Lyth and A. Riotto, Phys. Rept. **314**, 1 (1999).

[11] A. D. Linde, arXiv:hep-th/0503203.

[12] A. D. Linde, Phys. Lett. B **129** 177 (1983).

[13] J. E. Lidsey, A. R. Liddle, E. W. Kolb, E. J. Copeland, Rev. Mod. Phys. **69**, 373 (1997).

[14] A. R. Liddle and D. H. Lyth, *Cosmological inflation and large-scale structure*, Cambridge University Press (2000).

[15] B. A. Bassett, S. Tsujikawa and D. Wands, Rev. Mod. Phys. **78**, 537 (2006).

[16] C. Armendariz-Picon, T. Damour and V. F. Mukhanov, Phys. Lett. B **458**, 209 (1999).

[17] J. Garriga and V. F. Mukhanov, Phys. Lett. B **458**, 219 (1999).

[18] D. Seery and J. E. Lidsey, JCAP **0506**, 003 (2005).

[19] X. Chen, M. x. Huang, S. Kachru and G. Shiu, JCAP **0701**, 002 (2007).

[20] A. G. Riess *et al.* [Supernova Search Team Collaboration], Astron. J. **116**, 1009 (1998).

[21] S. Perlmutter *et al.* [Supernova Cosmology Project Collaboration], Astrophys. J. **517**, 565 (1999).

[22] V. Sahni and A. A. Starobinsky, Int. J. Mod. Phys. D **9**, 373 (2000); P. J. E. Peebles and B. Ratra, Rev. Mod. Phys. **75**, 559 (2003); T. Padmanabhan, Phys. Rept. **380**, 235 (2003); E. J. Copeland, M. Sami and S. Tsujikawa, Int. J. Mod. Phys. D **15**, 1753 (2006).

[23] S. Weinberg, Rev. Mod. Phys. **61**, 1 (1989).

[24] Y. Fujii, Phys. Rev. D **26**, 2580 (1982); C. Wetterich, Nucl. Phys B. **302**, 668 (1988); B. Ratra and J. Peebles, Phys. Rev D **37**, 321 (1988); T. Chiba, N. Sugiyama and T. Nakamura, Mon. Not. Roy. Astron. Soc. **289**, L5 (1997).

[25] R. R. Caldwell, R. Dave and P. J. Steinhardt, Phys. Rev. Lett. **80**, 1582 (1998).

[26] T. Chiba, T. Okabe and M. Yamaguchi, Phys. Rev. D **62**, 023511 (2000).

[27] C. Armendariz-Picon, V. F. Mukhanov and P. J. Steinhardt, Phys. Rev. Lett. **85**, 4438 (2000); C. Armendariz-Picon, V. F. Mukhanov and P. J. Steinhardt, Phys. Rev. D **63**, 103510 (2001).

[28] S. Capozziello, Int. J. Mod. Phys. **D 11**, 483, (2002).

[29] S. Capozziello, V. F. Cardone, S. Carloni and A. Troisi, Int. J. Mod. Phys. **D**, 12, 1969 (2003); S. M. Carroll, V. Duvvuri, M. Trodden and M. S. Turner, Phys. Rev. D **70**, 043528 (2004).

[30] L. Amendola, Phys. Rev. D **60**, 043501 (1999); J. P. Uzan, Phys. Rev. D **59**, 123510 (1999); T. Chiba, Phys. Rev. D **60**, 083508 (1999); N. Bartolo and M. Pietroni, Phys. Rev. D **61** 023518 (2000).

[31] G. R. Dvali, G. Gabadadze and M. Porrati, Phys. Lett. B **485**, 208 (2000).

[32] A. Nicolis, R. Rattazzi and E. Trincherini, Phys. Rev. D **79**, 064036 (2009).

[33] A. R. Liddle, P. Parsons and J. D. Barrow, Phys. Rev. D **50**, 7222 (1994).

[34] E. W. Kolb, arXiv:hep-ph/9910311 (1999).

[35] K. Freese, J. A. Frieman and A. V. Olinto, Phys. Rev. Lett. **65**, 3233 (1990).

[36] A. D. Linde, Phys. Rev. D **49**, 748 (1994).

[37] E. J. Copeland, A. R. Liddle, D. H. Lyth, E. D. Stewart and D. Wands, Phys. Rev. D **49**, 6410 (1994).

[38] D. Polarski and A. A. Starobinsky, Nucl. Phys. B **385**, 623 (1992); D. Langlois, Phys. Rev. D **59**, 123512 (1999).

[39] A. A. Starobinsky and J. Yokoyama, arXiv:gr-qc/9502002; A. A. Starobinsky, S. Tsujikawa and J. Yokoyama, Nucl. Phys. B **610**, 383 (2001).

[40] F. Lucchin and S. Matarrese, Phys. Rev. D **32**, 1316 (1985); J. Yokoyama and K. i. Maeda, Phys. Lett. B **207**, 31 (1988).

[41] P. J. E. Peebles and A. Vilenkin, Phys. Rev. D **59**, 063505 (1999).

[42] M. Fairbairn and M. H. G. Tytgat, Phys. Lett. B **546**, 1 (2002); A. Feinstein, Phys. Rev. D **66**, 063511 (2002).

[43] N. Arkani-Hamed, P. Creminelli, S. Mukohyama and M. Zaldarriaga, JCAP **0404**, 001 (2004).

[44] J. R. Ellis, N. Kaloper, K. A. Olive and J. Yokoyama, Phys. Rev. D **59**, 103503 (1999); S. W. Hawking, T. Hertog and H. S. Reall, Phys. Rev. D **63**, 083504 (2001); K. i. Maeda and N. Ohta, Phys. Lett. B **597**, 400 (2004).

[45] M. Gasperini and G. Veneziano, Astropart. Phys. **1**, 317 (1993).

[46] N. Arkani-Hamed, H. C. Cheng, M. A. Luty and S. Mukohyama, JHEP **0405**, 074 (2004).

[47] A. Sen, JHEP **0204**, 048 (2002).

[48] E. Silverstein and D. Tong, Phys. Rev. D **70**, 103505 (2004); M. Alishahiha, E. Silverstein and D. Tong, Phys. Rev. D **70**, 123505 (2004).

[49] F. Piazza and S. Tsujikawa, JCAP **0407**, 004 (2004).

[50] J. M. Bardeen, Phys. Rev. D **22**, 1882 (1980); H. Kodama and M. Sasaki, Prog. Theor. Phys. Suppl. **78**, 1 (1984); V. F. Mukhanov, H. A. Feldman and R. H. Brandenberger, Phys. Rept. **215**, 203 (1992).

[51] V. N. Lukash, Sov. Phys. JETP **52**, 807 (1980); D. H. Lyth, Phys. Rev. D **31**, 1792 (1985); M. Sasaki, Prog. Theor. Phys. **76**, 1036 (1986).

[52] E. Komatsu *et al.* [WMAP Collaboration], Astrophys. J. Suppl. **180**, 330 (2009).

[53] D. Baumann, arXiv:0907.5424 [hep-th].

[54] D. H. Lyth, Phys. Rev. Lett. **78**, 1861 (1997).

[55] G. R. Dvali and S. H. H. Tye, Phys. Lett. B **450**, 72 (1999); S. Kachru *et al.*, JCAP **0310**, 013 (2003); D. Baumann, A. Dymarsky, I. R. Klebanov and L. McAllister, JCAP **0801**, 024 (2008); S. Panda, M. Sami and S. Tsujikawa, Phys. Rev. D **76**, 103512 (2007); D. Baumann *et al.*, JHEP **03**, 093 (2009).

[56] J. J. Blanco-Pillado *et al.*, JHEP **09**, 002 (2006).

[57] J. P. Conlon and F. Quevedo, JHEP **01**, 146 (2006).

[58] N. Bartolo, S. Matarrese and A. Riotto, Phys. Rev. D **65**, 103505 (2002).

[59] J. M. Maldacena, JHEP **0305**, 013 (2003).

[60] K. Koyama, Class. Quant. Grav. **27**, 124001 (2010).

[61] F. Bernardeau and J. P. Uzan, Phys. Rev. D **66**, 103506 (2002); D. Seery and J. E. Lidsey, JCAP **0509**, 011 (2005); C. T. Byrnes, M. Sasaki and D. Wands, Phys. Rev. D **74**, 123519 (2006); D. Langlois, S. Renaux-Petel, D. A. Steer and T. Tanaka, Phys. Rev. D **78**, 063523 (2008); F. Arroja, S. Mizuno and K. Koyama, JCAP **0808**, 015 (2008).

[62] A. R. Liddle, A. Mazumdar and F. E. Schunck, Phys. Rev. D **58**, 061301 (1998).

[63] S. Tsujikawa, Phys. Rev. D **73**, 103504 (2006).

[64] A. De Felice and S. Tsujikawa, Living Rev. Rel. **13**, 3 (2010).

[65] K. i. Maeda, Phys. Rev. D **37**, 858 (1988); L. Amendola, S. Capozziello, M. Litterio and F. Occhionero, Phys. Rev. D **45**, 417 (1992).

[66] K. i. Maeda, Phys. Rev. D **39**, 3159 (1989).

[67] L. Kofman, A. D. Linde and A. A. Starobinsky, Phys. Rev. Lett. **73**, 3195 (1994); Phys. Rev. D **56**, 3258 (1997).

[68] S. Tsujikawa, K. i. Maeda and T. Torii, Phys. Rev. D **60**, 123505 (1999).

[69] N. Makino and M. Sasaki, Prog. Theor. Phys. **86**, 103 (1991); R. Fakir, S. Habib and W. Unruh, Astrophys. J. **394**, 396 (1992).

[70] T. Futamase and K. i. Maeda, Phys. Rev. D **39**, 399 (1989).

[71] R. Fakir and W. G. Unruh, Phys. Rev. D **41**, 1783 (1990).

[72] E. Komatsu and T. Futamase, Phys. Rev. D **59**, 064029 (1999); S. Tsujikawa and B. Gumjudpai, Phys. Rev. D **69**, 123523 (2004).

[73] S. Tsujikawa, K. i. Maeda and T. Torii, Phys. Rev. D **61**, 103501 (2000).

[74] F. L. Bezrukov and M. Shaposhnikov, Phys. Lett. B **659**, 703 (2008).

[75] D. J. Eisenstein *et al.* [SDSS Collaboration], Astrophys. J. **633**, 560 (2005).

[76] M. Dine, R. Rohm, N. Seiberg and E. Witten, Phys. Lett. B **156**, 55 (1985).

[77] I. Affleck, M. Dine and N. Seiberg, Nucl. Phys. B **256**, 557 (1985).

[78] S. Kachru, R. Kallosh, A. D. Linde and S. P. Trivedi, Phys. Rev. D **68**, 046005 (2003).

[79] L. Susskind, arXiv:hep-th/0302219.

[80] F. Denef and M. R. Douglas, JHEP **0405**, 072 (2004); R. Blumenhagen *et al.,* Nucl. Phys. B **713**, 83 (2005).

[81] A. Y. Kamenshchik, U. Moschella and V. Pasquier, Phys. Lett. B **511**, 265 (2001); M. C. Bento, O. Bertolami and A. A. Sen, Phys. Rev. D **66**, 043507 (2002).

[82] H. Sandvik, M. Tegmark, M. Zaldarriaga and I. Waga, Phys. Rev. D **69**, 123524 (2004).

[83] R. R. Caldwell and E. V. Linder, Phys. Rev. Lett. **95**, 141301 (2005).

[84] P. Binetruy, Phys. Rev. D **60**, 063502 (1999).

[85] P. Brax and J. Martin, Phys. Lett. B **468**, 40 (1999).

[86] A. D. Linde, "Inflation and quantum cosmology", in: Three hundred years of gravitation, Eds.: S. W. Hawking and W. Israel, Cambridge Univeristy Press (1987), 604.

[87] R. Kallosh *et al.,* JCAP **0310**, 015 (2003).

[88] J. A. Frieman, C. T. Hill, A. Stebbins and I. Waga, Phys. Rev. Lett. **75**, 2077 (1995).

[89] A. A. Starobinsky, JETP Lett. **68**, 757 (1998); T. Nakamura and T. Chiba, Mon. Not. Roy. Astron. Soc. **306**, 696 (1999); T. Chiba and T. Nakamura, Phys. Rev. D **62**, 121301 (2000); T. D. Saini, S. Raychaudhury, V. Sahni and A. A. Starobinsky, Phys. Rev. Lett. **85**, 1162 (2000).

[90] R. R. Caldwell, Phys. Lett. B **545**, 23 (2002).

[91] C. Bonvin, C. Caprini and R. Durrer, Phys. Rev. Lett. **97**, 081303 (2006).

[92] A. D. Dolgov and M. Kawasaki, Phys. Lett. B **573**, 1 (2003).

[93] L. Amendola, D. Polarski and S. Tsujikawa, Phys. Rev. Lett. **98**, 131302 (2007).

[94] T. Chiba, Phys. Lett. B **575**, 1 (2003); G. J. Olmo, Phys. Rev. D **72**, 083505 (2005); I. Navarro and K. Van Acoleyen, JCAP **0702**, 022 (2007).

[95] Y. S. Song, W. Hu and I. Sawicki, Phys. Rev. D **75**, 044004 (2007).

[96] W. Hu and I. Sawicki, Phys. Rev. D **76**, 064004 (2007).

[97] A. A. Starobinsky, JETP Lett. **86**, 157 (2007).

[98] V. Muller, H. J. Schmidt and A. A. Starobinsky, Phys. Lett. B **202**, 198 (1988); V. Faraoni, Phys. Rev. D **72**, 061501 (2005).

[99] L. Amendola, R. Gannouji, D. Polarski and S. Tsujikawa, Phys. Rev. D **75**, 083504 (2007).

[100] S. Tsujikawa, Phys. Rev. D **77**, 023507 (2008).

[101] S. A. Appleby and R. A. Battye, Phys. Lett. B **654**, 7 (2007).

[102] L. Amendola and S. Tsujikawa, Phys. Lett. B **660**, 125 (2008).

[103] H. Motohashi, A. A. Starobinsky and J. Yokoyama, Prog. Theor. Phys. **123**, 887 (2010).

[104] S. Tsujikawa, Phys. Rev. D **76**, 023514 (2007).

[105] S. Capozziello and S. Tsujikawa, Phys. Rev. D **77**, 107501 (2008).

[106] J. Khoury and A. Weltman, Phys. Rev. Lett. **93**, 171104 (2004).

[107] T. Kobayashi and K. i. Maeda, Phys. Rev. D **78**, 064019 (2008).

[108] T. Kobayashi and K. i. Maeda, Phys. Rev. D **79**, 024009 (2009).

[109] S. Tsujikawa, T. Tamaki and R. Tavakol, JCAP **0905**, 020 (2009).

[110] A. Upadhye and W. Hu, Phys. Rev. D **80**, 064002 (2009).

[111] E. Babichev and D. Langlois, Phys. Rev. D **80**, 121501 (2009); Phys. Rev. D **81**, 124051 (2010).

[112] C. Deffayet, Phys. Lett. B **502** (2001), 199; C. Deffayet, G. R. Dvali and G. Gabadadze, Phys. Rev. D **65** (2002), 044023.

[113] M. Fairbairn and A. Goobar, Phys. Lett. B **642** , 432 (2006); R. Maartens and E. Majerotto, Phys. Rev. D **74**, 023004 (2006);Y. S. Song, I. Sawicki and W. Hu, Phys. Rev. D **75**, 064003 (2007).

[114] A. Lue, R. Scoccimarro and G. D. Starkman, Phys. Rev. D **69**, 124015 (2004); K. Koyama and R. Maartens, JCAP **0601**, 016 (2006).

[115] C. de Rham *et al.,* Phys. Rev. Lett. **100**, 251603 (2008).

[116] C. Deffayet, G. R. Dvali, G. Gabadadze and A. I. Vainshtein, Phys. Rev. D **65**, 044026 (2002); M. Porrati, Phys. Lett. B **534**, 209 (2002).

[117] A. I. Vainshtein, Phys. Lett. B **39**, 393 (1972).

[118] A. De Felice and S. Tsujikawa, Phys. Rev. Lett. **105**, 111301 (2010).

Non-linear perturbations from cosmological inflation

David Wands[1 (a)]

[(a)] *Institute of Cosmology and Gravitation, University of Portsmouth, Dennis Sciama Building, Portsmouth, PO1 3FX, United Kingdom*

Abstract

In this talk I will discuss various ways in which non-linear perturbations produced during inflation give distinctive signatures of the physical processes at work in the very early universe.

1 Introduction

It is a pleasure to be back in Kyoto and an honour to participate in this meeting celebrating the 60th birthdays of Professors Maeda and Nakamura. I was lucky enough to meet Kei-ichi Maeda for the first time towards the end of my PhD when he came to visit my supervisor, John Barrow, at the University of Sussex. Prof Maeda was a visitor for a month or more, so we had plenty of opportunity to discuss research. Of course Maeda-san was very approachable and easy to talk with, and so we soon had the outline of a paper [1]. That formed the basis for a continuing collaboration, my first visit to Tokyo ten years ago, and many visits since and papers with many other Japanese researchers.

In this talk I will try to give an overview, no doubt biased and incomplete, of recent work to characterise non-linear inhomogeneous perturbations in cosmology and in particular those produced in different models of inflation in the very early universe. The main point I wish to emphasise is that inhomogeneities beyond the first-order perturbations conventionally studied, can offer distinctive observational predictions of the physical processes at work during and after inflation. We have become adept at producing a power spectrum of primordial density perturbations that is consistent with observational constraints ($\Delta^2_{\mathcal{R}} = (2.430 \pm 0.091) \times 10^{-9}$ and spectral index $n = 0.968 \pm 0.012$ [2]) from a range of models with suitably tuned parameters, but there is additional information in the higher-order correlators of the primordial density field, as well as tensor perturbations.

2 Extended inflation

The work of Maeda and Japanese JGRG community has highlighted the central role played by gravity in cosmological inflation. Inflation is an accelerated expansion, usually framed in terms of a background homogeneous and isotropic (FRW) background cosmology obeying the Einstein equations of general relativity. The symmetry of the background spacetime limits the gravitational equations to the familiar Friedmann constraint equation for the Hubble rate, H, plus the evolution equation for the acceleration. Once we introduce inhomogeneous perturbations we have constraint and evolution equations for energy and momentum, which can be conveniently decomposed into scalar, vector and tensor perturbations on the maximally symmetric background space [4]. The non-linearity of general relativity is only apparent once we go beyond linear perturbations and go to second order and beyond. Often inflation is described in terms of minimally coupled scalar fields in four-dimensional general relativity, but sometimes gravity itself drives the inflationary dynamics, through modifications to general relativity and/or higher-dimensional geometry. Starobinsky's original inflation model was itself driven by the curvature of spacetime, considering the effective expansion in fourth-order gravity [3].

As this meeting also celebrates the 20th anniversary of the JGRG society I thought it would be interesting to look back at where inflation stood back in 1990, when I was just beginning as a research student. If you look back at the proceedings of the first JGRG meeting you will find papers by Kitada and Maeda [5], and Maeda and Sakai [6] investigating aspects of one particular theoretical model.

[1] Email address: david.wands@port.ac.uk

One particularly simple and elegant model of inflation - the hot topic in 1990 - was extended inflation proposed by La and Steinhardt [7]. It implemented Guth's old inflation [8] driven by a supercooled false vacuum energy density in an extended gravity theory - Brans and Dicke's gravity [9] with a dynamical effective gravitational "constant" determined by a scalar field: $G\text{eff} \propto M_{\rm Pl}^{-2} \propto \Phi^{-1}$.

The dynamics thus followed from the simple Lagrangian

$$\mathcal{L} = \Phi R - \frac{\omega}{\Phi}\left(\nabla\Phi\right)^2 - M_{\rm GUT}^4 \tag{1}$$

where R is the Ricci scalar and the false vacuum energy density is required to be around the GUT scale, $M_{\rm GUT}^4$. Extended inflation solved the graceful exit problem of old inflation because even with a constant false vacuum energy, the Hubble rate decreases in Brans-Dicke gravity as the Φ field grows, gravity becomes weaker and the Hubble constant decreases. This was soon generalised to other scalar-tensor theories by Barrow and Maeda [10] and Accetta and Steinhardt [11].

Intriguingly, extended inflation offers a dynamical solution to the hierarchy between the Planck scale and the GUT scale. Brans-Dicke gravity has no instrinsic mass scale, just the dimensionless parameter ω. But extended inflation fixes the value of the Planck scale at the end of inflation by the requirement that the phase transition completes [12, 14].

The false vacuum decays to the true vacuum via spontaneous bubble nucleation. The Coleman-de Luccia instanton [13] describes the tunneling of a self-gravitating scalar field. The physical decay rate (per unit volume per unit time) is given by a constant

$$\Gamma \simeq M_{\rm GUT}^4 \exp\left(-S_E\right) . \tag{2}$$

where the Euclidean action of the instanton, S_E, is a dimensionless shape parameter governed by the height of the barrier relative to the false vacuum energy. Whether or not the transition completes is governed by the percolation parameter which describes the nucleation rate per Hubble volume per Hubble time

$$\frac{\Gamma}{H^4} \sim \frac{M_{\rm Pl}^4}{M_{\rm GUT}^4} \exp\left(-S_E\right) . \tag{3}$$

In general relativity, where the expansion rate in the false vacuum is fixed, this is a constant. So the phase transition either completes too quickly (before sufficient inflation has taken place) for $\Gamma \gg H^4$ or not at all if $\Gamma \ll H^4$. In Brans-Dicke gravity inflation can start close to the Planck scale

$$H \sim \frac{M_{\rm GUT}^2}{M_{\rm Pl}} \sim M_{\rm Pl} . \tag{4}$$

with $\Gamma/H^4 \ll 1$ for a strongly first-order transition with $S_E > 1$, but then the percolation parameter grows as the Planck scale, $M_{\rm Pl}$, grows and $H \sim M_{\rm GUT}^2/M_{\rm Pl}$ decreases. The phase transition completes, and inflation ends, only when the Hubble rate has dropped sufficiently to give $\Gamma/H^4 \sim 1$ and hence

$$M_{\rm Pl} \sim M_{\rm GUT} \exp(S_E/4) . \tag{5}$$

So the Planck scale at the end of inflation is set relative to the GUT scale by the shape of the dimensionless potential. Like all good solutions to the hierarchy problem it identifies the ratio between mass scales with an exponential of a dimensionless number, in this case $S_E \simeq 30$.

The linear scalar and tensor perturbations - quantum fluctuations of the free fields - are most easily calculated by a conformal transformation to the Einstein frame, neatly described in another of Maeda's influential papers [15]. The model recovers a small red tilt for both scalar and tensor modes, and achieves sufficient inflation, so long as ω is large enough. The Brans-Dicke parameter also needs to be large enough to be compatible with current solar system bounds today.

The problem (as was soon realised by Erick Weinberg [12]) comes from non-linear perturbations. The nucleated bubbles are highly inhomogeneous with the energy density of the interior transfered to the relativistic bubble walls. For large ω the expansion becomes quasi-exponential, with an almost constant Hubble parameter and thus almost constant percolation parameter, Γ, so the distribution of bubbles at the end of inflation becomes almost scale invariant. This is the "big bubble problem" of extended

inflation [16]. The percolation rate must be suppressed on large scales so that the number of large bubbles, which would be observable on the cosmic microwave background (CMB) sky, is suppressed, and this is inconsistent with an almost scale-invariant distribution of linear density perturbations ($n \simeq 1$) in Brans-Dicke gravity [2].

The quality and quantity of data from the CMB sky has improved dramatically since the first detection of primordial anisotropies was announced by the CoBE satellite in 1992 [19]. But even then the bounds on the spectral index of linear perturbations($n > 0.8$) were incompatible with bounds from the spectrum of non-linear bubble perturbations in Brans-Dicke gravity [20].

3 Hybrid inflation

The problem with modifying gravity in order to achieve the graceful exit from inflation is that it can only affect the Hubble rate, or equivalently the ratio between the false vacuum and the Planck mass, and this is a relatively inefficient way to change the percolation parameter (3). Equation (2) for the physical decay rate offers a more efficient way to trigger a sudden transition; change the shape, S_E, which appears in the exponent. This is the basis for hybrid inflation, proposed by Linde [21, 22], which remains one of the most common models used to describe inflation today.

Hybrid inflation is also driven by the vacuum energy density of one field trapped in a false vacuum, while a second field evolves. Inflation ends when the dynamical field triggers a phase transition, which may be first-order or second-order [23], but unlike extended inflation it is the shape of the vacuum potential that changes rather than the mass scales. Explicit coupling between the fields rapidly destabilises the false vacuum and inflation comes to an abrupt end.

Consider the original hybrid inflation model [21–23] which is described by a slowly rolling inflaton field, ϕ, and the "waterfall field", χ, with a potential energy

$$V(\phi,\chi) = \left(M^2 - \frac{\sqrt{\lambda}}{2}\chi^2\right)^2 + \frac{1}{2}m^2\phi^2 + \frac{1}{2}\gamma\phi^2\chi^2 \,. \tag{6}$$

The effective mass of the waterfall field in the false vacuum state ($\chi = 0$) is

$$m_\chi^2(\phi) = \gamma\left(\phi^2 - \phi_c^2\right) \,. \tag{7}$$

where we define $\phi_c^2 \equiv 2\lambda^{1/2}M^2/\gamma$. Thus the false vacuum is stabilised for $\phi^2 > \phi_c^2$, while for $\phi^2 < \phi_c^2$ there is a tachyonic instability leading to a second-order phase transition from $\chi = 0$ to $|\chi| = 2M/\sqrt{\lambda}$.

The simple potential (6) for a real scalar field, χ, has two discrete minima at $\chi = \pm 2M/\sqrt{\lambda}$. Thus regions which settle into distinct true vacuum states are separated by domain walls leading to cosmological catastrophe at late times. However vacuum states with higher-dimensional vacuum manifolds may have cosmic strings (for a complex field with an S^1 vacuum manifold, $|\chi| = 2M/\sqrt{\lambda}$), monopoles (for an SO(3) symmetric field with an S^2 vacuum manifold) or no topologically stable defects for higher-dimensional vacua. The formation of cosmic defects plays an important role in constraints on particular hybrid models [23, 24, 26].

Primordial density perturbations arise due to first-order fluctuations in the inflaton field, $\delta\phi$, along the classical trajectory and requiring these to match observations is used to constrain the model parameters [23]. Hybrid inflation requires at least one further field and we should also consider the role of fluctuations in this field. However, so long as the waterfall field remains massive, $m_\chi^2 > H^2$, then there are effectively no classical perturbations in the χ field on super-Hubble scales during inflation. Eventually the tachyonic instability in the χ field does lead to the exponential growth of long-wavelength perturbations at the end of inflation but the waterfall field retains the steep blue spectrum of the initial quantum fluctuations [25].

[2] "Hyperextended" inflation models [10, 11] were also considered, but these required a large value of $\omega(\Phi)$, in order to obtain an almost scale-invariant spectrum of linear perturbations when large scales left the Hubble-horizon, which then decreased rapidly before the end of inflation to have a rapidly rising bubble spectrum on small scales, before recovering large ω (or stabilising the Brans-Dicke field by some other means) to recover the general relativistic limit by the present [17, 18].

Non-linear inhomogeneities are thus produced in the density by the phase transition, either bubble nucleation and collisions in first-order models, or tachyonic growth of fluctuations and tachyonic preheating [27, 28] in second-order transitions, but these are only significant on scales of order the Hubble-horizon at the end of inflation [25, 29, 30], unless the waterfall field remains light for an extended period during inflation. The case of an extended phase transition which takes place during inflation is an interesting case that requires further study [24, 31, 32].

4 Second-order gravitational waves

We have very little information about the primordial density perturbation on the Hubble scale at the end of inflation as the primordial perturbation has decayed away in the radiation era, erased by free-streaming, and reprocessed by non-linearities in the subsequent matter era. The only information we expect to have access to would be gravitational relics: possibly primordial black holes from large metric distortions, or gravitational waves.

Bubble collisions after a first-order phase transition or violent preheating at the end of inflation are just two of the possible mechanisms proposed as a source of a stochastic background of cosmological gravitational waves that could be detected by gravitational wave detectors currently being built or planned in future. Other possible sources of non-linearities are cosmic strings or self-ordering scalar fields. Gravitational waves must be generated at some level from free (first-order) fluctuations of the metric during inflation, but the amplitude is constrained to be small on scales probed by CMB experiments and necessarily smaller on scales accessible by direct detectors given the red-tilted spectrum predicted by inflation.

However we know that there must be a second-order background of gravitational waves generated from the scattering of the first-order primordial density perturbations [33–37] which are observed in the CMB or large-scale structure. Currently we have only upper limits on the amplitude of a stochastic gravitational wave background, but this observation can still be used to place limits on the primordial density perturbation on scales much smaller than those probed by the CMB or large-scale structure [39–41].

If we extract the transverse and tracefree part of the Einstein equations, expanded to second-order about a spatially flat FRW metric we obtain [38]

$$h_{ij}'' + 2\mathcal{H}h_{ij}' + k^2 h_{ij} = S_{ij}^{TT} \tag{8}$$

where S_{ij}^{TT} is the transverse, tracefree part of the source term

$$\begin{aligned} S_{ij} &= 2\Phi\partial_i\partial_j\Phi - 2\Psi\partial_i\partial_j\Phi + 4\Psi\partial_i\partial_j\Psi + \partial_i\Phi\partial_j\Phi - \partial^i\Phi\partial_j\Psi - \partial^i\Psi\partial_j\Phi + 3\partial^i\Psi\partial_j\Psi \\ &\quad - \frac{4}{3(1+w)\mathcal{H}^2}\partial_i(\Psi' + \mathcal{H}\Phi)\partial_j(\Psi' + \mathcal{H}\Phi) - \frac{2c_s^2}{3w\mathcal{H}^2}\left[3\mathcal{H}(\mathcal{H}\Phi - \Psi') + \nabla^2\Psi\right]\partial_i\partial_j(\Phi - \Psi) \end{aligned} \tag{9}$$

and $w = P/\rho$ is the equation of state and $c_s^2 = P'/\rho'$ is the adiabatic sound speed. We have neglected any first-order tensor or vector perturbations and assumed only scalar perturbations, expressed in terms of the longitudinal gauge metric perturbations Φ and Ψ [4]. At early times in the radiation-dominated era we have $w = c_s^2 = 1/3$ and $\Phi = \Psi = (2/3)\Delta_{\mathcal{R}}$ =constant on scales much larger than the Hubble scale at that time.

In the standard hot big bang cosmology, primordial density perturbations generate gravitational waves (with similar wavelengths) as modes re-enter the Hubble scale during the radiation dominated era after inflation [37]. The resulting stochastic background is conventionally expressed as a fractional density relative to the critical density. For an almost scale-invariant primordial power spectrum, $\Delta_{\mathcal{R}}^2(k)$, we have

$$\Omega_{gw,0}(k) = F_{\rm rad}\,\Omega_{\gamma,0}\,\Delta_{\mathcal{R}}^4(k)\,. \tag{10}$$

The gravitational wave background is only weakly dependent on the comoving wavenumber, k, with $F_{\rm rad} \simeq 33$ for a scale-invariant spectrum [37]. If the density perturbation spectrum has a sharp, localised peak at $k = k_{\rm pk}$, then the resulting gravitational wave background is sharply rising [39]

$$\Omega_{gw,0}(k) = 29\Omega_{\gamma,0}\,\Delta_{\mathcal{R}}^4(k_{\rm pk})\left(\frac{k}{k_{\rm pk}}\right)^2\,, \tag{11}$$

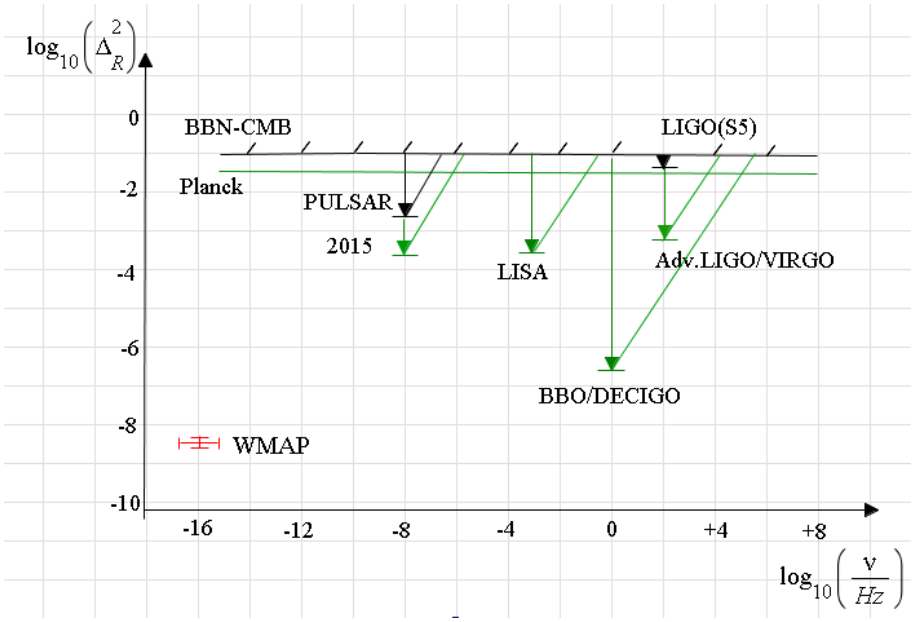

Figure 1: Constraints on the primordial density perturbation, $\Delta^2_{\mathcal{R}}$, obtained from gravitational waves produced during the radiation era [40]. Black lines denote current constraints from gravitational waves detectors and BBN. Green lines denote constraints expected from future gravitational waves detectors. WMAP gives a direct measurement (shown in red) of the primordial density perturbation on very low frequencies.

with an abrupt cut-off at $k = 2k_{\rm pk}$. In either case the observed bounds on $\Omega_{gw,0}$ on a range of scales today places bounds on the primordial density perturbation on the corresponding comoving scale in the early universe. Current and future bounds are shown in Figure 1. For example, future space-based experiments such as DECIGO [42] could place a bound on the primordial density perturbation at the level of $\Delta^2_{\mathcal{R}} \sim 3\times 10^{-7}$ on comoving scales $k \sim 10^{-8}{\rm m}^{-1}$. On the other hand current bounds from pulsar timing arrays require $\Delta^2_{\mathcal{R}} < 5\times 10^{-3}$ on comoving scales $k^{-1} \sim 1{\rm pc}$, which is already sufficient to rule out the formation of primordial black holes in the intermediate mass range $M_{\rm BH} \sim 10^3 M_\odot$ [39].

5 Second-order density perturbations and non-Gaussianity

The source terms like Eq. (9) also appear at second- and higher-order in the dynamical equations for scalar metric and density perturbations. Given that the observed primordial density perturbations are small, $\Delta^2_{\mathcal{R}} \sim 10^{-9}$, one might expect these higher-order effects to be negligible. But in canonical, slow-roll inflationary models, the first-order density perturbations come from vacuum fluctuations of the free, non-interacting quantum fields. Once stretched to super-Hubble scales, these fluctuations are well-described by a Gaussian random field, and linear evolution preserves the Gaussian nature of the distribution. Second- and higher-order terms in the field equations have a non-Gaussian distribution as the fluctuations on different wavelengths become correlated. Thus although second-order terms are generally expected to be small their contribution may be distinguished from that of the first-order terms.

In recent years, prompted by the influential work of Maldacena [43], researchers have begun to consider how the non-Gaussianity of primordial density perturbations can be used to systematically explore different possible higher-order terms describing different physical interactions in alternative inflationary models. At the same time observers have developed matched-filtering techniques to extract optimal estimators for theoretical templates for non-Gaussianity.

A simple technique for exploring primordial non-Gaussianity during or after inflation is the non-linear extension [44] of the δN-approach [45–47]. This identifies the primordial density perturbation, ζ, with the perturbation in the local expansion, $N = \int H dt$, from an initial flat hypersurface during inflation

to a final uniform-density hypersurface after inflation. For perturbations on scales far larger than the Hubble scale during inflation, we expect the local expansion to be determined by the local field values at that time, $N(\varphi_I)$.

The initial field values themselves can be constructed as a perturbative expansion

$$\varphi^I(t_i, \mathbf{x}) = \bar{\varphi}^I(t_i) + \delta_1\varphi^I(t_i, \mathbf{x}) + \frac{1}{2}\delta_2\varphi^I(t_i, \mathbf{x}) + \dots \tag{12}$$

where $\bar{\varphi}^I(t_i)$ is the classical background field, $\delta_1\varphi^I$ are the first-order vacuum fluctuations of the free field, and $\delta_2\varphi^I$ and higher-terms are generated by non-linear interactions of the fields. We can give a perturbative expansion of the primordial perturbation

$$\begin{aligned}
\zeta &= N(\varphi^I) - N(\bar{\varphi}^I) && (13)\\
&= \zeta_1 + \frac{1}{2}\zeta_2 + \dots && (14)\\
&= N_I\delta_1\varphi^I + \frac{1}{2}\left[\sum_I N_I\delta_2\varphi^I + \sum_{I,J} N_{IJ}\delta_1\varphi^I\delta_1\varphi^J\right] + \dots && (15)
\end{aligned}$$

where $N_I = \partial N/\partial\varphi^I$, $N_{IJ} = \partial^2 N/\partial\varphi^I\partial\varphi^J$, etc.

First order terms give the leading, second-order contribution to the power spectrum or two-point function

$$\langle\zeta(\mathbf{x}_1)\zeta(\mathbf{x}_2)\rangle \simeq \sum_{I,J} N_I N_J \langle\delta_1\varphi^I(\mathbf{x}_1)\delta_1\varphi^J(\mathbf{x}_2)\rangle\,. \tag{16}$$

Since the bispectrum or 3-point function vanishes for a Gaussian field, the leading, fourth-order contribution to the primordial 3-point function is dependent upon the second-order terms, giving

$$\begin{aligned}
\langle\zeta(\mathbf{x}_1)\zeta(\mathbf{x}_2)\zeta(\mathbf{x}_3)\rangle \simeq\ & \sum_{I,J,K} N_I N_J N_K \left(\langle\delta_1\varphi^I(\mathbf{x}_1)\delta_1\varphi^J(\mathbf{x}_2)\delta_2\varphi^K(\mathbf{x}_3)\rangle + \text{perms}\right)\\
&+ \sum_{I,J,K,L} N_I N_J N_{KL}\left(\langle\delta_1\varphi^I(\mathbf{x}_1)\delta_1\varphi^J(\mathbf{x}_2)\delta_1\varphi^K(\mathbf{x}_3)\delta_1\varphi^L(\mathbf{x}_3)\rangle + \text{perms}\right)\,. \qquad (17)
\end{aligned}$$

It is instructive to rotate from an arbitrary basis in field space into adiabatic perturbations along the background trajectory [59]

$$d\sigma = \frac{\sum_I \dot{\varphi}^I d\varphi^I}{\sqrt{\sum_J (\dot{\varphi}^J)^2}}\,, \tag{18}$$

and the remaining directions, χ^I, orthogonal to the background trajectory such that $\sum_I \dot{\varphi}^I d\chi^I = 0$ (assuming for simplicity a flat metric in field space). Since ζ is non-linearly conserved in the large-scale limit [60] we know that adiabatic field perturbations lead to a primordial perturbation [55, 61]

$$\begin{aligned}
\zeta|_{\rm ad} &= N_{,\sigma}\delta\sigma + \frac{1}{2}N_{,\sigma\sigma}\delta\sigma^2 + \dots && (19)\\
&= \frac{H}{\dot{\sigma}}\delta\sigma + \frac{1}{2}\frac{\dot{H}}{\ddot{\sigma}}\delta\sigma^2 + \dots && (20)\\
&= -\frac{1}{\sqrt{2\epsilon}M_{\rm Pl}}\delta\sigma + \frac{1}{2}\frac{1}{2\epsilon M_{\rm Pl}^2}(2\epsilon - \eta)\,\delta\sigma^2 + \dots && (21)
\end{aligned}$$

where ϵ and η are the usual slow-roll parameters for a canonical inflaton field. Thus the non-Gaussianity due to adiabatic perturbations of weakly-coupled (Gaussian) fields is suppressed by slow-roll parameters, $\mathcal{O}(\epsilon, \eta)$, and unlikely to ever be observed. Any observable non-Gaussianity must come from either intrinsic non-Gaussianity of the field perturbations, due to interactions on sub-Hubble scales, and/or non-adiabatic perturbations in multi-field models.

The first line in Eq. (17) corresponds to the intrinsic non-linearity of the field. This is expected to be small for canonical, weakly-coupled fields during slow-roll inflation, of order the slow-roll parameter $\epsilon \equiv \dot{H}/H^2 \ll 1$. For it to be significant on sub-Hubble scales during inflation implies that the fields

have significant self-interaction terms on sub-Hubble scales, which is possible in models of inflation with non-canonical kinetic terms, such as DBI inflation [48] or k-inflation [49]. An alternative possibility is that the initial vacuum state, perhaps at the Planck scale, itself contains non-Gaussianities, e.g., [50].

The second line corresponds to non-Gaussianity that is generated even if the initial field perturbations are Gaussian, due to the non-linear dependence of the expansion upon the initial field values. In this case the resulting primordial density perturbation, $\zeta(\mathbf{x})$, is a local function of initially Gaussian fields, $\delta_1\varphi^I(\mathbf{x})$, and hence this is known as local-type non-Gaussianity [51]. It arises due to the non-linear expansion history on super-Hubble scales either during inflation, due to coupled field dynamics [52], or after inflation in modulated reheating scenarios, where one or more fields control the reheating process after the end of inflation [53], or in the curvaton scenario due to the late decay of a weakly coupled field [54].

These different physical processes can be distinguished in terms of the shape of the bispectrum. In Fourier space the primordial bispectrum is commonly written as

$$B_\zeta(k_1,k_2,k_3) = \frac{6}{5} f_{\rm NL}(k_1,k_2,k_2)\left[P_\zeta(k_1)P_\zeta(k_2) + 2\text{perms}\right] . \tag{22}$$

where the primordial power spectrum is given by $P_\zeta(k) = \Delta^2_{\mathcal{R}}(k)/(4\pi k^3)$.

For non-Gaussianity described by a local function of a single Gaussian field $f_{\rm NL}$ is independent of wavenumber. Thus the bispectrum peaks at poles of the power spectra $P(k)$, corresponding to a squeezed triangle $k_1 = -|\mathbf{k}_2+\mathbf{k}_3| \to 0$ and permutations. This is now tightly constrained by both CMB and large-scale structure data which requires $-5 < f_{\rm NL} < 70$ at 95% confidence limit [2].

Non-Gaussianity generated on sub-Hubble scales by non-canonical fields during inflation generally gives a primordial bispectrum which peaks at values $k_1 \sim k_2 \sim k_3$. This equilateral-type non-Gaussianity is primarily constrained by CMB data, which requires $-214 < f_{\rm NL}^{\rm equil} < 266$ at 95% confidence limit [2].

Reducing all the possible forms of non-Gaussianity down to a single number such as $f_{\rm NL}$ allows us to place tight constraints with the current data, but hides the diversity of possible forms of non-linearity and the information potentially available in the distribution of primordial density perturbations. Constraints on the 4-point function or trispectrum are currently weak but offer one obvious way to distinguish between inflationary models with similar bispectra [55]. Even the bispectrum may contain additional information in models where the non-Gaussianity is scale-dependent [56]. This may be due either to a single field whose non-linearity evolves with time during inflation, such as a curvaton coupled to the inflaton [57], or non-Gaussianity due to multiple Gaussian fields whose power spectra have different scale dependence [58].

6 Conclusions

Although observations of a nearly scale-invariant spectrum of primordial density perturbations about a spatially flat FRW universe are consistent with many models of inflation in the very early universe, they will probably never be considered proof that inflation really happened. We would like to find properties of the universe which are produced by inflation, but not likely to be necessary features of any model for the origin of structure. Evidence of deviations from an exactly scale-invariant spectrum [2] is perhaps the first evidence for the dynamical origin for primordial perturbations. An almost scale-invariant power spectrum of gravitational waves produced from vacuum fluctuations during inflation is of course another generic feature of inflation that is not otherwise required by any astronomical considerations. But conversely such first order gravitational waves would tell us little about the physical processes driving inflation.

We can go beyond the primordial power spectrum to seek signatures predicted by specific realisations of inflation. In a perturbative approach interactions lead first to a non-vanishing 3-point function or bispectrum, and the shape of this bispectrum reflects the nature of the interactions, either scattering on sub-Hubble scales, which produces an equilateral-type bispectrum, or local evolution on super-Hubble scales, which produces a squeezed bispectrum shape. Non-Gaussianity of the primordial distribution thus offers a systematic way of building up a picture of the physical interactions in the early universe. Superimposed on this there will be intrinsic non-linearities in the subsequent radiation- and matter-dominated eras, which we have shown, give rise to some level of gravitational waves and a mixture of

local- and equilateral-type non-Gaussianity in the CMB anisotropies [62] which may ultimately limit the level of primordial non-Gaussianity we can observe.

More speculatively different models of inflation may be distinguished by non-perturbative phenomena such as topological defects or the spectrum of inhomogeneous bubbles and their gravitational waves spectra generated by phase transitions during or at the end of inflation as in models of hybrid or extended inflation.

Acknowledgements

I am grateful to the organisers of JGRG20 for the invitation to participate in this anniversary meeting. I am also grateful to my many collaborators in Japan and elsewhere, especially Kei-ichi Maeda and Misao Sasaki, for their contributions to the work I have described here. My work is supported by the UK STFC grant ST/H002774/1.

References

[1] R. Easther, K. i. Maeda and D. Wands, Phys. Rev. D **53**, 4247 (1996) [arXiv:hep-th/9509074].

[2] E. Komatsu *et al.* [WMAP Collaboration], Astrophys. J. Suppl. **192**, 18 (2011). [arXiv:1001.4538 [astro-ph.CO]].

[3] A. A. Starobinsky, Phys. Lett. B **91**, 99 (1980).

[4] K. A. Malik, D. Wands, Phys. Rept. **475**, 1-51 (2009). [arXiv:0809.4944 [astro-ph]].

[5] Y. Kitada, K. -i. Maeda, Phys. Rev. **D45**, 1416-1419 (1992).

[6] N. Sakai, K. -i. Maeda, Prog. Theor. Phys. **90**, 1001-1018 (1993).

[7] D. La, P. J. Steinhardt, Phys. Rev. Lett. **62**, 376 (1989).

[8] A. H. Guth, Phys. Rev. **D23**, 347-356 (1981).

[9] C. Brans, R. H. Dicke, Phys. Rev. **124**, 925-935 (1961).

[10] J. D. Barrow, K. -i. Maeda, Nucl. Phys. **B341**, 294-308 (1990).

[11] P. J. Steinhardt, F. S. Accetta, Phys. Rev. Lett. **64**, 2740 (1990).

[12] E. J. Weinberg, Phys. Rev. **D40**, 3950 (1989).

[13] S. R. Coleman, F. De Luccia, Phys. Rev. **D21**, 3305 (1980).

[14] A. R. Liddle, D. Wands, Phys. Rev. **D46**, 3655-3658 (1992).

[15] K. -i. Maeda, Phys. Rev. **D39**, 3159 (1989).

[16] A. R. Liddle, D. Wands, Mon. Not. Roy. Astron. Soc. **253**, 637-648 (1991).

[17] A. R. Liddle, D. Wands, Phys. Rev. **D45**, 2665-2673 (1992).

[18] A. M. Green, A. R. Liddle, Phys. Rev. **D54**, 2557-2563 (1996). [astro-ph/9604001].

[19] G. F. Smoot, C. L. Bennett, A. Kogut *et al.*, Astrophys. J. **396**, L1-L5 (1992).

[20] A. R. Liddle, D. H. Lyth, Phys. Lett. **B291**, 391-398 (1992). [astro-ph/9208007].

[21] A. D. Linde, Phys. Lett. B **259**, 38 (1991).

[22] A. D. Linde, Phys. Rev. **D49**, 748-754 (1994). [astro-ph/9307002].

[23] E. J. Copeland, A. R. Liddle, D. H. Lyth *et al.*, Phys. Rev. **D49**, 6410-6433 (1994). [astro-ph/9401011].

[24] J. Garcia-Bellido, A. D. Linde and D. Wands, Phys. Rev. D **54**, 6040 (1996) [arXiv:astro-ph/9605094].

[25] J. Fonseca, M. Sasaki and D. Wands, JCAP **1009**, 012 (2010) [arXiv:1005.4053 [astro-ph.CO]].

[26] R. Jeannerot, J. Rocher, M. Sakellariadou, Phys. Rev. **D68**, 103514 (2003). [hep-ph/0308134].

[27] G. N. Felder, J. Garcia-Bellido, P. B. Greene, L. Kofman, A. D. Linde and I. Tkachev, Phys. Rev. Lett. **87**, 011601 (2001) [arXiv:hep-ph/0012142].

[28] E. J. Copeland, S. Pascoli and A. Rajantie, Phys. Rev. D **65**, 103517 (2002) [arXiv:hep-ph/0202031].

[29] D. H. Lyth, arXiv:1005.2461 [astro-ph.CO].

[30] A. A. Abolhasani and H. Firouzjahi, arXiv:1005.2934 [hep-th].

[31] L. Randall, M. Soljacic and A. H. Guth, Nucl. Phys. B **472**, 377 (1996) [arXiv:hep-ph/9512439].

[32] N. Barnaby and J. M. Cline, Phys. Rev. D **75**, 086004 (2007) [arXiv:astro-ph/0611750].

[33] K. Tomita, Prog. Theor. Phys. **37**, 831 (1967).

[34] S. Matarrese, O. Pantano and D. Saez, Phys. Rev. Lett. **72**, 320 (1994) [arXiv:astro-ph/9310036].

[35] H. Noh and J. c. Hwang, Phys. Rev. D **69**, 104011 (2004).

[36] K. Nakamura, Prog. Theor. Phys. **117**, 17 (2007) [arXiv:gr-qc/0605108].

[37] K. N. Ananda, C. Clarkson and D. Wands, Phys. Rev. D **75**, 123518 (2007) [arXiv:gr-qc/0612013].

[38] D. Baumann, P. J. Steinhardt, K. Takahashi and K. Ichiki, Phys. Rev. D **76**, 084019 (2007) [arXiv:hep-th/0703290].

[39] R. Saito and J. Yokoyama, Phys. Rev. Lett. **102**, 161101 (2009) [arXiv:0812.4339 [astro-ph]].

[40] H. Assadullahi and D. Wands, Phys. Rev. D **81**, 023527 (2010) [arXiv:0907.4073 [astro-ph.CO]].

[41] E. Bugaev and P. Klimai, Phys. Rev. D **81**, 023517 (2010) [arXiv:0908.0664 [astro-ph.CO]].

[42] S. Kawamura *et al.*, J. Phys. Conf. Ser. **120**, 032004 (2008).

[43] J. M. Maldacena, JHEP **0305**, 013 (2003) [arXiv:astro-ph/0210603].

[44] D. H. Lyth and Y. Rodriguez, Phys. Rev. Lett. **95**, 121302 (2005) [arXiv:astro-ph/0504045].

[45] A. A. Starobinsky, JETP Lett. **42**, 152 (1985) [Pisma Zh. Eksp. Teor. Fiz. **42**, 124 (1985)].

[46] M. Sasaki and E. D. Stewart, Prog. Theor. Phys. **95**, 71 (1996) [arXiv:astro-ph/9507001].

[47] D. Wands, K. A. Malik, D. H. Lyth and A. R. Liddle, Phys. Rev. D **62**, 043527 (2000) [arXiv:astro-ph/0003278].

[48] M. Alishahiha, E. Silverstein and D. Tong, Phys. Rev. D **70**, 123505 (2004) [arXiv:hep-th/0404084].

[49] D. Seery and J. E. Lidsey, JCAP **0506**, 003 (2005) [arXiv:astro-ph/0503692].

[50] R. Holman and A. J. Tolley, JCAP **0805**, 001 (2008) [arXiv:0710.1302 [hep-th]].

[51] D. Wands, Class. Quant. Grav. **27**, 124002 (2010) [arXiv:1004.0818 [astro-ph.CO]].

[52] F. Bernardeau and J. P. Uzan, Phys. Rev. D **66**, 103506 (2002) [arXiv:hep-ph/0207295].

[53] M. Zaldarriaga, Phys. Rev. D **69**, 043508 (2004) [arXiv:astro-ph/0306006].

[54] D. H. Lyth, C. Ungarelli and D. Wands, Phys. Rev. D **67**, 023503 (2003) [arXiv:astro-ph/0208055].

[55] C. T. Byrnes, M. Sasaki and D. Wands, Phys. Rev. D **74**, 123519 (2006) [arXiv:astro-ph/0611075].

[56] C. T. Byrnes, M. Gerstenlauer, S. Nurmi, G. Tasinato and D. Wands, JCAP **1010**, 004 (2010) [arXiv:1007.4277 [astro-ph.CO]].

[57] C. T. Byrnes, K. Enqvist and T. Takahashi, JCAP **1009**, 026 (2010) [arXiv:1007.5148 [astro-ph.CO]].

[58] C. T. Byrnes, S. Nurmi, G. Tasinato and D. Wands, JCAP **1002**, 034 (2010) [arXiv:0911.2780 [astro-ph.CO]].

[59] C. Gordon, D. Wands, B. A. Bassett and R. Maartens, Phys. Rev. D **63**, 023506 (2001) [arXiv:astro-ph/0009131].

[60] D. H. Lyth, K. A. Malik and M. Sasaki, JCAP **0505**, 004 (2005) [arXiv:astro-ph/0411220].

[61] D. Langlois, F. Vernizzi and D. Wands, JCAP **0812**, 004 (2008) [arXiv:0809.4646 [astro-ph]].

[62] C. Pitrou, J. P. Uzan and F. Bernardeau, JCAP **1007**, 003 (2010) [arXiv:1003.0481 [astro-ph.CO]].

Black Holes in Effective String Theory

Takashi Torii[1(a)] and Nobuyoshi Ohta[2(b)]

[(a)] *Department of General Education, Osaka Institute of Technology, Asahi-ku, Osaka 535-8585*
[(b)] *Department of Physics, Kinki University, Higashi-Osaka, Osaka 577-8502*

Abstract

We study black hole solutions in the Einstein gravity with Gauss-Bonnet term, the dilaton and the Maxwell gauge field in various dimensions. The spacetime is asymptotically flat and the solutions have static and spherical symmetry. We focus on the effect of the higher order correction term of the dilaton field and found that it gives little effect on the solutions except for the five-dimensional case. The charged black hole solution does not have the extreme limit by the coupling to the dilaton field.

1 Introduction

One of the long-standing problems in theoretical physics is how to reconcile gravity with quantum theory. Superstring theory is the leading candidate for quantum gravity. In order to study the geometrical properties and strong gravitational phenomena, it is still difficult to apply full superstring theory itself. In this situation, it is appropriate to investigate these problems by using the effective low-energy field theories including string quantum corrections.

Many works have been done on black hole solutions in dilatonic gravity, and various properties have been studied since the work in Refs. [1]. On the other hand, it is known that there are higher-order quantum corrections from string theories. It is thus important to ask how these corrections may modify the results. Several works have studied the effects of higher order terms, but most of the work considers theories without dilaton, which is one of the most important ingredients in the string effective theories. Hence it is most significant to study black hole solutions and their properties in the theory with the higher order corrections and dilaton. The simplest higher order correction is the Gauss-Bonnet (GB) term coupled to dilaton in heterotic string theories.

In our previous paper [2], we have studied asymptotically flat black hole solutions with the GB correction term and dilaton without a cosmological constant in various dimensions from 4 to 10 with $(D-2)$-dimensional hypersurface of curvature signature $k=+1$. We have then presented our results on black hole solutions with the cosmological constant with $(D-2)$-dimensional hypersurface with $k=0,\pm1$ [3–5]. In the string perspective, it is also interesting to examine asymptotically non-flat black hole solutions with possible application to AdS/CFT and dS/CFT correspondences in mind. However, in our previous work, we do not consider the higher order term of the dilaton field as in many other works. Hence in this work we investigate the effects of such term on the properties of the black holes. We also include the U(1) gauge field in the system to examine whether coupling of the dilaton field affect the gauge field.

2 Dilatonic Einstein-Gauss-Bonnet-Maxwell theory

We consider the following low-energy effective action for a heterotic string in one scheme:

$$S=\frac{1}{2\kappa_D^2}\int d^Dx\sqrt{-g}\left[R-\frac{1}{2}(\partial\phi)^2-\frac{1}{4}e^{-\gamma\phi}F^2+\alpha_2 e^{-\gamma\phi}\left\{R^2_{\rm GB}+\frac{3}{16}\mu(\partial\phi)^4\right\}\right], \tag{1}$$

where κ_D^2 is a D-dimensional gravitational constant, ϕ is a dilaton field, $\gamma=1/2$, F is a gauge field, $\alpha_2=\alpha'/8$ is a numerical coefficient given in terms of the Regge slope parameter, and $R^2_{\rm GB}=R_{\mu\nu\rho\sigma}R^{\mu\nu\rho\sigma}-$

[1]Email address: torii@ge.oit.ac.jp
[2]Email address: ohtan@phys.kindai.ac.jp

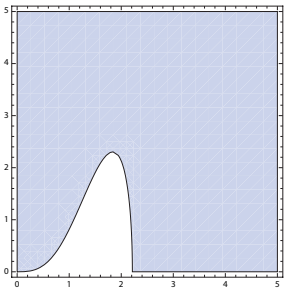

Figure 1: The region where the discriminant of the quadratic equation for ϕ'_H is positive in $D = 4$. The horizontal axis is $e^{\gamma\phi_H/2} r_H$ and the vertical axis is $e^{\gamma\phi_H} e_1$.

$4R_{\mu\nu}R^{\mu\nu} + R^2$ is the GB correction. In the original derivation of the effective action, it was first derived in the Einstein frame from the S-matrix calculation in string theory and then transformed into the string frame. Also it is convenient to interpret our results in the Einstein frame. Hence we have transformed this into the Einstein frame, reduced to D dimensions, and used the field redefinition ambiguity $\delta g_{\mu\nu} = \alpha'[a_1 R_{\mu\nu} + a_2 \nabla_\mu\phi\nabla_\nu\phi + g_{\mu\nu}\{a_3 R + a_4(\nabla\phi)^2 + a_5\nabla^2\phi\}]$ and $\delta\phi = \alpha'[b_1 R + b_2(\partial\phi)^2 + b_3\nabla^2\phi]$, up to higher order terms. We have also set $H = 0$. The constant μ is introduced to see the difference of the solutions with and without the higher order term of the dilaton field. In the above process, higher order terms are dropped. This is allowed because the effective low-energy action can be determined up to field redefinition when it is read off from the scattering amplitudes computed in string theories. All this means that there is no absolutely preferred form of the action if they are related this way, and one cannot claim which system is better.

Let us consider the static spacetime and adopt the metric and field strength

$$ds_D^2 = -B(r)e^{-2\delta(r)}dt^2 + B^{-1}dr^2 + r^2 h_{ij}dx^i dx^j, \quad F_{0r} = f(r)', \tag{2}$$

where $h_{ij}dx^i dx^j$ represents the line element of a $(D-2)$-dimensional hypersurface with constant curvature $(D-2)(D-3)k$ and volume Σ_k for $k = \pm 1, 0$. A prime denoted the derivative with respect to r.

In this paper we study spherically symmetric solutions ($k = 1$). The field equation for the Maxwell field is easily integrated to give

$$f' = \frac{e_1}{r^{D-2}} e^{\gamma\phi - \delta}, \tag{3}$$

where e_1 is a constant corresponding to the charge. Hence our task is reduced to setting boundary conditions for the fields B, δ and dilaton ϕ and integrate the above set of equations.

Let us first examine the boundary conditions of the black hole spacetime. We assume the following boundary conditions for the metric functions:

1. The existence of a regular black hole horizon r_H: $B_H = 0, \quad B'_H > 0, \quad |\delta_H| < \infty, \quad |\phi_H| < \infty$.
2. The nonexistence of singularities outside the event horizon: $B(r) > 0, \quad |\delta| < \infty, \quad |\phi| < \infty$.

Here and in what follows, the values of various quantities at the horizon are denoted with subscript H.

3. Asymptotic flatness at spatial infinity (as $r \to \infty$):

$$B \sim 1 - \frac{2M}{r^{D-3}}, \quad \delta(r) \sim \frac{\delta_1}{r}, \quad \phi \sim \frac{\phi_1}{r}, \tag{4}$$

with finite constants M, δ_1, ϕ_1, where M corresponds to the mass parameter of the black hole.

By the equation of the dilaton field with the regularity condition at the horizon, we obtain the quadratic equation determining ϕ'_H. The $(\partial\phi)^4$-term in Eq. (1) does not contribute to the boundary

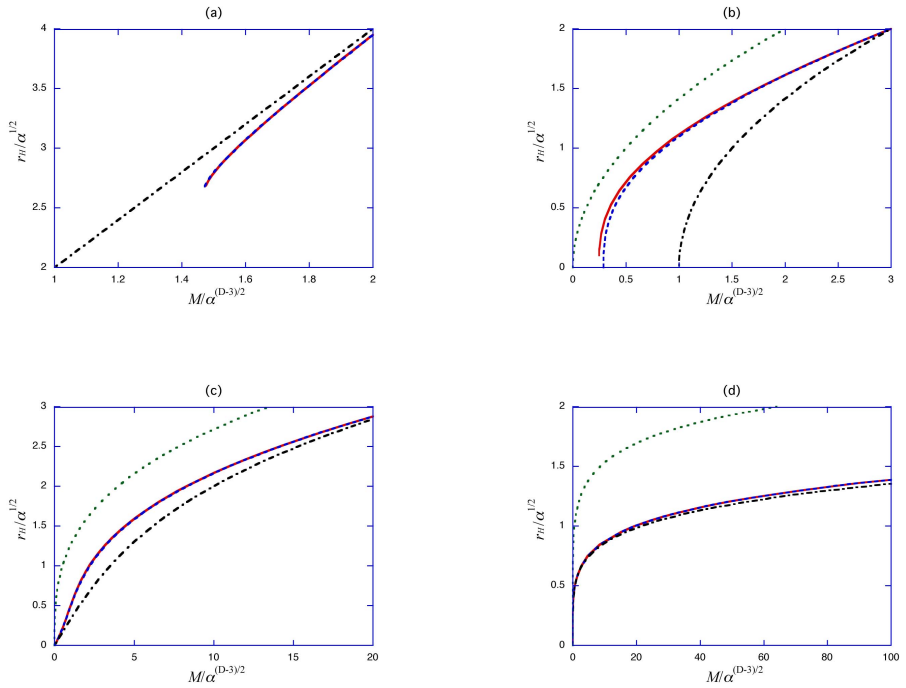

Figure 2: The M-r_H diagram of the neutral solution ($e_1 = 0$) in Einstin-GB-dilaton system with the higher order term of the dilaton field (red solid line), in Einstin-GB-dilaton system without the higher order term of the dilaton field (blue dashed line), in Einstin-GB system (black dot-dashed line), and in GR (green doted line) (a) $D = 4$, (b) $D = 5$, (c) $D = 6$, and (d) $D = 10$.

condition of the dilaton field at the horizon. For the $D = 4$ case, there is a parameter region where the quadratic equation has no real solution. The region where the discriminant is positive is depicted in Fig. 1. For $e = 0$, the boundary is $r_H e^{\gamma\phi_H/2} > 24^{1/4} \approx 2.192$. For $e^{\gamma\phi_H} e_1 > 2.3032$, the discriminant is positive for all r_H.

It is useful to consider several scaling symmetries of our field equations (or our model). Firstly, α_2 can be scaled out by the following scaling as $r \to r/{\alpha_2}^{1/2}$, $M \to M/{\alpha_2}^{(D-3)/2}$, $e_1 \to e_1/{\alpha_2}^{(D-2)/2}$. The field equations also have a shift symmetry:

$$\phi \to \phi - \phi_*, \quad r \to e^{\gamma\phi_*/2} r, \quad e_1 \to e^{(D-2)\gamma\phi_*/2} e_1. \tag{5}$$

where ϕ_* is an arbitrary constant. The third one is the shift symmetry under

$$\delta \to \delta - \delta_*, \quad t \to e^{-\delta_*} t, \tag{6}$$

with an arbitrary constant δ_*, which may be used to shift the asymptotic value of δ to zero.

3 Black hole solutions

It will be instructive to compare our results with the non-dilatonic case. When the dilaton field is absent (i.e., Einstein-GB-Maxwell system), we substitute $\phi \equiv 0$ and $\gamma = 0$. For the $D \geq 5$ case, the field equations can be integrated to yield [7]

$$B = 1 - \frac{2m(r)}{r^{D-3}}, \quad \delta = 0, \tag{7}$$

where

$$m(r) = \frac{r^{D-1}}{4\alpha_2(D-3)_4} \left[-1 \pm \sqrt{1 + \frac{8(D-3)_4 \bar{M}}{r^{D-1}} - \frac{(D-4)e_1^2}{8(D-2)r^{2(D-2)}}} \right], \tag{8}$$

and $\bar{M}$ is an integration constant corresponding to the asymptotic value $m(\infty)$ for the plus sign in Eq. (8). In the $\alpha_2 \to 0$ limit, the solutions with the plus sign approach the Reissner-Nortström solutions. This means that they can be considered to be the solution with GB correction to GR. On the other hand, the solutions with the minus sign do not have such a limit. For these reasons, we call the solutions with plus (minus) sign the (non-)GR branch.

In the dilatonic case, since the basic equations do not have non-trivial analytical solutions, we have to resort to the numerical method. Firstly we consider the neutral solution ($e_1 = 0$). The relation between the mass and the horizon radius of the black holes in various dimensions are shown in Fig. 2. We find that the relations are qualitatively same as those of solutions without the higher order term of the dilaton field ($\mu = 0$) except for the 5-dimensional case[2].

In the $D = 5$ case, there is the lower limit for the mass and the horizon radius of the black holes as in the 4-dimensional case. In $D = 4$ the lower limit is determined by the condition at the horizon shown in Fig. 1, while the second derivative of the dilaton field diverges at some radius outside of the event horizon in the lower limit in $D = 5$.

For the charged solutions, we depict the relation between the mass and horizon radius in $D = 5$ in Fig. 3. The electric charge is $e_1 = 5$. The charged Boulware-Deser solution [7] have the extreme limit where the black hole horizon and the inner horizon coincide. The extreme solution has the lowest mass and is the smallest black hole solution. The dilatonic solution also has the lowest limit solution. It is not, however, the extreme solution and the horizon is not degenerate. At this solution, the field variables diverges as in the neutral black hole solution. As a result, there is no extreme solution even for the charged black hole in the dilatonic case.

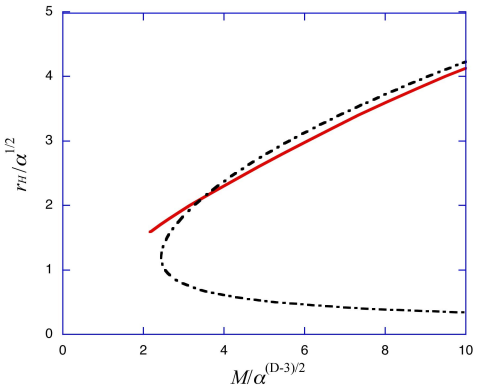

Figure 3: The M-r_H diagram of the charged solution ($e_1/{\alpha_2}^{(D-2)/2} = 5$) in Einstin-GB-dilaton system with the higher order term of the dilaton field (red solid line) and in Einstin-GB system (black dot-dashed line) in $D = 5$.

References

[1] G. W. Gibbons and K. Maeda, Nucl. Phys. **B298** (1988) 741; D. Garfinkle, G. T. Horowitz, and A. Strominger, Phys. Rev. D **43** (1991) 3140.

[2] Z. K. Guo, N. Ohta and T. Torii, Prog. Theor. Phys. **120** (2008) 581 [arXiv:0806.2481 [gr-qc]].

[3] Z. K. Guo, N. Ohta and T. Torii, Prog. Theor. Phys. **121** (2009) 253 [arXiv:0811.3068 [gr-qc]].

[4] N. Ohta and T. Torii, Prog. Theor. Phys. **121** (2009) 959 [arXiv:0902.4072 [hep-th]].

[5] N. Ohta and T. Torii, Prog. Theor. Phys. **122** (2009) 1477 [arXiv:0908.3918 [hep-th]].

[6] N. Ohta and T. Torii, Prog. Theor. Phys. **124** (2010) 207 [arXiv:1004.2779 [hep-th]].

[7] D. G. Boulware and S. Deser, Phys. Rev. Lett. **55** (1985) 2656; Phys. Lett. B **175** (1986) 409.

Quantum state of universe before big bounce

Fumitoshi Amemiya[1] and Tatsuhiko Koike[2]

Department of Physics, Keio University, 3-14-1 Hiyoshi, Kohoku-ku, 223-8522 Yokohama, Japan

Abstract

A gauge-invariant quantum theory of the flat Friedmann-Robertson-Walker (FRW) universe with dust is studied in terms of the Ashtekar variables. We use the reduced phase space quantization which has following advantages: (i) fundamental variables are all gauge invariant, (ii) there exists a physical time evolution of gauge-invariant quantities, so that the problem of time is absent and (iii) the reduced phase space can be quantized in the same manner as in ordinary quantum mechanics. Analyzing the dynamics of a wave packet, we show that the classical initial singularity is replaced by a big bounce in quantum theory. A possible interpretation of the result is that the wave function of the universe has been in superposition of states representating right-handed and left-handed systems before the big bounce.

1 Introduction

One of the motivations of quantum cosmology is to shed light on quantum nature of the initial singularity. However, there exists potential problems that have not been completely resolved yet. A problem is about what should be interpreted as observables in classical and quantum gravity [1, 2]. A canonical formulation of general relativity (GR) is a constrained system with first-class constraints in which the spacetime diffeomorphisms are interpreted as gauge transformations. In gauge theories, only gauge-invariant quantities are observables. However, there are technical and conceptual difficulties in the realization of the idea especially in GR. In many works, gauge-variant quantities are used as observables. This issue must be seriously considered especially in quantum gravity because it is substantially related to the problem of time [3].

In this paper, we shall construct and analyze a gauge-invariant quantum theory of the flat FRW universe with the Brown-Kuchař dust [4] in terms of the Ashtekar variables [5, 6]. We use the reduced phase space quantization method where the so-called relational formalism [7, 8] is used to construct the classical reduced phase space spanned by gauge-invariant quantities, and then the system is quantized in the same manner as in ordinary quantum mechanics. The quantization gives a possible resolution to the problem of time. As for the dynamics of the universe, we consider the motion of a wave packet and evaluate the expectation value of the scale factor. It is shown that the expectation value has a non-zero minimum, that is, the initial singularity is replaced by a big bounce in quantum theory. The remarkable point is that the big bounce mixes the states representing right-handed and left-handed systems. See [9, 10] for details of the work. In this paper we adopt the unit in which $c = 1$.

2 Reduced phase space of the flat Friedmann-Robertson-Walker universe with dust

In the Ashtekar formulation [5, 6], the variables (A_a^i, E_i^a) form a canonically conjugate pair where A_a^i is a SU(2) connection and E_i^a is an orthonormal triad with density weight 1. In the flat FRW model, the Ashtekar variables can be written in terms of only one independent components $\tilde{c}$ and $\tilde{p}$ [11],

$$A_a^i = \tilde{c}(t)\omega_a^i, \quad E_i^a = \tilde{p}(t)X_i^a, \tag{1}$$

[1]Email address: famemiya@rk.phys.keio.ac.jp
[2]Email address: koike@phys.keio.ac.jp

where ω^i are bases of left invariant one-forms and X_i are invariant vector fields dual to the one-forms. These variables have relations to the scale factor a such that

$$|\tilde{p}| = a^2, \quad \tilde{c} = \mathrm{sgn}(p)\frac{\gamma}{N}\dot{a}, \tag{2}$$

where γ is the so-called Barbero-Immirzi parameter, N is the lapse function and the dot denotes the derivative with respect to t. Note that, while the scale factor is restricted to be nonnegative, $\tilde{p}$ ranges over the entire real line, carrying an orientation of triads determined by the sign of $\tilde{p}$. We here consider a compact universe to avoide the divergence of the three-space integral and in particular we only consider the case of three-dimensional torus, where we take a cube of coordinate range $0 \leq x, y, z \leq V^{\frac{1}{3}}$, and identify the opposite faces.

If we define new variables as $p := V^{\frac{2}{3}}\tilde{p}$ and $c := V^{\frac{1}{3}}\tilde{c}$, the total action for gravity plus the Brown-Kuchař dust [4] is written as

$$S_{\mathrm{tot}} = \int dt \left[\frac{3}{\kappa\gamma}p\dot{c} + P_T\dot{T} - NH_{\mathrm{tot}}\right], \tag{3}$$

where $\kappa = 8\pi G$, T is the proper time measured along the particle flow lines when the equations of motion hold, P_T is its conjugate momentum and the Hamiltonian constraint takes the form

$$H_{\mathrm{tot}} = H_{\mathrm{grav}} + H_{\mathrm{dust}} = -\frac{3}{\kappa\gamma^2}c^2\sqrt{|p|} + P_T = 0. \tag{4}$$

The key observation of the relational formalism [7, 8] to define gauge-invariant quantities is as follows. Take two gauge-variant functions F and T on the phase space, and choose one of the functions T as a clock. Then, the value of F at $T = \tau$ is gauge-invariant even if F and T themselves are gauge variant. Suppose a phase space has a $2n$-dimension ($n \geq 2$), and there are canonical coordinates $(q^a, p_a, a = 1, \cdots, n)$ such that $\{q^a, p_b\} = \delta^a_b$. We will denote a first-class constraint by H and a phase space point by $y = (q^a, p_a)$. Under the gauge transformation generated by H, a point y is mapped to $y \mapsto \alpha^t_H(y)$, where t is a gauge parameter. That is, $\alpha^t_H(y)$ is a gauge flow generated by H starting from y. Then we can define the gauge-invariant quantity $O^\tau_F(y)$ as

$$O^\tau_F(y) := F(\alpha^t_H(y))|_{T(\alpha^t_H(y))=\tau}. \tag{5}$$

A constraint equation $H = 0$ is said to be of deparametrized form if it is written as $H(q^a, T, p_a, P_T) = P_T + h(q^a, p_a) = 0$ with some phase space coordinates $\{q^a, T; p_a, P_T\}$. In the deparametrized theories, the reduced phase space is spanned by the gauge-invariant quantities $\left(O^\tau_{q^a}(y), O^\tau_{p_a}(y)\right)$ associated with q^a and p_a with the simple symplectic structure $\left\{O^\tau_{q^a}(y), O^\tau_{p_b}(y)\right\} = \delta^a_b$. The physical Hamiltonian H_{phys} is obtained by replacing q^a and p_a in $h(q^a, p_a)$ with $O^\tau_{q^a}(y)$ and $O^\tau_{p_a}(y)$: $H_{\mathrm{phys}}\left(O^\tau_{q^a}(y), O^\tau_{p_a}(y)\right) := h\left(O^\tau_{q^a}(y), O^\tau_{p_a}(y)\right)$. The Hamiltonian generates the time evolution of the gauge-invariant quantity associated with a function F which depends only on q^a and p_a: $\frac{\partial O^\tau_F(y)}{\partial\tau} = \{H_{\mathrm{phys}}, O^\tau_F(y)\}$.

In the present case, it is natural to choose the function T as the clock variable. Then, the reduced phase space is coordinatized by the gauge-invariant quantities $C(\tau) := O^\tau_c(y)$ and $P(\tau) := O^\tau_p(y)$ associated with c and p with very simple symplectic structure

$$\{C(\tau), P(\tau)\} = \frac{\kappa\gamma}{3}. \tag{6}$$

Moreover, we can obtain the physical Hamiltonian H_{phys} by replacing c and p in $H_{\mathrm{grav}}(c, p)$ with C and P,

$$H_{\mathrm{phys}} = -\frac{3}{\kappa\gamma^2}C(\tau)^2\sqrt{|P(\tau)|}. \tag{7}$$

3 Quantization

In this section, we shall quantize the system on the reduced phase space obtained in the previous section. Now the physical variables are operators and the Poisson bracket $\{\bullet, \bullet\}$ is replaced with the commutation

relation $(1/i\hbar)[\bullet,\bullet]$. Thus (6) becomes the canonical commutation relation

$$[\hat{C},\hat{P}] = \frac{i\kappa\gamma\hbar}{3}. \tag{8}$$

Let us choose the ordinary Schrödinger representation in which the operators $\hat{P}$ and $\hat{C}$, respectively, act on a wave function $\Psi(P)$ in the following way: $\hat{P}\Psi(P) = P\Psi(P)$, $\hat{C}\Psi(P) = \frac{i\hbar\kappa\gamma}{3}\frac{\partial\Psi(P)}{\partial P}$. As a concrete example, we choose the following operator ordering for the Hamiltonian,

$$\hat{H}_{\rm phys} = -\frac{3}{\kappa\gamma^2}\sqrt{|\hat{P}|}\hat{C}^2. \tag{9}$$

Then the Schrödinger equation takes the simplest form,

$$i\hbar\frac{\partial\Psi}{\partial\tau} = \frac{\kappa\hbar^2}{3}\sqrt{|P|}\frac{\partial^2\Psi}{\partial P^2}. \tag{10}$$

Since the present Hamiltonian is different from the ordinary kinematical term, we choose the Hilbert space as $\mathcal{H} = L^2(\mathbb{R}, |P|^{-\frac{1}{2}}dP)$ in order to make the Hamiltonian (9) Hermitian up to surface term. $\hat{H}_{\rm phys}$ is somewhat singular at the origin $P = 0$, it is indeed self-adjoint in $\mathcal{H}$.

4 Dynamics of the universe

Let us now analyze the dynamics of a wave packet. The procedure is as follows. First, we prepare an initial wave packet $\Psi(P, 0)$ at some nonzero P. Then, we numerically evolve it backward in time by the Schrödinger equation (10) and evaluate the expectation value of $|P|$ as a function of the internal time $\tilde{\tau}$. Here we consider $|P|$ because both the positive and negative P correspond to the universe of the same size with different orientation of triads. For simplicity, we here choose the initial wave function as a Gaussian wave packet

$$\Psi(P,0) = C_0 \exp\left(-\frac{(P-P_0)^2}{2\sigma^2} - ik_0P\right), \tag{11}$$

where C_0 is the normalization constant. Fig. 1(a) show the absolute value of the wave function as a function of P and τ, and the expectation value of $|P|$ is plotted as a function of the time τ in Fig. 1(b).

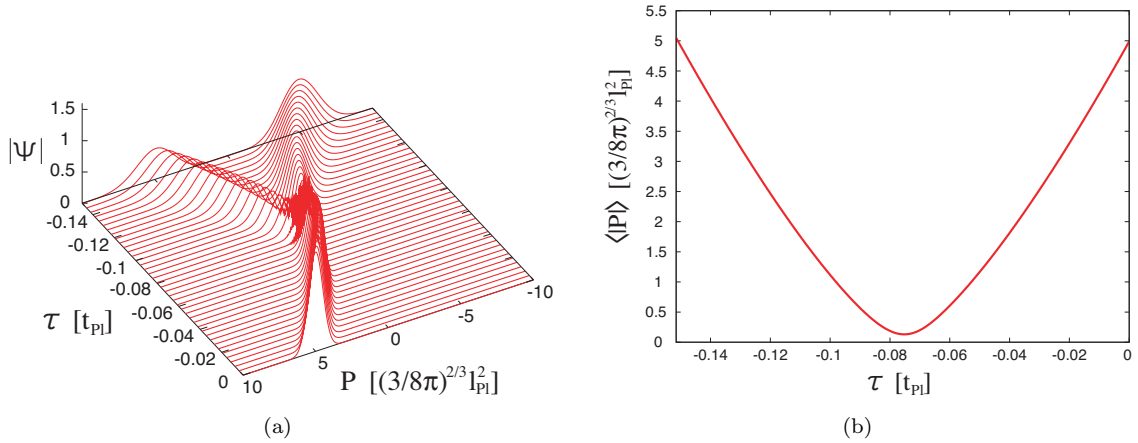

(a) (b)

Figure 1: Fig.(a) shows the absolute value of the wave function as a function of τ and P. Fig.(b) shows the expectation values of $|P|$ as a functions of τ.

We can see from Fig. 1(a) that a part of the wave packet is reflected and the rest is transmitted at the origin. We here remind that the sign of P determines an orientation of triads, which correspond to a

right-handed and left-handed systems respectively. Thus, the result indicates that if the present state of the universe is in a right-handed system, the past state is in superposition of the states of a right-handed and left-handed systems. As for the expectation value of $|P|$, Fig. 1(b) indicates that the expectation value never goes to zero and bounces at a nonzero minimum. That is, the initial singularity is replaced by a big bounce in the present model.

5 Conclusions

A gauge-invariant quantum theory of the flat FRW universe with dust has been studied in terms of the Ashtekar variables. We have first constructed the classical reduced phase space of the system by using the relational formalism and then have quantized the reduced system. The advantages of the quantization method are as follows: (i) fundamental variables are gauge-invariant quantities, (ii) a natural time evolution of the gauge-invariant quantities exists, so that the problem of time is absent and (iii) the reduced phase space can be quantized in the same manner as in ordinary quantum mechanics because there are no constraints in the reduced phase space. In the obtained quantum theory, we have analyzed the dynamics of a wave packet and have shown that the expectation value of P has a non-zero minimum, that is, the initial singularity is replaced by a big bounce in quantum theory. The interpretation of the wave packet is that if the present state of the universe is in a right-handed system, the past state has been in a superposition of the states of a right-handed and left-handed systems.

Achnowledgement

This work was supported in part by Global COE Program "High-Level Grobal Cooperation for Leading-Edge Platform on Access Spaces (C12)".

References

[1] P. G. Bergmann, Rev. Mod. Phys. **33** 510 (1961).

[2] C. Rovelli, Class. Quant. Grav. **8**, 1895 (1991); Phys. Rev. D **65**, 124013 (2002).

[3] For a comprehensive review on the problem of time, see e.g. C. J. Isham, arXiv:gr-qc/9210011.

[4] J. D. Brown and K. V. Kuchař, Phys. Rev. D **51**, 5600 (1995).

[5] A. Ashtekar, Phys. Rev. Lett. **57**, 2244 (1986); Phys. Rev. D **36**, 1587 (1987).

[6] J. F. Barbero G., Phys. Rev. D **51**, 5507 (1995).

[7] B. Dittrich, Gen. Rel. Grav. **39**, 1891 (2007).

[8] T. Thiemann, Class. Quant. Grav. **23**, 1163 (2006).

[9] F. Amemiya and T. Koike, Phys. Rev. D **80**, 103507 (2009).

[10] F. Amemiya and T. Koike, Phys. Rev. D **82**, 104007 (2010).

[11] A. Ashtekar, M. Bojowald and J. Lewandowski, Adv. Theor. Math. Phys. **7**, 233 (2003).

Light propagation in time-dependent gravitational field

Hideyoshi Arakida[1]

School of Education, Waseda University, Tokyo 169-8050

Abstract

We attempt to calculate the gravitational time delay in a time-dependent gravitational field, especially in Robertson-McVittie spacetime. To this end, we adopt the time transfer function method proposed by Le Poncin-Lafitte *et al.* (2004) and Teyssandier and Le Poncin-Lafitte (2008) and we re-examine the global cosmological effect on light propagation in the solar system. We also apply the obtained results to the secular increase in the astronomical unit, reported by Krasinsky and Brumberg (2004), and we show that the leading order terms of the time-dependent component due to cosmological expansion is 9 orders of magnitude smaller than the observed value of $d\mathrm{AU}/dt$, i.e., 15 ± 4 [m/century].

1 Time Transfer Function

The time transfer functions that give the travel time of the light ray/signal are formally expressed as follows [1, 2]:

$$t_B - t_A = \mathcal{T}_e(t_A, \vec{x}_A, \vec{x}_B) = \frac{1}{c}\left[R_{AB} + \Delta_e(t_A, \vec{x}_A, \vec{x}_B)\right] \tag{1}$$

$$= \mathcal{T}_r(\vec{x}_A, t_B, \vec{x}_B) = \frac{1}{c}\left[R_{AB} + \Delta_r(\vec{x}_A, t_B, \vec{x}_B)\right], \tag{2}$$

where $\mathcal{T}_e(t_A, \vec{x}_A, \vec{x}_B)$ is the emission time transfer function in spacial coordinates $\vec{x}_A, \vec{x}_B$ and t_A is the emission time of the signal, $\mathcal{T}_r(\vec{x}_A, t_B, \vec{x}_B)$ is the reception time transfer function in spacial coordinates $\vec{x}_A, \vec{x}_B$ and t_B is the reception time of the signal, $R_{AB} = |\vec{x}_B - \vec{x}_A|$, and Δ_e and Δ_r are the emission time delay function and reception time delay function, respectively. Δ_e and Δ_r characterize the gravitational time delay. In (1) and (2), Henceforth, A denotes the emission and B denotes the reception.

Δ_e and Δ_r can be iteratively calculated up to any order of approximation; nevertheless, now we only need the 1st order formulae, i.e.,

$$\Delta_e^{(1)} = \frac{R_{AB}}{2}\int_0^1 \left[g_{(1)}^{00} - 2N_{AB}^i g_{(1)}^{0i} + N_{AB}^i N_{AB}^j g_{(1)}^{ij}\right] d\mu \tag{3}$$

$$\Delta_r^{(1)} = \frac{R_{AB}}{2}\int_0^1 \left[g_{(1)}^{00} - 2N_{AB}^i g_{(1)}^{0i} + N_{AB}^i N_{AB}^j g_{(1)}^{ij}\right] d\lambda, \tag{4}$$

where $g_{(1)}^{\mu\nu}$ indicates the 1st order perturbation with respect to $\eta^{\mu\nu}$ and $N_{AB}^i = (x_B^i - x_A^i)/R_{AB}$. In (3) and (4), integration is carried out along the straight line

$$t(\mu) = t_A + \mu T_{AB}, \quad x(\mu) = x_A + \mu(x_B - x_A) \quad \text{for} \quad \Delta_e^{(1)}, \tag{5}$$

$$t(\lambda) = t_B - \lambda T_{AB}, \quad x(\lambda) = x_B - \lambda(x_B - x_A) \quad \text{for} \quad \Delta_r^{(1)}, \tag{6}$$

where T_{AB} is the time lapse between A and B along the straight line. Then, we can put $T_{AB} = R_{AB}/c$.

[1]Email address: arakida@edu.waseda.ac.jp

2 Gravitational Time Delay in Robertson-McVittie Spacetime

The Robertson-McVittie (RM) metric is expressed in standard comoving form [3, 4] as

$$ds^2 = -\left[\frac{1-\frac{GM}{2c^2ra(t)}}{1+\frac{GM}{2c^2ra(t)}}\right]^2 c^2dt^2 + \left[1+\frac{GM}{2c^2ra(t)}\right]^4 a^2(t)(dr^2+r^2d\Omega^2), \tag{7}$$

where $d\Omega^2 = d\theta^2 + \sin^2\theta d\phi^2$, M is the mass of the central gravitating body, and $a(t)$ is a scale factor. (7) reduces to the Schwarzschild solution when $a(t) = 1$, and it reduces to the FLRW cosmological model for the curvature parameter $k = 0$ when $M = 0$.

The various observational models of the solar system are currently formulated in some kind of proper coordinate system such as the barycentric celestial reference system (BCRS) based on the post-Newtonian framework [5], instead of the cosmological comoving frame. Hence, to compare the effects formulated using the proper coordinates with the cosmological ones within the same framework, we adopt the radial transformation

$$R = a(t)r\left[1+\frac{GM}{2c^2ra(t)}\right]^2, \tag{8}$$

we convert (7) into the virtually proper coordinate system [3, 6–10]. Thus, (7) is rewritten as

$$ds \simeq -\left(1-\frac{2GM}{c^2R}-\frac{H^2R^2}{c^2}\right)c^2dt^2 - \frac{2HR}{c}\left(1+\frac{GM}{c^2R}\right)cdtdR + \left(1+\frac{2GM}{c^2R}\right)dR^2 + R^2d\Omega^2, \tag{9}$$

where $H = H(t) = \dot{a}(t)/a(t)$ is the Hubble parameter.

As mentioned in previous section, the light path used in the computation is rectilinear so that the rectangular coordinate system can be used instead of the spherical coordinate system. By coordinate transformation,

$$x = R\sin\theta\cos\phi, \quad y = R\sin\theta\sin\phi, \quad z = R\cos\theta, \tag{10}$$

and (9) becomes (see [14, 15])

$$ds^2 = -\left(1-\frac{2GM}{c^2R}-\frac{H^2R^2}{c^2}\right)c^2dt^2 - \frac{2Hx^i}{c}\left(1+\frac{2GM}{c^2R}\right)cdtdx^i + \left(\delta_{ij}+\frac{2GM}{c^2R^3}x^ix^j\right)dx^idx^j, \tag{11}$$

where $R = \sqrt{x^2+y^2+z^2}$. To simplify the computation, the straight line used in integration is parallel to the x-axis Hence, (11) reduces to

$$ds^2 = -\left(1-\frac{2GM}{c^2R}-\frac{H^2R^2}{c^2}\right)c^2dt^2 - \frac{2Hx}{c}\left(1+\frac{2GM}{c^2R}\right)cdtdx + \left(1+\frac{2GM}{c^2R^3}x^2\right)dx^2, \tag{12}$$

where $y = b =$ constant (b is the impact factor), $z = 0$, $R = \sqrt{x^2+b^2}$, and in this case, we may put $N^i_{AB} = N^x_{AB} = (x_B - x_A)/R_{AB}$. This approach is similar to the one described in [16], (see Section 40.4 and Fig. 40.3 of [16]). In (12), we see the Hubble parameter $H(t)$, which generally is an arbitrary function of time t. Hence, we suppose that $H(t)$ changes adiabatically because the time lapse of a light ray/signal observed in the solar system is much shorter than the age of the universe, $T_{\rm U} \approx 10^{10}$ [yr]:

$$H(t) \simeq H_0 + \left.\frac{dH}{dt}\right|_0 t, \quad \left|\left.\frac{dH}{dt}\right|_0\right| \approx \frac{H_0}{T_{\rm U}} \approx 10^{-24} \ \ [1/(\text{s yr})], \tag{13}$$

where $H_0 \approx 10^{-17}$ [1/s]. Therefore $dH/dt|_0 > 0$ implies accelerating expansion of the universe; otherwise, it implies decelerating expansion.

The time delay functions Δ_e and Δ_r can be resolved into the following components:

$$\Delta_e(x_A, t_A, x_B) = \hat{\Delta}(x_A, x_B) + \bar{\Delta}(x_A, x_B) + \bar{\Delta}_e(x_A, t_A, x_B), \tag{14}$$

$$\Delta_r(x_A, x_B, t_B) = \hat{\Delta}(x_A, x_B) + \bar{\Delta}(x_A, x_B) + \bar{\Delta}_r(x_A, x_B, t_B), \tag{15}$$

where $\hat{\Delta}(x_A, x_B)$ corresponds to the Shapiro time delay, $\bar{\Delta}(x_A, x_B)$ is due to the static component of cosmological expansion (H_0 in (13)), and $\bar{\Delta}_e(x_A, t_A, x_B)$, $\bar{\Delta}_r(x_A, x_B, t_B)$ are due to the time-dependent (secular) component of cosmological expansion ($dH/dt|_0$ in (13)). By the straightforward calculations from (3), (4), (12), and (13), we obtain following results:

$$\hat{\Delta}(x_A, x_B) = \frac{GM}{c^2}\left[2\ln\left|\frac{x_B+\sqrt{x_B^2+b^2}}{x_A+\sqrt{x_A^2+b^2}}\right| - \left(\frac{x_B}{\sqrt{x_B^2+b^2}} - \frac{x_A}{\sqrt{x_A^2+b^2}}\right)\right] \tag{16}$$

$$\begin{aligned}\bar{\Delta}(x_A, x_B) &= -\varepsilon\frac{H_0}{c}(x_B^2 - x_A^2) + \frac{H_0^2}{6c^2}\left[x_B^3 - x_A^3 + 3b^2(x_B - x_A)\right] \\ &- \varepsilon\frac{4GMH_0}{c^3}\left(\sqrt{x_B^2+b^2} - \sqrt{x_A^2+b^2}\right)\end{aligned} \tag{17}$$

$$\begin{aligned}\bar{\Delta}_e(x_A, t_A, x_B) &= \left.\frac{dH}{dt}\right|_0\left(-\frac{\varepsilon}{c}\left[(x_B^2 - x_A^2)t_A + \frac{1}{3}(2x_B^2 - x_Ax_B - x_A^2)T_{AB}\right]\right. \\ &+ \frac{H_0}{3c^2}\left\{\left[x_B^3 - x_A^3 + 3b^2(x_B - x_A)\right]t_A\right. \\ &+ \left.\frac{1}{4}\left[3x_B^3 - x_Ax_B^2 - x_A^2x_B - x_A^3 + 6b^2(x_B - x_A)\right]T_{AB}\right\} \\ &- \varepsilon\frac{2GM}{c^3R_{AB}}\left\{\left[(x_B - 2x_A)T_{AB} + 2(x_B - x_A)t_A\right]\sqrt{x_B^2+b^2}\right. \\ &+ \left.\left.\left[x_AT_{AB} - 2(x_B - x_A)t_A\right]\sqrt{x_A^2+b^2} - b^2T_{AB}\ln\left|\frac{x_B+\sqrt{x_B^2+b^2}}{x_A+\sqrt{x_A^2+b^2}}\right|\right\}\right)\end{aligned} \tag{18}$$

$$\begin{aligned}\bar{\Delta}_r(x_A, x_B, t_B) &= \left.\frac{dH}{dt}\right|_0\left(-\frac{\varepsilon}{c}\left[(x_B^2 - x_A^2)t_B - \frac{1}{3}(x_B^2 + x_Ax_B - 2x_A^2)T_{AB}\right]\right. \\ &+ \frac{H_0}{3c^2}\left\{\left[x_B^3 - x_A^3 + 3b^2(x_B - x_A)\right]t_B\right. \\ &- \left.\frac{1}{4}\left[x_B^3 + x_Ax_B^2 + x_A^2x_B - 3x_A^3 + 6b^2(x_B - x_A)\right]T_{AB}\right\} \\ &+ \varepsilon\frac{2GM}{c^3R_{AB}}\left\{\left[x_BT_{AB} - 2(x_B - x_A)t_B\right]\sqrt{x_B^2+b^2}\right. \\ &- \left.\left.\left[(2x_B - x_A)T_{AB} - 2(x_B - x_A)t_B\right]\sqrt{x_A^2+b^2} - b^2T_{AB}\ln\left|\frac{x_B+\sqrt{x_B^2+b^2}}{x_A+\sqrt{x_A^2+b^2}}\right|\right\}\right)\end{aligned} \tag{19}$$

where $\varepsilon = N^x_{AB} = 1$ for $x_B - x_A > 0$ and $\varepsilon = -1$ for $x_B - x_A < 0$. ε is derived from the term $-2N^i_{AB}g^{0i}_{(1)}$ in (3) and (4).

3 Application to Secular Increase in Astronomical Unit

The Secular increase in the astronomical unit (AU), reported by Krasinsky and Brumberg (2004) [11], is an unexplained physical phenomenon observed in the solar system. This anomaly was discovered while analyzing planetary radar and spacecraft (mainly Martian landers/orbiters) ranging data and improving the various astronomical constants including AU. Krasinsky and Brumberg estimated

$$\frac{d\mathrm{AU}}{dt} = 15 \pm 4 \text{ [m/cy]}. \tag{20}$$

as the most appropriate value. Subsequently $d\mathrm{AU}/dt \simeq 20$ [m/cy] was separately evaluated by Pitjeva at the Institute of Applied Astronomy (IAA), Russia, and by Standish at the Jet Propulsion Laboratory (JPL), USA.

It should be emphasized that the increase in AU does not imply the expansion of a planetary orbit or the equivalent increase in the orbital period of a planet. According to Krasinsky [18], the observations do

not reveal any such traces. Further, the determination error of inner planetary orbits in the latest lunar-planetary ephemerides (e.g. DE of JPL and EPM of IAA) is also smaller than the observed $d\mathrm{AU}/dt$, i.e., 15 [m/cy] (see Table 4 of [12]). Therefore, the observed $d\mathrm{AU}/dt$ value may relate with not the dynamic aspect of planetary motion but the propagation of a light ray/signal.

Previously, some attempts have been made to explain the secular trend in terms of cosmological expansion [11, 13, 17]. In particular, Krasinsky and Brumberg (2004) and Arakida (2009) considered its contribution to light propagation. However, it is generally difficult to compute the time-dependent geodesic of null rays; hence, the approach of the farmer is somewhat qualitative, whereas that of the latter is essentially restricted to discussion in static spacetime.

Now, on the basis of the results obtained in previous section, let us re-examine whether the cosmological effect relates with the observed $d\mathrm{AU}/dt$. It is appropriate to regard the coefficients of t_A and t_B in (18) and (19) as secular terms owing to cosmological expansion. Then, if we assume that $dH/dt|_0 \approx 10^{-24}$ [1/(s yr)] from (13), the leading order of magnitude of coefficients is approximately 10^{-10} [m/yr] $= 10^{-8}$ [m/cy] because x_A and x_B are of the order of a few [AU] or 10^{11} [m] in the solar system. Unfortunately, this is approximately 9 orders of magnitude smaller than the evaluated $d\mathrm{AU}/dt$, i.e., 15 [m/cy]. Therefore, the time-dependent effect due to cosmological expansion does not induce the secular increase in AU.

References

[1] Le Poncin-Lafitte, C., Linet, B., Teyssandier, P., Class. Quantum Phys. , **21**, 4463 (2004).

[2] Teyssandier, P. Le Poncin-Lafitte, C., Class. Quantum Phys. , **25**, 145020 (2008).

[3] Robertson, H. P., Phil. Mag., **7**, 845 (1928).

[4] McVittie, G. C., Mon. Not. R. Astron. Soc. , **93**, 325 (1933)

[5] Soffel, M. H. *et al.*, AJ, **126**, 2687 (2003).

[6] Järnefelt, G., Ann. Acad. Soc. Sci. Fennicae, **A45**, 3 (1940).

[7] Järnefelt, G., Arkiv Matem. Astron. Fys, **27**, 1 (1940).

[8] Nolan, B. C., Class. Quantum Phys. , **16**, 1227 (1999).

[9] Nolan, B. C., Class. Quantum Phys. , **16**, 3183 (1999).

[10] Carrera, M., Giulini, D., Rev. Mod. Phys., **82**, 169 (2010).

[11] Krasinsky, G., Brumberg, V., Celect. Mech. Dyn. Astron., **90**, 267 (2004).

[12] Pitjeva, E. V., Solar Syst. Res., **39**, 176 (2005).

[13] Arakida, H., New Astron., **14**, 264 (2009).

[14] Brumberg, V. A., Reliativistskaia Nebesnaia Mekhanika, Nauka, Moskva (1972).

[15] Brumberg, V. A., Essential Relativistic Celestial Mechanics, Adam Hilger, Bristol, Philadelphia and New York (1991).

[16] Misner, C. W., Thorne, K. S., Wheeler, J. A., Gravitation, Freeman, New York (1970).

[17] Mashhoon, B., Mobed, N., Singh, D., Class. Quantum Phys. , **24**, 5031 (2007)

[18] Krasinsky, G. A., private communications (2007)

Gravity on a multifractal

Gianluca Calcagni[1]

Max Planck Institute for Gravitational Physics (Albert Einstein Institute)
Am Mühlenberg 1, D-14476 Golm, Germany

Abstract

Despite their diversity, many of the most prominent candidate theories of quantum gravity share the property to be effectively lower-dimensional at small scales. In particular, dimension two plays a fundamental role in the finiteness of these models of Nature. Thus motivated, we entertain the idea that spacetime is a multifractal with integer dimension 4 at large scales, while it is two-dimensional in the ultraviolet. Consequences for particle physics, gravity and cosmology are discussed.

In 1884, Edwin A. Abbott published his satirical novella *Flatland: A Romance of many dimensions*, where a Square living in the $(2+1)$-dimensional Flatland envisions different geometries. While it is easy for it to imagine worlds of lower dimensions such as Pointland and Lineland, it takes the intervention of a Sphere to have the Square realize the possibility of Spaceland (our world) and even more fantastic cosmos which even the Sphere cannot fathom.

This book has been entertaining generations of teachers, mathematicians and physicists, keeping vivid in the public imagination the possibility that the universe, after all, might be more than a matter of spheres. In fact, the notion of higher dimensions has been considered most seriously by the scientific community, from Kaluza–Klein to brane-world scenarios. The latter can be motivated by perturbative string theory, where the number of spacetime dimensions is higher than four. The brane-world has been a popular playground where issues such as the hierarchy problem have found fresh insight [1].

On the other side of the story, models in lower dimensions are extremely helpful in addressing a number of physical and technical problems which are harder to tackle in $4D$. However, the dimensionality of spacetime is a fixed ingredient, so while in the case of brane and string scenarios the unobserved extra dimensions are explained via compactification or other mechanisms, lower-dimensional theories are typically regarded as toy, albeit very interesting, models of reality.

Nevertheless, there is another meaning in which a model can be "lower-dimensional". Independent theories such as causal dynamical triangulations, asymptotically safe gravity, spin-foam models, and Hořava–Lifshitz gravity all exhibit a running of the spectral dimension d_S of spacetime such that at short scales $d_S \sim 2$ [2]. This number is no chance and plays an important role in quantum gravity, not only in reference to the richness of worldsheet string theory, but also because gravity as a perturbative field theory is renormalizable near two dimensions [3].

Is it possible to construct a field theory of matter and gravity which is effectively two-dimensional at small space-time scales and four-dimensional in the infrared? Here we wish to argue for a positive answer, whose details can be found in [4]. In homage to Abbott's novella, one would have liked to call the short-scale world a Lineland, but this would have been misleading. Nowadays we know that there exist geometric objects which are not curves or sheets or solids even if they have integer dimension. Fractals have required a revision and extension of the concept of "dimension", the Hausdorff definition being just one example. In many cases, often presented in rich pictorials, fractals have noninteger dimensions, but there exist instances where a dust or a curve can fill the ambient space enough to achieve integer dimensionality [5]. Multifractals are objects with scale-dependent Hausdorff dimension.

The problem now is to encode in the structure of spacetime the dimensional flow typical of multifractals. This can be done by promoting the Lebesgue measure in the integral defining any field theory action to a generic Lebesgue–Stieltjes measure:

$$d^D x \to d\varrho(x)\,, \qquad [\varrho] = -D\alpha \neq -D\,, \tag{1}$$

[1]Email address: calcagni@aei.mpg.de

whereϱ is a (possibly very irregular) distribution, square brackets denote the engineering dimension in momentum units, and $0 < \alpha < 1$ is a parameter which is related with the operational definition of the Hausdorff dimension $d_{\rm H}$ as follows. In fact, the latter determines the scaling of a Euclidean volume (or mass distribution) of characteristic size R, $V(R) \sim R^{d_{\rm H}}$. Taking $\varrho \sim d(r^{D\alpha})$,

$$V(R) \sim \int_{D\text{-ball}} d\varrho_{\rm Eucl}(x) \sim \int_0^R dr\, r^{D\alpha-1} \sim R^{D\alpha}, \tag{2}$$

thus showing that

$$\alpha = \frac{d_{\rm H}}{D}. \tag{3}$$

Consider a Lorentz-covariant Lagrangian density $\mathcal{L}$; this can be the total Lagrangian of gravity and matter on a manifold $\tilde{\mathcal{M}}$ endowed with metric $g_{\mu\nu}$, where $\mu = 0, 1, \ldots, D-1$ and D is the topological (positive integer) dimension of $\tilde{\mathcal{M}}$. To make the universe a multifractal $\mathcal{M}$, we replace the standard measure in the action with a nontrivial Stieltjes measure:

$$S = \int_{\mathcal{M}} d\varrho(x)\, \sqrt{-g}\mathcal{L}\,. \tag{4}$$

We assume $\mathcal{M}$ has no boundary; the case with boundary should share most of the same qualitative features. If ϱ is absolutely continuous, it can be written as $d\varrho(x) = v(x)d^D x$, where v is a Lorentz scalar. We can choose

$$v(X) = X^{D(\alpha-1)} + M^{D(1-\alpha)}\,, \tag{5}$$

where M is a constant mass and $X = t$ or $X = |\mathbf{x}|$ depending on whether we want to define a "timelike" or "spacelike" multifractal. The metric $g_{\mu\nu}$ and the scalar v are independent degrees of freedom which constitute the composite geometric structure (metric and fractal) of $\mathcal{M}$. A fractal must shortly evolve to a smooth configuration. We expect M to be about the Planck mass, although the lower bound from particle physics actually seems to be much lower, $M > 300 \div 400$ GeV [6].

Equation (5) is inspired by results in classical mechanics, according to which integrals on fractals can be approximated by Weyl or fractional integrals which, in turn, are particular Lebesgue–Stieltjes integrals. The order of the fractional integral $D\alpha$ has a natural interpretation in terms of the Hausdorff dimension of $\mathcal{M}$ [7]. Fractional integrals find applications in a range of disciplines, from statistics to finance to engineering. In one dimension, different values of α mediate between full-memory ($\alpha = 1$) and Markov processes ($\alpha = 0$), where α corresponds to the fraction of states preserved at a given time. Loosely speaking, in our case it is the "fraction of spacetime dimensionality" felt by an observer living in $\mathcal{M}$, which is equally divided among the D directions for the isotropic weight (5).

The Lorentz scalar v may contribute a kinetic term if interpreted as part of the field dynamics, otherwise it is excluded from the calculus of variations. We must stress that Eq. (5) is a very special case of Stieltjes measure and it is quite possible that realistic models with fractal behaviour do not admit an absolutely continuous measure. In that case, it is not yet clear how to work out the details of the theory.

Otherwise, properties of the class of models satisfying Eq. (5) are well illustrated by a scalar field theory [4]. The engineering dimension of the scalar field is zero when α has the critical value $\alpha = \alpha_* \equiv 2/D$. The dimension of spacetime is well constrained to be 4 from particle physics to cosmological scales and starting at least from the last scattering era. Therefore, $D = 4$ for phenomenological reasons. The properties of the field causal propagator in configuration space depend on the value of α. By making use of momentum-space results, one can see that the superficial degree of divergence of the Feynman-like diagrams of the theory is lower than in $4D$. This is promising but not sufficient to demonstrate the effectiveness and viability of a renormalization group flow. At any rate, at the classical level the system does flow from a lower-dimensional configuration to a smooth D-dimensional one. This is clear from the definition (5) of the measure weight and its scaling properties when $\alpha < 1$, as already discussed. Therefore, at least the phenomenological valence of the model is guaranteed.

If $M \sim m_{\rm Pl}$, it is likely that UV effects be important only during the very early universe. This is suggested also by a minisuperspace analysis of the model [4], indicating that UV cosmological solutions with zero intrinsic curvature do not exist unless one allows for exotic matter fields (or condensates)

violating the null energy condition. On the other hand, at late times an imprint of the nontrivial short-scale geometry might survive as a running cosmological constant. The latter appears as a source term in the Noether conservation law for the Hamiltonian H: in Minkowski, the energy of the system is

$$\mathcal{E}(t) = H(t) + \Lambda(t) = H(t) + \int^t dt \int d\mathbf{x}\, \dot{v}\mathcal{L}\,. \tag{6}$$

In general, the physical D-momentum dissipates, which might constitute a unitarity problem at the quantum level. In nonrelativistic fractal models this is a direct result of the nonautonomous character of the action; translation invariance is broken *explicitly*. In our relativistic scenario, v is a scalar with implicit coordinate dependence, a geometric factor defined for a $D\alpha$-dimensional physical world which enters the definition of Poisson brackets. This is a key difference with respect to scalar-tensor theories and results in a *deformation of the Poincaré algebra*. In this precise sense, also relativistic fractals break translation invariance.

However, the system also admits a conservative interpretation. One can also regard v as an independent "dilaton-like" field rescaling the total Lagrangian density in the D-dimensional ambient spacetime. In that case, one can define the Poisson brackets as usual (no Stieltjes measure within) and show that Poincaré invariance is preserved. Dissipation occurs relatively between parts of a *conservative* system. Quantization would follow through, although an UV observer would experience an effective probability flow through his world-fractal.

We have just said that translation invariance is not broken explicitly in relativistic fractal field theory. For instance, the use of a nontrivial measure weight might lead to the idea that translation invariance be violated by the expression for the propagator. This is not the case, as we show here in more detail than in [4]. Consider a free scalar field with action

$$S_0 = -\frac{1}{2}\int d\varrho(x)\,\phi(x)\,f(\Box)\,\phi(x)\,, \tag{7}$$

where we keep the kinetic operator $f(\Box)$ general. The free Lorentzian partition function Z_0 in the presence of a local source J is

$$Z_0[J] \equiv \int [\mathcal{D}\phi]\, e^{i[S_0 + \int d\varrho(x)\, J(x)\phi(x)]} \equiv \int [\mathcal{D}\phi]\, e^{iS_J}\,. \tag{8}$$

Using the definition of the D-dimensional Dirac distribution with nontrivial measure

$$\delta_\varrho(k) = \frac{1}{(2\pi)^D}\int d\varrho(x)\, e^{-ik\cdot x} \tag{9}$$

and the Fourier–Stieltjes transform of the field $\phi(x) = (2\pi)^{-D}\int d\varrho(k)\,\tilde{\phi}(k)\, e^{ik\cdot x}$, we obtain

$$\begin{aligned} S_J &= \frac{1}{2}\int d\varrho(x)\int\frac{d\varrho(k_1)}{(2\pi)^D}\int\frac{d\varrho(k_2)}{(2\pi)^D}\, e^{i(k_1+k_2)\cdot x}\left[-\tilde{\phi}(k_1)f(-k_2^2)\tilde{\phi}(k_2) + \tilde{J}(k_1)\tilde{\phi}(k_2) + \tilde{J}(k_2)\tilde{\phi}(k_1)\right] \\ &= \frac{1}{2}\int\frac{d\varrho(-k)}{(2\pi)^D}\left[-\tilde{\phi}(-k)f(-k^2)\tilde{\phi}(k) + \tilde{J}(-k)\tilde{\phi}(k) + \tilde{J}(k)\tilde{\phi}(-k)\right] \\ &= \frac{1}{2}\int\frac{d\varrho(-k)}{(2\pi)^D}\left[-\tilde{\varphi}(-k)f(-k^2)\tilde{\varphi}(k) + \frac{\tilde{J}(-k)\tilde{J}(k)}{f(-k^2)}\right], \end{aligned} \tag{10}$$

where

$$\tilde{\varphi}(k) \equiv \tilde{\phi}(k) - \frac{\tilde{J}(k)}{f(-k^2)}\,. \tag{11}$$

Modulo the measure, we have followed exactly the same steps as in ordinary quantum field theory. Equation (8) becomes

$$\begin{aligned} Z_0[J] &= \left\{\int[\mathcal{D}\varphi]\exp\left[-\frac{i}{2}\int\frac{d\varrho(-k)}{(2\pi)^D}\tilde{\varphi}(-k)f(-k^2)\tilde{\varphi}(k)\right]\right\}\exp\left[\frac{i}{2}\int\frac{d\varrho(-k)}{(2\pi)^D}\frac{\tilde{J}(-k)\tilde{J}(k)}{f(-k^2)}\right] \\ &= Z_0[0]\exp\left[\frac{i}{2}\int\frac{d\varrho(-k)}{(2\pi)^D}\frac{\tilde{J}(-k)\tilde{J}(k)}{f(-k^2)}\right]. \end{aligned} \tag{12}$$

The exponent can be written as

$$\int \frac{d\varrho(-k)}{(2\pi)^D} \frac{\tilde{J}(-k)\tilde{J}(k)}{f(-k^2)} = \int \frac{d\varrho(-k)}{(2\pi)^D} \int d\varrho(x) \int d\varrho(y)\, e^{ik\cdot(x-y)} \frac{J(x)J(y)}{f(-k^2)}\,,$$

so that, if $\varrho(-k) = \varrho(k)$, the free partition function reads

$$Z_0[J] = Z_0[0] \exp\left[\frac{i}{2} \int d\varrho(x) \int d\varrho(y)\, J(x)G(x-y)J(y)\right]\,, \tag{13}$$

where

$$G(x-y) = \frac{1}{(2\pi)^D} \int d\varrho(k)\, \frac{e^{ik\cdot(x-y)}}{f(-k^2)}\,. \tag{14}$$

Therefore, we have recovered the usual definition of the propagator as the solution of the Green equation

$$f(\Box)\, G(x-y) = \delta_\varrho(x-y)\,. \tag{15}$$

Other details and other features of the scalar field on an effective (multi)fractal spacetime can be found in [4]. These properties are shared also by the gravitational sector when the latter is switched on. There, one can see that the bare Newton's constant is dimensionless for $\alpha = \alpha_*$, thus suggesting renormalizability [4]. Physical implications of the UV propagator, renormalization, and the hierarchy problem will require further attention.

References

[1] N. Arkani-Hamed, S. Dimopoulos, and G.R. Dvali, Phys. Lett. B **429**, 263 (1998); L. Randall and R. Sundrum, Phys. Rev. Lett. **83**, 3370 (1999); L. Randall and R. Sundrum, Phys. Rev. Lett. **83**, 4690 (1999).

[2] J. Ambjørn, J. Jurkiewicz, and R. Loll, Phys. Rev. Lett. **95**, 171301 (2005); O. Lauscher and M. Reuter, J. High Energy Phys. **0510**, 050 (2005); L. Modesto, Class. Quantum Grav. **26**, 242002 (2009); D. Benedetti, Phys. Rev. Lett. **102**, 111303 (2009); P. Hořava, Phys. Rev. Lett. **102**, 161301 (2009).

[3] R. Gastmans, R. Kallosh, and C. Truffin, Nucl. Phys. B **133**, 417 (1978); S.M. Christensen and M.J. Duff, Phys. Lett. B **79**, 213 (1978); S. Weinberg, in *General Relativity, an Einstein Centenary Survey*, ed. by S.W. Hawking and W. Israel (Cambridge University Press, Cambridge, 1979); H. Kawai and M. Ninomiya, Nucl. Phys. B **336**, 115 (1990).

[4] G. Calcagni, Phys. Rev. Lett. **104**, 251301 (2010); G. Calcagni, J. High Energy Phys. **1003**, 120 (2010).

[5] K. Falconer, *Fractal geometry*, Wiley, New York (2003).

[6] V.I. Shevchenko, arXiv:0903.0565.

[7] F.B. Tatom, Fractals **3**, 217 (1995); F.-Y. Ren, J.-R. Liang, X.-T. Wang, and W.-Y. Qiu, Chaos, Solitons and Fractals **16**, 107 (2003); V.E. Tarasov, Chaos **14**, 123 (2004).

Waterfall field in hybrid inflation and curvature perturbation

Jinn-Ouk Gong[1(a)] and Misao Sasaki[2(b)]

[(a)] *Instituut-Lorentz for Theoretical Physics, Universiteit Leiden, 2333 CA Leiden, The Netherlands*
[(b)] *Yukawa Institute for Theoretical Physics, Kyoto University, Kyoto 606-8502*

Abstract

We study the contribution of the waterfall field to the curvature perturbation at the end of hybrid inflation. In particular we clarify the parameter dependence analytically under reasonable assumptions on the model parameters. After calculating the mode function of the waterfall field, we use the δN formalism and confirm the previously obtained result that the power spectrum is very blue with the index 4 and is absolutely negligible on large scales. However, we also find that the resulting curvature perturbation is highly non-Gaussian and hence we calculate the bispectrum. We find that the bispectrum is at leading order independent of momentum and exhibits its peak at the equilateral limit, though it is unobservably small on large scales.

1 Introduction

Hybrid inflation [1] is an interesting realization with two field contents, the usual inflaton field ϕ which drives slow-roll inflation and the waterfall field χ which terminates inflation by triggering an instability, a "waterfall" phase transition. Previously, it has been assumed that χ becomes momentarily massless only at the time of waterfall and very heavy otherwise, and thus does not contribute to the curvature perturbation $\mathcal{R}$ on large scales: only the quantum fluctuations of ϕ contributes to $\mathcal{R}$ and we can follow the well-known calculations of single field case, with the energy density of the universe being dominated by a non-zero vacuum energy.

This naive picture has been receiving a renewed interest [2, 3] with the common qualitative results that the power spectrum of the curvature perturbation induced by the waterfall field is very blue and extremely small on large scales. However, quantitatively it is not clear if they all agree or not. In particular, in Ref. [3] the δN formalism was employed to derive the power spectrum, but the dependence on the model parameters was not explicitly presented.

Here, we provide another complementary view. We adopt a few reasonable assumptions on the model parameters and solve the mode functions of χ in terms of the number of e-folds analytically. Then using the δN formalism we calculate the corresponding $\mathcal{R}$ induced by χ explicitly.

2 Mode function solution of waterfall field

Before we begin explicit computations, first of all we make the physical picture clear. Our purpose is to calculate the contribution of the waterfall field χ to the curvature perturbation $\mathcal{R}$. This is only possible when χ becomes dynamically relevant. While χ is well anchored at its minimum during the phase of slow-roll inflation and hence does not participate in the inflationary dynamics, it controls the physical processes from the moment of waterfall till the end of inflation. Thus, in the context of the δN formalism, if we can find the evolution of χ during this phase as a function of the number of e-folds N, it amounts to finding $\mathcal{R}$ by the geometrical identity $\mathcal{R} = \delta N$. Therefore, our aim in this section is to calculate $\chi = \chi(N)$ starting from the moment of waterfall. We will directly use this result to calculate $\mathcal{R}$ in the next section.

We consider the potential of the two fields, the inflaton ϕ and the waterfall field χ, as

$$V(\phi, \chi) = \frac{\lambda}{4}\left(\frac{M^2}{\lambda} - \chi^2\right)^2 + \frac{1}{2}m^2\phi^2 + \frac{1}{2}g^2\phi^2\chi^2 \,. \tag{1}$$

[1]Email address: jgong@lorentz.leidenuniv.nl
[2]Email address: misao@yukawa.kyoto-u.ac.jp

We note that during the most period of inflation of our interest, it is assumed that the vacuum energy $V_0 = M^4/(4\lambda)$ dominates so that the Hubble parameter is effectively a constant, $H = H_0$. This is a good approximation even after the waterfall phase transition until the last moment of inflation. The slow-roll and the waterfall conditions are $m^2/H_0^2 \ll 1$ and $M^2/H_0^2 \equiv \beta \gg 1$, respectively. Note that before waterfall, $\phi^2 > \phi_c^2 \equiv M^2/g^2$, χ is well anchored at its minimum $\chi = 0$ so it is itself the same as its fluctuation, $\chi = \delta\chi$. Then after the waterfall transition, $\delta\chi$ becomes unstable and $\delta\chi^2$ starts to grow rapidly, and inflation ends when the inflaton starts to roll fast, which happens when the term $g^2\delta\chi^2$ exceeds m^2 in the effective mass squared of the inflaton. Here we adopt the mean field approximation, i.e. we replace $g^2\delta\chi^2$ by its expectation value $g^2\langle\delta\chi^2\rangle$, which should be valid for the motion of the homogeneous inflaton field ϕ. We also assume that the nonlinear term $\lambda\delta\chi^2$ in the equation of $\delta\chi$ can be neglected until the end of inflation. That is, we assume

$$M^2 \gg \frac{\lambda}{g^2} m^2 \gtrsim \lambda\langle\delta\chi^2\rangle\,. \tag{2}$$

Then, using the background solution $\phi = \phi_c e^{-rn}$ where $n = N - N_c$ is the number of e-folds measured relative to the time of the waterfall transition and $r \equiv 3/2 - \sqrt{9/4 - m^2/H_0^2} \approx m^2/(3H_0^2) \ll 1$ and neglecting the nonlinear term in accordance with the assumption (2), we obtain the equation for $\delta\chi$ in the Fourier space in terms of n as

$$\delta\chi_{\boldsymbol{k}}'' + 3\delta\chi_{\boldsymbol{k}}' + \left[\frac{k^2}{k_c^2} e^{-2n} + \beta\left(e^{-2rn} - 1\right)\right]\delta\chi_{\boldsymbol{k}} = 0\,, \tag{3}$$

where $k_c = a_c H_0$.

We can find the solution of (3) by using the WKB approximation and the large scale limit ($k \to 0$) [4]. With $\alpha \equiv \sqrt{2r\beta} \gg 1$, the evolution of the large and short scale modes are given by

$$|\delta\chi_{L,S}(n)| = |\delta\chi_{L,S}(n=0)|\, A\, \exp\left(\frac{2}{3}\alpha n^{3/2} - \frac{3}{2}n - \frac{1}{4}\log n\right)\,, \tag{4}$$

where $A \equiv 3^{2/3}\Gamma(2/3)/[2\sqrt{\pi}\alpha^{1/6}]$ and the "initial" amplitudes are

$$|\delta\chi_L(n=0)| = \frac{2\sqrt{\pi}}{3^{2/3}\Gamma(2/3)} \frac{H_0}{\sqrt{2k_c^3}\alpha^{1/3}}\,, \tag{5}$$

$$|\delta\chi_S(n=0)| = \frac{H_0}{\sqrt{2k}k_c}\,. \tag{6}$$

3 Curvature perturbation induced by waterfall field

In this section, we calculate the curvature perturbation $\mathcal{R}$ by using (4) in the context of the δN formalism. In the δN formalism the spacetime geometry is spatially smoothly varying over super-horizon scales while each Hubble horizon size region is regarded as a homogeneous and isotropic universe. Hence we first need to smooth over the horizon scale H_0^{-1},

$$\delta\chi^2(n,\boldsymbol{x}) = \delta\chi_L^2(n,\boldsymbol{x}) + \left\langle\delta\chi_S^2(n)\right\rangle = \left[\delta\chi_L^2(0) + \int_{k_c}^{\alpha k_c} \frac{d^3k}{(2\pi)^3}\delta\chi_S^2(0)\right] A^2 \exp\left(\frac{4}{3}\alpha n^{3/2} - 3n\right)\,, \tag{7}$$

where $\delta\chi_L^2(0)$ and hence $\delta\chi^2(n)$ is spatially varying on super-horizon scales, and $\left\langle\delta\chi_S^2(0)\right\rangle = \alpha^2 H_0^2/(8\pi^2)$ which follows from (6). Note that we have omitted the logarithmic dependence term on n in the exponent, which is sub-dominant when we evaluate at $n = n_f = \mathcal{O}(1)$. We have also subtracted the contribution from the modes with $k > \alpha k$ since they remain stable and behave in the same way as the flat Minkowski vacuum modes, in accordance with the regularization we adopted, i.e. $\langle\delta\chi^2(n)\rangle = 0$ at $n < 0$. Neglecting $-3n$ in the exponential for simplicity since $\alpha \gg 1$, splitting $n = \bar{n} + \delta n$ and expanding in terms of δn, (7) is written as

$$\delta\chi^2(\bar{n}+\delta n) = \left[1 + \frac{\delta\chi_L^2(0)}{\langle\delta\chi_S^2(0)\rangle}\right]\left\langle\delta\chi_S^2(0)\right\rangle A^2 \exp\left(\frac{4}{3}\alpha\bar{n}^{3/2}\right)\left(1 + 2\alpha\bar{n}^{1/2}\delta n + \cdots\right)\,, \tag{8}$$

where $\langle \delta\chi_S^2 \rangle \gg \delta\chi_L^2$ as discussed above.

Now we evaluate δn at a later time, say, at the end of inflation $n = n_f$. Here it is important to note that the end of inflation is controlled by the value of $\delta\chi^2$ at each spatial point, namely,

$$\delta\chi^2(n_f, \boldsymbol{x}) = \frac{m^2}{g^2} = \langle \delta\chi^2(n_f) \rangle \,. \tag{9}$$

Analogous to the case when the value of the inflaton field determines the end of inflation hypersurface, this condition determines the end of inflation hypersurface on which the energy density is uniform (at leading order approximation where the contribution of the inflaton to the energy density is negligible). Then, we find

$$1 \approx \left[1 + \frac{\delta\chi_L^2(0)}{\langle \delta\chi_S^2(0) \rangle}\right] \left(1 + 2\alpha n_f^{1/2} \delta n\right) \,, \tag{10}$$

where we have truncated at linear order in δn. Inverting this relation, we can write the curvature perturbation generated between the moment of phase transition and the end of inflation as

$$\mathcal{R}(\boldsymbol{x}) = \delta n \approx -\frac{1}{2\alpha n_f^{1/2}} \frac{\delta\chi_L^2(0, \boldsymbol{x})}{\langle \delta\chi_S^2(0) \rangle} \,. \tag{11}$$

This explicitly shows that the spectrum of $\mathcal{R}$ is determined by the spectrum of $\delta\chi_L^2$.

4 Correlation functions

Moving to the Fourier space, the power spectrum is defined by

$$\langle \mathcal{R}(\boldsymbol{k}) \mathcal{R}(\boldsymbol{q}) \rangle \equiv (2\pi)^3 \delta^{(3)}(\boldsymbol{k} + \boldsymbol{q}) P_{\mathcal{R}}(k) = \frac{1}{4\alpha^2 n_f} \frac{\left\langle \left(\delta\chi^2\right)_{\boldsymbol{k}} \left(\delta\chi^2\right)_{\boldsymbol{q}} \right\rangle}{\langle \delta\chi_S^2 \rangle^2} = \frac{16\pi^4}{\alpha^6 n_f H_0^4} \left\langle \left(\delta\chi^2\right)_{\boldsymbol{k}} \left(\delta\chi^2\right)_{\boldsymbol{q}} \right\rangle \,. \tag{12}$$

Before waterfall, $\delta\chi$ is purely quantum and it can be expressed in terms of the creation and annihilation operators $a_{\boldsymbol{k}}^\dagger$ and $a_{\boldsymbol{k}}$ as

$$\delta\chi = \int \frac{d^3k}{(2\pi)^3} e^{i\boldsymbol{k}\cdot\boldsymbol{x}} \delta\chi_{\boldsymbol{k}} = \int \frac{d^3k}{(2\pi)^3} e^{i\boldsymbol{k}\cdot\boldsymbol{x}} \left(a_{\boldsymbol{k}} \chi_k + a_{-\boldsymbol{k}}^\dagger \chi_k^*\right) \,, \tag{13}$$

where $a_{\boldsymbol{k}}^\dagger$ and $a_{\boldsymbol{k}}$ satisfy the canonical commutation relations $\left[a_{\boldsymbol{k}}, a_{\boldsymbol{q}}^\dagger\right] = (2\pi)^3 \delta^{(3)}(\boldsymbol{k} - \boldsymbol{q})$, otherwise zero, and the mode function χ_k follows the same equation as that of $\delta\chi$. Since the Fourier component of $\delta\chi^2$ is written as a convolution, we have to correlate four creation and annihilation operators with different momenta,

$$\left\langle \left(\delta\chi^2\right)_{\boldsymbol{k}} \left(\delta\chi^2\right)_{\boldsymbol{q}} \right\rangle = \int \frac{d^3p d^3l}{(2\pi)^{3\cdot 2}} \left\langle \left(\delta\chi_{\boldsymbol{p}} \delta\chi_{\boldsymbol{k}-\boldsymbol{p}}\right) \left(\delta\chi_{\boldsymbol{l}} \delta\chi_{\boldsymbol{q}-\boldsymbol{l}}\right) \right\rangle \,. \tag{14}$$

To calculate the above, we should note that what we are interested in are connected graphs, correlating *different* $(\delta\chi^2)_{\boldsymbol{k}}$'s. Thus only taking into account the meaningful contractions, we can easily find

$$\begin{aligned} &\left\langle \left(\delta\chi_{\boldsymbol{p}} \delta\chi_{\boldsymbol{k}-\boldsymbol{p}}\right) \left(\delta\chi_{\boldsymbol{l}} \delta\chi_{\boldsymbol{q}-\boldsymbol{l}}\right) \right\rangle \\ &= \chi_p \chi_{|\boldsymbol{k}-\boldsymbol{p}|} \chi_l^* \chi_{|\boldsymbol{q}-\boldsymbol{l}|}^* (2\pi)^{3\cdot 2} \left[\delta^{(3)}(\boldsymbol{p} + \boldsymbol{q} - \boldsymbol{l}) \delta^{(3)}(\boldsymbol{k} - \boldsymbol{p} + \boldsymbol{l}) + \delta^{(3)}(\boldsymbol{p} + \boldsymbol{l}) \delta^{(3)}(\boldsymbol{k} - \boldsymbol{p} + \boldsymbol{q} - \boldsymbol{l})\right] \,. \end{aligned} \tag{15}$$

Thus, eliminating one of the momenta using the delta functions, and using the remaining delta function $\delta^{(3)}(\boldsymbol{k} + \boldsymbol{q})$ to replace $\boldsymbol{q}$ with $-\boldsymbol{k}$, we find

$$\left\langle \left(\delta\chi^2\right)_{\boldsymbol{k}} \left(\delta\chi^2\right)_{\boldsymbol{q}} \right\rangle = 2 \int d^3p |\chi_p|^2 \left|\chi_{|\boldsymbol{k}-\boldsymbol{p}|}\right|^2 \delta^{(3)}(\boldsymbol{k} + \boldsymbol{q}) \,. \tag{16}$$

However, from (5), we have already seen that the super-horizon mode χ_k is independent of k, and thus can be pulled out of the integral. Hence, we only have to integrate over the relevant super-horizon scale momentum, for which the upper limit is $k = k_c$. Therefore, using (5), we finally obtain

$$\left\langle \left(\delta\chi^2\right)_{\boldsymbol{k}} \left(\delta\chi^2\right)_{\boldsymbol{q}} \right\rangle = (2\pi)^3\delta^{(3)}(\boldsymbol{k}+\boldsymbol{q}) \frac{4}{3^{11/3}\left[\Gamma(2/3)\right]^4} \alpha^{-4/3} \frac{H_0^4}{k_c^3} \,. \tag{17}$$

Since this expression has, as it should, the correct delta function dependence, we can readily extract the power spectrum $\mathcal{P}_\mathcal{R}$. Noting (12) we find

$$\mathcal{P}_\mathcal{R} \equiv \frac{k^3}{2\pi^2} P_\mathcal{R} = \frac{32\pi^2}{3^{11/3}\left[\Gamma(2/3)\right]^4} \frac{\alpha^{-22/3}}{n_f} \left(\frac{k}{k_c}\right)^3 , \tag{18}$$

where the numerical coefficient reads $32\pi^2/\left\{3^{11/3}\left[\Gamma(2/3)\right]^4\right\} \approx 1.67255$. Thus, with $n_f = \mathcal{O}(1)$, the maximum amplitude is found at $k = k_c$ as $\mathcal{P}_\mathcal{R} \sim \alpha^{-22/3}$ which is already much smaller than unity for $\alpha \gg 1$. For larger scales, it is exponentially suppressed and thus becomes absolutely negligible: for example, for a scale that exited the horizon at 50 e-folds before waterfall, it is suppressed by a factor $(e^{-50})^3 \approx 10^{-65}$. As already discussed in the previous section, setting $\mathcal{P}_\mathcal{R} \propto k^{n_\mathcal{R}-1}$, the spectrum is very blue with the index $n_\mathcal{R} = 4$.

We can proceed almost identically to compute the bispectrum. It is given by

$$\begin{aligned} &\langle \mathcal{R}(\boldsymbol{k}_1)\mathcal{R}(\boldsymbol{k}_2)\mathcal{R}(\boldsymbol{k}_3)\rangle = (2\pi)^3\delta^{(3)}(\boldsymbol{k}_1+\boldsymbol{k}_2+\boldsymbol{k}_3) B_\mathcal{R}(\boldsymbol{k}_1,\boldsymbol{k}_2,\boldsymbol{k}_3) \\ &= \left(\frac{-1}{2\alpha n_f^{1/2}} \frac{1}{\langle \delta\chi_S^2\rangle}\right)^3 \int \frac{d^3q_1 d^3q_2 d^3q_3}{(2\pi)^{3\cdot 3}} \left\langle \left(\delta\chi_{\boldsymbol{q}_1}\delta\chi_{\boldsymbol{k}_1-\boldsymbol{q}_1}\right)\left(\delta\chi_{\boldsymbol{q}_2}\delta\chi_{\boldsymbol{k}_2-\boldsymbol{q}_2}\right)\left(\delta\chi_{\boldsymbol{q}_3}\delta\chi_{\boldsymbol{k}_3-\boldsymbol{q}_3}\right)\right\rangle , \end{aligned} \tag{19}$$

where after choosing meaningful contractions we have

$$\begin{aligned} &\int \frac{d^3q_1 d^3q_2 d^3q_3}{(2\pi)^{3\cdot 3}} \left\langle \left(\delta\chi_{\boldsymbol{q}_1}\delta\chi_{\boldsymbol{k}_1-\boldsymbol{q}_1}\right)\left(\delta\chi_{\boldsymbol{q}_2}\delta\chi_{\boldsymbol{k}_2-\boldsymbol{q}_2}\right)\left(\delta\chi_{\boldsymbol{q}_3}\delta\chi_{\boldsymbol{k}_3-\boldsymbol{q}_3}\right)\right\rangle \\ &= 8\delta^{(3)}(\boldsymbol{k}_1+\boldsymbol{k}_2+\boldsymbol{k}_3) \frac{4\pi k_c^3}{3} \left[\frac{2\sqrt{\pi}}{3^{2/3}\Gamma(2/3)} \frac{H_0}{\sqrt{2k_c^3}\alpha^{1/3}}\right]^6 . \end{aligned} \tag{20}$$

Comparing this expression with the definition of the bispectrum, we find

$$B_\mathcal{R}(\boldsymbol{k}_1,\boldsymbol{k}_2,\boldsymbol{k}_3) = -\frac{16(2\pi)^7}{3^5\left[\Gamma(2/3)\right]^6} \frac{\alpha^{-11}}{n_f^{3/2}k_c^6} , \tag{21}$$

where the numerical coefficient reads $16(2\pi)^7/\left\{3^5[\Gamma(2/3)]^6\right\} \approx 4128.89$. To leading order, the bispectrum has no momentum dependence, and thus the dimensionless shape function $(k_1k_2k_3)^2 B_\mathcal{R}(\boldsymbol{k}_1,\boldsymbol{k}_2,\boldsymbol{k}_3)$ exhibits its maximum amplitude at the equilateral limit $k_1 = k_2 = k_3$. This is anticipated, since the curvature perturbation produced by the waterfall field is *intrinsically* highly non-Gaussian. Note, however, that this bispectrum is completely unobservable on large scales: in the equilateral limit, multiplying k^6, we see for example that it is exponentially suppressed by a factor of $(e^{-50})^6 \approx 10^{-130}$ for a scale that exited the horizon at 50 e-folds before the waterfall. Thus this bispectrum is totally hopeless to be detected on large scales.

References

[1] A. D. Linde, Phys. Lett. B **259**, 38 (1991) ; A. D. Linde, Phys. Rev. D **49**, 748 (1994) [arXiv:astro-ph/9307002].

[2] D. H. Lyth, arXiv:1005.2461 [astro-ph.CO] ; A. A. Abolhasani and H. Firouzjahi, arXiv:1005.2934 [hep-th].

[3] J. Fonseca, M. Sasaki and D. Wands, JCAP **1009**, 012 (2010) [arXiv:1005.4053 [astro-ph.CO]].

[4] J. O. Gong and M. Sasaki, arXiv:1010.3405 [astro-ph.CO].

$f(R)$ modified gravity and its cosmological and solar-system tests

Je-An Gu[1]

Leung Center for Cosmology and Particle Astrophysics (LeCosPA), National Taiwan University, Taipei 10617, Taiwan, R.O.C.

Abstract

In this paper we highlight our work in arXiv:1009.3488, where we test the $f(R)$ theory of modified gravity via the cosmological observations and the solar-system experiments.

The $f(R)$ theory of modified gravity with the following gravity action was proposed for explaining the cosmic acceleration at the present epoch [1–3].

$$S = \frac{1}{2\kappa^2}\int d^4x\sqrt{-g}\ \left[R + f(R)\right], \tag{1}$$

where $f(R)$ is a general function of the Ricci scalar, representing the deviation from general relativity (GR), and κ is the gravitational coupling. As an essence of cosmology, this theory needs to pass the cosmological test. As a theory of modified gravity, it needs to pass the local gravity test. In Ref. [4] we test the $f(R)$ modified gravity via the cosmological observations about (1) the cosmic expansion and (2) the cosmic structures and via (3) the solar-system experiments. This work will be highlighted in the present paper, as follows.

Cosmic-expansion test

It is well known that for any given expansion history $H(z)$ (where H is the Hubble expansion rate and z is the redshift) one can reconstruct $f(R)$ which generates the required $H(z)$. The $f(R)$ models constructed in this way are called "designer $f(R)$".

For the construction of the designer $f(R)$ models, we consider the expansion rate $H(z)$ parameterized via the constant equation of state of effective dark energy, $w_{\rm eff}$, and that via the Chevallier-Polarski-Linder (CPL) parametrization [5, 6], $w_{\rm CPL}(z) = w_0 + w_a z/(1+z)$, with the current observational constraints [7]:

$$w_{\rm eff} = \text{ constant } = -0.980 \pm 0.053\ (68\%\ \text{CL}), \tag{2}$$

$$w_0 = -0.93 \pm 0.13,\ w_a = -0.41^{+0.72}_{-0.71}\ (68\%\ \text{CL}). \tag{3}$$

In this case the designer $f(R)$ is parameterized by the parameters of $w(z)$, the initial condition of $f(R)$, and other cosmological parameters q_j. That is, $f(R) = f(R;\{w_0, w_a, f_{Ri}, q_j\})$, where f_{Ri} is the initial value of f_R and $f_R \equiv df/dR$. These models by design can pass the current cosmic-expansion test.

After constructing the designer $f(R;\{w_0, w_a, f_{Ri}, q_j\})$, we test them via the cosmic-structure observations and the solar-system experiments.

Cosmic-structure test

Regarding the cosmic structures, the key quantities for distinguishing between GR and modified gravity are the two ratios, Ψ/Φ and $G_{\rm eff}/G_N$. The scalar metric perturbations, Ψ and Φ, are defined with the perturbed Robertson-Walker metric in the conformal Newtonian gauge:

$$ds^2 = -\left[1 + 2\Psi(\vec{x}, t)\right] dt^2 + a^2\left[1 - 2\Phi(\vec{x}, t)\right] d\vec{x}^2. \tag{4}$$

[1]Email address: jagu@ntu.edu.tw

The effective gravitational coupling $G_{\rm eff}$ is operationally defined by the following evolution equation of the matter density perturbation ($\delta_m \equiv \delta\rho_m/\rho_m$), while G_N is the Newtonian gravitational constant.

$$\ddot{\delta}_m + 2H\dot{\delta}_m - 4\pi G_{\rm eff}\rho_m\delta_m \cong 0, \tag{5}$$

which is valid for the sub-horizon perturbations at late times.

In GR these two ratios are both unity, while in $f(R)$ modified gravity they are complicated functions of the length scale and time: For a sub-horizon Fourier mode with the wave number k at late times,

$$\frac{\Psi}{\Phi}(k,a) \cong \frac{1+4\frac{k^2}{a^2}\frac{f_{RR}}{1+f_R}}{1+2\frac{k^2}{a^2}\frac{f_{RR}}{1+f_R}}, \tag{6}$$

$$\frac{G_{\rm eff}(k,a)}{G_N} \cong \frac{G_{\rm eff}(k,a)}{\kappa^2/8\pi} \cong \frac{1}{1+f_R}\frac{1+4\frac{k^2}{a^2}\frac{f_{RR}}{1+f_R}}{1+3\frac{k^2}{a^2}\frac{f_{RR}}{1+f_R}}, \tag{7}$$

where $f_R \equiv df/dR$ and $f_{RR} \equiv d^2f/dR^2$.

For the designer $f(R;\{w_0, w_a, f_{Ri}, q_j\})$ we constructed, we found that for all $\{w_0, w_a\}$ and for most of the initial conditions f_{Ri} the theoretical prediction of the ratio Ψ/Φ at $k = 0.01h/\text{Mpc}$ and $a = 1$ is very close to 2, which is around the margin of the current observational bound [8]:

$$1 \le \Psi/\Phi < 1.996 \quad \text{for} \quad k = 0.01h/\text{Mpc and } a = 1. \tag{8}$$

Only within a narrow range of f_{Ri} this ratio can be significantly smaller than 2 and fit the above constraint well. Accordingly, a fine-tuning of the initial condition of $f(R)$ is required for the designer $f(R)$ modified gravity to survive the cosmic-structure test.

Solar-system test

For the solar-system test, we consider the $f(R)$ modified gravity with the chameleon mechanism [9] and obtain the solar-system constraints of the general $f(R)$ [10]:

$$-10^{-15} \lesssim f_R \le 0 \quad \text{for} \quad R/H_0^2 \sim 10^5, \tag{9}$$

$$0 \le Rf_{RR} < 2/5 \quad \text{for} \quad R/H_0^2 \gtrsim 10^5. \tag{10}$$

We then look for the the viable designer $f(R;\{w_{\rm eff}, f_{Ri}\})$ (for constant $w_{\rm eff}$) models, which satisfy the above constraints, by surveying the parameter space $\{w_{\rm eff}, f_{Ri}\}$ around the GR point $\{-1, 0\}$.

We found the viable region extremely small. The deviation of the viable $\{w_{\rm eff}, f_{Ri}\}$ from the GR point $\{-1, 0\}$ is tiny:

$$|1 + w_{\rm eff}| < 10^{-9}, \tag{11}$$

$$|f_{Ri}| < 10^{-36}. \tag{12}$$

The ratios, Ψ/Φ and $G_{\rm eff}/G_N$, in these viable designer models are very close to unity (the GR prediction):

$$\left|\frac{\Psi}{\Phi} - 1\right| < 10^{-6}, \tag{13}$$

$$\left|\frac{G_{\rm eff}}{G_N} - 1\right| < 10^{-6}. \tag{14}$$

Accordingly, these viable models are indistinguishable from GR, considering both the current and the future observations in sight.

To sum up, among the designer $f(R;\{w_0, w_a, f_{Ri}\})$ models under our consideration, only those closely mimicking GR (with a cosmological constant) can pass the solar-system test. As a result, regarding the frequently studied designer $f(R)$ models constructed with respect to $w_{\rm eff} = -1$, the solar-system test has ruled out those of cosmological interest, i.e., distinct from ΛCDM in the prediction of cosmic structures (Ψ/Φ and $G_{\rm eff}/G_N$).

Acknowledgments

This work is supported by the Dark Energy Working Group of the Leung Center for Cosmology and Particle Astrophysics (LeCosPA) and by the Taiwan National Science Council (NSC) under Project No. NSC 98-2112-M-002-007-MY3.

References

[1] S. Capozziello, S. Carloni and A. Troisi, Recent Res. Dev. Astron. Astrophys. **1**, 625 (2003) [arXiv:astro-ph/0303041].

[2] S. M. Carroll, V. Duvvuri, M. Trodden and M. S. Turner, Phys. Rev. D **70**, 043528 (2004) [arXiv:astro-ph/0306438].

[3] S. Nojiri and S. D. Odintsov, Phys. Rev. D **68**, 123512 (2003) [arXiv:hep-th/0307288].

[4] W.-T. Lin, Je-An Gu and P. Chen, arXiv:1009.3488 [astro-ph.CO].

[5] M. Chevallier and D. Polarski, Int. J. Mod. Phys. D **10**, 213 (2001) [arXiv:gr-qc/0009008].

[6] E. V. Linder, Phys. Rev. Lett. **90**, 091301 (2003) [arXiv:astro-ph/0208512].

[7] E. Komatsu *et al.*, arXiv:1001.4538 [astro-ph.CO].

[8] T. Giannantonio, M. Martinelli, A. Silvestri and A. Melchiorri, JCAP **1004**, 030 (2010) [arXiv:astro-ph/0909.2045].

[9] J. Khoury and A. Weltman, Phys. Rev. Lett. **93**, 171104 (2004) [arXiv:astro-ph/0309300]; Phys. Rev. D **69**, 044026 (2004) [arXiv:astro-ph/0309411].

[10] Je-An Gu and Wei-Ting Lin, *in preparation.*

Black hole candidates and the Kerr bound

Tomohiro Harada[1](a) and Rohta Takahashi(b)

(a) *Department of Physics, Rikkyo University, Toshima, Tokyo 175-8501, Japan*
(b) *Cosmic Radiation Laboratory, the Institute of Physical and Chemical Research, 2-1 Hirosawa, Wako, Saitama 351-0198, Japan*

Abstract

The specific angular momentum of a Kerr black hole must not be larger than its mass in the geometrical units. The observational confirmation of this bound which we call a Kerr bound directly suggests the existence of a black hole. On the other hand, the violation of this bound may suggest the existence of a superspinning object which might be suggested from a string theory argument. In order to investigate observational testability of this bound by using the X-ray energy spectrum of black hole candidates, we calculate the energy spectra from an optically thick and geometrically thin accretion disk of a superspinning object which is described by a Kerr metric but whose specific angular momentum is larger than its mass, and then compare the spectra of this object with those of a black hole. Based on this calculation, we present that the observational confirmation of the Kerr bound is very hard but the violation of it may be detectable if only the continuum X-ray spectrum of the disk is available.

1 Introduction

Black hole candidates will be directly observed by radio interferometers by X-ray satellites and gravitational wave detectors in the near future. Although these candidates are most likely to be black holes, it is not obvious to confirm that. In principle, to prove that black hole candidates are really black holes, we have to show that the observed data cannot be explained by anything else. In this relation, there is an argument that if we can show that a sufficiently large amount of mass, say, above the model-independent maximum mass of neutron stars $\sim 3M_\odot$, is compactified within the size comparable with its gravitational radius, general relativity assures that it is a black hole. It turns out however that this argument crucially depends on the cosmic censorship hypothesis [1, 2]. The singularity theorems predict the existence of spacetime singularities in generic spacetimes, where the spacetime curvature is singular in typical cases. The cosmic censorship hypothesis is an unproven hypothesis about the properties of spacetimes which are solutions to the Einstein equation with physically reasonable matter fields and with generic initial data. It claims that spacetime singularities formed in physical gravitational collapse are covered by horizons and hidden from any or distant observers. Thus, the cosmic censorship hypothesis ensures the future predictability of the classical theory including general relativity. On the other hand, since quantum gravity should replace classical general relativity in the Planckian regime, singular spacetimes in classical theory might be modified to regular ones in some sense. If this is true, the cosmic censorship hypothesis for the classical theory should be reconsidered in the new context. One of the interesting possibilities is that naked-singular solutions of the classical Einstein equation are physically significant in the low-curvature region but largely modified to be smooth spacetimes around singularities in the classical solutions due to quantum gravity effects. This article is based on Takahashi and Harada [3]. We use the geometrical units, where $c = G = 1$.

The Kerr metric is a solution to the vacuum Einstein equation. This solution is stationary, axisymmetric and asymptotically flat. The metric is given by

$$\begin{aligned} ds^2 &= -\left(1-\frac{2Mr}{\Sigma}\right)dt^2 - \frac{4aMr\sin^2\theta}{\Sigma}dtd\phi + \frac{\Sigma}{\Delta}dr^2 + \Sigma d\theta^2 \\ &\quad + \left(r^2+a^2+\frac{2Mra^2\sin^2\theta}{\Sigma}\right)\sin^2\theta d\phi^2, \end{aligned}$$

[1]Email address: harada@rikkyo.ac.jp

where $\Sigma = r^2 + a^2 \cos^2\theta$, $\Delta = r^2 - 2Mr + a^2$, and M and a are the mass and the Kerr parameter, respectively. We put $a_* \equiv a/M$ as the nondimensional Kerr parameter. The Kerr solution has a curvature singularity at $r = 0$ and $\theta = \pi/2$, where $\Sigma = 0$ and this is called a ring singularity. For $|a_*| \leq 1$, the solution has an event horizon at $r = r_H$, where r_H is a larger root of $\Delta = 0$. We can see that the ring singularity is covered by an event horizon. For $|a_*| > 1$, there is no event horizon and the ring singularity is therefore not covered by a horizon. A singularity which is not covered by a horizon is called a naked singularity. Therefore, the condition $|a_*| \leq 1$ must be satisfied for the singularity to be covered and we call this condition the Kerr bound on the Kerr parameter.

Here we should mention an important example where the naked singularity is remedied due to quantum gravity effects in string theory [4]. There is a solution called the BMPV solution of supergravity in (4+1) dimensions. This solution describes a black hole in some region of the parameter space as a sub-extremal case but has a naked singularity in other region as a super-extremal case. This naked singularity is actually excised by a domain wall of strings and D-branes, if stringy effects are taken into account. Although the Kerr solution has not yet been dealt with in the same context, we can assume that the naked singularity in the super-extremal Kerr solution is excised as well due to stringy effects and this regular object is called a superspinar. Figure 1 shows this assumption schematically. In this connection, we should also mention that it is suggested that we might overspin a sub-extremal black hole to a super-extremal object by plunging a test body [5].

Figure 1: The schematic figure of the remedy of a naked singularity due to stringy effects.

2 The standard accretion disk in the general Kerr spacetime

We newly invent the consistent accretion disk model for the superspinar. We generalise the general relativistic standard accretion disk model around a black hole [6] to a superspinar. We adopt the following assumptions. The disk is axisymmetric, steady-state, geometrically thin and optically thick. The angular momentum of the fluid is transferred by the viscous torque and the dissipative energy is used to thermalise the disk. The local thermal equilibrium holds in the disk fluid. The inner edge is torque free and given by the innermost stable circular orbit (ISCO). Then, we find the solution of the fluid equation in the background Kerr metric. Given a Kerr spacetime, the accretion flow is fixed by two parameters, the accretion rate $\dot{M}$ and the radius of the outer edge $r_{\rm max}$. The accretion rate must be sub-Eddington for the consistency of the model. The result is not sensitive to the choice of $r_{\rm max}$ if it is chosen to be sufficiently large. Figure 2(a) shows the present accretion disk model schematically.

It is well known that the Kerr black hole has an ISCO. As a_* is increased from 0 to 1, $r_{\rm ISCO}$, the radius of the ISCO, decreases from $6M$ to M, while $r_{\rm H}$, the horizon radius, decreases from $2M$ to M. In fact, the Kerr spacetime has an ISCO even for $a_* > 1$. As a_* is increased from 1, $r_{\rm ISCO}$ continues to decrease to $2/3$ at $a_* = 4\sqrt{2}/(3\sqrt{3}) \simeq 1.09$, takes a minimum there and turns to increase. $r_{\rm ISCO}$ is greater than its Schwarzschild value $6M$ for $a_* > 8\sqrt{6}/3 \simeq 6.53$. This is shown in Fig. 2(b).

The efficiency ϵ of emission can be calculated as $1 - E_{\rm ISCO}$, where $E_{\rm ISCO}$ is the specific energy of the particle orbiting the ISCO. Figure 3(a) shows the efficiency as a function of the spin parameter a_*, where only the short-dashed line and the solid line are relevant to the present accretion disk model. The efficiency is ~ 5.7 % for the Schwarzschild black hole $a_* = 0$ and increases to ~ 42 % for $a_* = 1^-$. Then, it jumps to the maximum value $\sim 157.7\%$. The efficiency is larger than 100% for $1 < a_* \lesssim 1.09$. It then decreases to ~ 42 % for $a_* = 5/3 \simeq 1.67$ and continues to decrease as a_* is increased further. Note that the efficiency becomes ~ 5.7 % again for $a_* \simeq 6.53$. Figure 3(b) shows the temperature profiles of the

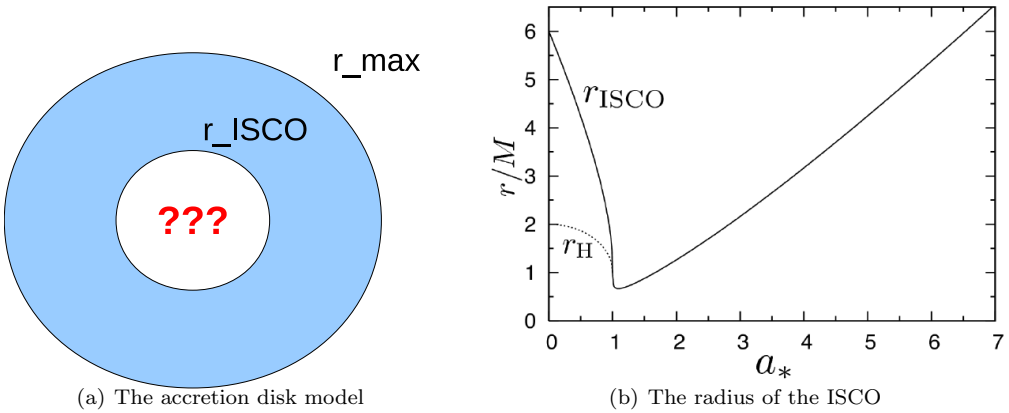

(a) The accretion disk model (b) The radius of the ISCO

Figure 2: (a) The schematic figure of the accretion disk model in the general Kerr spacetime and (b) the radius of the ISCO as a function of the Kerr parameter [3].

accretion disks. We can see that there appears a peaky spike near the inner edge for $1 < a_* \lesssim 1.09$ due to the high efficiency of the disk. We should note that for a superspinar with $1.09 \lesssim a_* \lesssim 6.53$, there is a black hole counterpart with very similar temperature structure.

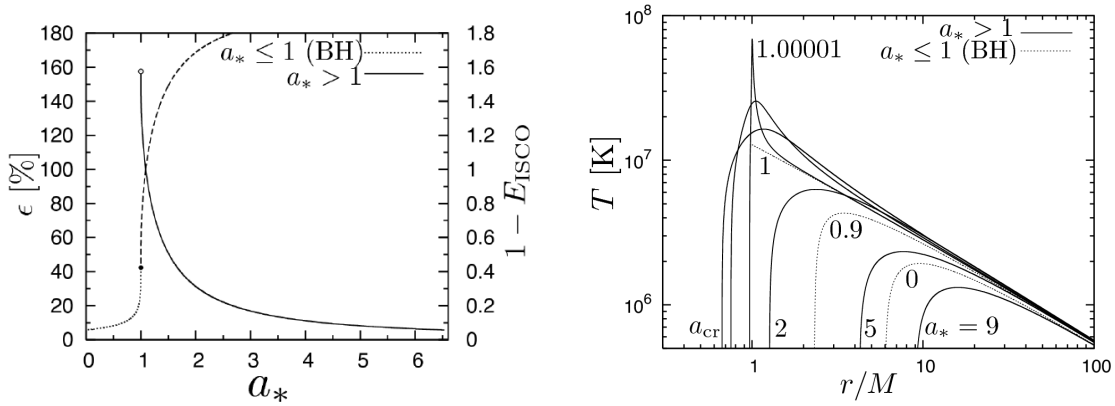

(a) The energy efficiency (b) The temperature profile

Figure 3: (a) The energy efficiency $\epsilon = 1 - E_{\rm ISCO}$ as a function of the Kerr parameter and (b) the temperature profiles of the accretion disks for the different values of the Kerr parameter [3].

3 The X-ray spectrum from the accretion disk

In addition to the dynamics and thermodynamics of the accretion disk, we assume that the dissipative energy due to the viscous torque is fully converted to the locally black-body radiation. We solve the general relativistic radiative transfer, including all kinematical general relativistic effects through the spacetime metric and the motion of the fluid. We neglect the absorption, emission and reflection by the surrounding gases for simplicity. We assume there is no emission and no absorption by the superspinar at the centre.

Figure 4(a) shows the predicted energy spectra for the different spin parameter values. For $1 \lesssim a_* \lesssim 1.67$, the spectrum extends to higher energy compared to black holes. For $a_* \gtrsim 6.53$, the photon energy is lower compared to black holes. However, surprisingly, any black hole has its superspinar counterpart which

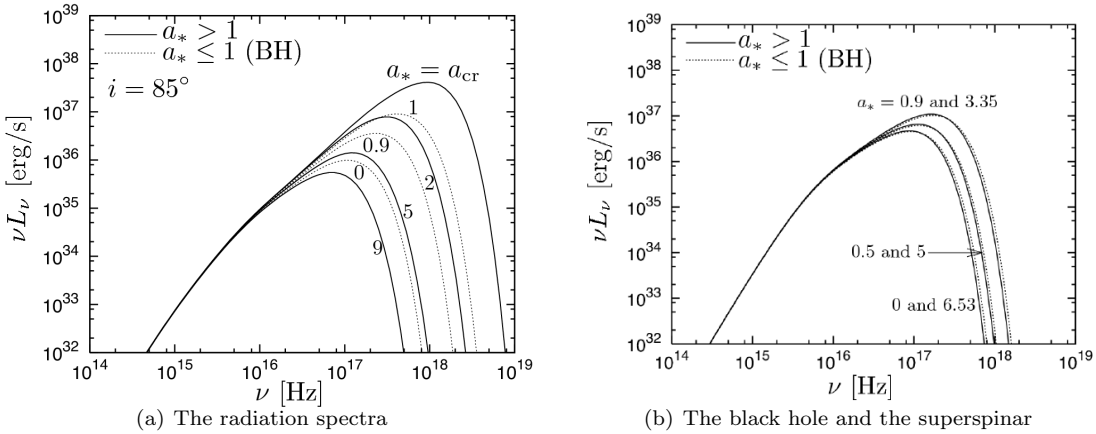

(a) The radiation spectra (b) The black hole and the superspinar

Figure 4: (a) The spectra of the emission from the disk with the different values of the Kerr parameter and (b) the demonstration of the similarity of the spectra between the black hole and the superspinar counterpart [3].

gives a very similar X-ray spectrum. This is demonstrated in Fig. 4(b). In contrast, for a superspinar with $1 \lesssim a_* \lesssim 1.67$ or $a_* \gtrsim 6.53$, there is no black hole counterpart.

4 Summary

In the present settings, it is very challenging to distinguish black holes from superspinars only by the X-ray spectrum observation. In contrast, some of the superspinars can be clearly distinguished from black holes. In other words, we can potentially find the violation of the Kerr bound by the X-ray spectrum observation. The present disk and radiation model might be too simple. It is interesting to study the observational testability of the Kerr bound with other accretion models, such as Radiatively Inefficient Accretion Flow (RIAF). See Takahashi and Harada [3] for further details.

References

[1] Penrose R., 1969, Riv. Nuovo Cim. **1**, 252

[2] Penrose R., 1979, in *General Relativity and Einstein Centenary Survey*, edited by S. W. Hawking and W. Israel (Cambridge University Press, Cambridge, England, 1979)

[3] Takahashi R., Harada T., 2010 Class. Quant. Grav. **27**, 075003

[4] Gimon E. G., Horava P., 2009, Phys. Lett. B**672**, 299

[5] Jacobson T., Sotiriou T. P., 2009, Phys. Rev. Lett. **103**, 141101; **103**, 209903(E)

[6] Page D. N., Thorne K. S., 1974, Astrophys. J. **191**, 499

Gauge invariant second order Boltzman equation

Atsushi Naruko[1(a)], Cyril Pitrou[2(b)], Koyama Kazuya[3(b)], and Misao Sasaki[4(a)]

[(a)] *Yukawa Institute, Kyoto University, Kyoto 606-8502*
[(b)] *Institute of Cosmology and Gravitation, University of Portsmouth, Dennis Sciama Building Burnaby Road, Portsmouth PO1 3FX, UK*

Abstract

In this talk, we show the second order Boltzmann equation with polarisation without specifying any gauges. In order to describe a polarisation of photon, we introduce a tensor-valued distribution function. We derive the gauge transformation rules for metric, momentum and distribution function. We correct the previous results for gauge transformtion rule of distribution function in which some terms were missed. The tensor-valued distribution function is a tensor on two dimensional polarisation surface, therefore, we have to consider the change of polarisation surface as well as its transformation rules as a tensorial quantity in the gauge transformation. For a consistency, we check the gauge invariance of the derived equation. Finally, we give a short comment on the observed temperature.

1 Introduction

The non-Gaussianity in the Cosmic Microwave Background is the one of the hottest topics in Cosmology because the non-Gaussianity can be a new window for the information of primordial universe. It is often said that the simplest inflation model predicts the very tiny non-Gaussianity, therefore if non-Gaussianity is detected, this simplest model can be ruled out. From the recent studies, we know a lot of models which predict large non-Gaussianity. Therfore, from the observations of non-Gaussianity, we may constrain inflationary models.

On the other hand, the non-linear evolution of perturbations generates the so-called late time non-Gaussianity. This becomes the noise for primordial non-Gaussianity. Fortunately, if cosmological parameters are given, we can calculate this late time non-Gaussianity without ambiguity by solving second order Boltzmann equation. Then, in principle, they can be completely subtracted.

Along this direction, the second order Boltzmann equation was written down in the Poisson gauge in [1, 2]. In [3], this equation was solved numerically and they reported that $f_{\rm NL}^{\rm local} \sim 5$ can be generated. We have to consider this late time non-Guassianity seriously and estimate it correctly. Although their calculation were performed in the Poisson gauge, at a linear level, the synchronous gauge was used for the numerical calculation. Therefore there could be some inconsistency in such a calculation.

For this purpose, we write down the second order Boltzmann equation without specifying gauges. We derive the gauge transformation rules for metric, momentum and distriabution function. Finally we check the gauge invariance of the derived equation.

2 Preparations

We shall use the ADM formalism to write down the expression of the perturbed metric. In general, the metric can be decomposed in this formalism as

$$ds^2 = a^2(\eta)\left[-N^2 d\eta^2 + \gamma_{ij}(dx^i + N^i d\eta)(dx^j + N^j d\eta)\right] \tag{1}$$

[1]Email address: naruko@yukawa.kyoto-u.ac.jp
[2]Email address: Cyril.Pitrou@port.ac.uk
[3]Email address: kazuya.koyama@port.ac.uk
[4]Email address: misao@yukawa.kyoto-u.ac.jp

where N is a lapse, N^i is a shift and γ_{ij} is a spatial metric. We consider perturbations around the flat Friedmann-Robertson-Walker spacetime and we then define the perturbations as

$$N = 1 + \alpha, \qquad \gamma_{ij} = \delta_{ij} + 2h_{ij}. \tag{2}$$

Any perturbation X will be expanded into a first-order and a second order parts as

$$X = X^{(1)} + \frac{1}{2}X^{(2)} \tag{3}$$

The photon momentum satisfies the null condition $P^\mu P_\mu = 0$, thus there are only three independent components. Using the components of the momentum in the local inertial frame $p^{(a)} \equiv e^{(a)}_\mu P^\mu$, we consider the conformal energy q and the direction $n^{(i)}$ of the photon as independent variables;

$$q \equiv \sqrt{a^2\delta_{(i)(j)}p^{(i)}p^{(j)}} = ap^{(0)}, \qquad n^{(i)} \equiv \frac{p^{(i)}}{p^{(0)}}, \qquad \delta_{(i)(j)}n^{(i)}n^{(j)} = 1, \tag{4}$$

$$e^{(0)}_\mu = a(1+\alpha)\delta^0{}_\mu, \qquad e^{(i)}_\mu = a\left[\left(N^i + h^i{}_k N^k\right)\delta^0{}_\mu + \left(\delta^i{}_j + h^i{}_j - \frac{1}{2}h^{ik}h_{kj}\right)\delta^j{}_\mu\right]. \tag{5}$$

We introduce the tensor-valued distribution function $f_{\mu\nu}$ to express the polarisation. Since the distribution function will be defined on a two-dimensional polarisation surface, it has only four degrees of freedom. These four degrees of freedom can be extracted by decomposing $f_{\mu\nu}$ into a trace part, a symmetric traceless part and an anti-symmetric part as

$$f_{\mu\nu}(x^\mu, q, n^{(i)}) \equiv \frac{1}{2}I(x^\mu, q, n^{(i)})S_{\mu\nu} + P_{\mu\nu}(x^\mu, q, n^{(i)}) + \frac{1}{2}V(x^\mu, q, n^{(i)})\epsilon_{\rho\mu\nu\sigma}e^\rho_0 d^\sigma \tag{6}$$

where $S_{\mu\nu}$ is a screen projector and its definition is

$$S_{\mu\nu}(P^\mu) \equiv g_{\mu\nu} + e^{(0)}_\mu e^{(0)}_\nu - d_\mu d_\nu, \qquad d^\mu \equiv (g^\mu{}_\nu + e^{(0)\mu}e^{(0)}_\nu)P^\nu \tag{7}$$

And also, the anti-symmetric tensor is defined by

$$\epsilon_{\alpha\beta\gamma\delta} = \epsilon_{[\alpha\beta\gamma\delta]}, \qquad \epsilon_{0123} = \sqrt{-g}. \tag{8}$$

Here I is the intensity and V the degree of circular polarization. As for $P_{\mu\nu}$, it encodes the two degrees of linear polarisation (so called Q and U in Stokes parameter).

3 Boltzmann equation

The distribution matrix satisfies the Boltzmann equation

$$\frac{\mathcal{D}f_{\alpha\beta}}{\mathcal{D}\lambda} = C_{\alpha\beta} \tag{9}$$

where $\mathcal{D}/\mathcal{D}\lambda$ is the covariant derivative along a photon trajectory $x^\mu(\lambda)$ and $C_{\mu\nu}$ is the collision term. The explicit form of $\mathcal{D}f_{\alpha\beta}/\mathcal{D}\lambda$ is

$$\frac{\mathcal{D}f_{\alpha\beta}}{\mathcal{D}\lambda} = \nabla_\mu f_{\alpha\beta}\frac{dx^\mu}{d\lambda} + \frac{\partial f_{\alpha\beta}}{\partial q}\frac{dq}{d\lambda} + \frac{\partial f_{\alpha\beta}}{\partial n^{(i)}}\frac{dn^{(i)}}{d\lambda} \tag{10}$$

where ∇_μ is the covariant derivative. Projecting the equation with the screen projector, we can show that the physical distribution matrix satisfies the following equation

$$S_\rho{}^\mu S_\sigma{}^\nu \frac{\mathcal{D}f_{\mu\nu}}{\mathcal{D}\lambda} = c_{\mu\nu} \tag{11}$$

where $c_{\mu\nu} = S_\mu{}^\alpha S_\nu{}^\beta C_{\alpha\beta}$. After short calculation, the left hand side is decomposed into the I, V and $P_{\mu\nu}$ parts similarly to Eq. (6);

$$S_\rho{}^\mu S_\sigma{}^\nu \frac{\mathcal{D} f_{\mu\nu}}{\mathcal{D}\lambda} = S_\rho{}^\mu S_\sigma{}^\nu \left(\frac{1}{2}\frac{\mathcal{D} I}{\mathcal{D}\lambda} S_{\mu\nu} + \frac{\mathcal{D} P_{\mu\nu}}{\mathcal{D}\lambda} + \frac{1}{2}\frac{\mathcal{D} V}{\mathcal{D}\lambda}\epsilon_{\gamma\mu\nu\delta} e^\gamma_{(0)} d^\delta \right). \tag{12}$$

We also decompose the collision term in the same way as

$$c_{\mu\nu}(x^\mu, q, n^{(i)}) \equiv \frac{1}{2} C^I(x^\mu, q, n^{(i)}) S_{\mu\nu} + C^P_{\mu\nu}(x^\mu, q, n^{(i)}) + \frac{1}{2} C^V(x^\mu, q, n^{(i)}) \epsilon_{\rho\mu\nu\sigma} e^\rho_{(0)} d^\sigma \tag{13}$$

We can write down the second order Boltzmann equation for intensity as

$$\begin{aligned}
\frac{\mathcal{D} I}{\mathcal{D}\lambda} = {} & \frac{q}{a^2 N}\frac{\partial I}{\partial \eta} + \frac{q}{a^2}\left(n^{(i)} - \delta^{ik} h_{kj} n^{(j)} - \frac{N^i}{N} + \frac{3}{2}\delta^{ij} h_{jk} \delta^{kl} h_{lm} n^{(m)} \right) \frac{\partial I}{\partial x^i} \\
& + \frac{q^2}{a^2}\Big\{ -\alpha_{,i} n^{(i)} + (\delta_{jk} N^k{}_{,i} - \dot{h}_{ij}) n^{(i)} n^{(j)} + \alpha(\alpha_{,i} - \delta_{jk} N^k{}_{,i} n^{(j)} + \dot{h}_{ij} n^{(j)}) n^{(i)} \\
& \qquad + (\alpha_{,i} - \delta_{lm} N^m{}_{,i} n^{(l)} + 2\dot{h}_{il} n^{(l)}) \delta^{ik} h_{jk} n^{(j)} + (N^k{}_{,i} h_{jk} + N^k h_{ij,k}) n^{(i)} n^{(j)} \Big\} \frac{\partial I}{\partial q} \\
& + \frac{q}{a^2}(n^{(i)} n^{(j)} - \delta^{ij}) \Big\{ \alpha_{,j} - \delta_{kl} N^l{}_{,j} n^{(k)} + \dot{h}_{jk} n^{(k)} + (h_{jl,k} - h_{kl,j}) n^{(k)} n^{(l)} \Big\} \frac{\partial I}{\partial n^{(i)}} = C^I
\end{aligned} \tag{14}$$

where $\dot{}$ means the derivative with rigard to η. We can write down the equation for $P_{\mu\nu}$ and V, although we don't give the expression here.

4 Gauge dependence

One of our goals is to check the gauge invariance of the Boltzmann equation. For this, we first derive the transformation rules under the gauge transformation. The gauge transformation up to the second order is given by

$$x^\mu \to \tilde{x}^\mu = x^\mu + \xi^\mu \qquad \xi^\mu = \xi^{(1)\mu} + \frac{1}{2}\xi^{(2)\mu} \tag{15}$$

From now on, we derive the gauge transformation rules for metric, momentum, and the distribution function. We will write the component of ξ^μ as $\xi^\mu = (T, L^i)$.

Gauge transformation of metric at second order are given by

$$g_{\alpha\beta} \to \tilde{g}_{\alpha\beta} = g_{\alpha\beta} - \mathcal{L}_\xi g_{\alpha\beta} + \frac{1}{2}\mathcal{L}_\xi(\mathcal{L}_\xi g_{\alpha\beta}) + \frac{1}{2}\mathcal{L}_{\xi\xi} g_{\alpha\beta} \tag{16}$$

$\xi\xi$ means $\xi^\mu{}_{,\nu}\xi^\nu$. Up to the second order, the ADM variables transform as

$$\begin{aligned}
\tilde{\alpha} = {} & \alpha - \mathcal{H}T - \dot{T} + \frac{1}{2}(\mathcal{H}^2 + \dot{\mathcal{H}})T^2 + \mathcal{H}(2\dot{T}T + T_{,i}L^i) - \mathcal{H}\alpha T \\
& - \alpha\dot{T} - \dot{\alpha}T - \alpha_{,i}L^i + N^i T_{,i} + \ddot{T}T + \dot{T}^2 + \dot{T}_{,i}L^i + \frac{1}{2}\delta^{ij} T_{,i} T_{,j}
\end{aligned} \tag{17}$$

$$\begin{aligned}
\tilde{N}^i = {} & N^i + \delta^{ij} T_{,j} - \dot{L}^i + 2\delta^{ij}\alpha T_{,j} - N^i \dot{T} - \dot{N}^i T + N^j L^i{}_{,j} - N^i{}_{,j} L^j - 2\delta^{ik}\delta^{jl} h_{jk} T_{,l} \\
& - \delta^{ij}(2T_{,j}\dot{T} + T\dot{T}_{,j}) + T\ddot{L}^i + \dot{T}\dot{L}^i + \delta^{jk} T_{,j} L^i{}_{,k} - \delta^{ij} T_{,jk} L^k + \dot{L}^i{}_{,j} L^j
\end{aligned} \tag{18}$$

$$\begin{aligned}
2\tilde{h}_{ij} = {} & 2h_{ij} - 2\mathcal{H}T\delta_{ij} - (\delta_{ik} L^k{}_{,j} + \delta_{jk} L^k{}_{,i}) - 4\mathcal{H} h_{ij} T + (2\mathcal{H}^2 + \dot{\mathcal{H}})\delta_{ij} T^2 + 2\mathcal{H}\delta_{ij}(\dot{T}T + T_{,k} L^k) \\
& + 2\mathcal{H}T(\delta_{ik} L^k{}_{,j} + \delta_{kj} L^k{}_{,i}) - N^k(\delta_{ik} T_{,j} + \delta_{jk} T_{,i}) - 2\dot{h}_{ij} T - 2h_{ij,k} L^k - 2(h_{ik} L^k{}_{,j} + h_{jk} L^k{}_{,i}) \\
& - T_{,i} T_{,j} + T(\delta_{ik}\dot{L}^k{}_{,j} + \delta_{kj}\dot{L}^k{}_{,i}) + (\delta_{ik} T_{,j} + \delta_{kj} T_{,i})\dot{L}^k \\
& + \delta_{kl} L^k{}_{,i} L^l{}_{,j} + (\delta_{ik} L^k{}_{,jl} + \delta_{kj} L^k{}_{,il}) L^l + (\delta_{ik} L^l{}_{,j} + \delta_{kj} L^l{}_{,i}) L^k{}_{,l}
\end{aligned} \tag{19}$$

where $\mathcal{H}$ is conformal hubble parameter defined by $\mathcal{H} \equiv \dot{a}/a$.

Then using the transformation rules for P^μ and metric, we obtain the transformation rule for q;

$$\tilde{q} = q + \delta q = q\left\{1 + \mathcal{H}T + T_{,i}n^{(i)} + \frac{1}{2}(\dot{\mathcal{H}} + \mathcal{H}^2)T^2 + (\mathcal{H}T - \dot{T})T_{,i}n^{(i)} + \frac{1}{2}\delta^{jl}T_{,j}T_{,l} + T_{,i}(\alpha n^{(i)} - \delta^{ik}h_{kj}n^{(i)})\right\} \tag{20}$$

In the same way, the gauge transformation rule of $n^{(i)}$ is given by

$$\tilde{n}^{(i)} = n^{(i)} + \delta n^{(i)} = n^{(i)} + (\delta^{ij} - n^{(i)}n^{(j)})T_{,j} + \frac{1}{2}\delta^{ik}(\delta_{kl}L^l{}_{,j} - \delta_{jl}L^l{}_{,k})n^{(j)} \tag{21}$$

Using the transformation rules for metric and momentum, we find the gauge transformation rule for the distribution function

$$\tilde{f}_{\alpha\beta} = f_{\alpha\beta} - \mathcal{L}_\xi f_{\alpha\beta} - \delta q\frac{\partial f_{\mu\nu}}{\partial q} - \delta n^i\frac{\partial f_{\mu\nu}}{\partial n^i} - \frac{a^2}{q}T_{,i}(P_\alpha f^i{}_\beta + f_\alpha{}^i P_\beta) \tag{22}$$

The last two terms were missed in [1]. These terms come from the gauge transformation of projection tensor $S_{\mu\nu}$ and physically means the change of screen.

Although we don't show the detailed calculation, using the derived gauge transformation rules for metric, momentum and distribution function, we can show the gauge invariance of the second order Boltzmann equation. This fact gives the consistency check for the derived gauge transformation rule.

5 comment on observed temperature

In all the literature, the second order temperature anisotropies are calculated in the Poisson gauge with a specific choice of the local inertial frame. Strictly speaking this is not the temperature anisotopies that we observe. Thus one needs to change the local inertial frame or perform the gauge transformation. At the first order, this is not an issue. Since the first order gauge transformation rule of temperature is given by;

$$\Theta \to \Theta + \mathcal{H}T + T_{,i}n^{(i)} \tag{23}$$

the change of the gauge and the local inertial frame only affects the monopole $\ell = 0$ and dipole $\ell = 1$ if we expands the temperature aniostropies into multipole components. Thus the $\ell \geq 2$ modes are not affected by the change of observers. However this is no longer the case at the second order. In the second order gauge transformation, there are terms that are convolutions of the first order temperature anisotorpies and the gauge transformation functions. These terms affect the observed temperatures even for the $\ell > 2$ modes. Thus a care must be taken when we compare theoretical predictions to observations.

References

[1] C. Pitrou, Class. Quant. Grav. **26**, 065006 (2009) [arXiv:0809.3036 [gr-qc]].

[2] M. Beneke and C. Fidler, Phys. Rev. D **82**, 063509 (2010) [arXiv:1003.1834 [astro-ph.CO]].

[3] C. Pitrou, J. P. Uzan and F. Bernardeau, JCAP **1007**, 003 (2010) [arXiv:1003.0481 [astro-ph.CO]].

Effectiveness of Empirical Mode Decomposition in Search for Gravitational Wave Signals

Yuta Hiranuma[1](a), Makoto Saito(a), Masamoto Saito(a), Ken-ichi Oohara [2](a), Hirotaka Takahashi [3](b),(c), Alexander Stroeer(d) L. Blackburn(e) and Jordan B. Camp(f)

(a) *Graduate School of Science and Technology, Niigata University, Niigata 950-2181, Japan*
(b) *Department of Humanities, Yamanashi Eiwa College, Yamanashi, 400-8555 Japan*
(c) *Earthquake Research Institute, The University of Tokyo, Tokyo 113-0032, Japan*
(d) *Center for Gravitational Wave Astronomy, The University of Texas at Brownsville, Brownsville, Texas 78520, USA*
(e) *Laboratory for Gravitational Physics, Goddard Space Flight Center, Greenbelt, Maryland 20771, USA*

Abstract

The Hilbert-Huang transform is a novel, adaptive approach to time series analysis that does not make assumptions about the data form. This algorithm is adaptive and does not impose a basis set on the data, and thus the time-frequency decomposition is not limited by time-frequency uncertainty spreading. Because of its high time-frequency resolution, it will have important applications to the detection of gravitational wave signal. As a first step, we demonstrate a possibility of the application of a Hilbert-Huang transform to the search for gravitational waves.

1 Introduction

The Hilbert-Huang transform (HHT) is the combination of the well-known Hilbert spectral analysis and the empirical mode decompositon developed recently by Huang et al.[1]. It presents a fundamentally new approach to the analysis of time series data. Its essential feature is the use of an adaptive time-frequency decomposition that does not impose a fixed basis set on the data, and therefore, unlike Fourier or Wavelet analysis, its application is not limited by the time-frequency uncertainty relation. This leads to a highly efficient tool for the investigation of transient and nonlinear features. The HHT is applied to various fields including materials damage detection [2], biomedical monitoring [3] [4], etc. Because gravitational wave detectors, such as LIGO, Virgo and LCGT, have a great variety of nonlinear and transient signals, the HHT has the promise of being a powerful new tool in the search for gravitational waves. We will, therefore, demonstrate a possibility of the application of the HHT to data analysis of gravitational waves.

2 Brief Description of Hilbert-Huang Transform

The HHT consists of two components; empirical mode decomposition (EMD) and Hilbert spectral analysis. In this section, we introduce briefly both components of HHT. It will be shown that the Hilbert transform (HT) can lead to an apparent time-frequency-energy description of a time series. However, this description may not be consistent with physically meaningful definitions of instantaneous frequency and instantaneous amplitude, since the HT is based on Cauchy's integral formula of holomorphic functions tending to zero fast enough at infinity. The EMD can generate components of the time series whose HT can lead to physically meaningful definitions of these two instantaneous quantities, and hence the combination of EMD and HT provides a more physically meaningful time-frequency-energy description of a time series.

Hereafter, we assume that the input $x(t)$ is given by sampling a continuous signal at the discrete time, $t = t_i$ for $i = 0, 1, \cdots, N$.

[1]Email address: yuta@astro.sc.niigata-u.ac.jp
[2]Email address: oohara@astro.sc.niigata-u.ac.jp
[3]Email address: hirotaka@y-eiwa.ac.jp

2.1 Empirical Mode Decomposition

The EMD has implicitly a simple assumption that, at any given time, the data may have many coexisting oscillatory modes of significantly different frequencies, one superimposed on the other. The each component is defined as an intrinsic mode function (IMF) that satisfies the following conditions: (i) In the whole data set, the number of extrema and the number of zero crossings must either equal or differ at most by one. (ii) At any data point, the mean value of the upper and the lower envelopes defined using the local maxima and the local minima, respectively, is zero.

With the above definition of an IMF, we can then decompose any function through a sifting process. The sifting starts with identifying all the local extrema and then connecting all the local maxima (minima) by a cubic spline to form the upper (lower) envelope. The upper and lower envelopes usually encompass all the data between them. Their mean is designated as $m_1(t)$. The difference between the input $x(t)$ and $m_1(t)$ is the first protomode, $h_1(t)$, namely, $h_1(t) = x(t) - m_1(t)$. By construction, h_1 is expected to satisfy the definition of an IMF. However, that is usually not the case since changing a local zero from a rectangular to a curvilinear coordinate system may introduce new extrema, and further adjustments are needed. Therefore, a repeat of the above procedure is necessary. This sifting process serves two purposes; (a) to eliminate background waves on which the IMF is riding and (b) to make the wave profiles more symmetric. The sifting process has to be repeated as many times as is required to make the extracted signal satisfy the definition of an IMF. In the iterating processes, h_1 can only be treated as a proto-IMF, which is treated as the data in the next iteration: $h_1(t) - m_{11}(t) = h_{11}(t)$. After k times of iterations, $h_{1(k-1)}(t) - m_{1k}(t) = h_{1k}(t)$; the approximate local envelope symmetry condition is satisfied, and h_{1k} becomes the IMF c_1, that is, $c_1(t) = h_{1k}(t)$.

The approximate local envelope symmetry condition in the sifting process is called the stoppage criterion. The several different types of stoppage criterion were adopted. In this article, we use the Cauchy types of stoppage criterion [1]:

$$\sum_{i=0}^{N} \left|m_{1k}(t_i)\right|^2 \Big/ \sum_{i=0}^{N} \left|h_{1k}(t_i)\right|^2 < \epsilon \tag{1}$$

with a predetermined value ϵ.

The first IMF should contain the finest scale or the shortest-period oscillation in the signal, which can be extracted from the data by $x(t) - c_1(t) = r_1(t)$. The residue, r_1, still contains longer-period variations. This residual is then treated as the new data and subjected to the same sifting process as described above to obtain an IMF of lower frequency. The procedure can be repeatedly applied to all subsequent r_n, and the result is $r_{n-1}(t) - c_n(t) = r_n(t)$. The decomposition process finally stops when the residue, r_n, becomes a monotonic function or a function with only one extremum from which no more IMF can be extracted. Thus, the original data are decomposed into n IMFs and a residue obtained, r_n, which can be either the adaptive trend or a constant: $x(t) = \sum_{j=1}^{n} c_j(t) + r_n(t)$.

2.2 Hilbert Spectral Analysis

The purpose of the development of HHT is to provide an alternative view of the time-frequency-energy paradigm of data. In this approach, the nonlinearity and nonstationarity can be dealt with better than by using the traditional paradigm of constant frequency and amplitude. One way to express the nonstationarity is to find instantaneous frequency (IF) and instantaneous amplitude (IA). This was the reason why Hilbert spectral analysis was included as a part of HHT.

For any function $x(t)$, its Hilbert transform (HT) $y(t)$ is

$$y(t) = \frac{1}{\pi} P \int_{-\infty}^{\infty} \frac{x(\tau)}{t - \tau} d\tau, \tag{2}$$

where P is the Cauchy principal value of the singular integral. Although it is not trivial to calculate the Cauchy principal value numerically, the HT can be obtained using the Fourier transform or the FFT of $x(t)$ and the convolution theorem, since the HT is the convolution of $x(t)$ and $1/(\pi t)$. Assuming the

function $x(t)$ is the real part of a holomorphic function $F(z)$ on the real axis $z = t$, the HT $y(t)$ will be its imaginary part, that is,

$$F(t) = x(t) + iy(t) = a(t)e^{i\theta(t)}, \tag{3}$$

where

$$a(t) = \sqrt{x(t)^2 + y(t)^2} \qquad \text{and} \qquad \theta(t) = \tan^{-1}\left\{\frac{y(t)}{x(t)}\right\}. \tag{4}$$

Here $a(t)$ is the instantaneous amplitude and $\theta(t)$ is the instantaneous phase function. The instantaneous frequency is given by

$$f(t) = \frac{1}{2\pi}\frac{d\theta(t)}{dt} = \frac{1}{2\pi a^2}\left(x\frac{dy}{dt} - y\frac{dx}{dt}\right). \tag{5}$$

With both amplitude and frequency, we can express the amplitude (or energy, the square of amplitude) in terms of a function of time and frequency, $H(\omega, t)$. The marginal spectrum can then be defined as

$$h(\omega) = \int_0^T H(\omega, t)dt, \tag{6}$$

where $[0, T]$ is the temporal domain within which the data is defined. The marginal spectrum represents the accumulated amplitude (energy) over the entire data span in a probabilistic sense and offers a measure of the total amplitude (or energy) contribution from each frequency value, serving as an alternative spectrum expression of the data to the traditional Fourier spectrum.

3 Demonstration of HHT as Gravitational Wave Data Analysis

To illustrate the application of the HHT to data analysis of gravitational waves (GW), we look at the identification of a signal in white Gaussian noise. Our principal motivation is in analyzing data from GW detectors such as LIGO, Virgo and LCGT. GW signals at the sensitivity of the current detector are not expected to show rates exceeding one per year at SNR > 8. The adaptive and high time-frequency resolution features of the HHT are well suited to GW analysis.

We focus in this article on simulations with time series data composed of stationary white Gaussian noise and GW signals well separated in time. As an example, we inject a 20 solar mass black hole binary merger and ringdown signal [5] with SNR = 7 into white Gaussian noise at 16 kHz sampling rate. The merger signal is shown in the top panel of Fig.1 and the time series of signal in white Gaussian noise is shown in the lower panel of Fig.1.

Although, in this article, we do not discuss in detail, we have made the modifications, which is called Ensemble Empirical Mode Decomposition (EEMD) [6], to HHT application to the GW data analysis. The purpose of introducing EEMD is to average over errors in the EMD process. EEMD is also an algorithm, which contains the following steps: (1) Add a white noise series to the targeted data; (2) decompose the data with added white noise into IMFs; (3) repeat steps (1) and (2) again and again but with different white noise series each time; and (4) the ensemble means of corresponding IMFs of the decompositions are obtained as the final result. In this article, we set a EMD ensemble number and EMD stoppage criterion 200 and $\epsilon = 0.01$ respectively.

The top panel of Fig.2 shows the results of EEMD. The green, blue and red lines show 2nd, 3rd and 4th IMFs. The black line shows injected signal. In the 2nd and 3rd IMFs, the signal can be seen, largely separate from the noise. The middle and lower panels of Fig.2 show the instantaneous amplitude and frequency derived from the Hilbert transform of 2nd, 3rd and 4th IMFs. The black line shows the instantaneous amplitude and frequency of injected signal without noise. The instantaneous amplitude and frequency of 2nd plus 3rd IMFs display similar behavior of the instantaneous frequency and power of injected signal. Thus, there is a possibility that we can identify a targeted signal and extract information about the signal frequency and power evolution in time.

4 Summary

In this article, we briefly reviewed the analysis algorithm of the HHT. As a fist step, we demonstrated the application of the HHT to GW data analysis. To illustrate the application of the HHT to GW analysis,

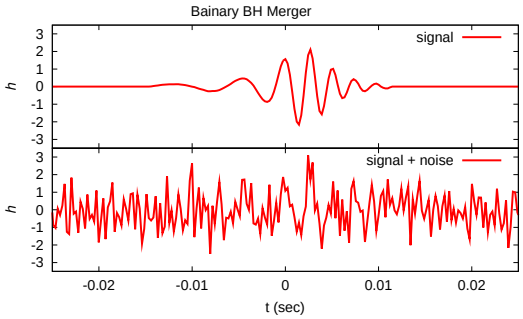

Figure 1: 20 solar mass black hole binary merger and ringdown signal [5]. The upper and lower panels show the pure signal and the signal in white Gaussian noise with SNR=7, respectively.

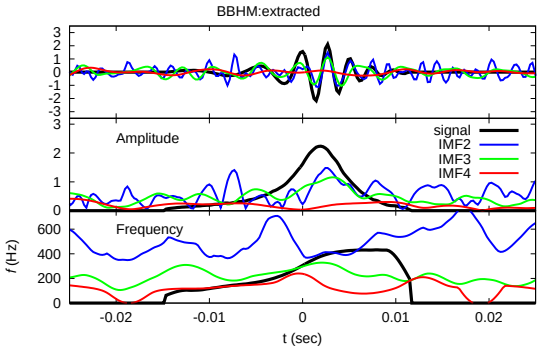

Figure 2: IMFs 2, 3, 4 and original signal. The middle and lower panels display instantaneous amplitude and frequency, respectively.

we looked at the identification of a signal in white Gaussian noise. As the result, we found that there was a possibility that we could identify a targeted signal and extract information about the signal frequency and power evolution in time.

In future, because HHT is empirical method, we need more systematic simulations to investigate the property of the HHT. Many more details of the results of systematic simulations will be discussed elsewhere.

Acknowledgment

This work has been supported in part by JSPS Grant-in-Aid for Scientific Research No.20540260.

References

[1] N. E. Huang, S. R. Long and Z. Shen, Adv. Appl. Mech. **32**, 59 (1996);
N. E. Huang et al. Proc. R. Soc. London A **454**, 903 (1998);
N. E. Huang, Z. Shen and S. R. Long, Annu. Rev. Fluid Mech. **31**, 417 (1999).

[2] J. Yang et al., Journal of Engineering Mechanics American Society of Civil Engineers **130**, 85 (2004).

[3] V. Novak et al., Biomed. Eng. Online **3**, 39 (2004).

[4] *Hilbert-Huang Transform and its Applications*, edited by N. Huang et al. (World Scientific, Singapore, 2005).

[5] J. G. Baker, J. Centrella, D. I. Choi, M. Koppitz, and J. van Meter1 Phys. Rev. D **73**, 104002 (2006);
J. G. Baker, J. Centrella, D. I. Choi, M. Koppitz, and J. van Meter1 Phys. Rev. Lett. **96**, 111102 (2006).

[6] *Ensemble Empirical Mode Decomposition: A Noise Assisted Data Analysis Method*, Z. Wu, N. Huang. (Center for Ocean-Land-Atmosphere Studies, 2005).

Creation of D9-brane–anti-D9-brane Pairs from Hagedorn Transition of Closed Strings – its application to cosmology

Kenji Hotta[1(a)],

(a) *Department of Physics, Hokkaido University, Sapporo 060-0810*

Abstract

It is well known that one-loop free energy of closed strings diverges above the Hagedorn temperature. One explanation for this divergence is that a 'winding mode' in the Euclidean time direction becomes tachyonic above the Hagedorn temperature. The Hagedorn transition of closed strings has been proposed as a phase transition via condensation of this winding tachyon. But we have not known the stable minimum of the potential of this winding tachyon so far. On the other hand, we have previously calculated the finite temperature effective potential of open strings on D-brane–anti-D-brane pairs, and shown that a phase transition occurs near the Hagedorn temperature and D9-brane–anti-D9-brane pairs become stable. In this article, we present a conjecture that *D9-brane–anti-D9-brane pairs are created by the Hagedorn transition of closed strings*, and describe some circumstantial evidences. We also discuss its application to cosmology.

1 Hagedorn Transition of Closed Strings

Since the early days of string theory, it was observed that perturbative string gas has an interesting thermodynamic property. The string gas has a characteristic temperature called the Hagedorn temperature. We can compute the one-loop free energy of strings by using path integral in Matsubara method. The one-loop free energy of strings diverges above this temperature.

One explanation for this divergence is that a 'winding mode' in the Euclidean time direction becomes tachyonic above the Hagedorn temperature. Sathiapalan [1], Kogan [2] and Atick and Witten [3] have proposed the Hagedorn transition of closed strings via condensation of this winding tachyon. They advocated that the Hagedorn temperature is not really a limiting temperature but rather is associated with a phase transition. Atick and Witten argued further from the world sheet point of view. The insertion of the winding tachyon vertex operator means the creation of a tiny hole in the world sheet which wraps around the compactified Euclidean time. Thus, the addition of the winding tachyon vertex operator to the world sheet action induces the creation of a sea of such holes. At low temperature, sphere world sheet does not contribute to the free energy, since it cannot wrap the compactified Euclidean time. But if we consider the condensation of winding tachyon above the Hagedorn temperature, the sphere world sheet is no longer simply connected and it contributes to the free energy above the Hagedorn temperature. It should be noted that these modes can be interpreted as winding tachyon only in the Matsubara formalism, namely, if we perform the Wick rotation of the time direction and compactified it with period β. We cannot identify which modes condensate to what extent in Lorentzian time when this winding tachyon condensates in the Euclidean time.

Significant effort has been devoted to find out the stable minimum of the potential of this winding tachyon. But we have not known the stable minimum yet. It is difficult to compute the potential of closed string tachyon because this potential has to be calculated by closed string field theory and this theory has not been well-established.

2 Brane–anti-brane Pairs at Finite Temperature

We have previously discussed the behavior of brane-antibrane pairs at finite temperature in the constant tachyon background [4]. At zero temperature, the spectrum of open strings on these unstable branes

[1]Email address: khotta@particle.sci.hokudai.ac.jp

contains a tachyon field T. In the brane–antibrane configuration, we have $T = 0$, and the potential of this tachyon field has a local maximum at $T = 0$. If we assume that the tachyon potential has a non-trivial minimum, it is hypothesized that the tachyon falls into it. Sen conjectured that the potential height of the tachyon potential exactly cancels the tension of the original brane-antibrane pairs [5]. This implies that these unstable brane systems disappear at the end of the tachyon condensation.

Although brane-antibrane pairs are unstable at zero temperature, there are the cases that they become stable at finite temperature. We have calculated the finite temperature effective potential of open strings on these branes based on boundary string field theory. For the D9-brane–$\overline{\text{D9}}$-brane pairs, a phase transition occurs at slightly below the Hagedorn temperature and the D9-$\overline{\text{D9}}$ pairs become stable above this temperature. On the other hand, for the Dp-brane–$\overline{\text{D}p}$-brane pairs with $p \leq 8$, such a phase transition does not occur. We thus concluded that not a lower dimensional brane-antibrane pairs but D9-$\overline{\text{D9}}$ pairs are created near the Hagedorn temperature. Let us call this phase transition brane-antibrane pair creation transition. Although we only describe the case of brane-antibrane pairs, almost the same argument holds for the case of non-BPS D-branes. This work is generalized to the case that Dp-brane and $\overline{\text{D}p}$-brane are separated by Calò and Thomas [6].

3 Creation of D9-brane–$\overline{\text{D9}}$-brane Pairs from Hagedorn Transition of Closed Strings

Let us consider the relationship between above two phase transitions. Let us return to the argument of Atick and Witten about the meaning of the condensation of the winding tachyon [3]. The insertion of the winding tachyon vertex operator corresponds to the creation of a tiny hole in the world sheet which wraps around the compactified Euclidean time, and the condensation of winding tachyon induces an infinite number of tiny holes in the world sheet. But what is the hole of closed string world sheet? Let us try to think about it from a different point of view. If we identify the boundary of a hole created by winding tachyon vertex operator with a boundary of open string on a D9-$\overline{\text{D9}}$ pair, the insertion of winding tachyon vertex operator means the insertion of the boundary of open strings, which wraps the compactified Euclidean time once, in the tiny hole limit. Then the sphere world sheet which is no longer simply connected is naturally reinterpreted as higher-loop open string world sheet. If we enlarge the size of this hole, we can describe open strings with arbitrary boundary. Therefore, we present a following conjecture :

D9-brane–$\overline{\text{D9}}$-brane pairs are created by the Hagedorn transition of closed strings.

That is, above two phase transitions are two aspects of one phase transition. In the sense that $T = 0$ is the perturbative vacuum of open strings, this is a phase transition from closed string vacuum to open string vacuum. In other words, the stable minimum of the Hagedorn transition is the open string vacuum.

4 Circumstantial Evidences

Here we describe some circumstantial evidences for this conjecture. First, if we consider the thermodynamic balance on D9–$\overline{\text{D9}}$ pairs, we can show that energy flows from closed strings to open strings and open strings dominate the total energy. This is because we can reach the Hagedorn temperature for closed strings by supplying finite energy, while we need infinite energy to reach the Hagedorn temperature for open strings on these branes. This implies that, as the temperature increases, the creation of D9–$\overline{\text{D9}}$ pairs begins before closed strings are highly excited.

Secondly, one-loop free energy of open strings on a D9-$\overline{\text{D9}}$ pair approaches to the propagator of winding tachyon in the closed string vacuum limit, as is sketched in Fig. 1. This is an example that we can identify the closed string sphere world sheet with winding tachyon vertex operators with the open string world sheet in the closed string vacuum limit. Atick and Witten consider only closed string vacuum and looking for stable minimum in winding tachyon space. But it is reasonable to look for the stable minimum in all the open string tachyon space.

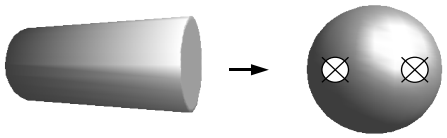

Figure 1: The cylinder world sheet (left) approaches to the sphere world sheet with two winding tachyon vertices insertion (right).

Thirdly, we can show that the finite temperature effective potential at the open string vacuum becomes the global minimum in entire space of the open string tachyon field near the Hagedorn temperature.

In the case of a D9-$\overline{\text{D9}}$ pair, the potential energy at $T = 0$ is given by

$$V \simeq - \frac{2v_9}{\pi {\beta_H}^9 (\beta - \beta_H)}, \tag{1}$$

where β_H is the inverse of the Hagedorn temperature and v_9 is the 9-dimensional volume of the system that we are considering. From this we can see that this potential energy decreases limitlessly as the temperature approaches to the Hagedorn temperature. It is natural to think that the open string vacuum becomes the global minimum near the Hagedorn temperature. This is the property that the stable minimum of the Hagedorn transition is expected to have.

5 Application to Cosmology

The spacetime-filling branes are very advantageous in the sense that all the lower-dimensional D-branes in type II string theory are realized as topological defects through tachyon condensation from non-BPS D9-branes and D9-$\overline{\text{D9}}$ pairs. We can identify the topological charge as the Ramond-Ramond charge of the resulting D-branes. These D-brane charges can be classified using K-theory [7]. Thus, if non-BPS D9-branes exist in the early universe, various kinds of branes may form through tachyon condensation [8]. It would be interesting to examine the possibility that our Brane World forms as a topological defect in a cosmological context. We have studied the homogeneous and isotropic tachyon condensation as a first step towards 'Brane World Formation Scenario'. In this article, we describe only the simplest case. For other cases, see Ref. [9].

The low energy effective action for tree level closed strings is described by type IIA supergravity. For simplicity, we shall focus on 10-dimensional metric $g_{\mu\nu}$, and set the other fields to zero or some constants. Then the action is given by

$$S_E = - \frac{1}{2\kappa^2} \int d^{10}x \sqrt{-g}\, \mathcal{R}. \tag{2}$$

We must also consider the action for non-BPS D9-branes. For simplicity, we only deal with the zero temperature case. The BSFT action for a linear tachyon profile in the flat spacetime is derived in Ref. [10]. Let us focus on tachyon T in the open string spectrum, as well as graviton $g_{\mu\nu}$ in the closed string one, and assume that the action in the curved spacetime is given by

$$S_T = \mu \int d^{10}x \sqrt{-g}\, e^{-\alpha T^2} \mathcal{F}\left(\lambda \nabla_\mu T \nabla^\mu T\right), \tag{3}$$

where α, λ and μ are constants, and

$$\mathcal{F}(z) = \sqrt{\pi}\, \Gamma(z+1) \left\{ \Gamma\left(z + \frac{1}{2}\right) \right\}^{-1}. \tag{4}$$

The total action we consider is the sum of (2) and (3). We assume that the universe is homogeneous and isotropic, and that the spatial curvature is flat. In order to perform the numerical calculation,

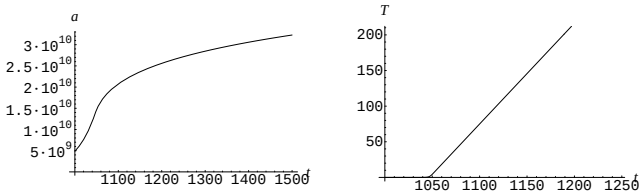

Figure 2: The time evolution of the scale factor $a(t)$ (left) and the tachyon field $T(t)$ (right) in the case of Einstein gravity coupled to tachyon field. We have set $a(0) = 1$. The initial condition for the tachyon is $T = 10^{-10}$ and $\dot{T} = 0$ at $t = 1000$. We choose such a small initial value of T in order to show the inflation phase exists before the decelerated expansion phase.

we must choose an initial condition. It is expected that, even if non-BPS D9-branes are stable near the Hagedorn temperature initially, they become unstable because the energy density decreases as the universe expands. Then the tachyon starts to roll down from the local maximum of the potential at $T = 0$. When the tachyon remains at $T = 0$, the solution for the equations of motion is de Sitter solution. Thus, it is reasonable to choose the initial condition which is close to the de Sitter solution. We calculate the numerical solution as is depicted in Fig. 2. From this we can see that the tachyon asymptotically approaches to a linear function of t. Sugimoto and Terashima have pointed out that $T \to t/\sqrt{\lambda} + \text{const.}$ as $t \to \infty$, and that it is related to tachyon matter [11]. This comes from the divergence of $\mathcal{F}(z)$ and its derivative at $z = -1$. As we can see from Fig. 2, the scale factor asymptotically approaches to a constant as $t \to \infty$. This is because the energy density of the tachyon field asymptotically approaches to zero and we are considering the case that the spatial curvature is zero. The inflation phase continues for a long time if we choose small initial value of T.

Acknowledgments

The author would like to thank the organizers of workshop for giving him an opportunity of participation.

References

[1] B. Sathiapalan, Phys. Rev. **D35** (1987) 3277.

[2] I. Kogan, JETP Lett. **45** (1987) 709.

[3] J. J. Atick and E. Witten, *Nucl. Phys.* **B310** (1988) 291.

[4] K. Hotta, JHEP **0212** (2002) 072, hep-th/0212063; JHEP **0309** (2003) 002, hep-th/0303236; Prog. Theor. Phys. **112** (2004) 653, hep-th/0403078.

[5] A. Sen, JHEP **9808** (1998) 012, hep-th/9805170.

[6] V. Calò, S. Thomas, JHEP **0806** (2008) 093, arXiv:0802.2453.

[7] E. Witten, JHEP **9812** (1998) 019, hep-th/9810188; P. Horava, Adv. Theor. Math. Phys. **2** (1999) 1373, hep-th/9812135.

[8] M. Majumdar and A. -C. Davis, JHEP **0203** (2002) 056, hep-th/0202148.

[9] K. Hotta, JHEP **0603** (2006) 070, hep-th/0601133.

[10] D. Kutasov, M. Marino and G. W. Moore, hep-th/0010108; M. Marino, JHEP **0106** (2001) 059, hep-th/0103089.

[11] S. Sugimoto and S. Terashima, JHEP **0207** (2002) 025, hep-th/0205085.

Generalized Hidden Symmetries and the Kerr-Sen Black Hole

Tsuyoshi Houri[1]

Osaka City University Advanced Mathematical Institute (OCAMI),
3-3-138 Sugimoto, Sumiyoshi, Osaka, 558-8585 JAPAN

Abstract

We study an extension of Killing-Yano symmetry in the presence of totally skew-symmetric torsion, which is called generalized hidden symmetry. Such a symmetry gives rank-2 irreducible Killing tensors which don't in general commute. We further study Kerr-Sen black hole spacetime and its generalizations in hetelotic supergravity theory. It is shown that these spacetimes possess generalized Killing-Yano symmetry and the torsion is identified with 3-form flux naturally.

1 Introduction

Killing–Yano symmetry has been studied as a fundamental hidden symmetry which plays a crucial role in black hole spacetimes. It is known that in the four-dimensional Kerr spacetime [1], all the symmetries necessary for separability of the geodesic, Klein-Gordon and Dirac equations, are described by a Killing–Yano tensor [2]. Higher-dimensional solutions describing rotating black holes have attention in the recent developments of superstring and supergravity theories. It was demonstrated that the vacuum rotating black hole solutions (with spherical horizon topology) [3–5] have Killing–Yano symmetry and generalize separability of Hamilton-Jacobi equation [6–9], Klein-Gordon equation [10, 11] and Dirac equation [12]. In this presentation we discuss a Killing–Yano symmetry in the presence of skew-symmetric torsion. The spacetimes with skew-symmetric torsion occur naturally in supergravity theories, where the torsion may be identified with a 3-form field strength. Black hole spacetimes of such theories are natural candidates to admit the Killing–Yano symmetry with torsion. This generalized symmetry was first introduced by Bochner and Yano [13] from the mathematical point of view and recently rediscovered [14–16] as a hidden symmetry of the Chong–Cvetic–Lü–Pope rotating black hole of $D = 5$ minimal gauged supergravity [17]. Furthermore, this was found in the Kerr–Sen black hole solution [18, 19] of effective string theory and its higher-dimensional generalizations [20]. The discovered generalized symmetry shears almost identical properties with its vacuum cousin; it gives rise symmetries that imply separability of the Hamilton–Jacobi, Klein-Gordon, and Dirac equations in this background [21].

2 Generalized Killing-Yano symmetries

We first recall some notations concerning a connection with totally skew-symmetric torsion. Let T_{abc} be a 3-form and ∇^T_a be a connection defined by

$$\nabla^T_a Y^b = \nabla_a Y^b + \frac{1}{2} T_{cab} Y^c \ , \tag{1}$$

where ∇_a is the Levi-Civita connection. The connection ∇^T_a satisfies a metricity condition $\nabla^T_a g_{bc} = 0$, and preserves the geodesics. For a p-form $\psi_{a_1 \cdots a_p}$ the covariant derivative is calculated as

$$\nabla^T_a \psi_{b_1 \cdots b_p} = \nabla_a \psi_{b_a \cdots b_p} + \frac{1}{2} T_{ca[b_1} \psi^c{}_{b_2 \cdots b_p]} \ . \tag{2}$$

We further define an exterior derivative d^T and a co-exterior derivative δ^T by

$$(d^T \psi)_{a_1 \cdots a_{p+1}} = \frac{1}{p!} \nabla^T_{[a_1} \psi_{a_2 \cdots a_{p+1}]} \ , \quad (\delta^T \psi)_{a_1 \cdots a_{p-1}} = -\nabla^{T\,c} \psi_{c a_1 \cdots a_{p-1}} \ . \tag{3}$$

[1]Email address: houri@sci.osaka-cu.ac.jp

A *generalized conformal Killing-Yano (GCKY) tensor* k was introduced as a p-form satisfying for any vector field X

$$\nabla^T_X k = \frac{1}{p+1} X \lrcorner d^T k - \frac{1}{D-p+1} X^* \wedge \delta^T k \ , \tag{4}$$

where $\lrcorner$ and $\wedge$ stand for an inner and a wedge product, respectively. A GCKY p-form f obeying $\delta^T f = 0$ is called a *generalized Killing-Yano (GKY) tensor*, and a GCKY p-form h obeying $d^T h = 0$ is called a *generalized closed conformal Killing-Yano (GCCKY) tensor*.

Proposition 2.1 *GCKY tensors possess the following basic properties:*

1. *A GCKY 1-form is equal to a conformal Killing 1-form.*
2. *The Hodge star $*$ maps GCKY p-forms into GCKY $(D-p)$-forms. In particular, the Hodge star of a GCCKY p-form is a GKY $(D-p)$-form and vice versa.*
3. *When h_1 and h_2 is a GCCKY p-form and q-form, then $h_3 = h_1 \wedge h_2$ is a GCCKY $(p+q)$-form.*
4. *Let k be a GCKY p-form for a metric g and a torsion 3-form T. Then, $\tilde{k} = \Omega^{p+1} k$ is a GCKY p-form for the metric $\tilde{g} = \Omega^2 g$ and the torsion $\tilde{T} = \Omega^2 T$.*
5. *Let k be a GCKY p-form. Then*

$$Q_{ab} \equiv k_{ac_1\cdots c_{p-1}} k_b{}^{c_1\cdots c_{p-1}} \tag{5}$$

is a rank-2 conformal Killing tensor. In particular, Q is a rank-2 Killing tensor if k is a GKY tensor.

We define a $2j$-form $h^{(j)}$ as $h^{(j)} = h \wedge h \wedge \cdots \wedge h$ where the wedge products are taken $j-1$ times such as $h^{(0)} = 1$, $h^{(1)} = h$, $h^{(2)} = h \wedge h$, $\cdots$. If we put the dimension $D = 2n + \varepsilon$, where $\varepsilon = 0$ for even dimensions and $\varepsilon = 1$ for odd dimensions, $h^{(j)}$ are non-trivial only for $j = 0, \cdots, n-1+\varepsilon$, i.e., $h^{(j)} = 0$ for $j > n - 1 + \varepsilon$. Since the wedge product of two GCCKY tensors is again a GCCKY tensor, $h^{(j)}$ are GCCKY tensors for all j. Moreover the Hodge dual of the GCCKY tensors $h^{(j)}$ gives rise to the GKY tensors $f^{(j)} = *h^{(j)}$. For odd dimensions, since $h^{(n)}$ is a rank-$2n$ GCCKY tensor, $f^{(n)}$ is a Killing vector. Given these GKY tensors $f^{(j)}$ $(j = 0, \ldots, n-1)$, one can construct the rank-2 Killing tensors

$$K^{(j)}_{ab} = \frac{1}{(D-2j-1)!(j!)^2} f^{(j)}_{ac_1\cdots c_{D-2j-1}} f^{(j)c_1\cdots c_{D-2j-1}}_b \ , \tag{6}$$

obeying the equation $\nabla_{(a} K^{(j)}_{bc)} = 0$, and

$$[K^{(j)}, K^{(\ell)}]^T_{abc} \equiv K^{(j)}_{e(a} \nabla^{Te} K^{(\ell)}_{bc)} - K^{(\ell)}_{ea} \nabla^{Te} K^{(j)}_{bc)} = 0 \ . \tag{7}$$

This means that the integrals of motion generated from Killing tensors don't commute with respect to Poisson bracket.

When the torsion is absent, it is shown that δh is a Killing vector. On the other hand, when the torsion is present, neither $\delta^T h$ nor δh are in general Killing vectors. Such a torsion anomaly appears everywhere in considering geometry with the GCCKY 2-form. For instance, it is seen in separability of field equations. Separation of variables in differential equations is deeply related to the existence of symmetry operators, which commute between themselves and whose number is that of dimensions. It is known that such symmetry operators can be generated by a CCKY 2-form in the absence of torsion. In the presence of torsion, however, the commutator between a symmetry operator generated by a Killing tensor and the laplacian don't vanish in general. This means that a GCCKY 2-form no longer generates symmetry operators for Klein-Gordon equation. Similarly, it is known that the GCCKY 2-form doesn't in general generates symmetry operators for Dirac equation, while it is possible for CCKY tensor.

2.1 Kerr–Sen Black Hole

Let us see an example of spacetimes admitting a GCCKY 2-form. Actually, it can be shown that $(2n+\varepsilon)$-dimensional metric

$$g = \sum_{\mu=1}^{n} \frac{U_\mu}{X_\mu} dx_\mu^2 + \sum_{\mu=1}^{n} \frac{X_\mu}{U_\mu} \left(\sum_{k=0}^{n-1} A_\mu^{(k)} d\psi_k - \sum_{\nu=1}^{n} \frac{N_\nu}{HU_\nu} \sum_{k=0}^{n-1} A_\nu^{(k)} d\psi_k \right)^2 + \varepsilon \frac{c}{A^{(n)}} \left(\sum_{k=0}^{n} A^{(k)} d\psi_k - \sum_{\nu=1}^{n} \frac{N_\nu}{HU_\nu} \sum_{k=0}^{n-1} A_\nu^{(k)} d\psi_k \right)^2 , \tag{8}$$

where c is a constant, admits a GCCKY 2-form h. It is convenient to introduce an orthonormal basis $\{e^\mu, e^{\hat{\mu}}, e^0\}$,

$$e^\mu = \sqrt{\frac{U_\mu}{X_\mu}} dx_\mu \ , \quad e^{\hat{\mu}} = \sqrt{\frac{X_\mu}{U_\mu}} \left(\sum_{k=0}^{n-1} A_\mu^{(k)} d\psi_k - \sum_{\nu=1}^{n} \frac{N_\nu}{HU_\nu} \sum_{k=0}^{n-1} A_\nu^{(k)} d\psi_k \right) ,$$
$$e^0 = \frac{c}{A^{(n)}} \left(\sum_{k=0}^{n} A^{(k)} d\psi_k - \sum_{\nu=1}^{n} \frac{N_\nu}{HU_\nu} \sum_{k=0}^{n-1} A_\nu^{(k)} d\psi_k \right) , \tag{9}$$

in which g, h and the torsion T are written as

$$g = \sum_{\mu=1}^{n} \left(e^\mu e^\mu + e^{\hat{\mu}} e^{\hat{\mu}} \right) + \varepsilon e^0 e^0 \ ,$$
$$h = \sum_{\mu=1}^{n} x_\mu \, e^\mu \wedge e^{\hat{\mu}} \ , \quad T = -\left(\sum_{\mu=1}^{n} \frac{\partial_\mu H}{H} \, e^\mu \wedge e^{\hat{\mu}} \right) \wedge \sum_{\nu=1}^{n} \sqrt{\frac{X_\nu}{U_\nu}} \, e^{\hat{\nu}} \ . \tag{10}$$

Here the metric functions are given as

$$U_\mu = \prod_{\nu \neq \mu} (x_\mu^2 - x_\nu^2) \ , \quad H = 1 + \sum_{\mu=1}^{n} \frac{N_\mu}{U_\mu} \ ,$$
$$A_\mu^{(k)} = \sum_{\substack{1 \le \nu_1 < \cdots < \nu_k \le n \\ \nu_i \neq \mu}} x_{\nu_1}^2 \cdots x_{\nu_k}^2 \ , \quad A^{(k)} = \sum_{1 \le \nu_1 < \cdots < \nu_k \le n} x_{\nu_1}^2 \cdots x_{\nu_k}^2 \ , \quad A_\mu^{(0)} = A^{(0)} = 1 \ , \tag{11}$$

and the functions X_μ and N_μ depend on the single variable x_μ: $X_\mu(x_\mu)$, $N_\mu(x_\mu)$.

In considering an effective theory of hetelotic supergravity,

$$S = \int e^\phi \Big(* R + * d\phi \wedge d\phi - * F \wedge F - \frac{1}{2} * H \wedge H \Big) \ , \tag{12}$$

where $F = dA$ and $H = dB - A \wedge dA$, the metric g and the 3-form field strength H identified with the torsion T are required to satisfy the equations of motion

$$R_{ab} - \nabla_a \nabla_b \phi - F_a{}^c F_{bc} - \frac{1}{4} H_a{}^{cd} H_{bcd} = 0 \ ,$$
$$d\Big(e^\phi * F \Big) = e^\phi * H \wedge F \ , \quad d\Big(e^\phi * H \Big) = 0 \ ,$$
$$(\nabla\phi)^2 + 2\nabla^2 \phi + \frac{1}{2} F_{ab} F^{ab} + \frac{1}{12} H_{abc} H^{abc} - R = 0 \ . \tag{13}$$

These equations determine the unknown functions X_μ and N_μ as

$$X_\mu = \sum_{k=0}^{n-1} c_k x_\mu^{2k} + 2m_\mu x_\mu^{1-\varepsilon} + \varepsilon \frac{(-1)^n \tilde{c}}{x_\mu^2} \ , \quad N_\mu = 2m_\mu x_\mu^{1-\varepsilon} s^2 \ , \tag{14}$$

where $s = \sinh\delta$, $c = \cosh\delta$, $c_{n-1} = -1$, and m_μ $(\mu = 1, \cdots, n)$, c_k $(k = 0, \cdots, n-2)$, $\tilde{c}$ and δ are arbitrary constants. In addition, the Maxwell potential A and the dilaton field ϕ become

$$A = \frac{c}{s}\sum_{\mu=1}^{n}\frac{N_\mu}{HU_\mu}\sum_{k=0}^{n-1}A_\mu^{(k)}d\psi_k \ , \quad \phi = \log H \ . \tag{15}$$

When we take the special choices of the constants, the solutions represent charged rotating black hole solutions including the Kerr-Sen black hole [18, 19] and its higher-dimensional generalizations [20]. The torsion anomalies vanish on these black hole spacetimes, and hence one can expect that integrable structures [22–25] are subject to a generalized Killing-Yano symmetry.

3 Conclusion

We have studied an extension of Killing-Yano symmetry in the presence of 3-form torsion. We have demonstrated that, when the torsion is an arbitrary 3-form, one obtains various torsion anomalies and the implications of the existence of the generalized Killing-Yano symmetry are relatively weak compared with ordinary Killing-Yano symmetry. However, in the spacetimes where there is a natural 3-form obeying the appropriate field equations, these anomalies disappear and the concept of generalized Killing-Yano symmetry may become very powerful.

References

[1] R. P. Kerr, *Gravitational field of a spinning mass as an example of algebraically special metrics*, *Phys. Rev. Lett.* **11** (1963) 237–238.

[2] K. Yano, *Some remarks on tensor fields and curvature*, *Ann. Math.* **55** (1952) 328–347.

[3] R. C. Myers and M. J. Perry, *Black holes in higher dimensional space-times*, *Ann. Phys. (N.Y.)* **172** (1986) 304–347.

[4] G. W. Gibbons, H. Lü, D. N. Page, and C. N. Pope, *Rotating black holes in higher dimensions with a cosmological constant*, *Phys. Rev. Lett.* **93** (2004) 171102, [hep-th/0409155].

[5] W. Chen, H. Lü, and C. N. Pope, *General Kerr-NUT-AdS metrics in all dimensions*, *Class. Quantum Grav.* **23** (2006) 5323–5340, [hep-th/0604125].

[6] D. Kubizňák and V. P. Frolov, *Hidden symmetry of higher dimensional Kerr-NUT-AdS spacetimes*, *Class. Quantum Grav.* **24** (2007) F1–F6, [gr-qc/0610144].

[7] D. N. Page, D. Kubizňák, M. Vasudevan, and P. Krtouš, *Complete integrability of geodesic motion in general higher-dimensional rotating black hole spacetimes*, *Phys. Rev. Lett.* **98** (2007) 061102, [hep-th/0611083].

[8] P. Krtouš, D. Kubizňák, D. N. Page, and V. P. Frolov, *Killing-Yano tensors, rank-2 Killing tensors, and conserved quantities in higher dimensions*, *J. High Energy Phys.* **02** (2007) 004, [hep-th/0612029].

[9] T. Houri, T. Oota, and Y. Yasui, *Closed conformal Killing-Yano tensor and geodesic integrability*, *J. Phys.* **A41** (2008) 025204, [arXiv:0707.4039].

[10] V. P. Frolov, P. Krtouš, and D. Kubizňák, *Separability of Hamilton-Jacobi and Klein-Gordon equations in general Kerr-NUT-AdS spacetimes*, *J. High Energy Phys.* **02** (2007) 005, [hep-th/0611245].

[11] A. Sergyeyev and P. Krtouš, *Complete Set of Commuting Symmetry Operators for the Klein-Gordon Equation in Generalized Higher-Dimensional Kerr-NUT-(A)dS Spacetimes*, *Phys. Rev.* **D77** (2008) 044033, [arXiv:0711.4623].

[12] T. Oota and Y. Yasui, *Separability of Dirac equation in higher dimensional Kerr- NUT-de Sitter spacetime*, *Phys. Lett.* **B659** (2008) 688–693, [arXiv:0711.0078].

[13] K. Yano and S. Bochner, *Curvature and Betti numbers.* Annals of Mathematics Studies, no. 32., Princeton University Press, Princeton, USA, 1953.

[14] S.-Q. Wu, *Separability of a modified Dirac equation in a five- dimensional rotating, charged black hole in string theory*, *Phys. Rev.* **D80** (2009) 044037, [arXiv:0902.2823].

[15] D. Kubiznak, H. Kunduri, and Y. Yasui, *Generalized Killing-Yano equations in D=5 gauged supergravity*, *Phys. Lett.* **B678** (2009) 240–245, [arXiv:0905.0722].

[16] S.-Q. Wu, *Separability of massive field equations for spin-0 and spin-1/2 charged particles in the general non-extremal rotating charged black holes in minimal five-dimensional gauged supergravity*, *Phys. Rev.* **D80** (2009) 084009, [arXiv:0906.2049].

[17] Z. W. Chong, M. Cvetic, H. Lu, and C. N. Pope, *General non-extremal rotating black holes in minimal five- dimensional gauged supergravity*, *Phys. Rev. Lett.* **95** (2005) 161301, [hep-th/0506029].

[18] A. Sen, *Rotating charged black hole solution in heterotic string theory*, *Phys. Rev. Lett.* **69** (1992) 1006–1009, [hep-th/9204046].

[19] S. F. Hassan and A. Sen, *Twisting classical solutions in heterotic string theory*, *Nucl. Phys.* **B375** (1992) 103–118, [hep-th/9109038].

[20] D. D. K. Chow, *Symmetries of supergravity black holes*, arXiv:0811.1264.

[21] T. Houri, D. Kubiznak, C. Warnick, and Y. Yasui, *Symmetries of the Dirac operator with skew-symmetric torsion*, arXiv:1002.3616.

[22] A. Burinskii, *Some properties of the Kerr solution to low-energy string theory*, *Phys. Rev.* **D52** (1995) 5826–5831, [hep-th/9504139].

[23] T. Okai, *Global structure and thermodynamic property of the four- dimensional twisted Kerr solution*, *Prog. Theor. Phys.* **92** (1994) 47–66, [hep-th/9402149].

[24] P. A. Blaga and C. Blaga, *Bounded radial geodesics around a Kerr–Sen black hole*, *Class. Quantum Grav.* **18** (2001) 3893–3905.

[25] K. Hioki and U. Miyamoto, *Hidden symmetries, null geodesics, and photon capture in Sen black hole*, *Phys. Rev.* **D78** (2008) 044007, [arXiv:0805.3146].

A General Dark Energy Model

Changyu Huang[1](a,b), Qing Zhang[2](a) and Yong-Chang Huang[3](a,c)

(a) *Institute of Theoretical Physics, Beijing University of Technology, Beijing, 100124, China*
(b) *Institute of Theoretical Physics, Chinese Academy of Sciences, Beijing, 100190, China*
(c) *CCAST (World Lab.), P.O.Box 8730, Beijing, 100080, China*

Abstract

This Letter generally deduces a general dark energy model in Einstein's special relativity, which just shows a general dark energy may generally exist not being necessary in general relativity.

1 Introduction

Special Relativity is, built up by Einstein, a kind of special spacetime theory [1]. It overcomes the difficulties relative to Galilean transformation ((i) the equations of electromagnetic fields do not obey the Galilean transformation; (ii) the speed of light c is a constant —— the results of Michelson - Morley experiment; (iii) Particles move with high-speed), it generalized Lorentz invariant property of the equations of electromagnetic fields to the situation of mechanics. In addition, it expanded and modified Newtonian spacetime, thus Einstein gave the creation of a new era of Einstein's space-time theory. Beside, Poincare etc, had some contributions to the modern theory of special relativity [2]. Newtonian mechanics is the case of special relativity in the low-speed approximation.

2 A general dark energy model

For convenience of discussion, we first review some main relative results to be used in this Letter, then generally deduce a general dark energy model in Einstein's special relativity. Using proper time $d\tau = dt\sqrt{1-v^2/c^2}$ ($v = \frac{dl}{dt}$ ($l^2 = \Delta\mathbf{x}\cdot\Delta\mathbf{x}$) is the velocity of the object in the reference frame) and generalizing the speed to four dimensions, we may set up the Four-velocity

$$u_\alpha = \frac{dx_\alpha}{d\tau} = \frac{1}{\sqrt{1-v^2/c^2}}\frac{dx_\alpha}{dt} = \frac{v_\alpha}{\sqrt{1-v^2/c^2}},\ \alpha = 0,1,2,3. \tag{1}$$

Utilizing the invariance of the interval $\triangle x^0\triangle x_0+\triangle x^1\triangle x_1+\triangle x^2\triangle x_2+\triangle x^3\triangle x_3=c^2\triangle\tau\triangle\tau$, then we have $u^0u_0+u^1u_1+u^2u_2+u^3u_3=c^2=\eta^{\mu\nu}u_\mu u_\nu$. Therefore, we obtain

$$2\eta^{\mu\nu}u_\mu\frac{du_\nu}{d\tau}=2u_\mu\frac{du^\mu}{d\tau}=0. \tag{2}$$

Eq.(2) shows that the relation of 4-vector u_μ and $du^\mu/d\tau$ is vertical.
With Eq.(1), we define the four-momentum as

$$p_\alpha=m_0u_\alpha=m_0dx_\alpha/d\tau,\ \alpha=0,1,2,3. \tag{3}$$

Then the fourth component of the four-momentum is

$$p_4=m_0u_4=m_0ic/\sqrt{1-\beta^2}, \tag{4}$$

[1]Email address: cyhuang520@hotmail.com
[2]Email address: qingzhang@emails.bjut.edu.cn
[3]Email address: ychuang@bjut.edu.cn

the space component of the four-momentum is

$$p_i=\frac{m_0}{\sqrt{1-v^2/c^2}}\frac{dx_i}{dt}=mv_i,\ (m=m_0/\sqrt{1-\frac{v^2}{c^2}}). \tag{5}$$

In the equations of the special relativity, for an object acted by four-force K_μ, and considering Eq.(3), we have

$$K_\mu=\frac{dp_\mu}{d\tau}=m_0\frac{du_\mu}{d\tau}, \tag{6}$$

multipling Eq.(2) with m_0 , we achieve

$$u_\mu m_0 du^\mu/d\tau=u_\mu K^\mu=0, \tag{7}$$

Eq. (7) shows that 4-vector u_μ is vertical to K^μ. With Eq.(6), we have

$$K_i=\frac{dp_i}{d\tau}=\frac{1}{\sqrt{1-\frac{v^2}{c^2}}}\frac{d(mv_i)}{dt}=\frac{1}{\sqrt{1-\frac{v^2}{c^2}}}F_i. \tag{8}$$

The forth component of four-force is

$$K_4=\frac{dp_4}{d\tau}=m_0\frac{d\mu_4}{d\tau}. \tag{9}$$

Substituting Eq.(8) and (9) into (7), we obtain

$$u_4K^4+u_iK^i=u_4\frac{dp^4}{d\tau}+u_i\frac{1}{\sqrt{1-\frac{v^2}{c^2}}}F^i=0. \tag{10}$$

Then, we have

$$\frac{dp^4}{d\tau}=\frac{i}{c\sqrt{1-\frac{v^2}{c^2}}}v_iF^i, \tag{11}$$

$\mathbf{v}\cdot\mathbf{F}$ is the power of the force $\mathbf{F}$, and the power is equal to the rate of increase of energy with time, i.e., $\frac{dE}{dt}$, thus we have

$$\frac{dp^4}{d\tau}=\frac{i}{c\sqrt{1-\frac{v^2}{c^2}}}\frac{dE}{dt}=\frac{i}{c}\frac{dE}{d\tau}. \tag{12}$$

Therefore, we obtain

$$\frac{dp_4}{d\tau}=\frac{i}{c}\frac{dE}{d\tau}. \tag{13}$$

Then, we achieve

$$p_4=\frac{i}{c}E+C_{01}, \tag{14}$$

where C_{01} is an integral constant, satisfies $\frac{C_{01}}{d\tau}=0$. It means that C_{01} is independent of the proper time or time. Therefore, C_{01} has a clear physical significance, which is relative to dark energy, cosmological constant and zero-point energy in quantum field theory. When neglecting C_{01}, it reduces to Einstein's theory of special relativity. Thus, using Eq.(4) we obtain

$$p_4=\frac{i}{c}E+C_{01}=\frac{m_0ic}{\sqrt{1-\beta^2}}. \tag{15}$$

Thus, we achieve a general energy

$$E=m_0c^2/\sqrt{1-\beta^2}+E_{01}=mc^2+E_{01}, \tag{16}$$

where $E_{01}=icC_{01}$ is a general invariant energy as a general dark energy, because its dimension is energy. In particular, it is just the dark energy that causes the accelerating expansion of the universe or relative to cosmological constant and so on, and which is determined by the relative cosmological experimental data.

3 Discussion and conclusion

When neglecting E_{01} , Eq.(16) reduces to the Einstein's Mass-Energy relation $E{=}m_0c^2/\sqrt{1{-}\beta^2}{=}mc^2$, which is another way to deduce the Einstein's Mass-Energy relation. It means that the achieved theory is consistent. $E{=}mc^2$ means that any matter has the great power, which predicts the existence of matter energy. Any rest object has a great rest energy $E_0{=}m_0c^2$. Combining Eqs. (8) and (12), we have $K_\mu{=}(\mathbf{K},i\mathbf{K}{\cdot}\mathbf{v}/c)$. If v changed, then $\dot{v}{\neq}0$, it is a non-inertial reference frame. In fact, the $\mathbf{F}{=}m\mathbf{a}$ is equivalent to $\mathbf{F}{=}d\mathbf{p}/dt$ in Newtonian physics. In the discussion above, we find that the former is not suitable for generalizing, becuase the property of m and $\mathbf{a}$ is not well defined. While the latter is a well defined vector, once we replace dt with $d\tau$, and generalize the 3-momentum to 4-momentum, it is just the relation between 4-force and 4-acceleration, which looks like the Newton's second law in four dimensional expression.

Therefore, we generally deduces a general dark energy model in Einstein's special relativity, which just shows that a general dark energy may generally exist, which is not necessary to exist in general relativity.

Acknowledgment: The work is partly supported by National Natural Science Foundation of China (Grant No. 10435080) and Beijing Natural Science Foundation (Grant No. 1072005).

References

[1] W. G. Dixon, W. Graham, Special relativity: the foundation of macroscopic physics, Cambridge University Press (1978).

[2] W. Rindler, Relativity: special, general, and cosmological, New York, Oxford University Press (2006).

Renormalization Group Flow and the Dark Energy Problem

Shoichi Ichinose[1]

Laboratory of Physics, School of Food and Nutritional Sciences, University of Shizuoka
Shizuoka 422-8526, Japan

Abstract

Casimir energy is calculated for 5D scalar theory in the *warped* geometry. A new regularization, called *sphere lattice regularization*, is taken. The regularized configuration is *closed-string like*. We numerically evaluate Λ(4D UV-cutoff), ω(5D bulk curvature, extra space UV-boundary parameter) and T(extra space IR-boundary parameter) dependence of Casimir energy. 5D Casimir energy is *finitely* obtained after the *proper renormalization procedure*. The *warp parameter* ω suffers from the *renormalization effect*. Regarding Casimir energy as the main contribution to the cosmological term, we examine the dark energy problem.

1. Introduction In the quest for the unified theory, the higher dimensional (HD) approach is a fascinating one from the geometrical point. Historically the initial successful one is the Kaluza-Klein model, which unifies the photon, graviton and dilaton from the 5D space-time approach. The HD theories , however, generally have the serious defect as the quantum field theory(QFT) : un-renormalizability. The HD quantum field theories, at present, are not defined within the QFT.

In 1983, the Casimir energy in the Kaluza-Klein theory was calculated by Appelquist and Chodos[1]. They took the cut-off (Λ) regularization and found the quintic (Λ^5) divergence and the finite term. The divergent term shows the *unrenormalizability* of the 5D theory, but the finite term looks meaningful[2] and, in fact, is widely regarded as the right vacuum energy which shows *contraction* of the extra axis.

In the development of the string and D-brane theories, a new approach to the renormalization group was found. It is called *holographic renormalization*. We regard the renormalization group flow as a curve in the bulk. The flow goes along the extra axis. The curve is derived as a dynamical equation such as Hamilton-Jacobi equation. It originated from the AdS/CFT correspondence. Spiritually the present basic idea overlaps with this approach.

2. Casimir Energy of 5D Scalar Theory In the warped geometry, $ds^2 = \frac{1}{\omega^2 z^2}(\eta_{\mu\nu}dx^\mu dx^\nu + dz^2)$, we consider the 5D massive *scalar* theory with $m^2 = -4\omega^2$ (< 0). $\mathcal{L} = \sqrt{-G}(-\frac{1}{2}\nabla^A\Phi\nabla_A\Phi - \frac{1}{2}m^2\Phi^2)$. The Casimir energy E_{Cas} is given by

$$\mathrm{e}^{-T^{-4}E_{Cas}} = \int \mathcal{D}\Phi \exp\{i\int d^5X\mathcal{L}\}\Big|_{\text{Euclid}} = \exp\sum_{n,p}\{-\frac{1}{2}\ln(p_E^2 + M_n^2)\},\ p_E^2 \equiv p_1^2+p_2^2+p_3^2+p_4^2, \quad (1)$$

where M_n is the eigenvalues of the following operator.

$$\{s(z)^{-1}\hat{L}_z + {M_n}^2\}\psi_n(z) = 0 \quad , \quad \hat{L}_z \equiv \frac{d}{dz}\frac{1}{(\omega z)^3}\frac{d}{dz} - \frac{m^2}{(\omega z)^5} \quad , \quad (2)$$

where $s(z) = \frac{1}{(\omega z)^3}$. Z_2 parity is imposed as: $\psi_n(z) = -\psi_n(-z)$ for $P = -$; $\psi_n(z) = \psi_n(-z)$ for $P = +$. The expression (1) is the familiar one of the Casimir energy. It is re-expressed in a *closed* form using the heat-kernel method and the propagator as follows. First we can express it, using the heat equation solution, as ($\omega/T = \mathrm{e}^{\omega l}$, l is the periodicity in y-coordinate: $y \to y + 2l, \omega|z| = \mathrm{e}^{\omega|y|}$),

$$\mathrm{e}^{-T^{-4}E_{Cas}} = (\text{const}) \times \exp\left[T^{-4}\int\frac{d^4p}{(2\pi)^4}2\int_0^\infty \frac{1}{2}\frac{dt}{t}\mathrm{Tr}\ H_p(z,z';t)\right] \quad ,$$

$$\mathrm{Tr}\ H_p(z,z';t) = \int_{1/\omega}^{1/T} s(z)H_p(z,z;t)dz \quad , \quad \{\frac{\partial}{\partial t} - (s^{-1}\hat{L}_z - p^2)\}H_p(z,z';t) = 0 \quad . \quad (3)$$

[1]Email address: ichinose@u-shizuoka-ken.ac.jp

The heat kernel $H_p(z,z';t)$ is formally solved, using the Dirac's bra and ket vectors $(z|, |z)$, as $H_p(z,z';t) = (z|\mathrm{e}^{-(-s^{-1}\hat{L}_z+p^2)t}|z')$. We here introduce the position/momentum propagators $G_p^{\mp}$: $G_p^{\mp}(z,z') \equiv \int_0^\infty dt\, H_p(z,z';t)$. They satisfy the following differential equations of *propagators*.

$$(\hat{L}_z - p^2 s(z))G_p^{\mp}(z,z') = \begin{cases} \epsilon(z)\epsilon(z')\hat{\delta}(|z|-|z'|) & \mathrm{P}=-1 \\ \hat{\delta}(|z|-|z'|) & \mathrm{P}=1 \end{cases}, \quad p^2 = p_\mu p^\mu = -p_0^2 + p_1^2 + p_2^2 + p_3^2 \tag{4}$$

$G_p^{\mp}$ can be expressed in a *closed* form. Taking the *Dirichlet* condition at all fixed points, the expression for the fundamental region $(1/\omega \le z \le z' \le 1/T)$ is given by

$$G_p^{\mp}(z,z') = \mp\frac{\omega^3}{2} z^2 z'^2 \frac{\{\mathbf{I}_0(\frac{\tilde{p}}{\omega})\mathbf{K}_0(\tilde{p}z) \mp \mathbf{K}_0(\frac{\tilde{p}}{\omega})\mathbf{I}_0(\tilde{p}z)\}\{\mathbf{I}_0(\frac{\tilde{p}}{T})\mathbf{K}_0(\tilde{p}z') \mp \mathbf{K}_0(\frac{\tilde{p}}{T})\mathbf{I}_0(\tilde{p}z')\}}{\mathbf{I}_0(\frac{\tilde{p}}{T})\mathbf{K}_0(\frac{\tilde{p}}{\omega}) - \mathbf{K}_0(\frac{\tilde{p}}{T})\mathbf{I}_0(\frac{\tilde{p}}{\omega})}, \tag{5}$$

where $\tilde{p} \equiv \sqrt{p^2}, p^2 \ge 0$. I_0 and K_0 are modified Bessel functions. We can express Casimir energy as,

$$-E_{Cas}^{\Lambda,\mp}(\omega,T) = \int \frac{d^4p_E}{(2\pi)^4}\Big|_{\tilde{p}\le\Lambda} \int_{1/\omega}^{1/T} dz\; F^{\mp}(\tilde{p},z), F^{\mp}(\tilde{p},z) = \frac{2}{(\omega z)^3}\int_{\tilde{p}}^{\Lambda} \tilde{k}\; G_k^{\mp}(z,z)d\tilde{k}, \tag{6}$$

where $\tilde{p} = \sqrt{p_E^2}$. The momentum symbol p_E indicates Euclideanization. Here we introduce the UV cut-off parameter Λ in the 4D momentum space.

3. UV and IR Regularization and Evaluation of Casimir Energy The integral region of the above equation (6) is displayed, in Fig.1, as a rectangle. In the figure, we introduce the regularization cut-offs for the 4D-momentum integral, $\mu \le \tilde{p} \le \Lambda$. For simplicity, we take the following IR cutoff of 4D momentum : $\mu = \Lambda \cdot \frac{T}{\omega} = \Lambda \mathrm{e}^{-\omega l}$.

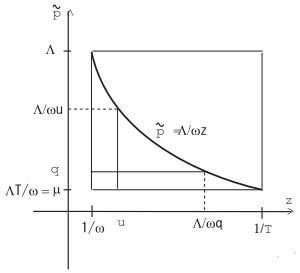

Fig.1 Rectangle region of (z,$\tilde{p}$) for the integration (6). The hyperbolic curve was proposed[3].

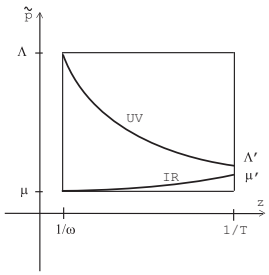

Fig.2 Region of ($\tilde{p}$,z) for the integration (present proposal).

Importantly, (6) shows the *scaling* behavior for large values of Λ and $1/T$. From a *close* numerical analysis, we have confirmed : (4A) $E_{Cas}^{\Lambda,-}(\omega,T) = \frac{2\pi^2}{(2\pi)^4} \times \left[-0.0250\frac{\Lambda^5}{T}\right]$. The Λ^5-divergence, (4A), shows the notorious problem of the higher dimensional theories. We have proposed an approach to solve this problem and given a legitimate explanation within the 5D QFT[4, 5]. See Fig.2. The IR and UV cutoffs *change* along the etra axis. Their S^3-radii are given by $r_{IR}(z) = 1/\tilde{p}_{IR}(z)$ and $r_{UV}(z) = 1/\tilde{p}_{UV}(z)$. The 5D volume region bounded by B_{UV} and B_{IR} is the integral region of the Casimir energy E_{Cas}. (We call this regularization *sphere lattice regularization* because one big 4D-ball (radius r_{IR}) are made of many small 4D-balls (cells, radius r_{UV}). See Fig.12 of Ref.[6]) The forms of $r_{UV}(z)$ and $r_{IR}(z)$ can be determined by the *minimal area principle*: $3 + \frac{4}{z}r'r - \frac{r''r}{r'^2+1} = 0, r' \equiv \frac{dr}{dz}, r'' \equiv \frac{d^2r}{dz^2}, 1/\omega \le z \le 1/T$. We have confirmed, by *numerically* solving the above differential eqation (Runge-Kutta), those curves that show the flow of renormalization really appear. The results imply the *boundary conditions* determine the property of the renormalization flow.

4. Weight Function and the Meaning We consider another approach which respects the *minimal area principle*. Let us introduce, instead of restricting the integral region, a *weight function* $W(\tilde{p},z)$ in

the $(\tilde{p}, z)$-space for the purpose of *suppressing* UV and IR divergences of the Casimir Energy.

$$-E_{Cas}^{\mp\, W}(\omega, T) \equiv \int \frac{d^4 p_E}{(2\pi)^4} \int_{1/\omega}^{1/T} dz\ W(\tilde{p}, z) F^{\mp}(\tilde{p}, z) \quad , \quad \tilde{p} = \sqrt{p_4^2 + p_1^2 + p_2^2 + p_3^2} \quad ,$$

$$\begin{cases} (N_1)^{-1} \mathrm{e}^{-(1/2)\tilde{p}^2/\omega^2 - (1/2) z^2 T^2} \equiv W_1(\tilde{p}, z),\ N_1 = 1.711/8\pi^2 & \text{elliptic suppr.} \\ (N_2)^{-1} \mathrm{e}^{-\tilde{p} z T/\omega} \equiv W_2(\tilde{p}, z),\ N_2 = 2\frac{\omega^3}{T^3}/8\pi^2 & \text{hyperbolic suppr.1} \\ (N_8)^{-1} \mathrm{e}^{-1/2(\tilde{p}^2/\omega^2 + 1/z^2 T^2)} \equiv W_8(\tilde{p}, z),\ N_8 = 0.4177/8\pi^2 & \text{reciprocal suppr.1} \end{cases} \tag{7}$$

where $F^{\mp}(\tilde{p}, z)$ are defined in (6). They (except W_2) give, after normalizing the factor Λ/T, *only* the *log-divergence*.

$$E_{Cas}^{W}/\Lambda T^{-1} = -\alpha\omega^4 \left(1 - 4c \ln(\Lambda/\omega) - 4c' \ln(\Lambda/T)\right) \quad , \tag{8}$$

where the numerical values of α, c and c' are obtained depending on the choice of the weight function[6]. This means the 5D Casimir energy is *finitely* obtained by the ordinary renormalization of the warp factor ω. (See the final section.)

In the previous work[5], we have presented the following idea to define the weight function $W(\tilde{p}, z)$. In the evaluation (7), the $(\tilde{p}, z)$-integral is over the rectangle region shown in Fig.1 (with $\Lambda \to \infty$ and $\mu \to 0$). Following Feynman[7], we can replace the integral by the *summation* over *all possible pathes* $\tilde{p}(z)$.

$$-E_{Cas}^{W}(\omega, T) = \int \mathcal{D}\tilde{p}(z) \int_{1/\omega}^{1/T} dz\ S[\tilde{p}(z), z], S[\tilde{p}(z), z] = \frac{2\pi^2}{(2\pi)^4} \tilde{p}(z)^3 W(\tilde{p}(z), z) F^{\mp}(\tilde{p}(z), z). \tag{9}$$

There exists the *dominant path* $\tilde{p}_W(z)$ which is determined by the minimal principle : $\delta S = 0$. Dominant Path $\tilde{p}_W(z)$: $\frac{d\tilde{p}}{dz} = -\frac{\partial \ln(WF)}{\partial z} / \left(\frac{3}{\tilde{p}} + \frac{\partial \ln(WF)}{\partial \tilde{p}}\right)$. Hence it is fixed by the weight function $W(\tilde{p}, z)$. On the other hand, there exists another independent path: the minimal surface curve $r_g(z)$. Minimal Surface Curve $r_g(z)$: $3 + \frac{4}{z} r' r - \frac{r'' r}{r'^2 + 1} = 0$, $\frac{1}{\omega} \le z \le \frac{1}{T}$. It is obtained by the *minimal area principle*: $\delta A = 0$ where

$$ds^2 = (\delta_{ab} + \frac{x^a x^b}{(r r')^2}) \frac{dx^a dx^b}{\omega^2 z^2} \equiv g_{ab}(x) dx^a dx^b, A = \int \sqrt{g}\ d^4 x = \int_{1/\omega}^{1/T} \frac{\sqrt{r'^2 + 1}\ r^3}{\omega^4 z^4} dz. \tag{10}$$

Hence $r_g(z)$ is fixed by the *induced geometry* $g_{ab}(x)$. Here we put the *requirement*[5]: (4A) $\tilde{p}_W(z) = \tilde{p}_g(z)$, where $\tilde{p}_g \equiv 1/r_g$. This means the following things. We *require* the dominant path coincides with the minimal surface line $\tilde{p}_g(z) = 1/r_g(z)$ which is defined independently of $W(\tilde{p}, z)$. $W(\tilde{p}, z)$ is defined here by the induced geometry $g_{ab}(x)$. In this way, we can connect the integral-measure over the 5D-space with the geometry. We have confirmed the coincidence by the numerical method.

In order to most naturally accomplish the above requirement, we can go to a *new step*. Namely, we *propose* to *replace* the 5D space integral with the weight W, (7), by the following *path-integral*. We *newly define* the Casimir energy in the higher-dimensional theory as follows.

$$-\mathcal{E}_{Cas}(\omega, T, \Lambda) = \int_{1/\Lambda}^{1/\mu} d\rho \int \begin{matrix} r(\omega^{-1}) \\ = r(T^{-1}) \\ = \rho \end{matrix} \prod_{a,z} \mathcal{D}x^a(z) F(\frac{1}{r}, z) \exp\left[-\int_{1/\omega}^{1/T} \frac{\sqrt{r'^2 + 1}\ r^3}{2\alpha' \omega^4 z^4} dz\right], \tag{11}$$

where $\mu = \Lambda T/\omega$ and the limit $\Lambda T^{-1} \to \infty$ is taken. The string (surface) tension parameter $1/2\alpha'$ is introduced. (Note: Dimension of α' is [Length]^4.) $F(\tilde{p}, z)$ is defined in (6) and represents the contribution from the *field-quantization* of the bulk scalar (or EM) fields. (This proposal is shown to be valid in arXiv:1004.2573, 1010.5558.)

5. Discussion and Conclusion When c and c' in (8) are sufficiently small we find the renormalization group function for the warp factor ω as

$$\omega_r = \omega(1 - c \ln(\Lambda/\omega) - c' \ln(\Lambda/T)) \ , \ \beta \equiv \frac{\partial}{\partial(\ln \Lambda)} \ln \frac{\omega_r}{\omega} = -c - c' \quad . \tag{12}$$

No local counterterms are necessary.

Through the Casimir energy calculation, in the higher dimension, we find a way to quantize the higher dimensional theories within the QFT framework. The quantization *with respect to the fields* (except the gravitational fields $G_{AB}(X)$) is done in the standard way. After this step, the expression has the summation *over the 5D space(-time) coordinates or momenta* $\int dz \prod_a dp^a$. We have proposed that this summation should be replaced by the *path-integral* $\int \prod_{a,z} \mathcal{D}p^a(z)$ with the *area* action (Hamiltonian) $A = \int \sqrt{\det g_{ab}}\ d^4x$ where g_{ab} is the *induced* metric on the 4D surface. This procedure says the 4D momenta p^a (or coordinates x^a) are *quantum statistical* operators and the extra-coordinate z is the inverse temperature (Euclidean time). We recall the similar situation occurs in the standard string approach. The space-time coordinates obey some uncertainty principle[8].

Recently the dark energy (as well as the dark matter) in the universe is a hot subject. It is well-known that the dominant candidate is the cosmological term. The cosmological constant λ appears as: (5A) $R_{\mu\nu} - \frac{1}{2}g_{\mu\nu}R - \lambda g_{\mu\nu} = T_{\mu\nu}^{matter}, S = \int d^4x\sqrt{-g}\{\frac{1}{G_N}(R+\lambda)\} + \int d^4x\sqrt{-g}\{\mathcal{L}_{matter}\}, g = \det\ g_{\mu\nu}$. We consider here the 3+1 dim Lorentzian space-time ($\mu,\nu = 0,1,2,3$). The constant λ observationally takes the value : (5B) $\frac{1}{G_N}\lambda_{obs} \sim \frac{1}{G_N {R_{cos}}^2} \sim m_\nu^4 \sim (10^{-3}eV)^4, \lambda_{obs} \sim \frac{1}{R_{cos}^2} \sim 4\times 10^{-66}(eV)^2$, where $R_{cos} \sim 5\times 10^{32}\mathrm{eV}^{-1}$ is the cosmological size (Hubble length), m_ν is the neutrino mass. On the other hand, we have theoretically so far : (5C) $\frac{1}{G_N}\lambda_{th} \sim \frac{1}{{G_N}^2} = {M_{pl}}^4 \sim (10^{28}eV)^4$. We have the famous huge discrepancy factor : (5D) $\frac{\lambda_{th}}{\lambda_{obs}} \sim N_{DL}^2, N_{DL} \equiv M_{pl}R_{cos} \sim 6\times 10^{60}$, where N_{DL} is here introduced as the Dirac's large number. If we use the present result, we can obtain a natural choice of T, ω and Λ as follows. By identifying $T^{-4}E_{Cas} = -\alpha_1 \Lambda T^{-1}\omega^4/T^4$ with $\int d^4x\sqrt{-g}(1/G_N)\lambda_{ob} = R_{cos}^2(1/G_N)$, we obtain the following relation: (5E) $N_{DL}^2 = R_{cos}^2\frac{1}{G_N} = -\alpha_1\frac{\omega^4\Lambda}{T^5}$. The warped ($\mathrm{AdS}_5$) model predicts the cosmological constant *negative*, hence we have interest only in its absolute value. We take the following choice for Λ and ω : (5F) $\Lambda = M_{pl} \sim 10^{19}GeV, \omega \sim \frac{1}{\sqrt[4]{G_N {R_{cos}}^2}} = \sqrt{\frac{M_{pl}}{R_{cos}}} \sim m_\nu \sim 10^{-3}\mathrm{eV}$.

As shown above, we have the standpoint that the cosmological constant is mainly made from the Casimir energy. We do not yet succeed in obtaining the value α_1 negatively, but succeed in obtaining the finiteness of the cosmological constant and its gross absolute value. The smallness of the value is naturally explained by the renormalization group flow. Because we already know the warp parameter ω *flows* (12), the $\lambda_{obs} \sim 1/R_{cos}^2 \propto \omega^4$, says that the *smallness of the cosmological constant comes from the renormalization group flow* for the non asymptotic-free case ($c + c' < 0$ in (12)).

The IR parameter T, the normalization factor Λ/T in (8) and the IR cutoff $\mu = \Lambda\frac{T}{\omega}$ are given by : (5G) $T = R_{cos}^{-1}(N_{DL})^{1/5} \sim 10^{-20}eV, \frac{\Lambda}{T} = (N_{DL})^{4/5} \sim 10^{50}, \mu = M_{pl}N_{DL}^{-3/10} \sim 1GeV \sim m_N$, where m_N is the nucleon mass. The degree of freedom of the universe (space-time) is given by : (5H) $\frac{\Lambda^4}{\mu^4} = \frac{\omega^4}{T^4} = N_{DL}^{6/5} \sim 10^{74} \sim (\frac{M_{pl}}{m_N})^4$.

References

[1] T. Appelquist and A. Chodos, Phys.Rev.Lett.**50**(1983)141

[2] S. Ichinose, Phys.Lett.**152B**(1985),56

[3] L. Randall and M.D. Schwartz, *JHEP* **0111** (2001) 003, hep-th/0108114

[4] S. Ichinose and A. Murayama, Phys.Rev.**D76**(2007)065008, hep-th/0703228

[5] S. Ichinose, Prog.Theor.Phys.**121**(2009)727, ArXiv:0801.3064v8[hep-th]

[6] S. Ichinose, ArXiv:0812.1263[hep-th]

[7] R.P. Feynman, *Statistical Mechanics*, W.A.Benjamin,Inc., Massachusetts, 1972

[8] T. Yoneya, Prog.Theor.Phys.**103**(2000)1081

Stable Bound Orbits around Black Rings

Takahisa Igata[1], Hideki Ishihara[2] and Yohsuke Takamori[3]

Department of Mathematics and Physics,
Graduate School of Science, Osaka City University, Osaka 558-8585, Japan

Abstract

We study stable bound orbits of a free particle around a black ring. Unlike the higher-dimensional black hole case, we find that there exist stable bound orbits in toroidal spiral shape near the black ring axis and stable circular orbits on the axis. However, a range of thickness parameter of the black ring solution which has the stable bound orbits has a upper bound at a critical value. The critical thickness value is determined analytically as the degenerate point of the innermost and outermost stable bound orbit on the ring axis.

In higher dimensions, there is a wide variety of black hole solutions in contrast to four dimensions. In the framework of the vacuum Einstein gravity, in addition to a generalization of the Kerr metric derived by Myers and Perry in [2], we have the metrics of the black object solutions with various topology of event horizon [3]. Indeed, Emparan and Reall found the five-dimensional black ring solution which has horizon topology $S^2 \times S^1$ in [4]. The existence of the black ring solution shows multiplicity of higher-dimensional black objects. Namely, the black hole uniqueness theorem does not hold in higher-dimensional spacetime as the same form in the case of four-dimensional black hole.

Among many ways of investigating black objects, the study of a free particle motion is a basic approach to understanding physical features of black objects. In recent years, free particle motion in the black ring geometry is studied by several authors [5]. In particular, Hoskisson has investigated extensively geodesics in the black ring geometry in [6]. He has shown that the separation of variable of the Hamilton-Jacobi equation for geodesics does not occur in the ring coordinates.

In this report, we then will focus on existence of stable bound orbits around a black ring. It is worth pointing out that there is no stable bound circular orbit in the higher-dimensional Schwarzschild solution. In contrast, we show that there exist stable bound orbits far from a black ring. The difference of geometry between a black hole and a black ring is clearly distinguishable by geodesic motions.

We begin by giving the geometry of the black ring. The metric is written in the form

$$\begin{aligned} ds^2 &= -\frac{F(y)}{F(x)}\left(dt - CR\frac{1+y}{F(y)}d\psi\right)^2 \\ &\quad + \frac{R^2}{(x-y)^2}F(x)\left(-\frac{G(y)}{F(y)}d\psi^2 - \frac{dy^2}{G(y)} + \frac{dx^2}{G(x)} + \frac{G(x)}{F(x)}d\phi^2\right), \end{aligned} \tag{1}$$

with the range of the ring coordinates $-1 < x < 1$, $-\infty < y < -1$, where

$$F(\xi) = 1 + \lambda\xi, \quad G(\xi) = (1-\xi^2)(1+\nu\xi), \quad C = \sqrt{\lambda(\lambda-\nu)\frac{1+\lambda}{1-\lambda}}, \tag{2}$$

and R, ν, and λ are the parameters of the solution. The three parameters all have a physical interpretation: R, ν, and λ denote the ring radius, the thickness of the ring, the rotation velocity of the ring, respectively, where the parameter range is

$$R > 0, \quad 0 < \lambda \leq \nu < 1. \tag{3}$$

[1]Email address: igata@sci.osaka-cu.ac.jp
[2]Email address: ishihara@sci.osaka-cu.ac.jp
[3]Email address: takamori@sci.osaka-cu.ac.jp

The parameter λ is determined by the regularity conditions at the two rotation axes of the ring in terms of ν as follows:

$$\lambda = \frac{2\nu}{1+\nu^2}. \tag{4}$$

The black ring metrics are stationary and axisymmetric, with Killing vectors ∂_t, ∂_ϕ, and ∂_ψ. The fixed point of ψ-rotation generated by ∂_ψ, which we refer to as the ring axis, exists at $y=-1$, and the fixed point of ϕ-rotation generated by ∂_ϕ, which we refer to as the equatorial plane, exists at $x=\pm 1$. Furthermore, this metric appears to have a singularity at $y=-1/\nu, -1/\lambda, -\infty$. Evaluation of curvature invariants such as $R_{abcd}R^{abcd}$ shows that the singularity at $y=-\infty$ is a true, curvature singularity. The singularities in the metric components at $y=-1/\nu$ and $y=-1/\lambda$ are coordinate singularities, corresponding to the event horizon and the ergo surface with $S^2\times S^1$ topology, respectively.

We turn to a discussion of geodesic motion in the black ring geometry. Let p_μ be 5-momentum of a particle with rest mass m, we obtain the Hamiltonian of geodesic motion as

$$H = \frac{1}{2}\left[\frac{(x-y)^2}{R^2}\frac{G(x)}{F(x)}p_x^2 - \frac{(x-y)^2}{R^2}\frac{G(y)}{F(x)}p_y^2 + E^2\left(U_{\rm eff}+\frac{m^2}{E^2}\right)\right], \tag{5}$$

where

$$U_{\rm eff} = -\frac{F(x)}{F(y)} - \frac{C^2(x-y)^2(y+1)^2}{G(y)F(x)F(y)} + \frac{(x-y)^2}{R^2G(x)}\ell_\phi^2 - \frac{F(y)(x-y)^2}{R^2G(y)F(x)}\ell_\psi^2 + 2\frac{C(x-y)^2(y+1)}{RG(y)F(x)}\ell_\psi \tag{6}$$

is the effective potential of the geodesic motion and E denotes $-p_t$, and ℓ_ϕ, ℓ_ψ denote p_ϕ/E, p_ψ/E, respectively. The three components, p_t, p_ϕ, and p_ψ, yield constants of motion since the black ring metric admits three commutable Killing vectors.

In what follows, in order to give intuitive picture of particle motion, we use ζ-ρ coordinates which are defined as

$$\zeta = R\frac{\sqrt{y^2-1}}{x-y}, \quad \rho = R\frac{1-x^2}{x-y}. \tag{7}$$

In the flat limit, the black ring metric reduces to the flat metric in the form $ds^2 = -dt^2 + d\zeta^2 + \zeta^2 d\psi^2 + d\rho^2 + \rho^2 d\phi^2$.

Let us consider stationary particle motion determined by

$$U_{\rm eff}(\zeta_{\rm st},\rho_{\rm st}) + \frac{m^2}{E^2} = 0, \quad \frac{\partial U_{\rm eff}}{\partial\zeta}(\zeta_{\rm st},\rho_{\rm st}) = \frac{\partial U_{\rm eff}}{\partial\rho}(\zeta_{\rm st},\rho_{\rm st}) = 0, \tag{8}$$

i.e., $(\zeta_{\rm st},\rho_{\rm st})$ are positions of the extrema of $U_{\rm eff}$. Restricting attention to stable bound orbits, we impose in addition to equation (8) the requirement that

$$\det\mathcal{H}(\zeta_{\rm s},\rho_{\rm s}) > 0, \quad \frac{\partial^2 U_{\rm eff}}{\partial\rho^2}(\zeta_{\rm s},\rho_{\rm s}) > 0, \tag{9}$$

where

$$\mathcal{H}(\zeta,\rho) = \begin{pmatrix} \frac{\partial^2 U_{\rm eff}}{\partial\rho^2}(\zeta,\rho) & \frac{\partial^2 U_{\rm eff}}{\partial\rho\partial\zeta}(\zeta,\rho) \\ \frac{\partial^2 U_{\rm eff}}{\partial\zeta\partial\rho}(\zeta,\rho) & \frac{\partial^2 U_{\rm eff}}{\partial\zeta^2}(\zeta,\rho) \end{pmatrix}, \tag{10}$$

so that $(\zeta_{\rm s},\rho_{\rm s})$ denote positions of local minima of $U_{\rm eff}$.

In Figure 1, the domains of $(\zeta_{\rm s},\rho_{\rm s})$ are drawn by solving the conditions (8) and (9) numerically. The figure shows that there are stable bound orbits on and near the ring axis of the black ring geometry while there is no stable bound orbit on the equatorial plane. The orbits on the time slice of the Killing time have toroidal spiral shape near the ring axis and circular shape on the ring axis, which is generated by the two axial Killing vectors.

In figure 1, it is not clear whether outermost stable bound orbits exist in the case of $\nu=0.2$ and how much the value of ν at which the domain of stable bound orbits disappears is. Therefore, let us discuss

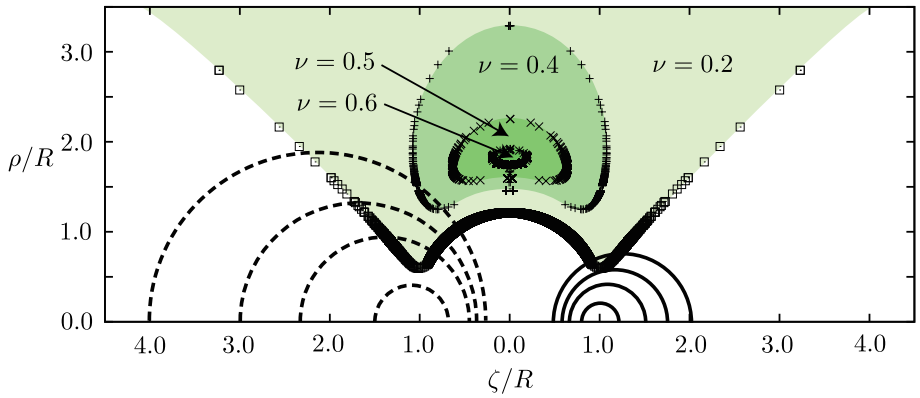

Figure 1: The shaded region shows the domain of stable bound orbits in the black ring spacetime for each ν. The dashed and solid semicircles show the ergo surfaces and the event horizon, respectively, where $\nu = 0.2, 0.4, 0.5$, and 0.6 from the small one to the large one.

innermost and outermost stable circular orbits in the black ring geometry. To simplify the discussion here, we focus attention on the ring axis. If $\ell_\psi = 0$, the form of $U_{\rm eff}$ expanded in ζ near the ring axis is

$$U_{\rm eff} \simeq \quad U_{\rm axis} + \frac{4\nu R^2}{(\rho^2+R^2)^3}\left[\frac{\ell_\phi^2(\rho^2+R^2)^2}{((1+\nu)R^2+(1-\nu)\rho^2)^2} - \frac{(1+\nu)^3R^4-(1-\nu)^3\rho^4}{R^2(1-\nu)^3(1+\nu)^2+(1-\nu)^5\rho^2}\right]\zeta^2, \tag{11}$$

where

$$U_{\rm axis} = -1 - \frac{4R^2\nu}{(1-\nu)^2(R^2+\rho^2)} + \frac{\ell_\phi^2(R^2+\rho^2)}{R^2\rho^2(1+\nu)+(1-\nu)\rho^4}. \tag{12}$$

We impose condition (8) on equation (12) and solve the equation for ℓ_ϕ, then we have

$$\ell_\phi = \frac{2\rho_{\rm st}^2(R^2(1+\nu)+\rho_{\rm st}^2(1-\nu))}{(1-\nu)(R^2+\rho_{\rm st}^2)}\sqrt{\frac{\nu}{(R^2+\rho_{\rm st}^2)^2-\nu(\rho_{\rm st}^4+2\rho_{\rm st}^2R^2-R^4)}}, \tag{13}$$

where we chose the positive root without loss of generality. Substituting equation (13) into equation (11), we solve equation, $\det\mathcal{H} = 0$, where the equation, in this case, reduces to

$$\frac{\partial^2 U_{\rm eff}}{\partial\rho^2}(\zeta=0,\rho_{\rm O}) = 0 \quad \text{or} \quad \frac{\partial^2 U_{\rm eff}}{\partial\zeta^2}(\zeta=0,\rho_{\rm I}) = 0, \tag{14}$$

where $\rho_{\rm O}$ and $\rho_{\rm I}$ denote radius of the outermost stable circular orbit and the innermost stable circular orbit, respectively. Figure 2 shows the plot of the solutions of equation (14) in ν-ρ plane. The radii of outermost stable circular orbits approach infinity as ν decreases. Indeed, we can find that there are stable circular orbits with infinite radii in the case of $0 < \nu < 1/3$. Details of this discussion is found in the our paper [7].

In addition, the two curves intersect at the critical value of the thickness, ν_0. By solving equations $\partial U_{\rm eff}/\partial\rho = 0$, $\partial^2 U_{\rm eff}/\partial\rho^2 = 0$, $\partial^2 U_{\rm eff}/\partial\zeta^2 = 0$, with $U_{\rm eff}$ in the form of equation (11) simultaneously, we obtain the exact expression for ν_0:

$$\begin{aligned}\nu_0 = \frac{1}{2}\Bigg(145 - 24\left(\frac{2}{3+\sqrt{41}}\right)^{1/3} + 6\left(4(3+\sqrt{41})\right)^{1/3}\Bigg)^{1/2} - \Bigg[6\left(\frac{2}{3+\sqrt{41}}\right)^{1/3} - 3\left(\frac{3+\sqrt{41}}{2}\right)^{1/3} \\ + \frac{1783}{2}\Bigg(145 - 24\left(\frac{2}{3+\sqrt{41}}\right)^{1/3} + 6\left(4(3+\sqrt{41})\right)^{1/3}\Bigg)^{-1/2} + \frac{145}{2}\Bigg]^{1/2} + \frac{13}{2}\end{aligned} \tag{15}$$

$$= 0.65379\cdots.$$

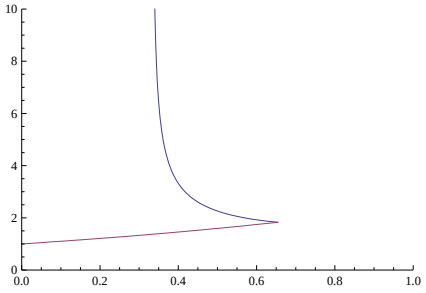

Figure 2: (ν-ρ plane) The top curve shows the radii of the outermost stable circular orbits, $\rho_{\rm O}$, and the bottom curve shows the radii of the innermost stable circular orbits, $\rho_{\rm I}$.

Therefore, we find that there exist stable bound orbits only in the case of $\nu < \nu_0$ on the ring axis. In fact, the statement holds in the whole black ring geometry within the limit of accuracy of the numerical calculations.

In this report, we have discussed stable bound orbits of a free particle in the black ring geometry. By using the way of an effective potential of a free particle motion, we show the existence of stable bound orbits in the black ring spacetime which is a characteristic property of the black ring geometry unlike the black hole case. In addition, the characteristic value of the thickness parameter of the black ring solution were found by the analysis in the ring axis. The stable bound orbits exist only in the case of $\nu < \nu_0 \simeq 0.65379$.

References

[1] R. Emparan and H. S. Reall, Living Rev. Relativity 11, (2008), 6. URL (cited on 3 Jun. 2010): http://www.livingreviews.org/lrr-2008-6 .

[2] R. C. Myers and M. J. Perry, Annals Phys. **172**, 304 (1986).

[3] T. Mishima and H. Iguchi, Phys. Rev. D **73**, 044030 (2006)
H. Elvang and P. Figueras, JHEP **0705**, 050 (2007)
H. Iguchi and T. Mishima, Phys. Rev. D **75**, 064018 (2007) [Erratum-ibid. D **78**, 069903 (2008)]
J. Evslin and C. Krishnan, Class. Quant. Grav. **26**, 125018 (2009)
K. Izumi, Prog. Theor. Phys. **119**, 757 (2008)
H. Elvang and M. J. Rodriguez, JHEP **0804**, 045 (2008)

[4] R. Emparan and H. S. Reall, Phys. Rev. Lett. **88**, 101101 (2002)

[5] M. Nozawa and K. i. Maeda, Phys. Rev. D **71**, 084028 (2005)
H. Elvang, R. Emparan and A. Virmani, JHEP **0612**, 074 (2006)
A. Sahay and G. Sengupta, JHEP **0706**, 006 (2007)

[6] J. Hoskisson, Phys. Rev. D **78**, 064039 (2008)

[7] T. Igata, H. Ishihara and Y. Takamori, Phys. Rev. D **82**, 101501 (2010)

[8] T. Igata, H. Ishihara and Y. Takamori, in preparation

Perturbation solutions to the lnes equation for multiple lens planes

Koji Izumi and Hideki Asada
Faculty of Science and Technology, Hirosaki University, Hirosaki 036-8561, Japan

Abstract

Continuing work initiated in an earlier publication (Asada, 2009, MNRAS, **394**, 818), we make a systematic attempt to determine, as a function of lens and source parameters, the positions of images by multi-plane gravitational lenses. By extending the previous single-plane work, we present a method of Taylor-series expansion to solve the multi-plane lens equation in terms of mass ratios. The advantage of this method is that it allows a systematic iterative analysis and clarifies the dependence on lens and source parameters. In concordance with the multi-plane lensed-image counting theorem that the lower bound on the image number is 2^N for N planes with a single point mass on each plane, our iterative results show directly that 2^N images are always realized as the minimum number of lensed images.

1 Introduction

Gravitational lensing has become one of important subjects in modern astronomy and cosmology (e.g., Schneider 2006, Weinberg 2008). It has many applications as gravitational telescopes in various fields ranging from extra-solar planets to dark matter and dark energy at cosmological scales (e.g., Refregier 2003 for a review). For instance, it is successful in detecting extra-solar planetary systems (Schneider and Weiss 1986, Mao and Paczynski 1991, Gould and Loeb 1992, Bond et al. 2004, Beaulieu et al. 2006). Gaudi et al. (2008) have found an analogy of the Sun-Jupiter-Saturn system through lensing. In recent, gravitational lensing has been used to constrain modified gravity at cosmological scale (Reyes et al. 2010).

It has long been a challenging problem to express the image positions as functions of lens and source parameters (Asada 2002, Asada, Hamana and Kasai 2003 and references therein). For this purpose, we present a method of Taylor-series expansion to solve the multi-plane lens equation in terms of mass ratios by extending the previous single-plane work (Asada 2009).

For N point lenses, Witt (1990) succeeded in recasting the lens equation into a single-complex-variable polynomial. This is in an elegant form and thus has been often used in investigations of point-mass lenses. The single-variable polynomial due to N point lenses on a single plane has the degree of N^2+1, though the maximum number of images is known as $5(N-1)$ (Rhie 2001, 2003, Khavinson and Neumann 2006, 2008). This means that unphysical roots are included in the polynomial (for detailed discussions on the disappearance and appearance of images near fold and cusp caustics for general lens systems, see also Petters, Levine and Wambsganss (2001) and references therein). Following Asada (2009), we consider the lens equation in dual complex variables, so that we can avoid inclusions of unphysical roots.

2 Basic Formulation

2.1 Multi-plane lens equation

We consider lens effects by N point masses, each of which is located at different distance D_i $(i=1,2,\cdots N)$ from the observer. For this case, we prepare N lens planes and assume the thin-lens approximation for each lens plane (Blandford, Narayan 1986, Yoshida, Nakamura, Omote 2005).

First of all, angular variables are normalised in the unit of the angular radius of the Einstein ring as

$$\theta_E = \sqrt{\frac{4GM_{tot}D_{1S}}{c^2 D_1 D_S}}, \tag{1}$$

where we put the total mass on the first plane at D_1, G denotes the gravitational constant, c means the light speed, M_{tot} is defined as the total mass $\sum_{i=1}^{N} M_i$ and D_1, D_S and D_{1S} denote distances between the observer and the first mass, between the observer and the source, and between the first mass and the source, respectively.

Recursively one can write down the multi-plane lens equation (Blandford and Narayan 1986, Schneider et al. 1992). In the vectorial notation, the double-plane lens equation is written as

$$\begin{aligned} \boldsymbol{\beta} &= \boldsymbol{\theta} - \left(\nu_1 \frac{\boldsymbol{\theta} - \boldsymbol{\ell}_1}{|\boldsymbol{\theta} - \boldsymbol{\ell}_1|^2} \right. \\ &\left. + \nu_2 d_2 \frac{\boldsymbol{\theta} - \nu_1 \delta_2 \dfrac{\boldsymbol{\theta} - \boldsymbol{\ell}_1}{|\boldsymbol{\theta} - \boldsymbol{\ell}_1|^2} - \boldsymbol{\ell}_2}{|\boldsymbol{\theta} - \nu_1 \delta_2 \dfrac{\boldsymbol{\theta} - \boldsymbol{\ell}_1}{|\boldsymbol{\theta} - \boldsymbol{\ell}_1|^2} - \boldsymbol{\ell}_2|^2} \right), \end{aligned} \tag{2}$$

where $\boldsymbol{\beta}$, $\boldsymbol{\theta}$, $\boldsymbol{\ell}_1$ and $\boldsymbol{\ell}_2$ denote the positions of the source, image, first and second lens objects, respectively. Here, ν_i denotes the mass ratio of each lens object, and we define d_2 and δ_2 as

$$d_2 \equiv \frac{D_1 D_{2s}}{D_2 D_{1s}}, \tag{3}$$

$$\delta_2 \equiv \frac{D_S D_{12}}{D_2 D_{1S}}. \tag{4}$$

It is convenient to use complex variables when algebraic manipulations are done. In a formalism based on complex variables, two-dimensional vectors for the source, image and lens positions are denoted as $w = \beta_x + i\beta_y$, $z = \theta_x + i\theta_y$, and $\epsilon_i = \ell_{ix} + i\ell_{iy}$, respectively. Figure 1 shows our notation for the multi-plane lens system. Here, z is on the complex plane corresponding to the first lens object that finally deflects light rays and thus z means the direction of a lensed image.

By employing this formalism, the double-plane lens equation is rewritten as

$$w = z - \left(\frac{1-\nu}{z^*} + \frac{\nu d_2}{z^* - \epsilon^* - \dfrac{(1-\nu)\delta_2}{z^*}} \right), \tag{5}$$

where the asterisk $*$ means the complex conjugate and we use the identity as $\nu_1 + \nu_2 = 1$ to delete ν_1 and ν denotes ν_2. Note that we choose the center of the complex coordinate as the first mass. Then, we have $\epsilon_1 = 0$ and simply denote $\epsilon \equiv \epsilon_2$, which is the projected relative position of the second mass with respect to the first one. The lens equation is non-analytic because it contains not only z but also z^*.

2.2 Iterative solutions

The mass ratio does not exceed the unity by its definition. Therefore, we use a simple-minded method of making expansions in terms of the mass ratios. One can delete ν_1 by noting the identity as $\sum_i \nu_i = 1$. And the location of the first lens is chosen as the origin of the complex coordinates.

Formal solutions are expressed in Taylor series as

$$z = \sum_{p_2=0}^{\infty} \sum_{p_3=0}^{\infty} \cdots \sum_{p_N=0}^{\infty} \nu_2^{p_2} \nu_3^{p_3} \cdots \nu_N^{p_N} z_{(p_2)(p_3)\cdots(p_N)}, \tag{6}$$

where the coefficients $z_{(p_2)(p_3)\cdots(p_N)}$ are independent of any ν_i. What we have to do is to determine each coefficient $z_{(p_2)(p_3)\cdots(p_N)}$ iteratively.

At the zeroth order, we have always a single-plane lens equation as the limit of $\nu_1 \to 1$ ($\nu_2 = \cdots = \nu_N \to 0$). We have the two roots for it. In addition, we have more roots for a multi-plane lens equation as *seeds* for our iterative calculations. An algorithm for doing such things is explained in next section.

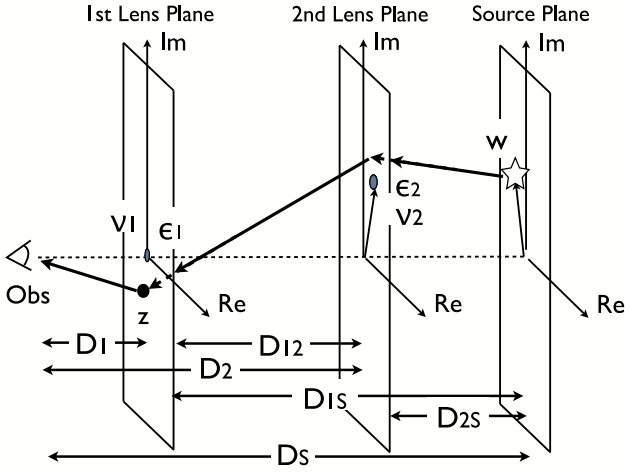

Figure 1: Notation: The source and image positions on complex planes are denoted by w and z, respectively. Locations of N masses are denoted by ϵ_i for $i = 1, \cdots, N$. Here, we assume the thin lens approximation for each deflector. The several distances among the observer, source and each lens object are also defined.

3 Image Positions

3.1 Double lens planes

At zeroth order ($\nu_2 \to 0$), the double-plane lens equation becomes simply

$$w = z_{(0)} - \frac{1}{z^*_{(0)}}, \tag{7}$$

which is rewritten as

$$z_{(0)} z^*_{(0)} - 1 = w z^*_{(0)}. \tag{8}$$

The L.H.S. of the last equation is purely real so that the R.H.S. must be real. Unless $w = 0$, therefore, one can put $z_{(0)} = Aw$ by introducing a certain real number A. By substituting $z_{(0)} = Aw$ into Eq. (8), one obtains a quadratic equation for A as

$$ww^* A^2 - ww^* A - 1 = 0. \tag{9}$$

This is solved as

$$\begin{aligned} A &= \frac{1}{2}\left(1 \pm \sqrt{1 + \frac{4}{ww^*}}\right) \\ &\equiv A_\pm, \end{aligned} \tag{10}$$

which gives $z_{(0)}$ as $A_\pm w$.

In the particular case of $w = 0$, Eq. (8) becomes $|z_{(0)}| = 1$, which is nothing but the Einstein ring. In the following, we assume a general case of $w \neq 0$.

We must consider $z_{(0)} = A_\pm w$, separately,

Table 1 shows a numerical example of image positions obtained iteratively and their convergence.

$z_{(1)}$ tells us an order-of-magnitude estimate of the effect by a separation between the two lens planes. Such a depth effect is characterised by δ_2, which enters the iterative expressions through z_+ and z_-.

Table 1: Example of image positions by the double-plane lens. We choose $\nu_1 = 9/10$, $\nu_2 = 1/10$, $\epsilon = 3/2$, $w = 2$, $D_1/D_S = 2/5$, $D_2/D_S = 3/5$. Iterative results (denoted as '0th'. '1st', '2nd' and '3rd') show a good convergence for the value (denoted as 'Num') that is obtained by numerically solving the lens equation.

Images	1	2	3	4
0th.	2.414213	-0.414213	1.780776	-0.280776
1st.	2.434312	-0.390217	1.731605	-0.276050
2nd.	2.430981	-0.388713	1.732327	-0.275043
3rd.	2.431474	-0.388781	1.732190	-0.274861
Num	2.431396	-0.388766	1.73220	-0.274833

4 Conclusion

We made a systematic attempt to determine, as a function of lens and source parameters, the positions of images by multi-plane gravitational lenses (Izumi, Asada 2010). We presented a method of Taylor-series expansion to solve the multi-plane lens equation in terms of mass ratios.

In concordance with the multi-plane lensed-image counting theorem that the lower bound on the image number is 2^N for N planes with a single point mass on each plane, our iterative results show directly that 2^N images are always realized as the minimum number of lensed images.

It is left as a future work to compare the present result with state-of-art numerical simulations.

Acknowledgments

The authors would like to thank M. Kasai and R. Takahashi for stimulating conversations. This work was supported in part by a Japanese Grant-in-Aid for Scientific Research from the Ministry of Education, No. 19035002.

References

[1] Asada H., 2002a, A&A, 390, L11

[2] Asada H., Hamana T., Kasai M., 2003, A&A, 397, 825

[3] Beaulieu J. P., et al., 2006, Nature, 439, 437

[4] Blandford R., Narayan R., 1986, ApJ, 310, 568

[5] Bond I. A., et al., 2004, ApJ, 606, L155

[6] Bourassa R. R., Kantowski R., Norton T. D., 1973, ApJ, 185, 747

[7] Bourassa R. R., Kantowski R., 1975, ApJ, 195, 13

[8] Gaudi B. S., et al., 2008, Science, 319, 927

[9] Gould A., Loeb A., 1992, ApJ, 396, 104

[10] Izumi K., Asada., 2010, arXiv:1012.0070

[11] Khavinson D., Neumann G., 2006, Proc. Amer. Math. Soc. 134, 1077

[12] Khavinson D., Neumann G., 2008, Not. Amer. Math. Soc. 55, 666

[13] Mao S., Paczynski B., 1991, ApJ, 374, 37L

[14] Refregier A., 2003, ARAA, 41, 645

[15] Reyes R., 2010, Nature, 464, 256

[16] Rhie S. H., 2001, arXiv:astro-ph/0103463

[17] Rhie S. H., 2003, arXiv:astro-ph/0305166

[18] Schneider P., Weiss A., 1986, A&A. 164, 237

[19] Schneider P., Ehlers J., Falco E. E., 1992, *Gravitational Lenses* (Heidelberg, Springer-Verlag)

[20] Schneider P., 2006, *Extragalactic Astronomy And Cosmology: An Introduction* (Heidelberg, Springer-Verlag)

[21] van der Waerden B. L., 1966, *Algebra I* (Heidelberg, Springer-Verlag)

[22] Weinberg S., 2008, *Cosmology* (Oxford, Oxford Univ. Press)

[23] Witt H. J., 1990, A&A. 236, 311

[24] Yoshida H., Nakamura K., Omote M., 2005, MNRAS, 358, 39

Non-Gaussianity from Lifshitz Scalar

Keisuke Izumi[1(a)], Takeshi Kobayashi[2(b)] and Shinji Mukohyama[3(a)]

[(a)] *Institute for the Physics and Mathematics of the Universe (IPMU), The University of Tokyo, 5-1-5 Kashiwanoha, Kashiwa, Chiba 277-8583, Japan*
[(b)] *Institute for Cosmic Ray Research, The University of Tokyo, 5-1-5 Kashiwanoha, Kashiwa, Chiba 277-8582, Japan*

Abstract

A Lifshitz scalar with the dynamical critical exponent $z = 3$ obtains scale-invariant, super-horizon field fluctuations without the need of an inflationary era. Since this mechanism is due to the special scaling of the Lifshitz scalar and persists in the presence of unsuppressed self-couplings, the resulting fluctuation spectrum can deviate from a Gaussian distribution. We study the non-Gaussian nature of the Lifshitz scalar's intrinsic field fluctuations, and show that primordial curvature perturbations sourced from such field fluctuations can have large non-Gaussianity of order $f_{\rm NL} = O(100)$, which will be detected by upcoming CMB observations. We compute the bispectrum and trispectrum of the fluctuations, and discuss their configurations in momentum space. In particular, the bispectrum is found to take various shapes, including the local, equilateral, and orthogonal shapes. Intriguingly, all integrals in the in-in formalism can be performed analytically.

1 introduction

Hořava-Lifshitz gravity [1] is attracting much attention as one of candidates for the theory of quantum gravity because of its power-counting renormalizability, which is realized by the Lifshitz scaling

$$\vec{x} \to b\vec{x}, \qquad t \to b^z t, \tag{1}$$

with the dynamical critical exponent $z \geq 3$ in the ultraviolet (UV). There are many attempts to investigate properties and implications of this theory [2, 3].

It is natural to suppose that not only gravitational fields but also other fields exhibit the same Lifshitz scaling in the UV. Even if they classically have different scalings, quantum corrections should render them to have the same scaling. A Lifshitz scalar with $z = 3$ can produce the primordial scale-invariant perturbations even without inflation [2]. It is noteworthy that this value of z is the minimal value for which gravity is power-counting renormalizable.

In order to discern this production mechanism of the primordial perturbation from others, we need to investigate distinct features in observables such as the cosmic microwave background. In this respect, non-Gaussianity has been considered as one of the promising approaches to distinguish production mechanisms. For this reason, there are on-going efforts to detect or constrain non-Gaussian nature of the primordial perturbation [4]. Towards identification of the production mechanism by future observations, theoretical analyses of non-Gaussianity in various cosmological scenarios have been performed [5–7].

We focus on primordial non-Gaussianity from a Lifshitz scalar and calculate its bispectrum and trispectrum. With the dynamical critical exponent $z = 3$, the scaling dimension of the Lifshitz scalar is zero and, thus, nonlinear terms in the action are unsuppressed unless forbidden by symmetry or driven to small values by renormalization. It is those nonlinear terms that we expect to produce non-Gaussianity. It turns out that the produced bispectrum can be large enough to be observed in future observations. We find three independent cubic terms dominant in the UV, each of which gives different shape dependence of the bispectrum. Roughly speaking, they correspond to local, equilateral and orthogonal shapes, respectively.

This presentation is based on our paper [8].

[1]Email address: keisuke.izumi@ipmu.jp
[2]Email address: takeshi.kobayashi@ipmu.jp
[3]Email address:shinji.mukohyama@ipmu.jp

2 Order estimate for $f_{\rm NL}$

We shall present order estimates for the bispectrum of curvature perturbations and the corresponding nonlinear parameter $f_{\rm NL}$.

We assume that perturbations of the Lifshitz scalar are almost linearly transformed to curvature perturbations. In our calculation of the bispectrum and trispectrum of curvature perturbations, we thus take into account the linear term only. In particular,

$$\langle\zeta\zeta\rangle \simeq \mu^{-2}\langle\phi\phi\rangle\,, \quad \langle\zeta\zeta\zeta\rangle \simeq \mu^{-3}\langle\phi\phi\phi\rangle\,. \tag{2}$$

This treatment is justified by the fact that perturbations of the Lifshitz scalar have large non-Gaussianity.

We review the mechanism for generation of scale-invariant cosmological perturbations from a Lifshitz scalar [2]. Let us consider the Lifshitz scalar ϕ, specialized to the case with $z = 3$, in a flat FRW background

$$ds^2 = -dt + a(t)^2\delta_{ij}dx^i dx^j, \tag{3}$$

to investigate generation of cosmological perturbations. The action for the perturbation ϕ is then written as

$$S_\phi = \frac{1}{2}\int dtd^3x\; a(t)^3\left[(\partial_t\phi)^2 + \phi\mathcal{O}\phi + O(\phi^3)\right], \tag{4}$$

where

$$\mathcal{O} = \frac{1}{M^4a(t)^6}\Delta^3 - \frac{s}{M^2a(t)^4}\Delta^2 + \frac{c_s^2}{a(t)^2}\Delta - m^2, \tag{5}$$

M and m are mass scales and s and c_s^2 are dimensionless constants. In the UV, the quadratic action for ϕ is simply

$$S_2 = \frac{1}{2}\int dtd^3x\, a(t)^3\left\{(\partial_t\phi)^2 + \frac{1}{M^4a(t)^6}\phi\Delta^3\phi\right\}. \tag{6}$$

The scaling dimension of ϕ is zero,

$$\phi \to b^0\phi, \tag{7}$$

and its power-spectrum should be scale-invariant. Since ϕ is scale-invariant and there is only one scale M in the UV quadratic action (6), we expect that the power-spectrum should be roughly

$$\langle\phi\phi\rangle \sim M^2. \tag{8}$$

We shall adopt the so called in-in formalism [5, 9] to calculate the bispectrum and trispectrum of the Lifshitz scalar. The leading contribution to the bispectrum is given by the following formula (see the next section for details)

$$\langle\phi\phi\phi\rangle = i\left\langle\left[\int dtH_3, \phi\phi\phi\right]\right\rangle, \tag{9}$$

where H_3 represents cubic terms in the interaction Hamiltonian. Dominant terms in $\int dtH_3$ are marginal ones, i.e. those terms whose scaling dimensions are zero. Actually, there are three (and only three) independent marginal cubic operators in the action in the UV:

$$S_3 = \int dtd^3x\,\frac{1}{M^5a(t)^3}\left\{\alpha_1\phi^2\Delta^3\phi + \alpha_2(\Delta^2\phi)(\partial_i\phi)^2 + \alpha_3(\Delta\phi)^3\right\}, \tag{10}$$

where α_i are dimensionless parameters. (The fist term can be forbidden by the shift symmetry if one likes.) Evidently, validity of perturbative expansion (in the in-in formalism) requires α_i be smaller than unity. The corresponding cubic operators in the interaction Hamiltonian are

$$H_3(t) = -\int d^3x\,\frac{1}{M^5a^3}\left\{\alpha_1\phi^2\Delta^3\phi + \alpha_2(\Delta^2\phi)(\partial_i\phi)^2 + \alpha_3(\Delta\phi)^3\right\}. \tag{11}$$

Each of these dominant cubic terms includes six spatial derivatives and gives zero scaling dimension to $\int dt H_3$. Combining this with the fact that the scaling dimension of ϕ is zero, we conclude that the bispectrum of ϕ given by (9) should be scale-independent, and thus

$$\langle \phi\phi\phi \rangle \sim \alpha M^3, \tag{12}$$

where α stands for the most dominant one among α_i $(i = 1, 2, 3)$.

Roughly speaking, the non-linear parameter $f_{\rm NL}$ is defined so that

$$f_{\rm NL} \sim \frac{\langle \zeta\zeta\zeta \rangle}{\langle \zeta\zeta \rangle^2}. \tag{13}$$

Thus, combining this with (2), (8) and (12), we obtain

$$f_{\rm NL} \sim \alpha \left(\frac{M}{\mu} \right)^{-1} \sim 3 \times 10^3 \alpha. \tag{14}$$

Here, we have used the COBE normalization [4], $\mathcal{P}_\zeta^{1/2} \simeq 4.9 \times 10^{-5}$.

As already stated, validity of perturbative expansion requires that the dimensionless parameters α_i be smaller than unity. We find from the order estimate (14) that $f_{\rm NL}$ can be large, e.g. as large as $O(100)$, even if α_i are reasonably small.

3 Conclusions

We have studied non-Gaussianity in the intrinsic fluctuations of a Lifshitz scalar which follows an anisotropic scaling with $z = 3$. Our work is based on [2], which pointed out that its special dispersion relation in the UV can lead to generation of super-horizon field perturbations. Since the scaling dimension of a Lifshitz scalar with $z = 3$ is zero, the resulting field perturbations become scale-invariant whether or not the scalar's self-couplings are small. This leads to our main point that curvature perturbations generated from such field fluctuations necessarily leave large non-Gaussianity in the sky, unless the field's self-couplings are forbidden by some symmetry, or the field exhibits some sort of asymptotic freedom. This is to be contrasted with perturbations generated through cosmic inflation, where largely non-Gaussian intrinsic fluctuations are in most cases incompatible with scale-invariance.

The Lifshitz scalar's self-coupling terms containing spatial derivatives produce non-Gaussianities with various configurations in momentum space. In particular, the bispectrum of the field fluctuations includes shapes which are similar to that of the local, equilateral, and orthogonal forms. (However, we emphasize that the local, equilateral, and orthogonal shapes do not form a complete basis set for the bispectrum obtained. We also note that the results of the effective field theory approach in [10] do not apply to our case, where Lorentz symmetry is explicitly broken, and non-Gaussianity is sourced by marginal terms in the action.) Upon computing the correlation functions, we have carried out expansions in terms of the interaction Hamiltonian. Within the domain of applicability of such perturbative expansion, i.e. the self-couplings less than unity, we have seen that the Lifshitz scalar's field fluctuations can lead to significant non-Gaussianity in the primordial curvature perturbations. In particular, when curvature perturbations are sourced linearly from the field fluctuations, their bispectrum saturates the current observational limit for the orthogonal and equilateral forms, as the self-couplings α_2 and α_3 in (10) approach unity. Since naively there is no reason for such self-couplings to be suppressed, we can expect large non-Gaussianity to be produced from Lifshitz scalar fluctuations, which may be detected by upcoming CMB observations. On the other hand, for the local-type bispectrum, observational constraints require α_1 to be as small as $O(10^{-2}-10^{-3})$ (the level of tuning depends on α_1's sign). However, such self-couplings sourcing local-type non-Gaussianity can be forbidden by a shift symmetry.

The field fluctuations generated in the mechanism of [2] obtain a scale-invariant spectrum. However, when one takes into account the renormalization-group flow of the parameters of the theory (e.g. M in (6)), the spectrum may become tilted. A time-dependent background value $\Phi_0(t)$ may also give rise to similar effects. How strong the tilt becomes, as well as the scale-dependence of the non-Gaussianity, remains to be understood. While we have studied fluctuations of scalar fields, the scalar graviton which

can show up in Hořava-Lifshitz gravity may also obtain fluctuations in a similar manner. It would be interesting to investigate the possibility that such scalar graviton generates the primordial curvature perturbations. (Ref. [11] works in this direction. See [12] for some issues related to the scalar graviton, including non-perturbative continuity of the limit in which general relativity is supposed to be recovered. See also [13] for a recent attempt to eliminate the scalar graviton from the theory.) Furthermore, when considering cosmic inflation in Hořava-Lifshitz gravity, due to the field fluctuations freezing-out at the time of sound horizon $(M^2H)^{-1/3}$ exit, the well-known relations in slow-roll inflation between various cosmological observables and the slow-roll parameters are expected to be modified. Aspects of cosmic inflation in Hořava-Lifshitz gravity are also worthy of study in details.

References

[1] P. Horava, Phys. Rev. D **79**, 084008 (2009) [arXiv:0901.3775 [hep-th]].
P. Horava, Phys. Rev. Lett. **102**, 161301 (2009) [arXiv:0902.3657 [hep-th]].

[2] S. Mukohyama, JCAP **0906**, 001 (2009) [arXiv:0904.2190 [hep-th]].

[3] S. Maeda, S. Mukohyama and T. Shiromizu, Phys. Rev. D **80**, 123538 (2009) [arXiv:0909.2149 [astro-ph.CO]].
S. Mukohyama, K. Nakayama, F. Takahashi and S. Yokoyama, Phys. Lett. B **679**, 6 (2009) [arXiv:0905.0055 [hep-th]].
S. Mukohyama, Phys. Rev. D **80**, 064005 (2009) [arXiv:0905.3563 [hep-th]].
S. Mukohyama, JCAP **0909**, 005 (2009) [arXiv:0906.5069 [hep-th]].
K. Izumi and S. Mukohyama, Phys. Rev. D **81**, 044008 (2010) [arXiv:0911.1814 [hep-th]].

[4] E. Komatsu *et al.*, arXiv:1001.4538 [astro-ph.CO].

[5] J. M. Maldacena, JHEP **0305**, 013 (2003) [arXiv:astro-ph/0210603].

[6] M. Alishahiha, E. Silverstein and D. Tong, Phys. Rev. D **70**, 123505 (2004) [arXiv:hep-th/0404084].
D. Langlois, S. Renaux-Petel, D. A. Steer and T. Tanaka, Phys. Rev. Lett. **101**, 061301 (2008) [arXiv:0804.3139 [hep-th]].
D. Langlois, S. Renaux-Petel, D. A. Steer and T. Tanaka, Phys. Rev. D **78**, 063523 (2008) [arXiv:0806.0336 [hep-th]]. N. Arkani-Hamed, P. Creminelli, S. Mukohyama and M. Zaldarriaga, JCAP **0404**, 001 (2004) [arXiv:hep-th/0312100].

[7] D. Seery and J. E. Lidsey, JCAP **0701**, 008 (2007) [arXiv:astro-ph/0611034].
K. Izumi and S. Mukohyama, JCAP **1006**, 016 (2010) [arXiv:1004.1776 [hep-th]].

[8] K. Izumi, T. Kobayashi and S. Mukohyama, JCAP **1010**, 031 (2010) [arXiv:1008.1406 [hep-th]].

[9] S. Weinberg, Phys. Rev. D **72**, 043514 (2005) [arXiv:hep-th/0506236].

[10] C. Cheung, P. Creminelli, A. L. Fitzpatrick, J. Kaplan and L. Senatore, JHEP **0803**, 014 (2008) [arXiv:0709.0293 [hep-th]].

[11] B. Chen, S. Pi and J. Z. Tang, JCAP **0908**, 007 (2009) [arXiv:0905.2300 [hep-th]].

[12] S. Mukohyama, arXiv:1007.5199 [hep-th].

[13] P. Horava and C. M. Melby-Thompson, arXiv:1007.2410 [hep-th].

[14] X. Gao, arXiv:0904.4187 [hep-th].

Q balls in thermal logarithmic potential [1]

Kohei Kamada[2(a),(b)], Takeshi Chiba[(c)], Shinta Kasuya[(d)] and Masahide Yamaguchi[(e)]

[(a)] *Department of Physics, Graduate School of Science, The University of Tokyo, Tokyo 113-0033, Japan*
[(b)] *Research Center for the Early Universe (RESCEU), Graduate School of Science, The University of Tokyo, Tokyo 113-0033, Japan*
[(c)] *Department of Physics, College of Humanities and Sciences, Nihon University, Tokyo 156-8550, Japan*
[(d)] *Department of Information Sciences, Kanagawa University, Kanagawa 259-1293, Japan*
[(e)] *Department of Physics and Mathematics, Aoyama Gakuin University, Sagamihara 229-8558, Japan*

Abstract

Time evolution of the Q ball in thermal logarithmic potential is studied using lattice simulations. We confirm that the Q ball transforms from the thick-wall type to the thin-wall type when the thermal logarithmic term in the potential is overcome by a mass term with a positive coefficient of radiative corrections as the temperature decreases due to the cosmic expansion. We also discuss the effects of this phenomenon on the detectability of gravitational waves from the Q-ball formation.

1 Introduction

A Q ball is a non-topological soliton, which consists of scalar fields that carry global $U(1)$ charge Q. Its existence and stability are guaranteed by finite Q and it is often generated in the Affleck-Dine (AD) mechanism for baryogenesis. Recently, it is claimed that gravitational waves (GWs) are generated at the Q-ball formation [3], which may be detected by the next generation gravitational wave detectors such as DECIGO and BBO. However, the detailed study of the subsequent evolution and the decay of Q balls revealed it to be difficult even by those next generation gravitational wave detectors [2].

The properties of the AD mechanism and the Q ball depend on the supersymmetry (SUSY) breaking mechanism, because the effective potential of the relevant scalar field (AD field) quite differs for the different mediation mechanism. Consequently, there are various types of Q balls. Among them, the thermal log type Q ball, whose effective potential is dominated by thermal logarithmic term, possesses an interesting feature. As the universe expands, the cosmic temperature decreases and so does the thermal logarithmic potential. Thus, the properties of thermal log type Q ball will change with time. Moreover, zero-temperature potential eventually overcomes the thermal potential and then the type of Q ball changes [2]. If the zero-temperature potential itself allows a Q-ball solution, the type of Q ball changes to the corresponding type.

It may then be naively expected that the Q balls would be destroyed if the zero-temperature potential alone does not allow a Q-ball solution. Recently, however, it was shown that even if the zero-temperature potential alone does not allow a Q-ball solution, the total potential (the thermal logarithmic term and a mass term with a positive radiative correction) *does* allow a Q-ball solution, which would result in the transformation from the thermal log type of the Q ball into the thin-wall type [4]. Since the scenario would be changed in this case, it is important to investigate whether the field configuration dynamically transforms from one type of the Q ball to the other.

Here, we perform numerical simulations on the lattice to see the time evolution of the configuration of the AD field in the potential with a thermal logarithmic term and a mass term with a positive coefficient for radiative corrections, where the latter term alone does not allow a Q-ball solution. We confirm that the thermal log type Q ball transforms to the thin-wall type Q ball found in Ref. [4]. We also find that there is a tiny parameter region where the GWs from Q-ball formation may be detected by future detectors such as DECIGO or BBO only in the case of Q balls in thermal potential [2].

[1] This presentation is based on [1, 2].

[2] Email address: kamada@resceu.s.u-tokyo.ac.jp

2 Properties of Q balls

We are interested in the Q-ball properties in the potential with both a thermal logarithmic term and a mass term with a positive coefficient for one-loop radiative correction,

$$V_{\rm tot} = V_{\rm thermal} + V_{\rm grav}, \tag{1}$$

$$V_{\rm thermal} \simeq \begin{cases} T^2|\Phi|^2, & \text{for } |\Phi| \ll T \\ T^4 \log\left(\frac{|\Phi|^2}{T^2}\right), & \text{for } |\Phi| \gg T \end{cases} \tag{2}$$

$$V_{\rm grav} = m_\phi^2 |\Phi|^2 \left[1 + K \log\left(\frac{|\Phi|^2}{\Lambda^2}\right)\right], \tag{3}$$

where Φ is the complex AD field and T is the cosmic temperature. The upper term in $V_{\rm thermal}$ represents the thermal mass from the thermal plasma and the lower one represents the two-loop finite temperature effects coming from the running of the gauge coupling $g(T)$ which depends on the AD field value. Note that even before the reheating from the inflaton decay has not completed, there exists thermal plasma from the partial inflaton decay as a subdominant component of the universe. $V_{\rm grav}$ denotes a soft mass term due to gravity-mediated SUSY breaking, where $m_\phi \sim \mathcal{O}(\text{TeV})$. The second term in the bracket is the one-loop radiative correction, and Λ is the renormalization scale. Here we assume $K > 0$ ($K \simeq 0.01 - 0.1$) so that $V_{\rm grav}$ alone does not allow a Q-ball solution.

At larger temperature when the field starts the oscillation, the potential is dominated by the thermal logarithmic term $V_{\rm thermal}$, and the thermal log type Q balls form [4]. The properties of this type Q ball are similar to those of the gauge-mediation type Q ball [4],

$$\phi_0(T) \sim TQ^{1/4}, \qquad \omega(T) \sim \sqrt{2}\pi T Q^{-1/4}, \qquad E(T) \sim \frac{4\pi\sqrt{2}}{3} T Q^{3/4}, \qquad R(T) \sim \frac{Q^{1/4}}{\sqrt{2}T}, \tag{4}$$

where Q is the charge stored in a Q ball, $\phi_0 = \sqrt{2}|\Phi_0|$ is the AD field value at the center of Q ball, ω is the angular velocity of the AD field, E is the energy stored in a Q ball, and R is its radius. Since the charge Q is the conserved quantity, whose value is determined at the Q-ball formation, the parameters of Q balls change as the temperature decreases according to Eq. (4).

As the temperature decreases further, $V_{\rm grav}$ will eventually dominate the potential at ϕ_0. In our previous study in Ref. [2], we assumed that Q balls are destroyed and turn into almost homogeneous AD field quickly at this moment, because the potential (3) alone does not allow a Q-ball solution. Recently, however, one of the present authors pointed out that a Q-ball solution *does* exist even in this situation [4]. Although the soft mass term overcomes the thermal logarithmic term at large field values, the latter will dominate the potential at smaller field values. As a result, in the light of charge conservation, a thin-wall type Q-ball solution exists. We shall call it the thermal thin-wall type Q ball. The properties of the Q ball are written as

$$\phi_0(T) \sim c(T/m_\phi K^{1/2}) \frac{T^2}{m_\phi K^{1/2}}, \qquad \omega \sim \alpha(T) m_\phi, \qquad E \sim \alpha(T) m_\phi Q, \qquad R \sim \left(\frac{m_\phi K Q}{c\alpha T^4}\right)^{1/3}, \tag{5}$$

where $c(T/m_\phi K^{1/2})$ and $\alpha(T)$ are slowly increasing functions of T and they are of order of unity at the temperature we are interested in. For example, $c(10) \simeq 2.5, c(10^2) \simeq 3.4, c(10^3) \simeq 4.1, c(10^4) \simeq 4.6, c(10^5) \simeq 5.1, c(10^6) \simeq 5.5, c(10^7) \simeq 6.0$ and so on. $\alpha(T)$ is expressed as

$$\alpha^2 = 1 + K\left(\log\left(\frac{c^2T^4}{2m^2K\Lambda^2}\right) + \frac{1}{c^2}\log\left(\frac{c^2T^2}{2m_\phi^2 K}\right)\right), \tag{6}$$

and its temperature dependence is stronger than that of c.

It is true that such a Q-ball solution exists but not clear that the field configuration follows from the thermal log type Q ball to the thermal thin-wall one. In order to tell how the configuration of the AD field evolves, we perform numerical studies on the lattices.

3 Time evolution and type transformation of the Q ball

Here, we investigate the time evolution of the Q ball in the potential of the thermal logarithmic term and the soft mass term with positive radiative corrections by using lattice simulations. Since we are primarily interested in the transformation of a Q ball, here we limit ourselves to a single Q ball assuming the spherical symmetry of the field configuration, and solve the 1-dimensional partial differential equations in the radial direction by using the staggered leapfrog method with second order accuracy both in time and in space.

The time evolution of the field configuration is shown in Fig. 1 for $Q \simeq 1.0 \times 10^9$. The axes are rescaled with respect to the scale factor a so that the rescaled radius is almost constant for the thick-wall type. We can see that the configuration of the Q ball changes from the thick-wall to the thin-wall types. This coincides with the feature of the transformation of the Q-ball solution found in Ref. [4].

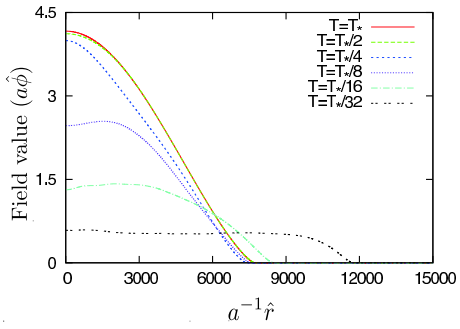

Figure 1: Configurations of the AD field for $Q \simeq 1.0 \times 10^9$ at the time of $T = T_*, T_*/2, T_*/4, T_*/8, T_*/16$, and $T_*/32$ from the top to the bottom, respectively. Q-ball configuration changes from the thick-wall to the thin-wall types.

The temperature dependence of the field value at the Q-ball center and the Q-ball radius with various charges of the Q ball are shown in Fig. 2. Here blue crosses, red x's, and green stars represent numerical results for $Q \simeq 2.5 \times 10^8, 1.0 \times 10^9$, and 3.0×10^9, respectively. Corresponding lines are the analytic estimates (4) and (5) up to numerical coefficients for each case (blue: $Q \simeq 2.5 \times 10^8$, red: $Q \simeq 1.0 \times 10^9$, green: $Q \simeq 3.0 \times 10^9$): At high temperature, $\phi_0 \propto TQ^{1/4}, R \propto T^{-1}Q^{1/4}, \omega \propto TQ^{-1/4}$ for the thermal log type Q ball, while, at low temperature, $\phi_0 \propto T^2, R \propto T^{-4/3}Q^{1/3}, \omega =$ const. for the thermal thin-wall type Q ball. We show the analytical estimates of the field value and the angular velocity in Eq. (5) with purple line in Fig. 2(a), since they are independent of charge Q. We can see that the analytical estimates (4) and (5) are well reproduced by the lattice simulations. One exception is the angular velocity at low temperature. This could be understood by the factor $\alpha(T)$ in Eq. (5), which decreases as T gets lower. We can therefore conclude that the Q ball really transforms from the thermal log type to the thermal thin-wall type in the potential considered here.

4 Detectability of gravitational waves

Now we see the detectability of the GWs from Q-ball formation. The present density parameter $\Omega^0_{\rm GW}$ and frequency f_0 of the GWs are given by

$$\Omega^0_{\rm GW} = \Omega^f_{\rm GW} \left(\frac{a_f}{a_0}\right)^4 \left(\frac{H_f}{H_0}\right)^2, \tag{7}$$

$$f_0 = f_f \left(\frac{a_f}{a_0}\right), \tag{8}$$

where the subscript f and 0 represents the parameters are evaluated at the time of Q-ball formation and the present. They strongly depend on the cosmic history after Q-ball formation. In particular, the

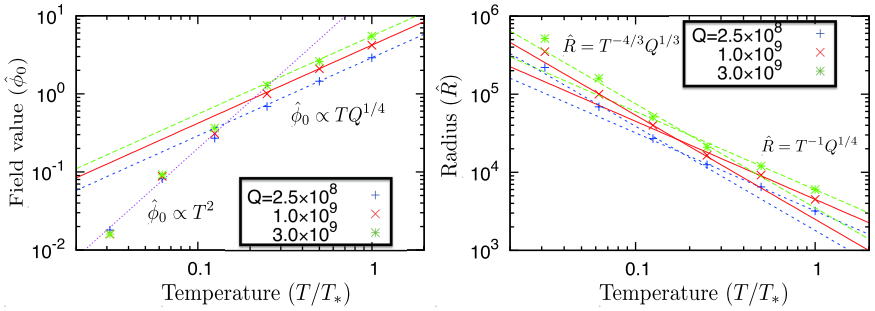

(a) Field value at the center of Q ball (b) Radius of Q ball

Figure 2: Temperature dependence of Q ball properties. Blue crosses, red x's, and green stars represent the numerical results for $Q \simeq 2.5 \times 10^8, 1.0 \times 10^9$, and 3.0×10^9, respectively. Lines correspond to analytical estimates (4) and (5) up to numerical coefficients.

existence of Q-ball dominated era severely constrains the detectability of GWs, which is determined by the SUSY breaking mechanism, its model parameters and initial conditions. Anyway, we can calculate them by evaluating the Hubble parameter when Q balls dominate the energy density of the Universe and they decay.

As a result, we can find that in the gauge-mediated SUSY-breaking model, if the reheating temperature is $T_R \simeq 10^{10}$ GeV and the initial field value of the AD field is $\phi_{\rm osc} \simeq M_G$ with $m_{3/2} \simeq 10$GeV and $M_F \simeq 10^4$ GeV, the present density parameter of the GWs from the Q-ball formation can be as large as $\Omega^0_{\rm GW} \simeq 10^{-16}$ and their frequency is $f_0 \simeq 10$ Hz [1, 2]. Thus, it is difficult but not impossible to detect them by next-generation gravitational detectors like DECIGO or BBO, but the parameter region for detectable GWs is very small. Moreover, we can find that it is almost impossible to detect GWs from Q-ball formation in other cases. In other cases when the thermal logarithmic potential drives the Q-ball formation, though the present amounts of the GWs from the Q-ball formation can be as large as $\Omega^0_{\rm GW} \simeq 10^{-8}$, the frequencies of such GWs are turned out to be very high. Thus, the identification of such GWs may determine the decay rate of inflaton or the initial condition of the AD mechanism.

We would like to comment on baryogenesis. Generally speaking, including the present case, the amount of produced baryon asymmetry is typically large for the case that AD condensates or Q-balls (almost) dominate the energy density of the Universe so that the present radiations and baryons are attributed to their decays. This is simply because the number densities of radiations and baryons are of the same order unless the (CP-violating) A-terms are suppressed by some symmetry. Thus, it is difficult to explain GWs and baryogenesis simultaneously. Once the GWs from the Q-ball formation are detected, we have the following two possibilities. In the case that such Q-balls are responsible for the present baryon asymmetry, the A-terms are suppressed by symmetry reason. The second option is that Q-balls are irrelevant for baryogenesis, which is realized for the AD fields with $B - L = 0$.

References

[1] T. Chiba, S. Kasuya, K. Kamada and M. Yamaguchi, Phys. Rev. D **82**, 103534 (2010) [arXiv:1007.4235 [hep-ph]].

[2] T. Chiba, K. Kamada and M. Yamaguchi, Phys. Rev. D **81**, 083503 (2010) [arXiv:0912.3585 [astro-ph.CO]].

[3] A. Kusenko and A. Mazumdar, Phys. Rev. Lett. **101**, 211301 (2008) [arXiv:0807.4554 [astro-ph]]; A. Kusenko, A. Mazumdar and T. Multamäki, Phys. Rev. D **79**, 124034 (2009) [arXiv:0902.2197 [astro-ph.CO]].

[4] S. Kasuya, Phys. Rev. D **81**, 083507 (2010) [arXiv:1002.4032 [hep-ph]].

Weyl invariant Dirac-Born-Infeld-Einstein theory

Nahomi Kan[1(a)], Takuya Maki[2(b)], and Kiyoshi Shiraishi[3(c)]

[(a)] *Yamaguchi Junior College, Hofu-shi, Yamaguchi 747–1232, Japan*
[(b)] *Japan Women's College of Physical Education, Setagaya, Tokyo 157-8565, Japan*
[(c)] *Yamaguchi University, Yamaguchi-shi, Yamaguchi 753–8512, Japan*

Abstract

We consider a Weyl invariant extension of Dirac-Born-Infeld type gravity. An appropriate choice of the metric hides the scalar degree of freedom which is required by the local scale invariance of the action at the first sight, and then a vector field acquires mass. Moreover, nonminimal couplings of the vector field and curvatures are induced, which may be suitable to the vector inflation scenario.

1 Introduction

The cosmological inflation is proposed as some resolutions for the important cosmological problems, *e.g.* the flatness, horizon and monopole problems. Most of successful models are based on models of classical scalar fields, although we have not known the reason of the existence of such fields in the theory of elementary particle physics. Another inflation scenario, which is called the vector inflation, is proposed by Ford [1] and some authors [2–4]. In such recent models [3, 4], the massive vector field couples nonminimally to gravity. The Lagrangian density in the model [3] is expressed as

$$\mathcal{L} = \sqrt{-g}\left[\frac{R}{16\pi} - \frac{1}{4}F_{\mu\nu}F^{\mu\nu} - \frac{1}{2}\left(m^2 - \frac{R}{6}\right)A_\mu A^\mu\right], \tag{1}$$

where $F_{\mu\nu} = \partial_\mu A_\nu - \partial_\nu A_\mu$ and the Newton constant is unity ($G = 1$). If we assume the spatially flat universe with the metric

$$ds^2 = -dt^2 + a^2(t)d\mathbf{x}^2\,, \tag{2}$$

and A_i ($i = 1, 2, 3$) depends only on t and $A_0 = 0$, then the equation of motion of the vector field A_i becomes the following form

$$\ddot{B}_i + 3\frac{\dot{a}}{a}\dot{B}_i + m^2 B_i = 0\,, \tag{3}$$

where $B_i \equiv A_i/a$. Eq. (3) is very similar to the one for a homogeneous scalar field in the Friedmann-Lemaître-Robertson-Walker universe. Moreover, the energy density is expressed as $\sim \dot{B}_i^2$, which is also similar to the one for the scalar field. Thus the approximately isotropic ansatz can be justified.

We have studied the vector inflation scenario [5] with Weyl invariance [6]. We found that the choice of the frame yields the mass of the Weyl gauge field, but the nonminimal coupling term is lost [5]. We need to generalize further the gravitation theory.

Dirac-Born-Infeld-Einstein (DBIE) theory was considered by Deser and Gibbons [7] and have been studied by many authors [8]. The Lagrangian density of DBIE theory takes the following type

$$\mathcal{L} \sim \pm\sqrt{-\det(g_{\mu\nu} \pm \alpha R_{\mu\nu})}\,, \tag{4}$$

where $R_{\mu\nu}$ is the Ricci tensor and the α is a constant. Originally, electromagnetism of the Dirac-Born-Infeld (DBI) type has been considered as a candidate of the nonsingular theory of electric fields. Therefore the DBIE theory as the highly-nonlinear theory is also expected as a theory of gravity suffered from no argument of singularity.

We take notice of the nonlinearity in the DBIE theory and expect that the Weyl invariant DBIE theory realizes the suitable scenario of the cosmological inflation.

[1]Email address: kan@yamaguchi-jc.ac.jp
[2]Email address: maki@jwcpe.ac.jp
[3]Email address: shiraish@yamaguchi-u.ac.jp

2 Weyl's gauge gravity theory

In this section, we briefly review the Weyl's gauge transformation to construct the gauge invariant Lagrangian. Consider the transformation of metric in D dimensions

$$g_{\mu\nu} \to g'_{\mu\nu} = e^{2\Lambda(x)} g_{\mu\nu} \,, \tag{5}$$

where $\Lambda(x)$ is an arbitrary function of the coordinates x^μ. We can define the field with weight $d = -\frac{D-2}{2}$ which transforms as

$$\Phi \to \Phi' = e^{-\frac{D-2}{2}\Lambda(x)} \Phi \,. \tag{6}$$

In order to construct the locally invariant theory, we consider the covariant derivative of the scalar field

$$\tilde{\partial}_\mu \Phi \equiv \partial_\mu \Phi - \frac{D-2}{2} A_\mu \Phi \,, \tag{7}$$

where A_μ is a Weyl's gauge invariant vector field. Under the Weyl gauge field transformation

$$A_\mu \to A'_\mu = A_\mu - \partial_\mu \Lambda(x) \,, \tag{8}$$

we obtain the transformation of the covariant derivative of the scalar field as

$$\tilde{\partial}_\mu \Phi \to e^{-\frac{D-2}{2}\Lambda(x)} \tilde{\partial}_\mu \Phi \,. \tag{9}$$

The modified Christoffel symbol and the modified curvature are given as follows

$$\tilde{\Gamma}^\lambda_{\mu\nu} \equiv \frac{1}{2} g^{\lambda\sigma} \left(\tilde{\partial}_\mu g_{\sigma\nu} + \tilde{\partial}_\nu g_{\mu\sigma} - \tilde{\partial}_\sigma g_{\mu\nu} \right) \,, \tag{10}$$

$$\tilde{R}^\mu{}_{\nu\rho\sigma}[g,A] \equiv \partial_\rho \tilde{\Gamma}^\mu_{\nu\sigma} - \partial_\sigma \tilde{\Gamma}^\mu_{\nu\rho} + \tilde{\Gamma}^\mu_{\lambda\rho} \tilde{\Gamma}^\lambda_{\nu\sigma} - \tilde{\Gamma}^\mu_{\lambda\sigma} \tilde{\Gamma}^\lambda_{\nu\rho} \,, \tag{11}$$

where $\tilde{\partial}_\mu g_{\sigma\mu} \equiv \partial_\mu g_{\sigma\mu} + 2A_\mu g_{\sigma\mu}$. The Ricci curvature is generalized as

$$\begin{aligned} \tilde{R}_{\nu\sigma}[g,A] &\equiv \tilde{R}^\mu{}_{\nu\mu\sigma}[g,A] \\ &= R_{\nu\sigma} + F_{\nu\sigma} - [(D-2)\nabla_\sigma A_\nu + g_{\nu\sigma}\nabla_\mu A^\mu] + (D-2)\left(A_\nu A_\sigma - A_\lambda A^\lambda g_{\nu\sigma}\right) \,, \end{aligned} \tag{12}$$

where the field strength of the vector field is given by $F_{\mu\nu} \equiv \partial_\mu A_\nu - \partial_\nu A_\mu$, which is gauge invariant as $F_{\mu\nu} \to F'_{\mu\nu} = F_{\mu\nu}$. Note that under the Weyl's gauge transformation, The Ricci curvature (12) is invariant

$$\tilde{R}_{\nu\sigma}[g,A] \to \tilde{R}_{\nu\sigma}[g',A'] = \tilde{R}_{\nu\sigma}[g,A] \,. \tag{13}$$

3 Weyl invariant Dirac-Born-Infeld gravity

We can use the Weyl invariant Ricci tensor $\tilde{R}_{\mu\nu}$ in the DBI gravity. We should also use a combination $\Phi^{\frac{4}{D-2}} g_{\mu\nu}$ instead of the metric tensor, because it is not Weyl invariant. Note that the scalar Φ compensates the dimensionality of the metric. The use of $\tilde{R}_{\mu\nu}$ and $\Phi^{\frac{4}{D-2}} g_{\mu\nu}$ in the DBI type action leads to the theory of gravity, a vector field, and unexpectedly, a scalar field.

Now we introduce the following independently Weyl invariant tensors into the determinant in the DBI theory

$$\begin{aligned} &\Phi^{\frac{4}{D-2}} g_{\nu\sigma} \,, \quad \tilde{R}^S_{\nu\sigma}[g,A] \,, \quad \tilde{R}[g,A] g_{\nu\sigma} \,, \quad F_{\nu\sigma} \,, \quad \Phi^{-2} \tilde{\partial}_\nu \Phi \tilde{\partial}_\sigma \Phi \,, \\ &\Phi^{-2} g^{\lambda\mu} \tilde{\partial}_\lambda \Phi \tilde{\partial}_\mu \Phi g_{\nu\sigma} \,, \quad \tilde{\nabla}_\sigma (\Phi^{-1} \tilde{\partial}_\nu \Phi) + \tilde{\nabla}_\nu (\Phi^{-1} \tilde{\partial}_\sigma \Phi) \,, \quad \tilde{\nabla}^\mu (\Phi^{-1} \tilde{\partial}_\mu \Phi) g_{\nu\sigma} \,, \end{aligned} \tag{14}$$

where

$$\tilde{R}^S_{\nu\sigma}[g,A] = R_{\nu\sigma} - \left[\frac{D-2}{2} (\nabla_\sigma A_\nu + \nabla_\nu A_\sigma) + g_{\nu\sigma} \nabla_\mu A^\mu \right] + (D-2)\left(A_\nu A_\sigma - A_\lambda A^\lambda g_{\nu\sigma}\right) \,, \tag{15}$$

and

$$\tilde{R}[g,A] \equiv g^{\nu\sigma}\tilde{R}_{\nu\sigma}[g,A] = R - 2(D-1)\nabla_\mu A^\mu - (D-1)(D-2)A_\mu A^\mu \,. \tag{16}$$

We choose those as symmetric tensors are not traceless.[4] Using the Weyl invariant tensors (14), our model is described by the Lagrangian density

$$\mathcal{L} = -\sqrt{-\det M_{\mu\nu}} + (1-\lambda)\sqrt{-\det(\Phi^{\frac{4}{D-2}} g_{\mu\nu})}\,, \tag{17}$$

with

$$\begin{aligned} M_{\mu\nu} \equiv\ & \Phi^{\frac{4}{D-2}} g_{\mu\nu} - \alpha_1 \tilde{R}^S_{\mu\nu}[g,A] - \alpha_2 \tilde{R}[g,A] g_{\mu\nu} + \beta F_{\mu\nu} \\ & + \gamma_1 \Phi^{-2}\tilde{\partial}_\mu\Phi\tilde{\partial}_\nu\Phi + \gamma_2\Phi^{-2} g^{\lambda\sigma}\tilde{\partial}_\lambda\Phi\tilde{\partial}_\sigma\Phi g_{\mu\nu} \\ & - \gamma_3\left[\tilde{\nabla}_\mu(\Phi^{-1}\tilde{\partial}_\nu\Phi) + \tilde{\nabla}_\nu(\Phi^{-1}\tilde{\partial}_\mu\Phi)\right] - \gamma_4\, g^{\lambda\sigma}\tilde{\nabla}_\lambda(\Phi^{-1}\tilde{\partial}_\sigma\Phi) g_{\mu\nu}\,, \end{aligned} \tag{18}$$

where α_1, α_2, β, γ_1, γ_2, γ_3, γ_4 and λ are dimensionless constants.[5] Furthermore the Lagrangian density can be expressed by the new metric conformally related to the original one and new variables. If we choose

$$\hat{g}_{\mu\nu} \equiv f^{-2}\Phi^{\frac{4}{D-2}} g_{\mu\nu}\,, \tag{19}$$

where a mass scale f was introduced, and

$$\hat{A}_\mu \equiv A_\mu - \frac{2}{D-2}\partial_\mu \ln\Phi\,, \tag{20}$$

we can rewrite the Lagrangian density (17) as

$$\mathcal{L} = -\sqrt{-\det \hat{M}_{\mu\nu}} + (1-\lambda) f^D \sqrt{-\hat{g}}\,, \tag{21}$$

where $\hat{g} = \det \hat{g}_{\mu\nu}$ and

$$\hat{M}_{\mu\nu} = f^2\hat{g}_{\mu\nu} - \alpha_1\tilde{R}_{\mu\nu} - \alpha_2\tilde{R}\hat{g}_{\mu\nu} + \beta\hat{F}_{\mu\nu} + \gamma_1'\hat{A}_\mu\hat{A}_\nu + \gamma_2'\hat{g}^{\rho\sigma}\hat{A}_\rho\hat{A}_\sigma\hat{g}_{\mu\nu} + \gamma_3'\left(\hat{\nabla}_\mu\hat{A}_\nu + \hat{\nabla}_\nu\hat{A}_\mu\right) + \gamma_4'\,\hat{\nabla}^\rho\hat{A}_\rho\,\hat{g}_{\mu\nu}\,, \tag{22}$$

in which γ_1', γ_2', γ_3' and γ_4' are dimensionless constants rewritten by the set of the former, α_1, α_2, γ_1, γ_2, γ_3 and γ_4. Note that the scalar field $\Phi(x)$ is hidden away in the Lagrangian (21). The expansion of the determinant in (21) yields the non-minimal coupling term to gravity of the vector field and the induced curvature term as well as the ordinary scalar curvature and the gauge sector.[6] Therefore (21) is the promising Lagrangian for describing the vector inflation.

4 Cosmology of Weyl's gauge gravity

We consider cosmological aspect of the theory described by the Lagrangian (21). We assume the four dimensional flat universe and take the isotropic metric

$$ds^2 = -dt^2 + a^2(t)d\mathbf{x}^2\,. \tag{23}$$

We also assume that only $A_1(t)$ is homogeneously evolving, and $A_2 = A_3 = A_0 = 0$. By these ansatze, we look for the condition that the vector field behaves much like a scalar field at classical homogeneous level. Substituting the ansatze into (22), and after some calculation, we can extract the part of the Lagrangian which includes bilinear and higher-order of the vector field A_1. If we choose the parameters

[4] Judging from the number of fields and derivatives, the term $\Phi^{-\frac{4}{D-2}} g^{\lambda\mu}F_{\nu\lambda}F_{\sigma\mu}$ is allowed in the same order. But this term is different from others in the point that it includes two kinds of fields except for the metric. We discarded this marginally possible term here.

[5] If we demand that the terms with lowest derivatives in the expansion of the Weyl invariant Lagrangian density (17) look like the one of scalar-tensor theory, we must choose as $\alpha_1 + 4\alpha_2 > 0$ and $\gamma_1 + 4\gamma_2 + 4\gamma_3 + 8\gamma_4 > 0$, for $D = 4$.

[6] The expansion of the determinant is known for various dimensions.

as $\beta^2 = \frac{1}{2}\left(5\alpha_1\gamma_1' + 12\alpha_2\gamma_1' + 12\alpha_1\gamma_2' + 48\alpha_2\gamma_2'\right)$ and $(\gamma_3')^2 = -\frac{1}{2}\alpha_1\gamma_1'$, we find that the vector-field part becomes

$$a^3\left[\frac{1}{2}(\beta^2 - \gamma_3'^2)\dot{B}_1^2 - \frac{f^2}{2}(\gamma_1' + 4\gamma_2')B_1^2 - \frac{1}{8}\left(-\gamma_1'^2 + 4\gamma_1'\gamma_2' + 8\gamma_2'^2\right)B_1^4 + \cdots\right], \tag{24}$$

where $B_1 = \frac{A_1}{a}$, which acts as a scalar field.

We can tune the parameters to obtain the model of the realistic inflation. If $\alpha_2 = \gamma_1 = \gamma_2 = \gamma_3 = \gamma_4 = 0$, or these parameters take small values in comparison with α_1, there is only one parameter α_1 in the model. Unfortunately, the effective mass for B_1 may be large in this simple model. Another tuning of the parameters is also possible. If we choose appropriate parameters, the chaotic inflation [9] is practicable via the self-interaction of the scalar field B_1.

5 Summary and Outlook

We investigated Weyl invariant Dirac-Born-Infeld gravity. The choice of an appropriate frame breaks the Weyl invariance, and the vector field acquires mass as well as non-minimal coupling to gravity, and curvatures are induced. Therefore the Weyl invariant DBIE theory is expected to be a candidate for a model which causes an inflationary universe. We also examined slow development of the massive vector field and indicated that several scenarios of the inflation are possible by tuning of parameters appropriately.

Future works are in order. Numerical calculation and large simulation will be needed to understand the minute meaning of the Weyl invariant DBI gravity, because of the local inhomogenuity of the direction as well as the strength of vector fields is important for thorough understanding.[7] The inflation along with a fast evolution, known as the DBI inflation, is also interesting. The similar scenario is feasible in our model, though the higher-derivatives make the detailed analysis difficult. The higher-dimensional cosmology in the Weyl invariant DBI gravity is worth studying because of its rich content. Incidentally, DBI gravity in three dimensions is eagerly studied, which is related to new massive gravity theory. We think that the Weyl invariant extension is also of much interest.

Acknowledgements

The authors would like to thank K. Kobayashi for useful comments, and also the organizers of JGRG20.

References

[1] L. H. Ford, Phys. Rev. **D40** (1989) 967.

[2] A. B. Burd and J. E. Lidsey, Nucl. Phys. **B351** (1991) 679.

[3] A. Golovnev, V. Mukhanov, V. Vanchurin, JCAP 0806:009 (2008).

[4] A. Golovnev and V. Vanchurin, Phys. Rev. **D79** (2009) 103524. `arXiv:0903.2977 [astro-ph].CO`.

[5] T. Maki, Y. Naramoto and K. Shiraishi, Acta Phys. Polonica **B41** (2010) 1195.

[6] R. Utiyama, Prog. Theor. Phys. **50** (1973) 2080; W. F. Kao,Phys. Rev. **D61** (2000) 047501; P. Jain, S. Mitra, S. Panda and N. K. Singh, `arXiv:1010.3483 [hep-ph]` and references therein.

[7] S. Deser and G. W. Gibbons, Class. Quant. Grav. **15** (1998) L35 [hep-th/9803049].

[8] M. N. R. Wohlfarth, Class. Quant. Grav. **21** (2004) 1927 [hep-th/0310067]; D. N. Vollick, Phys. Rev. **D69** (2004) 064030; Phys. Rev. **D72** (2005) 084026; gr-qc/0601136; J. A. Nieto, Phys. Rev. **D70** (2004) 044042.

[9] A D Linde, Phys. Lett. **B129** (1983) 177.

[7] The calculation will be slightly simplified if we use a scalar auxiliary field.

Gravitational collapse in Painlevé-Gullstrand coordinates

Yuki Kanai[1], Masaru Siino[2] and Akio Hosoya[3]

Department of Physics, Tokyo Institute of Technology, Tokyo 152-8551

Abstract

We construct an exact solution for the spherical gravitational collapse in a single coordinate patch. To describe the dynamics of collapse, we use a generalized form of the Painlevé-Gullstrand coordinates in the Schwarzschild spacetime. The time coordinate of the form is the proper time of a free-falling observer so that we can describe the collapsing star not only outside but also inside the event horizon in a single coordinate patch. We show the both solutions corresponding to the gravitational collapse from infinity and from a finite radius.

1 Introduction

Numerous studies have been done on the properties of the black hole and the formation by gravitational collapse. The standard method of describing a spherical contraction of a uniformly distributed dust star [1, 2] is making a physically reasonable junction of the two different spacetimes corresponding to the interior and exterior regions of the collapsing body. The interior and exterior solutions are given by the FLRW metric and the Schwarzschild metric, respectively, and described in different coordinate systems. Although it is nothing wrong to construct solutions in such a manner, one cannot describe the dynamics of the collapsing star in terms of the coordinates of the observer outside the event horizon. The main purpose of this paper is to describe the both regions inside and outside the horizon by a single coordinate system in a physical way.

The Painlevé-Gullstrand coordinates of the Schwarzschild solution [3, 4] is, in fact, the key to a simple physical picture of black hole and gravitational collapse. Unlike the Schwarzschild form, the Painlevé-Gullstrand metric tensor has an off-diagonal element so that it is regular at the Schwarzschild radius and has a singularity only at the origin of the spherical coordinates. In other words, the surfaces of constant-time traverse the event horizon to reach the singularity. Therefore, the Painlevé-Gullstrand coordinates are convenient for exploring the geometry of collapsing star and black hole both inside and outside the horizon altogether by a single coordinate patch. This feature results from the fact that this coordinate system adopts a time coordinate as measured by an observer who is at rest at infinity and freely falls straightforward to the origin. We note that the physics of the collapsing matter is best described by its proper time, i.e., the Painlevé-Gullstrand time coordinate. In the present work, we generalize the Painlevé-Gullstrand metric to incorporate gravitational collapse.

2 Painlevé-Gullstrand coordinates

In this section, we derive generalized Painlevé-Gullstrand coordinates $(t_{\rm p}, r, \theta, \phi)$. We say here "generalized" in the sense that we introduce free-falling observers who start not only from infinity but also from other general points. The following mathematical derivation of the generalized Painlevé-Gullstrand coordinates is close to the derivation in [5], but the physical situation and the time coordinate are different.

The time coordinate $t_{\rm p}$ of this family is the proper time τ of an observer who freely falls radially from rest. Let us start with the Schwarzschild metric given in the standard form

$$ds^2 = -f(r){dt_{\rm s}}^2 + f^{-1}(r)dr^2 + r^2\left(d\theta^2 + \sin^2\theta d\phi^2\right), \tag{1}$$

[1]Email address: kanai@th.phys.titech.ac.jp
[2]Email address: msiino@th.phys.titech.ac.jp
[3]Email address: ahosoya@th.phys.titech.ac.jp

where $f(r) = 1 - 2M/r$. In the Schwarzschild spacetime, the normalized four-velocity ${u_{\rm s}}^{\mu}$ of an observer at the spacetime coordinates ${x_{\rm s}}^{\mu}(\tau)$ is defined by ${u_{\rm s}}^{\mu} = d{x_{\rm s}}^{\mu}/d\tau \equiv \dot{x}_{\rm s}{}^{\mu}$ with τ being the proper time, and can be explicitly written as ${u_{\rm s}}^{\mu} = \left(\dot{t}_{\rm s},\, \dot{r},\, \dot{\theta},\, \dot{\phi}\right) = \left(\varepsilon/f\,,\, -\sqrt{\varepsilon^2 - f},\, 0,\, 0\right)$, where ε is a constant of motion. Since we choose the Painlevé-Gullstrand time coordinate $t_{\rm p}$ as the proper time of the free-falling observer, the geodesic is orthogonal to the surfaces $t_{\rm p} =$ constant and the geodesic tangent vector $u_{{\rm s}\mu}$ is equal to the gradient of $t_{\rm p}$: $u_{{\rm s}\mu} = -\partial t_{\rm p}({x_{\rm s}}^{\mu})/\partial {x_{\rm s}}^{\mu}$, that is to say,

$$dt_{\rm p} = \varepsilon dt_{\rm s} + \frac{\sqrt{\varepsilon^2 - f}}{f} dr. \tag{2}$$

Consequently, the Painlevé-Gullstrand metric takes the form

$$ds^2 = -{dt_{\rm p}}^2 + \frac{1}{\varepsilon^2}\left(dr + v(r)dt_{\rm p}\right)^2 + r^2 d\Omega^2, \tag{3}$$

where $v(r) = \sqrt{\varepsilon^2 - f(r)}$ is radially free-falling velocity. The observer in geodesic motion have the normalized four-velocity

$${u_{\rm p}}^{\mu} = \left(\dot{t}_{\rm p},\, \dot{r},\, \dot{\theta},\, \dot{\phi}\right) = (1,\, -v,\, 0,\, 0)\,. \tag{4}$$

Note that the metric form (3) is different from that given by Martel and Poisson [5], for our time coordinate is ε times larger than theirs. This is because our metric is characterized by the free fall from various points at rest, while theirs by the free fall from infinity at various initial velocities.

The important point to note is that the metric (3) indicates an analogue of the conservation of energy in the Newtonian mechanics,

$$E = \frac{1}{2}\left(\frac{dr}{dt_{\rm p}}\right)^2 + \Phi(r), \tag{5}$$

where $E = (\varepsilon^2 - 1)/2$ is a conserved energy and $\Phi(r) = -M/r$ is a gravitational potential energy of a central force field. In particular, if the particle freely falls from rest at infinity, the conserved energy E is zero (i.e., $\varepsilon = 1$) and the metric (3) reduces to the standard form given by Painlevé and Gullstrand:

$$ds^2 = -{dt_{\rm p}}^2 + \left(dr + \sqrt{\frac{2M}{r}}dt_{\rm p}\right)^2 + r^2 d\Omega^2. \tag{6}$$

For a free fall from infinity, the radial velocity v is the Newtonian escape velocity $\sqrt{2M/r}$. It is obvious from the metric (3) and (6) that the Painlevé-Gullstrand coordinates are regular at the horizon $r = 2M$. This enables us to deal with the geometry of black hole both inside and outside the horizon.

In the subsequent sections, we will consider the solution of the Einstein equation with matter. In general, the energy E and the mass M are functions of $t_{\rm p}$ and r, not constant values. With the physical picture in mind and motivated by (3), we make the ansatz for the metric in the generalized Painlevé-Gullstrand form

$$ds^2 = -{dt_{\rm p}}^2 + \frac{1}{1 + 2E(t_{\rm p}, r)}\Big(dr + v(t_{\rm p}, r)dt_{\rm p}\Big)^2 + r^2 d\Omega^2, \tag{7}$$

where

$$v(t_{\rm p}, r) = \sqrt{2E(t_{\rm p}, r) + \frac{2m(t_{\rm p}, r)}{r}}. \tag{8}$$

3 Spherical gravitational collapse—from infinity

We solve the Einstein equation in the spherical gravitational collapse from infinity. According to Birkhoff's theorem, the Schwarzschild solution is the only solution of the vacuum Einstein equation for a spherically symmetric spacetime. In particular, even if matter distribution is not static but moving in a spherically symmetric way, the exterior vacuum region is given by the Schwarzschild metric. As shown in the previous

section, we can express the Schwarzschild metric in the Painlevé-Gullstrand form (6). Meanwhile, for the matter solution in the case of the gravitational collapse, the metric is assumed to be of the form

$$ds^2 = -{dt_\mathrm{p}}^2 + \left(dr + \sqrt{\frac{2m(t_\mathrm{p}, r)}{r}}dt_\mathrm{p}\right)^2 + r^2 d\Omega^2, \tag{9}$$

that is, the generalized form (7) with $E = 0$. For simplicity, we consider the Einstein equation with uniformly distributed dust matter, $G_{\mu\nu} = 8\pi T_{\mu\nu} = 8\pi\rho(t_\mathrm{p})u_{\mathrm{p}\mu}u_{\mathrm{p}\nu}$, and then obtain the solution of the mass function

$$m(t_\mathrm{p}, r) = \frac{4\pi}{3}r^3\rho(t_\mathrm{p}), \quad \rho(t_\mathrm{p}) = \frac{1}{6\pi {t_\mathrm{p}}^2}. \tag{10}$$

Let $R(t_\mathrm{p})$ be the surface radius of the star at time t_p and M be the mass inside the surface. It is natural to impose a boundary condition at the surface $r = R(t_\mathrm{p})$, that is, the mass,

$$m(t_\mathrm{p}, r)|_{r=R(t_\mathrm{p})} = \frac{4\pi}{3}R^3(t_\mathrm{p})\rho(t_\mathrm{p}) \equiv M, \tag{11}$$

of the star is constant, and then the radius of the boundary is given by

$$R(t_\mathrm{p}) = \left(\frac{9M}{2}(-t_\mathrm{p})^2\right)^{1/3}. \tag{12}$$

This means that the surface of the star is at rest at infinity and its radius monotonically decreases to zero as $t_\mathrm{p} \to 0$. In addition, the motion of the surface is geodesic. From simple calculations, the exterior metric (6) and the interior metric (9) turn out to be smoothly matched at the boundary surface $r = R(t_\mathrm{p})$. Therefore, we can describe the geometry of all the spacetime by a single coordinate system $(t_\mathrm{p}, r, \theta, \phi)$.

4 Spherical gravitational collapse—from a finite radius

We show the solution of the collapse from a finite radius. The standard model of a collapsing star is collapse from rest at a finite initial radius. It is not trivial to apply the idea of the Painlevé-Gullstrand coordinates to the situation of the collapse starting with a finite radius.

To begin with, we consider the boundary surface that freely falls from rest at a radius R_0. At the surface, the conservation law (5) gives the energy

$$E = -\frac{M}{R_0} \tag{13}$$

and the infall velocity

$$V(t_\mathrm{p}) = \sqrt{\frac{2M}{R(t_\mathrm{p})} - \frac{2M}{R_0}} \tag{14}$$

where $R(t_\mathrm{p})$ is the surface radius smaller than the initial radius R_0.

Next, when we assume that the exterior solution ranges from the contracting surface radius $R(t_\mathrm{p})$ to the initial radius R_0 (i.e., $R(t_\mathrm{p}) < r < R_0$), the energy remains the same as (13),

$$E_+ = -\frac{M}{R_0}, \tag{15}$$

and therefore the infall velocity becomes

$$v_+(r) = \sqrt{\frac{2M}{r} + 2E_+} = \sqrt{\frac{2M}{r} - \frac{2M}{R_0}} \tag{16}$$

in the exterior region. The exterior metric is therefore given by

$$ds_+^2 = -{dt_\mathrm{p}}^2 + \frac{1}{1 - \dfrac{2M}{R_0}}\left(dr + \sqrt{\frac{2M}{r} - \frac{2M}{R_0}}dt_\mathrm{p}\right)^2 + r^2 d\Omega^2. \tag{17}$$

Finally, in the interior region $0 < r < R(t_{\rm p})$, since the energy is now a function of time and radius coordinates, we make the ansatz

$$E_{-}(t_{\rm p}, r) = -\frac{m(t_{\rm p}, r)}{R_0 \dfrac{r}{R(t_{\rm p})}} \tag{18}$$

for the energy and

$$v_{-}(t_{\rm p}, r) = \sqrt{\frac{2m(t_{\rm p}, r)}{r} + 2E_{-}(t_{\rm p}, r)} = \sqrt{\frac{2m(t_{\rm p}, r)}{r}\left(1 - \frac{R(t_{\rm p})}{R_0}\right)} \tag{19}$$

for the velocity in the generalized Painlevé-Gullstrand metric (7).

In the case of the uniformly distributed dust, we can solve the Einstein equation taking into account the boundary condition as before. The mass function reduces to

$$m(t_{\rm p}, r) = \frac{4\pi}{3} r^3 \rho(t_{\rm p}), \quad \rho(t_{\rm p}) = \frac{3M}{4\pi R^3(t_{\rm p})}, \tag{20}$$

where the surface radius and the time coordinate are

$$R(t_{\rm p}) = \frac{R_0}{2}\left(1 + \cos\eta\right), \quad t_{\rm p} = \sqrt{\frac{{R_0}^3}{8M}}\left(\eta + \sin\eta\right), \tag{21}$$

respectively, and the parameter η takes the value from 0 to π. This interior solution

$$ds_{-}^2 = -{dt_{\rm p}}^2 + \frac{1}{1 - \dfrac{2M}{R_0}\left(\dfrac{r}{R(t_{\rm p})}\right)^2}\left(dr + \sqrt{\frac{2M}{R(t_{\rm p})} - \frac{2M}{R_0}}\,\frac{r}{R(t_{\rm p})}dt_{\rm p}\right)^2 + r^2 d\Omega^2 \tag{22}$$

is smoothly matched with the exterior metric (17) at the boundary surface $r = R(t_{\rm p})$. In fact, when the initial radius is large enough to satisfy $R_0 \gg M$, the energy and the velocity in the both regions become the same as those of the collapse from infinity.

5 Summary

For the description of gravitational collapse of a dust star, we have introduced the generalized Painlevé-Gullstrand coordinates with the time coordinate being the proper time of a free-falling observer. We gave the solutions of the Einstein equation in the cases of the collapse from a finite radius as well as from infinity. The metric describes both the interior and exterior regions of the star, which smoothly match at the surface of the star. More precisely, the metric is of C^1 class, while the metric component is of C^{1-} class. The choice of the Painlevé-Gullstrand time coordinate enables us to write the solutions inside and outside the event horizon in a single coordinate patch.

References

[1] J. R. Oppenheimer and H. Snyder, Phys. Rev. **56**, 455 (1939).

[2] C. W. Misner, K. S. Thorne and J. A. Wheeler, *Gravitation* (Freeman, San Francisco, 1973).

[3] P. Painlevé, C. R. Acad. Sci. (Paris) **173**, 677 (1921).

[4] A. Gullstrand, Arkiv. Mat. Astron. Fys. **16**, 1 (1922).

[5] K. Martel and E. Poisson, Am. J. Phys. **69**, 476 (2001).

Angular momentum at null infinity in five dimensions

Kentaro Tanabe[1](a), Norihiro Tanahashi[2](b) and Tetsuya Shiromizu[3](c)

(a) *Yukawa Institute, Kyoto University, Kyoto 606-8502*
(b) *Department of Physics, University of California, Davis, CA 95616, USA*
(c) *Department of Physics, Kyoto University, Kyoto 606-8502*

Abstract

Using the Bondi coordinates, we discuss the angular momentum at null infinity in five dimensions and address the Poincare covariance of the Bondi angular momentum. We also show the angular momentum loss/gain law due to gravitational waves. In four dimensions, the angular momentum at null infinity has the supertranslational ambiguity and then it is known that we cannot construct well-defined angular momentum there. On the other hand, we would stress that we can define angular momentum at null infinity without any ambiguity in higher dimensions. This is because of the non-existence of supertranslations in higher dimensions.

1 Introduction

Inspired by the recent progress of the string theory, the importance of the gravity theory in higher dimensional space-times is steadily growing. However, there are still many remaining issues to be investigated in higher dimensions. One issue among them is the asymptotic structure. For asymptotically flat space-times, the asymptotic structure is defined at spatial and null infinites. The asymptotic structure at spatial infinity (spi) is well-defined by conformal embedding in four and higher dimensions [1]. The asymptotic structure at null infinity in four dimensions is well studied by many authors [2, 3]. On the other hand, there are only a few work about the asymptotic structure at null infinity in higher dimensions. Indeed, asymptotic flatness has been defined by using conformal completion method in only even dimensions [4–6] and by using the Bondi coordinates in five dimensions [7].

The asymptotic symmetry at null infinity in four dimensions is semi-direct product of the Lorentz group and the supertranslational group, which is an infinite dimensional translational group. The presence of supertranslations implies the infinite number of the direction of translation, while the Poincare group has only four directions in four dimensions. Because of this infinite directions of translation, we cannot construct well-defined angular momentum in four dimensions. There are many attempts to define of angular momentum at null infinity in four dimensions, whereas all those definitions are suffered from supertranslational ambiguity. On the other hands, in five dimensions, since asymptotic symmetry is the Poincare group [7], we can expect that angular momentum at null infinity can be defined without any ambiguities. The purpose of this paper is to discuss angular momentum at null infinity in five dimensions. We will see that angular momentum can be defined well and show the Poincare covariance of the Bondi angular momentum.

2 Bondi coordinate and Einstein equations

In the Bondi coordinates $x^a = (u, r, \theta, \phi, \psi)$ the metric can be written as

$$ds^2 = -\frac{Ve^B}{r^2}du^2 - 2e^B dudr + r^2 h_{AB}(dx^A + U^A du)(dx^B + U^B du), \tag{1}$$

[1]Email address: tanabe@yukawa.kyoto-u.ac.jp
[2]Email address: tanahashi@ms.physics.ucdavis.edu
[3]Email address:shiromizu@tap.scphys.kyoto-u.ac.jp

where

$$h_{AB} = \begin{pmatrix} e^{C_1} & \sin\theta\sinh D_1 & \cos\theta\sinh D_2 \\ \sin\theta\sinh D_1 & e^{C_2}\sin^2\theta & \sin\theta\cos\theta\sinh D_3 \\ \cos\theta\sinh D_2 & \sin\theta\cos\theta\sinh D_3 & e^{C_3}\cos^2\theta \end{pmatrix}, \tag{2}$$

where $x^A = (\theta, \phi, \psi)$ and we adopted the gauge condition satisfying $\det h_{AB} = \sin^2\theta\cos^2\theta$. $u = \text{const.}$ are null hypersurfaces and the periods of the coordinates θ, ϕ and ψ are $\pi/2$, 2π and 2π, respectively. From the gauge condition, e^{C_3} can be written as

$$e^{C_3} = \frac{1 + e^{C_2}\sinh^2 D_2 + e^{C_1}\sinh^2 D_3 - 2\sinh D_1 \sinh D_2 \sinh D_3}{e^{C_1+C_2} - \sinh^2 D_1}. \tag{3}$$

Then h_{AB} have five functional freedom. In the following we will identify C_1, C_2, D_1, D_2, D_3 as those freedom. In this coordinate system, null infinity is represented by $r = \infty$ and the metric at null infinity is

$$ds^2 = -du^2 - 2dudr + r^2(d\theta^2 + \sin^2\theta d\phi^2 + \cos^2\theta d\psi^2). \tag{4}$$

To investigate the asymptotic structure at null infinity, we have to solve the Einstein equations near null infinity. Here note that five dimensional space-times have five degree of freedom of gravitational fields. If we identify h_{AB} as the freedom of gravitational field, C_1, C_2, D_1, D_2, D_3 can be expanded as

$$C_1(u, r, x^A) = \frac{C_{11}(u,x^A)}{r\sqrt{r}} + \frac{C_{12}(u,x^A)}{r^2} + \frac{C_{13}(u,x^A)}{r^2\sqrt{r}} + \frac{C_{14}(u,x^A)}{r^3} + O(r^{-7/2}) \tag{5}$$

$$C_2(u, r, x^A) = \frac{C_{21}(u,x^A)}{r\sqrt{r}} + \frac{C_{22}(u,x^A)}{r^2} + \frac{C_{23}(u,x^A)}{r^2\sqrt{r}} + \frac{C_{24}(u,x^A)}{r^3} + O(r^{-7/2}) \tag{6}$$

$$D_1(u, r, x^A) = \frac{D_{11}(u,x^A)}{r\sqrt{r}} + \frac{D_{12}(u,x^A)}{r^2} + \frac{D_{13}(u,x^A)}{r^2\sqrt{r}} + \frac{D_{14}(u,x^A)}{r^3} + O(r^{-7/2}) \tag{7}$$

$$D_2(u, r, x^A) = \frac{D_{21}(u,x^A)}{r\sqrt{r}} + \frac{D_{22}(u,x^A)}{r^2} + \frac{D_{23}(u,x^A)}{r^2\sqrt{r}} + \frac{D_{24}(u,x^A)}{r^3} + O(r^{-7/2}) \tag{8}$$

$$D_3(u, r, x^A) = \frac{D_{31}(u,x^A)}{r\sqrt{r}} + \frac{D_{32}(u,x^A)}{r^2} + \frac{D_{33}(u,x^A)}{r^2\sqrt{r}} + \frac{D_{34}(u,x^A)}{r^3} + O(r^{-7/2}). \tag{9}$$

From Einstein equations $R_{rA} = 0$, we can see that U^A can be expanded as

$$U^A = \frac{U_1^A(u,x^A)}{r^2\sqrt{r}} + \frac{U_2^A(u,x^A)}{r^3} + \frac{U_3^A(u,x^A)}{r^3\sqrt{r}} + \frac{U_4^A(u,x^A)}{r^4} + O(r^{-9/2}), \tag{10}$$

and coefficients U_n^A can be written by $C_{1n}, C_{2n}, D_{1n}, D_{2n}, D_{3n}$, for example,

$$U_1^\theta = \frac{2}{5}\left[\frac{1}{\sin\theta\cos^2\theta}\frac{\partial}{\partial\theta}(\sin\theta\cos^2\theta C_{11}) + \frac{1}{\sin\theta}\frac{\partial}{\partial\phi}D_{11} + \frac{1}{\cos\theta}\frac{\partial}{\partial\psi}D_{21} - \frac{1}{\sin\theta\cos\theta}C_{21}\right]. \tag{11}$$

Next, let us define the Bondi angular momentum from uA components of the metric. Near null infinity, $g_{u\phi}$ and $g_{u\psi}$ are expanded as

$$g_{u\phi} = \frac{1}{\sqrt{r}}\sin^2\theta U_1^\phi + \frac{1}{r}\sin^2\theta U_2^\phi + \frac{1}{r\sqrt{r}}\sin^2\theta U_3^\phi + \frac{1}{r^2}j^\phi + O(r^{-5/2}) \tag{12}$$

$$g_{u\psi} = \frac{1}{\sqrt{r}}\cos^2\theta U_1^\psi + \frac{1}{r}\cos^2\theta U_2^\psi + \frac{1}{r\sqrt{r}}\cos^2\theta U_3^\psi + \frac{1}{r^2}j^\psi + O(r^{-5/2}), \tag{13}$$

where

$$j^\phi = \sin\theta D_{11}U_1^\theta + \sin^2\theta C_{21}U_1^\phi + \sin\theta\cos\theta D_{31}U_1^\psi + \sin^2\theta U_4^\phi \tag{14}$$

$$j^\psi = \cos\theta D_{21}U_1^\theta + \sin\theta\cos\theta D_{31}U_1^\phi - \cos^2\theta(C_{11} + C_{21})U_1^\psi + \cos^2\theta U_4^\psi. \tag{15}$$

We define the Bondi angular momenta, $J^{\phi}_{\rm Bondi}$ and $J^{\psi}_{\rm Bondi}$, will be naturally defined by

$$J^{\phi}_{\rm Bondi}(u) \;=\; -\frac{1}{4\pi}\int_{S^3} j^{\phi} d\Omega\,,\; J^{\psi}_{\rm Bondi}(u) \;=\; -\frac{1}{4\pi}\int_{S^3} j^{\psi} d\Omega. \tag{16}$$

From $R_{uA} = 0$, we can derive the evolution equations of angular momentum $J^{\phi}_{\rm Bondi}$ and $J^{\psi}_{\rm Bondi}$. The evolution equation of $J^{\phi}_{\rm Bondi}$ by gravitational waves can be expressed as

$$\frac{d}{du}J^{\phi}_{\rm Bondi}(u) \;=\; -\frac{1}{4\pi}\int_{S^3}\left[\left(\frac{\partial j^{\phi}}{\partial u}\right)_{\rm radiation} + \left(\frac{\partial j^{\phi}}{\partial u}\right)_{\rm total\ derivative}\right] d\Omega, \tag{17}$$

where $(\partial j^{\phi}/\partial u)_{\rm radiation}$ is the radiation part given by

$$\begin{aligned}
\left(\frac{\partial j^{\phi}}{\partial u}\right)_{\rm radiation} \;=\;& -\frac{1}{4}\frac{\partial C_{11}}{\partial \phi}\frac{\partial C_{11}}{\partial u} - \frac{1}{8}\frac{\partial C_{21}}{\partial \phi}\frac{\partial C_{11}}{\partial u} - \frac{1}{8}\frac{\partial C_{11}}{\partial \phi}\frac{\partial C_{21}}{\partial u} - \frac{1}{4}\frac{\partial C_{21}}{\partial \phi}\frac{\partial C_{21}}{\partial u} \\
& -\frac{1}{4}\frac{\partial D_{21}}{\partial \phi}\frac{\partial D_{21}}{\partial u} + \frac{1}{10}\tan\theta\frac{\partial D_{31}}{\partial u}\left(\frac{\partial C_{11}}{\partial \psi} + \frac{\partial C_{21}}{\partial \psi}\right) + \frac{3}{20}\tan\theta\frac{\partial D_{31}}{\partial \psi}\frac{\partial C_{11}}{\partial u} \\
& +\frac{2}{5}\tan\theta\frac{\partial D_{31}}{\partial \psi}\frac{\partial C_{21}}{\partial u} - \frac{1}{4}\frac{\partial D_{11}}{\partial \phi}\frac{\partial D_{11}}{\partial u} + \frac{3}{20}\tan\theta\frac{\partial D_{11}}{\partial u}\frac{\partial D_{21}}{\partial \psi} - \frac{3}{20}\tan\theta\frac{\partial D_{11}}{\partial \psi}\frac{\partial D_{21}}{\partial u} \\
& -\frac{1}{4}\tan\theta\frac{\partial C_{11}}{\partial \psi}\frac{\partial D_{31}}{\partial u} - \frac{1}{10}\tan\theta\frac{\partial C_{21}}{\partial u}\frac{\partial D_{31}}{\partial \psi} - \frac{2}{5}\tan\theta\frac{\partial D_{31}}{\partial u}\frac{\partial C_{21}}{\partial \psi} - \frac{1}{4}\frac{\partial D_{31}}{\partial u}\frac{\partial D_{31}}{\partial \phi} \\
& +\frac{3}{20\cos^2\theta}\frac{\partial D_{31}}{\partial u}\frac{\partial}{\partial \theta}(\sin\theta\cos^2\theta D_{21}) - \frac{3}{20}\cos\theta\frac{\partial}{\partial \theta}(\tan\theta D_{31})\frac{\partial D_{21}}{\partial u} \\
& +\frac{3}{20\cos^2\theta}\frac{\partial D_{11}}{\partial u}\frac{\partial}{\partial \theta}(\sin\theta\cos^2\theta C_{11}) - \frac{3}{20}\cos\theta\frac{\partial C_{11}}{\partial u}\frac{\partial}{\partial \theta}(\tan\theta D_{11}) \\
& +\frac{3}{20\sin\theta\cos\theta}\frac{\partial C_{21}}{\partial u}\frac{\partial}{\partial \theta}(\sin^2\theta\cos\theta D_{11}) - \frac{3}{20}\sin\theta\frac{\partial C_{21}}{\partial \theta}\frac{\partial D_{11}}{\partial u} \\
& -\frac{3}{20\cos\theta}\frac{\partial}{\partial u}(C_{21}D_{11})
\end{aligned} \tag{18}$$

and since $(\partial j^{\phi}/\partial u)_{\rm total\ derivative}$ is the total derivative part which has no contribution to the evolution for the angular momentum by gravitational waves, we do not write its explicit form here. The evolution equation for $J^{\psi}_{\rm Bondi}$ has same form. For the details, see [8].

3 Asymptotic symmetry and Poincare covariance of angular momentum

Asymptotic symmetry is defined as the transformation group which preserve the boundary conditions of at null infinity. By infinitesimal transformations ξ^a, the metric is transformed as $g_{ab} \to g_{ab} + \delta g_{ab}$, where

$$\delta g_{ab} \;=\; \nabla_a \xi_b + \nabla_b \xi_a. \tag{19}$$

In Ref. [7], it was shown that the asymptotic symmetry at null infinity in five dimensions is Poincare group and the generator of the translations is represented as $\xi^u = -f(x^A)$ where the function $f(x^A)$ is

$$f(x^A) \;=\; a_u + a_x \sin\theta\cos\phi + a_y \sin\theta\sin\phi + a_z\cos\theta\cos\psi + a_w\cos\theta\sin\psi. \tag{20}$$

The global charges associated with asymptotic symmetry (the Poincare group), which is angular momentum M_{ab} should be transformed under translations as

$$M_{ab} \to M_{ab} + 2P_{[a}\omega_{b]}, \tag{21}$$

where $f = \hat{x}^a\omega_a$ and $\hat{x}^a = (1, \hat{x}^i)$ and $\hat{x}^i = (\sin\theta\cos\phi, \sin\theta\sin\phi, \cos\theta\cos\psi, \cos\theta\sin\psi)$. P^a is a Bondi momentum [8]. However, we are considering dynamical space-times which has no exact timelike Killing

vector. This means that the quantities M_{ab} would change due to gravitational waves under translations ($u \to u - f(x^A)$). Then, the expected transformations of M_{ab} under translation are

$$M_{ab}(u) \quad \to \quad M_{ab}(u-f) + 2P_{[a}(u)\omega_{b]} \;=\; M_{ab}(u) + 2P_{[a}(u)\omega_{b]} - \left(f\frac{d}{du}M_{ab}(u) \right)_{\text{radiation}}. \tag{22}$$

In fact, we can show this transformation as follows. By the translations, j^ϕ is transformed as

$$j^\phi \quad \to \quad j^\phi - \alpha(x^A)\frac{\partial j^\phi}{\partial u} + (\delta j^\phi)_{\text{non radiation}} + (\text{total derivative terms}), \tag{23}$$

where we do not write the explicit form of above terms. For the details, see [8]. Using the solutions for U^A, we can show that

$$J^\phi_{\text{Bondi}} \quad \to \quad J^\phi_{\text{Bondi}} - \frac{1}{4\pi}\int_{S^3}\left[-\alpha(x^A)\left(\frac{\partial j^\phi}{\partial u} \right)_{\text{radiation}} \right] d\Omega + \frac{3}{16\pi}\int_{S^3} m(u,x^A)\frac{\partial \alpha}{\partial \phi} d\Omega. \tag{24}$$

This transformation is equivalent to $M_{\hat{x}\hat{y}} \to M_{\hat{x}\hat{y}} + 2P_{[\hat{x}}\omega_{\hat{y}]} - (fdM_{\hat{x}\hat{y}}/du)_{\text{radiation}}$. This stands for the Poincare covariance of the Bondi angular momentum. In the same way, we can show the Poincare covariance of angular momentum J^ψ_{Bondi}.

4 Summary

In this paper, we defined the Bondi angular momentum at null infinity in five dimensions and showed the Poincare covariance of the Bondi angular momentum. In addition, we successfully confirmed the Bondi angular momentum loss/gain due to gravitational wave. Asymptotic symmetry at null infinity is an infinite dimensional translational group (supertranslations) in four dimensions, not a four dimensional group. Then this implies that the angular momentum at null infinity has always ambiguities. Contrasted with this, it is shown that asymptotic symmetry at null infinity is the Poincare group in five dimensions. Then we can define the Bondi angular momentum at null infinity in a Poincare covariant way without any ambiguities.

References

[1] K. Tanabe, N. Tanahashi and T. Shiromizu, J. Math. Phys. **50**, 072502 (2009) [arXiv:0902.1583 [gr-qc]].

[2] H. Bondi, M. G. J. van der Burg and A. W. K. Metzner, Proc. Roy. Soc. Lond. A **269**, 21 (1962).

[3] R. K. Sachs, Proc. Roy. Soc. Lond. A **270**, 103 (1962).

[4] S. Hollands and A. Ishibashi, J. Math. Phys. **46**, 022503 (2005) [arXiv:gr-qc/0304054].

[5] S. Hollands and A. Ishibashi, arXiv:hep-th/0311178.

[6] A. Ishibashi, Class. Quant. Grav. **25**, 165004 (2008) [arXiv:0712.4348 [gr-qc]].

[7] K. Tanabe, N. Tanahashi and T. Shiromizu, J. Math. Phys. **51**, 062502 (2010) [arXiv:0909.0426 [gr-qc]].

[8] K. Tanabe, N. Tanahashi and T. Shiromizu, arXiv:1010.1664 [gr-qc].

On Non-Linear Effects of BSW Mechanism

Masashi Kimura[(a)], Ken-ichi Nakao[(a)], and Hideyuki Tagoshi[(b)]

[(a)] *Department of Mathematics and Physics, Osaka City University, Osaka 558-8585*
[(b)] *Department of Earth and Space Science, Osaka University, Osaka 560-0043*

Abstract

In this presentation, in order to draw some implications concerning the effects of gravity generated by colliding particles in the BSW mechanism., we study a collision of two spherical dust shells based on the paper [1]. We show that the energy of two colliding shells in the center of mass frame *observable from infinity* has an upper limit due to their own gravity.

1 Introduction

Recently, Banados, Silk and West (BSW) showed that two test particles can collide with arbitrarily high energy in the center of mass (CM) frame near an extremal Kerr black hole, even though these particles were at rest at infinity in the infinite past [2]. We call this mechanism the BSW mechanism. If this mechanism was really workable, it might be possible to probe Planck-scale physics by observing the neighborhood of an extreme or almost extreme Kerr black hole. However, it is not yet clear whether particles can really be accelerated with sufficient efficiency to produce collisions with Planckian energies. To answer this question, it is necessary to consider, among other things, the effect of particle size, the effect of gravitational radiation on the trajectories of the particles, and the effect of the gravity generated by the particles themselves at the event horizon. In this presentation, we focus on the third effect.

2 Particle Collision around Extreme Charged Black Holes

Since the large CM energy of the particles produces strong gravity, we must take this into account when evaluating how large the CM energy can become in the BSW mechanism. However, it is difficult to treat the effects of gravity due to the particles, partly because Kerr spacetime is not very symmetric.

A mechanism similar to the BSW mechanism has been reported for Reissner-Nordström spacetime [3]. In this case, we can see the effects of the gravity generated by the colliding objects, since Reissner-Nordström spacetime is more symmetric than Kerr spacetime. This will be carried out in the next section. For now, we will ignore the effects of gravity.

The metric and gauge 1-form of Reissner-Nordström spacetime is

$$ds^2 = -f dt^2 + f^{-1} dr^2 + r^2(d\theta^2 + \sin^2\theta d\phi^2), \qquad A_a = \frac{Q}{r}(dt)_a, \tag{1}$$

where $f = 1 - 2M/r + Q^2/r^2$, M and Q being the mass parameter and the charge, respectively. In the case of $M^2 \geq Q^2$, the equation $f = 0$ has two positive roots, $r = r_\pm := M \pm \sqrt{M^2 - Q^2}$.

The action of a charged test particle subjected to the Lorentz force is given by

$$S \;=\; -m \int d\tau - q \int \sum_{\mu=0}^{3} A_\mu \frac{dx^\mu}{d\tau} d\tau, \tag{2}$$

where τ, m and q are the proper time, inertial mass and charge of the test particle, respectively. From the minimal action principle, we obtain its equation of motion. Without loss of generality, we may assume that the orbit of the particle is confined to the equatorial plane $\theta = \pi/2$. We can easily integrate the time and azimuthal components of the equation of motion and obtain

$$\frac{dt}{d\tau} = \frac{1}{f}\left(\mathcal{E}_{\rm c} - \frac{q}{m} A_t\right) \qquad \text{and} \qquad \frac{d\phi}{d\tau} = \frac{\ell_{\rm c}}{r^2}, \tag{3}$$

where $\mathcal{E}_{\rm c}$ and $\ell_{\rm c}$ are integration constants which correspond to the specific energy and angular momentum of the particle, respectively. We assume that $\mathcal{E}_{\rm c}$ is positive. By using the normalization condition of the 4-velocity and the above results, we obtain the energy equation

$$\left(\frac{dr}{d\tau}\right)^2 + V = 0, \qquad \text{with} \qquad V = -\left(\mathcal{E}_{\rm c} - \frac{qQ}{mr}\right)^2 + \left(1 - \frac{2M}{r} + \frac{Q^2}{r^2}\right)\left(1 + \frac{\ell_{\rm c}^2}{r^2}\right). \tag{4}$$

For simplicity, hereafter, we consider a particle radially falling toward the black hole, i.e., the case of $\ell_{\rm c} = 0$. If the background spacetime is extreme $Q = M$ and the charge of the particle is $q = \mathcal{E}_{\rm c} m$, the effective potential becomes

$$V = -\frac{(\mathcal{E}_{\rm c}^2 - 1)(r - M)^2}{r^2}. \tag{5}$$

From the above equation, we can see that this charged test particle asymptotically approaches the future degenerate horizon $r = r_{\pm} = M$, i.e., the outward null if $\mathcal{E}_{\rm c} > 1$.

We consider another particle with an identical inertial mass m to the charged particle but with a vanishing charge, which is also radially falling toward the black hole. Then, let us consider the collision between this neutral particle and the charged particle with the effective potential (5). We assume that the specific energy of the neutral particle is equal to that of the charged particle, $\mathcal{E}_{\rm c}$. We can easily see that, by this assumption, the absolute value of the velocity of the neutral particle is larger than that of the charged particle at the same radial coordinate. Hence, the charged particle corresponds to the 1st particle, whereas the neutral particle corresponds to the 2nd particle. The square of the CM energy at the collision event is obtained as

$$E_{\rm cm}^2 = \sqrt{-g_{ab}p^a p^b} = \sqrt{2}m\sqrt{1 - g_{ab}u^a_{(1)}u^b_{(2)}} \tag{6}$$

$$= \frac{2m^2 r}{r - M}\left[1 - \frac{M}{r} + \mathcal{E}_{\rm c}^2 - \sqrt{\mathcal{E}_{\rm c}^2 - 1}\sqrt{\mathcal{E}_{\rm c}^2 - \left(1 - \frac{M}{r}\right)^2}\right]. \tag{7}$$

We can easily see that the CM energy diverges in the limit $r \to r_{\pm} = M$. This is similar to the BSW mechanism.

It is still difficult to treat the gravity of particles in Reissner-Nordström spacetime. Here, it is worthwhile to note that the world line of a radially moving test particle is equivalent to the trajectory of an infinitesimally thin spherical test shell by virtue of the symmetry of Reissner-Nordström spacetime. Since the CM energy at the collision event between two shells is the same as that given by Eq. (6) (see Eq.(12) in Sec.4), an indefinitely large CM energy is realizable also in this case. The gravity generated by an infinitesimally thin spherical shell can be treated analytically by the Israel formalism [4]. In the next section, we study the effects of the gravity of a thin spherical charged shell.

3 Infinitesimally thin spherical charged dust shell

In this section, we study the gravity generated by a thin spherical shell with a non-vanishing charge. An infinitesimally thin shell is equivalent to a singular timelike hypersurface Σ which divides spacetime into two regions V_1 and V_2 (see Fig.1).

We consider a spherically symmetric dust shell whose surface stress-energy tensor is given by $S^{ab} = \sigma u^a u^b$, where σ is the energy density per unit area, which is assumed to be non-negative, and u^a can be regarded as the 4-velocity of the shell. We assume that this dust shell may have a non-vanishing charge. According to the Birkhoff's theorem, the spacetime except on the shell itself is Reissner-Nordström spacetime, and hence the metric in the region V_i is given as

$$ds^2 = -f_{(i)}dt_{(i)}^2 + f_{(i)}^{-1}dr^2 + r^2(d\theta^2 + \sin^2\theta d\phi^2), \tag{8}$$

where $f_{(i)}$ is $f_{(i)} = 1 - 2M_i/r + Q_i^2/r^2$. Here, note that all coordinates except for the time t are common to both V_1 and V_2. We assume $M_i \geq |Q_i|$ and denote the roots of $f_{(i)} = 0$ by $r = r_{\pm}^{(i)} := M_i \pm \sqrt{M_i^2 - Q_i^2}$.

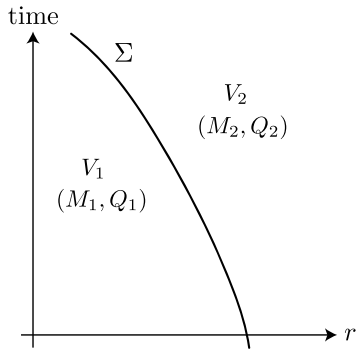

Figure 1: Schematic spacetime diagram of a spherical timelike shell.

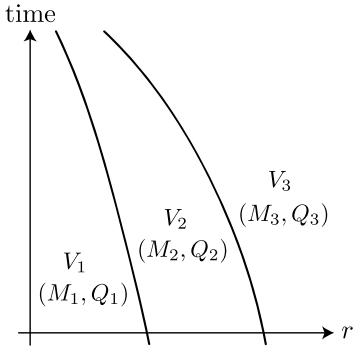

Figure 2: Schematic spacetime diagram of two spherical timelike shells.

In this coordinate system, the components of the 4-velocity u^a are $u^\mu_{(i)} = \left(dt_{(i)}/d\tau, dr/d\tau, 0, 0\right)$, where τ is chosen so that $u^a u_a = -1$.

Using the normalization condition of the 4-velocity, the constraint of Einstein equation leads to $\mu := 4\pi\sigma r^2 = \text{const}$. This equation means that the proper mass μ of the shell is conserved. From the Israel formalism [4] and the normalization condition of the 4-velocity, we obtain the energy equation for the shell as

$$\left(\frac{dr}{d\tau}\right)^2 + V_{\rm shell} = 0, \qquad \text{with} \qquad V_{\rm shell} = -\left(\mathcal{E} - \frac{q\langle Q\rangle}{\mu r}\right)^2 + 1 - \frac{2\langle M\rangle}{r} + \frac{\langle Q\rangle^2}{r^2} - \left(\frac{\mu}{2r}\right)^2 + \left(\frac{q}{2r}\right)^2, \quad (9)$$

where $\mathcal{E} := (M_2 - M_1)/\mu, \langle M\rangle := (M_2 + M_1)/2, \langle Q\rangle := (Q_2 + Q_1)/2$, and $q := Q_2 - Q_1$. Thus, we may call $\mathcal{E}$ the specific energy of the shell, and we assume that it is positive. We can see that the effective potential (9) has almost the same form as that for a charged test particle (4) with $\ell_{\rm c} = 0$, or equivalently, that for a spherical charged test shell. The differences between Eqs. (4) with $\ell_{\rm c} = 0$ and (9) are regarded as the self-gravity and self-electric interaction terms.

Let us investigate whether the charged dust shell can asymptotically approach an outward null hypersurface as in the case of the charged test shell. The outside of the shell is the region V_2, and the BH horizon in this region is $r = r_+^{(2)} := M_2 + \sqrt{M_2^2 - Q_2^2}$ which is the outward null hypersurface. Hence, we search for the condition which guarantees $r = r_+^{(2)}$ to be the asymptote of the singular hypersurface Σ. This task is equivalent to solving $V(r_+^{(2)}) = 0$ and $dV(r)/dr|_{r=r_+^{(2)}} = 0$ in terms of the parameters, Q_2, M_2, μ, q and $\mathcal{E}$. We have

$$Q_2 = M_2, \qquad q^2 - 2M_2 q + 2M_2\mathcal{E}\mu - \mu^2 = 0. \quad (10)$$

The condition $Q_2 = M_2$ implies that region V_2 is an extreme Reissner-Nordström spacetime. If the above conditions hold, the effective potential becomes

$$V_{\rm shell} = -\frac{(\mathcal{E}^2 - 1)(r - M_2)^2}{r^2}. \quad (11)$$

Namely, if this charged dust shell is contracting and $\mathcal{E} > 1$, it asymptotically approaches the outward null hypersurface $r = M_2$. Hence, it is likely that a BSW-type mechanism can occur in this system.

4 effect of gravity generated by colliding shells in BSW process

In this section, we consider collisions of two spherical dust shells and discuss the CM energy at the collision event. These two shells divide the spacetime into three regions, V_1, V_2 and V_3, before the collision (see Fig.2). We assume that the inner shell is the same as that considered in the preceding

section, whose parameters satisfy conditions (10). We also assume that, as in Sec. 2, the outer shell is composed of neutral dust and has the same specific energy $\mathcal{E}$ as the inner charged shell. Because the outer shell is neutral, we have $Q_2 = Q_3$. Further, both shells are assumed to have an identical proper mass, $\mu_{\rm out} = \mu_{\rm in} = \mu$.

The energy of the colliding shells in this frame, which is also called the CM energy $E_{\rm cm}$, is given by

$$E_{\rm cm} = \int T^{ab}_{\Sigma} \bar{u}_a \bar{u}_b r^2 \sin\theta d\bar{\lambda} d\theta d\phi = \sqrt{2}\mu\sqrt{1 - g_{ab}u^a_{\rm in}u^b_{\rm out}}, \tag{12}$$

where T^{ab}_{Σ} is the total stress-energy tensor of the shells, $\bar{\lambda}$ is the proper length in the direction of $\bar{n}^a$. As expected, the CM energy of the shells takes the same form as that of the particles.

As shown in the preceding section, the outward null hypersurface $r = r^{(2)}_{\pm} = M_2$ is the asymptote of the inner shell. Thus, as in the case of the test shells, the closer the relative velocity between the inner and outer shells approaches to the speed of light, the closer the collision event approaches to the BH horizon in V_2, i.e., $r = r^{(2)}_{\pm}$. As a result, the CM energy at the collision event can be indefinitely large, even if the gravity of the colliding shells is taken into account. However, we should note that if the two shells collide inside the BH horizon in V_3, i.e., $r \leq r^{(3)}_{+} = M_3 + \sqrt{M_3^2 - Q_3^2}$, distant observers like us could not see the collision of these shells. We should also note that $r^{(3)}_{+}$ is larger than $r^{(2)}_{\pm}$ by virtue of the gravity generated by the outer shell. Thus, the observable CM energy is less than that of the collision at $r = r^{(3)}_{+}$ given in accordance with Eq. (12) as

$$E_{\rm cm}(r = r^{(3)}_{+}) = \sqrt{2}\mu\sqrt{1 - \frac{1}{\sqrt{\mu}}\frac{Y}{2\sqrt{\mathcal{E}(3\mathcal{E}\mu + 2M_1)} + 2\mathcal{E}\sqrt{\mu}}}, \tag{13}$$

where the function Y is given by

$$\begin{aligned} Y \;=\; & \sqrt{\mathcal{E}^2 - 1}\sqrt{2(\mathcal{E}\mu + M_1) + 2(\mathcal{E} - 1)\left(\sqrt{\mathcal{E}\mu(3\mathcal{E}\mu + 2M_1)} + 2\mathcal{E}\mu + M_1\right) + \mu} \\ & \times\sqrt{-2(\mathcal{E}\mu + M_1) + 2(\mathcal{E} + 1)\left(\sqrt{\mathcal{E}\mu(3\mathcal{E}\mu + 2M_1)} + 2\mathcal{E}\mu + M_1\right) + \mu} \\ & -\mathcal{E}\left(2\mathcal{E}\left(\sqrt{\mathcal{E}\mu(3\mathcal{E}\mu + 2M_1)} + 2\mathcal{E}\mu + M_1\right) + \mu\right). \end{aligned} \tag{14}$$

We can see from the above result that the CM energy at the collision event between these shells has an upper limit in the observable domain $r > r^{(3)}_{+}$, and this limit is determined by the mass M_1 of the "central black hole" and the proper mass of the two shells. Here, we should note that in order that the outer shell overtakes the inner shell, $(u^r_{\rm out})^2 - (u^r_{\rm in})^2$ should be positive at $r = r^{(3)}_{+}$. We can see that this condition holds from $\left[(u^r_{\rm out})^2 - (u^r_{\rm in})^2\right]_{r=r^{(3)}_{+}} > 0$.

In the case that the mass M_1 of the central black hole is much larger than the proper masses of the shells μ, the observable CM energy becomes $E_{\rm cm} \simeq 2^{1/4}\mathcal{E}^{1/4}\sqrt{\mathcal{E} - \sqrt{\mathcal{E}^2 - 1}}M_1^{1/4}\mu^{3/4}$. We can see from this equation that the observable CM energy is not indefinitely large. Thus, when estimating the size of the observable CM energy, the gravity caused by the colliding objects must not be ignored, even if their initial energy is very small. Our result suggests that an upper limit also exists for the total energy of colliding particles in the center of mass frame in the observable domain in the BSW process due to the gravity of the particles.

References

[1] M. Kimura, K. i. Nakao and H. Tagoshi, Phys. Rev. D **83**, 044013 (2011) [arXiv:1010.5438 [gr-qc]].

[2] M. Banados, J. Silk and S. M. West, Phys. Rev. Lett. **103**, 111102 (2009) [arXiv:0909.0169 [hep-ph]].

[3] O. B. Zaslavskii, JETP Lett. **92**, 571 (2010) [arXiv:1007.4598 [gr-qc]].

[4] W. Israel, Nuovo Cim. B **44S10**, 1 (1966).

Non-equilibrium Condensation Process in a Holographic Superconductor

Shunichiro Kinoshita[1](a), Keiju Murata,(b) and Norihiro Tanahashi(c)

(a) *Yukawa Institute for Theoretical Physics, Kyoto University, Kyoto 606-8502*
(b) *DAMTP, University of Cambridge, Centre for Mathematical Sciences, Wilberforce Road, Cambridge, CB3 0WA, United Kingdom*
(c) *Department of Physics, University of California, Davis, CA 95616, USA*

Abstract

We study the non-equilibrium condensation process in the holographic superconductor. When the temperature T is smaller than a critical temperature T_c, there are two black hole solutions, the Reissner-Nordström-AdS black hole and a black hole with a scalar hair. In the boundary theory, they can be regarded as the supercooled normal phase and the superconducting phase, respectively. We consider perturbations on supercooled Reissner-Nordström-AdS black holes and study their non-linear time evolution to know about physical phenomena associated with rapidly-cooled superconductors. We find that, for $T < T_c$, the initial perturbations grow exponentially and, eventually, spacetimes approach the hairy black holes. We also clarify how the relaxation process from a far-from-equilibrium state proceeds in the boundary theory by observing the time dependence of the superconducting order parameter. Finally, we study the time evolution of event and apparent horizons and discuss their correspondence with the entropy of the boundary theory. Our result gives a first step toward the holographic understanding of the non-equilibrium process in superconductors.

1 Introduction

Recently, the duality between the superconductor and gravity theory has been proposed [1–3] as a new application of the AdS/CFT correspondence, in which the simplest gravity theory is given by Einstein-Maxwell-charged scalar theory with negative cosmological constant. In this gravity theory one of static solutions is the well-known Reissner-Nordström-AdS black hole solution, in which the scalar field vanishes. It is known that this solution is unstable when the temperature T is lower than a critical temperature T_c. In consequence of the instability, it is expected that the scalar field will condense into a non-vanishing profile and eventually the black hole will have the scalar hair breaking the $U(1)$-gauge symmetry spontaneously. For low temperature $T < T_c$, such a static solution has been constructed numerically. It was shown that the solution has similar properties with superconductors [3]. Thus, the instability of the Reissner-Nordström-AdS black hole for low temperature was identified with the superconducting phase transition. In the same way, the Reissner-Nordström-AdS and hairy black holes in the gravitational theory were identified with the normal and superconducting phases of a superconductor realized within the dual field theory, respectively. Such holographic superconductors are considered as a hopeful approach to understand the property of strongly correlated electron systems.

The non-equilibrium process of strongly correlated systems such as superconductors is not fully understood because of difficulties in its theoretical treatment. The AdS/CFT correspondence offers a novel approach to this longstanding problem. To understand non-equilibrium process of strongly correlated systems, we should simply solve classical dynamics of gravitational systems in the bulk thanks to the duality. For near equilibrium dynamics of superconductor, there are several approaches from the holography. However, very little progress has been made in the regime that the theory is far from equilibrium. In this work, we give a holographic approach to understand the non-equilibrium process of superconductors.

As we mentioned before, for low temperature $T < T_c$ there are two phases of black holes in the gravity side, the Reissner-Nordström-AdS and the hairy black holes, and they are regarded as supercooled

[1]Email address: kinosita@yukawa.kyoto-u.ac.jp

normal phase and superconducting phases, respectively. In this work, we consider small perturbations on the supercooled Reissner-Nordström-AdS black holes and study non-linear time evolution of them. Because of the instability of the Reissner-Nordström-AdS black holes, the initial perturbations will grow exponentially at the beginning of the time evolution. It is expected that the exponential growth is saturated due to the non-linear effect and the spacetimes will approach static solutions. It is believed that the final states of the time evolution are the hairy black holes obtained in [3], but there is no proof. Studying non-linear time evolutions of the Einstein-Maxwell-charged scalar system, we will show that the final states are given by the hairy black holes. We are also interested in dynamics of the phase transition on the boundary theory. To reveal the non-equilibrium process, we observe the time dependence of the superconducting order parameter and study how the normal phase goes to superconducting phase in the boundary theory in the middle of the time evolution. Finally, we study the time evolution of event and apparent horizons. See also [4] in detail.

2 Equations of motion

We consider the 4-dimensional Einstein-Maxwell-charged scalar theory with negative cosmological constant, whose action is given by

$$S = \int d^4x\sqrt{-g}\left[R + \frac{6}{L^2} - \frac{1}{4}F_{\mu\nu}F^{\mu\nu} - |\partial_\mu\psi - iqA_\mu\psi|^2 - m^2|\psi|^2\right] , \tag{1}$$

where L is the AdS curvature scale and q is the $U(1)$-charge of the complex scalar field ψ. The field strength is defined by $F = dA$ as usual. This theory is introduced in [1–3] as a gravity dual of a superconductor. In addition to the diffeomorphism symmetry, this action has the local $U(1)$ symmetry, $A \to A + d\lambda$ and $\psi \to e^{iq\lambda}\psi$, where λ is an arbitrary scalar function. Hereafter, we take the unit of $L = 1$ and set $m^2 = -2$.

For simplicity, we assume that the spacetime has the plane symmetry. Using the diffeomorphism and $U(1)$ gauge symmetries together with the assumed plane symmetry, we can take the metric ansatz without loss of generality as

$$\begin{aligned} ds^2 &= -\frac{1}{z^2}\left[F(t,z)dt^2 + 2dtdz\right] + \Phi(t,z)^2(dx^2+dy^2) , \\ A &= \alpha(t,z)dt , \\ \psi &= \psi(t,z) . \end{aligned} \tag{2}$$

We use the ingoing Eddington-Finkelstein coordinates, (t,z). In these coordinates, the AdS boundary is located at $z = 0$. These coordinates are convenient for our numerical calculations since we can easily extend time slices defined by constant-t surfaces into the inside of the event horizon and also set the AdS boundary to be a constant-z plane. Note that diffeomorphism and $U(1)$ gauge symmetries have not been completely fixed, because the form of the variables (2) is invariant under the residual symmetry, $1/z \to 1/z + g(t)$, $\alpha \to \alpha + \partial_t\lambda(t)$ and $\psi \to e^{iq\lambda(t)}\psi$. These residual gauge symmetries will be fixed by the boundary conditions. The complete set of the equations of motion are given by

$$(\Phi D\Phi)' - \frac{\Phi^2}{4z^2}\left(\frac{1}{2}z^4\alpha'^2 + m^2|\psi|^2 - 6\right) = 0 , \tag{3}$$

$$2z^2(D\psi)' + iqz^2\alpha'\psi + 2z^2\Phi^{-1}(D\Phi)\psi' + 2z^2\Phi^{-1}\Phi' D\psi + m^2\psi = 0 , \tag{4}$$

$$(z^2(z^{-2}F)')' - z^2\alpha'^2 + 4\Phi^{-2}(D\Phi)\Phi' - (\psi^{*\prime}D\psi + \psi' D\psi^*) = 0 , \tag{5}$$

$$2z^2(D\alpha)' + z^4(z^{-2}F)'\alpha' + 4z^2\Phi^{-1}(D\Phi)\alpha' - 2iq(\psi D\psi^* - \psi^* D\psi) = 0 , \tag{6}$$

and

$$\Phi^{-2}C_1 \equiv -2\Phi^{-1}D^2\Phi - \left(F' - \frac{2}{z}F\right)\Phi^{-1}D\Phi - |D\psi|^2 = 0 , \tag{7}$$

$$\Phi^{-2}C_2 \equiv -2z^3\Phi^{-1}(z\Phi'' + 2\Phi') - z^4|\psi'|^2 = 0 , \tag{8}$$

$$\Phi^{-2}C_3 \equiv -z^2[z^2\alpha'' + 2z\alpha' + 2z^2\Phi^{-1}\Phi'\alpha' + iq(\psi\psi^{*\prime} - \psi^*\psi')] = 0 , \tag{9}$$

where $' \equiv \partial_z$ and derivative operator D is defined as

$$\begin{aligned} &D\Phi = \partial_t\Phi - F\partial_z\Phi/2 \ , \quad D^2\Phi = \partial_t(D\Phi) - F\partial_z(D\Phi)/2 \ , \quad D\alpha = \partial_t\alpha - F\partial_z\alpha/2 \ , \\ &D\psi = \partial_t\psi - F\partial_z\psi/2 - iq\alpha\psi \ , \quad D\psi^* = \partial_t\psi^* - F\partial_z\psi^*/2 + iq\alpha\psi^* \ . \end{aligned} \tag{10}$$

Here, the operator $\partial_t - F\partial_z/2$ represents the derivative along the outgoing null vector. We regard Eqs. (3-6) as evolution equations and Eqs. (7-9) as constraint equations. We solve the evolution equations for the time evolution and use the constraint equations only at the AdS boundary and the initial surface to give the boundary conditions for the time evolution.

One of static solutions of the equations of motion is merely the Reissner-Nordström-AdS black hole solution (with planar horizon), which is given by $F = 1 - 2Mz^3 + \frac{1}{4}Q^2z^4$, $\Phi = z^{-1}$, $\alpha = Qz$ and $\psi = 0$. Parameters M and Q are proportional to mass and charge of the black hole, respectively. For this solution, the complex scalar field has a trivial configuration $\psi = 0$. That is, this black hole has no "hair" except for the mass and electric charge. The event horizon is located at $z = z_+$ determined by $F(z_+) = 0$. In terms of the horizon radius z_+, we can rewrite M as

$$M = \frac{1}{2z_+^3}\left(1 + \frac{1}{4}Q^2z_+^4\right) \ . \tag{11}$$

The temperature of the black hole is given by

$$T = -\frac{1}{4\pi}\frac{dF}{dz}\bigg|_{z=z_+} = \frac{12 - z_+^4Q^2}{16\pi z_+} \ . \tag{12}$$

It is known that this solution is unstable when the temperature T is smaller than a critical temperature T_c. The numerical value of the T_c is obtained in [1–3]. In consequence of the instability, it is expected that the scalar field will grow and eventually the black hole will have the scalar hair. Thus, the $U(1)$-gauge symmetry is spontaneously broken due to condensation of the complex scalar field. Indeed, for low temperature $T < T_c$ at fixed charge Q, static solutions of the hairy black hole with $\psi \neq 0$ exist and have been constructed numerically [3]. Similarly to the previous case, the temperature of the hairy black hole is given by $T = -\frac{1}{4\pi}\frac{dF}{dz}\big|_{z=z_+}$, where $F(z_+) = 0$.

This instability was identified with the superconducting phase transition in the dual theory [1–3]. In this work, we will investigate the dynamical process of the superconducting phase transition in the view of the gravity theory. Since we are taking the ingoing Eddington-Finkelstein coordinates (2), our time slices are given by null surfaces. We consider a slightly-perturbed Reissner-Nordström-AdS spacetime as initial data, and study non-linear time evolution from it. At the AdS boundary, we give appropriate boundary conditions. Inside the event horizon, we excise a region before encountering the singularity for the numerical calculation.

3 Numerical Results

In this section, we summarize the numerical results obtained by the evolution scheme of the previous section. In Section 3.1, we describe the free parameter and the initial conditions. We summarize the general properties of the bulk field dynamics in Section 3.2. After that, we study the dynamics of the order parameter of the boundary theory, which is the boundary value of the bulk scalar field, in Section 3.3. In Section 3.4, we focus on the dynamics of the event and the apparent horizons.

3.1 Initial data and parameters

We should specify the $\psi(t = 0, z)$, M and Q on the initial surface. We treat M and Q as fixed parameters since they are conserved quantities in our setting. Without loss of generality, we can fix one of the parameters using a residual coordinate transformation. In our numerical calculation, we put $M = \left(1 + Q^2/4\right)/2$. This condition implies that the *horizon radius* of the initial black hole is set to unity

(see Eq. (11))[2]. As for the initial data of ψ, we consider the Gaussian perturbation on the Reissner-Nordström-AdS spacetime as

$$\psi(t=0,z) = \frac{\mathcal{A}}{\sqrt{2\pi}\,\delta} z^2 \exp\left[-\frac{(z-z_m)^2}{2\delta^2}\right] \tag{13}$$

with $\mathcal{A} = 0.01$, $\delta = 0.05$ and $z_m = 0.3$. We tried several other initial conditions and found that they yield qualitatively the same results. Thus, we will show below the results only for the initial data given by Eq. (13).

3.2 Dynamics of bulk fields

First of all, we show the dynamics of the bulk scalar field. In Figure 1, we depict the dynamics of the amplitude of the complex scalar, $|\psi(t,z)|$, for $q = 1.0$ and $T/T_c = 0.5$ at the initial state. The critical temperature T_c is evaluated for a fixed charge Q[3]. We can find that much of the wave packet of the initial perturbation (13) is instantaneously absorbed in the horizon within $tT_c \lesssim 0.06$. Because of the remnant of the wave packet, which is the unstable mode contained in the initial perturbation (13), the scalar density grows exponentially for $tT_c \lesssim 6$. The exponential growth is saturated by the nonlinear effect at $tT_c \sim 6$. In $tT_c \gtrsim 6$, the scalar density approaches a static solution. As in Figure 2, we can find that the static solution coincides with the hairy black hole solution obtained in [3]. Thus, our result gives numerical proof of the conjecture that the final state of the instability of the Reissner-Nordström-AdS black hole is the hairy black hole. Our result also implies that, for the most symmetric perturbations, the hairy black holes are stable. It is worth noting that this phase transition from the initial Reissner-Nordström-AdS black hole to the final hairy black hole is a dynamical process under the fixed mass and charge. It implies that the temperature of the initial state and that of the final state are different in general. Indeed, the temperature of the final hairy black hole increases compared to the initial temperature due to the phase transition.

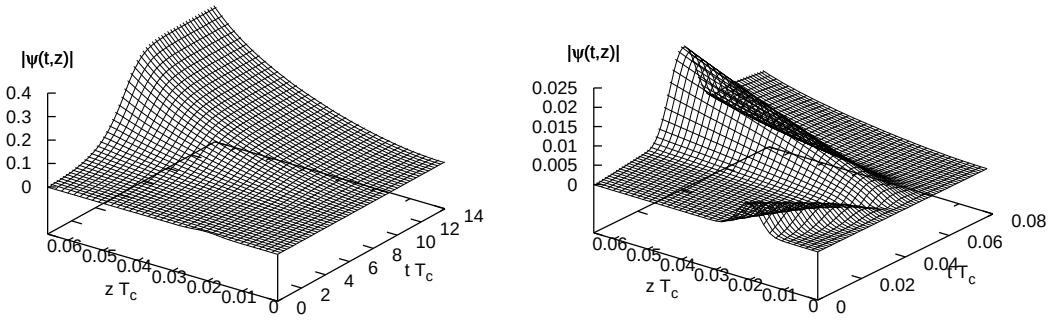

(a) $0 \le tT_c \le 14$ (b) $0 \le tT_c \le 0.08$

Figure 1: The dynamics of the scalar field for $q = 1.0$ and initial temperature $T/T_c = 0.5$. In Figure (a), we depict the dynamics of the amplitude of the complex scalar field, $|\psi(t,z)|$, on (t,z)-plane for $0 \le tT_c \le 14$. In Figure (b), we depict $|\psi(t,z)|$ for $0 \le tT_c \le 0.08$ in order to focus on the behavior of the wave packet of the initial perturbation.

3.3 Dynamics of the order parameter

In following subsections, we show some results from the numerical solutions that are relevant to the dual theory. In this subsection, we describe the non-linear dynamics of the order parameter of the boundary theory.

[2]To be accurate, the z_+ defined by Eq. (11) slightly differs from the apparent horizon position for our initial data, because we will give small perturbations on the Reissner-Nordström-AdS solutions.

[3] For $q = 1.0$, 1.5 and 2.0, the critical temperature T_c is respectively given by $T_c/\sqrt{Q} = 0.03589$, 0.08421 and 0.1234.

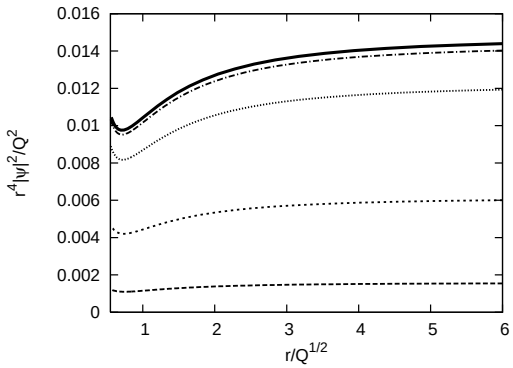

Figure 2: The function $r^4|\psi|^2/Q^2$ is depicted on fixed time slices, where r is circumference radius defined by $r = \Phi$. From bottom to top, the curves correspond to $tT_c = 5.15$, 6.44, 7.73 and 9.02. The top solid curve correspond to that of the hairy black hole. We can see that the solution approaches the hairy black hole.

From the asymptotic form of the numerical solution $\psi(t, z)$, we can read off $\psi_2(t)$ defined by $\psi(t, z) = \psi_1(t)z + \psi_2(t)z^2 + \cdots$. The coefficient $\psi_2(t)$ is regarded as the superconducting order parameter in dual theory and so we set $\psi_1(t) = 0$. Following [2, 3], we define the order parameter on the boundary theory as $\langle \mathcal{O}_2(t) \rangle \equiv \sqrt{2}\,\psi_2(t)$. In Figure 3, we depict the time dependence of the order parameter $(q|\langle \mathcal{O}_2(t) \rangle|)^{1/2}/T_c$, for $q = 1.5$ and $T/T_c = 0.2$, 0.4, 0.6, 0.8, 1.1, 1.2 and 1.4. The sharp signal at the small t is caused by the initial perturbation (13). For $T > T_c$, the initial perturbation dissipates and the order parameter converges to zero. On the other hand, for $T < T_c$, the order parameter grows exponentially and approaches a non-trivial value. We find that, for $T < T_c$, the more rapidly the order parameter converges to its final value for lower temperature.

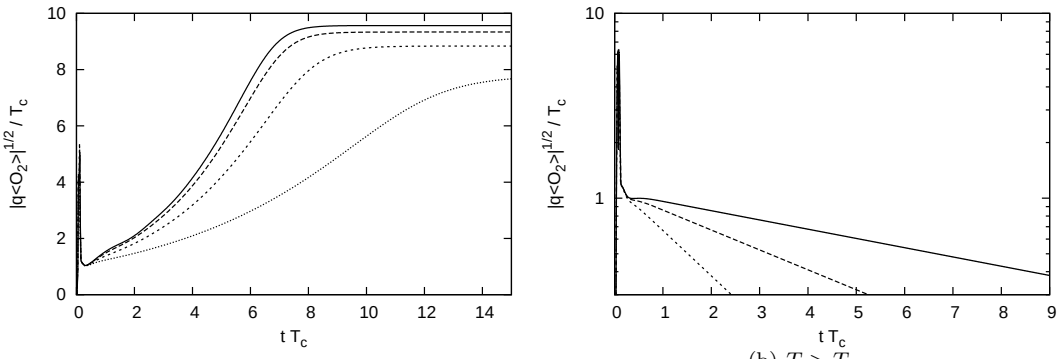

(a) $T < T_c$ (b) $T > T_c$

Figure 3: The dynamics of the order parameter is depicted for $q = 1.5$. In Figure (a), the curves from top to bottom correspond to $T/T_c = 0.2$, 0.4, 0.6 and 0.8. In Figure (b), the curves from top to bottom correspond to $T/T_c = 1.1$, 1.2 and 1.4. Note that the vertical axis in Figure (b) is logarithmic scale, while that is linear scale in Figure (a).

3.4 Evolution of horizons

Now, we investigate the time evolution of apparent and event horizons. The apparent horizon $z = z_{\rm AH}(t)$ can be determined from $D\Phi(t, z_{\rm AH}(t)) = 0$. We determine the event horizon $z = z_{\rm EH}(t)$ as follows. For sufficiently late time, spacetimes settle static solutions. Thus, at late time, the event horizon can be easily determined by $F(t, z_{\rm EH}(t)) = 0$. To determine the event horizon for any t, we solve the null geodesic

equations, $\dot{z}_{\rm EH}(t) = -F(t, z_{\rm EH}(t))/2$, backward along the tangent to the event horizon at late time. Then, we obtain null geodesic generators of the event horizon and find the location of the event horizon $z = z_{\rm EH}(t)$. Once we know the $z_{\rm EH}(t)$ and $z_{\rm AH}(t)$, we can calculate the area of event and apparent horizons as

$$\text{Area(event/apparent horizon)} = \Phi(t, z_{\rm EH/AH}(t))^2 \ . \tag{14}$$

In Figure 4, we depict the time evolution of the area of the horizons. We find that the area of the horizons monotonically increase by the time evolution and the event horizon has larger area than that of the apparent horizon. We also see that, after the final state has settled to equilibrium, the apparent horizon and the event horizon coincide. In addition, the two horizons seem to coincide even at the initial state. Thus, it is quite likely that we can regard the area of the horizon as the entropy at the initial state.

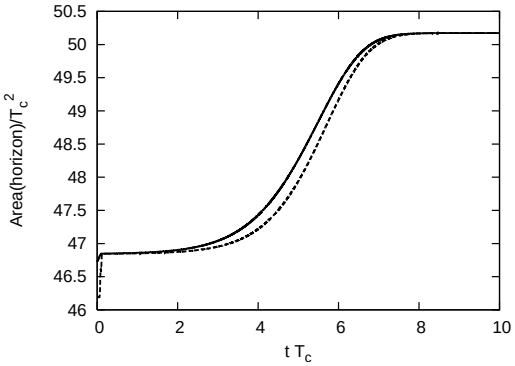

Figure 4: The time evolution of the area of event and apparent horizons are depicted for $q = 1.5$ and $T/T_c = 0.4$ at the initial state. Solid and dashed curves correspond to the area of event and apparent horizons respectively.

References

[1] S. S. Gubser, Phys. Rev. D **78**, 065034 (2008) [arXiv:0801.2977 [hep-th]].

[2] S. A. Hartnoll, C. P. Herzog and G. T. Horowitz, Phys. Rev. Lett. **101**, 031601 (2008) [arXiv:0803.3295 [hep-th]].

[3] S. A. Hartnoll, C. P. Herzog and G. T. Horowitz, JHEP **0812**, 015 (2008) [arXiv:0810.1563 [hep-th]].

[4] K. Murata, S. Kinoshita and N. Tanahashi, JHEP **1007**, 050 (2010) [arXiv:1005.0633 [hep-th]].

Inflation driven by the Galileon field

Tsutomu Kobayashi[1(a)], Masahide Yamaguchi[2(b)] and Jun'ichi Yokoyama[3(a,c)]

[(a)] *Research Center for the Early Universe (RESCEU), Graduate School of Science, The University of Tokyo, Tokyo 113-0033, Japan*
[(b)] *Department of Physics, Tokyo Institute of Technology, Tokyo 152-8551, Japan*
[(c)] *Institute for the Physics and Mathematics of the Universe (IPMU), the University of Tokyo, Kashiwa, Chiba, 277-8568, Japan*

Abstract

We propose a new class of inflation model, *G-inflation*, which has a Galileon-like nonlinear derivative interaction of the form $G(\phi,(\nabla\phi)^2)\Box\phi$ in the Lagrangian with the resultant equations of motion being of second order. It is shown that (almost) scale-invariant curvature fluctuations can be generated even in the exactly de Sitter background and that the tensor-to-scalar ratio can take a significantly larger value than in the standard inflation models, violating the standard consistency relation. Furthermore, violation of the null energy condition can occur without any instabilities. As a result, the spectral index of tensor modes can be blue, which makes it easier to observe quantum gravitational waves from inflation by the planned gravitational-wave experiments such as LISA and DECIGO as well as by the upcoming CMB experiments such as Planck and CMBpol.

Inflation in the early universe is now a part of the standard cosmology to solve the horizon and flatness problem as well as to account for the origin of density/curvature fluctuations. It is most commonly driven by a scalar field dubbed as inflaton, and the research on inflationary cosmology has long been focused on the shape of the inflaton potential in the particle physics context. Its underlying physics is now being probed using precision observations of the cosmic microwave background and large scale structure which are sensitive only to the dynamical nature of the inflaton. Reflecting this situation, a number of novel inflation models have been proposed extending the structure of the kinetic function.

In this article, we propose a new class of inflation models, for which the scalar field Lagrangian is of the form

$$\mathcal{L}_\phi = K(\phi,X) - G(\phi,X)\Box\phi, \tag{1}$$

where K and G are general function of ϕ and $X := -\nabla_\mu\phi\nabla^\mu\phi/2$. The most striking property of this generic Lagrangian (1) is that it gives rise to derivatives no higher than two both in the gravitational- and scalar-field equations. In the simplest form the nonlinear term may be given by $G\Box\phi \propto X\Box\phi$, which has recently been discussed in the context of the so-called *Galileon* field [1, 2]. The general form $G(\phi,X)\Box\phi$ may be regarded as an extension of the Galileon-type interaction $X\Box\phi$ while maintaining the field equations to be of second-order [3]. So far the phenomenological aspects of the Galileon-type scalar field have been studied mainly in the context of dark energy and modified gravity. In this article, we discuss primordial inflation induced by this type of fields. See also [4, 5].

Now let us start investigating our model in detail. Assuming that ϕ is minimally coupled to gravity, the total action is given by

$$S = \int \mathrm{d}^4x\sqrt{-g}\left[\frac{M_{\rm Pl}^2}{2}R + \mathcal{L}_\phi\right]. \tag{2}$$

The energy-momentum tensor $T_{\mu\nu}$ derived from the action reads

$$T_{\mu\nu} = K_X\nabla_\mu\phi\nabla_\nu\phi + Kg_{\mu\nu} - 2\nabla_{(\mu}G\nabla_{\nu)}\phi + g_{\mu\nu}\nabla_\lambda G\nabla^\lambda\phi - G_X\Box\phi\nabla_\mu\phi\nabla_\nu\phi. \tag{3}$$

[1]Email address: tsutomu"at"resceu.s.u-tokyo.ac.jp
[2]Email address: gucci"at"phys.titech.ac.jp
[3]Email address: yokoyama"at"resceu.s.u-tokyo.ac.jp

The equation of motion of the scalar field is equivalent to $\nabla_\nu T_\mu^{\ \nu} = 0$. Here and hereafter we use the notation K_X for $\partial K/\partial X$ etc.

Taking the homogeneous and isotropic background, $\mathrm{d}s^2 = -\mathrm{d}t^2 + a^2(t)\mathrm{d}\mathbf{x}^2$, $\phi = \phi(t)$, let us study inflation driven by the Galileon-like scalar field (1), which we call "*G-inflation*." The energy-momentum tensor (3) has the form $T_\mu^{\ \nu} = \mathrm{diag}(-\rho, p, p, p)$ with

$$\rho = 2K_X X - K + 3G_X H\dot{\phi}^3 - 2G_\phi X, \quad p = K - 2\left(G_\phi + G_X\ddot{\phi}\right)X. \tag{4}$$

Here, ρ has an explicit dependence on the Hubble rate H. The gravitational field equations are thus given by

$$3M_{\rm Pl}^2 H^2 = \rho, \quad -M_{\rm Pl}^2\left(3H^2 + 2\dot{H}\right) = p, \tag{5}$$

and the scalar field equation of motion reads

$$\begin{aligned} &K_X\left(\ddot{\phi} + 3H\dot{\phi}\right) + 2K_{XX}X\ddot{\phi} + 2K_{X\phi}X - K_\phi - 2\left(G_\phi - G_{X\phi}X\right)\left(\ddot{\phi} + 3H\dot{\phi}\right) \\ &+6G_X\left[(HX)^{\cdot} + 3H^2X\right] - 4G_{X\phi}X\ddot{\phi} - 2G_{\phi\phi}X + 6HG_{XX}X\dot{X} = 0. \end{aligned} \tag{6}$$

These three equations constitute two independent evolution equations for the background. Note that the appearance of the terms proportional to the Hubble parameter in Eqs. (4) and (6) reflects the fact that the Galileon symmetry is broken in the curved spacetime even if we constrain our functional form of the Lagrangian which possess its symmetry in the Minkowski spacetime.

We begin with constructing an exactly de Sitter background, taking K and G as

$$K(\phi, X) = K(X), \quad G(\phi, X) = g(\phi)X. \tag{7}$$

In this case, inflation is driven purely kinematically, although G-inflation does not preclude a potential-driven inflationary solution with an explicit ϕ-dependence in $K(\phi, X)$ in general; see Eq. (1). If $g(\phi) =$ const, *i.e.*, the Lagrangian has a shift symmetry $\phi \to \phi +$ const, we have an exactly de Sitter solution satisfying $\dot{\phi} =$const,

$$3M_{\rm Pl}^2 H^2 = -K, \quad \mathcal{D} := K_X + 3gH\dot{\phi} = 0. \tag{8}$$

Let us now provide a simple example:

$$K = -X + \frac{X^2}{2M^3\mu}, \quad g = \frac{1}{M^3}, \tag{9}$$

where M and μ are parameters having dimension of mass. The de Sitter solution is given by

$$X = M^3\mu x, \quad H^2 = \frac{M^3}{18\mu}\frac{(1-x)^2}{x}, \tag{10}$$

where x $(0 < x < 1)$ is a constant satisfying $(1-x)/x\sqrt{1-x/2} = \sqrt{6}\mu/M_{\rm Pl}$. For $\mu \ll M_{\rm Pl}$, it can be seen that $x \simeq 1 - \sqrt{3}\mu/M_{\rm Pl}$ and hence the Hubble rate during inflation is given in terms of M and μ as $H^2 \simeq M^3\mu/(6M_{\rm Pl}^2)$. As the first term in $K(X)$ has the "wrong" sign, one may worry about ghost-like instabilities. However, as we will see shortly, this model is free from ghost and any other instabilities.

We now move on to study scalar perturbations in this model using the unitary gauge with $\delta\phi = 0$ and

$$\mathrm{d}s^2 = -(1+2\alpha)\mathrm{d}t^2 + 2a^2\partial_i\beta\mathrm{d}t\mathrm{d}x^i + a^2(1+2\mathcal{R}_\phi)\mathrm{d}\mathbf{x}^2. \tag{11}$$

In this gauge we have $\delta T_i^{\ 0} = -G_X\dot{\phi}^3\partial_i\alpha$, and hence this gauge does not coincide with the comoving gauge $\delta T_i^{\ 0} = 0$. Consequently, $\mathcal{R}_\phi$ in general differs from the comoving curvature perturbation $\mathcal{R}_c$. This point highlights the difference between the present model and the standard k-inflationary model described simply by $\mathcal{L}_\phi = K(\phi, X)$. It will turn out that the variable $\mathcal{R}_\phi$ is subject to an analogous wave equation to the familiar Sasaki-Mukhanov equation.

Expanding the action (2) to second order in the perturbation variables and then substituting the Hamiltonian and momentum constraint equations to eliminate α and β, we obtain the following quadratic action for $\mathcal{R}_\phi$:

$$S^{(2)} = \frac{1}{2}\int \mathrm{d}\tau \mathrm{d}^3x\, z^2 \left[\mathcal{G}(\mathcal{R}'_\phi)^2 - \mathcal{F}(\vec{\nabla}\mathcal{R}_\phi)^2\right], \tag{12}$$

where

$$z := \frac{a\dot{\phi}}{H - G_X\dot{\phi}^3/2M_{\rm Pl}^2}, \tag{13}$$

$$\mathcal{F} := K_X + 2G_X\left(\ddot{\phi} + 2H\dot{\phi}\right) - 2\frac{G_X^2}{M_{\rm Pl}^2}X^2 + 2G_{XX}X\ddot{\phi} - 2\left(G_\phi - XG_{\phi X}\right), \tag{14}$$

$$\mathcal{G} := K_X + 2XK_{XX} + 6G_XH\dot{\phi} + 6\frac{G_X^2}{M_{\rm Pl}^2}X^2 - 2\left(G_\phi + XG_{\phi X}\right) + 6G_{XX}HX\dot{\phi}, \tag{15}$$

and the prime represents differentiation with respect to the conformal time τ. The squared sound speed is therefore $c_s^2 = \mathcal{F}/\mathcal{G}$. To avoid ghost and gradient instabilities we require the conditions $\mathcal{F} > 0$ and $\mathcal{G} > 0$. One should note that the above equations have been derived without assuming any specific form of $K(\phi, X)$ and $G(\phi, X)$.

It is now easy to check whether a given G-inflation model is stable or not. In the simplest class of models (7), we have

$$\mathcal{F} = -\frac{K_X}{3} + \frac{XK_X^2}{3K},\ \mathcal{G} = -K_X + 2XK_{XX} - \frac{XK_X^2}{K}, \tag{16}$$

where the "slow-roll" suppressed terms are ignored. For the previous toy model (9) one obtains $\mathcal{F} = x(1-x)/6(1-x/2)$ and $\mathcal{G} = 1 - x + (1-x/2)^{-1}$. Since $0 < x < 1$, both $\mathcal{F}$ and $\mathcal{G}$ are positive. In this model, the sound speed is smaller than the speed of light: $c_s^2 \le (4\sqrt{2}-5)/21 \simeq 0.031 < 1$.

The power spectrum of $\mathcal{R}_\phi$ generated during G-inflation can be evaluated by writing the perturbation equation in the Fourier space as

$$\frac{\mathrm{d}^2u_k}{\mathrm{d}y^2} + \left(k^2 - \frac{\tilde{z}_{,yy}}{\tilde{z}}\right)u_k = 0, \tag{17}$$

where $\mathrm{d}y = c_s\,\mathrm{d}\tau$, $\tilde{z} := (\mathcal{F}\mathcal{G})^{1/4}z$, and $u_k := \tilde{z}\mathcal{R}_{\phi,k}$. Let us again focus on the class of models (7). Note that the sound speed c_s may vary rapidly in the present case, and hence one cannot neglect $\epsilon_s := \dot{c}_s/Hc_s$ even when working in leading order in "slow-roll." Indeed, one finds $\epsilon_s \simeq \eta X(\mathcal{G}_X/\mathcal{G} - \mathcal{F}_X/\mathcal{F})$. With some manipulation, one obtains $\tilde{z}_{,yy}/\tilde{z} \simeq (-y)^{-2}[2 + 3\epsilon\mathcal{C}(X)]$ with

$$\mathcal{C}(X) := \frac{K}{K_X}\frac{Q_X}{Q}, \quad Q(X) := \frac{(K - XK_X)^2}{18M_{\rm Pl}^4Xc_s^2\sqrt{\mathcal{F}\mathcal{G}}}. \tag{18}$$

It should be emphasized that scalar fluctuations are generated even from exactly de Sitter inflation. This is because, as mentioned before, the Galileon symmetry is broken in the de Sitter background, which is manifest from $\dot{\phi} = $ const. This situation is in stark contrast with other inflation models: scalar fluctuations cannot be generated from the de Sitter background with $\dot{\phi} = 0$ in usual potential-driven inflation, while the exactly de Sitter background cannot be realized in k-inflation.

The normalized mode is given in terms of the Hankel function as

$$u_k = \frac{\sqrt{\pi}}{2}\sqrt{-y}H_\nu^{(1)}(-ky), \quad \nu := \frac{3}{2} + \epsilon\,\mathcal{C}, \tag{19}$$

from which it is straightforward to obtain the power spectrum and the spectral index:

$$\mathcal{P}_{\mathcal{R}_\phi} = \left.\frac{Q}{4\pi^2}\right|_{c_sk=1/(-\tau)}, \quad n_s - 1 = -2\epsilon\,\mathcal{C}. \tag{20}$$

The behavior of tensor perturbations in G-inflation is basically the same as in the usual inflation models and is completely determined geometrically. Therefore, the power spectrum and the spectral index of primordial gravitational waves are given by $\mathcal{P}_T = (8/M_{\rm Pl}^2)(H/2\pi)^2$ and $n_T = -2\epsilon$. However, it would be interesting to point out that the tensor spectrum can be blue in G-inflation with possible violation of the NEC. The positive tensor spectral index not only is compatible with current observational data, but also broadens the limits on cosmological parameters. Moreover, the amplitude of tensor fluctuation with such a blue spectral index is relatively enhanced for large frequencies, which makes its direct detection easier.

As a concrete example, let us come back again to the previous toy model (9), in which the tensor-to-scalar ratio is given by

$$r \simeq \frac{16\sqrt{6}}{3}\left(\frac{\sqrt{3}\mu}{M_{\rm Pl}}\right)^{3/2} \quad \text{for} \quad \mu \ll M_{\rm Pl}. \tag{21}$$

With the properly normalized scalar perturbation, $\mathcal{P}_{\mathcal{R}_\phi} = 2.4 \times 10^{-9}$, we can easily realize large r to saturate the current observational bound, exceeding the predictions of the chaotic inflation models. For example, for $M = 0.00425 \times M_{\rm Pl}$ and $\mu = 0.032 \times M_{\rm Pl}$ we find $r = 0.17$, which is large enough to be probed by the PLANCK satellite. Note that neither the standard consistency relation, $r = -8n_T$, nor the k-inflation-type consistency relation, $r = -8c_s n_T$, holds in our model.

In summary, we have proposed a novel inflationary mechanism driven by the Galileon-like scalar field. Our model —*G-inflation*— is a new class of inflation models with the term proportional to $\Box\phi$ in the Lagrangian, which opens a new branch of inflation model building. Contrary to the most naive expectation, the interaction of the form $G\left(\phi, (\nabla\phi)^2\right)\Box\phi$ gives rise to derivatives no higher than two in the field equations [3]. In this sense, G-inflation is distinct also from ghost condensation and B-inflation. After G-inflation, the universe is reheated through the gravitational particle production with successful thermal leptogenesis. We have also shown that G-inflation can generate (almost) scale-invariant density perturbations, possibly together with a large amplitude of primordial gravitational waves. These facts have great impacts on the planned and ongoing gravitational wave experiments and CMB observations. In a forthcoming paper we shall compute the non-Gaussianity of the curvature perturbation from G-inflation, which would be a powerful discriminant of the scenario in addition to the violation of the standard consistency relation.

References

[1] A. Nicolis, R. Rattazzi and E. Trincherini, Phys. Rev. D **79**, 064036 (2009).

[2] C. Deffayet, G. Esposito-Farese and A. Vikman, Phys. Rev. D **79**, 084003 (2009); C. Deffayet, S. Deser and G. Esposito-Farese, Phys. Rev. D **80**, 064015 (2009).

[3] C. Deffayet, O. Pujolas, I. Sawicki and A. Vikman, arXiv:1008.0048 [hep-th].

[4] T. Kobayashi, M. Yamaguchi and J. Yokoyama, Phys. Rev. Lett. **105**, 231302 (2010) [arXiv:1008.0603 [hep-th]].

[5] K. Kamada, T. Kobayashi, M. Yamaguchi and J. Yokoyama, arXiv:1012.4238 [astro-ph]; T. Kobayashi, M. Yamaguchi and J. Yokoyama, *to appear*.

Scalar field dynamics in nonminimally coupled hybrid inflation

Seoktae Koh[1]

Center for Quantum Spacetime, Sogang University, Shinsu-dong 1, Mapo-gu, Seoul, 121-742, South Korea

Abstract

We study the dynamics of a scalar field which is coupled to gravity nonminimally in hybrid inflation. If the ϕ^2 term in the hybrid potential is dominant over ϕ^4 term, the potential has an maximum at $\phi = \phi_e$. Whereas if ϕ^4 term is dominant over the ϕ^2 term, the potential has a minimum at $\phi = \phi_e$. Since the observable quantities such as power spectrum, spectral indices, and tensor-to-scalar ratio are invariant under the conformal transformation, we compute the observable quantities in Einstein frame.

1 Introduction

The nonminimal coupling to gravity in inflation have drawn attention recently *e.g.* in Higgs inflation [1] in which the nonminimal coupling makes it possible to be $\lambda \sim \mathcal{O}(0.1-1)$ and resolve the discrepancy between the inflation scale ($10^{16}GeV$) and electroweak scale ($100GeV$) for large nonminimal coupling. In addition, the inflation model from the high energy theory such as string theory provides the nonminimal coupling terms naturally.

Hybrid inflation is physically well motivated in string theory or high energy [2]. Inflation can be terminated naturally through the tachyonic instability. During inflation, since the waterfall field is massive, it stays along $\chi = 0$. If ϕ reach to $\phi_c = \sqrt{\lambda v^2/g^2}$, the tachyonic instability begins and the inflation ends. Even if the nonminimal coupling of inflaton to gravity is taken into account [3] [4] [5], since it does not change the dynamics of the waterfall field, the tachyonic instability condition is not changed.

In this paper, we investigate the dynamics of the inflaton in hybrid inflation in which the inflaton is coupled to gravity nonminimally. Inflation would be terminated via tachyonic instability or the violation of the slow-roll conditions. And then using the conformal invariance of the power spectrum of the curvature and tensor perturbations [6] [4][7], we compute the spectral indices and the tensor-to-scalar ratio.

2 Background

We start with the hybrid inflation action in which the inflaton is coupled to gravity nonminimally

$$S = \int d^4\sqrt{-g}\left[\frac{1}{2\kappa^2}(1-\kappa^2\xi\phi^2)R - \frac{1}{2}(\partial\phi)^2 - \frac{1}{2}(\partial\chi)^2 - V(\phi,\chi)\right], \tag{1}$$

where $\kappa^2 = 8\pi/m_{pl}^2$ and ξ is the nonminimal coupling parameter. In this work, we only focus on the case of $\xi < 0$.

Varying the action (1) yields the equations of motion

$$H^2 = \frac{\kappa^2}{3(1-\kappa^2\xi\phi^2)}\left[6\xi H\phi\dot{\phi} + \frac{1}{2}(\dot{\phi}^2+\dot{\chi}^2) + V\right], \tag{2}$$

$$\dot{H} = \frac{\kappa^2}{1-\kappa^2\xi\phi^2}\left[\xi\{\dot{\phi}^2 + \phi\ddot{\phi} - H\phi\dot{\phi}\} - \frac{1}{2}(\dot{\phi}^2+\dot{\chi}^2)\right], \tag{3}$$

$$\ddot{\phi} + 3H\dot{\phi} - \frac{\kappa^2\xi\phi(1-6\xi)\dot{\phi}^2 - \kappa^2\xi\phi\dot{\chi}^2}{1-\kappa^2\xi\phi^2(1-6\xi)} + \frac{4\kappa^2\xi\phi V + (1-\kappa^2\xi\phi^2)V_\phi}{1-\kappa^2\xi\phi^2(1-6\xi)} = 0, \tag{4}$$

$$\ddot{\chi} + 3H\dot{\chi} + V_\chi = 0 \tag{5}$$

[1]Email address: steinkoh@sogang.ac.kr

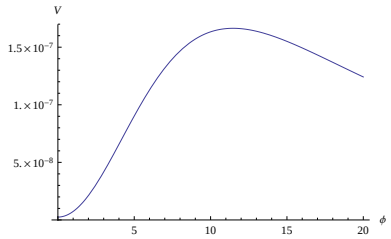

Figure 1: $\lambda = g^2 = 1, v^2 = 10^{-4} m_{pl}^2, m^2 = 10^{-8} m_{pl}^2, \xi = -3 \times 10^{-4}$

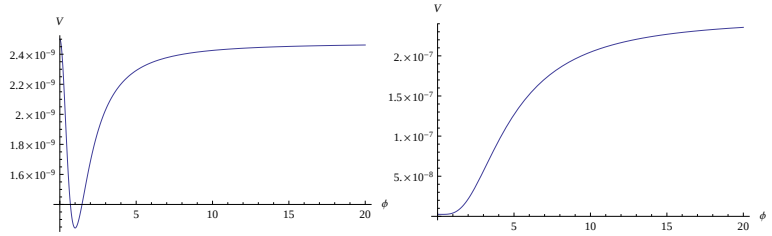

(a) ϕ^4 (b) ϕ^4

Figure 2: $\lambda = g^2 = 1, v^2 = 10^{-4} m_{pl}^2, \mu = 10^{-8}$, (a) $\xi = -4 \times 10^{-2}$ (b) $\xi = -4 \times 10^{-3}$

The potential of the hybrid inflation takes the following form

$$V(\phi, \chi) = \frac{\lambda}{4}(\chi^2 - v^2)^2 + \frac{1}{2} m^2 \phi^2 + \frac{1}{4}\mu\phi^4 + \frac{1}{2} g^2 \phi^2 \chi^2 \tag{6}$$

where v the vacuum expectation value, λ, g and μ are dimensionless parameters and m is the mass of the inflaton. We add the $\mu\phi^4$ term to the conventional hybrid inflation potential in order to make flat potential in the large ϕ limit. The mass of the χ field becomes $m_\chi^2 = -\lambda v^2 + g^2\phi^2$. When ϕ reaches to $\phi_c \equiv \sqrt{\lambda v^2/g^2}$, the effective mass of χ turns to negative value and then the tachyonic instability begins. Since we are interested in the dynamics of the inflaton during accelerating phase, we set to $\chi = 0$.

Through the conformal transformation, $\hat{g}_{\mu\nu} = \Omega^2(\phi) g_{\mu\nu}$, where $\Omega^2(\phi) = 1 - \kappa^2 \xi \phi^2$, the action (1) can be transformed to the canonical form in Einstein frame

$$S = \int d^4x \sqrt{-\hat{g}} \left[\frac{1}{2\kappa^2} \hat{R} - \frac{1}{2} \hat{g}^{\mu\nu} \hat{\nabla}_\mu \varphi \hat{\nabla}_\nu \varphi - \frac{1}{2\Omega^2} \hat{g}^{\mu\nu} \hat{\nabla}_\mu \chi \hat{\nabla}_\nu \chi - \hat{V}(\varphi, \chi) \right] \tag{7}$$

where

$$\varphi = \int F(\phi) d\phi, \quad F(\phi) = \frac{\sqrt{1 - \kappa^2 \xi \phi^2 (1 - 6\xi)}}{\Omega^2(\phi)}, \tag{8}$$

$$\hat{V}(\varphi, \chi) = \frac{1}{\Omega^4(\phi)} V(\phi, \chi) \tag{9}$$

We plot the potential $\hat{V}(\phi, \chi)$ in Einstein frame in Fig. 1 for $\mu = 0$ and in Fig. 2 for $m^2 = 0$. Along $\chi = 0$, the potential (9) in the Einstein frame has the extremum at ϕ_e

$$\phi_e = \sqrt{\frac{-m^2 - \kappa^2 \xi \lambda v^4}{\mu + \kappa^2 \xi m^2}}. \tag{10}$$

While for $m^2 = 0$, the extremum turns out to be maximum value at which has $\hat{V}_e = \frac{m^4}{4\kappa^2 |\xi| (m^2 - 2\kappa^2 |\xi| \lambda v^4)}$, for $\mu = 0$, it corresponds to the minimum value and the potential has $\hat{V}_e = \frac{\mu \lambda v^4}{4(\kappa^2 |\xi|^2 \lambda v^4 + \mu)}$. For $\mu = 0$, as $|\xi|$ increases, ϕ_e decreases. But as $|\xi|$ increases, ϕ_e is increasing for $m^2 = 0$.

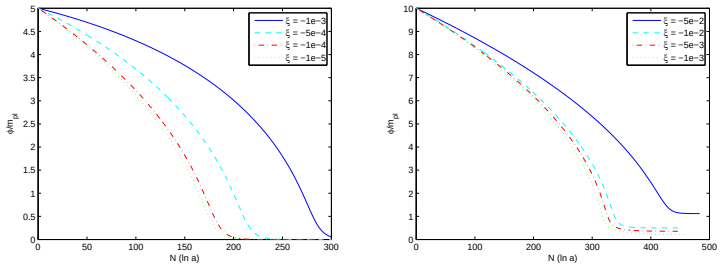

(a) $\mu = 0$ (b) $m^2 = 0$

Figure 3: $\lambda = g^2 = 1, v^2 = 10^{-4} m_{pl}^2$, (a) $m^2 = 10^{-8} m_{pl}^2, \mu = 0$ (b) $m^2 = 0, \mu = 10^{-8}$

We compute the background equations (2),(3), (4) and (5) numerically (see Fig. 3). As an initial condition, we set $\phi_i = 5 m_{pl} < \phi_e$ for $\mu = 0$ (Fig. 3-(a)) and $\phi_i = 10 m_{pl} > \phi_e$ for $m^2 = 0$ (Fig. 3-(b)). We found that enough number e-folds can be obtained for given parameter values. For $m^2 = 0$, since as $|\xi|$ increases, the minimum value ϕ_e increases, the inflaton rolls toward to the $\phi_e \neq 0$.

3 Observations

Since the curvature perturbation $\mathcal{R}$ and tensor perturbation h are invariant under the conformal transformation [6] , we use the results in Einstein frame for power spectrum [4]

$$\mathcal{P}_{\mathcal{R}} = \frac{\kappa^6}{12\pi^2} \frac{\hat{V}^3}{\hat{V}_\phi^2} \left(\frac{d\varphi}{d\phi} \right)^2, \quad \mathcal{P}_h = 2\kappa^2 \left(\frac{\hat{H}}{2\pi} \right)^2 = \frac{2\kappa^4 \hat{V}}{3\pi^2} \tag{11}$$

From these results, we can compute the spectral indices of the curvature and tensor perturbations and the tensor-to-scalar ratio

$$n_s - 1 = \frac{d \ln \mathcal{P}_{\mathcal{R}}}{d \ln k} = -6\epsilon + 2\eta, \quad n_t = \frac{d \ln \mathcal{P}_h}{d \ln k} = -2\epsilon, \quad r = \frac{\mathcal{P}_h}{\mathcal{P}_{\mathcal{R}}} = 16\epsilon, \tag{12}$$

where

$$\epsilon = \frac{1}{2\kappa^2} \left(\frac{d\phi}{d\varphi} \right)^2 \left(\frac{\hat{V}_\phi}{\hat{V}} \right)^2, \quad \eta = \frac{1}{\kappa^2} \left(\frac{d\phi}{d\varphi} \right)^2 \left[\hat{V}_{\phi\phi} - \frac{\hat{V}_\phi d^2\varphi/d\phi^2}{d\varphi/d\phi} \right]. \tag{13}$$

In Fig. 4, we plot the evolution of n_s and r for $\mu = 0$ (Fig. 4-(a)) and for $m^2 = 0$ (Fig. 4-(b)). In order to compare with observations, we draw the lines $n_s = 0.96$, $r = 0.2$ (WMAP bound) and $r = 0.03$ (PLANCK bound). In the large field dominated region, the spectrum shows red ($n_s < 1$). As ϕ evolves to the vacuum dominated regime, the spectrum changes from red to blue ($n_s > 1$).

4 Conclusion and Discussion

We have investigated the inflaton dynamics during inflationary phase with a hybrid inflation potential when an inflaton is coupled to gravity nonminimally. Since the water fall field stays at the false vacuum during inflation, it is very convenient to use conformal transformation to the Einstein frame. In addition, the observable quantities such as the power spectrum, spectral indices, and tensor-to-scalar ratio are invariant under the conformal transformation.

The hybrid potential has an extremum value at $\phi = \phi_e$ and is decreasing (increasing) as $|\xi|$ increases for $\mu = 0$ ($m^2 = 0$). Therefore depending on ξ, ϕ field rolls toward to $\phi_e \neq 0$ instead of $\phi = 0$. If ϕ starts off from the large value, the power spectrum shows the red spectrum which is similar to chaotic inflation and then changes to the blue spectrum around the vacuum dominated regime. More general potential cases are investigated in Ref. [5]

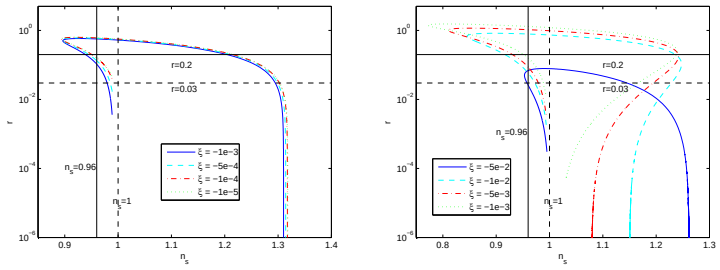

(a) $\mu = 0$ (b) $m^2 = 0$

Figure 4: $\lambda = g^2 = 1, v^2 = 10^{-4} m_{pl}^2$, (a) $m^2 = 10^{-8} m_{pl}^2, \mu = 0$ (b) $m^2 = 0, \mu = 10^{-8}$

References

[1] F. L. Bezrukov and M. Shaposhnikov, Phys. Lett. B **659**, 703 (2008) [arXiv:0710.3755 [hep-th]].
A. O. Barvinsky, A. Y. Kamenshchik and A. A. Starobinsky, JCAP **0811**, 021 (2008) [arXiv:0809.2104 [hep-ph]].
A. De Simone, M. P. Hertzberg and F. Wilczek, Phys. Lett. B **678**, 1 (2009) [arXiv:0812.4946 [hep-ph]].
C. P. Burgess, H. M. Lee and M. Trott, JHEP **0909**, 103 (2009) [arXiv:0902.4465 [hep-ph]].

[2] A. D. Linde, Phys. Rev. D **49**, 748 (1994) [arXiv:astro-ph/9307002];
J. Garcia-Bellido and D. Wands, Phys. Rev. D **54**, 7181 (1996) [arXiv:astro-ph/9606047];
J. Garcia-Bellido, A. D. Linde and D. Wands, Phys. Rev. D **54**, 6040 (1996) [arXiv:astro-ph/9605094].

[3] T. Futamase and K. i. Maeda, Phys. Rev. D **39**, 399 (1989).

[4] S. Tsujikawa and B. Gumjudpai, Phys. Rev. D **69**, 123523 (2004) [arXiv:astro-ph/0402185].

[5] S. Koh and M. Minamitsuji, arXiv:1011.4655 [hep-th].

[6] N. Makino and M. Sasaki, Prog. Theor. Phys. **86**, 103 (1991);
J. c. Hwang, Class. Quant. Grav. **14**, 1981 (1997) [arXiv:gr-qc/9605024].

[7] S. Koh, J. Korean Phys. Soc. **49**, S787 (2006) [arXiv:astro-ph/0510030].

N-body simulation on the MOdified Gravity

Takayuki Suzuki [1(a)]

[(a)] *Department of Physics, Yamaguchi University, Yamaguchi city, Yamaguchi prefecture 171-8501*

Abstract

MOG is abbreviated name for MOdified Gravity developed by John Moffat(2005). It also called Scalar Tensor Vector Gravity(STVG).its added a vector field to Brans-Dicke theory. It can explain a galactic rotary curve and the structure formation without dark matter. Without dark energy,acceleration universe too. I carried out verification from the viewpoint of N-body simulation.

1 Introduction

The standard model of cosmology today, the ΛCDM model, provides an excellent fit to cosmological observations, but at a substantial cost: according to this model, *about 95% of the universe is invisible and undetectable(=dark energy and dark matter)*. This fact provides a strong incentive to seek alternative explanations that can account for cosmological observations without resorting to dark matter or dark energy. For gravitational theories designed to challenge the ΛCDM model, the bar is set increasingly higher by recent discoveries. Not only do such theories have to explain successfully the velocity dispersions, rotational curves, and gravitational lensing of galaxies and galaxy clusters, the theories must also be in accord with cosmological observations, notably the acoustic power spectrum of the cosmic microwave background (CMB), the matter power spectrum of galaxies, and the recent observation of the luminosity-distance relationship of high-z supernovae, which is seen as evidence for "dark energy".

Modified Gravity (MOG) [1] has been used successfully to account for galaxy cluster masses [8], the rotation curves of galaxies [5][6], velocity dispersions of satellite galaxies, and globular clusters [11]. It was also used to offer an explanation for the Bullet Cluster [6] without resorting to cold dark matter. Remarkably, MOG also meets the challenge posed by cosmological observations. In the paper(arXiv:0710.0364)[4],it is demonstrated that MOG produces an acoustic power spectrum, a matter power spectrum, and a luminosity-distance relationship that are in good agreement with observations, and require no dark matter nor dark energy.

However,these are claims by the developer and collaboraters.Therefore it needs objective verifications. This study carried out verification of MOG on galctic scale from the viewpoint of N-body simulation. But,such study is already accomplished by Brandao et al.(2010)[7].The result was negative for the Moffatian model. They claim that the Moffatian potential cannot maintain exponential disks in dynamical equilibrium and therefore cannot be consistent with observations. However, they did not precisely formulate N-body simulation on MOG. In this study,I performed formulation to the N-body simulation on MOG in comformity with Moffat el al.(2009)[13].

2 Theory of MOG

2.1 Action

The action of Moffat theory is constructed as follows [1]. STVG is formulated using the action principle. In the following discussion, a metric signature of $[+,-,-,-]$ will be used; the speed of light is set to $c = 1$, and we are using the following definition for the Ricci tensor: $R_{\mu\nu} = \partial_\alpha \Gamma^\alpha_{\mu\nu} - \partial_\nu \Gamma^\alpha_{\mu\alpha} + \Gamma^\alpha_{\mu\nu}\Gamma^\beta_{\alpha\beta} - \Gamma^\alpha_{\mu\beta}\Gamma^\beta_{\alpha\nu}$. We begin with the Einstein-Hilbert Lagrangian:$\mathcal{L}_G = -\frac{1}{16\pi G}(R + 2\Lambda)\sqrt{-g}$, where R is the trace of the Ricci tensor, G is the gravitational constant, g is the determinant of the metric tensor $g_{\mu\nu}$, while Λ is

[1]Email address: n003wa@yamaguchi-u.ac.jp

the cosmological constant. Introducing the Proca action Maxwell-Proca Lagrangian for the STVG vector field ϕ_μ:

$$\mathcal{L}_\phi = -\frac{1}{4\pi}\omega\left[\frac{1}{4}B^{\mu\nu}B_{\mu\nu} - \frac{1}{2}\mu^2\phi_\mu\phi^\mu + V_\phi(\phi)\right]\sqrt{-g}, \tag{1}$$

where $B_{\mu\nu} = \partial_\mu\phi_\nu - \partial_\nu\phi_\mu$, μ is the mass of the vector field, ω characterizes the strength of the coupling between the fifth force and matter, and V_ϕ is a self-interaction potential. The three constants of the theory, G, μ and ω, are promoted to scalar fields by introducing associated kinetic and potential terms in the Lagrangian density:

$$\mathcal{L}_S = -\frac{1}{G}\left[\frac{1}{2}g^{\mu\nu}\left(\frac{\nabla_\mu G\nabla_\nu G}{G^2} + \frac{\nabla_\mu\mu\nabla_\nu\mu}{\mu^2} - \nabla_\mu\omega\nabla_\nu\omega\right) + \frac{V_G(G)}{G^2} + \frac{V_\mu(\mu)}{\mu^2} + V_\omega(\omega)\right]\sqrt{-g}, \tag{2}$$

where ∇_μ denotes covariant differentiation with respect to the metric $g_{\mu\nu}$, while V_G, V_μ, and V_ω are the self-interaction potentials associated with the scalar fields. The STVG action integral takes the form$S = \int(\mathcal{L}_G + \mathcal{L}_\phi + \mathcal{L}_S + \mathcal{L}_M)\, d^4x$, where $\mathcal{L}_M$ is the ordinary matter Lagrangian density.

2.2 Weak field approximation of MOG

The field equations of STVG can be developed from the action integral using the variational principle. First a test particle Lagrangian is postulated in the form$\mathcal{L}_{\rm TP} = -m + \alpha\omega q_5\phi_\mu u^\mu$, where m is the test particle mass, α is a factor representing the nonlinearity of the theory, q_5 is the test particle's fifth-force charge, and $u^\mu = dx^\mu/ds$ is its four-velocity. Assuming that the fifth-force charge is proportional to mass,$q_5 = \kappa m$, the value of $\kappa = \sqrt{G_N/\omega}$ is determined and the following equation of motion is obtained in the spherically symmetric, static and weak gravitational field of a point mass of mass M:

$$\ddot{r} = -\frac{G_N M}{r^2}\left[1 + \alpha - \alpha(1 + r/\lambda)e^{-r/\lambda}\right] \tag{3}$$

where G_N is Newton's constant of gravitation. Further study of the field equations allows a determination of α and λ for a point gravitational source of mass M in the form $\lambda = 1/\mu = \frac{\sqrt{M}}{D}$,$\alpha = \frac{19M}{(\sqrt{M}+E)^2}$, while for the constants D and E various astronomical observation yield the following values: $D \simeq 6250 M_\odot^{1/2}\mathrm{kpc}^{-1}$, $E \simeq 25000 M_\odot^{1/2}$,

In the weak-field approximation, STVG produces a Yukawa-like modification of the gravitational force due to a point source. Intuitively, this result can be described as follows: far from a source gravity is stronger than the Newtonian prediction, but at shorter distances, it is counteracted by a repulsive fifth force due to the vector field.

MOG advocate that we recognize this strong gravity appearing by leaving for far away as dark matter. $[1 + \alpha - \alpha(1 + r/\lambda)e^{-r/\lambda}]$ in Eq.3 is able to interpreted as effective gravitational constant. Fig.1 shows relation between mass scale / distance scale and effective G. The maximum of effective G and the effective range grow large depending on the mass of object.(See Fig. 2) Therefore it can explain an effect of the dark matter of every scale.

The reason that the MOG can explain galactic flat rotary curves without dark matter halo is as follows. Fig.3 shows effective gravitatonal constant of $10^{10}M_\odot$(It comparable to Galaxy disk). On galaxy disk scale ,G_{eff} is in proportion to a radius.Remember equation of Kepler motion. The revolution velocity of object having the circular orbit:$v = \sqrt{\frac{GM}{r}}$. If G_{eff} is in proportion to r, velocity is constant.

The above is qualitative explanation, but agreement of observed rotation velocity by Doppler effect is identified as predicted rotation velocity by brightness in 100 galaxy[5][6]. As usual in this kind of study, they consider only centrifugal equilibrium, which means in the end that their galaxy model is gstatic.h The aim of this study is to probe if the Moffat model is gdynamicallyh consistent, as it should be in order to be considered a realistic model. Instead of using a gstatic galaxy,h where the centrifugal equilibrium is usually adopted, we probe the Moffat gravity dynamically via numerical N-body simulations.

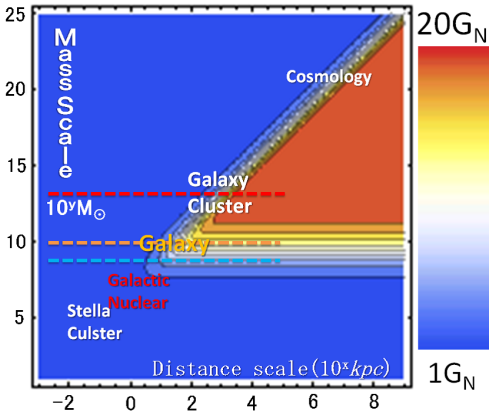

Figure 1: Relation between scale and effective G.
x-axis shows a distance scale.
y-axis shows mass of the gravity source.

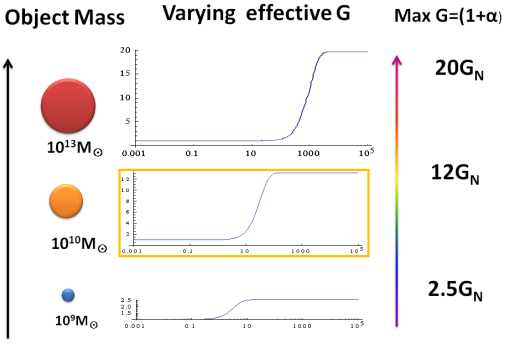

Figure 2:
Effective G and distance from the object.
The example of three different weight's objects:
$10^9 M_\odot$,$10^{10} M_\odot$,$10^{13} M_\odot$

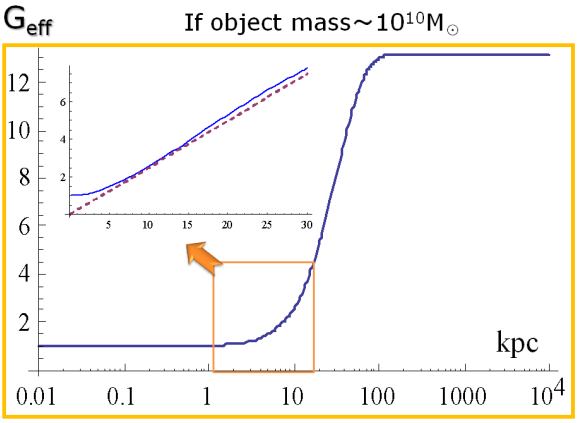

Figure 3: Relation between effective G and distance from the object.
if object mass is $10^{10} M_\odot$ ~Galactic disk,On disk scale,G_{eff} is in proportion to r.

3 Techniques and detail of N-body simulations

The gravity acceleration equation of the STVG in a weak gravitational field is shown in the Eq.3. But,This equtaion is adaped only gravitational field of ga point massh. It is not applied simple superposition principle of forces without self-contradiction. The precedent study by Brandao [7] formulated it based on MSTG(Metric-Skew-Tensor Gravity) which is previous version of MOG. Brandao's formulation is insufficient for latest version of MOG (=STVG). They treat MOG as simple Yukawa gravity.Yukawa-effective range is fixed as $13.96kpc$. But,STVG is not simple Yukawa gravity.Yukawa-effective range(=λ)and increase of effective G(=α) are depend on neighboring mass distribution. Every combination of an interacting particle(i-j) have λ_{ji} and α_{ji}.

The mutual gravity between the particle by STVG is written in Moffat el al.(2009)[13]. I let an equation written in the paper become disintegration. And the following expressions are derived by adapt itself to many body system.

$$a_i = -\sum_j \frac{G_N m_j(\vec{r_j}-\vec{r_i})}{(|r_j-r_i|^2+eps^2)^{3/2}}\left[1+\alpha_{ji}-\alpha_{ji}(1+\frac{|r_j-r_i|}{\lambda_{ji}})e^{-|r_j-r_i|/\lambda_{ji}}\right] \quad (4)$$

$$\lambda_{ji} = \frac{\sqrt{M_{eff}}}{D}, \alpha_{ji} = \frac{19M_{eff}}{(\sqrt{M_{eff}}+E)^2}, M_{eff} = -\sum_l m_l exp(\frac{|r_l - r_j|}{|r_j - r_i|}) \tag{5}$$

This calculation needs the information of all particles whenever It calculate force between two particles. That is why the calculation number of times becomes $\mathcal{O}(N^3)$. The parameter of the initial condition adopted the value of the table.These are comparable to our galaxy. Intential mass distribution is exponential profile($\rho(r) \sim \exp(-r/R_d)$) .From observation,it is well-known that a spiral galaxy of density distribution is described as expnetial profile. And we calculated dynamics evolution for 6.0 Gry.

1R	(radius)	40kpc
1M	(mass)	$4 \times 10^{10} M_\odot$
1T	(time)	0.6Gry
1V	(velocity)	65km/s

Table 1: The standardization of the unit

R_d(scale length of disk)	4.0kpc
Z_d(scale length of disk height)	0.4kpc
M_d(total mass of disk)	$4 \times 10^{10} M_\odot$
eps(softening length)	1.25kpc
Nbody(number of particles)	2000

Table 2: Intential parameters

Because of the calculation number of times,if there is much number of the particles,the exact calculation is not able to carried out. There is too little number of the particles 2000 to perform galactic N-body simulation. We can reduce calculation number of times by defining to an individual particle with thegmass shellh which is a state in Fig.4.

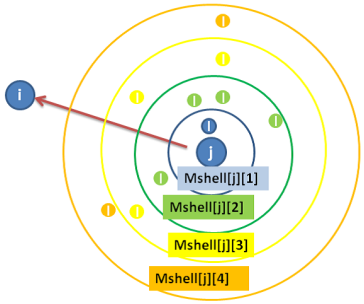

Figure 4: Image of mass shell

With this approximation method, we calculated for the model of 10,000 particles and 30,000 particles. Nurmerical calculation were carried out on the general-purpose PC farm at Center for Computational Astrophysics, CfCA, of National Astronomical Observatory of Japan. Because of a non-parallel computer, it was not possible to perform more large scale calculations.

We pay attention to it whether flat rotary curve and exponetial disk are maintained for long time like a precedent study.

4 Results of simulations

At first we introduce the result by the precision calculation of 2048 particles. Like the precedent study, the mean of the rotation velocity(=rotation curve) kept a flat state(Fig. 5). Velocity dispersion of individual particles grow large comparing with an initial state. Because this has little number of the particles,it is caused by the fact that proximity dispersion occurs frequently. About brightness distribution, the exponetial disk has changed(Fig. 6). The vertical axis of the graph is described $-2.5log\rho$(This ρ is density projected onto the sky). It is in proportion to magnitude.If it can draw a straight line on this graph,exponential profile will be formed. The result of the simulation shows that the brightness distribution in the center deviates from exponetial profile. In the galactic center, brightness distribution varied from exponential profile to de Vaucouleurs profile($\rho(r) \sim \exp(-r^{1/4})$). But,this anomaly may be nonphysical nurmerical artifacts by a little number of the particles.

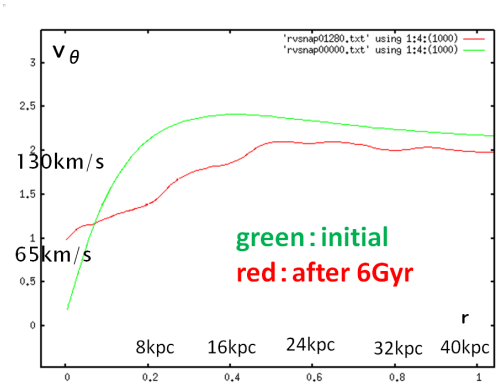

Figure 5:
Time development of rotation curve(Nbody=2000). the rotation velocity dropped,but kept a flat state

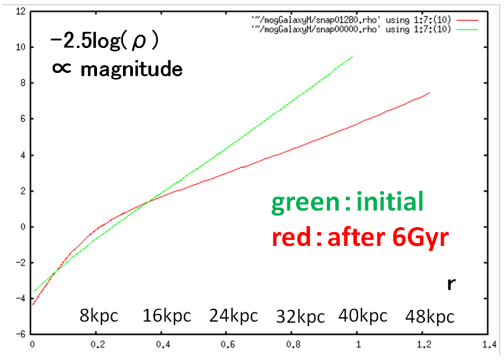

Figure 6: Time development of brightness distribution
(Nbody=2000).In the galactic center, brightness distribution varied from exponential profile.

The result when the number of the particles increased by means of mass shell approximation method is as follows.

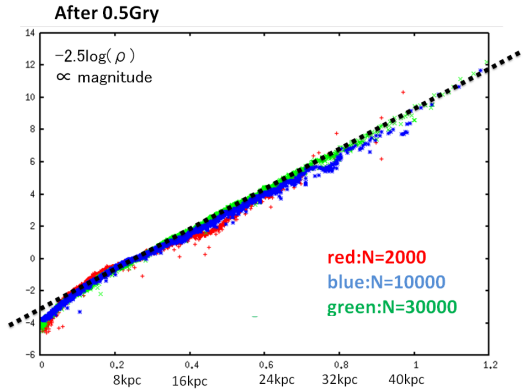

Figure 7: Particle number and brightness distribution(After 0.5Gyr). N=2000 has begun to change from initial distribution, but N=10000 and N=30000 keep the initial state.

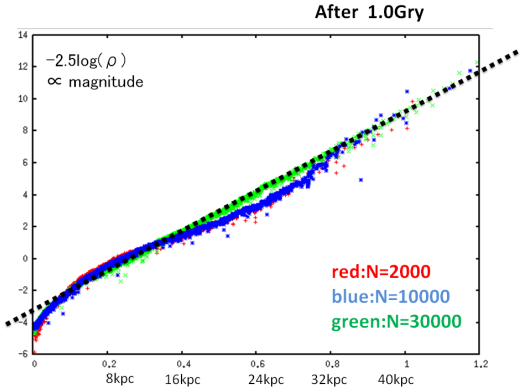

Figure 8: Particle number and brightness distribution(After 1.0Gyr). Also N=10000 has begun to slip off, but N=30000 keeps a straight line(=exponential profile) yet.

As for the model with much number of the particles, the change of the mass distribution becomes slow. But 6.0 Gyrs later, the brightness distribution of the center is denatured even if the number of the particles increase to 30000.

5 Conclusion

The result of the simulation shows that the galactic flat rotation curve is stability in MOG in the long term. However, like a precedent study by Brandao [7], the exponetial disk was not stabile. In the galactic center, brightness distribution varied from exponential profile to de Vaucouleurs profile. But,this anomaly may be nonphysical nurmerical artifacts by a little number of the particles. The change of the brightness distribution is dissolved by increasing the number of the particles. When it used more particles, it is a point at issue whether we can find stability over cosmic age of the exponential disk. We will carry out simulation of the large number of particles with a parallel calculation and tree method in future.

6 Acknowledgments

Nurmerical calculation were carried out on the general-purpose PC farm at Center for Computational Astrophysics, CfCA, of National Astronomical Observatory of Japan.

References

[1] J. W. Moffat,JCAP(03):004, 2006.

[2] J. W. Moffat and V. T. Toth,Class. Quant. Grav. **26** 085002, 2009.

[3] V. T. Toth,[[gr-qc]arXiv:1011.5174].

[4] J. W. Moffat and V. T. Toth[[astro-ph]arXiv:0710.0364].

[5] J. R. Brownstein and J. W. Moffat, Astrophys. J., **636**, P721-P741, 2006.

[6] J. R. Brownstein, [arXiv:0908.0040 [astro-ph]].

[7] C. S. S. Brandao and J. C. N. de Araujo, Astrophs. J. **717**, 849 (2010), [arXiv:1006.1000].

[8] J. R. Brownstein and J. W. Moffat, Mon. Not. R. Astron. Soc., **367**, 527, 2006.

[9] J. R. Brownstein and J. W. Moffat, Mon. Not. R. Astron. Soc., **382**, 29, 2007.

[10] J. W. Moffat and V. T. Toth, [arXiv:1005.2685 [astro-ph]].

[11] J.W. Moffat and V. T. Toth, Astrophys. J., **680**, 1158, 2008.

[12] J. W. Moffat and V. T. Toth, [arXiv:0901.1927 [astro-ph]].

[13] J. W. Moffat and V. T. Toth, Mon. Not. Roy. Astron. Soc., **397**,P.1885-P.1892, 2009.

[14] J. W. Moffat and V. T. Toth, [arXiv:1001.1564 [gr-qc]].

[15] J. W. Moffat and V. T. Toth, Mon. Not. Roy. Astron. Soc., **395**, L25-L28, 2009.

Feynman propagators in Riemann-Cartan space-times: A momentum-space representation

Chih-Hung Wang [1](a),(b) and Yu-Huei Wu[2](b),(c)

(a) *Department of Physics, Tamkang University, Tamsui, Taipei 251, Taiwan.*
(b) *Department of Physics, National Central University, Chungli 320, Taiwan.*
(c) *Center for Mathematics and Theoretical Physics, National Central University, Chungli 320, Taiwan.*

Abstract

The construction of generalized normal coordinates has been accomplished by using autoparallels, instead of geodesics, in an arbitrary Riemann-Cartan spacetime. With the aid of generalized Riemann-normal coordinates and their associated orthonormal frames, we obtain a momentum-space representation of the Feynman propagator for scalar fields. By using dimensional regularization, the renormalization of one-loop effective Lagrangians of free scalar fields is then derived. When torsion vanishes, our resulting momentum-space representation returns to the standard Riemannian results.

1 Introduction

General relativity (GR) was developed almost a century ago and has been considered as one of the most successful classical theories of gravity. Nevertheless, GR is established (by hypothesis) in the pseudo-Riemannian (i.e. torsion free) framework, so the conservation law of angular-momentum does not involve intrinsic spin of elementary particles, i.e. there is no spin-orbit coupling. In most of the torsion theories of gravity, e.g. Einstein-Cartan theory and Poincaré gauge theory of gravity (PGT), the intrinsic spin does play a significant role and becomes the source of torsion field. Hence, Riemann-Cartan spacetime, which is characterized by a metric g and a metric-compatible connection ∇, provides a natural geometrical structure to cooperate with the intrinsic spin. Moreover, recent astrophysical observations, e.g. supernova Type Ia observations, indicate that the expansion of the present Universe is in an *accelerating* phase, and it is contrary to the prediction of standard cosmological model, which is based on GR plus the known matter fields. Hence, a new cosmological model beyond the standard model is necessary. A recent development on torsion cosmology yields a power-law inflation in the early Universe [1] by considering quadratic curvature effects. Do these quadratic curvature effects come from the vacuum polarization of quantum fields in background (classical) curved spacetime with torsion? It leads us to study the renormalization of quantum fields in Riemann-Cartan spacetime.

Quantum field theory in the pseudo-Riemannian structure of spacetime has been extensively investigated [2]. The covariant approach to study the renormalization of stress-energy tensor was discussed by using DeWitt-Schwinger proper-time method with some regularization methods. It requires to introduce a bi-scalar world-function $\sigma(x,x')$, i.e. one-half the square of the geodesic distance between x and x', and then solve a heat kernel equation in the *normal* neighborhood of a point x', which is defined by the exponential map. The generalization of proper-time formulation to Riemann-Cartan spacetime has been considered [4, 5]. However, it immediately encounter with a question: which curve, autoparallel or geodeisc, should be used to construct the exponential map? In [4], it applied DeWitt-Schwinger ansatz to solve a heat kernel equation in Riemann-Cartan spacetime by using *autoparallels*. However, we found that these curves are not autoparallels since the one-half the square of the *autoparallel distance* $\sigma(x,x')$ satisfies the equation $\sigma(x,x') = \frac{1}{2}g^{\mu\nu}\nabla_\mu\sigma\nabla_\nu\sigma$ (see Eq. (3.8) in [4]), which is actually the geodesic equation. It turns out that geodesic interval $\sigma(x,x')$ is more suitable for applying DeWitt-Schwinger ansatz in Riemann-Cartan spacetime.

Besides the DeWitt-Schwinger proper-time representation, Bunch and Parker developed a momentum-space representation, which is useful for discussing the renormalizability of interacting fields, e.g. $\lambda\phi^4$

[1]Email address: chwang@phy.ncu.edu.tw
[2]Email address: yhwu@mail.phy.ncu.edu.tw

theory, in a general pseudo-Riemannian structure of spacetime [3]. By constructing the Riemann-normal coordinates in the normal neighborhood of an original point x', they solved the Feynman Green's function $G(x,x')$ of free scalar and Dirac fields in the large wave number k approximation and also showed the equivalence of momentum-space and proper-time representations. The method of momentum-space representation can be naturally extended to Riemann-Cartan spacetime. The major difference is that the background field variables are changed from the metric tensor $g = g_{\mu\nu}dx^\mu \otimes dx^\nu$ to orthonormal co-frames $\{e^a = e^a{}_\mu dx^\mu\}$ and connection 1-forms $\{\omega^a{}_b = \omega^a{}_{b\mu}dx^\mu\}$, so we should construct generalized normal coordinates $\{x^\mu\}$, where the coefficients of $e^a{}_\mu$ and $\omega^a{}_{b\mu}$ in the Taylor series expansions can be systematically expressed in terms of full curvature, torsion and the covariant derivative ∇_μ at the original point x'. The generalized normal coordinates are established by using autoparallels, which is defined by $\nabla_{\gamma'}\gamma' = 0$, and the detail constructions will be presented in the following section.

In this paper, we use the units $\hbar = c = 1$, and for n dimensional spacetime, the metric signature is $(-,+,\cdots,+)$. The Greek indices $\alpha,\beta,\gamma\cdots$ are referred to coordinate indices and the Latin indices $a,b,\cdots$ referred to frame indices. Both types of indices run from 0 to $n-1$.

2 Generalized normal coordinates

Consider an autoparallel $\gamma_v : \lambda \mapsto \gamma_v(\lambda) \in M$ with its initial values $\gamma_v(0) = x'$ and $\gamma_v'(0) = v$, where M denotes a n-dimensional Riemann-Cartan spacetime. Provided $\gamma_v(1)$ exists, the exponential map $\exp_{x'} : T_{x'}M \mapsto M$ is then defined in an open neighborhood $\mathcal{U}$ of x' by $\exp_{x'}(v) \equiv \gamma_v(1) \in M$, where $T_{x'}M$ denotes the tangent space to M at x'. Using $\exp_{x'}$ with an orthonormal frame $\{\hat{X}_a\}$ at x', we obtain the generalized normal coordiantes x^α

$$\Psi^\alpha(\exp_{x'} v) = x^\alpha, \tag{1}$$

where Ψ^α is a coordinate chart and $v = \sum_{\alpha=0}^{n-1}\delta^a{}_\alpha\, x^\alpha \hat{X}_a$ with $\delta^a{}_\alpha = \mathrm{diag}(1,\cdots,1)$. In the following, $\hat{}$ on any tensor field Z denotes $Z|_{x^\alpha=0}$ (i.e. Z at x'). A natural induced coordinate basis $\{\partial_\alpha\}$, by construction, has $\{\hat{\partial}_\alpha = \delta^a{}_\alpha \hat{X}_a\}$.

It will be useful to introduce generalized normal hyper-spherical coordinates $\{\lambda,\, p^\alpha\}$ defined by $x^\alpha = \lambda\, p^\alpha$, where λ is the radial coordinate with affine parametrization and p^a are the direction cosines of tangent vectors of autoparallels γ_{∂_α} at x' satisfying $\sum_{\alpha=0}^{n-1} p^\alpha p^\alpha = 1$. From the inverse relations $\lambda^2 = \sum_{\alpha=0}^{n-1} x^\alpha x^\alpha$, one has $\partial_\lambda = p^\alpha\partial_\alpha$, $\partial_\lambda p^\alpha = 0$, and $v = \lambda\hat{\partial}_\lambda$. It should be mentioned that $\hat{Z} = Z|_{\lambda=0}$ denotes the initial value of any tensor field Z in hyper-spherical coordinates $\{\lambda,\, p^\alpha\}$. Using $\{\lambda,\, p^\alpha\}$, we can parallel transport $\{\hat{X}_a\}$ along autoparallels $\gamma_{\partial_\lambda}$ to set up a field of orthonormal frames $\{X_a\}$ and its dual co-frame field $\{e^a\}$ on $\mathcal{U}$. So orthonormal co-frames satisfy

$$\nabla_{\partial_\lambda} e^a = 0, \tag{2}$$

i.e. $i_{\partial_\lambda}\omega^a{}_b = \omega^a{}_b(\partial_\lambda) = 0$, with its initial value $\hat{e}^a = \delta^a{}_\alpha\, \widehat{dx^\alpha} = \delta^a{}_\alpha\, p^\alpha \widehat{d\lambda}$. Since ∂_λ are tangent vectors of autoaparallels, we further obtain $\partial_\lambda(e^a(\partial_\lambda)) = 0$. From the above generalized normal coordinates construction and the associated orthonormal (co)-frames setting on $\mathcal{U}$, we obtain

$$e^a = \delta^a{}_\alpha\, p^\alpha d\lambda + \mathcal{A}^a{}_\mu\, dp^\mu, \qquad\qquad \omega^a{}_b = \mathcal{C}^a{}_{b\mu}\, dp^\mu \tag{3}$$

with the initial values $\hat{\mathcal{A}}^a \equiv \hat{\mathcal{A}}^a{}_\mu\, dp^\mu = 0$, and $\hat{\mathcal{C}}^a{}_b = \hat{\mathcal{C}}^a{}_{b\mu}\, dp^\mu = \widehat{\omega^a{}_b(\partial_\mu)}\, dp^\mu = 0$.

Since we have completely constructed the generalized normal coordinates with the associated orthonormal co-frames $\{e^a\}$ on $\mathcal{U}$, the next step is to expand the fundamental variables $\{e^a\}$ and $\{\omega^a{}_b\}$ with respect to radial variable λ and then to express their coefficients in terms of the full curvature $\hat{R}^a{}_{bcd}$, torsion $\hat{T}^a{}_{bc}$ and their covariant derivative ∇_α. It can be accomplished by using Cartan structure equations :

$$de^a = -\omega^a{}_b \wedge e^b + \mathrm{T}^a, \qquad\qquad d\omega^a{}_b = -\omega^a{}_c \wedge \omega^c{}_b + \mathrm{R}^a{}_b \tag{4}$$

where $\mathrm{T}^a = \frac{1}{2}\, T^a{}_{bc}\, e^b \wedge e^c$ and $\mathrm{R}^a{}_b = \frac{1}{2}\, R^a{}_{bcd}\, e^c \wedge e^d$ are torsion 2-forms and curvature 2-forms in the co-frame fields $\{e^a\}$. Substituting Eq. (3) into Eq. (4) and equating the forms containing $d\lambda \wedge dp^\alpha$ on

each side gives ordinary differential equations for $\mathcal{A}^a$ and $\mathcal{C}^a{}_b$:

$$\mathcal{A}'^a = \delta^a{}_\alpha\, dp^\alpha + \mathcal{C}^a{}_b\, \delta^b{}_\alpha\, p^\alpha + T^a{}_{bc}\, \delta^b{}_\alpha\, p^\alpha \mathcal{A}^c, \qquad \mathcal{C}'^a{}_b = R^a{}_{bcd}\, \delta^c{}_\alpha\, p^\alpha \mathcal{A}^d, \tag{5}$$

where $'$ denotes the radial derivative ∂_λ. $\mathcal{A}'^a$ and $\mathcal{C}'^a{}_b$ denote $(\partial_\lambda \mathcal{A}^a{}_b)\, dp^b$ and $\mathcal{C}'^a{}_b = (\partial_\lambda \mathcal{C}^a{}_{bc})\, dp^c$, respectively. In the following, we will use the notations $dp^a \equiv \delta^a{}_\alpha\, dp^\alpha$ and $p^a \equiv \delta^a{}_\alpha\, p^\alpha$. By successively differentiating Eq. (5) with respect to λ and then evaluating the results at $\lambda = 0$, one can obtain $\hat{\mathcal{A}}'^{\cdots a}$ and $\hat{\mathcal{C}}'^{\cdots a}{}_b$ in terms of $\hat{R}^a{}_{bcd}$, $\hat{T}^a{}_{bc}$, and their radial derivative ∂_λ. The discussion of renormalization of the one-loop effective action W requires to calculate $\hat{\mathcal{A}}'^{\cdots a}$ and $\hat{\mathcal{C}}'^{\cdots a}{}_b$ to *fifth*-order (see [6] for the detail results). Here, we only present the results to third-order. To first order in λ one find $\hat{\mathcal{A}}'^a = dp^a$ and $\hat{\mathcal{C}}'^a{}_b = 0$. The curvature and torsion start to appear at the second order:

$$\hat{\mathcal{A}}''^a = \hat{T}^a{}_{bc}\, p^b\, dp^c, \qquad \hat{\mathcal{C}}''^a{}_b = \hat{R}^a{}_{bcd}\, p^c\, dp^d. \tag{6}$$

At the third order, which have one radial derivative of the curvature and torsion:

$$\hat{\mathcal{A}}'''^a = \hat{R}^a{}_{bcd}\, p^b p^c dp^d + 2\hat{T}'^a{}_{bc}\, p^b dp^c + \hat{T}^a{}_{bc}\, \hat{T}^c{}_{de}\, p^b p^d dp^e, \tag{7}$$

$$\hat{\mathcal{C}}'''^a{}_b = 2\hat{R}'^a{}_{bcd}\, p^c dp^d + \hat{R}^a{}_{bcd}\, \hat{T}^d{}_{ef}\, p^c p^e dp^f. \tag{8}$$

Although these expressions involve the radial derivative ∂_λ, it can be changed to covariant derivative $\nabla_{\partial_\lambda}$ by using Eq. (2), e.g.

$$\nabla_{\partial_\lambda} R^a{}_{bcd} \equiv (\nabla_{\partial_\lambda} R)(e^a, X_b, X_c, X_d) = \nabla_{\partial_\lambda} \left(R(e^a, X_b, X_c, X_d)\right) \equiv \partial_\lambda R^a{}_{bcd}. \tag{9}$$

Moreover, it is understood that any tensor-field components $Z^{a\cdots b}{}_{c\ldots d}$ satisfy

$$\hat{Z}^{a\cdots b}{}_{c\ldots d} = \delta^a{}_\alpha \cdots \delta^b{}_\beta\, \delta^\gamma{}_c \cdots \delta^\delta{}_d\, \hat{Z}^{\alpha\cdots\beta}{}_{\gamma\ldots\delta}, \tag{10}$$

so there is no difference of using the Greek or Latin indices for any tensor-field components at the original point x'. In the following, we will adapt the Greek indices on any tensor-field components at x'.

3 Momentum-space representation of the Feynman propagator of a scalar field and its renormalization

To find the one-loop vacuum polarization of a scalar field in Riemann-Cartan spacetime, we need to solve Feynman Green's function $G(x, x')$, which satisfies $\sqrt{|g(x)|}\, \left[-\star^{-1}\, d \star d + m^2 + \xi R\right] G(x, x') = \delta(x - x')$, where $|g(x)| \equiv |\det g_{ab}(x)|$, and then take the coincident limit $x \to x'$. It is known that one-loop vacuum polarization contains ultraviolet divergences, so the regularization is necessary. Though $G(x, x')$ cannot be solved in general background curved spacetime, ultraviolet divergences can still be obtained by solving $G(x, x')$ in generalized normal coordinates with large wave-number k approximation. Furthermore, we will use the dimensional regularization to handle these divergent terms.

The approximate solution of $G(x, x')$ in the general normal coordiantes yields (see [6] for more detail calculations)

$$G(x, x') = \frac{i \triangle^{1/2}(x, x')}{(4\pi)^{n/2}} \int_0^\infty ids(is)^{-n/2} \times \exp[-im^2 s - (\sigma/2is)] F(x, x'; is), \tag{11}$$

where $\sigma(x, x') = \frac{1}{2} x^\alpha x_\alpha$ is half the square of the autoparallel distance between x and x', and the determinant $\triangle(x, x') = -|g(x)|^{-1/2} \det[-\partial_\mu \partial_{\nu'} \sigma] |g(x')|^{-1/2}$ reduces to $|g(x)|^{-1/2}$ in generalized normal coordinates. $F(x, x'; is) = 1 - \frac{1}{4}\hat{T}_\alpha x^\alpha + a_{\alpha\beta} x^\alpha x^\beta + (a + b_\alpha x^\alpha + c_{\alpha\beta} x^\alpha x^\beta) is + c(is)^2$. It should be pointed out that the calculations of coefficients b_α, $c_{\alpha\beta}$, and c are limited in the background *totally* anti-symmetric torsion fields. So the ultraviolet divergences of one-loop effective Lagrangian density in four-dimensional spacetime can be obtained

$$L_{div} = \lim_{n \to 4} \frac{1}{(32\pi^2)} \left[m^4 \Gamma(-\frac{n}{2}) + m^2 a(x') \Gamma(-\frac{n}{2} + 1) + c(x') \Gamma(-\frac{n}{2} + 2) \right], \tag{12}$$

where

$$a(x') = (\frac{1}{6}-\xi)\hat{R} - \frac{1}{4}\hat{T}_\alpha\hat{T}^\alpha + \frac{1}{3}\widehat{\nabla_\alpha T^\alpha} - \frac{1}{8}\hat{T}_{\alpha\beta\gamma}\hat{T}^{\alpha\beta\gamma} - \frac{1}{6}\hat{T}_{\alpha\beta\gamma}\hat{T}^{\gamma\beta\alpha}, \quad (13)$$

$$c(x') = \frac{1}{2}\left[(\frac{1}{6}-\xi)\hat{R} + \frac{1}{24}\hat{T}_{[\alpha\beta\gamma]}\hat{T}^{[\alpha\beta\gamma]}\right]^2 + \frac{1}{3}\left(\overset{(4)}{\mathcal{P}}{}^{\alpha}{}_{\alpha} - \frac{1}{2}\xi\widehat{\Box R}\right), \quad (14)$$

It turns out that the divergent terms are entirely geometrical and involve only $a(x')$ and $c(x')$. By adding the counterterms, which contain bare coefficients, into the gravitational Lagrangian, the infinite quantities of L_{div} can be absorbed into bare coefficients to obtain renormalized physical quantities.

4 Conclusion and outlook

We obtain the momentum-space representation of the Feynman propagator of a free massive scalar field in Riemann-Cartan spacetime. Moreover, the proper-time representation in n-dimensional Riemann-Cartan spacetime has been derived from our momentum-space representation. It leads us to find the divergences of the one-loop effective action by using dimensional regularization. It turns out that the divergences of one-loop effective action of the scalar field are purely geometrical and involve full curvature, torsion and their covariant derivatives. When torsion vanishes, our momentum-space representation agrees with the results in [3]. Since the momentum-space representation is useful for studying the renormalizability of interacting fields in the pseudo-Riemannian structure of spacetime, our future work will be to investigate the renormalizability of interacting scalar fields and also spin 1/2 field in Riemann-Cartan spacetime.

References

[1] Chih-Hung Wang and Yu-Huei Wu, Class. Quantum Grav. **26**, 045016 (2009).

[2] N. D. Birrell and P. C. W. Davies, *Quantum fields in curved space,* (Cambridge University Press, Cambridge, England, 1982).

[3] T. S. Bunch and L. Parker, Phys. Rev. D **20**, 2499 (1979).

[4] W. H. Goldthorpe, Nucl. Phys. B**170**, 307 (1980).

[5] H. T. Nieh and M. L. Yan, Ann. Phys. **138**, 237 (1982).

[6] Chih-Hung Wang and Yu-Huei Wu, Phys. Rev. D **82**, 064007 (2010)

Non-axisymmetric instabilities of toroidal magnetic field in neutron stars

Kenta Kiuchi[1 (a)], Shijun Yoshida[(b)] and Masaru Shibata[(a)]

[(a)] *Yukawa Institute, Kyoto University, Kyoto 606-8502*
[(b)] *Astronomical Institute, Tohoku University, Sendai 980-8578*

Abstract

We explore the instabilities of neutron star with toroidal magnetic fields. General relativistic magnetohydrodynamical simulations are performed in the framework of Numerical Relativity. The magnetized neutron stars are potentially unstable against the Taylor and/or Parker instability. We confirm this linear analysis prediction and explore the non-linear phase of these instabilities.

1 Introduction

The aim of this paper is to clarify the stabilities of neutron stars with strong toroidal magnetic fields against non-axisymmetric perturbation. The motivation comes from the fact that super magnetized neutron stars of $\sim 10^{15}$G, magnetars, and magnetized proto-neutron stars born after the magnetically-driven supernovae are likely to have such strong toroidal magnetic fields. Long-term, three-dimensional general relativistic magneto-hydrodynamic simulations are performed, preparing isentropic neutron stars with toroidal magnetic fields in equilibrium as initial conditions. To explore the effects of rotations on the stability, simulations are done for both non-rotating and rigidly rotating models. We find the emergence of the Parker and/or Tayler instabilities in both the non-rotating and rotating models. For both non-rotating and rotating models, the Parker instability is the primary instability as predicted by the local linear perturbation analysis. It is found that rapid rotation is not enough to suppress the Parker instability, and this finding does not agree with the perturbation analysis. The reason for this is that rigidly and rapidly rotating stars are marginally stable, and hence, in the presence of stellar pulsations by which the rotational profile is deformed, unstable regions with negative gradient of angular momentum profile are developed. After the onset of the instabilities, a turbulence is excited. Contrary to the axisymmetric case, the magnetic fields never reach an equilibrium state after the development of the turbulence. Isentropic neutron stars with strong toroidal magnetic fields are likely to be always unstable against the Parker instability. A turbulence motion is induced and maintained for a long time. This conclusion is different from that in axisymmetric simulations and suggests that three-dimensional simulation is indispensable for exploring the formation of magnetars or prominence activities of magnetars such as giant flares.

2 Method and initial conditions

The stability of magnetized neutron stars are studied by three dimensional GRMHD simulation assuming that the ideal MHD condition holds. In this paper we focus on the Parker and/or Tayler instabilities against non-axisymmetric perturbations. The simulation is performed upgrading our axisymmetric GRMHD numerical code to that for three dimensions [4]. Neutron stars with toroidal magnetic fields in equilibrium, employed as initial conditions, are computed by the code described in Kiuchi & Yoshida [3]. We assume the toroidal magnetic field profile to be given by $b_{(\varphi)} = B_0 u^t (\rho h \alpha^2 \gamma_{\varphi\varphi})^k \gamma_{\varphi\varphi}^{-1/2}/\sqrt{4\pi}$ where k and B_0 are constants which determine the field profile and strength, respectively. The regularity condition of magnetic fields near the axis of $\varpi = 0$ requires $k \geq 1$. Thus, the magnetic field is confined inside the neutron star. Because of $\gamma_{\varphi\varphi} \propto \varpi^2$ for $\varpi \to 0$, the toroidal magnetic filed is proportional to ϖ^{2k-1} near the axis. The profile of $k = 1$ is stable against axisymmetric perturbations but may be unstable

[1]Email address: kiuchi@yukawa.kyoto-u.ac.jp

against non-axisymmetric ones (see also Acheson [1]). Hence in this paper, we focus on the profile of $k = 1$. Magnetic field strength, B_0, is chosen so as to satisfy $8 \times 10^{-3} \leq H/|W| \leq 5 \times 10^{-2}$ with H and W being the magnetic field energy and gravitational binding energy. The initial conditions for the non-rotating/rotating model are specified to be such that the neutron star has a realistic compactness. Γ-law equation of state with $\Gamma = 2$ is used.

3 Result

3.1 Non-rotating case

We study the stability for non-rotating model. The simulations are performed for a sufficiently long time, more than ten times of the averaged Alfvén time scale or several thousands of time in units of M_0. This is necessary to clarify whether or not any MHD instability, which grows approximately on an Alfvén time scale, sets in and to determine the final fate after the onset of the instabilities. Figures 1 and 2 plot the evolution of the rest-mass density and magnetic energy density on the equatorial plane and in one of meridian (x-z) planes, respectively, for the non-rotating model. The panels (a)–(c) in these figures show that the magnetic field near the stellar surface is disturbed by the Parker instability, and leaks out of the stellar surface. Because the plasma beta is small and thus the matter inertia is small near the stellar surface (as shown below), the matter is dragged by the magnetic force and consequently the stellar surface is distorted. Here, the plasma beta is the ratio of the fluid pressure to the magnetic pressure, $\beta_{\rm plasma} \equiv 8\pi P/b^2 \propto \rho^2/b^2_{(\varphi)} \propto 1/\gamma_{\varphi\varphi}$ assuming $\Gamma = 2$ and $k = 1$. The minimum value of the plasma beta is initially ≈ 2 at the stellar surface, and after the onset of the Parker instability, the leak-out magnetic field loop produces even lower beta plasma near the stellar surface. As a result, a weak wind expanding outward is driven. On the other hand, the ingoing magnetic field loop enhances a turbulent motion in the neutron star. During the transition from the state shown in panel (c) to (d) in Figures 1 and 2, the initial magnetic field profile is completely destroyed and turbulent magnetic field is produced. During the development of the turbulence, the Tayler instability does not appear to play an important role. However, the region near the axis of $\varpi = 0$ is not stable against this instability and thus no mechanism seems to help stabilizing there. The toroidal magnetic fields initially prepared behave like a rubber belt, which fastens the "waist" of neutron stars. The disappearance of the coherent toroidal magnetic fields, therefore, results in the expansion of the star as shown in the panel (d) of Figures 1 and 2. After the magnetic field becomes turbulent, the star stably oscillates around the hypothetical quasi-stationary state. Although the density profile relaxes to a quasi-stationary state, the turbulent motion is maintained. Figures 1 and 2 specifically show that the meridional circular motion is induced by the displacement of the toroidal magnetic field line. The magnetic field configuration never reaches to any equilibrium state in contrast to the axisymmetric case [2]. The growth time scale of the instability is approximately proportional to the Alfvén time scale. Therefore, we can conclude that the primary instability is the Parker instability as expected in the linear analysis.

3.2 Rotating case

We study the stability for two rigidly rotating model. Again, long-term simulations are performed as in the non-rotating model. We find that the instability is not suppressed by the presence of rapid rotation for all the places inside the neutron star. This result is totally different from that in the axisymmetric case [2], in which the rapid rotation suppresses the onset of the interchange instability. Moreover, the linear perturbation analysis predicts that rigidly and rapidly rotation can suppress the instability. We find that the magnetic field profile *near the stellar surface* is deformed, in the same manner as found for the non-rotating model. During the subsequent evolution, the coherent magnetic field structure is totally destroyed and a turbulent motion is excited. The surface expands because the plasma beta near the surface is below unity due to the leak-out of the magnetic field. Because the coherent toroidal magnetic field which fastens the waist of the neutron star disappears, the radius of the neutron star increases. All these features are essentially the same as for the non-rotating model. It is interesting to note that the stellar surface in the rotating model expands whereas the central part contracts due to the redistribution of the magnetic field profile. Contrary to the rotating model, the coherent profile of the magnetic fields

near the stellar center in the non-rotating model disappears after the onset of the instability, which results in the systematic expansion of the star as mentioned in the previous subsection. It is also interesting to note that the non-axisymmetric instability sets in only near the stellar surface (not in the central region). Namely, only the Parker instability in the outer region plays an important role for the rotating models.

The local linear perturbation analysis predicts that our rigidly rotating models is stable. Thus, our numerical result does not seem to agree with that in the linear analysis. However, this is not the case, because our rotating model is close to a marginally stable state and is destabilized by a slight nonlinear perturbation to the rotational velocity. The evolution of the angular velocity profile reveals the slight deviation from the constant profile and the emergence of the negative gradients, in particular, near the stellar surface during the evolution. This time variation is due to the oscillation of the neutron star which is initially triggered by a perturbation of numerical origin. Note that the initial conditions we gave are in equilibria, but a small numerical error associated with the finite grid resolution induces a perturbation and then the neutron stars start oscillating around their equilibrium states. Although the perturbation is induced by a numerical error in this case, it is quite natural to expect that any star in nature oscillates and thus the precisely rigid rotation is not realized. Once the angular velocity profile has the negative gradient, the instability criterion could be satisfied because the instability criterion is satisfied even for a small angular velocity gradient [1].

4 Summary

We explored the non-axisymmetric instability of neutron stars with purely toroidal magnetic fields. Preparing the non-rotating and rotating neutron stars in equilibrium as the initial conditions, the three-dimensional GRMHD simulations were performed. For the non-rotating models, the local linear perturbation analysis predicts that the Parker instability would be the primary instability and we confirmed this. Due to the Parker instability, a turbulent state is developed and the initially coherent magnetic field profile is totally varied. The magnetic field profile never reaches an equilibrium state. This fact is in sharp contrast with that in the axisymmetric instability of Kiuchi et al. [2]. The growth time scale of the Parker instability depends on the magnetic field strength, i.e., the Alfvén time scale, and this result also agrees with the local linear perturbation analysis. The present result strongly suggests that three-dimensional treatment is crucial to clarify the instability of a neutron star with toroidal magnetic fields. In other words, any a priori assumption of the spacetime symmetry (e.g., axisymmetric symmetry) could prevent from deriving the correct conclusion.

We also explored the instability of rigidly and rapidly rotating neutron stars. The linear analyses have suggested that rapid rotation could play a role as a stabilizing agent. We confirm that the rapid rotation stabilizes the Tayler instability, which may occur near the axis of $\varpi = 0$ in the non-rotating case. However, we find that the Parker instability which is relevant near the stellar surface may not be stabilized by the rapid rotation. The reason is that by a perturbative oscillation, neutron stars may have a region in which the gradient in the angular velocity profile is negative ($\partial\Omega/\partial\varpi < 0$). This negative gradient can induce the Parker instability in the case that the neutron star has rapid rotation and weak magnetic fields. As in the non-rotating model, a turbulent state is subsequently developed in the outer region of the neutron star. This result also gives us a message that the three-dimensional simulation is essential for investigating a magnetic field instability.

References

[1] Acheson, D. J., 1978, Phil. Trans. Roy. Soc. Lond. A, 289, 459

[2] Kiuchi, K., Shibata, M., and Yoshida, S., 2008, Phys. Rev. D 78, 024029

[3] Kiuchi, K., and Yoshida, S., 2008, Phys. Rev. D 78, 044045

[4] Kiuchi, K., Yoshida, S., and Shibata, M. submitted to Astron. Astrophys. in 2011

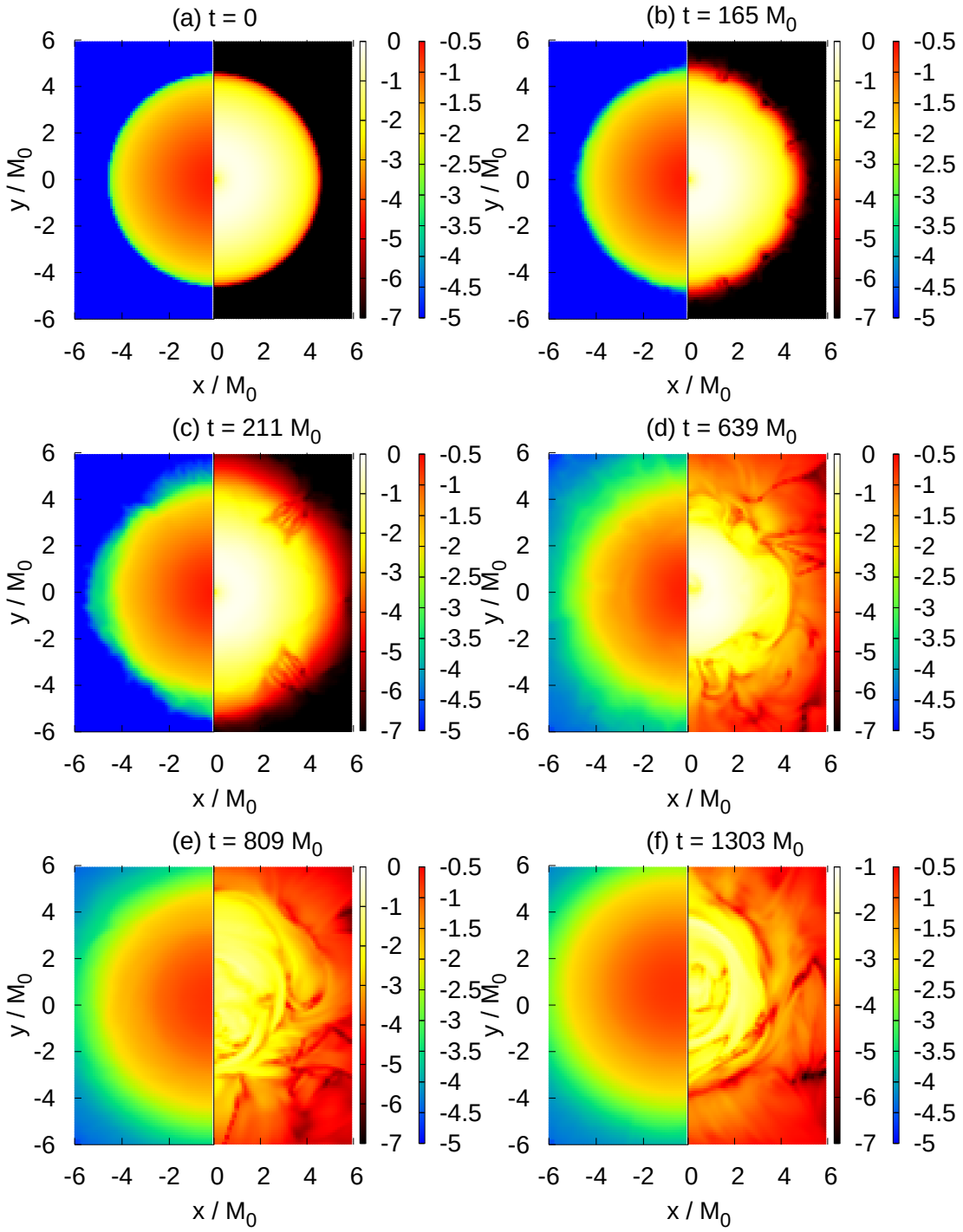

Figure 1: The evolution of rest-mass density (left) and magnetic energy density (right) on the equator for the non-rotating model. Both of them are plotted in the logarithmic scale. The coordinate time at each slice is shown in each panel.

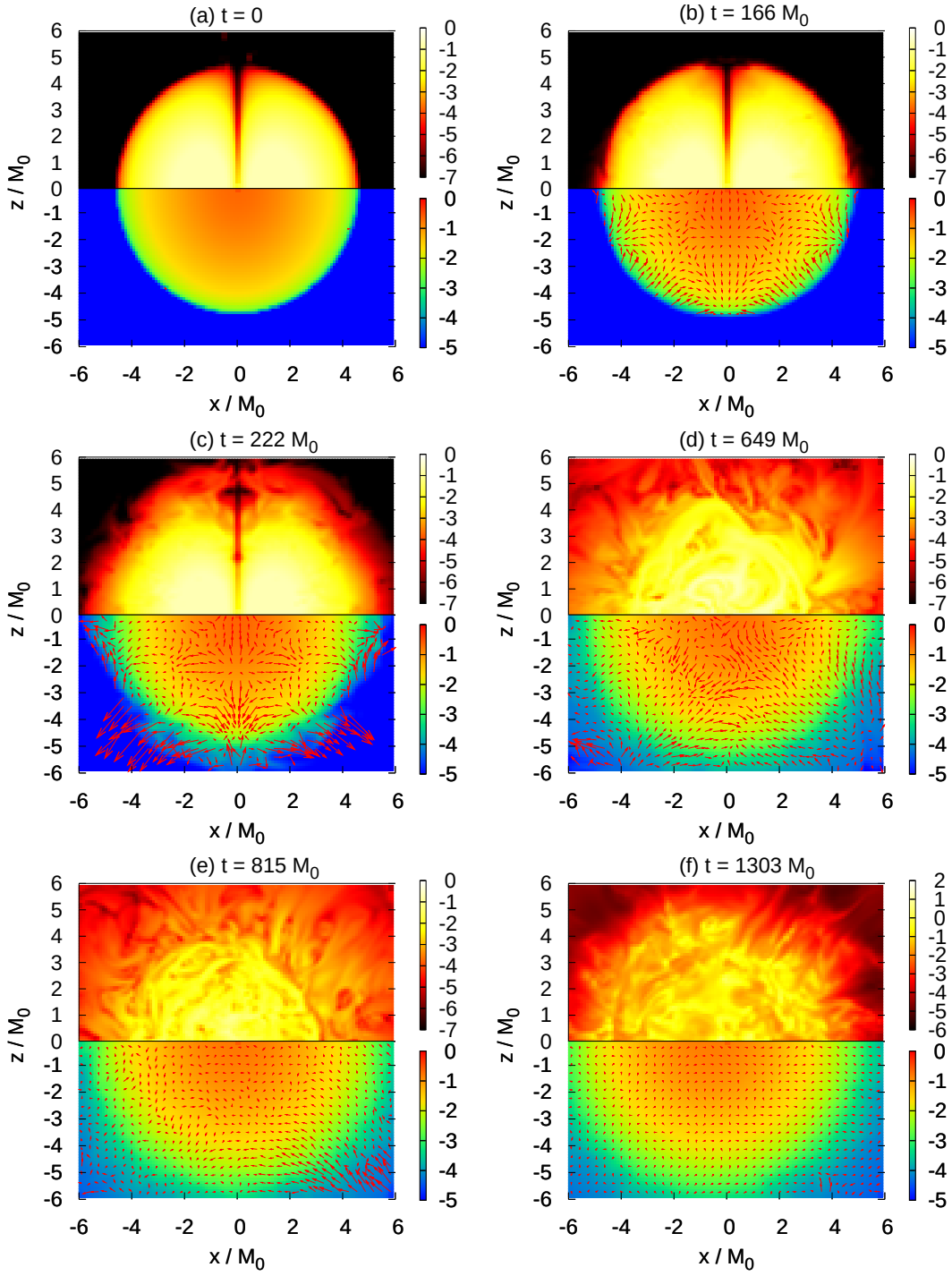

Figure 2: The evolution of the rest-mass density (bottom) and magnetic energy density (top) on a meridian (x-z) plane for the non-rotating model in the logarithmic scale. The arrows indicate the velocity fields.

Dynamics of membranes with symmetry and projection formalism

Hiroshi Kozaki[1(a)], Tatsuhiko Koike[2(b)] and Hideki Ishihara[3(b)]

[(a)] *Department of General Education, Ishikawa National College of Technology, Tsubata, Ishikawa 929-0392, Japan*
[(b)] *Department of Physics, Keio University, Yokohama 223-8522, Japan*
[(c)] *Department of Mathematics and Physics, Graduate school of Science, Osaka City University, Osaka 558-8585, Japan*

Abstract

We investigate dynamics of membrane with cohomogeneity-one symmetry. The cohomogeneity-one membrane has world surface foliated by two-dimensional orbits of isometry group. We show that the Nambu-Goto equations of motion reduce to geodesic equations in the orbit space. We also clarify the form of the metric provided to the orbit space. The generalization to higher dimensional object with cohomogeneity-one symmetry in higher dimensional spacetime is discussed.

1 Introduction

Extended objects gather much attention in cosmology. The examples are topological defects such as cosmic strings and domain walls which are produced during phase transitions in the early Universe. In the brane-world universe models, the Universe itself is also an extended object embedded in a higher dimensional spacetime.

The dynamics of the extended object is governed by partial differential equations (PDEs) because the trajectory is a surface and its embedding is determined by PDEs. On the other hand, the dynamics of a particle is governed by ordinary differential equations (ODEs). PDEs are much more difficult to solve, and then, exact solutions of extended objects are not known so much.

One way to find exact solutions is to assume symmetry. Stationary strings[1–7] and the generalization called cohomogeneity-one strings[8, 9] are the examples. A cohomogeneity-one string is defined, roughly speaking, as the one whose world surface is homogeneous in one direction. In the case that the homogeneous direction is timelike, the string is stationary. By assuming the cohomogeneity-one symmetry, the Nambu-Goto equations of motion reduces to the geodesic equation in the orbit space endowed with some metric. $U(1)$ membranes are the examples of membranes with symmetry. Hoppe assumed $U(1)$ symmetry on the membrane world surface and observed that the equations of motion for the membrane reduces to those of string[10]. The exact solutions are obtained by Trzetrelewski and Zheltukhin[11]. Higher dimensional objects with symmetry are also investigated as ξ-branes which are the special case of cohomogeneity-one symmetry[12].

In this article, we consider membranes with cohomogeneity-one symmetry and show that the Nambu-Goto equations of motion reduces to geodesic equations in the orbit space. Furthermore, we write down the metric of the orbit space.

2 Cohomogeneity-one membranes

A trajectory of the membrane is a three-dimensional surface which is embedded in a spacetime $(\mathcal{M}, g)$. Hereinafter, we assume that the spacetime $(\mathcal{M}, g)$ admits an isometry group G which spans two-dimensional orbits and that the orbits are not null. The group action on the orbits are divided into two types: simply transitive actions and multiply transitive actions. In the case that the group action is simply transitive,

[1]Email address: kozaki@ishikawa-nct.ac.jp
[2]Email address: koike@phys.keio.ac.jp
[3]Email address: ishihara@sci.osaka-cu.ac.jp

$\dim G = 2$ and two independent Killing vector fields are tangent to the orbit. In the case of the multiply transitive action, $\dim G = 3$ because two-dimensional orbits cannot admit isometry group G such that $\dim G$ is larger than $2(2+1)/2 = 3$. In this case, the orbits are maximally symmetric and three independent Killing vector fields are tangent to the orbits.

We define a cohomogeneity-one membrane such that its world surface, say Σ, is foliated by two-dimensional orbits of G. When we identify the points in $\mathcal{M}$ which are connected by the action of G, $\mathcal{M}$ reduces to an orbit space $\mathcal{M}/G$ and Σ reduces to a curve, say C, in $\mathcal{M}/G$. Let π be a projection from $\mathcal{M}$ to $\mathcal{M}/G$, Σ is represented as a preimage $\pi^{-1}(C)$. Then, the embedding of Σ is completely determined by C, and the problem is reduced to finding C such that $\pi^{-1}(C)$ satisfies the equations of motion. Because a curve is governed by ODEs in general, the equations of motion of cohomogeneity-one membranes are reduced to ODEs. In the following, we show that the Nambu-Goto equations of motion reduces to geodesic equations in $\mathcal{M}/G$ and clarify that what kind of metric are provided to $\mathcal{M}/G$.

2.1 $\dim G = 2$

In the case of $\dim G = 2$, two independent Killing vector fields, say $\boldsymbol{\xi}_I$ $(I = 1, 2)$, are tangent to the orbit. The vector space spanned by $\boldsymbol{\xi}_I$ becomes a Lie algebra with respect to the commutator of vector fields. The structure of two-dimensional Lie algebra is classified into two classes; commutative and solvable. In the case of commutative Lie algebra, it has been already clarified that the Nambu-Goto equations of motion reduce to geodesic equations. In the following, we shall take different method so that we can apply it to solvable Lie algebra.

First, we shall set up a coordinate in $\mathcal{M}$ by making use of the G orbits. We take an orbit $\mathcal{O}_0$ and a two-dimensional surface $\mathcal{S}$ which intersects with each orbit at one point. Coordinates on $\mathcal{O}_0$ and $\mathcal{S}$ are denoted by x^i $(i = 1, 2)$ and y^p $(p = 3, 4)$ respectively. Because all orbits intersect with $\mathcal{S}$ at different points on $\mathcal{S}$, we can label the orbit as $\mathcal{O}(y^p)$ by using the coordinate y^p of the intersection. The orbits $\mathcal{O}(y^p)$ do not intersect with each other and fill the spacetime. We extend the internal coordinate y^p of $\mathcal{S}$ to spacetime coordinate such a way that y^p is constant on $\mathcal{O}(y^p)$.

Group action moves $\mathcal{S}$ to another surface $\mathcal{S}'$ which also intersects with each orbit at one point. In the case that $\mathcal{S}'$ intersects with $\mathcal{O}_0$ at x^i, we write $\mathcal{S}'$ as $\mathcal{S}(x^i)$. Surfaces $\mathcal{S}(x^i)$ $(x^i \in \mathcal{O}_)$ also do not intersect with each other and fill the spacetime. Then, we can extend x^i to the coordinate of $\mathcal{M}$ so that x^i is constant on $\mathcal{S}(x^i)$. Combining extended x^i and y^p, we set up a coordinate (x^i, y^p) in $\mathcal{M}$. With respect to (x^i, y^p), G action moves is written as $G : (x^i, y^p) \mapsto (x'^i, y^p)$, i.e., y^p is invariant under the G action.

Next, we shall write the spacetime metric with respect to the coordinate (x^i, y^p). Because the group action is simply transitive on the orbit, we have invariant dual basis χ^I in $\mathcal{O}_0$;

$$\mathcal{L}_{\xi_I} \chi^J = 0, \tag{1}$$

where $\mathcal{L}$ denotes the Lie derivative in $\mathcal{O}_0$. With respect to the coordinate x^i in $\mathcal{O}_0$, χ^I is written as

$$\chi^I = \chi^I_i(x) dx^i. \tag{2}$$

We can extend the 1-forms χ^I in $\mathcal{O}_0$ to those defined in $\mathcal{M}$ by taking x^i as spacetime coordinate in Eq.(2). The extended χ^I are also invariant under G action. By using χ^I, we can write the metric as

$$ds^2 = g_{pq} dy^p dy^q + 2 g_{pI} dy^p \chi^I + g_{IJ} \chi^I \chi^J. \tag{3}$$

The metric functions g_{pq}, g_{pI} and g_{IJ} do not depend on x^i because isometry group G moves x^i.

The orbits are labeled by y^p. Then, we can also take y^p as a coordinate of $\mathcal{M}/G$. The projection $\pi : \mathcal{M} \to \mathcal{M}/G$ is described as $\pi : (x^i, y^p) \mapsto y^p$. Here, we rewrite the metric as

$$ds^2 = g_{IJ}(\chi^I + N^I_p dy^p)(\chi^J + N^J_q dy^q) + h_{pq} dy^p dy^q, \tag{4}$$

where

$$g_{IJ} N^J_p = g_{Ip}, \tag{5}$$

$$h_{pq} = g_{pq} - g_{IJ} N^I_p N^J_q. \tag{6}$$

constant curvature space(time)	Bianchi type	$[\boldsymbol{\xi}_1, \boldsymbol{\xi}_2]$	$[\boldsymbol{\xi}_2, \boldsymbol{\xi}_3]$	$[\boldsymbol{\xi}_3, \boldsymbol{\xi}_1]$
Euclid space E^2	VII_0	0	$-\boldsymbol{\xi}_1$	$\boldsymbol{\xi}_2$
sphere S^2	IX	$\boldsymbol{\xi}_3$	$\boldsymbol{\xi}_1$	$\boldsymbol{\xi}_2$
hyperbolic space H^2	VIII	$\boldsymbol{\xi}_3$	$-\boldsymbol{\xi}_1$	$\boldsymbol{\xi}_2$
Minkowski spacetime $E^{1,1}$	VI_0	0	$-\boldsymbol{\xi}_2$	$-\boldsymbol{\xi}_1$
de Sitter spacetime dS^2	VIII	$\boldsymbol{\xi}_3$	$-\boldsymbol{\xi}_1$	$\boldsymbol{\xi}_2$
anti-de Sitter spacetime AdS^2	VIII	$\boldsymbol{\xi}_3$	$-\boldsymbol{\xi}_1$	$\boldsymbol{\xi}_2$

Table 1: Lie algebras of isometry groups of the maximally symmetric space(time)

We can regard h_{pq} as the metric in $\mathcal{M}/G$ so that the projection π is a Riemann submersion. When we identify the points connected by group actions of G, the cohomogeneity-one world surface reduces to a curve C in $\mathcal{M}/G$. The metric h_{pq} measures the length of C in $\mathcal{M}/G$, so that it agrees with the length of a *lift* curve c in $\mathcal{M}$ which are measured orthogonally to the orbits.

The volume element of Σ is given as a product of the area element of the orbits and the line element of c which are orthogonally measured to the orbits. The orthogonally measured line element of c agrees with the line element of C, and then, it is given as

$$dL = \sqrt{|h_{pq}(y) dy^p dy^q|}. \tag{7}$$

The area element on the orbit is given as

$$dA = \sqrt{|\det g_{IJ}(y)|}\chi^1 \wedge \chi^2. \tag{8}$$

Hence, the Nambu-Goto action is

$$S = \iint_\Sigma dA dL = \mathcal{E} \int_C \sqrt{|(\det g_{IJ}) h_{pq} dy^p dy^q|}, \tag{9}$$

where

$$\mathcal{E} = \int_{\text{orbit}} \chi^1 \wedge \chi^2. \tag{10}$$

Therefore, the problem is reduced to solving the geodesic equations in the orbit space endowed with the metric $(\det g_{IJ}) h_{pq}$.

2.2 $\dim G = 3$

In the case of $\dim G = 3$, three independent Killing vector fields, say $\boldsymbol{\xi}_I$ $(I = 1, 2, 3)$, are tangent to the two-dimensional orbit. Then, the two-dimensional orbit is a space of constant curvature. Let $\mathfrak{g}$ be a Lie algebra spanned by $\boldsymbol{\xi}_I$. The structure of $\mathfrak{g}$ is same as the constant curvature space. Following the Bianchi classification of three dimensional Lie algebras, we summarize the possible structure of $\mathfrak{g}$ in Table 1.

In the case that the spacetime admits two-dimensional orbits with constant curvature K, the metric is written as[13, 14]

$$ds^2 = Y^2[(dx^1)^2 + \epsilon \Sigma^2(x^1, k)(dx^2)^2] + e^{2\lambda}(dy^3)^2 - \epsilon e^{2\nu}(dy^4)^2. \tag{11}$$

where Y, λ and ν are functions of y^3 and y^4,

$$\epsilon = \begin{cases} +1 & \text{(spacelike orbit)} \\ -1 & \text{(timelike orbit)} \end{cases}, \tag{12}$$

and

$$\Sigma(x^1, k) = (\sin x^1, x^1, \sinh x^1) \text{ for } k = KY^2 = (1, 0, -1). \tag{13}$$

We can consider x^1 and x^2 as the coordinates in the orbits and y^3 and y^4 as the parameters which distinguish the orbits. Then, the map $\pi : (x^1, x^2, y^3, y^4) \mapsto (y^3, y^4)$ is a projection from $\mathcal{M}$ to $\mathcal{M}/G$.

The last two terms of Eq.(11) is the 2-metric in $\mathcal{M}/G$ such that the projection is Riemann submersion. Following the similar derivation in $\dim G = 2$ case, the Nambu-Goto action is

$$S = \int_\Sigma dv = \int_{\text{orbit}} \sqrt{|\epsilon\Sigma^2(x^1,k)|}dx^1dx^2 \int_C \sqrt{|Y^4(y)(e^{2\lambda}(dy^3)^2 - \epsilon e^{2\nu}(dy^4)^2)|}. \tag{14}$$

Therefore, the problem is reduced to solving the geodesic equations in $\mathcal{M}/G$ with the metric

$$ds^2_{\mathcal{M}/G} = Y^4(e^{2\lambda}(dy^3)^2 - \epsilon e^{2\nu}(dy^4)^2). \tag{15}$$

3 Conclusion

We have studied dynamics of the Nambu-Goto membrane with cohomogeneity-one symmetry in four dimensional spacetime $(\mathcal{M}, g)$. The cohomogeneity-one symmetry means that the world surface is foliated by two-dimensional orbits of isometry group G in $(\mathcal{M}, g)$. By virtue of the symmetry on the world surface, the equations of motion reduces to the geodesic equations in the orbit space $\mathcal{M}/G$. In this case, the metric is of the form $\det(g_{IJ})h_{pq}$ where g_{IJ} is the metric on the G orbit and h_{pq} is a metric in $\mathcal{M}/G$ such that the projection $\pi : \mathcal{M} \to \mathcal{M}/G$ is a Riemann submersion.

In this article, we have considered dynamics of cohomogeneity-one membrane in four dimensional spacetime. The results may be valid for higher dimensional cohomogeneity-one objects in higher dimensional spacetime in two cases. One is the case that the group action is simply transitive on orbit and the other is that the orbit is maximally symmetric. In the other cases, the equations of motion may reduce to geodesic equations but we do not know the metric form.

References

[1] V. P. Frolov, V. Skarzhinsky, A. Zelnikov and O. Heinrich, Phys. Lett. B **224**, 255 (1989)

[2] H. J. de Vega, A. L. Larsen and N. G. Sanchez, Nucl. Phys. B **427**, 643 (1994)

[3] A. L. Larsen and N. G. Sanchez, Phys. Rev. D **50**, 7493 (1994)

[4] Larsen A L and Sanchez N G, Phys. Rev. D **51** 6929 (1995)

[5] de Vega H J and Egusquiza I L, Phys. Rev. D **54** 7513 (1996)

[6] V. P. Frolov, S. Hendy and J. P. De Villiers, Class. Quant. Grav. **14**, 1099 (1997)

[7] Ogawa K, Ishihara H, Kozaki H, Nakano H and Saito S, Phys. Rev. D **78** 023525 (2008)

[8] Ishihara H and Kozaki H, Phys. Rev. D **72** 061701(R) (2005)

[9] Koike T, Kozaki H and Ishihara H, Phys. Rev. D **77** 125003 (2008)

[10] J. Hoppe, arXiv:0805.4738 [hep-th]

[11] M. Trzetrzelewski and A. A. Zheltukhin, Phys. Lett. B **679**, 523 (2009)

[12] D. Kubiznak and V. P. Frolov, JHEP **0802**, 007 (2008)

[13] H. Goenner and J. Stachel, J. Math. Phys. 11, 3358 (1970)

[14] H. Stephani, D. Kramer, M. A. H. MacCallum and C. Hoenselaers, *Exact Solutions of Einstein's Field Equations* (Cambridge University Press, Cambridge, 2003)

Backreaction problem in Bose-Einstein condensates: an analogy with curved spacetime

Yasunari Kurita[1], Michikazu Kobayashi[(b)], Hideki Ishihara[(c)], Makoto Tsubota[(c)].

[(a)] *Kanagawa Institute of Technology, Atsugi, Kanagawa 243-0292, Japan*
[(b)] *Department of Pure and Applied Sciences, The University of Tokyo, Komaba, Tokyo 153-8902, Japan*
[(c)] *Department of Physics, Osaka City University, Osaka 558-8585, Japan*

Abstract

We discuss particle creation phenomena in Bose–Einstein condensates in terms of conserving gapless mean field theory. The particle creation spectrum accompanied by backreaction effect can be calculated by rediagonalizing the Bogoliubov–de Gennes (BdG) Hamiltonian in the mean field theory. An expression for an effective metric affected by quantum backreaction is shown.

As is well-known, spacetime dynamics causes particle creation as a result of change in definition of particles [1]. A famous example of particle creation is Hawking radiation from dynamically formed black holes [2]. It is commonly believed that black holes evaporates as a result of Hawking radiation, which is an example of backreaction of particle creation to background spacetime. However, a precise description of the backreaction of quantum particle creation to classical spacetime dynamics has not been developed yet [3] (for recent progress see, for example, [4, 5]).

Particle creation has some striking features. The spectrum of particle creation is generally very wide. It does not keep symmetry of background spacetime dynamics. For example, spherically symmetric black holes formed via spherically symmetric gravitational collapse emits non-spherically symmetric radiation as well as spherically symmetric one. These properties are not belong to resonances or perturbations in field theory. Therefore, particle creation is a non-trivial field theoretical phenomenon and is completely different from resonances or perturbations. Theoretically, it is considered that particle creation occurs even in condensed matter systems.

It is well-known that there is analogy between a wave propagating in curved spacetime and a sound wave propagating in a fluid [6]. In this analogy, fluid flow corresponds to spacetime. The effective spacetime metric is determined by information of the background fluid flow. The sound wave can then be seen as a field in curved spacetime. This analogy enables us to use fluid systems to study many field theoretical phenomena in curved spacetime [7, 8].

One advantage of using such an analogy is the possibility of observing quantum effects experimentally. It is important to consider quantum fluids to investigate quantum effects precisely. Bose–Einstein condensates (BECs) in trapped cold atoms [9, 10] are some of the best systems in this context [11]. Acoustic black holes has been recently reported for the first time in BEC [12]. One of the simplest methods for realizing a sonic horizon is just to expand a BEC [13].

From theoretical points of view, in BECs, quantum theory for elementary excitation is known, which gives theoretical basis for studying particle creation. It is known that Bogoliubov theory for BECs precisely corresponds to quantum field theory (QFT) in curved spacetime. In this formulation, particle creation in BECs can be formulated in terms of rediagonalization of the BdG Hamiltonian [14, 15], representing change in definition of quasiparticles. However, in the Bogoliubov theory, particle number of the condensate is conserved, and the backreaction to the condensate can not be taken into account. Therefore, we have to consider another theory.

Recently, Kita [16–19] formulated a new mean field theory for BECs that both satisfies conservation laws and has gapless excitations. It is thus a promising theory for describing BEC systems. By use of this theory, particle creation that includes backreaction effects in BECs at zero temperature was formulated in [20], where the particle creation spectrum corrected by backreaction effects is obtained. By considering the analogy, we seek to obtain a model representing the quantum backreaction effect in the effective

[1]Email address: kurita@gen.kanagawa-it.ac.jp[(a)]

spacetime metric and to obtain some implications for QFT in curved spacetime. In this paper, we give a brief review of discussion in this topic given in [20].

In particle creation in BECs system, Bogoliubov quasiparticles will be created as a result of non-trivial dynamics of background condensates. Without considering backreaction effect, it is known that dynamics of condensates obeys Gross–Pitaevskii (GP) equation. In Kita theory, backreaction effects are accompanied and the equation for condensate wave function Ψ is given by

$$i\hbar\frac{\partial\Psi}{\partial t} = \left(\hat{L} + U_0|\Psi|^2\right)\Psi + 2U_0\langle\phi^\dagger\phi\rangle\Psi + U_0\langle\phi\phi\rangle\Psi^*, \tag{1}$$

where $\hat{L} = \hat{K} + V_{\rm ext} - \mu$. $\hat{K} = -\frac{\hbar^2}{2m}\nabla^2$ is the kinetic energy operator and μ is the chemical potential. $V_{\rm ext}$ is the trapping potential for Bose gases. The extended GP equation (Eq. (1)) includes quasiparticle pair correlations $\langle\phi^\dagger\phi\rangle$ and $\langle\phi\phi\rangle$. These correlations are obtained from renormalized Green's function [19] and we assume that these quantities are finite. The condensate wave function Ψ can be rewritten in terms of the condensate number density n_0 and the phase S as:

$$\Psi = \sqrt{n_0}e^{iS}. \tag{2}$$

The total number of condensate particles is given by

$$N_0 := \int |\Psi|^2 d^3x = \int n_0 d^3x. \tag{3}$$

In general, N_0 is time dependent in this theory.

Bogoliubov quasi-particles are seen as elementary excitations, obeying Bogoliubov-de Gennes (BdG) equations. The time-dependent BdG equation can be represented as

$$i\hbar\partial_t\mathbf{\Phi} = \mathbf{H}\mathbf{\Phi} \tag{4}$$

where the BdG Hamiltonian is given by

$$\mathbf{H} = \begin{pmatrix} W + 2U_0\langle\phi^\dagger\phi\rangle & U_0\Psi^2 - U_0\langle\phi\phi\rangle \\ -U_0\Psi^{*2} + U_0\langle\phi^\dagger\phi^\dagger\rangle & -W - 2U_0\langle\phi^\dagger\phi\rangle \end{pmatrix}, \tag{5}$$

where we have defined $W := \hat{K} + V_{\rm ext} - \mu + 2n_0U_0$. $\mathbf{\Phi}$ is a two-component vector composed of fields for Bogoliubov quasiparticles ϕ and its conjugate $\phi^\dagger$

$$\mathbf{\Phi}(t,\mathbf{x}) = \begin{pmatrix} \phi(t,\mathbf{x}) \\ \phi^\dagger(t,\mathbf{x}) \end{pmatrix}. \tag{6}$$

These quasiparitcle fields ϕ, $\phi^\dagger$ can be expanded by use of a set of eigen vectors for the BdG Hamiltonian $(u_k, -v_k^*)$ as

$$\begin{aligned} \begin{pmatrix} \phi \\ \phi^\dagger \end{pmatrix} &= \sum_{k\neq 0}\left[\hat{\gamma}_k\begin{pmatrix} u_k \\ -v_k^* \end{pmatrix} + \hat{\gamma}_k^\dagger\begin{pmatrix} -v_k \\ u_k^* \end{pmatrix}\right] \\ &\quad + (\hat{\gamma}_0 - \hat{\gamma}_0^\dagger)\begin{pmatrix} \varphi_0 \\ -\varphi_0^* \end{pmatrix}. \end{aligned} \tag{7}$$

The operators $\hat{\gamma}_m$ and $\hat{\gamma}_n^\dagger$ $(m, n = 0, 1, 2, \cdots)$ satisfy the boson commutation relation $[\hat{\gamma}_m, \hat{\gamma}_n^\dagger] = \delta_{mn}$, and these can be interpreted as annihilation and creation operators of quasiparticles, respectively.

After some calculation, it is found that condensates behaves like perfect fluids, which implies that the fluid/spacetime analogy can be considered. By considering the effective equation for sound wave in BECs within the Kita theory, we obtain the effective spacetime metric as

$$g_{\mu\nu} := \frac{mc_s}{U_0X}\begin{pmatrix} -(c_s^2 - v_0^2) & -v_{0a} \\ -v_{0b} & \delta_{ab} \end{pmatrix}, \tag{8}$$

where $a, b = 1, 2, 3$. The sound velocity can be described as

$$c_s := \sqrt{\frac{n_0 U_0 X}{m}}, \tag{9}$$

where the quantity X has been defined as

$$X := 1 - \frac{\langle \tilde{\phi}\tilde{\phi} \rangle + \langle \tilde{\phi}^\dagger \tilde{\phi}^\dagger \rangle}{2n_0}. \tag{10}$$

Note that X is real. The effective metric includes contributions from quasiparticle pair correlations. If we drop the contributions and set $X = 1$, then the effective metric becomes the well-known metric without the backreaction (see, for example, [8]). We find that the correction to the effective metric appears in the form of $U_0 X$. However, the backreaction effect is not included only in X: the quantities n_0 and v_0 are affected by the backreaction effect through the pair correlation terms in the extended GP equations.

Now, we consider the time evolution of condensate for $t_1 < t < t_2$ accompanied with the initial and final quasi-static condensates. Then, the complete sets that diagonalize the BdG Hamiltonian at $t = t_1$ and $t = t_2$ will be different in general, and annihilation and creation operators that define quasiparticle states will change. The particle number operator of j-th mode at the time $t = t_2$ is denoted by $\hat{N}_j$. By rediagonalizing the BdG Hamiltonian in Kita theory, the expression for the particle creation spectrum can be obtained as

$${}_{(1)}\langle 0|\hat{N}_j|0\rangle_{(1)} = \sum_{k\neq 0} |B_{jk}|^2, \tag{11}$$

where

$$B_{jk} = \int_{t=t_2} d^3x \left(v_j^{(2)} u_k^{(1)*} - u_j^{(2)*} v_k^{(1)} \right), \tag{12}$$

and $|0\rangle_{(1)}$ is the initial vacuum. The functions $u_j^{(i)}$ and $v_j^{(i)}$ $(i = 1, 2)$ are elements of the complete set that diagonalizes the BdG Hamiltonian at time $t = t_i (i = 1, 2)$. If the right-hand side of Eq. (11) is not zero, quasiparticles will appear at $t = t_2$. This is the formula for the particle creation spectrum in Kita theory. The spectrum given by Eq. (11) includes the backreaction effect. It should be noted that this particle creation spectrum is obtained within condensed matter theory. By use of the fluid/spacetime analogy, we can calculate it by use of a well-known way of QFT in curved spacetime. This expression (12) agrees with one calculated by QFT in effective spacetime [20]. Furthermore, the spectrum is the same, apparently, as one obtained within Bogoliubov theory [14]. But the wave functions $u_j^{(i)}$, $v_j^{(i)}$ obey the equation affected by the backreaction and are quantitatively different from those in Bogoliubov theory [14], in general.

These results imply that the usual prescription for particle creation in QFT in curved spacetime might give the correct result. In the analogy, the explicit backreaction effect appears only in the effective spacetime metric. The BdG Hamiltonian rediagonalization formulation provides a rigorous result for particle creation from a theoretical point of view, in the sense that the hydrodynamic approximation (which is assumed in constructing the analogy) is not required in this formulation.

References

[1] See, for example, N. D. Birrell and P. C. W. Davies, "*Quantum fields in curved space*", Cambridge Univ. Press (1982).

[2] S. W. Hawking, *Nature* **248**, 30 (1974); S. W. Hawking, Commun. Math. Phys. **43**, 199 (1975) [Erratum-ibid. **46**, 206 (1976)].

[3] See, for example, R. M. Wald, "*Quantum Field Theory in Curved Spacetime and Black Hole Thermodynamics*", The University of Chicago Press (1994).

[4] C. Maia and R. Schutzhold, Phys. Rev. D **76**, 101502 (2007) [arXiv:0706.4010 [gr-qc]].

[5] R. Schutzhold and C. Maia, J. Phys. A **41**, 164065 (2008).

[6] W. G. Unruh, Phys. Rev. Lett. **46**, 1351 (1981).

[7] *Artificial Black Holes*, edited by M. Novello, M. Visser, and G. Volovik (World Scientific, 2002).

[8] C. Barceló, S. Liberati and M. Visser, Living Rev. Rel. **8**, 12 (2005).

[9] M. H. Anderson, J. R. Ensher, M. R. Matthews, C. E. Wieman, and E. A. Cornell, Science **269**, 198 (1995).

[10] K. B. Davis, M.-O. Mewes, M. R. Andrews, N. J. van Druten, D. S. Durfee, D. M. Kurn, and W. Ketterle, Phys. Rev. Lett. **75**, 3969 (1995).

[11] L. J. Garay, J. R. Anglin, J. I. Cirac and P. Zoller, Phys. Rev. Lett. **85**, 4643 (2000).

[12] O. Lahav, A. Itah, A. Blumkin, C. Gordon, J. Steinhauer, arXiv:0906.1337.

[13] Y. Kurita and T. Morinari, Phys. Rev. A **76**, 053603 (2007).

[14] Y. Kurita, M. Kobayashi, T. Morinari, M. Tsubota and H. Ishihara, Phys. Rev. A **79**, 043616 (2009).

[15] C. Barceló, L. J. Garay, and G. Jannes, Phys. Rev. D **82**, 044042 (2010).

[16] T. Kita, J. Phys. Soc. Jpn. **74**, 1891 (2005).

[17] T. Kita, J. Phys. Soc. Jpn. **75**, 044603 (2006).

[18] T. Kita, J. Phys. Soc. Jpn. **74**, 3397 (2005).

[19] T. Kita, Phys. Rev. B **80**, 214502 (2009).

[20] Y. Kurita, M. Kobayashi, H. Ishihara and M. Tsubota Phys. Rev. A **82**, 053602 (2010).

Gravitational waves from spinning black hole-neutron star binaries

Koutarou Kyutoku[(a)], Masaru Shibata[(a)], Hirotada Okawa[(a)] and Keisuke Taniguchi[(b)]

[(a)] *Yukawa Institute for Theoretical Physics, Kyoto University, Kyoto 606-8502*
[(b)] *Graduate School of Arts and Sciences, University of Tokyo, Komaba, Meguro, Tokyo 153-8902*

Abstract

We report our recent results obtained from numerical-relativity simulations of black hole-neutron star binary mergers with a variety of equations of state and black hole spins. The tidal disruption of the neutron star occurs even for high mass-ratio binaries of $M_{\rm BH}/M_{\rm NS} = 5$, if the black hole has a sufficiently large prograde spin. Information about the equation of state at high density can be obtained from observations of gravitational waves, especially from the cutoff frequency shown in the spectra.

1 Introduction

Compact object binaries are ones of the most promising sources of gravitational waves for ground-based laser-interferometric detectors such as (Advanced) LIGO, VIRGO and LCGT [3, 6]. Since gravitational waves are more transparent to the matter than the electromagnetic waves and neutrinos, gravitational waves from the merger of a black hole (BH)-neutron star (NS) or NS-NS binary are expected to be an unique tool to investigate the radius and equation of state (EOS) of the NS. In such circumstances, theoretical calculations of gravitational-wave templates are strongly required to extract physical information from observed gravitational waves. At the same time, such binaries are also important for high-energy astrophysics because the BH-hot, massive accretion disk system as a remnant of the BH-NS binary merger is a possible progenitor of a short-hard gamma-ray burst (GRB) [7]. To validate this merger scenario, theoretical calculation of the BH-NS binary merger is again required to show that the BH-disk system is actually formed.

Numerical relativity is the unique approach to investigate the merger phase of BH-NS binary coalescences, in which the nonlinearity of general relativity and the hydrodynamic effect of the NS are important. Especially, whether the tidal disruption of the NS occurs during the merger or not is the most important question, since (i) the tidal disruption imprints information about the NS radius and EOS on the gravitational waveforms, and (ii) the merger scenario of short-hard GRBs requires the NS tidal disruption.

The NS EOS and the BH spin are crucial ingredients for the tidal disruption. By an approximate estimation by Newtonian gravity, the ratio of the radius at which the mass shedding $r_{\rm MS}$ to the radius of innermost stable circular orbit (ISCO) of the BH $r_{\rm ISCO}$ is written as

$$\frac{r_{\rm MS}}{r_{\rm ISCO}} \propto \frac{M_{\rm BH}}{r_{\rm ISCO}} \frac{R_{\rm NS}}{M_{\rm NS}} \left(\frac{M_{\rm NS}}{M_{\rm BH}}\right)^{2/3}, \tag{1}$$

where $M_{\rm BH}$, $M_{\rm NS}$ and $R_{\rm NS}$ are the mass of the BH, mass of the NS and radius of the NS, respectively. This ratio must be sufficiently large so that the NS tidal disurption occurs outside the BH ISCO and the remnant disk is formed. We can rewrite this expression as

$$\frac{r_{\rm MS}}{r_{\rm ISCO}} \propto \xi^{-1} \mathcal{C}^{-1} Q^{-2/3}, \tag{2}$$

where $\xi \equiv r_{\rm ISCO}/M_{\rm BH}$ is the ratio between the ISCO radius and the BH mass, $\mathcal{C} \equiv M_{\rm NS}/R_{\rm NS}$ is the NS compactness and $Q \equiv M_{\rm BH}/M_{\rm NS}$ is the mass ratio of the BH to the NS.(Here and throughout this paper, the geometrical unit in which $G = c = 1$ is assumed.) This expression shows the importance of the BH spin and the NS EOS. The BH spin determines the radius of a fixed mass BH. If the BH spin is

prograde (i.e., parallel to the orbital angular momentum), ξ becomes smaller by a factor of $\lesssim 6$ than in the nonspinning BH case. The NS EOS determines the radius of a fixed mass NS and hence compactness, $\mathcal{C}$, which becomes smaller when the EOS is stiffer.

Motivated by these facts, we investigate the effect of the BH spin and NS EOS on the coalescences of BH-NS binaries by numerical-relativity simulations. We mainly focus on how the information of the NS radius and EOS can be extracted from gravitational waves and their spectra via the NS tidal disruption. We briefly describe our numerical method in Sec. 2 and report some of our results in Sec. 3, and Sec. 4 is devoted to a summary.

2 Methods

We employ a quasiequilibrium state of the BH-NS binary as an initial condition for the numerical simulation. We compute the quasiequilibrium state as a solution of the initial value problem of general relativity [1] within the moving-puncture framework. Formulation and numerical methods are summarized in Ref. [4] except for issues related to the BH spin. The spin of the BH is controlled via a so-called Bowen-York extrinsic curvature [1], and determined to give a desired value of the BH spin evaluated on the apparent horizon within the isolated-horizon framework [2]. We systematically choose physical parameters of the BH-NS binary, i.e., the NS mass, BH mass and BH spin. We denote the nondimensional spin parameter of the BH as $a \equiv S_{\rm BH}/M_{\rm BH}^2$, where $S_{\rm BH}$ is the spin angular momentum of the BH.

To investigate the effect of the EOS systematically, we also adopt several piecewise polytropic EOSs for the cold, zero temperature NS matter. Piecewise polytropic EOS is a phenomenologically parameterized EOS, which mimics a nuclear-theory based EOS, of the form

$$P(\rho) = \kappa_i \rho^{\Gamma_i} \text{ for } \rho_{i-1} \le \rho \le \rho_i \ (1 \le i \le n), \tag{3}$$

where ρ is the rest-mass density, P is the pressure, n is the number of the pieces used to parameterize an EOS and $(\kappa_i, \Gamma_i, \rho_i)$ are parameters to specify each piece of polytrope. (See Ref. [8] for more detail.) In this paper, we focus only on the case of $n = 2$, i.e., different polytropes for the crust and core of the NS, for simplicity. In this work, we adopt five piecewise polytropic EOS systematically to investigate the effect of the NS EOS.

We perform dynamical simulations using an AMR code SACRA [10]. We solve the Einstein equation in the BSSN formalism with the moving-puncture gauge conditions, and solve hydrodynamic equations using the high-resolution central scheme of Kurganov and Tadmor with third-order piecewise parabolic interpolation in SACRA. Details of the formulation, gauge condition, numerical schemes and methods of diagnostics are the same as described in Ref. [5] and references therein. We adopt piecewise polytropic EOSs for the cold part EOS, and adopt simple Γ-law ideal gas EOS for the thermal part EOS.

3 Results

The mass of the remnant disk is a reasonable indicator of the strength of the NS tidal disruption. We plot the ratio of the mass of the remnant disk to the baryon rest-mass of the NS for HB EOS and $M_{\rm NS} = 1.35 M_\odot$ cases as a function of a in Fig. 1. The disk mass increases as the BH spin increases for each mass ratio, and the disk mass is as large as $\gtrsim 0.01 M_\odot$, which is required for the disk to be a progenitor of the GRB, irrespective of the mass ratio concerned here if the BH spin is as large as $a \gtrsim 0.75$. Aside from the difference in the disk mass according to the different stiffness of the EOS, this trend of increase holds irrespective of the NS EOS and explained by the contraction of the BH ISCO due to the prograde BH spin. Such formation of a massive disk from a high mass-ratio binary of $Q \sim 5$, or equivalently massive BH of $M_{\rm BH} \sim 6.75 M_\odot$, is not expected if the BH is nonspinning [9]. The fact that the NS tidal disruption occurs for a high mass-ratio binary is important in an astrophysical sense, since the typical mass of the stellar mass BH is assumed to be $\gtrsim 5 M_\odot$ from a population synthesis studies, and hence a low mass-ratio BH-NS binary of $Q \sim 2$ is not realistic.

Information of the NS tidal disruption can be written from a gravitational-wave spectrum, especially via a cutoff frequency $f_{\rm cut}$ [5]. Figure 2 shows the gravitational-wave spectra obtained from $(Q, M_{\rm NS}, a) = (5, 1.35 M_\odot, 0.75)$ binaries with several EOSs. We also plot the spectrum obtained from a

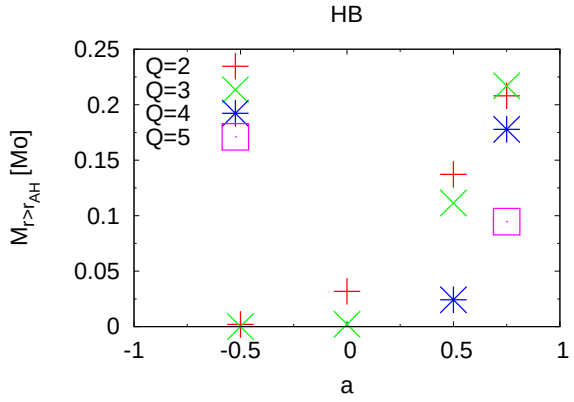

Figure 1: The ratio of the mass of the remnant disk to the baryon rest-mass of the NS as a function of the nondimensional spin parameter of the BH for HB EOS and $M_{\rm NS}$.

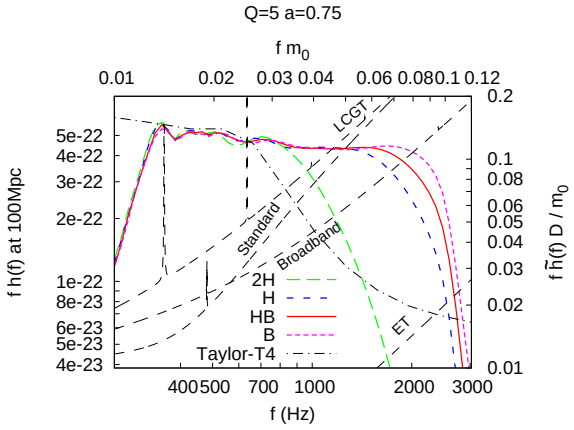

Figure 2: Gravitational-wave spectra from $(Q, M_{\rm NS}, a) = (5, 1.35M_\odot, 0.75)$ binaries. Transverse light-blue line is the spectrum calculated by a post-Newtonian formula. Black dashed lines are planned noise curves of next- and third-generation gravitational-wave detectors.

post-Newtonian formula and planned noise curves of next- and third-generation gravitational-wave detectors. The spectrum at low frequency of $f \lesssim 1$ kHz agrees with the post-Newtonian spectrum, since the finite size effect of the NS does not play an important role. In the late inspiral phases of $f \gtrsim 1$ kHz, this post-Newtonian formula used here is not sufficient to model the inspiral of a strongly gravitating binary due to the strong nonlinear gravity. The inspiral is terminated when the NS is tidally disrupted by the tidal force field of the BH, and hence the spectra shown in Fig. 2 show the damping around $f_{\rm cut} \sim 2$ kHz, which is closely related to the NS tidal disruption and depends strongly on the NS EOS. It should be noted that $f_{\rm cut}$ does not depend on the NS EOS very much if the NS tidal disruption does not occur, since $f_{\rm cut}$ approximately agrees with the quasinormal-mode frequency of the remnant BH, which is determined primarily by the mass ratio of the binary and the BH spin.

In order to investigate what gravitational waves tell us, we extract $f_{\rm cut}$ by a systematic fitting procedure from each spectrum for $a = 0.75$. Figure 3 shows the cutoff frequency times the total mass of the system, $f_{\rm cut}m_0$, as a function of the NS compactness, $\mathcal{C}$. This plot includes results obtained by $M_{\rm NS} \neq 1.35M_\odot$ models, and hence difference between $\mathcal{C}$ and $R_{\rm NS}$ is important. This figure indicates the existence of a strong correlation between $f_{\rm cut}m_0$ and $\mathcal{C}$ as an approximate power law,

$$f_{\rm cut}m_0 \propto \mathcal{C}^p, \tag{4}$$

where p is a power depending on Q and a. This correlation will give us an unique opportunity to know the

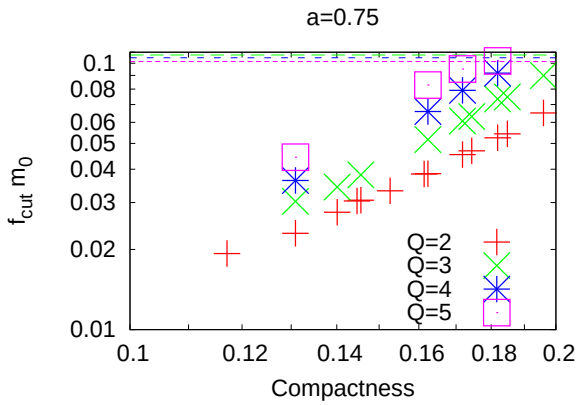

Figure 3: $f_{\rm cut} m_0 - \mathcal{C}$ for $a = 0.75$ models.

NS compactness, and hence the radius and EOS of the NS. Again, it is important that such a relationship holds for a high mass-ratio binary of $Q \gtrsim 4$, which is assumed to be an astrophysically realistic one, when the BH has a sufficiently large prograde spin. If the BH is nonspinning and the NS tidal disruption does not occur, $f_{\rm cut}$ does not show the strong correlation with the NS quantities such as the radius and compactness for $Q \gtrsim 3$.

4 Summary

We performed numerical-relativity simulations of BH-NS binary mergers in order to clarify the effects of the BH spin and the NS EOS on the NS tidal disruption and related outcomes of the mergers. We find that the NS tidal disruption occurs even for high mass-ratio binaries of $Q \lesssim 5$ if the BH has a prograde spin, and the gravitational-wave spectra of such events will give us the information about the NS radius and EOS. This suggests that gravitational-wave astronomy with the BH-NS binary will be a strong tool to investigate the NS radius and the EOS at high density. Accordingly, the mass of the remnant disk is sufficiently massive as $\gtrsim 0.01 M_\odot$ so that the merger remnant of high mass-ratio binary is a potential central engine of the GRB. More detailed results and discussion will be reported in near future.

References

[1] G. B. Cook Living Rev. Relativity **3**, 5 (2000)

[2] G. B. Cook, B. F. Whiting Phys. Rev. D **76**, 041501 (2007)

[3] K. Kuroda and The LCGT Collaboration Class. Quantum Phys. **27**, 084004 (2010)

[4] K. Kyutoku, M. Shibata, K. Taniguchi Phys. Rev. D **79**, 124018 (2009).

[5] K. Kyutoku, M. Shibata, K. Taniguchi Phys. Rev. D **82**, 044049 (2010).

[6] The LIGO Scientific Collaboration and The Virgo Collaboration Nature **460**, 990 (2009)

[7] E. Nakar Phys. Rep. **442**, 166 (2007)

[8] J. S. Read, B. D. Lackey, B. J. Owen, J. L. Friedman Phys. Rev. D **79**, 124032 (2009)

[9] M. Shibata, K. Kyutoku, T. Yamamoto, K. Taniguchi Phys. Rev. D **79**, 044030 (2009)

[10] T. Yamamoto, M. Shibata, K. Taniguchi Phys. Rev. D **78**, 064054 (2008)

Horava gravity coupled to the Brans-Dicke field

Tae Hoon Lee[1 (a)], Joohan Lee[(b)], and Phillial Oh[(c)]

[(a)] *Department of Physics, Soongsil University, Seoul 156-743 Korea*
[(b)] *Department of Physics, University of Seoul, Seoul 130-743 Korea*
[(c)] *Department of Physics, Sungkyunkwan University, Suwon 440-746 Korea*

Abstract

We seek a Brans-Dicke type generalization of Horava-Lifshitz gravity, and we show that such a generalization is possible within the detailed balance condition. The resulting theory reduces classically, in the low energy limit, to the usual Brans-Dicke theory with a negative cosmological constant for certain values of parameters.

1 Introduction

A new theory of gravity has been recently proposed by Horava[1]. This theory, being based on anisotropic scaling of space and time, breaks the spacetime symmetry. It has a much better UV behavior than the theories with the spacetime diffeomorphism symmetry, but expected to reduce to Einstein's gravity in the infrared limit, thereby recovering the spacetime diffeomorphism symmetry. Physical constants such as the speed of light, Newton's constant, and cosmological constant all emerge from the relevant deformation of the non-relativistic theory at short distance. These interesting features as well as other related findings have received a great deal of attention[2, 3].

Even if we consider classical limit of gravity there are many alternative theories and extensions of the Einstein theory. In particular, various gravity models with scalar fields have been considered and a possible role of the scalar fields in explaining the behavior of the universe in the early stage as well as the late stage has been investigated[4, 5]. Therefore, it would be interesting to see if Horava's theory can be extended in such a way that in the infrared limit it reduces to those alternative theories. In this regard, of particular interest would be the one with a non-minimally coupled scalar field because ordinary minimally coupled scalar source had already been investigated[1, 6]. Typical example would be the Brans-Dicke theory[7].

From the next section of this paper, we extend the Horava-Lifshitz gravity to include the Brans-Dicke field as a concrete example of the non-minimally coupled scalar field. It turns out that such an extension is possible within the context of the detailed balance condition, which reduces to the four-dimensional Brans-Dicke theory with negative cosmological constant when only the lowest order derivative terms are kept and parameters of the theory are chosen to satisfy certain conditions. There are many known problems with the detailed balance condition[8]. However, one can break the condition if necessary. In any case, it will be interesting to see if the detailed balance condition can be maintained when we try to non-minimally generalize the Horava-Lifshitz gravity.

2 Horava-Lifshitz gravity coupled to the Brans-Dicke field

Let us consider the four-dimensional Brans-Dicke theory[7], where the action is given by

$$S = \int d^4x\sqrt{-g}\left(\phi R - \omega\phi^{-1}g^{\mu\nu}\partial_\mu\phi\partial_\nu\phi\right). \tag{1}$$

Decomposition of this action into $(3+1)$ form, including the speed of light, c, yields (See Ref. [9], for instance.)

$$\sqrt{-g}\phi R \simeq N\sqrt{q}\phi\left(\mathcal{R} + c^{-2}(K_{ab}K^{ab} - K^2)\right) - 2N\sqrt{q}c^{-2}K\pi - 2N\sqrt{q}D^2\phi, \tag{2}$$

$$-\sqrt{-g}\omega\phi^{-1}g^{\mu\nu}\partial_\mu\phi\partial_\nu\phi = N\sqrt{q}\omega\phi^{-1}c^{-2}\pi^2 - N\sqrt{q}\omega\phi^{-1}D^a\phi D_a\phi, \tag{3}$$

[1]Email address: thlee@ssu.ac.kr

where the four metric g is decomposed into the lapse function N, the shift vector N^a and the three metric q_{ab}, and the corresponding three-dimensional covariant derivative and its scalar curvature are denoted respectively by D_a, $\mathcal{R}$. The Brans-Dicke parameter is assumed positive, $\omega > 0$. In the first equation irrelevant total divergence terms were dropped out. The time derivatives of the three-metric and the scalar field are encoded in the following quantities;

$$K_{ab} \equiv \frac{1}{2N}(\dot{g}_{ab} - D_a N_b - D_b N_a),\ \pi \equiv \frac{1}{N}(\dot{\phi} - N^a \partial_a \phi). \tag{4}$$

Using the above result the Brans-Dicke action can be split into the two parts $S_{BD} = S^K_{BD} + S^V_{BD}$, where the kinetic and potential parts can be written after re-scaling of the scalar field ϕ and the corresponding field π as

$$S^K_{BD} = \int dt\, d^3x N\sqrt{q}\left(\phi(K_{ab}K^{ab} - K^2) - 2K\pi + \omega\phi^{-1}\pi^2\right), \tag{5}$$

$$S^V_{BD} = c^2 \int dt\, d^3x N\sqrt{q}\left(\phi\mathcal{R} - 2D^2\phi - \omega\phi^{-1}D^a\phi D_a\phi\right). \tag{6}$$

Note the factor of c^2 in front of the potential term. For the later purpose regarding the detailed balance condition it is important to express the kinetic part in the following matrix form;

$$S^K_{BD} = \int dt\, d^3x N\sqrt{q} \begin{pmatrix} K_{ab} & \pi \end{pmatrix} \begin{pmatrix} \phi G^{abcd} & -q^{ab} \\ -q^{cd} & \omega\phi^{-1} \end{pmatrix} \begin{pmatrix} K_{cd} \\ \pi \end{pmatrix}, \tag{7}$$

where

$$G^{abcd} = \frac{1}{2}\left(q^{ac}q^{bd} + q^{ad}q^{bc}\right) - q^{ab}q^{cd}. \tag{8}$$

The matrix in the middle of the kinetic part of the action can be regarded as the supermetric on the space of (q_{ab}, ϕ), naturally extending the DeWitt metric on the space of three-metrics.

We intend to construct a Brans-Dicke type extension of Horava-Lifshitz gravity with the detailed balance condition. So, we choose the action of the form, $S_{HLBD} = S^K_{HLBD} + S^V_{HLBD}$, where the kinetic part is

$$S^K_{HLBD} = \int dt d^3x N\sqrt{q} \begin{pmatrix} K_{ab} & \pi \end{pmatrix} \begin{pmatrix} \phi G^{abcd}(\lambda) & -q^{ab} \\ -q^{cd} & \omega\phi^{-1} \end{pmatrix} \begin{pmatrix} K_{cd} \\ \pi \end{pmatrix} \tag{9}$$

and the potential part is of the form

$$S^V_{HLBD} = -\int dt d^3x N\sqrt{q} \begin{pmatrix} \frac{\delta W}{\delta q_{ab}} & \frac{1}{2}\frac{\delta W}{\delta \phi} \end{pmatrix} \begin{pmatrix} \phi G^{abcd}(\lambda) & -q^{ab} \\ -q^{cd} & \omega\phi^{-1} \end{pmatrix}^{-1} \begin{pmatrix} \frac{\delta W}{\delta q_{cd}} \\ \frac{1}{2}\frac{\delta W}{\delta \phi} \end{pmatrix} \tag{10}$$

for some suitable choice of function $W(q, \phi)$. The supermetric $G^{abcd}(\lambda)$ was slightly deformed compared to the Eq. (8) to include the parameter λ as usual, $G^{abcd}(\lambda) \equiv \frac{1}{2}\left(q^{ac}q^{bd} + q^{ad}q^{bc}\right) - \lambda q^{ab}q^{cd}$. The factor of two was inserted in front of the variation of W with respect to ϕ to compensate for different normalization in time derivatives in Eqs.(4) and (5). It is a straightforward matter to calculate the inverse supermetric. It comes out to be of form

$$\begin{pmatrix} \phi^{-1}\mathcal{G}_{abcd} & -Aq_{ab} \\ -Aq_{cd} & B\phi \end{pmatrix}, \tag{11}$$

where $\mathcal{G}_{abcd} = \frac{1}{2}\left(q_{ac}q_{bd} + q_{ad}q_{bc}\right) - \bar{\lambda}q_{ab}q_{cd}$, with $A = \frac{1}{\omega(3\lambda-1)+3}$, $B = \frac{3\lambda-1}{\omega(3\lambda-1)+3}$, $\bar{\lambda} = \frac{1+\omega\lambda}{\omega(3\lambda-1)+3}$. Note that this inverse supermetric is well-defined even for $\lambda = 1/3$ contrary to the pure gravity case and becomes singular instead when $\lambda = (\omega - 3)/3\omega$, for instance when $\lambda = 1$ and $\omega = -3/2$ corresponding to the conformal scalar case (We assume $\omega > 0$ in this work.). If we take the limit of $\omega \to \infty$, A and B vanish and $\bar{\lambda} = \lambda/(3\lambda - 1)$, reproducing the pure gravity case.

We choose

$$W = c_1 \int d^3x\sqrt{q}\phi(\mathcal{R} - 2\Lambda_b) - c_2 \int d^3x\sqrt{q}\omega\phi^{-1}D^a\phi D_a\phi. \tag{12}$$

In general all possible marginal and relevant terms can be included. The above choice of W corresponds to keeping only terms important in the infrared limit. Then, after a straightforward calculation Eq. (10) can be written as

$$\begin{aligned} S^V_{HLBD} &= \int dt\, d^3x N\sqrt{q}\left\{\alpha\phi+\beta(\phi\mathcal{R}-\frac{c_2}{c_1}\omega\phi^{-1}D^a\phi D_a\phi)+\gamma(-2D^2\phi)\right\} \\ &- \int dt\, d^3x N\sqrt{q}\left(Q^{ab}\phi^{-1}\mathcal{G}_{abcd}Q^{cd}-2AQ^{ab}q_{ab}Q+B\phi Q^2\right), \end{aligned} \tag{13}$$

where $\alpha=(c_1\Lambda_b)^2\frac{3\omega+7-3\lambda}{\omega(3\lambda-1)+3}$, $\beta=-(c_1)^2\Lambda_b\frac{\omega+5-3\lambda}{\omega(3\lambda-1)+3}$, $\gamma=-(c_1)^2\Lambda_b\frac{2(\omega+1)-\frac{c_2}{c_1}\omega(4-3\lambda)}{\omega(3\lambda-1)+3}$, and

$$Q^{ab}\equiv c_1\left(-\phi(\mathcal{R}^{ab}-\frac{1}{2}\mathcal{R}q^{ab})+D^aD^b\phi-q^{ab}D^2\phi\right),\ Q\equiv c_1\frac{\mathcal{R}}{2}-c_2\left(-\omega\phi^{-1}D^2\phi+\frac{\omega}{2}\phi^{-2}D^a\phi D_a\phi\right). \tag{14}$$

The second line of Eq. (13) has quadratic terms only.

When $c_1=c_2$ and $\lambda=1$, the theory recovers four-dimensional diffeomorphism symmetry, as one can see from the fact that in the infrared limit the potential part of the action becomes

$$S^V_{BDHL}|_{IR}=-(c_1)^2\Lambda_b\frac{\omega+2}{2\omega+3}\int dt\, d^3x N\sqrt{q}\left(\phi(\mathcal{R}-2\Lambda)-2D^2\phi-\omega\phi^{-1}D^a\phi D_a\phi\right), \tag{15}$$

where

$$\Lambda=\frac{3\omega+4}{2(\omega+2)}\Lambda_b. \tag{16}$$

This expression coincides with that of the Brans-Dicke theory except that the cosmological constant term is present. Comparison with the kinetic part yields the speed of light

$$c^2=-(c_1)^2\Lambda_b\frac{\omega+2}{2\omega+3}. \tag{17}$$

As in the case of the Horava gravity the constant Λ_b must be negative, consequently allowing only negative cosmological constant Λ. The Newton constant is related to the expectation value of the scalar field $<\phi>$ as follows,

$$G_N=\frac{c^2}{16\pi<\phi>}. \tag{18}$$

Now, we consider the homogeneous, isotropic cosmology. We restrict ourself to the case of $\lambda=1$, $c_1=c_2$, and set the speed of light to unity, i.e., $c=1$. We choose vanishing shift vector $N^a=0$, and the three-metric to be the usual maximally symmetric ones with curvature constant $k=-1,0,+1$,

$$ds^2=a^2(t)\left(\frac{dr^2}{1-kr^2}+r^2(d\theta^2+\sin^2\theta d\phi^2)\right). \tag{19}$$

In this case the higher derivative terms become greatly simplified due to homogeneity and isotropy,

$$Q^{ab}=kc_1\frac{\phi}{a^2}q^{ab},\quad Q=6kc_1\frac{1}{a^2}. \tag{20}$$

Independent field equations can be chosen to be

$$\begin{aligned} 3H^2+3H\frac{\dot\phi}{\phi}-\frac{1}{2}\omega(\frac{\dot\phi}{\phi})^2 &= \frac{1}{2}\phi^{-1}\rho_m-(\frac{3k}{a^2}-\Lambda)-\frac{1}{2}(\frac{B^2}{a^4}), \\ (2\omega+3)\left(\frac{\ddot\phi}{\phi}+3H\frac{\dot\phi}{\phi}\right) &= \frac{1}{2}\phi^{-1}(\rho_m-3p_m)+2\Lambda+\frac{B^2}{a^4}, \end{aligned} \tag{21}$$

together with the usual form of the continuity equation for the matter density ρ_m for consistency, where $H\equiv(\dot a/a)$ is the Hubble constant and

$$B^2=\frac{3\omega}{2\omega+3}(kc_1)^2=\frac{3\omega(3\omega+4)}{2(\omega+2)}\frac{k^2}{(-\Lambda)}. \tag{22}$$

The first equation in Eq. (21) is the Friedmann equation of the Brans-Dicke theory with a negative cosmological term and the dark radiation term included. In the absence of those two terms the equations simply become those of the usual Brans-Dicke theory[10].

3 Summary

To summarize, we have constructed a Brans-Dicke type extension of the Horava-Lifshitz gravity maintaining the detailed balance condition. We have investigated its low energy limit and shown that the resulting theory is the Brans-Dicke theory with a negative cosmological constant and a dark radiation term. Although we focused on the Brans-Dicke theory in this paper the analysis can be generalized to other non-minimally coupled scalar field gravity theory. It would be interesting to investigate cosmological aspects of the resulting theories.

acknowledgments The research of THL was supported by the Basic Science Research Program through the National Research Foundation of Korea(NRF) funded by Ministry of Education, Science and Technology(2010-0012692).

References

[1] P. Horava, *JHEP* **0903** (2009) 020; P. Horava, *Phys. Rev.* **D79** (2009) 084008; P. Horava, *Phys. Rev. Lett.* **102** (2009) 161301.

[2] G. Calcagni, *JHEP* **09**, (2009) 112.

[3] H. Lu, J. Mei, and C. N. Pope, *Phys. Rev. Lett.* **103**, (2009) 091301; E. Kiritsis and G. Kofinas, *Nucl. Phys.* **B821**, (2009) 467; T. Takahashi and J. Soda, *Phys. Rev. Lett.* **102**, (2009) 231301; R. Brandenberger, *Phys. Rev.* **D80**, (2009) 043516; S. Mukohyama, *JCAP* **0906**, (2009) 001; R.-G. Cai, L.-M. Cao, and N. Ohta, *Phys. Rev.* **D80**, (2009) 024003; H. Nastase, arXiv:0904.3604; A. Kehagias and K. Sfetsos, *Phys. Lett.* **B678**, (2009) 123; X. Gao, arXiv:0904.4187; M. Li and Y. Pang, *JHEP* **0908**, (2009) 015; T. P. Sotiriou, M. Visser, and S. Weinfurtner, *JHEP* **0910**, (2009) 033; R.-G. Cai, Y. Liu, and Y.-W. Sun, *JHEP* **0906**, (2009) 010; Y.-S. Piao, *Phys. Lett.* **B681**, (2009) 1; R.-G. Cai, B. Hu, and H.-B. Zhang, *Phys. Rev.* **D80**, (2009) 041501; R.-G. Cai, L.-M. Cao, and N. Ohta, *Phys. Lett.* **B679**, (2009) 504; M. I. Park, *JHEP* **0909**, (2009) 123.

[4] B. Ratra and P.J.E. Peebles, *Phys. Rev.* **D37** (1988) 3406; R.R Caldwell, R. Dave and P.J. Steinhardt, *Phys. Rev. Lett.* **80**, (1998) 1582.

[5] C. Armendariz-Picon, V. Mukhanov and P.J. Steinhardt, *Phys. Rev. Lett.* **85**, (2000) 4438; T. Okabe and M. Yamaguchi, *Phys. Rev.* **D62**, (2000) 023511; M. Malquarti, E.J. Copland, A.R. Liddle and M. Trodden, *Phys. Rev.* **D67**, (2003) 123503.

[6] S. Mukohyama, *JCAP* **0906**, (2009) 001; E. Kiritsis and G. Kofinas, *Nucl. Phys.* **B821**, (2009) 467; B. Chen and Qing-Guo Huang, *Phys. Lett.* **B683**, (2010) 108.

[7] C. Brans and R. H. Dicke, *Phys. Rev.* **124**, (1961) 925.

[8] G. Calcagni, *Phys. Rev.* **D81** (2010) 044006; C. Bogdanos and E. N. Saridakis, *Class. Quant. Grav.* **27** (2010) 075005; T. Sotiriou, M. Visser and S. Weinfurtner, *Phys. Rev. Lett.* **102**, (2009) 251601.

[9] B. Kelleher, *Class. Quantum Grav.* **21**, (2004) 483.

[10] Hongsu Kim, *Mon. Not. Roy. Astron. Soc.* **364**, (2005) 813.

The power spectrum of the magnetic fields generated by the second-order perturbations during the pre-recombination era

Satoshi Maeda[1(a)], Keitaro Takahashi[2(b)], Tsutomu Kobayahi[3(c)] and Tetusya Shiromizu[4(a)]

[(a)] *Department of Physics, Kyoto University, Department of Physic, Kyoto, 606-8502*
[(b)] *Department of Physics, Nagoya University, Chikusa-ku, Nagoya, 464-8602*
[(c)] *Research Center for the Early Universe (RESCEU),Graduate School of Science, The University of Tokyo, Tokyo 113-0033*

Abstract

The origin of the large-scale magnetic fields is one of the interesting problem in modern cosmology. In the previous work, we showed the possibility of generating the primordial magnetic fields at the pre-recombination era using the second-order perturbation theory and the tight coupling approximation for the Thomson scattering. Finally we obtained the power spectrum of the magnetic fields which consists of the slip term and the vorticity term. The remaining task is the numerical evaluation of it. In this proceeding, we obtain a contribution from the slip term using the numerical integration and present the simple estimation of the power.

1 Introduction

The magnetic fields are well known in the all scale, sun, galaxies and clusters of the galaxies and the strength is about μGauss. The origin of the large-scale magnetic fields is especially important in the modern cosmology[1]. If primordial large-scale magnetic field is present, it may serve as seeds for the magnetic fields in galaxies and clusters which are amplified through the dynamo mechanism after galaxy formation[2].

Many people suggest many mechanisms of the generation of the primordial magnetic fields on a large scale. The one of these mechanism is the generation at the pre-recombination era[3–6]. The standard inflationary scenario predicts the generation of the scalar (and tensor) perturbations which explain the fluctuations of the cosmic microwave background and the seeds for the large scale structure. The first-order vector perturbations like magnetic fields can not be generated in the standard inflationary scenario. However, there are the possible of the generation of the vector perturbation when we consider up to the send-order perturbations. When we consider the pre-recombination era, photons are strongly coupled with protons and electrons via the Thomson scattering. Since the proton's and electron's Thomson cross section is different, the difference of the velocities is generated. In the result, the rotational current and the magnetic field is produced.

2 The previous work

In the previous work[6], we consider the above mechanism and using the second-order cosmological perturbation theory and tight coupling approximation for the Thomson scattering and give the evolution equation of the magnetic fields:

$$(a^3 B^i)' = \frac{1-\beta^3}{1+\beta}\frac{\sigma_T}{e}a^2\bar{\rho}_\gamma^{(0)}\left[\frac{2a^2\mathcal{H}}{\bar{\alpha}^{(0)}}\omega^{(2)i} + \epsilon^{ijk}\frac{\bar{R}^{(0)}}{1+\bar{R}^{(0)}}\partial_j\Delta_b^{(I,1)}\delta v_{(\gamma b)k}^{(I,1)}\right]. \tag{1}$$

[1]Email address: smaeda@tap.scphys.kyoto-u.ac.jp
[2]Email address: keitaro@a.phys.nagoya-u.ac.jp
[3]Email address: tsutomu@resceu.s.u-tokyo.ac.jp
[4]Email address: shiromizu@tap.scphys.kyoto-u.ac.jp

where a is the scale factor and $\mathcal{H} = a'/a$, $\beta = m_e/m_p$, $\bar{R}^{(0)} = 3\bar{\rho}_b^{(0)}/4\bar{\rho}_\gamma^{(0)}$,

$$\bar{\alpha}^{(0)} = \frac{(1+\beta^2)(1+\bar{R}^{(0)})}{1+\beta}\frac{a\sigma_T\bar{\rho}_\gamma^{(0)}}{m_p}, \quad \Delta_b^{(I,1)} = \int d\eta \partial_i \delta v_{(\gamma b)}^{(I,1)i}, \quad \delta v_{(\gamma b)i}^{(I,1)} = \frac{1}{\bar{\alpha}^{(0)}}\left[\mathcal{H}v_i^{(1)} - \frac{1}{4}\frac{\partial_i \delta\bar{\rho}_\gamma^{(1)}}{\bar{\rho}_\gamma^{(0)}}\right] \tag{2}$$

and the prime denotes the derivative with respect to conformal time η. And $\omega^{(2)}$ represents the photon's vorticity. We make the curl the equation of motion of the total momentum conservation and obtain the vorticity evolution equation:

$$(a^2\omega^{(2)i})' + \frac{\mathcal{H}\bar{R}^{(0)}}{1+\bar{R}^{(0)}}a^2\omega^{(2)i} = \frac{\bar{R}^{(0)})}{2(1+\bar{R}^{(0)})^2}\epsilon^{ijk}\partial_j\Delta_b^{(I,1)}\bar{\alpha}^{(0)}\delta v_{(\gamma b)k}^{(I,1)}. \tag{3}$$

We find that the vorticity itself is sourced by the product of the first-order perturbation in the vorticity evolution equation. We find from eq.(1) and eq.(3) that the sources of the magnetic fields are the product of the first-order perturbations We call the first and second term in eq.(1) as the vorticity and slip term.

Since the source is only written by first-order cosmological perturbations, we can calculate the power spectrum of the magnetic fields by solving the linear Einstein equation. The result is the following:

$$\begin{aligned}\frac{2\pi^2}{k^3}P_B(k,\eta) &= \left(\frac{1-\beta^3}{1+\beta}\frac{\sigma_T\rho_{\gamma 0}}{ea^3}\right)^2(2\pi^2)^2\int d^3p\int_0^\eta d\eta_1\int_0^\eta d\eta_2 \times \\ &\times|\vec{k}\times\vec{p}|^2\frac{P_\psi(p)}{p^3}\frac{P_\psi(|\vec{k}-\vec{p}|)}{|\vec{k}-\vec{p}|^3}a^{-2}(\eta_1)a^{-2}(\eta_2)\{g(\vec{k},\vec{p},\eta_1)+f(\vec{k},\vec{p},\eta_1)\}\times \\ &\times\{g(\vec{k},\vec{p},\eta_2)-g(\vec{k},\vec{k}-\vec{p},\eta_2)+f(\vec{k},\vec{p},\eta_2)-f(\vec{k},\vec{k}-\vec{p},\eta_2)\},\end{aligned} \tag{4}$$

where $y_1 = p\eta/\sqrt{3}$, $y_2 = |\vec{k}-\vec{p}|\eta/\sqrt{3}$, $P(\eta) = \mathcal{H}\bar{R}^{(0)}/1+\bar{R}^{(0)}$,

$$f(\vec{k},\vec{p},\eta) = \frac{1}{(2\pi)^{3/2}}\frac{\bar{R}^{(0)}}{1+\bar{R}^{(0)}}\frac{1}{\bar{\alpha}^{(0)}}\frac{\eta^2}{4}p^4|\vec{k}-\vec{p}|^2\frac{j_1(y_2)}{y_2}\int_0^\eta d\eta'\left(\frac{(\eta')^2}{\bar{\alpha}^{(0)}}\frac{j_1(y_1')}{y_1'}\right), \tag{5}$$

$$\begin{aligned}g(\vec{k},\vec{p},\eta) &= \frac{1}{4\eta\bar{\alpha}^{(0)}}\frac{1}{(2\pi)^{3/2}}e^{-\int_0^\eta P(\eta')d\eta'}p^4|\vec{k}-\vec{p}|^2\times \\ &\times\int_0^\eta d\eta'\frac{\bar{R}^{(0)}}{(1+\bar{R}^{(0)})^2}(\eta')^2\frac{j_1(y_2')}{y_2'}\int_0^{\eta'}d\eta''\left(\frac{(\eta'')^2}{\bar{\alpha}^{(0)}}\frac{j_1(y_1'')}{y_1''}\right)e^{\int_0^{\eta'}P(\eta'')d\eta''},\end{aligned} \tag{6}$$

$$P_\psi(k) = \frac{9}{4}\Delta_{\mathcal{R}}^2(k_0)\left(\frac{k}{k_0}\right)^{n_s-1}. \tag{7}$$

Here $j_1(x)$ is the spherical Bessel function of the first kind and order one. In recent measurements, $n_s \simeq 1.0$ and $\Delta_{\mathcal{R}}^2(k_0 = 0.002\text{Mpc}) \simeq 2.5\times10^{-9}$.

3 The numerical result

Before we take a numerical calculation, we note the range of the wave-number integral. The photon's perturbations on a smaller scale than the Silk scale are suppressed by the Silk damping. But we do not consider this effect in the above calculation. It causes the divergence of the wave-number integral in eq.(4). The photon's density and velocity perturbations on the smaller scale than the Silk scale, p_{Silk}^{-1}, do not contribute to the generation of the magnetic fields because of the Silk damping. So we set $p_{\max} = p_{Silk}$ as the upper limit of the wave-number integral. And the contribution of the large-scale perturbation should be important when the perturbations enter the horizon. Hence the lower limit of the wave-number integral is $p_{\min} = p_{\rm H}$. We mention that the Silk scale depends on the time, $p_{Silk} \simeq 4.3\times10^{-6}a^{-3/2}(\text{Mpc})^{-1}$ and the horizon scale depends also on the time, $p_{\rm H} = 1/\eta$. The integral region is a gray region in the figure 1.

We take the numerical integration of the slip term and show the result in the figure 2. The figure shows the magnetic fields, $\sqrt{k^3P_B}$. The power on a large scale is k^2 and one on a small scale is $k^{-1.3}$ in this figure. The scale of the folding corresponding to the Silk scale at the time we consider and we find that the generation of the magnetic fields is suppressed on smaller scale than the Silk scale. The amplitude of the magnetic field is about 10^{-20} Gauss with Mpc scale.

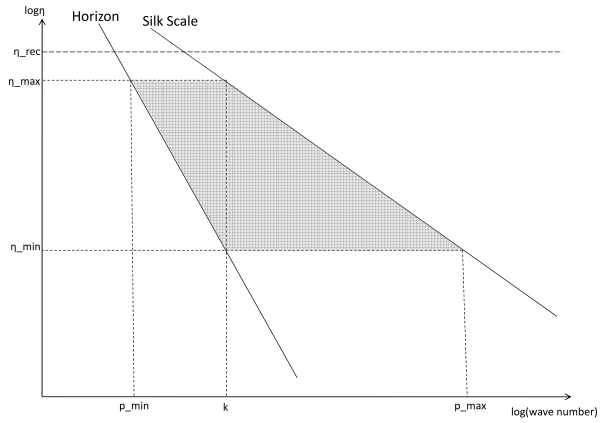

Figure 1: the integral region

4 A simple estimation of the power

In this section, we derive the power using a simple calculation. We write simply the power spectrum of the slip term

$$P_B \simeq k^3 \int d^3p |\vec{k}\times\vec{p}|^2 \frac{1}{p^3}\frac{1}{|\vec{k}-\vec{p}|^3}\int_0^\eta d\eta_1 a^{-2}(\eta_1) f(\vec{k},\vec{p},\eta_1)\int_0^\eta d\eta_2 a^{-2}(\eta_2)\left\{f(\vec{k},\vec{p},\eta_2)-f(\vec{k},\vec{k}-\vec{p},\eta_2)\right\} \quad (8)$$

and

$$f(\vec{k},\vec{p},\eta) \simeq \frac{\bar{R}^{(0)}}{1+\bar{R}^{(0)}}\frac{1}{\bar{\alpha}^{(0)}}\frac{\eta^2}{4}p^4|\vec{k}-\vec{p}|^2\frac{j_1(y_2)}{y_2}\int_0^\eta d\eta'\left(\frac{(\eta')^2}{\bar{\alpha}^{(0)}}\frac{j_1(y_1')}{y_1'}\right). \quad (9)$$

We replace $p\eta$ into $p\eta/\sqrt{3}$ for simplicity. As $1+\bar{R}^{(0)}\sim 1$, $\bar{R}^{(0)}\propto a\propto\eta$ and $\bar{\alpha}^{(0)}\propto a^{-3}\propto\eta^{-3}$ at the radiation dominant era,

$$f(\vec{k},\vec{p},\eta)\simeq\eta^5p^4zj_1(p\eta z)\int_0^\eta d\eta'(\eta')^4j_1(p\eta') \text{ and } f(\vec{k},\vec{k}-\vec{p},\eta)\simeq\eta^5p^4z^3j_1(p\eta)\int_0^\eta d\eta'(\eta')^4j_1(p\eta' z), \quad (10)$$

where we define $z\equiv|\vec{k}-\vec{p}|/p$.

We consider a shorter wave length than the horizon, $p\eta >> 1$ and $k\eta >> 1$ and then Eq.(10) is approximately represented by

$$f(\vec{k},\vec{p},\eta)\simeq\frac{p\eta^7}{2}\Big(\sin(p\eta+pz\eta)+\sin(p\eta-pz\eta)\Big) \text{ and } f(\vec{k},\vec{k}-\vec{p},\eta)\simeq\frac{p\eta^7 z}{2}\Big(\sin(p\eta+pz\eta)-\sin(p\eta-pz\eta)\Big). \quad (11)$$

The integration of η_1 is

$$\int d\eta_1\frac{1}{(\eta_1)^2}f(\vec{k},\vec{p},\eta_1)\simeq\eta^5\left[\frac{1}{1+z}\cos(p\eta+pz\eta)+\frac{1}{1-z}\cos(p\eta-pz\eta)\right]. \quad (12)$$

And integration of η_2 is

$$\int d\eta_2\frac{1}{(\eta_2)^2}\left[f(k,\vec{p},\eta_2)-f(\vec{k},\vec{k}-\vec{p},\eta_2)\right]\simeq\eta^5\left[\frac{1-z}{1+z}\cos(p\eta+pz\eta)-\frac{1+z}{1-z}\cos(p\eta-pz\eta)\right]. \quad (13)$$

Therefore we obtain the simple form of the power spectrum,

$$\begin{aligned} P_B \simeq\ & \frac{k^5\eta^{10}}{pz^3}\left[\frac{1-z}{(1+z)^2}\cos^2(p\eta+pz\eta)\right. \\ & \left.-\frac{2z}{(1+z)(1-z)}\cos(p\eta+pz\eta)\cos(p\eta-pz\eta)-\frac{1+z}{(1-z)^2}\cos^2(p\eta-pz\eta)\right]. \end{aligned} \quad (14)$$

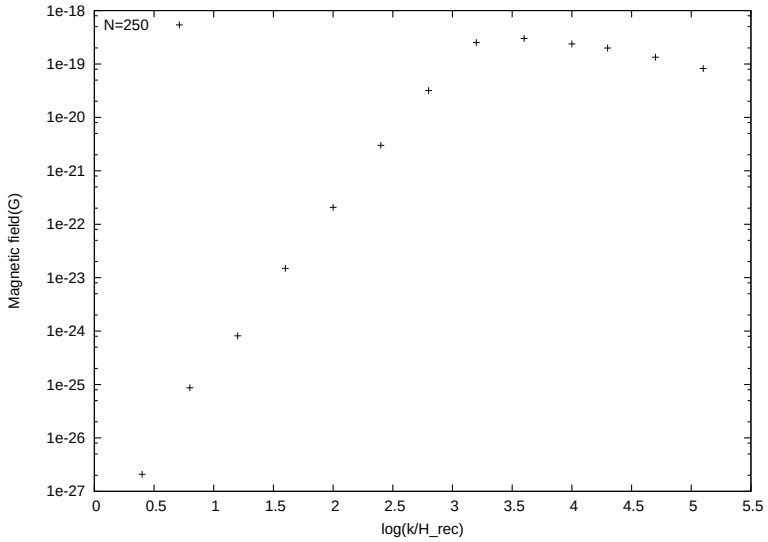

Figure 2: the magnetic field

We take a leading term in the above equation and obtain $P_B \propto\sim k^3 p\eta^{10}$. On $k < k_{Silk}$, $p \sim k$ and $\eta \sim$ Const. and the magnetic fields are $B \propto k^2$. On $k > k_{Silk}$, $p \sim k$ and $\eta \propto k^{-2/3}$ and it is $B \propto k^{-1.3}$. These are consistent of the numerical integration.

5 Summary

We calculate the power spectrum and take numerical integration of the slip term. We show that the power is k^2 on the large scale and $k^{-1.3}$ on the small scale. Especially, we find that the magnetic fields on the small scale is suppressed by the silk dumping. A remaining work is the evaluation of the vorticity term. We will prepare it soon.

References

[1] L. M. Widrow, Rev. Mod. Phys. **74**, 775 (2002); M. Giovannini, Int. J. Mod. Phys. D **13**, 391(2004).

[2] A. C. Davis, M. Lilley and O. Tornkvist, Phys. Rev. D **60**, 021301 (1999).

[3] S. Matarrese, S. Mollerach, A. Notari and A. Riotto, Phys. Rev. D **71**, 043502 (2005).

[4] K. Ichiki, K. Takahashi, N. Sugiyama, H. Hanayama and H. Ohno, Science **311**, 827 (2006); K. Ichiki, K. Takahashi, N. Sugiyama, H. Hanayama and H. Ohno, arXiv:astro-ph/0701329; K. Takahashi, K. Ichiki and N. Sugiyama, Phys. Rev. D **77**, 124028 (2008).

[5] T. Kobayashi, R. Maartens, T. Shiromizu and K. Takahashi, Phys. Rev. D **75**, 103501 (2007).

[6] S. Maeda, S. Kitagawa, T. Kobayashi and T. Shiromizu, Class. Quant. Grav. **26**, 135014 (2009).

Multi-black strings in five-dimensional Einstein-Maxwell theory

Ken Matsuno[1], Hideki Ishihara[2], Masashi Kimura[3], and Takamitsu Tatsuoka[4]

Department of Mathematics and Physics, Graduate School of Science, Osaka City University, 3-3-138 Sugimoto, Sumiyoshi-ku, Osaka 558-8585, Japan

Abstract

We consider dyonically charged static black strings in the five-dimensional Einstein-Maxwell theory. We obtain three types of analytic solutions, i.e., electrically charged ones, magnetically charged ones and dyonically charged ones with a constant extra dimension. We also construct dyonically charged multi-black strings with a constant extra dimension.

1 Introduction

In the context of string theory and brane world models, investigations on black hole solutions in higher dimensions have attracted a lot of attention (see [1] for review). For example, in five-dimensional spacetimes, unlike in four-dimensional spacetimes, where the only allowed horizon topology is a two-sphere, we can have different more interesting horizon topologies such as black holes with a horizon topology of a three-sphere, black rings with a horizon topology of a direct product of a two-sphere and a circle, and a black lens in which the horizon geometry is a Lens space $L(p;q)$.

The five-dimensional vacuum black string, a direct product of the four-dimensional Schwarzschild black hole and a circle, is one of simple examples of higher-dimensional black holes. In this report, we generalize such vacuum black strings to the charged ones. Especially, we consider dyonically charged static black strings in the five-dimensional Einstein-Maxwell theory. We obtain three types of analytic solutions, i.e., electrically charged ones, magnetically charged ones and dyonically charged ones with a constant extra dimension. We also construct dyonically charged multi-black strings with a constant extra dimension.

2 Solutions

We start from the five-dimensional Einstein and the Maxwell equations,

$$R_{\mu\nu} = 2\left(T_{\mu\nu} - \frac{T}{3}g_{\mu\nu}\right), \quad \nabla_\mu F^{\mu\nu} = 0. \tag{1}$$

We consider five-dimensional dyonically charged static spacetimes with a compactified extra dimension. The ansatz of the metric and the gauge potential are

$$ds^2 = -\alpha^2(\rho)dt^2 + \beta^2(\rho)d\rho^2 + \gamma^2(\rho)d\Omega_{S^2}^2 + \delta^2(\rho)dw^2, \tag{2}$$

$$\boldsymbol{A} = A_t(\rho)dt + A_\phi(\theta)d\phi, \tag{3}$$

where $d\Omega_{S^2}^2 = d\theta^2 + \sin^2\theta d\phi^2$ denotes a metric of the unit two-sphere, the functions α, β, γ, δ and A_t depend only on ρ, and the function A_ϕ depends only on θ. When we take a coordinate condition such as $\beta = \alpha\delta\gamma^2$, then the gauge potential $\boldsymbol{A} = Q\left(\int \alpha^2 d\rho\right)dt + P\cos\theta d\phi$ solves the Maxwell equation, where Q and P denote an electric and a magnetic charges, respectively. Then the Einstein equation gives the equations of motion,

$$\frac{\alpha'}{\alpha}\frac{\delta'}{\delta} + \frac{\delta'}{\delta}\frac{\gamma'}{\gamma} + \frac{\gamma'}{\gamma}\frac{\alpha'}{\alpha} + \frac{\gamma'}{\gamma}\left(\frac{\alpha'}{\alpha} + \frac{\delta'}{\delta} + \frac{\gamma'}{\gamma}\right) + \alpha^2\left(P^2\delta^2 + Q^2\right) - (\alpha\delta\gamma)^2 = 0, \tag{4}$$

[1]Email address: matsuno@sci.osaka-cu.ac.jp
[2]Email address: ishihara@sci.osaka-cu.ac.jp
[3]Email address: mkimura@sci.osaka-cu.ac.jp
[4]Email address: tatsuoka@sci.osaka-cu.ac.jp

$$\left(\frac{\alpha'}{\alpha}\right)' = \frac{2\alpha^2}{3}\left(P^2\delta^2 + 2Q^2\right), \tag{5}$$

$$\left(\frac{\delta'}{\delta}\right)' = \frac{2\alpha^2}{3}\left(P^2\delta^2 - Q^2\right), \tag{6}$$

$$\left(\frac{\gamma'}{\gamma}\right)' = (\alpha\delta\gamma)^2 - \frac{2\alpha^2}{3}\left(2P^2\delta^2 + Q^2\right), \tag{7}$$

respectively, where the prime denotes the derivative with respect to ρ. Combing Eqs. (5)-(7), we obtain an analytic solution as

$$\alpha\delta\gamma = c_1/\sinh(c_1\rho + c_2), \tag{8}$$

where c_i $(i = 1,\ 2)$ are constants. For general Q and P, we could not find a set of analytic solutions to Eqs. (5)-(7). In the following subsections, we study some special cases, i.e., electrically charged $(Q \neq 0,\ P = 0)$ solutions, magnetically charged $(Q = 0,\ P \neq 0)$ ones and dyonically charged $(Q,\ P \neq 0)$ ones with a constant extra dimension.

2.1 Electrically charged solutions

When the magnetic charge vanishes, $P = 0$, we obtain a set of analytic solutions to Eqs. (5)-(7) as

$$\alpha^2(\rho) = \frac{c_1^2}{u^2\sinh^2(c_1\rho)}, \quad \delta^2(\rho) = \frac{c_5 u}{c_1}e^{c_2\rho}\sinh(c_1\rho), \quad \gamma^2(\rho) = \frac{c_3^2 u e^{-c_2\rho}\sinh(c_1\rho)}{c_1 c_5\sinh^2(c_3\rho + c_4)}, \tag{9}$$

where $u^2 = 4Q^2/3$ and c_i $(i = 1, \ldots, 5)$ are constants. Substituting the solution (9) into Eq. (4), we have $c_3^2 = \left(3c_1^2 + c_2^2\right)/4$. It would be easy to see the geometry of the solution (9) in a new coordinate system. We introduce the coordinate and the constants as $e^{\rho} = \nu\left(1 - 2M/r\right)$, $a = -2c_1$, $b = c_1 + c_2$, $\tilde{\alpha} = u/\left(8c_1c_5M^2\nu^{a+b}\right)$, $\tilde{\beta} = u/\left(8c_1c_5M^2\nu^b\right)$, $c_4 = \nu^{-1/2}$ and choose the constant as $c_3 = 1/2$ without loss of generality. After rescaling the coordinates as $t \to 4c_5M^2\nu^{a/2+b}t$, $w \to w/\left(2c_5M\nu^{a/2+b}\right)$, we have the metric and the gauge potential in the forms

$$ds^2 = -h^{-2}f^a dt^2 + h\left(f^{-a-b}dr^2 + f^{1-a-b}r^2 d\Omega_{S^2}^2 + f^b dw^2\right), \tag{10}$$

$$\boldsymbol{A} = \pm\sqrt{\frac{3\tilde{\alpha}}{4\tilde{\beta}}}\frac{dt}{h}, \tag{11}$$

where the functions f, h and the relation between parameters a and b are, respectively, given by

$$f(r) = 1 - 2M/r, \quad h(r) = \tilde{\alpha} - \tilde{\beta}f^a(r), \quad a^2 + b^2 + ab = 1. \tag{12}$$

When the Maxwell field (11) vanishes, $\tilde{\alpha} \to 1$ and $\tilde{\beta} \to 0$, the function $h \to 1$ and the metric (10) reduces to that of vacuum Kaluza-Klein solitons [2]. As same as vacuum Kaluza-Klein solitons, for general a and b, the charged solution (10) has a naked curvature singularity at $r = 2M$.

To obtain black string solutions, we choose the parameters such that $a = 1$, $b = 0$. In this case, introducing the coordinate and the constants as $R = r\sqrt{\tilde{\alpha} - \tilde{\beta}} + 2M\tilde{\beta}\left(\tilde{\alpha} - \tilde{\beta}\right)^{-1/2}$, $R_1 = 2M\tilde{\alpha}\left(\tilde{\alpha} - \tilde{\beta}\right)^{-1/2}$, $R_2 = 2M\tilde{\beta}\left(\tilde{\alpha} - \tilde{\beta}\right)^{-1/2}$ and rescaling the coordinates as $t \to t\left(\tilde{\alpha} - \tilde{\beta}\right)$, $w \to w\left(\tilde{\alpha} - \tilde{\beta}\right)^{-1/2}$, the metric (10) and the gauge potential (11) are rewritten as

$$ds^2 = -\frac{(R - R_1)(R - R_2)}{R^2}dt^2 + \frac{R}{R - R_1}dR^2 + R\left(R - R_2\right)d\Omega_{S^2}^2 + \frac{R}{R - R_2}dw^2, \tag{13}$$

$$\boldsymbol{A} = \pm\frac{\sqrt{3R_1R_2}}{2}\frac{dt}{R}. \tag{14}$$

We see that the metric (13) and the gauge potential (14) coincide with those of five-dimensional electrically charged static black strings in [3]. When $R_1 > R_2 > 0$, the horizon is located at $R = R_1$, and the curvature singularity at $R = R_2$ is concealed behind it. At infinity, $R = \infty$, the metric (13) asymptotically approaches a direct product of the four-dimensional Minkowski spacetime and a compactified extra dimension, i.e., the black sting (13) is asymptotically locally flat.

2.2 Magnetically charged solutions

When the electric charge vanishes, $Q = 0$, we obtain a set of analytic solutions to Eqs. (5)-(7) as

$$\alpha^2(\rho) = \frac{c_2 e^{-c_1\rho}}{v\sinh(c_2\rho + c_3)}, \quad \delta^2(\rho) = \frac{c_2 e^{c_1\rho}}{v\sinh(c_2\rho + c_3)}, \quad \gamma^2(\rho) = \frac{c_4^2 v^2 \sinh^2(c_2\rho + c_3)}{c_2^2 \sinh^2(c_4\rho + c_5)}, \tag{15}$$

where $v^2 = 4P^2/3$ and c_i $(i = 1, \ldots, 5)$ are constants. Substituting the solution (15) into Eq. (4), we have $c_4^2 = \left(c_1^2 + 3c_2^2\right)/4$. In order to see the geometry of the solution (15) easily, we introduce the coordinate and the constants as $e^\rho = 1 - 2M/r$, $a = -c_1 - c_2$, $b = c_1 - c_2$, $\tilde{\alpha} = ve^{c_3}/(4c_2 M)$, $\tilde{\beta} = v/(4c_2 M e^{c_3})$ and choose the constants as $c_4 = 1/2$, $c_5 = 0$ without loss of generality. After rescaling the coordinates as $t \to \sqrt{2M}t$, $w \to \sqrt{2M}w$, we have the metric and the gauge potential in the forms

$$ds^2 = h^{-1}\left(-f^a dt^2 + f^b dw^2\right) + h^2\left(f^{-a-b}dr^2 + f^{1-a-b}r^2 d\Omega_{S^2}^2\right), \tag{16}$$

$$\boldsymbol{A} = \pm\sqrt{3\tilde{\alpha}\tilde{\beta}}(a+b)M\cos\theta d\phi, \tag{17}$$

where the functions f, h and the relation between parameters a and b are, respectively, given by

$$f(r) = 1 - 2M/r, \quad h(r) = \tilde{\alpha} - \tilde{\beta}f^{a+b}(r), \quad a^2 + b^2 + ab = 1. \tag{18}$$

When the Maxwell field (17) vanishes, $\tilde{\alpha} \to 1$ and $\tilde{\beta} \to 0$, the function $h \to 1$ and the metric (16) reduces to that of vacuum Kaluza-Klein solitons [2]. As same as vacuum Kaluza-Klein solitons, for general a and b, the charged solution (16) has a naked curvature singularity at $r = 2M$.

To obtain black string solutions, we choose the parameters such that $a = 1$, $b = 0$. In this case, introducing the coordinate and the constants as $R = \left(\tilde{\alpha} - \tilde{\beta}\right)r + 2M\tilde{\beta}$, $R_1 = 2M\tilde{\alpha}$, $R_2 = 2M\tilde{\beta}$ and rescaling the coordinates as $t \to t\sqrt{\tilde{\alpha} - \tilde{\beta}}$, $w \to w\sqrt{\tilde{\alpha} - \tilde{\beta}}$, the metric (16) and the gauge potential (17) are rewritten as

$$ds^2 = -\frac{R - R_1}{R}dt^2 + \frac{R^2}{(R - R_1)(R - R_2)}dR^2 + R^2 d\Omega_{S^2}^2 + \frac{R - R_2}{R}dw^2, \tag{19}$$

$$\boldsymbol{A} = \pm\frac{\sqrt{3R_1R_2}}{2}\cos\theta d\phi. \tag{20}$$

We see that the metric (19) and the gauge potential (20) coincide with those of five-dimensional magnetically charged static black strings, which asymptote to locally flat spacetimes [4]. When $R_1 > R_2 > 0$, the horizon is located at $R = R_1$, and the curvature singularity at $R = 0$ is concealed behind it.

2.3 Dyonically charged solutions with a constant extra dimension

When the size of extra dimension becomes constant everywhere, $\delta = \text{const.}$, we obtain a set of analytic solutions to Eqs. (5)-(7) as

$$\alpha^2(\rho) = \frac{c_1^2}{2Q^2\sinh^2(c_1\rho)}, \quad \delta^2 = \left(\frac{Q}{P}\right)^2 = \text{const.}, \quad \gamma^2(\rho) = \frac{2P^2\sinh^2(c_1\rho)}{\sinh^2(c_2\rho + c_3)}, \tag{21}$$

where c_i $(i = 1,\ 2,\ 3)$ are constants. Substituting the solution (21) into Eq. (4), we have $c_1 = c_2$. In order to see the geometry of the solution (21) easily, we introduce the coordinates and the constants as $T = \sqrt{2}c_1 t/\left[Q(e^{c_3} - e^{-c_3})\right]$, $R = \gamma = \sqrt{2}P\sinh(c_1\rho)/\sinh(c_1\rho + c_3)$, $W = wQ/P$, $R_\pm = \sqrt{2}Pe^{\pm c_3}$. Then the metric and the gauge potential are rewritten as

$$ds^2 = -\frac{(R - R_+)(R - R_-)}{R^2}dT^2 + \frac{R^2}{(R - R_+)(R - R_-)}dR^2 + R^2 d\Omega_{S^2}^2 + dW^2, \tag{22}$$

$$\boldsymbol{A} = \pm\sqrt{\frac{R_+R_-}{2}}\left(\frac{dT}{R} + \cos\theta d\phi\right). \tag{23}$$

For $R_+ > R_- > 0$, the solution (22) describes a non-extremal dyonically charged static black string with a constant extra dimension, where the horizons and the curvature singularity are located at $R = R_\pm$ and $R = 0$, respectively. When two horizons degenerate, $R_- \to R_+$, the solution (22) reduces to an extremal black string solution. In this case, we can generalize such single extremal black string to multi-black strings.

The forms of the metric and the gauge potential of charged static multi-black strings are

$$ds^2 = -H^{-2}dT^2 + H^2 ds^2_{\mathbb{E}^3} + dW^2, \tag{24}$$

$$\sqrt{2}\boldsymbol{A} = H^{-1}dT + \boldsymbol{\omega}, \tag{25}$$

where $ds^2_{\mathbb{E}^3} = dx^2 + dy^2 + dz^2$ is a metric on the three-dimensional Euclid space $\mathbb{E}^3$, the function H and the 1-form $\boldsymbol{\omega}$ are, respectively, given by

$$H = 1 + \sum_i \frac{M_i}{|\boldsymbol{R} - \boldsymbol{R}_i|}, \tag{26}$$

$$\boldsymbol{\omega} = \sum_i M_i \frac{z - z_i}{|\boldsymbol{R} - \boldsymbol{R}_i|} \frac{(x - x_i)dy - (y - y_i)dx}{(x - x_i)^2 + (y - y_i)^2}, \tag{27}$$

with the constants M_i, and $\boldsymbol{R} = (x,\ y,\ z)$ denotes a position vector on $\mathbb{E}^3$. The function H is a harmonic function on $\mathbb{E}^3$ with point sources located at $\boldsymbol{R} = \boldsymbol{R}_i = (x_i,\ y_i,\ z_i)$ and the 1-form $\boldsymbol{\omega}$ is determined by $\nabla \times \boldsymbol{\omega} = \nabla H$. To avoid the existence of singularities on and outside the black string horizons, we choose the parameters such that $M_i > 0$. Then the solution (24) describes dyonically charged multi-black strings, which are located at $\boldsymbol{R} = \boldsymbol{R}_i$, in the spacetime with a constant extra dimension.

3 Summary and discussion

We have considered dyonically charged static black strings in the five-dimensional Einstein-Maxwell theory. In dyonically charged case, where both an electric charge Q and a magnetic charge P exist, we have not found an analytic general solution. In some special cases, we have obtained analytic solutions, i.e., electrically charged ($Q \neq 0,\ P = 0$) ones (10), magnetically charged ($Q = 0,\ P \neq 0$) ones (16) and dyonically charged ($Q,\ P \neq 0$) ones with a constant extra dimension (22). We have also constructed dyonically charged multi-black strings with a constant extra dimension (24).

We note that the multi-black string solutions in the five-dimensional Einstein-Maxwell theory (24) coincide with those uplifted from the four-dimensional equal charged dyonic Majumdar-Papapetrou solutions with constant dilaton fields [5]. By uplifting the same four-dimensional solutions to the five-dimensional Einstein system, we obtain different multi-black object solutions [6]. The metric is

$$ds^2 = -H^{-2}dt^2 + H^2\left(dx^2 + dy^2 + dz^2\right) + \left(\sqrt{2}H^{-1}dt + dw + \sqrt{2}\boldsymbol{\omega}\right)^2, \tag{28}$$

where the function H and the 1-form $\boldsymbol{\omega}$ are given by Eqs. (26) and (27), respectively. We expect that the solution (28) describes rotating Kaluza-Klein vacuum multi-black holes with a twisted constant extra dimension. We leave the analysis for the future.

References

[1] R. Emparan and H.S. Reall, Living Rev. Rel. **11**, 6 (2008).

[2] D.J. Gross and M.J. Perry, Nucl. Phys. B **226**, 29 (1983).

[3] G.T. Horowitz and K. Maeda, Phys. Rev. D **65**, 104028 (2002).

[4] U. Miyamoto, Phys. Lett. B **659**, 380 (2008).

[5] H.J. Sheinblatt, Phys. Rev. D **57**, 2421 (1998).

[6] R.R. Khuri and T. Ortin, Phys. Lett. B **373**, 56 (1996).

Dynamical solutions in the Nishino-Salam-Sezgin model

Masato Minamitsuji

Department of Physics, School of Science and Technology, Kwansei Gakuin University, Gakuen 2-1, Sanda, 669-1337 Japan

Abstract

We investigate the static and dynamical solutions in the 3-form background of the six-dimensional Nishino-Salam-Sezgin model, which is usually referred to as the Salam-Sezgin model. We take the background of the 3-form field acting on the internal space and timelike dimensions without the $U(1)$ gauge field strength. We firstly review the static solution. The dynamical solutions are obtained by exchanging the roles of the radial and timelike coordinates. Our cosmological solution leads to the ordinary three-space which expands faster than two internal two dimensions. In particular, when two internal dimensions are stabilized, the three-dimensional sapce expands as the universe filled with the stiff matter.

1 Introduction

Six-dimensional models have been recognized as the important playground to study cosmology and gravity with extra dimensions compactified by fluxes of antisymmetric tensor fields. The warped, flux compactification solutions were reported in the context of Nishino-Salam-Sezgin (NSS) six-dimensional supergravity [1, 2]. Note that this model is usually referred to as the Salam-Sezgin model especially when compactification is discussed. However, the compactification on S^2, which was found by Salam and Sezgin, was constructed in the theory first proposed by Nishino and Sezgin. Therefore, it is more suitable for us to refer to the model as the NSS model.

In order to explore the cosmology, one useful approach is to use the dynamical solutions. In this direction, exact dynamical solutions were obtained in [3]. The field components of the bosonic part of the NSS model are the gravity, the $U(1)$-gauge field, Kalb-Ramond 2-form (i.e., 3-form field strength) and the dilaton. In Refs. [3], warped time dependent solutions with the $U(1)$-field strength, without the Kalb-Ramond 3-form field strength in the NSS model, were explored. The solutions have all six dimensions evolving in time. There are three types of the exact time dependent solutions: The purpose of this work is to present the other classes of time dependent solutions in the NSS model in the presence of the nonvanishing 3-form field strength but in the absence of the $U(1)$ field strength. Our solutions are obtained by exchanging the roles of the radial coordinate and the time coordinate in the static solutions obtained recently in Ref. [4]. For more details, see our recent publications [5, 6].

2 Warped static solutions in the Nishino-Salam-Sezgin model

2.1 Theory

The action of the bosonic part of the NSS supergravity [2] is given by

$$I = \int d^6x\sqrt{-g}\left[\frac{1}{2\kappa^2}(R-(\partial\phi)^2) - \frac{1}{4}e^{-\phi}F_{\mu\nu}^2 - \frac{1}{12}e^{-2\phi}H_{\mu\nu\rho}^2 - \frac{g^2}{2}e^{\phi}\right], \tag{1}$$

where ϕ is the dilaton, $H = dB$ is the field strength for the Kalb-Ramond field B and $F = dA$ is the field strength for the $U(1)$ gauge field A. The parameters g and κ are gauge and gravitational coupling constants, respectively. Most of the preceding works have discussed the $U(1)$ field acting on the internal space dimensions, $F \neq 0$, with the vanishing 3-form $H = 0$. Instead, we consider the nonvanishing 3-form field acting on the internal space and timelike dimensions $H \neq 0$, with the vanishing $U(1)$ field $F = 0$.

2.2 Solutions

The type of solutions depends on the signature of

$$f_2^2 = 2f_1^2 - 4\big(G_\phi - G_w\big)^2 - \frac{32}{3}G_\phi^2, \tag{2}$$

where f_1, G_ϕ and G_w are constants, which appear in integrating the Einstein equations and the dilaton equation of motion. For $f_2^2 > 0$

$$\begin{aligned} ds^2 &= \frac{e^{-2(2G_\phi - G_w)y}}{\cosh^{\frac{1}{2}}[f_1(y-y_1)]\,|\sinh[f_2(y-y_2)]|^{\frac{1}{2}}}\Big[-dt^2 + |\sinh[f_2(y-y_2)]|e^{2\left(\frac{7}{3}G_\phi - G_w\right)y}\sum_{i=1}^{3}(dx^i)^2\Big] \\ &+ \frac{e^{-2G_\phi y}|\sinh[f_2(y-y_2)]|^{\frac{1}{2}}}{\cosh^{\frac{5}{2}}[f_1(y-y_1)]}\Big[\frac{2c^2f_1^4}{\kappa^2 g^4 f_2^2}dy^2 + e^{-2(G_w - G_\phi)y}\frac{\cosh^2[f_1(y-y_1)]}{\sinh[f_2(y-y_2)]}d\theta^2\Big], \\ e^\phi &= \frac{g^2 f_2^2}{2f_1^2c^2}e^{2G_\phi y}\frac{\cosh^{\frac{1}{2}}[f_1(y-y_1)]}{\big|\sinh[f_2(y-y_2)]\big|^{\frac{1}{2}}}, \quad H = \frac{\sqrt{2}f_2^3 g^2}{4\kappa f_1^2 c^2}\frac{1}{\sinh^2[f_2(y-y_2)]}dt\wedge dy\wedge d\theta, \end{aligned} \tag{3}$$

where c, y_1 and y_2 are the other integration constants. For $f_2^2 < 0$

$$\begin{aligned} ds^2 &= \frac{e^{-2(2G_\phi - G_w)y}}{\cosh^{\frac{1}{2}}[f_1(y-y_1)]\,|\sin[|f_2|(y-y_2)]|^{\frac{1}{2}}}\Big[-dt^2 + |\sin[|f_2|(y-y_2)]|e^{2\left(\frac{7}{3}G_\phi - G_w\right)y}\sum_{i=1}^{3}(dx^i)^2\Big] \\ &+ \frac{e^{-2G_\phi y}|\sin[|f_2|(y-y_2)]|^{\frac{1}{2}}}{\cosh^{\frac{5}{2}}[f_1(y-y_1)]}\Big[\frac{2c^2f_1^4}{\kappa^2 g^4|f_2|^2}dy^2 + e^{-2(G_w - G_\phi)y}\frac{\cosh^2[f_1(y-y_1)]}{|\sin[|f_2|(y-y_2)]|}d\theta^2\Big], \\ e^\phi &= \frac{g^2|f_2|^2}{2f_1^2c^2}e^{2G_\phi y}\frac{\cosh^{\frac{1}{2}}[f_1(y-y_1)]}{|\sin[|f_2|(y-y_2)]|^{\frac{1}{2}}}, \quad H = \frac{\sqrt{2}|f_2|^3 g^2}{4\kappa f_1^2 c^2}\frac{1}{\sin^2[|f_2|(y-y_2)]}dt\wedge dy\wedge d\theta. \end{aligned} \tag{4}$$

For $f_2^2 = 0$

$$\begin{aligned} ds^2 &= \frac{e^{-2(2G_\phi - G_w)y}}{\cosh^{\frac{1}{2}}[f_1(y-y_1)]|y-y_2|^{\frac{1}{2}}}\Big[-dt^2 + |y-y_2|e^{2\left(\frac{7}{3}G_\phi - G_w\right)y}\sum_{i=1}^{3}(dx^i)^2\Big] \\ &+ \frac{e^{-2G_\phi y|y-y_2|^{1/2}}}{\cosh^{\frac{5}{2}}[f_1(y-y_1)]}\Big[\frac{2c^2f_1^4}{\kappa^2 g^4}dy^2 + e^{-2(G_w - G_\phi)y}\frac{\cosh^{\frac{1}{2}}[f_1(y-y_1)]}{|y-y_2|}d\theta^2\Big], \\ e^\phi &= \frac{g^2}{2c^2f_1^2}e^{2G_\phi y}\frac{\cosh^{\frac{1}{2}}[f_1(y-y_1)]}{|y-y_2|^{\frac{1}{2}}}, \quad H = \frac{\sqrt{2}g^2}{4\kappa f_1^2c^2}\frac{1}{|y-y_2|^2}dt\wedge dy\wedge d\theta. \end{aligned} \tag{5}$$

3 Time dependent solutions

3.1 Solutions

By exchanging the roles of the t and y, we can obtain the cosmological solutions given by

$$\begin{aligned} ds^2 &= \frac{e^{-2G_\phi t}\cosh^{\frac{1}{2}}[f_2(t-t_2)]}{|\sinh[f_1(t-t_1)]|^{\frac{5}{2}}}\Big[-\frac{2c^2f_1^4}{\kappa^2 g^4 f_2^2}dt^2 + e^{\frac{8}{3}G_\phi t}\sinh^2[f_1(t-t_1)]\sum_{i=1}^{3}\big(dx^i\big)^2\Big] \\ &+ \frac{e^{-2(2G_\phi - G_w)t}}{|\sinh[f_1(t-t_1)]|^{\frac{1}{2}}\cosh^{\frac{1}{2}}[f_2(t-t_2)]}\Big[dy^2 + e^{4(G_\phi - G_w)t}d\theta^2\Big], \\ e^\phi &= \frac{f_2^2 g^2}{2c^2f_1^2}\frac{|\sinh[f_1(t-t_1)]|^{\frac{1}{2}}}{\cosh^{\frac{1}{2}}[f_2(t-t_2)]}e^{2G_\phi t}, \quad H = \frac{\sqrt{2}f_2^3 g^2}{4\kappa f_1^2c^2}\frac{1}{\cosh^2[f_2(t-t_2)]}dt\wedge dy\wedge d\theta, \end{aligned} \tag{6}$$

where

$$f_2^2 = 2f_1^2 - 4\big(G_w - G_\phi\big)^2 - \frac{32}{3}G_\phi^2, \tag{7}$$

is assumed to be positive. Although there are the other type of solutions with the oscillating metric components, we now focus on the cosmological case.

3.2 Cosmological evolutions

Let us discuss the cosmological behavior of our solutions. Therefore, we investigate the late-time behavior $t \gg t_1, t_2$. Then, we obtain the asymptotic form of the metric at the later times:

$$ds^2 \approx -dT^2 + T^{2q_1}\sum_{i=1}^{3}(dx^i)^2 + T^{2q_v}dy^2 + T^{2q_w}d\theta^2, \tag{8}$$

where T is the cosmic proper time, and q_1, q_v and q_w are the powers of the cosmic expansion in the 3-space and two-dimensional internal space, defined by

$$q_1 := \frac{f_2 - f_1 + \frac{4}{3}G_\phi}{f_2 - 5f_1 - 4G_\phi}, \quad q_v := \frac{-f_2 - f_1 - 4(2G_\phi - G_w)}{f_2 - 5f_1 - 4G_\phi}, \quad q_w := \frac{-f_2 - f_1 - 4G_w}{f_2 - 5f_1 - 4G_\phi}, \tag{9}$$

respectively. Here, we omit unimportant numerical coefficients. In Fig. 2, we show q_1 as the functions of $g_w := \frac{G_w}{|f_1|}$ and $g_\phi := \frac{G_\phi}{|f_1|}$. The power of the fastest three-space expansion is given by $q_{1,\max} = \frac{9+4\sqrt{3}}{33} \approx 0.483$ for $g_w = g_\phi = -\frac{\sqrt{3}}{4}$, which is less than the radiation-dominated universe $\frac{1}{2}$ For the same value of $g_w = g_\phi$, $q_v = q_w$ takes the minimal value $q_{v,\min} = q_{w,\min} = \frac{1-2\sqrt{3}}{11} \approx -0.224$. These powers of $(q_{1,\max}, q_{(v,w),\min})$ are the same as in the time dependent solution in the 2-form backgrond of NSS model [7]. Thus, it is not enough to explain the present cosmic acceleration. In Fig. 3, the solid (black) curve shows the region where solutions of $f_2^2 > 0$ exist. The thick (red) curve shows the points below which $q_1 > q_v$, while in the left side to the dashed (blue) curve, $q_1 > q_w$. The dotted line shows $g_w = g_\phi$. Therefore, in the region surrounded by these three curves, q_1 is positive and greater than q_v and q_w. Thus, the ordinary three space can expand faster than the y- and θ-directions in the small region of the

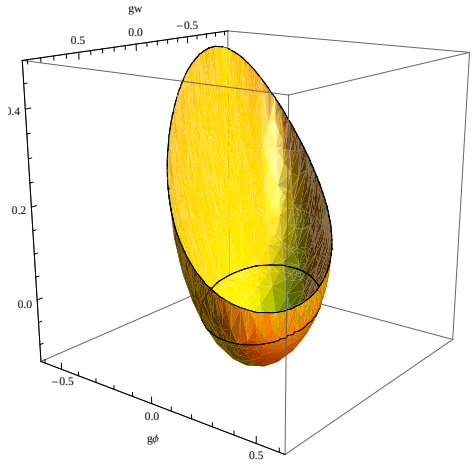

Figure 1: q_1 is shown as the function of g_w and g_ϕ. The solid curve shows the level of $q_1 = 0$.

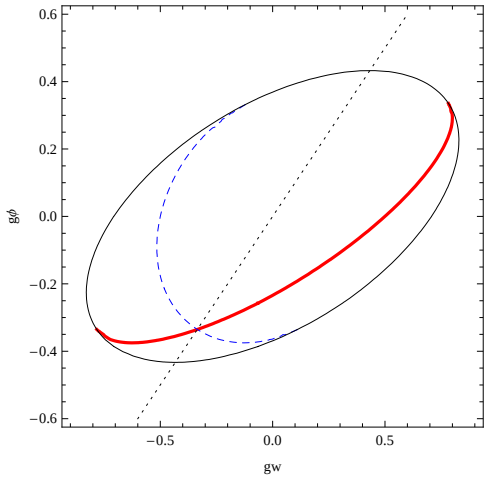

Figure 2: The solid (black) curve shows the region where solutions of $f_2^2 > 0$ exist. The thick (red) curve shows the points below which $q_1 > q_v$, while in the left side to the dashed (blue) curve, $q_1 > q_w$. The dotted line shows $g_w = g_\phi$.

negative g_w and g_ϕ which is surrounded by three different curves.

On the other hand, the internal dimensions are stabilized, $q_v = q_w = 0$, for $f_2 = -f_1 - 4G_\phi$. Then, $q_1 = \frac{1}{3}$ and therefore the expansion law of the three-dimensional space follows that of the universe filled with the stiff matter.

4 Conclusions

We derived the time dependent solutions in the 3-form background in the six-dimensional Nishino-Salam-Sezgin model and discussed their properties, after reviewing the warped static solutions obtained in [4]. The time dependent solutions are obtained, by exchanging the role of space and time from the above static solutions. Focusing on the solutions with the non-oscillating metric components with time, we investigated the cosmological evolutions obtained from the late-time behaviors. Although in a region of the parameter space the ordinary three-dimensional space can expand faster than both the internal directions, the power of the fastest expansion is approximately 0.483 and is not enough to explain the acceleration of the universe. On the other hand, when two internal dimensions are stabilized, the three-dimensional sapce expands as the universe filled with the stiff matter.

Other than the solutions discussed in this article, we have also investigated the dynamical 1-brane solutions in the NSS model. Readers who are interested in these solutions should refer to Refs. [5, 6] for more details.

Acknowledgments

The author would like to thank the coauthors of [5, 6], Prof. Maeda, Prof. Ohta and Dr. Uzawa, for fruitful discussions in completing these works.

References

[1] Y. Aghababaie *et al.*, JHEP **0309**, 037 (2003) [arXiv:hep-th/0308064]; G. W. Gibbons, R. Guven and C. N. Pope, Phys. Lett. B **595**, 498 (2004) [arXiv:hep-th/0307238]; C. P. Burgess, F. Quevedo, G. Tasinato and I. Zavala, JHEP **0411**, 069 (2004) [arXiv:hep-th/0408109].

[2] H. Nishino and E. Sezgin, Phys. Lett. B **144**, 187 (1984); A. Salam and E. Sezgin, Phys. Lett. B **147**, 47 (1984); H. Nishino and E. Sezgin, Nucl. Phys. B **278**, 353 (1986).

[3] A. J. Tolley, C. P. Burgess, C. de Rham and D. Hoover, New J. Phys. **8**, 324 (2006) [arXiv:hep-th/0608083];

[4] H. R. Afshar and S. Parvizi, JHEP **0910**, 086 (2009) [arXiv:0906.0707 [hep-th]].

[5] M. Minamitsuji, N. Ohta and K. Uzawa, Phys. Rev. D **81**, 126005 (2010) [arXiv:1003.5967 [hep-th]].

[6] K. i. Maeda, M. Minamitsuji, N. Ohta and K. Uzawa, Phys. Rev. D **82**, 046007 (2010) [arXiv:1006.2306 [hep-th]].

[7] K. i. Maeda and H. Nishino, Phys. Lett. B **154**, 358 (1985); K. i. Maeda and H. Nishino, Phys. Lett. B **158**, 381 (1985).

Oscillating Universe in Hořava-Lifshitz Gravity

Kei-ichi Maeda[1](a)(b), Yosuke Misonoh[2](a) and Tsutomu Kobayashi[3](c)

(a) *Department of Physics, Waseda University, Okubo 3-4-1, Shinjuku, Tokyo 169-8555, Japan*
(b) *RISE, Waseda University, Okubo 3-4-1, Shinjuku, Tokyo 169-8555, Japan*
(c) *Research Center for the Early Universe (RESCEU), Graduate School of Science, The University of Tokyo, Tokyo 113-0033, Japan*

Abstract

We study the dynamics of isotropic and homogeneous universes in the generalized Hořava-Lifshitz gravity, and classify all possible evolutions of vacuum spacetime. In the case without the detailed balance condition, we find a variety of phase structures of vacuum spacetimes depending on the coupling constants as well as the spatial curvature K and a cosmological constant Λ. A bounce universe solution is obtained for $\Lambda > 0, K = \pm 1$ or $\Lambda = 0, K = -1$, while an oscillation spacetime is found for $\Lambda \geq 0, K = 1$, or $\Lambda < 0, K = \pm 1$.

1 Introduction

Recently Hořava proposed a power-counting renormalizable theory of gravity [1], which has attracted much attention over the past year. In Hořava's theory, Lorentz symmetry is broken and it exhibits a Lifshitz-like anisotropic scaling in the ultraviolet (UV), $t \to \ell^z t, \vec{x} \to \ell \vec{x}$, with the dynamical critical exponent $z = 3$. (For this reason the theory is called Hořava-Lifshitz (HL) gravity.) Anisotropic scaling leads higher curvature terms in action with arbitrary coupling constants. In the original HL gravity, the so-called detailed balance condition is assumed, which limit these coupling constants. However, this condition can be loosened. In application to cosmology, a possibility of big bang initial singularity avoidance is indicated, which is led by higher curvature terms in the action come from anisotropic scaling. We study the dynamics of isotropic and homogeneous universe without any matters in the generalized HL gravity, and discuss the conditions for non-singular solutions i.e. bouncing and oscillating solutions.

2 Hořava-Lifshitz gravity and the coupling constants

The basic variables in HL gravity are the lapse function, N, the shift vector, N_i, and the spatial metric, g_{ij}. These variables are subject to the action [1, 2]

$$S = \frac{1}{2\kappa^2} \int dt d^3x \sqrt{g} N \left(\mathscr{L}_K - \mathscr{V}_{\rm HL}[g_{ij}] \right), \tag{1}$$

where $\kappa^2 = 1/M_{\rm PL}^2$ and the kinetic term is given by

$$\mathscr{L}_K = \mathcal{K}_{ij} \mathcal{K}^{ij} - \lambda \mathcal{K}^2 \tag{2}$$

with

$$\mathcal{K}_{ij} := \frac{1}{2N} \left(\dot{g}_{ij} - \nabla_i N_j - \nabla_j N_i \right) \tag{3}$$

being the extrinsic curvature. The potential term $\mathscr{V}_{\rm HL}$ will be defined shortly. In general relativity we have $\lambda = 1$, only for which the kinetic term is invariant under general coordinate transformations. In HL

[1]Email address: maeda@waseda.jp
[2]Email address: y"underscore"misonou@moegi.waseda.jp
[3]Email address: tsutomu@resceu.s.u-tokyo.ac.jp

gravity, however, Lorentz symmetry is broken in exchange for renormalizability and the symmetry of the theory is invariance under the foliation-preserving diffeomorphism transformations,

$$t \to \bar{t}(t), \quad x^i \to \bar{x}^i(t, x^j). \tag{4}$$

As implied by the symmetry (4) it is most natural to consider the projectable version of HL gravity, for which the lapse function is dependent only on t: $N = N(t)$ [1]. Since the Hamiltonian constraint is derived from the variation with respect to the lapse function, in the projectable version of the theory the resultant constraint equation is not imposed locally at each point in space, but rather is an integration over the whole space. In the cosmological setting, the projectability condition results in an additional dust-like component in the Friedmann equation [see Eq. (7) below] [3].

The most general form of the potential $\mathscr{V}_{\rm HL}$ is given by [2]

$$\begin{aligned}\mathscr{V}_{\rm HL} &= 2\Lambda + g_1\mathcal{R} + \kappa^2\left(g_2\mathcal{R}^2 + g_3\mathcal{R}^i_j\mathcal{R}^j_i\right) + \kappa^3 g_4\epsilon^{ijk}\mathcal{R}_{i\ell}\nabla_j\mathcal{R}^\ell_k \\ &\quad +\kappa^4\Big(g_5\mathcal{R}^3 + g_6\mathcal{R}\,\mathcal{R}^i_j\mathcal{R}^j_i + g_7\mathcal{R}^i_j\mathcal{R}^j_k\mathcal{R}^k_i + g_8\mathcal{R}\Delta\mathcal{R} + g_9\nabla_i\mathcal{R}_{jk}\nabla^i\mathcal{R}^{jk}\Big)\,,\end{aligned} \tag{5}$$

where Λ is a cosmological constant, $\mathcal{R}^i_j$ and $\mathcal{R}$ are the Ricci and scalar curvatures of the 3-metric g_{ij}, respectively, and g_i's ($i = 1, ..., 9$) are the dimensionless coupling constants. Requiring a stability of flat spacetime, we impose following conditions [see [4]]: $g_1 < 0, \quad g_9 > 0$. By a suitable rescaling of time, we then set $g_1 = -1$. In what follows, we adopt the unit of $\kappa^2 = 1 (M^2_{\rm PL} = 1)$ for brevity.

3 FLRW universe in Hořava-Lifshitz gravity

We discuss an isotropic and homogeneous vacuum universe in Hořava-Lifshitz gravity. Note that such a vacuum spacetime is not realized in general relativity.

Assuming a FLRW spacetime, which metric is given by

$$ds^2 = -dt^2 + a^2\left(\frac{dr^2}{1-Kr^2} + r^2 d\Omega^2\right)\,, \tag{6}$$

with $K = 0$ or ± 1. We find the Friedmann equation as

$$H^2 + \frac{2}{(3\lambda-1)}\frac{K}{a^2} = \frac{2}{3(3\lambda-1)}\left[\Lambda + \frac{g_{\rm d}}{a^3} + \frac{g_{\rm r}}{a^4} + \frac{g_{\rm s}}{a^6}\right]\,, \tag{7}$$

where $H = \dot{a}/a$,

$$\begin{aligned} g_{\rm d} &:= 8C\,. \\ g_{\rm r} &:= 6(g_3 + 3g_2)K^2\,, \\ g_{\rm s} &:= 12(9g_5 + 3g_6 + g_7)K^3\,. \end{aligned} \tag{8}$$

A constant C may appear from the projectability condition and could be "dark matter"[2]. For a flat universe ($K = 0$), the higher curvature terms do not give any contribution, and then the dynamics is almost trivial. Hence, in this paper, we discuss only non-flat universe ($K = \pm 1$). Note that imposing detailed balance condition, $g_r > 0$ and $g_r = 0$.

If $\lambda = 1$, we find a usual Friedmann equation for an isotropic and homogeneous universe in GR with a cosmological constant, dust, radiation and stiff matter. If $g_{\rm d}, g_{\rm r}$, and $g_{\rm s}$ are non-negative, such a spacetime gives a conventional FLRW universe model. However, since those coefficients come from higher curvature terms, their positivity is not guaranteed. Rather some of them could be negative. As a result, we find an unconventional cosmological scenario, which we shall discuss here. In what follows, we assume that $\lambda > 1/3$, but do not fix it to be unity.

Here we assume $C = 0$ just for simplicity. The Friedmann equation is written as

$$\frac{1}{2}\dot{a}^2 + \mathcal{U}(a) = 0\,, \tag{9}$$

where

$$\mathcal{U}(a) = \frac{1}{3\lambda - 1}\left[K - \frac{\Lambda}{3}a^2 - \frac{g_{\rm r}}{3a^2} - \frac{g_{\rm s}}{3a^4}\right] . \tag{10}$$

Since the scale factor a changes as a particle with zero energy in this "potential" $\mathcal{U}$, the condition $\mathcal{U}(a) \leq 0$ gives the possible range of a when the universe evolves. So we can classify the "motion" of the universe by the signs of K and Λ, and by the values of $g_{\rm r}$ and $g_{\rm s}$. For the case of $\Lambda \neq 0$, introducing the curvature scale ℓ which is defined by

$$\frac{\Lambda}{3} = \frac{\epsilon}{\ell^2} , \tag{11}$$

where $\epsilon = \pm 1$, we can rescale the variables and rewrite the "potential" $\mathcal{U}$ by the rescaled variables as

$$\mathcal{U}(a) = \frac{1}{3\lambda - 1}\left[K - \epsilon\tilde{a}^2 - \frac{\tilde{g}_{\rm r}}{3\tilde{a}^2} - \frac{\tilde{g}_{\rm s}}{3\tilde{a}^4}\right] , \tag{12}$$

where $\tilde{a} = a/\ell$, $\tilde{g}_{\rm r} = g_{\rm r}/\ell^2$, and $\tilde{g}_{\rm s} = g_{\rm s}/\ell^4$. Using this potential and variables, we can discuss the fate of the universe without specifying the value of Λ.

A static universe will appear if we find a solution $a = a_S(> 0)$ which satisfies $\mathcal{U}(a_S) = 0$ and $\mathcal{U}'(a_S) = 0$. If $\Lambda \neq 0$ ($\epsilon = \pm 1$), it happens if there is a relation between $\tilde{g}_{\rm r}$ and $\tilde{g}_{\rm s}$, which is defined by

$$\tilde{g}_{\rm s} \quad = \quad \tilde{g}_{\rm s}^{[\epsilon,K](\pm)}(\tilde{g}_{\rm r}) := \frac{1}{9\epsilon^2}\left[2K - 3\epsilon K\tilde{g}_{\rm r} \pm 2(1 - \epsilon\tilde{g}_{\rm r})^{3/2}\right] . \tag{13}$$

This gives the curve $\Gamma_{\epsilon,K(\pm)}$ on the $\tilde{g}_{\rm r}$-$\tilde{g}_{\rm s}$ plane, which gives the boundary between two different phases of spacetime. If $\Lambda = 0$, we find

$$g_{\rm s} = -\frac{K}{12}g_{\rm r}^2 , \tag{14}$$

which is found from (13) in the limit of $\epsilon = 0$. The corresponding curve on the $g_{\rm r}$-$g_{\rm s}$ plane is denoted by $\Gamma_{0,K}$. We summarize our result in Figure 3 to 3. In these figures, we denote $\mathcal{BB}$ is big bang, $\mathcal{BC}$ is big crunch, $\mathcal{dS}$ is de Sitter universe, $\mathcal{M}$ is Milne universe, *bounce* is bouncing universe, *oscillation* is oscillating universe and $\mathcal{S}$ is static universe. There are two types of static universes: one is stable ($\mathcal{S}_{\rm s}$) and the other is unstable ($\mathcal{S}_{\rm u}$).

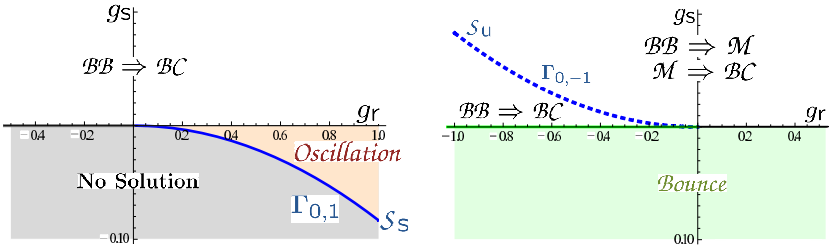

(a) $K = 1$ (b) $K = -1$

Figure 1: Phase diagram of spacetimes for $\Lambda = 0$. The oscillating universe is found only for the case of $K = 1$. The stable and unstable static universes ($\mathcal{S}_{\rm s}$ and $\mathcal{S}_{\rm u}$) exist on the boundary $\Gamma_{0,1}$ and $\Gamma_{0,-1}$, respectively.

4 Conclusion

We have study the classification of vacuum FLRW universe in generalized HL gravity. As we have evaluated, the oscillation period and amplitude are expected to be the Planck scale or the scale ℓ defined

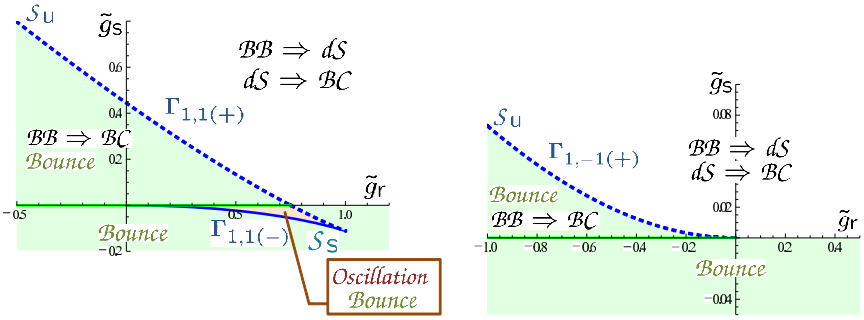

(a) $K = 1$ (b) $K = -1$

Figure 2: Phase diagram of spacetimes for $\Lambda > 0$. The oscillating universe is found only for the case of $K = 1$. The static universes ($\mathcal{S}_s$ and $\mathcal{S}_u$) exist on the boundaries $\Gamma_{1,K(\pm)}$.

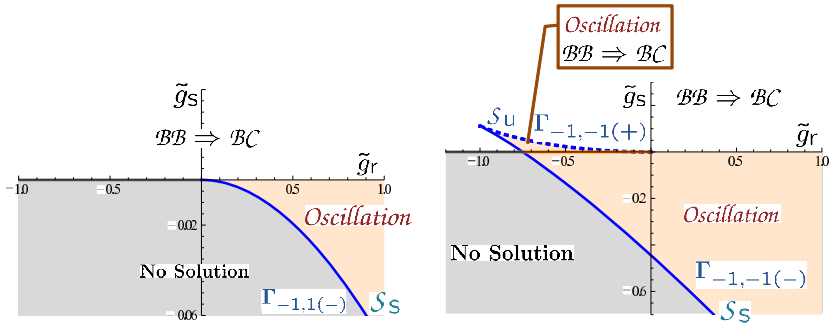

(a) $K = 1$ (b) $K = -1$

Figure 3: Phase diagram of spacetimes for $\Lambda < 0$. The oscillating universe is found for both $K = \pm 1$. The static universe exists on the boundary $\Gamma_{-1,1(-)}$ $(K = 1)$ and on $\Gamma_{-1,-1(\pm)}$ $(K = -1)$.

by a cosmological constant Λ, unless the coupling constants are unnaturally large. Hence it cannot be a cyclic universe, which period is macroscopic such as the age of the universe. To find more realistic universe, we discuss further in [4]. We also have another extension of the present FLRW spacetime to anisotropic one. It may be interesting and important not only to study the dynamics of Bianchi spacetime but also to analyze the stability of the FLRW universe against anisotropic perturbations.

References

[1] P. Hořava, Phys. Rev. D **79**, 084008 (2009).

[2] T. P. Sotiriou, M. Visser and S. Weinfurtner, Phys. Rev. Lett. **102**, 251601 (2009); T. P. Sotiriou, M. Visser and S. Weinfurtner, JHEP **0910**, 033 (2009).

[3] S. Mukohyama, Phys. Rev. D **80**, 064005 (2009).

[4] K-i. Maeda, Y. Misonoh and T. Kobayashi, Phys. Rev. D **82**, 064024 (2010).

Trispectrum estimator in equilateral type non-Gaussian models

Shuntaro Mizuno[1] and Kazuya Koyama[2]

Institute of Cosmology and Gravitation, University of Portsmouth, Portsmouth PO1 3FX, UK.

Abstract

We investigate an estimator to measure the primordial trispectrum in equilateral type non-Gaussian models such as k-inflation, single field DBI inflation and multi-field DBI inflation models from Cosmic Microwave Background (CMB) anisotropies. The shape of the trispectrum whose amplitude is not constrained by the bispectrum in the context of effective theory of inflation and k-inflation is known to admit a separable form of the estimator for CMB anisotropies. We show that this shape is 87% correlated with the full quantum trispectrum in single field DBI inflation, while it is 33% correlated with the one in multi-field DBI inflation when curvature perturbation is originated from purely entropic contribution. This suggests that $g_{\rm NL}^{equil}$, the amplitude of this particular shape, provides a reasonable measure of the non-Gaussianity from the trispectrum in equilateral non-Gaussian models. We relate model parameters such as the sound speed, c_s and the transfer coefficient from entropy perturbations to the curvature perturbation, $T_{\mathcal{R}S}$ with $g_{\rm NL}^{equil}$, which enables us to constrain model parameters in these models once $g_{\rm NL}^{equil}$ is measured in WMAP and Planck.

1 Introduction

The statistical properties of primordial fluctuations provide crucial information on the physics of the very early universe [1]. In the simplest single field inflation models where the scalar field has a canonical kinetic term and quantum fluctuations are generated from the standard Bunch-Davis vacuum, non-Gaussianity of the fluctuations is too small to be observed even with future experiments. Thus the detection of non-negligible departures from Gaussinaity of primordial fluctuations will have a huge impact on the models of early universe. So far, most of the studies have focused on the leading order non-Gaussianity measured by the three-point function of Cosmic Microwave Background (CMB) anisotropies, i.e. the bispectrum. However, future experiments like Planck [2] can also prove the higher order statistics like the trispectrum. Actually, the trispectrum gives information that cannot be obtained from the bispectrum.

In the local type non-Gaussian models, the primordial curvature perturbation ζ is modeled as

$$\zeta = \zeta_g + \frac{3}{5} f_{\rm NL}^{local} (\zeta_g^2 - \langle \zeta_g^2 \rangle) + \frac{9}{25} g_{\rm NL}^{local} \zeta_g^3 \tag{1}$$

where ζ_g is a Gaussian variable. In this model, the bispectrum has maximum amplitude for the squeezed configurations in the Fourier space where one of wavenumbers is small compared with others. In these models, the trispectrum indeed gives very interesting tests on multi-field inflation models. Also the trispectrum can constrain the cubic-order non-linearities in primordial curvature perturbation, $g_{\rm NL}^{local}$ that cannot be constrained by the bispectrum measurements. Estimators to measure the trispectrum in the local-type non-Gaussianity have been developed and the kurtosis based estimator have been used to obtain constraints on the amplitude of the trispectrum, $-7.4 < g_{\rm NL}^{local}/10^5 < 8.2$ at 95% confidence level from the WMAP 5-year data [3].

There are another class of non-Gaussian models. A typical example is Dirac-Born-Infled (DBI) inflation [4] In this model, like k-inflation, the inflaton field has non-canonical kinetic term and non-linear derivative interactions can give rise to large non-Gaussianity of quantum fluctuations. In these models, the amplitude of the bispectrum has a peak typically for the equilateral configuration in the Fourier space. The shape of the trispectrum is more complicated. For example, for the bispectrum, the equilateral condition $k_1 = k_2 = k_3$ completely specifies the shape of the bisepctrum, but this is not the case for

[1]Email address: shuntaro.mizuno@port.ac.uk
[2]Kazuya.Koyama@port.ac.uk

the trispectrum. The shape of the trispectrum has been analyzed in several inflationary models such as single field DBI inflation [5], multi-field DBI inflation [7] and the models motivated by effective theory of inflation [8, 9].

Regardless of these efforts, since the form of the trispectrum is generally very complicated, estimators for the trispectrum in this class of non-Gaussian models have not been implemented yet so far. It was suggested that the form of trispectrum given by

$$T_\zeta(\mathbf{k}_1,\mathbf{k}_2,\mathbf{k}_3,\mathbf{k}_4) = \frac{g_{\rm NL}^{equil}}{k_1k_2k_3k_4(\frac{k_1+k_2+k_3+k_4}{4})^5}\mathcal{P}_\zeta(k)^3\,, \tag{2}$$

represents the shape of the trispectrum in equilateral non-Gaussian models very well.

This trispectrum (2) appears in DBI inflation as a contribution from the fourth order interacting Hamiltonian (the "contact interaction") [5, 6]. In the effective theory of inflation, it was shown that the trispectrum of this shape can have the amplitude that is not constrained by the bispectrum measurements [8]. In Ref. [6] , it was suggested that this trispectrum can be used to construct an estimator because by introducing the integral $1/M^n = (1/\Gamma(n))\int_0^\infty t^{(n-1)}e^{-Mt}$, this function is factorisable. Therefore, in this paper which is based on [10], we compare the shapes of trispectra in single field and multi-field DBI inflation with Eq. (2) based on a shape correlator introduced by Regan et.al [11] and investigate whether the estimator constructed from the trispectrum (2) represents the shapes of trispetrum in these models.

2 The shape correlator

Here, we review the shape correlator introduced by Regan et al. [11]. First we exploit the symmetry of the trispectrum to define the *reduced* trispectrum as follows [12]. We rewrite the definition of the trispectrum as

$$\begin{aligned}\langle\zeta(\mathbf{k_1})\zeta(\mathbf{k_2})\zeta(\mathbf{k_3})\zeta(\mathbf{k_4})\rangle_c &= (2\pi)^3\int d^3K\big[\delta(\mathbf{k_1}+\mathbf{k_2}-\mathbf{K})\delta(\mathbf{k_3}+\mathbf{k_4}+\mathbf{K})\big(\mathcal{T}_\zeta(\mathbf{k_1},\mathbf{k_2},\mathbf{k_3},\mathbf{k_4};\mathbf{K})\\ &\quad+\mathcal{T}_\zeta(\mathbf{k_2},\mathbf{k_1},\mathbf{k_3},\mathbf{k_4};\mathbf{K})+\mathcal{T}_\zeta(\mathbf{k_1},\mathbf{k_2},\mathbf{k_4},\mathbf{k_3};\mathbf{K})+\mathcal{T}_\zeta(\mathbf{k_2},\mathbf{k_1},\mathbf{k_4},\mathbf{k_3};\mathbf{K})\big)\\ &\quad+(\mathbf{k_2}\leftrightarrow\mathbf{k_3})+(\mathbf{k_2}\leftrightarrow\mathbf{k_4})\big]\,.\end{aligned} \tag{3}$$

Then we need to consider only the reduced trispectrum $\mathcal{T}_\zeta$ from one particular arrangement of the vectors, such as $\mathcal{T}_\Phi(\mathbf{k_1},\mathbf{k_2},\mathbf{k_3},\mathbf{k_4};\mathbf{k_{12}})$ with $\mathbf{k_{12}}=\mathbf{k_1}+\mathbf{k_2}$ and form the other contributions by considering permutations. Here, for the later convenience, we use the symmetrised reduced trispectrum

$$\begin{aligned}\mathcal{T}_\zeta^{sym}(\mathbf{k_1},\mathbf{k_2},\mathbf{k_3},\mathbf{k_4};\mathbf{k_{12}}) &\equiv \frac{1}{4}\big[\mathcal{T}_\zeta(\mathbf{k_1},\mathbf{k_2},\mathbf{k_3},\mathbf{k_4};\mathbf{k_{12}})+\mathcal{T}_\zeta(\mathbf{k_2},\mathbf{k_1},\mathbf{k_3},\mathbf{k_4};\mathbf{k_{12}})\\ &\quad+\mathcal{T}_\zeta(\mathbf{k_1},\mathbf{k_2},\mathbf{k_4},\mathbf{k_3};\mathbf{k_{12}})+\mathcal{T}_\zeta(\mathbf{k_2},\mathbf{k_1},\mathbf{k_4},\mathbf{k_3};\mathbf{k_{12}})\big]\,,\end{aligned} \tag{4}$$

and from now on we omit the superscript *sym* for simplicity.

The reduced trispectrum is a function of six variables. We can choose them to be $(k_1,k_2,k_3,k_4,k_{12},\theta_4)$ where θ_4 represents the deviation of the quadrilateral from planarity which is specified by the triangle (k_1,k_2,k_{12}). We find that in terms of these variables $k_{14}=|\mathbf{k_1}+\mathbf{k_4}|$ is expressed as

$$\begin{aligned}k_{14}^2 &= k_1^2+k_4^2-\frac{1}{2k_{12}^2}(k_1^2+k_{12}^2-k_2^2)(k_4^2+k_{12}^2-k_3^2)\\ &\quad\pm\frac{1}{2k_{12}^2}\sqrt{4k_1^2k_{12}^2-(k_1^2+k_{12}^2-k_2^2)^2}\sqrt{4k_4^2k_{12}^2\cos^2\theta_4-(k_4^2+k_{12}^2-k_3^2)^2}\,,\end{aligned} \tag{5}$$

which implies that the valid range of $\cos\theta_4$ is constrained by

$$|\cos\theta_4| \geq \frac{|k_4^2+k_{12}^2-k_3^2|}{2k_{12}k_4}\,. \tag{6}$$

Motivated by the relation between the CMB trispectrum and the trispectrum for ζ, the shape function for the reduced trispectrum is defined as

$$S_\mathcal{T}(k_1,k_2,k_3,k_4,k_{12},\theta_4) = (k_1k_2k_3k_4)^2k_{12}\mathcal{T}_\zeta(k_1,k_2,k_3,k_4;k_{12},\theta_4)\,. \tag{7}$$

Regan et al. [11] proposed to define an overlap between two different shape functions $S_{\mathcal{T}}$ and $S_{\mathcal{T}'}$ as

$$F(S_{\mathcal{T}}, S_{\mathcal{T}'}) = \int d\mathcal{V}_k \int d(\cos\theta_4) S_{\mathcal{T}}(k_1, k_2, k_3, k_4, k_{12}, \theta_4) S_{\mathcal{T}'}(k_1, k_2, k_3, k_4, k_{12}, \theta_4) w(k_1, k_2, k_3, k_4, k_{12}) \,, \quad (8)$$

where w is an appropriate weight function. The weight function should be chosen such that $S^2 w$ in k space produces the same scaling as the estimator in l space and we adopt the one used in Ref. [11],

$$w(k_1, k_2, k_3, k_4, k_{12}) = \frac{1}{k_{12}(k_1 + k_2 + k_{12})(k_3 + k_4 + k_{12})} \,. \quad (9)$$

With this choice of weight, the shape correlator is defined as

$$\bar{\mathcal{C}}(S_{\mathcal{T}}, S_{\mathcal{T}'}) = \frac{F(S_{\mathcal{T}}, S_{\mathcal{T}'})}{\sqrt{F(S_{\mathcal{T}}, S_{\mathcal{T}}) F(S_{\mathcal{T}'}, S_{\mathcal{T}'})}} \,. \quad (10)$$

3 Shape correlations and theoretical predictions for $g_{\rm NL}^{\rm equil}$

In this section, we study the overlap between Eq. (2) and the trispectra in single field and multi-field DBI inflation. First, we find that the shape function for the trispectrum (2), single field DBI inflation and multi-field DBI inflation as follows:

$$S_{\mathcal{T}}^{equil} = \frac{64}{3} \mathcal{P}_\zeta^3 g_{\rm NL}^{equil} S_{\mathcal{T}}^{c_1} \,, \quad (11)$$

$$S_{\mathcal{T}}^{DBI(\sigma)} = \frac{H^{12}}{\dot{\phi}^6 c_s^4} \left[-3 S_{\mathcal{T}}^{c_1} + \frac{1}{64} S_{\mathcal{T}}^{s_1} + \frac{1}{64} S_{\mathcal{T}}^{s_2} - \frac{1}{64} S_{\mathcal{T}}^{s_3} \right] , \quad (12)$$

$$S_{\mathcal{T}}^{DBI(s)} = \frac{H^{12}}{\dot{\phi}^6 c_s^4} T_{\mathcal{R}S}^4 \left[-\frac{1}{8} S_{\mathcal{T}}^{c_2} + \frac{1}{576} S_{\mathcal{T}}^{s_1} + \frac{1}{64} S_{\mathcal{T}}^{\tilde{s}_2} + \frac{1}{192} S_{\mathcal{T}}^{\tilde{s}_3} \right] , \quad (13)$$

where $S_{\mathcal{T}}^{c_1}$, $S_{\mathcal{T}}^{c_2}$, $S_{\mathcal{T}}^{s_1}$, $S_{\mathcal{T}}^{s_2}$, $S_{\mathcal{T}}^{s_3}$, $S_{\mathcal{T}}^{\tilde{s}_2}$ and $S_{\mathcal{T}}^{\tilde{s}_3}$ are given in [10]. Table 1 provides a summary of correlations among $S_{\mathcal{T}}^{equil}$, $S_{\mathcal{T}}^{DBI(\sigma)}$ and $S_{\mathcal{T}}^{DBI(s)}$. In addition to the correlation considering full configurations dealing with five dimensional parameter space, for comparisons, we also consider the configurations limited with $k_1 + k_2 = k_3 + k_4$ and equilateral configurations ($k_1 = k_2 = k_3 = k_4$).

Making use of these shape correlations, we give theoretical predictions for $g_{\rm NL}^{equil}$. In order to express the amplitude of the trispectra in single field DBI inflation and multi-field DBI inflation in terms of $g^{\rm equil_{NL}}$, we rewrite Eqs. (12) and (13) so that the normalisation is chosen so that when $g_{\rm NL}^{equil} = 1$ and $\bar{\mathcal{C}}(S_{\mathcal{T}}^{DBI(\sigma,\, s)}, S_{\mathcal{T}}^{equil}) = 1$, the following conditions are satisfied,

$$\begin{aligned} F(S_{\mathcal{T}}^{DBI(\sigma,\, s)}, S_{\mathcal{T}}^{DBI(\sigma,\, s)}) &= F(S_{\mathcal{T}}^{equil}, S_{\mathcal{T}}^{equil}) \,, \\ F(S_{\mathcal{T}}^{DBI(\sigma,\, s)}, S_{\mathcal{T}}^{equil}) &> 0 \,. \end{aligned} \quad (14)$$

Of course, $\bar{\mathcal{C}}(S_{\mathcal{T}}^{DBI(\sigma,\, s)}, S_{\mathcal{T}}^{equil}) = 1$ is not true in reality and this factor will enhance the amplitude of the signal for a given $g_{\rm NL}^{equil}$. This term is necessary because when we use the estimator related with $S_{\mathcal{T}}^{equil}$ for the signal whose shape is characterised by $S_{\mathcal{T}}^{DBI(\sigma,\, s)}$, the observed signal is suppressed by $\bar{\mathcal{C}}(S_{\mathcal{T}}^{DBI(\sigma,\, s)}, S_{\mathcal{T}}^{equil})$ and it is necessary to compensate this.

4 Conclusion

It is well known that there are many interesting early universe models that predict equilateral type primordial non-Gaussianity motivated by string theory and effective field theory. Taking into account the fact that future experiments such as Planck can prove even next order statistics, it is important to

	Overlap-full	$\epsilon = 1$	equilateral	theoretical prediction for $g_{\rm NL}^{equil}$	$f_{\rm NL}^{equil}$
equilateral shape	1	1	1	$(3X^3c_s^2P_{,4X})/(16P_{,X})$	$f_{\rm NL}^{equil}$
single DBI	0.87	0.90	0.92	$17/c_s^4$	$-0.36/c_s^2$
multi DBI	0.33	0.60	0.85	$2.2/(c_s^4T_{\mathcal{R}S}^2)$	$-0.36/(c_s^2T_{\mathcal{R}S}^2)$

Table 1: Shape correlations. We also summarise theoretical predictions for $g_{\rm NL}^{equil}$ and $f_{\rm NL}^{equil}$ in the model with equilateral shape motivated by effective theory of inflation, single field DBI inflation and multi-field DBI inflation these models.

study the primordial trispectrum in these models. Therefore, in this work we have presented a method to estimate primordial trispectrum in equilateral type non-Gaussian models such as k-inflation model, single field DBI inflation and multi-field DBI inflation. Our method is based on the following two facts. One is that the equilateral shape given by Eq. (2) becomes factorisable by introducing the integral $1/M^n = (1/\Gamma(n))\int_0^\infty t^{(n-1)}e^{-Mt}$ as was suggested in Ref. [6]. The other is that in terms of the shape correlation proposed by Ref. [11], we can relate the amplitudes of trispectra with different shapes.

We have shown that the shape is 87% correlated with the one in single field DBI inflation, while it is 33% correlated with that in multi-field DBI inflation when the curvature perturbation is originated from purely entropic perturbations during inflation. Then, we have given theoretical predictions for $g_{\rm NL}^{equil}$, which enables us to constrain this type of non-Gaussian models from future experiments. For the model with equilateral shape motivated by k-inflation, we obtained $g_{\rm NL}^{equil} = (3X^3c_s^2P_{,4X})/(16P_{,X})$, while for single field DBI inflation and multi-field DBI inflation, $g_{\rm NL}^{equil} = 17/c_s^4$ and $g_{\rm NL}^{equil} = 2.2/(c_s^4T_{\mathcal{R}S}^2)$, respectively. To obtain this value, instead of matching the amplitudes of the shape functions at a specific point in the parameter space, we have adopted an overlap function, $F(S_{\mathcal{T}}, S_{\mathcal{T}'})$, defined in Eq. (8), which involves integration over five-parameters. Finally, although this work is limited to consider k-inflation, single field DBI inflation and multi-field DBI inflation, it is recognised that the ghost inflation and the cosmology based on a Lifshitz scalar field give equilateral type non-Gaussianity and the their shape dependences of the trispectra were calculated. As a natural extension of this work, it is worth applying the method proposed in this paper to the models mentioned above [13].

References

[1] N. Bartolo, E. Komatsu, S. Matarrese and A. Riotto, Phys. Rept. **402**, 103 (2004).

[2] http://www.rssd.esa.int/index.php?project=Planck

[3] J. Smidt, A. Amblard, A. Cooray, A. Heavens, D. Munshi and P. Serra, arXiv:1001.5026 [astro-ph.CO].

[4] E. Silverstein and D. Tong, Phys. Rev. D **70** (2004) 103505.

[5] F. Arroja, S. Mizuno, K. Koyama and T. Tanaka, Phys. Rev. D **80**, 043527 (2009).

[6] X. Chen, B. Hu, M. x. Huang, G. Shiu and Y. Wang, JCAP **0908** (2009) 008.

[7] S. Mizuno, F. Arroja and K. Koyama, Phys. Rev. D **80** (2009) 083517.

[8] L. Senatore and M. Zaldarriaga, arXiv:1004.1201 [hep-th].

[9] N. Bartolo, M. Fasiello, S. Matarrese and A. Riotto, JCAP **1009**, 035 (2010).

[10] S. Mizuno and K. Koyama, JCAP **1010** (2010) 002.

[11] D. Regan, E. Shellard, and J. Fergusson, Phys. Rev. D **82**, 023520 (2010)

[12] W. Hu, Phys. Rev. D **64**, 083005 (2001).

[13] K. Izumi, S. Mizuno and K. Koyama, in preparation

Target space structure of 5-dimensional Einstein-Maxwell-Chern-Simons theory with non-SUGRA coupling

Yoshiyuki Morisawa[1]

Faculty of Liberal Arts and Sciences, Osaka University of Economics and Law, Gakuonji 6-10, Yao, Osaka 581-8511

Abstract

We investigate the geometrical properties of the target space of the five-dimensional Einstein-Maxwell-Chern-Simons system admitting two commuting spacelike Killing vector fields whose Chern-Simons coupling constant is the non-SUGRA value.

1 Introduction

As well known, the five-dimensional Einstein-Maxwell-Chern-Simons system admitting two commuting spacelike Killing vector fields whose Chern-Simons coupling constant is the SUGRA value can be reduced to the three-dimensional gravity-coupled sigma-model. Then the target space is the homogeneous space $G_{2(2)}/SO(4)$ [1, 2]. The solution generating methods using target space symmetry yield fruitful results. Assuming one more timelike symmetry, one can discuss black hole uniqueness as a boundary value problem using the Mazur identity [3].

However, this is not the case of the non-SUGRA value coupling constant. Although the five-dimensional Einstein-Maxwell-Chern-Simons system admitting two commuting spacelike Killing vector fields can also be reduced to the three-dimensional gravity-coupled sigma-model, the target space is not homogeneous and the Mazur identity is not applicable there. In this short article, we investigate the geometrical properties of this non-homogeneous target space. The target space is derived in Sec. 2. We show the symmetry of target space in Sec. 3 and the existence of the totally geodesic submanifolds in Sec. 4. In Sec. 5, we calculate the sectional curvature of the target space, then we also discuss the applicability of the Bunting identity.

2 Reduction of 5D EMCS system with 2KVs

We consider the five-dimensional Einstein-Maxwell-Chern-Simons system and assume that the spacetime admits two commuting spacelike Killing vector fields ξ_1,ξ_2. Then, the metric can be written in the form

$$g = f^{-1}\gamma_{ij}dx^i dx^j + f_{IJ}(dx^I + w^I{}_i dx^i)(dx^J + w^J{}_j dx^j), \tag{1}$$

where $I, J = 1, 2$, $i, j = 3, 4, 5$, $f = \det(f_{IJ})$ and γ_{ij}, $w^I{}_i$ and the gravitational potential $f_{IJ} = g(\xi_I, \xi_J)$ are independent on the coordinates x^I. We define the twist 1-form ω_I by

$$\omega_I = *(\xi_1 \wedge \xi_2 \wedge d\xi_I), \tag{2}$$

and then we obtain

$$d\omega_I = 2 * (\xi_1 \wedge \xi_2 \wedge R(\xi_I)). \tag{3}$$

Using these f_{IJ} and ω_I, the Ricci tensor R with respect to g and the Ricci tensor ${}^{(\gamma)}R$ with respect to the three-metric γ_{ij} are related to each other by

$$\begin{aligned} {}^{(\gamma)}R_{ij} = {} & f^{-2}\gamma_{im}\gamma_{jn}R^{mn} + f^{-1}f^{IJ}R_{IJ}\gamma_{ij} \\ & + \frac{1}{4}f^{-2}f_{,i}f_{,j} + \frac{1}{4}f^{IJ}f^{KL}f_{IK,i}f_{JL,j} + \frac{1}{2}f^{-1}f^{IJ}\omega_{Ii}\omega_{Jj}. \end{aligned} \tag{4}$$

[1]Email address: morisawa@keiho-u.ac.jp

Next, we consider the Maxwell field $F = dA$ and assume that $\mathcal{L}_{\xi_I} A = 0$. We define the electric 1-forms E_I and the magnetic 1-form B by

$$E_I = -\iota_I F, \tag{5}$$
$$B = *(\xi_1 \wedge \xi_2 \wedge F). \tag{6}$$

The Maxwell equation $dF = 0$ ensures the local existence of the electric potentials Φ_I such that

$$d\Phi_I = E_I. \tag{7}$$

From the Maxwell equation $d * F = -4\beta F \wedge F$, we can show that there locally exists the magnetic potential Ψ such that

$$d\Psi + 4\beta\epsilon^{PQ}\Phi_P d\Phi_Q = B, \tag{8}$$

where ϵ^{PQ} is the totally skew-symmetric symbol such that $\epsilon^{12} = 1$. Using these potentials Φ_I, Ψ, and the Einstein equation $R = \alpha(T - \frac{\mathrm{tr}T}{3}g)$ (where T is the stress-energy tensor of the Maxwell field), Eq. (4) can be written by

$$\begin{aligned} {}^{(\gamma)}R_{ij} = {} & \frac{1}{4}f^{-2}f_{,i}f_{,j} + \frac{1}{4}f^{IJ}f^{KL}f_{IK,i}f_{JL,j} + \frac{1}{2}f^{-1}f^{IJ}\omega_{Ii}\omega_{Jj} \\ & +\alpha\left[f^{IJ}\Phi_{I,i}\Phi_{J,j} + f^{-1}(\Psi_{,i} + 4\beta\epsilon^{IJ}\Phi_I\Phi_{J,i})(\Psi_{,j} + 4\beta\epsilon^{KL}\Phi_K\Phi_{L,j})\right], \end{aligned} \tag{9}$$

and Eq. (3) ensures the local existence of the twist potentials λ_I such that

$$\omega_I = d\lambda_I + \alpha(\Psi d\Phi_I - \Phi_I d\Psi) - \frac{8}{3}\alpha\beta\epsilon^{PQ}\Phi_I\Phi P d\Phi_Q. \tag{10}$$

We can also derive the equation of motion of the potentials f_{IJ}, λ_I, Φ_I and Ψ.

Finally, the Einstein-Maxwell-Chern-Simons system reduces to the equations derived from the action

$$S = \int d^3x\sqrt{|\gamma|}\gamma^{ij}\left({}^{(\gamma)}R - G_{AB}\frac{\partial X^A}{\partial x^i}\frac{\partial X^B}{\partial x^j}\right), \tag{11}$$

which describes the three-dimensional gravity-coupled sigma-model with the eight scalar fields $X^A = \{f_{11}, f_{12}, f_{22}, \lambda_1, \lambda_2, \Phi_1, \Phi_2, \Psi\}$ and the target space metric G. Here G_{AB} is given by

$$\begin{aligned} G_{AB}dX^A \otimes dX^B = {} & \frac{1}{4}f^{IJ}f^{KL}(df_{IJ} \otimes df_{KL} + df_{IK} \otimes df_{JL}) + \frac{1}{2}f^{-1}f^{IJ}\omega_I \otimes \omega_J \\ & +\alpha[f^{IJ}d\Phi_I \otimes d\Phi_J + f^{-1}B \otimes B], \end{aligned} \tag{12}$$

where

$$B = d\Psi + 4\beta\epsilon^{PQ}\Phi_P d\Phi_Q, \tag{13}$$
$$\omega_I = d\lambda_I + \alpha(\Psi d\Phi_I - \Phi_I d\Psi) - \frac{8}{3}\alpha\beta\epsilon^{PQ}\Phi_I\Phi_P d\Phi_Q. \tag{14}$$

Here α is the parameter to absorb the normalization of the gauge field, β is related to the coupling constant of the Chern-Simons term, and $\alpha = 24\beta^2$ means the SUGRA value.

The Ricci tensor for this target space

$${}^{(G)}Ric = -4G + \frac{4(\alpha - 24\beta^2)}{3}(f^{IJ}d\Phi_I \otimes d\Phi_J - f^{-1}B \otimes B) \tag{15}$$

shows the target space is Einstein space when $\alpha = 24\beta^2$.

3 Target space symmetry with non-SUGRA value coupling constant

For the SUGRA value coupling constant $\alpha = 24\beta^2$, the target space has the fourteen Killing vector fields which are generators of $G_{2(2)}$ symmetry, and the target space is the homogeneous space $G_{2(2)}/SO(4)$.

On the other hand, the target space with $\alpha \neq 24\beta^2$ has only nine Killing vector fields:

$$K_1 = \frac{\partial}{\partial\lambda_1}, \tag{16}$$

$$K_2 = \frac{\partial}{\partial\lambda_2}, \tag{17}$$

$$K_3 = \Phi_1\frac{\partial}{\partial\Phi_1} + \Psi\frac{\partial}{\partial\Psi} + 2\lambda_1\frac{\partial}{\partial\lambda_1} + \lambda_2\frac{\partial}{\partial\lambda_2} + 2f_{11}\frac{\partial}{\partial f_{11}} + f_{12}\frac{\partial}{\partial f_{12}}, \tag{18}$$

$$K_4 = \Phi_2\frac{\partial}{\partial\Phi_2} + \Psi\frac{\partial}{\partial\Psi} + \lambda_1\frac{\partial}{\partial\lambda_1} + 2\lambda_2\frac{\partial}{\partial\lambda_2} + f_{12}\frac{\partial}{\partial f_{12}} + 2f_{22}\frac{\partial}{\partial f_{22}}, \tag{19}$$

$$K_5 = \Phi_1\frac{\partial}{\partial\Phi_2} + \lambda_1\frac{\partial}{\partial\lambda_2} + f_{11}\frac{\partial}{\partial f_{12}} + 2f_{12}\frac{\partial}{\partial f_{22}}, \tag{20}$$

$$K_6 = \Phi_2\frac{\partial}{\partial\Phi_1} + \lambda_2\frac{\partial}{\partial\lambda_1} + 2f_{12}\frac{\partial}{\partial f_{11}} + f_{22}\frac{\partial}{\partial f_{12}}, \tag{21}$$

$$K_7 = \frac{\partial}{\partial\Psi} - \alpha\Phi_I\frac{\partial}{\partial\lambda_I}, \tag{22}$$

$$K_8 = \frac{\partial}{\partial\Phi_1} - 4\beta\Phi_2\frac{\partial}{\partial\Psi} + \alpha\Psi\frac{\partial}{\partial\lambda_1} + \frac{4}{3}\alpha\beta\Phi_2\Phi_J\frac{\partial}{\partial\lambda_J}, \tag{23}$$

$$K_9 = \frac{\partial}{\partial\Phi_2} + 4\beta\Phi_1\frac{\partial}{\partial\Psi} + \alpha\Psi\frac{\partial}{\partial\lambda_2} - \frac{4}{3}\alpha\beta\Phi_1\Phi_J\frac{\partial}{\partial\lambda_J}. \tag{24}$$

We obtain the commutation relations as follows:

	K_1	K_2	K_7	K_8	K_9	K_3+K_4	K_3-K_4	K_5	K_6
K_1						$3K_1$	K_1	K_2	
K_2						$3K_2$	$-K_2$		K_1
K_7				$2\alpha K_1$	$2\alpha K_2$	$2K_7$			
K_8			$-2\alpha K_1$		$8\beta K_7$	K_8	K_8	K_9	
K_9			$-2\alpha K_2$	$-8\beta K_7$		K_9	$-K_9$		K_8
K_3+K_4	$-3K_1$	$-3K_2$	$-2K_7$	$-K_8$	$-K_9$				
K_3-K_4	$-K_1$	K_2		$-K_8$	K_9			$2K_5$	$-2K_6$
K_5	$-K_2$			$-K_9$			$-2K_5$		K_3-K_4
K_6		$-K_1$			$-K_8$		$2K_6$	$-K_3+K_4$	

These form a non-semisimple Lie algebra. We denote this algebra by g_9.

g_9 has a structure like Bianchi I "$\times$" V "$\times$" IX. g_9 has the ideal $\{K_1, K_2, K_7\}$, which forms Bianchi type I algebra. The quotient $g_9/\{K_1, K_2, K_7\}$ has the ideal $\{K_8, K_9, K_3 + K_4\}$, which forms Bianchi type V algebra. Then $(g_9/\{K_1, K_2, K_7\})/\{K_8, K_9, K_3 + K_4\}$ forms $su(2)$ (type IX).

4 Totally geodesic submanifolds

We can easily confirm that the target space with $\alpha \neq 24\beta^2$ is not homogeneous. However, some submanifolds of this target space are homogeneous and embedded as totally geodesic submanifolds.

The five-dimensional submanifold restricted by $\Phi_1 = const.$, $\Phi_2 = const.$, and $\Psi = const.$ is the homogeneous space $SL(3,R)/SO(3)$ and corresponds to the target space for the five-dimensional pure gravity system.

The four-dimensional submanifold restricted by $\lambda_1 = const.$, $\lambda_2 = const.$, and $\Phi_1 = \Phi_2 = 0$ corresponds to the target space for the static solutions including the Reissner-Nordström solution. The Killing vector fields of this submanifold form $su(2) \times su(2)$.

The four-dimensional submanifolds restricted by $\lambda_2 = const.$ and $f_{12} = \Phi_1 = \Psi = 0$ or restricted by $\lambda_1 = const.$ and $f_{12} = \Phi_2 = \Psi = 0$ are also homogeneous and totally geodesic. These correspond to the restricted solution spaces where Ida and Uchida provided the solution generating method for the five-dimensional Einstein-Maxwell system [4] and Hollands and Yazadjiev proved the uniqueness theorem for the five-dimensional Einstein-Maxwell black holes [5]. The Killing vector fields of these submanifolds form $su(2) \times su(2)$.

5 Black hole uniqueness

Assuming the existence of another timelike Killing vector field, the system consists of the three-dimensional gravity-coupled sigma-model with the eight scalar fields reduced to the two-dimensional sigma-model with the eight scalar fields. When the target space is homogeneous, one can use the Mazur identity to discuss uniqueness property of black hole solutions as a boundary value problem.

Although the target space is not homogeneous, the Bunting identity can be used to show black hole uniqueness when the target space has negative semi-definite sectional curvature. We calculate the sectional curvature of the target space and obtain that it is negative semi-definite for $96/11 \leq \alpha/\beta^2 \leq 288/5$. The SUGRA value $\alpha/\beta^2 = 24$ is included in this range.

Kunz and Navarro-Lerida [6] showed that black holes are not uniquely characterized by their global charges when the Chern-Simons coupling constant increases beyond some value (λ=2 in their notation). The parameter range corresponding to negative semi-definite sectional curvature can be written by $5/12 \leq \lambda^2 \leq 11/4$. λ=2 is out of this range, hence our result is consistent with theirs.

6 Summary

We investigate the geometrical properties of the target space of the five-dimensional Einstein-Maxwell-Chern-Simons theory with non-SUGRA value coupling constant admitting two commuting spacelike Killing vector fields. The target space has the nine Killing vector fields and is not homogeneous. However, in some parameter range, it has negative semi-definite sectional curvature and the Bunting identity is applicable.

Acknowledgement

This short article is based on the collaboration with Daisuke Ida, Akihiro Ishibashi, and Yukinori Yasui.

References

[1] S. Mizoguchi and N. Ohta, Phys. Lett. B **441**, 123 (1998) [arXiv:hep-th/9807111].

[2] A. Bouchareb, G. Clement, C. M. Chen, D. V. Gal'tsov, N. G. Scherbluk and T. Wolf, Phys. Rev. D **76**, 104032 (2007) [Erratum-ibid. D **78**, 029901 (2008)] [arXiv:0708.2361 [hep-th]].

[3] S. Tomizawa, Y. Yasui and A. Ishibashi, Phys. Rev. D **79**, 124023 (2009) [arXiv:0901.4724 [hep-th]].

[4] D. Ida and Y. Uchida, Phys. Rev. D **68**, 104014 (2003) [arXiv:gr-qc/0307095].

[5] S. Hollands and S. Yazadjiev, Class. Quant. Grav. **25**, 095010 (2008) [arXiv:0711.1722 [gr-qc]].

[6] J. Kunz and F. Navarro-Lerida, Mod. Phys. Lett. A **21**, 2621 (2006) [arXiv:hep-th/0610075].

Classification of Future Phantom-to-Normal Oscillations in $f(R)$ Gravity

Hayato Motohashi[1 (a,b)], Alexei A. Starobinsky[2 (b,c)] and Jun'ichi Yokoyama[3 (b,d)]

[(a)] *Department of Physics, Graduate School of Science, The University of Tokyo, Tokyo 113-0033, Japan*
[(b)] *Research Center for the Early Universe (RESCEU), Graduate School of Science, The University of Tokyo, Tokyo 113-0033, Japan*
[(c)] *L. D. Landau Institute for Theoretical Physics, Moscow 119334, Russia*
[(d)] *Institute for the Physics and Mathematics of the Universe (IPMU), The University of Tokyo, Kashiwa, Chiba 277-8568, Japan*

Abstract

We consider oscillations of the dark energy effective equation of state $w_{\rm DE}$ around the phantom divide line $w_{\rm DE} = -1$ in the future evolution of viable cosmological models in $f(R)$ gravity. We present an analytical condition for the existence of an infinite number of such oscillations and numerically determine the region of model parameters where it is satisfied. It is shown that the amplitude of the oscillations decreases very fast with the increase of the present mass of scalaron, which is the scalar particle appearing in $f(R)$ gravity. As a result, the effect quickly becomes very small and its beginning is shifted to the remote future.

1 Introduction

$f(R)$ gravity is a natural generalization of the Einstein gravity which can provide a self-consistent and nontrivial alternative to the ΛCDM model of the present Universe [1–3], as well as a viable model of inflation in the early Universe [4]. This theory adopts a new phenomenological function of the Ricci scalar R, $f(R)$. As compared to the Einstein gravity, it contains a new scalar degree of freedom, in quantum language – a new scalar particle dubbed "scalaron" in [4]. Thus, this generalization is *nonperturbative*. Scalaron is a massive particle which mass depends on R.

To distinguish $f(R)$ gravity as the model for "present Dark Energy (DE)" which is responsible for the current cosmic acceleration (as opposed to "primordial DE" which drove inflation in the early Universe) from the standard ΛCDM model, it is useful to focus on two parameters, the effective equation-of-state (EoS) parameter for dark energy $w_{\rm DE}$ and the gravitational growth index γ. The latter is defined as $d\ln\delta/d\ln a \equiv \Omega_m(z)^{\gamma(z)}$ where $\delta \equiv \delta\rho_m/\rho_m$ and $\Omega_m \equiv 8\pi G\rho_m/3H^2$ are matter density fluctuation and density parameter for matter, respectively. In $f(R)$ gravity, $w_{\rm DE}$ is time dependent and γ is time and scale dependent, whilst $w_{\rm DE} \equiv -1$ and $\gamma \simeq 6/11$ in the ΛCDM model. Viable $f(R)$ models generically exhibit crossing of the phantom divide $w_{\rm DE} = -1$, similar to a more general case of scalar-tensor gravity. Time and scale dependency of γ generates an additional transfer function for matter density fluctuations that constraints the region of viable model parameters [5–7].

It was noted recently that the EoS parameter $w_{\rm DE}$ oscillates around the de Sitter solution in the future evolution of viable $f(R)$ models of dark energy[8]. However, it has not been clarified yet whether the phantom crossing occurs infinitely many times or not, and under which condition. Although this property is not observable since it refers to the remote future, it is very interesting from the theoretical point of view. Here we derive this conditions for a general $f(R)$ gravity, and present results of numerical calculations for a specific viable model.

[1]Email address: motohashi"at"resceu.s.u-tokyo.ac.jp
[2]Email address: alstar"at"landau.ac.ru
[3]Email address: yokoyama"at"resceu.s.u-tokyo.ac.jp

2 Conditions

$f(R)$ gravity is defined by the following action:

$$S = \frac{1}{16\pi G}\int d^4x\sqrt{-g}f(R) + S_m, \tag{1}$$

where $f(R)$ is a function of Ricci scalar and S_m denotes the matter action. Field equations are derived as

$$R_{\mu\nu} - \frac{1}{2}g_{\mu\nu}R = 8\pi G(T_{\mu\nu} + T^{\rm DE}_{\mu\nu}), \tag{2}$$

$$8\pi G T^{\rm DE}_{\mu\nu} = (1-F)R_{\mu\nu} - \frac{1}{2}(R-f)g_{\mu\nu} + (\nabla_\mu\nabla_\nu - g_{\mu\nu}\Box)F, \tag{3}$$

where $F = df/dR$ and $T^{\rm DE}_{\mu\nu}$ is the energy-momentum tensor for effective DE. The trace equation is

$$RF - 2f + 3\Box F = 8\pi G T. \tag{4}$$

In de Sitter regime, matter density decreases rapidly as $\rho \propto e^{-3H_1 t}$. It follows from Eq. (4), that a constant value of the Ricci scalar $R = R_1 = \text{const.}$ characterizing the de Sitter regime should be a root of the algebraic equation

$$2f_1 = R_1 F_1, \tag{5}$$

where $f_1 \equiv f(R_1)$ and $F_1 \equiv F(R_1)$. Effective dark energy at de Sitter regime is characterized by $8\pi G\rho_{\rm DE,1} = -8\pi G P_{\rm DE,1} = \frac{R_1}{4}$, thus $w_{\rm DE,1} = -1$.

To investigate stability of the de Sitter solution and to find the condition for the existence of oscillations around it, we use the first order of perturbation theory with respect to $\delta R \equiv R - R_1$. The evolution equation for δR is derived from Eq. (4),

$$\delta R'' + 3\delta R' + \frac{1}{3H_1^2}\left(\frac{F_1}{F_{R1}} - R_1\right)\delta R = \frac{8\pi G\rho_m}{3F_{R1}H_1^2}. \tag{6}$$

where prime denotes the derivative with respect to number of e-folding $N \equiv \ln a = -\ln(1+z)$ and $F_{R1} \equiv F_R(R_1) \equiv dF(R_1)/dR$. We include the matter density term $\rho_m = \rho_{m0}e^{-3N}$ into the right-hand side since $\delta R_{\rm dec}$ is much smaller than background quantities at the de Sitter stage.

The solution for Eq. (6) takes the form $\delta R = \delta R_{\rm dec} + \delta R_{\rm osc}$, where $\delta R_{\rm osc}$ is the homogeneous solution with an integration constant and $\delta R_{\rm dec} = \frac{8\pi G\rho_{m0}}{F_1 - R_1F_{R1}}e^{-3N}$ is the special solution for the full equation. Whilst $\delta R_{\rm dec}$ is a monotonically decaying mode, $\delta R_{\rm osc}$ may have oscillatory behaviour. The de Sitter solution is future stable, $dR_{\rm osc} \to 0$ for $t \to \infty$, if the following stability condition is satisfied:

$$\frac{F_1}{F_{R1}} > R_1. \tag{7}$$

Further, the criterion for the existence of an infinite number of oscillations around the de Sitter asymptote for $t \to \infty$ is obtained by setting negative the discriminant of the second order algebraic equation for characteristic exponents of homogeneous solutions of Eq. (6):

$$\frac{F_1}{F_{R1}} > \frac{25}{16}R_1. \tag{8}$$

If this condition is satisfied, $\delta R_{\rm osc} = Ae^{-3N/2}\sin(\omega N + \phi)$, where $\omega \equiv 2\sqrt{\frac{F_1}{R_1F_{R1}} - \frac{25}{16}}$, and A and ϕ are integration constants.

The perturbation of EoS parameter $\delta w_{\rm DE} = (\delta P_{\rm DE} + \delta\rho_{\rm DE})/\rho_{\rm DE,1}$ is calculated from $8\pi G(\rho_{\rm DE} + P_{\rm DE}) = -2\dot{H} - 8\pi G\rho_m$. We decompose $\delta w_{\rm DE} \equiv \delta w_{\rm dec} + \delta w_{\rm osc}$ as

$$\delta w_{\rm dec} = \frac{4}{R_1}\left(\frac{1}{F_1 - R_1F_{R1}} - 1\right)8\pi G\rho_{m0}(1+z)^3 \tag{9}$$

$$\delta w_{\rm osc} = A(1+z)^{3/2}\frac{4}{R_1}\left[-\frac{R_1F_{R1}}{3F_1}\omega\cos(\omega N + \phi) + \frac{1}{3}\left(\frac{5R_1F_{R1}}{2F_1} - 1\right)\sin(\omega N + \phi)\right]. \tag{10}$$

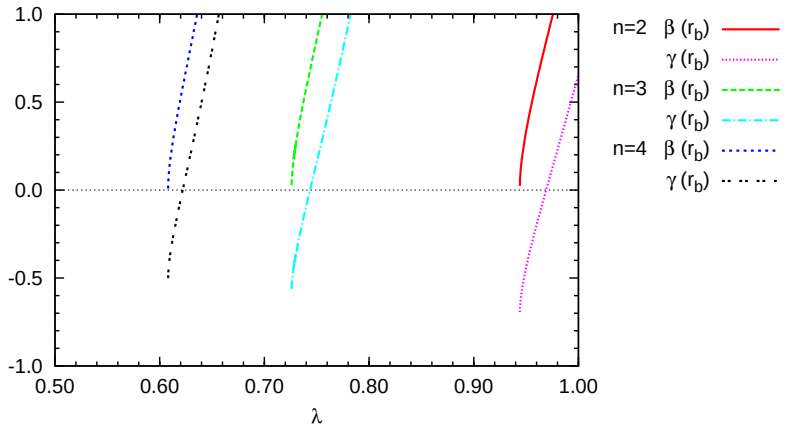

Figure 1: The parameter region $\gamma(r_b) < 0 < \beta(r_b)$ corresponds to stable de Sitter solution without the oscillatory behaviour.

3 The specific model

Hereafter, we consider the following viable cosmological model of present DE in $f(R)$ gravity [3]:

$$f(R) = R + \lambda R_s \left[\left(1 + \frac{R^2}{R_s^2} \right)^{-n} - 1 \right], \tag{11}$$

where n and λ are model parameters, and R_s is determined by the present observational data, namely, the ratio R_s/H_0^2 is well fit by a simple power-law $R_s/H_0^2 = c_n \lambda^{-p_n}$ with $(n, c_n, p_n) = (2, 4.16, 0.953)$, $(3, 4.12, 0.837)$, and $(4, 4.74, 0.702)$, respectively[5].

From Eq. (5), the de Sitter curvature is given by

$$\alpha(r) \equiv r + 2\lambda \left[\frac{1 + (n+1)r^2}{(1+r^2)^{n+1}} - 1 \right] = 0, \tag{12}$$

where $r \equiv R_1/R_s$. It is obvious that the Minkowski space, $r = 0$, is one of the solutions. We denote the other positive solutions for $\alpha(r) = 0$ as $r_a \equiv R_{1a}/R_s$ and $r_b \equiv R_{1b}/R_s$. We can estimate r_a and r_b by considering limiting cases. For $r \ll 1$, $\alpha(r) \simeq r[1 - 2\lambda(n+1)^2 r^3]$, and for $r \gg 1$, $\alpha(r) \simeq r - 2\lambda$. Therefore, for large n and λ the de Sitter solutions are given by $r = r_a \simeq [2\lambda(n+1)^2]^{-1/3}$ and $r = r_b \simeq 2\lambda$. Numerical analysis shows that this approximation is enough close to the exact answer even for $n = 2$ and $\lambda = 3$.

Once one obtained the de Sitter solutions, one can check their stability and oscillatory behaviour around them by using the stability condition and the oscillation condition derived in Eq. (7) and (8),

$$\beta(r) \equiv \frac{(1+r^2)[(1+r^2)^{n+1} - 2n\lambda r]}{2n\lambda[(2n+1)r^2 - 1]} - r > 0, \tag{13}$$

$$\gamma(r) \equiv \frac{(1+r^2)[(1+r^2)^{n+1} - 2n\lambda r]}{2n\lambda[(2n+1)r^2 - 1]} - \frac{25}{16} r > 0. \tag{14}$$

Since $\gamma(r) = \beta(r) - 9r/16$, there is no oscillation for the unstable de Sitter state, as it should be. From these criteria, we note that $r = r_a$ and r_b are unstable and stable, respectively.

For fixed n and various values of λ, we obtain λ_β and λ_γ as roots of $\beta(r_b) = 0$ and $\gamma(r_b) = 0$ respectively. Now the whole range of λ can be divided into 3 regions $\lambda < \lambda_\beta$, $\lambda_\beta < \lambda < \lambda_\gamma$, and $\lambda > \lambda_\gamma$, in which the de Sitter solution $r = r_b$ is stable with oscillations, stable without oscillations, and unstable correspondingly. Although for the most of the parameters values the stable de Sitter solution with oscillations is realized, there exists a parameter region corresponding to the stable de Sitter solution

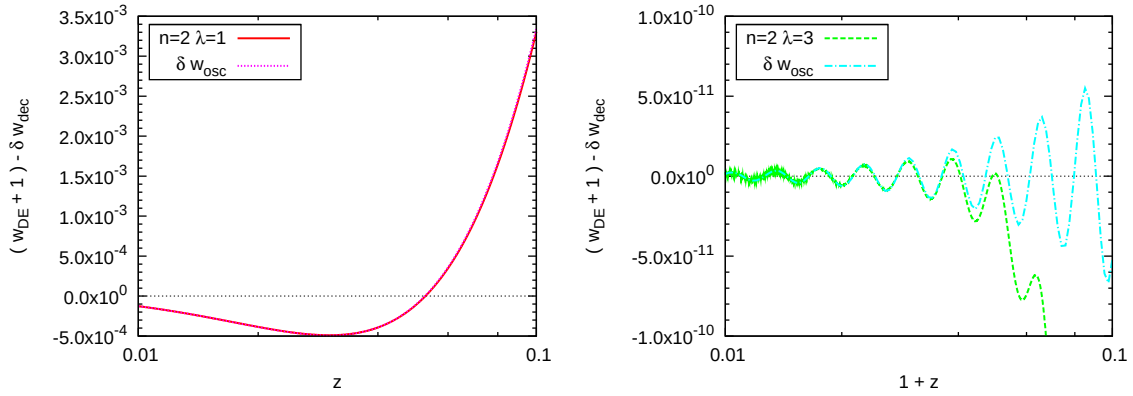

Figure 2: Numerical results for $(1+w)-\delta w_{\rm dec}$ using the analytic solution for $\delta w_{\rm osc}$.

without oscillations. Fig. 1 suggests that such parameter regions are $0.944<\lambda<0.970$, $0.726<\lambda<0.744$ and $0.608<\lambda<0.622$ for $n=2,\ 3$ and 4 respectively.

We integrate the evolution equation numerically. The initial condition is taken to be the same as in the ΛCDM model at $z=10$. The present time is identified as the moment when $\Omega_m=0.27$. Fig. 2 depicts oscillations of the EoS parameter for $n=2$ and $\lambda=1,\ 3$. We subtract $\delta w_{\rm dec}$ and present $\delta w_{\rm osc}$ using the analytic solution for it.

4 Conclusion

We have considered future oscillations of the effective EoS parameter $w_{\rm DE}$ for dark energy in $f(R)$ gravity around the phantom divide $w_{DE}=-1$. They occur due to scalaron oscillations around the future stable de Sitter solution in the first order of perturbations theory. We have derived the analytical expression, Eq. (8), for the existence of an infinite number of such oscillations. There are two types of models which correspond to stable de Sitter solutions with and without oscillations. An analytic solution for the EoS perturbation $\delta w_{\rm DE}$ is obtained which contains a monotonically decaying part $\delta w_{\rm dec}$ and a damped oscillatory part $\delta w_{\rm osc}$. This is confirmed by numerical calculations for a specific viable cosmological $f(R)$ model.

References

[1] W. Hu and I. Sawicki, Phys. Rev. D **76**, 064004 (2007) [arXiv:0705.1158].

[2] S. A. Appleby and R. A. Battye, Phys. Lett. B **654**, 7 (2007) [arXiv:0705.3199].

[3] A. A. Starobinsky, JETP Lett. **86**, 157 (2007) [arXiv:0706.2041].

[4] A. A. Starobinsky, Phys. Lett. B **91** (1980) 99.

[5] H. Motohashi, A. A. Starobinsky and J. Yokoyama, Prog. Theor. Phys. **123**, 887 (2010) [arXiv:1002.1141].

[6] H. Motohashi, A. A. Starobinsky and J. Yokoyama, Int. J. Mod. Phys. D **18**, 1731 (2009) [arXiv:0905.0730].

[7] H. Motohashi, A. A. Starobinsky and J. Yokoyama, Prog. Theor. Phys. **124**, 541 (2010) [arXiv:1005.1171].

[8] K. Bamba, C. Q. Geng and C. C. Lee, JCAP **1011**, 001 (2010) [arXiv:1007.0482].

Construction of gauge-invariant variables for linear-order metric perturbations on some background spacetimes

Kouji Nakamura[1]

Optical and Infrared Astronomy Division, National Astronomical Observatory of Japan, 2-21-1, Osawa, Mitaka, Tokyo 181-8588, Japan

Abstract

Gauge-invariant treatments of general-relativistic higher-order perturbations on generic background spacetime is proposed. We show the fact that the linear-order metric perturbation is decomposed into gauge-invariant and gauge-variant parts, which was the important premise of this general framework. This means that the development the higher-order gauge-invariant perturbation theory on generic background spacetime is possible.

1 Introduction

Perturbation theories are powerful techniques in many area of physics and lead physically fruitful results. In particular, in general relativity, the construction of exact solutions is not so easy and known exact solutions are often too idealized, though there are many known exact solutions to the Einstein equation. Furthermore, in natural phenomena, there always exist "fluctuations". To describe this, the *linear* perturbation theories around some background spacetime are developed, and are used to describe fluctuations of our universe, gravity of stars, and gravitational waves from strongly gravitating sources.

Besides the development of the general-relativistic linear-order perturbation theory, higher-order general-relativistic perturbations also have very wide applications, for example, cosmological perturbations, black hole perturbations, and perturbation of a neutron star. In spite of these applications, there is a delicate issue in general-relativistic perturbations, which is called *gauge issue*. General relativity is based on general covariance. and this general covariance, the *gauge degree of freedom*, which is an unphysical degree of freedom of perturbations, arises in general-relativistic perturbations. To obtain physical results, we have to fix this gauge degree of freedom or to treat some invariant quantities. This situation becomes more complicated in higher-order perturbations. For this reason, it is worthwhile to investigate higher-order gauge-invariant perturbation theory from a general point of view.

According to this motivation, the general framework of higher-order general-relativistic gauge-invariant perturbation theory has been discussed[3, 4] and applied to cosmological perturbations[1, 2]. This framework is based on a conjecture (Conjecture 1 below) which roughly states that *we have already known the procedure to find gauge-invariant variables for a linear-order metric perturbations*. The main purpose of this article is to give the outline of a proof of this conjecture.

2 General framework of the higher-order gauge-invariant perturbation theory

In any perturbation theory, we always treat two spacetime manifolds. One is the physical spacetime $(\mathcal{M}, \bar{g}_{ab})$, which is our nature itself, and we want to describe $(\mathcal{M}, \bar{g}_{ab})$ by perturbations. The other is the background spacetime $(\mathcal{M}_0, g_{ab})$, which is prepared as a reference to calculate perturbations by us. We note that these two spacetimes are distinct.

Further, in any perturbation theory, we write equations for the perturbation of the variable Q like

$$Q(\text{“}p\text{”}) = Q_0(p) + \delta Q(p). \tag{1}$$

[1]Email address: kouji.nakamura@nao.ac.jp

Equation (1) gives a relation between variables on different manifolds. Actually, $Q(\text{“}p\text{”})$ in Eq. (1) is a variable on $\mathcal{M}$, while $Q_0(p)$ and $\delta Q(p)$ are variables on $\mathcal{M}_0$. Further, since regard Eq. (1) as a field equation, this is an implicit assumption of the existence of a point identification map $\mathcal{M}_0 \to \mathcal{M} : p \in \mathcal{M}_0 \mapsto \text{“}p\text{”} \in \mathcal{M}$. This identification map is a *gauge choice* in perturbation theories[5].

To develop this understanding of the “gauge”, we introduce an infinitesimal parameter λ and $(n+1)+1$-dimensional manifold $\mathcal{N} = \mathcal{M} \times \mathbb{R}$ ($n+1 = \dim \mathcal{M}$) so that $\mathcal{M}_0 = \mathcal{N}|_{\lambda=0}$ and $\mathcal{M} = \mathcal{M}_\lambda = \mathcal{N}|_{\mathbb{R}=\lambda}$. On $\mathcal{N}$, the gauge choice is regarded as a diffeomorphism $\mathcal{X}_\lambda : \mathcal{N} \to \mathcal{N}$ such that $\mathcal{X}_\lambda : \mathcal{M}_0 \to \mathcal{M}_\lambda$. Further, we introduce a gauge choice $\mathcal{X}_\lambda$ as an exponential map with a generator ${}^{\mathcal{X}}\eta^a$ which is chosen so that its integral curve in $\mathcal{N}$ is transverse to each $\mathcal{M}_\lambda$ everywhere on $\mathcal{N}$. Points lying on the same integral curve are regarded as the “same” by the gauge choice $\mathcal{X}_\lambda$.

The first- and the second-order perturbations of the variable Q on $\mathcal{M}_\lambda$ are defined by the pulled-back $\mathcal{X}_\lambda^* Q$ on $\mathcal{M}_0$ induced by $\mathcal{X}_\lambda$, and expanded as

$$\mathcal{X}_\lambda^* Q = Q_0 + \lambda \, \pounds_{{}^{\mathcal{X}}\eta} Q\big|_{\mathcal{M}_0} + \frac{1}{2}\lambda^2 \, \pounds^2_{{}^{\mathcal{X}}\eta} Q\Big|_{\mathcal{M}_0} + O(\lambda^3), \tag{2}$$

$Q_0 = Q|_{\mathcal{M}_0}$ is the background value of Q and all terms in Eq. (2) are evaluated on $\mathcal{M}_0$. Since Eq. (2) is just the perturbative expansion of $\mathcal{X}_\lambda^* Q_\lambda$, the first- and the second-order perturbations of Q are given by ${}^{(1)}_{\mathcal{X}}Q := \pounds_{{}^{\mathcal{X}}\eta} Q\big|_{\mathcal{M}_0}$ and ${}^{(2)}_{\mathcal{X}}Q := \pounds^2_{{}^{\mathcal{X}}\eta} Q\Big|_{\mathcal{M}_0}$, respectively.

When we have two gauge choices $\mathcal{X}_\lambda$ and $\mathcal{Y}_\lambda$ with the generators ${}^{\mathcal{X}}\eta^a$ and ${}^{\mathcal{Y}}\eta^a$, respectively, and when these generators have the different tangential components to each $\mathcal{M}_\lambda$, $\mathcal{X}_\lambda$ and $\mathcal{Y}_\lambda$ are regarded as *different gauge choices*. The *gauge-transformation* is regarded as the change of the gauge choice $\mathcal{X}_\lambda \to \mathcal{Y}_\lambda$, which is given by the diffeomorphism $\Phi_\lambda := (\mathcal{X}_\lambda)^{-1} \circ \mathcal{Y}_\lambda : \mathcal{M}_0 \to \mathcal{M}_0$. The diffeomorphism Φ_λ does change the point identification. Φ_λ induces a pull-back from the representation $\mathcal{X}_\lambda^* Q_\lambda$ to the representation $\mathcal{Y}_\lambda^* Q_\lambda$ as $\mathcal{Y}_\lambda^* Q_\lambda = \Phi_\lambda^* \mathcal{X}_\lambda^* Q_\lambda$. From general arguments of the Taylor expansion, the pull-back Φ_λ^* is expanded as

$$\mathcal{Y}_\lambda^* Q_\lambda = \mathcal{X}_\lambda^* Q_\lambda + \lambda \pounds_{\xi_{(1)}} \mathcal{X}_\lambda^* Q_\lambda + \frac{1}{2}\lambda \left(\pounds_{\xi_{(2)}} + \pounds^2_{\xi_{(1)}} \right) \mathcal{X}_\lambda^* Q_\lambda + O(\lambda^3), \tag{3}$$

where $\xi^a_{(1)}$ and $\xi^a_{(2)}$ are the generators of Φ_λ. From Eqs. (2) and (3), each order gauge-transformation is given as

$${}^{(1)}_{\mathcal{Y}}Q - {}^{(1)}_{\mathcal{X}}Q = \pounds_{\xi_{(1)}} Q_0, \quad {}^{(2)}_{\mathcal{Y}}Q - {}^{(2)}_{\mathcal{X}}Q = 2\pounds_{\xi_{(1)}} {}^{(1)}_{\mathcal{X}}Q + \left\{ \pounds_{\xi_{(2)}} + \pounds^2_{\xi_{(1)}} \right\} Q_0. \tag{4}$$

We also employ the *order by order gauge invariance* as a concept of gauge invariance[2]. We call the kth-order perturbation ${}^{(p)}_{\mathcal{X}}Q$ is gauge invariant iff ${}^{(k)}_{\mathcal{X}}Q = {}^{(k)}_{\mathcal{Y}}Q$ for any gauge choice $\mathcal{X}_\lambda$ and $\mathcal{Y}_\lambda$.

Based on the above set up, we proposed a procedure to construct gauge-invariant variables of higher-order perturbations[3]. First, we expand the metric on the physical spacetime $\mathcal{M}_\lambda$, which is pulled back to the background spacetime $\mathcal{M}_0$ through a gauge choice $\mathcal{X}_\lambda$ as $\mathcal{X}_\lambda^* \bar{g}_{ab} = g_{ab} + \lambda {}_{\mathcal{X}}h_{ab} + \frac{\lambda^2}{2} {}_{\mathcal{X}}l_{ab} + O^3(\lambda)$. Although this expression of metric perturbations depends entirely on the gauge choice $\mathcal{X}_\lambda$, henceforth, we do not explicitly express the index of the gauge choice $\mathcal{X}_\lambda$ in the expression if there is no possibility of confusion. The important premise of our proposal was the following conjecture[3] for h_{ab} :

Conjecture 1. *For a second-rank tensor h_{ab}, whose gauge transformation is given by (4), there exist a tensor $\mathcal{H}_{ab}$ and a vector X^a such that h_{ab} is decomposed as*

$$h_{ab} =: \mathcal{H}_{ab} + \pounds_X g_{ab}, \tag{5}$$

where $\mathcal{H}_{ab}$ and X^a are transformed as

$${}_{\mathcal{Y}}\mathcal{H}_{ab} - {}_{\mathcal{X}}\mathcal{H}_{ab} = 0, \qquad {}_{\mathcal{Y}}X^a - {}_{\mathcal{X}}X^a = \xi^a_{(1)} \tag{6}$$

under the gauge transformation (4), respectively.

We call $\mathcal{H}_{ab}$ and X^a are the *gauge-invariant part* and the *gauge-variant part* of h_{ab}, respectively.

Although Conjecture 1 is nontrivial on generic background spacetime, once we accept this conjecture, we can always find gauge-invariant variables for higher-order perturbations[3]. Using Conjecture 1, the second-order metric perturbation l_{ab} is decomposed as

$$l_{ab} =: \mathcal{L}_{ab} + 2\pounds_X h_{ab} + \left(\pounds_Y - \pounds_X^2\right) g_{ab}, \tag{7}$$

where ${}^{\mathcal{Y}}\mathcal{L}_{ab} - {}^{\mathcal{X}}\mathcal{L}_{ab} = 0$ and ${}^{\mathcal{Y}}Y^a - {}^{\mathcal{X}}Y^a = \xi^a_{(2)} + [\xi_{(1)}, X]^a$. Furthermore, using the first- and second-order gauge-variant parts, X^a and Y^a, of the metric perturbations, gauge-invariant variables for an arbitrary tensor field Q other than the metric can be defined by

$${}^{(1)}\mathcal{Q} := {}^{(1)}Q - \pounds_X Q_0, \quad {}^{(2)}\mathcal{Q} := {}^{(2)}Q - 2\pounds_X {}^{(1)}Q - \left\{\pounds_Y - \pounds_X^2\right\} Q_0. \tag{8}$$

These definitions (8) also imply that any perturbation of first and second order is always decomposed into gauge-invariant and gauge-variant parts. These decomposition formulae are universal[2, 4]. Further, when we impose order by order equations for the perturbations, any perturbative equations are automatically given in gauge-invariant form[2, 4].

Thus, based only on Conjecture 1, we have developed the general framework of second-order general relativistic perturbation theory without detail information of the background metric g_{ab}.

3 Decomposition of the linear-order metric perturbation

Now, we show the outline of a proof of Conjecture 1. To do this, we only consider the background spacetimes which admit ADM decomposition. Therefore, the background spacetime $\mathcal{M}_0$ considered here is $n+1$-dimensional spacetime which is described by the direct product $\mathbb{R}\times\Sigma$. Here, $\mathbb{R}$ is a time direction and Σ is the spacelike hypersurface ($\dim\Sigma = n$). The background metric g_{ab} is given as

$$g_{ab} = -\alpha^2 (dt)_a (dt)_b + q_{ij}(dx^i + \beta^i dt)_a (dx^j + \beta^j dt)_b. \tag{9}$$

In this article, we only consider the case where $\alpha = 1$ and $\beta^i = 0$, for simplicity. The proof shown here is extended to general case[7].

To consider the decomposition (5) of h_{ab}, first, we consider the components of the metric h_{ab} as $h_{ab} =: h_{tt}(dt)_a(dt)_b + 2h_{ti}(dt)_{(a}(dx^i)_{b)} + h_{ij}(dx^i)_a(dx^j)_b$. Under the gauge-transformation (4), these components $\{h_{tt}, h_{ti}, h_{ij}\}$ are transformed as

$${}^{\mathcal{Y}}h_{tt} - {}^{\mathcal{X}}h_{tt} = 2\partial_t\xi_t, \quad {}^{\mathcal{Y}}h_{ti} - {}^{\mathcal{X}}h_{ti} = \partial_t\xi_i + D_i\xi_t + 2K^j{}_i\xi_j, \quad {}^{\mathcal{Y}}h_{ij} - {}^{\mathcal{X}}h_{ij} = 2D_{(i}\xi_{j)} + 2K_{ij}\xi_t. \tag{10}$$

where K_{ij} is the extrinsic curvature of Σ and D_i is the covariant derivative associate with the metric q_{ij} ($D_i q_{jk} = 0$). In our case, $K_{ij} = -\frac{1}{2}\partial_t q_{ij}$. Inspecting gauge-transformation rules (10), we introduce a new symmetric tensor $\hat{H}_{ab}$ whose components are given by $\hat{H}_{tt} := h_{tt}$, $\hat{H}_{ti} := h_{ti}$, $\hat{H}_{ij} := h_{ij} - 2K_{ij}X_t$. Here, we assume the existence of the variable X_t whose gauge-transformation rule is given by ${}^{\mathcal{Y}}X_t - {}^{\mathcal{X}}X_t = \xi_t$. This assumption is confirmed later soon. Since the components $\hat{H}_{ti}$ and $\hat{H}_{ij}$ are a vector and a symmetric tensor on Σ, respectively, $\hat{H}_{ti}$ and $\hat{H}_{ij}$ are decomposed as[6]

$$\hat{H}_{ti} = D_i h_{(VL)} + h_{(V)i}, \quad D^i h_{(V)i} = 0, \tag{11}$$

$$\hat{H}_{ij} = \frac{1}{n} q_{ij} h_{(L)} + 2\left(D_{(i}h_{(TV)j)} - \frac{1}{n} q_{ij} D^l h_{(TV)l}\right) + h_{(TT)ij}, \quad D^i h_{(TT)ij} = 0, \tag{12}$$

$$h_{(TV)i} = D_i h_{(TVL)} + h_{(TVV)i}, \quad D^i h_{(TVV)i} = 0. \tag{13}$$

The one-to-one correspondence between $\{\hat{H}_{ti},\ \hat{H}_{ij}\}$ and $\{h_{(VL)}, h_{(V)i}, h_{(L)}, h_{(TVL)}, h_{(TVV)i}, h_{(TT)ij}\}$ is guaranteed by the existence of the Green functions of operators $\Delta := D^i D_i$ and $\mathcal{D}^{ij} := q^{ij}\Delta + \left(1 - \frac{2}{n}\right) D^i D^j + {}^{(n)}R^{ij}$, where ${}^{(n)}R^{ij}$ is the Ricci curvature on Σ. Here, we assume their existence. Gauge-transformation rules for $\{h_{tt},\ h_{(VL)},\ h_{(V)i},\ h_{(L)},\ h_{(TVL)},\ h_{(TVV)i},\ h_{(TT)ij}\}$ are summarized as

$${}^{\mathcal{Y}}h_{tt} - {}^{\mathcal{X}}h_{tt} = 2\partial_t\xi_t, \quad {}^{\mathcal{Y}}h_{(TT)ij} - {}^{\mathcal{X}}h_{(TT)ij} = 0, \tag{14}$$

$${}^{\mathcal{Y}}h_{(VL)} - {}^{\mathcal{X}}h_{(VL)} = \partial_t\xi_{(L)} + \xi_t + \Delta^{-1}\left[2D_i\left(K^{ij}D_j\xi_{(L)}\right) + D^k K\xi_{(V)k}\right], \tag{15}$$

$${}^{\mathcal{Y}}h_{(V)i} - {}^{\mathcal{X}}h_{(V)i} = \partial_t\xi_{(V)i} + 2K^j{}_i D_j\xi_{(L)} + 2K^j{}_i\xi_{(V)j} - D_i\Delta^{-1}\left[2D_i\left(K^{ij}D_j\xi_{(L)}\right) + D^k K\xi_{(V)k}\right], \tag{16}$$

$${}^{\mathcal{Y}}h_{(L)} - {}^{\mathcal{X}}h_{(L)} = 2D^i\xi_i, \quad {}^{\mathcal{Y}}h_{(TVL)} - {}^{\mathcal{X}}h_{(TVL)} = \xi_{(L)}, \quad {}^{\mathcal{Y}}h_{(TVV)l} - {}^{\mathcal{X}}h_{(TVV)l} = \xi_{(V)l}, \quad . \tag{17}$$

where we decompose $\xi_i =: D_i\xi_{(L)} + \xi_{(V)i}$, $D^i\xi_{(V)i} = 0$.

We first find the variable X_t in the definition of $\hat{H}_{ab}$. From the above gauge-transformation rules, we see that the combination $X_t := h_{(VL)} - \partial_t h_{(TVL)} - \Delta^{-1}\left[2D_i\left(K^{ij}D_j h_{(TVL)}\right) + D^k K h_{(TVV)k}\right]$ satisfy ${}_{\mathcal{Y}}X_t - {}_{\mathcal{X}}X_t = \xi_t$. We also find the variable $X_i := h_{(TV)i} = D_i h_{(TVL)} + h_{(TVV)i}$ satisfy the gauge-transformation rule ${}_{\mathcal{Y}}X_i - {}_{\mathcal{X}}X_i = \xi_i$.

Inspecting gauge-transformation rules (14)–(17) and using the variables X_t and X_i, we find gauge-invariant variables as follows:

$$
\begin{aligned}
-2\Phi &:= h_{tt} - 2\partial_t\hat{X}_t, \quad -2n\Psi := h_{(L)} - 2D^i\hat{X}_i, \quad \chi_{ij} := h_{(TT)ij}, && (18)\\
\nu_i &:= h_{(V)i} - \partial_t h_{(TVV)i} - 2K^j{}_i\left(D_j h_{(TVL)} + h_{(TVV)j}\right)\\
&\quad + D_i\Delta^{-1}\left[2D_i\left(K^{ij}D_j h_{(TVL)}\right) + D^k K h_{(TVV)k}\right]. && (19)
\end{aligned}
$$

Actually, it is straightforward to confirm the gauge-invariance of these variables. In terms of the variables Φ, Ψ, ν_i, χ_{ij}, X_t, and X_i, original components of h_{ab} is given by

$$
\begin{aligned}
h_{tt} &= -2\Phi + 2\partial_t X_t, \quad h_{ti} = \nu_i + D_i X_t + \partial_t X_i + 2K^j{}_i X_j, && (20)\\
h_{ij} &= -2\Psi q_{ij} + \chi_{ij} + D_i X_j + D_j X_i + 2K_{ij}X_t. && (21)
\end{aligned}
$$

Comparing Eq. (5), a natural choice of $\mathcal{H}_{ab}$ and X_a are

$$
\mathcal{H}_{ab} = -2\Phi(dt)_a(dt)_b + 2\nu_i(dt)_{(a}(dx^i)_{b)} + (-2\Psi q_{ij} + \chi_{ij})(dx^i)_a(dx^i)_b, \quad X_a = X_t(dt)_a + X_i(dx^i). \quad (22)
$$

These show that the linear-order metric perturbation h_{ab} is decomposed into the form Eq. (5).

4 Discussion

In our proof, we assumed the existence of the Green functions for the derivative operators Δ and $\mathcal{D}^{ij}$. This implies that we have ignored the modes which belong to the kernel of these derivative operators. To includes these modes into our consideration, different treatments of perturbations will be necessary. We call this problem as *zero-mode problem*. We leave this zero-mode problem as a future work.

Although this zero-mode problem should be resolved, we confirmed the important premise of our general framework of second-order gauge-invariant perturbation theory on generic background spacetime. This means that we have the possibility of applications of our framework for the second-order gauge-invariant perturbation theory to perturbations on generic background spacetime. Furthermore, the similar development will be also possible for the any order perturbation in two-parameter case[3]. Thus, we may say that wide applications of our gauge-invariant perturbation theory are opened. We also leave these developments as future works.

The author deeply acknowledged to Professor Masa-Katsu Fujimoto in National Astronomical Observatory of Japan for his various support.

References

[1] K. Nakamura, Phys. Rev. D **74** (2006), 101301(R); Prog. Theor. Phys. **117** (2007), 17; Prog. Theor. Phys. **121** (2009), 1321; Advances in Astronomy, **2010** (2010), 576273.

[2] K. Nakamura, Phys. Rev. D **80** (2009), 124021.

[3] K. Nakamura, Prog. Theor. Phys. **110**, (2003), 723.

[4] K. Nakamura, Prog. Theor. Phys. **113** (2005), 481.

[5] J. M. Stewart and M. Walker, Proc. R. Soc. London A **341** (1974), 49; J. M. Stewart, Class. Quantum Grav. **7** (1990), 1169; *Advanced General Relativity* (Cambridge University Press, Cambridge, 1991).

[6] J. W. York, Jr. J. Math. Phys. **14** (1973), 456; Ann. Inst. H. Poincaré **21** (1974), 319.

[7] K. Nakamura, in preparation.

CMB Polarization in Einstein-Aether Theory[1]

Masahiro Nakashima[2(a,b)] and Tsutomu Kobayashi[3(b)]

[(a)] *Department of Physics, Graduate School of Science, The University of Tokyo, Tokyo 113-0033, Japan*
[(b)] *Research Center for the Early Universe (RESCEU), Graduate School of Science, The University of Tokyo, Tokyo 113-0033, Japan*

Abstract

We study the impact of modifying the vector sector of gravity on the CMB polarization. We employ the Einstein-aether theory as a concrete example. The Einstein-aether theory admits dynamical vector perturbations generated during inflation, leaving imprints on the CMB polarization. We derive the perturbation equations of the aether vector field in covariant formalism and compute the CMB B-mode polarization using the modified CAMB code. It is found that the amplitude of the B-mode signal from the aether field can surpass the one from the inflationary gravitational waves. The shape of the spectrum is clearly understood in an analytic way using the tight coupling approximation.

Motivated mainly by the mystery of the dark components of the Universe, modification of gravity law from standard general relativity (GR) has been explored much. It is commonly made by adding an extra scalar degree of freedom as in $f(R)$ theories. It is also possible to modify the spin-2 sector as in massive gravity and bi-gravity theories. In this paper, we are going to consider a hypothetical *vector* degree of freedom of gravity. Specifically, we shall focus on the Einstein-aether (EA) theory proposed by Jacobson and Mattingly [2], in which a fixed norm vector field with a Lorentz-violating vacuum expectation value takes part in the gravitational interaction.

The purpose of the present paper is to clarify the impact of the aether vector field on the CMB polarization. The CMB polarization arises from all the three types of cosmological perturbations, i.e., scalar, vector, and tensor perturbations. Among them, the vector perturbations most effectively generate the B-mode polarization [3], though the effect has been less investigated because the vector mode decays unless sourced, *e.g.*, by topological defects or the neutrino anisotropic stress [4]. Modifying the vector sector of gravity would add yet another possibility of producing vector perturbations, leaving a unique signature in the CMB polarization due to nontrivial dynamics of the aether field.

The action of the EA theory is given by

$$\mathcal{S}=\frac{1}{2\kappa}\int d^4x\sqrt{-g}[\mathcal{R}-c_1\nabla_aA^b\nabla^aA_b-c_2(\nabla_bA^b)^2-c_3\nabla_aA^b\nabla_bA^a \\ -c_4A^aA^b\nabla_aA^c\nabla_bA_c]+\lambda(A_bA^b-1)]+\mathcal{S}_m, \tag{1}$$

where $\kappa=8\pi G$, $\mathcal{R}$ is the Ricci scalar, A_a is the aether field, and $\mathcal{S}_m$ is the action of ordinary matter. Variation with respect to A^a yields the equation of motion for the aether and variation with respect to the Lagrange multiplier λ gives the fixed norm constraint, $A_aA^a=1$. In the rest of the paper we use the following abbreviations: $c_{13}=c_1+c_3, c_{14}=c_1+c_4, \alpha=c_1+3c_2+c_3$.

To describe background cosmology and the evolution of vector perturbations, we employ the covariant equations obtained by the method of $3+1$ decomposition. We begin with splitting physical quantities with respect to observer's 4-velocity u^a. Following the usual procedure, the projection tensor is defined as $h_{ab}:=g_{ab}-u_au_b$. We define time derivative as $\dot{T}^{a\cdots}_{b\cdots}:=u^c\nabla_cT^{a\cdots}_{b\cdots}$ and covariant spatial derivative as $D^aT^{b\cdots}_{c\cdots}:=h^a_ih^b_j\cdots h^k_c\cdots\nabla^iT^{j\cdots}_{k\cdots}$. The energy-momentum tensor for each matter component and ∇_au_b are expressed respectively as

$$T^{(i)}_{ab}=\rho^{(i)}u_au_b-p^{(i)}h_{ab}+2q^{(i)}_{(a}u_{b)}+\pi^{(i)}_{ab}, \quad \nabla_au_b=\frac{1}{3}\theta h_{ab}+\sigma_{ab}+\omega_{ab}-u_a\dot{u}_b. \tag{2}$$

[1] Complete details will be presented in a longer paper [1].
[2] Email address: nakashima@resceu.s.u-tokyo.ac.jp
[3] Email address: tsutomu@resceu.s.u-tokyo.ac.jp

The energy-momentum tensor for the aether, $T^{(A)}_{ab}$, is also written in the same form as above. The expansion θ may be written as $\theta = 3\dot{S}/S$, where S is the averaged scale factor.

At zeroth order, $A^a = u^a$, so that the energy density and the pressure of the aether are given respectively by $\rho^{(A)} = \alpha\theta^2/6$ and $p^{(A)} = -\alpha(2\dot{\theta} + \theta^2)/6$. The Friedman equation is thus given by $3\mathcal{H}^2 = \kappa S^2\rho/(1-\alpha/2)$ where ρ is the total energy density of ordinary matter and we have introduced the conformal Hubble parameter, $\mathcal{H} := S\theta/3$. The background effect of the aether is just to rescale the gravitational constant κ.

Let us move on to the dynamics of vector perturbations. We choose u_a to be hypersurface orthogonal, so that $\dot{u}_b = 0$ at linear order. At this order, the aether field can be written as $A_b = u_b + D_bV^{(s)} + V_b$, where $V^{(s)}$ corresponds to a scalar perturbation which we do not consider in this paper, while V_b a vector perturbation that satisfies $D_bV^b = 0$. Each perturbation variable can be expanded using the transverse eigenfunctions $Q^{\pm}_{a\cdots}$: $V_a = \sum VQ^{\pm}_a$, $q^{(i)}_a = \sum q^{(i)}Q^{\pm}_a$, $\sigma_{ab} = \sum(k/S)\sigma Q^{\pm}_{ab}$, and $\pi^{(i)}_{ab} = \sum\Pi^{(i)}Q^{\pm}_{ab}$, where k is the eigenvalue. It is convenient to write the relevant equations in terms of the coefficient functions V, $q^{(i)}$, ...

From the equation of motion for the aether, we obtain the evolution equation for V:

$$c_{14}\left[V'' + 2\mathcal{H}V' + \left(\mathcal{H}^2 + \mathcal{H}'\right)V\right] + \alpha\left(\mathcal{H}^2 - \mathcal{H}'\right)V + c_1k^2V = -\frac{c_{13}}{2}k^2\sigma. \tag{3}$$

This shows that the fluctuation of the aether obeys the wave equation which is similar to the evolution equation for cosmological tensor perturbations. The crucial difference is the effective mass term which is dependent on the expansion rate $\mathcal{H}$ and the model parameters. The fluctuation of the aether leads to the effective heat-flux vector $q^{(A)}_a = -c_{13}D^b[\sigma_{ab} + D_{(a}V_{b)}]$, which gives rise to the additional contribution to the momentum constraint equation. The momentum constraint under the influence of the aether is thus given by

$$k^2\sigma = \frac{1}{1+c_{13}}\left(2\kappa S^2\sum_i q^{(i)} - c_{13}k^2V\right). \tag{4}$$

Here, $q^{(i)}$ is determined through the individual matter equations. In calculating the CMB power spectrum we simultaneously solve the equations of motion for other ordinary matter and the multipole moment equations for photons and neutrinos, as well as the equations derived above.

We now fix the initial condition for each variable at the early radiation-dominant epoch. This is done by a series expansion in terms of the conformal time η, following [4], but now taking into account the presence of the aether. Neglecting the $\mathcal{O}(k^2)$ terms, the perturbed equation of motion for the aether can be solved to give

$$V = \mathcal{A}_k\eta^\nu\left[1 + \mathcal{O}(\eta)\right], \quad \nu := \frac{-1 + \sqrt{1 - 8\alpha/c_{14}}}{2}, \tag{5}$$

implying that V can grow on superhorizon scales. Here, we have dropped the decaying mode solution which is not regular at $\eta \to 0$. The coefficient $\mathcal{A}_k$ is determined from the primordial spectrum of the aether fluctuation [5]. Requiring that scalar isocurvature modes do not grow, we consider the range $0 \le \nu \le 1$ [5]. As for the other variables, the appropriate early time solutions are found to be

$$\sigma = -\frac{\nu^*}{\nu^* + 4R^*}\frac{c_{13}}{1+c_{13}}\mathcal{A}_k\eta^\nu, \quad q^{(\gamma)} = q^{(b)} = q^{(\nu)} = 0, \quad \frac{\Pi^{(\nu)}}{\rho^{(\nu)}} = -\frac{8}{15(1+\nu)}\frac{\nu^*}{\nu^* + 4R^*}\frac{c_{13}}{1+c_{13}}\mathcal{A}_k k\eta^{1+\nu}, \tag{6}$$

where we defined $R^* := [(1-\alpha/2)/(1+c_{13})]\rho^{(\nu)}/(\rho^{(\gamma)} + \rho^{(\nu)})$ and $\nu^* := (5/2)(1+\nu)(2+\nu)$, with the superscripts γ, b, and ν denoting photons, baryons, and neutrions, respectively.

In the AE theory, primordial vector perturbations are generated quantum mechanically during inflation. Once the inflation model and the reheating history are specified, one can determine the primordial spectrum of the vector perturbation and hence $\mathcal{A}_k$, as discussed in [5]. We separate the issue of the perturbation evolution during inflation from the subsequent evolution, and set simply $\mathcal{A}_k = \mathcal{A}_0k^{(n_v-3)/2}$ (*i.e.*, the primordial spectrum $\mathcal{P}_V \propto k^{n_v}$), where $\mathcal{A}_0$ is a constant.

We have completed the numerical calculation using all the ingredients derived above and the CAMB code [6] modified so as to incorporate the presence of the aether. An example of our numerical results

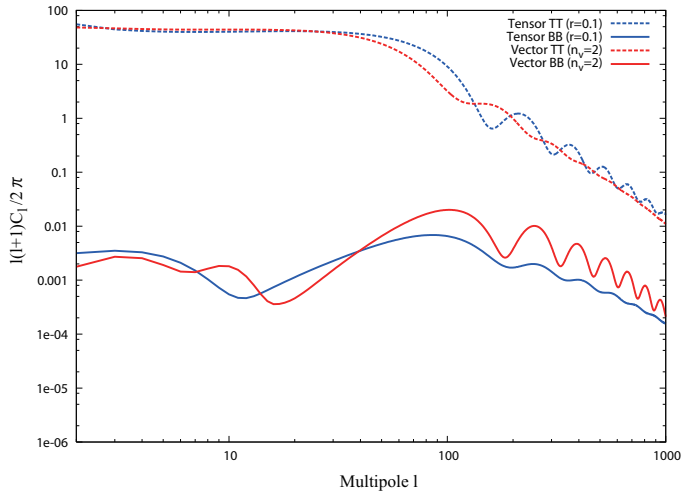

Figure 1: CMB B-mode polarization and temperature anisotropy power spectra in the EA theory. For comparison, those from the tensor perturbation in standard general relativity are also plotted in the case of the tensor-to-scalar ratio $r = 0.1$. In this figure, $c_1 = -0.2, c_{13} = -0.3, c_{14} = -\alpha = -0.2$, and dimensionless primordial power spectra are $\mathcal{P}_V \propto k^{n_v}$ and $\mathcal{P}_T \propto k^0$.

is presented in the Fig. 1. For comparison, we show contributions from inflationary gravitational waves in GR, assuming that the tensor-to-scalar ratio is given by $r = 0.1$. The amplitude $\mathcal{A}_0$ is adjusted so that the low-ℓ TT spectrum from the vector perturbation has the same magnitude as this primordial tensor contribution. We see in this case that the BB spectrum in the EA theory is larger than that from primordial tensor modes at $\ell \gtrsim 100$, and hence the B-mode is potentially detectable in future CMB observations aiming to detect $r = \mathcal{O}(0.1) - \mathcal{O}(0.01)$.

Let us try to understand the shape of the B-mode angular power spectrum C_ℓ^{BB} in the EA theory in an analytic way. We start with the integral solution for the moment B_ℓ^V of the B-mode polarization in the covariant formalism:

$$B_\ell^V(\eta_0) = -\frac{\ell-1}{\ell+1}\int^{\eta_0} d\eta \dot{\tau} e^{-\tau}\Psi_\ell(x)\zeta, \quad x = k(\eta_0 - \eta), \tag{7}$$

with $\Psi_\ell(x) = \ell j_\ell(x)/x$ and $\zeta = (3/4)I_2 - (9/2)E_2$. Here, $j_\ell(x)$ is a spherical Bessel function, τ is the optical depth, I_ℓ is the angular moment of the fractional photon density distribution, and E_ℓ is the moment of the E-mode polarization. Using the tight coupling approximation, we obtain

$$\zeta \simeq \frac{4k}{15\dot{\tau}}\sigma \simeq -\frac{4k}{15\dot{\tau}}\frac{c_{13}}{1+c_{13}}V \tag{8}$$

It turns out that ignoring $q^{(i)}$ in Eq. (4) is a good approximation. We thus arrive at [5]

$$V'' + 2\mathcal{H}V' + c_v^2 k^2 V + \left[\left(1+\frac{\alpha}{c_{14}}\right)\mathcal{H}^2 - \left(1-\frac{\alpha}{c_{14}}\right)\mathcal{H}'\right]V \simeq 0, \quad c_v^2 = \frac{c_1}{c_{14}}\left[1 - \frac{c_{13}^2}{2c_1(1+c_{13})}\right]. \tag{9}$$

On superhorizon scales we find $V \propto S^\nu$ in the radiation-dominant stage, as already derived, and $V \propto S^{\nu_m/2}$ with $\nu_m = (-3+\sqrt{1-24\alpha/c_{14}})/2$ in the matter-dominant stage. On subhorizon scale, V simply decays similarly to tensor perturbations, $V \propto S^{-1}$. These relations can be mapped into the wavenumber dependence of V at recombination ($\eta = \eta_{\rm rec}$) as $V \propto \mathcal{A}_k$ ($k < 1/c_v\eta_{\rm rec}$), $V \propto k^{-2-\nu_m}\mathcal{A}_k$ ($1/c_v\eta_{\rm rec} < k < 1/c_v\eta_{\rm eq}$), and $V \propto k^{-1-\nu}\mathcal{A}_k$ ($1/c_v\eta_{\rm eq} < k$), where $\eta_{\rm eq}$ refers to the radiation-matter equality time.

The CMB B-mode power spectrum is roughly expressed as $C_\ell^{BB} \sim \int \mathcal{P}_V(k) B_\ell^V B_\ell^V d\ln k$. Using the approximation $\dot{\tau}e^{-\tau} \simeq \delta(\eta - \eta_{\rm rec})$, $B_\ell^V(\eta_0)$ can be written as $B_\ell^V(\eta_0) \simeq (k/\dot{\tau})[c_{13}/(1+c_{13})]V(\eta_{\rm rec})\Psi_\ell[k(\eta_0 - \eta_{\rm rec})]$. ($\eta_0$ is the present time.) Since the projection factor $\Psi_\ell(x)$ has a peak at $\ell \simeq x$, the angular power spectrum reduces approximately to

$$C_\ell^{BB} \sim \left(\frac{V}{\mathcal{A}_k}\right)^2_{k=\ell/(\eta_0-\eta_{\rm rec})} \int k^{2+n_v}[\Psi_\ell(k(\eta_0 - \eta_{\rm rec}))]^2 d\ln k. \tag{10}$$

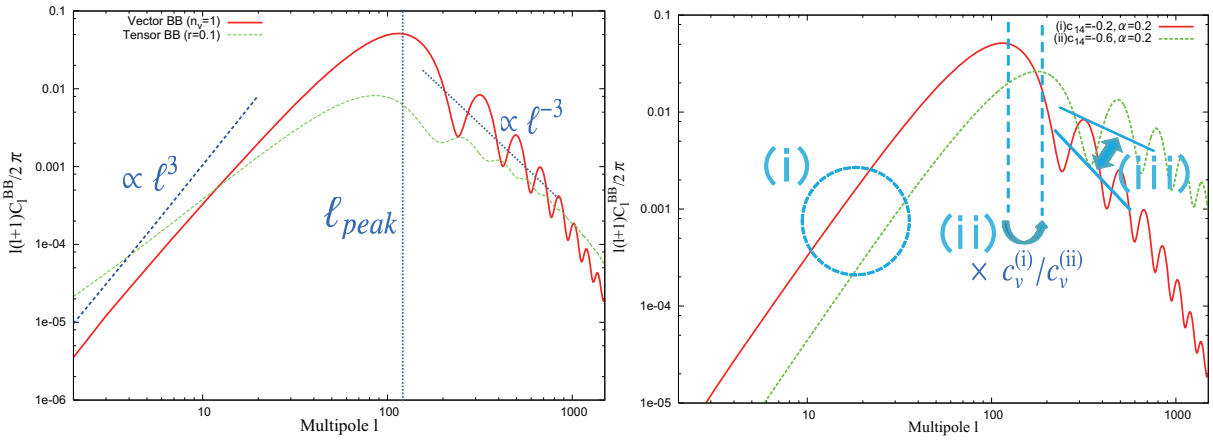

Figure 2: (a) Scaling for the illustrative case with $n_v = 1$ and $\alpha = -c_{14} = 0.2$. The other parameters are given by $c_{13} = -0.3$, and $c_1 = -0.1$; (b) Parameter dependence of the spectrum. In the two examples c_{14} is different while the other parameters are fixed as $n_v = 1$, $c_{13} = -0.3$, and $c_1 = -0.1$. The primordial amplitudes are arbitrary.

For example, for $n_v = 1$ and $c_{14} = -\alpha$, the above integral can be evaluated to give the scaling $\ell(\ell+1)C_\ell^{BB} \propto \ell^3$ ($\ell < \ell_{\rm rec} := (\eta_0 - \eta_{\rm rec})/c_v\eta_{\rm rec}$), ℓ^{-3} ($\ell_{\rm rec} < \ell < \ell_{\rm eq} := (\eta_0 - \eta_{\rm eq})/c_v\eta_{\rm eq}$), and ℓ^{-1} ($\ell_{\rm eq} < \ell$), showing a peak at $\ell_{\rm peak} \sim \ell_{\rm rec}$. This behavior can indeed be seen in Fig. 2(a), though the scaling at $\ell > \ell_{\rm eq}$ is hidden by the other effect and hence is not obvious. (Here, for comparison, the B-mode spectrum from tensor perturbations in standard GR are also plotted.)

We can also gain an understanding of how the shape of the angular power spectrum depends on the model parameters. From Fig. 2(b) one can confirm the following three things: (i) since the angular power spectrum on the largest scales $\ell < \ell_{\rm rec}$ depends only on the primordial spectrum, the plotted examples show the same scaling; (ii) the peak position is inversely proportional to the sound velocity of the aether vector perturbation c_v; (iii) the difference of the small scale scaling arises due to the difference of the growth rate of V on superhorizon scales. The detailed discussion on the analytic estimate will be provided in [1].

References

[1] M. Nakashima and T. Kobayashi, *to appear*.

[2] T. Jacobson and D. Mattingly Phys. Rev. D **64** (2001) 024028.

[3] W. Hu and M. White Phys. Rev. D **56** (1997) 596.

[4] A. Lewis Phys. Rev. D **70** (2004) 043518.

[5] C. Armendariz-Picon, N. F. Sierra and J. Garriga JCAP **1007** (2010) 010.

[6] A. Lewis, A. Challinor and A. Lasenby Astrophys. J. **538** 473 (2000).

Inflation from a Supersymmetric Axion Model

Masahiro Kawasaki[(a,b)], Naoya Kitajima[(a)] and Kazunori Nakayama[(c)]

[a] *Institute for Cosmic Ray Research, University of Tokyo, Kashiwa, Chiba 277-8582, Japan*
[b] *Institute for the Physics and Mathematics of the Universe, University of Tokyo, Kashiwa, Chiba 277-8568, Japan*
[c] *KEK Theory Center, Institute of Particle and Nuclear Studies, KEK, Tsukuba, Ibaraki 305-0801, Japan*

Abstract

We show that a supersymmetric axion model naturally induces a hybrid inflation with the waterfall field identified as a Peccei-Quinn scalar. The Peccei-Quinn scale is predicted to be around 10^{15}GeV for reproducing the large-scale density perturbation of the Universe. After the built-in late-time entropy-production process, the axion becomes a dark matter candidate. Several cosmological implications are discussed.

1 Introduction

The standard model in particle physics has succeeded to describe the physics below the electroweak scale. It is not, however, a complete theory because of the theoretical problems. One is the strong CP problem. Despite the expectation of the existence of the CP-violating θ-term in the Lagrangian, $\mathcal{L} = (\theta g_s^2/32\pi^2) G^a_{\mu\nu}\tilde{G}^{\mu\nu a}$ with $\theta \sim \mathcal{O}(1)$, experimentally it is constrained as $\theta \lesssim 10^{-10}$. This is solved by the Peccei-Quinn (PQ) mechanism [1, 2], in which the axion, pseudo-Nambu-Goldstone boson associated with the spontaneous breakdown of the global $\mathrm{U}(1)_{\mathrm{PQ}}$ symmetry, dynamically relaxes the θ to nearly zero. Another problem is the gauge hierarchy problem, which states that the huge difference between the weak scale and the grand unified theory scale requires unnatural fine tuning. In the framework of supersymmetry (SUSY), this problem does not arise. Thus it is well motivated that we consider the SUSY axion model.

In this letter we point out that inflation naturally takes place in the SUSY axion model [3]. It takes the form of hybrid inflation where the waterfall field is identified with the PQ scalar and the end of inflation is the PQ phase transition. The idea was already noticed in Ref. [4], but the discussion there was far from complete, considering developments on the SUSY hybrid inflation model thereafter [5]. Particularly, the PQ symmetry breaking scale, f_a, is determined as $f_a \sim 10^{15}$GeV by the condition that the cosmological density perturbation is in a correct magnitude. This seems to be too large, since the axion coherent oscillation might have abundance much larger than the dark matter. However, we point out that due to the post inflationary dynamics of the flat direction in the scalar potential, the axion is diluted, and it can take a role of dominant component of the dark matter. Therefore this model provides a simultaneous solution to the hierarchy and strong CP problems, inflation and dark matter in a simple and unified framework.

2 Model and cosmological implications

Our model is described by the following Kähler and superpotential,

$$K = |S|^2 + |\Psi|^2 + |\bar{\Psi}|^2, \tag{1}$$

$$W = \kappa S(\Psi\bar{\Psi} - f_a^2) + \lambda\Psi X\bar{X} + kSY\bar{Y} + W_0, \tag{2}$$

where S, Ψ and $\bar{\Psi}$ are gauge singlets, $X(\bar{X})$ and $Y(\bar{Y})$ have some gauge charges, and κ, λ and k are coupling constants, which are taken to be real and positive. Here we keep minimal Kähler potentials only, and effects of non-minimal terms will be discussed later. The constant term $W_0 (= m_{3/2}M_P^2$ where $m_{3/2}$ denotes the gravitino mass and M_P is the reduced Planck scale) ensures that the cosmological constant

	S	Ψ	$\bar{\Psi}$	X	$\bar{X}$	Y	$\bar{Y}$
$\mathrm{U}(1)_{\mathrm{PQ}}$	0	$+1$	-1	$-1/2$	$-1/2$	0	0
$\mathrm{U}(1)_R$	$+2$	0	0	$+1$	$+1$	0	0

Table 1: Charge assignments on the field content.

is nearly zero in the present Universe. This superpotential possesses a global $\mathrm{U}(1)_{\mathrm{PQ}}$ symmetry, which is anomalous at the quantum level, and also has the $\mathrm{U}(1)_R$ symmetry whose charge assignments are shown in Table. 1. After Ψ and $\bar{\Psi}$ obtain vacuum expectation values (VEV), this PQ symmetry is spontaneously broken and there appears a pseudo-Nambu-Goldstone boson, which dynamically cancels the strong CP phase and solves the strong CP problem.

This is nothing other than the SUSY version of the hadronic (or KSVZ) axion model [6], if X and $\bar{X}$ have color charge. In this case we can choose Y and $\bar{Y}$ as minimal SUSY standard model (MSSM) Higgses : $Y = H_u$ and $\bar{Y} = H_d$. For a certain choice of k, a sizable μ-term is generated after S gets a VEV, as we will see later.

It is also possible to choose X and $\bar{X}$ to be MSSM Higgses : $X = H_u, \bar{X} = H_d$. In this case, the present model describes the SUSY version of the DFSZ axion model [7]. In this case Y and $\bar{Y}$ are additional chiral supermultiplets. It is also allowed to introduce some additional chiral supermultiplets like heavy quarks in the KSVZ model. In order to maintain gauge coupling unification, these additional multiplets may belong to fundamental representations of SU(5).

One may notice that the first term in the superpotential (2) introduced to stabilize the PQ scalar at large field value coincides with that used for the hybrid inflation, after identification of S with the inflaton and $\Psi(\bar{\Psi})$ with the waterfall fields. Thus we reach the interesting possibility : the PQ sector for solving the strong CP problem naturally causes inflation. We do not need any additional fields and interactions. According to a recent analysis including the effect of constant term in the superpotential (2) [5], the correct magnitude of the density perturbation is reproduced for $f_a \sim 10^{15}$GeV and $\kappa \sim 10^{-3}$ if $m_{3/2} \simeq 1$ TeV. At first sight this may seem to be disappointing, because such large PQ symmetry breaking scale leads to axion overproduction, as is well known. In this inflationary scenario, the PQ symmetry is restored during inflation and broken after that. Thus the phase of the axion takes random values for different patch of the Universe, and it is not allowed to tune the initial misalignment angle to avoid the axion overproduction.

However, the situation is much better than the first thought. This is because the late-time entropy production mechanism, which dilutes the axion abundance to the acceptable level, is already built in the present model. Therefore, the large PQ scale, $f_a \sim 10^{15}$GeV, is rather an appealing feature considering that the axion can take a role of the dominant component of dark matter after the entropy-production process.

Now we discuss the scalar field dynamics after inflation. The scalar potential is given by

$$V = \kappa^2 |\Psi\bar{\Psi} - f_a^2|^2 + \kappa^2 |S|^2 (|\Psi|^2 + |\bar{\Psi}|^2). \tag{3}$$

Here we have taken $X = \bar{X} = 0$ since they quickly settle at the origin due to the Hubble mass term during inflation. The global minimum is located at $S = 0$ and $\Psi\bar{\Psi} = f_a^2$. In other words, there is a flat direction along which the scalar fields do not feel the potential, ensured by the $\mathrm{U}(1)_{\mathrm{PQ}}$ symmetry extended to a complex U(1) due to the holomorphy. The SUSY breaking effect lifts up the flat direction, saxion, and gives a mass of order $m_{3/2}$,

$$V_{\mathrm{SB}} = c_1 m_{3/2}^2 |\Psi|^2 + c_2 m_{3/2}^2 |\bar{\Psi}|^2, \tag{4}$$

where c_1 and c_2 are $\mathcal{O}(1)$ constants. This stabilizes the flat direction at $|\Psi| \simeq |\bar{\Psi}| \simeq f_a$. We denote deviation from this minimum along the flat direction as σ, and call it as saxion. The Ψ field also receives a finite-temperature effective potential, $V_T \simeq \alpha_s^2 T^4 \log \Psi$, where α_s is the QCD gauge coupling constant, coming from two-loop effects even if heavy quarks are decoupled from thermal bath.

After inflation ends, the inflaton S and waterfall fields $\Psi(\bar{\Psi})$ oscillates around the minimum, $S = 0, |\Psi| = |\bar{\Psi}| = f_a$, noting that the flat direction at this stage obtains a mass of $\kappa|S|$. The scalar degrees

perpendicular to this direction, which fully mixes with S, decays much earlier than the saxion since they have masses of $m_S \sim \kappa f_a$. The decay is induced by the third term in (2), and the reheating temperature is around $T_{\rm R} \sim 10^{11}$GeV for $m_S \sim 10^{12}$GeV and $k \sim \kappa$. After that, the thermal logarithmic comes to dominate and drives the saxion to $|\bar{\Psi}| \sim \alpha_s M_P$ where the effective thermal mass becomes equal to the Hubble parameter, and the saxion stops there until the thermal effect becomes irrelevant. When the Hubble parameter decreases to $\sim m_{3/2}$, the mass term dominates over the thermal correction, and the saxion begins to oscillate around the minimum, $|\Psi| \sim |\bar{\Psi}| \sim f_a$, with an initial amplitude of $\sigma_i \sim \alpha_s M_P$. The abundance of the saxion coherent oscillation, in terms of the energy density to entropy ratio, is then given by

$$\begin{aligned} \frac{\rho_\sigma}{s} &= \left(\frac{90}{\pi^2 g_*}\right)^{1/4} \frac{\sqrt{m_\sigma M_P}}{8} \frac{\sigma_i^2}{M_P^2} \\ &\simeq 1 \times 10^8 \text{GeV} \left(\frac{m_\sigma}{1\text{TeV}}\right)^{1/2} \left(\frac{\sigma_i}{\alpha_s M_P}\right)^2 , \end{aligned} \tag{5}$$

where $m_\sigma (\sim m_{3/2})$ is the saxion mass. This comes to dominate the Universe well before the QCD phase transition. In the case of KSVZ model, the saxion decays into gluons with the rate

$$\Gamma_{\sigma \to gg} = \frac{\alpha_s^2}{32\pi^3} \frac{m_\sigma^3}{f_a^2}. \tag{6}$$

Then the Universe is reheated again by the saxion decay. The temperature after the saxion decay is estimated as

$$T_\sigma \sim 3 \text{ MeV} \left(\frac{m_\sigma}{10\text{TeV}}\right)^{3/2} \left(\frac{10^{15}\text{GeV}}{f_a}\right), \tag{7}$$

and hence is compatible with the lower bound on the reheating temperature for $m_\sigma \gtrsim 10$TeV. Notice that the saxion also decays into a SUSY particle pair and then produces the lightest SUSY particles (LSP) nonthermally, which easily exceed the dark matter abundance. Thus we need to introduce small R-parity violation in order for the LSP to decay well before BBN begins, or to assume SUSY particles are heavy enough not to be produced by the saxion decay. In the case of DFSZ model, the saxion decays into Higgs pair or fermion pairs. For example, the decay width into the lightest Higgs boson pair is

$$\Gamma_{\sigma \to hh} = \frac{1}{8\pi} \frac{m_\sigma^3}{f_a^2} \left(\frac{\mu}{m_\sigma}\right)^4 , \tag{8}$$

where $\mu = \lambda \langle \Psi \rangle$ gives the higgsino mass, and hence we obtain

$$T_\sigma \sim 5 \text{ MeV} \left(\frac{m_\sigma}{1\text{TeV}}\right)^{3/2} \left(\frac{10^{15}\text{GeV}}{f_a}\right) \left(\frac{\mu}{m_\sigma}\right)^2 . \tag{9}$$

Thus in this case we need $m_\sigma \sim 1$ TeV and decay into a SUSY particle pair can naturally be forbidden.

Now let us discuss the abundance of the axion, gravitino and axino after the dilution by the saxion decay. The axion abundance, in terms of the density parameter, after the dilution is estimated as [8]

$$\Omega_a h^2 \simeq 5 \times 10^{-2} \left(\frac{T_\sigma}{1\text{MeV}}\right) \left(\frac{f_a}{10^{15}\text{GeV}}\right)^2 , \tag{10}$$

hence it is consistent with the WMAP observation of the dark matter abundance. This is appealing, since the PQ scale $f_a \sim 10^{15}$GeV is required for generating the density perturbation of the Universe, while this large PQ scale leads to the efficient late-time entropy production, making the axion plausible candidate of dark matter. Note that the axion does not have an isocurvature perturbation in this model, since the PQ symmetry is restored during inflation.

As for the gravitino, they are produced both thermally and nonthermally from the inflaton decay, but diluted sufficiently. The thermally produced gravitino abundance, in terms of the number to entropy ratio, is estimated as

$$Y_{3/2} \simeq 1 \times 10^{-22} \left(\frac{1\text{TeV}}{m_\sigma}\right)^{1/2} \left(\frac{T_{\rm R}}{10^{11}\text{GeV}}\right) \left(\frac{T_\sigma}{1\text{MeV}}\right) \left(\frac{\alpha_s M_P}{\sigma_i}\right)^2 . \tag{11}$$

This satisfies the bound on the unstable gravitino abundance from BBN $m_{3/2}Y_{3/2} \lesssim 10^{-13}$-$10^{-9}$GeV for $m_{3/2} \sim$ 1-10TeV for an unstable gravitino.

The axino, which is the fermionic superpartner of the axion, might also have significant effects on cosmology [9]. The axino abundance from thermal production, after the dilution, is given by

$$Y_{\tilde{a}} \simeq 1 \times 10^{-19} \left(\frac{1\text{TeV}}{m_\sigma}\right)^{1/2} \left(\frac{T_\text{R}}{10^{11}\text{GeV}}\right) \left(\frac{T_\sigma}{1\text{MeV}}\right) \left(\frac{10^{15}\text{GeV}}{f_a}\right)^2 \left(\frac{\alpha_s M_P}{\sigma_i}\right)^2 . \tag{12}$$

In the present model, the axino mass is generated once the A-term potential is included : $V_A = A\kappa S f_a^2 +$ h.c. with $A \sim m_{3/2}$. Then S has a VEV of $\sim A/\kappa$, and it gives an axino mass of $m_{\tilde{a}} = \kappa\langle S\rangle \sim A$. Thus the axino mass is comparable to the gravitino. If the axino is not the LSP, it has a similar lifetime to the saxion in the KSVZ model, and it decays before BBN. The constraint is given as $Y_{\tilde{a}} \lesssim 10^{-12}$ so as not to produce too much LSPs. If the axino is the LSP, the bound reads $m_{\tilde{a}} Y_{\tilde{a}} \lesssim 4 \times 10^{-10}$GeV. In both cases, the constraint is satisfied as is seen in Eq. (12).

3 Conclusion

To summarize, we have shown that a simple SUSY axion model naturally causes hybrid inflation. The PQ symmetry breaking scale is fixed to be around 10^{15}GeV so that the correct magnitude of cosmological density perturbation is reproduced. Taking into account the post inflationary dynamics of the scalar fields contained in the model, the late-time entropy production necessarily occurs and the axion coherent oscillation can be the dark matter. This provides a solution to the strong CP and gauge hierarchy problems and simultaneously explains a cosmic inflation and the presence of dark matter.

This work was supported by Grant-in-Aid for Scientific research from the Ministry of Education, Science, Sports, and Culture (MEXT), Japan, No.14102004 (M.K.) and No. 21111006 (M.K. and K.N.) and also by World Premier International Research Center Initiative (WPI Initiative), MEXT, Japan.

References

[1] R. D. Peccei and H. R. Quinn, Phys. Rev. Lett. **38**, 1440 (1977).

[2] For reviews, see J. E. Kim, Phys. Rept. **150**, 1 (1987); J. E. Kim and G. Carosi, arXiv:0807.3125 [hep-ph].

[3] M. Kawasaki, N. Kitajima and K. Nakayama, arXiv:1008.5013 [hep-ph], to appear in Phys.Rev.D.

[4] E. J. Copeland, A. R. Liddle, D. H. Lyth, E. D. Stewart and D. Wands, Phys. Rev. D **49**, 6410 (1994).

[5] See K. Nakayama, F. Takahashi and T. T. Yanagida, JCAP **1012**, 010 (2010) [arXiv:1007.5152 [hep-ph]] and references therein.

[6] J. E. Kim, Phys. Rev. Lett. **43**, 103 (1979); M. A. Shifman, A. I. Vainshtein and V. I. Zakharov, Nucl. Phys. B **166**, 493 (1980).

[7] M. Dine, W. Fischler and M. Srednicki, Phys. Lett. B **104**, 199 (1981); A. R. Zhitnitsky, Sov. J. Nucl. Phys. **31**, 260 (1980) [Yad. Fiz. **31**, 497 (1980)].

[8] M. Kawasaki, T. Moroi and T. Yanagida, Phys. Lett. B **383**, 313 (1996).

[9] K. Rajagopal, M. S. Turner and F. Wilczek, Nucl. Phys. B **358**, 447 (1991); M. Kawasaki, K. Nakayama and M. Senami, JCAP **0803**, 009 (2008) [arXiv:0711.3083 [hep-ph]].

Gravitational waves from Q-balls in gravity mediation

Takashi Hiramatsu[1(a)], Fuminobu Takahashi[2(b)] and Masahide Yamaguchi[3(c)]

[(a)] *Yukawa Institute for Theretical Physics, Kyoto University, Kyoto 606-8502*
[(b)] *Institute for the Physics and Mathematics of the universe, The University of Tokyo, Kashiwa, Chiba 277-8568, Japan*
[(c)] *Department of Physics, Tokyo Institute of Technology, Tokyo 152-8551, Japan*

Abstract

We estimate gravitational waves produced during the formation of Q-balls associated with the Affleck-Dine mechanism in the gravity mediation on 3D lattice simulations. As a preliminary result, we find that the peak amplitude at the Q-ball formation epoch comes up to $\Omega_{\rm GW} \sim 10^{-3}(\Phi_{in}/M_{\rm pl})^4$ at the scale of physical size of Q-balls, $k \approx 0.06m$.

1 Introduction

The gravitational wave (GW), as it is coupled to the energy-momentum tensor, must be ubiquitous in nature, although its small amplitude and weak interaction make the direct detection extremely challenging. There are many on-going and planned direct gravitational wave detection experiments such as DECIGO [1], and the sensitivity will be greatly improved in the near future.

In cosmology, the gravitational waves may provide us with valuable information on the evolution of the universe. Recently, another interesting source of GWs is proposed, which is a non-topological soliton, Q-ball [2–4]. It was noticed in Refs. [5–8] that Q-balls play an important role in a context of the Affleck-Dine (AD) mechanism [9]. The mechanism utilizes a flat direction of the supersymmetric standard model (SSM), which possesses a non-zero baryon (or lepton) number. A flat direction responsible for the AD mechanism is referred to as the AD field (denoted by Φ in the following). The AD field Φ develops a large expectation value during inflation, and it starts to oscillate after inflation when the cosmic expansion rate becomes comparable to its mass. The baryon number is effectively created at the onset of the oscillations. Finally, Φ decays into the ordinary quarks, leaving the universe with a right amount of the baryon asymmetry. It was realized however that, soon after the onset of oscillations, the AD field experiences spatial instabilities and deforms into clumpy Q-balls which absorb most of the baryon asymmetry [7]. Thus, such a violent change of the scalar field and its energy-momentum tensor can produce significant amount of GWs [3, 4]. Detailed calculations with a realistic decay rate of a Q-ball, unfortunately, shows that there is a finite but small parameter region where such GWs may be detected by future detectors such as DECIGO or BBO [10]. In these analyses, the initial amplitudes and typical wavelengths of GWs are estimated analytically by use of the instability bands of the Q-ball formation. However, the Q-ball formation is a quite non-linear process, which necessitates numerical approach to the formation, the subsequent evolution, and the associated GW emissions. Such a numerical analysis was first done in Ref. [4].

Recently, two of the authors (TH and FT) and Kawasaki studied the Q-ball formation in the AD mechanism in gravity mediation, and found that before the Q-balls are formed, complicated structure like a web is developed. Also, if the ellipticity is large, the Q-ball relaxation proceeds in a violent way. Those processes could produce a large amount of gravitational waves with a distinctive spectrum. The purpose of this paper is to estimate the gravitational wave spectrum and amplitude in the Q-ball formation, based on a sophisticated numerical code developed in Ref. [11].

[1]Email address: hiramatz@yukawa.kyoto-u.ac.jp
[2]Email address: fuminobu.takahashi@ipmu.jp
[3]Email address: gucci@phys.titech.ac.jp

2 Q-ball dynamics

In the gravity-mediated SUSY breaking model, the AD field typically has a potential of the following form,

$$V(\Phi) = m^2|\Phi|^2\left[1 + K\log\left(\frac{|\Phi|^2}{M_*^2}\right)\right] - cH^2|\Phi|^2 + \frac{\lambda^2}{M^{2n-6}}|\Phi|^{2n-2}, \tag{1}$$

where Φ is a complex scalar field parametrizing the flat direction. The evolution equation of the scalar field Φ is given by

$$\Phi'' + 2\mathcal{H}\Phi' - \nabla^2\Phi + m^2a^2\Phi\left[1 + K + K\log\left(\frac{|\Phi|^2}{M_*^2}\right)\right] - \mathcal{H}^2\Phi = 0, \tag{2}$$

where $K = -0.01 \sim -0.1$[8], the prime represents the derivative with respect to the conformal time and ∇^2 is defined as the Laplacian with respect to the comoving coordinate. In this paper, we restrict our analysis to the epoch between the end of inflation and the reheating era, where the scale factor behaves as $a \propto \tau^2$ like the matter-dominant case. In addition, the non-renormalizable term (the last term being proportional to λ) does not directly contribute to the late-time evolution of the scalar field, so we fix $\lambda = 0$, and, for simplicity, $c = 1$. In this paper, we also fix $K = -0.1$, while we present the dependence of some properties of Q-balls on K in Ref. [11].

3 Simulation setup

The potential (1) is invariant under the U(1) rotation of Φ, and therefore the charge Q is preserved. In general, however, there is a U(1)-violating term arising from the A-term $\propto (\Phi^n + \Phi^{*n})$. This term kicks the AD field into the angular direction at the onset of oscillations, giving a nonzero U(1) charge, or equivalently, the angular momentum in the complex Φ plane. To realise this situation without adding the A-term to the potential, according to our previous study [11], we parametrize the homogeneous part of the initial condition as

$$\Phi(t_{\rm in}) = M_*, \quad \dot{\Phi}(t_{\rm in}) = i\epsilon M_*, \tag{3}$$

where the dot represents the derivative with respect to the cosmic time. The initial charge density is then $q(t_{\rm in}) = -i(\Phi^*\dot{\Phi} - \Phi\dot{\Phi}^*) \sim 2\epsilon M_*^2$. In the following analysis we take $\epsilon = 1$ and 0. Also we add small fluctuations to the above initial condition, $|\delta\Phi/\Phi| = 10^{-7}$, following Ref. [12].

We use a comoving box as a computational domain whose physical size at the initial time is $L = H^{-1}(\tau_{\rm in}) = m^{-1}$, and the number of grid is 256^3. On the boundaries, we impose the periodic boundary condition. To evolve Φ, we implement the 3 stages 4th-order simplectic integrator developed by Yoshida [13]. The spatial derivatives, i.e. the Laplacian operator in Eq. (2), are estimated with the 4th-order finite difference.

According to Ref. [14], we estimate the energy spectrum of the gravitational waves during the Q-ball formation. From the perturbed metric in the flat universe, $ds^2 = a^2\left(-d\tau^2 + (\delta_{ij} + h_{ij})dx^i dx^j\right)$, the gravitational waves sourced by the AD field obey the following equation,

$$\frac{\partial^2\widetilde{\chi}_{ij}}{\partial\tau^2} + \left(k^2 - \frac{2}{\tau^2}\right)\widetilde{\chi}_{ij} = 16\pi G a(\tau)\widetilde{B}_{ij}(\boldsymbol{k},\tau), \tag{4}$$

where $\widetilde{\chi_{ij}}(\boldsymbol{k},\tau)$ is the Fourier components of $\chi_{ij}(\boldsymbol{x},\tau) \equiv a(\tau)h_{ij}(\boldsymbol{x},\tau)$, and $\widetilde{B}_{ij}(\boldsymbol{k},\tau)$ is that of $B_{ij}(\boldsymbol{x},\tau) = \partial_i\phi\partial_j\phi^* + \partial_i\phi^*\partial_j\phi$. The special solution of this equation can be written by

$$\widetilde{\chi}_{ij}(\boldsymbol{k},\tau) = \frac{16\pi G}{k^2}\left\{\overline{C}_{ij}^{(1)}(\boldsymbol{k},\tau)\xi_1(\tau) + \overline{C}_{ij}^{(2)}(\boldsymbol{k},\tau)\xi_2(\tau)\right\}, \tag{5}$$

where

$$\overline{C}_{ij}^{(1)}(\boldsymbol{k},\tau) = -\int_{\tau_0}^{\tau} k d\tau'\,\xi_2(\tau')a(\tau')\widetilde{B}_{ij}(\boldsymbol{k},\tau'), \qquad \xi_2(\tau) = \frac{k\tau\sin k\tau + \cos k\tau}{k\tau}, \tag{6}$$

$$\overline{C}_{ij}^{(2)}(\boldsymbol{k},\tau) = \int_{\tau_0}^{\tau} k d\tau'\,\xi_1(\tau')a(\tau')\widetilde{B}_{ij}(\boldsymbol{k},\tau'), \qquad \xi_1(\tau) = \frac{k\tau\cos k\tau - \sin k\tau}{k\tau}, \tag{7}$$

where we assume $\widetilde{B}_{ij}(\boldsymbol{k},\tau)=0$ for $\tau<\tau_0$. The energy density of the gravitational waves is given by

$$\rho_{\rm GW}(\tau)=\frac{1}{32\pi G a(\tau)^4}\langle\chi'_{ij}(\tau)\chi'_{ij}(\tau)\rangle_{V,T}=\frac{G}{2\pi^2a^4V}\int dkd\Omega(|\overline{C}^{(1)}_{ij}|^2+|\overline{C}^{(2)}_{ij}|^2), \tag{8}$$

where $\langle\cdots\rangle_{V,T}$ represents the average over the spatial volume and the duration during which a wave with a wave number k passes over, namely, $T=2\pi/k$, and $V=m^3$ is the comoving volume. Then the energy spectrum at the time τ is given by

$$\Omega_{\rm GW}(k,\tau)\equiv\frac{1}{\rho_c}\frac{d\rho_{GW}}{d\log k}=\frac{4G^2k}{3\pi H_0^2aV}\int d\Omega(|\overline{C}^{(1)}_{ij}|^2+|\overline{C}^{(2)}_{ij}|^2), \tag{9}$$

where we used $\rho_c=3H^2/(8\pi G)$ and $H=H_0a^{-3/2}$ in the matter dominant era.

4 Gravitational wave spectrum

At this stage, our numerical results to be presented here are still preliminary. We would like to emphasise that there remains some subtle points to be discussed more.

4.1 A case of $\epsilon=1$

Figure 1 shows the time evolution of gravitational wave spectrum in the case with $\epsilon=1$. At the early epoch, the power gradually grows on large scales which corresponds to the scale of filamentary structure appearing before Q-ball formation found in [11]. Around $\tau\sim20$, the power on intermediate scales rapidly grows. This implies that the filamentary structure collapses into Q-balls, and a large amount of gravitational waves is radiated. At this time, we found that the peak appears around $k\approx0.06m$, while a naive estimation of the Q-ball size is $k\approx\sqrt{|K|}m\sim0.3m$. These values are consistent with each other if including some neglected numerical factors.

We also have performed the simulation with $L=4$, four times larger box (the volume is 64 times larger) than that of Fig. 1. As shown in Fig. 2, we found that the spectrum behaves as $\Omega_{\rm GW}\propto k^3$ on large scales, which agrees with with the suggestion given in Ref. [14]. On the other hand, the spectrum behaves mostly as $\Omega_{\rm GW}\propto k^{-2}$. At this preliminary stage of our numerical calculations, this is not consistent with their result, and also the result of Ref. [15], in which they have clamed $\Omega_{\rm GW}\propto k^{-1}$.

After $\tau\gtrsim21$, we can see no extra production of gravitational waves, and the power starts to decay due to the cosmic expansion, $\Omega_{\rm GW}\propto1/a$. However, around the peak, the amplitude keeps to grow gradually, and eventually becomes $\Omega_{GW}\approx\mathcal{O}(10^{-3})$. The amplitude at the final time of our simulation is 10^3 times larger than that obtained in [4]. Hence we should discuss the discrepancy carefully.

4.2 A case of $\epsilon=0$

Even if $\epsilon=0$, the basic behaviour of the GW spectrum is the same as that in the previous case. According to our previous work [11], for small ϵ, there is the secondary formation epoch around $26\lesssim\tau\lesssim29$ when a quite large number of anti-Q-balls are formed around the original Q-balls formed at earlier time. This process seems so violent. Nevertheless, we cannot see any significant changes on the gravitational wave spectrum until $\tau=31$ shown in Fig. 3. Rather, the amplitude starts to decay due to the cosmic expansion after the prouction of GWs accompanying the Q-ball formation was terminated. Consequently, we expect that the second formation process is actually not so violent as to generate extra amounts of gravitational waves.

5 Discussion and Conclusions

In this paper, we have studied the production of gravitational waves (GWs) accompanying the gravity-mediation type Q-ball formation in 3D lattice simulations.

We have found that the amplitude of GWs monotonically grows as the filamentary structure develops in the early epoch of the simulations, and at the Q-ball formation epoch, the amplitude on small scales

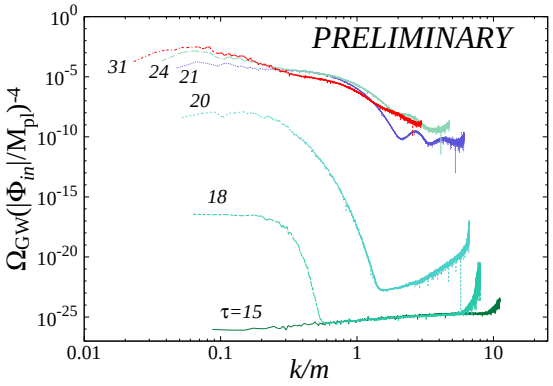

Figure 1: Time evolution of gravitational wave specrum during Q-ball formation. The number on far left of each line indicates the conformal time.

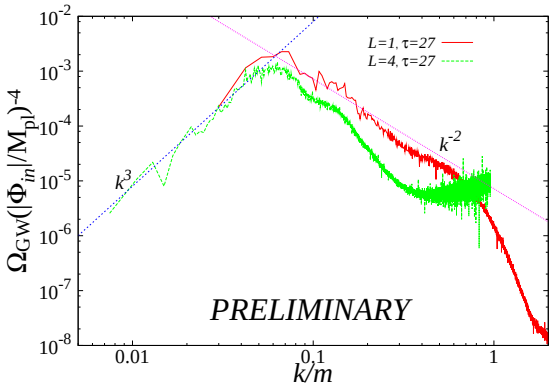

Figure 2: Spectra from simulations with different box sizes at $\tau = 27$. The red solid line is $L = 1$ and the green dotted line is $L = 4$.

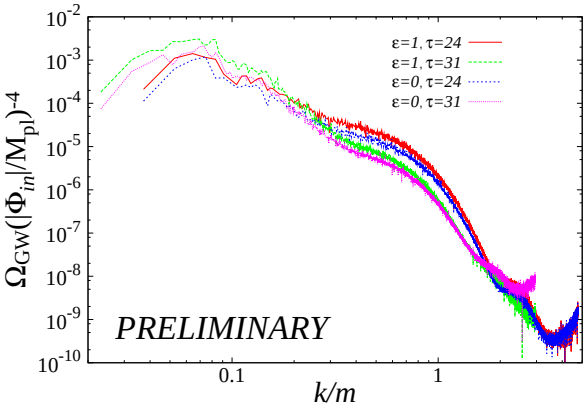

Figure 3: The spectra with $\epsilon = 1$ at $\tau = 24$ (red solid), and $\epsilon = 0$ at $\tau = 24$ (green dotted), and at $\tau = 31$ (blue dashed).

is rapidly enhanced. As a result, the peak appears around $k \approx 0.06m$ in the power spectrum of GWs, $\Omega_{\rm GW}$, and the feature is also confirmed in a simulation with a larger box. As for the case with $\epsilon = 0$, in which there is the secondary formation of anti-Q-balls, we could not observe the extra production of GWs in this epoch contrary to our expectations.

We numerically found that the peak amplitude evolves up to $\Omega_{\rm GW} \sim O(10^{-3})(\Phi_{in}/M_{\rm pl})^4$. This value is not consistent with the result in Kusenko et al.[4], which has reported $\Omega_{\rm GW} \sim O(10^{-5})$. In our simulations, however, there are some subtle points to be addressed. We would like to report our final outcomes in the near future.

References

[1] N. Seto, S. Kawamura and T. Nakamura, Phys. Rev. Lett. **87**, 221103 (2001) [arXiv:astro-ph/0108011]; S. Kawamura *et al.*, Class. Quant. Grav. **23**, S125 (2006).

[2] S. R. Coleman, Nucl. Phys. B **262**, 263 (1985) [Erratum-ibid. B **269**, 744 (1986)].

[3] A. Kusenko and A. Mazumdar, Phys. Rev. Lett. **101**, 211301 (2008) [arXiv:0807.4554 [astro-ph]].

[4] A. Kusenko, A. Mazumdar and T. Multamaki, arXiv:0902.2197 [astro-ph.CO].

[5] A. Kusenko, Phys. Lett. B **405**, 108 (1997) [arXiv:hep-ph/9704273].

[6] G. R. Dvali, A. Kusenko and M. E. Shaposhnikov, Phys. Lett. B **417**, 99 (1998) [arXiv:hep-ph/9707423].

[7] A. Kusenko and M. E. Shaposhnikov, Phys. Lett. B **418**, 46 (1998) [arXiv:hep-ph/9709492].

[8] K. Enqvist and J. McDonald, Phys. Lett. B **425**, 309 (1998) [arXiv:hep-ph/9711514].

[9] I. Affleck and M. Dine, Nucl. Phys. B **249**, 361 (1985); M. Dine, L. Randall and S. D. Thomas, Nucl. Phys. B **458**, 291 (1996) [arXiv:hep-ph/9507453].

[10] T. Chiba, K. Kamada and M. Yamaguchi, Phys. Rev. D **81**, 083503 (2010) [arXiv:0912.3585 [astro-ph.CO]].

[11] T. Hiramatsu, M. Kawasaki and F. Takahashi, JCAP **1006**, 008 (2010) [arXiv:1003.1779 [hep-ph]].

[12] S. Kasuya and M. Kawasaki, Phys. Rev. D **62**, 023512 (2000) [arXiv:hep-ph/0002285].

[13] H. Yoshida, Phys. Lett. A **150** (1990) 262.

[14] J. F. Dufaux, A. Bergman, G. N. Felder, L. Kofman and J. P. Uzan, Phys. Rev. D **76**, 123517 (2007) [arXiv:0707.0875 [astro-ph]].

[15] A. Mazumdar and I. M. Shoemaker, arXiv:1010.1546 [hep-ph].

Rotating black holes in fake supergravity

Masato Nozawa[1(a)], and Kei-ichi Maeda[2(b)]

(a) *Department of Physics, Waseda University, Okubo 3-4-1, Shinjuku, Tokyo 169-8555, Japan*
(b) *Waseda Research Institute for Science and Engineering, Okubo 3-4-1, Shinjuku, Tokyo 169-8555, Japan*

Abstract

In recent series of papers, we found an arbitrary dimensional, time-evolving and spatially-inhomogeneous solutions in Einstein-Maxwell-dilaton gravity with particular couplings. Similar to the supersymmetric case the solution can be arbitrarily superposed in spite of nontrivial time-dependence, since the metric is specified by a set of harmonic functions. When each harmonic has a single point source at the center, the solution describes a spherically symmetric charged black hole with regular Killing horizons and the spacetime approaches asymptotically to the Friedmann-Lemaˆtre-Robertson-Walker (FLRW) universe. We discuss in this paper that in 5-dimensions this equilibrium condition traces back to the 1st-order Killing spinor equation in fake supergravity coupled to arbitrary U(1) gauge fields and scalars. We present a 5-dimensional, asymptotically FLRW, rotating black-hole solution admitting a nontrivial Killing spinor, which is a spinning generalization of our previous solution. We discuss physical properties and causal structures of solutions with nonvanishing angular momentum.

1 Introduction

Black holes in our universe commonly form via the gravitational collapse of massive stars. If a great deal of time has past from the formation of the hole, the system settles down to equilibrium states. Therefore the stationary black holes have been intensively studied in the literature. Black hole solutions out of equilibrium, on the other hand, have been much less understood thus far, irrespective of the fact that the dynamical black holes are of great importance in the early stages of the universe. However, it is in general difficult to construct the black hole spacetime in the dynamical background. If a black hole is put on the homogeneous and isotropic FLRW universe on which the standard cosmological scenario lays the foundation, the background universe will become inhomogeneous, and at the same time the black hole will continue to grow and/or deform by swallowing ambient matters. Thus, the fact that the spacetime is time-evolving and spatially inhomogeneous enforces us to solve nonlinear partial differential equations for the geometry, as well as for the matter fields.

Consequently the cosmological black holes obtained thus far admit a number of symmetries. Prime examples are the Schwarzschild-de Sitter black holes and the Reissner-Nordström-de Sitter black holes. These are exact solutions in Einstein-Maxwell-$\Lambda(>0)$ system and each solution describes a black hole in the de Sitter universe. The supersymmetry requires the negative cosmological constant, so that this theory is not supersymmetric. Nevertheless, Kastor and Traschen [1] have shown that the Reissner-Nordström-de Sitter black holes can be arbitrary superposed. This is the generalization of Majumdar-Papapetrou solution in the de Sitter background. The Kastor-Traschen solution describes coalescing black holes in the contracting de Sitter universe (or splitting white holes in the expanding de Sitter universe) and inherits some salient characteristics from the Majumdar-Papapetrou solution. The reason why multicenter metric is in mechanical equilibrium irrespective of the time-dependence is attributed to the first-order "BPS equation" which is obtainable via Wick rotation of the AdS curvature radius [2], allowing the complete linearization of field equations. Since these "BPS" states are not truly supersymmetric in the usual sense, they are referred to as pseudo-supersymmetric and the corresponding theory is called a "fake" supergravity.

[1]Email address: nozawa@gravity.phys.waseda.ac.jp
[2]Email address: maeda@waseda.jp

Recent series of papers of present authors [3, 4] have found solutions similar to the Kastor-Traschen metric. The solution is specified by a set of harmonic functions, but approaches to the FLRW universe asymptotically. When a single point source is placed at the center, we demonstrated that the solution actually describes a charged black hole in the FLRW cosmology [5, 6]. Though these metrics were shown to be the exact solutions of Einstein-Maxwell-dilaton system in arbitrary dimensions, we can show that the 5-dimensional solutions of [3, 6] in fact satisfy the 1st-order BPS equation in fake supergravity. Some time-dependent black hole solutions have been available so far [7], but their properties and causal structures are yet to be explored. We discuss these issues in 5-dimensional fake supergravity with arbitrary number of U(1) gauge fields and scalar fields. For the details of the present article, we refer the reader to reference [8].

2 $\mathrm{U}(1)^N$-fake supergravity in five-dimensions

Let us start from the usual 5-dimensional minimal gauged supergravity coupled to N abelian vector multiplets. The bosonic action involves graviton, U(1) gauge fields $A^{(I)}$ $(I = 1, ..., N)$ with real scalars ϕ^A $(A = 1, ..., N-1)$,

$$S = \frac{1}{2\kappa_5^2}\int \left({}^5R + 2\mathfrak{g}^2 V\right) \star_5 1 - \mathcal{G}_{AB}\mathrm{d}\phi^A \wedge \star_5 \mathrm{d}\phi^B - G_{IJ}F^{(I)} \wedge \star_5 F^{(J)} - \frac{1}{6}C_{IJK}A^{(I)} \wedge F^{(J)} \wedge F^{(K)}\,, \quad (1)$$

where $F^{(I)} = \mathrm{d}A^{(I)}$ are the field strengths of gauge fields, $\mathcal{G}_{AB}$ is the metric of the potential space for ϕ^A, $\mathfrak{g}(\in \mathbb{R})$ is the coupling constants corresponding to the reciprocal of the AdS curvature radius. The constants $C_{IJK} = C^{IJK}$ are totally symmetric in (IJK). The N-scalars X^I are constrained by $\mathcal{V} := (1/6)C_{IJK}X^IX^JX^K = 1$. Defining $X_I := (1/6)C_{IJK}X^JX^K$, the metric G_{IJ} and its inverse G^{IJ} define the very special geometry,

$$G_{IJ} := -\frac{1}{2}\left.\frac{\partial^2}{\partial X^I \partial X^J}\ln \mathcal{V}\right|_{\mathcal{V}=1} = \frac{9}{2}X_IX_J - \frac{1}{2}C_{IJK}X^K\,, \qquad G^{IJ} = 2X^IX^J - 6C^{IJK}X_K\,, \quad (2)$$

The potential V is determined by the superpotential as $V = 27C^{IJK}V_IV_JX_K$, where V_I are constants. The supersymmetry transformations generated by a spinor ϵ are given by

$$\delta\Psi_\mu = \hat{\nabla}_\mu\epsilon\,, \qquad \delta\lambda_A = \mathcal{D}_A\epsilon\,, \quad (3)$$

which specify the variations of gravitino and dilatino, respectively.

Here, if we consider a non-compact gauging of R-symmetry, an imaginary coupling arises, $\mathfrak{g} \to ik$ $(k \in \mathbb{R})$. Since only the R-symmetry is gauged, the imaginary coupling reflects the non-compactness of R-symmetry. The Lagrangian (1) is neutral under the R-symmetry, so that the theory is free from the ghost-like contribution. This theory is called a *fake supergravity*. Assuming that the first-order equations (3) make sense after the Wick-rotation, we are led to the pseudo-Killing spinor equations. The explicit forms are

$$\left[\nabla_\mu + \frac{3k}{2}V_IA^{(I)}_\mu + \frac{i}{8}X_I\left(\gamma_\mu{}^{\nu\rho} - 4\delta_\mu{}^\nu\gamma^\rho\right)F^{(I)}_{\nu\rho} + \frac{i}{2}k\gamma_\mu X^IV_I\right]\epsilon = 0\,, \quad (4)$$

$$\left[\frac{3}{8}\gamma^{\mu\nu}F^{(I)}_{\mu\nu}\frac{\partial}{\partial\phi^A}X_I - \frac{i}{2}\mathcal{G}_{AB}\gamma^\mu\partial_\mu\phi^B - \frac{3}{2}kV_I\frac{\partial}{\partial\phi^A}X^I\right]\epsilon = 0\,. \quad (5)$$

Here, the supercovariant derivative operator is no longer hermitian for $k \in \mathbb{R}$. This implies that we are unable to use ϵ to prove the positive energy theorem in the usual manner.

Inferring from the supersymmetric solutions, we assume the standard metric ansatz,

$$\mathrm{d}s_5^2 = -f^2(\mathrm{d}t + \omega)^2 + f^{-1}h_{mn}\mathrm{d}x^m\mathrm{d}x^n\,, \quad (6)$$

where h_{mn} is the metric of 4-space orthogonal to $V = \partial/\partial t$. In what follows, indices $m, n, ...$ are raised and lowered by h_{mn} and its inverse h^{mn}. The one-form ω corresponds to the U(1) fibration over the transverse base space $(\mathcal{B}, h_{mn})$. We assume $\mathcal{L}_Vh_{\mu\nu} = 0$ and $\mathcal{L}_V\omega = 0$. Setting

$$f^{-3} = \frac{1}{6}C^{IJK}H_IH_JH_K\,, \qquad A^{(I)} = fX^I(\mathrm{d}t + \omega)\,, \qquad X_I = \frac{1}{3}fH_I\,, \quad (7)$$

we find that the spacetime satisfies the Maxwell equations and the 1st-order equations (4) and (5), provided that the base space $(\mathcal{B}, h_{mn})$ is hyper-Kähler (with anti-self-dual complex structures), and

$$\mathrm{d}\omega + \star_h \mathrm{d}\omega = 0\,, \qquad H_I(t, x^m) = 6kV_I t + \bar{H}_I(x^m)\,, \qquad \mathrm{i}\gamma^0\epsilon = \epsilon\,, \qquad \epsilon = f^{1/2}\epsilon_0\,, \tag{8}$$

where $\bar{H}_I$ are the harmonics on the base space and ϵ_0 is a constant spinor. The Einstein equations and the scalar field equations are ensured by (4) and (5). Since the functions H_I obey Laplace equations, the metric can be superposed in spite of the nontrivial time-dependence.

3 Global structures

To be concrete, let us consider the "STU-theory," which is defined by the conditions such that $C_{123} = C_{(123)} = 1$ and the other C_{IJK}'s vanish. For simplicity, let us choose the flat space $\mathbb{R}^4$ as a base space. We work with the hyperspherical coordinates $(r, \vartheta, \phi_1, \phi_2)$. Assuming that the solution preserves the SU(2)-left action, the anti-self-duality for $\mathrm{d}\omega$ is solved by

$$\omega = \frac{j}{r^2}\left(\sin^2\vartheta \mathrm{d}\phi_1 + \cos^2\vartheta \mathrm{d}\phi_2\right)\,, \tag{9}$$

where j is a constant corresponding to the angular momentum. We further specialize to the case in which all harmonics have a single point source at the center with the same charges. In this case the function f can be written as

$$f = H_T^{-n/3} H_S^{-1+n/3}\,, \qquad H_T := \frac{t}{t_0} + \frac{Q}{r^2}\,, \qquad H_S := 1 + \frac{Q}{r^2}\,, \tag{10}$$

where $t_0 := (6kV_I)$ and n counts the number of nonvanishing V_I's. Under these restrictions one has two Abelian gauge fields and a single unconstrained scalar. This metric (10) admits an enhanced symmetries $\mathrm{U}(2) \simeq \mathrm{SU}(2) \times \mathrm{U}(1)$, which allows a reducible Killing tensor. The spacetime points where $H_T = 0$ and $H_S = 0$ correspond to the timelike singularities.

Changing to the new time slice $\bar{t} \propto t^{1-n/3}$ for $n = 1, 2$ and $\bar{t} = t_0 \ln(t/t_0)$ for $n = 3$, one easily finds that each solution (10) approaches as $r \to \infty$ to the 5-dimensional flat FLRW universe,

$$\mathrm{d}s_5^2 = -\mathrm{d}\bar{t}^2 + a^2 \delta_{mn} \mathrm{d}x^m \mathrm{d}x^n\,, \tag{11}$$

where the scale factor obeys $a \propto \bar{t}^{n/[2(3-n)]}$ for $n = 1, 2$ and $a \propto e^{\bar{t}/2t_0}$ for $n = 3$. When the rotation vanishes $j = 0$, the metric (10) reduces to the one found in [3, 6]. The $n = 1$ case is derivable from the intersecting branes in intersecting M-branes in 11-dimensional supergravity [3]. For the $n = 3$ case, the potential of a scalar field is constant, giving rise to a positive cosmological constant.

When one takes the limit in which r goes to zero *with t kept finite*, the solution (10) approaches to a deformed $\mathrm{AdS}_2 \times S^3$:

$$\mathrm{d}s^2_{r\to 0} = -\left(\frac{r^2}{Q}\right)^2 \left[\mathrm{d}t + \frac{j}{r^2}(\sin^2\vartheta \mathrm{d}\phi_1 + \cos^2\vartheta \mathrm{d}\phi_2)\right]^2 + \left(\frac{Q}{r^2}\right)^2 \mathrm{d}r^2 + Q\mathrm{d}\Omega_3^2\,, \tag{12}$$

where $\mathrm{d}\Omega_3^2$ denotes the unit line-element of S^3. This is the same as the near-horizon geometry of a BMPV black hole [9], implying that $r = 0$ is a point at the tip of an infinite throat. Hence the spacetime is expected to describe a rotating black hole in the FLRW universe.

It is noteworthy, however, that this metric (12) does *not* describe the geometry of a neighborhood of "would-be horizon" since we have fixed the time-coordinate when taking the $r \to 0$ limit. As pointed out in [5, 6] the null surfaces piercing the throat correspond to the infinite redshift ($t \to +\infty$) and blueshift ($t \to -\infty$) surfaces. The structures of these null surfaces can be analyzed by taking appropriate "near-horizon" limit. The genuine near-horizon geometries are captured by the scaling limit $t \to t/\epsilon^2$, $r \to \epsilon r$ with $\epsilon \to 0$. After taking the scaling limit, one obtains a stationary geometries since $\xi = t(\partial/\partial t) - (r/2)(\partial/\partial r)$ is the Killing field which defines the Killing horizons. It is interesting to observe that the spacetime admits (asymptotic) Killing horizons in spite of the fact that the original metric

is time-dependent. It follows that the ambient matters fail to accrete onto the hole, which may be attributed to the equilibrium states specified by the pseudo-supersymmetries. A close inspection shows that the horizon is nonextremal and rotating unless the parameters are finely tuned. This property is in sharp contrast with the supersymmetric cases.

In the presence of rotation ($j \neq 0$), the spacetime suffers from causal violation. Defining the areal radius of S^2 by $R := |r| f^{-1/2}$, we can define the velocity of light surface $R_L := j^{1/3}$. Inside the velocity of light surface, there appear closed timelike curves. Since $R = 0$ surfaces correspond spacetime singularities, the spacetime regions around the singularities are causally ill-behaved. The whole spacetime geometries can be deduced by solving the geodesics numerically. The two-dimensional conformal diagrams allow useful visualization, which can be found in reference [8].

4 Concluding remarks

We have considered 5-dimensional fake supergravity and discussed properties of pseudo-supersymmetric spinning black holes. These black holes are in equilibrium in the dynamical background, as seen from the fact that the area of the hole remains constant in time. This is reminiscent of the usual supersymmetric black holes. However, the present horizons are nonextremal and rotating, which cannot be shared by supersymmetric black holes. The solution (10) can be dimensionally uplifted or reduced other spacetime dimensions. Specifically, the 11-dimensional solution (with $n = 1$) describes the M2/M2/M2-branes with rotation in the Kasner universe. We leave it to the future work whether other solutions with $n \neq 1$ can be understood in the context of intersecting branes.

Recently, all pseudo-supersymmetric solutions in 4- and 5-dimensional fake de Sitter fake supergravity were classified using the spinorial geometry method [10]. It is interesting to investigate whether more general solutions with nonvanishing torsion describe black hole solutions.

References

[1] D. Kastor and J. Traschen, Phys. Rev. D **47**, 5370 (1993) [arXiv: hep-th/9212035].

[2] L. A. J. London, Nucl. Phys. B **434** (1995) 709.

[3] K. Maeda, N. Ohta and K. Uzawa, JHEP **0906**, 051 (2009) [arXiv:0903.5483 [hep-th]].

[4] G. W. Gibbons and K. Maeda, Phys. Rev. Lett. **104**, 131101 (2010) [arXiv:0912.2809 [gr-qc]].

[5] K. Maeda and M. Nozawa, Phys. Rev. D **81**, 044017 (2010) [arXiv:0912.2811 [hep-th]].

[6] K. Maeda and M. Nozawa, Phys. Rev. D **81**, 124038 (2010) [arXiv:1003.2849 [gr-qc]].

[7] K. Behrndt and M. Cvetic, Class. Quant. Grav. **20**, 4177 (2003) [arXiv:hep-th/0303266]; D. Klemm and W. A. Sabra, JHEP **0102**, 031 (2001) [arXiv:hep-th/0011016].

[8] M. Nozawa and K. i. Maeda, arXiv:1009.3688 [hep-th], to appear in PRD.

[9] J. P. Gauntlett, R. C. Myers and P. K. Townsend, Class. Quant. Grav. **16**, 1 (1999) [arXiv:hep-th/9810204].

[10] J. B. Gutowski and W. A. Sabra, arXiv:0903.0179 [hep-th]; J. Grover, J. B. Gutowski, C. A. R. Herdeiro and W. Sabra, Nucl. Phys. B **809**, 406 (2009) [arXiv:0806.2626 [hep-th]].

No-dipole-hair theorem for higher-dimensional static black holes

Roberto Emparan[1(a)], Seiju Ohashi[2(b)] and Tetsuya Shiromizu[3(b)]

[(a)] *Institució Catalana de Recerca i Estudis Avançats (ICREA), Passeig Lluís Companys 23, E-08010 Barcelona, Spain and*
Departament de Física Fonamental and Institut de Ciències del Cosmos, Universitat de Barcelona, Martí i Franquès 1, E-08028 Barcelona, Spain
[(b)] *Department of Physics, Kyoto University, Kyoto 606-8502*

Abstract

We prove that static black holes in n-dimensional asymptotically flat spacetime cannot support nontrivial electric p-form field strengths when $(n+1)/2 \leq p \leq n-1$. This implies, in particular, that static black holes cannot possess dipole hair under these fields.

1 Introduction

Motivated by superstring theory, higher dimensional black holes has been attracted much attention [1]. In higher-dimensional static (electro)vacuum spacetime, the uniqueness thoerem holds. But, if one puts matter fields, it's highly nontrivial whether uniqueness theorem holds or not.

In this article we prove the impossibility of dipole hair for static black holes. The proof follows the one employed in the uniqueness theorem of higher-dimensional static black holes [2–5].

Together with the gauge dipole, we will also consider the inclusion of scalar fields and scalar hair. Bekenstein proved that a static black hole can not have scalar hair in four dimensions [6]. This no-hair theorem is easily extended to higher dimensions since the dimensionality does not enter into the proof. However, this type of proof cannot be applied to systems where the scalar field couples to higher form fields.

2 No-dipole-hair theorem

We consider n-dimensional asymptotically flat solutions of theories described by the class of Lagrangians

$$\mathcal{L} = R - \frac{1}{2}(\partial\phi)^2 - \frac{1}{p!}e^{-\alpha\phi}H_{(p)}^2, \tag{1}$$

where R is the n-dimensional Ricci scalar, ϕ is a dilaton with coupling α, and $H_{(p)}$ is the field strength of a $(p-1)$-form field potential $B_{(p-1)}$,

$$H_{(p)} = dB_{(p-1)}. \tag{2}$$

Since we are interested in asymptotically flat spacetimes, we take $p \leq n-1$. A form field with $p = n$ does not have any dynamical degree of freedom and behaves like a cosmological constant, which would prevent asymptotic flatness.

We only consider electric fields of $H_{(p)}$. Note that via electric-magnetic duality we can always trade a magnetic charge or dipole under $H_{(p)}$ for an electric one under $H_{(n-p)}$. However, we do not consider the possibility of simultaneous presence of dipoles and monopole charges of electric and magnetic type, *e.g.*, in $n = p+2$ one can have solutions with both magnetic monopole charge and electric dipole of $H_{(p)}$.

The metric of a static spacetime can be written as

$$ds^2 = g_{MN}dx^M dx^N = -V^2(x^i)dt^2 + g_{ij}(x^k)dx^i dx^j, \tag{3}$$

[1]Email address: emparan@ub.edu
[2]Email address: ohashi@tap.scphys.kyoto-u.ac.jp
[3]Email address: shiromizu@tap.scphys.kyoto-u.ac.jp

where x^i are spatial coordinates on $x^0 = t$ =const. surfaces Σ. In these coordinates, the event horizon is located at $V = 0$, *i.e.*, the Killing horizon. The static ansatz for the $(p-1)$-form potential is of the form

$$B_{(p-1)} = \varphi_{i_1 \cdots i_{p-2}}(x^k) dt \wedge dx^{i_1} \wedge \cdots \wedge dx^{i_{p-2}}. \tag{4}$$

Then the only nontrivial component of the field strength is $H_{0i_1 \cdots 1_{p-1}}$. The metric components and the potential do not depend on t.

We shall prove the following theorem:

No-dipole-hair theorem: The only static, asymptotically flat black hole solution for the theories (1) with electric p-form field strength, with $(n+1)/2 \leq p \leq n-1$, *is the Schwarzschild-Tangherlini solution.*

From the Einstein equation we have

$$^{(n-1)}R = \frac{e^{-\alpha\phi}}{(p-1)!V^2} H_0{}^{i_1 \cdots i_{p-1}} H_{0i_1 \cdots i_{p-1}} + \frac{1}{2}(D\phi)^2 \tag{5}$$

and

$$D^2 V = \frac{n-p-1}{(n-2)(p-1)!} \frac{e^{-\alpha\phi}}{V} H_0{}^{i_1 \cdots i_{p-1}} H_{0i_1 \cdots i_{p-1}}. \tag{6}$$

where D_i is the covariant derivative with respect to g_{ij} and $^{(n-1)}R$ is Ricci scalar on Σ.

The asymptotic behavior of V, g_{ij}, and $H_{(p)}$ is

$$V = 1 - \frac{m}{r^{n-3}} + O(1/r^{n-2}) \tag{7}$$

$$g_{ij} = \delta_{ij}\left(1 + \frac{2}{n-3}\frac{m}{r^{n-3}}\right) + O(1/r^{n-2}) \tag{8}$$

$$H_{0i_1 \cdots i_{p-1}} = O(1/r^{n-p+1}). \tag{9}$$

Observe that the falloff of $H_{(p)}$ is the appropriate one for a dipole field, or higher multipole components. In our proof this decay rate could be relaxed to that of a monopole field, $O(1/r^{n-p})$. However, as we explained in the introduction, when $p > 2$ electric monopole charges are incompatible with asymptotic flatness.

We also assume regularity on the event horizon. To this effect, we compute the curvature invariant

$$\begin{aligned} R_{MNKL}R^{MNKL} = {}& {}^{(n-1)}R_{ijkl}{}^{(n-1)}R^{ijkl} \\ & + \frac{4(n-2)}{(n-3)V^2\rho^2}[k_{ab}k^{ab} + k^2 + \mathcal{D}_a\rho\mathcal{D}^a\rho]. \end{aligned} \tag{10}$$

Here we have used the fact that the spatial metric can be written as

$$g_{ij}dx^i dx^j = \rho^2 dV^2 + h_{ab}dx^a dx^b, \tag{11}$$

where x^a is the coordinate on the level surfaces of V. $\mathcal{D}_a$ is the covariant derivative with respect to h_{ab}. k_{ab} is the extrinsic curvature of V =const. surface and $\rho := |D^i V D_i V|^{-1/2}$. Then, from Eq. (10), one can easily see that

$$k_{ab}|_{V=0} = \mathcal{D}_a\rho|_{V=0} = 0 \tag{12}$$

hold on the event horizon. From the Einstein equation, we can also easily see that regularity implies $H_{0i_1 \cdots i_{p-1}} = 0$ on the event horizon; see Eq. (5).

Let us consider the conformal transformation defined by

$$\tilde{g}_{ij} = \Omega_{\pm}^2 g_{ij} \tag{13}$$

where

$$\Omega_\pm = \left(\frac{1 \pm V}{2}\right)^{\frac{2}{n-3}} =: \omega_\pm^{\frac{2}{n-3}}. \tag{14}$$

This conformal transformation is the same as the one employed in the proof for the vacuum case [2, 4]. Now we have two manifolds, $(\tilde{\Sigma}^+, \tilde{g}^+)$ and $(\tilde{\Sigma}^-, \tilde{g}^-)$. The Ricci scalar of $\tilde{\Sigma}^\pm$ is

$$\Omega_\pm^{2\ (n-1)}\tilde{R}_\pm = \frac{1}{(p-1)!}\frac{e^{-\alpha\phi}}{V^2}\frac{\lambda_\pm}{\omega_\pm}H_0{}^{i_1\cdots i_{p-1}}H_{0i_1\cdots i_{p-1}} + \frac{1}{2}(D\phi)^2, \tag{15}$$

where

$$\lambda_\pm := \frac{1 \mp \frac{3n-4p-1}{n-3}V}{2}. \tag{16}$$

Since $0 \le V \le 1$, the $\lambda_\pm$ are positive-definite if

$$\frac{n+1}{2} \le p \le n-1. \tag{17}$$

Under this condition the positivity of ${}^{(n-1)}\tilde{R}_\pm$ follows. We will use this result later.

On $\tilde{\Sigma}^+$ the asymptotic behavior of the metric becomes

$$\tilde{g}^+_{ij} = \left(1 + O(1/r^{n-2})\right)\delta_{ij} \tag{18}$$

and therefore the ADM mass vanishes there. On $\tilde{\Sigma}^-$, the metric behaves like

$$\begin{aligned}\tilde{g}^-_{ij}dx^i dx^j &= \frac{(m/2)^{4/(n-3)}}{r^4}\delta_{ij}dx^i dx^j + O(1/r^5)\\ &= (m/2)^{4/(n-3)}(d\rho^2 + \rho^2 d\Omega^2_{n-2}) + O(\rho^5),\end{aligned} \tag{19}$$

where we set $\rho := 1/r$. From this, we see that infinity on Σ corresponds to a point, which we denote as q.

Let us construct a new manifold $(\tilde{\Sigma}, \tilde{g}_{ij}) := (\tilde{\Sigma}^+, \tilde{g}^+_{ij}) \cup (\tilde{\Sigma}^-, \tilde{g}^-_{ij}) \cup \{q\}$ by gluing the two manifolds $(\tilde{\Sigma}^+, \tilde{g}^+_{ij})$ and $(\tilde{\Sigma}^-, \tilde{g}^-_{ij})$ along the surface $V = 0$ and adding the point q. The calculations above imply that $(\tilde{\Sigma}, \tilde{g}_{ij})$ has zero mass and non-negative Ricci scalar. Note also that near the point q (which corresponds to $r \to \infty$) we have ${}^{(n-1)}\tilde{R}_- = O(r^{-(n-3)})$, so $\tilde{\Sigma}^-$ is regular at q . Thus $\tilde{\Sigma}$ is a Riemannian manifold with non-negative Ricci scalar and zero ADM mass. Then, by the positive energy theorem [8], $\tilde{\Sigma}$ is flat. So the metric $\tilde{g}_{ij}$ is flat and

$$H_{0i_1\cdots i_{p-1}} = 0 \quad \text{and} \quad \phi = \text{const} \tag{20}$$

hold. That is, asymptotically flat static black holes in n dimensions cannot support an electric dipole p-form field strength with p in the range (17), nor a nontrivial scalar field.

Once we have ruled out the possibility of nontrivial p-form and scalar fields, the problem is exactly the same as in vacuum and the results of [2] imply the uniqueness of the Schwarzschild-Tangherlini solution. For the sake of completeness, we briefly review this argument.

We have seen that $\tilde{\Sigma}^+$ must be flat space. In addition, we can check that the extrinsic curvature of the surface $V = 0$ on $\tilde{\Sigma}^+$ is proportional to its induced metric with a constant coefficient. According to Kobayashi and Nomizu [9], such a surface in flat space is spherically symmetric. Next, we define the function v by

$$v = \frac{2}{1+V}. \tag{21}$$

It is easy to see that it is a harmonic function on flat space $\tilde{\Sigma}^+$, that is,

$$\partial^2 v = 0. \tag{22}$$

The boundary corresponding to the horizon is spherically symmetric. So the problem is reduced to the familiar one of an electrostatic potential with spherical boundary in flat space. We can easily see that the level surfaces of v are spherically symmetric in the full region of $\tilde{\Sigma}^+$. So we have shown that Σ is spherically symmetric and then the spacetime must be the Schwarzschild-Tangherlini spacetime. This completes our proof.

3 Outlook

We have proven a no-dipole-hair theorem for p-form fields with p in the range (17). The proof can be straightforwardly extended to theories containing several electric form fields $H_{(p_i)}$ of different rank p_i, each with its own coupling α_i to the dilaton, as long as each of the p_i satisfies (17).

As mentioned above, the upper bound on p is a natural one given the requirement of asymptotic flatness. But the physical motivation for the lower bound, if any, is unclear. Could static black holes support dipoles when $p < (n+1)/2$? The answer when $p = 2$ is known: the uniqueness theorem of [3] affirms that a static black hole can have electric monopole charge, but not any higher multipole. However, here we are more interested in $p > 2$ where monopoles are not allowed. For instance, could there be static black holes in $n \geq 6$ with electric three-form, *i.e.*, string, dipole? The heuristic argument presented in the introduction would seem to run counter to this possibility, but maybe this argument misses a way to balance or cancel the tension of dipole sources that does not involve centrifugal forces. If this were the case it would be a striking new feature of static black holes afforded by higher dimensions. Alternatively, and more simply, maybe our no-dipole-hair theorem can be strengthened to rule out all p-form dipoles whenever $p \leq n-1$. This issue seems worthy of further investigation.

References

[1] R. Emparan and H. S. Reall, Living Rev. Relativity **11**, 6 (2008) [arXiv:0801.3471 [hep-th]].

[2] G. W. Gibbons, D. Ida and T. Shiromizu, Prog. Theor. Phys. Suppl. **148**, 284 (2002) [arXiv:gr-qc/0203004].

[3] G. W. Gibbons, D. Ida and T. Shiromizu, Phys. Rev. Lett. **89**, 041101 (2002) [arXiv:hep-th/0206049]; Phys. Rev. D **66**, 044010 (2002) [arXiv:hep-th/0206136].

[4] S. Hwang, Geometriae Dedicata **71**, 5 (1998).

[5] M. Rogatko, Phys. Rev. D **67**, 084025 (2003) [arXiv:hep-th/0302091],

[6] J. D. Bekenstein, Phys. Rev. D **5**, 1239 (1972).

[7] M. Rogatko, Phys. Rev. D **70**, 044023 (2004) [arXiv:hep-th/0406041],

[8] E. Witten, Commun. Math. Phys. **80**, 381 (1981),

[9] S. Kobayashi and K. Nomizu, *Foundations of Differential Geometry*, (Interscience, New York, 1969), Vol. II, Sec. VII, Theorem 5.1.

Observational constraints on assisted k-inflation

Junko Ohashi[1] and Shinji Tsujikawa[2]

Department of Physics, Faculty of Science, Tokyo University of Science, 1-3 Kagurazaka, Shinjuku-ku, Tokyo 162-8601, Japan

Abstract

The k-inflation models can give rise to large non-Gaussianities of primordial density perturbations because the field propagation speed is different from the speed of light. For assisted k-inflation models in which multiple scalar fields join an effective single-field attractor, we evaluate three observables: (i) the spectral index n_s of curvature perturbations, (ii) the tensor-to-scalar ratio r, and (iii) the non-Gaussianity parameter f_{nl}. This will be useful to constrain such models from future high-precision observations of the temperature anisotropies in Cosmic Microwave Background (CMB).

1 Introduction

Inflation has been the backbone of the high-energy cosmology over the past 30 years. Originally it was proposed to solve the horizon, flatness and monopole problems plagued in Big Bang cosmology [1]. Furthermore, inflation generally predicts almost scale-invariant adiabatic density perturbations [2]. This prediction is consistent with the observations of the CMB temperature anisotropies measured by WMAP [3]. One can distinguish between a host of inflationary models by comparing the theoretical prediction of the spectral index n_s of curvature perturbations and the tensor-to-scalar ratio r with observations.

In the next few years, the measurement of CMB temperature anisotropies by the Planck satellite will provide more high-precision observational data. In particular the non-Gaussianity parameter f_{nl} of primordial density perturbations may be constrained by about one order of magnitude better than the bounds constrained by WMAP. This will give additional important information to discriminate between many inflation models.

The standard inflation driven by a canonical scalar field ϕ with a potential $V(\phi)$ usually predicts small non-Gaussianities with $|f_{nl}| \ll 1$ for primordial perturbations [4, 5]. However the k-inflation models [6] described by the Lagrangian density $p(\phi, X)$, where $X = -(\nabla\phi)^2/2$ is the field kinetic energy, can give rise to large non-Gaussianities [7, 8]. This is related with the fact that for the Lagrangian including a non-linear kinetic term of X the propagation speed c_s is different from 1 (in the unit where the speed of light is $c = 1$).

In the models motivated by particle physics such as superstring and supergravity theories, there are many scalar fields that can be responsible for inflation (see e.g. [9]). In some cases, even if each field is unable to lead to cosmic acceleration, the presence of many fields allows a possibility for the realization of inflation through the so-called assisted inflation mechanism [10]. In Ref. [10] it was shown that many canonical fields with exponential potentials $V_i(\phi_i) = c_i e^{-\lambda_i \phi_i}$ evolve to give dynamics matching a single field with the effective slope $\lambda_{\rm eff} = \left(\sum_{i=1} 1/\lambda_i^2\right)^{-1/2}$. Since $\lambda_{\rm eff}$ is smaller than λ_i, the presence of multiple fields can lead to sufficient amount of inflation.

Ref. [11] showed that the Lagrangian density $p = \sum_{i=1}^{n} X_i g(Y_i)$, where $g(Y_i)$ is an arbitrary function in terms of $Y_i = X_i e^{\lambda_i \phi_i}$, leads to assisted inflation as in the case of the canonical fields with exponential potentials (see also Refs. [12, 13]). Moreover, since this assisted Lagrangian covers the k-inflation models such as the dilatonic ghost condensate [12] and the DBI inflation [14], the primordial non-Gaussianities can be large if $c_s^2 \ll 1$. We shall study the theoretical prediction of the three observables n_s, r, f_{nl} to confront assisted k-inflation models with observations.

[1]Email address: j1209610@ed.kagu.tus.ac.jp
[2]Email address: shinji@rs.kagu.tus.ac.jp

2 K-inflation model

The single-field k-inflation models with non-standard kinetic terms are described by the action [6]

$$S = \int d^4x\sqrt{-g}\left[M_{\rm pl}^2 R/2 + p(\phi, X)\right] , \tag{1}$$

where g is a determinant of the metric $g_{\mu\nu}$, $M_{\rm pl}$ is a reduced Planck mass, R is a scalar curvature, p is a general function in terms of the field ϕ and a kinetic term $X = -g^{\mu\nu}\partial_\mu\phi\partial_\nu\phi/2$. The pressure p and the energy density ρ of the scalar field are given, respectively, by

$$p = p(X, \phi) , \qquad \rho = 2Xp_{,X} - p , \tag{2}$$

where $p_{,X} \equiv \partial p/\partial X$.

In the flat Friedmann-Lemaître-Robertson-Walker (FLRW) background with a scale factor $a(t)$ the equations of motion are

$$3M_{\rm pl}^2 H^2 = \rho , \qquad \dot\rho + 3H(\rho + p) = 0 , \tag{3}$$

where $H \equiv \dot a/a$ is the Hubble parameter. The field propagation is defined by

$$c_s^2 \equiv \frac{p_{,X}}{\rho_{,X}} = \frac{p_{,X}}{p_{,X} + 2Xp_{,XX}} , \tag{4}$$

If p has a non-linear term of X, then c_s is different from 1. It is convenient to introduce "slow variation parameters", as

$$\epsilon \equiv -\frac{\dot H}{H^2} , \qquad \eta \equiv \frac{\dot\epsilon}{H\epsilon} , \qquad s \equiv \frac{\dot c_s}{Hc_s} . \tag{5}$$

In Ref. [15] the primordial scalar power spectrum $\mathcal{P}_S$ was derived, as

$$\mathcal{P}_S = \frac{H^2}{8\pi^2 M_{pl}^2\, c_s\, \epsilon} , \tag{6}$$

where the expression is evaluated at the time of horizon exit at $c_s k = aH$ (k is a comoving wavenumber). The spectral index n_s is

$$n_s - 1 = \left.\frac{d\ln\mathcal{P}_S}{d\ln k}\right|_{c_s k = aH} = -2\epsilon - \eta - s . \tag{7}$$

As long as $\epsilon, |\eta|, |s|$ are much smaller than 1, the scalar power spectrum is close to scale-invariant.

The tensor power spectrum $\mathcal{P}_T$ and its spectral index n_T are given by

$$\mathcal{P}_T = \frac{2H^2}{\pi^2 M_{pl}^2} , \qquad n_T = \left.\frac{d\ln\mathcal{P}_T}{d\ln k}\right|_{c_s k = aH} = -2\epsilon . \tag{8}$$

From Eqs. (7) and (8) the tensor-to-scalar ratio is

$$r \equiv \mathcal{P}_T/\mathcal{P}_S = 16\epsilon c_s = -8c_s n_T . \tag{9}$$

The primordial scalar non-Gaussianities can be evaluated by considering three-point correlation $\langle\mathcal{R}(\mathbf{k}_1)\mathcal{R}(\mathbf{k}_2)\mathcal{R}(\mathbf{k}_3)\rangle$ for the curvature perturbation $\mathcal{R}$. In the equilateral case ($|\mathbf{k}_1| = |\mathbf{k}_2| = |\mathbf{k}_3|$) the non-Gaussianity parameter f_{nl} is given by [7, 8]

$$f_{nl}|_{\rm equilateral} = 0.28\left(1 - 1/c_s^2\right) - 0.02(\epsilon/\epsilon_X)\, s + 1.53\,\epsilon + 0.42\,\eta , \tag{10}$$

where $\epsilon_X \equiv -(\dot X/H^2)(\partial H/\partial X)$. Note that our sign convention of f_{nl} coincides with that in the WMAP paper [3].

3 Observational constraints on inflation models

Let us proceed to recent observational constraints on the three inflationary parameters n_s, r, and f_{nl}. From the WMAP 7 year data combined with the distance measurements from the baryon acoustic oscillations in the distribution of galaxies and the Hubble constant (H_0) measurement, the scalar spectral index and the tensor-to-scalar ratio, in the case of no runnings of scalar and tensor perturbations, are constrained to be [3]

$$n_s = 0.963 \pm 0.012 \ (68\% \ \mathrm{CL}) \,, \qquad r < 0.24 \ (95\% \ \mathrm{CL}) \,. \tag{11}$$

The bound on the non-Gaussianity parameter $f_{nl}|_{\mathrm{equil}}$ is

$$f_{nl}|_{\mathrm{equil}} = 26 \pm 140 \ (68\% \ \mathrm{CL}) \,. \tag{12}$$

We can distinguish between many inflation models by comparing the theoretical prediction of these parameters with observations.

4 Assisted k-inflation model

We consider the following Lagrangian density with n scalar fields

$$p = \sum_{i=1}^{n} X_i \, g(Y_i) \,, \tag{13}$$

where $X_i = -g^{\mu\nu}\partial_\mu\phi_i\partial_\nu\phi_i/2$, $g(Y_i)$ is an arbitrary function in terms of $Y_i \equiv X_i e^{\lambda_i\phi_i}$ for each field, and λ_i's are constants. The multiple fields evolve to give dynamics matching an effective single-field model $p = Xg(Y)$ with [11]

$$\frac{1}{\lambda^2} = \sum_{i=1}^{n} \frac{1}{\lambda_i^2} \,. \tag{14}$$

Originally the Lagrangian density $p = Xg(Y)$ with $Y = Xe^{\lambda\phi}$ was derived for the existence of scaling solutions [12, 13], but it was later found that the multi-field system described by (13) can lead to assisted inflation with λ smaller than λ_i [11].

Considering autonomous equations of the effective single-field system with $p(X, \phi) = Xg(Y)$, one can show that there is an inflation attractor characterized by the condition $\dot{\phi}/H = \lambda/p_{,X}$ [11], i.e.

$$\lambda^2 = \frac{6\,(g + Yg')^2}{g + 2\,Yg'} \,, \tag{15}$$

where a prime represents a derivative with respect to Y. The stability of this solution requires that $\lambda^2 < 2\,(g + Yg')$. For given $g(Y)$, it follows that Y is constant. The parameters ϵ and c_s^2 are given by

$$\epsilon = \frac{3\,(g + Yg')}{g + 2\,Yg'} \,, \qquad c_s^2 = \frac{g + Yg'}{g + 5\,Yg' + 2\,Y^2 g''} \,, \tag{16}$$

which are functions of Y only. Hence we have $\epsilon = const.$ and $c_s^2 = const.$ on the attractor, which gives $\eta = 0$ and $s = 0$. Therefore the three inflationary observables reduce to

$$n_s = 1 - 2\,\epsilon \,, \quad r = 16\,\epsilon\, c_s \,, \quad f_{nl}|_{\mathrm{equil}} = 0.28\left(1 - 1/c_s^2\right) + 1.53\,\epsilon \,. \tag{17}$$

If $c_s^2 \ll 1$, then the non-Gaussianity parameter f_{nl} can be large ($|f_{nl}| \gg 1$).

The standard slow-roll inflation model with an exponential potential $V(\phi) = ce^{-\lambda\phi}$ corresponds to the choice $g(Y) = 1 - c/Y$. In this case we obtain the following relations

$$c_s^2 = 1 \,, \qquad \lambda^2 = \frac{6\,Y}{Y + c} \,, \qquad \epsilon = \frac{3\,Y}{Y + c} \,. \tag{18}$$

The three inflationary observables can be written in terms of a single parameter λ:

$$n_s = 1 - \lambda^2 \,, \qquad r = 8\lambda^2 \,, \qquad f_{nl} = 0.765\lambda^2 \,. \tag{19}$$

From the observational constraint (11) we require that $\lambda^2 \ll 1$ and hence $f_{nl} \ll 1$. On the other hand, the assisted k-inflation models based on the dilatonic ghost condensate [12] and the DBI inflation [14] can give rise to large f_{nl} accessible to the upper bound given in (12). We will leave the detailed analysis of such cases in a separate publication [16].

5 Conclusion

We have evaluated the three observables n_s, r, and f_{nl} for the assisted k-inflation model described by the effective single-field Lagrangian density $p(X, \phi) = Xg(Y)$ with $Y = Xe^{\lambda\phi}$. Since Y is constant on the assisted inflation attractor, the three observables can be expressed in terms of a single parameter: Y or λ. The field propagation speed c_s is also a function of Y only and is different from 1 in general. The non-Gaussianity parameter f_{nl} can be large in k-inflation models, whereas $f_{nl} \ll 1$ in standard slow-roll inflation since $c_s = 1$. It will be of interest to constrain the allowed parameter space of assisted k-inflation models from the joint analysis of WMAP and other observations.

References

[1] A. A. Starobinsky, Phys. Lett. B **91** (1980) 99; D. Kazanas, Astrophys. J. **241** L59 (1980); K. Sato, Mon. Not. R. Astron. Soc. **195**, 467 (1981); A. H. Guth, Phys. Rev. D **23**, 347 (1981).

[2] V. F. Mukhanov and G. V. Chibisov, JETP Lett. **33**, 532 (1981); A. H. Guth and S. Y. Pi, Phys. Rev. Lett. **49** (1982) 1110; S. W. Hawking, Phys. Lett. B **115**, 295 (1982); A. A. Starobinsky, Phys. Lett. B **117** (1982) 175.

[3] E. Komatsu *et al.*, arXiv:1001.4538 [astro-ph.CO].

[4] N. Bartolo, S. Matarrese and A. Riotto, Phys. Rev. D **65**, 103505 (2002).

[5] J. M. Maldacena, JHEP **0305**, 013 (2003).

[6] C. Armendariz-Picon, T. Damour and V. F. Mukhanov, Phys. Lett. B **458**, 209 (1999).

[7] D. Seery and J. E. Lidsey, JCAP **0506**, 003 (2005).

[8] X. Chen, M. x. Huang, S. Kachru and G. Shiu, JCAP **0701**, 002 (2007).

[9] D. H. Lyth and A. Riotto, Phys. Rept. **314**, 1 (1999).

[10] A. R. Liddle, A. Mazumdar and F. E. Schunck, Phys. Rev. D **58**, 061301 (1998).

[11] S. Tsujikawa, Phys. Rev. D **73**, 103504 (2006).

[12] F. Piazza and S. Tsujikawa, JCAP **0407**, 004 (2004).

[13] S. Tsujikawa and M. Sami, Phys. Lett. B **603**, 113 (2004).

[14] E. Silverstein and D. Tong, Phys. Rev. D **70**, 103505 (2004); M. Alishahiha, E. Silverstein and D. Tong, Phys. Rev. D **70**, 123505 (2004).

[15] J. Garriga and V. F. Mukhanov, Phys. Lett. B **458**, 219 (1999).

[16] J. Ohashi and S. Tsujikawa, *in preparation*.

Dynamics of flat anisotropic cosmological models in Lovelock gravity

Sergey Pavluchenko[1]

Special Astrophysical Observatory, Russian Academy of Sciences, Nizhnij Arkhyz, 369167 Russia

Abstract

In this report we summarize the main results obtained in past several years of our study the cosmological dynamics of flat anisotropic models in Lovelock gravity. With all results already published, there are features that are, in our opinion, essential to understanding the dynamics, but that were "left behind" the articles. Hence in addition to the results themselves we decided add a discussion of these features as well as mark the problems that are still remain unsolved.

1 Introduction

Although the idea of extra dimensions [1] is as old as General Relativity, real surge in interest was caused by the development of string theory in 70s-80s. String theories naturally could be formulated only in higher number of spatial dimensions, and the cosmological aspect of such theories also attracted an attention. Studing the low-energy limit of such theories, the researches found that the Lagrangians should have terms that are squared on curvature: R^2 and $R_{\mu\nu}R^{\mu\nu}$ [2], as well as $R_{\mu\nu\lambda\rho}R^{\mu\nu\lambda\rho}$ [3]. Later, it was demonstrated [4] that the only combination of quadratic terms that leads to ghost-free nontrivial gravitation interaction is the Gauss-Bonnet term:

$$L_{GB} = R_{\mu\nu\lambda\rho}R^{\mu\nu\lambda\rho} - 4R_{\mu\nu}R^{\mu\nu} + R^2.$$

This term is an topological invariant in 3 spatial dimensions but gives nontrivial contribution to the Lagrangian in (4+1) and in higher dimensions. Lovelock [5] derived the generic Lagrangian (Lovelock Lagrangian) of the order n, that contains n-th power of curvature contribution that is topological invariant if the number of spatial dimensions $D < 2n$ but nontrivial for $D \geqslant 2n$. So that Lovelock Lagrangian could be considered as a natural generalization of Gauss-Bonnet term in higher dimensions, though the fact that quadratic corrections of string theory is equal to Gauss-Bonnet term (2nd order Lovelock contribution) is a pure coincidence – cubic string correction does not equal to the 3rd order Lovelock term.

So we study the dynamics of flat anisotropic models in Lovelock gravity. The chioce of flat anisotropic models is motivated by several reasons – firstly, flat models are the simplest to deal with; they also have the same asymptotics in low-curvature regime as the models with some nontrivial Lie algebra in spatial part. Regarding anisotropy – anisotropic models form a more general class of geometries with Friedman models as a part of it; the presence of matter often leads to isotropisation turning anisotropic models into Friedman models. At this point, let us clarify the meaning of "flatness" of the model considered. Following Landau and Lifshits [6] let us introduce "spatial curvature tensor" P_{ijkl} with definition that coinside with that of Riemann tensor $R_{\nu\mu\lambda\rho}$ but with only spatial indices (so the Christoffel symbols are also computed with only spatial part). Now we call a model "spatially flat" if $P_{ijkl} = 0$ (obviously, $R_{\nu\mu\lambda\rho}$ might have non-zero components so the model would have non-zero Riemann curvature) and work with this kind of model. In three-dimensional case Bianchi classification is applied and all anisotropic models are divided into 9 classes – from Bianchi-I to Bianchi-IX (see [6]), and only one of them – Bianchi-I – is flat; its line element has a form $dl^2 = \mathrm{diag}(a^2(t), b^2(t), c^2(t))$. The classification of higher-dimensional anisotropic models is much more complicated (so far only (4+1) is fully classified [7]), but the form of flat model remains the same – its metric is $ds^2 = \mathrm{diag}(-c^2dt^2, a_1^2(t), a_2^2(t), \ldots, a_D^2(t))$ for $(D+1)$-dimensional model.

The manuscript is structured as follows: in next section we describe our study of generic Lagrangian and equations of motion for flat anisotropic models, and discuss the results. Then, we focus on the

[1]Email address: sergey.pavluchenko@gmail.com

(4+1)-dimensional model as an example of case with even number of spatial dimensions. The model in question is studied numerically both in vacuum and in presence of matter in the form of a perfect fluid; finally, we generalize the results on the higher number of spatial dimensions.

2 Generic Lagrangian and equations of motion

The details of the Lagrangian and equations of motion derivation could be found in [8]. Here we give the final result and discuss the difference between the cases with odd and even number of spatial dimensions. We consider "pure" Lovelock gravity (i.e., without Einstein-Hilbert contribution to the Lagrangian) with only highest possible correction taken into account. This is a good approach to the high-curvature regime – indeed, in this regime the leading one is the highest-order curvature correction. First, let us have a look on the constraint equation: in case $D = 2n + 1$ it takes the form

$$\sum_{k_1>k_2>\ldots k_{2n}} H_{k_1} H_{k_2} \ldots H_{k_{2n}} = \frac{\rho}{2n-1}, \tag{1}$$

$$\text{while in case } D = 2n \text{ it becomes} \quad H_1 H_2 \ldots H_{2n} = \frac{\rho}{2n-1}, \tag{2}$$

where $H_i = \dot{a}_i/a_i$ is the Hubble parameter that corresponds to i-th spatial dimension. One can see that due to different number of spatial dimensions in case $D = 2n + 1$ we have a sum of $2n$-multiplications, while in $D = 2n$ case this sum limits to one term. In vacuum case ($\rho = 0$) this difference is crucial – from (2) one can see that in case $D = 2n$ one of Hubble parameters should always be equal to zero, while in $D = 2n + 1$ case it is not so. If the Universe is not vacuum but filled with a perfect fluid with density ρ, the situation for the case $D = 2n$ changes drastically – none of Hubble parameters could be equal to zero. Thus, even small amount of matter completely changes the dynamics of the models with even number of spatial dimensions. On the contrary, there is no such change in case of odd number of spatial dimensions (1), so addition of matter "smoothly" changes its dynamics.

Not only constraint equations, but dynamical equations are also different for these two cases – in case $D = 2n + 1$ i-th dynamical equation has the form (other dynamical equations could be obtained from this one via cyclic index transmutation)

$$\sum_{\substack{m=1\\m\neq i}}^{D} \left[(\dot{H}_m + H_m^2) \sum_{\substack{\{j_1, j_2, \ldots j_{2n-2}\}\neq\{i,m\}\\ j_1>j_2>\ldots j_{2n-2}}} H_{j_1} H_{j_2} \ldots H_{j_{2n-2}} \right] + (2n-1)\ H_{k_1} H_{k_2} \ldots H_{k_{2n}} + p = 0, \tag{3}$$

$$\text{while in case } D = 2n \text{ it becomes} \quad \sum_{\substack{m=1\\m\neq i}}^{D} (\dot{H}_m + H_m^2)\ H_{j_1} H_{j_2} \ldots H_{j_{2n-2}} + p = 0, \tag{4}$$

where p is the pressure of the ideal fluid (vanishes in the vacuum case). The difference between (3) and (4) is obvious – second sum in (3)(inside the brackets) limits to only one term in (4) while the second term (with $(2n-1)$ multiplier) vanishes.

Finally, the models with even number of spatial dimensions have a "special solution" with $p = 0$. If we look for the solutions in power-law form, we can rewrite scale factors as $a_i(t) = t^{p_i}$ with p_i called Kasner exponents [9]. Expressing H_i and $\dot{H}_i$ through p_i and substituting them into (4) one can find that $p_i \equiv 1$ is valid solution.

3 (4+1)-dimensional case

In this section we review the results of numerical investigation of (4+1)-dimensional Einstein-Gauss-Bonne model (see [10] for details). We interested in both – future and past – asymptotics so we take both contributions – Einstein and Gauss Bonnet – into account. First we consider the vacuum case; we

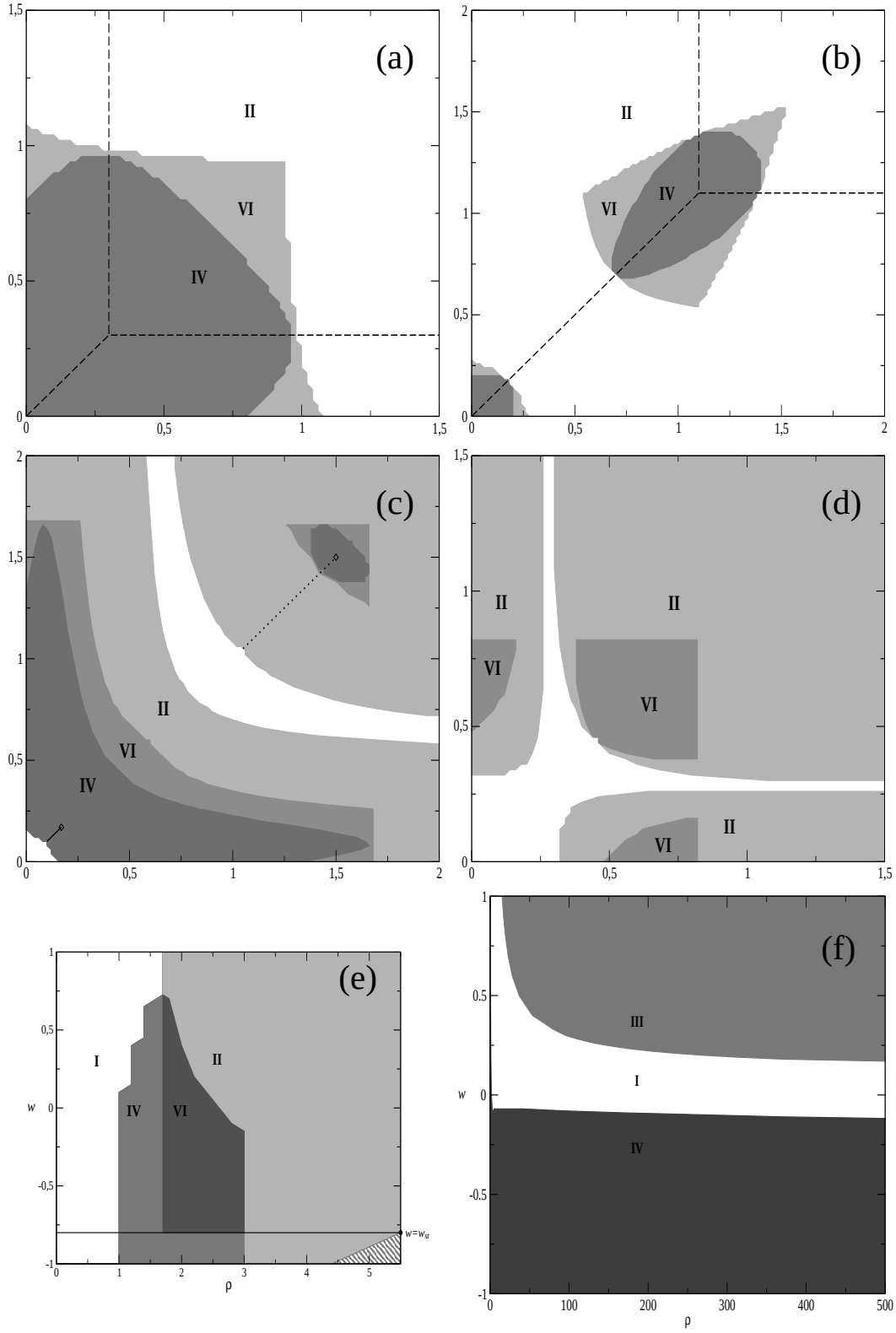

Figure 1: An examples of 2D scans over $H_1^{(0)}$ and $H_2^{(0)}$ with positive ((a) and (b)) as well as negative ((c) and (d)) value for $H_3^{(0)}$ for vacuum model. In (e) and (f) panels we demonstrate typical pattern for negative (e) and positive (f) triads in the presence of matter.

Table. Classification of possible trajectories

From	To	Design.
Standard singularity	Kasner	I
	Recollaps	II
	Non-standard sing.	III
Non-standard. sing.	Kasner	IV
	Recollaps	V
	Non-standard sing.	VI

make scans over the initial values of three Hubble parameter and calculate the fourth from constraint equation. Then we numerically calculate the equations of motion to reveal its future and past behavior, Table summarize all possible trajectories. In Fig. 1a–1d we present an example of our resuls – 2D "slices" of the resulting 3D picture in the $(H_1^{(0)}, H_2^{(0)}, H_3^{(0)})$ space. Figures 1a and 1b give example for positive and increasing $H_3^{(0)}$ while Figs. 1c and 1d – for negative and decreasing. One can see that these two cases have different dynamics – although type-II dominate in both of them and type-IV and type-VI decreasing, in case of positive $H_3^{(0)}$ they never vanish while if $H_3^{(0)}$ is negative they eventually do.

Finally let us investigate the influence the matter in form of perfect fluid exerts upon the dynamics of the model considered. We add matter to all vacuum regimes and scan over density and the equation of state $w = p/\rho$. We found that, almost independently of the vacuum transition, all transition maps on (ρ, w)-plane looks like either Fig. 1e of 1f. In presence of matter the constraint equation that we use to find $H_4^{(0)}$ takes a form

$$H_4^{(0)} = -\frac{2H_1^{(0)}H_2^{(0)} + 2H_1^{(0)}H_3^{(0)} + 2H_2^{(0)}H_3^{(0)} - \rho_0}{2H_1^{(0)} + 2H_2^{(0)} + 2H_3^{(0)} + 24\alpha H_1^{(0)}H_2^{(0)}H_3^{(0)}}. \tag{5}$$

One can see that depending on sign of the denominator, growth of ρ_0 leads either to increasing of $H_4^{(0)}$ or to decreasing. We call triads $(H_1^{(0)}, H_2^{(0)}, H_3^{(0)})$ that lead to former case as "positive" while those that lead to the latter – as "negative". Behavior of negative triads is shown in Fig. 1e, of positive – in Fig. 1f. Figure 1f also demonstrates presence of type-I transition – the only one that might have a connection with our Universe (in vacuum case the measure of type-I transitions is zero). Thus, addition of matter not only demonstrates interesting regime separation but also adds the regimes that are absent in vacuum.

Finally, I'd' like to thank the Organizing Committee for their hospitality during the workshop and for financial support.

References

[1] G. Nordström, Phys. Z. **15**, 504 (1914).

[2] J. Scherk and J.H. Schwarz, Nucl. Phys. **B81**, 118 (1974).

[3] P. Candelas, G.T. Horowitz, A. Strominger, and E. Witten, Nucl. Phys. **B258**, 46 (1985).

[4] B. Zwiebach, Phys. Lett. B **156**, 315 (1985).

[5] D. Lovelock, J. Math. Phys. (N.Y.) **12**, 498 (1971).

[6] L.D. Landau and E.M. Lifshitz, *The Classical Theory of Fields*, (Pergamon Press, Oxford, 2002).

[7] S. Hervik, Class. Quant. Grav. **19**, 5409 (2002).

[8] S. Pavluchenko, Phys. Rev. D **80**, 107501 (2009).

[9] E. Kasner, Am. J. Math., **43**, 217 (1921).

[10] S. Pavluchenko, Phys. Rev. D **82**, 104021 (2010).

Time evolution of potential dominated scalar-tensor cosmologies in the general relativity limit

Margus Saal[1(a)], Laur Järv[2(b)] and Piret Kuusk[3(b)]

[(a)] *Tartu Observatory, EE-61602 Tõravere, Tartumaa, Estonia*
[(b)] *Institute of Physics, University of Tartu, Riia 142, EE-51014 Tartu, Estonia*

Abstract

We consider Friedmann-Lemaître-Robertson-Walker flat cosmological models in the framework of general Jordan frame scalar-tensor theories of gravity with arbitrary coupling function and potential. At the era when the energy density of the potential dominates over the energy density of ordinary matter, we use a nonlinear approximation of the decoupled scalar field equation for the regime close to the so-called limit of general relativity where the local weak field constraints are satisfied. The nonlinear equation for the scalar field can be solved analytically in cosmological time. We focus to the models that asymptotically converge to general relativity and make some implications about the cosmological dynamics near this limit. In particular, the effective equation of state parameter $\mathrm{w_{eff}}$ is used to illustrate possible cosmological dynamics near this limit.

1 Introduction

The current expansion of the Universe can be accommodated in a cosmological model with a suitable cosmological constant Λ which is equivalent to an additional matter component with an equation of state (EoS) $\mathrm{w_\Lambda} = \mathrm{p_\Lambda}/\rho_\Lambda = -1$. However, recent data are not excluding the possibility that the EoS of dark energy is changing in the cosmological time [1, 2]. This circumstance gives additional encouragement to consider generalized theories of gravity which involve the possibility for a variable EoS of dark energy.

In this paper we consider the Friedmann-Lemaître-Robertson-Walker (FLRW) flat cosmological models in the framework of general scalar-tensor theory of gravity (STG) in a late Universe. We expect that at late times the energy density of scalar potential dominates over the energy density of matter at cosmological scales (we take $\rho_m = 0$) and the STG is close to general relativity (GR) (referred as 'the limit of GR' or 'GR point'). Among the other arguments, the latter assumption is strongly motivated by local weak field tests [3, 4] i.e. the limits of observed values of parametrized post-Newtonian (PPN) parameters $|\beta - 1| < 10^{-4}$, $|\gamma - 1| < 10^{-5}$ and the time variation of the gravitational constant $|\dot{G}/G| < 10^{-13}$. Therefore it is of particular interest to study the solutions of STG near the 'GR point'. The following is a brief review of our earlier publications [5–8].

2 Equations and approximation method

General scalar-tensor gravity in the Jordan frame is governed by the action

$$S = \frac{1}{2\kappa^2}\int d^4x\sqrt{-g}\left[\Psi R(g) - \frac{\omega(\Psi)}{\Psi}\nabla^\rho\Psi\nabla_\rho\Psi - 2\kappa^2 V(\Psi)\right]. \tag{1}$$

Here $\omega(\Psi)$ is a coupling function (we assume $2\omega(\Psi)+3 \geq 0$ to avoid ghosts in the Einstein frame), $V(\Psi) \geq 0$ is a potential, and κ^2 is the non-variable part of the effective gravitational constant $\frac{\kappa^2}{\Psi}$. In

[1]Email address: margus@fi.tartu.ee
[2]Email address: laur.jarv@ut.ee
[3]Email address: piret@fi.tartu.ee

order to keep the latter positive we assume that $0 < \Psi < \infty$. The field equations for the flat FLRW line element $ds^2 = -dt^2 + a(t)^2\left(dr^2 + r^2(d\theta^2 + \sin^2\theta d\varphi^2)\right)$ read

$$H^2 = -H\frac{\dot\Psi}{\Psi} + \frac{1}{6}\frac{\dot\Psi^2}{\Psi^2}\,\omega(\Psi) + \frac{\kappa^2}{\Psi}\frac{V(\Psi)}{3}\,, \tag{2}$$

$$2\dot H + 3H^2 = -2H\frac{\dot\Psi}{\Psi} - \frac{1}{2}\frac{\dot\Psi^2}{\Psi^2}\,\omega(\Psi) - \frac{\ddot\Psi}{\Psi} + \frac{\kappa^2}{\Psi}\,V(\Psi)\,, \tag{3}$$

$$\ddot\Psi = -3H\dot\Psi - \frac{1}{2\omega(\Psi)+3}\,\frac{d\omega(\Psi)}{d\Psi}\,\dot\Psi^2 + \frac{2\kappa^2}{2\omega(\Psi)+3}\,\left[2V(\Psi) - \Psi\,\frac{dV(\Psi)}{d\Psi}\right], \tag{4}$$

where $H \equiv \dot a/a$. Upon introducing the notation

$$A(\Psi) \equiv \frac{d}{d\Psi}\left(\frac{1}{2\omega(\Psi)+3}\right), \qquad W(\Psi) \equiv 2\kappa^2\left(2V(\Psi) - \frac{dV(\Psi)}{d\Psi}\Psi\right) \tag{5}$$

and substituting H from Eq. (2) in Eq. (4), we get

$$\ddot\Psi = \left(\frac{3}{2\Psi} + \frac{1}{2}A(\Psi)(2\omega(\Psi)+3)\right)\dot\Psi^2 \pm \frac{1}{2\Psi}\sqrt{3(2\omega(\Psi)+3)\dot\Psi^2 + 12\kappa^2\Psi V(\Psi)}\,\dot\Psi + \frac{W(\Psi)}{2\omega(\Psi)+3}\,. \tag{6}$$

In the limit $\frac{1}{(2\omega(\Psi)+3)} \to 0$, $\dot\Psi \neq 0$ the system faces a spacetime curvature singularity, since H diverges, and likewise behaves $\ddot\Psi$. At first the limit (a) $\frac{1}{(2\omega(\Psi)+3)} \to 0$ and (b) $\dot\Psi \to 0$ seems only slightly less mathematically precarious for the equations are left just indeterminate (contain terms $\frac{0}{0}$). Yet the latter situation is of particular physical importance, as the experiments in the Solar System (where local matter density dominates over the scalar potential), i.e. the limits of observed values of PPN parameters and the time variation of the gravitational constant [3, 4], suggest the present cosmological background value of the scalar field to be very close to the limit (a)-(b). As in this limit the STG PPN parameters coincide with those of general relativity we may tentatively call (a)-(b) 'the limit of GR' or 'GR point'. Let us define $\Psi_\star$ by $\frac{1}{2\omega(\Psi_\star)+3} = 0$ and make two additional assumptions (c) $A_\star \equiv A(\Psi_\star) \neq 0$ and (d) $\frac{1}{2\omega+3}$ is differentiable at $\Psi_\star$.

In what follows we focus around the point in the phase space, which corresponds to the limit of GR, $\Psi = \Psi_\star + x$, $\dot\Psi = \dot\Psi_\star + y = y$, where x and y span the neighbourhood of first order small distance from $(\Psi_\star,\, \dot\Psi_\star)$. As phase space variables x and y are independent from each other, their ratio y/x is indeterminate at $(x = 0,\, y = 0)$. We can expand in series

$$\frac{1}{2\omega(\Psi)+3} = \frac{1}{2\omega(\Psi_\star)+3} + A_\star x + \ldots \approx A_\star x\,, \tag{7}$$

$$(2\omega(\Psi)+3)\dot\Psi^2 = \frac{y^2}{0 + A_\star x + \ldots} = \frac{y^2}{A_\star x}(1 + O(x)) \approx \frac{y^2}{A_\star x}\,. \tag{8}$$

In approximate equations we must recognize the term $\frac{y^2}{x}$ as being the same order as x and y. Thus, keeping the term $\frac{y^2}{x}$ in the approximation of Eq. (6) we obtain a second order nonlinear differential equation [7, 8]

$$\ddot x + C_1\,\dot x - C_2\,x = \frac{\dot x^2}{2x} \tag{9}$$

and the corresponding first order system reads

$$\dot x = y\,, \qquad \dot y = \frac{y^2}{2x} - C_1\,y + C_2\,x\,. \tag{10}$$

Here we have defined the values of some parameters at $(\Psi_\star,\, \dot\Psi_\star)$ as

$$C_1 \equiv \pm\sqrt{\frac{3\kappa^2 V(\Psi_\star)}{\Psi_\star}}\,, \qquad C_2 \equiv A_\star\,W_\star\,, \tag{11}$$

where $W_\star \equiv W(\Psi_\star)$ and $V(\Psi_\star) \geq 0$. The three parameters $A_\star$, $W_\star$, C_1 determine the leading terms in expansions of the two functions $\omega(\Psi)$, $V(\Psi)$ which specify a STG. The phase trajectories for the nonlinear approximate system (10) near 'GR point' are classified and analysed in [7]. The fixed points and corresponding eigenvalues in the case of linear system (neglecting the term $y^2/2x$) are found in [6].

3 Solutions in cosmological time

The general solution of Eq. (9) reads

$$\pm\, x(t) = e^{-C_1 t}\left[M_1 e^{\frac{1}{2}t\sqrt{C}} - M_2 e^{-\frac{1}{2}t\sqrt{C}}\right]^2, \qquad C > 0\,, \tag{12}$$

$$= e^{-C_1 t}\left[M_1 t - M_2\right]^2, \qquad C = 0\,, \tag{13}$$

$$= e^{-C_1 t}\left[N_1 \sin(\frac{1}{2}t\sqrt{|C|}) - N_2 \cos(\frac{1}{2}t\sqrt{|C|})\right]^2, \quad C < 0\,, \tag{14}$$

where $C = \sqrt{C_1^2 + 2C_2}$ and M_1, M_2, N_1, N_2 are constants of integration determined by initial conditions. In order to successfully meet the observational constraints, let us now focus upon solutions which approach the GR limit asymptotically in time (PPN parameters approch the GR values $\beta = 1$ and $\gamma = 1$ as $t \to \infty$). Our results [6–8] allow one to immediately decide whether any STG with particular $\omega(\Psi)$ and $V(\Psi)$ is viable or not. Furthermore, the behavior of solutions which approach GR can be classified under two characteristic types: (i) exponential or linear exponential convergence ($C > 0$ or $C = 0$) (ii) damped oscillations around GR ($C < 0$).

For the evolution of the universe in scalar-tensor cosmology we may envisage a realistic scenario where during the matter domination era the scalar field has already dynamically relaxed sufficiently close to the GR limit. Later when the cosmological energy density of the potential becomes more significant, the solutions given here can be taken to provide a rough description. As an illustration for dynamics given by solutions (12)-(14), we use the effective barotropic index which determines the behaviour of dark energy. The same approximation scheme introduced in previous chapter allows to expand the effective barotropic index as (the expansion of H, $\dot{H}$ and PPN parameters, see [8])

$$\mathrm{w_{eff}} \equiv -1 - \frac{2\dot{H}}{3H^2} \approx -1 + \frac{1}{C_1^2 \Psi_\star}\left[\frac{3}{2}\left(1 + \frac{1}{\Psi_\star A_\star}\right)\frac{\dot{x}^2}{x} - 4C_1\dot{x} + 3C_2 x\right] + \ldots\,. \tag{15}$$

Among the models for which the 'GR point' works as an attractor, we can determine whether a model in the theory characterized by distinct parameters $(C_1, C_2, A_\star)$ approaches the de Sitter spacetime from the quintessence side ($\mathrm{w_{eff}} > -1$) or from the phantom side ($\mathrm{w_{eff}} < -1$). Note that a necessary condition for crossing the so-called phantom divide, $\mathrm{w_{eff}} = -1$, is vanishing of the second term in Eq. (15). Depending on the model, exponential solutions may cross the phantom divide line at most twice before approaching $\mathrm{w_{eff}} = -1$ from either above or below. In the oscillating type of solutions the dark energy effective barotropic index oscillates either in the quintessence regime ($\mathrm{w_{eff}} > -1$), phantom regime ($\mathrm{w_{eff}} < -1$), or crossing the phantom divide line once or twice during each period.

As an illustration, Figure 1 depicts the dynamics of $\mathrm{w_{eff}}$ for three sample solutions in different STG models:

$$\omega(\Psi) = \frac{3\Psi}{2(1-\Psi)}\,, \qquad \kappa^2 V(\Psi) = \frac{2}{3}\left[1 + (1-\Psi)^2\right]\,, \tag{16}$$

$$\omega(\Psi) = \frac{5\Psi}{7(1-\Psi)}\,, \qquad \kappa^2 V(\Psi) = 3e^{3(1-\Psi)}\,, \tag{17}$$

$$\omega(\Psi) = \frac{\Psi}{2(1-\Psi)}\,, \qquad \kappa^2 V(\Psi) = 3e^{3(1-\Psi)}\,. \tag{18}$$

The first model belongs to the class with $C > 0$, $C_1 > 0$, $C_2 < 0$ and the sample solution shows a monotonic quintessence type convergence towards de Sitter. The second model belongs to the class with $C < 0$, $C_1 > 0$, $C_2 < 0$ and is characterized by damped oscillations in the quintessence regime. The third

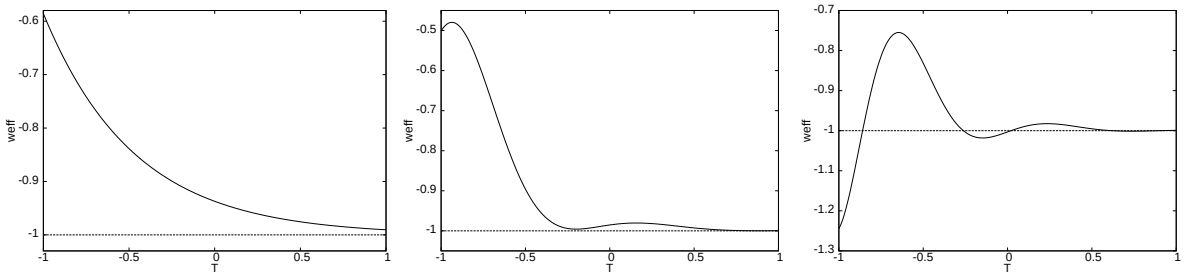

Figure 1: Examples of the time evolution of $w_{\rm eff}$ for different STG models: (16) left, (17) middle, (18) right. The evolution is measured in the units of the analogue of Hubble time, $T = H_\star\, t = \frac{C_1}{3}\, t$, and present moment is chosen to be at $T = 0$.

model also belongs to the same class as previous example but exhibits oscillations through the phantom divide line. The initial conditions of these solutions have been chosen such that the corresponding PPN parameters are within observationally allowed limits. We may notice that it is possible to have the period of oscillations to be about the same order of magnitude as the age of the Universe.

4 Summary

We have proposed and solved a nonlinear approximate equation (9) for decoupled scalar field in the framework of STG FLRW flat cosmological models describing the era when the energy density of the scalar potential dominates over the energy density of the ordinary matter and the universe has evolved close to the limit of GR (which acts as an attractor for certain classes of STG). The behaviour of solutions can be used to analyse the cosmological expansion near the 'GR point' where the weak field constraints are satisfied. Solutions which approach GR can be classified under two characteristic types: (i) exponential or linear exponential convergence, and (ii) damped oscillations around general relativity.

Acknowledgements

M.S. research is supported by the Estonian Science Foundation Postdoctoral research Grant No. JD131. L.J. and P.K. acknowledge the Estonian Science Foundation Grant No. 7185 and the Estonian Ministry for Education Science Support Grant No. SF0180013s07.

References

[1] Q. G. Huang, M. Li, X. D. Li and S. Wang Phys. Rev. D **80**, 083515 (2009).

[2] R. G. Cai, Q. Su and H. B. Zhang JCAP **1004**, 012 (2010).

[3] B. Bertotti, L. Iess and P. Tortora Nature **425**, 374 (2003).

[4] C. M. Will Living Rev. Rel. **9**, 3 (2005).

[5] L. Järv, P. Kuusk and M. Saal Phys. Rev. D **76**, 103506 (2007).

[6] L. Järv, P. Kuusk and M. Saal Phys. Rev. D **78**, 083530 (2008).

[7] L. Järv, P. Kuusk and M. Saal Phys. Rev. D **81**, 104007 (2010).

[8] L. Järv, P. Kuusk and M. Saal Phys. Lett. B **694**, 1 (2010).

Gravitational self-force effect on eccentric orbits in Schwarzschild geometry

Norichika Sago[1(a)]

(a) *Yukawa Institute for Theoretical Physics, Kyoto University, Kyoto 606-8502*

Abstract

We investigate the gravitational self-force effect on eccentric orbits in Schwarzschild spacetime. We derive the formulas of the post-geodesic corrections in some gauge-invariant quantities (e.g. the fundamental frequencies) in terms of the metric perturbation and the self-force in the Lorenz gauge. With the derived formulas and the numerical data obtained by the self-force calculation code we developed recently, we evaluate these corrections numerically for some sets of orbital parameters. In the circular limit, we find a gauge-invariant relation between the conservative correction in the periapsis advance and the dimensionless gravitational potential. This relation is used to explore both weak-field and strong-field aspects of the Effective One Body formalism.

1 Introduction

The problem of the gravitational self-force (GSF) on a point mass orbiting a black hole is one of the open issues in general relativity, and is well-motivated by the forthcoming gravitational wave observations which require a template bank of accurate waveforms. A breakthrough toward solving this issue has been given by Mino, Sasaki and Tanaka [1] and Quinn and Wald [2], deriving the formal expression of GSF under the Lorenz gauge condition. Since then, a number of studies have been devoted to develop a practical method of calculating the GSF based on their formulation. The "mode sum" scheme is considered as a promising method among ones proposed so far, and has been implemented in several studies to calculate the GSF in practice. See [3] for reviews.

Recently, based on the mode sum scheme, we developed a numerical code to compute the GSF for bound orbits in Schwarzschild geometry [4]. With the GSF data obtained by the code, we can now investigate the GSF effects on the motion of a point mass by evaluating the corrections in some quantities related to the orbit. For example, we calculated the correction in the gauge-invariant "redshift" parameter (the time component of 4-velocity of a point mass) which is proposed by Detweiler for comparison with post-Newtonian (PN) theory [5]. In [6], we compared the two results obtained in the Lorenz and Regge-Wheeler gauges and found a good agreement between them, even in strong gravitational field. We also computed the GSF correction in the orbital frequency of the innermost stable circular orbit (ISCO) [7]. More recently, we derived the GSF effect in the periapsis advance of eccentric orbits [8]. Especially, we showed that the results at the circular limit can be used to compare with post-Newtonian theory, and to explore both weak-field and strong-field aspects of the Effective One Body (EOB) formalism [9].

In this manuscript, we give a brief summary of our recent works on investigating the GSF effects on eccentric orbits in Schwarzschild geometry. The details of the analysis and the results are shown in [8, 9]. Throughout this paper, we denote the masses of a orbiting point particle and a central Schwarzschild black hole as μ and M, respectively.

2 Geodesic orbit

In this section, we give a brief review of the geodesic orbits in Schwarzschild geometry. The radial component of the geodesic equations is given

$$\left(\frac{dr_p}{d\tau}\right)^2 = R(r_p); \quad R(r) \equiv E^2 - f(r)\left(1+\frac{L^2}{r^2}\right), \tag{1}$$

[1]Email address: sago@yukawa.kyoto-u.ac.jp

where $f(r) = 1 - 2M/r$, τ is the proper time along the orbit, $r_p(\tau)$ is the orbital radius. E and L are the specific energy and angular momentum parameters of the particle, which conserve along the geodesic orbit. An eccentric orbit is bounded in the range of $r_- \leq r \leq r_+$, where $r_\pm$ satisfy $R(r_-) = R(r_+) = 0$ and $4M < r_- \leq r_+$. r_- and r_+ correspond to the radii at the periapsis and apoapsis respectively. We can define a alternative parametrization of eccentric orbits from (r_-, r_+) so that

$$p \equiv \frac{2r_-r_+}{M(r_+ + r_-)}, \quad e \equiv \frac{r_+ - r_-}{r_+ + r_-}, \tag{2}$$

where p is called as the (dimensionless) semi-latus rectum, and e is the eccentricity. With this parametrization, the radial motion is given by

$$r_p(\chi) = \frac{pM}{1 + e\cos\chi}, \tag{3}$$

where χ is a monotonically increasing parameter ("radial phase") along the worldline [10]. By using χ, we reexpress the t and φ components of the geodesic equations as

$$\begin{aligned} \frac{dt_p}{d\chi} &= t_\chi(\chi; E, L) \equiv \frac{E}{f(r_p)}\left[E^2 - f(r_p)\left(1 + \frac{L^2}{r_p^2}\right)\right]^{-1/2}\left(\frac{dr_p}{d\chi}\right), \\ \frac{d\varphi_p}{d\chi} &= \varphi_\chi(\chi; E, L) \equiv \frac{L}{r_p^2}\left[E^2 - f(r_p)\left(1 + \frac{L^2}{r_p^2}\right)\right]^{-1/2}\left(\frac{dr_p}{d\chi}\right). \end{aligned} \tag{4}$$

By integrating Eq. (4) over χ, we define the radial period and the increase of the phase for one radial period as

$$T \equiv \int_0^{2\pi} t_\chi(\chi; E, L)d\chi, \quad \Phi \equiv \int_0^{2\pi} \varphi_\chi(\chi; E, L)d\chi. \tag{5}$$

Now we can define the periapsis advance

$$\delta \equiv \Phi/(2\pi) - 1 > 0, \tag{6}$$

which represents the fractional difference between two frequencies

$$\Omega_\varphi = (1 + \delta)\,\Omega_r, \tag{7}$$

where $\Omega_r \equiv 2\pi/T$ and $\Omega_\varphi = \Phi/T$ are the radial and azimuthal frequencies respectively.

3 Results of GSF calculation

3.1 GSF correction in periapsis advance

The periapsis advance corrected by the conservative piece of the GSF can be given by replacing (E, L) in Eqs. (5) and (6) with the perturbed ones,

$$\tilde{\delta} = \frac{1}{2\pi}\int_0^{2\pi} \varphi_\chi(\chi; \tilde{E}, \tilde{L})d\chi, \tag{8}$$

where $\tilde{E}$ and $\tilde{L}$ are the perturbed values of the energy and angular momentum parameters, which are no longer constant along the orbit. The GSF correction in the periapsis advance is defined as

$$\Delta\delta = \tilde{\delta} - \delta = \frac{1}{2\pi}\int_0^{2\pi} \Delta\varphi_\chi(\chi; E, L)d\chi + O(\mu^2) \tag{9}$$

with

$$\Delta\varphi_\chi = \left.\frac{\partial\varphi_\chi}{\partial E}\right|_{E,L}\Delta E + \left.\frac{\partial\varphi_\chi}{\partial L}\right|_{E,L}\Delta L,$$

where ΔE and ΔL are the corrections in (E, L) calculated from the conservative piece of the GSF (Their explicit forms will be shown in [8]). In Fig. 1, we plot $\Delta\delta$ as functions of p for some fixed values of eccentricity.

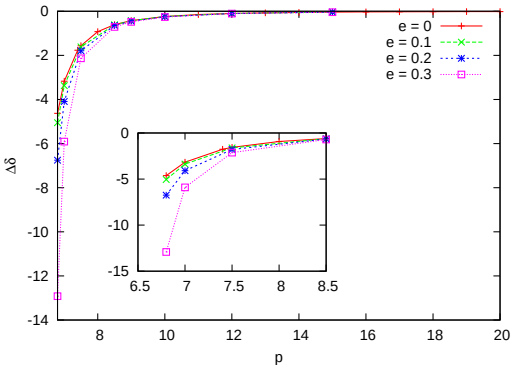

Figure 1: Conservative GSF correction in the periapsis advance. We plot $\Delta\delta$ as functions of p for some fixed values of e. The inset shows an expansion of the small-x range of the plot.

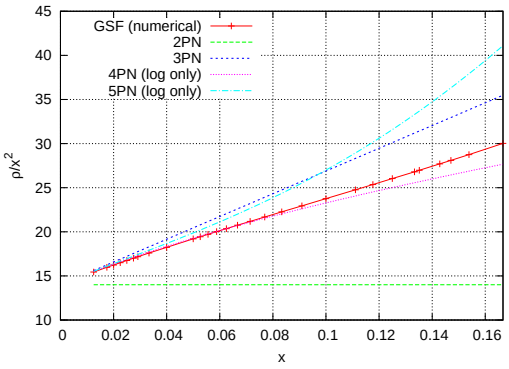

Figure 2: Conservative $O(\mu)$ correction in $W(x)$. We plot the GSF data and some PN forms of $\rho(x)/x^2$. As for 4PN and 5PN, we include only the known logarithmic terms.

3.2 Comparison with EOB/PN approach

Several ways to use the GSF results in calibrating the EOB model was discussed in [11]. Here we focus on one of them, investigating the circular limit of the ratio between the squares of the radial and azimuthal frequencies. This quantity can be written in the following form:

$$\lim_{e\to 0}\left(\tilde{\Omega}_r/\tilde{\Omega}_\varphi\right)^2 \equiv W(x) = 1 - 6x + (\mu/M)\rho(x) + O\left((\mu/M)^2\right), \tag{10}$$

where $x \equiv [(M+\mu)\tilde{\Omega}_\varphi]^{2/3}$ is the dimensionless gravitational potential, $\rho(x)$ can be related to the circular limit of $\Delta\delta$ as expected from Eq. (7). It should be noticed that the two frequencies and $\rho(x)$ are "gauge invariant" within a class of physically reasonable gauges and that the fact makes it possible to perform comparison between the results of different methods. In Fig. 2, we plot $\rho(x)$ (divided by x^2) estimated by the GSF computation for slightly eccentric orbits. On the other hand, $\rho(x)$ can be written in the form of the PN expansion

$$\rho^{\rm PN}(x) = \rho_2 x^2 + \rho_3 x^3 + (\rho_4^c + \rho_4^{\log}\ln x)x^4 + (\rho_5^c + \rho_5^{\log}\ln x)x^5 + O(x^6), \tag{11}$$

where ρ_2, ρ_3, $\rho_4^{\log}$ and $\rho_5^{\log}$ are known by the PN expansion of the EOB functions

$$\rho_2 = 14, \qquad \rho_3 = \frac{397}{2} - \frac{123}{16}\pi^2, \qquad \rho_4^{\log} = \frac{2512}{15}, \qquad \rho_5^{\log} = -\frac{11336}{7}. \tag{12}$$

In Fig. 2, we also show the plots of $\rho(x)$ predicted by the EOB/PN approach. Here "2PN" and "3PN" mean the forms through $O(x^2)$ and $O(x^3)$, respectively. As for the 4PN and 5PN, only the known logarithmic terms are included. We find a good agreement between the GSF and EOB/PN results for small x (large orbital radius).

3.3 Determination of unknown PN coefficients

The agreement of $\rho(x)$ between the GSF and EOB/PN suggests that we can use the GSF results to estimate the unknown PN coefficients by fitting. Our strategy for this purpose is as follows. We fit our GSF results to a set of PN models from 5PN to 8PN with all known PN coefficients $(\rho_2, \rho_3, \rho_4^{\log}, \rho_5^{\log})$ at their analytic values, and record the best-fit values of unknown PN coefficients with the values of χ^2 and L^∞ norm (i.e., the maximum value of the absolute difference between a data point and the best-fit model). And then, we extract values and rough error margins of the fitting coefficients. See Table VII in [9], where the results from this analysis are listed. Based on the list, we roughly estimate the "best guess" values as

$$\rho_4^c = 69^{+7}_{-4}, \qquad \rho_5^c = -4800^{+400}_{-1200}, \qquad \rho_6^{\log} < 0. \tag{13}$$

We have no meaningful information on ρ_6^c and higher order PN coefficients because the errors are dominant.

4 Summary and discussion

In this article, we investigated the GSF effects on the motion of a particle in Schwarzschild geometry. We presented (1) the GSF corrections on the periapsis advance for eccentric orbits, (2) the comparison between the GSF and EOB/PN results of the periapsis advance function $\rho(x)$ in the circular limit, (3) a demonstration of a calibration of the EOB/PN model with the GSF results.

Due to the errors in our current calculation of the GSF, we could not obtain a strong constraint on the unknown PN coefficients of the EOB functions. An improvement of the GSF computation will make it possible to determine the coefficients more accurately, to access the higher PN coefficients, and to put a stronger constraint on the EOB model.

We may use a rational function (Padé model) for fitting, instead of a Taylor-expanded function. This strategy was originally introduced to accelerate the convergence of the PN expansions. It is expected that the information on the GSF in strong field points (say, $x = 1/6$) will improve the Padé model. In fact, we observed that an good global representation of $\rho(x)$ can be obtained by a Padé approximant which combines 3PN knowledge at $x = 0$ with GSF information at $x = 1/6$. Such models may be useful for calibration of the EOB functions in both weak-field and strong-field regions. The details of the analysis and the utility are discussed in [9].

We should also mention that the GSF results for small eccentric orbits give us the information on only two EOB functions, $a(x)$ and $\bar{d}(x)$. To obtain the information on another EOB function $q(u, p_r)$, we need to consider the GSF dynamics of large-eccentricity orbits [11]. Investigations in this direction should be carried out in future works.

References

[1] Y. Mino, M. Sasaki and T. Tanaka, Phys. Rev. D **55**, 3457 (1997) [arXiv:gr-qc/9606018].

[2] T. C. Quinn and R. M. Wald, Phys. Rev. D **56**, 3381 (1997) [arXiv:gr-qc/9610053].

[3] L. Barack, Class. Quant. Grav. **26**, 213001 (2009) [arXiv:0908.1664 [gr-qc]].

[4] L. Barack and N. Sago, Phys. Rev. D **81**, 084021 (2010) [arXiv:1002.2386 [gr-qc]].

[5] S. Detweiler, Phys. Rev. D **77**, 124026 (2008) [arXiv:0804.3529 [gr-qc]].

[6] N. Sago, L. Barack and S. Detweiler, Phys. Rev. D **78**, 124024 (2008) [arXiv:0810.2530 [gr-qc]].

[7] L. Barack and N. Sago, Phys. Rev. Lett. **102**, 191101 (2009) [arXiv:0902.0573 [gr-qc]].

[8] L. Barack and N. Sago, in preparation.

[9] L. Barack, T. Damour and N. Sago, Phys. Rev. D **82**, 084036 (2010) [arXiv:1008.0935 [gr-qc]].

[10] C. Cutler, D. Kennefick and E. Poisson, Phys. Rev. D **50**, 3816 (1994).

[11] T. Damour, Phys. Rev. D **81**, 024017 (2010) [arXiv:0910.5533 [gr-qc]].

Rapidly Rotating Dynamic Black Holes through Gravitational Collapse

Motoyuki Saijo [1](a),(b)

(a) *Department of Physics, Rikkyo University, Toshima, Tokyo 171-8501*
(b) *Research Center for Measurement in Advanced Science, Rikkyo University, Toshima, Tokyo 171-8501*

Abstract

We investigate the properties of rapidly rotating black hole generated by gravitational collapse of rotating relativistic stars by means of $3+1$ hydrodynamic simulations in general relativity. Here we focus on the multipole moment of the dynamical black hole to extract some features in dynamical spacetime. We find that the dynamic black hole approaches to a stationary Kerr black hole after the damping timescale of the dynamic black hole from black hole formation. Therefore the existence of the quasi-periodic gravitational waves after the ringdown may connect to the instability of the fluid fragments around the black hole, which forms a disk.

There are variety of black holes (BHs) in nature, which are classified into three different mass scales. The first category is the supermassive BH. There are plenty of evidence that the supermassive BH exists in the center of most galaxy, and they seem to rotate very rapidly [1]. The typical mass range of this category is around $10^5 M_\odot - 10^{10} M_\odot$ ($M_\odot$: solar mass). However the formation scenario of the supermassive BH is still not certain. The second category is the intermediate mass BH ($10^2 M_\odot - 10^3 M_\odot$). There are some candidates of them at M82. Since the intermediate mass stars have not been found yet, those category of BH formation scenario has to go through the production of smaller size object. Merger of steller size holes or stars, or the collision of massive stars and collapse is the typical scenario to form an intermediate mass BH. The last category is the stellar mass BH ($3M_\odot - 50M_\odot$), whose candidates are in our galaxy. Binary coalescence of the stars or collapse of the stars is the typical scenario to form such object.

Nowadays, we can produce a dynamic BH in computer thanks to the triumph of numerical relativity. We have two representative scenarios to form a dynamic BH promptly. We neglect the accretion process, since the standard timescale for this is quite longer than the dynamical timescale. The first one is the merger of binary BHs. In a phenomenological sense, there may exist an upper limit for the spin of the newly formed BH. From the non-spinning individual BHs, the final maximum spin of the newly formed BH is $J_{\rm BH}/M_{\rm BH}^2 = 0.69M$ ($J_{\rm BH}$: total angular momentum of the BH, $M_{\rm BH}$: gravitational mass of the BH), while the arbitrary spinning individual BHs lead to final BH spin of $J_{\rm BH}/M_{\rm BH}^2 = 0.93M$. Suppose the plunge phase of the binary BHs can be characterised by the ones at ISCO (innermost stable circular orbit around the BH), there could have a certain condition that the binary BHs can collide. This picture can explain the existence of an upper limit to the spin of the newly formed BH.

The second one is gravitational collapse of uniformly rotating relativistic stars. In this scenario, the maximum spin of the BH do exist in the following manner. First, a star contracts itself until the mass shedding limit, conserving the mass and angular momentum of the system. Then, the star evolves along the mass shedding sequence quasi-stationary, releasing the mass and angular momentum, assuming that the system contains sufficient angular momentum. Once the star reaches the critical onset of collapse because of relativistic gravitation, the star begins to collapse. From the collapse of uniformly rotating supermassive star, the final spin of the newly formed BH is around $J_{\rm BH}/M_{\rm BH}^2 \approx 0.75$.

Here we relax the condition of uniformly rotational configuration of the star to produce a highly spinning dynamic BH. Differential rotational configuration of the star enable us to impose larger angular momentum in the system than the uniformly rotational case, since it relax the mass-shedding limit. Using this idea, we have succeeded in producing a dynamic BH of spin $J_{\rm BH}/M_{\rm BH}^2 \approx 0.98M$ in the previous paper

[1]Email address: saijo@rikkyo.ac.jp

Table 1: Two different radially unstable rotating equilibrium stars for BH formation

Model	$R_{\rm p}/R_{\rm e}{}^{(a)}$	$\rho_0^{\max(b)}$	$M^{(c)}$	$T/W^{(d)}$	$J^{(e)}/M^2$	$M/R^{(f)}$
I	0.450	1.56×10^{-5}	4.88	0.108	0.99	2.56×10^{-2}
II	0.425	1.56×10^{-5}	5.07	0.118	1.03	2.63×10^{-2}

(a): Ratio of the polar proper radius to the equatorial proper radius
(b): Maximum rest mass density
(c): Gravitational mass
(d): Ratio of the rotational kinetic energy to the gravitational binding energy
(e): Total angular momentum
(f): Circumferential radius

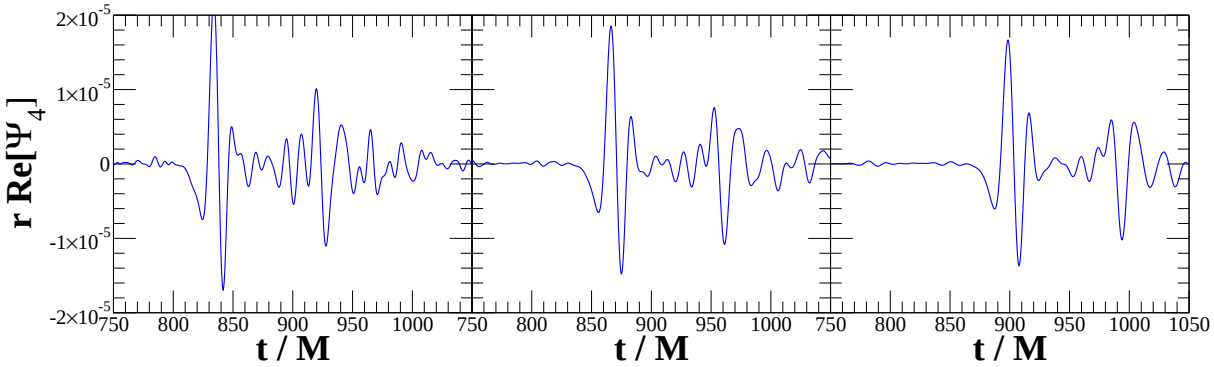

Figure 1: Gravitational waveform for model II. We monitor the real part of the Weyl scalar Ψ_4, which represents the plus mode of outgoing gravitational waves at null infinity. The observer is located in the x-direction of the equatorial plane at $x = 63.15M$, $94.72M$, $126.30M$ from the left panel, respectively. Note that the apparent horizon appears in the hypersurface after $t = 770.40M$. Hereafter M is the gravitational mass of the equilibrium star.

[2]. Here we focus on the dynamical configuration of BH itself in this paper by using the multipole moment of the curvatures on the apparent horizon. We try to answer the following questions. Can the newly formed BH be represented as stationary Kerr BH after some dynamical time from the BH formation? Is it useful to use multipole moment of the dynamic BH to extract the properties of dynamic BH, namely to find the cause of quasi-periodic gravitational waves after the ringdown? To answer those questions, three spatial dimensional general relativistic hydrodynamics is necessary. A more detailed discussion will be presented in Ref. [4]. Throughout this paper, we use the geometrized units in $G = c = 1$ and adopt Cartesian coordinates (x, y, z) with the coordinate time t.

We choose radially unstable supermassive stars for evolution in order to focus on the property of the dynamic BH. The equilibrium configuration we choose is summarised in Table 1, with a Γ-law equation of state with $\Gamma = 4/3$. We show the gravitational waveforms using the Weyl scalar Ψ_4 through gravitational collapse in Fig. 1. The Weyl scalar Ψ_4 contains both outgoing waves and back scattered waves by the curvature when we measure it in finite radius from the centre. We therefore monitor the waveform at three different locations, and investigate all of them. Since all three locations are considered as radiation zone from the source, the gravitational field of all three locations is weak and therefore back-scattered waves only plays a secondary role. The outgoing waves are propagating towards spatial infinity as time goes on, the features of the outgoing waves can be seen in all three locations with a positive direction of a time shift. For example, the left, middle, and right panel of Fig. 1 has a peak at $t \approx 833M$, $867M$, $900M$. The time lag between each panel roughly corresponds to the distance between the observers, using the fact that gravitational waves propagate with the speed of light. From all three waveforms we find that the outgoing waves contains three features. First, there exists a burst wave as the collapse goes on. Next, there is a damping wave once the BH forms. The damping waves corresponds to a characteristic oscillation of the dynamic BH. Finally, there is a continuous wave after the damping one.

In order to identify the cause of the continuous waves after the ringdown, we first investigate the

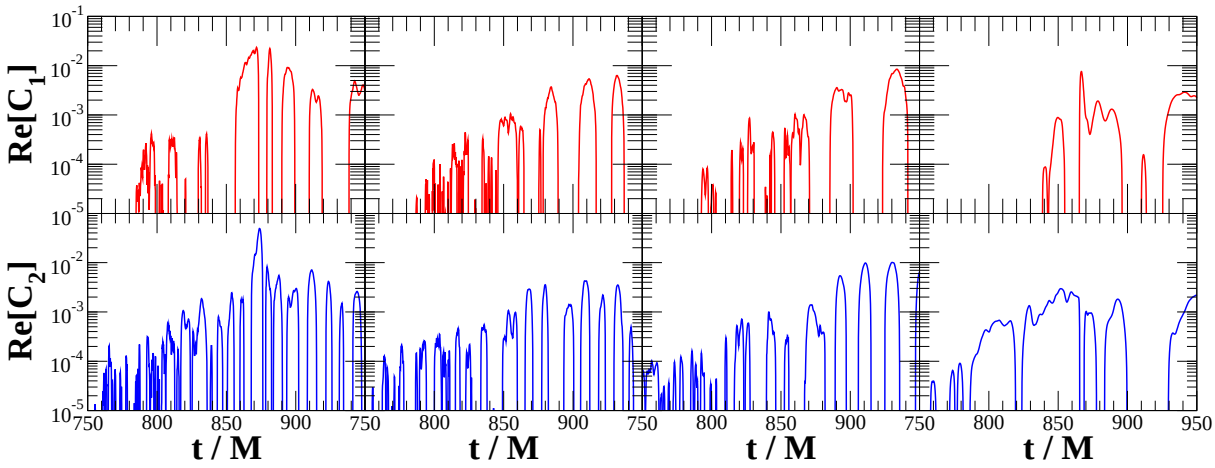

Figure 2: The $m = 1$ (red line) and the $m = 2$ (blue line) diagnostics of the rest mass density along the equatorial ring for model II. We measure the diagnostics in the equatorial plane at the radius $r = 0.987M$, $1.973M$, $3.947M$, $9.867M$ from the left panel, respectively.

azimuthal modes of the rest mass density. We introduce the following diagnostics at a certain radius of a ring in the equatorial plane as

$$C_m = \frac{1}{2\pi D_{\rm ring}} \int_0^{2\pi} \rho e^{im\varphi}\, d\varphi,$$

with a normalisation of $D_{\rm ring} (\equiv C_0)$, a mean density of the ring at a certain radius in the equatorial plane. We investigate $m = 1$ and $m = 2$ diagnostics at four different locations for model II in Fig. 2. Although the saturation amplitude for different locations is different for each m diagnostics, we find the following features. The azimuthal diagnostics begin to amplify efficiently after the apparent horizon appears in the hypersurface. This feature raise the question whether the amplification of the azimuthal diagnostics is directly connected to the configuration of the dynamic BH. The saturation amplitude of $m = 1$ and $m = 2$ diagnostics are quite similar at the same location, indicates that the cause of this amplification is $m = 1$. The saturation amplitude decreases as the location radius becomes far from the BH. This feature suggests us that the matter which is very close to the BH may play a key role for generating the quasi-periodic waveform after the ringdown.

Next, we investigate the BH configuration, namely the apparent horizon configuration, to identify the cause of the continuous waves. We apply the method of Jasiulek [3] for computing the multipole moment of the curvature on the horizon. In order to avoid the coordinate dependent variables, we introduce an averaged quantities on the trapped surface and compute the multipole moment. Like the definition of variance, we introduce the following multipole moment of the scalar 2-curvature ${}^2R$ and the imaginary part of the Weyl scalar $\Im\Psi_2$ as [3]

$$\begin{aligned} \mu_n({}^2\mathcal{R}) &= \langle(\langle {}^2\mathcal{R}\rangle - {}^2\mathcal{R})^n\rangle, \\ \mu_n(\Im\Psi_2) &= \langle(\langle \Im\Psi_2\rangle - \Im\Psi_2)^n\rangle, \end{aligned}$$

where the bracket of a physical quantity $\langle Q\rangle$ represents the averaged quantity on the BH horizon

$$\langle Q\rangle = \frac{1}{A}\int Q\, dA,$$

where A is the area of the horizon. We show the multipole moment of ${}^2R$ and $\Im\Psi_2$ on the apparent horizon throughout the evolution in Fig. 3. Note that we use the angular momentum of the dynamic BH as the dipole term of the $\Im\Psi_2$ on the horizon, and its gravitational mass is computed from the area law. Using the gravitational mass and angular momentum of the dynamic BH mentioned above, we compute the multipole moment of the dynamic BH and compare with those of Kerr. We find the following two

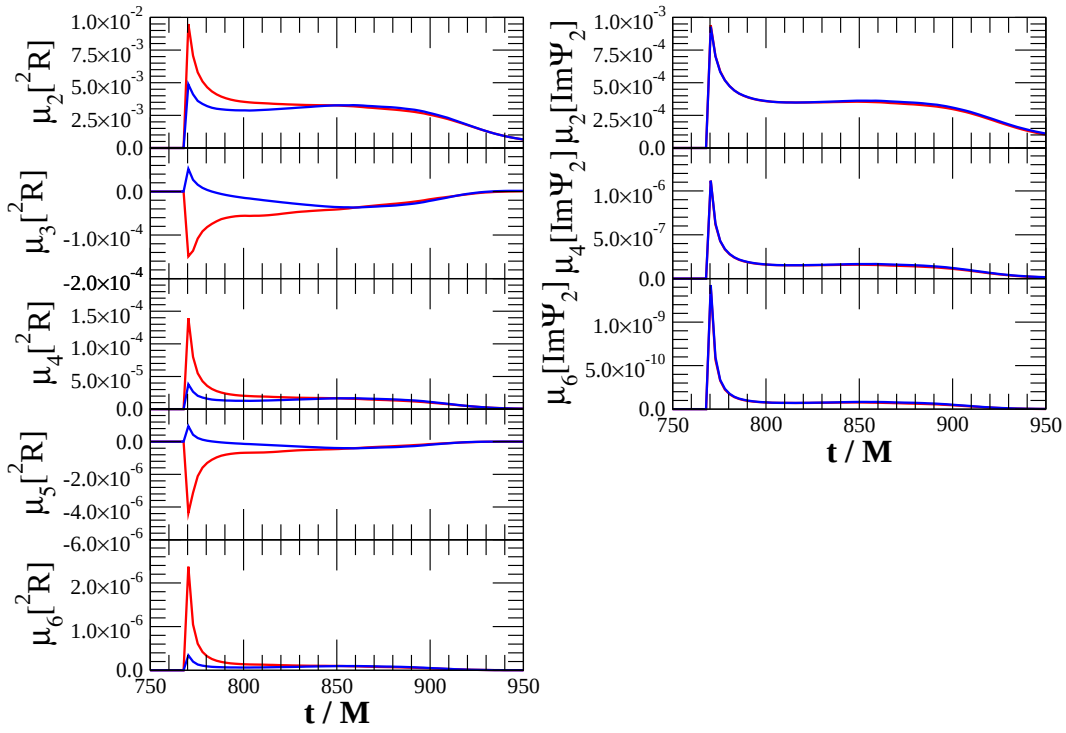

Figure 3: Multipole moment of the Ricci scalar R (left side of panels) and the imaginary part of the Weyl scalar Ψ_2 (right side of panels) of the dynamic black hole for model II through evolution. Red line represent the one from our dynamic BH, while blue line is the one from a Kerr using the gravitational mass and the angular momentum of the dynamic BH.

features. One is that after around $100M$ from the formation of the dynamic BH [2], the dynamic BH can be represented as Kerr BH within the relative error of several percents. In fact, the two lines of the multipole in Fig. 3 have a coincidence after $t \approx 850M$. Therefore the BH configuration almost becomes Kerr after $t \approx 100M$ of the BH formation. This statement suggests that the cause of the continuous wave may be related to the matter instability, since BH configuration is almost a Kerr, which does not produce gravitational waves. The other is that odd multipole moment have large deviation from the multipole moment of Kerr. This may be the fact of the nonaxisymmetric configuration of the rotating dynamic BH, which represents the violated phenomenon of the BH formation. One caution from this feature is that BH mass and angular momentum are settled down after $\approx 100M$, which is almost the same time that the BH is almost regarded as Kerr. Therefore we cannot extract the "stationary" mass and angular momentum of the dynamic BH by quasinormal ringing in theory. Those ringing waves represent the vibration of a transient dynamic BH.

We investigate the properties of the dynamic BH through gravitational collapse by means of three dimensional hydrodynamic simulations in general relativity.

We investigate the multipole moment of the curvature on the horizon and compare them with the multipole moment of Kerr, using the gravitational mass and angular momentum of the dynamic BH. We find that after $\approx 100M$ from the BH formation, the dynamic BH is described by Kerr. The timescale is in the same order of the damping timescale of the rapidly rotating BH.

We also investigate the cause of the quasi-periodic waves of gravitational waves after the ringdown. Since the configuration of dynamic BH becomes Kerr after the damping timescale of the stationary BH, quasi-periodic waves may be generated by the instability of the fluid fragments. Indeed we find the evidence of the amplification in our azimuthal diagnostics of the rest mass densities. In order to identify the cause, we need another approach to examine this problem, which is a future study in this field.

[2] We define the formation time of the BH as the first appearance of the apparent horizon in our hypersurface.

References

[1] M. Rees, in *The Future of Theoretical Physics and Cosmology*, edited by G. W. Gibbons, E. P. S. Shellard and S. J. Rankin (Cambridge Univ. Press, Cambridge, 2003), 17.

[2] M. Saijo and I. Hawke, Phys. Rev. D **80**, 64001 (2009).

[3] M. Jasiulek, Class. Quantum Grav. **26**, 245008 (2009).

[4] M. Saijo, in preparation.

Parametric amplification of the inflaton fluctuations induced by a heavy scalar field

Ryo Saito[1 (a),(b)], Masahiro Nakashima[2 (a),(b)] Yu-ichi Takamizu[3 (b)] and Jun'ichi Yokoyama[4 (b),(c)]

[(a)] *Department of Physics, Graduate School of Science, The University of Tokyo, Tokyo 113-0033, Japan*
[(b)] *Research Center for the Early Universe (RESCEU), Graduate School of Science, The University of Tokyo, Tokyo 113-0033, Japan*
[(c)] *Institute for the Physics and Mathematics of the Universe, The University of Tokyo, Chiba 277-8568, Japan*

Abstract

We investigate a possible effect of a heavy scalar field on the inflaton flucutations. A scalar field whose mass exceeds the Hubble scale can oscillate even in the inflationary era, and could modulate a dispersion relation of the inflaton field through derivative couplings. This modification leads to the parametric resonance and an enhancement of the fluctuations.

1 Introduction

Simple slow-roll single-field inflation models predict nearly scale-invariant power spectrum of primordial fluctuations. Then we usually parametrize the spectrum over the observable range of scales simply with two or three parameters: amplitude, tilt, and running. This parametrization, however, could be oversimplified one and miss valuable information on the physics behind inflation. In fact, some groups have reported the discrepancy between the prediction from the power-law spectrum and the Cosmic Microwave Background (CMB) data [1]. In this paper, we show that oscillations of a heavy scalar field, whose mass exceeds the Hubble scale, during inflation can induce an enhancement of the inflaton fluctuations through the parametric resonance and the feature in the power spectrum could contain information on natures of the heavy scalar field.

2 The model

We consider a model with a heavy scalar field χ with mass $m \gg H$ which couples to the inflaton field ϕ in the following manner,

$$S_m \equiv -\int \mathrm{d}x^4\sqrt{-g}\left[\frac{1}{2}(\partial\phi)^2 + V(\phi) + \frac{1}{2}(\partial\chi)^2 + \frac{m^2}{2}\chi^2 + K_d\right], \tag{1}$$

with

$$K_d \equiv \frac{\lambda_{d1}}{4\Lambda_d^4}(\partial\chi)^2(\partial\phi)^2 + \frac{\lambda_{d2}}{4\Lambda_d^4}(\partial\chi\cdot\partial\phi)^2. \tag{2}$$

The potential $V(\phi)$ is only assumed to be sufficiently flat; $\epsilon_V \ll 1,\ |\eta_V| \ll 1$ where

$$\epsilon_V \equiv \frac{M_p^2}{2}\left(\frac{V'}{V}\right)^2, \quad \eta_V \equiv M_p^2\frac{V''}{V}, \tag{3}$$

[1]Email address: r-saito'at'resceu.s.u-tokyo.ac.jp
[2]Email address: nakashima'at'resceu.s.u-tokyo.ac.jp
[3]Email address: takamizu'at'resceu.s.u-tokyo.ac.jp
[4]Email address: yokoyama'at'resceu.s.u-tokyo.ac.jp

are the slow-roll parameters. Here, $M_p = 2.4 \times 10^{18}$ GeV is the reduced Planck mass. Moreover, χ is assumed to be subdominant; $f_\chi \ll 1$ where

$$f_\chi \equiv \frac{\rho_\chi}{\rho} \simeq \frac{\dot{\chi}^2 + m^2\chi^2}{6M_p^2H^2}, \tag{4}$$

is a fraction of energy density of χ to the total one. We assume that χ decays with a rate Γ, which satisfies $H \ll \Gamma \ll m$.

The couplings K_d are the most general ones at the leading order in $1/\Lambda_d$ in a model with a parity symmetry $\phi \to -\phi$ and a shift symmetry $\phi \to \phi + c$ imposed to ensure flatness of the potential. We do not consider the couplings between $\partial\phi$ and χ for simplicity, which can be suppressed by imposing a shift symmetry on χ. The symmetries also allow higher order terms in $1/\Lambda_d$, though we have suppressed them in Eq. (1). To ensure that contributions from these terms can be safely neglected, we assume hereafter that background values of the fields satisfy conditions,

$$\dot{\phi},\ \dot{\chi} \ll \Lambda_d^2. \tag{5}$$

We have also suppressed terms $(\partial\phi)^4$ and $(\partial\chi)^4$, because they have little effect on our analysis under the above conditions.

As the inflaton ϕ slowly rolls down the potential and the amplitude of the heavy scalar field χ decreases monotonically, we can neglect the effects of the couplings to obtain the solutions for the background evolution,

$$\pi_\phi(t) \simeq -\frac{V'}{3H}, \qquad \text{(slow roll solution)}, \tag{6}$$

$$\chi(t) \simeq \chi_0 e^{-\Gamma t}\cos(mt), \tag{7}$$

if the conditions (5) are satisfied at the onset of the oscillations, $t = 0$. Here, π_ϕ is a conjugate momentum for ϕ. Inflation is realized if the slow-variation parameter is small; $\epsilon \ll 1$ where

$$\epsilon \equiv -\frac{\dot{H}}{H^2}. \tag{8}$$

Using the Friedman equation and the background field equations, we can estimate ϵ in this model as,

$$\epsilon \simeq \epsilon_V + 6f_\chi \sin^2(mt), \tag{9}$$

where we have neglected the higher order terms in ϵ_V and f_χ. Hence, the conditions (3), (4), and (5) are sufficient for realizing inflation. Note that the slow-variation parameter $\eta \equiv \dot{\epsilon}/H\epsilon$ is not so small due to the second term during the oscillations. In order that the slow-roll solution (6) be consistent, the acceleration $\dot{\pi}_\phi$ should be smaller than the dissipation term $3H\pi_\phi$; $\dot{\pi}_\phi/3H\pi_\phi \ll 1$. Substituting the solution (6), we obtain

$$\begin{aligned}\frac{\dot{\pi}_\phi}{3H\pi_\phi} &\simeq \frac{V''}{V'}\frac{\dot{\phi}}{H} - \frac{\dot{H}}{H^2} \\ &\simeq -\eta_V + \epsilon,\end{aligned} \tag{10}$$

which shows that the solution (6) can be used consistently under the conditions (3), (4), and (5).

3 Parametric resonance with the oscillations of the heavy scalar field

In the previous section, we saw that the oscillations of the heavy scalar field do not much affect the background evolution provided that the conditions (3), (4), and (5) are satisfied. In this section, we show that the inflaton fluctuations can be enhanced through the parametric resonance with the oscillations of χ even in this case.

First, we derive an evolution equation for the inflaton fluctuations. The heavy scalar field χ oscillates with a frequency $m \gg H$, then the resonance occurs on scales much smaller than the horizon. Hence, we can neglect contributions from the metric fluctuations during the resonance because they are much smaller than those in the scalar fields on the subhorizon scales. Furthermore, the fluctuations in the heavy scalar field can be neglected because they do not contribute to the resonance. To eliminate the gauge degrees of freedom in the metric fluctuations, a gauge is fixed to the flat slicing, where the spatial metric becomes $a^2\delta_{ij}$.

Neglecting the contributions from the fluctuations in the metric and the heavy scalar field, a second-order action in the inflaton fluctuations, φ, can be written as,

$$S_2 \simeq \int \mathrm{d}t\mathrm{d}^3x \, \frac{z_\phi^2}{2}\left[\dot{\varphi}^2 - c_s^2(\nabla\varphi)^2/a^2\right], \tag{11}$$

where

$$z_\phi^2 = a^3\left[1 + (\lambda_{d1} + 2\lambda_{d2})\,\frac{\dot{\chi}^2}{2\Lambda_d^4}\right], \tag{12}$$

$$c_s^2 = 1 + (\lambda_{d1} - 2\lambda_{d2})\,\frac{\dot{\chi}^2}{2\Lambda_d^4} + O\left(\frac{\dot{\chi}^4}{\Lambda_d^8}\right). \tag{13}$$

Here, we have neglected the potential term, $V''\varphi^2 \simeq -3\eta_V H^2\varphi^2$, which is much smaller than the term $(\nabla\varphi)^2/a^2$ during the resonance. Note that this implies that it is difficult to induce the parametric resonance by a potential term without affecting the background. The action (11) leads to the following evolution equation in the Fourier space for the inflaton fluctuations,

$$\ddot{v}_{\mathbf{k}} + \left[c_s^2\left(\frac{k}{a}\right)^2 - \frac{\ddot{z}_\phi}{z_\phi}\right]v_{\mathbf{k}} = 0, \tag{14}$$

where $v \equiv z_\phi\varphi$. Neglecting the higher order terms in $\dot{\chi}/\Lambda_d^2$, c_s^2 and $\ddot{z}_\phi/z_\phi$ are estimated to be

$$c_s^2 \simeq 1 + (\lambda_{d1} - 2\lambda_{d2})\frac{m^2\hat{\chi}_0^2}{2\Lambda_d^4}\sin^2(mt), \tag{15}$$

$$\begin{aligned}\frac{\ddot{z}_\phi}{z_\phi} &\simeq \frac{3}{4}(3-2\epsilon)H^2 + 3mH(\lambda_{d1} + 2\lambda_{d2})\frac{m^2\hat{\chi}_0^2}{2\Lambda_d^4}\sin(2mt) + m^2(\lambda_{d1} + 2\lambda_{d2})\frac{m^2\hat{\chi}_0^2}{2\Lambda_d^4}\cos(2mt)\\ &\simeq m^2\left[(\lambda_{d1} + 2\lambda_{d2})\frac{m^2\hat{\chi}_0^2}{2\Lambda_d^4}\cos(2mt) + O\left(\frac{H}{m}\right)\right],\end{aligned} \tag{16}$$

where $\hat{\chi}_0 \equiv \chi_0 e^{-\Gamma t}$, which can be considered as a constant during the oscillations. Substituting Eq. (15) and Eq. (16) into Eq. (14), we can rewritten Eq. (14) in the form of the Mathieu equation,

$$\frac{\mathrm{d}^2 v_{\mathbf{k}}}{\mathrm{d}z^2} + [A_k - 2q\cos(2z)]\,v_{\mathbf{k}} = 0, \tag{17}$$

where $z \equiv mt$, $A_k \equiv (k/am)^2$, and

$$q \equiv -(\lambda_{d1} - 2\lambda_{d2})\frac{m^2\hat{\chi}_0^2}{8\Lambda_d^4}\left(\frac{k}{am}\right)^2 + (\lambda_{d1} + 2\lambda_{d2})\frac{m^2\hat{\chi}_0^2}{4\Lambda_d^4}. \tag{18}$$

Here, the value of q is smaller than unity because $m\chi/\Lambda_d \sim \dot{\chi}/\Lambda_d \ll 1$ as assumed in the previous section, and the adiabaticity is mildly violated. Hence the resonance is narrow, which occurs in a narrow instability band, $|A_k - 1| < q$. The parametric resonance occurs when the modes are redshifted to this instability band; $(1 - \tilde{q}/2)m < k/a < (1 + \tilde{q}/2)m$ where

$$\tilde{q} \equiv (\lambda_{d1} + 6\lambda_{d2})\frac{m^2\hat{\chi}_0^2}{8\Lambda_d^4} \equiv 7q_0 e^{-2\Gamma t}. \tag{19}$$

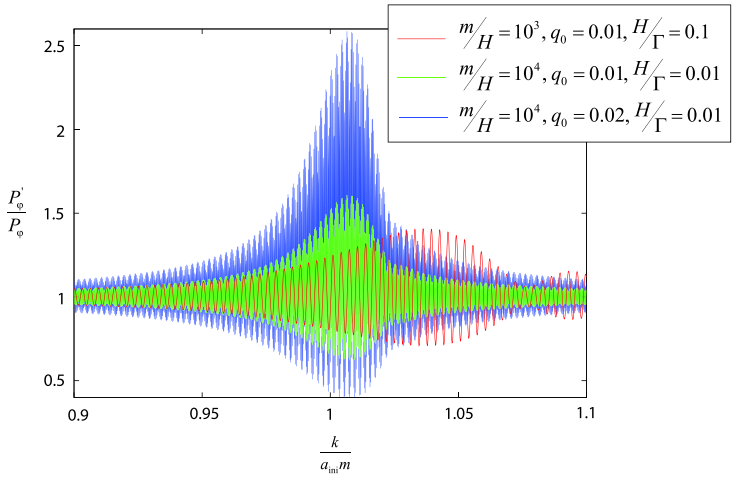

Figure 1: A feature in the power spectrum induced by the parametric resonance. The shape of the feature reflects the nature of the heavy scalar field, m, Γ, and q_0. Here, $a_{\rm ini}$ is the scale factor at the initial time.

After the oscillations cease, we can use the standard evolution equation for the inflaton field in a single-field inflation model. Hence, the parametric resonance continues at most for $\Delta z \sim (m/H)\min(7\tilde{q}_0, H/\Gamma)$, and the degree of the amplification can be largely understood by the Floquet theory as $\sim \exp\left(\int \tilde{q}/2\mathrm{d}z\right) \sim \exp(7q_0\Delta z/2)$. Therefore, the parametric resonance can induce nonnegligible modulation in the power spectrum thanks to the large factor m/H, which reflects a large number of oscillations of the heavy scalar field during the Hubble time.

In Fig. 1, we have depicted the modulated power spectrum for the inflaton fluctuations P'_φ normalized by the unmodulated one P_φ. The power spectra have been shown for different values of parameters. The resultant power spectrum has a peak because modes with smaller k already lie outside the resonance band at the initial time and modes with larger k cross the resonance band after the oscillations damped out. This also implies that the peak width for smaller and larger k are determined by q_0 and Γ/H, respectively. Inversely, we can read q_0 and Γ/H from the peak width. Then we can also read m from the peak height.

4 Summary and conclusion

In this paper, we have discussed that a heavy scalar field could induce the parametric amplification of the inflation fluctuations and an observable feature in their power spectrum without any large impact on the background expansion. Since a heavy scalar field (a scalar field whose mass exceeds the Hubble scale) has suppressed fluctuations and its vacuum expectation value could spoil the flatness of the inflaton potential, it is usually difficult to consider its major effects on the inflaton fluctuations in a controllable way. Therefore, information on the heavy scalar field is difficult to obtain. We have found that the derivative couplings do not spoil the inflationary expansion and could induce nonnegligible modulation in the power spectrum through the parametric resonance between the inflaton fluctuations and the oscillations of the heavy scalar field. The modulated spectrum is determined by natures of the heavy scalar field, so that we could know them from fine structures in the observed power spectrum. If this is correct, it is expected that its effects are also observed in the bispectrum. We estimate the modulation in the bispectrum in future work.

References

[1] D. Tocchini-Valentini, Y. Hoffman and J. Silk, Mon. Not. Roy. Astron. Soc. **367**, 1095 (2006); K. Ichiki, R. Nagata and J. Yokoyama, Phys. Rev. D **81**, 083010 (2010).

Deformation of an Expanding Void in Redshift Space

Nobuyuki Sakai[1(a)], Kei-ichi Maeda[2(b)] and Roland Triay[3(c)]

[(a)] *Department of Education, Yamagata University, Yamagata 990-8560, Japan*
[(b)] *Department of Physics & RISE, Waseda University, Shinjuku, Tokyo 169-8555, Japan*
[(c)] *Centre de Physique Théorique, CNRS Luminy Case 907, 13288 Marseille Cedex 9, France*

Abstract

We investigate the dynamics of a spherical void in the FLRW universe and discuss its observational consequences in redshift space. We show that a void is prolonged in the line of sight and that the deformation ratio depends on the dynamics of the background universe. Our results together with a future deep sky survey of galaxy distribution will confirm the existence of a cosmological constant.

1 Introduction

The existence of local voids with a radius larger than $100h^{-1}$Mpc is suggested by recent observational and theoretical studies. Granett et al. measured hot and cold spots on the cosmic microwave background associated with superclusters and supervoids, which were identified in the Sloan Digital Sky Survey Luminous Red Galaxy catalog [1]. Subsequently, Inoue et al. estimated the integrated Sachs-Wolfe effect due to spherically symmetric super-structures and found that observed cold and hot spots respectively imply presence of nonlinear voids and clusters with a radius $100 \sim 200h^{-1}$Mpc [2].

In this paper, we investigate the dynamics of a single spherical void embedded in the Friedmann-Lemaître-Robertson-Walker (FLRW) universe and discuss its observational consequences in redshift space. Especially, we focus on whether we can judge the existence of a cosmological constant by observing voids in redshift space. We expect that an expanding void is deformed, which is analogous but in the opposite way to the "fingers of God" effect or the Kaiser effect for a cluster in redshift space [3].

2 Dynamics of a Void

Let us consider a spherical shell that defines the boundary of a void. We assume that both the inner region $(-)$ and the outer region $(+)$ are described by the FLRW metrics. Both spacetimes satisfy the Friedmann equation with dust and a cosmological constant,

$$H_\pm^2 + \frac{k_\pm}{a_\pm^2} = \frac{8\pi G}{3}\rho_\pm, \qquad H_\pm = \frac{\dot{a}_\pm}{a_\pm}, \qquad \rho_\pm = \rho_{\rm vac} + \rho_\pm^{(m)}. \tag{1}$$

The equations of motion of the shell were originally derived by Maeda and Sato [4], and later they were rewritten in a more convenient expression [5] that we use here. To integrate them, we should give the initial values of the radius of a void, its velocity, the ratio of the inner expansion rate to the outer one, the density contrast, and the density parameter, and the dimensionless cosmological constant,

$$R, \quad v, \quad \frac{H^-}{H_+}, \quad \delta \equiv \frac{\rho_-^{(m)}}{\rho_+^{(m)}} - 1, \quad \Omega \equiv \frac{8\pi G\rho^{(m)_+}}{3H_+^2}, \quad \text{and} \quad \lambda \equiv \frac{\Lambda}{3H_+^2}, \tag{2}$$

at the initial time t_i (or the corresponding initial redshift z_i). Here we choose $z_i = 100$, $v_i = 0$ and $H_i^-/H_i^+ = 1$; however, the dynamics does not depend on these values as long as the "decaying mode" becomes negligibly small. In order to discuss comparison between our theoretical calculation and observation, the remaining model parameters Ω, λ, δ and R should be given at the present time t_0, i.e., Ω_0, λ_0, δ_0 and R_0. Hereafter we omit the subscript $+$.

[1]Email address: nsakai@e.yamagata-u.ac.jp
[2]Email address: maeda@waseda.jp
[3]Email address: triay@cpt.univ-mrs.fr

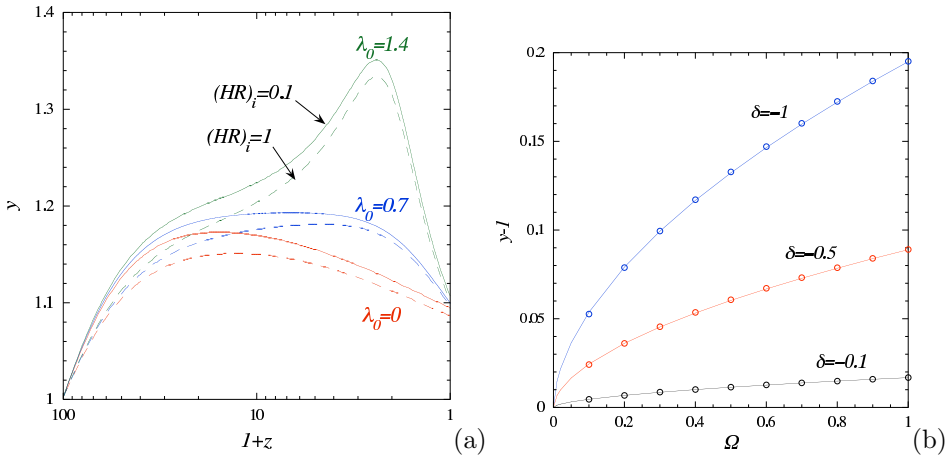

Figure 1: (a) Time-variation of $y(z)$ for an empty void with $\Omega_0 = 0.3$. (b) y versus Ω and δ for $\Omega + \lambda = 1$. The circles and the continuous lines correspond respectively to our numerical results and to Eq. (4).

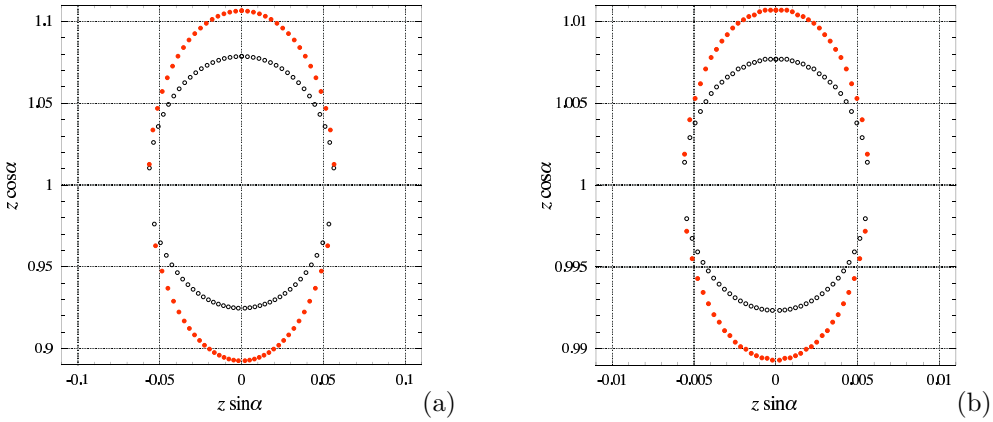

Figure 2: The image of a void at $z_V = 1$ in redshift space of the universe with $\Omega_0 = 0.3$ and $\lambda_0 = 0.7$. The observer is located at the origin. We show two voids with different scales, i.e., (a) $R_0 = 0.1H_0^{-1}$ and (b) $0.01H_0^{-1}$. The red dots and the black circles denote the image of the expanding shell and the reference image of the r =constant surface, respectively.

In order to compare the present general relativistic results with the Newtonian approximation [6], we define a "proper kinematics" of the shell as

$$y \equiv \frac{dR/dt}{HR} = 1 + \frac{f'v}{HR}, \quad f' = \sqrt{1 - \frac{kR^2}{a^2}}, \tag{3}$$

and present our numerical result in Fig. 1(a). We fix $\Omega_0 = 0.3$ and see how the dynamics depends on λ_0 and R_i. The result for the sub-horizon void confirms the previous result in the Newtonian approximation. The difference in dynamics between the sub-horizon void and the horizon-scale void is small; that is, the relativistic effect is small.

Because real voids may not be empty, it is also important to investigate how the shell velocity depends on the density contrast δ. We survey the shell velocity in the flat universe ($\Omega + \lambda = 1$), and show the numerical results by circles in Fig. 1(b). From this figure, we find that the velocity y highly depend on δ as well as Ω. For a practical purpose, we present a fitting formula,

$$y - 1 = \frac{v}{HR} = \frac{\Omega^{0.56}}{6}(|\delta| + 0.1|\delta|^2 + 0.07|\delta|^3), \quad \text{for} \quad \Omega + \lambda = 1, \tag{4}$$

which is shown by the solid curves in Fig. 1(b). They approximate our numerical data very well. The maximal difference between the numerical data and the formula (4) is less than one percent.

3 A void in redshift space

Next, we discuss how expanding voids look in redshift space. Our analysis method is as follows.
(i) Solve our equations of motion of the void shell to find $r = r(z)$ and $v = v(z)$.
(ii) For a given angle of sight from an observer, α, find the intersecting points of the light path with the shell and the time z when the photon is emitted.
(iii) Calculate the redshift of the void shell, z_s, for each angle α.
(iv) Draw the shape, i.e. $(z_x, z_y) = (z_s(\alpha)\cos\alpha,\ z_s(\alpha)\sin\alpha)$, in redshift space.

Figure 2 shows the image of a void, whose center is located at $z_V = 1$, with two scales,$R_0 = 0.1H_0^{-1}$ and $0.01H_0^{-1}$. Note that the observed void size is given by $R_V(z_V) \equiv a_0 r(z_V) = R_0 \times r(z_V)/r(0) < R_0$, because the photons were emitted at z_V. A void shape is prolonged in the direction of the line of sight mainly by the Doppler effects, which is the opposite deformation to the Kaiser effect because of the opposite direction of the peculiar velocity. Though the deformation in redshift space is proportional to the void size as $\Delta z_s \sim v \sim 0.1HR$, the ratio of two radii $(\Delta z_{||}/\Delta z_\perp)$ is almost independent of the void size.

The larger void with $R_0 = 0.1H_0^{-1}$ in the $\Omega_0 = 0.3$ universe in Fig. 2 (a) also showsa small front-back asymmetry. This is due to the evolutionary effect of the shell radius $r(t)$. On the other hand, for the smaller void with $R_0 \sim 0.01H_0^{-1}$ in Fig. 2 (b) the front-back asymmetry does not exist. It is because the evolutionary effect is negligible for the smaller void. This asymmetry could be used to test whether the observed void is an isolated one or not.

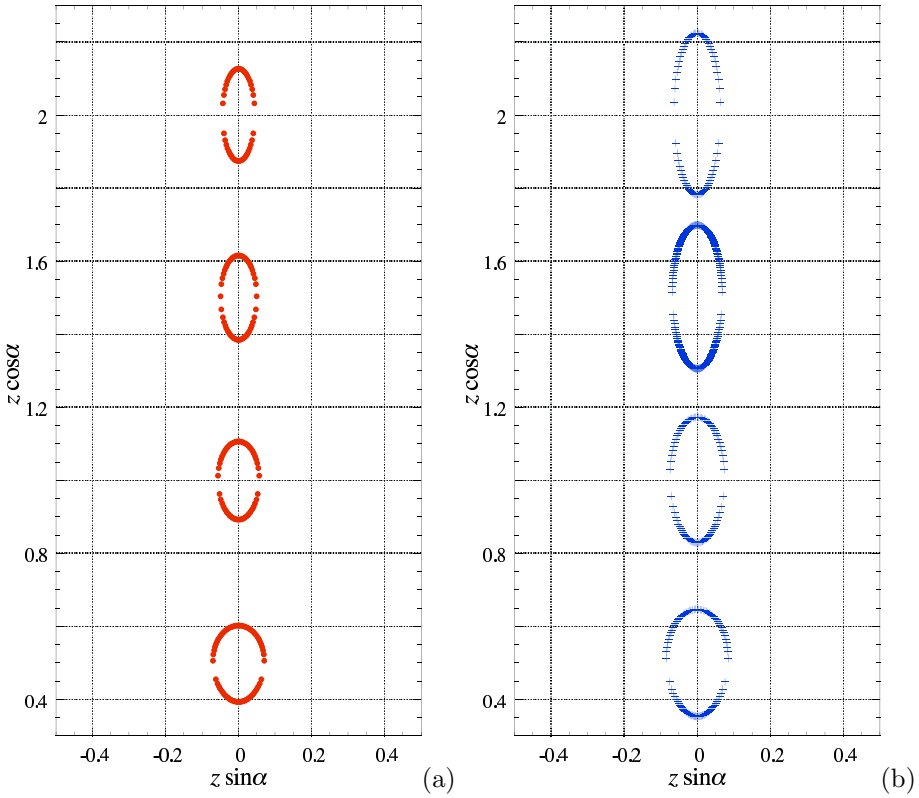

Figure 3: The images of four empty voids at $z_V = 0.5, 1, 1.5$ and 2 in redshift space for $\Omega_0 = 0.3$ and $\lambda_0 = 0.7$ (a) and those for t$\Omega_0 = 1$and $\lambda_0 = 0$ (b). We choose $R_0 = 0.1H_0^{-1}$.

In Fig. 3 (a), we present how voids look like in redshift space by showing four equivalent voids at $z_V = 0.5, 1, 1.5$ and 2. The present size is chosen as $R_0 = 0.1H_0^{-1}$. We can easily see the change of the vhoid shapes in terms of the distance z_V. When we have several equivalent voids in the universe, the observed void size $R_V(z_V)$ gets smaller as the distance z_V increases. As a result, $\Delta z_\perp$, which corresponds

to the observed void size in redshift space, decreases. However, we find that as z_V increases, $\Delta z_{||}$ increases at least in the large z_V region. This is because the Doppler effect overcomes the above evolutionary effect.

In Fig.3 (b), for reference, we show the shapes of four voids in the $\Omega_0 = 1$ universe. Comparing the shape change in two different cosmological models, we find the deformation ratio of a void in the $\Omega_0 = 1$ universe is larger than that in the $\Omega_0 = 0.3$. In order to show how much the shape is deformed quantitatively, we define the deformation ratio by $\mathcal{R} = \Delta z_{||}/\Delta z_{\perp}$, which is the ratio of the semi-major axis to the semi-minor axis of the approximate ellipse.

Figure 4 (a) confirms that, as z_V increases, $\Delta z_{\perp}$ decreases while $\Delta z_{||}$ increases. Only for neighbor voids in the universe with $\Omega_0 = 0.3$ and $\lambda_0 = 0.7$, $\Delta z_{||}$ as well as $\Delta z_{\perp}$ decrease due to the evolutionary effect. In Fig. 4 (b), we show the deformation ratio with respect to the distance z_V. The ratio $\mathcal{R}$ increases as the distance z_V increases. We also find the ratio $\mathcal{R}$ higly depends on the background cosmological model, which may give us some information on a cosmological constant.

Acknowledgements. This work was supported by KAKENHI (No. 22111502 and No. 22540291) and by the Waseda University Grants for Special Research Projects.

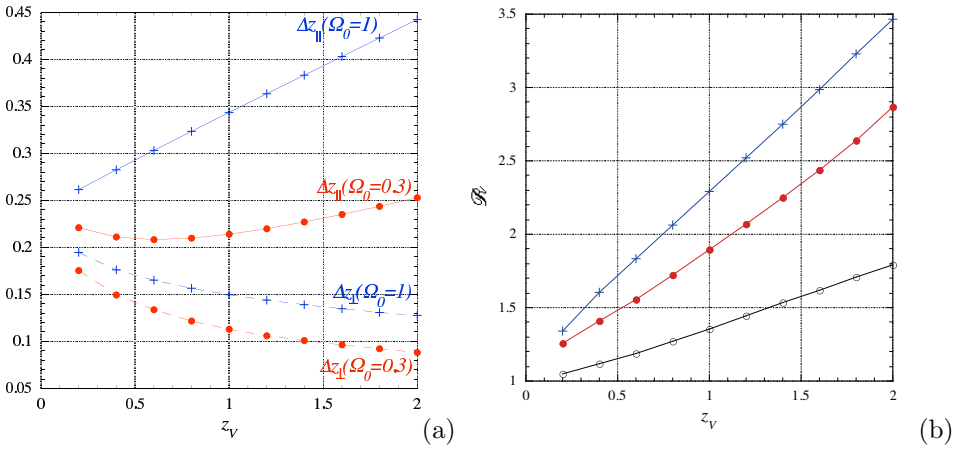

Figure 4: (a) The semi-major axis $\Delta z_{||}$ and the semi-minor axis $\Delta z_{\perp}$ in terms of the distance z_V. (b) The deformation ratio $\mathcal{R}$ of the shape of a void in the red shift space, which is defined by $\mathcal{R} = \Delta z_{||}/\Delta z_{\perp}$. The black line with circles represents the reference values of r = constant surface.

References

[1] B. R. Granett, M. C. Neyrinck and I. Szapudi, Astrophys. J. **683** (2008) L99.

[2] K. T. Inoue, N. Sakai, K. Tomita, Astrophys. J. **724** (2010) 12.

[3] R.P. Kirshner, A. Oemler, P.L. Schechter, S.A. Shectman, Astrophys. J. **248** (1981) L57; M. Davis, P.J.E. Peebles, *ibid.* **267** (1983) 465; A.J. Bean, R.S. Ellis, T. Shanks, G. Efstathiou, B.A. Peterson, Mon. Not. R. Astron. Soc. **205** (1983) 605; N. Kaiser, *ibid.* **227** (1987)1.

[4] K. Maeda and H. Sato, Prog. Theor. Phys. **70** (1983) 772; 1273.

[5] N. Sakai, K. Maeda and H. Sato, Prog. Theor. Phys. **89** (1993) 1193.

[6] H.H. Fliche and R. Triay, gr-qc/0607090 – to appear in JCAP; R. Triay and H.H. Fliche, Prog. Theor. Phys. *Suppl.* **172** (2008) 40.

AdS Black Hole Solution in Dilatonic Einstein-Gauss-Bonnet Gravity

Kei-ichi Maeda[1](a),(b),Nobuyoshi Ohta[2](d) and Yukinori Sasagawa[3](a)

(a) *Department of Physics, Waseda University, Shinjuku, Tokyo 169-8555, Japan*
(b) *Advanced Research Institute for Science and Engineering, Waseda University, Shinjuku, Tokyo 169-8555, Japan*
(d) *Department of Physics, Kinki University, Higashi-Osaka, Osaka 577-8502, Japan*

Abstract

We find AdS spacetime with a linear dilaton field is exact in effective action of string theory, which is described by gravity with Gauss-Bonnet curvature correction terms coupled to dilaton field in string frame. The AdS radius is determined by the number of dimensions and the coupling constants of curvature corrections. We numerically construct asymptotically AdS black hole solutions with a linear dilaton field in Einstein Gauss-Bonnet gravity coupled to dilaton field in string frame, when the spacetime possesses hyperbolic symmetry. We find the solution is a kind of solitonic solution.

1 Introduction

The Einstein-Gauss-Bonnet Gravity is a higher curvature generalization of Einstein gravity. Higher curvature theory is considered as quantum corrected model of gravity. In string theory, dilaton field plays important role, and appears coupled to the higher curvature terms. Black hole solutions in Gauss-Bonnet theory coupled with dilaton field in Einstein frame is studied for asymptotically flat case in [1]. The effect of truncation of terms from the conformal transformation between Einstein frame and String frame for the case of asymptotically flat black hole solutions is studied in [2].

The asymptotically non flat spacetimes, however, are also important. The asymptotically anti-de Sitter spacetime is especially interesting in the context of anti-de Sitter/conformal field theory (AdS/CFT) correspondence. AdS/CFT correspondence is a widely-believed conjecture which suggests that there exists a duality between bulk gravity and boundary conformal theory. Taking account into some quantum effects, i.e., the higher curvature correction terms, one may examine a strong coupling region via AdS/CFT. It may provide another confirmation for the conjecture. The asymptotically AdS spacetime in the truncated DEGB models were also analysed [3–5].

In Einstein Maxwell-dilaton gravity, linear dilaton solutions whose asymptotic behaviours are not AdS nor dS are studied in [6]. Some of such solutions are obtainable from asymptotically AdS or dS solution with suitable compactification. We discuss asymptotically linear dilaton and AdS black hole solutions in the presence of higher curvature corrections which arise in String theory. This work is based on [7]. In [7] we also present cosmological solutions and horizonless regular asymptotically AdS solutions. We extend the results on exact AdS spacetime solution for the action with even-order higher Lovelock curvature correction terms coupled to dilaton field in string frame.

2 Exact AdS spacetime with a linear dilaton field in dilatonic Einstein Gauss-Bonnet gravity

In this paper, we first focus on the D-dimensional Einstein Gauss-Bonnet gravity coupled to a dilaton field. The most general action in a string frame is given by

$$S_S = \frac{1}{2\kappa_D^2}\int d^Dx\sqrt{-g}\,e^{-2\phi}\left(R[g]+4\nabla_\mu\phi\nabla^\mu\phi+\alpha_2 R^2_{GB}\right), \tag{1}$$

[1]Email address: maeda@gravity.phys.waseda.ac.jp
[2]Email address: ohtan@phys.kindai.ac.jp
[3]Email address: yukinori@gravity.phys.waseda.ac.jp

where κ_D^2 is the D-dimensional gravitational constant, ϕ is a dilaton field. R^2_{GB} is Gauss-Bonnet terms defined by $R^2_{GB} = R^2 - 4R_{\mu\nu}R^{\mu\nu} + R^{\mu\nu\rho\sigma}R_{\mu\nu\rho\sigma}$. In order to consider AdS spacetime we adopt an ansatz as,

$$ds^2 = -\left(r^2/\ell^2\right)dt^2 + \left(\ell^2/r^2\right)dr^2 + r^2 d\boldsymbol{r}^2_{D-2}, \qquad \phi = p/2\ \ln\left[r^2/\ell^2\right] \tag{2}$$

where ℓ is an AdS radius and $d\boldsymbol{r}^2_{D-2}$ denotes the $(D-2)$-dimensional flat Euclidean space. This type of dilaton field is often referred as "Linear dilaton". With the ansatz (2), we find two out of the three field equations derived from the action (1) are independent.

$$\left[D_1 - 4(D-1)p + 4p^2\right]\ell^2 - \tilde{\alpha}_2 D_1 = 0\,, \qquad \ell^2 - 2(1+2p)\tilde{\alpha}_2 = 0\,. \tag{3}$$

From the second equation we obtain AdS radius ℓ

$$\ell = \sqrt{2(1+2p)}\,\tilde{\alpha}_2^{1/2}\,, \tag{4}$$

where p is given by the following cubic equation:

$$16p^3 - 8(2D-3)p^2 + 4(D-1)(D-2)p + D(D-1) = 0\,. \tag{5}$$

We find one real solution for Eq. (5), which gives an AdS space for $\alpha_2 > 0$ and a dS space for $\alpha_2 < 0$. We show the explicit solutions in Table 1. This analysis is easily extended to the Lovelock gravity,see appendix in [7].

Table 1: We present the rescaled AdS radius and dilaton power p from 4 dimensions to 10 dimensions

D	4	5	6	7	8	9	10
$\ell/\tilde{\alpha}_2^{1/2}$	0.861486	0.891094	0.910355	0.923867	0.933859	0.941543	0.947634
p	-0.314461	-0.301488	-0.292813	-0.286618	-0.281977	-0.278374	-0.275497

3 Asymptotically AdS black hole solutions in DEGB

3.1 Boundary conditions for asymptotically AdS black hole solutions

In this section we focus on black hole solutions whose asymptotic behaviour is AdS spacetime with Linear dilaton in Dilatonic Einstein Gauss-Bonnet theory. To find a black hole solution, we assume a maximally symmetric and static spacetime, whose metric form is given by

$$ds^2 = -f(r)e^{-2\delta(r)}dt^2 + f(r)^{-1}dr^2 + r^2 d\Sigma_k^2, \tag{6}$$

We numerically solve the field equation from horizon to infinity imposing suitable boundary conditions at horizon. Since we are interested in the regular black hole solutions, we impose regularity at horizon. At the event horizon (r_H), the metric function f vanishes. The condition for the finite variables and their derivatives at r_H gives us the quadratic equation for ϕ'_H: $a(\phi'_H r_H)^2 + b\phi'_H r_H + c = 0$ where a, b, and c are the functions of ρ_H, D and k. If the discriminant is negative there is no real value of f'_H, which means that no regular horizon exists. The condition for the discriminant to be non-negative gives some constraint on ρ_H^2 for given D and $\tilde{\alpha}_2$. Since $\tilde{\alpha}_2$ is a fundamental coupling constant, it gives some constraints on the horizon radius r_H. Since the case where $k = 1$ is studied in [2] here we focus on the case where $k = -1$. If $D = 4 \sim 10$, assuming $\tilde{\alpha}_2 > 0$, we find the allowed values for a regular event horizon, which are summarized in Table 2. In any dimensions higher than three, we always find a small gap in the parameter space of horizon radius, where there is no regular horizon.

In order to impose the boundary condition at infinity, we assume that spacetime approaches the solution (2) as $r \to \infty$. Since we will look for a black hole solution, we may have to find the mass. In the case of the Schwarzschild AdS black hole, the metric is given by $\delta = 0$ and $f(r) = r^2/\ell^2 + k + \mu/r^{D-3}$. So we expect the mass term appears in a negative higher power of r/ℓ. Assuming analyticity of spacetime at infinity, we expand the variables around the AdS spacetime by an integer-power series of r/ℓ, we find that non-trivial even power terms are given only by known parameters (D, k, and p). There is no freedom for a mass term. For the case of $k \neq 0$, we obtain a kind of a solitonic solution without a mass term, which may depend on a horizon radius r_H.

Table 2: The allowed values for a regular horizon radius are shown ($\rho_H := r_H/\tilde{\alpha}_2^{1/2}$) with $k = -1$ in (a). The equality gives a double root of ϕ'_H. In any dimension equal and higher than 4, there are gaps in which there is no regular horizon. We show the ranges of the horizon radii in which numerically solved asymptotically AdS black hole solutions exist in (b).

(a)

D	condition for regular horizon with $k = -1$
4	$\rho_H \leq 1.6566722$ or $2.4494897 \leq \rho_H$
5	$\rho_H \leq 1.5458773$ or $2.6272504 \leq \rho_H$
6	$\rho_H \leq 1.4951145$ or $2.7522118 \leq \rho_H$
7	$\rho_H \leq 1.4684167$ or $2.8514273 \leq \rho_H$
8	$\rho_H \leq 1.4528824$ or $2.9349158 \leq \rho_H$
9	$\rho_H \leq 1.4431206$ or $3.0076296 \leq \rho_H$
10	$\rho_H \leq 1.4366113$ or $3.0724201 \leq \rho_H$

(b)

D	range of obtained horizon radius
4	None
5	$0.00000000 < \rho_H \leq 0.70708722$
6	$0.51441011 \leq \rho_H \leq 0.89442653$
7	$0.63601600 \leq \rho_H \leq 0.99996864$
8	$0.70519140 \leq \rho_H \leq 1.06901380$
9	$0.75043583 \leq \rho_H \leq 1.11800344$
10	$0.78292643 \leq \rho_H \leq 1.15467074$

Hence, in order to extract a mass term, we have to assume non-analytic expansion at infinity as

$$f(r) = \bar{f}(r) + \frac{\mu}{r^\nu} + \cdots , \tag{7}$$

where $\bar{f}(r)$ is given by integer power terms obtained by the expansion and ν is a positive but non-integer number. Inserting this expression into the basic equations, we find $\nu = D - 3 - 2p$. μ is an arbitrary constant as expected. We shall call it a "mass" term, although it may not give a proper mass.

3.2 Numerical results for asymptotically AdS black hole solution

Now we present our numerical results. A detail of analysis is given in [7]. In the case of $k = -1$, we find AdS black hole solutions whose asymptotic structure is AdS spacetime numerically in dimension higher than 4. The ranges of the horizon radii in which numerically solved black hole solutions exist are summarized in Table 2 (b) This solution is a dilatonic analogue of the "non-GR branch" or "AdS branch" of the black hole solution in the non-dilatonic EGB theory. Similar to the case of "AdS branch" of EGB theory the horizon radius of our solutions do not depend on the conditions for regularity but the conditions for the horizon to describe the black hole properly$f'(r_H) > 0$ for $f(r_H) = 0$.

The specific heat C_V of a black hole solution is given by $C_V = T\left(\frac{\partial S}{\partial T}\right)_V$. We show the relation between the specific heat and the temperature in Fig. 1. The specific heat is positive for our solutions similar to that of AdS black hole in the non-dilatonic EGB gravity for $k = -1$ [8]. Since the specific heat is always positive for our solution as shown in Fig. 1, we do not expect the Hawking-Page transition.

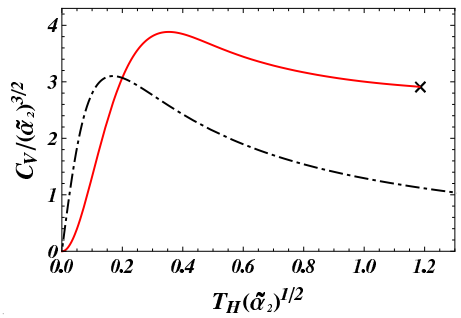

(a) C_V-T relation in five dimensions

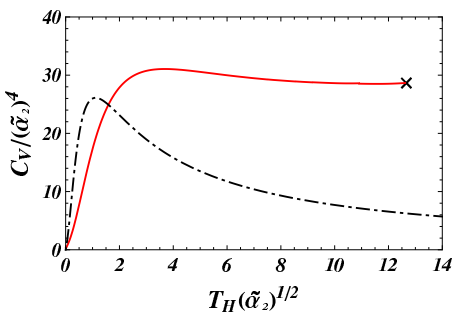

(b) C_V-T relation in ten dimensions

Figure 1: The relations between specific heat and temperature (a) in five dimensions and (b) in ten dimensions in the case of $k = -1$. The solid line in red and dot-dashed line in black correspond to the cases of the DEGB and EGB models, respectively. The maximum-temperature points are denoted by $\times$.

To extract the "mass" term, we introduce the following variables as

$$m[r] \equiv -r^{D-3-2p}\left(f[r]-\bar{f}[r]\right)\ , \qquad \Phi[r] \equiv r^{D-1-2p}\left(\phi[r]-\bar{\phi}[r]\right)\ , \tag{8}$$

$$\bar{f}[r] := \left(\frac{r}{\ell}\right)^2\left[1+\sum_{n=1}^{D-3} f_n\left(\frac{r}{\ell}\right)^{-n}\right]\ , \qquad e^{\bar{\phi}[r]} := \left(\frac{r}{\ell}\right)^p\left[1+\sum_{n=1}^{D-1}\phi_n\left(\frac{r}{\ell}\right)^{-n}\right]\ , \tag{9}$$

We depict the horizon radius-"mass" term at infinity ($\mu_f = m\ (r\to\infty)$) relations for 5 and 10 dimensions in Fig. 2. The "scalar charge" μ_Φ at infinity ($\mu_\Phi = \Phi\ (r\to\infty)$) behaves in qualitatively the same as "mass" term. The "mass" term and "scalar charge" in odd dimensions behave like those in 5 dimensions, while in even dimensions in 10 dimensions.

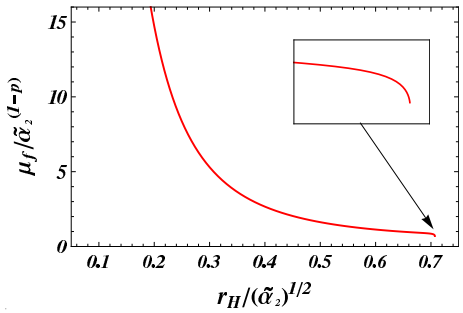

(a) "mass" term in 5 dimensions

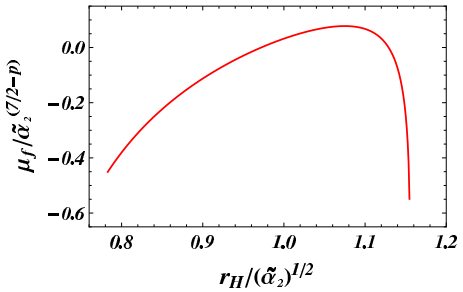

(b) "mass" term in 10 dimensions

Figure 2: We depict the horizon radius-"mass" term relations in 5 dimensions and 10 dimensions. The horizon radius-μ_Φ relations in 5 dimensions and 10 dimensions behave similarly.

4 Summary

In the dilatonic Einstein-Gauss-Bonnet (DEGB) gravity, we have obtained the exact AdS spacetimes with a planar symmetry and constructed the asymptotically AdS black holes numerically. These solutions are the dilatonic generalization of AdS spacetime and the "AdS branch" of black hole solutions in the Einstein-Gauss-Bonnet (EGB) gravity. A dilaton field, which diverges logarithmically at infinity, plays the role of a negative cosmological constant. The allowed horizon radii for asymptotically AdS black holes seem to be inherited from those of the corresponding solutions in the AdS branch in the EGB gravity.

As for the thermodynamical properties of the black holes, the entropy and temperature are well defined and their behaviours are similar to those of the "AdS branch" solution with a hyperbolic horizon in the EGB gravity. However, we could not define the proper mass and charge, although we have introduced "mass" term and "scalar charge", which may carry some physical properties of the black holes. It makes difficult for us to continue our discussion on thermodynamics such as the first law further. This strange behaviour of "mass" and "charge" may come from the fact that a dilaton field diverges logarithmically at infinity.

References

[1] Z. K. Guo, N. Ohta and T. Torii, Prog. Theor. Phys. **120**, 581 (2008).

[2] K. Maeda, N. Ohta, Y. Sasagawa Phys. Rev. D **80**, 104032 (2009).

[3] Z. K. Guo, N. Ohta and T. Torii, Prog. Theor. Phys. **121**, 253 (2009).

[4] N. Ohta and T. Torii, Prog. Theor. Phys. **121**, 959 (2009).

[5] N. Ohta and T. Torii, Prog. Theor. Phys. **122**, 1477 (2009).

[6] R. G. Cai, A. Wang Phys. Rev. D **D70**, 084042 (2004).

[7] K. Maeda, N. Ohta, Y. Sasagawa [arXiv:1012.0568[hep-th]].

[8] R. G. Cai, Phys. Rev. D **D65**, 084014 (2002).

Black hole and accretion disk formation in the collapsar model

Yuichiro Sekiguchi[1] [(a),(b)],

[(a)] *Yukawa Institute, Kyoto University, Kyoto 606-8502*
[(b)] *Division of Theoretical Astronomy, National Astronomical Observatory of Japan, Tokyo 181-8588*

Abstract

Recent studies of modeling a progenitor of long gamma-ray bursts (LGRBs) suggest that progenitors of LGRBs might have a core with higher entropy than that of ordinary presupernove. Based on the above suggestion, we performed fully general relativistic, two-dimensional simulations of collapse of *higher entropy* core to a black hole. As for the microphysics, we took into account a realistic EOS, weak interaction processes such as electron capture and pair-neutrino processes, and neutrino cooling by a recently develpoed general relativistic leakage scheme. The initial core is simply modeled by a equilibrium configuration with constant entropy and electron fraction. We found that (1) the core experiences gas pressure dominated bounce before it collapses to a black hole as in previsou simulations. (2) After the black hole formation, a thin accretion disk is formed. (3) Shock waves are formed at the inner part of the disk as infalling matters strike the disk. (4) The thin disk expands to be a thick torus accumulating the thermal energy generated at the shocks. (4) Convection occurs inside the torus because of the formation of negative entropy gradient. (5) As a result, neutrino luminosity shows violent time variability. We clarify the mechanism of these results. We also discuss importance of black hole spin on the dynamics and properties of the accretion flows around the black hole.

1 Introduction

Gamma-ray bursts (GRBs) have been one of the outstanding problems in astrophysics since their discovery. The large amount of energy release, short duration, and variability timescale indicates that GRBs may be associated with accretion processes onto a stellar-mass size black hole [1].

Although progenitors of GRBs have not been fully clarified yet, there is accumulating observational evidence that LGRBs are associated with collapse of massive stars [2]. Recent observations indicate that LGRBs may prefer a low metallicity environment [3, 4]. Therefore, gravitational collapse of population III (Pop III) stars, which are formed out of metal-free gas, may be accompanied by LGRB at a very high redshift [5]. On the other hand, it is recently showed that a single star can fulfill the requirements of the collapsar models if it is initially rapidly rotating ($\gtrsim 50\%$ of the Keplerian velocity at the equatorial surface) and of low metallicity ($Z/Z_\odot \lesssim 0.1$) [7**?**].

There have been other progenitor models of LGRBs (for a recent review, see[8]). Some authors [9] proposed binary-interaction models, in which the tidal force in a close binary keeps a helium star in synchronous, rapid rotation. It is also sugested that [10] a helium star in a close binary with a compact companion (i.e., neutron star or black hole) can retain sufficient angular momentum to form a progenitor of a GRB. Fryer and Heger [11] suggested a binary-merger model and showed that a merger of two helium cores during the common-envelope inspiral phase can produce a rapidly rotating core which satisfies the requirement of the collapsar models.

All of them are anomalous in the sense that they are quite different from the progenitors of ordinary supernovae. Qualitatively speaking, the progenitor models have larger angular momentum and *higher entropy* (and hence, more massive). The chemically homogeneous models predict a well-mixed, larger core with higher central entropy than the ordinary supernova core. It is also expected that the object formed after the binary merger will have a higher entropy, if the mass ratio of merging stars is not far from unity [12].

[1]Email address: sekig@yukawa.kyoto-u.ac.jp

Such a massive stellar core may collapse directly to a black hole without producing any explosion (Type III collapsar) [13]. In this article, we perform fully general relativistic simulations of collapse of rapidly rotating, higher entropy core in the context of the Type III collapsar, taking into account detailed microphysics, that is, a realistic equation of state (EOS), weak interaction processes such as electron capture and pair-neutrino processes, and neutrino cooling.

2 Setting

2.1 Hydrodynamic equations in general relativistic leakage scheme

Recently, I developed a fully general relativistic hydrodynamic code implementing a realistic equation of state, self-consistent electron and positron captures, and neutrino cooling by a general relativistic leakage scheme [14]. We follow this paper in solving hydrodynamic equations for which the readers may refer to the details. We assume the axial and equatorial symmetry of the spacetime and the hydrodynamics equations are solved in the cylindrical coordinates (ϖ, φ, z) where $\varpi = \sqrt{x^2+y^2}$.

2.1.1 Energy-momentum conservation equation

The basic equations of general relativistic hydrodynamics with neutrinos are

$$\nabla_\alpha (T^{\rm Total})^\alpha_\beta = \nabla_\alpha \left[(T^{\rm F})^\alpha_\beta + (T^\nu)^\alpha_\beta \right] = 0, \tag{1}$$

where $(T^{\rm Total})_{\alpha\beta}$ is the total energy-momentum tensor, and $(T^{\rm F})_{\alpha\beta}$ and $(T^\nu)_{\alpha\beta}$ are the energy-momentum tensor of fluids and neutrinos, respectively. The neutrino energy-momentum tensor is decomposed into 'trapped-neutrino' ($(T^{\nu,{\rm T}})_{\alpha\beta}$) and 'streaming-neutrino' ($(T^{\nu,{\rm S}})_{\alpha\beta}$) parts as

$$(T^\nu)_{\alpha\beta} = (T^{\nu,{\rm T}})_{\alpha\beta} + (T^{\nu,{\rm S}})_{\alpha\beta}. \tag{2}$$

Here, the trapped-neutrinos phenomenologically represent neutrinos which interact sufficiently frequently with matter and are thermalized, and the streaming-neutrino part describes a phenomenological flow of neutrinos streaming out of the system.

The streaming-neutrinos are produced with a leakage rate $Q^{\rm leak}_\alpha$ according to

$$\nabla_\beta (T^{\nu,{\rm S}})^\beta_\alpha = Q^{\rm leak}_\alpha. \tag{3}$$

On the other hand, the trapped-neutrino part is combined with the fluid part as

$$T_{\alpha\beta} \equiv (T^{\rm F})_{\alpha\beta} + (T^{\nu,{\rm T}})_{\alpha\beta}. \tag{4}$$

Then the equation for $T_{\alpha\beta}$ is

$$\nabla_\beta T^\beta_\alpha = -Q^{\rm leak}_\alpha. \tag{5}$$

We solve Eqs (3) and (5) for the energy-momentum conservation equation.

The energy-momentum tensor of the fluid and trapped-neutrino parts ($T_{\alpha\beta}$) is treated as that of the perfect fluid,

$$T_{\alpha\beta} = (\rho + \rho\varepsilon + P) u_\alpha u_\beta + P g_{\alpha\beta}, \tag{6}$$

where ρ and u^α are the rest mass density and the 4-velocity. The specific internal energy density (ε) and the pressure (P) are the sum of contributions from the baryons (free protons, free neutrons, α-particles, and heavy nuclei), leptons (electrons, positrons, and *trapped-neutrinos*), and the photons.

The streaming-neutrino part, on the other hand, is set to be a general form of

$$(T^{\nu,{\rm S}})_{\alpha\beta} = E n_\alpha n_\beta + F_\alpha n_\beta + F_\beta n_\alpha + P_{\alpha\beta}, \tag{7}$$

where $F_\alpha n^\alpha = P_{\alpha\beta} n^\alpha = 0$. In order to close the system, we need an explicit expression of $P_{\alpha\beta}$. In this paper, we adopt a simple form $P_{\alpha\beta} = \chi E \gamma_{\alpha\beta}$ with $\chi = 1/3$. This approximation may work well in high density regions but will violate in low density regions. However, the violation will not affect the dynamics because the total amount of streaming-neutrinos emitted in low density regions will be small.

2.1.2 Lepton-number conservation equations

The conservation equations of the lepton fractions are written schematically as

$$\frac{dY_e}{dt} = -\gamma_e, \tag{8}$$

$$\frac{dY_{\nu_e}}{dt} = \gamma_{\nu_e}, \quad \frac{dY_{\bar{\nu}_e}}{dt} = \gamma_{\bar{\nu}_e}, \tag{9}$$

$$\frac{dY_{\nu_x}}{dt} = \gamma_{\nu_x}, \tag{10}$$

where Y_e, Y_{ν_e}, $Y_{\bar{\nu}_e}$, and Y_{ν_x} denote the electron fraction, the electron neutrino fraction, the electron anti-neutrino fraction, and μ and τ neutrino and anti-neutrino fractions, respectively. The source terms are given by $\gamma_e = \gamma_{\nu_e}^{\rm local} - \gamma_{\bar{\nu}_e}^{\rm local}$, $\gamma_{\nu_e} = \gamma_{\nu_e}^{\rm local} - \gamma_{\nu_e}^{\rm leak}$, $\gamma_{\bar{\nu}_e} = \gamma_{\bar{\nu}_e}^{\rm local} - \gamma_{\bar{\nu}_e}^{\rm leak}$, and $\gamma_{\nu_x} = \gamma_{\nu_x}^{\rm local} - \gamma_{\nu_x}^{\rm leak}$, where $\gamma^{\rm local}$'s and $\gamma^{\rm leak}$'s are the local production and leakage rates of each neutrino, respectively. Because $\gamma_\nu^{\rm local}$'s are characterized by the timescale of weak-interaction processes $t_{\rm wp} \sim |Y_e/\dot{Y}_e|$ which can be much shorter than the dynamical timescale, the direct and explicit solution of Eqs (8)–(10) will be unstable. Therefore we follow the procedure proposed in [14] to solve the equations stably in an explicit manner.

First, in each timestep n, the conservation equation of the *total* lepton fraction ($Y_l = Y_e - Y_{\nu_e} + Y_{\bar{\nu}_e}$),

$$\frac{dY_l}{dt} = -\gamma_l, \tag{11}$$

is solved together with the conservation equation of Y_{ν_x}, Eq. (10), in advance of solving whole of the lepton conservation equations (Eqs. (8) – (10)). Then, assuming that the β-equilibrium is achieved, values of the lepton fractions in the β-equilibrium (Y_e^β, $Y_{\nu_e}^\beta$, and $Y_{\bar{\nu}_e}^\beta$) are calculated from the evolved Y_l.

Second, regarding $Y_{\nu_e}^\beta$ and $Y_{\bar{\nu}_e}^\beta$ as the maximum allowed values of the neutrino fractions in the next timestep $n+1$, the source terms are limited so that Y_ν's in the timestep $n+1$ cannot exceed Y_ν^β 's. Then, the whole of the lepton conservation equations (Eqs. (8) – (10)) are solved explicitly using these limiters.

Third, the conditions $\mu_p + \mu_e < \mu_n + \mu_{\nu_e}$ and $\mu_n - \mu_e < \mu_p + \mu_{\bar{\nu}_e}$ are checked, where μ_p, μ_n, μ_e, μ_{ν_e} and $\mu_{\bar{\nu}e}$ are the chemical potentials of protons, neutrons, electrons, electron neutrinos, and electron anti-neutrinos, respectively. If both conditions are satisfied, the values of the lepton fractions in the timestep $n+1$ are set to be those in the β-equilibrium value; Y_e^β, $Y_{\nu_e}^\beta$, and $Y_{\bar{\nu}_e}^\beta$. On the other hand, if either or both conditions are not satisfied, the lepton fractions in the timestep $n+1$ is set to be those obtained by solving whole of the lepton-number conservation equations.

2.2 Microphysics

2.2.1 Equation of state

In this paper, we employ an EOS by Shen et al [15], which is derived by the relativistic mean field theory based on the relativistic Brückner-Hartree-Fock theory. The thermodynamical quantities of dense matter at various sets of (ρ, Y_p, T) are calculated to construct the numerical data table for simulation. The table covers a wide range of density $10^{5.1}$–$10^{15.4}$ g/cm^3, electron fraction 0.0–0.56, and temperature 0–100 MeV, which are required for supernova simulation.

To consistently calculate the pressure and the internal energy of the electron and positron, the charge neutrality condition $Y_p = Y_e$ should be solved to determine the electron chemical potential μ_e for each value of the baryon rest-mass density ρ and the temperature T in the EOS table. Then, assuming that the electrons and positrons obey the Fermi-Dirac distribution, the number density, the pressure, and the internal energy density of electrons and positrons are calculated.

The pressure and the specific internal energy density of photons are given by $P_r = a_r T^4/3$ and $\varepsilon_r = a_r T^4/\rho$, where a_r is the radiation constant $a_r = (\pi^2 k_B^4)/(15c^3\hbar^3)$ and c is the velocity of light.

In this paper, the trapped-neutrinos are assumed to interact sufficiently frequently with matter that be thermalized. Therefore they are described as ideal Fermi gases with the matter temperature. Then, from the neutrino fractions Y_ν, the chemical potentials of neutrinos are calculated by solving $Y_\nu = Y_\nu(\mu_\nu, T)$. Using the chemical potentials, μ_ν, and the matter temperature, the pressure and the internal energy of the trapped-neutrinos are calculated in the same manner as for electrons.

2.2.2 Weak interaction and leakage rate

The leakage rates are defined by [14]

$$Q_\nu^{\rm leak} = (1 - e^{-b\tau_\nu})Q_\nu^{\rm diff} + e^{-b\tau_\nu} Q_\nu^{\rm local}, \tag{12}$$
$$\gamma_\nu^{\rm leak} = (1 - e^{-b\tau_\nu})\gamma_\nu^{\rm diff} + e^{-b\tau_\nu} \gamma_\nu^{\rm local}, \tag{13}$$

where τ_ν is the optical depth of neutrinos and b is a parameter which is typically set as $b^{-1} = 2/3$. Then, because $Q_\nu^{\rm leak}$ may be regarded as the emissivity of neutrinos measured in the *fluid rest frame*, $Q_\alpha^{\rm leak}$ is defined as

$$Q_\alpha^{\rm leak} = Q_\nu^{\rm leak} u_\alpha. \tag{14}$$

As the local production reactions of neutrinos, the electron and positron captures ($\gamma_{\nu_e}^{\rm ec}$ and $\gamma_{\bar\nu_e}^{\rm pc}$), the electron-positron pair annihilation ($\gamma_{\nu_e\bar\nu_e}^{\rm pair}$ for electron-type neutrinos and $\gamma_{\nu_x\bar\nu_x}^{\rm pair}$ for the other type), the plasmon decays ($\gamma_{\nu_e\bar\nu_e}^{\rm plas}$ and $\gamma_{\nu_x\bar\nu_x}^{\rm plas}$), and the Bremsstrahlung processes ($\gamma_{\nu_e\bar\nu_e}^{\rm Brems}$ and $\gamma_{\nu_x\bar\nu_x}^{\rm Brems}$), are considered in this paper. Then, the local rates for the neutrino fractions are

$$\gamma_{\nu_e}^{\rm local} = \gamma_{\nu_e}^{\rm ec} + \gamma_{\nu_e\bar\nu_e}^{\rm pair} + \gamma_{\nu_e\bar\nu_e}^{\rm plas} + \gamma_{\nu_e\bar\nu_e}^{\rm Brems}, \tag{15}$$
$$\gamma_{\bar\nu_e}^{\rm local} = \gamma_{\bar\nu_e}^{\rm pc} + \gamma_{\nu_e\bar\nu_e}^{\rm pair} + \gamma_{\nu_e\bar\nu_e}^{\rm plas} + \gamma_{\nu_e\bar\nu_e}^{\rm Brems}, \tag{16}$$
$$\gamma_{\nu_x}^{\rm local} = \gamma_{\nu_x\bar\nu_x}^{\rm pair} + \gamma_{\nu_x\bar\nu_x}^{\rm plas} + \gamma_{\nu_x\bar\nu_x}^{\rm Brems}. \tag{17}$$

Similarly, the local neutrino energy emission rate $Q_\nu^{\rm local}$ is given by

$$Q_\nu^{\rm local} = Q_{\nu_e}^{\rm ec} + Q_{\bar\nu_e}^{\rm pc} + 2\,(Q_{\nu_e\bar\nu_e}^{\rm pair} + Q_{\nu_e\bar\nu_e}^{\rm plas} + Q_{\nu_e\bar\nu_e}^{\rm Brems}) + 4\,(Q_{\nu_x\bar\nu_x}^{\rm pair} + Q_{\nu_x\bar\nu_x}^{\rm plas} + Q_{\nu_x\bar\nu_x}^{\rm Brems})\,. \tag{18}$$

The explicit forms of the local rates in Eqs. (15)–(18) will be found in [14].

We follow the recent work by Rosswog and Liebendörfer [16] for the diffusive neutrino emission rates $\gamma_\nu^{\rm diff}$ and $Q_\nu^{\rm diff}$ in Eqs (12) and (13). The explicit forms of $\gamma_\nu^{\rm diff}$ and $Q_\nu^{\rm diff}$ will be found in [14].

2.3 Initial condition and Grid

We construct approximate initial models in the following manner. We first calculate a spherical equilibrium configuration with a constant electron fraction of $Y_e = 0.5$ and with a constant entropy per baryon $s = 8k_B$. We set the central density to be $\rho_c \approx 10^8$ g/cm^3. The corresponding central temperature is $T_c \approx 9 \times 10^9$ K. Following Nakazato et al. [17], we define the boundary of the iron core to be where the temperature is 5×10^9 K. Then the mass and the radius of the iron core are $M_{\rm iron} \approx 13 M_\odot$ and $R_{\rm iron} \approx 7000$ km. We adopt a wider region of $R_{\rm init} \approx 14000$ km with mass of $M_{\rm init} \approx 23 M_\odot$.

At the current status, little is known about the angular momentum distribution in the progenitor core. Therefore we add the following rotation profile model

$$\Omega(\varpi) = \Omega_0 \exp\left[-\frac{1}{2}\frac{R_c^2}{(\varpi^2 + R_c^2)}\right] \exp\left[-\frac{\varpi^2}{R_0^2}\right], \tag{19}$$

where Ω, R_0 and R_c are parameters which control the degree of differential rotation. We fix the values of R_0 and R_c as $R_0 = R_{\rm init}/5$ and $R_c = R_{\rm init}/8$ and vary Ω_0 as 0, 0.4, 0.5 and 0.6 (hereafter referred to

	$\Phi_c \le 0.0125$	$\le \Phi_c \le 0.025$	$\le \Phi_c \le 0.05$	$\le \Phi_c \le 0.1$	$\Phi_c \le 0.2$	$\Phi_c \ge 0.2$
Δx_0	10.1	4.8	2.2	0.98	0.45	0.22
δ	0.008	0.0075	0.007	0.0065	0.006	0.0065
N	316	412	524	652	796	960
L (km)	14600	13300	11800	10100	8700	7700

Table 1: Summary of the regridding procedure. The values of the minimum grid spacing Δx_0 (in units of km), the non-uniform-grid factor δ, and the grid number N for each range of $\Phi_c = 1 - \alpha_c$ are listed.

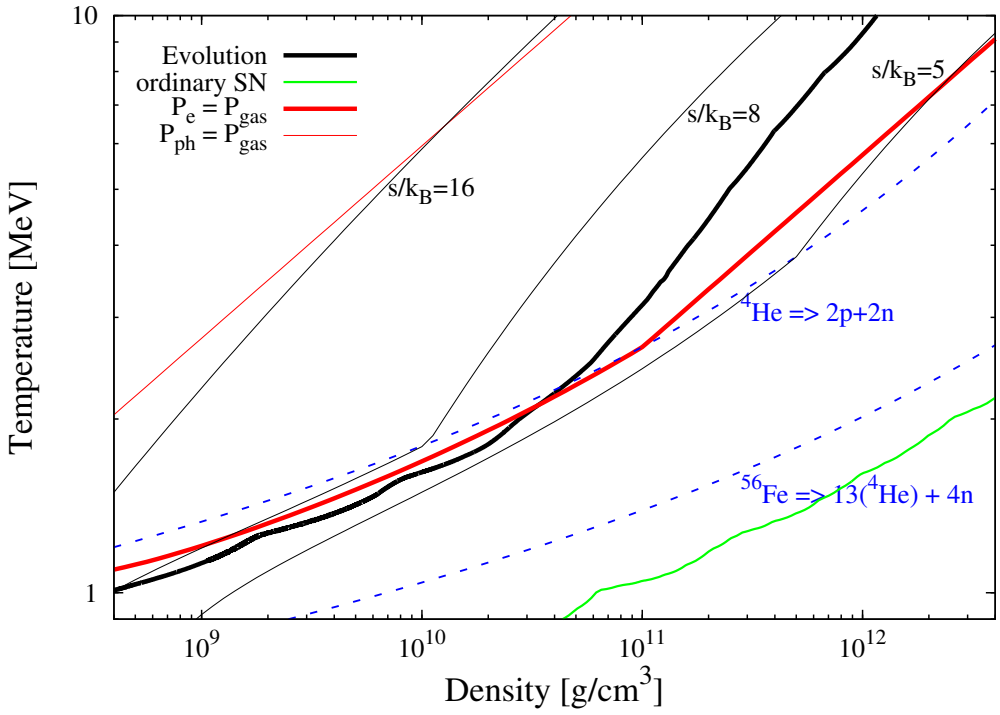

Figure 1: Evolution path of the central values of density and temperature for the spherical model in ρ-T plane (thick black solid curve). The thick and thin red solid curves show the boundary at which the condition $P_e = P_{\rm gas}$ or $P_r = P_{\rm gas}$ is satisfied. The thin black solid curves show evolution paths with constant entropy per baryon for $s/k_B = 5$, 8 and 16. The two blue dashed curves denote the value of (ρ, T) with which ^{56}Fe or ^{4}He will be half by mass due to the photo-dissociation. An evolution path of the central values of density and temperature for a usual supernova core is shown together (solid green curve).

as spherical, slowly rotating, moderately rotating, and rapidly rotating models). It should be addressed that the initial models adopted in this paper are *slowly rotating* in the sense the rotation imposed is much smallar than that considered in previous studies.

In numerical simulations, we adopt a nonuniform grid, in which the grid spacing is increased as $dx_{j+1} = (1+\delta)dx_j$, $dz_{l+1} = (1+\delta)dz_l$, where $dx_j \equiv x_{j+1} - x_j$, $dz_l \equiv z_{l+1} - z_l$, and δ is a constant. In addition, a regridding technique [18] is adopted to assign a sufficiently large number of grid points inside the collapsing core, saving the CPU time efficiently (see Table 1).

3 Results

As in the collapse of an ordinary supernova core for which the central value of entropy per baryon is $s/k_B \sim 1$, gravitational collapse is triggered by the electron capture and the photo-dissociation of heavy nuclei. In the present case, the photo-dissociation is more important for destabilizing the core because of the higher value of the entropy per baryon ($s/k_B = 8$). Due to the photo-dissociation, most of irons are resolved into heliums. As the collapse proceeds, heliums are resulved into free nucleons (p, n).

3.1 Gas pressure dominated bounce

It is known that an ordinary supernova core experiences a bounce when the central density exceeds the nuclear density ($\rho_{\rm nuc} \sim 2 \times 10^{14}$ g/cm^3) where the pressure increases drastically due to the repulsive nuclear force. In the present case, by contrast, the collapse is not decelerated by the nuclear force but by

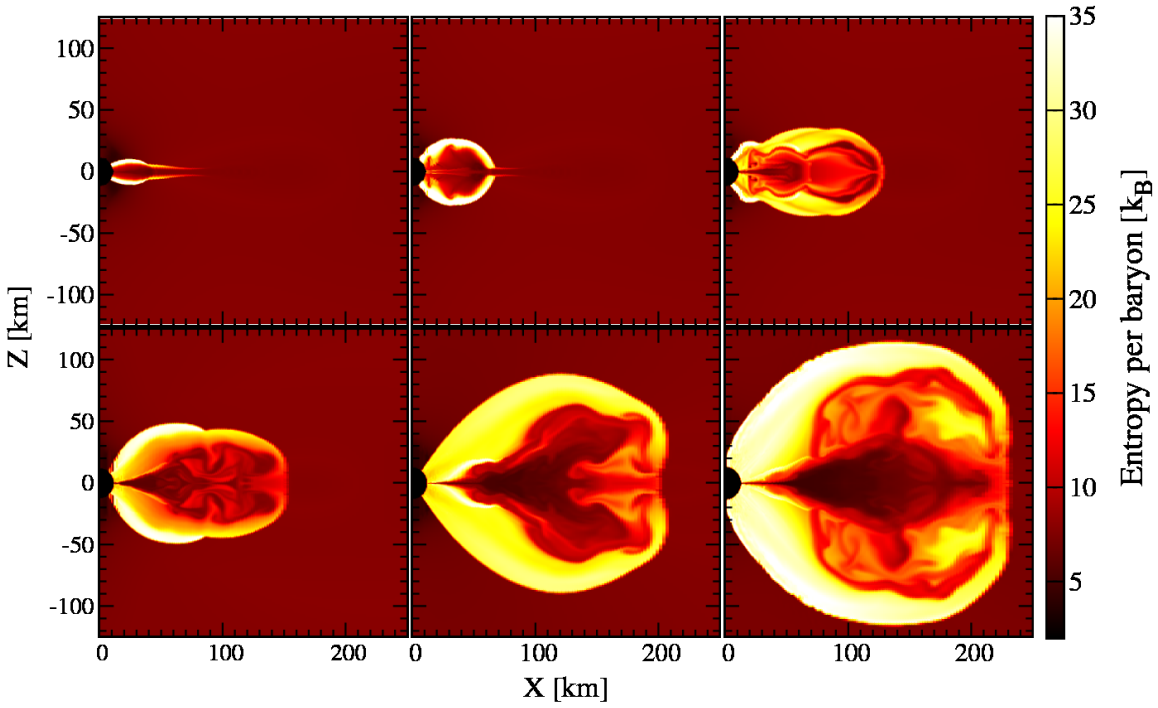

Figure 2: Contours of entropy per baryon at $t \approx 1578$ (top left), 1584 (top middle), 1591 (top right), 1644 (bottom left), 1706 (bottom middle) and 1800 ms (bottom right) for the moderately rotating model.

the thermal gas pressure $P_{\rm gas}$ [17]. Because the adiabatic index of non-relativistic gas is $\Gamma = 5/3$, which is much larger than that for the degenerate pressure of electrons (P_e), for which $\Gamma \approx 4/3$, the collapse is halted. The central density at bounce is below the nuclear density ($\approx 2 \times 10^{12}$ g/cm^3) and the central value of the temperature is ≈ 13 MeV.

The thick red curve in Figure 1 indicates the boundary in the ρ-T plane where the condition $P_e = P_{\rm gas}$ is satisfied ($P_e > P_{\rm gas}$ in the right-side of this curve). Evolution path of the central density and temperature in the ρ-T plane (the thick black curve in Figure 1) crosses the condition $P_e = P_{\rm gas}$, and hence, the pressure is dominated by the thermal gas pressure for $\rho \gtrsim 3 \times 10^{10}$ g/cm^3. Note that the pressure of the photon ($P_{\rm ph}$) is much smaller than the gas pressure in the density and temperature region considered here; the thin red curve in Figure 1 shows where the condition $P_{\rm ph} = P_{\rm gas}$ is satisfied.

It is also clear from Figure 1 that ordinary supernova cores do not experience the thermal-pressure dominated bounce. We plot an evolution path of collapse of an supernova core , simulated in [14], in Figure 1 (see the green curve).

3.2 Black hole and thin accretion disk formation

In the moderately rotating model, the apparent horizon is first formed at $t \approx 1373$ ms with mass of $\approx 6.5 M_\odot$ and spin paramter of ≈ 0.6. Soon after the apparent horizon is formed, a thin accretion disk is formed around the black hole.

At the same time, shocks are formed at the inner part of the disk, converting the kinetic energy of the infall into the thermal energy. However, the thermal energy is immediately carried away by neutrinos because the cooling timescale of neutrino emission, $t_{\rm cool}$, is very small due to the low density and small pressure scale height of the disk, H. Here, the neutrino-cooling timescale is given by $t_{\rm cool} \sim H\tau_\nu/c$.

The pressure scale height may be approximately determined by the following balance relation

$$\frac{P_{\rm disk} - P_{\rm ram}}{H} \sim \frac{G M_{\rm BH} \rho_s H}{R_{\rm disk}^3}, \tag{20}$$

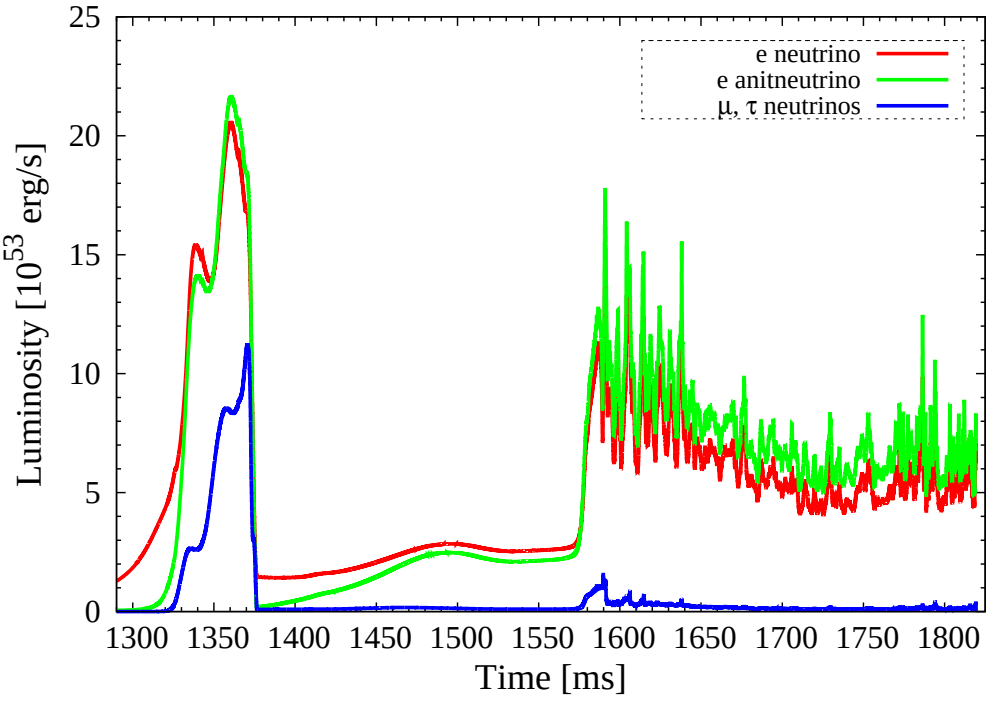

Figure 3: Time evolution of neutrino luminosities for moderately rotating model.

where $R_{\rm disk}(\approx r_{\rm ISCO})$, $\rho_{\rm disk}$, and $P_{\rm disk}$ are characteristic radius, density, and pressure of the disk, and $P_{\rm ram}$ is the ram pressure of the infalling matter, respectively. Equation (20) gives

$$\frac{H}{R_{\rm disk}} \sim \left(\frac{P_{\rm disk}-P_{\rm ram}}{10^{30}\ {\rm dyn/cm^2}}\right)^{1/2} \left(\frac{\rho_{\rm disk}}{10^{10}\ {\rm g/cm^3}}\right)^{1/2}. \tag{21}$$

Because the density and temperature are low due to the rapid advection and the copious neutrino emission, $P_{\rm disk}-P_{\rm ram}$ is very small, and hence, $H/R_{\rm disk} \ll 1$.

3.3 Disk expansion and torus formation

As matters with higher specific angular momentum in the outer region fall onto the disk, $t_{\rm cool}$ increases because neutrino optical depth and the pressure scale height increase. When density and pressure scale height become sufficiently large, the neutrino-cooling timescale becomes longer than the advection timescale onto black hole, and consequently, neutrinos are *trapped* in the accretion flow. The accretion timescale decreases because the angular momentum of the disk increases. Then, thermal energy generated by the shock heating begins to be stored efficiently and the internal energy of the disk increases (see the top-left panel in Figure 2).

As the thermal energy is stored, the disk height H increases according to Eq. (20). The density and the temperature ($T_{\rm disk}$) inside the disk eventually increase to be $\sim 10^{11}$ g/cm^3 and $\sim 5\times10^{11}$ K (and hence, $P_{\rm disk}\sim 10^{30}$ dyn/cm^2). At the same time, the ram pressure decreases to be $\lesssim 0.1P_{\rm disk}$ ($\ll P_{\rm disk}$) because the density of the infalling matter decreases to $\lesssim 10^9$ g/cm^3. Consequently, H increases to be $\sim R_{\rm disk}$ (see the top-middle panel in Figure 2). Then, the approximate balance relation (20) changes to

$$(P_{\rm disk}-P_{\rm ram}) \sim \frac{GM_{\rm BH}\rho_{\rm disk}}{H}. \tag{22}$$

Because the binding due to the gravitational force by the black hole decreases as H increases, the disk expands forming shock waves.

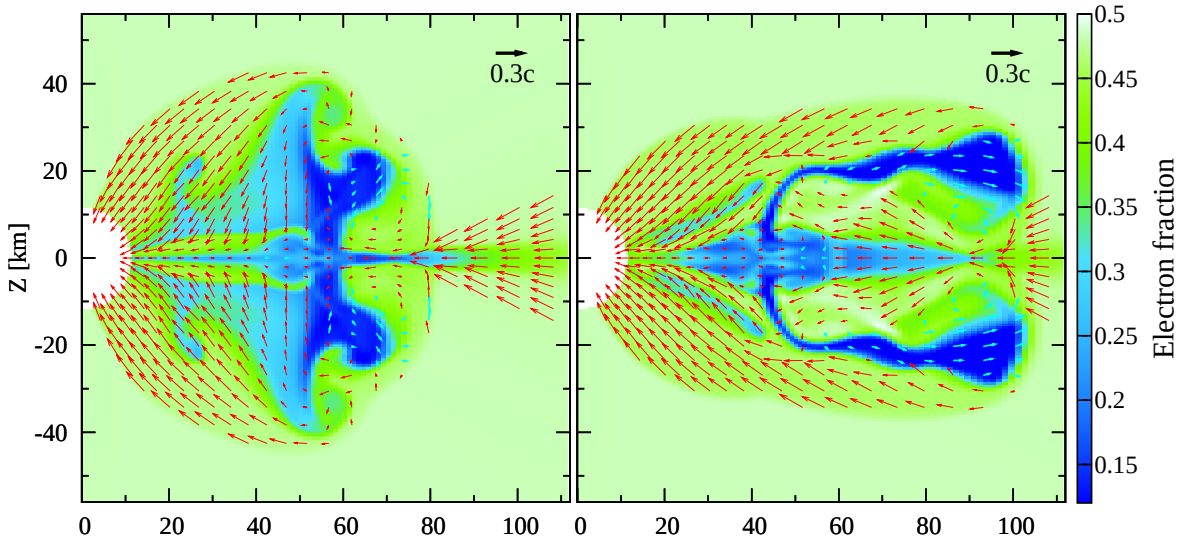

Figure 4: Contours of electron fraction with velocity fields at $t \approx 1589$ (left panel) and 1590 (right panel).

The neutrino opacities decrease as the disk expands (density and temperature decreases), and accordingly, the shock wave is stalled and the disk relaxes to a new geometrically thick state. Subsequently, the shock becomes standing accretion shock and expands gradually because matters with higher specific angular momentum falls onto the shock and because the ram pressure of the infall matters continues to decrease (see the bottom panels in Figure 2).

3.4 Convective activities

After the formation of the geometrically thick torus, convective motions are excited in the torus and the shocked region. The shock heating will be more efficient at the inner part of the disk because the kinetic energy of infall matters is larger (see the top-left panel in Figure 2). On the other hand, the neutrino cooling will be less efficient at the inner part of the disk because the disk is more optically thick to neutrinos. Then, the entropy per baryon becomes higher in the inner part of the disk and consequently, regions of negative entropy gradient are formed. Also, because neutrinos are trapped and β-equilibrium is achieved at the inner part of the disk, the total lepton fraction increases inward. These tendencies are enhanced as the accretion of matters with higher angular momentum proceeds.

Such configurations are known to be unstable to convection: The condition for convective instability to occur is given by the so-called Solberg-Hoiland criterion

$$N_{\rm SH}^2 = N_{\rm BV}^2 + \kappa^2 < 0, \tag{23}$$

where $N_{\rm BV}$ is the Brunt-Väisälä frequency and κ is the epicyclic frequency.

Figure 4 plots contours of electron fraction with velocity fields of matters. The convective flows cannot proceed freely because there is accretion flows outside the torus. Interacting with the thin accretion flows, a part of the convective flows is swerved to form finger-like structure (see the top-right panel in Figure 4). Note that there is velocity shear at the interface between the convective fingers and the accretion flows (see the right panel in Figure 4), and hence, the Kelvin-Helmholtz instability could be developed at the interface, generating turbulent motions.

Associated with the convective motions, shock waves are formed and accretion flows show very complicated features. Because of interplay of the neutrino-trapping, the Kelvin-Helmholtz instability, and the convective shock, the accretion flows remain convectively unstable. Figure 5 shows the Solberg-Hoiland

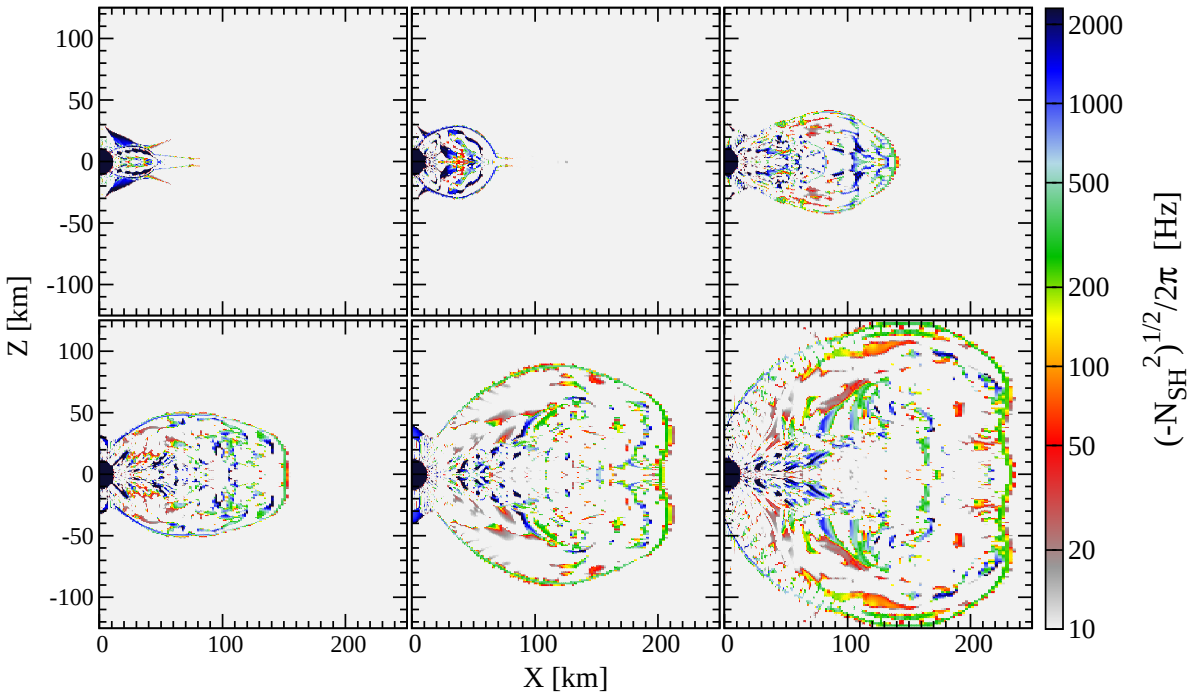

Figure 5: Contours of the frequency in Eq. (23) for the moderately rotating model. The selected timesclices are the same as those in Figure 2.

frequency, $N_{\rm SH}$ defined in Eq. (23). As this figure shows, the region below the shock remains convectively unstable.

As a natural consequence of the convective activities of accretion flows, neutrino luminosities vary violently in time (see Figure 3). Such time-variability may be associated with the observed time-variability of GRB light curves. Furthermore, electrons in the convective regions are only weakly degenerate due to the high entropy and temperature. Consequently, electron neutrinos and electron antineutrinos are approximately identically emitted. This is favorable for the pair annihilation of neutrinos to electron-positron pairs because its rate is proportional to $L_\nu L_{\bar\nu}$.

4 Discussions

The spin of a black hole plays crucial role on the dynamics of accretion flows. As clearly shown by [19], an accretion disk around a rapidly rotating black hole is remarkably different from that around a Schwarzschild black hole. The inner edge of the disk around a rotating black hole extends much closer to the black hole, and consequently, the temperature and density of the disk reach higher values. These have significant effects on the properties of disk against neutrinos.

Here, it should be noted that the trapping of neutrinos and occurrence of convective motions are not likely to be special consequences of the high mass accretion rate ($\dot{M} \sim 10 M_\odot$ s^{-1}) achieved in our models. According to the result by [19], the neutrino trapping occurs even with a moderate mass accretion rate of $\dot{M} \sim M_\odot$ s^{-1} for accretion flows around a rapidly rotating Kerr black hole. For accretion flows around a Schwarzschild black hole, by contrast, the neutrino trapping does not occur even with a high mass accretion rate of $\dot{M} \sim 10 M_\odot$ s^{-1}. This indicates that the black hole spin plays a crucial role on the properties of accretion flows around a black hole.

They also find that the neutrino trapping occurs in the vicinity of the black hole ($r \lesssim 20 G M_{\rm BH}/c^2$), as in our case. This indicates the importance of resolving the regions close to the black hole because the

seed of convection is formed there.

Similar convective accretion flows as found in the present simulation were first predicted by Narayan and Yi [20] in studies of a self-similar solution of advection-dominated accretion flows (ADAFs), and were coined as convection-dominated accretion flows (CDAFs). While the CDAF-like accretion flows are formed in the outer region of the torus, flows in the inner region are similar to those of neutrino-domineted accretion flows (NDAFs) [21]. As found in the present simulation, the accretion flows in collapsar will be characterized by the inner NDAF-like and outer CDAF-like flows. As suggested by [22], the former may produce a GRB and the later may make a supernova explosions.

Acknowledgments

The author thanks to T. Shiromizu and T. Fukushige for their grateful aids. Numerical computations were performed on the NEC SX-9 at the data analysis center of NAOJ and on the NEC SX-8 at YITP in Kyoto University. This work is supported by the Grant-in-Aid for Scientific Research (21018008, 21105511, 21340051).

References

[1] T. Piran, T., Phys. Rep., 314, 575 (1999).

[2] S. E. Woosley and J. S. Bloom, Ann. Rev. Astron. Astrophys 44, 507 (2006).

[3] A. S. Fruchter et al., Nature 441, 463 (2006).

[4] M. Modjaz et al., Astron. J. 135, 1136 (2008).

[5] V. Bromm and A. Loeb, Astrophys. J. 642, 382 (2002).

[6] S.-C. Yoon and N. Langer, Astron. Astrophys. 443, 643 (2005); S.-C. Yoon, N. Langer, and C. Norman, Astron. Astrophys. 460, 199 (2006)

[7] S. E. Woosley and A. Heger, Astrophys. J. 637, 914 (2006).

[8] C. L. Fryer et al., Publ. Astron. Soc. Pacific, 119, 1211 (2007).

[9] R. G. Izzard, E. Ramirez-Ruiz, and C. A. Tout, Mon. Not. R. Astron. Soc. 348, 1215 (2004); P. Podsiadlowski et al., Astrophys. J. 607, L17 (2004)

[10] E. P. J. van den Heuvel and S.-C. Yoon, Astrophys. Space Sci. 311, 177 (2007); M. Cantiello et al., Astron. Astrophys. 465, L29 (2007).

[11] C. L. Fryer and A. Heger, Astrophys. J. 623, 302 (2005)

[12] T. K. Suzuki et al., Astrophys. J. 668, 435 (2007); E. Gaburov, J. C. Lombardi, and S. Portegies Zwart, Mon. Not. R. Astron. Soc. 383, L5 (2008)

[13] A. Heger et al., Astrophys. J. 591, 288 (2003).

[14] Y. Sekiguchi, Class. Quant. Grav. 27, 114107 (2010); Prog. Theor. Phys. 124, 331 (2010).

[15] H. Shen, H. Toki, K. Oyamatsu, and K. Sumiyoshi, Nucl. Phys. A, 637, 435 (1998).

[16] S. Rosswog and M. Liebendörfer, Mon. Not. R. Astron. Soc. 342, 673 (2003).

[17] K. Nakazato, K. Sumiyoshi and S. Yamada, Astrophys. J. 666, 1140 (2007).

[18] M. Shibata and S. L. Shapiro, Astrophys. J. Lett. 572, 39 (2002).

[19] W.-X. Chen and A. M. Beloborodov, Astrophys. J. 657, 383 (2007).

[20] R. Narayan and I. Yi, Astrophys. J. Lett. 428, 13 (1994).

[21] R. Popham, S. E. Woosley and C. Fryer, Astrophys. J. 518, 356 (1999).

[22] R. Narayan, T. Piran and P. Kumar, Astrophys. J. 557, 949 (2001).

Curvaton with a double well potential

Ki-Young Choi[1 (a)] and Osamu Seto[2 (b)]

[(a)] *Department of Physics, Pusan National University, Busan 609-735, Korea*
[(b)] *Department of Architecture and Building Engineering, Hokkai-Gakuen University, Sapporo 062-8605, Japan*

Abstract

We study the curvature perturbation in the presence of a curvaton with a double well potential and give analytical expressions for the solution of field equation and a non-linear parameters f_{NL} with emphasizing the differences from the simple quadratic potential. We show that the level of non-Gaussianity and the tensor-to-scalar ratio depends crucially on the reheating temperature as well as the curvaton self coupling constant for a given initial amplitude of the curvaton.

1 Introduction

Cosmic inflation solves various problems in the standard Big Bang cosmology such as the flatness, the horizon, and the monopole problems [1]. A single field inflation model predicts that its density perturbation is nearly scale-invariant [2] and almost Gaussian with the corresponding nonlinearity parameter f_{NL} much less than unity [3]. Thus, the non-Gaussianity could be an important observable to check the simplest single field inflation and discriminate between various mechanisms of density perturbation generation. A mechanism to generate a large non-Gaussianity is the "curvaton" scenario [4–8], where a light scalar field σ called "curvaton" becomes the seed of the density perturbation. If the curvaton energy density is subdominant at its decay time, the large non-Gaussianity is generated in general [9]. Another important measure of the inflation is the gravitational wave background produced during the inflation [10] parametrized by the tensor-to-scalar ratio r_T, because it directly indicates the energy scale of inflation. r_T in curvaton models is also modified from that in the single field inflation.

Curvaton scenarios have been often modeled by a scalar field σ with a quadratic potential $V = \frac{1}{2}m_\sigma^2\sigma^2$ [11–13].Beyond the simplest model of curvaton, there are various possibilities; e.g., a non-negligible inflaton perturbation [14], multiple curvatons [15], and non-quadratic terms corrections [16]. It has been mostly assumed that the mass squared at the origin of field is positive as above. However, there is no reason that the true minimum is located at the origin. A moduli field, which is a promising candidate of curvaton [6], or the Peccei-Quinn field, to solve the strong CP problem, usually has the large vacuum expectation value (VEV). In this paper, we examine a curvaton model with a double well potential where it develops non-vanishing VEV [17].

For the small initial amplitude of curvaton, it shows the features of curvaton with a pure quadratic potential. For the range of the initial amplitude where the transition between quadratic and quartic potential occurs, the non-Gaussianity can be negatively very large with observable tensor-to scalar ratio. Even for a higher initial amplitude, the behavior changes again due to the the different phase of the background energy density when the curvaton starts oscillation depending on the reheating temperature.

2 A curvaton model with a double well potential

We consider a real scalar curvaton with a double well potential whose Lagrangian density is given by

$$\mathcal{L} = -\frac{1}{2}(\partial\sigma)^2 - V(\sigma), \qquad \text{and} \quad V(\sigma) = \frac{\lambda}{4}\left(\sigma^2 - v^2\right)^2, \tag{1}$$

[1]Email address: kiyoung.choi@pusan.ac.kr
[2]Email address: seto@physics.umn.edu

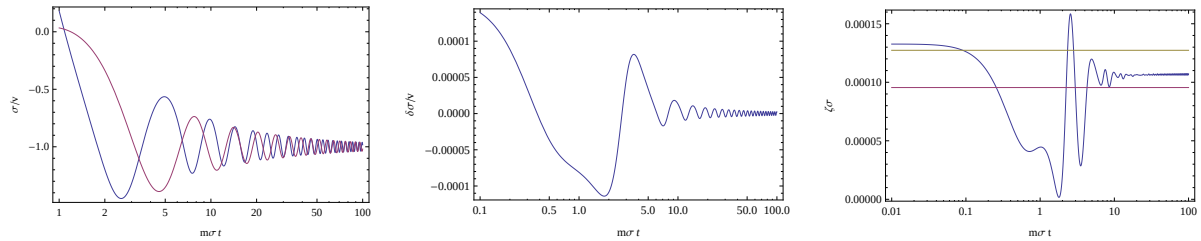

Figure 1: The evolution of σ (left), $\delta\sigma$ (center), and ζ_σ (right) for $\sigma_{\rm os} = 5v$. Here, we assume $\delta\sigma_* = H_*/(2\pi)$ with $H_* = 10^{-3}v$. The purple (blue) line in the left figure expresses the analytic solution given by Eq. (2) (the numerical solution). The green (purple) line in the right figure expresses the analytic formula of ζ_σ at $t_{\rm os}(t_v)$ without including the amplification effect.

with λ and v being respectively the self coupling constant and a large enough VEV not to form a domain wall [18, 19]. The decay rate of σ depends on its interactions with light particles and is assumed to be given by $\Gamma_\sigma \simeq m_\sigma^3/v^2$. m_σ denotes the mass at $\langle\sigma\rangle = v$. This kind of decay rate formula is realized, for instance, for the radial direction of Peccei-Quinn field in the hadronic axion model [20].

3 Cosmological evolution of σ

When the Hubble parameter H becomes comparable with the effective mass, the curvaton starts to oscillate with the initial amplitude $\sigma_{\rm os}$. After the oscillation amplitude decreases enough so that the field cannot go across the potential hill around the origin, the field can settle down at one of the two degenerate and distinct vacua. σ_v denotes the amplitude of the order of v where the transition from quartic oscillation to quadratic one occurs. At the late time, the evolution of σ can be well expressed as

$$\sigma(t) \simeq v\Theta(\sigma_{\rm os}) + \frac{\sigma_{2\rm os}}{(m_\sigma t)^{3/4}} \sin m_\sigma t, \tag{2}$$

where $\Theta(\sigma_{\rm os}) = 1$ or -1 depends on $\sigma_{\rm os}$. The amplitude of the oscillation $\sigma_{2\rm os}$ can be estimated by using the simple scaling law [21]. The left panel of Fig. 1 shows good agreement between the analytic approximated solutions (2) drawn by the purple line and the full numerical solutions drawn by the blue line. If the initial amplitude satisfies $v < \sigma_* < \sigma_v$, the curvaton field starts to oscillate initially in the potential dominated by quadratic term. For such a case, we obtain $\sigma_{2\rm os} \simeq (\sigma_* - v\Theta)(m_\sigma/2H_{\rm os})^{3/4}$.

4 Power spectrum and non-Gaussianity

For a small initial amplitude of the curvaton field $v < \sigma_* < \sigma_v$, the oscillation starts when the quadratic term dominates. The fluctuation $\delta\sigma$ has an additional dependence on $H_{2\rm os}$ compared to the simple curvaton model with quadratic potential. The non-trivial behavior from this is shown in Fig. 2. For the pure quadratic potential limit $\sigma_{\rm os} \simeq v$, the expression of ζ_σ is reduced to the known results [11–13].

Next, we consider a large initial amplitude of the curvaton field $\sigma_* \gg v$. At the early stage of oscillation, the field evolution is due to the quartic potential and highly nonlinear. When σ crosses the origin, $\delta\sigma$ has effectively the negative mass, which leads to the amplification of the fluctuation $\delta\sigma$. The center of Fig. 1 shows the amplification and evolution of the field fluctuation $\delta\sigma$ and the curvature perturbation ζ_σ for $\sigma_{\rm os} = 5v$. However, this enhancement occurs only for limited conditions of $\sigma_{\rm os}$ near the VEV transition initial expectation value. Indeed, this is not significant for $\sigma_{\rm os} = 5v$. From now on, we consider cases without this enhancement.

Since the total curvature perturbation of radiation after the curvaton decay is conserved, it can be calculated at the time of the curvaton decay. For a large initial amplitude $\sigma_* \gg \sigma_v$, the nonlinearity parameters are given for high T_R as

$$f_{NL} = \left(\frac{\tilde{r}}{1+\tilde{r}}\right)^2 \frac{5}{6}\left(\frac{1}{R} - 2 - R\right) > -2, \tag{3}$$

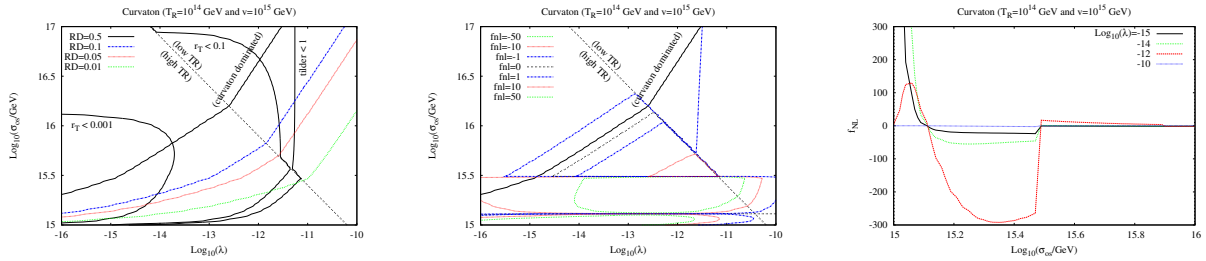

Figure 2: Left: The contour plots of R and r_T. Here we used $v = 10^{15}$ GeV and $T_R = 10^{14}$ GeV. Center: The contour plot of f_{NL} in the same plane of the left. Right: The plots for f_{NL} with the fixed λ.

and for a low T_R as

$$f_{NL} = \left(\frac{\tilde{r}}{1+\tilde{r}}\right)^2 \frac{5}{6}(-2-R)\,. \tag{4}$$

Here $R \equiv 3\rho_\sigma/(4\rho_r + 3\rho_\sigma)|_{H=\Gamma_\sigma}$ with $\rho_\sigma(\rho_r)$ being the energy density of curvaton (radiation). $\tilde{r}$ is defined as the ratio of the contribution to the perturbation from the curvaton to that from the inflaton. While the sizable $f_{NL} \sim 100$ is obtained with a small ratio $R \sim 10^{-2}$ for a high T_R, such a large non-Gaussianity is not possible for a low T_R due to the cancellations in the coefficients of the inverse of R-terms.

The tensor to scalar ratio r_T is given by

$$r_T \quad = \quad \frac{P_T}{P_\zeta} = \frac{16\epsilon}{(1-R)^2(1+\tilde{r})} \leq 16\epsilon. \tag{5}$$

The equality is satisfied when R goes to 0 which is the pure single field case. If the amplitude is large enough, the gravitational wave background is detectable through the measurement of the B-mode polarization in the cosmic microwave background anisotropy by Planck.

In Fig. 2, the contour plots of gravitational wave background and R (left window) and f_{NL} (central window) are shown with observational constraints in the plane parameters of λ and σ_*. Here we have fixed VEV $v = 10^{15}$ GeV, and the reheating temperature $T_R = 10^{14}$ GeV. The observational constraints include the tensor-to-scalar ratio $r_T = 0.1$ and 10^{-3} for the expected sensitivity of B-mode detection by Planck and future instruments. As can be seen in the figures, the large σ_* or the large λ region is excluded by the null detection of gravitational wave. For a larger initial amplitude where the curvaton oscillation starts before reheating, corresponding to low-T_R, the non-Gaussianity is significantly suppressed because of the cancellation as discussed after Eq. (4). For the initial amplitude $v < \sigma_* < \sigma_v$, the sign of f_{NL} changes nontrivially and is positive for $v < \sigma_* \lesssim 1.8v$ and negative for $1.8v < \sigma_* \lesssim \sigma_v$. This difference is due to the σ dependent effective mass in a double well potential, which is constant in the pure quadratic potential. The right window of Fig. 2 shows the σ_* dependence of f_{NL} for a given λ for $T_R = 10^{14}$ GeV.

5 Conclusion

We have studied the density perturbation and the observables such as large non-Gaussianity and gravitational wave background generated by a curvaton whose potential is flat with small self-coupling in a double well type. We have found three interesting features. One is the tachyonic amplification of the fluctuation by the negative mass squared at the origin, for a particular initial value $\sigma_{\rm os}$ which periodically appear in the parameter space. We have shown that, except for these tuned boundaries, the density perturbation and other nonlinear parameters are well approximated by analytic formula. The second is the suppression of non-Gaussianity even for very subdominant curvaton, if the reheating temperature after inflation is very low, i.e. the curvaton starts oscillation before inflaton decay. The other is the non-trivial behavior of f_{NL} even when the curvaton field starts oscillation trapped at one of the minima. Here we have shown the features of this double well potential which can be observed in the experiments. Therefore, if both large nonlinearity and B-mode polarization is detected, the potential of the curvaton or thermal history of the early Universe will be well constrained.

References

[1] A. A. Starobinsky, JETP Lett. **30** 682 (1979) [Pisma Zh. Eksp. Teor. Fiz. **30** 719 (1979)];
K. Sato, Mon. Not. Roy. Astron. Soc. **195**, 467 (1981);
A. H. Guth, Phys. Rev. D **23**, 347 (1981).

[2] S. W. Hawking, Phys. Lett. B **115**, 295 (1982);
A. A. Starobinsky, Phys. Lett. B **117**, 175 (1982);
A. H. Guth and S. Y. Pi, Phys. Rev. Lett. **49**, 1110 (1982).

[3] J. M. Maldacena, JHEP **0305**, 013 (2003).

[4] S. Mollerach, Phys. Rev. D **42** 313 (1990).

[5] D. H. Lyth and D. Wands, Phys. Lett. B **524**, 5 (2002).

[6] T. Moroi and T. Takahashi, Phys. Lett. B **522**, 215 (2001) [Erratum-ibid. B **539**, 303 (2002)].

[7] K. Enqvist and M. S. Sloth, Nucl. Phys. B **626**, 395 (2002).

[8] for a recent review on local type non-Gaussianity, see e.g., C. T. Byrnes and K. Y. Choi, Adv. Astron. **2010**, 724525 (2010); D. Wands, Class. Quant. Grav. **27**, 124002 (2010).

[9] D. H. Lyth, C. Ungarelli and D. Wands, Phys. Rev. D **67**, 023503 (2003).

[10] B. Allen, Phys. Rev. D **37**, 2078 (1988); V. Sahni, Phys. Rev. D **42**, 453 (1990).

[11] N. Bartolo, S. Matarrese and A. Riotto, Phys. Rev. D **69** 043503 (2004).

[12] D. H. Lyth and Y. Rodriguez, Phys. Rev. Lett. **95** 121302 (2005).

[13] M. Sasaki, J. Valiviita and D. Wands, Phys. Rev. D **74** 103003 (2006).

[14] D. Langlois and F. Vernizzi, Phys. Rev. D **70**, 063522 (2004);
F. Ferrer, S. Rasanen and J. Valiviita, JCAP **0410**, 010 (2004);
T. Moroi and T. Takahashi, Phys. Rev. D **72** 023505 (2005);
K. Ichikawa, T. Suyama, T. Takahashi and M. Yamaguchi, Phys. Rev. D **78**, 023513 (2008).

[15] K. Y. Choi and J. O. Gong, JCAP **0706** 007 (2007).

[16] K. Enqvist and S. Nurmi, JCAP **0510** 013 (2005);
Q. G. Huang and Y. Wang, JCAP **0809** 025 (2008);
K. Enqvist and T. Takahashi, JCAP **0809**, 012 (2008); JCAP **0912**, 001 (2009);
K. Enqvist, S. Nurmi, O. Taanila and T. Takahashi, JCAP **1004**, 009 (2010);
C. T. Byrnes, K. Enqvist and T. Takahashi, JCAP **1009** 026 (2010).

[17] K. Choi and O. Seto, Phys. Rev. D **82**, 103519 (2010) .

[18] A. D. Linde, Phys. Lett. B **259** 38 (1991).

[19] S. Kasuya, M. Kawasaki and T. Yanagida, Phys. Lett. B **409**, 94 (1997);
S. Kasuya and M. Kawasaki, Phys. Rev. D **56**, 7597 (1997); Phys. Rev. D **58**, 083516 (1998).

[20] J. E. Kim, Phys. Rev. Lett. **43**, 103 (1979);
M. A. Shifman, A. I. Vainshtein and V. I. Zakharov, Nucl. Phys. B **166**, 493 (1980).

[21] K. Enqvist, S. Nurmi, G. Rigopoulos, O. Taanila and T. Takahashi, JCAP **0911**, 003 (2009).

A note on trapped surfaces in the Oppenheimer-Snyder solution

Masahiro Shimano[1], Naoki Tsukamoto[2], Kohji Yaijma[3] and Tomohiro Harada[4]

Department of Physics, Rikkyo University, Toshima, Tokyo 171-8501, Japan

Abstract

Although an event horizon defines a black hole, it is difficult to explain a boundary of dynamical black holes. A trapped surface is a candidate of the boundary of dynamical black holes, and is studied in various spacetimes and settings. Usually, there is no trapped surface in a Minkowski region, however, Bengtsson and Senovilla showed an interesting result as follows: in a self-similar Vaidya spacetime, they considered non-spherical trapped surfaces and showed that trapped surfaces can extend into the Minkowski region, if and only if a mass function rises fast enough [1]. In this paper we extend Bengtsson and Senovilla's way in a Oppenheimer-Snyder solution. We match two kinds of two-surfaces and construct trapped surfaces which pass through an apparent horizon.

1 Introduction

A boundary of a region in a spacetime that cannot be observed from infinity is called event horizon. The event horizon defines a boundary between an inside and an outside of a black hole. Moreover, this horizon has a teleological property: an entire future history of the spacetime must be known before a position of the event horizon can be determined. Since the event horizon is defined at future timelike infinity, a shape of the event horizon does not change. However, some quantum effect might deform the boundary of dynamical black holes. It might be impossible to explain the boundary of dynamical black holes with the event horizon.

Eardley conjectured that the boundary of the region which contains marginally outer trapped surfaces coincide with the event horizon [2]. A surface called outer trapped surface is the closed spacelike two-surface and whose outer null expansion is negative. This conjecture is very interesting, because we can translate the event horizon with outer trapped surface, i.e., we can define the event horizon constructively. In a Vaidya spacetime, Ben-Dov showed that Eardley's conjecture is true [3]. However, the outer trapped surface cannot be considered in the general spacetime, because it is defined only in asymptotically flat spacetimes [4]. Moreover, the outer trapped surface only consider an outer null ray. There remains a possibility of which we can observe an inner null ray. Since the black hole is an invisible region, to define this region we should consider a notion of which both null rays cannot be observed.

A surfaces called trapped surface defines the boundary of an invisible region. The trapped surface is a closed spacelike two-surface and whose both null expansions are negative. Since the black hole cannot be observed even from infinity, its boundary might be defined with the trapped surface. Usually, there is no trapped surface in a Minkowski spacetime. However, in the Vaidya spacetime it was showed that trapped surfaces can extend into the Minkowski region. Numerical results of Schnetter and Krishnan showed that an outer boundary of trapped surfaces can extend into the Minkowski region [5]. Moreover, Bengtsson and Senovilla considered the self-similar Vaidya spacetime, and they analytically showed that trapped surfaces can extend into the Minkowski region, if and only if a mass function rises fast enough [1].

In this paper, we extend Bengtsson and Senovilla's way into a Oppenheimer-Snyder solution, and consider the relation between the trapped surface and an apparent horizon. The surface called apparent horizon is the boundary of a trapped region. A portion of hypersurface which contains trapped surfaces is called trapped region. Therefore, usually, trapped surface does not extend outside the apparent horizon. However, by using Bengtsson and Senovilla's way we construct a non-spherical trapped surface and show that this trapped surface passes through the apparent horizon.

[1]Email address: shimano@rikkyo.ac.jp
[2]Email address: 09la008b@rikkyo.ac.jp
[3]Email address: 09la010t@rikkyo.ac.jp
[4]Email address: harada@rikkyo.ac.jp

2 Oppenheimer-Snyder solution

The Oppenheimer-Snyder solution describes a process of a gravitational collapse to the black hole. In this paper, for simplicity, we consider a collapse of a homogeneous dust from infinity. A metric inside the dust is a flat Friedmann-Robertson-Walker(FRW) solution, while the metric outside the dust is a Schwarzschild solution. These metrics are joined smoothly on a common boundary which is the surface of the collapsing dust.

The metric inside the collapsing dust is given by

$$ds_-^2 = -dt + a^2(t)\left(dr^2 + r^2 d\theta^2 + r^2 \sin^2\theta d\phi^2\right), \tag{1}$$

where t is proper time on comoving world lines, and $a(t)$ is the scale factor. Substituting this metric into the Einstein equation, we get the Friedmann equation

$$\left(\frac{a'}{a}\right)^2 = \frac{8\pi G\rho}{3}, \tag{2}$$

where ρ is a energy density of the dust, G is a gravitational constant, and a over-dash denotes a differentiation with respect to t. Because the dust has not a pressure, the dust's energy density satisfies $\rho a^3 = C$ from the energy-momentum conservation law, where C is a constant. Substituting this energy density into Eq. (2), after some calculations, we obtain

$$a(\eta) = \frac{2\pi G}{3} C(-\eta)^2, \tag{3}$$

where we have introduced comoving time η which satisfies a relation $d\eta = dt/a$, and we have assumed $a = 0$ at $\eta = 0$. The collapse begins at $\eta = -\infty$ when $a = \infty$, and it ends at $\eta = 0$ when $a = 0$. We assume that the hypersurface Σ coincides with the surface of the collapsing dust, which is located at $r = r_c$ in our comoving coordinates. The induced metric of Σ is given by

$$ds^2_{\Sigma_{\text{inside}}} = a^2(\eta)\left\{-d\eta^2 + r_c^2\left(d\theta^2 + \sin^2\theta d\phi^2\right)\right\}. \tag{4}$$

On the other hand, the metric outside the dust is given by

$$ds^2 = -f d\tau^2 + f^{-1} d\chi^2 + \chi^2\left(d\theta^2 + \sin^2\theta d\phi^2\right), \tag{5}$$

where $f = 1 - 2m/r$ and m is a gravitational mass of the collapsing dust. In this metric, the surface of the collapsing dust Σ is described by the parametric equations $\chi = \bar{R}(\eta)$ and $\tau = \bar{T}(\eta)$, where η is the same η that appears in Eq. (3). The induced metric of Σ is given by

$$ds^2_{\Sigma_{\text{outside}}} = -(F\dot{\bar{T}}^2 - F^{-1}\dot{\bar{R}}^2)d\eta^2 + \bar{R}^2(\eta)\left(d\theta^2 + \sin^2\theta d\phi^2\right), \tag{6}$$

where $F = 1 - 2m/\bar{R}$, and a over-dot is the differentiation with respect to η.

Because the induced metric must be the same on both sides of the hypersurface Σ, we have

$$F\dot{\bar{T}}^2 - F^{-1}\dot{\bar{R}}^2 = a^2, \quad a^2 r_c^2 = \bar{R}^2. \tag{7}$$

Moreover, the extrinsic curvature also must be coincide with both sides of Σ. Then we get relations

$$a\dot{\beta} - \dot{a}\beta = 0, \quad a^2 = F^2\dot{\bar{T}}^2, \tag{8}$$

where $\beta = F\dot{\bar{T}} = \sqrt{\dot{\bar{R}}^2 + a^2 F}$. By using Eqs. (3), (7), (8), and $F = 1 - 2m/\bar{R}$, we obtain

$$C = \frac{3}{4\pi G}\frac{m}{r_c^3}, \quad \bar{R} = \frac{m}{2r_c^2}(-\eta)^2. \tag{9}$$

Substituting Eq. (9) into Eq. (8), after integrating with respect to η, we get

$$\bar{T} = -\frac{m}{2r_c^3}(-\eta)^3 - \frac{2m}{r_c}(-\eta) - 2m\ln\left(\frac{(-\eta) - 2r_c}{(-\eta) + 2r_c}\right) + 2m\left(20 + \ln\left(\frac{1}{3}\right)\right), \tag{10}$$

where we have considered $\bar{T} = 0$ at $-\eta = 4r_c$. Moreover, the relation of both coordinates on the hypersurface Σ is given by

$$\left(\frac{\partial}{\partial\tau}\right) = \frac{F\dot{\bar{T}}}{a}\left(\frac{\partial}{\partial\eta}\right) - \frac{\dot{\bar{R}}}{a}\left(\frac{\partial}{\partial r}\right), \quad \left(\frac{\partial}{\partial\chi}\right) = -\frac{\dot{\bar{R}}}{aF}\left(\frac{\partial}{\partial\eta}\right) + \frac{\dot{\bar{T}}}{a}\left(\frac{\partial}{\partial r}\right). \tag{11}$$

3 Trapped surface

In the Oppenheimer-Snyder spacetime, we consider two kinds of two-surfaces to obtain trapped surface which passes through the apparent horizon. One is the surface in which η and r are the function of ρ, and in which $\theta = \pi/2$. We call this surface *constant inclination surface* (CIS), and consider this surface in the inside of the collapsing dust. The other is the surface in which θ and v are the function of ρ, and in which $\chi = \chi_0$, where v is the ingoing null coordinate $v = \tau + \chi + 2m\ln|(\chi - 2m)/(2m)|$. We call this surface *constant radius surface* (CRS), and consider this surface in the outside of the collapsing dust. In order to get the trapped surface which passes through the apparent horizon, we bend these two-surfaces and match these on the hypersurface Σ.

In the inside of the collapsing dust, we bend the CIS into a quadratic curve

$$\eta = \eta_0 + \frac{E}{2}r^2, \tag{12}$$

where η_0 and E are constants. Both null expansions of this surface are

$$\vartheta_\pm = -\frac{1}{a\sqrt{1-E^2r^2}}\left[E(E^2r^2-2) + \frac{4}{(-\eta)}\right]. \tag{13}$$

If χ_0 satisfies

$$0 < \chi_0 < 1.6m, \tag{14}$$

both null expansions are negative.

On the other hand, in the outside of the collapsing dust, we bend the CRS into a quadrant of a circle

$$\theta^2 + (z - z_c)^2 = \frac{\pi^2}{4}, \tag{15}$$

where $z = v/\chi_0$ and $z_c = v_c/\chi_0$ is a constant. Both null expansions of this CRS are negative, if the inequality

$$\left(\frac{m}{\chi_0} - 1\right)\sqrt{\frac{2m}{\chi_0} - 1} > \frac{4}{\pi} \tag{16}$$

is satisfied. The solution of this inequality is

$$0 < \chi_0 < 0.68514m, \tag{17}$$

where we have assumed $\theta = \pi/2$ at $z = z_c$.

In order to match the CRS with the CIS on the hypersurface Σ, we match the derivative and the position of these surfaces on Σ. From Eq. (12) we obtain the derivative $d\eta/dr$ of the CIS on Σ as follows

$$\frac{d\eta}{dr} = Er. \tag{18}$$

A value of this derivative is positive. On the other hand, by using Eq. (11), we get the derivative of the CRS which is expressed by the coordinate of the inside of the collapsing dust as

$$\frac{d\eta}{dr} = \frac{(-\eta)}{2r_c}, \tag{19}$$

where we have assumed $\theta = \pi/2$ on matching point. The value of this derivative is positive too. Since both derivatives are positive, we can smoothly match the derivative. Moreover, by substituting Eq. (18) into Eq. (19) we decide the matching time

$$\eta_c = -2Er_c^2. \tag{20}$$

On this matching point, since the two-surface is $\chi = \chi_0$ and $\theta = \pi/2$, both null expansions are

$$\vartheta_{\pm} = \frac{1}{2\chi_0}\left(1 - \frac{m}{\chi_0}\right)\left(\frac{2m}{\chi_0} - 1\right)^{-1/2}. \tag{21}$$

If χ_0 satisfies

$$0 < \chi_0 < m, \tag{22}$$

both null expansions are negative.

Combining inequalities (14), (17) and (22), we can summarise that the trapped surface is constructed, if χ_0 satisfies the inequality (17).

Now, we shall check whether the trapped surface passes through the apparent horizon or not. Usually, the apparent horizon $r_{\rm AH}$ in the inside of the collapsing dust given by

$$r_{\rm AH} = \frac{a}{a'} = \frac{m}{4r_c^3}(-\eta)^3. \tag{23}$$

The apparent horizon appears $r_{\rm AH} = 2m$ when $\eta = -2r_c$, and ends $r_{\rm AH} = 0$ when $\eta = 0$. Therefore, if η_0 in Eq. (12) has a nonzero negative value, our trapped surface passes through the apparent horizon. Substituting Eq. (20) into Eq. (12) with $\eta = \eta_c$, we get

$$\eta_0 = -\frac{5}{2}Er_c. \tag{24}$$

Thus, η_0 has the nonzero negative value, and we could construct the trapped surface passes through the apparent horizon.

4 Conclusion

In the Vaidya spacetime, Bengtsson and Senovilla showed the interesting result: the trapped surface can extend into the flat region. In this paper, we have extended this result into the Oppenheimer-Snyder spacetime, and have shown that the trapped surface can pass through the apparent horizon. In order to get the trapped surface we have used two kinds of two-surfaces (we have called these surfaces CIS and CRS, respectively), and have bent the CIS and the CRS into the quadrant curve and the quadrant of the circle, respectively. We have matched the CIS and the CRS smoothly on the collapsing dust's surface Σ, and have shown that this matched surface are trapped surface, if χ_0 satisfies $0 < \chi_0 < 0.68514m$. Moreover, we have shown that this trapped surface passes through the apparent horizon.

References

[1] I. Bengtsson, and J. M. M. Senovilla, Phys. Rev. D **79**, 024027 (2009).

[2] D. M. Eardley, Phys. Rev, D **57**, 2299 (1998).

[3] I. Ben-Dov, Phys. Rev, D **75**, 064007 (2007).

[4] S. W. Hawking and G. F. R. Ellis, *Large Scale Structure of Spacetime* (Cambridge University Press, Cambridge, 1972).

[5] E. Schnetter and B. Krishnan, Phys. Rev, D **73**, 021502(R) (2006).

The CMB bispectrum from vector-mode perturbations induced by primordial magnetic fields

Maresuke Shiraishi[1(a)], Daisuke Nitta[(a)], Shuichiro Yokoyama[(a)], Kiyotomo Ichiki[(a)] and Keitaro Takahashi[(a)]

[(a)] *Department of Physics and Astrophysics, Nagoya University, Aichi 464-8602, Japan*

Abstract

We calculate CMB bispectrum of vector modes induced from primordial magnetic fields. We take into account the full angular dependence of the bispectrum and discuss the amplitude and also the shape of the bispectrum. In the squeezed limit, we estimate a typical values of the normalized reduced bispectrum as $\ell_1(\ell_1+1)\ell_3(\ell_3+1)|b_{\ell_1\ell_2\ell_3}| \sim 2\times10^{-19}$, for the strength of the primordial magnetic field smoothed on 1Mpc scale $B_{1\mathrm{Mpc}} = 4.7\mathrm{nG}$ assuming nearly scale-invariant spectrum of magnetic fields. We find that a new constraint on the magnetic field strength will be placed as $B_{1\mathrm{Mpc}} < 10\mathrm{nG}$ if PLANCK will place a limit on the nonlinearity parameter of local-type configuration as $|f_{\mathrm{NL}}^{\mathrm{local}}| < 5$.

1 Introduction

Non-Gaussianity of primordial curvature perturbation has been recently focused on as a powerful tool to probe the mechanism of generating the seed of structures in our Universe [1, 2]. Current observations of cosmic microwave background (CMB) anisotropies (and also large scale structure (LSS)) indicate that the statistics of the primordial curvature perturbation is almost Gaussian. Although it is difficult to detect the primordial non-Gaussianity by analyzing only the power spectrum, the bispectrum of the primordial fluctuation is an useful observable to detect the non-Gaussianity for such weakly non-Gaussian fluctuations.

On the other hand, there are a lot of sources of CMB bispectrum other than the primordial non-Gaussianity, e.g., nonlinear evolution of the temperature fluctuations, cosmic string and so on. Primordial magnetic fields (PMFs) may also become the source of the CMB temperature anisotropies and give a highly non-Gaussian contribution. In several studies [3, 4], the authors investigated the contribution to the bispectrum of the CMB temperature fluctuations from the scalar mode PMFs and roughly estimated the limit of the amplitude of the PMFs. As is well known, however, PMFs excite not only the scalar fluctuation but also the vector and tensor fluctuations. In particular, it has been known that the vector contribution may dominate the scalar one on small scales. Hence, the future CMB experiments, for example, Planck satellite [5], is expected to give a tighter constraint of the amplitude of the PMFs from the vector contribution induced from the magnetic fields. In this paper, following the discussion in Ref. [6], we investigate the CMB bispectrum of the vector perturbation induced from the PMFs without neglecting the angular dependence.

2 Formulation of the vector bispectrum induced from PMFs

Let us consider the stochastic PMFs $B^b(x^b,\tau)$ on the homogeneous background Universe which is characterized by the Friedmann-Robertson-Walker metric; $ds^2 = a(\tau)^2[-d\tau^2+\delta_{bc}dx^b dx^c]$, where τ is a conformal time and a is a scale factor. The expansion of the Universe makes the amplitude of the magnetic fields decay as $1/a^2$ and hence we can draw off the time dependence as $B^b(x^b,\tau) = B^b(\mathbf{x})/a^2$. The Fourier component of the anisotropic stress generated from PMFs is given by the convolution of B_a as

$$\Pi_{Bab}(\mathbf{k}) = -\frac{1}{4\pi\rho_{\gamma,0}}\int\frac{d^3\mathbf{k}'}{(2\pi)^3}B_a(\mathbf{k}')B_b(\mathbf{k}-\mathbf{k}')\ , \tag{1}$$

[1]Email address: mare@a.phys.nagoya-u.ac.jp

where $\rho_{\gamma,0}$ denotes the present energy density of photons. The index is lowered by δ_{ab} and the summation is implied for repeated indices. Assuming that $B^a(\mathbf{x})$ is a Gaussian field, the power spectrum of the PMFs $P_B(k)$ is defined by

$$\langle B_a(\mathbf{k})B_b(\mathbf{p})\rangle = (2\pi)^3\frac{P_B(k)}{2}P_{ab}(\hat{\mathbf{k}})\delta(\mathbf{k}+\mathbf{p}) \ , \tag{2}$$

with a projection tensor $P_{ab}(\hat{\mathbf{k}}) = \delta_{ab} - \hat{k}_a\hat{k}_b$, which comes from the divergence free nature of the PMF. Here $\hat{\mathbf{k}}$ denotes a unit vector. Although the form of the power spectrum $P_B(k)$ is strongly dependent on the production mechanism, we, here, assume a simple power law shape given by

$$P_B(k) = \frac{(2\pi)^{n_B+5}}{\Gamma(n_B/2+3/2)k_{1\mathrm{Mpc}}^3}B_{1\mathrm{Mpc}}^2\left(\frac{k}{k_{1\mathrm{Mpc}}}\right)^{n_B} \ , \tag{3}$$

where $B_{1\mathrm{Mpc}}$ denotes the magnetic field amplitude smoothed on a scale 1Mpc and n_B is a spectral index. The vector anisotropic stress fluctuations are defined as $\Pi_{Bv}^{(\pm1)} = \hat{k}_a\epsilon_b^{(\mp1)}\Pi_{Bab}$, where $\epsilon_a^{(\mp1)}$ is a normalized divergenceless polarization vector which satisfies the orthogonal condition; $\hat{k}^a\epsilon_a^{(\mp1)} = 0$. Since the statistics of the magnetic fields B^a are assumed to be a Gaussian, one can easily find that the statistics of the vector anisotropic stress fluctuations is highly non-Gaussian. Hence the bispectrum, which is calculated as

$$\begin{aligned}\left\langle\prod_{i=1}^3\Pi_{Bv}^{(\lambda_i)}(\mathbf{k_i})\right\rangle &= \left[\prod_{i=1}^3\int d^3\mathbf{k}_\mathbf{i}'P_B(k_i')\right]\delta(\mathbf{k_1}-\mathbf{k_1'}+\mathbf{k_3'})\delta(\mathbf{k_2}-\mathbf{k_2'}+\mathbf{k_1'})\delta(\mathbf{k_3}-\mathbf{k_3'}+\mathbf{k_2'})/\left(-4\pi\rho_{\gamma,0}\right)^3 \\ &\times\frac{1}{8}\hat{k}_{1a}\epsilon_b^{(-\lambda_1)}\hat{k}_{2c}\epsilon_d^{(-\lambda_2)}\hat{k}_{3e}\epsilon_f^{(-\lambda_3)}[P_{ad}(\hat{\mathbf{k}_1'})P_{be}(\hat{\mathbf{k}_3'})P_{cf}(\hat{\mathbf{k}_2'})+7\text{ perms.}] \ ,\end{aligned} \tag{4}$$

has the non-zero value. Here λ means two helicities: $\lambda_1,\lambda_2,\lambda_3 = \pm1$ and "7 perms" denotes the symmetric 7 terms under the permutations of indices: $a\leftrightarrow b$, $c\leftrightarrow d$, or $e\leftrightarrow f$.

The CMB temperature fluctuation is expanded into spherical harmonics as $\frac{\Delta T(\hat{\mathbf{n}})}{T}\equiv\sum_{\ell m}a_{\ell m}Y_{\ell m}(\hat{\mathbf{n}})$. Then the angle-averaged bispectrum can be defined as [1]

$$B_{\ell_1\ell_2\ell_3} \equiv \sum_{m_1m_2m_3}\begin{pmatrix}\ell_1 & \ell_2 & \ell_3\\ m_1 & m_2 & m_3\end{pmatrix}\left\langle\prod_{i=1}^3 a_{\ell_i m_i}\right\rangle, \tag{5}$$

where the matrix is the Wigner-3j symbol. Let us consider $B_{\ell_1\ell_2\ell_3}$ induced from $\Pi_{Bv}^{(\pm1)}$ where $a_{\ell m}$ is given by

$$a_{\ell m} = (-i)^\ell\int\frac{k^2dk}{2\pi^2}\mathcal{T}_\ell(k)\sum_{\lambda=\pm1}\lambda\Pi_{Bv,\ell m}^{(\lambda)}(k) \ , \quad \Pi_{Bv,\ell m}^{(\pm1)}(k) \equiv \int d^2\hat{\mathbf{k}}\Pi_{Bv}^{(\pm1)}(\mathbf{k})_{\mp1}Y_{\ell m}^*(\hat{\mathbf{k}}) \ . \tag{6}$$

Here $\mathcal{T}_\ell(k)$ denotes the transfer function and ${}_{\mp1}Y_{\ell m}(\hat{\mathbf{k}})$ is spin-1 spherical harmonic function. In Ref. [8], one can find a more general formulation of $a_{\ell m}$ generated from vector or tensor perturbations. By making use of these equations, we obtain the CMB bispectrum induced from the vector anisotropic stress $\Pi_{Bv}^{(\pm1)}$ which is given by

$$\begin{aligned}B_{\ell_1\ell_2\ell_3} &= \left[\prod_{j=1}^3(-i)^{\ell_j}\int\frac{k_j^2dk_j}{2\pi^2}\mathcal{T}_{\ell_j}(k_j)\int_0^{k_D}k_j'^2dk_j'P_B(k_j')\right]/(-4\pi\rho_{\gamma,0})^3 \\ &\times\sum_{LL'L''}\sum_{S,S',S''=\pm1}\sum_{\lambda_1,\lambda_2,\lambda_3=\pm1}\lambda_1\lambda_2\lambda_3\begin{Bmatrix}\ell_1 & \ell_2 & \ell_3\\ L' & L'' & L\end{Bmatrix} \\ &\times f_{L''L\ell_1}^{S''S\lambda_1}(k_3',k_1',k_1)f_{LL'\ell_2}^{SS'\lambda_2}(k_1',k_2',k_2)f_{L'L''\ell_3}^{S'S''\lambda_3}(k_2',k_3',k_3) \ ,\end{aligned} \tag{7}$$

$$\begin{aligned}f_{L''L\ell}^{S''S\lambda}(r_3,r_2,r_1) &\equiv \frac{2(8\pi)^{3/2}}{3}\sum_{L_1L_2L_3}\int_0^\infty y^2dy j_{L_3}(r_3y)j_{L_2}(r_2y)j_{L_1}(r_1y) \\ &\times\lambda(-1)^{\ell+L_2+L_3}(-1)^{\frac{L_1+L_2+L_3}{2}}I_{L_1L_2L_3}^{0\ 0\ 0}I_{L_31L''}^{0S''-S''}I_{L_21L}^{0S-S}I_{L_1\ell2}^{0\lambda-\lambda}\begin{Bmatrix}L'' & L & \ell\\ L_3 & L_2 & L_1\\ 1 & 1 & 2\end{Bmatrix}\end{aligned} \tag{8}$$

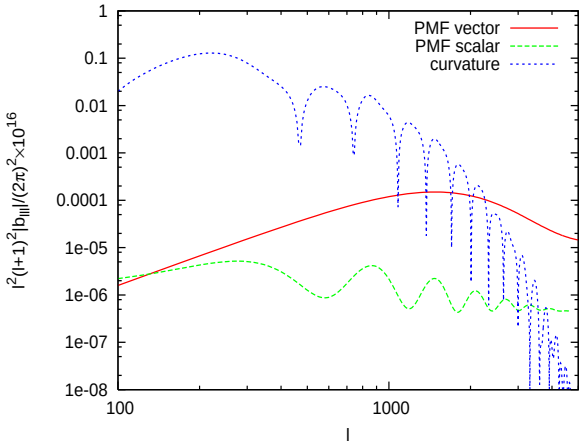

Figure 1: Absolute values of the normalized reduced bispectra of temperature fluctuation for a configuration $\ell_1 = \ell_2 = \ell_3$. The lines correspond to the spectra generated from vector anisotropic stress (red solid line), scalar isotropic stress (green dashed line) and primordial non-Gaussianity with $f_{\rm NL}^{\rm local} = 5$ (blue dotted line). The PMF parameters are fixed to ($n_B = -2.9$ and $B_{1\rm Mpc} = 4.7$nG) and the other cosmological parameters are fixed to the mean values limited from WMAP-7yr data reported in Ref. [2].

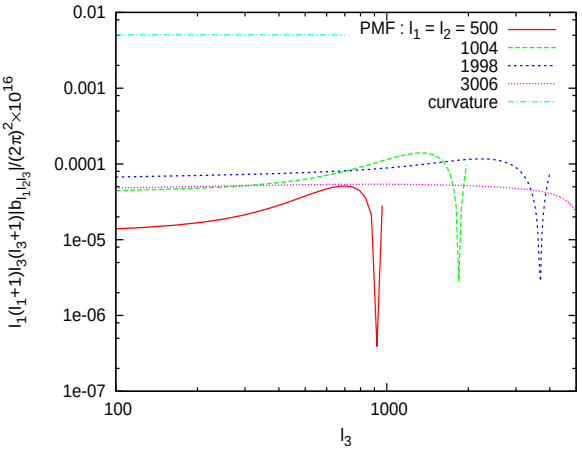

Figure 2: Absolute values of the normalized reduced bispectra of temperature fluctuation given by Eq. (7) and generated from primordial non-Gaussianity as a function of ℓ_3 with ℓ_1 and ℓ_2 fixed to some values as indicated. Each parameter is fixed to the same values defined in Fig. 1.

Here we have integrated complicated angular dependencies by expanding in terms of spin spherical harmonic functions and expressed them with the Wigner symbols. More details can be seen in Ref. [6].

3 Results

Here we show the result of the CMB temperature bispectrum induced from the vector anisotropic stress $\Pi_{Bv}^{(\lambda)}$.

In Fig. 1, we show the reduced bispectra of temperature fluctuation induced by the PMFs defined as [1] $b_{\ell_1\ell_2\ell_3} \equiv \sqrt{\frac{(4\pi)}{(2\ell_1+1)(2\ell_1+2)(2\ell_1+3)}} \begin{pmatrix} \ell_1 & \ell_2 & \ell_3 \\ 0 & 0 & 0 \end{pmatrix}^{-1} B_{\ell_1\ell_2\ell_3}$, for $\ell_1 = \ell_2 = \ell_3$. One can see that the overall behavior, such as the peak location at $\ell \sim 1500$, is very similar to that of the angular power spectrum C_ℓ from vector mode as calculated in Ref. [7]. On the other hand, the amplitude is smaller than to $C_\ell^{3/2}$, which is expected by a naive order of magnitude estimate. It is because the configuration of multipoles, corresponding to the angle of wave number vectors, is limited to the conditions placed by the Wigner symbols. By this effect, $b_{\ell\ell\ell}$ is suppressed by a factor ℓ^{-2} from $C_\ell^{3/2}$. This is the reason that our constraint from vector bispectrum on the PMF is not so much stronger than expected from the scalar counterpart.

For comparison, we also compute the CMB bispectrum sourced from scalar mode isotropic stress of the PMFs. The amplitude at large scale is consistent with the results of previous studies [3] although we newly consider the full angular dependence. From this figure, we can confirm that in the bispectrum, the vector mode dominates at small scales, specifically $\ell \sim 1500$, in the same manner as the angular power spectrum.

In Fig. 2, we also show the reduced bispectrum $b_{\ell_1\ell_2\ell_3}$ with respect to ℓ_3 with setting $\ell_1 = \ell_2$. From this figure, we can see that the normalized reduced bispectrum of the vector magnetic mode is nearly flat

as

$$\ell_1(\ell_1+1)\ell_3(\ell_3+1)|b_{\ell_1\ell_2\ell_3}| \sim 2\times 10^{-19}\left(\frac{B_{1\mathrm{Mpc}}}{4.7\mathrm{nG}}\right)^6, \tag{9}$$

and it is clear that $b_{\ell_1\ell_2\ell_3}$ for $n_B = -2.9$ dominates in $\ell_1 = \ell_2 \gg \ell_3$. This seems to mean the shape of CMB bispectrum generated from vector anisotropic stress of PMF is close to the local-type configuration if the power spectrum of PMF is nearly scale invariant. Therefore, in order to obtain a valid constraint on the magnitude of PMF, the bispectrum induced from PMF should be compared with that from the local-type primordial non-Gaussianity, which is estimated as $\ell_1(\ell_1+1)\ell_3(\ell_3+1)b_{\ell_1\ell_2\ell_3} \sim 4\times 10^{-18} f_{\mathrm{NL}}^{\mathrm{local}}$ [9]. From these equations, the relation between the magnitudes of the PMF and $f_{\mathrm{NL}}^{\mathrm{local}}$ is derived as

$$\left(\frac{B_{1\mathrm{Mpc}}}{1\mathrm{nG}}\right) \sim 7.74\ |f_{\mathrm{NL}}^{\mathrm{local}}|^{1/6} \quad (\text{for } \mathrm{n_B} = -2.9)\ . \tag{10}$$

By making use of the above relation, we can place the upper bound of strength of the PMF. If we assume $|f_{\mathrm{NL}}^{\mathrm{local}}| < 100$: as considered in Ref. [3], we obtain $B_{1\mathrm{Mpc}} < 17\mathrm{nG}$, which is stronger by a factor of two than estimated in Ref. [3]. On the other hand, from current observational lower bound from WMAP 7-yr data mentioned in Sec. 1, namely $f_{\mathrm{NL}}^{\mathrm{local}} > -10$, we derive $B_{1\mathrm{Mpc}} < 11\mathrm{nG}$. Furthermore, if we use the observational data of PLANCK experiment [5] which is expected to reach $|f_{\mathrm{NL}}^{\mathrm{local}}| < 5$, we will meet $B_{1\mathrm{Mpc}} < 10\mathrm{nG}$.

So far, constraints on the PMFs have been derived mainly from the power spectrum of CMB, dark matter clustering, and the structure formation. However, it has been reported that the PMF parameters have some degeneracy with the other cosmological parameters, such as neutrino masses. From this fact and the non-Gaussian nature of the magnetic field induced fluctuations, the CMB bispectrum will give us supplementary and complementary information about the PMF parameters. By translating the current bound on the local-type non-Gaussianity from the CMB bispectrum into the bound on the amplitude of the magnetic fields, we obtain a new limit. : $B_{1\mathrm{Mpc}} < 11\mathrm{nG}$. This is a rough estimate and a tighter constraint is expected if one considers the full ℓ contribution by using an appropriate estimator of the magnetic field bispectrum.

Due to the complicated discussions and mathematical manipulations, here we only show the temperature bispectrum from the vector mode of the PMFs. A full treatment of the bispectra of CMB temperature and polarization from the vector and scalar modes will be presented elsewhere.

4 References

References

[1] E. Komatsu and D. N. Spergel, Phys. Rev. **D63**, 063002 (2001), astro-ph/0005036.

[2] E. Komatsu et al. (2010), 1001.4538.

[3] T. R. Seshadri and K. Subramanian, Phys. Rev. Lett. **103**, 081303 (2009), 0902.4066.

[4] C. Caprini, F. Finelli, D. Paoletti, and A. Riotto, JCAP **0906**, 021 (2009), 0903.1420.

[5] [Planck Collaboration] (2006), astro-ph/0604069.

[6] M. Shiraishi, D. Nitta, S. Yokoyama, K. Ichiki and K. Takahashi, arXiv:1009.3632 [astro-ph.CO].

[7] J. R. Shaw and A. Lewis, Phys. Rev. **D81**, 043517 (2010), 0911.2714.

[8] M. Shiraishi, S. Yokoyama, D. Nitta, K. Ichiki, and K. Takahashi, Phys. Rev. **D82**, 103505 (2010), 1003.2096.

[9] A. Riotto, in *Inflationary Cosmology*, edited by M. Lemoine, J. Martin, & P. Peter (2008), vol. 738 of *Lecture Notes in Physics, Berlin Springer Verlag*, pp. 305–+.

The effect of multi-field interactions on false vacuum decay

Kazuyuki Sugimura[1(a)], Daisuke Yamauchi[2(a)] and Misao Sasaki[3(a)]

[(a)] *Yukawa Institute for Theoretical Phyics, Kyoto University, Kyoto 606-8502*

Abstract

Multi-field tunneling from false vacuum at the beginning of slow-roll inflation is favored in the picture of string-landscape. We investigate the multi-field tunneling using the method of instanton with gravity. We find multi-field instanton solutions in certain classes of potential numerically as well as perturbatively. Then we study the nature of the obtained instantons.

1 Introduction

Recently, many observations indicate that there was slow-roll inflation in the erarly universe. But the mechanism of how slow-roll inflation began is not known.

Recent advancements in string theory lead us to the picture of string landscape [4]. It predicts the exisitence of many scalar fields with many potential minima. Then, it is reasonable to expect that the universe experienced quantum tunneling that involved many scalar fields before the beginning of slow-roll inflation. Therefore we will consider a model in which multi-scalar fields tunnel from the false vacuum to the true vacuum. Slow-roll inflation is assumed to start after the tunneling. Such a model is called mutli-field open inflation because the metric for the true vacuum bubble which is created by quantum tunneling is that of open Friedman-Lemaitre-Robertson-Walker(FLRW) universe.

Open inflation was well studied in 1990's[3, 6], when observations indicated that universe was open. Of course, present observations indicate that the universe is almost flat, and there is no motivation for considering an inflation model with a negative spatial curvature. However, there is still a possibility that the universe is almost flat but not exactly flat; $1 - \Omega_{\rm total} \lesssim 0.01$. In fact this may be a consequence of string landscape [5].

Quantum tunneling of a scalar field with gravity is usually described with the method of instanton with gravity, which was proposed by S. Coleman and F. De Luccia[1, 2]. In this method, instanton, which is a solution of Euclidean Equation Of Motion (EOM), plays a major role in estimating the decay rate of false vacuum and in describing the time evolution of a nucleated bubble. Here we apply the method of instanton to multi-field quantum tunneling with gravity.

Multi-field open inflation was not studied seriously in the research of open inflation in 1990's, because string landscape was not known and considering multi-field tunneling seemed a little artificial. Thus not much has been known about multi-field instantons, not to mention the existence condition.

In order to establish the method of instanton in multi-field quantum tunneling with gravity, we first investigate the existance of instanton solutions numerically as well as perturbatively. We find multi-field instantons can be constructed in certain types of potential. Then we study the nature of the obtained instantons. In particular, we discuss the validity of the semiclassical approximation, on which the method of instanton is based, from various aspects.

2 Multi-field instanton

We investigate the application of the method of instanton to multi-field quantum tunneling with gravity. Single-field gravitational instanton method was proposed by S. Coleman and F. De Luccia[2], and there is natural extension to the multi-field case.

[1]Email address: sugimrua@yukawa.kyoto-u.ac.jp
[2]Email address: yamauchi@yukawa.kyoto-u.ac.jp
[3]Email address: misao@yukawa.kyoto-u.ac.jp

First, we write down the formulation for multi-field gravitaional instanton method, by extending the single-field gravitational instanton method. O(4)-symmetry of instanton is assumed as in the single-field case. Therefore, Euclidean metric is written as

$$ds^2 = dt^2 + a(t)^2 d\Omega^2. \tag{1}$$

Here, t is radial coordinate, and Ω is usual S_3 metric. $a(t)$ is like scale factor in FLRW universe. Euclidean action with scalar fields σ, ϕ is written as

$$S_E[\sigma,\phi,a] = 2\pi^2 \int dt a^3 \left(\left(\frac{1}{2}\dot{\sigma}^2 + \frac{1}{2}\dot{\phi}^2 + V(\sigma,\phi) \right) - \frac{3}{\kappa}\left(\frac{\dot{a}^2}{a^2} + \frac{1}{a^2} \right) \right) \tag{2}$$

Here, $\dot{}$ means derivative of t.

Instanton $\sigma(t), \phi(t), a(t)$ is the solution of classical Eucildean EOMs, which is obtained by varying Euclidean action(2).

$$\frac{\ddot{a}}{a} + \frac{\kappa}{3}\left(\dot{\sigma}^2 + \dot{\phi}^2 + V(\sigma,\phi) \right) = 0 \tag{3}$$

$$\ddot{\sigma} + 3\frac{\dot{a}}{a}\dot{\sigma} - \frac{\partial V(\sigma,\phi)}{\partial \sigma} = 0 \tag{4}$$

$$\ddot{\phi} + 3\frac{\dot{a}}{a}\dot{\phi} - \frac{\partial V(\sigma,\phi)}{\partial \phi} = 0. \tag{5}$$

When you solve the first equation, $a(t)$ takes zero at the two value of t, which we define $t = 0$ and $t = t_{end}$.

From the regularity at the center of spherical coordinate, boundary conditions for instanton is obtained.

$$\dot{a}(0) = \dot{a}(t_{end}) = 1 \tag{6}$$

$$\dot{\sigma}(0) = \dot{\sigma}(t_{end}) = 0 \tag{7}$$

$$\dot{\phi}(0) = \dot{\phi}(t_{end}) = 0. \tag{8}$$

Instanton is the solution satisfying these EOMs and boudary conditions.

Decay rate Γ can be estimated using instanton.

$$\Gamma \propto \exp\left[-S_E[\sigma,\phi,a] - S_E[\sigma_F,\phi_F,a_F] \right]. \tag{9}$$

Here, $S_E[\sigma_F,\phi_F,a_F]$ is the Euclidean action for the trivial solution when two scalar fields stay at the false vacuum.

This is a natural extension of single-field gravitational instanton method. Now, let's apply this method to multi-filed tunneling.

3 Existance of Instanton

We study the multi-field tunneling in the system where the potential for scalar fields σ and ϕ is Fig. 1. Linde and Mezulumian first proposed this type of potential for multi-field open inflation[3].

In order to investigate the tunneling, we assume the form of potential.

$$V(\sigma,\phi) = V_{tun}(\sigma) + V_{int}(\sigma,\phi) \tag{10}$$

$$V_{int}(\sigma,\phi) \sim \begin{cases} \frac{1}{2}m^2\phi^2 & \sigma \sim \sigma_F \\ \lambda m^3 \phi & \sigma \sim \sigma_T \end{cases}. \tag{11}$$

Here, σ_T is the value of σ outside the potential barrier, and σ_F is the value of σ at the false vacuum.

$V_{tun}(\sigma)$ is the dominant part for tunneling and we call σ tunneling field. If the effect of ϕ and V_{int} can be ignored, there is single-field type instanton for σ and $V_{tun}(\sigma)$.

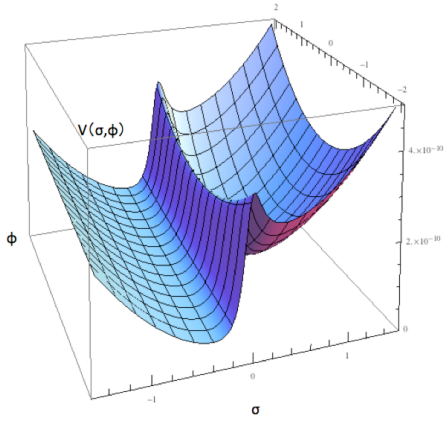

Figure 1: Potential $V(\sigma, \phi)$

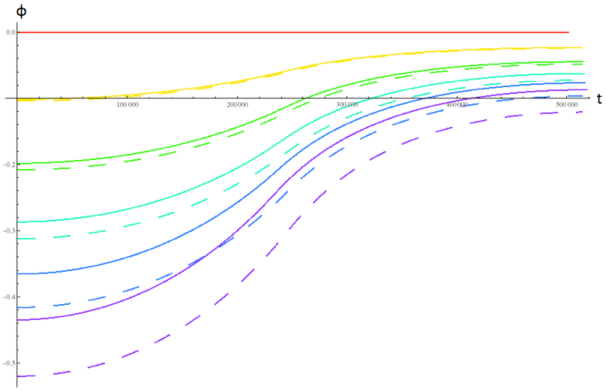

Figure 2: Instanton $\phi(t)$. Vertical axis is $\phi(t)$ and horizontal axis is t. The parameter is $V_{tun}(\sigma_F) = m^2 = 10^{-10}$, $\lambda m = 0$(red), $\lambda m = 0.05$(yellow), $\lambda m = 0.1$(green), $\lambda m = 0.15$(light blue), $\lambda m = 0.2$(blue), and $\lambda m = 0.25$(purpule). All dimensionful values are written in Planck unit. Solid line : numerical method. Dashed line : perturbative method.

$V_{int}(\sigma, \phi)$ is interaction term. This type of potential is obtained when we expand the potential $V(\sigma, \phi)$ around $\phi = 0$ which is the false vacuum value for ϕ. Before the tunneling slow-roll field ϕ is confined by the mass-type potential at false vacuum. Only after the tunneling ϕ can slow-roll on the potential. This is the mechanics that starts slow-roll inflation.

We now have EOMs, boundary conditions, and potential, which are needed to construct an instanton. Then, we will indicate that instanton does exist in multi-field system, by constructing a mutli-field instanton.

Firstly, we try to construct an instanton in numerical way using shooting method, which is useful to get a solution for the system with differential equations and boundary conditons. As a result, we construct an instanton(Fig.2).

Secondly, we try to construct an instanton in perturbative way. Exact instanton $\sigma(t)$ and $a(t)$ is approximated with the instanton obtained with ignoring the effect of V_{int}. When parmeter λ in (11) is eqaul to zero $\phi(t)$ stays at false vacuum. Hence, we adopt parmeter λ as a perturbation parameter. Further, we approximate $\sigma(t)$ as the thin-wall instanton for calculation convinience. Under these approximations, we analytically construct an instanton $\phi(t)$(Fig.2).

In Fig.2, you can see that the instanton obtained with numerical method and with perturbative method agrees well when the effect of V_{int} is small.

In summary, we find that multi-field gravitational instanton does exist in certain potential by constructing an instanton.

4 Effect of Interaction

Here, we study the nature of the instanton obtained in the last section. We focus on when the effect of interaction for instanton is significant. Method of instanton is derived with semi-classical approximation, therefore the physical meaning of instanton is restricted. It is important to investigate the instanton as the mathematical solution of EOMs and boundary conditions from physical viewpoint.

In order to get the condition when the effect of interaction for instanton is significant, we study the nature of instanton $\phi(t)$ because $\phi(t)$ has the information of the effect of interaction for instanton. If the effect of interaction is ignored, instanton $\phi(t)$ stays at the false vacuum. We find that by checking following two conditions we can decide whether the effect of interaction for instanton is significant.

Fist condition is whether the dispersion of instanton $\phi(t)$ is larger than the initial quantum fluctuation. When the typical quautum dispersion of ϕ, $\sqrt{\langle\phi^2\rangle}$, is much larger than that of instanton, the change of

ϕ in instanton cannot be seen in the broad quantum fluctuation, and the instanton $\phi(t)$ doesn't have physical meaning. We check whether following condition is satisfied.

$$|\phi(0)| \gg \sqrt{\langle\phi^2\rangle}. \tag{12}$$

Here, $\phi(0)$ is the value of instanton $\phi(t)$ at the center of bubble, and the value of ϕ at the false vacuum is zero.

Second condition is whether semi-classical approximation is appropriate. In the case the classical action for instanton ϕ is much smaller than the quantum fluctuation contribution, instanton ϕ has no physical meaning. We check whether following condition is satisfied.

$$S[\phi]/\hbar \gg 1 \tag{13}$$

Here, $S[\phi]$ is typical value for the part of classical action which instanton $\phi(t)$ contributes to. Typical contribution for the action from quantum fluctuation is $O(\hbar)$, because wave funciton typically spreads to the state whose action is different from the action of classical path by $O(\hbar)$.

We check these two conditions for the instanton obtained in perturbative way in the last section. As a result we find following condition for the potential in the last section that when the effect of interaction in instanton is significant.

Conditions are obtained in terms of λ, m, R_W, H. Here, R_W is a radius of thin-wall bubble and H is typical Hubble parameter for the instanton $a(t)$.

For the case $m^2 \gg H^2$, the typical dispersion of quantum fluctuation is supressed because of large mass, and (12) is always satisfied except when λ is strictly zero. Hence, the effect of interaction in instanton is significant when $m^2 \gg H^2$.

On the other hand, for the case $m^2 \ll H^2$, the condition is

$$\lambda \gg \max\left(\frac{1}{m^2 R_W^2}, \frac{1}{m^2 R_W^2}\frac{H^2}{m^2}\right). \tag{14}$$

Whether this condition is satisfied depends on the potential of the sysetem. Therefore, checking this condition is necessary in the annalysis of quantum tunneling when $m^2 \ll H^2$.

5 Conclusion

We found that multi-field instanton with gravity does exists in multi-field open inflation. After that, using the obtained instanton, we studied when the effect of interaction for instanton is significant. As a result we got a condition for that.

Acknowledgments

This work is supported in part by Monbukagaku-sho Grant-in-Aid for the Global COE programs, The Next Generation of Physics, Spun from Universality and Emergence at Kyoto University, by JSPS Grant-in-Aid for Scientific Research (A) No. 21244033, and by Grant-in-Aid for Creative Scientific Research No. 19GS0219.

References

[1] S. Coleman, Phys. Rev. D **15**, 2929 (1977).

[2] S. Coleman and F. De Luccia, Phys. Rev. D **21**, 3305 (1980).

[3] A. Linde and A. Mezhlumian, Phys. Rev. D **52**, 6789 (1995).

[4] L. Susskind, arXiv:hep-th/0302219 (2003).

[5] B. Freivogel, M. Kleban, M. Rodriguez Martinez and L. Susskind, JHEP **0603**, 039 (2006).

[6] J. Garriga, X. Montes, M. Sasaki, T. Tanaka, Nucl. Phys. B **551**, 317 (1999).

Gamma-ray bursts of the first generation of stars

Yudai Suwa[1(a)], and Kunihito Ioka[(b)]

[(a)] *Yukawa Institute for Theoretical Physics, Kyoto University, Kyoto 606-8502*
[(b)] *KEK Theory Center and the Graduate University for Advanced Studies (Sokendai), Tsukuba 305-0801*

Abstract

We show that a relativistic gamma-ray burst (GRB) jet can potentially pierce the envelope of very massive first generation star (Population III; Pop III) by using the stellar density profile to estimate both the jet luminosity (via accretion) and its penetrability. The jet breakout is possible even if the Pop III star has a supergiant hydrogen envelope without mass loss, thanks to the long-lived powerful accretion of the envelope itself. While the Pop III GRB is estimated to be energetic $E_{\gamma,\rm iso} \sim 10^{55}$ erg, the supergiant envelope hides the initial bright phase into the cocoon component, leading to a GRB with a long duration $\sim 1000(1+z)$ sec and an ordinary isotropic luminosity $\sim 10^{52}$ erg s^{-1} ($\sim 10^{-9}$ erg cm^{-2} s^{-1} at redshift $z \sim 20$). The neutrino-annihilation is not effective for Pop III GRBs because of a low central temperature, while the magnetic mechanism is viable. We also derive analytic estimates of the breakout conditions, which are applicable to various progenitor models. The GRB luminosity and duration are found to be very sensitive to the core and envelope mass, providing possible probes of the first luminous objects at the end of the high redshift dark ages.

1 Introduction

One of the most important goals in modern cosmology is to understand how the first stars, so-called Population III (PopIII) stars, formed at the end of the dark ages, and how they transformed the initially simple, homogeneous universe into a state of ever increasing complexity. The first stars are predicted to have been predominantly very massive with $\gtrsim 100 M_\odot$.

GRBs are very luminous and able to be seen from very early epoch of the universe. In fact, the most distant observed object in the universe is GRB 090423, which was discovered by *Swift* at a redshift of z=8.26. GRBs produced at $z \gtrsim 10$ are also detectable so that even the first stars, which is thought to be generated $z \sim 20$, could be observed using GRBs if the first stars produce GRBs.

2 Progenitor structure

In this study, we investigate the activity of GRB central engine using the structure of progenitors. First, we explain the progenitor density profiles used in this study. We employ two progenitors; Pop III star and Walf-Rayet star. These stars correspond to progenitors of First GRBs and ordinary GRBs, respectively.

The density profiles of investigated models are shown in the left panel of Fig. 1. Red line shows the density profile of Pop III star with 915 $M_\odot$, model Y-1 of [1]. Blue indicates the GRB progenitor with 16 $M_\odot$, model 16TI of [2].

We can calculate the accretion rate, $\dot{M}$, using these density profiles. The accretion timescale of matter at radius r falling to the center of the star is roughly equal to the free-fall timescale, $t_{\rm ff} \approx \sqrt{2r^3/GM_r}$, where r is the radius from the center of the star, G is the gravitational constant, and M_r is the mass inside r, respectively. We then can evaluate the accretion rate at the center using $t_{\rm ff}$ as $\dot{M} = dM_r/dt_{\rm ff}$. In the right panel of Fig. 1, mass accretion rates of investigated models are shown. The origin of time in this figure is set at the time of the black hole (BH) mass (central mass) being $3M_\odot$. The accretion rate should be related to the activity of the central engine, and that of Pop III star is much larger than the other progenitors. Therefore, the GRBs of Pop III stars are expected to be more energetic than ordinary GRBs.

[1]Email address: suwa@yukawa.kyoto-u.ac.jp

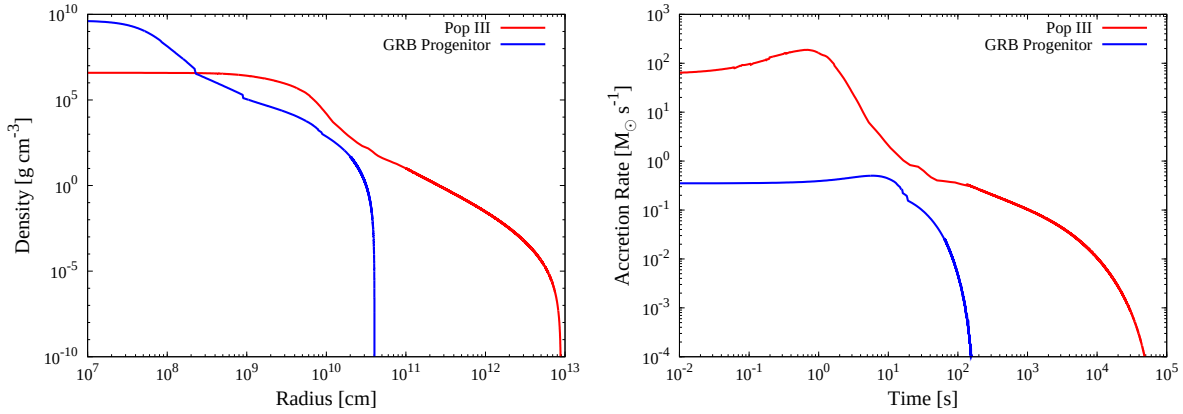

Figure 1: (*Left*): The density profiles of Pop III (red) and ordinary GRB progenitor (blue). (*Right*): The accretion rate of investigated progenitors calculated using density profiles.

3 Jet Models and penetration of stellar envelope

In this study we employ the *collapsar* model, which is a widely accepted scenario for the central engine of longer-lasting GRBs. In this scenario a BH accompanied by the stellar collapse produces a relativistic jet, which is strongly suggested by observations. The greatest uncertainty in this scenario is the mechanism for converting the disk binding energy or BH rotation energy into directed relativistic outflows. There are two proposed candidates of jet production in vicinity of the central engine: neutrino annihilation and magnetohydrodynamical (MHD) mechanisms. Although there are plentiful studies about these mechanisms, we have no concrete consensus for the available energy injection rate from central engine into the jet. Therefore, we employ following two simple models mimicking the jet producing mechanisms.

(A) MHD process: A jet is driven by magnetic fields that are generated by accreting matter. In this case the jet injection luminosity is given by $L_j \propto \dot{M}$, where $\dot{M}$ is the accretion rate.

(B) Neutrino-annihilation process: A jet is driven by annihilation of neutrinos ($\nu\bar{\nu} \rightarrow e^- e^+$), which are copiously radiated by "hyperaccretion flow" [3]. As for neutrino-annihilation process, jet injection luminosity can be written in $L_j \propto \dot{M}^{9/4} M_{\rm BH}^{-3/2}$, where $M_{\rm BH}$ is the mass of BH [4].

Next, we consider the propagation of shock, which is driven by the jet emitted by the central engine. We assume a relativistic jet ($\Gamma_j \gg 1$) as it strikes the stellar matter to obtain the evolution of the jet head. There are two shocks in this situation: a forward shock (FS) that accelerates the external material to a Lorentz factor Γ_h, and a reverse shock (RS) that decelerates the head of the jet to Γ_h. Balancing the energy density behind the FS with that above the RS, one can obtain the Lorentz factor of shock wave. There are two limits for this equation: ultra-relativistic one, $\Gamma_h \sim L_{\rm iso}^{1/4} r^{-1/2} \rho^{-1/4}$, where $L_{\rm iso}$ is isotropic luminosity of a jet [5], and non-relativistic one, $\beta_h \sim L_{\rm iso}^{1/2} r^{-1} \rho^{-1/2}$, where β_h is the velocity of FS in unit of the speed of light, c [6]. Here we combine these equations empirically as following:

$$\beta_h \Gamma_h^2 \approx 18 \left(\frac{L_{\rm iso}}{10^{52}\ {\rm erg\ s^{-1}}} \right)^{1/2} \left(\frac{r}{10^{12}\ {\rm cm}} \right)^{-1} \left(\frac{\rho}{10^{-7}\ {\rm g\ cm^{-3}}} \right)^{-1/2}. \quad (1)$$

This approximation leads the same relation with [6] for non-relativistic case ($\Gamma_h \approx 1$) and agree with [5] to within 40% for ultra-relativistic case ($\beta_h \approx 1$). The crossing time of the FS is also given by

$$t_h \approx \frac{r}{\Gamma_h^2 \beta_h c}. \quad (2)$$

As for the relativistic FS, the crossing time is much shorter than the light crossing time due to its large Lorentz factor.

Combining Eqs. (1) and (2), we obtain the necessary isotropic jet luminosity for the FS to reach the

Table 1: Model Summary

Model	Mass $[M_\odot]$	Mechanism	$t_{\rm b}$ [s]	Energy of GRB $[10^{52}$ erg]	Energy of Cocoon $[10^{52}$ erg]	T_{90} [s]	$E_{\rm iso}$ $[10^{54}$ erg]
GRB	16	MHD	4.7	1.0	0.23	49	2.6
		Neutrino	2.8	1.0	0.42	10	2.6
Pop III	915	MHD	690	45	57	1500	120
		Neutrino	—	—	—	—	—

radius r as

$$L_{\rm iso} \approx 3\times10^{52}\ {\rm erg\ s^{-1}} \left(\frac{r}{10^{12}\ {\rm cm}}\right)^4 \left(\frac{\rho}{10^{-7}\ {\rm g\ cm^{-3}}}\right) \left(\frac{t}{1\ {\rm sec}}\right)^{-2}. \tag{3}$$

If the jet luminosity decrease slower than t^{-2}, the jet luminosity can achieve this value at the late phase. We can follow the evolution of the FS by equating L_j and Eq. (3) for each point.

Here, we divide the energetics of the jet into two component: GRB emitter (relativistic component) and cocoon (non-relativistic component). When the Lorentz factor of the FS, Γ_h, is smaller than the inverse of the opening angle of the jet, θ_j, the shocked material may escape sideways and form the cocoon [7], which leads avoidance of baryon loading problem. With this scenario, injected energy before the shock breakout through the stellar surface goes to the energy of cocoon and that after breakout goes to GRB emitter. Therefore, we can calculate the energy budget of GRB emitter and cocoon after the determination of the jet breakout time, t_b. We define t_b as the maximum time obtained by Eq. (3).

Our calculation procedure for GRB of Pop III is following: First, we determine the overall factor of jet luminosity (depending on mechanism) using GRB progenitor to make the total energy of GRB emitter $E_{\rm tot} = 10^{52}$ erg[2]. In this estimation we assume that the half opening angle of jet $\theta_j = 5^\circ$, which is necessary for connection between $L_{\rm iso}$ and $L_j (= L_{\rm iso}\theta_j^2)$. As for the MHD process, $L_{j,51} = 1.1\dot{M}_0$ and $t_{\rm b} = 4.7$ s, where $L_{j,51} = L_j/10^{51}$ erg s^{-1} and $\dot{M}_0 = \dot{M}/M_\odot$ s^{-1}. On the other hand, for neutrino-annihilation process $L_{j,51} = 76\dot{M}_0^{9/4} M_{\rm BH}^{-3/2}$ and $t_{\rm b} = 2.8$ s, where $M_{\rm BH}$ is in the unit of $M_\odot$. We estimate the expected duration of the burst with the period which 90 percent of the burst's energy is emitted, T_{90}. Both models reproduce the typical duration of burst of ~ 10 s (see Table 1). The energy of cocoon (injected energy before shock breakout) is smaller than that of GRB emitter. The isotropic *kinetic* energy of GRB emitter is $\sim 10^{54}$ erg, corrected by the jet opening angle, $\theta_j = 5^\circ$.

Now we can calculate the evolution of the FS for the case of Pop III star using above luminosities. We find that neutrino-annihilation process does *not* produce GRB because the FS stalls inside the envelope due to rapidly decreasing jet luminosity (so-called "failed GRB"). On the other hand, MHD process can supply enough energy for jet to penetrate the envelope and produce GRB. The total energy of GRB jet (injected energy after breakout) is ~ 45 times larger than ordinary GRB and the duration is much longer ($T_{90} \sim 1000$ s). It should be noted that the energy contained in cocoon component is larger than GRB emitter so that the afterglow could be brighter than typical GRBs occurring at the local universe.

Considering the Pop III GRB at redshift z, the duration is

$$T_{\rm GRB} = T_{90}(1+z) \approx 30000\ {\rm s} \left(\frac{1+z}{20}\right), \tag{4}$$

which is much longer than the canonical duration of GRBs, ~ 20 s. The total isotropic-equivalent energy of Pop III GRB is

$$E_{\gamma,{\rm iso}} = \varepsilon_\gamma E_{\rm iso} \approx 1.2\times10^{55} \left(\frac{\varepsilon_\gamma}{0.1}\right)\ {\rm erg}, \tag{5}$$

where ε_γ is the conversion efficiency from the jet kinetic energy to gamma rays (see Table 1). It should be noted that this value is comparable to the largest $E_{\gamma,{\rm iso}}$ ever observed, $\approx 9\times10^{54}$ erg for GRB

[2]Note that $E_{\rm tot}$ is not total energy of gamma rays because there must be conversion from jet kinetic energy to gamma rays. Though the efficiency of conversion is unclear, it is typically the order of 0.1. Therefore, we employ $E_{\rm tot} = 10^{52}$ erg that could lead total *physical* energy of GRB $\sim 10^{51}$ erg.

080916C [8]. This value is smaller than the estimation of [9, 10] because we consider the hidden (cocoon) component. Since the large isotropic energy is stretched over the long duration, the expected flux just after the breakout is not so bright,

$$F = \frac{\varepsilon_\gamma L_{\rm iso}}{4\pi r_L^2} \sim 10^{-9} \text{ erg cm}^{-2} \text{ s}^{-1}, \tag{6}$$

where r_L is the luminosity distance, which is smaller than the *Swift* Burst Array Telescope (BAT) sensitivity, $\sim 10^{-8}$ erg cm^{-2} s^{-1}. However, there must be a large variety of the luminosity as ordinary GRBs so that more luminous but rare events might be observable by BAT. Although the cocoon component has a large energy, the velocity is so low that it is also difficult to observe. If the cocoon component interacts with the dense wind or ambient medium, it might be observable. This is an interesting future work.

4 Summary

We have investigated the jet propagation in the very massive Population III stars assuming the accretion-to-jet conversion efficiency of the observed normal GRBs. We find that the jet can potentially break out the stellar surface even if the Pop III star has a massive hydrogen envelope thanks to the long-lasting accretion of the envelope itself. Although the total energy injected by the jet is as large as $\sim 10^{54}$ erg, more than half is hidden in the stellar interior and the energy injected before the breakout goes into the cocoon component. The large envelope accretion can activate the central engine so that the duration of Pop III GRB is very long if the hydrogen envelope exists. As a result, the luminosity of Pop III GRB is modest, being comparable to that of ordinary GRBs. More detailed discussions can be found in [11].

References

[1] T. Ohkubo, K. Nomoto, H. Umeda, N. Yoshida, and S. Tsuruta, Astrophys. J. **706**, 1184 (2009).

[2] S. E. Woosley, and A. Heger, Astrophys. J. **637**, 914 (2006).

[3] A. I. MacFadyen, and S. E. Woosley, Astrophys. J. **524**, 262 (1999).

[4] I. Zalamea, and A. M. Beloborodov, arXiv:1003.0710 (2010).

[5] P. Mészáros, and E. Waxman, Phys. Rev. Lett. **87**, 171102 (2001).

[6] E. Waxman, and P. Mészáros, Astrophys. J. **584**, 390 (2003).

[7] C. D. Matzner, Mon. Not. R. Astron. Soc. **345**, 575 (2003).

[8] A. A. Abdo et al., Science, **323**, 1688 (2009).

[9] S. S. Komissarov, and M. V. Barkov, Mon. Not. R. Astron. Soc. **402**, L25 (2010)

[10] P. Mészáros, and M. J. Rees, Astrophys. J. **715**, 967 (2010)

[11] Y. Suwa, and K. Ioka, Astrophys. J. **726**, 107 (2011).

Temporal enhancement of large scale curvature perturbation in multiple curvaton decays

Teruaki Suyama[1(a)], and Jun'ichi Yokoyama[2(a)]

[(a)] *Research Center for the Early Universe, The University of Tokyo, 4-3-1, Hongo, Bunkyo-ku, Tokyo 113-0033, Japan*

Abstract

If more than one curvaton dominate the Universe at different epochs from each other, the curvature perturbation can be temporarily enhanced. The trace of the enhancement is left in higher order correlation functions, that is, as non-Gaussianity. We first confirm the enhancement by the numerical calculation. We then derive analytic expression of the full order curvature perturbation and provide the non-linearity parameters $f_{\rm NL}$, $\tau_{\rm NL}$ and $g_{\rm NL}$, with a consistency relation among them.

1 Introduction

In [1], a scenario where multiple curvatons dominate at different epochs was studied. There, although not emphasized, it was implicitly shown that if the two curvatons dominate the Universe at different epochs from each other, the curvature fluctuations may evolve dramatically different way than the standard case. That is they can grow to an amplitude much larger than the observed value, 10^{-5}, when the first curvaton dominates and decays, and then they are moderated to the observed amplitude when the second curvaton dominates and decays. Thus in this scenario the curvature perturbation can be temporarily enhanced.

At first glance, this temporal enhancement seems to have little effect on observables since it occurs much before the big-bang nucleosynthesis, not to mention the observation time. But, this is not the case. As pointed out in [1], large possibly detectable non-Gaussian perturbations can be generated. If we denote by $\zeta_{\rm max}$ the maximum amplitude of the curvature perturbation when it is enhanced, the so-called $f_{\rm NL}$ parameter is given by $f_{\rm NL} \simeq \zeta_{\rm max}/10^{-5} \gg 1$, under the assumption that the curvature perturbation is sourced only by the first decaying curvaton fluctuations. For example, if $\zeta_{\rm max} = 10^{-3}$, then we get $f_{\rm NL} \simeq 100$.

The present paper aims to take up this temporal enhancement of the curvature perturbation in two curvaton model, to provide a detailed analysis of the generation and evolution of fluctuations and the non-linearity parameters of the bi- and tri-spectrum.

2 Decays of two curvatons and generation of perturbations

2.1 Evolution of the background quantities

In this subsection, we see how the background quantities evolve in time. The evolution equations for the background quantities are given by

$$\dot{\rho}_1 + 3\mathcal{H}\rho_1 = -a\Gamma_1\rho_a, \tag{1}$$

$$\dot{\rho}_2 + 3\mathcal{H}\rho_2 = -a\Gamma_2\rho_2, \tag{2}$$

$$\dot{\rho}_r + 4\mathcal{H}\rho_r = a\Gamma_1\rho_a + a\Gamma_2\rho_2, \tag{3}$$

$$\mathcal{H}^2 = \frac{8\pi G}{3}(\rho_a + \rho_2 + \rho_r)a^2, \tag{4}$$

Where ρ_1, ρ_2 are the energy density of the first and secondly decaying curvaton, respectively, and ρ_r is the radiation energy density. Γ_1 and Γ_2 are the decay rate of the first and secondly decaying curvaton, respectively. We also define $\dot{} \equiv d/d\eta$, $\mathcal{H} \equiv \dot{a}/a$ and η is the conformal time.

[1]Email address: suyama@resceu.s.u-tokyo.ac.jp
[2]Email address: yokoyama@resceu.s.u-tokyo.ac.jp

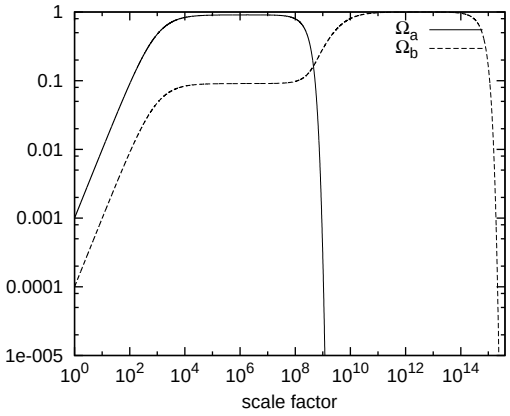

Figure 1: The evolution of Ω_1 and Ω_2. We chose $\Omega_{1,\mathrm{ini}}/\Omega_{2,\mathrm{ini}} = 10$ and $\Gamma_2/\Gamma_1 = 10^{-10}$.

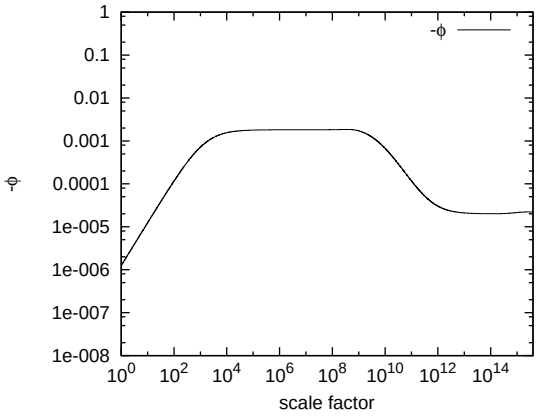

Figure 2: The evolution of ϕ. Since ϕ is negative, we plot $-\phi$. We chose $\Omega_{1,\mathrm{ini}}/\Omega_{2,\mathrm{ini}} = 10, \delta_{1,\mathrm{ini}} = 10^{-2}, \delta_{2,\mathrm{ini}} = 10^{-4}, \Gamma_2/\Gamma_1 = 10^{-10}$.

The designing situation in this paper is that both two curvatons dominate the universe at different epochs. We give in Fig.1 a typical evolution of Ω_1 and Ω_2.

2.2 Evolution of the linear curvature perturbation

In Fig.2, we show a typical evolution of ϕ, the curvature perturbation in the Newtonian gauge, which is obtained by solving numerically the perturbation equations. Since we assume that inflaton fluctuation contributes little to the curvature perturbation, we have imposed the condition that both δ_r and ϕ vanish at the outset. The parameters used in Fig.2 are such that $\delta_{1,\mathrm{ini}} = 10^{-2}$ and $\delta_{2,\mathrm{ini}} = 10^{-4}$. The parameters for the background are the same as the ones used in Fig.1.

From Fig.2, we can clearly see that ϕ is being enhanced until the secondly decaying curvaton dominates. The order of ϕ at this time is roughly $\delta_{1,\mathrm{ini}}$ (we will provide exact analytic expression later.). As the σ_2-field dominates, ϕ decays to $\Omega_{r,2}\delta_{1,\mathrm{ini}} + \delta_{2,\mathrm{ini}}$, where $\Omega_{r,2} \ll 1$ is Ω_r evaluated at the time when the σ_2-field decays. Therefore, the enhanced value of the curvature perturbation is determined by $\delta_{1,\mathrm{ini}}$ and the final value is determined by either $\Omega_{r,2}\delta_{1,\mathrm{ini}}$ or $\delta_{2,\mathrm{ini}}$, whichever is greater.

2.3 Full order curvature perturbation

We can derive analytic expressions for the enhanced value and the final value of the curvature perturbation up to any order in perturbation. To this end, we adopt δN formalism which is a powerful method to

evaluate the curvature perturbation on super-horizon scales.

Using this formalism, we find that the full non-linear expression of ζ at the final time η_f is given by

$$\zeta(\eta_f,\vec{x}) = \frac{1}{4}\log\left\{(1+\epsilon_\Gamma)\Omega_1^{4/3}(\eta_*)(1+\delta_{1,\mathrm{ini}}(\vec{x}))^{4/3} + \left(\frac{\Gamma_1}{\Gamma_2}\right)^{2/3}\Omega_2^{4/3}(\eta_*)(1+\delta_{2,\mathrm{ini}}(\vec{x}))^{4/3}\right\} - \frac{1}{4}\log\left\{(1+\epsilon_\Gamma)\Omega_1^{4/3}(\eta_*) + \left(\frac{\Gamma_1}{\Gamma_2}\right)^{2/3}\Omega_2^{4/3}(\eta_*)\right\}, \tag{5}$$

where $\epsilon_\Gamma \simeq 1.183$ is a numerical value and η_* is a time much before the first decaying curvaton dominates the universe. At linear order in the density contrasts, this equation reduces to

$$\zeta(\eta_f,\vec{x}) \approx \frac{1}{3}s\delta_{1,\mathrm{ini}}(\vec{x}) + \frac{1}{3}\delta_{2,\mathrm{ini}}(\vec{x}). \tag{6}$$

where a parameter s is defined by

$$s \equiv (1+\epsilon_\Gamma)\left(\frac{\Gamma_2}{\Gamma_1}\right)^{2/3}\left(\frac{\Omega_{1,*}}{\Omega_{2,*}}\right)^{4/3}, \tag{7}$$

which roughly represents the fraction of the radiation from σ_1-field decay at the time of σ_2-field decay.

We can also derive the maximum magnitude of the enhanced ζ. Since the σ_2-field is subdominant when ζ is enhanced, $\zeta_{\max}$ is completely sourced by the σ_1-field perturbation. This means that $\zeta_{\max}$ is equal to the final curvature perturbation in the single curvaton model in which the curvaton dominates the universe before its decay. Therefore, $\zeta_{\max}$ can be obtained by the second term in (6) with δ_2 replaced by δ_1:

$$\zeta_{\max}(\vec{x}) = \frac{1}{3}\delta_{1,\mathrm{ini}}(\vec{x}). \tag{8}$$

2.4 Non-Gaussianity

Eq. (5) is the fully non-linear expression of the curvature perturbation. By using this equation, we can calculate any order correlation functions. Here, we calculate the three and four-point functions (bi- and tri-spectra) which are now becoming important observables to extract information of the early universe.

The curvature perturbation given by Eq. (5) is the so-called local type for which the curvature perturbation depends on the source fields at the same point. In such a case, it is known that the bispectrum and trispectrum are parametrized by a single constant f_{NL} and two constants τ_{NL} and g_{NL}, respectively (for the definition of these parameters, see e. g. [2]).

Let us define a new parameter $r \equiv \delta_{2,\mathrm{ini}}/(s\delta_{1,\mathrm{ini}})$ which represents the contribution of $\delta_{2,\mathrm{ini}}$ to ζ compared to that of $\delta_{1,\mathrm{ini}}$. If $r = 0$, then ζ is solely sourced by the a-field fluctuations. If $r \gg 1$, then ζ is mostly sourced by the b-field fluctuations. With this parameter, the non-linearity parameters for two curvaton case are given by

$$f_{\mathrm{NL}} = -\frac{(15r^2+80)r^2s-25}{12(r^2+1)^2s} = \frac{25}{12(r^2+1)^2s} + \mathcal{O}(1), \tag{9}$$

$$\tau_{\mathrm{NL}} = \frac{(9r^4+112r^2+64)r^2s^2-80r^2s+25}{4(r^2+1)^3s^2} = \frac{25}{4(r^2+1)^3s^2} + \mathcal{O}\left(\frac{1}{s}\right), \tag{10}$$

$$g_{\mathrm{NL}} = \frac{(225r^4+3300r^2)r^2s^2-1500r^2s+125}{108(r^2+1)^3s^2} = \frac{125}{108(r^2+1)^3s^2} + \mathcal{O}\left(\frac{1}{s}\right). \tag{11}$$

Since s enters f_{NL} in the denominator, $s \ll 1$, which is satisfied in the situation we are interested in, is a necessary condition to have large f_{NL}. This condition can be qualitatively understood by expanding (6) to second order in $\delta\sigma_1$:

$$\zeta = \frac{1}{3}s\left(2\frac{\delta\sigma_1}{\sigma_1} + \left(\frac{\delta\sigma_1}{\sigma_1}\right)^2\right) = \zeta_g + \frac{3}{4s}\zeta_g^2, \tag{12}$$

where we have set $\delta_2 = 0$ and $\zeta_g \equiv \frac{2}{3}s\frac{\delta\sigma_1}{\sigma_1}$ is the Gaussian part of ζ. We see that the second order coefficient which is, apart from the numerical factor, nothing more than $f_{\rm NL}$ contains an enhancement factor $1/s$. This mechanism to get large $f_{\rm NL}$ is exactly the same as the single curvaton case in which $f_{\rm NL}$ is inversely proportional to a fraction of the curvaton energy density at the time when it decays into the radiation.

Since $f_{\rm NL}$ is bounded to be $|f_{\rm NL}| \lesssim 100$ from the observations, s can not be smaller than 10^{-2} if $\delta_2 = 0$. Correspondingly, the observationally allowed maximum curvature perturbation when it is enhanced is at most $10^{-5}/s \simeq 10^{-3}$. However, things change when δ_2 is also allowed to take non-zero amplitude. From (9), we find that if the b-field fluctuations contribute more to the curvature perturbation than the a-field fluctuations, i.e. $r \gtrsim 1$, then $f_{\rm NL}$ is suppressed by a factor r^{-4} compared to a case with $r = 0$. Therefore, s smaller than 10^{-2} can satisfy the bound $|f_{\rm NL}| \lesssim 100$ if r is suitably chosen. In particular, if $r \gtrsim s^{-1/4} \gg 1$, then $f_{\rm NL}$ becomes as small as $\mathcal{O}(1)$. At this level of $f_{\rm NL}$, non-primordial non-linear effects become important and it will not be easy to extract primordial $f_{\rm NL}$ from observations. Interestingly, in this case, we find from (10) and (11) that $\tau_{\rm NL},\ g_{\rm NL} \gtrsim \mathcal{O}(s^{-1/2}) \gg 1$. Therefore, strong non-Gaussianity appears in the trispectrum but not in the bispectrum. In such a case, the trispectrum would be useful to search for non-Gaussianity.

From (10) and (11), we can also derive a unique relation between $\tau_{\rm NL}$ and $g_{\rm NL}$ as

$$\frac{\tau_{\rm NL}}{g_{\rm NL}} = \frac{27}{5} + \mathcal{O}\left(\frac{1}{f_{\rm NL}}\right), \tag{13}$$

which will be useful to observationally discriminate two curvaton model from the other models that generate large non-Gaussianity.

3 Conclusion

If more than one curvaton dominate the Universe at different epochs from each other, the curvature perturbation can be temporarily enhanced. The trace of the enhancement is left in higher order correlation functions, that is, as non-Gaussianity. In this paper, sticking ourselves to the case of two curvatons, we confirmed that such enhancement actually occurs by numerically solving the linearized perturbation equations. We then derived the analytic expression of the full order curvature perturbation by using the δN formalism, which enables us to evaluate any higher order correlation functions. We also provided the expressions of the non-linearity parameters $f_{\rm NL},\ \tau_{\rm NL}$ and $g_{\rm NL}$, with a unique consistency relation between $\tau_{\rm NL}$ and $g_{\rm NL}$. If the final curvature perturbation is dominated by the secondly decaying curvaton fluctuations, then we have $f_{\rm NL} = \mathcal{O}(1)$ and $\tau_{\rm NL},\ g_{\rm NL} \gg 1$. Hence in such a case, the strong signal of non-Gaussianity comes from the trispectrum.

References

[1] H. Assadullahi, J. Valiviita and D. Wands, Phys. Rev. D **76**, 103003 (2007) [arXiv:0708.0223 [hep-ph]].

[2] T. Suyama, T. Takahashi, M. Yamaguchi and S. Yokoyama, arXiv:1009.1979 [astro-ph.CO].

Extreme charged black hole in braneworld with cosmological constant

Ryotaku Suzuki[1(a)], Tetsuya Shiromizu[2(a)] and Norihiro Tanahashi[3(b)]

[(a)] *Department of Physics, Kyoto University, Kyoto 606-8502*
[(b)] *Department of Physics, UC Davis*

Abstract

Application of the AdS/CFT correspondence to the Randall-Sundrum models may predict that there is no static solution for black holes with a radius larger than the bulk curvature scale. When the black hole has an extremal horizon, however, the correspondence suggests that the black hole can stay static. We focus on the effects of cosmological constant on the brane on such extremal brane-localized black holes. We observe that the positive cosmological constant restricts the black hole size on the brane as in ordinary four-dimensional general relativity. The maximum black hole size differs from that in four-dimensional general relativity case due to the nonlinear term in the effective Einstein equation. In the negative cosmological constant case, we obtain an implication on the Newton constant in the Karch-Randall model.

1 Randall-Sundrum model and black hole

In the Randall-Sundrum (RS) braneworld models [1–3], static solutions of black holes localized on the brane have not found yet. For this issue, the following conjecture has been proposed based on the adS/CFT correspondence [4–6]. According to the correspondence, a five-dimensional classical brane-localized black hole is dual to a four-dimensional black hole that emits the Hawking radiation. Since the latter one cannot be static due to the Hawking radiation emission, it is suggested by the duality that there is no static brane-localized black hole which is larger than the bulk curvature radius.

Here, one might realize that the adS/CFT correspondence also tells that static solutions may present when the black hole horizon is extreme [7] since the horizon temperature is zero and the Hawking radiation will not be emitted. Indeed, the authors of Ref. [7] constructed the near-horizon geometry of such extreme charged static black hole localized on the asymptotically flat brane and studied its properties.

In our study, we shall consider the near-horizon geometry of extreme charged black hole localized on the brane with non-vanishing cosmological constant to study the properties of the brane-localized black holes in more generalized settings. We also intend to reveal the non-trivial property of the gravity in the braneworld model with negative cosmological constant, the Karch-Randall model. For detailed analysis, see our paper [8].

2 Models

The model we consider in this paper is the RS braneworld model, which consists of five-dimensional asymptotically anti-de Sitter (adS) bulk spacetime and a four-dimensional brane with positive tension in it. The action of this model is given by

$$S = \frac{1}{2\kappa_5^2}\int_M d^5x\sqrt{-g}\left({}^{(5)}R + \frac{12}{l^2}\right) + \frac{1}{\kappa_5^2}\int_{\partial M} d^4x\sqrt{-h}K + \int_{\text{brane}} d^4x\sqrt{-h}\left(-\sigma - \frac{1}{2\kappa_4^2}F_{\mu\nu}F^{\mu\nu}\right), \quad (1)$$

where M is the bulk spacetime and ∂M is its outer boundary. $h_{\mu\nu}$ is the induced metric on the brane. $\kappa_5^2 = 8\pi G_5$ and $\kappa_4^2 = 8\pi G_4$ are the five and four-dimensional gravitational coupling, respectively. l is the bulk curvature radius. σ and $F_{\mu\nu}$ are the brane tension and the field strength of the Maxwell field living on the brane. K is the trace of the extrinsic curvature $K_{\mu\nu} = \frac{1}{2}\mathcal{L}_n h_{\mu\nu}$ of ∂M, where $\mathcal{L}_n$ is the Lie derivative with the unit normal vector n of the brane. We impose the Z_2-symmetry about the brane.

[1]Email address: ryotaku@tap.scphys.kyoto-u.ac.jp
[2]Email address: shiromizu@tap.scphys.kyoto-u.ac.jp
[3]Email address: tanahashi@ms.physics.ucdavis.edu

3 Near-horizon geometry

We consider a static brane-localized black hole whose horizon is made to be extreme by the Maxwell field on the brane. A static black hole has constant surface gravity on its horizon. Then, when the horizon is extremal on the intersection with the brane, the whole part of the horizon in the bulk will also be extremal. For such an extremal horizon, we can take the near-horizon limit and analyze its properties. It is proved that the near-horizon geometry of a static extreme black hole can be written in a warped product of a two-dimensional Lorentzian space and a compact manifold as [9]

$$ds^2 = A(x)^2 d\Sigma^2 + g_{ab}dx^a dx^b, \tag{2}$$

where $d\Sigma^2$ is a two-dimensional Lorentzian metric M_2 of constant curvature $2k$. When the metric describes the black hole spacetime, k should be negative and then M_2 is two-dimensional AdS spacetime (adS_2). We also assume that $g_{ab}dx^a dx^b$ has $SO(3)$ symmetry. Choosing the coordinates $x^a = (\rho, \theta, \phi)$, the near-horizon geometry becomes

$$ds^2 = A(\rho)^2 d\Sigma^2 + d\rho^2 + R(\rho)^2 d\Omega^2, \tag{3}$$

where $d\Omega^2$ is the metric of the two-dimensional unit sphere.

We assume the horizon to be compact, which implies that $R(\rho)$ vanishes somewhere. Then, we set the "origin" of ρ as $R(\rho = 0) = 0$. We solve the bulk Einstein equation from $\rho = 0$ and the initial parameter at $\rho = 0$ is $A(0) = A_0$. The bulk equations have three free parameters $\{A_0, k, l\}$. We can set $l = 1$ without losing generality.

Assuming that the brane position is at $\rho = \rho_0$, the induced metric on the brane is defined as

$$ds^2_{\mathrm{brane}} = |k| L_1^2 d\Sigma^2 + L_2^2 d\Omega^2, \tag{4}$$

where L_1 and L_2 are proper radii of M_2 and S^2 defined by

$$L_1^2 \equiv |k|^{-1} A(\rho_0)^2, \quad L_2^2 \equiv R(\rho_0)^2. \tag{5}$$

The induced cosmological constant Λ_4 on the brane is determined by the brane tension as

$$\Lambda_4 \equiv -\frac{3}{l^2} + \frac{\kappa_5^4 \sigma^2}{12}. \tag{6}$$

For convenience, we use the normalized tension α,

$$\alpha = \sqrt{1 + \frac{l^2 \Lambda_4}{3}} = \frac{l\kappa_5^2 \sigma}{6} = \frac{\sigma}{\sigma_{RS}}. \tag{7}$$

Moreover, we define the total charge Q on the brane

$$Q = \frac{1}{4\pi} \int_{S^2} *F. \tag{8}$$

After solving the bulk equations to $\rho = \rho_0$, we impose the Israel's junction condition on the brane which relates the bulk solution to α and Q.

4 Results

4.1 Positive cosmological constant case: $\alpha > 1$

In $\alpha > 1$ case, positive cosmological constant is induced on the brane and the brane geometry becomes asymptotically de Sitter spacetime. We observed a restriction on the black hole size in the sense that the black hole size $R(\rho_0)$ has an upper bound which depends on α.

The size of the black hole horizon in de Sitter spacetime is known to be restricted by the cosmological constant in the ordinary general relativity. From our result, we can confirm that the same restriction holds even in the braneworld setup.

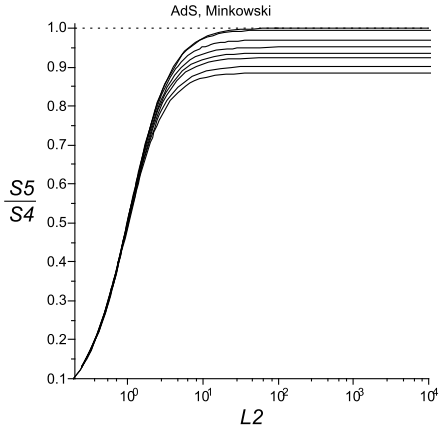

Figure 1: $L_2 = R(\rho_0)$ dependence of the entropy ratio S_5/S_4 for the brane solutions which are asymptotically adS($\alpha < 1$) or flat($\alpha = 1$). Each lines correspond to $\alpha = 1, 0.9995, 0.995, 0.99, 0.985, 0.98, 0.97$ and 0.96 from the top.

Comparing the braneworld upper limit $\alpha_{\rm max}^{\rm BW}$ with the upper limit $\alpha_{\rm max}^{\rm 4D}$ in the ordinary four-dimensional general relativity, we can see that

$$\alpha_{\rm max}^{\rm BW} > \alpha_{\rm max}^{\rm 4D} = \sqrt{1 + \frac{1}{6L_2^2}} \tag{9}$$

is satisfied. It tells us that the restriction on the black hole size is weaker in the braneworld model. The value of $\alpha_{\rm max}^{\rm BW}$ is given by $k = 0$ solution.

The difference in the cosmological constant is evaluated as

$$\Lambda_4^{\rm 4D} - \Lambda_4^{\rm BW} = 3\Big((\alpha_{\rm max}^{\rm 4D})^2 - (\alpha_{\rm max}^{\rm BW})^2\Big) \simeq -\frac{1}{16L_2^4}. \tag{10}$$

This, in fact, is consistent with the value which can be read off from the effective Einstein equation on the brane in [10] at the leading order.

4.2 Negative cosmological constant case: $\alpha < 1$

In the anti-de Sitter brane case, we observed discrepancies between the near-horizon geometry of the brane-localized black hole from that of the four-dimensional extreme adS-RN black hole. We found that the adS_2 radius and the charge are smaller than those of four-dimensional adS-RN black holes, and confirmed that those discrepancies vanish in the flat brane limit ($\alpha \to 1$).

In the large black hole limit,

$$\frac{L_1^2}{{L_{1(4D)}}^2} = 1 - \frac{3}{2}(1-\alpha) + \mathcal{O}\big((1-\alpha)^2 \log(1-\alpha)\big), \tag{11}$$

$$\frac{Q^2}{{Q_{4D}}^2} = \frac{G_4}{G_5}(1 + 2(1-\alpha)\log(1-\alpha) + \mathcal{O}(1-\alpha)). \tag{12}$$

We also calculated the five and four-dimensional black hole entropies. In the large black hole limit,

$$\frac{S_5}{S_4} = \frac{G_4}{G_5}\frac{A_5}{A_4} = \frac{G_4}{G_5}\Big(1 + 2\,(1-\alpha)\log\,(1-\alpha) + \mathcal{O}\,(1-\alpha)\Big). \tag{13}$$

When the black hole is much larger than the AdS curvature radius, the two entropies are expected to coincide by AdS/CFT correspondence. Then, Eq. (13) may imply the change in G_4 as

$$\begin{aligned}\frac{G_5}{G_4} &= 1 + 2(1-\alpha)\log(1-\alpha) + \cdots \\ &= 1 + \frac{l^2}{L^2}\log\left(\frac{2l^2}{L^2}\right) + \cdots .\end{aligned} \tag{14}$$

This is interesting because the charge ratio (Eq. (12)) also becomes unity at the leading order in such G_4 choise.

In the Karch-Randall model, it is suggested by Ref. [11] that the four-dimensional gravity weakens as $G_4/G_5 \approx 1 - \mathcal{O}\left(l^2/L^3\right)\mathcal{R}$ for $L \lesssim \mathcal{R} \lesssim L^3/l^2$, where $\mathcal{R}$ is the separation of two gravitating objects, due to small four-dimensional graviton mass. However, the formula for G_4/G_5 we proposed in this paper, Eq. (14), has a different form from it. It may be peculiar that our formula is independent of the black hole size, while the formula of Ref. [11] depends on propagation distance $\mathcal{R}$ of the gravity. It will be interesting to investigate whether these two formulae are compatible or not.

References

[1] L. Randall and R. Sundrum, Phys. Rev. Lett. **83**, 3370 (1999) [arXiv:hep-ph/9905221].

[2] L. Randall and R. Sundrum, Phys. Rev. Lett. **83**, 4690 (1999) [arXiv:hep-th/9906064].

[3] For review, R. Maartens and K. Koyama, arXiv:1004.3962.

[4] R. Emparan, A. Fabbri and N. Kaloper, JHEP **0208**, 043 (2002) [arXiv:hep-th/0206155].

[5] T. Tanaka, Prog. Theor. Phys. Suppl. **148**, 307 (2003) [arXiv:gr-qc/0203082].

[6] R. Emparan, J. Garcia-Bellido and N. Kaloper, JHEP **0301**, 079 (2003) [arXiv:hep-th/0212132].

[7] A. Kaus and H. S. Reall, JHEP **0905**, 032 (2009) [arXiv:0901.4236 [hep-th]].

[8] R. Suzuki, T. Shiromizu and N. Tanahashi, Phys. Rev. D **82**, 085029 (2010) [arXiv:1007.1820 [hep-th]].

[9] H. K. Kunduri, J. Lucietti and H. S. Reall, Class. Quant. Grav. **24**, 4169 (2007) [arXiv:0705.4214 [hep-th]].

[10] T. Shiromizu, K. i. Maeda and M. Sasaki, Phys. Rev. D **62**, 024012 (2000) [arXiv:gr-qc/9910076].

[11] N. Kaloper and L. Sorbo, JHEP **0508**, 070 (2005) [arXiv:hep-th/0507191].

Linear Instability of Lovelock Black Holes

Tomohiro Takahashi[1] and Jiro Soda[2]

Department of Physics, Kyoto University, Kyoto 606-8502

Abstract

We study the stability of static black holes in Lovelock theory which is a natural higher dimensional generalization of Einstein theory. We derive master equation for all type perturbation. Using these equations, we examine the stability of Lovelock black holes. Then we show that there exist a function whose behavior determine the stability of black holes.

1 Introduction

The possibility of higher dimensional black hole creation at the LHC would be the most fascinating prediction of the braneworld with large extra-dimensions.[1] However, not all black holes are produced in LHC; black hole which is not stable can not be produced because such black hole solutions are not attracter solutions. So it is important to examine the stability of black holes in higher dimensions.

By the way, the energy scale of black hole production is Planck scale where String theory affects. We should recall that string theory predicts Einstein theory only in the low energy limit.[3] In string theory, there are higher curvature corrections in addition to the Einstein-Hilbert term.[3] Thus, it is natural to extend gravitational theory into those with higher power of curvature in higher dimensions. It is Lovelock theory that belongs to such class of theories.[2, 4] In Lovelock theory, it is known that there exist static spherical symmetric black hole solutions [5] . Hence, it is natural to suppose black holes produced at the LHC are of this type.[6] Thus, it is important to study the stability of these Lovelock black holes.

We mainly concentrate on tensor type perturbation and scalar type perturbation in this proceedings.

2 Lovelock Black Holes

In this section, we review Lovelock theory and Lovelock black hole solution.

The most general divergence free symmetric tensor constructed out of a metric and its first and second derivatives has been obtained by Lovelock.[2] The corresponding Lagrangian can be constructed from m-th order Lovelock terms

$$\mathcal{L}_m = \frac{1}{2^m}\delta^{\lambda_1\sigma_1\cdots\lambda_m\sigma_m}_{\rho_1\kappa_1\cdots\rho_m\kappa_m} R_{\lambda_1\sigma_1}{}^{\rho_1\kappa_1}\cdots R_{\lambda_m\sigma_m}{}^{\rho_m\kappa_m} \ , \tag{1}$$

where $R_{\lambda\sigma}{}^{\rho\kappa}$ is the Riemann tensor in D-dimensions and $\delta^{\lambda_1\sigma_1\cdots\lambda_m\sigma_m}_{\rho_1\kappa_1\cdots\rho_m\kappa_m}$ is the generalized totally antisymmetric Kronecker delta.

By construction, the Lovelock terms vanish for $2m > D$. It is also known that the Lovelock term with $2m = D$ is a topological term. Thus, Lovelock Lagrangian in D-dimensions is defined by

$$L = \sum_{m=0}^{k} c_m \mathcal{L}_m \ , \tag{2}$$

where we defined the maximum order $k \equiv [(D-1)/2]$ and c_m are arbitrary constants. Here, $[z]$ represents the maximum integer satisfying $[z] \leq z$. Hereafter, we set $c_0 = -2\Lambda$, $c_1 = 1$ and $c_m = a_m/m$ $(m \geq 2)$

[1]Email address: takahashi@tap.scphys.kyoto-u.ac.jp
[2]Email address: jiro@tap.scphys.kyoto-u.ac.jp

for convenience. Taking variation of the Lagrangian with respect to the metric, we can derive Lovelock equation

$$0 = \mathcal{G}_\mu^\nu = \Lambda\delta_\mu^\nu - \sum_{m=1}^{k} \frac{1}{2^{(m+1)}} \frac{a_m}{m} \delta^{\nu\lambda_1\sigma_1\cdots\lambda_m\sigma_m}_{\mu\rho_1\kappa_1\cdots\rho_m\kappa_m} R_{\lambda_1\sigma_1}{}^{\rho_1\kappa_1} \cdots R_{\lambda_m\sigma_m}{}^{\rho_m\kappa_m} \ . \tag{3}$$

As is shown in Refs. [5], there exist static exact solutions of Lovelock equation. Let us consider the following metric

$$ds^2 = -f(r)dt^2 + \frac{dr^2}{f(r)} + r^2\bar{\gamma}_{ij}dx^i dx^j \ , \tag{4}$$

where $\bar{\gamma}_{ij}$ is the metric of $n \equiv D-2$-dimensional constant curvature space with a curvature κ=1,0 or -1. Substituting this ansatz into (3) and defining a new variable $\psi(r)$ by

$$f(r) = \kappa - r^2\psi(r) \ , \tag{5}$$

we obtain an algebraic equation

$$W[\psi] \equiv \sum_{m=2}^{k} \left[\frac{a_m}{m} \left\{ \prod_{p=1}^{2m-2} (n-p) \right\} \psi^m \right] + \psi - \frac{2\Lambda}{n(n+1)} = \frac{\mu}{r^{n+1}} \ . \tag{6}$$

In (6), we used $n = D-2$ and μ is a constant of integration which is related to the ADM mass.

After this we assume $\mu > 0$, $a_m > 0$ and $\Lambda = 0$. In this case, one of the solution of (6) is asymptotic flat branch which satisfies $\partial_\psi W[\psi] > 0$. We only consider this branch hereafter.

3 tensor perturbation

In this section, we examine the stability under tensor perturbations.

We start from the master equation for tensor perturbations (see [7])

$$-f^2\chi'' - \left(f^2\frac{T''}{T'} + \frac{2f^2}{r} + ff' \right)\chi' + \frac{(2\kappa+\gamma_t)f}{(n-2)r}\frac{T''}{T'}\chi = \omega^2\chi \ , \tag{7}$$

where ω is a frequency and we have defined a key function

$$T(r) = r^{n-1}\partial_\psi W[\psi] \ . \tag{8}$$

Note that $T > 0$ under our assumption. In (7), χ is the master variable and γ_t is eigenvalue of tensor harmonics which is given by $\gamma_t = \ell(\ell+n-1)-2$, $(\ell = 2, 3, 4\cdots)$ for $\kappa = 1$ and positive real numbers for $\kappa = -1, 0$.

As we will soon see, the master equation (7) can be transformed into the Schrödinger form. To do this, we have to impose the condition

$$T'(r) > 0 \ , \quad (\text{for } r > r_H) \ . \tag{9}$$

This is necessary for no ghost mode. Indeed, if there is a region $T'(r) < 0$ outside the horizon, the kinetic term of perturbations has a wrong sign. Hereafter, we call this the ghost instability.

When the condition (9) is fulfilled, introducing a new variable $\Psi(r) = \chi(r)r\sqrt{T'(r)}$ and switching to the coordinate r^*, defined by $dr^*/dr = 1/f$, we can rewrite Eq.(7) as

$$-\frac{d^2\Psi}{dr^{*2}} + V_t(r(r^*))\Psi = \omega^2\Psi \ , \tag{10}$$

where

$$V_t(r) = \frac{(2\kappa+\gamma_t)f}{(n-2)r}\frac{d\ln T'}{dr} + \frac{1}{r\sqrt{T'}} f\frac{d}{dr}\left(f\frac{d}{dr} r\sqrt{T'} \right) \tag{11}$$

is an effective potential.

Let us define the operator

$$\mathcal{H} \equiv -\frac{d^2}{dr^{*2}} + V_t \tag{12}$$

acting on smooth functions defined on $I = (r_H^*, \infty)$. Then, (10) is the eigenequation and ω^2 is eigenvalue of $\mathcal{H}$. We also define the inner products as

$$(\varphi_1, \varphi_2) = \int_I \varphi_1^* \varphi_2 dr^* \ . \tag{13}$$

After this, we show that there exist negative energy states if T'' has negative region outside of horizon. In order to prove this, the inequality

$$\frac{(\varphi, \mathcal{H}\varphi)}{(\varphi, \varphi)} \geq \omega_0^2 \tag{14}$$

is useful. Here, φ is an arbitrary test function and ω_0^2 means the lowest eigenvalue. This inequality shows that there exist negative energy state if we can find a φ which satisfies $(\varphi, \mathcal{H}\varphi) < 0$.

We assume T'' has negative region. Under this assumption, we can choose φ as the smooth function that has compact support in the region where $T^{''}$ is negative. Using such test function, $(\varphi, \mathcal{H}\varphi)$ becomes

$$(\varphi, \mathcal{H}\varphi) = \int_I |D\varphi|^2 dr^* + (2\kappa + \gamma_t) \int_{r_H}^{\infty} \frac{|\varphi|^2}{(n-2)r} \frac{d \ln T^{'}}{dr} dr \ . \tag{15}$$

where $D = \frac{d}{dr^*} - f \frac{d}{dr} \ln (r\sqrt{T'})$. Because of the assumption for T' and φ, it is easily seen that the first term is positive and the second term is negative. Therefore, considering sufficient large γ_t mode, this inner product must be negative. This means that negative energy state exist if T' has negative region.

Note that this instability is dynamical. Then, we call this as dynamical instability in order to distinguish this from the ghost instability which is caused by negativity of $T^{'}(r)$.

We want to summarize this subsection. If $T^{'}$ has negative region outside the horizon $r > r_H$, Lovelock black holes have the ghost instability. Even if $T^{'}$ is always positive, Lovelock black holes have the dynamical instability if $T^{''}$ has a negative region outside the horizon. Therefore, Lovelock black holes are stable under tensor perturbations if and only if $T^{'}$ and $T^{''}$ are always positive outside the horizon.

4 scalar perturbation

In this section, we examine the stability of Lovelock black holes under scalar perturbations.

Using the master variable Ψ, we can write down the master equation (see [7])

$$-\partial_{r^*}^2 \Psi + V_s(r)\Psi = \omega^2 \Psi \ . \tag{16}$$

Here, the effective potential reads

$$\begin{aligned} V_s(r) \quad = \quad & 2\gamma_s f \frac{(rNT)^{'}}{nNTr^2} \\ & -\frac{f}{N}\partial_r (f\partial_r N) + 2f^2 \frac{N'^2}{N^2} - \frac{f}{T}\partial_r (f\partial_r T) + 2f^2 \frac{T'^2}{T^2} + 2f^2 \frac{N^{'}T^{'}}{NT} \ , \end{aligned} \tag{17}$$

where we have defined

$$N(r) = \frac{-2nf + 2\gamma_s + nrf^{'}}{r\sqrt{T'}} \ . \tag{18}$$

For scalar perturbations, eigenvalues of scalar harmonics γ_s are given by $\gamma_s = \ell(\ell + n - 1)$ for $\kappa = 1$ and positive real numbers for $\kappa = 0, -1$. The above master equation is obtained by assuming $T' > 0$. Hence, tensor perturbations have no ghost instability. We also define $\mathcal{H} \equiv -d^2/dr^{*2} + V_s$.

After this, we show that black holes are unstable if $2T^{'2} - TT^{''}$ has a negative region outside the horizon. In order to prove this statement, we can use the same approach as tensor perturbation; that is, we find the test function φ which leads $(\varphi, \mathcal{H}\varphi) < 0$.

We assume $2T'^2 - TT''$ has negative region. Then we can choose test function φ as a smooth function which has compact support on the region where $2T'^2 - TT'' < 0$. Using such a function, $(\varphi, \mathcal{H}\varphi)$ can be bounded as

$$\begin{aligned}(\varphi, \mathcal{H}\varphi) &= \int dr^* \left[|D\varphi|^2 + \tilde{V} |\varphi|^2 \right] \\ &< \int dr^* |D\varphi|^2 + \gamma_s \int dr^* \frac{f}{nrTT'} \left(2T^{'2} - TT^{''} \right) |\varphi|^2 \ , \end{aligned} \tag{19}$$

where $D = -d^2/dr^{*2} + f\partial_r(\ln N) + f\partial_r(\ln T)$ and we use

$$\begin{aligned}\tilde{V} &= 2\gamma_s f \frac{(rNT)'}{nNTr^2} \\ &= \frac{2\gamma_s f}{nr} \left[\frac{2(\gamma_s - n\kappa)}{2(\gamma_s - n\kappa) + \frac{n(n+1)\mu}{T}} \frac{T'}{T} - \frac{1}{2} \frac{T''}{T'} \right] \\ &< \frac{\gamma_s f}{nrTT'} \left[2T'^2 - TT'' \right] \ . \end{aligned} \tag{20}$$

In the last inequality, we use $T > 0$, $T' > 0$ and $\mu > 0$.

We assume $T > 0$, $T^{'} > 0$ and choose φ as the smooth function which has compact support in the region $2T^{'2} - TT^{''} < 0$, so the first term in (19) must be positive and the second term in (19) must be negative. Therefore, by taking the limit $\gamma_s \to \infty$, the last line of Eq.(19) becomes negative, which means the lowest eigenvalue ω_0^2 is negative. Hence, black holes are dynamically unstable.

In summary, we can say that "If $T^{'}$ has a negative region, black holes have the ghost instability under tensor perturbations. Even if $T^{'}$ is always positive, Lovelock black holes have the dynamical instability under scalar perturbations if $2T^{'2} - TT^{''}$ has a negative region".

5 conclusion

We examine the stability of Lovelock black holes in all dimensions. We derive master equation for tensor and scalar type perturbations. Using this equations, we examine the stability of Lovelock black holes. Then, we show that behavior of a function $T(r)$ determines the stability.

One of our future work is examining the meaning of $T(r)$. If this function has thermodynamical meanings, it is interesting because dynamical stability and thermodynamics are related in Lovelock theory.

References

[1] S. B. Giddings and S. D. Thomas, Phys. Rev. D **65**, 056010 (2002) [arXiv:hep-ph/0106219]; S. B. Giddings and M. L. Mangano, Phys. Rev. D **78**, 035009 (2008) [arXiv:0806.3381 [hep-ph]].

[2] D. Lovelock, J. Math. Phys. **12** (1971) 498.

[3] D. G. Boulware and S. Deser, Phys. Rev. Lett. **55**, 2656 (1985).

[4] C. Charmousis, Lect. Notes Phys. **769**, 299 (2009) [arXiv:0805.0568 [gr-qc]];
C. Garraffo and G. Giribet, Mod. Phys. Lett. A **23**, 1801 (2008) [arXiv:0805.3575 [gr-qc]].

[5] J. T. Wheeler, Nucl. Phys. B **273**, 732 (1986).

[6] A. Barrau, J. Grain and S. O. Alexeyev, Phys. Lett. B **584**, 114 (2004) [arXiv:hep-ph/0311238].

[7] T. Takahashi and J. Soda, arXiv:1008.1385 [gr-qc].

Beyond δN formalism for a single scalar field

Yuichi Takamizu[1(a)], Shinji Mukohyama[2(b)] and Misao Sasaki[3(c)]

[(a)] *Research Center for the Early Universe (RESCEU), The University of Tokyo, Tokyo 113-0033*
[(b)] *Institute for the Physics and Mathematics of the Universe (IPMU), The University of Tokyo, 5-1-5 Kashiwanoha, Kashiwa, Chiba 277-8582*
[(c)] *Yukawa Institute for Theoretical Physics Kyoto University, Kyoto 606-8502*

Abstract

We develop a theory of nonlinear cosmological perturbations on superhorizon scales for a single scalar field with a general kinetic term and a general form of the potential. We employ the ADM formalism and the spatial gradient expansion approach and show the nonlinear theory called the *beyond* δN-formalism as the next-leading order in the expansion to the so-called δN-formalism as the leading order. We obtain the general solution for a full nonlinear version of the curvature perturbation valid up through the second-order in the expansion and find the solution satisfies a nonlinear second-order differential equation as an extension of the equation for the linear curvature perturbation on the comoving hypersurface. The formalism developed in this paper allows us to calculate the superhorizon evolution of a primordial non-Gaussianity beyond δN-formalism.

1 Introduction

The PLANCK satellite launched last year is expected to bring us much finer data and it is hoped that non-Gaussianity may actually be detected. As a consequence, non-Gaussianity from inflation has been a focus of much attention in recent years. To study possible origins of non-Gaussianity, the δN-formalism [2, 4, 5] turned out to be a powerful tool for the estimation of non-Gaussianity. We investigate a possible origin of non-Gaussianity, namely, non-Gaussianity due to a temporary non-slow roll stage on superhorizon scales. In order to investigate such a case, however, the δN-formalism is not sufficient since it is equivalent to the leading order approximation in the spatial gradient expansion. Thus, to evaluate such situation, it is necessary to develop a nonlinear theory of cosmological perturbations valid up through the next-leading order in the gradient expansion.

2 Beyond δN-Formalism

In this section, we will briefly review the nonlinear theory of cosmological perturbations valid up to $O(\epsilon^2)$ in the spatial gradient expansion and follow the previous works [6, 7], where ϵ is the ratio of the Hubble length scale $1/H$ to the characteristic length scale of perturbations L, used as a small expansion parameter, $\epsilon \equiv 1/(HL)$, of the superhorizon scales. First of all, we show the main result in our formula for the nonlinear curvature perturbation, $\mathcal{R}_c^{\rm NL}$,

$$\mathcal{R}_c^{\rm NL\prime\prime} + 2\frac{z'}{z}\mathcal{R}_c^{\rm NL\prime} + \frac{c_s^2}{4}K^{(2)}[\,\mathcal{R}_c^{\rm NL}\,] = O(\epsilon^4)\,, \tag{1}$$

which shows two full-nonlinear effects;

1. Nonlinear variable: $\mathcal{R}_c^{\rm NL}$ including full-nonlinear curvature perturbation, δN
2. Source term: $K^{(2)}[\mathcal{R}_c^{\rm NL}]$ is a nonlinear function of curvature perturbations.

In (1), the prime denotes conformal time derivative and z is a well-known Mukhanov-Sasaki variable. The explicit forms of both the definition of $\mathcal{R}_c^{\rm NL}$ and the source term $K^{(2)}[X]$, that is the Ricci scalar of

[1]Email address: takamizu@resceu.s.u-tokyo.ac.jp
[2]Email address: shinji.mukohyama@ipmu.jp
[3]Email address: misao@yukawa.kyoto-u.ac.jp

the metric X, will be also seen later, in (5) and in (8), respectively. Of course, in the linear limit, it can be reduced to the well-known equation for the curvature perturbation on comoving hypersurfaces,$\mathcal{R}_c^{\mathrm{Lin}\prime\prime} + 2\frac{z'}{z}\mathcal{R}_c^{\mathrm{Lin}\prime} - c_s^2\,\Delta[\mathcal{R}_c^{\mathrm{Lin}}] = 0$.

We will briefly summarize our formula and show the above results in the following. Throughout this paper we consider a minimally-coupled single scalar field described by an action of the form $I = \int d^4x\sqrt{-g}P(X,\phi)$, where $X = -g^{\mu\nu}\partial_\mu\phi\partial_\nu\phi$. Note that we do not assume the explicit forms of both kinetic term and its potential, that can be given as arbitrary function of $P(X,\phi)$. We adopt the ADM decomposition and employ the gradient expansion. In the ADM decomposition, the metric is expressed as $ds^2 = -\alpha^2dt^2 + \gamma_{ij}(dx^i + \beta^i dt)(dx^j + \beta^j dt)$, where α is the lapse function, β^i is the shift vector and Latin indices run over $1,2,3$. We introduce the extrinsic curvature K_{ij} defined by $K_{ij} = -\frac{1}{2\alpha}\left(\partial_t\gamma_{ij} - D_i\beta_j - D_j\beta_i\right)$, where D is the covariant derivative compatible with the spatial metric γ_{ij}. As a result, the basic equations are reduced to the first-order equations for the dynamical variables (γ_{ij},K_{ij}), with the two constraint equations (the so-called Hamiltonian and Momentum constraint). We further decompose them as $\gamma_{ij} = a^2e^{2\zeta}\tilde{\gamma}_{ij}$ and $K_{ij} = a^2e^{2\zeta}\left(\frac{1}{3}K\tilde{\gamma}_{ij} + \tilde{A}_{ij}\right)$ where $a(t)$ is the scale factor of the background FRW universe and $\det\tilde{\gamma}_{ij} = 1$. Next, we will employ the gradient expansion. In this approach we introduce a flat FRW universe ($a(t)$, $\phi_0(t)$) as a background. As discussed, we consider the perturbations on superhorizon scales, therefore we consider $\epsilon \equiv 1/(HL)$ as a small expansion parameter and systematically expand equations by ϵ. We assume the condition for the gradient expansion; $\partial_t\tilde{\gamma}_{ij} = O(\epsilon^2)$. This corresponds to assuming the absence of any decaying modes at the leading-order in the expansion. This is justified in most of the inflationary models.

When we focus on a contribution arising from the scalar-type perturbations, we may choose the gauge in which $\tilde{\gamma}_{ij}$ approaches the flat metric,

$$\tilde{\gamma}_{ij}\,(t\to\infty) = \delta_{ij}, \tag{2}$$

where in reality the limit $t\to\infty$ may be reasonably interpreted as an epoch close to the end of inflation. We take the *comoving slicing, time-orthogonal* gauge:

$$\delta\phi_c(t,x^i) = \beta_c^i(t,x^i) = O(\epsilon^3), \tag{3}$$

where $\delta\phi \equiv \phi - \phi_0$ denotes a fluctuation of a scalar field. The subscript c denotes this gauge throughout this paper. Now we turn to the problem of properly defining a nonlinear curvature perturbation to $O(\epsilon^2)$ accuracy. Hereafter we will use the expression $\mathcal{R}_c$ on comoving slices to denote it. Let us consider the linear curvature perturbation which is given as $\mathcal{R}^{\mathrm{Lin}} = \left(H_L^{\mathrm{Lin}} + \frac{H_T^{\mathrm{Lin}}}{3}\right)Y$, where, following the notation in [1], the spatial metric in the linear limit is expressed as $\gamma_{ij} = a^2(\delta_{ij} + 2H_L^{\mathrm{Lin}}Y\delta_{ij} + 2H_T^{\mathrm{Lin}}Y_{ij})$. These expressions in the linear theory correspond to the metric components in our notation as $\zeta = H_L^{\mathrm{Lin}}Y$ and $\tilde{\gamma}_{ij} = \delta_{ij} + 2H_T^{\mathrm{Lin}}Y_{ij}$. Notice that the variable ζ_c reduces to $\mathcal{R}_c^{\mathrm{Lin}}$ at leading-order in the gradient expansion, but not at second-order and it will be also similar to the nonlinear theory. Thus to define a nonlinear generalization of the linear curvature perturbation, we need nonlinear generalizations of H_LY and H_TY. Our nonlinear ζ is an apparent natural generalization of $H_L^{\mathrm{Lin}}Y$ as $H_LY = \zeta$. As for H_TY, however, the generalization is non-trivial. It corresponds to the $O(\epsilon^2)$ part of $\tilde{\gamma}_{ij}$ and we have obtained a general solution of the dynamical equation for $\tilde{\gamma}_{ij}$ as a first-order differential equation in [6, 7] and the time-dependent part includes the following solution; $\tilde{\gamma}_{ij}(t) \ni C_{ij}^{(2)}\int\frac{dt'}{a^3(t')}$ with the Momentum constraint: $e^{3\ell^{(0)}}\partial_iC^{(2)} = 6f_{(0)}^{jk}\partial_j\left[e^{3\ell^{(0)}}C_{ki}^{(2)}\right]$. The explicit forms of solutions can be seen in [6]. Here we attach the superscript (m) to a quantity of $O(\epsilon^m)$, and both $\ell^{(0)}$ and $f_{ij}^{(0)}$ will be denoted as the leading-order metric. Our aim is to derive the scalar-type solution $C^{(2)}$ from the tensor $C_{ij}^{(2)}$ by using the constraint eq. As shown in [7], it can be done by introducing the inverse Laplacian operator Δ^{-1} on the flat background and we defined the nonlinear generalization of H_TY as

$$H_TY = E \equiv -\frac{3}{4}\Delta^{-1}\left[\partial^ie^{-3\ell^{(0)}}\partial^je^{3\ell^{(0)}}(\ln\tilde{\gamma})_{ij}\right]. \tag{4}$$

It is easy to see that $E \ni C^{(2)}$ which we expected. At leading-order, the only non-trivial quantities for the spatial metric, ζ and $\tilde{\gamma}_{ij}$, are given by $\zeta = \ell^{(0)}(x^k) + O(\epsilon^2)$ and $\tilde{\gamma}_{ij} = f_{ij}^{(0)}(x^k) + O(\epsilon^2)$, where $\ell^{(0)}(x^k)$ is an

arbitrary function of the spatial coordinates $\{x^k\}$ $(k = 1, 2, 3)$ and $f^{(0)}_{ij}(x^k)$ is a (3×3)-matrix function of the spatial coordinates with a unit determinant, respectively. Throughout this paper, we choose $f^{(0)}_{ij} = \delta_{ij}$ consistent with the gauge condition of (2). On the other hand, $\ell^{(0)}$ represents a conserved comoving curvature perturbation, which is denoted by the so-called δN term from some final uniform density (or comoving) hypersurface to the initial flat hypersurface at $t = t_*$, namely, $\ell^{(0)} = \delta N(t_*, x^i)$.

With these definitions of $H_L Y$ and $H_T Y$, we can define the nonlinear curvature perturbation valid up through $O(\epsilon^2)$ as

$$\mathcal{R}^{\rm NL}_c \equiv \zeta_c + \frac{E_c}{3}\,. \tag{5}$$

It is easy to show that this nonlinear quantity can be reduced to $\mathcal{R}^{\rm Lin}_c$ in the linear limit. As clear from (4), finding $H_T Y$ generally requires a spatially non-local operation, however, in the comoving slicing, time-orthogonal gauge with the asymptotic condition on the spatial coordinates (2), we find it is possible to obtain the explicit form of $H_T Y$ without any non-local operation as seen in [7]. Finally, we can derive a nonlinear second-order differential equation that $\mathcal{R}^{\rm NL}_c$ (5) satisfies at $O(\epsilon^2)$ accuracy by introducing the conformal time η, defined by $d\eta = dt/a(t)$ and the Mukhanov-Sasaki variable $z = \frac{a}{H}\sqrt{\frac{\rho+P}{c_s^2}}$. The result can be reduced to a simple equation of the form (1) as a natural extension of the linear version. We also obtain the solution of the nonlinear equation (1) as

$$\mathcal{R}^{\rm NL}_c(\eta) = \ell^{(0)} + \frac{1}{4}\big[F(\eta) - F_*\big]K^{(2)} + \big[D(\eta) - D_*\big]C^{(2)} + O(\epsilon^4), \tag{6}$$

where

$$D(\eta) = 3\mathcal{H}_* \int_\eta^0 \frac{z^2(\eta_*)}{z^2(\eta')} d\eta'\,, \quad F(\eta) = \int_\eta^0 \frac{d\eta'}{z^2(\eta')} \int_{\eta_*}^{\eta'} z^2 c_s^2(\eta'') d\eta''\,. \tag{7}$$

Here $D_* = D(\eta_*)$, $F_* = F(\eta_*)$ and $\mathcal{H}_*$ denotes the conformal Hubble parameter $\mathcal{H} = d\ln a/d\eta$ at $\eta = \eta_*$ which we take the time as some after the horizon crossing. Note that $t \to \infty$ corresponds to $\eta \to 0$ in the conformal time. Thus the functions D and F vanish asymptotically at late times, $D(0) = F(0) = 0$. Deviation of the solution (6) can be easily understood as follows. The second-order differential equation (1) contains two solutions, i.e. decaying mode and growing mode. We can find that the function $D(\eta)$ satisfies $D'' + 2\frac{z'}{z}D' = 0$ in the long-wavelength limit, i.e. no source term in (1). It corresponds to the decaying mode in the linear theory. On the other hand, the function $F(\eta)$ corresponds to the source term in (1), satisfying $F'' + 2\frac{z'}{z}F' + c_s^2 = 0$, as the $O(\epsilon^2)$ correction to a constant mode at the leading-order, i.e. as the growing mode in the linear theory, which is taken the form $1 + F(\eta)K^{(2)} + O(\epsilon^4)$.

Moreover the equation (1) includes two 'constants' of integration, or arbitrary spatial functions, which in general appear as the initial conditions. Let us consider the spatial functions; $\ell^{(0)}, C^{(2)}$ and $K^{(2)}$. Here the last one is related to the Ricci scalar of the 0th-order spatial metric as

$$K^{(2)}[\ell^{(0)}] = R\left[e^{2\ell^{(0)}}\delta_{ij}\right] = -2(2\Delta\ell^{(0)} + \delta^{ij}\partial_i\ell^{(0)}\partial_j\ell^{(0)})e^{-2\ell^{(0)}}. \tag{8}$$

Then we have the two arbitrary spatial functions: $\ell^{(0)}$ and $C^{(2)}$, which are related to the number of physical degrees of freedom for the initial conditions. Therefore they have to be determined by matching a solution of n-th order perturbation solved inside the horizon to this superhorizon solution at $\eta = \eta_*$.

3 Application

In this subsection, we calculate the bispectrum of our nonlinear curvature perturbation by assuming that $\mathcal{R}^{\rm Lin}_{c,\boldsymbol{k}}(\eta_k)$ is a Gaussian random variable with the horizon crossing time; $\eta_k = -\frac{r}{k}$ ($0 < r \ll 1$). We assume the leading order contribution to the bispectrum comes from the terms second order in $\mathcal{R}^{\rm Lin}_{c,\boldsymbol{k}}(\eta_k)$. The final result can be obtained by

$$\zeta_{\boldsymbol{k}} = G(k)\ \mathcal{R}^{\rm Lin}_{c,\boldsymbol{k}}(\eta_k) + H(k)\ \left\{\int \frac{d^3k' d^3k''}{(2\pi)^3}(4k'^2 - \delta_{ij}k'^i k''^j)\mathcal{R}^{\rm Lin}_{c,\boldsymbol{k}'}(\eta_{k'})\mathcal{R}^{\rm Lin}_{c,\boldsymbol{k}''}(\eta_{k''})\delta^3(-\boldsymbol{k} + \boldsymbol{k}' + \boldsymbol{k}'')\right\}, \tag{9}$$

where $G(k) = 1 + \frac{\tilde{D}_k}{3\mathcal{H}(\eta_k)}\frac{\mathcal{R}'_c}{\mathcal{R}_c}\big|_{\eta=\eta_k} k^2\tilde{F}_k$, $H(k) = \frac{1}{2}\tilde{F}_k$, $\tilde{D}_k = \tilde{D}(\eta_k)$ and $\tilde{F}_k = \tilde{F}(\eta_k)$. Here we defined the integrals $\tilde{D}$ and $\tilde{F}$ obtained by replacements η_k with η_* in their definitions of (7). In particular, it can

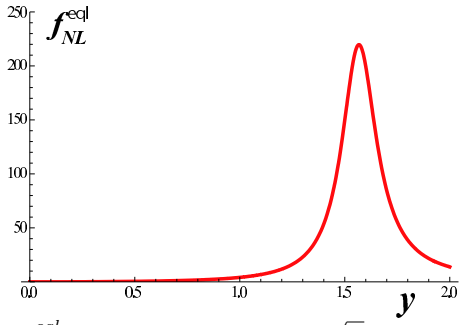

Figure 1: $f_{NL}^{eql}(k)$ as a function of $y = \sqrt{T}k/k_0$ for $T = 10^2$.

deal with the case when there is a temporary violation of slow-roll conditions. As one application of our formalism, we consider Starobinsky's model [3], which is described by the potential having its slope's step as $V(\phi) = V_0 + A_+(\phi - \phi_0)$ for $\phi > \phi_0$ or $V_0 + A_-(\phi - \phi_0)$ for $\phi < \phi_0$, where $A_+ > A_- > 0$ is assumed. The advantage of this model is that it allows analytical treatment of linear perturbations as well as of the background evolution, provided that V_0 dominates in the potential. If $A_+ \gg A_-$, and for ϕ initially large and positive, the slow-roll condition is violated right after ϕ falls below ϕ_0. We find that a large non-Gaussianity can be generated even on superhorizon scales due to this temporary suspension of slow-roll inflation as shown in Fig. 1. We have found that non-Gaussianity can become large if the parameter $T \approx A_+/A_-$, which characterises the ratio of the slope before and after the transition, is large. For $T \gg 1$, we have found that the non-Gaussianity parameter for the bispectrum $f_{NL}(k_1, k_2, k_3)$ is peaked at the wavenumbers forming an equilateral triangle, $k = k_1 = k_2 = k_3$, denoted by $f_{NL}^{eql}(k)$. It is found to be positive and takes the maximum value $f_{NL}^{eql}(k) \simeq 2T$ at $\sqrt{T}k/k_0 \simeq 1.5$ where k_0 is the comoving wavenumber that crosses the horizon at the time when the potential slope changes. This implies that, even for a relatively small T, say for $T = 10$, it is possible to generate a fairly large non-Gaussianity $f_{NL} \sim 20$ at wavenumber $k \simeq 0.5k_0$.

4 Summary

We have developed a theory of nonlinear cosmological perturbations on superhorizon scales for a single scalar field with a general kinetic term and a general form of the potential to the second-order in the spatial gradient expansion. The solution to this order is necessary to evaluate correctly the final amplitude of the curvature perturbation for models of inflation with a temporary violation of the slow-roll condition. We have introduced a reasonable variable that represents the nonlinear curvature perturbation on comoving slices $\mathcal{R}_c^{\rm NL}$, which reduces to the comoving curvature perturbation $\mathcal{R}_c^{\rm Lin}$ in the linear limit. Then we have found that $\mathcal{R}_c^{\rm NL}$ satisfies a nonlinear second-order differential equation, (1), as a natural extension of the linear second-order differential equation. Since the evolution of superhorizon curvature perturbations is genuinely due to the $O(\epsilon^2)$ effect, our formulation can be used to calculate the primordial non-Gaussianity beyond the δN formalism which is equivalent to leading order in the gradient expansion. As one application of our formalism, we have investigated Starobinsky's model [3] in which there is a temporary non-slow-roll stage during inflation due to a sudden change of the potential slope. We have found that non-Gaussianity can become large if the ratio of the slope before and after the transition is large.

References

[1] H. Kodama and M. Sasaki, Prog. Theor. Phys. Suppl. **78** 1 (1984).

[2] A. A. Starobinsky, JETP Lett. **42**, 152 (1985).

[3] A. A. Starobinsky, JETP Lett. **55**, 489 (1992).

[4] Y. Nambu and A. Taruya, Class. Quant. Grav. **13**, 705 (1996).

[5] M. Sasaki and E. D. Stewart, Prog. Theor. Phys. **95**, 71 (1996).

[6] Y. Takamizu and S. Mukohyama, JCAP **0901**, 013 (2009).

[7] Y. Takamizu, S. Mukohyama, M. Sasaki and Y. Tanaka, JCAP **1006**, 019 (2010).

Unified picture of Q-balls and boson stars via catastrophe theory

Takashi Tamaki[1(a)] and Nobuyuki Sakai[2(b)]

(a) *Department of Physics, Nihon University, Fukushima 963-8642*
(b) *Department of Education, Yamagata University, Yamagata 990-8560*

Abstract

We make an analysis of Q-balls and boson stars via catastrophe theory.

1 Introduction

Among non-topological solitons which appear in $U(1)$-symmetric scalar fields, objects existing even in flat spacetime are called Q-balls [1], while objects supported by strong gravity are called boson stars [2]. Although the difference in theory between Q-balls and boson stars is solely the model parameters, the investigations of their properties have been carried out separately. This is because Q-balls and boson stars have been discussed in different contexts of particle physics or astrophysics. The purpose of the present paper is to obtain a unified picture of equilibrium solutions and their stability of Q-balls and boson stars. Gravitating Q-balls, or Q-stars, which are intermediate objects between Q-balls in flat spacetime and boson stars, have also been discussed [3–5]. Therefore, a unified analysis of Q-balls and boson stars is also important for the study of astrophysical models [6].

2 Analysis method of equilibrium Q-balls and boson stars

We begin with the action

$$\mathcal{S} = \int d^4x\sqrt{-g}\left(\frac{\mathcal{R}}{16\pi G} - \frac{1}{2}g^{\mu\nu}\partial_\mu\boldsymbol{\phi}\cdot\partial_\nu\boldsymbol{\phi} - V(\phi)\right), \tag{1}$$

where $\boldsymbol{\phi} = (\phi_1,\ \phi_2)$ is a SO(2)-symmetric scalar field and $\phi \equiv \sqrt{\boldsymbol{\phi}\cdot\boldsymbol{\phi}} = \sqrt{\phi_1^2+\phi_2^2}$. We assume a spherically symmetric and static spacetime, $ds^2 = -\alpha^2(r)dt^2 + A^2(r)dr^2 + r^2(d\theta^2+\sin^2\theta d\varphi^2)$. For the scalar field, we assume $(\phi_1,\phi_2) = \phi(r)(\cos\omega t, \sin\omega t)$.

Because of the symmetry, there is a conserved charge called Q-ball charge,

$$Q \equiv \int d^3x\sqrt{-g}g^{\mu\nu}(\phi_1\partial_\nu\phi_2 - \phi_2\partial_\nu\phi_1) = \omega I, \quad \text{where} \quad I \equiv 4\pi\int\frac{Ar^2\phi^2}{\alpha}dr. \tag{2}$$

As for Q-balls, which are present even in flat spacetime, we suppose the potential,

$$V_3(\phi) := \frac{m^2}{2}\phi^2 - \mu\phi^3 + \lambda\phi^4 \quad \text{with} \quad m^2,\ \mu,\ \lambda > 0\ , \tag{3}$$

which we call V_3 Model. Rescaling the quantities as

$$\tilde{t} \equiv mt, \quad \tilde{r} \equiv mr, \quad \tilde{\omega} \equiv \frac{\omega}{m}, \quad \tilde{\mu} \equiv \frac{\mu}{\sqrt{\lambda}m}, \quad \kappa \equiv \frac{m^2G}{\lambda}, \quad \tilde{\phi} \equiv \frac{\sqrt{\lambda}}{m}\phi, \quad \tilde{V} \equiv \frac{\lambda}{m^4}V_3, \quad \tilde{Q} \equiv \lambda Q, \tag{4}$$

the field equations are rewritten as

$$A' + \frac{A}{2\tilde{r}}(A^2-1) = 4\pi\kappa\tilde{r}A^3\left(\frac{\tilde{\phi}'^2}{2A^2} + \frac{\tilde{\omega}^2\tilde{\phi}^2}{2\alpha^2} + \tilde{V}\right), \tag{5}$$

[1]Email address: tamaki@ge.ce.nihon-u.ac.jp
[2]Email address: nsakai@e.yamagata-u.ac.jp

$$\alpha' + \frac{\alpha}{2\tilde{r}}(1-A^2) = 4\pi\kappa\tilde{r}\alpha A^2\left(\frac{\tilde{\phi}'^2}{2A^2} + \frac{\tilde{\omega}^2\tilde{\phi}^2}{2\alpha^2} - \tilde{V}\right), \tag{6}$$

$$\tilde{\phi}'' + \left(\frac{2}{\tilde{r}} + \frac{\alpha'}{\alpha} - \frac{A'}{A}\right)\tilde{\phi}' + \left(\frac{\tilde{\omega}A}{\alpha}\right)^2\tilde{\phi} = A^2\frac{d\tilde{V}}{d\tilde{\phi}}. \tag{7}$$

Let us discuss how we apply catastrophe theory to the present Q-ball or boson star system. An essential point is to choose *behavior variable*(*s*), *control parameter*(*s*) and a *potential* in the Q-ball or boson star system appropriately. In [7] we argued that the total energy of the scalar field,

$$E_\phi \equiv \int d^3x \left\{\frac{\omega^2\phi^2}{2} + \frac{(\phi')^2}{2} + V\right\}, \tag{8}$$

is appropriate for a *potential* because the variation of E_ϕ under fixed Q, $\delta E_\phi/\delta\phi|_Q = 0$, reproduces the equilibrium field equation. A nontrivial issue in curved spacetime is the choice of the corresponding total energy since there are many definitions for total energy. However, we can conclude that the Hamiltonian energy E is appropriate which reduces to $E = \frac{M}{2}$, where M is the gravitational mass. We also use the normalized quantity $\tilde{E} \equiv \frac{\lambda}{m}E$.

Because the charge Q and the model parameter(s) of $V(\phi)$ can be given by hand, they should be regarded as *control parameters*. In flat spacetime, V_3 Model essentially has only one parameter, $\tilde{\mu}^2$. In curved spacetime, on the other hand, the normalized gravitational constant κ is another *control parameter*, which represents the strength of gravity.

To discuss a *behavior variable* we consider an one-parameter family of perturbed field configurations $\phi_x(r)$ near the equilibrium solution $\phi(r)$. Because $dE[\phi_x]/dx = (\delta E/\delta\phi_x)d\phi_x/dx = 0$ when ϕ_x is an equilibrium solution, x is a *behavior variable*. Although an explicit choice for x is not unique, we choose $\tilde{\omega}^2$ and $\tilde{\phi}(0)$ as *behavior variables*.

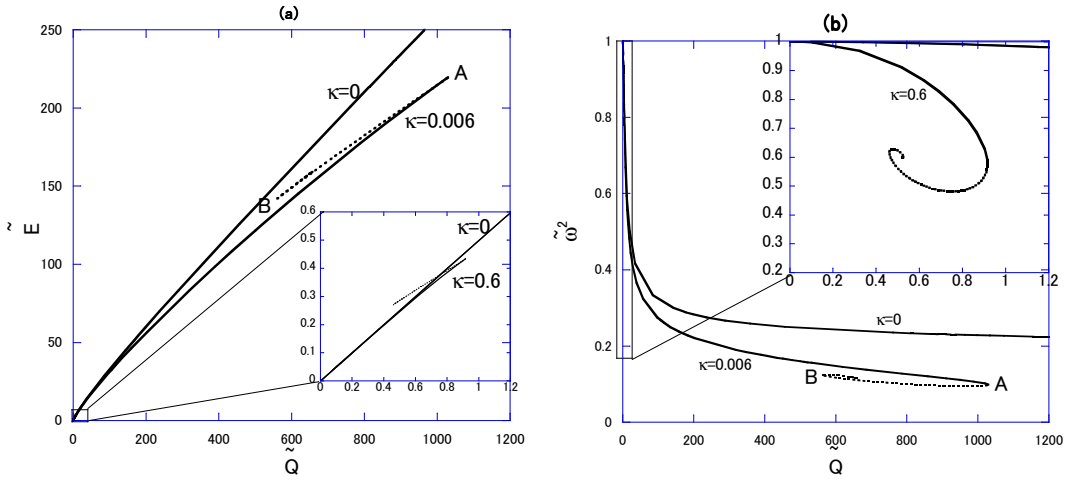

Figure 1: (a) $\tilde{Q}$-$\tilde{E}$ relation and (b) $\tilde{Q}$-$\tilde{\omega}^2$ relation for $\tilde{\mu}^2 = \frac{5}{3}$ in V_3 Model.

3 Stability of gravitating Q-balls and boson stars

3.1 Q-balls

We fix $\tilde{\mu}^2 = \frac{5}{3}$ as an example. Figure 1 shows a plot of $\tilde{Q}$ versus $\tilde{E}$ and that of $\tilde{Q}$ versus $\tilde{\omega}^2$ for equilibrium Q-ball solutions. In the case of $\kappa = 0$ there is one-to-one correspondence between $\tilde{Q}$ and $\tilde{E}$ while cusp structures appear in the case of $\kappa \neq 0$, as shown in (a). The maximum of $\tilde{Q}$ (labeled as A for $\kappa = 0.006$)

and the local minimum (labeled as B for $\kappa = 0.006$) appear in the case of gravitating Q-balls. At the point B, another cusp strcture appears and is far smaller than that at the point A. This sequences of cusp structure continue and we stopped calculation where the 4th cusp structure appears. The $\tilde{Q}$-maximum for $\kappa = 0.6$ is far smaller than that for $\kappa = 0.006$.

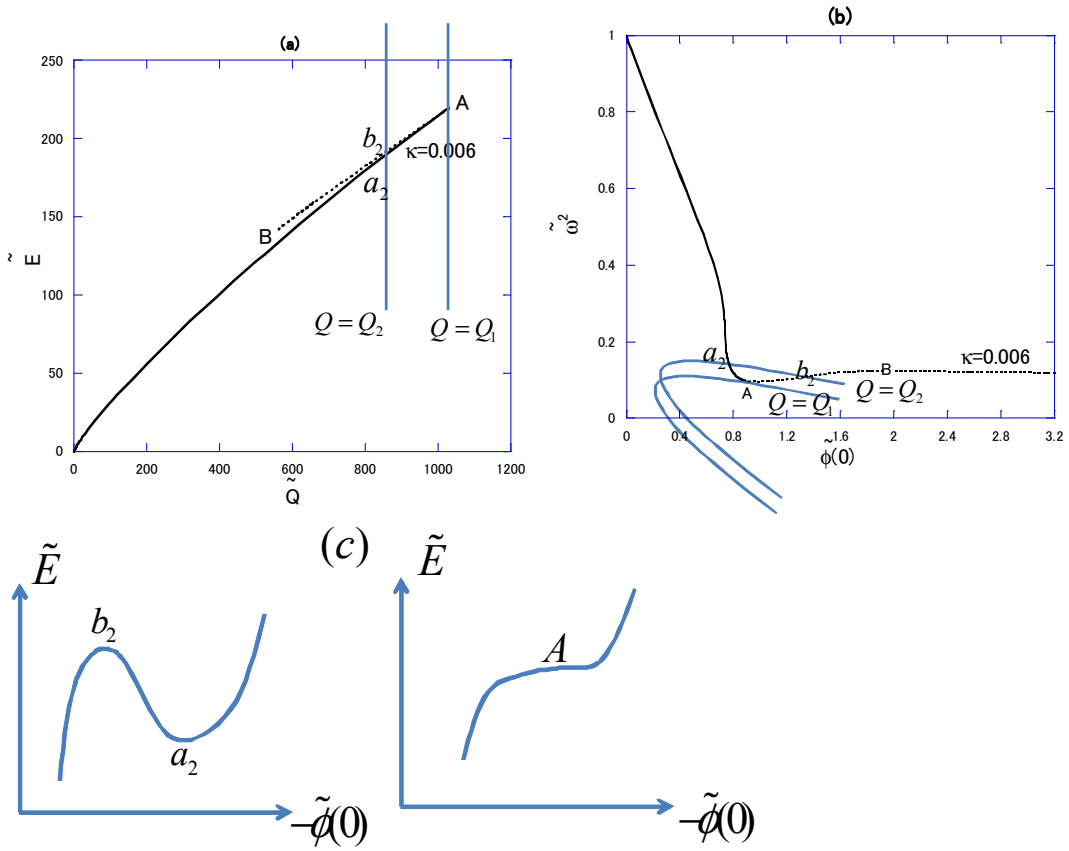

Figure 2: Stability interpretation via catastrophe theory for $\tilde{\mu}^2 = \frac{5}{3}$ for the gravitating case with $\kappa = 0.006$ (The qualitative properties are same for other κ).

We explain our interpretation via catastrophe theory by exemplifying the case with $\tilde{\mu}^2 = \frac{5}{3}$ and $\kappa = 0.006$ (Qualitative properties are not changed for other κ.). We identify $\tilde{Q}$ =const. lines in Fig. 2 (a) with the quadratic curves in Fig. 2 (b). If we adopt the view point that stability changes at the point A as we mentioned above and observe Fig. 2 (b), we notice that $(-\tilde{\phi}(0))$ is more appropriate for a *behavior variable* than $\tilde{\omega}^2$. Then, as we show in (c), a_2, b_2 and A can be interpreted as the potential minimum, maximum and the inflection point, respectively.

This case can be understood using the fold catastrophe $f(u) = u^3 + tu$ where u and t are the *bahavior variable* identified with $(-\tilde{\phi}(0))$ and the *control parameter* identified with $\tilde{Q}$, respectively.

We should reveal what causes the difference from the flat case. Naively speaking, solutions having larger $|A-1|$ at its peak have larger $(-\tilde{\phi}(0))$. We have confirmed that, independent of κ, solutions having $|A-1| \sim 1$ correspond to solutions expressed by dotted lines in Fig. 1. Therefore, we can suppose that the intrinsic difference from the flat case can be characterized by $|A-1|$.

3.2 Boson stars

Now we discuss boson stars with the potential V_3 with $\mu = 0$. Figure 3 shows plots of (a) $\tilde{Q}$-$\tilde{E}$, (b) $\tilde{Q}$-$\tilde{\omega}^2$ for equilibrium solutions of boson stars. Degenerate cusp and spiral structures are seen as in the case of gravitating Q-balls for $\tilde{\mu}^2 = \frac{5}{3}$. We have confirmed $|A-1| \sim 1$ at its peak in the solutions corresponding to the spiral curves or near the stability change points. We therefore conclude that, if gravity is so strong

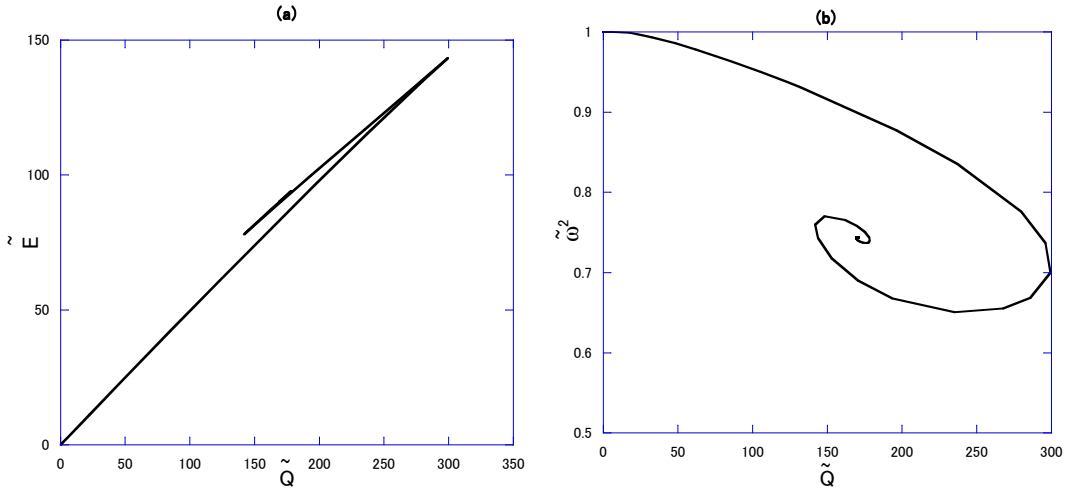

Figure 3: (a)$\tilde{Q}$-$\tilde{E}$, (b)$\tilde{Q}$-$\tilde{\omega}^2$ relations in the model of boson stars for $\kappa = 0.006$.

as $|A-1| \sim 1$ at its peak, catastrophic structures of Q-balls approach those of boson stars, regardless of the potential shape.

4 Conclusion and discussion

We have reanalyzed stability of gravitating Q-balls for a V_3 model and boson stars for a V_3 model with $\mu = 0$. For solutions with $|g^{rr} - 1| \sim 1$ at its peak, stability of Q-balls has been lost regardless of the potential parameters. As a result, phase relations, such as $\tilde{Q}$-$\tilde{E}$, approach those of boson stars, which tell us a unified picture of Q-balls and boson stars. Therefore, if we discuss the possibility of Q-balls or boson stars as dark matter candidates, our work would be useful.

References

[1] S. Coleman, Nucl. Phys. **B262**, 263 (1985).

[2] For a review of boson stars, see, P. Jetzer, Phys. Rep. **220**, 163 (1992). F. E. Schunck and E. W. Mielke, Class. Quantum Grav. **20**, R301 (2003).

[3] R. Friedberg, T. D. Lee, and Y. Pang, Phys. Rev. D **35**, 3658 (1987);

[4] B. W. Lynn, Nucl. Phys. **B321**, 465 (1989); S. B. Selipsky, *ibid.* **B321**, 430,1989; S. Bahcall, *ibid.* **B325**, 606 (1989); A. Prikas, Phys. Rev. D **66**, 025023 (2002); Y. Verbin, *ibid.* **76**, 085018 (2007).

[5] T. Multamaki and I. Vilja, Phys. Lett. B **542**, 137 (2002).

[6] T. Tamaki and N. Sakai, Phys. Rev. D **81**, 124041 (2010).

[7] N. Sakai and M. Sasaki, Progress of Theoretical Physics, **119**, 929 (2008).

Time Dependent Meta Stable Vacua in M-theory

Makoto Tanabe[1(a)], and Ryo Wakebe[2(a)]

[(a)] *Department of Physics, Waseda University, Tokyo 169-8555*

Abstract

We study the time dependent solutions with intersecting M5-brane with non-trivial extra dimension in M-theroy. Conforming to the meta-stable intersecting brane solution in type IIA super string theory, we must smear the flat extra coordinate, and put in the monopole for M5-brane. Which solution preserves the 1/8 supersymmetries, and we can add the time dependence to this solution with dynamical supersymmetry breaking. After the breaking supersymmetries, we find the time-dependent NS5-brane and the extra D0-brane in type IIA string theory. However the scale factor proportional to minus fifth root of the cosmic time in Einstein flame, thus we must find another method to add the time-dependece in order to find the inflationary universe.

1 Supersymmetric Static Solution in M-theory

In this section we construct the static intersecting M-brane solution in M-theory, which solution can be expended to supersymmetric vacua given in [1, 2]. First we consider the action for M-theory is given by

$$S = \frac{1}{16\pi G_{11}} \int \left(\mathcal{R} * 1 - \frac{1}{2} F_4 \wedge * F_4 \right) , \tag{1}$$

where $F_4 = dC_3, D_4 = *F_7 = *dC_6$ and $\mathcal{R}$ is the Ricci scalar of spacetime metric $g_{\mu\nu}$. The equation of motion are written in as follow ; $\mathcal{R}_{\mu\nu} = \frac{1}{2}\left[F^2_{\mu\nu} - \frac{1}{3}F^2 g_{\mu\nu}\right]$, where $F^2_{\mu\nu} = F_{\mu\rho\sigma\lambda}F_\nu{}^{\rho\sigma\lambda}/3!$, and $F^2 = F_{\mu\nu\rho\sigma}F^{\mu\nu\rho\sigma}/4!$. We consider the configuration of intersecting M-brane as $M5 \perp M5 \perp M5$ case, then the metric ansatz are given by

$$\begin{aligned} ds^2 = (H_A H_B H_C)^{2/3} \Bigg[& (H_A H_B H_C)^{-1} \sum_{i=0}^{3} dx_i^2 + dr^2 + \sum_{\alpha=1}^{2} H_A^{-1} dy_\alpha^2 \\ & + \sum_{\rho=1}^{2} \left(\frac{H_B}{H_D}\right)^{-1} dz_\rho^2 + \left(\frac{H_C}{H_D}\right)^{-1} dw_\mu^2 + (H_C H_D)^{-1} d\tilde{w}_\nu^2 \Bigg] , \end{aligned} \tag{2}$$

where $d\tilde{w}^\nu = dw^\nu + A^\nu_\rho(z^\sigma)dz^\rho + A^\nu_\sigma(z^\rho)dz^\sigma$. The metric function H_A, H_B and H_C are only depend on the coordinate r, and $H_D = H_D(w, z)$. For simplicity we assume the constraint

$$\frac{\partial_a H_D}{H_D} = A^\nu_a \frac{\partial_\nu H_D}{H_D} = 0 , \quad \frac{1}{2}\partial_{[a} A^\nu_{b]} = \frac{H_C H_D}{H_B}\frac{\partial_\mu H_D}{H_D} \tag{3}$$

H_D must be depend on w^μ coordinate ($H_D = H_D(\mu)$) in the first equation. The last equation is equivalent to the Hodge dual in ten-dimensional compactified spacetime. The gauge ansatz $C_6 = C_A + C_B + C_C$ are given by

$$C_A = H_A^{-1}(r) dt \wedge dx^1 \wedge dx^2 \wedge dx^3 \wedge dy^1 \wedge dy^2 \tag{4}$$

$$C_B = H_B^{-1}(r) H_D(w^\mu) dt \wedge dx^1 \wedge dx^2 \wedge dx^3 \wedge dz^1 \wedge dz^2 \tag{5}$$

$$C_C = H_C^{-1}(r) dt \wedge dx^1 \wedge dx^2 \wedge dx^3 \wedge dw^\mu \wedge d\tilde{w}^\nu . \tag{6}$$

[1]Email address: tanabe@gravity.phys.waseda.ac.jp
[2]Email address: wakebe@gravity.phys.waseda.ac.jp

The Maxwell equation $dD_i = 0$ can be written in

$$\partial_r^2 H_A = \partial_r^2 H_B = \partial_r^2 H_C = 0\,. \tag{7}$$

The solution of the harmonic functions are given by $H_i = q_i + Q_i r$, and the rotating term is given by $A_\rho = Q_\rho z^\sigma$, $A_\sigma = Q_\sigma z^\rho$ and $H_D = q_D + Q_D w^\mu$.

The Killing spinor equation is consistent with the supersymmetric translation for gravitino, which is given by

$$\delta\psi_M = \left[\nabla_M + \frac{1}{4} e^{\tilde{a}}{}_M \omega_M{}^{\tilde{b}\tilde{c}} \Gamma_{\tilde{b}\tilde{c}} + \frac{1}{4!3!2!} e^{\tilde{a}}{}_M \left(\Gamma_{\tilde{a}}{}^{\tilde{b}\tilde{c}\tilde{d}\tilde{e}} - 8\delta_{\tilde{a}}^{\tilde{b}} \Gamma^{\tilde{c}\tilde{d}\tilde{e}}\right) F_{\tilde{b}\tilde{c}\tilde{d}\tilde{e}}\right] \zeta = 0\,. \tag{8}$$

In this below we skip tilde in flame space for simplicity. We can calculate Killing spinor equation with convenient expression of our metric ansatz (2). First we assume three spinor condition as $\Gamma^{z_1 z_2 w_1 w_2 r} = \Gamma^{y_1 y_2 w_1 w_2 r} = \Gamma^{y_1 y_2 z_1 z_2 r} = 1$, and these condition related M5-brane's chirarity as $\Gamma^{x_0 x_1 x_2 x_3 y_1 y_2} = \Gamma^{x_0 x_1 x_2 x_3 z_1 z_2} = \Gamma^{x_0 x_1 x_2 x_3 w_1 w_2} = -1$, which space-time coordinate occupied by each M5-branes. Thus this intersecting M-brane solution preserve 1/8 supersymmetries in eleven dimension. However we must put the extra condition for spinor ζ to satisfy the Killing spinor equation as

$$\zeta = (H_A H_B H_C)^{-1/12} \zeta_0\,, \tag{9}$$

and ζ_0 is the constant spinor. In this below, we use this metric and we can solve the equation of metric functions.

2 Time Dependent Solution

Adding the time-dependece to the static solution, there are two kind of solutions. In M-theory the four-form fields strength are only allowed. Thus we assume the time dependent solution without additional form field.

First we can add the linear time-coordinate function for the harmonic function H_A as $H_A = q_A t + Q_A r$, which solution are related to the Uzawa's solution [3]. Next we can add the time dependent function for the eleven dimensional monopole as $\mathcal{A} = A_\rho(z^\sigma) dz^\rho + A_\sigma(z^\rho) dz^\sigma + A_\mu(t) dw - u + A_t(w^\mu) dt$, and the new monopole condition $\partial_t A_\mu - \partial_\mu A_t = 0$ appears. The solution which satisfy the new monopole condition is linear function as $A_\mu = Q_\mu t$ and $A_t = Q_t w^\mu$. These two possible ways can be combine al together. Therefore we consider the solution with time-dependent harmonic function $H_A(t, r)$ and the time-dependent monopole function $\mathcal{A}(t, z^\rho, z^\sigma, w^\mu)$.

Now we compactify the w^ν direction with some conformal transformation, we find the intersecting time-dependent solution in type IIA super string theory, as

$$ds_{10}^2 = (H_A H_B) \left(\frac{H_C}{H_D}\right)^{1/2} \left[(H_A H_B H_C)^{-1} d\mathbf{x}^2 + dr^2 + H_A^{-1} d\mathbf{y}^2 + \left(\frac{H_B}{H_D}\right)^{-1} d\mathbf{z}^2 + \left(\frac{H_C}{H_D}\right)^{-1} dw_\mu^2\right]$$

$$\phi = \frac{3}{4} \log(H_A H_B H_C)^{2/3} (H_C H_D)^{-1} \tag{10}$$

$$\mathcal{A} = A_t dt + A_\mu dw^\mu + *\left(\log H_D d\mathbf{x} \wedge d\mathbf{y} \wedge dr\right) \tag{11}$$

$$\mathcal{B} = \frac{3}{2} * \left(H_A^{-1} d\mathbf{x} \wedge d\mathbf{y} + H_B^{-1} H_D d\mathbf{x} \wedge d\mathbf{z}\right) \tag{12}$$

$$\mathcal{C} = * \left(H_C^{-1} d\mathbf{x} \wedge dw^\mu\right)\,. \tag{13}$$

In type IIA theory, this solution are related to the intersecting D-brane system as NS5-NS5-D0-D4-D6 system. Because of the time-dependence of the monopole, an extra D0-brane is added in the ordinary model given by [2]. In the view of the four dimensional Einstein flame, the scale factor is proportional to $a(t) \sim t^{-5}$. This solutions are not suitable for the cosmological solution, therefore we must find the another method to make a time dependent solution which gives accelerating universe solution.

References

[1] K. A. Intriligator, N. Seiberg and D. Shih, gDynamical SUSY breaking in meta-stable vacua,h JHEP 0604, 021 (2006) [arXiv:hep-th/0602239].

[2] H. Ooguri and Y. Ookouchi, gMeta-stable supersymmetry breaking vacua on intersecting branes,h Phys. Lett. B 641, 323 (2006) [arXiv:hep-th/0607183].

[3] K. Maeda, N. Ohta, K. Uzawa, "Dynamics of intersecting brane systems – Classification and their applications –," JHEP 0906:051,2009 [arXiv:0903.5483[hep-th]].

The final fate of instability of Reissner-Nordström-AdS black holes

Jun-ichirou Koga[1](a), Kengo Maeda[2](b) and Shunsuke Fujii[3](c)

(a) *Research Institute for Science and Engineering, Waseda University, Shinjuku, Tokyo 169-8555*
(b) *Faculty of Engineering, Shibaura Institute of Technology, Saitama, 330-8570*
(c) *Iwate Prefectural Morioka First High School, Iwate, 020-8515*

Abstract

We investigate dynamical and thermodynamical instability of the 4-d Reissner–Nordström–anti de–Sitter (RN-AdS) black holes. In accordance with the holographic model of superconductor, we find, by computing the quasi-normal mode, that the RN-AdS black holes are unstable below the critical temperature. We also calculate the difference of the entropy between the RN-AdS black hole and the hairy black hole that emerges below the critical temperature. It is shown that the hairy black hole carries larger entropy than the RN-AdS black hole in the micro-canonical ensemble, which implies that the RN-AdS black holes evolve towards the hairy black holes, due to the instability.

1 Introduction

Based on AdS/CFT correspondence, the simplest model of holographic superconductor [1] has been constructed in the theory described by the bulk action

$$S = \int \sqrt{-g}\, d^4x \left[R + \frac{6}{L^2} - \frac{F^{ab}F_{ab}}{4} - m^2|\psi|^2 - (\bar{D}^a\bar{\psi})(D_a\psi) \right], \tag{1}$$

where L is the scale of the cosmological constant, $D_a = \nabla_a - iqA_a$, and m and q are the mass and the charge of the scalar field ψ, respectively. (See for reviews [2–4]). In this model, we have the RN-AdS black hole as the unique solution in the bulk when the temperature of the black hole is high enough, which corresponds to the normal state in the boundary field theory. However, at some critical temperature T_c, there emerges the so-called marginally stable solution [5], which is a black hole solution with a tiny scalar hair, and it is argued that the emergence of this solution signals instability of the RN-AdS black holes below T_c, implying phase transition at T_c. Although this argument of instability seems natural, it has not been explicitly shown so far whether the RN-AdS black holes are really unstable below T_c, and whether they evolve, due to this instability, towards black holes with the scalar hair, which correspond to the superconducting state in the holographic superconductor.

In order to clarify the dynamical and thermodynamical aspects of this instability of the RN-AdS black hole, we computed [6] the quasi-normal mode on the background of the RN-AdS black hole, and the difference of the entropy between the RN-AdS black hole and the hairy black hole in the micro-canonical ensemble near T_c. We will describe here the primary analyses and results presented in [6].

2 Quasi-normal modes

We first analyze the quasi-normal mode of the scalar filed ψ on the 4-d RN-AdS black hole background near T_c. The metric and the gauge potential of this black hole are given by

$$ds^2 = -f(r)dt^2 + \frac{dr^2}{f(r)} + r^2 d\Omega_2^2, \qquad A_\mu dx^\mu = \Phi(r)dt = \rho\left(\frac{1}{r_+} - \frac{1}{r}\right)dt, \tag{2}$$

[1]Email address: koga@waseda.jp
[2]Email address: maeda302@sic.shibaura-it.ac.jp
[3]Email address: fujii@th.phys.titech.ac.jp

where $f(r) = k - 2M/r + \rho^2/4r^2 + r^2/L^2$, k is the curvature of the 2-d Einstein subspace, and M, ρ, and r_+ are the mass, the charge, and the horizon radius of the black hole, respectively. The holographic model of superconductor has a planar horizon, and hence $k = 0$ in this case. Although we considered in [6] all the cases of k, we thus focus here on the case of $k = 0$.

The boundary condition for the quasi-normal mode of the scalar field ψ is imposed such that ψ is purely in-going near the horizon. By writing as

$$\psi = e^{-i\omega t}\,(1-u)^{-i\omega/2\kappa}\,\Psi(u), \tag{3}$$

where u is the new radial coordinate defined by $u \equiv r_+/r$ and κ is the surface gravity, this boundary condition is found to require that the new variable $\Psi(u)$ is regular on the horizon. On the other hand, we impose the Dirichlet boundary condition $\psi \to 0$ at infinity. Then, the scalar field equation derived from Eq. (1) yields the asymptotic form of $\Psi(u)$ as $\Psi(u) \to u^{\Delta_+}$, where $\Delta_+ \equiv 3/2 + \sqrt{9/4 + m^2L^2}$.

We now consider the perturbation *of* the RN-AdS black hole near T_c. We perturb the horizon radius r_+, the surface gravity κ, the metric function $f(u)$, and the gauge field $\Phi(u)$ (the latter two now being considered as functions of u), as

$$r_+ = r_c + \delta r_+, \qquad \kappa = \kappa_c + \delta\kappa, \qquad f(u) = f_c(u) + \delta f(u), \qquad \Phi(u) = \Phi_c(u) + \delta\Phi(u), \tag{4}$$

where the subscript c stands for quantities at T_c. We also note that the quasi-normal frequency ω approaches zero when $T = \kappa/2\pi \to T_c$, according to the critical slowing down [7]. Since we have the marginally stable solution $\Psi_0(u)$ at T_c, we can write $\Psi(u)$ as

$$\Psi(u) = \Psi_0(u) + \omega\Psi_1(u), \tag{5}$$

where it is understood that ω is also small near T_c. Then, the leading and the next-to-leading order terms of the scalar field equation derived from Eq. (1) are written as

$$\mathcal{D}\,\Psi_0(u) = 0, \qquad \omega\,\mathcal{D}\,\Psi_1(u) = j_1(u) + \omega\, j_2(u), \tag{6}$$

where $\mathcal{D}$ is a Sturm-Liouville differential operator, and the source terms (the right-hand side) in the second equation are divided into those which do not depend on ω (the first term) and those which are linear in ω (the second term). Under the boundary condition we imposed above, the differential operator $\mathcal{D}$ is shown to be Hermitian. Thus, by considering the inner product of $\omega\,\mathcal{D}\,\Psi_1(u)$ and $\Psi_0(u)$, and employing Eq. (6), we obtain

$$\omega = -\left(\int_0^1 j_1(u)\,\Psi_0(u)\,du\right) \Big/ \left(\int_0^1 j_2(u)\,\Psi_0(u)\,du\right). \tag{7}$$

In order to evaluate the frequency of the quasi-normal mode, we substitute the numerical solution of $\Psi_0(u)$ into Eq. (7), and perform the integration in Eq. (7) numerically. The imaginary part ω_I of (7) for $\rho L = 60$, normalized by $-r_c^2/\delta r_+$, is shown in the left panel of Figure 1. We see that $\omega_I < 0$ for $\delta r_+ > 0$, and $\omega_I > 0$ for $\delta r_+ < 0$. Since we have $\delta r_+(T - T_c) > 0$ for ρ fixed, we see that the RN-AdS black holes with $T > T_c$ are dynamically stable, while those with $T < T_c$ are dynamically unstable.

3 Entropy

Now we consider the perturbative solution of the hairy black hole near T_c, and compare its entropy with that of the RN-AdS black hole in the micro-canonical ensemble. To do so, we take the ansatz

$$ds^2 = -g(y)d\tau^2 + \frac{dy^2}{g(y)} + R^2(y)d\Omega_2^2, \qquad A_\mu dx^\mu = \phi(y)d\tau, \qquad \psi = \psi(y), \tag{8}$$

where the radial coordinate y is related to r as $y = r/r_c$ for the background RN-AdS solution at T_c, and we consider the perturbation of these field variables near T_c as

$$\psi(y) = \epsilon^{1/2}\psi_1(y) + \cdots,\ g(y) = g_c(y) + \epsilon g_1(y) + \cdots,\ R(y) = r_c y + \epsilon R_1(y) + \cdots,\ \phi(y) = \phi_c(y) + \epsilon\phi_1(y) + \cdots,$$

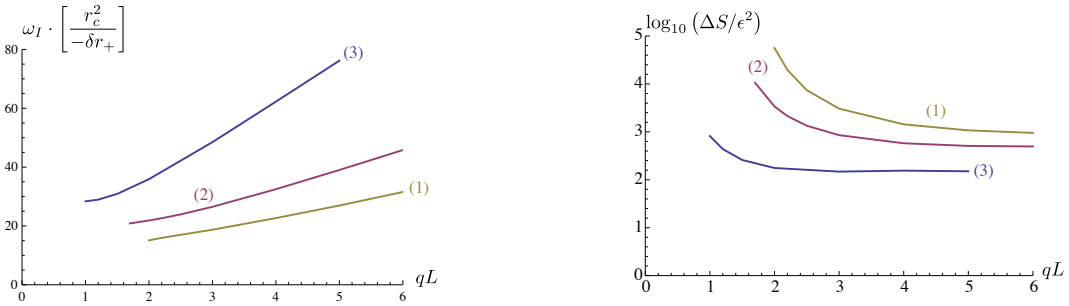

Figure 1: The imaginary part ω_I of the quasi-normal frequency is shown in the left panel, and the difference of the entropy ΔS is shown in the right panel, for $k = 0$ and $\rho L = 60$. The line (1) represents the result for $m^2L^2 = 7/4$, the line (2) for $m^2L^2 = 0$, and the line (3) for $m^2L^2 = -2$.

as well as the perturbation of the temperature T as

$$T = T_c + \epsilon T_1 + \cdots , \tag{9}$$

where the subscript c stands for quantities at T_c. Thus, the small parameter ϵ measures the deviation from the phase transition point ($T = T_c$). The field equations derived from Eq. (1) are then written in terms of the perturbed variables as

$$\frac{\left(y^2 g_c \psi_1'\right)'}{y^2} = \left(m^2 - \frac{q^2\phi_c^2}{g_c}\right)\psi_1, \ \frac{\left(y^2\phi_1'\right)'}{y^2} = \frac{2q^2\phi_c\psi_1^2}{g_c} - \frac{2}{r_c}\left(\frac{R_1'}{y} - \frac{R_1}{y^2}\right)\phi_c', \ R_1'' = -\frac{r_c y}{2}\left(\frac{q^2\phi_c^2\psi_1^2}{g_c^2} + \psi_1'^2\right),$$
$$\frac{(yg_1)'}{y^2} = -\frac{1}{2}\phi_c'\phi_1' - \frac{m^2}{2}\psi_1^2 + \frac{1}{2}g_c\psi_1'^2 + \frac{q^2}{2g_c}\phi_c^2\psi_1^2 - \frac{1}{r_c}\left(g_c' + \frac{2g_c}{y}\right)\left(\frac{R_1'}{y} - \frac{R_1}{y^2}\right)g_c' - \frac{2kR_1}{r_c^3 y^3}.$$

From these forms of the field equations, we see that once we have the solution of ψ_1 at hand, other perturbed field variables are given by quadratures, and hence integration constants in those quadratures are determined from the asymptotic behavior of these variables. Since we are concerned here with the micro-canonical ensemble, we require that these variables behave asymptotically such that the mass M and the charge ρ of the hairy black hole ($\psi_1 \neq 0$) are the same as those of the RN-AdS black hole ($\psi_1 = 0$) not only at T_c but also away from T_c. In what follows, we shall fix the charge ρ of the black hole, and set ϵ in terms of the mass M as

$$\epsilon = \frac{M_c - M}{M_c}, \tag{10}$$

where M_c is the mass at T_c.

Then, we apply the first law of black hole thermodynamics with $\rho = \text{const.}$, i.e., $\delta S = \delta M/T$, in order to obtain the entropies of the hairy black hole and the RN-AdS black hole. By using Eqs. (9) and (10), and integrating the first law, we obtain

$$S(\epsilon) = S_c - \int_0^\epsilon \frac{M_c}{T} d\epsilon = S_c - \frac{M_c}{T_c}\epsilon + \frac{1}{2}\frac{M_c T_1}{T_c^2}\epsilon^2 + \cdots , \tag{11}$$

where $S(\epsilon)$ is the entropy of the black hole with the mass M defined by Eq. (10) in terms of ϵ, and S_c is the entropy at T_c. Note that the hairy black hole and the RN-AdS black hole with the same M have the same value of ϵ. Therefore, the difference $\Delta S \equiv S_{\text{hairy}} - S_{\text{RNAdS}}$ between the entropy S_{hairy} of the hairy black hole and S_{RNAdS} of the RN-AdS black hole arises at order of ϵ^2 as

$$\Delta S = \frac{1}{2}\frac{M_c \Delta T_1}{T_c^2}\epsilon^2, \tag{12}$$

where ΔT_1 is the difference of the temperature perturbation T_1 between the hairy and the RN-AdS black holes, which is expressed as

$$\frac{\Delta T_1}{T_c} = \frac{\psi_1^2(1)}{4} + \frac{1}{2}\int_1^\infty \left(\frac{y g_c' \psi_1'}{g_c} - \frac{m^2\psi_1}{g_c}\right)\psi_1 dy + \frac{1}{L^2 g_c'(1)}\int_1^\infty \frac{y(y-1)}{g_c}\left(\frac{kL^2}{r_c^2} + 3 + y(2+y)\right)\frac{q^2\phi_c^2\psi_1^2}{g_c} dy.$$

The behavior of ΔS for $\rho L = 60$, normalized by ϵ^2, is shown in the right panel of Figure 1. We see that the entropy of the hairy black hole is larger than that of the RN-AdS black hole.

4 Conclusion and discussion

We first investigated the quasi-normal mode of the scalar field on the background of the RN-AdS black hole. We found that the imaginary part of the quasi-normal mode frequency changes its sign at T_c, and it is positive when the temperature of the black hole is smaller than T_c, which indicates that the RN-AdS black holes are dynamically unstable below T_c. We also found that the hairy black hole with the same mass and charge as the RN-AdS black hole possesses larger entropy than the RN-AdS black hole. These results support the scenario underlying the holographic model of superconductor, where the phase transition is expected to occur at T_c, and the RN-AdS black holes below T_c evolve towards the hairy

black holes. Although we presented here the numerical results only for the case where the 2-d Einstein subspace has planar symmetry ($k = 0$), the same instability has been found [6] to occur also in the cases of $k = 1$ and $k = -1$, i.e., without depending on the topology of the 2-d Einstein subspace.

It is worthwhile mentioning the aspect of this instability from the viewpoint of the bulk spacetime. The electric charge flux $\mathcal{F}$ through the horizon due to the instability and the charge density σ outside the hairy black hole are computed near T_c as

$$\mathcal{F} \equiv j_a k^a|_{r=r_c} = 4\,\omega_I \rho\, q^2 e^{2\omega_I t} \int_0^1 \frac{(1-u)\Psi_0^2(u)}{u^4 f_c(u)} du, \qquad \sigma \equiv j_a n^a = 2\,\epsilon\,\rho\, q^2 \frac{(1-y^{-1})}{r_c^2\sqrt{g_c(y)}} \psi_1^2(y), \tag{13}$$

where j_a is the electric current density carried by the scalar field, k^a is the future-directed null Killing vector tangent to the horizon, and n^a is the past-directed unit normal to the $\tau =$ const. hypersurface. We thus see that both $\mathcal{F}$ and σ have the same sign as ρ below T_c, which implies that the charge of the same sign as the black hole charge ρ has been extracted from the black hole. We also note that the energy-momentum tensor of the scalar field alone is *not* conserved, because it is interacting with the gauge field, as well as gravity. Although we fixed the gauge field as the background in deriving the quasi-normal mode, the back reaction of the scalar field onto the gauge field, which is at higher order in the present perturbation analysis, transfers energy of the gauge field to the scalar field. Thus, the scalar field gains energy from the gauge field, and drops into the black hole the electric charge of the sign opposite to that of the black hole.

References

[1] S. A. Hartnoll, C. P. Herzog, and G. T. Horowitz, J. High Energy Phys. **12**, 015 (2008).

[2] S. A. Hartnoll, Class. Quantum Grav. **26**, 224002 (2009).

[3] C. P. Herzog, J. Phys. A **42**, 343001 (2009).

[4] G. T. Horowitz, arXiv:1002.1722 [hep-th].

[5] S.S. Gubser, Phys. Rev. D **78**, 065034 (2008).

[6] K. Maeda, S. Fujii, and J. Koga Phys. Rev. D **81**, 124020 (2010).

[7] K. Maeda, M. Natsuume, and T. Okamura, Phys. Rev. D **78**, 106007 (2008); Phys. Rev. D **79**, 126004 (2009).

Infrared divergence and the gauge-invariant initial vacuum

Yuko Urakawa[1(a)], and Takahiro Tanaka[2(b)]

(a) *Department of Physics, Waseda University, Ohkubo 3-4-1, Shinjuku, Tokyo 169-8555, Japan*
(b) *Yukawa Institute, Kyoto University, Kyoto 606-8502*

Abstract

It has been an issue of debate whether the inflationary infrared(IR) divergences are physical or not. Our claim is that, at least, in single-field models, the answer is "No," and that the spurious IR divergence is originating from the careless treatment of the gauge modes. In our previous work we have explicitly shown that the IR divergence is absent in the genuine gauge-invariant quantity at the leading order in the slow-roll approximation. We extend our argument to include higher-order slow-roll corrections and the contributions from the gravitational waves. The key issue is to assure the gauge invariance in the choice of the initial vacuum, which is a new concept that has not been considered in conventional calculations.

1 Introduction

The precise measurements of the primordial fluctuation provide us with valuable information of the early universe. It is widely accepted that the primordial fluctuation originates from the quantum fluctuation of the inflaton field. In the last decades, it has been recognized that the perturbation theory in the inflationary universe might break down because of the infrared(IR) divergence from loop corrections. (For a recent review, see Ref. [1].) During inflation, massless fields are known to yield the scale invariant spectrum $P(k) \propto 1/k^3$ at linear order. These fields contribute to the one-loop diagram with the four point interaction as $\int \mathrm{d}^3k/k^3$, which leads to the logarithmic divergence.

It has been an issue of debate whether the IR divergences are physical or not. If it were really physical, there might be a possibility that loop corrections are observable. The possibility of secular growth of IR contributions has also been studied motivated as a possible explanation of the smallness of the cosmological constant. However, before we discuss implications of the IR effects, we need to carefully examine whether the reported IR divergences are not due to careless treatment. In our previous work [2], we pointed out the presence of gauge degrees of freedom in the frequently used gauges such as the comoving gauge and the flat gauge, and these gauge degrees of freedom are responsible for the IR divergences. There, we have shown that, if we fix the residual gauge degrees of freedom, the IR divergences automatically disappear in the single field model. (Multi-field case was discussed in a separate paper [3].)

In this paper, we reexamine our previous argument. If the IR divergences are really due to the residual gauge degrees of freedom, those divergences should disappear if we evaluate genuine gauge-invariant quantities even though we do not fix the residual gauge. Hence, the demonstration of the genuine gauge-invariance of computed results would be necessary to obtain reliable predictions, which are to be compared with observations. In this brief report we demonstrate more explicitly that the IR divergence in the curvature perturbation can be removed by looking at such genuine gauge-invariant quantities. In doing so, we shall notice that the choice of initial vacuum state is restricted. At the leading order in the slow-roll approximation, we find that a natural vacuum state is surprisingly limited to the Bunch-Davies vacuum state as far as we consider Gaussian vacuum state for the inflaton perturbation in the flat slicing at the initial time. We consider the single field inflation model whose action takes the form

$$S = \frac{M_{\rm pl}^2}{2} \int \sqrt{-g}\, [R - g^{\mu\nu}\phi_{,\mu}\phi_{,\nu} - 2V(\phi)]\mathrm{d}^4x \ , \tag{1}$$

where $M_{\rm pl}$ is the Planck mass and the scalar field Φ was rescaled so as to be non-dimensional.

[1]Email address: yuko@gravity.phys.waseda.ac.jp
[2]Email address: tanaka@yukawa.kyoto-u.ac.jp

2 Construction of gauge-invariant variables

In this section, we construct an example of genuine gauge-invariant quantities. Since the temporal slicing is already fixed, it is sufficient to address the gauge-invariance under the residual gauge transformation of the spatial coordinates. Genuine gauge-invariance is equivalent to complete gauge fixing. In this sense, if we give appropriate boundary conditions for the lapse and shift, the residual gauge degrees of freedom can be completely fixed. However, here arises a difficulty in fixing the gauge, if we wish to remove all arbitrariness regarding the choice of coordinates, such as the choice of the local region $\mathcal{O}$.

When we consider the universe with infinite volume, the conventional gauge-invariant perturbation theory is formulated using particular combinations of perturbed variables invariant under an arbitrary gauge transformation. The construction of such gauge-invariant variables is possible thanks to the absence of the ambiguity in the inverse Laplacian under the assumption that the perturbations remain finite at the spatial infinity. However, the same procedure does not work when we try to use only the information contained in the limited area $\mathcal{O}$. Under this restriction, genuine gauge-invariant quantities cannot be constructed by the combination of local quantities.

Keeping these in mind, as one example of the calculable genuine gauge-invariant variables, we consider n-point functions of the scalar curvature ${}^sR$, which we think is the easiest to evaluate. The scalar curvature ${}^sR$ does not remain invariant but transforms as a scalar quantity under the change of spatial coordinates. If we could specify its n arguments in a coordinate-independent manner, the n-point functions of the scalar quantity would be gauge-invariant. This can be partly achieved by specifying the n spatial points by the geodesic distances and the directional cosines from one reference point. Although we cannot specify the reference point in a coordinate independent manner, this remaining gauge dependence would not matter as long as we are interested in the correlation functions for a quantum state that respects the spatial homogeneity and isotropy of the universe.

As an example, we consider the two point function of ${}^sR$, whose arguments X^i_A $(A = 1, 2)$ are specified by solving the three-dimensional geodesic equation from $\lambda = 0$ to 1 with the initial "velocity" given by $\mathrm{d}x^i(\mathbf{X}, \lambda)/\mathrm{d}\lambda|_{\lambda=0} = e^i_{(j)}X^{(j)}$, where $e^i_{(j)}$ is an orthonormal triad basis at the reference point. We identify a point in the geodesic normal coordinates $X^{(i)}$ with the end point of the geodesic $x^i(\mathbf{X}, \lambda = 1)$. Noticing that, in the absence of the fluctuations, x^i coincides with the value of $X^{(i)}$, we expand $x^i(\mathbf{X})$ as $x^i(\mathbf{X}) := X^i + \delta x^i(\mathbf{X})$. Then, the expectation value of a product of

$$ {}^gR(\eta, \mathbf{X}) := {}^sR\left(\eta, \mathbf{X} + \delta\mathbf{x}(\mathbf{X})\right) = \sum_{n=0}^{\infty} \frac{\delta x^{i_1} \cdots \delta x^{i_n}}{n!} \partial_{i_1} \cdots \partial_{i_n} {}^sR(\eta, x^i)|_{x^i = X^i}, \tag{2} $$

should be surely gauge-invariant, unless the initial state fails to be gauge invariant.

3 IR regularity of genuine gauge-invariants

The genuine gauge-invariant quantities that we introduced should be finite in the local gauge, since the field itself is constructed to be free from IR divergence in this gauge by construction. However, since these quantities are really gauge-invariant, they should be finite even if we send the size of $\mathcal{O}$ to infinity. This limit is supposed to agree with the case when we calculate them in the infinite volume. In the rest of this paper we study the regularity of the gauge-invariant two point function introduced above in the conventional global gauge [4], focusing on the loop of longitudinal modes at the lowest order in the slow-roll approximation. Here we give only the outline of the calculation, deferring the detailed description to Ref. [5, 6]. We expand the gauge-invariant spatial curvature as ${}^sR = {}^gR_1 + {}^gR_2 + \cdots$, in terms of the interaction picture field operator. Here the subscript denotes the number of the contained interaction picture field operators. Then, one-loop contribution to the two point function starts with the quartic order,

$$ \langle {}^gR {}^gR \rangle_4 := \langle {}^gR_1 {}^gR_3 \rangle + \langle {}^gR_2 {}^gR_2 \rangle + \langle {}^gR_3 {}^gR_1 \rangle \ . \tag{3} $$

Using the fact that the IR divergence arises only from the contraction between interaction picture fields $\psi := \zeta_1$ without any derivative, we keep only the terms that are possibly divergent[3]. For instance, the terms that include more than two ψs with spatial or temporal derivatives do not yield divergences. (A more detailed explanation is presented in Sec.III of Ref. [6].) Hereafter, we denote an equality which is valid only when we neglect the terms irrelevant to IR divergences or higher order in the slow-roll approximation by "$\overset{\rm IR}{\approx}$". Then, abbreviating the unimportant pre-factor -2, we simply denote the scalar curvature ${}^sR$ as

$$ {}^sR \overset{\rm IR}{\approx} e^{-2\zeta}\partial^2\zeta \,. \tag{4}$$

In order to obtain the expression for ${}^sR$, we use the fact that in the flat slicing the interaction Hamiltonian is totally suppressed by the slow roll parameter [4]. We therefore solve the non-linear evolution of perturbation in the flat gauge, and transform the results into the $\delta\phi = 0$ gauge. Then, the contributions at the lowest order in slow-roll expansion to ζ arises only from the non-trivial gauge transformation given by [4]

$$ \zeta \overset{\rm IR}{\approx} \zeta_n + \zeta_n\partial_\rho\zeta_n + \frac{1}{2}\zeta_n^2\partial_\rho^2\zeta_n, \tag{5}$$

where $\zeta_n := -\rho'\varphi/\phi'$. Here φ is the inflaton perturbation in the flat gauge.

Solving the spatial geodesic equation on a η =constant hypersurface, we obtain $x^i \overset{\rm IR}{\approx} e^{-\zeta}X^i$, that is perturbed as

$$ \delta x^i \overset{\rm IR}{\approx} -(\psi+\zeta_2)X^i + \psi^2 X^i/2 \,. \tag{6}$$

Using Eqs. (4)-(6), the gauge-invariant scalar curvature is given by the following compact expressions:

$$\begin{aligned} &{}^gR_1(X) = \partial^2\psi|_{x^i=X^i},\ {}^gR_2(X) \overset{\rm IR}{\approx} \psi\partial^2(\partial_\rho - x^i\partial_i)\psi|_{x^i=X^i}, \\ &{}^gR_3(X) \overset{\rm IR}{\approx} \frac{1}{2}\psi^2\partial^2(\partial_\rho - x^i\partial_i)^2\psi|_{x^i=X^i}, \end{aligned} \tag{7}$$

where we defined $X := (\eta, \mathbf{X})$. Here we note that, for the Bunch-Davies vacuum, the positive frequency function of ψ satisfies

$$ (\partial_\rho - \mathbf{X}\cdot\partial_{\mathbf{X}})\psi_{\mathbf{k}} = -D_k\psi_{\mathbf{k}}, \quad D_k := \partial_{\log k} + 3/2 \tag{8}$$

Using Eqs. (6) and (8), the possibly divergent terms in $\langle {}^gR{}^gR\rangle_4$ can be summed up as

$$ \langle\{{}^gR(X_1),\, {}^gR(X_2)\}\rangle_4 \overset{\rm IR}{\approx} \frac{1}{2}\langle\psi^2\rangle\int\frac{{\rm d}(\log k)}{2\pi^2}\Big[\partial^2_{\log k}\left\{k^7\psi_{\mathbf{k}}(X_1)\psi^*_{\mathbf{k}}(X_2)\right\} + ({\rm c.c.})\Big], \tag{9}$$

where we symmetrized about X_1 and X_2. Since $\langle\psi^2\rangle$ is IR divergent, the regularity is maintained only when the integral in Eq. (9) vanishes exactly. This is actually realized, because thanks to the condition (8), this integral becomes total derivative. The usage of the invariant distance is requested also in Ref. [7], where the δN formalism is utilized. It is intriguing that, while the method is different, they have arrived at the same conclusion as we obtained.

4 Conclusion

In the global gauge that we used in this paper, the Hilbert space has not been reduced to the one composed only of the physical degrees of freedom and a part of gauge degrees of freedom are left unfixed. These residual gauge degrees of freedom include the overall spatial scale transformation corresponding to a constant shift of ζ in the $\delta\phi = 0$ gauge, which is the origin of the IR divergences. To remove IR divergences, hence, we had to impose the invariance of quantum states in the direction of this residual

[3]Here, the IR divergence means the appearance of the factor $\langle\psi^2\rangle$, although this factor is not necessarily divergent if the spectrum is bluer than the scale invariant one. Even in this case, the amplitude of $\langle\psi^2\rangle$ can suffer from a large amplification due to IR contributions compared with the amplitude of the linear spectrum.

gauge, which requests additional gauge invariance conditions. As we have seen above, at the lowest order of slow roll approximation, thanks to its scale-invariant property, the Bunch-Davies vacuum state provides the gauge-invariant initial vacuum. If we do not choose this vacuum, the quantum state is not invariant under the residual gauge transformation, and hence the two-point function fails to be regular.

We should note that at the higher order in the slow-roll approximation, the Bunch-Davies vacuum no longer yields the gauge-invariant initial state. We need to extend the condition (8) that guarantees the gauge-invariance of the quantum state, to include the slow-roll corrections. This extension is addressed in Ref. [6]. In this brief report, we have also neglected the transverse traceless metric perturbation, which can participate in the IR divergence. In Ref. [6], we also showed that the loop corrections from the graviton field are also regularized in the n-point functions of the gauge-invariant spatial curvature ${}^{g}R$. In this paper, we considered the single scalar field with the canonical kinetic term, but our argument can be extended to other single field models of inflation.

The way of quantization here in the global gauge is quiet different from that in the local gauge [2]. In the local gauge, we removed the residual gauge degrees of freedom that are associated with IR divergences by adapting additional gauge conditions. The IR regularity is then ensured without restricting the initial quantum state. This provides another way of quantization that also yields no artificial divergences. The relation between these two ways of quantization is far from trivial, because the global gauge and the local gauge is connected by a non-linear gauge transformation. (See also Sec. V of Ref. [6].)

References

[1] D. Seery, Class. Quantum Phys. **27**, 124005 (2010) [arXiv:1005.1649 [astro-ph.CO]].

[2] Y. Urakawa and T. Tanaka, Prog. Theor. Phys. **122**, 779 (2009) [arXiv:0902.3209 [hep-th]].

[3] Y. Urakawa and T. Tanaka, Prog. Theor. Phys. **122**, 1207 (2010) [arXiv:0904.4415 [hep-th]].

[4] J. M. Maldacena, JHEP **0305**, 013 (2003) [arXiv:astro-ph/0210603].

[5] Y. Urakawa and T. Tanaka, Phys. Rev. D **82**, 121301 (2010) [arXiv:1007.0468 [hep-th]].

[6] Y. Urakawa and T. Tanaka, arXiv:1009.2947 [hep-th].

[7] C. T. Byrnes, M. Gerstenlauer, A. Hebecker, S. Nurmi and G. Tasinato, arXiv:1005.3307 [hep-th].

Magnetized binary black holes and neutron stars in equiliblium

Kōji Uryū[1(a)], Eric Gourgoulhon[2(b)], and Charalampos Markakis[3(c)],

[(a)] *Department of Physics, University of the Ryukyus, Senbaru, Nishihara, Okinawa 903-0213, Japan*
[(b)] *Laboratoire Univers et Théories, UMR 8102 du CNRS, Observatoire de Paris, Université Paris Diderot, F-92190 Meudon, France*
[(c)] *Department of Physics, University of Wisconsin-Milwaukee, P.O. Box 413, Milwaukee, WI 53201*

Abstract

For helically symmetric Einstein-Maxwell spacetimes with magnetized perfect fluids, generalized thermodynamic laws – the zeroth law, the constancy of surface gravity and electric potential, and the first law, a variation formula for the Noether charge Q associated with a helical Killing vector – are derived. Applying Bekenstein and Oron's theory of ideal magnetohydrodynamics (MHD), the first law is written as $\delta Q = 0$ for a sequence of equilibrium solutions that models adiabatic binary inspiral due to gravitational wave emission. We introduce a possible formulation for computing such magnetized binary neutron stars and black holes in close circular orbits in quasi-equilibriums, and a project to develop computer code for such magnetized compact objects the Cocal code – Compact Object CALculator.

1 Introduction

A uniformly rotating neutron star is significantly deformed when the ratio of kinetic energy T to gravitational energy W becomes $T/|W| \sim 0.1$. When the averaged magnetic field energy, $\mathcal{M}$, becomes $\mathcal{M}/|W| \sim 0.01$, the contribution of the magnetic field to the structure of the neutron srar may not be neglected. This is estimated to occur for $B \gtrsim 10^{16}$[G]. Recent observations of anomalous X-ray pulsars, or soft γ-ray repeaters suggest that the neutron stars in these systems may be associated with strong magnetic fields around 10^{14} – 10^{15} G at the surface (see, e.g. [1]). We may expect that the interior magnetic field of such a strongly magnetized neutron star, a magnetar, is highly anisotropic, hence it is a few orders of magnitudes larger.

Such strong magnetic fields have not been found in binary neutron star systems. Moreover, in such old systems initial magnetic fields may decay during the long evolutional time to become inspiraling binary compact objects just before the merger. Hypothetically, however, strongly magnetized neutron stars or black holes may form binary neutron star or black hole - neutron star systems. For instance, the poloidal field seen as the surface magnetic field decays but the toroidal field stays strong enough to affect the structure of the compact objects.

In several numerical relativity simulations of magnetized binary neutron stars, it has been shown that, after binary inspiral and merger, the magnetic fields are amplified around 10 times by magnetic winding and the magnetorotational instability in post-merger, pre-collapse objects [2]. Such an object is likely to form a black hole and a magnetized toroid system, which becomes the source of a short γ-ray burst. It is desirable to prepare realistic initial data sets for such merger simulations calculated by solving the Einstein-Maxwell equations and a first integral of the MHD-Euler equation, assuming (quasi-)equilibrium. In this article, we model such magnetized binary compact objects in close circular orbits, assuming that the spacetime and magnetic fields satisfy helical symmetry and that the stars are in equilibrium [3–5]. In Sec. 2, we review the generalized thermodynamic laws and in Sec. 3 a formulation for computing such binary equilibriums. Derivations of these are detailed in [6] (hereafter FUS), and [7] (UGM).

[1]Email address: uryu@sci.u-ryukyu.ac.jp
[2]Email address: eric.gourgoulhon@obspm.fr
[3]Email address: markakis@uwm.edu

2 Generalized thermodynamic laws for charged and magnetized compact objects

2.1 Zeroth law

We consider a globally hyperbolic spacetime $(\mathcal{M}, g_{\alpha\beta})$. The field k^α is transverse to each Cauchy surface, not necessarily timelike everywhere, and generates a one-parameter family of diffeomorphisms χ_t. The action of χ_t on a spacelike sphere $\mathcal{S}$ on a Cauchy surface generates a timelike surface, $\mathcal{T}(\mathcal{S}) = \cup_t \chi_t(\mathcal{S})$, called the *history of* $\mathcal{S}$. Then, k^α is a *helical vector* field if there is a smallest $T > 0$ for which P and $\chi_T(P)$ are timelike separated for every point P outside of the history $\mathcal{T}(\mathcal{S})$. A vector k^α written as $k^\alpha = t^\alpha + \Omega\phi^\alpha$ is the helical vector, where t^α is a timelike vector and ϕ^α a spacelike vector that has circular orbits with a parameter length 2π (see, FUS).

Each Cauchy surface of a helically symmetric spacetime does not admit flat asymptotics. Therefore, the future (past) horizon $\mathcal{H}^\pm$ is defined as the boundary of the future(past) domain of outer communication $\mathcal{D}^\pm$ of a history $\mathcal{T}(\mathcal{S})$ of each spacelike sphere $\mathcal{S}$. If the history $\mathcal{T}(\mathcal{S})$ of a sphere $\mathcal{S}$ is in $\mathcal{D}^\pm$, the future (past) horizon agrees with the chronological past (future) of the history $\mathcal{T}$, $\mathcal{H}^\pm = \partial I^\mp(\mathcal{T})$.

The existence of a global helical symmetry assures that the horizon is a Killing horizon. With the null energy condition $R_{\alpha\beta}l^\alpha l^\beta \geq 0$ for any null vector l^α, the surface gravity κ defined on each connected component of the horizon $\mathcal{H}^\pm$ by

$$k^\beta \nabla_\beta k^\alpha \;=\; \kappa k^\alpha \tag{1}$$

is constant. The proof is given in FUS, in which conditions of theorems by Friedrich, Rácz, and Wald [8] are modified to make them suitable for helically symmetric spacetimes. Also the electric potential $\Phi^{\rm E}$ in the rotating frame defined by

$$E_\alpha \;=\; F_{\alpha\beta}k^\beta \;=\; -\nabla_\alpha \Phi^{\rm E}, \qquad \Phi^{\rm E} \;=\; A_\alpha k^\alpha + \text{const}, \tag{2}$$

is constant on $\mathcal{H}^\pm$, where the symmetry $\pounds_k A_\alpha = 0$ is assumed. Since E_α is null on $\mathcal{H}^\pm$, and $E_\alpha k^\alpha = 0$, E_α is parallel to the null generator on $\mathcal{H}^\pm$. Hence for any vector η^α tangent to $\mathcal{H}^\pm$, $\eta^\alpha E_\alpha = -\eta^\alpha \nabla_\alpha \Phi^{\rm E} = 0$. Therefore, as for the stationary and axisymmetric spacetimes shown by Carter [9, 10], the surface gravity κ and the electric potential $\Phi^{\rm E}$ in the rotating frame are constant on the horizon $\mathcal{H}^\pm$.

2.2 First law

Consider a family of spacetimes,

$$\mathcal{Q}(\lambda) := [g_{\alpha\beta}(\lambda), u^\alpha(\lambda), \rho(\lambda), s(\lambda), A_\alpha(\lambda), j^\alpha(\lambda)], \tag{3}$$

whose Lagrangian density is written

$$\mathcal{L} \;=\; \left(\frac{1}{16\pi}R \;-\; \epsilon \;-\; \frac{1}{16\pi}F_{\alpha\beta}F^{\alpha\beta} \;+\; A_\alpha j^\alpha\right)\sqrt{-g}, \tag{4}$$

where u^α, ρ, s, ϵ, and j^α are, respectively, the 4-velocity, baryon rest mass density, entropy per baryon mass, energy density, and electric 4-current. A generalized first law for the spacetime $\mathcal{Q}(\lambda)$ associated with the helical symmetry is derived as a variation formula of the Noether charge associated with the helical Killing vector defined by [11, 12]

$$Q(\lambda) = \oint_S Q^{\alpha\beta} dS_{\alpha\beta}, \tag{5}$$

$$\mathfrak{B}^\alpha(\lambda) \;=\; \frac{1}{16\pi}(g^{\alpha\gamma}g^{\beta\delta} - g^{\alpha\beta}g^{\gamma\delta})|_{\lambda=0}\, \mathring{\nabla}_\beta\, g_{\gamma\delta}(\lambda) \;+\; \frac{1}{4\pi}F^{\beta\alpha}|_{\lambda=0}\Big[A_\beta(\lambda) - \frac{1}{2}A_\beta(0)\Big] \;+\; \mathrm{O}(\lambda^2), \tag{6}$$

With this choice of $\mathfrak{B}^\alpha$, the charge $Q(\lambda)$ becomes finite and independent of the sphere S on which the charge $Q(\lambda)$ is evaluated, as long as S encloses all black holes and neutron stars.

To see this, we first check that $Q(0)$ is independent of S. The surface integral of (5) is rewritten in terms of integrals over a spacelike hypersurface Σ transverse to k^α and over the black hole boundary $\mathcal{B}_i$,

where $\mathcal{B}_i$ is the i-th connected component of $\Sigma \cap \mathcal{H}^+$. Since, the boundary of Σ is the union of the sphere S and $\mathcal{B}_i$, $\partial\Sigma = S \cup_i \mathcal{B}_i$, a difference $Q - \sum_i Q_i$ is calculated at $\lambda = 0$:

$$Q - \sum_i Q_i = -\frac{1}{8\pi}\int_\Sigma (G^\alpha{}_\beta k^\beta - 8\pi T_{\rm F}{}^\alpha{}_\beta) dS_\alpha - \frac{1}{16\pi}\int_\Sigma R k^\alpha dS_\alpha.$$
$$+ \int_\Sigma \left(\frac{1}{8\pi}\nabla_\gamma F^{\beta\gamma} A_\beta k^\alpha - \frac{1}{4\pi} k^\gamma A_\gamma \nabla_\beta F^{\alpha\beta}\right) dS_\alpha - \sum_i \frac{1}{4\pi}\int_{\mathcal{B}i} k^\gamma A_\gamma F^{\alpha\beta} dS_{\alpha\beta}. \quad (7)$$

where $Q_i(\lambda)$ is defined on $\mathcal{B}_i$ by

$$Q_i(\lambda) := \oint_{\mathcal{B}_i} Q^{\alpha\beta} dS_{\alpha\beta}, \quad (8)$$

$T_{\rm F}{}^\alpha{}_\beta$, the stress-energy tensor of the electromagnetic field, is defined by,

$$T_{\rm F}^{\alpha\beta} = \frac{1}{4\pi}\left(F^{\alpha\gamma}F^\beta{}_\gamma - \frac{1}{4} g^{\alpha\beta} F_{\gamma\delta} F^{\gamma\delta}\right). \quad (9)$$

To derive Eq. (7), we have also used a condition

$$\frac{1}{4\pi}\oint_S k^\gamma A_\gamma F^{\alpha\beta} dS_{\alpha\beta} = 0 \quad (10)$$

on the boundary sphere S to determine the constant of the electric potential $\Phi^{\rm E}$ in Eq. (2). Eq. (7) implies that $Q(0)$ does not depend on the sphere S as long as it encloses all black holes and neutron stars, because in the region where the sphere S is located, the integrand of the volume integrals in Eq. (7) vanishes when Einstein's and Maxwell's equations are satisfied.

Next, the variation $\delta Q := dQ/d\lambda$ in the Noether charge is evaluated in terms of perturbations of the baryon mass, entropy, circulation and electric current of each fluid element, and the surface areas and charges of the black holes. The detailed calculation is described in UGM: the variation δQ becomes

$$\delta Q = \int_\Sigma \left\{ \frac{T}{u^t}\Delta(s\,\rho u^\alpha\, dS_\alpha) + \frac{h - Ts}{u^t}\Delta(\rho u^\alpha\, dS_\alpha) + v^\beta \Delta(h u_\beta\, \rho u^\alpha\, dS_\alpha) - A_\beta k^\beta\, \Delta(j^\alpha dS_\alpha) \right.$$
$$\left. - (j^\alpha k^\beta - j^\beta k^\alpha)\Delta A_\beta\, dS_\alpha \right\} + \sum_i \left(\frac{1}{8\pi}\kappa_i \delta\mathcal{A}_i + \Phi_i^{\rm E}\,\delta Q_i^{\rm E}\right), \quad (11)$$

where T is the temperature, h is the relativistic specific enthalpy, and v^α is the spatial velocity defined by the following decomposition of the 4-velocity u^α with respect to the helical vector:

$$u^\alpha = u^t(k^\alpha + v^\alpha) \quad \text{with} \quad v^\alpha \nabla_\alpha t = 0 \quad \text{and} \quad u^t = u^\alpha \nabla_\alpha t. \quad (12)$$

The electric charge of each black hole $Q_i^{\rm E}$ is defined by

$$Q_i^{\rm E} := \frac{1}{4\pi}\oint_{\mathcal{B}i} F^{\alpha\beta} dS_{\alpha\beta}, \quad (13)$$

which is related to the total electric charge of the system $Q^{\rm E}$ by Stokes' theorem:

$$Q^{\rm E} := \frac{1}{4\pi}\oint_S F^{\alpha\beta} dS_{\alpha\beta}. = \int_\Sigma j^\alpha dS_\alpha + \sum_i Q_i^{\rm E}. \quad (14)$$

Note that the $\Phi_i^{\rm E}$, defined on each $\mathcal{B}_i$ by

$$\Phi_i^{\rm E} = -A^\alpha k_\alpha = \Phi^{\rm E} + C, \quad (15)$$

is constant. In the case of stationary and axisymmetric spacetimes, the mass variation formula derived by Carter [9, 10] can be derived from Eq. (11).

We can now verify that $Q(\lambda)$ is independent of the location of the 2-surface S, because the charge $Q(\lambda)$ at $\lambda = 0$ is shown to be independent of S, and the variation formula (11) implies that $dQ/d\lambda = \delta Q$ is independent of S as long as it encloses the fluid and black holes. Moreover, in UGM we have shown that the difference,

$$\delta\Big(Q - \sum_i Q_i - \frac{1}{4\pi}\int_{\partial\Sigma} k^\gamma A_\gamma F^{\alpha\beta} dS_{\alpha\beta}\Big) = \delta Q - \sum_i \Big(\frac{1}{8\pi}\kappa_i \delta\mathcal{A}_i + \Phi_i^{\rm E}\,\delta Q_i^{\rm E}\Big), \tag{16}$$

is invariant under a gauge transformation that respects the symmetry, and hence we verify that so is δQ.

2.3 Application of the first law to solution sequences in equilibrium

When inspiraling binary systems, or isolated neutron stars are evolving adiabatically – in a timescale much longer than the dynamical timescale – they may be modeled by a sequence of solutions in equilibrium. When the first law for a stationary and axisymmetric perfect fluid spacetime is applied to a sequence of rotating neutron star solutions whose local changes of rest mass and entropy are constant, the first law becomes $\delta M = \Omega\delta J$. This is a condition for applying the turning point theorem [13] to determine the stability of solutions. In this section, we consider an application of the first law (11) to a sequence of helically symmetric solutions that models inspiraling binary black holes and/or neutron stars, assuming that the neutron star matter is a perfect conductor.

For a perfectly conducting medium, the ideal MHD condition,

$$F_{\alpha\beta}u^\beta = 0, \tag{17}$$

is satisfied, and hence its curl is written

$$\pounds_u F_{\alpha\beta} = 0, \tag{18}$$

which is the magnetic flux conservation law, Alfven's law. For each solution in equilibrium, conservation of rest mass and entropy are assumed to be satisfied.

$$\pounds_u(\rho\sqrt{-g}) = 0, \quad \pounds_u s = 0. \tag{19}$$

When we consider a sequence of solutions along which the rest mass, entropy, and magnetic flux are all conserved, the perturbed conservation laws corresponding to the above Eqs. (18) and (19) are satisfied:

$$\Delta(\rho\sqrt{-g}) = 0, \quad \Delta s = 0, \quad \text{and} \quad \Delta F_{\alpha\beta} = 0. \tag{20}$$

For the black holes, we may assume that areas and charges are constant. With these assumptions, the first law (11) is rewritten

$$\delta Q = \int_\Sigma \left\{ v^\beta \Delta(h u_\beta\, \rho u^\alpha\, dS_\alpha) - A_\beta k^\beta\, \Delta(j^\alpha dS_\alpha) \right\}. \tag{21}$$

Here $\Delta F_{\alpha\beta} = 0$ with $F_{\alpha\beta} = (dA)_{\alpha\beta}$ [4], $\Delta(dA)_{\alpha\beta} = (d\Delta A)_{\alpha\beta}$, whence the Poincaré lemma implies that there exists a function Ψ such that $\Delta A_\alpha = \nabla_\alpha\Psi$. From a substitution of this to the last term in the volume integral of Eq. (11), the latter is shown to vanish. The remaining terms in Eq. (21) are related to the circulation of the magnetized flow.

For a perfect fluid without magnetic fields, the conservation of circulation is written as $\pounds_u\hat{\omega}_{\alpha\beta} = 0$ where $\hat{\omega}_{\alpha\beta} := (d(hu))_{\alpha\beta}$ is the vorticity tensor. When circulation is conserved along a sequence of solutions, it implies that $\Delta\hat{\omega}_{\alpha\beta} = 0$, and hence the first term in the integral of Eq. (21) vanishes [6]. In general, there is no such conservation law for the circulation of magnetized flow. However, Bekenstein and Oron [14] (Tarapov and Gorskii [15] for Newtonian MHD) have developed a formulation of ideal MHD, in which a generalized circulation of magnetized flow is conserved. Their theory begins with a Lagrangian in which the interaction term $A_\alpha j^\alpha$ in Eq. (4) is replaced by $F_{\alpha\beta}\rho u^\alpha q^\beta$, where the vector q^α is a Lagrange multiplier, and, after the variation, it results in a current of the form

$$j^\alpha = \nabla_\beta(\rho u^\alpha q^\beta - \rho u^\beta q^\alpha). \tag{22}$$

[4] For a one-form w_α, the exterior derivative $(dw)_{\alpha\beta}$ (within index notation) is defined by $(dw)_{\alpha\beta} := \nabla_\alpha w_\beta - \nabla_\beta w_\alpha$, and for a two-form $w_{\alpha\beta} = w_{[\alpha\beta]}$ by $(dw)_{\alpha\beta\gamma} := 3\,\nabla_{[\alpha} w_{\beta\gamma]} = \nabla_\alpha w_{\beta\gamma} + \nabla_\beta w_{\gamma\alpha} + \nabla_\gamma w_{\alpha\beta}$.

When a vector q^α is found to give the current (22), the Lorenz force term in the MHD-Euler equation

$$u^\beta (d(hu))_{\beta\alpha} = \frac{1}{\rho} F_{\alpha\beta} j^\beta \tag{23}$$

becomes

$$u^\beta \omega_{\beta\alpha} = 0, \tag{24}$$

where

$$\omega_{\alpha\beta} := (dw)_{\alpha\beta}, \quad w_\alpha := hu_\alpha + \eta_\alpha, \quad \eta_\alpha := F_{\alpha\beta} q^\beta, \tag{25}$$

because of a relation,

$$\frac{1}{\rho} F_{\alpha\beta} j^\beta = \frac{1}{\rho} F_{\alpha\beta} \left[\pounds_q (\rho u^\beta) + \rho u^\beta \nabla_\gamma q^\gamma \right] = (d\eta)_{\alpha\beta} u^\beta. \tag{26}$$

The MHD-Euler equation in this case (24) implies conservation of circulation for the magnetized flow, because its curl, with $(d\omega)_{\alpha\beta\gamma} = 0$, yields

$$\pounds_u \omega_{\alpha\beta} = 0, \tag{27}$$

and its perturbed conservation law becomes

$$\Delta \omega_{\alpha\beta} = 0. \tag{28}$$

Substituting the current (22) to the first law (11), we have

$$\begin{aligned} \delta Q &= \int_\Sigma \left\{ \frac{T}{u^t} \Delta dS + \frac{h - Ts}{u^t} \Delta dM_{\rm B} + v^\alpha \Delta dC_\alpha - v^\beta q^\gamma \Delta F_{\beta\gamma}\, dM_{\rm B} - (j^\alpha k^\beta - j^\beta k^\alpha) \Delta A_\beta\, dS_\alpha \right\} \\ &+ \sum_i \left(\frac{1}{8\pi} \kappa_i \delta \mathcal{A}_i + \Phi_i^{\rm E}\, \delta Q_i^{\rm E} \right), \end{aligned} \tag{29}$$

where we introduced the following notation

$$dM_{\rm B} := \rho u^\alpha dS_\alpha, \quad dS := s\, dM_{\rm B}, \quad dC_\alpha := (hu_\alpha + \eta_\alpha) dM_{\rm B}. \tag{30}$$

Applying the first law (29) to a sequence of solutions along which the quantities are conserved as in Eq. (20) and the circulation of magnetized flow is conserved as in Eq. (28), the first law becomes

$$\delta Q = 0, \tag{31}$$

or for asymptotically flat systems, such as in the post-Newtonian approximation, $\delta Q = \delta M - \Omega \delta J = 0$.

3 A formulation for calculating magnetized irrotational binary neutron stars in equilibrium

To compute solutions of binary compact objects in equilibrium, we apply a finite difference scheme, or a pseudo-spectral method, to a system of basic equations and numerically solve the system. Those equations include Einstein's equations, Maxwell's equations, the MHD-Euler equation, and the baryon mass conservation equation. Here, we assume that the flow is homentropic, and hence neutron-star matter is described by a one-parameter EOS.

For the gravitational field, the Isenberg - Wilson - Mathews formulation, the waveless formulation, or a full set of Einstein's equations assuming helical symmetry may be used. These formulations are based on a 3+1 decomposition of spacetime, and reliable numerical methods to solve these equations have been developed [16–18]. We expect that Maxwell's equations can be solved using analogous formulations and applying one of numerical methods used in these references.

However, for the MHD-Euler equation, when stationarity or helical symmetry is imposed, it is no longer an evolution equation, and as a result it is difficult to integrate numerically. In usual methods

[16–18], a numerical solution is calculated from a first integral, a sufficient condition, of the (MHD-) Euler equation with an assumption that the flow is either corotational or irrotational. Therefore, finding the first integral of the MHD-Euler equation is a key, and also a restriction, for computing equilibrium solutions considered in the previous section successfully.

As shown in Sec. 2.3, when the Bekenstein-Oron 4-current (22) is introduced, the relativistic MHD-Euler equation for ideal MHD flows takes the form (24). If we assume that the generalized momentum (25) of the magnetized flow respects the helical symmetry, $\pounds_k w_\alpha = 0$, then a first integral is immediately derived for corotational and irrotational flows, in a way fully analogous with the non-magnetized case [19] : the Cartan identity $k^\beta \omega_{\beta\alpha} = \pounds_k w_\alpha - \nabla_\alpha(w_\beta k^\beta)$ reduces to $k^\beta \omega_{\beta\alpha} = -\nabla_\alpha(w_\beta k^\beta)$ and, for an irrotational flow ($\omega_{\beta\alpha} = 0$), or for a corotational one [u^α colinear to k^α so that (24) implies $k^\beta \omega_{\beta\alpha} = 0$], we get the first integral $w_\alpha k^\alpha = \text{const}$.

The generalized momentum w_α, however, does not necessarily respect the helical symmetry because q^α is not a physical quantity: it can be written

$$\pounds_k w_\alpha \;=\; \pounds_k \eta_\alpha \;=\; F_{\alpha\beta} \pounds_k q^\beta \;\neq\; 0. \tag{32}$$

In fact, if one assumes $\pounds_k w_\alpha = 0$ for a corotational flow, no Lorenz force is exerted on the matter. In this case, enforcing helical symmetry to the MHD-Euler equation (24), we first isolate the Lie derivative with respect to k^α,

$$\nabla_\alpha \left(\frac{h}{u^t} + w_\beta v^\beta \right) \;+\; \pounds_k w_\alpha \;+\; v^\beta (dw)_{\beta\alpha} \;=\; 0. \tag{33}$$

With the assumption that the flow coupled with the magnetic field is irrotational, the velocity potential Φ is introduced:

$$w_\alpha = h u_\alpha \;+\; \eta_\alpha = \nabla_\alpha \Phi. \tag{34}$$

Then, we have four variables for the matter, two thermodynamic variables and two variables for the velocity fields, $\{h, p, \Phi, u^t\}$. The set of equations to solve for these four variables is supplemented by a one-parameter EOS, $p = p(h)$, and the normalization of the 4-velocity $u_\alpha u^\alpha = -1$. The velocity potential Φ is obtained from the rest mass conservation equation which is an elliptic equation for Φ with Neumann boundary conditions. An additional degree of freedom may be obtained from the first integral if it exists. Substituting Eqs. (32) and (34) to Eq. (33), we have

$$\nabla_\alpha \left(\frac{h}{u^t} + \pounds_v \Phi \right) \;-\; \pounds_k q^\beta (dA)_{\beta\alpha} \;=\; 0. \tag{35}$$

Hence the integrability condition for a magnetized irrotational flow is that the last term be a gradient of a function, $\pounds_k q^\beta (dA)_{\beta\alpha} = \nabla_\alpha f$, or using the Cartan identity,

$$\pounds_{[k,q]} F_{\alpha\beta} \;=\; 0, \tag{36}$$

where $[k, q]^\alpha := \pounds_k q^\alpha$.

It is not at all trivial to find a vector q^α that satisfies both the integrability condition (36) and the ideal MHD condition (17); q^α is not freely specifiable. Instead of solving for a q^α that satisfies both conditions, we assume

$$q^\alpha = q^t k^\alpha \quad \text{with} \quad \pounds_k q^t = f(A_\alpha k^\alpha), \tag{37}$$

and claim that we are free to choose q^α as above at least instantaneously on an initial hypersurface Σ. Then, the first integral is written,

$$\frac{h}{u^t} \;+\; \pounds_v \Phi \;+\; \int \pounds_k q^t \, d(A_\alpha k^\alpha) \;=\; \mathcal{E} \;=\; \text{const}. \tag{38}$$

It is likely that solutions with neutron stars and strong magnetic fields computed from Eq. (38) may not be strictly in equilibrium. Nonetheless, such solutions with strong magnetic fields that satisfy a set of hydrostationary equations will serve as interesting initial data sets for numerical relativity merger simulations, and for further studies of such strongly magnetized compact binaries.

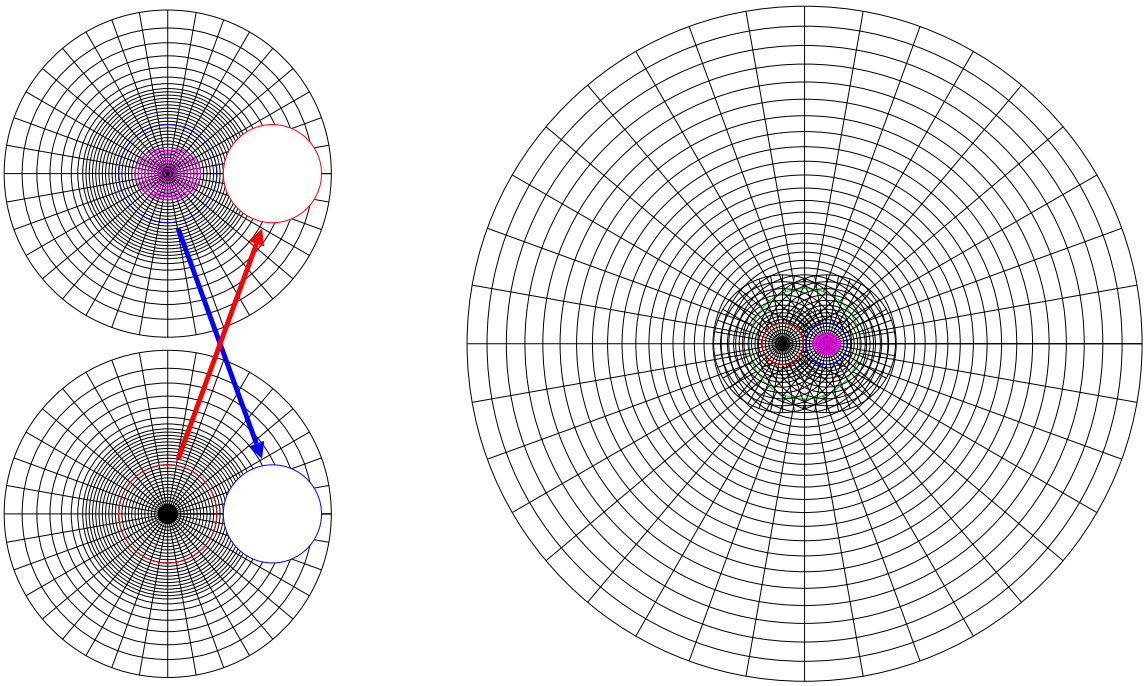

Figure 1: Example of the grid structure of Cocal code for the black hole-neutron star binary. Left panel: the coordinate grids for a black hole and a neutron star. Between these grids, the value of potential on the red (blue) circle is mapped to the empty red (blue) circle. Right panel: a third patch to cover an asymptotics may be introduced to reduce the memory and CPU time, or to compute standing wave solution.

4 Numerical method – Cocal code –

Several numerical methods have been developed for computing equilibria of various self-gravitating objects, including rapidly rotating stars, black hole - toroid systems, and close binary systems. One of the methods for computing solutions of stationary axisymmetric spacetimes with high density matter is known as the KEH method named after Komatsu, Eriguchi and Hachisu, which is the relativistic version of the Hachisu's extension of the self-consistent field method (HSCF method) for rapidly rotating stars [20].

Based on KEH method, we have been developing a new Cocal code for computing compact objects, including a rapidly rotating neutron star, a neutron star/black hole - toroid system, binary neutron stars, black hole - neutron star binaries, binary black holes, and all the above with magnetic fields. Cocal is the abbreviation of "Compact Object CALculator", and also means a seagull in Triestino (Trieste dialect of Italian). The ideas of Cocal code project are to make the simplest code for computing such compact objects. Those include the followings: no symmetry is assumed for the 3D computational domain, a 2nd order finite difference scheme is used on the spherical grids, and a multipole expansion of a Green's function is used to solve the Poisson/Helmholtz equation. Cocal code is written in Fortran 90.

In Fig.1, a plan for the grid structure of the Cocal code for the case with a black hole – neutron star binary is shown. As shown in the left panel, each spherical domain is centered at either the black hole or neutron star, and a spherical region surrounding a companion is excised. In an actual computation for solving Poisson equation, two spherical domains for each compact object is extended to the asymptotics. As the other option, third patch is introduced to cover the asymptotics as shown in the right panel of Fig.1. The third patch is used to reduce the memory and computing time sacrificing the simplicity of the code, and is necessary for solving Helmholtz equation accurately.

A contribution from the companion is calculated through the surface integral of Green's formula,

$$\phi(x) = -\frac{1}{4\pi}\int_V G(x,x')S(x')d^3x' + \frac{1}{4\pi}\int_{\partial V}\left[G(x,x')\mathring{D}_a\phi(x') - \phi(x')\mathring{D}_a G(x,x')\right]\hat{r}^a d^2x' \qquad (39)$$

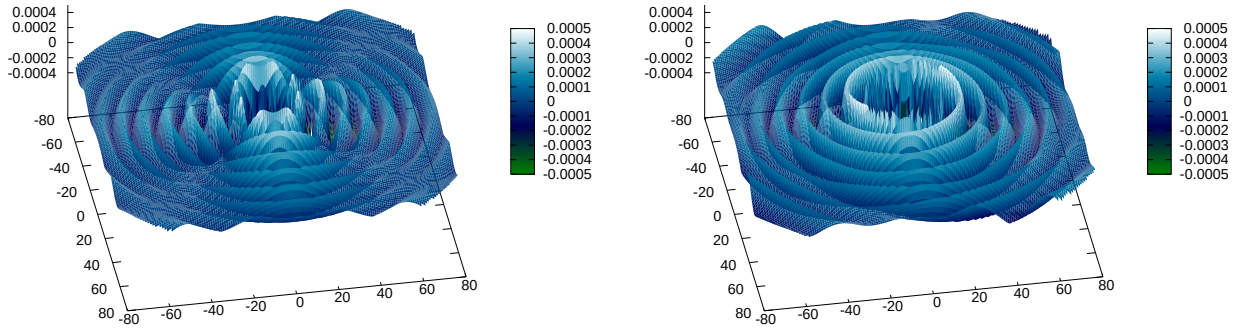

Figure 2: Solutions of Helmholtz equations Eqs. (40) and (41) with half-ingoing + half-outgoing Green's function (Left panel) and with outgoing Green's function (Right panel). A Contribution of the order of $O(r^{-1})$ is subtracted from each solution to show the patterns of the waves.

where $G(x, x')$ is the Green's function either for the flat Laplacian, or flat Helmholtz operator, expanded in multipole moments. The contributions from the curved geometry are collected in the source term $S(x')$.

In Fig. 2, a preliminary result for our Helmholtz solver is shown, in which the same toy problem considered in [21] is solved. Imposing a helical symmetry to a scalar wave equation, we have $(\mathring{\Delta} - \Omega^2\partial_\phi^2)\psi = \mathcal{S}$, and its multipole expansion gives a set of Helmholtz equations

$$(\mathring{\Delta} + m^2\Omega^2)\psi^{\ell m}Y_{\ell m} = \mathcal{S}^{\ell m}Y_{\ell m}, \quad \text{where} \quad \psi = \sum_{\ell m}\psi^{\ell m}Y_{\ell m}. \tag{40}$$

These are solved for standing waves generated from binary sources

$$\mathcal{S} = \sum_{\pm}\frac{q}{\sqrt{(2\pi\sigma^2)^3}}\exp\left(\pm\frac{|r^a - R^a|^2}{2\sigma^2}\right) \tag{41}$$

where parameters are set as $q = 1$, $a = 1$, $\sigma = 0.5$, and $\Omega = 0.3$. The result from the half-ingoing + half-outgoing Green's function in the left panel agree with that presented in [21]. As shown in the right panel, the same method works also for the case with outgoing Green's function. These solutions are calculated using a single spherical coordinate patch; a work is in progress to implement the multi-patch Fig. 1 in the Helmholtz solver.

5 Discussion

The thermodynamic laws derived for helically symmetric Einstein-Maxwell spacetimes with magnetized matter can be applied to a non-axisymmetirc single rotating star, or an axisymmetric rotating star beyond the stationary, axisymmetric *and circular* spacetime. Our plan is to construct models not only binary compact objects, but also a magnetar, as well as a proto neutron star which is likely to have a strong magnetic field that may affect the neutron-star structure.

Recently, the convergence of self-consistent field methods for computing non-rotating stellar equilibria was analyzed in [22], and it was found that the choice of parameters to be fixed during the iteration is essential for a convergent code. It seems reasonable to us that an analogous property holds for more general geometries, and empirically it is known that one can find a convergent scheme choosing the axis ratio, or positions of the surface of the star, as fixed parameters. Based on all the knowledge on formulations and numerical methods, Cocal code to compute various kinds of magnetized compact objects will be successfully developed in near future.

Acknowledgements

We thank Brandon Carter and John L. Friedman for enlightening discussions and suggestions. KU thanks Yoshiharu Eriguchi, Antonios Tsokaros, and Shin'ichiro Yoshida for discussions. This work was supported by JSPS Grant-in-Aid for Scientific Research(C) 20540275, MEXT Grant-in-Aid for Scientific Research on Innovative Area 20105004, NSF grants No. PHY0071044 and PHY0503366, NASA grant No. NNG05GB99G, and ANR grant 06-2-134423 *Méthodes mathématiques pour la relativité générale*. CM thanks the Greek State Scholarships Foundation for support during the early stages of this work and the Paris Observatory and the University of Wisconsin-Milwaukee for travel support. KU and EG acknowledge support from the JSPS Invitation Fellowship for Research in Japan (Short-term) and the invitation program of foreign researchers at the Paris Observatory.

References

[1] P. M. Woods, & C. Thompson, In "Compact stellar X-ray sources" edited by W. Lewin & M. van der Klis, Cambridge Astrophysics Series, No. 39, 547, Cambridge University Press (2006).

[2] Y. T. Liu, S. L. Shapiro, Z. B. Etienne and K. Taniguchi, Phys. Rev. D **78**, 024012 (2008); M. Anderson, E. W. Hirschmann, L. Lehner, S. L. Liebling, P. M. Motl, D. Neilsen, C. Palenzuela, J. E. Tohline, Phys. Rev. Lett. **100**, 191101 (2008). B. Giacomazzo, L. Rezzolla and L. Baiotti, arXiv:0901.2722 [gr-qc].

[3] J. K. Blackburn and S. Detweiler, Phys. Rev. D **46**, 2318 (1992); S. Detweiler, Phys. Rev. D **50**, 4929 (1994).

[4] A. Schild, Phys. Rev. 131, 2762 (1963).

[5] J. L. Friedman and K. Uryu, Phys. Rev. D **73**, 104039 (2006); M. M. Glenz and K. Uryu, Phys. Rev. D **76**, 027501 (2007).

[6] J. L. Friedman, K. Uryu and M. Shibata (FUS), Phys. Rev. D **65**, 064035 (2002) [Erratum-ibid. D **70**, 129904 (2004)]

[7] K. Uryu, E. Gourgoulhon and C. Markakis (UGM), Phys. Rev. D **82**, 104054 (2010)

[8] H. Friedrich, I. Rácz, and R. M. Wald, Comm. Math. Phys. **204**, 691 (1999).

[9] B. Carter, 'Black hole equilibrium states', in Black Holes (Les Astres Occlus), p. 57-214 (1973).

[10] B. Carter, 'The general theory of the mechanical, electromagnetic and thermodynamic properties of black holes', in General Relativity: An Einstein centenary survey, eds., S. W. Hawking & W. Israel, p. 294-369 (1979); B. Carter, 'Generalised mass variation formula for a stationary axisymmetric star or black hole with surrounding accretion disc', in Anneau d'accrétion sur les trous noires, (Faculté des Sciences, Angers), eds., I. Moret-Bailly & C. Latremolière, p. 166-182, (1979); B. Carter, 'Perfect fluid and magnetic field conservation laws in the theory of black hole accretion rings', in Active galactic nuclei. (A79-50785 22-90) Cambridge, Cambridge University Press, eds., C. Hazard,& S. Mitton, p. 273-300, (1979).

[11] R. M. Wald, Phys. Rev. D. **48**, R3427 (1993).

[12] V. Iyer and R. M. Wald, Phys. Rev. D. **52**, 4430 (1995).

[13] R. Sorkin, Astrophys. J. **249**, 254 (1981).

[14] J. D. Bekenstein and A. Oron, Phys. Rev. E **62**, 5594 (2000); J. D. Bekenstein and A. Oron, Found. Phys. **31**, 895 (2001);

[15] I. E. Tarapov, PMM U.S.S.R., 48, 275 (1984); V. B. Gorskii, PMM U.S.S.R., 50, 388 (1986).

[16] S. Bonazzola, E. Gourgoulhon, and J.-A. Marck, Phys. Rev. Lett. 82, 892 (1999); E. Gourgoulhon, P. Grandclement, K. Taniguchi, J.-A. Marck, S. Bonazzola, Phys. Rev. D 63, 064029 (2001); K. Taniguchi and E. Gourgoulhon, Phys. Rev. D 66, 104019 (2002); ibid. 68, 124025 (2003); M. Bejger, D. Gondek-Rosinska, E. Gourgoulhon, P. Haensel, K. Taniguchi and J. L. Zdunik, Astron. Astrophys. **431**, 297 (2005). K. Taniguchi and M. Shibata, Astrophys. J. Suppl. **188**, 187 (2010)

[17] K. Uryu and Y. Eriguchi, Phys. Rev. D 61, 124023 (2000); K. Uryu, M. Shibata, and Y. Eriguchi, Phys. Rev. D 62, 104015 (2000); K. Uryu, F. Limousin, J. L. Friedman, E. Gourgoulhon and M. Shibata, Phys. Rev. Lett. **97**, 171101 (2006); K. Uryu, F. Limousin, J. L. Friedman, E. Gourgoulhon and M. Shibata, Phys. Rev. D **80**, 124004 (2009).

[18] K. Taniguchi, T. W. Baumgarte, J. A. Faber and S. L. Shapiro, Phys. Rev. D **72**, 044008 (2005); K. Taniguchi, T. W. Baumgarte, J. A. Faber and S. L. Shapiro, Phys. Rev. D **74**, 041502(R) (2006); K. Taniguchi, T. W. Baumgarte, J. A. Faber and S. L. Shapiro, Phys. Rev. D **75**, 084005 (2007); K. Taniguchi, T. W. Baumgarte, J. A. Faber and S. L. Shapiro, Phys. Rev. D **77**, 044003 (2008); K. Kyutoku, M. Shibata, and K. Taniguchi, Phys. Rev. D **79**, 124018 (2009); F. Foucart, L. E. Kidder, H. P. Pfeiffer and S. A. Teukolsky, Phys. Rev. D **77**, 124051 (2008).

[19] H. Asada, Phys. Rev. D **57**, 7292 (1998); M. Shibata, Phys. Rev. D **58**, 024012 (1998); S. A. Teukolsky, Astrophys. J. , 504, 442 (1998)

[20] J. P. Ostriker, and J. W.-K. Mark, Astrophys. J. 151, 1075 (1968); I. Hachisu, Astrophys. J. Suppl. 62, 461 (1986); ibid. 61, 479 (1986); H. Komatsu, Y. Eriguchi, and I. Hachisu, Mon. Not. Roy. Astron. Soc. 237, 355 (1989)

[21] S. Yoshida, B. C. Bromley, J. S. Read, K. Uryu and J. L. Friedman, Class. Quant. Grav. **23**, S599 (2006).

[22] R. H. Price, C. Markakis and J. L. Friedman, J. Math. Phys. **50**, 073505 (2009).

Accelerating Cosmologies in Dilatonic Einstein-Gauss-Bonnet Gravity in the String Frame

Kei-ichi Maeda,[a,b,*] Nobuyoshi Ohta[c,†] and Ryo Wakebe[a,‡]

[(a)] *Department of Physics, Waseda University, Shinjuku, Tokyo 169-8555, Japan*
[(b)] *Waseda Research Institute for Science and Engineering, Shinjuku, Tokyo 169-8555, Japan*
[(c)] *Department of Physics, Kinki University, Higashi-Osaka, Osaka 577-8502, Japan*

Abstract

We study cosmological solutions in low-energy effective heterotic string theory, which consists of the Einstein gravity with the Gauss-Bonnet term and a dilaton. And there are non-linear self-interaction terms which looks like recently studied in context of "Galileon" cosmology. We study cosmological solutions with the self-interaction term which includes two arbitrary coupling parameter. We examine the time evolution of the solutions and the question of whether the solutions can describe accelerated expansion of our four-dimensional space in the Einstein frame. We found de-Sitter solutions in our four-dimension when these two parameter are related.

1 Introduction

The recent cosmological observation confirmed the existence of the early inflationary cosmological epoch as well as the accelareted expansion of the present universe. Though it is not difficult to construct cosmological models with theses features if one introduces scalar fields with suitable potentials, it is desirable to derive such a model from fundamental theories of particle physics without making special assumptions. The most promising candidates for such theories are the ten-dimensional superstrings or eleven-dimensional M theory, which are hoped to give models of accelarated expansion of the universe upon compactification to four dimensions.

The scale when the acceleration occurs in this type of models is basically governed by the Planck scale in higher ten or eleven dimensions. With phenomena at such high energy, it is expected that we cannot ignore quantum corrections such as higher derivative terms in the theories at least in the early universe. It is known that there are terms of higher orders in the curvature to the lowest effective supergravity action coming from superstings or M theory.

In particular, the leading quadratic correction for heterotic string theories is proportional th to Gauss-Bonnet (GB) combination. This model has been studied in some detail in Ref. [1] and it was shown that there are two exponentially expanding solutions, which may be called generalized de Sitter solutions since the size of the internal space also depends on time. Note, however, that this does not mean that the solutions describe accelerating expansion in four dimensions. Another interesting claim is that it is possible to obtain inflationary solutions if the coefficient of the GB term is negative, which is not the case in the effective theory of the heterotic string, and hence may not be relevant in our study. Moreover, most investigations consider a pure GB term without a dilaton, or assume a constant dilaton, which is not a solution of the heterotic string and they do not discuss cosmological solutions with a dynamical dilaton in higher dimensions. It is thus important to analyze a system including dynamical dilatons. There has also been an attempt to obtain inflationary solutions in M theory with higher-order quantum corrections. [2]

In the string frame, the Einstein-Hilbert curvature term is also coupled to the dilaton field. So usually we perform a conformal transformation to find the Einstein frame, in which the Einstein-Hilbert curvature term does not couple to the dilaton field. When we study cosmological solutions in the Einstein frame, only the Gauss-Bonnet term is taken into account as the quantum correction, but some additional terms

*E-mail address: maeda"at"waseda.jp
†E-mail address: ohtan"at"phys.kindai.ac.jp
‡E-mail address: wakebe"at"gravity.phys.waseda.ac.jp

appear through a conformal transformation compared with the string frame. It is not so obvious which frame is to be used in investigating solutions where strong gravitational effects become strong such as early universe. It is certainly natural to take the action in the string frame in string theory, and then it is important to check if the above additional terms make any difference in the results.

On the other hand, the effective action is defined as a field theory action generating the S-matrix which coincides with the massless sector of the (tree-level) string S-matrix. The generating functional for the string S-matrix can be represented as a path integral over surfaces with the free string action replaced by the generalized σ-model action describing the string propagating in a non-trivial background. Since the perturbative S-matrix does not change under local field redefinitions there exist a large class of effective action, which all correspond to the same string S-matrix. We investigate the effect of this ambiguity in the field redefinition on the cosmological solutions.

In this paper, we consider cosmological solutions with a dilaton field and the GB correction form heteotic string theory by extending the dynamical system method. We find that the field equations take the form of an autonomous system in the case of flat internal and external spaces in the string frame. We derive the fixed points and analyze their stability in the system. We also examine the time evolution of the solutions and investigate whether the solutions can describe (transient) accelerated expansion of our four dimensional space in the Einstein frame.

2 Higher order corrections including dilaton

It is known that there are also higher order corrections to dilaton. When we consider the effects of the higher order corrections in the metric, we should also include these terms. Because of the ambiguity in the field redefinition, their contributions are not unique. In a convenient parametrization after dropping NS-NS forms, they are given by [3] *

$$S = \frac{1}{2\kappa_D^2}\int d^D x\sqrt{-g}e^{-2\phi}\Big[R + 4(\nabla\phi)^2 + \alpha_2\Big(R^2_{GB} - 16(\nabla\phi)^4\Big)\Big]. \tag{1}$$

Under the field redefinition, we could also choose the form of the higher order terms with Riemann curvature squared only without higher order term in the dilaton. Of particular interest is the class of theories in which we do not have any higher order derivatives in the resulting field equation.

If we make the field redefinition

$$\begin{aligned} \delta g_{\mu\nu} &= \alpha_2\left\{b_1 R_{\mu\nu} + b_2\nabla_\mu\phi\nabla_\nu\phi + g_{\mu\nu}[b_3 R + b_4(\nabla\phi)^2 + b_5\Box\phi]\right\}, \\ \delta\phi &= \alpha_2\left\{c_1 R + c_2(\nabla\phi)^2 + c_3\Box\phi\right\}, \end{aligned} \tag{2}$$

with b's and c's being constants, we find

$$\begin{aligned} \delta S = \frac{1}{2\kappa_D^2}\sqrt{-g}e^{-2\phi}\alpha_2\Big[&b_1 R^2_{\mu\nu} + (b_2+4b_1)R_{\mu\nu}\nabla^\mu\phi\nabla^\nu\phi + \Big(2c_1 - \frac{1}{2}b_1 - \frac{D-2}{2}b_3\Big)R^2 \\ &+\Big(2c_2 - 8c_1 - \frac{b_2}{2} + 2Db_3 - \frac{D-2}{2}b_4\Big)R(\nabla\phi)^2 \\ &+\Big(2c_3 + 8c_1 - b_1 - 2(D-1)b_3 - \frac{D-2}{2}b_5\Big)R(\Box\phi) - (8c_2 - 4b_2 - 2Db_4)(\nabla\phi)^4 \\ &+[8c_2 - 8c_3 - 3b_2 - 2(D-1)b_4 + 2Db_5]\Box\phi(\nabla\phi)^2 + [8c_3 - 2(D-1)b_5](\Box\phi)^2\Big], \end{aligned} \tag{3}$$

up to $O(\alpha_2^2)$. Imposing the condition that higher derivative terms do not appear in the resulting field equations, we get

$$b_1 = 0, \quad b_5 = 4b_3, \quad c_1 = \frac{D-2}{4}b_3, \quad c_2 = -2b_3 + \frac{D-2}{4}b_4, \quad c_3 = (D-1)b_3, \tag{4}$$

*Another effective action has been obtained in Ref. [4]. After dropping the NS-NS 2-form and using the field redefinition, it is given in the Einstein frame. Translated into the string frame in order to compare with (1), there is a slightly difference in the coefficient of the last term, it is $-\frac{247}{16}$ instead of -16. However this difference affect the solution few.

where we chose $b_2 \equiv m$, $b_4 \equiv (3m+n)/2$. Hence we are left with two-parameter family of the theory,

$$S = \frac{1}{2\kappa_D^2}\int d^Dx\sqrt{-g}e^{-2\phi}\Big[R+4(\nabla\phi)^2+\alpha_2\Big\{R_{GB}^2+m\Big(R_{\mu\nu}-\frac{1}{2}Rg_{\mu\nu}\Big)\nabla^\mu\phi\nabla^\nu\phi \\ +n\Box\phi(\nabla\phi)^2-(16+2m+2n)(\nabla\phi)^4\Big\}\Big], \tag{5}$$

where m and n are free parameters.

3 Solutions with higher correction in string frame

Let us consider the metric in ten-dimensional space,

$$ds_{10}^2 = -e^{2u_0(t)}dt^2+e^{2u_1(t)}ds_3^2+e^{2u_2(t)}ds_6^2\,. \tag{6}$$

The external 3-dimensional and internal 6-dimensional spaces (ds_3^2 and ds_6^2) are chosen to be flat for simplicity.

Our cosmological model is higher dimensional, and there are two kinds of frames that we can consider to discuss cosmologies, the original frame and the Einstein frame in four dimensions. Instead, it is a new frame which is defined so as to eliminate the scalar fields which appear from the internal space by Kaluza-Klein compactification to the external space. This is the frame in which the Newton constant is truly constant. We must determine which frame is important for realizing an inflationary scenario. Since flatness and horizon problems should be accounted for in our four-dimensional spacetime, that is, in the Einstein frame, we should require inflation in the Einstein frame.

Now, let us examine if there is any region in which accelerating expansion is realized in the four-dimensional Einstein frame. The Einstein frame is obtained from

$$ds_{10} = e^{-(6u_2-2\phi)}ds_E^2+e^{2u_2}ds_6^2\,,\quad \text{where}\quad ds_E^2 = -d\tau^2+a^2(\tau)ds_3^2\,, \tag{7}$$

where we have defined the cosmic time τ and scale factor by

$$\frac{d\tau}{dt} = e^{(3u_2-\phi)}\,,\quad a(\tau) = e^{(u_1+3u_2-\phi)} \tag{8}$$

The condition for expansion is

$$\frac{da(\tau)}{d\tau} = \frac{da(\tau)}{dt}\frac{dt}{d\tau} = \left(\dot{u}_1+3\dot{u}_2-\dot{\phi}\right)e^{u_1} > 0\,, \tag{9}$$

and the condition for accelerated expansion is

$$\frac{d^2a(\tau)}{d\tau^2} = \frac{dt}{d\tau}\frac{d}{dt}\left\{\left(\dot{u}_1+3\dot{u}_2-\dot{\phi}\right)e^{u_1}\right\} \\ = \left\{\ddot{u}_1+3\ddot{u}_2-\ddot{\phi}+\dot{u}_1\left(\dot{u}_1+3\dot{u}_2-\dot{\phi}\right)\right\}e^{u_1-3u_2+\phi} > 0\,. \tag{10}$$

From the variation of the total action (5) with respect to u_0, u_1, u_2 and ϕ, we find four basic field equations:

$$F_0 \equiv F\left(u_0,\dot{u_0},\dot{u_1},\dot{u_2},\dot{\phi}\right)\,,\quad F_1 \equiv F\left(u_0,\dot{u_0},\dot{u_1},\dot{u_2},\dot{\phi},\ddot{u_0},\ddot{u_1},\ddot{u_2},\ddot{\phi}\right)\,, \\ F_2 \equiv F\left(u_0,\dot{u_0},\dot{u_1},\dot{u_2},\dot{\phi},\ddot{u_0},\ddot{u_1},\ddot{u_2},\ddot{\phi}\right)\,,\quad F_\phi \equiv F\left(u_0,\dot{u_0},\dot{u_1},\dot{u_2},\dot{\phi},\ddot{u_0},\ddot{u_1},\ddot{u_2},\ddot{\phi}\right)\,. \tag{11}$$

Since u_0 is a gauge freedom of time coordinate, we have four equations for three variables u_1, u_2 and ϕ. It looks like an over-determinant system. However, these four equations are not independent. In fact, we can derive the following equations after bothersome calculation,

$$\dot{F}_0+(3\dot{u}_1+6\dot{u}_2-2\dot{u}_0-2\dot{\phi})F_0 = 3\dot{u}_1F_1+6\dot{u}_2F_2+8\,\dot{\phi}F_\phi\,. \tag{12}$$

Therefore we calculate only three equations, which we choose F_0, F_1 and F_2.

This system is an autonomous system for $\dot{u_1}$, $\dot{u_2}$ and $\dot{\phi}$ if u_0 is zero. We can set $u_0 = 0$ by using time-reparametrization invariance. It is also possible to set $\alpha_2 = 1$ by choosing a suitable unit of time. We solved these autonomous system eqs. (11), and then we find some fixed points of these variables (we described them a, b and c) for several m and n.

In order to study the stabilities of the fixed points, we substitute linear perturbations $a \to a + \delta a$, $b \to b + \delta b$, $c \to c + \delta c$ about the fixed points into the field equations (11). To first order in these perturbations, we obtain two independent equations of motion, which can be written as

$$\begin{pmatrix} \delta a' \\ \delta b' \end{pmatrix} = \mathcal{M} \begin{pmatrix} \delta a \\ \delta b \end{pmatrix} \tag{13}$$

where $\mathcal{M}$ is a 2×2 matrix. Stability requires that both the eigenvalues of the matrix be negative.

4 Conclusion and Remarks

We found the scale factor of four-dimensional Einstein frame become exponential function at some fixed point. This is new feature obtained by introducing two parameters m and n which determines the strength of the coupling of new terms derived from field redefinition. In this case, these two parameter are not determined freely respectively, they are related each other. We also investigate the stability of these fixed points. We find the eigenvalues of $\mathcal{M}$ is only depend on a which is described the fixed point of u_1. If a is positive(negative), the eigenvalues are negative(positive), respectively. That is, expanding external space is stable, shrinking external space is unstable.

In this investigation, we consider flat external and internal space for simplicity. Therefore it need to investigate the curved space case. We find stable fixed points corresponding to the four-dimensional de-Sitter solution. If it goes on, the space eternally accelerating expansion, therefore we have to consider the way to finish the expansion. We also investigate detailed cosmological perturbation for these solution.

References

[1] H. Ishihara, Phys. Lett. B **176** (1986), 217.

[2] K. Bamba, Z. K. Guo and N. Ohta, Prog. Theor. Phys **118** (2007) 879[arXiv:0707.4334[hep-th]]].

[3] R. R. Metsaev and A. A. Tseytlin, Nucl. Phys. B **293** (1987) 385.

[4] D. J. Gross and J. H. Sloan, Nucl. Phys. B **291** (1987) 41.

High-velocity BH collision in 5 dimensions

Hirotada Okawa[1(a)], and Masaru Shibata[2(a)]

(a) *Yukawa Institute, Kyoto University, Kyoto 606-8502*

Abstract

We study the high-velocity collision of two black holes in five dimension by numerical relativity. We prepare two boosted black holes for the initial condition and perform simulations for two equal mass black holes of no spin. We show some results of five-dimensional simulations compared with four-dimensional simulations.

1 Introduction

Clarifying the nature of the gravity in higher-dimension spacetime has become an important issue since a possibility of BH formation in accelerators was pointed out. During the high-energy particle collision of small impact parameter in a higher-dimensional spacetime, two particle may merge to form a BH. Although BH will be evaporated soon by the Hawking radiation and the quantum gravity effect will be important in this phases, BH formation phases are described well in the context of General Relativity. And the numerical relativity simulation is the unique approach to study this phase because of highly nonliear nature.

In order to know the nature of the formed BH, we need to consider the dissipation of the gravitational wave. The radiated energy from the head-on collision of two test particles in 4 dimensions is given as

$$\frac{\mathrm{dE_{rad}}}{\mathrm{d}\omega \mathrm{d}\Omega} = \frac{2G}{(2\pi)^2} \frac{m^2 v^4 \sin^4\theta}{(1-v^2\cos\theta)^2} \tag{1}$$

,where v is the speed of particles[1]. Sperhake *et al.*[4] compared BH collisions with numerical relativity to test particle collisions in 4 dimensions.

We investigate the gravitational wave from the head-on collision of two BHs in 5 dimensions.

2 Numerical relativity in higher dimensions

We perform the 5-dimensional simulation with numerical relativity in higher dimensions[2]. We extend SACRA code[3] to 5 dimensions with U(1) symmetry. CARTOON method enables us to save machine resources.

In higher dimension, we can define the induced metric and the extrinsic curvature as the same as in 4 dimensions. We decompose the Einstein equation in the same expression as in 4 dimensions. In order to perform the stable simulation, we adopt BSSN formalism in higher dimension[2][5].

We construct the initial condition for the headon collision of two BHs by superimposing boosted BHs[6].

3 Results

After merger of two BHs in the headon collision in 5 dimensions, a formed BH can be regarded as Myers-Perry BH in the single rotation[7].

$$\mathrm{ds}^2 = -\mathrm{dt}^2 + \frac{\mu}{\Sigma}\left(\mathrm{dt} - \mathrm{a}\sin^2\theta \mathrm{d}\phi\right)^2 + \frac{\Sigma}{\Delta}\mathrm{dr}^2 + \Sigma \mathrm{d}\theta^2 + \left(\mathrm{r}^2+\mathrm{a}^2\right)\sin^2\theta \mathrm{d}\phi^2 + \mathrm{r}^2\cos^2\theta \mathrm{d}\chi \tag{2}$$

$$\Sigma = r^2 + a^2\cos^2\theta, \qquad \Delta = r^2 + a^2 - \mu \tag{3}$$

[1]Email address: okawa@yukawa.kyoto-u.ac.jp
[2]Email address: shibata@yukawa.kyoto-u.ac.jp

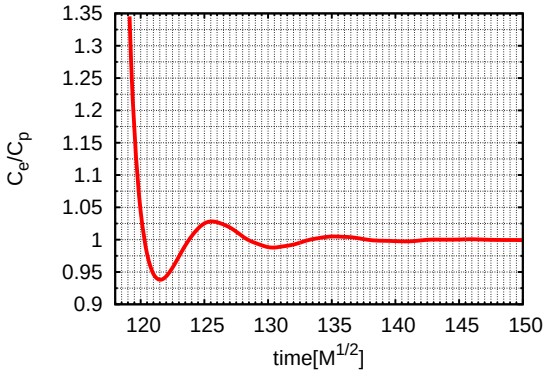

Figure 1: The time variation of the length of equator over that of meridian after merger of two BHs. This damping oscillation corresponds the quasi-normal mode of 5 dimensional Schwarzschild BH.

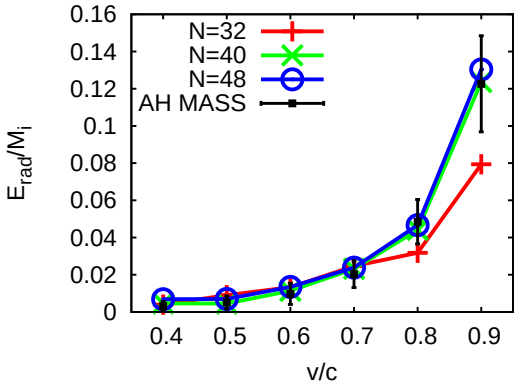

Figure 2: The radiated energy of gravitational wave from headon collision in 5 dimensions. The color shows the difference of the grid resolution. The black squares and their error bars are calculated from the formed BH mass.

From above expression, we calculate the mass parameter μ by using the area of horizon $\mathcal{A}_H$ and the length of the equator $\mathcal{C}_e$. The BH mass is related to the mass parameter as

$$M_{BH} = \frac{3\pi\mu}{8}. \tag{4}$$

We also see the quasi-normal mode of the BH in 5 dimensions by comparing the length of equator and that of meridian $\mathcal{C}_p$.

$$\mathcal{A}_H = \int_0^{2\pi}\int_0^{2\pi}\int_0^{\pi/2} \mathrm{d}\chi\mathrm{d}\phi\mathrm{d}\theta\ \mathrm{r}_+\mu\sin\theta\cos\theta = 2\pi^2\mu\mathrm{r}_+, \tag{5}$$

$$\mathcal{C}_p = \int_0^{\pi/2} \mathrm{d}\theta \sqrt{\mathrm{g_{rr}}\left(\frac{\mathrm{dr}}{\mathrm{d}\theta}\right)^2 + 2\mathrm{g_{r\theta}}\left(\frac{\mathrm{dr}}{\mathrm{d}\theta}\right) + \mathrm{g}_{\theta\theta}} = \sqrt{\mu}\mathrm{E}\left(\mathrm{a}/\sqrt{\mu}\right), \tag{6}$$

$$\mathcal{C}_e = \int_0^{2\pi} \mathrm{d}\phi \sqrt{\mathrm{g_{rr}}\left(\frac{\mathrm{dr}}{\mathrm{d}\phi}\right)^2 + 2\mathrm{g_{r\phi}}\left(\frac{\mathrm{dr}}{\mathrm{d}\phi}\right) + \mathrm{g}_{\phi\phi}} = \frac{2\pi\mu}{\mathrm{r}_+}, \tag{7}$$

where r_+ is the horizon radius and $E(z)$ is the elliptic function.

Fig.1 shows that the deformed BH by the high speed collision of two BHs settle down Schwarzschild BH. To estimate the radiated energy from the gravitational wave, we consider the energy balance between the initial total energy and the final total energy as follows.

$$E_{ini} = M_{BH} + E_{rad} \tag{8}$$

On the other hand, we can directly calculate the radiated energy by gravitational wave from headon collisions of two BHs in 5 dimensions using Landau-Lifshitz's pseudo tensor[8]. Fig.2 shows that the estimation from the energy balance and from LL pseudo tensor agree well. We also see the convergence with the simulation in high resolution.

The radiated energy from two test particle collision in 5 dimensions is given [9] as

$$\frac{E_{rad}}{M_{ini}} = E_\infty \frac{(\gamma-1)^2\left(\gamma^2+3\gamma+1\right)}{\gamma^3(\gamma+1)}. \tag{9}$$

E_∞ contains a cut-off frequency because of the test particle approximation. If we choose the quasi-normal mode as the cut-off frequency, Our results agree well in the region of not so high velocity collision.

4 Conclusion and Discussion

We perform simulations of the headon collision in 5 dimensions with numerical relativity by extending SACRA code. The mass of a formed BH is calculated from the area of horizon and the length of equator and the length of meridian. We estimate the radiated energy from the headon collision of two BHs by two different methods. Fist is by the energy balance between before merger and after merger. Second is by Landau and Lifshitz's pseudo tensor. The results shows both methods agree well in high resolution. We also compare the radiated energy from the headon collision of two BHs in 5 dimensions to the headon collision of two test particles in 5 dimensions. Two results have a good agreement in the low velocity collision.

References

[1] S. Weinberg, *Gravitation and Cosmology* (Wiley, New York, 1972).

[2] H. Yoshino, M. Shibata, Phys. Rev. D **80**, 084025 (2009).

[3] T. Yamamoto, M. Shibata, and K. Taniguchi, Phys. Rev. D **78**, 064054 (2008).

[4] U. Sperhake *et al.*, Phys. Rev. Lett. **103**, 131102 (2009).

[5] M. Shibata and T. Nakamura, Phys. Rev. D **52**, 5428 (1995); T. W. Baumgarte and S. L. Shapiro, Phys. Rev. D **58**, (1998).

[6] M. Shibata, H. Okawa, and T. Yamamoto, Phys. Rev. D **70**, 101501 (2008).

[7] R. Emparan and H. Reall, Living Rev. Relativity, **11**, (2008), 6.

[8] L. D. Landau and E. M. Lifshitz, *The Classical Theory of Fields* (Pergamon Press, Oxford,1962).

[9] V. Cardoso, O. Dias and J. Lemos, Phys. Phys. Rev. D **67**, 064026 (2006).

Anisotropic inflation and its imprints on the CMB

Masa-aki Watanabe[1 (a)], Sugumi Kanno[(b)] and Jiro Soda[(a)]

[(a)] *Department of Physics, Kyoto University, Kitashirakawa-oiwake-cho, Sakyo, Kyoto, 606-8502*
[(b)] *Department of Physics and Astronomy, Tufts University, Robinson Hall, 212 College Avenue,Medford, MA, 02155, USA*

Abstract

We study the imprints of anisotropic inflation on the CMB temperature fluctuations and polarizations. The statistical anisotropy stems not only from the direction dependence of curvature and tensor perturbations, but also from the cross correlation between curvature and tensor perturbations, and the linear polarization of tensor perturbations. We show that off-diagonal TB and EB spectra as well as on- and off-diagonal TT, EE, BB, TE spectra are induced from anisotropic inflation. We emphasize that the off-diagonal spectra induced by the cross correlation could be a characteristic signature of anisotropic inflation.

1 Primordial Statistical Anisotropy

Precise observations of the cosmic microwave background radiation (CMB) enable us to test the fundamental predictions of inflation on primordial fluctuations such as scale independence and Gaussianity. The statistical isotropy has been a robust prediction protected by the cosmic no-hair conjecture which claims that the inflation washes out classical anisotropy. Recently, however, its apparent violation has been reported and its origins including systematic effects have been widely discussed.[1][2]

In this paper, we discuss the statistical anisotropy from anisotropic inflation including tensor perturbations and show how they are imprinted in the two-point correlations of the CMB temperature fluctuations and polarizations. Then we compare signals of the primordial anisotropy induced by tensor perturbations with that induced purely by scalar perturbations, and see what we can expect as a signal peculiar to anisotropic inflation.

In the anisotropic inflation model, we have four kinds of anisotropy: (i) direction dependence in primordial power spectrum of scalar (curvature) perturbations, (ii) that in tensor perturbations, (iii) cross correlation between curvature perturbations and a linear polarization mode of tensor perturbations, and (iv) linear polarization of tensor perturbations.

It is convenient to express the primordial power spectra in the following way:

$$\langle R^s(\mathbf{k}) R^{s'}(\mathbf{k}')^* \rangle = P^{ss'}(\mathbf{k}) \delta^3(\mathbf{k} - \mathbf{k}'), \tag{1}$$

where primordial scalar perturbations is represented by R^0 and right- and left-handed circular polarizations of tensor perturbations are given by R^{+2} and R^{-2} respectively, while the delta function results from an assumption of statistical homogeneity (translational invariance). In the conventional isotropic inflation, where rotational invariance holds, $P^{ss'}(\mathbf{k})$ are proportional to $\delta_{ss'}$ and functions dependent only on $|s|$ and $|\mathbf{k}|$. When we consider the cross correlation (iii) and the linear polarization (iv), we need to take into account off-diagonal ($s \neq s'$) components.

Note that, unlike diagonal ones, these components change their values with the rotation of the polarization bases, hence the bases have to be specified. The simplest choice is to make use of spherical coordinates with a certain fixed preferred direction, i.e. $\sqrt{2}e_{ij}^{\pm 2} = e_{ij}^{\mathrm{d}} \pm i e_{ij}^{\times}$, $\sqrt{2}e_{ij}^{\mathrm{d}} = \mathbf{e}_i^{\theta}\mathbf{e}_j^{\theta} - \mathbf{e}_i^{\phi}\mathbf{e}_j^{\phi}$, $\sqrt{2}e_{ij}^{\times} = \mathbf{e}_i^{\theta}\mathbf{e}_j^{\phi} + \mathbf{e}_i^{\phi}\mathbf{e}_j^{\theta}$, here θ and ϕ are polar and azimuthal angles. This convention is adopted throughout this paper. The power spectra in linear polarization modes $\sqrt{2}R^{\mathrm{d}} = R^{+2} + R^{-2}$, $\sqrt{2}R^{\times} = i(R^{+2} - R^{-2})$ are similarly defined by $\langle R^{\alpha}(\mathbf{k}) R^{\beta *}(\mathbf{k}') \rangle = P^{\alpha\beta}(\mathbf{k}) \delta^3(\mathbf{k} - \mathbf{k}')$, where α, β denote $0, \mathrm{d}$ or $\times$. Then, the power spectra

[1] Email address: mwatanabe@tap.scphys.kyoto-u.ac.jp

of helicity bases are expressed by those of linear bases as

$$\begin{aligned} P^{0\pm2} &= (P^{0\mathrm{d}} \pm iP^{0\times})/\sqrt{2},\ P^{\pm20} = (P^{\mathrm{d}0} \mp iP^{\times0})/\sqrt{2}, \\ P^{+2+2} &= P^{-2-2} = (P^{\mathrm{dd}} + P^{\times\times})/2 \equiv P_t^{\mathrm{unp}} \\ P^{+2-2} &= P^{-2+2} = (P^{\mathrm{dd}} - P^{\times\times})/2 \equiv P_t^{\mathrm{pol}}, \end{aligned} \tag{2}$$

We hereafter neglect circular polarization of the tensor modes in this study.

We consider an anisotropic inflation model we proposed in [3]. The model includes a vector field coupled to the inflaton field ϕ through a kinetic term of the form $\mathcal{L}_{\mathrm{vec}} = -1/4 f(\phi)^2 F_{\mu\nu}F^{\mu\nu}$. The anisotropic inflation predicts the following modification to primordial power spectra [4]:

$$\begin{aligned} \text{i) } P^{00}(\mathbf{k}) &= P_{\mathrm{s}}(k)[1 + g\sin^2\theta], \quad \text{ii) } P_t^{\mathrm{unp}}(\mathbf{k}) = P_{\mathrm{t}}(k)[1 + g_h \sin^2\theta], \\ \text{iii) } P^{0\mathrm{d}}(\mathbf{k}) &= P^{\mathrm{d}0}(\mathbf{k}) = \sqrt{P_{\mathrm{s}}(k)P_{\mathrm{t}}(k)}g_c \sin^2\theta, \quad \text{iv) } P_t^{\mathrm{pol}}(\mathbf{k}) = P_{\mathrm{t}}(k) g_l \sin^4\theta, \end{aligned} \tag{3}$$

where $P_{\mathrm{s}}(k), P_{\mathrm{t}}(k)$ are isotropic parts of scalar and tensor power spectra, the θ is the angle between $\hat{\mathbf{k}}$ and a certain privileged direction, and $k \equiv |\mathbf{k}|$. For simplicity, here we neglected the scale dependence of g, g_h, g_l, g_c which is not significant for the scales relevant to the CMB. The model predicts the consistency relation $g_h = \frac{1}{4}\epsilon g,\ g_c = \sqrt{\epsilon} g$, where ϵ is a slow-roll parameter, in addition to the usual relation for tensor-to-scalar ratio $r = 2P_{\mathrm{t}}(k)/P_{\mathrm{s}}(k) = 16\epsilon$, and the linear polarization is relatively small $g_l \sim \mathcal{O}(g_h^2)$ and there is no cross correlation between scalar perturbations and cross mode tensor perturbations $P^{\times0} = P^{0\times} = 0$.

2 Angular Power Spectra

In this section, we evaluate the following angular power spectra:

$$C_{ll'mm'}^{XX'} \equiv \langle a_{lm}^X a_{l'm'}^{X'*} \rangle, \quad a_{lm}^X(\eta_o, \mathbf{x}_o) = \int d\Omega_{\hat{\mathbf{p}}} X(\hat{\mathbf{p}}, \eta_o, \mathbf{x}_o) Y_{lm}^*(\hat{\mathbf{p}}; \mathbf{e}). \tag{4}$$

where $*$ denotes complex conjugate and $X = T, E, B$ designates fluctuations in temperature and polarization modes of the CMB. The polar angle of spherical harmonics $Y_{lm}(\hat{\mathbf{p}}; \mathbf{e})$ is measured from the direction $\mathbf{e}$. In the presence of statistical anisotropy, the spectra $C_{ll'mm'}^{XX'}$ are generally dependent on the direction $\mathbf{e}$. In this paper, we make this direction coincide with the privileged direction of statistical anisotropy for simplicity. The fluctuation X can be expressed in terms of the primordial fluctuation with wavenumber $\mathbf{k}$ in the following way:

$$X(\hat{\mathbf{p}}, \eta_o, \mathbf{x}_o) = \int \frac{d^3\mathbf{k}}{(2\pi)^3} \sum_L \sum_{s=-2}^{2} R^s(\mathbf{k}) Y_{Ls}(\hat{\mathbf{p}}; \hat{\mathbf{k}}) \Delta_{Ls}^X(k, \eta_o) e^{i\mathbf{k}\cdot\mathbf{x}_o}. \tag{5}$$

where $s = 0, \pm2$ denote contributions from 3d-scalar, tensor mode, respectively. The vector modes are hereafter neglected for simplicity. Note that $Y_{Ls}(\hat{\mathbf{p}}; \hat{\mathbf{k}})$ explicitly indicates that the polar angle of the spherical harmonics is measured from the direction $\hat{\mathbf{k}}$ while the azimuthal angle is assumed to be defined by the polarization bases of R^s. And the transfer functions Δ satisfy the relations $\Delta_{L,-s}^M = \Delta_{L,s}^M,\ \Delta_{L,-s}^E = \Delta_{L,s}^E,\ \Delta_{L,-s}^B = -\Delta_{L,s}^B$. Substituting Eq.(5) into Eq.(4) and using the following formula

$$Y_{lm}(\hat{\mathbf{p}}; \hat{\mathbf{k}}) = \sqrt{\frac{4\pi}{2l+1}} \sum_{m'} Y_{lm'}(\hat{\mathbf{p}}; \mathbf{e})\ {}_{-m}Y_{lm'}^*(\hat{\mathbf{k}}; \mathbf{e})\ , \tag{6}$$

we have

$$C_{ll'mm'}^{XX'} = \int \frac{k^2 dk}{(2\pi)^6} \sum_{s,s'} \tilde{\Delta}_{l,s}^X(k, \eta_o) \tilde{\Delta}_{l',s'}^{X'}(k, \eta_o) \int d\Omega_{\hat{\mathbf{k}}} P^{ss'}(\mathbf{k})\ {}_{-s}Y_{lm}^*(\hat{\mathbf{k}}; \mathbf{e})\ {}_{-s'}Y_{l'm'}(\hat{\mathbf{k}}; \mathbf{e}), \tag{7}$$

where we defined $\tilde{\Delta}_{l,s}^X(k, \eta_o) \equiv \sqrt{\frac{4\pi}{2l+1}} \Delta_{l,s}^X(k, \eta_o)$, ${}_0Y_{lm} \equiv Y_{lm}$ and ${}_{\pm2}Y_{lm}$ denote spin weighted spherical harmonics. Hereafter, we omit the direction $\mathbf{e}$ for simplicity. Then $P^{ss'}$ is associated to the linear

polarizations and scalar-tensor correlation via Eq.(2) and the property of transfer function helps to simplify the expression.

Now, we can see the imprints of statistical anisotropy on the CMB. Here we exemplify the calculation of the spectra for (iii) cross correlation. For the spectra for (i)(ii) and (iv), please see [5].

We have TT,EE,TE spectra induced by the cross correlation of scalar perturbations and plus mode tensor perturbations:

$$C_{ll'mm'}^{XX'(\mathrm{iii})} = \frac{1}{\sqrt{2}} \int \frac{k^2 dk}{(2\pi)^6} \left[\tilde{\Delta}_{l0}^{X} \tilde{\Delta}_{l'2}^{X'} I_{ll'mm'}^{(\mathrm{iii})+} + (-1)^{l+l'+m+m'} \tilde{\Delta}_{l2}^{X} \tilde{\Delta}_{l'0}^{X'} I_{l',l,-m',-m}^{(\mathrm{iii})+} \right], \tag{8}$$

and TB,EB spectra:

$$C_{ll'mm'}^{XB(\mathrm{iii})} = \frac{1}{\sqrt{2}} \int \frac{k^2 dk}{(2\pi)^6} \tilde{\Delta}_{l0}^{X} \tilde{\Delta}_{l'2}^{B} I_{ll'mm'}^{(\mathrm{iii})-} \ . \tag{9}$$

Here, we have defined

$$I_{ll'mm'}^{(\mathrm{iii})\pm} = \int d\Omega_{\hat{\mathbf{k}}} P^{0\mathrm{d}}(\mathbf{k}) \ Y_{lm}^{*}(\hat{\mathbf{k}}) \left({}_{-2}Y_{l'm'}(\hat{\mathbf{k}}) \pm {}_{+2}Y_{l'm'}(\hat{\mathbf{k}}) \right) \ , \tag{10}$$

To derive these relations we used the property $P^{d0}(\mathbf{k}) = P^{0d}(-\mathbf{k})$ and ${}_{s}Y_{lm}^{*}(\mathbf{k}) = (-1)^{l+m} \ {}_{-s}Y_{l,-m}(-\mathbf{k})$.

The direction dependence of cross correlation is $\sin^2\theta$. Hence, TT,EE,TE spectra can be evaluated as:

$$\begin{aligned} I_{ll'mm'}^{(\mathrm{iii})+} &= 2\Big(\alpha_{l+2,m}^{-2}\delta_{l',l+2} + \alpha_{l,m}^{0}\delta_{l',l} + \alpha_{l-2,m}^{+2}\delta_{l',l-2}\Big)\delta_{mm'} g_c \sqrt{P_s(k)P_t(k)}, \\ I_{ll'mm'}^{(\mathrm{iii})-} &= 2\Big(\beta_{l+1,m}^{-1}\delta_{l',l+1} + \beta_{l-1,m}^{+1}\delta_{l',l-1}\Big)\delta_{mm'} g_c \sqrt{P_s(k)P_t(k)}\,, \end{aligned} \tag{11}$$

where the coefficients are given by:

$$\begin{aligned} \alpha_{l,m}^{+2} &\equiv \sqrt{\frac{l(l-1)(l+m+1)(l-m+1)(l+m+2)(l-m+2)}{(l+1)(l+2)(2l+1)(2l+3)^2(2l+5)}}\,, \\ \alpha_{l,m}^{-2} &\equiv \sqrt{\frac{(l+1)(l+2)(l+m)(l-m)(l+m-1)(l-m-1)}{(l-1)l(2l-3)(2l-1)^2(2l+1)}}\,, \\ \alpha_{l,m}^{0} &\equiv \frac{2\left\{3m^2 - l(l+1)\right\}}{(2l-1)(2l+3)} \sqrt{\frac{(l-1)(l+2)}{l(l+1)}}\,, \\ \beta_{l,m}^{+1} &\equiv 2m\sqrt{\frac{(l-1)(l+m+1)(l-m+1)}{l(l+1)(l+2)(2l+1)(2l+3)}}\,, \ \beta_{l,m}^{-1} \equiv -2m\sqrt{\frac{(l+2)(l+m)(l-m)}{(l-1)l(l+1)(2l+1)(2l-1)}}. \end{aligned} \tag{12}$$

3 Discussion

In the previous section, we have shown that the anisotropy related to tensor perturbations generally induces off-diagonal TB, EB spectra as well as on- and off-diagonal TT, EE, BB, TE spectra. Here we discuss its significance.

First, we compare the amplitudes of signals induced by the four components of anisotropy. In Fig 1, we have depicted contributions of each component to an off-diagonal TT correlation $\frac{l(l+1)}{2\pi}|C_{l,l+2,0,0}^{TT}|$. As for the parameter of anisotropy in scalar perturbations, we adopted the value $g = 0.3$ as a reference, which is just of the order of a systematic error in WMAP 5-year data obtained in [1]. We also assumed the tensor-to-scalar ratio to be $r = 0.3$. Then the other quantities can be determined by the consistency relations in our model: $r = 16\epsilon,\ g_h = \frac{1}{4}\epsilon g,\ g_c = \sqrt{\epsilon} g,\ g_l \sim g_h^2$.

We see that the contributions of tensor perturbations (ii),(iii) and (iv) are suppressed in comparison to that of (i). And, the cross correlation (iii) has the largest contribution next to (i). This reflects the hierarchy among $rg_h = \mathcal{O}(g\epsilon^2), \sqrt{r}g_c = \mathcal{O}(g\epsilon), rg_l = \mathcal{O}(g^2\epsilon^3)$. It is also true for EE and TE spectra.

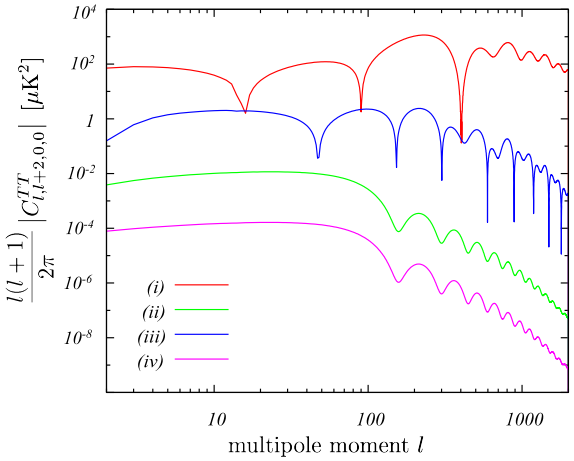

Figure 1: The TT spectra induced by (i) anisotropy in scalar perturbations, (ii) that in tensor perturbations, (iii) cross correlation, and (iv) linear polarization of tensor perturbations. The parameters are chosen as $g = 0.3,\ r = 0.3$.

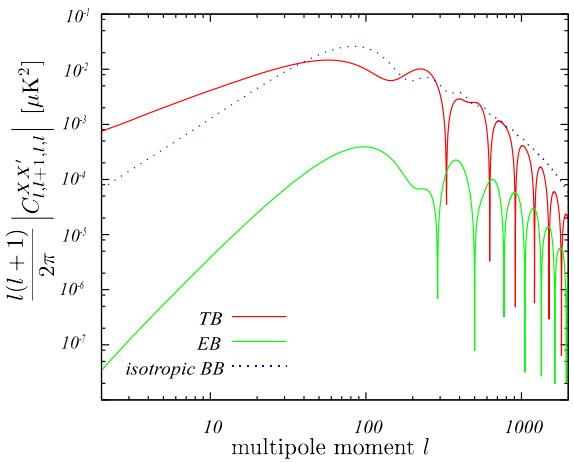

Figure 2: The TB and EB spectra induced by (iii) cross correlation. As a reference of magnitude, the conventional BB spectrum $l(l+1)C^{BB}_{llmm}/2\pi$ induced by isotropic part of the tensor perturbations is plotted with a dotted line. The parameters are chosen as $g = 0.3,\ r = 0.3$.

The ratio between (i), (ii) and (iii) are given by the slow-roll parameter ϵ (or tensor-to-scalar ratio r) and does not depend on the value of g.

Next we consider peculiar signals of anisotropic inflation. The components (ii), (iii), (iv) induce B mode polarization, and the largest correlation is produced by the cross correlation (iii). In Fig 2, we have depicted examples of TB and EB correlations $\frac{l(l+1)}{2\pi}|C^{TB}_{l,l+1,l,l}|$, $\frac{l(l+1)}{2\pi}|C^{EB}_{l,l+1,l,l}|$. The parameters are again $r = 0.3, g = 0.3$. As a reference, the conventional BB spectrum induced by the isotropic part of tensor perturbations $\frac{l(l+1)}{2\pi}C^{BB}_{llmm}$ (independent of m) is also plotted with a dotted line.

The ratio of TB correlation induced by cross correlation to the isotropic BB correlation is not dependent on ϵ (or r) for a fixed value of g in our anisotropic inflation model. For the optimistic value of $g \sim 0.3$, both amplitudes become comparable. This simple order estimation implies that the TB signal could be comparable to that of B mode correlation induced by primordial gravitational wave. Hence, we can conclude that anisotropic inflation is a potential source of off-diagonal TB correlation, in addition to other effects such as gravitational lensing and our peculiar velocity proposed so far.

References

[1] N. E. Groeneboom, L. Ackerman, I. K. Wehus and H. K. Eriksen, Astrophys. J. **722**, 452 (2010) [arXiv:0911.0150 [astro-ph.CO]].

[2] D. Hanson, A. Lewis and A. Challinor, Phys. Rev. D **81**, 103003 (2010) [arXiv:1003.0198 [astro-ph.CO]].

[3] M. a. Watanabe, S. Kanno and J. Soda, Phys. Rev. Lett. **102**, 191302 (2009) [arXiv:0902.2833 [hep-th]].

[4] T. R. Dulaney and M. I. Gresham, Phys. Rev. D **81**, 103532 (2010) [arXiv:1001.2301 [astro-ph.CO]]. A. E. Gumrukcuoglu, B. Himmetoglu and M. Peloso, Phys. Rev. D **81**, 063528 (2010) [arXiv:1001.4088 [astro-ph.CO]]. M. a. Watanabe, S. Kanno and J. Soda, Prog. Theor. Phys. **123**, 1041 (2010) [arXiv:1003.0056 [astro-ph.CO]].

[5] M. a. Watanabe, S. Kanno and J. Soda, arXiv:1011.3604 [astro-ph.CO].

Gravitational radiation and angular momentum flux from a spinning dynamical black hole

Yu-Huei Wu[1](a)(b) and Chih-Hung Wang[2](b)(c)(d)

(a) *Center for Mathematics and Theoretical Physics, National Central University, Chungli, 320, Taiwan.*
(b) *Department of Physics, National Central University, Chungli, 320, Taiwan.*
(c) *Department of Physics, Tamkang University, Tamsui, Taipei 25137, Taiwan.*
(d) *Institute of Physics, Academia Sinica, Taipei 115, Taiwan.*

Abstract

A four-dimensional asymptotic expansion scheme is used to study the next order effects of the nonlinearity near a spinning dynamical black hole. The angular momentum flux and energy flux formula are then obtained by asymptotic expansion and the compatibility of the coupling Newman-Penrose equations. After constructing the reference frame in terms of the compatible constant spinors, the energy-momentum flux is derived and it is related to the black hole area growth. Directly from the flux formula of the spinning dynamical horizon, we find that the physically reasonable condition on the positivity of the gravitational energy flux yields that the shear will monotonically decrease with time.

1 Introduction

In this paper, we use the Bondi-type coordinates to write the null tetrad for a spinning dynamical horizon (DH). The boundary conditions for the quasi-local horizons can be expressed in terms of Newman-Penrose (NP) coefficients from the Ashtekar's definition on DH. Unlike Ashtekar *et al*'s [1, 2] three dimensional analysis, we adopts a 4-dimensional asymptotic expansion to study the neighborhoods of generic isolated horizons (IHs) and dynamical horizons (DHs). Since the asymptotic expansion has been used to study gravitational radiations near the null infinity [6, 7], it offers a useful scheme to analyze gravitational radiations approaching another boundary of space-time, black hole horizons. We first set up a null frame with the proper gauge choices near quasi-local horizons and then expand Newman-Penrose (NP) coefficients, Weyl, and Ricci curvature with respect to radius. Their fall-off can be determined from NP equations, Bianchi equations, and exact solutions, e.g., the Vaidya solution. From the reduction and the decoupling of the equations governing the Weyl scalars, instead of assuming $\Psi_0, \Psi_1 = 0$ on DH, we set Ψ_1, Ψ_3 vanishing on a spinning DH. This serves as a *peeling property* for a spinning DH and is a similar setting with the perturbation method (Also see Chandrasekhar [5]). This approach allows one to see the next order contributions from the nonlinearity of the full theory for the quasi-local horizons. We have shown that the quasi-local energy-momentum flux formula for a non-rotating DH by using asymptotic expansion yields the same result as Ashtekar-Krishman flux [8, 9]. For slow rotating DH, we have presented our results in [8], however, it makes too many assumptions to be satisfactory. Furthermore, the flux formula has a shear (NP coefficient σ) and a angular momentum (NP coefficient π) coupling term. Since it is unclear whether the existence of this term carries any physical meaning or it may due to our assumptions, we thereby study the fast spinning case and extend our previous work on IHs and DHs into a more general case.It is known that DH is a three-dimensional spacelike hypersurface with its topology $R^1 \times S^2$, so the shape of its 2-dimentioanl cross section will depend on the gauge freedom of choosing foliation. One may image that there exists a gauge choice which can make DH's cross section looks like a 2-sphere. The existence of angular momentum will not change the boundary condition for the null infinity, however, it will affect the boundary conditions of a black hole. In GR, quasi-local mass expressions for Kerr solution disagree one another [3]. Different quasi-local expressions give different values of quasi-local mass for Kerr black hole. At null infinity, there is no generally accepted definition for angular momentum [11]. By the aid of using asymptotic constant spinor to define spin frame as the reference frame for our observation, mass and angular momentum flux can be calculated.

[1]Email address: yhwu@mail.phy.ncu.edu.tw
[2]Email address: chwang1101@phys.sinica.edu.tw, chwang@phy.ncu.edu.tw

2 Angular momentum and energy-momentum and their flux of a spinning DH

We choose the incoming null tetrad $n_a = \nabla_a v$ to be the gradient of the null hypersurface $v = const$. We then have $g^{ab}v_{,a}v_{,a} = 0$. It gives us the gauge conditions $\nu = \mu - \overline{\mu} = \gamma + \overline{\gamma} = \overline{\alpha} + \beta - \overline{\pi} = 0$. Then we further choose n^a flag plane parallel, it implies $\gamma = 0$. For the setting of outgoing null tetrad ℓ, we first choose ℓ to be a geodesic and use null rotation type III to make $\epsilon - \overline{\epsilon} = 0$. We choose $m, \overline{m}$ tangent to the cross section S, and thus $\rho \hat{=} \overline{\rho}, \pi \hat{=} \overline{\tau}$. In the comoving coordinate (v, r', x^2, x^3) we have $\ell^a = (1, U - \dot{R}_\Delta, X^2, X^3)$,$n^a = (0, -1, 0, 0)$, $m^a = (0, 0, \xi^2, \xi^3)$, where $\dot{R}_\Delta(v)$ is the rate of changing effective radius of DH and $r' = r - R_\Delta(v)$ and $R_\Delta(v)$ is effective radius of a spinning DH. Since we use $\kappa = \nu = 0, \sigma \neq 0, \lambda \neq 0$, therefore one can set $\Psi_1 \hat{=} \Psi_3 \hat{=} 0$ as *peeling properties for a spinning DH*. This is a similar with perturbation method and one may refer to p. 175 and p. 180 in [5]. The falloff of the Weyl scalars is algebraically general (this is a more general setting than [8] and [9]) on DH where

$$\Psi_1 = \Psi_3 = O(r'), \Psi_0 = \Psi_2 = \Psi_4 = O(1). \tag{1}$$

By considering Vaidya solution as our compared basis for matter field part, the falloff of the Ricci spinor components are

$$\Phi_{00} = O(1), \Phi_{22} = \Phi_{11} = \Phi_{02} = \Phi_{01} = \Phi_{21} = O(r'). \tag{2}$$

We adopt a similar idea of Bramson's asymptotic frame alignment for null infinity [4] and apply it to set up spinor frames for a spinning DH. We find the compatible conditions for spin frame are

$$\text{þ}_0\lambda_0^0 = 0, \text{ð}_0\lambda_0^0 + \sigma_0\lambda_1^0 = 0, \text{ð}_0\lambda_1^0 - \mu_0\lambda_0^0 = 0, \text{þ}_0\lambda_1^0 = -\overline{\text{ð}}_0\lambda_0^0. \tag{3}$$

Since there are gauge freedoms on choosing the foliation of DH, we then assume that there exists a natural foliation to make DH cross section S as a two sphere. Therefore, on a sphere with effective horizon radius $R_\Delta(v)$, one can set $\mu_0 = -\frac{1}{R_\Delta}$. Let P, μ_0 on a sphere with radius R_Δ, then $P \propto \frac{1}{R_\Delta}$. Moreover, the effective surface gravity is $\tilde{\kappa} = 2\epsilon_0 = \frac{1}{2R_\Delta}$, and then $\mu_0 = -4\epsilon_0$. Check the commutation relation $[\delta_0, D_0]\lambda_0$ and $[\delta_0, D_0]\sigma_0$, it implies $\ddot{R}_\Delta = 0$. This means that the horizon radius will not accelerate (no inflation). The dynamical horizon will increase with a constant speed. After applying these conditions, we list the main equations that will be used later (for detail, see [10])

(NR1) $\dot{R}_\Delta[-\frac{1}{2}(\Psi_2^0 + \overline{\Psi}_2^0) + \frac{1}{2}(\text{ð}_0\pi_0 + \overline{\text{ð}}_0\overline{\pi}_0) - \pi_0\overline{\pi}_0] = \Phi_{00}^0,$

(NR2) $\dot{\sigma}_0 = \dot{R}_\Delta[-\text{ð}_0\overline{\pi}_0 - \overline{\pi}_0^2 + \sigma_0\mu_0] + 2\epsilon_0\sigma_0 + \Psi_0^0,$

(NR4) $\frac{\overline{\sigma}_0\ddot{R}_0 - \dot{R}_\Delta\dot{\overline{\sigma}}_0}{(\dot{R}_\Delta)^2} = \dot{R}_\Delta\Psi_4^0 + \overline{\text{ð}}_0\pi_0 + \pi_0^2 + 2\frac{\overline{\sigma}_0\epsilon_0}{\dot{R}_\Delta} - \mu_0\overline{\sigma}_0,$

(NR7) $\text{Re}\Psi_2^0 = 2\mu_0\epsilon_0 - \pi_0\overline{\pi}_0 - \text{Re}\text{ð}_0\pi_0, \text{Im}\Psi_2^0 = -\text{Im}\text{ð}_0\pi_0,$

(NB2) $\dot{\Psi}_2^0 = \dot{R}_\Delta[3\mu_0 - \sigma_0\Psi_4^0] + \frac{\overline{\sigma}_0\Psi_0^0}{\dot{R}_\Delta} + \mu_0\Phi_{00}^0,$

(NR1)+(NR7) $2\text{Re}\text{ð}_0\pi_0 = \frac{\Phi_{00}^0}{\dot{R}_\Delta} + 2\mu_0\epsilon_0,$

(NR8) $\overline{\text{ð}}_0\sigma_0 = 0,$ **(NR9)** $-2\overline{\sigma}_0\overline{\pi}_0 = \dot{R}_\Delta\mu_0\pi_0, \sigma_0\overline{\text{ð}}_0\pi_0 = -\frac{1}{2}\dot{R}_\Delta\mu_0\overline{\text{ð}}_0\overline{\pi}_0,$

(NR3) $\dot{\pi}_0 = 2\dot{R}_\Delta\mu_0\pi_0,$ **(NR5)** $\dot{\alpha}_0 = \dot{R}_\Delta\alpha_0\mu_0 - \overline{\sigma}_0\overline{\pi}_0,$ **(NR6)** $\dot{\beta}_0 = \dot{R}_\Delta\mu_0(\overline{\pi}_0 + \beta_0) + \sigma_0\pi_0.$

We use an asymptotically rotating Killing vector ϕ^a for a spinning DH. It coincides with a rotating vector $\phi^\alpha \hat{=} \psi^a$ on a DH and is divergent free. It implies $\Delta_a\phi^a := S_{a0}^a S_a^{b0}\nabla_{b0}\phi^{a0} = 0$. Therefore, $\overline{m}_a\delta\phi^a = -m_a\overline{\delta}\phi^a$. Let $\phi^a = Am^a + B\overline{m}^a$, we get $A = -B$. Therefore, it exists a function f such that $\phi^a = \overline{\delta}fm^a - \delta f\overline{m}^a$, which is type $(0,0)$. Since f is type $(0,0)$, therefore $\delta f = \text{ð}f$. By using Komar integral, the quasi-local angular momentum on a spinning DH is

$$J(R_\Delta) = -\frac{1}{4\pi}\oint_S f\text{Im}\Psi_2^0 dS_\Delta. \tag{4}$$

From (NB2), we get $\text{Im}\dot{\Psi}_2^0 = 3\frac{\dot{R}_\Delta}{R_\Delta}\text{Im}\text{ð}_0\pi_0 = -3\frac{\dot{R}_\Delta}{R_\Delta}\text{Im}\Psi_2^0$. Together with $\frac{\partial}{\partial v}dS_\Delta = 2\frac{\dot{R}_\Delta}{R_\Delta}dS_\Delta$, the angular momentum flux for a spinning DH is

$$\dot{J}(R_\Delta) = -\frac{1}{4\pi}\oint_S(\dot{f} - \frac{\dot{R}_\Delta}{R_\Delta}f)\text{Im}\Psi_2^0 dS_\Delta = -\frac{1}{4\pi}\oint_S \text{Im}[(\text{ð}_0\dot{f} - \frac{\dot{R}_\Delta}{R_\Delta}\text{ð}_0 f)\pi_0]dS_\Delta. \tag{5}$$

We note that from $\frac{d}{dv}$ (NR7), it yields the same result. Here if $\pi_0 \neq 0$ and $f(v,\theta,\phi) = G(\theta,\phi)R_\Delta(v)$, then $\dot{J}(R_\Delta) = 0$. It then returns to the stationary case. If $\pi_0 = 0$, i.e., $\mathrm{Im}\Psi_2^0 = 0$, then J and $\dot{J} = 0$. It then returns to the non-rotating black hole.

By using the compatible constant spinor conditions for a spinning dynamical horizon (3) and the results of the asymptotic expansion, we get the quasi-local energy-momentum integral on a spinning dynamical horizon

$$\begin{aligned} I(R_\Delta) &= -\tfrac{1}{4\pi}\oint \mu_0 \lambda_0^0 \overline{\lambda}_{0'}^0 dS_\Delta \qquad \text{(i)} \\ &= -\tfrac{1}{4\pi}\oint \tfrac{\mathrm{Re}}{2\epsilon_0}[\Psi_2^0 + \delta_0\pi_0 + 2\beta_0\pi_0]\lambda_0^0\overline{\lambda}_{0'}^0 dS_\Delta. \quad \text{(ii)} \end{aligned}$$

In order to calculate flux we need the time related condition (3) of constant spinor of dynamical horizon and re-scale it. Then $\dot{\lambda}_0^0 = 0$. It's tedious but straightforward to calculate the flux expression. It largely depends on the non-radial NP equations and the second order NP coefficients. By using the results on two sphere foliation, we substitute them back into the energy-momentum flux formula to simplify our expression.

From (i): Apply time derivative to (i), and then we obtain the *quasi-local energy momentum flux for dynamical horizon*

$$\dot{I}(R_\Delta) = \frac{1}{4\pi}\oint \dot{\mu}_0 \lambda_0^0 \overline{\lambda}_{0'}^0 dS_\Delta. \tag{6}$$

where it is always *positive*. Here $\dot{\mu}_0$ is the *news function of DH* that always has mass gain. Integrate the above equation with respect to v and use the results on two sphere, we then have [10]

$$dI(R_\Delta) = \frac{1}{8\pi}\int {}^{(2)}R\lambda_{0'}^0\overline{\lambda}_0^0 dS_\Delta dR_\Delta. \tag{7}$$

From (ii): The total energy momentum flux F_{total} is equal to matter flux plus gravitational flux $F_{\text{total}} = F_{\text{matter}} + F_{\text{grav}}$. We can write the gravitational flux equal to the shear flux plus angular momentum flux $F_{\text{grav}} = F_\sigma + F_J$. The coupling of the shear σ_0 and π_0 can be transform into π_0 terms by using (NR9), then we obtain

$$dI(R_\Delta) = \frac{1}{8\pi}\int \frac{R_\Delta}{\dot{R}_\Delta}\{\frac{1}{\dot{R}_\Delta}\Phi_{00}^0 - 2\frac{\sigma_0\overline{\sigma}_0}{\dot{R}_\Delta}(\frac{\partial}{\partial v}\ln(R_\Delta^2\sigma_0\overline{\sigma}_0)) + 3\frac{\dot{R}_\Delta\pi_0\overline{\pi}_0}{R_\Delta}\}\lambda_0^0\overline{\lambda}_{0'}^0 dS_\Delta dR_\Delta. \tag{8}$$

where $dv = \frac{dR_\Delta}{\dot{R}_\Delta}$. Here we note that if one wants to observe positive shear flux $-\frac{\partial}{\partial v}\ln(R_\Delta^2\sigma_0\overline{\sigma}_0) \geq 0$, it implies that $\dot{\sigma}_0 \leq 0$, where $\dot{R}_\Delta, R_\Delta > 0$ have been considered. So the shear on a spinning DH is monotonically decreasing with respect to v.

Recall that the total flux of Ashtekar-Krishnan [2], we compare our expression with Ashtekar's expression. If we choose $N = \lambda_0^0\overline{\lambda}_{0'}^0$, then (8) together with (7) gives

$$dI(R_\Delta) = \frac{1}{8\pi}\int {}^{(2)}RNdS_\Delta dR_\Delta = \frac{1}{8\pi}\int \frac{R_\Delta}{\dot{R}_\Delta}\{\frac{1}{\dot{R}_\Delta}\Phi_{00}^0 + 2k\frac{\sigma_0\overline{\sigma}_0}{\dot{R}_\Delta} + 3\frac{\dot{R}_\Delta\pi_0\overline{\pi}_0}{R_\Delta}\}NdS_\Delta dR_\Delta \tag{9}$$

where we define $\frac{\partial}{\partial v}\ln(R_\Delta^2\sigma_0\overline{\sigma}_0) := -k$ for the convenience. In the special case $\frac{\partial}{\partial v}\ln(R_\Delta^2\sigma_0\overline{\sigma}_0) := -k$ where k is a constant, we then have

$$R_\Delta^2\sigma_0\overline{\sigma}_0 = Ae^{-kv}. \tag{10}$$

If $k > 0$, $\sigma_0 \searrow$. If $k < 0$, $\sigma_0 \nearrow$. Therefore, if we want to get positive gravitational flux, the shear σ_0 must decrease with time v and $k > 0$. On the contrary, the negative gravitational flux implies the shear must grow with time. The negative mass loss from shear flux will make the dynamical horizon grow with time is physically unreasonable. Therefore, the shear flux should be positive. This says that the shear on a spinning DH will decay to zero when time v goes to infinity and the amount of shear flux F_σ is finite.

$$\sigma_0 \to 0, |v| \to \infty. \tag{11}$$

Hence the dynamical horizon will settle down to an equilibrium state, i.e., isolated horizon.

Laws of black hole dynamics

LHS of eq. (9) can be written as $\frac{dI(R_\Delta)}{2} = \frac{\tilde{\kappa}}{8\pi} dA = \frac{dR_\Delta}{2}$ where $A = 4\pi R_\Delta^2$. For a time evolute vector $t^a = N\ell^a - \Omega\phi^a$, the difference of horizon energy dE^t can be calculated as follow

$$dE^t = \frac{1}{16\pi}\int \frac{R_\Delta}{\dot{R}_\Delta}\{\frac{1}{\dot{R}_\Delta}\Phi^0_{00} + 2k\frac{\sigma_0\overline{\sigma}_0}{\dot{R}_\Delta}\}N + [3N\pi_0\overline{\pi}_0 - 4\frac{\Omega}{\dot{R}_\Delta}\mathrm{Im}[(\eth_0\dot{f} - \frac{\dot{R}_\Delta}{R_\Delta}\eth_0 f)\pi_0]dV$$

and the generalized black hole first law for a spinning dynamical horizon is

$$\frac{\tilde{\kappa}}{8\pi}dA + \Omega dJ = dE^t. \tag{12}$$

3 Conclusions

We use a different peeling property from our earlier work [9][8]. This leads to a physical picture that captures a non-spherical symmetric collapse of a spinning star and formation of dynamical horizon that finally settle down to an isolated horizon. Further from the peeling property, if the shear flux is positive, it excludes the possibility for a spinning DH to absorb the gravitational radiation from nearby gravitational sources. The mass and momentum are carried in by the incoming gravitational wave and cross into dynamical horizon. We shall see that though it may exist outgoing wave on horizon, however, it will not change the boundary condition or make the contribution to the energy flux. A dynamical horizon forms inside the star and eat up all the incoming wave when it reaches the equilibrium state, i.e., isolated horizon. The NP equations are simplified by transforming to a new comoving coordinate and a foliation of 2-sphere for a spinning DH. The existence about how to make such a choice of the foliation will be a further mathematical problem. By using the compatibility of the coupling NP equations and the asymptotic constant spinors, the energy flux that cross into a spinning DH should be positive. The mass gain of a spinning DH can be quantitatively written as matter flux, shear flux and angular momentum flux. Further, a result come out that the shear flux must be positive implies the shear must monotonically decay with respect to time. This is physically reasonable since black hole cannot eat infinite amount of gravitational energy when there is no other gravitational source near a spinning DH. We further found that the mass and mass flux based on Komar integral can yield the same result [10]. Therefore, our results are unlikely expression dependent. For other quasi-local expressions remain the open question for the future study. It would be also interesting if one can generalize to a binary problem.

References

[1] A. Ashtekar, C. Beetle, and S. Fairhurst, Class. Quantum Grav. **17** 253-298 (2000) [arXiv:gr-qc/9907068] .

[2] A. Ashtekar, and B. Krishnan, Class. Quantum Grav. **20** 1031-1062 (2002) [arXiv:gr-qc/0207080].

[3] G. Bergqvist, Class. Quantum Grav. 9 1753-1768 (1992).

[4] B. D. Bramson, Proc. Roy. Soc. London **A341**, 451-461 (1975).

[5] S. Chandrasekhar, The Mathematical Theory of Black Hole, Oxford University Press (1983).

[6] A. R. Exton, E. T. Newman, and R. Penrose, J. Math. Phys. **10** 1566-1570 (1969).

[7] E. T. Newman and T. W. J. Unti, J. Math. Phys. **3**, 891-901 (1962).

[8] Y. H. Wu, PhD thesis, University of Southampton (2007).

[9] Y. H. Wu and C. H. Wang, Phys. Rev. D 80, 063002 (2009). arXiv:0906.1551v1 [gr-qc]

[10] Y. H. Wu and C. H. Wang, arXiv:1009.3331v2 [gr-qc] (2010)

[11] L. B. Szabados, Living Rev. Rel. (2004) (http://relativity.livingreviews.org/Articles/lrr-2004-4)

Probing the size of extra dimension from gravitational wave astronomy

Kent Yagi[1(a)], Norihiro Tanahashi[2(b)] and Takahiro Tanaka[3(c)]

[(a)] *Department of Physics, Kyoto University, Kyoto 606-8502*
[(b)] *Department of Physics, University of California, Davis, CA 95616*
[(c)] *Yukawa Institute, Kyoto University, Kyoto 606-8502*

Abstract

In Randall-Sundrum II (RS-II) braneworld model, it has been conjectured according to the AdS/CFT correspondence that brane-localized black hole (BH) larger than the bulk AdS curvature scale ℓ cannot be static , and it is dual to a 4 dimensional BH emitting the Hawking radiation through some quantum fields. In this scenario, the number of the quantum field species is so large that this radiation changes the orbital evolution of a BH binary. We derived the correction to the gravitational waveform phase due to this effect and estimated the upper bounds on ℓ by performing Fisher analyses. DECIGO/BBO is expected to detect 10^5 BH/NS binaries per year. Taking this advantage, we found that DECIGO/BBO can actually measure ℓ down to $\ell = 0.328$ μm for 5 year observation if we know that binaries are circular a priori. This is about 40 times smaller than the upper bound obtained from the table-top experiment.

1 Introduction

Randall and Sundrum [1] proposed a extra dimension model (RS-II model) which is super-string theory motivated and contains a positive tension brane (on which we live) in 5D AdS bulk with AdS curvature scale ℓ representing the characteristic size of the extra dimension. Ordinary matters are localized on it and gravitons are the only components that can propagate through the bulk. Although the model has a non-compact extra dimension, 4 dimensional general relativity is approximately reproduced on the positive tension brane. The current table-top experiment puts a constraint $\ell \leq 14$ μm [2]

So far, theoretically no brane-localized BHs larger than ℓ have been constructed either analytically or numerically. By employing the AdS/CFT correspondence [3] to the brane-localized BHs, it has been conjectured that such BHs cannot be static [4, 5]. Applying the AdS/CFT correspondence, a 5 dimensional BH is considered to be dual to a 4 dimensional BH associated with CFT fields. The latter system should evolve via Hawking emission from the BH. According to the dictionary of the AdS/CFT correspondence, the number of degrees of freedom of CFT is as large as $g_* \sim 10^{60}$ for $\ell = 10$ μm [6]. This enormously large factor enhances the BH evaporation rate considerably. For a BH with mass M, it is evaluated as [6]

$$\frac{dM}{dt} = -2.8 \times 10^{-7} \left(\frac{1\ M_\odot}{M}\right)^2 \left(\frac{\ell}{10\ \mu\mathrm{m}}\right)^2 M_\odot\ \mathrm{yr}^{-1} =: -C_{\dot{M}} \left(\frac{\ell}{M}\right)^2, \tag{1}$$

where $C_{\dot{M}}$ was defined as the coefficient of the mass loss rate for later use. This leads to the estimate of the lifetime of the BH as $\tau \simeq 1.2 \times 10^6 \left(\frac{M}{1\ M_\odot}\right)^3 \left(\frac{10\ \mu\mathrm{m}}{\ell}\right)^2$ yr which is much less than the age of the universe and may be tested from astrophysical observations [6].

Recently, McWilliams [7] estimated the constraints on ℓ by using the Laser Interferometer Space Antenna (LISA) [8]. A monochromatic binary signal of a galactic $(2+5)$ $M_\odot$ BH/NS binary at $f = 10^{-4}$ Hz puts a constraint $\ell \leq 22$ μm, assuming that it is in the inspiral phase. However, in order to perform more robust probe of the mass loss effect, we need to determine the change in the orbital separation, which cannot be detected from a monochromatic signal. Namely, we need to detect chirp (or anti-chirp)

[1]Email address: kent@tap.scphys.kyoto-u.ac.jp
[2]Email address: tanahashi@ms.physics.ucdavis.edu
[3]Email address: tanaka@yukawa.kyoto-u.ac.jp

GW signals from binaries. In detecting chirp signals from a stellar mass BH/NS binary, the Deci-Hertz Interferometer Gravitational Wave Observatory (DECIGO) [9, 10] and the Big Bang Observatory (BBO) [11], both having optimal sensitivities at 0.1-1 Hz, perform better than LISA.

Here, we first derive the correction to the GW phase due to the mass loss effect, which behaves like -4PN correction. Then, we perform the matched filtering analyses and estimate the possible constraint on ℓ by detecting GWs from BH/NS binaries with DECIGO/BBO. Since high event rate of $O(10^5\ \mathrm{yr}^{-1})$ has been predicted for DECIGO/BBO in GR, we can obtain rather strong constraint by performing statistical analyses.

2 Constraints with LISA obtained by McWilliams

LISA will detect an almost monochromatic GW signal from a galactic binary composed of a BH and a NS. The event rate for such a binary in the LISA frequency range is expected to be 1 yr^{-1} [12]. GW emission makes the orbital separation a smaller (inspiral) with the orbital decay rate given by $\dot{a}_{\rm GW} = -\frac{64}{5}\frac{\mu M_t^2}{a^3}$ [13] where $M_t = m + M$ is the total mass of the binary and $\mu = mM/M_t$ is the reduced mass. On the other hand, BH mass loss effect makes a larger (outspiral) whose rate is given by $\dot{a}_H = -\frac{\dot{M}}{M_t}a$ with the mass loss rate given in Eq. (1). This is derived from the conservation of the specific orbital angular momentum $j = \sqrt{M_t a}$ assuming that the radiation is emitted isotropically in the rest frame of the BH. There exists a critical separation $a_{\rm crit}$ where $\dot{a}_{\rm GW}$ and $\dot{a}_H$ balance. If the separation is larger than $a_{\rm crit}$, the mass loss effect dominates over the GW emission and the separation gets larger while if a is smaller than $a_{\rm crit}$, GW emission wins and the separation gets smaller. Typically, a galactic BH binary forms with its orbital period O(days) [14] whose GW frequency being slightly lower than the LISA sensitivity band. Therefore if its signal is detected at $f = 10^{-4}$ Hz, it means that GW emission effect is dominating over the mass loss effect. The inequality $a(f = 10^{-4}\ \mathrm{Hz}) \leq a_{\rm crit}$ leads to the constraint $\ell \leq 22\ \mu$m, where the typical BH and NS masses are assumed to be 5 $M_\odot$ and 2 $M_\odot$, respectively.

3 Constraints from the matched filtering analysis

3.1 Waveforms

First we study the GW waveform from a binary composed of two BHs with masses M and m (with $M \geq m$). The binaries of our interest satisfy the following conditions, $d\ln A/dt \ll d\phi/dt$ and $d^2\phi/dt^2 \ll (d\phi/dt)^2$, where A is the GW amplitude and ϕ is the phase in the time domain. Then, using the stationary phase approximation [13], the gravitational waveform in the Fourier domain is given as

$$\tilde{h}(f) = \frac{\sqrt{3}}{2}\mathcal{A}f^{-7/6}e^{i\Psi(f)}. \tag{2}$$

In this paper, we only keep the Newtonian quadrupole term for the amplitude and average it over the directions and the orientations of the binaries $\mathcal{A} = \frac{1}{\sqrt{30}\pi^{2/3}}\frac{\mathcal{M}_{z0}^{5/6}}{D_L}$, [15], where D_L is the luminosity distance and $\mathcal{M}_z$ is the redshifted chirp mass defined as $\mathcal{M}_z \equiv (1+z)M_t\eta^{3/5}$ with $\eta \equiv \frac{\mu}{M_t}$. The subscript 0 denotes the quantity at the time of coalescence. On the other hand, we keep the phase up to 2PN order. This is the so-called restricted 2PN waveform. The sky-averaged GW phase in the Fourier space is given as

$$\begin{aligned}\Psi(f) &= 2\pi f t(f) - \phi(f) - \pi/4 \\ &= 2\pi f t_0 - \phi_0 - \pi/4 + \frac{3}{128}(\pi\mathcal{M}_{z0}f)^{-5/3}\left[1 - \frac{25}{19968}C_{\dot{M}}CLx_0^{-4} + \left(\frac{3715}{756} + \frac{55}{9}\eta_0\right)x_0 - 16\pi x_0^{3/2}\right. \\ &\quad \left. + \left(\frac{15293365}{508032} + \frac{27145}{504}\eta_0 + \frac{3085}{72}\eta_0^2\right)x_0^2\right].\end{aligned} \tag{3}$$

The second term in the bracket is the "-4PN" correction term in GW phase due to the mass loss effect. $x \equiv v^2 \equiv (\pi M_{tz} f)^{2/3}$ is the squared velocity of the relative motion with M_{tz} representing the redshifted total mass ($M_{tz} \equiv (1+z)M_t$) and we have introduced a new parameter $L \equiv \frac{\ell^2}{M_{t0}^2}$. The coefficient C is given as $C = \frac{(3-26\eta_0+34\eta_0^2)+(-3+20\eta_0)\sqrt{1-4\eta_0}}{2\eta_0^4}$ for a BH/NS binary.

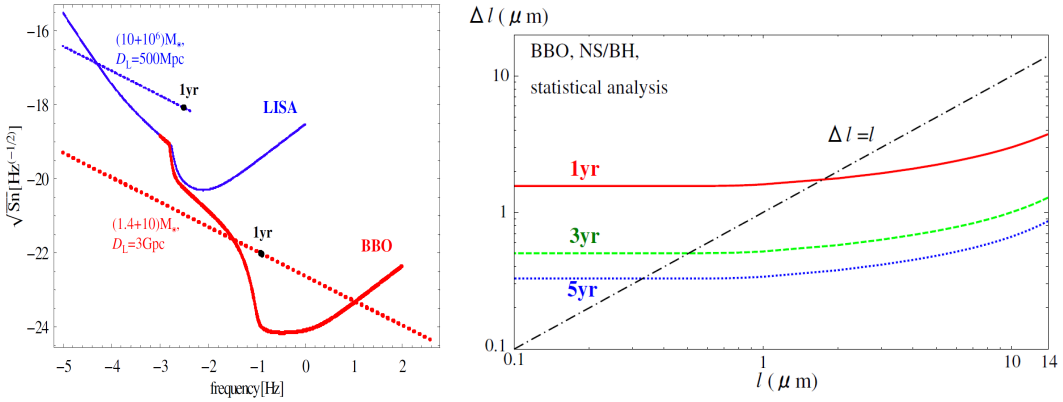

Figure 1: (left) The noise spectral density for BBO (thick solid curve) and LISA (thin solid curve). We also show the amplitudes of GWs from a $(10+10^6)\ M_\odot$ BH/BH binary at $D_L = 500$ Mpc (thin dotted line) and a $(1.4, +10)\ M_\odot$ BH/NS binary at $D_L = 3$ Gpc (thick dotted line). Each dot labelled "1 yr" represents the frequency at 1 yr before the binary reaches ISCO. (Right) The detection errors of ℓ with statistical analysis for 1 yr (red solid), 3 yr (green dashed) and 5 yr (blue dotted) observations of BH/NS binaries with BBO. The (black) dotted-dashed line represents $\Delta\ell = \ell$. If $\Delta\ell$ comes below this line, ℓ can be measured.

3.2 Fisher Analysis

The detected signal $s(t) = h(t) + n(t)$ both contains the GW signal $h(t)$ and the noise $n(t)$. Given a GW signal $s(t)$, the probability distribution that the parameter $\boldsymbol{\theta}$ is the true parameter set becomes $p(h(\boldsymbol{\theta})|s) \propto \exp\left[-\frac{1}{2}\Gamma_{ij}\Delta\theta^i\Delta\theta^j\right]$, where Γ_{ij} is called the Fisher matrix defined by $\Gamma_{ij} \equiv \left(\frac{\partial h}{\partial\theta^i}\middle|\frac{\partial h}{\partial\theta^j}\right)$. The inner product is defined as $(A|B) = 4\mathrm{Re}\int_0^\infty df\ \frac{\tilde{A}^*(f)\tilde{B}(f)}{S_h(f)}$ where the quantities with *tilde* are the Fourier components. $S_h(f)$ is called the noise spectral density shown in the left panel of Fig. 1, together with GW amplitudes of typical binaries. We take the high cutoff frequency of BBO as $f_{\rm high} = 100$Hz. Then, the variance of the parameter θ^i when other parameters have been marginalized is estimated as $\sigma_{\theta^i} = \sqrt{(\Gamma^{-1})_{ii}}$.

3.3 Numerical Calculations and Results

In this subsection, we explain how we perform the numerical calculations of the Fisher analyses. We take $\boldsymbol{\theta} = (\ln\mathcal{M}_0, \ln\eta_0, t_0, \phi_0, D_L, L)$ as binary parameters, setting $t_0 = \phi_0 = 0$ for the fiducial values and we assume that we know a binary is circular *a priori*. We evaluate the determination errors of these parameters, especially focusing on L, which can be turned into the one of ℓ as $\Delta\ell = (\Gamma^{-1})_{LL}^{1/4} M_{t0}$. We assume that the observation starts Tyr before coalescence. We take the integration range of $(f_{T\rm yr}, f_{\rm fin})$ with $f_{\rm fin} = \min\{f_{\rm high}, f_{\rm ISCO}\}$. Here $f_{T\rm yr}$ is the frequency at the time Tyr before the binary reaches the innermost stable circular orbit (ISCO), which is given as $f_{T\rm yr} = 4.149\times10^{-5}\left(\frac{\mathcal{M}_0}{10^6\ M_\odot}\right)^{-5/8} T^{-3/8}$, and $f_{\rm ISCO} = \frac{1}{6^{3/2}\pi M_{t0}}$ is the frequency at ISCO.

Following Ref. [16], we performed statistical analysis in order to take into account the advantage of high event rate. First, we estimate the determination errors of L for BH/NS binaries at various redshift z and BH mass M_0. Next we integrate these errors by z and M_0 with appropriate distribution functions. We use the results by Schneider *et al.* [17] for z evolution and we take flat mass distribution [14]. We also take into account the reduction of the event rate due to the enhanced Hawking radiation. The result of $\Delta\ell$ against ℓ is shown in the right panel of Fig. 1 for various observation times. If these lines are below $\Delta\ell = \ell$ (black dotted-dashed line), DECIGO/BBO can actually detect the size of ℓ rather than just putting constraint. For 5 year observation, it is possible to measure ℓ down to $\ell = 0.328\ \mu$m which is 40 times stronger than the current table-top experiment.

4 Conclusions and Discussions

In this paper, we obtained the possible upper bounds on the size of extra dimension ℓ in the RS-II braneworld scenario [1] by detecting GWs from BH/NS binaries with DECIGO/BBO. First, we derived the -4PN correction term due to this mass loss effect in the phase of the gravitational waveform. It is a negative PN correction since this mass loss effect is greater when the separation of a binary is larger. Then we performed Fisher analyses and estimated the upper bound on ℓ. By performing statistical analysis, we found that DECIGO/BBO can detect ℓ down to $\ell = 0.328$ μm for 5 yr observation if we know eccentricities *a priori*. This is almost 40 times stronger than the table-top one.

When we include eccentricities into binary parameters, and considering actual detection of ℓ, the detection limit becomes $\ell = 1.49$ μm. This is still 1 order of magnitude stronger than the table-top one. However, table-top experiments are performed model-independently whereas the results obtained here can only be applied to RS-II braneworld model. Therefore we cannot directly compare these results. Nevertheless, our results here show the strong potential of DECIGO/BBO in probing extra dimensional theories.

References

[1] L. Randall and R. Sundrum, Phys. Rev. Lett. **83**, 4690 (1999).

[2] E. G. Adelberger, B. R. Heckel, S. A. Hoedl, C. D. Hoyle, D. J. Kapner and A. Upadhye, Phys. Rev. Lett. **98**, 131104 (2007).

[3] J. M. Maldacena, Adv. Theor. Math. Phys. **2**, 231 (1998).

[4] R. Emparan, A. Fabbri and N. Kaloper, JHEP **0208**, 043 (2002).

[5] T. Tanaka, Prog. Theor. Phys. Suppl. **148**, 307 (2003).

[6] R. Emparan, J. Garcia-Bellido and N. Kaloper, JHEP **0301**, 079 (2003).

[7] S. T. McWilliams, Phys. Rev. Lett. **104**, 141601 (2010).

[8] K. Danzmann, Class. Quant. Grav. **14**, 1399 (1997).

[9] N. Seto, S. Kawamura and T. Nakamura, Phys. Rev. Lett. **87**, 221103 (2001).

[10] S. Kawamura *et al.*, Class. Quant. Grav. **23**, S125 (2006).

[11] E. S. Phinney *et al.*, *Big Bang Observer Mission Concept Study* (NASA), (2003).

[12] G. Nelemans, L. R. Yungelson, and S. F. Portegies Zwart, Astron and Astrophys. **375**, 890 (2001).

[13] C. Cutler and E. E. Flanagan, Phys. Rev. D **49**, 2658 (1994).

[14] K. Belczynski, V. Kalogera and T. Bulik, Astrophys. J. **572**, 407 (2001).

[15] E. Berti, A. Buonanno and C. M. Will, Phys. Rev. D **71**, 084025 (2005).

[16] K. Yagi and T. Tanaka, Prog. Theor. Phys. **123**, 1069 (2010).

[17] R. Schneider, V. Ferrari, S. Matarrese and S. F. Portegies Zwart, Mon. Not. Roy. Astron. Soc. **324**, 797 (2001).

Euler's collinear solution to three-body problem in GR

Kei Yamada and Hideki Asada
Faculty of Science and Technology,
Hirosaki University, Hirosaki 036-8561, Japan

Abstract

The three-body problem is reexamined in the framework of general relativity. The Newtonian three-body problem admits *Euler's collinear solution*, where three bodies move around the common center of mass with the same orbital period and always line up. The solution is unstable. Hence it is unlikely that such a simple configuration would exist owing to general relativistic forces dependent not only on the masses but also on the velocity of each body. However, we show that the collinear solution remains true with a correction to the spatial separation between masses.

1 Euler's collinear solution in the Newton gravity

The location of each mass M_I $(I = 1, 2, 3)$ is written as $\boldsymbol{X}_I \equiv (x_I, 0)$. Without loss of generality, we assume $x_3 < x_2 < x_1$. Let R_I define the relative position of each mass with respective to the center of mass $\boldsymbol{X}_G \equiv (x_G, 0)$, namely $R_I \equiv x_I - x_G$ ($R_I \neq |\boldsymbol{X}_I|$ unless $x_G = 0$). We choose $x = 0$ between M_1 and M_3. We thus have $R_3 < R_2 < R_1$, $R_3 < 0$ and $R_1 > 0$.

It is convenient to define an important ratio as $R_{23}/R_{12} = z$. Then we have $R_{13} = (1 + z)R_{12}$. The equation of motion in Newton gravity becomes

$$R_1\omega^2 = \frac{M_2}{R_{12}^2} + \frac{M_3}{R_{13}^2}, \tag{1}$$

$$R_2\omega^2 = -\frac{M_1}{R_{12}^2} + \frac{M_3}{R_{23}^2}, \tag{2}$$

$$R_3\omega^2 = -\frac{M_1}{R_{13}^2} - \frac{M_2}{R_{23}^2}, \tag{3}$$

where we define

$$\boldsymbol{R}_{IJ} \equiv \boldsymbol{X}_I - \boldsymbol{X}_J, \tag{4}$$

$$R_{IJ} \equiv |\boldsymbol{R}_{IJ}|. \tag{5}$$

First, we subtract Eq. (2) from Eq. (1) and Eq. (3) from Eq. (2) and use $R_{12} \equiv |\boldsymbol{X}_1 - \boldsymbol{X}_2|$ and $R_{23} \equiv |\boldsymbol{X}_2 - \boldsymbol{X}_3|$. Next, we compute a ratio between them to delete ω^2. Hence we obtain a fifth-order equation as [1]

$$(M_1 + M_2)z^5 + (3M_1 + 2M_2)z^4 + (3M_1 + M_2)z^3 - (M_2 + 3M_3)z^2 - (2M_2 + 3M_3)z - (M_2 + M_3) = 0. \tag{6}$$

Now we have a condition as $z > 0$. Descartes' rule of signs : the number of positive roots either equals to that of sign changes in coefficients of a polynomial or less than it by a multiple of two. According to this rule, Eq. (6) has the only positive root $z > 0$, though such a fifth-order equation cannot be solved in algebraic manners as shown by Galois. After obtaining z, one can substitute it into a difference, for instance between Eqs. (1) and (3). Hence we get ω.

2 What happens in GR ?

2.1 The EIH equation of motion for a many-body system

In order to include the dominant part of general relativistic effects, we take account of the terms at the first post-Newtonian order. Namely, the massive bodies obey the Einstein-Infeld-Hoffman (EIH) equation

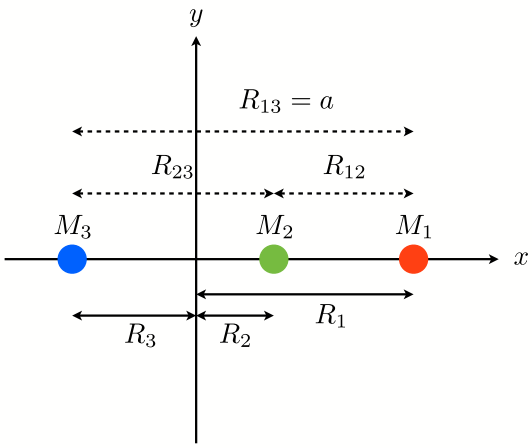

Figure 1: Schematic figure for a classical configuration of three masses denoted by M_1 , M_2 and M_3.

of motion as [2, 3]

$$\begin{aligned}\frac{d^2\boldsymbol{r}_K}{dt^2} &= \sum_{A\neq K}\boldsymbol{r}_{AK}\frac{1}{r_{AK}^3}\left[1-4\sum_{B\neq K}\frac{1}{r_{BK}}-\sum_{C\neq A}\frac{1}{r_{CA}}\left(1-\frac{\boldsymbol{r}_{AK}\cdot\boldsymbol{r}_{CA}}{2r_{CA}^2}\right)\right.\\ &\qquad\left.+\boldsymbol{v}_K^2+2\boldsymbol{v}_A^2-4\boldsymbol{v}_A\cdot\boldsymbol{v}_K-\frac{3}{2}\left(\frac{\boldsymbol{v}_A\cdot\boldsymbol{r}_{AK}}{r_{AK}}\right)^2\right]\\ &\quad-\sum_{A\neq K}(\boldsymbol{v}_A-\boldsymbol{v}_K)\frac{\boldsymbol{r}_{AK}\cdot(3\boldsymbol{v}_A-4\boldsymbol{v}_K)}{r_{AK}^3}\\ &\quad+\frac{7}{2}\sum_{A\neq K}\sum_{C\neq A}\boldsymbol{r}_{CA}\frac{1}{r_{AK}r_{CA}^3}.\end{aligned}$$

2.2 The seventh-order equation

Similarly to the above Newtonian case, we obtain a seventh-order equation as [4]

$$F(z) \equiv \sum_{k=0}^{7}A_k z^k = 0, \tag{7}$$

where we define the mass ratio as $\nu_I \equiv M_I/M$ for $M \equiv \sum_I M_I$ and

$$\begin{aligned}A_7 &= \frac{M}{a}\left[-4-2(\nu_1-4\nu_3)+2(\nu_1^2+2\nu_1\nu_3-2\nu_3^2)-2\nu_1\nu_3(\nu_1+\nu_3)\right],\\ A_6 &= 1-\nu_3+\frac{M}{a}\left[-13-(10\nu_1-17\nu_3)+2(2\nu_1^2+8\nu_1\nu_3-\nu_3^2)\right.\\ &\qquad\left.+2(\nu_1^3-2\nu_1^2\nu_3-3\nu_1\nu_3^2-\nu_3^3)\right],\end{aligned}$$

$$
\begin{aligned}
A_5 &= 2+\nu_1-2\nu_3+\frac{M}{a}\Big[-15-(18\nu_1-5\nu_3)+4(5\nu_1\nu_3+4\nu_3^2) \\
&\qquad +6(\nu_1^3-\nu_1\nu_3^2-\nu_3^3)\Big], \\
A_4 &= 1+2\nu_1-\nu_3+\frac{M}{a}\Big[-6-2(5\nu_1+2\nu_3)-4(2\nu_1^2-\nu_1\nu_3-4\nu_3^2) \\
&\qquad +2(3\nu_1^3+\nu_1^2\nu_3-2\nu_1\nu_3^2-3\nu_3^3)\Big], \\
A_3 &= -(1-\nu_1+2\nu_3)+\frac{M}{a}\Big[6+2(2\nu_1+5\nu_3)+4(-4\nu_1^2-\nu_1\nu_3+2\nu_3^2) \\
&\qquad -2(-3\nu_1^3-2\nu_1^2\nu_3+\nu_1\nu_3^2+3\nu_3^3)\Big], \\
A_2 &= -(2-2\nu_1+\nu_3)+\frac{M}{a}\Big[15+(-5\nu_1+18\nu_3)-4(4\nu_1^2+5\nu_1\nu_3) \\
&\qquad -6(-\nu_1^3-\nu_1^2\nu_3+\nu_3^3)\Big], \\
A_1 &= -(1-\nu_1)+\frac{M}{a}\Big[13+(-17\nu_1+10\nu_3)-2(-\nu_1^2+8\nu_1\nu_3+2\nu_3^2) \\
&\qquad -2(-\nu_1^3-3\nu_1^2\nu_3-2\nu_1\nu_3^2+\nu_3^3)\Big], \\
A_0 &= \frac{M}{a}\Big[4+2(-4\nu_1+\nu_3)-2(-2\nu_1^2+2\nu_1\nu_3+\nu_3^2)+2\nu_1\nu_3(\nu_1+\nu_3)\Big].
\end{aligned}
$$

This seventh-order equation is symmetric for exchanges between ν_1 and ν_3, only if one makes a change $z \to 1/z$. This symmetry seems to validate the complicated form of each coefficient.

Figure 2 shows a numerical example for $M_1 : M_2 : M_3 = 1 : 2 : 3$, $R_{12} = 1$ and $a/M = 100$, where the post-Newtonian correction is of the order of one percent. In this figure, we employ the inertial frame $(\bar{x}, \bar{y})$ but not the corotating frame (x, y). We assume $x_3 < x_2 < x_1$ throughout this paper. This figure suggests that as an alternative initial condition we can assume $x_1 < x_2 < x_3$, which is realized at $t = T/2$ (T=orbital period) in this figure. It is natural that this is a consequence of the parity symmetry in our formulation. It should be noted also that the location of each mass at $t = T/2$ is advanced compared with that at $t = T_N/2$ (a half of the *Newtonian* orbital period). This may correspond to the periastron advance (in circular orbits).

Finally, we focus on the restricted three-body problem so that we can put $z = z_N(1+\varepsilon)$ for the Newtonian root z_N. Substitution of this into Eq. (7) gives the post-Newtonian correction as

$$
\varepsilon = -\frac{\sum_k A_{PNk} z_N^k}{\sum_k k A_{Nk} z_N^k}, \tag{8}
$$

where A_{Nk} and A_{PNk} denote the Newtonian and post-Newtonian parts of A_k, respectively. For a binary system of comparable mass stars, the correction ε is $O(M/a)$. This implies that a corrected length is of the order of the Schwarzschild radius.

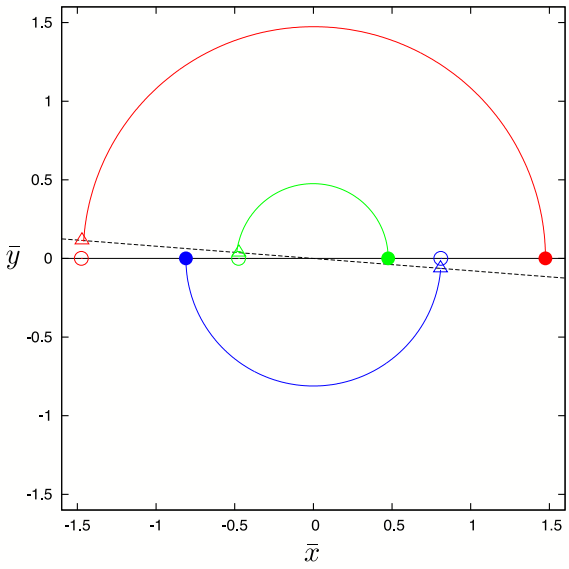

Fig 2: $M_1 : M_2 : M_3 = 1 : 2 : 3$, $a/M = 100$

For the Sun-Jupiter system, general relativistic corrections to L_1, L_2 and L_3 become $+30$, -38, $+1$ [m], respectively, where the positive sign is chosen along the direction from the Sun to the Jupiter. Such corrections suggest a potential role of the general relativistic three (or more) body dynamics for high precision astrometry in our solar system and perhaps also for gravitational waves astronomy.

3 Conclusion

We obtained a general relativistic version of Euler's collinear solution for the three-body problem at the post-Newtonian order [4]. Studying global properties of the seventh-order equation that we have derived is left as future work.

It is interesting also to include higher post-Newtonian corrections, especially 2.5PN effects in order to elucidate the secular evolution of the orbit due to the gravitational radiation reaction at the 2.5PN order. One might see probably a shrinking collinear orbit as a consequence of a decrease in the total energy and angular momentum, if such a radiation reaction effect is included. This is a testable prediction.

It may be important also to search other solutions, notably a relativistic counterpart of the Lagrange's triangle solution (so-called L_4 and L_5 in the restricted three-body problem). Clearly it seems much more complicated to obtain relativistic corrections to the Lagrange orbit.

References

[1] J. M. A. Danby, *Fundamentals of Celestial Mechanics* (William-Bell, VA, 1988).

[2] C. W. Misner, K. S. Thorne, J. A. Wheeler, *Gravitation*, (Freeman, New York, 1973).

[3] L. D. Landau and E. M. Lifshitz, *The Classical Theory of Fields* (Oxford: Pergamon 1962).

[4] K. Yamada and H. Asada Phys. Rev. D **82**, 104019 (2010).

Gravitational collapse in five dimensional space-time

Yuta Yamada[1] and Hisa-aki Shinkai[2]

Faculty of Information Science and Technology, Osaka Institute of Technology, 1-79-1 Kitayama, Hirakata, Osaka 573-0196, Japan

Abstract

We numerically investigate the gravitational collapse of collisionless particles in spheroidal configurations both in four and five-dimensional (5D) space-time. We repeat the simulation performed by Shapiro and Teukolsky (1991) that announced an appearance of a naked singularity, and also find that the similar results in 5D version. That is, in a collapse of a highly prolate spindle, the Kretschmann invariant blows up outside the matter and no apparent horizon forms. We also find that the collapses in 5D proceed rapidly than in 4D, and the critical prolateness for appearance of apparent horizon in 5D is loosened compared to 4D cases. We also show how collapses differ with spatial symmetries comparing 5D evolutions in single-axisymmetry, SO(3), and those in double-axisymmetry, U(1)×U(1).

1 Introduction

Motivated by the so-called "large extra-dimensional models", black-holes in higher dimensional space-time are extensively studied for a decade. Many interesting discoveries of new solutions have been reported, and their properties are also been revealing. However, fully relativistic dynamical features, such as the formation processes, stabilities and late-time fate, are still unknown and they are waiting to be studied.

In classical general relativity, there are two famous conjectures concerning the gravitational collapse. One is the *cosmic censorship conjecture* [1] which states that singularities are always clothed by event horizons. The other is the *hoop conjecture* [2] which states that black holes with horizons are formed when and only when a mass gets compacted into a small region. Shapiro and Teukolsky (ST91, hereafter) numerically showed that axisymmetric space-time with collisionless matter particles in spheroidal distribution will collapse to singularity, and there are no apparent horizon formed when the spheroids are highly prolate[3]. The behaviors supported the hoop conjecture.

Regarding to the 5D cases, the hoop conjecture is supposed to be replaced with the *hyper-hoop* version[4, 5], i.e. a criteria is not a hoop but a surface. In our previous work [6], we numerically constructed initial data sequences of non-rotating matter for 5D evolutions and examined the hyper-hoop conjecture using minimum *area* around the matter. The sequences suggest that a highly prolate spindle in 5D will form a naked singularity similar to the 4D cases.

In this note, we report our numerical simulations on gravitational collapse in axisymmetric space-time in (3+1)-dimensional space-time (4D, hereafter) and (4+1)-dimensional (5D) versions. We show that the naked singularity is formed for the gravitational collapse of spheroidal matter configuration in 5D. We also compare the dynamics between 4D and 5D. In 5D, two axes can be settled as rotational symmetric axes, so that we also compare gravitational collapses in axisymmetry with those in "doubly"-axisymmetric space-time.

2 Numerical code

We evolve five-dimensional axisymmetric [symmetric on z-axis, SO(3)] or doubly-axisymmetric [symmetric both on x and z-axes, U(1)×U(1)], asymptotically flat space-time (see Figure 1). For the comparison, we also performed four-dimensional axisymmetric space-time evolutions.

[1]Email address: yamada@is.oit.ac.jp
[2]Email address: shinkai@is.oit.ac.jp

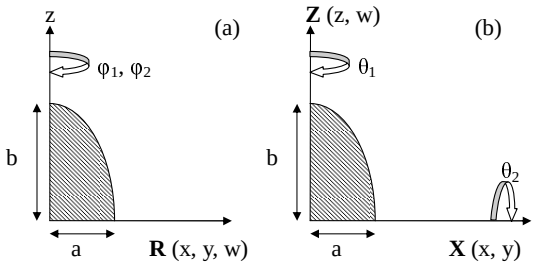

Figure 1: (above) we evolve five-dimensional (a) axisymmetric [SO(3)] or (b) double-axisymmetric [U(1)× U(1)], asymptotically flat space-time using the Cartesian grid. the initial matter configuration is expressed with parameters a and b.

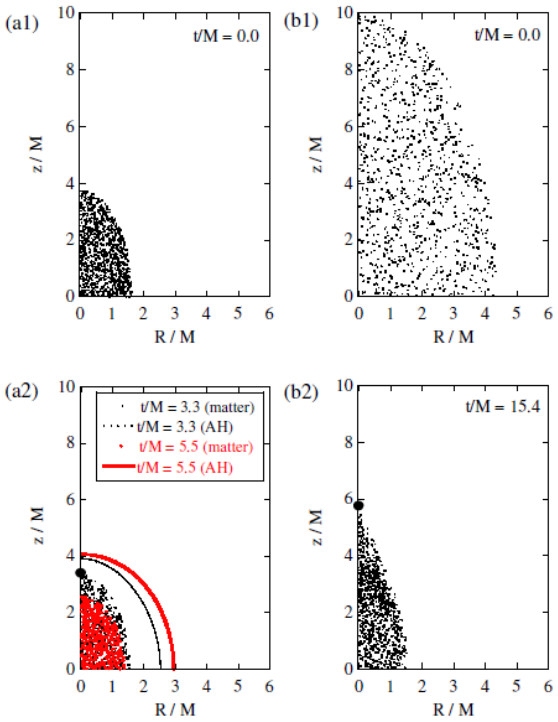

Figure 2: (right) Snapshots of 5D axisymmetric evolution with the initial matter distribution of $b/M = 4$ [Fig.(a1) and (a2); model 5DSβ in Table 1] and 10 [Fig.(b1) and (b2); model 5DSδ]. The big circle indicates the location of the maximum Kretschmann invariant $\mathcal{I}_{\rm max}$ at the final time at each evolution.

We start our simulation from time symmetric and conformally flat initial data, which are obtained by solving the Hamiltonian constraint equations [6]. The asymptotical flatness is imposed throughout the evolution, which settles the fall-off condition to the metric as $\sim 1/r$ for 4D cases and $\sim 1/r^2$ for 5D cases.

The matter is described with 5000 collisionless particles, which move along the geodesic equations. We smooth out the matter by expressing each particle with Gaussian density distribution function with its typical width is twice as much as the numerical grid. The particles are homogeneously distributed in a spheroidal shape, parametrized with a and b (Figure 1), or eccentricity $e = \sqrt{1 - a^2/b^2}$.

By imposing axisymmetry or double-axisymmetry, our model becomes practically a (2+1)-dimensional problem. We construct our numerical grids with the Cartesian coordinate (x, z), and apply the so-called Cartoon method [7] to recover the symmetry of space-time.

The space-time is evolved using the Arnowitt-Deser-Misner (ADM) evolution equations. It is known that the ADM evolution equations excite an unstable mode (constraint-violation mode) in long-term simulations [8, 9]. However, we are free from this problem since gravitational collapse occurs within quite short time. By monitoring the violation of constraint equations during evolutions, we confirm that our numerical code has second-order convergence, and also that the simulation continues in stable manner. The results shown in this report are obtained with numerical grids, 129×129×2×2. We confirmed that higher resolution runs do not change the physical results.

We use the maximal slicing condition for the lapse function α, and the minimal strain condition for the shift vectors β^i. Both conditions are proposed for avoiding the singularity in numerical evolutions [10], and the behavior of α and β^i roughly indicates the strength of gravity, conversely. The iterative Crank-Nicholson method is used for integrating ADM evolution equations, and the Runge-Kutta method is used for matter evolution equations.

For discussing physics, we search the location of apparent horizon (AH), calculate the Kretschmann invariant ($\mathcal{I} = R_{abcd}R^{abcd}$) on the spacial hypersurface.

b/M $(t=0)$	2.50	4.00	6.25	10.00
4D axisym.	4Dα	4Dβ	4Dγ	4Dδ
	AH-formed	no	no	no
	$e_{\rm AH}=0.90$			
	$e_{\rm f}=0.92$	$e_{\rm f}=0.89$	$e_{\rm f}=0.92$	$e_{\rm f}=0.96$
5D axisym. SO(3)	5DSα	5DSβ	5DSγ	5DSδ
	AH-formed	AH-formed	no	no
	$e_{\rm AH}=0.88$	$e_{\rm AH}=0.88$		
	$e_{\rm f}=0.82$	$e_{\rm f}=0.84$	$e_{\rm f}=0.88$	$e_{\rm f}=0.96$
5D double axisym. U(1)×U(1)	5DUα	5DUβ	5DUγ	5DUδ
	AH-formed	AH-formed	AH-formed	no
	$e_{\rm AH}=0.86$	$e_{\rm AH}=0.87$	$e_{\rm AH}=0.92$	
	$e_{\rm f}=0.79$	$e_{\rm f}=0.81$	$e_{\rm f}=0.90$	$e_{\rm f}=0.98$

Table 1: Model-names and the results of their evolutions whether we observed AH or not. The eccentricity e the collapsed matter configurations is also shown; $e_{\rm AH}$ and $e_{\rm f}$ are at the time of AH formed (if formed), and on the numerically obtained final hypersurface, respectively.

3 Results

We prepare several initial data keeping the total ADM mass and the eccentricity of distribution, $e=0.9$. By changing the initial matter distribution sizes, we observe the different final structures. Figure 2 shows snapshots of 5D axisymmetric evolutions of model $b/M=4$ and 10 (model 5DSβ and 5DSδ, respectively; see Table 1); the former collapses to a black hole while the latter collapses without AH formation.

All the models we tried result in forming a singularity (i.e., diverging $\mathcal{I}$). We stop our numerical evolutions when the shift vector is not obtained with sufficient accuracy due to the large curvature. For model 5DSδ, we integrated up to the coordinate time $t/M=15.4$ and the maximum of the Kretschmann invariant $\mathcal{I}_{\rm max}$ becomes $O(1000)$ on z-axis (see Figure 3), but AH is not formed.

When the initial matter is highly prolated, AH is not observed. This is consistent with 4D cases [3], and matches with the predictions from initial data analysis in 5D cases [5, 6]. The location of $\mathcal{I}_{\rm max}$ is on z-axis, and just outside of the matter. This is again the same with 4D cases [3]. The absence of AH with diverging $\mathcal{I}$ suggests a formation of naked singularity in 5D.

In order to compare the results with 4D and 5D, we reproduce the results of ST91. We then find that the $e=0.9$ initial data with $b/M=10$ (model 4Dδ) collapses without forming AH, and the code stops at the coordinate time $t=20.91$ with $\mathcal{I}_{\rm max}=84.3$ on the z-axis ($z/M=6.1$); all the numbers match quite well with ST91. (Note that our slicing conditions and coordinate structure is not the same with ST91.)

We also performed 5D collapses with doubly-axisymmetric [U(1)×U(1)] space-time. The matter and space-time evolve quite similar to 5D and 4D axisymmetric cases, but we find that the critical configurations for forming AH is different. Table 1 summarizes the main results of 4D and two 5D cases. We find that AH in 5D is formed in larger b initial data than 4D cases. This result is consistent with our prediction from the sequence of initial data [6]. AH criteria with initial b is loosened for 5D doubly-axisymmetric cases. We show the eccentricity, $e_{\rm AH}$ and $e_{\rm f}$, which tell us that the doubly-axisymmetric assumption makes collapse less sharp when it forms AH, and makes collapse similar to 4D cases when it does not form AH. Table 1 indicates that the eccentricity itself is not a guiding measure for AH formation.

In Figure 4, we plotted $\mathcal{I}$ at the point which gives $\mathcal{I}_{\rm max}$ on the final hypersurface as a function of proper time. We see that 5D-collapse is proceeding rapidly than 4D collapses. We also see that collapses in doubly-axisymmetric space-time is proceeding slowly than single axisymmetric cases.

4 Discussions

In this paper, we reported our numerical study of gravitational collapses in 5D space-time. The collapsing behaviors are quite similar to the cases in 4D, but we also found that (a) 5D-collapses proceed rapidly than 4D-collapses, (b) AH appears in highly prolate matter configurations than 4D cases, (c) doubly-axisymmetric [U(1)×U(1)] assumption makes collapse less sharp when it forms AH, and (d) the positive evidence for appearance of a naked singularity in 5D.

Up to this moment, we only checked the existence of apparent horizons, and not the event horizons. The system does not include any angular momentums. We are implementing our code to cover these studies.

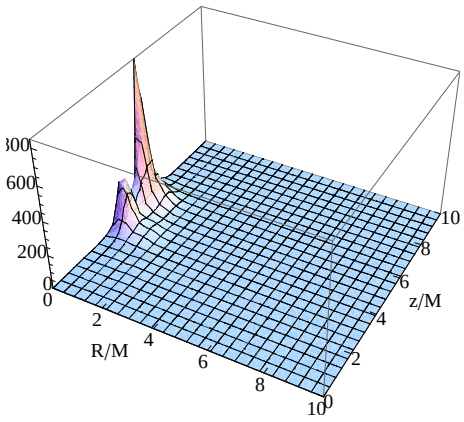

Figure 3: Kretschmann invariant $\mathcal{I}$ for model `5DS`δ at $t/M = 15.4$. The maximum is $O(1000)$, and its location is on z-axis, just outside of the matter.

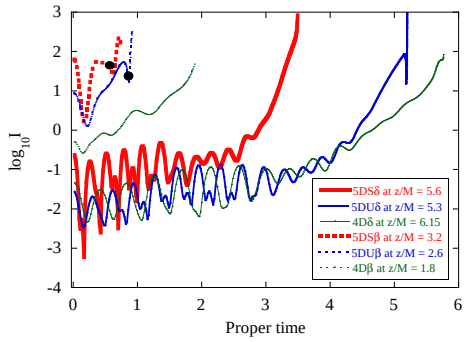

Figure 4: Kretschmann invariant $\mathcal{I}$ at the location of $\mathcal{I}_{\rm max}$ on the final hypersurface is plotted as a function of proper time at its location. labels indicate model-names in table 1. the time of ah formation (t=0.6 for model `5ds`β, t=0.9 for `5du`β) is shown by a dot.

We are now preparing our next detail report including the validity of hyper-hoop conjecture in 5D, and the cases of the ring objects.

This work was supported partially by the Grant-in-Aid for Scientific Research Fund of Japan Society of the Promotion of Science, No. 22540293. Numerical computations were carried out on Altix3700 BX2 at YITP in Kyoto University, and on the RIKEN Integrated Cluster of Clusters (RICC).

References

[1] R. Penrose, Riv. Nuovo Cimento **1**, 252 (1969).

[2] K. S. Thorne, in *Magic Without Magic*, ed. by J. R. Klauder (Freeman, San. Francisco), 231 (1972).

[3] S. L. Shapiro and S. A. Teukolsky, Phys. Rev. Lett. **66**, 994 (1991).

[4] D. Ida and K. Nakao, Phys. Rev. D **66**, 064026 (2002).

[5] C-M. Yoo, K. Nakao and D. Ida, Phys. Rev. D **71**, 104014 (2005).

[6] Y. Yamada and H. Shinkai, Class. Quant. Grav. **27**, 045012 (2010).

[7] M. Alcubierre, et al., Int. J. Mod. Phys. D**10**, 273 (2001).

[8] see e.g., H. Shinkai, J. Korean Phys. Soc. **54** 2513 (2009).

[9] H. Shinkai and G. Yoneda, Gen. Rel. Grav. **36** 1931 (2004).

[10] L. Smarr and J. W. York, Jr., Phys. Rev. D **17**, 2529 (1978).

Analytic model for CMB temperature fluctuations from cosmic (super-)strings

Daisuke Yamauchi[1(a)] Keitaro Takahashi[2(b)] Yuuti Sendouda[3(c)] Chul-Moon Yoo[4(a)] and Misao Sasaki[5(a)]

[(a)] *Yukawa Institute, Kyoto University, Kyoto 606-8502*
[(b)] *Department of Physics and Astrophysics, Nagoya University, Nagoya 494-8602, Japan*
[(c)] *APC, Université Paris 7, 10, rue Alice Domon et Léonie Duquet, 75205 Paris cedex 13, France*

Abstract

We present a new analytical method to calculate the small angle CMB temperature angular power spectrum due to cosmic (super-)string segments. In particular, using our method, we clarify the dependence on the intercommuting probability P. We find that the power spectrum is dominated by Poisson-distributed string segments. The power spectrum for a general value of P has a plateau on large angular scales and shows a power-law decrease on small angular scales. The resulting spectrum in the case of conventional cosmic strings is in very good agreement with the numerical result obtained by Fraisse et al.. Then we estimate the upper bound on the dimensionless tension of the string for various values of P by assuming that the fraction of the CMB power spectrum due to cosmic (super-)strings is less than ten percents at various angular scales up to $\ell = 2000$. We find that the amplitude of the spectrum increases as the intercommuting probability. As a consequence, strings with smaller intercommuting probabilities are found to be more tightly constrained.

1 Introduction

Cosmic strings are line-like topological defects formed in the early universe through spontaneous symmetry breaking in a wide range of inflationary models [1]. Since the string tension μ is directly related to the symmetry breaking energy scale, observational verification of the existence of cosmic strings will have profound implications to unified theories. Theoretically, recent developments in string cosmology suggest that inflation may be due to motions of branes in higher dimensions and various new types of strings, called cosmic superstrings, may be formed at the end of inflation [2]. One of the differences between cosmic superstrings and conventional field-theoretic strings is the value of the intercommuting probability P. It can be significantly smaller than unity for cosmic superstrings, while normally it is unity for field-theoretic strings [5].

Recent numerical simulations [3, 4] show that the small scale CMB temperature angular power spectrum due to cosmic strings with $P = 1$ behaves as a power law. One of our purposes of this paper is to derive this power-law behavior analytically and to extend it to the case of cosmic strings with $P < 1$. For our purpose, we adopt a simple model of string network for general values of the intercommuting probability P and consider long straight string segments which are located randomly between the last scattering surface (LSS) and the present time consistently with the string network model.

2 Angular power spectrum from cosmic (super-)string

In this section we will briefly review the angular power spectrum from cosmic (super-)strings incorporating intercommuting probability P, following the previous work [6].

[1]Email: yamauchi@yukawa.kyoto-u.ac.jp
[2]Email: keitaro@a.phys.nagoya-u.ac.jp
[3]Email: sendouda@apc.univ-paris7.fr
[4]Email: yoo@yukawa.kyoto-u.ac.jp
[5]Email: misao@yukawa.kyoto-u.ac.jp

2.1 Analytic string network model

In the velocity-dependent one-scale model, a string segment has two properties, the length ξ and the root-mean-square velocity $v_{\rm rms}$. The typical length ξ is defined by $\xi \equiv \sqrt{\mu/\rho_{\rm seg}}$ where $\rho_{\rm seg}$ is the total string energy density. In our treatment, we also take account of the energy loss due to loop formation. The characteristic time scale for loop formation is $\sim \xi/(Pv_{\rm rms})$ and the energy loss can be described as $\sim \tilde{c}Pv_{\rm rms}\rho_{\rm seg}/\xi$ where we have introduced $\tilde{c}$ as a constant which represents the efficiency of loop formation. Assuming $a(t) \propto t^\beta$ with the physical time $t = \int a(\eta)d\eta$, the equations of motion for $\gamma = 1/H\xi$ and $v_{\rm rms}$ are given by [6]

$$\frac{t}{\gamma}\frac{d\gamma}{dt} = 1 - \beta - \frac{1}{2}\beta\tilde{c}Pv_{\rm rms}\gamma - \beta v_{\rm rms}^2\,, \quad \frac{dv_{\rm rms}}{dt} = (1 - v_{\rm rms}^2)H\left[k(v_{\rm rms})\gamma - 2v_{\rm rms}\right], \tag{1}$$

where $k(v_{\rm rms}) = (2\sqrt{2}/\pi)(1 - 8v_{\rm rms}^6)/(1 + 8v_{\rm rms}^6)$ [7]. Hereafter we assume a matter-dominated era, $\beta = 2/3$, and we use $\tilde{c} \approx 0.23$ as the standard value [8]. It is known that a string network approaches the so-called scaling regime where the characteristic scale grows with the Hubble horizon size. We assume that the scaling is already realized by the time of the last scattering surface (LSS) and this means that $\gamma, v_{\rm rms}$ are constant in time.

2.2 Segment formalism

On small scale, for an exactly straight and uniformly moving segment the temperature fluctuation due to a string segment is given by [6]

$$\frac{\Delta T}{T}(\boldsymbol{\vartheta}) = -4G\mu\frac{v_{\rm rms}}{\sqrt{1 - v_{\rm rms}^2}}\alpha_{\rm seg}\left\{\arctan\left[\frac{\ell_{\rm co}^{-1} + \vartheta\cos\varphi}{\vartheta\sin\varphi}\right] + \arctan\left[\frac{\ell_{\rm co}^{-1} - \vartheta\cos\varphi}{\vartheta\sin\varphi}\right]\right\}, \tag{2}$$

where $\boldsymbol{\vartheta}\cdot\mathbf{e} = \vartheta\cos\varphi$, where $\mathbf{e}$ is the unit vector along the string, and $\boldsymbol{\vartheta}$ is the angular position vector relative to the middle point of the segment in a small patch of sky. We have introduced the angular scale $\ell_{\rm co} = d_{\rm A}/\xi$ corresponding to the correlation length of the segment, where d_A denotes the angular diameter distance from the observer. Note that $\alpha_{\rm seg}$ is a constant parameter depending on the set of angular parameters, which determines the configuration of a string. We can perform the Fourier transformation of the temperature fluctuation analytically:

$$a_{\boldsymbol{\ell}} = \frac{1}{2\pi}\int d^2\boldsymbol{\vartheta}\frac{\Delta T}{T}(\boldsymbol{\vartheta})e^{-i\boldsymbol{\ell}\cdot\boldsymbol{\vartheta}} = -\frac{8iG\mu v_{\rm rms}\alpha_{\rm seg}}{\sqrt{1 - v_{\rm rms}^2}\ell^2}\tan\varphi_\ell\sin\left(\frac{\ell}{\ell_{\rm co}}\cos\varphi_\ell\right), \tag{3}$$

where $\boldsymbol{\ell}\cdot\mathbf{e} = \cos\varphi_\ell$.

In order to compute the angular power spectrum of the temperature fluctuations due to cosmic (super-)strings, we use what we call the *segment formalism*. Since the observed sky map of temperature fluctuations due to segments appears as a superposition of those due to each segment, the Fourier transform of the total temperature fluctuations, $a_{\boldsymbol{\ell}}^{\rm tot}$, can be decomposed into each contribution of each string segment. In our treatment, we first introduce a segment index "i" to denote the contribution from each segment between LSS and the present. Then we have $a_{\boldsymbol{\ell}}^{\rm tot} = \sum a_{\boldsymbol{\ell}}^{(i)}$.

Asuming the statistical isotropy of the CMB, the angular power spectrum can be written as

$$C_\ell = \int\frac{d\varphi_\ell}{2\pi}\Big\langle\sum_i\big|a_{\boldsymbol{\ell}}^{(i)}\big|^2\Big\rangle + \int\frac{d\varphi_\ell}{2\pi}\Big\langle\sum_{i\neq j}a_{\boldsymbol{\ell}}^{(i)}a_{\boldsymbol{\ell}}^{(j)*}\Big\rangle, \tag{4}$$

where the integral over φ_ℓ is the large ℓ approximation of the sum over the azimuthal eigenvalues m ($-\ell \le m \le \ell$), and $\langle\cdots\rangle$ denotes the ensemble average. The ensemble average can be calculated by averaging over the parameter space. We assume uniform distributions of the angular parameters.

Long straight string segments are assumed to be distributed randomly between LSS and the present consistently with the string network model. This implies there is no correlation between two segments, $\langle a_{\boldsymbol{\ell}}^{(i)}a_{\boldsymbol{\ell}}^{(j)}\rangle = 0$ for $i \neq j$. Therefore, the explicit expression on small scale can be obtained as

$$C_\ell \approx \int_0^{z_{\rm LSS}}\frac{dz}{1+z}\frac{2\pi(8\gamma)^3v_{\rm rms}^2(G\mu)^2}{3(1 - v_{\rm rms}^2)\ell^4}\left(\sqrt{1+z} - 1\right)^2\int_{-\pi}^{\pi}\frac{d\varphi_\ell}{2\pi}\tan^2\varphi_\ell\sin^2\left(\frac{\ell}{\ell_{\rm co}(z)}\cos\varphi_\ell\right). \tag{5}$$

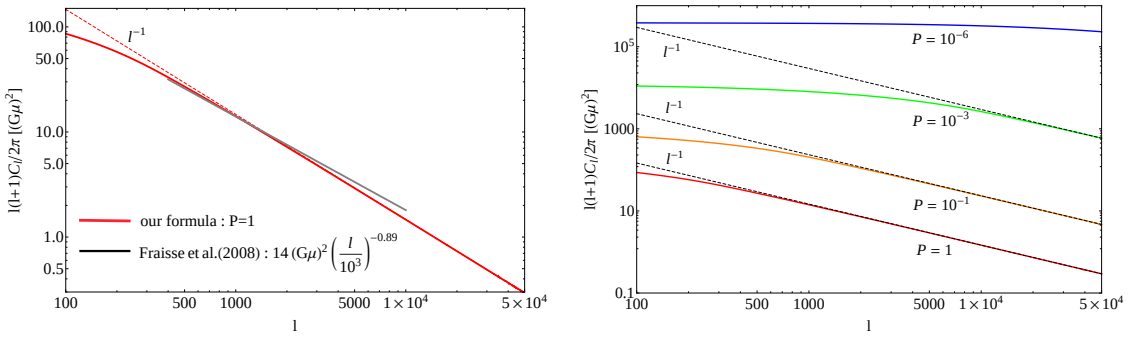

Figure 1: (Left) The angular power spectrum for $P = 1$ in units of $(G\mu)^2$. The red solid line is our result given by Eq. (5). The red dotted line shows the behavior $\propto \ell^{-1}$. The gray solid lines are power-law fit to previous numerical result by Fraisse et al. [3]. (Right) The angular power spectrum given by Eq. (5) in units of $(G\mu)^2$. The curves are, from bottom to top, for $P = 1$ (red), $P = 10^{-1}$ (orange), $P = 10^{-3}$ (green), and $P = 10^{-6}$ (blue).

The total CMB temperature angular power spectrum in the case of $P = 1$ is shown in Fig. 1. As seen from it, a typical amplitude of the power spectrum at $\ell = 10^3$ is $[\ell(\ell+1)/2\pi]C(\ell = 10^3) \approx 14(G\mu)^2$, and it behaves as ℓ^{-1} for large $\ell(\gg \ell_{\rm co}(z_{\rm LSS}))$ while it has a plateau for small $\ell(\lesssim \ell_{\rm co}(z_{\rm LSS}))$. As clearly seen, our result agrees very well with the numerical result by Fraisse et al. [3]. This strongly supports the validity of our approach.

In order to investigate the dependence on the intercommuting probability P, the angular power spectrum (5) is computed for various P. The results are shown in Fig. 1. We see that the overall amplitude of the spectrum increases as P decreases. This is because of the factor $\gamma^3 \propto P^{-3/2}$ in the formula (5), which describes the fact that the density of cosmic string segments is larger for smaller P. Also since $\ell_{\rm co}(z_{\rm LSS}) \propto P^{-1/2}$, we see that the transition from the plateau to the power law occurs at larger ℓ for smaller P.

2.3 Constraints on string tension

Let us discuss possible constraints on the string tension from our result. We plot the angular power spectrum for various values of P and $G\mu$ in Fig. 2. For comparison, we also plot the primary spectrum. An interesting observation is that as P decreases the amplitude due to strings increases, hence the tension of strings with smaller P is more tightly constrained.

It was pointed out in [9] that the CMB anisotropy spectrum is consistent with the presence of cosmic strings if the fraction of the power spectrum due to cosmic strings is about 10% or less at $\ell = 10$. In this paper we adopt a similar criterion and drive an upper bound on $G\mu$ as a function of P. Specifically, we consider the condition that the fraction of the power spectrum due to cosmic (super-)strings is less than 10% at $\ell = 10^2$, 5×10^2, 10^3 and 2×10^3. The result is shown in Fig. 2. As expected, the upper bound on $G\mu$ decreases as P decreases, because the amplitude of the power spectrum increases. Also, we see that the constraint becomes severer for larger ℓ because the contribution from cosmic strings decays very slowly as ℓ increases unlike the case of the primordial anisotropy which shows exponential dumping. For example, the upper bound at $\ell = 10^2$ is 2.1×10^6 for $P = 1$ and 3.1×10^{-8} for $P = 10^{-6}$, while that at $\ell = 10^3$ is 9.8×10^{-7} for $P = 1$ and 6.0×10^{-9} for $P = 10^{-6}$.

3 Summary

In this paper, we presented a new analytical method to calculate the small angle CMB power spectrum due to cosmic (super-)string segments, and investigated the dependence of the power spectrum on the intercommuting probability P. We found that the angular power spectrum on small scales can be well

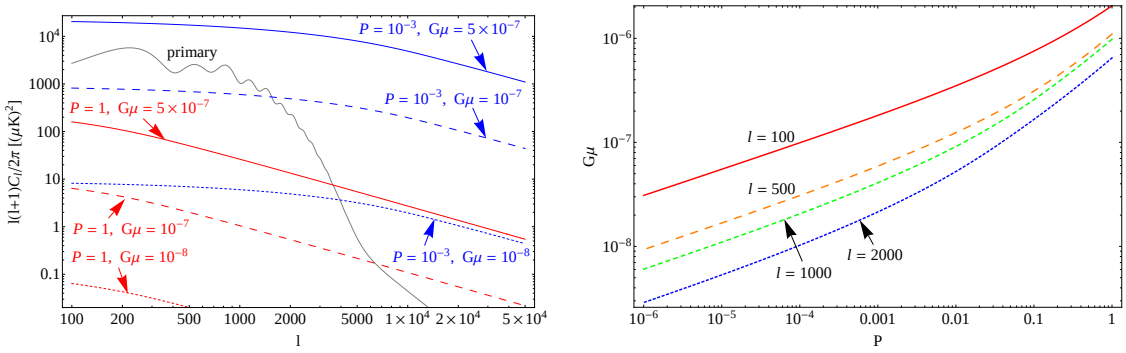

Figure 2: (Left) The angular power spectrum in units of μK^2. The red lines are for $P = 1$ and the blue lines are $P = 10^{-3}$. For both cases $G\mu = 5 \times 10^{-7}$, 10^{-7} and 10^{-8} from top to bottom. For comparison, the primary spectrum is shown in gray. (Right) Upper bound on $G\mu$ as a function of P at $\ell = 10^2$, 5×10^2, 10^3 and 2×10^3, assuming that the fraction of the spectrum due to cosmic (super-)strings is less than 10%.

approximated by the GKS effect due to Poisson-distributed mutually independent segments. Then we derived an analytical formula for the power spectrum valid for general values of P. The angular power spectrum is found to behave as ℓ^{-1} for large $\ell(> \ell_{\rm co}(z_{\rm LSS}))$ and have a plateau for small $\ell(< \ell_{\rm co}(z_{\rm LSS}))$, where $\ell_{\rm co}(z_{\rm LSS})$ is the angular scale corresponding the correlation length at LSS. Since $\ell_{\rm co}(z_{\rm LSS})$ is proportional to $P^{-1/2}$ in the scaling regime, the transition from a plateau to the power-law behavior is found to occur at larger ℓ as P decreases. Then using our result, we discussed an upper bound on the dimensionless tension $G\mu$ as a function of P. We found that strings with small P are more tightly constrained. This can be naturally explained by the fact that the amplitude of the spectrum increases as P decreases because of the increase in the number density of strings. These properties of the power spectrum are distinguishable features of cosmic superstrings that generally have a small intercommuting probability P. They may be used to detect cosmic superstrings in future experiments.

References

[1] R. Jeannerot, J. Rocher and M. Sakellariadou, Phys. Rev. D **68**, 103514 (2003).

[2] S. Sarangi and S. -H. H. Tye, Phys. Lett. B **536**, 185 (2002).

[3] A. A. Fraisse *et al.*, Phys. Rev. D **78**, 043535 (2008)

[4] N. Bevis *et al.*, Phys. Rev. D **82**, 065004 (2010); L. Pogosian *et al.*, JCAP **0902**, 013 (2009)

[5] M. G. Jackson, N. T. Jones and J. Polchinski, JHEP **0510**, 013 (2005); M. Eto *et al.*, Phys. Rev. Lett. **98**, 091602 (2007).

[6] K. Takahashi, A. Naruko, Y. Sendouda, D. Yamauchi, C. -M. Yoo and M. Sasaki, JCAP **0910**, 003 (2009); D. Yamauchi, Y. Sendouda, C. -M. Yoo, K. Takahashi, A. Naruko and M. Sasaki, JCAP **1005**, 033 (2010); D. Yamauchi, K. Takahashi, Y. Sendouda, C. M. Yoo and M. Sasaki, Phys. Rev. D **82**, 063518 (2010);

[7] C. J. A. Martins and E. P. S. Shellard, Phys. Rev. D **65**, 043514 (2002)

[8] C. J. A. Martins, J. N. Moore and E. P. S. Shellard, Phys. Rev. Lett. **92**, 251601 (2004)

[9] N. Bevis *et al.*, Phys. Rev. Lett. **100**, 021301 (2008)

Rotating Black Holes in Chern-Simons Modified Gravity

Kohkichi Konno[1],

Department of Natural and Physical Sciences, Tomakomai National College of Technology, Tomakomai 059-1275

Abstract

The Chern-Simons modification of general relativity requires the modification of the Kerr solution for a rotating black hole. We present approximate rotating black hole solutions in Chern-Simons modified gravity.

1 Introduction

Chern-Simons (CS) modified gravity is a theory in which the Einstein-Hilbert action is modified by the CS term [1]. It is interesting to note that the CS modified gravity can be obtained from several approaches to quantum gravity [2]. The remarkable characteristic of the CS term is to violate parity symmetry. This characteristic leads to the result that solutions for a rotating black hole in the CS modified gravity inevitably has a different form from that of the Kerr solution. However, the Schwarzschild solution still holds in the CS modified gravity. The latter fact ensures that the CS modified gravity survives under observational constraints at present. In the present work, we provide approximate solutions for a rotating black hole in the CS modified gravity.

This paper is organized as follows. In Sec. 2, we briefly review two models of the CS modified gravity. In Sec. 3, we provide approximate solutions for a rotating black hole in the two models (see [3–5] in detail). Finally, we provide a summary in Sec. 4. Throughout the paper, we use geometrized units with $c = G = 1$.

2 CS modified gravity

2.1 Non-dynamical CS modified gravity

The action of non-dynamical CS modified gravity is provided by [1]

$$I = \int d^4x\sqrt{-g}\left[-\frac{R}{16\pi}+\frac{\ell}{64\pi}\vartheta\, {}^*R^{\tau}{}_{\sigma}{}^{\mu\nu}R^{\sigma}{}_{\tau\mu\nu}+\mathcal{L}_{\rm m}\right], \tag{1}$$

where g is the determinant of the metric $g_{\mu\nu}$, $R \equiv g^{\alpha\beta}R_{\alpha\beta}$ ($R_{\alpha\beta} \equiv R^{\lambda}{}_{\alpha\lambda\beta}$) is the Ricci scalar, $R^{\tau}{}_{\sigma\alpha\beta} \equiv \partial_\beta\Gamma^{\tau}_{\sigma\alpha} - \cdots$ is the Riemann tensor ($\Gamma^{\alpha}_{\beta\gamma}$ is the Christoffel symbols), ℓ is a coupling constant, and $\mathcal{L}_{\rm m}$ is the Lagrangian density for matter. The dual Riemann tensor is defined by ${}^*R^{\tau}{}_{\sigma}{}^{\mu\nu} \equiv \frac{1}{2}\varepsilon^{\mu\nu\alpha\beta}R^{\tau}{}_{\sigma\alpha\beta}$, where $\varepsilon^{\mu\nu\alpha\beta}$ is the Levi-Civita tensor with $\varepsilon^{0123} \equiv 1/\sqrt{-g}$. In this model, ϑ is an external scalar function. The term $\sqrt{-g}\,{}^*R^{\tau}{}_{\sigma}{}^{\mu\nu}R^{\sigma}{}_{\tau\mu\nu}$ is mathematically called Chern-Pontryagin density. The Chern-Pontryagin density can be written as a total derivative of the CS topological current K^μ defined by

$$K^\mu = \varepsilon^{\mu\alpha\beta\gamma}\left[\Gamma^{\sigma}_{\alpha\tau}\partial_\beta\Gamma^{\tau}_{\gamma\sigma}+\frac{2}{3}\Gamma^{\sigma}_{\alpha\tau}\Gamma^{\tau}_{\beta\eta}\Gamma^{\eta}_{\gamma\sigma}\right], \tag{2}$$

Thus we have

$$\partial_\alpha\left(\sqrt{-g}K^\alpha\right) = \frac{1}{2}\sqrt{-g}\,{}^*R^{\tau}{}_{\sigma}{}^{\mu\nu}R^{\sigma}{}_{\tau\mu\nu}. \tag{3}$$

Hence the action (1) can be written in terms of the CS topological current,

$$I = \int d^4x\sqrt{-g}\left[-\frac{R}{16\pi}-\frac{\ell}{32\pi}\left(\partial_\alpha\vartheta\right)K^\alpha+\mathcal{L}_{\rm m}\right]. \tag{4}$$

[1]Email address: kohkichi@gt.tomakomai-ct.ac.jp

Therefore the gravitational theory provided by Eq. (4), i.e., Eq. (1) with non-vanishing $\partial_\alpha \vartheta$, is called *CS modified gravity*.

From the variation in the action with respect to the metric $g_{\mu\nu}$, we obtain the field equation

$$G^{\mu\nu} + \ell C^{\mu\nu} = -8\pi T_{\rm m}{}^{\mu\nu}, \tag{5}$$

where $G^{\mu\nu}$ is the Einstein tensor, $T_{\rm m}^{\mu\nu}$ is the energy-momentum tensor, and $C^{\mu\nu}$ is the Cotton tensor defined by

$$C^{\mu\nu} \equiv -\frac{1}{2}\left[(\nabla_\sigma \vartheta)\left(\varepsilon^{\sigma\mu\alpha\beta}\nabla_\alpha R^\nu{}_\beta + \varepsilon^{\sigma\nu\alpha\beta}\nabla_\alpha R^\mu{}_\beta\right) + (\nabla_\sigma \nabla_\tau \vartheta)\left({}^*R^{\tau\mu\sigma\nu} + {}^*R^{\tau\nu\sigma\mu}\right)\right]. \tag{6}$$

The covariant divergence of Eq. (5) leads to the constraint [1]

$${}^*R^\tau{}_\sigma{}^{\mu\nu} R^\sigma{}_{\tau\mu\nu} = 0. \tag{7}$$

This equation is called the Chern-Pontryagin constraint. Therefore the non-dynamical CS modified gravity is governed by Eq. (5) with the constraint (7).

2.2 Dynamical CS modified gravity

In dynamical CS modified gravity, the scalar function ϑ is replaced with a scalar field which behaves as a dynamical variable in the gravitational system. The action is provided by

$$I = \int d^4x\sqrt{-g}\left[-\frac{R}{16\pi} + \frac{\ell}{64\pi}\vartheta\, {}^*R^\tau{}_\sigma{}^{\mu\nu} R^\sigma{}_{\tau\mu\nu} - \frac{1}{2}g^{\mu\nu}(\partial_\mu\vartheta)(\partial_\nu\vartheta) + \mathcal{L}_{\rm m}\right], \tag{8}$$

where the kinematic term for ϑ is added, but a potential for ϑ is ignored. Then the field equations are given by

$$G^{\mu\nu} + \ell C^{\mu\nu} = -8\pi\left(T_{\rm m}{}^{\mu\nu} + T_\vartheta{}^{\mu\nu}\right), \tag{9}$$

$$g^{\mu\nu}\nabla_\mu\nabla_\nu\vartheta = -\frac{\ell}{64\pi}\, {}^*R^\tau{}_\sigma{}^{\mu\nu} R^\sigma{}_{\tau\mu\nu}. \tag{10}$$

The constraint (7) in the non-dynamical model is now replaced with the equation of motion (10) for the scalar field ϑ.

3 Slowly rotating black holes

We discuss slowly rotating black hole solutions in the two models of CS modified gravity. For this purpose, let us consider the perturbation of the Schwarzschild spacetime. In the non-dynamical model, the Schwarzschild metric satisfies both the field equation (5) and the constraint (7). Furthermore, the Schwarzschild metric satisfies the field equations (9) and (10) in the dynamical model under the condition in which the boundary condition $\vartheta \to 0$ at infinity is imposed. Thus we take the Schwarzschild metric as the background. To obtain slowly rotating black hole solutions, we consider the perturbed metric given by

$$\begin{aligned} ds^2 = &-\left(1-\frac{2M}{r}\right)(1+h(r,\theta))\,dt^2 + \left(1-\frac{2M}{r}\right)^{-1}(1+m(r,\theta))\,dr^2 \\ &+r^2(1+k(r,\theta))\left[d\theta^2 + \sin^2\theta\,(d\phi - \omega(r,\theta)\,dt)^2\right], \end{aligned} \tag{11}$$

where M is the mass of a black hole, the functions $h(r,\theta)$, $m(r,\theta)$, $k(r,\theta)$ and $\omega(r,\theta)$ are of the first order in $\epsilon \sim J/M^2$ (J is the angular momentum of the black hole). Here ϵ is considered to be a small parameter for the perturbation. Hereafter, we take account of equations up to the first order in ϵ. By substituting Eq. (11) into the field equations (5) and (7), or (9) and (10) and solving those equations, we can obtain the metric solutions.

3.1 Solutions in the non-dynamical model

We discuss a slowly rotating black hole in the non-dynamical model. From the Chern-Pontryagin constraint (7), we derive

$$(\nabla^\nu \vartheta)\, \frac{3M}{r^3} \sin\theta \ (\omega_{,r\theta} + 2\cot\theta\, \omega_{,r}) = 0, \tag{12}$$

where a subscript comma denotes the partial differentiation with respect to the coordinates. It should be noted that the function $\omega\,(r,\theta)$ only appears in Eq. (12). As the solution for Eq. (12), we find

$$\omega\,(r,\theta) = \frac{\varpi(r)}{\sin^2\theta}, \tag{13}$$

where ϖ is a function of r only. Equation (13) means that the function $\omega\,(r,\theta)$ is singular on the rotational axis ($\theta = 0$ and π), irrespective of the choice of the scalar function ϑ. Thus $g_{t\phi}$ does not vanish on the rotational axis unless $\varpi(r)$ is identically zero, and the shift vector $N_i \equiv g_{ti}$ $(i = r, \theta, \phi)$ is also singular on the rotational axis.

When we adopt $\vartheta = r\cos\theta/\mu_0$ (μ_0 is a constant), we can find the metric solution for a slowly rotating black hole which is given by [3]

$$\begin{aligned} ds^2 &= -\left(1-\frac{2M}{r}\right)dt^2 + \left(1-\frac{2M}{r}\right)^{-1} dr^2 + r^2\left(d\theta^2 + \sin^2\theta d\phi^2\right) \\ &\quad -2\left[C_1\left(1-\frac{2M}{r}\right) + \frac{C_2}{r}\left\{r^2 - 2Mr - 4M^2 + 4M(r-2M)\ln\left(r-2M\right)\right\}\right] dt d\phi, \end{aligned} \tag{14}$$

where C_1 and C_2 are constants. Although this solution has the singularity on the rotational axis, this spacetime can interestingly provide the flat rotation curves at a large distance from the black hole [4]. (See [6, 7] for other solutions in the non-dynamical model.)

3.2 Solutions in the dynamical model

Next we consider a slowly rotating black hole in the dynamical model. To obtain the solution, we have to remind that ϑ is a dynamical variable. The scalar field ϑ is assumed to be expanded as

$$\vartheta\,(r,\theta) = \vartheta^{(1)}\,(r,\theta) + O\left(\epsilon^2\right), \tag{15}$$

where $\vartheta^{(1)}\,(r,\theta) \sim O(\epsilon)$. Furthermore, we consider the coupling constant ℓ to be a small parameter and expand the field equations in a power series of ℓ. By solving the field equations (9) and (10), we can find the solution [5]

$$\vartheta = -\ell \frac{J}{128\pi M^2 r^4}\left(5r^2 + 10Mr + 18M^2\right)\cos\theta, \tag{16}$$

$$\begin{aligned} ds^2 &= -\left(1-\frac{2M}{r}\right)dt^2 + \left(1-\frac{2M}{r}\right)^{-1} dr^2 + r^2\left(d\theta^2 + \sin^2\theta d\phi^2\right) \\ &\quad -\frac{4J}{r}\left[1 - \ell^2 \frac{1}{3584\pi M r^5}\left(70r^2 + 120Mr + 189M^2\right)\right]\sin^2\theta dt d\phi, \end{aligned} \tag{17}$$

where J is the angular momentum of the black hole. In deriving Eqs. (16) and (17), we assumed the solutions of $\vartheta^{(1)} = 0$ and $\omega = -2J/r^3$ at order $\ell^0\epsilon$, where ω coincides with the first order approximation of the Kerr black hole. (The same solution was also obtained independently by Yunes and Pretorius [7].) From the $(t\phi)$-component of the metric in Eq. (17), we find that the frame-dragging effect is suppressed by the CS correction, because the second term of order ℓ^2 in the bracket is negative for any value of r. (See [5, 7] for astrophysical implications.)

4 Summary

We have discussed slowly rotating black hole solutions in the two models of CS modified gravity. In the non-dynamical model, the singularity like a spinning cosmic string appears on the rotational axis owing to the Chern-Pontryagin constraint. However, the solution for a slowly rotating black hole interestingly provides the flat rotation curves far away from the black hole. On the other hand, such a singularity does not appear in the dynamical model. The solution in the dynamical model reduces to the first order approximation of the Kerr solution when the coupling constant vanishes. To impose a severe observational constraint for the CS coupling constant using astrophysical objects, we need the solution for a rapidly rotating black hole, which will be obtained in the future work.

Acknowledgments

This work is based on the results [3–5, 8] of collaborations with Prof. T. Matsuyama, Prof. Y. Asano, and Prof. S. Tanda. The author thanks them for useful discussions.

References

[1] R. Jackiw and S.-Y. Pi Phys. Rev. D **68**, 104012 (2003).

[2] S. Alexander and N. Yunes Phys. Rep. **480**, 1 (2009).

[3] K. Konno, T. Matsuyama, and S. Tanda Phys. Rev. D **76**, 024009 (2007).

[4] K. Konno, T. Matsuyama, Y. Asano and S. Tanda Phys. Rev. D **78**, 024037 (2008).

[5] K. Konno, T. Matsuyama, and S. Tanda Prog. Theor. Phys. **122**, 561 (2009).

[6] D. Grumiller and N. Yunes Phys. Rev. D **77**, 044015 (2008).

[7] N. Yunes and F. Pretorius Phys. Rev. D **79**, 084043 (2009).

[8] K. Konno, T. Matsuyama, and S. Tanda Mod. Phys. Lett. A **25**, 2655 (2010).

Iso-curvature fluctuations in modulated reheating scenario

Shuichiro Yokoyama[1(a)], Kohei Kamada[(b)] and Kazunori Kohri[(c)]

[(a)] *Department of Physics and Astrophysics, Nagoya University, Aichi 464-8602*
[(b)] *RESCEU, Graduate School of Science, The University of Tokyo, Tokyo 113-0033*
[(c)] *Institute of Particle and Nuclear Studies, KEK, Ibaraki 305-0801*

Abstract

Modulated reheating scenario is one of the most attractive models that predict possible detections of primordial non-Gaussianity through future CMB observations such as the Planck satellite. We study the baryonic-isocurvature fluctuations in the Affleck-Dine baryogenesis with the modulated reheating scenario. We show that the simple Affleck-Dine baryogenesis would be incompatible with the modulated reheating scenario with respect to the current observational constraint on the baryonic-isocurvature fluctuations, like a gravitino dark matter scenario.

1 Introduction

Primordial non-Gaussianity of curvature fluctuation fluctuations is one of well discussed topics recently. From the recent result from WMAP 7-year data, the so-called local type non-linearity parameter $f_{\rm NL}$ is constrained as $-10 < f_{\rm NL} < 74$ [1]. If future observations confirm such a large value of $f_{\rm NL}$, we need some mechanism which generates large non-Gaussian primordial fluctuations. The modulated reheating scenario [2] , where a scalar field other than the inflaton is responsible for primordial fluctuations through the inhomogeneous reheating, is interesting mechanisms generating large non-Gaussianity.

Of course, it is important to check consistencies of the modulated reheating scenario with other observational constraints. In the modulated reheating scenario, the curvature perturbation is effectively governed by the fluctuation of the reheating temperature after inflation $\delta T_R/T_R$. Since most class of viable baryogenesis scenarios in modern cosmology depend on the reheating temperature, the modulated reheating may induce a large baryonic-isocurvature fluctuation. Some class of scenarios for dark-matter production also depend on the reheating temperature such as gravitino thermal/non-thermal production. In Ref. [3, 4], the authors shown that in this case the modulated reheating is severely constrained by observations of the cold dark matter (CDM)-isocurvature fluctuation.

Here, we consider baryogenesis in models with supersymmetric (SUSY) extension of standard model, especially so-called Affleck-Dine (AD) mechanism [5, 6], which is naturally realized even in the Minimal Supersymmetric Standard Model (MSSM) and agrees with observations in broad parameter regions [7]. Since good candidates for the light scalar field σ could be found in SUSY or supergravity (the local theory of SUSY), this direction of discussion should be naturally motivated.

2 Modulated Reheating Scenario

Here, we give a brief review of the modulated reheating scenario. In such scenario, we consider the decay rate of the inflaton, Γ, depending on a light scalar field, σ, which has a quantum fluctuation during inflation, that is, $\Gamma = \Gamma(\sigma)$.

In order to evaluate the curvature perturbation generated in the modulated reheating scenario, let us consider the e-folding number $N = \int d\ln a$, where a is a scale factor, measured between the end of inflation at $t = t_{\rm inf}$ and a time after the end of the complete reheating, $t_{\rm c}$. This can be written as

$$\begin{aligned} N &= \ln\left(\frac{a(t_{\rm c})}{a(t_{\rm inf})}\right) \\ &= \ln\left(\frac{a(t_{\rm reh})}{a(t_{\rm inf})}\right) + \ln\left(\frac{a(t_{\rm c})}{a(t_{\rm reh})}\right) , \end{aligned} \tag{1}$$

[1]Email address: shu@a.phys.nagoya-u.ac.jp

where $t_{\rm reh}$ represents a time at $d\ln a/dt = H = \Gamma$. For the quadratic inflaton potential, $V(\phi) \propto \phi^2$, during the inflaton oscillating phase after the inflation, the energy density of the Universe relying on the inflaton decays as $\rho \propto a^{-3}$ and the Hubble parameter, H, evolves as $H \propto \rho^{1/2}$. Since after the complete reheating the energy density of the Universe is dominated by the radiation ($\rho \propto a^{-4}$ and $H \propto a^{-2}$), the e-folding number given by Eq. (1) is rewritten as

$$\begin{aligned} N &= \ln\left(\frac{a(t_{\rm reh})}{a(t_{\rm inf})}\right) + \ln\left(\frac{a(t_{\rm c})}{a(t_{\rm reh})}\right) \\ &= -\frac{1}{6}\ln\left(\frac{\Gamma}{H(t_{\rm inf})}\right) + \frac{1}{2}\ln\left(\frac{H(t_{\rm inf})}{H(t_{\rm c})}\right) , \end{aligned} \tag{2}$$

where we have used $H(t_{\rm reh}) = \Gamma$. Then, the fluctuation of σ induces the modulated reheating and hence the fluctuation of the e-folding number is given by

$$\delta N = -\frac{1}{6}\frac{\delta\Gamma(\sigma)}{\Gamma(\sigma)} = -\frac{1}{6}\frac{\Gamma'}{\Gamma}\delta\sigma , \tag{3}$$

where $\Gamma'(\sigma) \equiv d\Gamma(\sigma)/d\sigma$. Based on δN formula, taking the final hypersurface at $t = t_{\rm c}$ to be a uniform energy density one, we have

$$\zeta(t_{\rm c}) = \delta N(t_{\rm c}, t_{\rm ini}) = -\frac{1}{6}\frac{\Gamma'}{\Gamma}\delta\sigma(t_{\rm ini}) , \tag{4}$$

where $\delta\sigma(t_{\rm ini})$ is the fluctuation of the field σ on the flat hypersurface and we have assumed that $\delta\sigma$ is almost constant and also almost Gaussian fluctuation after the horizon crossing time. In terms of the reheating temperature $T_R \propto \Gamma^{1/2}$, the above expression can be rewritten as

$$\delta N = -\frac{1}{3}\frac{\delta T_R}{T_R} . \tag{5}$$

Up to the second order, we have

$$\zeta \approx \delta N = -\frac{1}{6}\frac{\Gamma'}{\Gamma}\left[\delta\sigma + \frac{1}{2}\left(\frac{\Gamma''}{\Gamma'} - \frac{\Gamma'}{\Gamma}\right)\delta\sigma^2\right] . \tag{6}$$

Hence the power spectrum and the non-linearity parameter $f_{\rm NL}$ defined as

$$\langle\zeta(\mathbf{k})\zeta(\mathbf{k}')\rangle \equiv (2\pi)^3\frac{2\pi^2}{k^3}\mathcal{P}(k)\delta^{(3)}(\mathbf{k}+\mathbf{k}') , \tag{7}$$

$$\zeta = \zeta_{\rm lin} + \frac{3}{5}f_{\rm NL}\zeta_{\rm lin}^2 , \tag{8}$$

are respectively given by

$$\mathcal{P}(k) = \left(\frac{1}{6}\frac{\Gamma'}{\Gamma}\right)^2\left(\frac{H_{\rm inf}}{2\pi}\right)^2 , \tag{9}$$

$$f_{\rm NL} = 5\left(1 - \frac{\Gamma\Gamma''}{\Gamma'^2}\right) . \tag{10}$$

Hence, in the modulated reheating scenario we can easily get the large non-Gaussianity ($f_{\rm NL} \sim \mathcal{O}(10)$) by considering appropriate form of $\Gamma(\sigma)$ and also the power spectrum of primordial curvature fluctuations which is consistent with the current cosmological observations.

3 Affleck-Dine Baryogenesis Scenario

AD mechanism [5, 6] has been known as one of the powerful candidates for the successful baryogenesis mechanism. It can be realized by taking advantage of a flat direction along which scalar potential vanishes

in the global SUSY limit. Hereafter we call the complex scalar field that parameterizes the flat direction as AD field Φ and assume that it carries non-zero baryon charge β.

Though the scalar potential for the AD field vanishes in the global SUSY limit, it is lifted by non-renormalizable terms, the SUSY-breaking effect and some other effects. Let us consider a non-renormalizable superpotential for the AD field given by

$$W_{\rm nr} = \frac{\Phi^{n+3}}{(n+3)M_*^n}, \tag{11}$$

where M_* is the cut-off scale and the positive integer n depends on the flat direction. Including the SUSY breaking effect, the induced scalar potential reads

$$V = V_{\not S} + \frac{|\Phi|^{2n+4}}{M_*^{2n}} + \left(\frac{a_B m_{3/2}}{M_*^n} \Phi^{n+3} + \text{h.c.} \right) , \tag{12}$$

where $m_{3/2}$ is a gravitino mass and a_B is a complex numerical factor whose amplitude is of order of unity. $V_{\not S}$ is the soft SUSY breaking effect that depends on the SUSY breaking mechanism. The second term is the F-term that comes from non-renormalizable operator $W_{\rm nr}$. The last term represents the interaction between non-renormalizable operator and the SUSY breaking sector coming from supergravity effect, which breaks the $U(1)$ baryon symmetry and is called as the A-term.

During and after inflation, the AD field acquires the Hubble induced mass from the interaction between the AD field and the inflaton through the supergravity effect, which can be negative,

$$V_{\rm H} = -c_{\rm H} H^2 |\Phi|^2, \tag{13}$$

where $c_{\rm H}$ is a positive numerical factor of order of unity. Thus, the AD field evolves with the effective potential,

$$V_{\rm eff} = V + V_{\rm H}. \tag{14}$$

During and after inflation, when the Hubble parameter H is sufficiently large, the AD field settles down to the time-dependent potential minimum,

$$|\Phi| \simeq (H M_*^n)^{1/(n+1)}, \tag{15}$$

and traces its evolution. Note that there can be several non-renormalizable operators for the AD field but only the one with the smallest n determines the dynamics of the AD field. Thus hereafter we consider only smaller n ($n \leq 3$).

Let us consider the evolution of the AD field further. As the Hubble parameter decreases, the Hubble induced mass also gets small. Then, when $H_{\rm osc}^2 \simeq |V''_{\rm eff}|$, the AD field (more precisely its radial component) starts to oscillate around the origin. Here the dash denotes the derivative with respect to $\phi \equiv \sqrt{2}|\Phi|$, and hereafter the subscript "osc" indicates that the parameter or the variable is evaluated at the onset of the AD field oscillation.

At the onset of the oscillation, the AD field acquires an angular momentum due to the A-term, which represents the baryon asymmetry of the Universe n_B,

$$n_B(t_{\rm osc}) \simeq \beta m_{3/2} (H_{\rm osc} M_*^n)^{2/(n+1)} \sin(n\theta_{\rm inf} + \alpha), \tag{16}$$

where $\theta_{\rm inf}$ and α are the phases of Φ during inflation and the constant a_B in the third term of Eq. (12), respectively. Just after the onset of the AD field oscillation, $a^3 n_B$ is conserved since the CP-violating A-term comes to ineffective quickly. This is because the AD field value continues decreasing with time during the field oscillation due to the cosmic expansion. Since the entropy density decreases as $s \propto a^{-3}$ after the reheating if there is no late-time entropy production, the baryon-to-entropy ratio n_B/s is conserved. Thus its present value is estimated as

$$\left(\frac{n_B}{s} \right)_0 \simeq \frac{\beta m_{3/2} T_R}{M_G^2 H_{\rm osc}^2} (H_{\rm osc} M_*^n)^{2/(n+1)} \sin(n\theta_{\rm inf} + \alpha). \tag{17}$$

The Hubble parameter at the onset of the AD field oscillation is

$$H_{\rm osc} \simeq m_0(|\Phi|_{\rm osc}), \tag{18}$$

where $m_0(|\Phi|) \equiv V''_{\not S}(|\Phi|)$. Hence, from Eq. (17) we can find that the present value of the baryon-to-entropy ratio is proportional to the reheating temperature.

4 Result

Let us consider the baryonic-isocurvature fluctuation S_B, which is commonly defined as

$$S_B \equiv \frac{\delta n_B}{n_B} - \frac{\delta s}{s} = \frac{\delta(n_B/s)}{n_B/s} \ . \tag{19}$$

In the case where the baryon-to-entropy ratio depends on the reheating temperature, the baryonic-isocurvature fluctuation can be also generated in the modulated reheating scenario. From Eq. (**??**), we have

$$S_B = \frac{\delta(n_B/s)}{n_B/s} = \frac{\delta T_R}{T_R} \ . \tag{20}$$

Hence, in the case where the curvature perturbation originates mainly from the modulated reheating mechanism, from Eq. (5) and Eq. (20), we have

$$S_B = -3\zeta \ . \tag{21}$$

The current observational limit for the anti-correlated baryonic-isocurvature fluctuation is roughly given by $|S_B/\zeta| \lesssim O(0.1)$ and hence it means that this model seems to be conflict with current observations. This result is quite similar to that in the case where one consider the gravitino dark matter in the modulated reheating scenario [3]. However, in Ref. [7], we have shown that as for the AD baryogenesis scenario if one consider the thermal effect even before the reheating one can construct the successful AD baryogenesis scenario in modulated reheating scenario.

References

[1] E. Komatsu *et al.*, arXiv:1001.4538 [astro-ph.CO].

[2] G. Dvali, A. Gruzinov and M. Zaldarriaga, Phys. Rev. D **69**, 023505 (2004) [arXiv:astro-ph/0303591]. L. Kofman, arXiv:astro-ph/0303614.

[3] T. Takahashi, M. Yamaguchi, J. Yokoyama and S. Yokoyama, Phys. Lett. B **678**, 15 (2009).

[4] T. Takahashi, M. Yamaguchi and S. Yokoyama, Phys. Rev. D **80**, 063524 (2009)

[5] I. Affleck and M. Dine, Nucl. Phys. B **249**, 361 (1985).

[6] M. Dine, L. Randall and S. D. Thomas, Nucl. Phys. B **458**, 291 (1996) [arXiv:hep-ph/9507453].

[7] K. Kamada, K. Kohri and S. Yokoyama, arXiv:1008.1450 [astro-ph.CO].

Redshift drift in LTB universes

Chul-Moon Yoo[1(a)], Tomohiro Kai[2(b)] and Ken-ichi Nakao[3(b)]

[(a)] *Yukawa Institute for Theoretical Physics, Kyoto University, Kyoto 606-8502*
[(b)] *Department of Mathematics and Physics, Graduate School of Science, Osaka City University, Osaka 558-8585*

Abstract

We study the redshift drift, i.e., the time derivative of the cosmological redshift in the Lemaître-Tolman-Bondi (LTB) solution in which the observer is assumed to be located at the symmetry center. This solution has often been studied as an anti-Copernican universe model to explain the acceleration of cosmic volume expansion without introducing the concept of dark energy. One of decisive differences between LTB universe models and Copernican universe models with dark energy is believed to be the redshift drift. The redshift drift is negative in all known LTB universe models, whereas it is positive in the redshift domain $z \lesssim 2$ in Copernican models with dark energy. However, there have been no detailed studies on this subject. In the present paper, we prove that the redshift drift of an off-center source is always negative in the case of LTB void models. We also show that the redshift drift can be positive with an extremely large hump-type inhomogeneity. Our results suggest that we can determine whether we live near the center of a large void without dark energy by observing the redshift drift.

1 introduction

The standard cosmological model is based on the so-called Copernican principle that we are not located in a special position in the universe. This model can naturally explain almost all observational data, and consequently seems to imply that the Copernican principle is a reality. However, we should not blindly rely on this principle without observational justifications. Here, we should note that it is not clear at all how large the systematic errors would be in the determination of the cosmological parameters, if the Copernican principle is abandoned. Thus, it is an unavoidable task in observational cosmology to investigate possible "anti-Copernican" universe models and test if such models can be observationally excluded.

Almost all anti-Copernican universe models are based on the Lemaître-Tolman-Bondi (LTB) solution which describes the dynamics of a spherically symmetric dust. In order to check the LTB universe models observationally, it is crucial to find observable quantities which can reveal differences between the LTB universe models and Copernican universe models with the dark energy. One such quantity is believed to be the redshift drift, i.e., the time derivative of the cosmological redshift [1]. In the case of the ΛCDM model, which is the most likely Copernican model at present, the redshift drift is positive in the redshift domain $z \lesssim 2$, since the cosmological constant Λ causes repulsive gravity. By contrast, there is no exotic matter with the violation of the strong energy condition in the LTB solution. Thus, as long as there is no highly inhomogeneous structure, the redshift drift might be negative in LTB universe models. Although several authors have pointed out the importance of the redshift drift [1–4], there has been no detailed study of its general behavior in LTB universe models. It is the purpose of this paper to investigate it.

In Sec. 2, we briefly review the LTB solution. In Sec. 3, we derive the equation for the redshift drift. In Sec. 4, we define LTB void models and prove a theorem on the redshift drift in these models. In Sec. 5, we show that the redshift drift can be positive even in an LTB universe model, if an extremely large hump-type mass density distribution exists. Sec. 6 is devoted to the summary and discussion.

In this paper, we denote the speed of light and Newton's gravitational constant by c and G, respectively.

[1]Email address: yoo@yukawa.kyoto-u.ac.jp
[2]Email address: hirotomo203@gmail.com
[3]Email address: knakao@sci.osaka-cu.ac.jp

2 the LTB solution

As mentioned in the introduction, we consider a spherically symmetric inhomogeneous universe filled with dust. This universe is described by an exact solution of the Einstein equations, which is known as the Lemaître-Tolman-Bondi (LTB) solution. The metric of the LTB solution is given by

$$ds^2 = -c^2dt^2 + \frac{(\partial_r R(t,r))^2}{1-k(r)r^2}dr^2 + R^2(t,r)d\Omega^2, \tag{1}$$

where $k(r)$ is an arbitrary function of the radial coordinate r. The matter is dust whose stress-energy tensor is given by $T^{\mu\nu} = \rho u^\mu u^\nu$, where $\rho = \rho(t,r)$ is the mass density, and u^μ is the four-velocity of the fluid element. The coordinate system in Eq. (1) is chosen in such a way that $u^\mu = (c,0,0,0)$.

The circumferential radius $R(t,r)$ is determined by one of the Einstein equations, $\left(\frac{\partial R}{\partial t}\right)^2 = \frac{2GM(r)}{R} - c^2kr^2$, where $M(r)$ is an arbitrary function related to the mass density ρ by $\rho(t,r) = \frac{1}{4\pi R^2 \partial_r R}\frac{dM}{dr}$. $M(r)$ is known as the Misner-Sharp mass that is the quasi-local mass naturally introduced into the spherically symmetric spacetime[5]. In this paper, we assume that the Misner-Sharp mass is a monotonically increasing function of r in the domain of interest. This assumption is equivalent to the one that $\partial_r R$ is positive if ρ is positive.

Following Ref. [6], we write the solution of Einstein equations in the form,

$$R(t,r) = (6GM)^{1/3}[t - t_{\rm B}(r)]^{2/3}S(x), \quad x = c^2kr^2\left(\frac{t-t_{\rm B}}{6GM}\right)^{2/3}, \tag{2}$$

where $t_{\rm B}(r)$ is an arbitrary function which determines the big bang time, and $S(x)$ is an analytic function in $x < (\pi/3)^{2/3}$ (see Ref.[6] for the definition of $\mathcal{S}(x)$).

As shown in the above, the LTB solution has three arbitrary functions, $k(r)$, $M(r)$ and $t_{\rm B}(r)$. One of them is a gauge degree of freedom for the rescaling of r. In this paper, since M is assumed to be a monotonically increasing function of r, we can fix this freedom by setting $M = \frac{4}{3}\pi\rho_0 r^3$, where ρ_0 is the mass density at the symmetry center at the present time t_0, i.e., $\rho_0 = \rho(t_0, 0)$.

3 Equation for the redshift drift

In order to study the cosmological redshift and the redshift drift, we consider ingoing radial null geodesics. The cosmological redshift z of a light ray from a comoving source at r to the observer at the symmetry center $r = 0$ is defined by $z(r) := k^t(\lambda(r))/k^t(\lambda(0)) - 1$, where k^t is the time component of the null geodesic tangent, and λ is the affine parameter which can be regarded as a function of r. From the geodesic equations, we have the equation for the redshift z as

$$\frac{dz}{dr} = \frac{(1+z)\partial_t\partial_r R}{c\sqrt{1-kr^2}}. \tag{3}$$

The null condition leads to

$$\frac{dt}{dr} = -\frac{\partial_r R}{c\sqrt{1-kr^2}}. \tag{4}$$

We denote the trajectories of light rays observed by the central observer at $t = t_0$ and $t = t_0 + \delta t_0$, respectively, by

$$\begin{cases} z = z_{\rm lc}(r;t_0) \\ t = t_{\rm lc}(r;t_0) \end{cases} \tag{5}$$

and

$$\begin{cases} z = z_{\rm lc}(r;t_0+\delta t_0) =: z_{\rm lc}(r;t_0) + \delta z(r) \\ t = t_{\rm lc}(r;t_0+\delta t_0) =: t_{\rm lc}(r;t_0) + \delta t(r) \end{cases}. \tag{6}$$

Here, by their definitions, we have $t_{\rm lc}(0;t_0) = t_0$, $z_{\rm lc}(0;t) = 0$, $\delta z(0) = 0$ and $\delta t(0) = \delta t_0$. Substituting Eq. (6) into Eqs. (3) and (4), and regarding $\delta z(r)$ and $\delta t(r)$ as infinitesimal quantities, we obtain

$$\frac{d}{dr}\delta z = \frac{\partial_t\partial_r R}{c\sqrt{1-kr^2}}\delta z + \frac{(1+z)\partial_t^2\partial_r R}{c\sqrt{1-kr^2}}\delta t, \quad \frac{d}{dr}\delta t = \frac{-\partial_t\partial_r R}{c\sqrt{1-kr^2}}\delta t, \tag{7}$$

where we have used the fact that (5) satisfies Eqs. (3) and (4), and the arguments of $\partial_t\partial_r R$ and $\partial_t^2\partial_r R$ are $t = t_{\rm lc}(r, t_0)$ and r.

Hereafter, we consider the case where the cosmological redshift z is monotonically increasing with r. We say that such a model is *z-normal*. Then, we replace the independent variable r by $z = z_{\rm lc}(r; t_0)$. By using $\frac{d}{dr} = \frac{dz}{dr}\frac{d}{dz} = \frac{(1+z)\partial_t\partial_r R}{c\sqrt{1-kr^2}}\frac{d}{dz}$, we have

$$\frac{d}{dz}\delta z = \frac{\delta z}{1+z} + \frac{\partial_t^2\partial_r R}{\partial_t\partial_r R}\delta t, \quad \frac{d}{dz}\delta t = -\frac{\delta t}{1+z}. \tag{8}$$

We can easily integrate the above equation to obtain $\delta t = \frac{\delta t_0}{1+z}$. By using the above result, we obtain

$$\frac{d}{dz}\left(\frac{\delta z}{1+z}\right) = \frac{1}{(1+z)^2}\frac{\partial_t^2\partial_r R}{\partial_t\partial_r R}\delta t_0. \tag{9}$$

4 The redshift drift in LTB void models

We call an LTB universe model the LTB *void* model, if the following three conditions are satisfied. 1 the mass density is non-negative; 2 the mass density is increasing with r increasing in the domain $r > 0$ on a spacelike hypersurface of constant t; 3 $\partial_r R$ is positive; 4 z-normality.

Proposition 1 In LTB void models, $\partial_t^2\partial_r R$ is negative.

Proof. By Einstein equations, we obtain

$$\partial_t^2\partial_r R(t,r) = -\frac{G\partial_r M}{R^2} + \frac{2GM\partial_r R}{R^3} = 4\pi G\frac{\partial_r R}{R^3}\left(-\rho R^3 + 2\int_0^r \rho(t,x)R^2(t,x)\partial_r R(t,x)dx\right). \tag{10}$$

Since $\partial_r R$ is positive by the definition of LTB void models, we may replace the integration variable x by $R = R(t,x)$ and obtain

$$\partial_t^2\partial_r R(t,r) = 4\pi G\frac{\partial_r R}{R^3}\left(-\rho R^3 + 2\int_0^{R(t,r)} \rho R^2 dR\right) = -4\pi G\frac{\partial_r R}{R^3}\int_0^{R(t,r)}\left(\frac{d\rho}{dR}R^3 + \rho R^2\right)dR. \tag{11}$$

Since $d\rho/dR = (\partial_r R)^{-1}\partial_r\rho$ is positive in the domain of $R > 0$, the integrand in the last equality of the above equation is positive. Q.E.D.

Theorem In LTB void models, the redshift drift of an off-center source observed at the symmetry center is negative.

Proof. Since the cosmological redshift z vanishes at $r = 0$, z is non-negative by the assumption of z-normality. Further, the z-normality leads to $\partial_t\partial_r R > 0$ through Eq. (3). Then, since $\delta t_0 > 0$, we see from Eq. (9) that Proposition 1 leads to the following inequality $\frac{d}{dz}\left(\frac{\delta z}{1+z}\right) < 0$. Since δz should vanish at $z = 0$, we have $\delta z < 0$ for $z > 0$ from the above inequality. Q.E.D.

5 Redshift drift in LTB universe models with a large hump

In the preceding section, we showed that the redshift drift observed at the symmetry center is negative for $r > 0$ in LTB void models. Conversely, if there is a domain in which the mass density is decreasing with increasing r, the redshift drift might be negative. In this section, we show that it is true with hump-type mass density distributions. We consider the following two LTB universe models, (i): $k(r) = 0$ and $t_{\rm B}(r) = f(r; a, r_1, r_2)$ with $a = -1.7H_0^{-1}$, $r_1 = 0.12cH_0^{-1}$ and $r_2 = 0.9cH_0^{-1}$, (ii): $t_{\rm B}(r) = 0$ and $k(r) = f(r; a, r_1, r_2)$ with $a = -100c^{-2}H_0^2$, $r_1 = 0.1cH_0^{-1}$ and $r_2 = 0.2cH_0^{-1}$, where $f(r; a, r_1, r_2) = 0$ for $r < r_1$, $f(r; a, r_1, r_2) = a\left(r - r_1\right)^3\left(r_1^2 - 5r_1r_2 + 10r_2^2 + 3r_1r - 15r_2r + 6r^2\right)/(r_2 - r_1)^5$ for $r_1 \le r < r_2$ and $f(r; a, r_1, r_2) = a$ for $r_2 \le r$. In Figs.1 and 2, we show the redshift drifts of these models. Although we do not show the energy densities of these models, a large hump in the mass density distribution exists in each model as well as in $t_{\rm B}(r)$ or $k(r)$. Although there is a redshift domain with positive redshift drift in each example, the distance-redshift relations of these models do not agree with the observational data, and further, the inhomogeneities need to be very large.

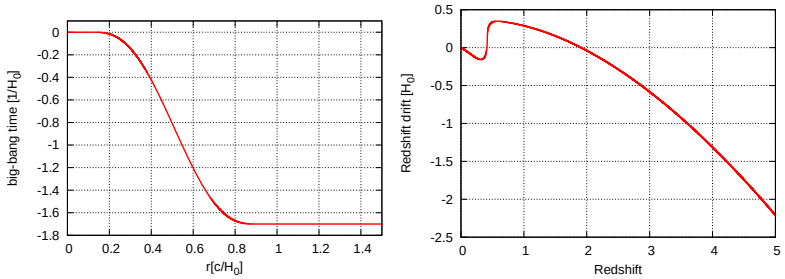

Figure 1: $t_{\rm B}(r)$(left panel) and $\delta z/\delta t_0$(right panel) of the model (i).

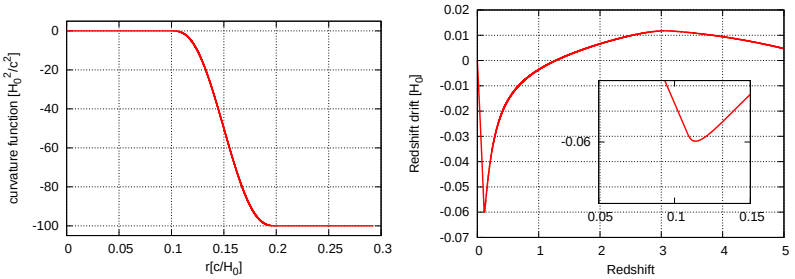

Figure 2: $k(r)$(left panel) and $\delta z/\delta t_0$(right panel) of the model (ii).

6 summary and discussion

In this paper, we studied the redshift drift in LTB universe models in which the observer is located at the symmetry center. We showed that, assuming that the mass density of the dust is positive, the redshift drift of an off-center source is negative if the mass density and the circumferential radius are increasing functions of the comoving radial coordinate. We also showed that if there is a very large hump structure around the symmetry center, the redshift drift can be positive. As a result, by observation of the redshift drift, we get a strong constraint on void-type universe models: if the redshift drift turns out to be positive in some redshift domain, LTB void models can be rejected.

Acknowledgements

We thank A. Nishizawa and K. Yagi for helpful discussions and comments. We would also like to thank all the participants of the Long-term Workshop on Gravity and Cosmology (GC2010: YITP-T-10-01) for fruitful discussions. This work is supported in part by JSPS Grant-in-Aid for Creative Scientific Research No. 19GS0219 and JSPS Grant-in-Aid for Scientific Research (C) No. 21540276.

References

[1] J.-P. Uzan, C. Clarkson, and G. F. R. Ellis, Phys. Rev. Lett. **100**, 191303 (2008), arXiv:0801.0068.

[2] P. Dunsby, N. Goheer, B. Osano, and J.-P. Uzan, (2010), arXiv:1002.2397.

[3] M. Quartin and L. Amendola, (2009), arXiv:0909.4954.

[4] C.-M. Yoo, T. Kai, and K.-i. Nakao, Prog. Theor. Phys. **120**, 937 (2008), arXiv:0807.0932.

[5] C. W. Misner and D. H. Sharp, Phys. Rev. **136**, B571 (1964).

[6] M. Tanimoto and Y. Nambu, Class. Quant. Grav. **24**, 3843 (2007), arXiv:gr-qc/0703012.

A new plane symmetric solution

Hongsheng Zhang[1],

Shanghai United Center for Astrophysics (SUCA), Shanghai Normal University, 100 Guilin Road, Shanghai 200234, P.R.China

Abstract

A new class of static plane symmetric solution of Einstein field equation generated by a perfect fluid source is put forward. A special family of this new solution is investigated in detail. The junction condition matching Taub metric is analyzed. The properties of geodesics of this solution are explored. It is found that this solution can be an appropriate simulation to the field of a uniformly accelerated observer in Newton mechanics.

1 introduction

Though considerable amounts of vacuum solutions of Einstein equation are known, but, frankly speaking, the physical interpretation of many of them remains unsettled [1]. As emphasized in [2], the key to physical interpretation is to find out the nature of the sources which generate these vacuum spaces. Singularity theorem is one of the most important and profound theorem in classical general relativity. For a deeper understanding and control of the singularities, the physical characters, such as mass densities, internal pressures, of the sources are imperative. For example in black hole solutions, where only singularity "generates" the whole space, investigating of how a matter distribution gives rise to the black hole space is necessary to judge the physical significance (or lack of it) of the complete analytic extensions of these solutions.

The static vacuum plane symmetric solution, Taub solution was obtained more than 50 years ago [3]. There is a serious time-like singularity in Taub space. People believe that the singularity should be superseded by some matter source, for some unsuccessful attempts to seek the sources, see [4].

We will present a new class of plane symmetric solution with perfect fluid source, which definitely violates the dominant energy condition. We will find that a special family of this solution is the proper source of the Taub metric.

We find a very general plane symmetric with 4 real parameters which solves the Einstein field equation with a perfect fluid source,

$$ds^2 = -f(z)^2dt^2 + dz^2 + e^{2az}f(z)^2e^{-2\left[az+\frac{h(z)\arctan\left(e^{az}\sqrt{\frac{w}{c}}\right)}{\sqrt{wc}}-dh(z)\right]}\left(dx^2+dy^2\right), \tag{1}$$

solves the Einstein field equation with a perfect fluid source. Here $a,\ w,\ c,\ d$ are 4 real parameters, and

$$f(z) = ce^{-az} + we^{az}, \tag{2}$$

$$h(z) = -ce^{-az} + we^{az}. \tag{3}$$

Clearly there are four Killing fields $\frac{\partial}{\partial t}$, $\frac{\partial}{\partial x}$, $\frac{\partial}{\partial y}$ and $-y\frac{\partial}{\partial x} + x\frac{\partial}{\partial y}$. The latter three span a Euclidean group G_3, which implies the plane symmetry. The metric (1) solves the Einstein field equation with a source in perfect fluid form

$$T = (\rho(z) + p(z))U \otimes U + p(z)g, \tag{4}$$

[1]Email address: hongshe@gmail.com

where T denotes the energy momentum tensor of the fluid, U stands for four-velocity of the fluid and g denotes the metric tensor. The exact forms of $p(z)$ and $\rho(z)$ are very involved,

$$\begin{aligned}\rho = \Big[&-16b^3c^4du^3 + 16b^4c^3du^5 + 12b^3c^4du^3 + 45b^2c^4u^2v^2 + 3b^7d^2cu^{10} + 12b^{7/2}c^{5/2}u^5v + 18b^2c^6d^2 - \\ &12b^4c^3du^5 + 45b^3c^5d^2u^2 + 18b^6c^2d^2u^8 + 45b^5c^3d^2u^6 + 18bc^5v^2 - 6b^6\sqrt{bc}du^{10}v + 18b^{9/2}c^{3/2}u^7v - \\ &16b^2c^4e^{2ar} - 120(bc)^{7/2}du^4v + 6b^5cu^8 + 6b^{11/2}c^{1/2}u^9v - 24b^2c^5du - 8bc^6/u + 24b^{3/2}c^{9/2}v + \\ &8\sqrt{bc}c^5u^{-1}v - 12b^{5/2}c^{7/2}u^3v + 45b^4c^2u^6v^2 + 8b^4c^2u^6 + 24b^5c^2du^7 + 60b^4c^4d^2u^4 - 90b^{9/2}c^{5/2}dv + \\ &b^{5/2}c^{9/2}du + 8b^6cdu^9 - 8bc^5 - 6\sqrt{bc}c^6u^{-2}v + 18b^5cu^8v^2 + 3c^6u^{-2}v^2 + 6bc^5 - 16b^2c^3u^4 + \\ &3bc^7d^2u^{-2} - 18b^{3/2}c^{9/2}uv - 6b^{1/2}c^{11/2}u^{-1}v - 8b^5cu^8 + 4b^3c^3u^4 - 18b^5c^2du^7 + 6bc^6d/u - \\ &16b^4c^2u^6 + 3b^6u^{10}v^2 - 36b^{3/2}c^{11/2}v + 16b^2c^3\sqrt{bc}u^3v - 16b^4c^3u^5v - 90b^2c^4\sqrt{bc}du^2v - 24b^5c^2u^7v + \\ &+8b^2c^4u^2 - 36b^5c\sqrt{bc}du^8v - 8b^5\sqrt{bc}v + 60b^3c^3u^4v^2 - 6b^6cdu^9\Big]\, a^2(bc)^{-1}(c+bu^2)^{-4}\,, \end{aligned} \tag{5}$$

$$\begin{aligned}p = -\Big[&4bc^6du^{-1} - 6b^2c^6d^2 - 2b^5\sqrt{bc}u^7v + 40b^3c^3\sqrt{bc}dv/u - 8b^3c^3u^2 + 2\sqrt{bc}c^6u^{-2}v - 6b^2c^5d/u - \\ &4bc^5 + 6b^5c^2du^5 - 15b^4c^2u^4v^2 - 8b^4c^3du^3 - 12b^5c^2du^5 - 6b^4c\sqrt{bc}u^5v - 4b^5cu^6 + \sqrt{bc}c^5vu^{-3} + \\ &2b^6cdu^7 + 2b^6\sqrt{bc}du^8v + 12b^4c\sqrt{bc}u^5v + 12b^5c\sqrt{bc}u^6v + 8b^3c^4du - 15b^2c^4v^2 - 6b^6c^2d^2u^6 - \\ &6bc^5u^{-2}v^2 - b^6u^8v^2 - 4b^6cdu^7 + 30b^2c^4\sqrt{bc}dv + 4b^4c^3du^3 + 8b^3c^3u^2 + 4b^5cu^6 + 6bc^4\sqrt{bc}v/u + \\ &12bc^5\sqrt{bc}u^{-2}v - 15b^3c^5d^2 + 30b^4c^2\sqrt{bc}u^4v + 8b^3c^2\sqrt{bc}u^3v + 4bc^5\sqrt{bc}u^{-2} - 2bc^6\sqrt{bc}du^{-3} - \\ &c^6u^{-4}v^2 - b^7cd^2u^8 - 4b^3c^4du + 4b^5\sqrt{bc}u^7v + 12b^2c^5d/u + 4b^2c^3\sqrt{bc}uv - bc^7d^2u^{-4} - 12bc^4\sqrt{bc}v/u + \\ &8b^2c^4 - 20b^4c^4d^2u^2 - 20b^3c^3u^2v^2 - 8b^3c^3\sqrt{bc}uv - 4c^5\sqrt{bc}u^{-3}v - 6b^5cu^6v^2\Big]\, a^2(bc)^{-1}(c+bu^2)^{-4}\,, \end{aligned} \tag{6}$$

where $u = e^{az}$, $v = \arctan\left(u\sqrt{\frac{b}{c}}\right)$.

The energy momentum tensor of metric (1) is too complicated to make further analysis. Alternatively we may concentrate on a special family of solution (1),

$$ds^2 = -e^{2az}dt^2 + dz^2 + e^{2(az+be^{az})}(dx^2+dy^2). \tag{7}$$

See our original articles [5] for how to reduce the general solution (1) to this simplified form (7). There are two free parameters a and b in the above solution. With the above metric $\rho(z)$ and $p(z)$, respectively given by (5), (6) for the original metric (1), are reduced to extraordinarily simple form

$$\rho(z) = -a^2(3 + 8be^{az} + 3b^2e^{2az}), \tag{8}$$

$$p(z) = a^2(3 + 4be^{az} + b^2e^{2az}), \tag{9}$$

where we have set $8\pi G \equiv 1$, and G, as usual, denotes the Newton gravitational constant. In this article we will concentrate on metric (7). Before studying the detailed properties of (7), we first investigate the various limitations of it. Obviously when $a = 0$ (7) degenerates to Minkowski metric. When $b = 0$, it becomes

$$ds^2 = dz^2 + e^{2az}(-dt^2 + dx^2 + dy^2), \tag{10}$$

which is just anti-de Sitter (AdS) metric in an unattractive coordinate system. Surely it describes a homogeneous and isotropic solution in all directions, not only a plane symmetric one.

2 geodesics

Free falling is natural state of a particle. Mathematically, its orbit is time-like or null geodesics. In fact, any test particle with the same initial position and velocity goes along the same orbit: It is just the (weak) equivalence principle. Fundamentally, we can derive the geodesics by the self-parallel equations,

$$\frac{d^2x^\mu}{d\tau^2} + \Gamma^\mu_{\alpha\beta}\frac{dx^\alpha}{d\tau}\frac{dx^\beta}{d\tau} = 0, \tag{11}$$

where $x^\mu = (t, z, x, y)$, Γ denotes the affine connection of metric (7), τ is an affine parameter along the geodesic. We can calculate the affine connections routinely and then solve the four coupled second order equations. Generally speaking it is not an easy work.

Alternatively, we advance a different way by applying the properties of Killing vectors. The velocity normalization imposes the constraint along a curve,

$$g(\frac{\partial}{\partial\tau}, \frac{\partial}{\partial\tau}) = g_{tt}\left(\frac{dt}{d\tau}\right)^2 + g_{zz}\left(\frac{dz}{d\tau}\right)^2 + g_{xx}\left(\frac{dx}{d\tau}\right)^2 + g_{yy}\left(\frac{dy}{d\tau}\right)^2 = \eta, \tag{12}$$

where g is the metric tensor whose components are given by (7), $\eta = -1, 0, 1$ for time-like, null, space-like curve, respectively. For a time-like curve, τ denotes the proper time; For a null curve, τ represents an affine parameter; and for a space-like curve, τ stands for the length parameter. The inner product of a Killing vector ξ and the tangent vector $T = \frac{\partial}{\partial\tau}$ of a geodesics is a constant along the geodesic. This result can be proved as follows,

$$\nabla_T(g(T, \xi)) = g(\nabla_T T, \xi) + g(T, \nabla_T \xi) = 0, \tag{13}$$

where ∇ is the derivative operator consisting with the metric g. The three Killing vectors $\frac{\partial}{\partial t}$, $\frac{\partial}{\partial x}$, and $\frac{\partial}{\partial y}$ yield

$$g(T, \frac{\partial}{\partial t}) = g_{tt}\frac{dt}{d\tau} = -E, \tag{14}$$

$$g(T, \frac{\partial}{\partial x}) = g_{xx}\frac{dx}{d\tau} = P_1, \tag{15}$$

$$g(T, \frac{\partial}{\partial y}) = g_{yy}\frac{dy}{d\tau} = P_2, \tag{16}$$

respectively. Here, E, P_1, P_2 are three constants. Physically, for a time-like geodesic E denotes the energy of a unit mass particle moving along it, P_1, P_2 are the momentum of unit mass particle along x and y direction, respectively. From now on we only consider time-like and null curves since the particles of realistic matter can run only along such curves.

First we consider the motion along z direction, that is x =constant, y =constant. In this case we should solve the equation set (12) and (14). Note that the geodesics along z direction will be the same as of an AdS, since the equations to determine it are exactly the same as that of AdS, say, (12) and (14). The reason is that the AdS metric (10) permits the Killing vector $\frac{\partial}{\partial t}$ and the tangent of the geodesic also needs to obey the normalization equation (12), where g_{tt} and g_{zz} are the same with (7). For time-like geodesic, the result reads

$$z = \frac{1}{a}\left[\ln E + \ln|\sin(a\tau + c_1)|\right], \tag{17}$$

$$t = -\frac{1}{aE}\cot(a\tau + c_1) + c_2, \tag{18}$$

where c_1, c_2 are integration constants. It is clear there is a maximum value of z. For such an observer, the bigger value of E, the farther it can go. There is an apparent problem for this observer. z and t will be divergent when $a\tau + c_1 \to n\pi$, where n is an integer. This indicates that z, t are not suitable coordinates at the neighborhood of $a\tau + c_1 = n\pi$. The case is very similar to the case of Schwarzschild coordinate t. The Schwarzschild coordinate t of a free falling observer will be divergent when it goes to the event horizon. To find a well-posed coordinate is not very difficult. For example, we set a new coordinate I to replace t,

$$I = \frac{2(c_2 - t)}{1 + (t - c_2)^2} = aE\sin(2(\tau + c_1)), \tag{19}$$

and a new coordinate J to replace z,

$$J = ae^z = E|\sin(a\tau + c_1)|. \tag{20}$$

It is easy to see that for any τ, both I and J keep finite.

Now we consider its 3-velocity measured by t. The 3-velocity is defined as

$$\vec{v} = \frac{dx^i}{dt}\frac{\partial}{\partial x^i}, \tag{21}$$

where i runs from 1 to 3. Here only the velocity in z direction does not vanish, whose magnitude reads,

$$v = [g_{zz}(\vec{v},\vec{v})]^{1/2} = \frac{dz}{d\tau}(\frac{dt}{d\tau})^{-1}. \tag{22}$$

By using (17) and (18), we arrive at,

$$v = \frac{a^2E^2(c_2-t)}{1+(c_2-t)^2a^2E^2}. \tag{23}$$

Expanding v about $t = c_2$, we obtain,

$$v = -a^2E^2(t-c_2) + a^4E^4(t-c_2)^3 + \mathcal{O}\left((t_2-c)^5\right). \tag{24}$$

In the region around $t = c_2$, constant acceleration is a fairly good approximation since there is no $(t-c_2)^2$ term in the expansion series. In (24), v is independent of z, x, y. In such a sense, the global effect of gravitation, not only the local effect, can be simulated by a field of a uniformly accelerating observer. One may doubt that this is a physical conclusion since a coordinate system can be rather arbitrary, that is, if we change a coordinate system whether this conclusion remains valid. We present a brief analysis of this point. $\frac{\partial}{\partial t}$ is the time-like Killing vector which denotes that the metric is static. Hence the coordinate t, as its integral curve, is unique (up to a constant factor). Similarly, the coordinates x, y are unique (up to constant factors). The coordinate z is orthogonal to all of them in the 4-dimensional space-time with $g_{zz} = 1$. Hence it is unique too. So our conclusion is physical.

For null curves, $\eta = 0$, we reach,

$$z = \frac{1}{a}\ln(aE\tau + c_3), \tag{25}$$

$$t = -\frac{1}{a^2E^2\tau + ac_3} + c_4, \tag{26}$$

where c_3, c_4 are integration constants.

For the most general case in which x and y are not constants, we have to solve the associated equation set (12, 14, 15, 16). For the details of the this case, see the our original article [5].

Acknowledgments. This work is supported by National Education Foundation of China under grant No. 200931271104, Shanghai Municipal Pujiang grant No. 10pj1408100, and and National Natural Science Foundation of China under Grant No. 11075106.

References

[1] H. Stephani, D. Kramer, C. Hoenselaers, E. Herlt, M. A MacCallum, Exact Solutions of Einstein's Field Equations , Cambridge University Press, 2003.

[2] W. B. Bonnor, M. A. P. Martins, Class. Quantum Grav. 8 (1991) 727.

[3] A.H. Taub, Ann.Math. 53 (1951) 472.

[4] J. Horsky and J. Novotny, J.Phys.A 2 (1969) 251; J. Ipser and P. Sikivie, Phys.Rev.D 30 (1984) 712; O,Gron and H.H. Soleng, Phys.Lett.A 165 (1992) 191; B.W. Bonnor, Gen. Rel. Grav. 24, 551 (1992); B. Jensen and J. Kucera, Phys. Lett. A195, 111 (1994); M.L. Bedran, M.O. Calvao, F.M. Paiva and I.D. Soares, Phys. Rev. D55, 3431 (1997); A F F Teixeira, gr-qc/0502013.

[5] H. s. Zhang, H. Noh and Z. H. Zhu, Phys. lett. B663,291(2008) [arXiv:0804.2931 [gr-qc]]; H. s. Zhang, H. Noh, Phys. Lett. B670, 271(2009),arXiv:0904.0063.

White Dwarf Pulsars as Possible Electron-Positron Factories

Kazumi Kashiyama[1](a), Kunihito Ioka[2](b) and Norita Kawanaka[3](b)

(a) *Department of Physics, Kyoto University, Kyoto 606-8502*
(b) *Theory Center, KEK(High Energy Accelerator Research Organization), Tsukuba 305-0801*

Abstract

We suggest that white dwarf pulsars can compete with neutron star pulsars for producing the excesses of cosmic ray positrons and electrons ($e^{\pm}$) observed by the PAMELA, ATIC/PPB-BETS, Fermi and H.E.S.S. experiments. A double degenerate white dwarf binary mergers into a white dwarf pulsar with rotational energy ($\sim 10^{50}$erg) comparable to a neutron star pulsar. The birth rate ($\sim 1/100$yr) is also similar, providing the right energy budget. Applying the neutron star theory, we show that the white dwarf pulsars can produce $e^{\pm}$, up to ~ 10TeV for high magnetic fields ($> 10^{8}$G). In contrast to the neutron star case, the adiabatic energy losses of $e^{\pm}$ are negligible since their injection continues after the nebula expansion. The long activity also enhances the nearby sources, potentially dominating the quickly cooled $e^{\pm}$ above TeV energy, detectable by the future AMS-02, CALET and CTA experiment.

1 Introduction

Recently, the cosmic-ray positron fraction (the ratio of positron to electrons plus positrons) has been measured by PAMELA satellite [1]. The observed positron fraction rises in the energy range of $10\text{GeV} < \epsilon_{e^{\pm}} < 100\text{GeV}$, contrary to the prediction of secondary positrons, which are generated from cosmic-rays propagating in the interstellar medium (ISM). The ATIC balloon experiment has also revealed that there is an excess above 300GeV and a possible peak at $\epsilon_{e^{\pm}} \sim 600\text{GeV}$ [2], which is also reported by PPB-BETS [3]. These obsevations strongly indicate nearby sources of $e^{\pm}$ pairs within $d \sim 1$kpc since high energy $e^{\pm}$ lose their energy during propagation. There are some candidates for the origin of $e^{\pm}$ excess in the energy range > 10GeV, such as a neutron star pulsar, a microquasar, a gammaray burst and dark matter annihilations or decays. Instead we might be observing the propagation effects ([4] and reference therein).

In addition, recently the Fermi Large Area Telescope has measured the electron spectrum up to ~ 1 TeV that is roughly proportional to $\sim {\epsilon_e}^{-3}$ without any spectral peak as reported by ATIC/PPB-BETS [5]. The H.E.S.S. collaboration also provides the electron spectrum [6], which is consistent with the Fermi result up to ~ 1 TeV and shows the steep drop of the flux above that energy. The Fermi data, however, should has a large systematic error in the high energy range (< 300GeV) where a significant fraction of electrons are removed to avoid a large hadron contamination, and so the real flux is estimated not by the pure experimental data but by the Monte Carlo simulations. On the other hand the ATIC data contains the larger statistical errors than Fermi data. Therefore we cannnot judge which observations are more reliable so far.

Here we investigate a possibility for white dwarves to become a new candidate for high energy $e^{\pm}$ sources. We consider especially white dwarf pulsars, which are naively speaking neutron star pulsar like white dwarves, which have strong magnetic field $B \sim 10^{8\text{-}9}$G and high angular frequency $\Omega \sim 0.1\text{s}^{-1}$. We limit ourselvese to discuss the energetics, and show white dwarf pulsars potentially become TeV energy $e^{\pm}$ source. We invite the interested reader to our paper [7].

[1]Email address: kashiyama@tap.scphys.kyoto-u.ac.jp
[2]Email address: kunihito.ioka@kek.jp
[3]Email address: norita@post.kek.jp

2 Energy budgets in white dwarf pulsars

Now we show that white dwarves potentially have enough rotational energy for producing high energy $e^{\pm}$ cosmic rays.

Neutron star pulsars, which are formed after the supernova (SN) explosions, are one of the most promising candidates for the astrophysical sources of high energy positrons. For the PAMELA positron excess, each neutron star pulsar should provide mean energy $\sim 10^{48}$ erg to positrons since the cosmic ray positrons have $\sim 0.1\%$ energy budget of cosmic ray protons, which require $\sim 10^{50}$ erg per each SN, and the positrons suffer cooling more than the protons. The intrinsic energy source is the rotational energy of a newborn neutron star, which is typically

$$E_{rot} \approx \frac{1}{2} I \Omega^2 \sim 10^{50} \left(\frac{M}{1.0 M_{\odot}} \right) \left(\frac{R}{10^6 \mathrm{cm}} \right)^2 \left(\frac{\Omega}{10^2 \mathrm{s}^{-1}} \right)^2 \mathrm{erg}, \tag{1}$$

where I is the moment of inertia. Then, if all the neutron star pulsars are born with the above rotation energy and the 1% energy is used for producing and accelerating $e^{\pm}$, the neutron star pulsars can supply enough amounts of $e^{\pm}$ for explaining the PAMELA positron excess.

Let us show that double degenerate white dwarf binary mergers can also supply enough amounts of ratational energy. Here we consider the mass $0.6 M_{\odot}$ and radius $R \sim 10^{8.7}$cm for each white dwarves, which are typical observed ones. Just after a merger of the binary, the rotational speed v_{rot} can be estimated as $v_{rot} \approx (GM/R)^{1/2} \sim 10^8$cm/s, which corresponds to the mass shedding limit, and the angular frequency is about $\Omega = v_{rot}/R \sim 0.1 \mathrm{s}^{-1}$. Then, the rotation energy of the merged object is

$$E_{rot} \approx \frac{1}{2} I \Omega^2 \sim 10^{50} \left(\frac{M}{1.0 M_{\odot}} \right) \left(\frac{R}{10^{8.7} \mathrm{cm}} \right)^2 \left(\frac{\Omega}{0.1 \mathrm{s}^{-1}} \right)^2 \mathrm{erg}, \tag{2}$$

which is comparable to the NS pulsar case in Eq.(1). The event rate η_{WD} of the double degenerate white dwarf mergers in our galaxy remains uncertain. Any theoritical estimate requires a knowledge of the initial mass function for binary stars, the distribution of their initial separation, and also the evolution of the system during periods of nonconservative mass transfer. Nevertheless, the estimates are generally in the range [8],

$$\eta_{WD} \sim 10^{-2}\text{–}10^{-3} \ /\mathrm{yr/galaxy}. \tag{3}$$

This is comparable to the typical birth rate of neutron star pulsars [9]. Therefore, from the viewpoint of energy budget in Eqs. (1), (2) and (3), the white dwarves are also good candidates for the high energy $e^{\pm}$ sources as the neutron star pulsars, if the merged binaries can efficiently produce and accelerate $e^{\pm}$.

The estimated merger rate is also similar to that of type Ia supernove (SNIa), which is one of the reason that the double degenerate white dwarf mergers are one of the candidates for SNIa. Since the typical white dwarve mass is $0.6 M_{\odot}$, the merged objects do not exceed the Chandrasekhr limit $1.4 M_{\odot}$ even without any mass loss. Then, they leave fast rotating white dwarves, as suggested by some recent simulations [10], and could become white dwarf pulsars. Here, we assume that almost all the double degenerate white dwarf mergers result in the white dwarf pulsars.

The accretion scenario is also another possibility for the fast rotating white dwarf formation. In the single degenerate binary, which consists of a white dwarf and a main sequence star, there exist mass transfer from the main sequence star to the white dwarf as the binary separation becomes smaller and the Roche radius becomes larger than the radius of the main sequence star. In this stage, the angular momentum is also transfered to the white dwarf, and the white dwarf can spin up to almost the mass shedding limit with the rotational energy as large as Eq.(2).

As the discussion above, white dwarf pulsars potentially could become TeV energy $e^{\pm}$ source based upon the energetics. However we have to look more closely whether white dwarf pulsars can

(i) produce $e^{\pm}$ pairs,

(ii) accelerate $e^{\pm}$ up to TeV.

We show that white dwarf pulasrs can meet the both conditions in our paper [7].

3 References

References

[1] Andriani, O. et al. 2008, Nature, 458, 607

[2] Chang, J. et al. 2008, Nature 456, 362

[3] Torii, S. et al. 2008b, arXiv:0809.0760

[4] Kawanaka, N., Ioka, K., Nojiri, M. M. 2010, APJ, 710, 958

[5] Abdo, A. A. et al. 2009, Phys. Rev. Lett. 102, 181101

[6] Aharonian, F. et al. 2009, A & A, 508, 561

[7] Kashiyama, K. et al. arXiv:1009.1141

[8] Iben, I. Jr.,& Tutukov, A. V. 1984, APJS, 54, 335

[9] Narayan, R. 1987, APJ, 319, 162

[10] Lorén-Aguilar, P., Isern, J. & García-Berro, E. 2009, A & A, 500, 1193